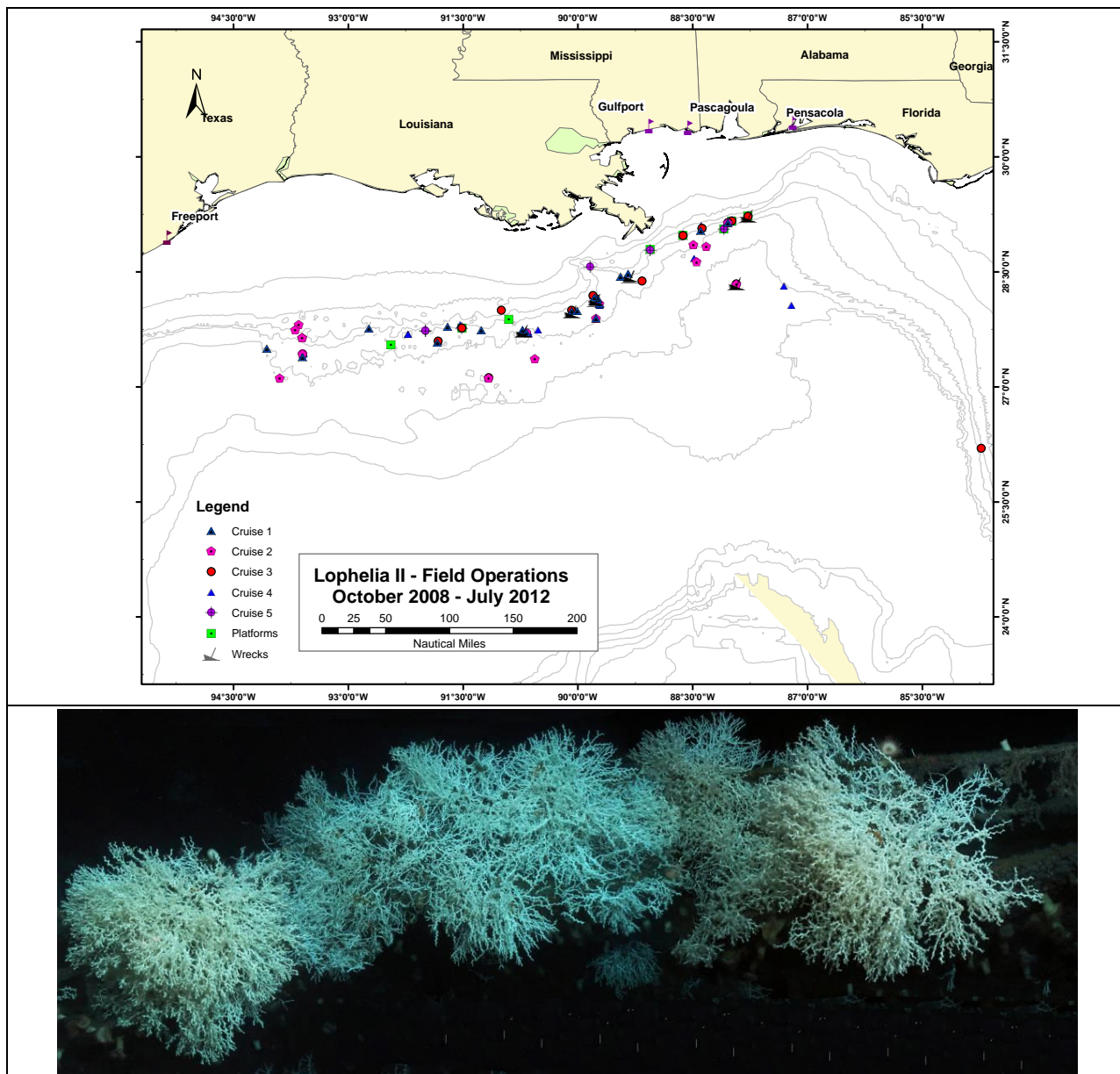# Exploration and Research of Northern Gulf of Mexico Deepwater Natural and Artificial Hard-Bottom Habitats with Emphasis on Coral Communities: Reefs, Rigs, and Wrecks—"Lophelia II"

# Volume I: Technical Report



**U.S. Department of the Interior**
**Bureau of Ocean Energy Management**
**Gulf of Mexico OCS Region**

BOEM
BUREAU OF OCEAN ENERGY MANAGEMENT

# Exploration and Research of Northern Gulf of Mexico Deepwater Natural and Artificial Hard-Bottom Habitats with Emphasis on Coral Communities: Reefs, Rigs, and Wrecks—"*Lophelia* II"

# Final Report

Authors

James M. Brooks
Charles Fisher
Erik Cordes
Iliana Baums
Bernie Bernard
Robert Church
Peter Etnoyer
Chris German
Elizabeth Goehring
Ian MacDonald
Harry Roberts
Tim Shank
Dan Warren
Susan Welsh
Gary Wolff
Douglas Weaver

# DISCLAIMER

This report was prepared under contract between the Bureau of Ocean Energy Management, (BOEM, previously the Minerals Management Service [MMS], then the Bureau of Ocean Energy Management, Regulation and Enforcement [BOEMRE]) and TDI-Brooks International, Inc. (TDI-BI). Study concept, oversight, and funding were provided by the US Department of the Interior, Bureau of Ocean Energy Management, Environmental Studies Program, Washington, DC, under Contract Number M08PC20028. This report has been technically reviewed by BOEM and it has been approved for publication. The views and conclusions contained in this document are those of the authors and should not be interpreted as representing the opinions or policies of the US Government, nor does mention of trade names or commercial products constitute endorsement or recommendation for use.

# REPORT AVAILABILITY

To download a PDF file of this Environmental Studies Program report, go to the US Department of the Interior, Bureau of Ocean Energy Management, Environmental Studies Program Information System website and search on OCS Study BOEM 2016-021. Copies can also be viewed at selected Federal Depository Libraries. See http://www.gpo.gov/libraries/. In the near future, you will also be able to get this report from the National Technical Information Service at the address below.

| | |
|---|---|
| U.S. Department of the Interior | U.S. Department of Commerce |
| Bureau of Ocean Energy Management | National Technical Information Service |
| Gulf of Mexico OCS Region | 5301Shawnee Rd. |
| Public Information Office (MS GM 355A) | Springfield, Virginia  22312 |
| 1201 Elmwood Park Blvd. | Phone: (703) 605-6000,1-800-553-6847 |
| New Orleans, Louisiana  70123-2394 | Fax: (703) 605-6900 |
| Phone:  (504) 736-2519, 1-800-200-GULF | Web site: http://www.ntis.gov/ |
| Fax:  (504) 736-2620 | |

# CITATION

# TABLE OF CONTENTS

# LIST OF FIGURES

xvi

xvii

xxiii

xxiv

# LIST OF TABLES

# 1   INTRODUCTION

## 1.1 OVERVIEW

This document represents TDI-Brooks' Final Report for the *Lophelia* II Project, Contract M08PC20038, issued by the U.S. Department of the Interior, Bureau of Ocean Energy Management, Regulation and Enforcement (now the Bureau of Ocean Energy Management [BOEM]) "Exploration and Research of Northern Gulf of Mexico Deepwater Natural and Artificial Hard Bottom Habitats with Emphasis on Coral Communities: Reef, Rigs, and Wrecks. This report provides detailed information regarding the five (5) cruises completed during the field operations phase, the study sites selection process and sites visited with full descriptions of the conditions encountered both physically and biologically.  The analytical results from the research effort includes community structure using photomosaics, trophic studies, laboratory experiments with *Lophelia pertusa*, archaeology, educational outreach and analyses of a *Lophelia*  mound piston core study and commercial fisheries impact on deepwater corals presented in 15 sections. This report is the final product of Contract M08PC20038.

## 1.2 BACKGROUND

Over the last half century, offshore exploration for hydrocarbons in the northern Gulf of Mexico (GoM) has advanced from the bays and inner shelf to the continental slope-to-continental rise transition.  Geophysical and geotechnical data collected in support of both exploration and production has been largely responsible for the foundation of our present understanding of slope geology.  This database emphasizes the extremely complex geological framework of the northern Gulf's continental slope and the surprisingly important role that the expulsion of subsurface fluids and gases has on shaping surficial geology and biology of the modern seafloor.  Regional topography of the slope consists of basins, knolls, ridges, and mounds derived from the dynamic adjustments of salt to the introduction of large volumes of sediment over long time scales. Superimposed on this underlying topography is a smaller class of mounds, flows, and hard-bottom areas that are the products of the transport of fluidized sediment, mineral-rich formation fluids, and hydrocarbons to the present sediment-water interface. The geologic response to the expulsion process is related both to the products being transported and the rate at which they arrive at the seafloor.  Mud volcanoes and mudflows are typical of rapid flux settings where fluidized sediment is involved.  Slow flux settings are mineral-prone.  Authigenic carbonate mounds, hard grounds, crusts, and nodules are common to settings where hydrocarbons are involved.

The authigenic carbonates that are a part of nearly every fluid-gas expulsion site provide the hard substrate necessary for many marine sessile organisms, particularly corals.  Consumption of hydrocarbons by microorganisms at expulsion sites is intimately associated with carbonate precipitation and the production of hard substrates. Aerobic methane oxidation produces $CO_2$ and decreases pH, favoring dissolution of carbonates (Aloisi et al., 2002). Anaerobic microbial sulfate reduction using hydrocarbon substrates causes sulfate depletion and simultaneous bicarbonate and hydrogen sulfide enrichments in sediments.  The increase in carbonate alkalinity of pore fluids produces calcium-magnesium carbonate by-products (Ritger et al, 1987; Roberts and Aharon, 1994).  These carbonates take the form of distinct mounds with relief of up to 10 m, larger boulders and blocks, and low relief slabs and hard grounds.

Recent manned submersible and remotely operated vehicle (ROV) dives to the middle and lower continental slope confirm the existence of these hard substrates to the deepest parts of the slope. Direct observation and sampling of expulsion sites started in the mid-1980s on the upper slope. We now know from analysis of three-dimensional (3-D)-seismic data and submersible- ROV dives that numerous expulsion sites with hard substrates provide habitat for deep-water corals over the slope's full depth range.

## 1.2.1 Deep-water Hard -Ground Communities

In the context of this study, deep hard-ground communities of the GoM comprise all of the biological communities inhabiting natural or artificial hard substrates, excluding the chemosynthetic seep communities. These communities consist of foundation species, those species that form large complex habitats at these sites, and their associated fauna ranging in size from large mobile fishes to microscopic meiofauna. The most prominent foundation species in these communities are the deep-water ("cold-water") corals. The terms "deep-water corals" or "cold-water corals" include relatives of the tropical reef-forming scleractinian corals, but also refer to a variety of other cnidarian taxa including antipatharians (black corals), gorgonians (including bamboo corals), alcyonaceans (soft corals), and stylasterine hydrocorals. Other taxa, including anemones and sponges are also significant contributors to the biogenic framework of these deep-water reef systems. When related to coral species, the term "deep water" refers to aphotic waters greater than 200 m depth.

In the GoM, deep-water corals are commonly found on seep-related authigenic carbonates. The most common species of reef-forming deep-water coral in the GoM is *Lophelia pertusa* (=*prolifera*). This species was first recovered in the late 1800s by the *U.S. Coast Survey Steamer Blake* (Cairns 1978). *L. pertusa* "reefs" in the GoM were first reported from a deep water trawl taken by the motor vessel (M/V) *Oregon* in 1955 (Moore and Bullis, 1960). Recently, submersible observations have located *L. pertusa* in numerous additional locations on the upper slope of the northern GoM (Schroeder 2002, Schroeder et al. 2005, Cordes et al. 2006, Cordes et al. 2008, CSA, 2007) and this study has contributed significantly to our knowledge on the distribution of this coral.

Deep-water corals have also been observed colonizing artificial substrates in the GoM. Previous studies have located coral communities on the shipwreck *Gulfpenn* in Mississippi Canyon (MC) lease block 497 (MC497). Two scleractinians, *Lophelia pertusa* and *Pourtalosmilia conferta*, were found on the *Gulfpenn* (Church et al. 2007). *P. conferta* was restricted to a solitary, medium size colony observed near the top of the starboard boom stanchion. *L. pertusa* was far more abundant, colonizing 12-15 percent of exposed surfaces and structures throughout the wreck. *L. pertusa* appears to have developed most successfully on surfaces or structures that have a vertical orientation (e.g. hull, bulwarks and sides of the superstructures) or that have an upright (e.g. davits, masts, booms and stacks), raised (e.g. catwalks and deck piping), or open (e.g. railings and rigging) construction. The most extensive coral growth occurs along the railing, bulwarks and hull on the starboard side and on the deck piping and catwalks. At numerous locations clusters of adjacent colonies have coalesced into an initial phase of 'thicket' building. The largest development is a 6 to 7 m high by 3 to 3.5 m wide aggregate of at least 5 or 6 coalescing colonies. *L. pertusa* was also found living on the sediment adjacent to the hull and colonizing wreckage scattered about in the

debris field northwest and west of the *Gulfpenn*. In this study, a sister-ship sunk in the same era, the *Gulfoil*, was discovered. It was also covered with extensive *L. pertusa* growth coalescing into the thicket phase. These shipwrecks and others are discussed in Chapter 10.

Increasing industry activity in deepwater has resulted in the creation of numerous platforms in water depths exceeding 300 m. In areas where hard substrates are limiting, these platforms may significantly increase the potential range of corals and other hard-ground fauna. Growth of *Lophelia pertusa* had previously been noted on the Pompano platform in Viosca Knoll (VK)989. This study continued the exploration and characterization *L. pertusa* growth rates and patterns on several platforms, and examination of their potential connection to other coral populations and surrounding deep-water communities.

### 1.2.2  Deep-water Coral Biology and Ecology

Although the existence of deep-water corals has been known since the first descriptions by Linnaeus in the mid 1700s (Cairns 2001) and the oceanographic research expeditions of the His Majesty's Ship (*H.M.S.) Challenger* and *H.M.S. Porcupine* in the late 1800s (Rogers 1999), we are still in the process of describing their distribution and basic elements of their biology and ecology. The popular conception of corals is that they are restricted to the shallow waters of tropical seas; however, 65% of the known 5,160 species of corals occur in waters deeper than 50 m across the globe (Roberts et al. 2009).

The most well-known deep-water coral species is *Lophelia pertusa,* a cosmopolitan coral found in water depths from 39 m in Norwegian fjords to over 3,000 m on the Mid-Atlantic Ridge and some seamounts (Bett 1997, Rogers 1999). Current knowledge suggests that distribution, abundance, and growth of *L. pertusa* is strongly influenced by environmental factors such as temperature, food supply, hydrography, dissolved oxygen concentration, and carbonate chemistry (Rogers 1999; Thiem et al. 2006; Davies et al. 2010; Guinotte et al. 2006), and each subspecies varies according to latitude, depth, surface productivity, seafloor topography, and position on the ocean conveyor belt (Broecker 1991). *L. pertusa* is typically associated with temperatures from 4 to 12°C (Frederiksen et al. 1992; Freiwald et al. 1997), dissolved oxygen concentrations from 3 to 5 mL·L$^{-1}$, and a relatively constant salinity from 35 to 37 (Roberts et al. 2003). There have been no previous studies characterizing the aragonite saturation state adjacent to *L. pertusa* reefs, although this is considered to be a significant factor in the worldwide distribution of scleractinians (Davies and Guinotte 2011). *L. pertusa* exhibits patchy distribution at local spatial scales, suggesting an influence of current regime on food delivery (Genin et al. 1986; Becker et al. 2009) and larval supply (Roberts et al. 2009).

*L. pertusa* develops from individual polyps, to larger "thickets", to massive reef structures. It has separate sexes and exhibits seasonality in reproduction with spawning apparently occurring in September to October in the GoM (Brooke and Schroeder 2007), and February in the Northeast Atlantic (Waller and Tyler 2005). Gametes are released and fertilized externally, producing lecithotrophic planula larvae (Waller and Tyler 2005), which require hard substrata for settlement (Wilson 1979). Individual branches of coral grow slowly, and previous estimates of linear extension rates range from 2-30 mm·yr$^{-1}$, although pioneer colonies on man-made substrates may grow much faster (Mortensen and Rapp 1998; Gass and Roberts 2006). As the branches of the colony grow, new polyps are added via intra-tentacular budding. The rate of addition of new polyps

in *L. pertusa* is poorly characterized, with most recent estimates approaching 1 polyp every 2 to 3 years, though with a high level of uncertainty (Sabatier et al. 2012). Several studies of *L. pertusa* reveal patterns of allometric growth, the differential extension of select parts of a colony relative to the whole (e.g. Mortensen 2001; Brooke and Young 2009), with younger polyps growing significantly faster than older polyps (Maier et al. 2009). Small, young colonies consisting of living, white coral polyps are normally positioned along the edge of rocky outcrops or authigenic carbonates. As they grow, larger thickets of coral are usually comprised of a periphery of living coral surrounding a central dead portion of coral skeleton that serve as substrate for secondary settlement of *L. pertusa* and other species of deep-water corals (Wilson 1979). Larger, reef-like structures may cover extensive areas. The largest known continuous reef structure is roughly oval in shape covering 13 km along its axis and 300 m in diameter and consists of coral matrices up to 35 m thick (Freiwald et al. 1999). Carbon ($^{14}$C) dating has placed the age of dead corals at the center of similar (but much smaller) structures in the GoM at over 40,000 years (Neumann et al. 1977).

Deep-water corals are important sources of habitat heterogeneity on continental shelves worldwide. They create habitat for a diverse group of associated fauna that may occur in abundances orders of magnitude above that on the surrounding seafloor (Jensen and Frederiksen 1992). In the Northeast Atlantic alone, over 1,300 species have been recorded living in and on *L. pertusa* habitats in physical and photographic samples (Rogers 1999; Roberts et al. 2006; Henry and Roberts 2007). On two reef structures alone in Norway, 256 species were recorded from recovered coral blocks (Jensen and Frederiksen 1992). In the Porcupine Seabight in the Northeast Atlantic, 313 taxa were collected in 7 box core samples from coral mounds (Henry and Roberts 2007). The diversity of the community on these reefs rivals the diversity of many tropical zooxanthellate coral reefs (Rogers 1999). However, these studies all involved dredge and box core samples that include species that are likely not be intimately associated with coral structure but inhabit the sediments beneath the coral framework and in the case of dredges perhaps as much as 100s of m away. In the GoM, 68 taxa of large macrofauna and megafauna (> 1 mm sieve size) were found in closely associated with *L. pertusa* in quantitative community collections obtained with custom collection devices deployed from a submersible (Cordes et al. 2008). Photographic surveys indicate that a variety of invertebrate and fish species occur primarily and possibly exclusively in these habitats (Ross and Quattrini 2007; Lessard-Pilon et al. 2010). Some associated species appear to have very specific interactions with *L. pertusa* including the polychaete *Eunice* sp. which may help to assemble coral structure and the coralivorous gastropod *Coralliophila* sp. (Cordes et al. 2008; Becker et al. 2009).

While *L. pertusa* remains the best-known deep-water corals species in the GoM in particular and the world in general, many other species of deep-water corals exist and are not as well studied. The number of described deep-water scleractinian coral species now exceeds the number of described shallow-water scleractinians (Cairns 2001). In the GoM, 63 species of azoozanthellate scleractinians have been reported (Cairns 1993). In addition to *L. pertusa*, 3 other species are known to form reef-like structures. *Madrepora oculata* is a cosmopolitan reef-forming species that has been found down to 1,500 m depth (Cairns 1978). *Enallopsammia profunda* is found to 2,165 m depth and is another common component of the deep-water reef-forming coral assemblage (Rogers 1999). *Solenosmilia variabilis* has been documented in waters to 3,383 m (Cairns 1978). This species is a contributor to coral frameworks in the Atlantic (Rogers 1999) and is the most

common deep-water reef species on Southwest Pacific seamounts (Koslow et al. 2001). All three of these species were observed and collected at a recently discovered site in Green Canyon (GC) 852 during the Minerals Management Service (MMS) /National Oceanic and Atmospheric Administration (NOAA) funded characterization of chemosynthetic communities in the deep GoM (Roberts et al. 2007). There are also at least 5 species of solitary scleractinians that contribute to the species richness of the deep-water coral community below 1,000 m in the GoM (Cairns 1978).

In addition to scleractinian corals, a number of gorgonian and antipatharian corals are present in deep waters in the GoM (Cairns 1978; Cairns 1993). They can occur in the same areas with extensive development of scleractinian corals as well as in areas lacking reef-building hard corals. In either case these taxa add significant habitat heterogeneity and vertical relief. Gorgonians (Anthozoa: Octocorallia: Gorgonacea) are some of the most common and conspicuous sessile coral reef fauna in the shallow GoM and Caribbean Sea (Cairns 1977), and occur worldwide deeper than 4,200 m (Bayer 1956). Gorgonians create habitat for associated species of fish (Etnoyer and Warrenchuk 2007), invertebrates (Buhl-Mortensen and Mortensen 2005), and microbial fauna (Penn et al 2006). Gorgonians are also relatively long-lived organisms, with single colonies of *Primnoa reseadiformis* estimated to be between 150 (Andrews et al. 2002) and 500 years old (Risk et al. 2002). Recent reviews of octocoral diversity in the GoM place the total number of species at 162 (Cairns and Bayer 2009). Gorgonacea in the Gulf occur from intermediate to abyssal depths (Isididae, 250-2,800 m; Primnoidae 200-1400 m) (Etnoyer, unpublished data). The most common deep-water species include the endemic primnoid *Callogorgia americana delta* that forms extensive stands at many of the Green Canyon sites and on carbonate blocks in Viosca Knoll (VK) 826, and the broadly distributed bamboo coral *Acanella eburnea*. Precious corals (*Corallium* spp.) are rare, but one colony was recently sampled at GC852 during the Chemo III project.

Forty-two species of antipatharians have been recorded from the western Atlantic and about 30 of these have been found in the GoM (Cairns et al., 1993). The greatest species diversity occurs in a depth range of about 20 to 200 m, however, some GoM species have been reported from depths greater than 300 m, including *Elatopathes abietina* (Pourtales), *Bathypathes patula* Brook, *Aphanipathes pedata* Gray, *Stylopathes columnaris* (Duchassaing and Michelotti), *Sibopathes macrospina* (Opresko)*, Tanacetipathes hirta* (Gray), *Parantipathes tetrasticha* (Pourtales), and *Leiopathes glaberrima* (Esper). Other antipatharian taxa that might be expected to occur in deep waters in the GOM are species of the genera *Chrysopathes* spp., *Heliopathes*, and *Acanthopathes*. Although many antipatharian species form colonies of relatively small size, some are large enough to create habitat for many other marine organisms (see Yoklavich and Love, 2005). There is, however, very little information on the habitat-forming species in the deep waters of the GoM, and very little is known about the distribution of antipatharians in the deep sea in general. In deep reef and upper slope habitats, antipatharians can be a major component of the sessile benthic fauna, and it is likely that they play a similar role in the deep sea – particularly in locations characterized by distinct topographic features, hard bottom, and relatively fast currents, such as many of the hard grounds of the GoM slope.

## 1.2.3 Deep-sea Environmental Issues and Impacts

With the current push to expand energy reserves in U.S. territorial waters, the activities of energy companies in the deep GoM will continue to increase. As of April 2013, 5,891 active leases are currently held by industry, with a significant portion (74%) concentrated within the north-central

GoM. Lease statistics from 2000 to 2012 show an expansion of industry interest into progressively deeper waters; in 2012, 58% of industry bids in the north-central GoM were made for areas deeper than 200 m.

Exploration and extraction of energy reserves impact hard-bottom communities in the GoM because the formation and occurrence of authigenic carbonates is strongly correlated with chemosynthetic activity associated with hydrocarbon seeps in this region (Formolo et al. 2004). Therefore, the substrate for coral settlement is largely tied to the occurrence of existing or relict hydrocarbon seeps in the GoM. In shallow water corals, direct exposure to hydrocarbons can cause reductions in growth and fecundity, prevention of settlement, and even whole colony mortality (Loya and Rinkevich 1980). In the vicinity of oil platforms in the GoM, increased abundances of poly-aromatic hydrocarbons (PAHs) and metals (Ba, Hg, Pb, and Zn) as well as organic enrichment resulting from the discharge of well cuttings have been shown to lead to changes in infaunal community structure (Peterson et al., 1996). Drilling discharges of cuttings and fluids will smother fauna, cause some mortality and alter both the geological and geochemical habitat. Such impacts may be greater in deep development due to increased use of multiple wells drilled through a single seafloor template and use of bio-active synthetic drilling fluids. The dependence of deep hard-ground fauna on very sparse suspended detritus may make these communities especially sensitive to the added particulate influx since this may clog filter apparatus and lead to stress responses. In addition, the chains and wire ropes used to anchor floating deep-water oil platforms to the bottom have been implicated as the cause of damage to *Lophelia* reefs in the Viosca Knoll region of the Gulf (Schroeder 2002). Once sites of significant coral abundance have been identified, the standoff and site approval requirements of Notice to Leessees (NTL) 2000-G20 should provide adequate protection from routine operations. In a more general sense, the establishment of a deep-water coral research program in the deep GoM prior to significant anthropogenic disturbance will provide us with a background against which to measure future impacts and may improve our understanding of other deep-water coral habitats in areas which have already been impacted by human activity.

The current lack of a significant deep-water fishery in the GoM also makes this an ideal setting for the study of deep-water coral habitats in the absence of impact from such fisheries. In other regions, the past and ongoing fishery pressure on populations of deep water fishes with long life spans such as rockfish (*Sebastes* spp.), orange roughy (*Hoplostethus atlanticus*), and pelagic armourhead (*Pseudopentaceros wheeleri*) has resulted in significant damage to coral communities from deep-water fisheries (Rogers 1999, Koslow *et al*. 2001, Roberts et al. 2002). The deepest commercial fisheries for bottom-dwelling fishes in the GoM remain in waters overlying the continental shelf. However, the presence of economically viable fishery species such as the longfin hake (*Phycis chesteri*), wreckfish (*Polyprion americanus),* blackbelly rosefish (*Heliocolenus dactylopterus*) and numerous grenadiers (Macrouridae) in deep waters (McEachran and Fechhelm 1998) and specifically at *L. pertusa* banks (Sulak et al. 2007) suggests that there may be current fishery activity that has been largely undocumented, and that a larger commercial deep-water fishery in the GoM may yet develop.
The correlation between the distribution of deep-water corals and the location of deep water human activity has led to recent conservation efforts on the behalf of deep-water corals. For example, the Darwin Mounds off Scotland (Masson et al. 2003) were recently proposed by the European Union as Special Areas of Conservation. The *Lophelia* reefs off Norway are protected under the Coral

Protection Regulation of 1999 (Fossa *et al*. 2002). In the areas surrounding the Azores, Madeira, and Canary Islands, all bottom trawling is prohibited in depths > 200 m. Off New Zealand and Australia, seamounts are closed to dredging and trawling, and a marine protected area (MPA) was established to protect the scleractinian *Solensmilia variabilis* (Koslow *et al*. 2001). In 2005, the Aleutian Islands Habitat Conservation Area was established covering nearly 1 million km$^2$ for deepwater coral protection off Alaska. Bottom trawling is restricted in two conservation areas in Atlantic Canada and in canyons near George's Bank off the New England coast. Off the southeast U.S. coast, a MPA exists for *Oculina varicosa* off the coast of Florida and a large deep-water coral Habitat Area of Particular Concern has been proposed. In the GoM, the high-density *L. pertusa* portion of Viosca Knoll 826 has been proposed as a conservation area. To compliment these activities in the U.S., the 2007 reauthorization of the Magnuson-Stevens Fishery Conservation and Management Act called for the Deep Sea Coral Research and Technology Program to locate, map, and monitor activity in locations where deep-sea corals are known or likely to occur. In addition to the establishment of long term monitoring stations, the predictive capacity for determination of areas where corals are "likely to occur" was developed as a prime focus of the proposed research here and will be a significant tool for future management of deep coral communities in the GoM.

## 1.3 OBJECTIVES OF THE PROJECT

A primary goal of this study was to obtain a robust predictive capability for the occurrence of rich cnidarian (primarily scleractinian coral) hard-ground communities in the deep GoM. To achieve this long-term goal, this study accomplished eight interrelated and interdependent objectives:

1) Discovered and described numerous new locations at greater than 300 m depth in the GoM with extensive coral community development.
2) Established long term monitoring stations at many of these locations to allow study of natural and anthropogenic change over time.
3) Characterized the newly discovered communities geologically and biologically, and determined the primary factors that contribute to the biogeographic patterns of deep coral community biodiversity in the GoM.
4) Conducted laboratory experiments that provide a more comprehensive understanding of the fundamental processes that control the occurrence and distribution of *L. pertusa* in the GoM.
5) Gathered field data that constrain the environmental conditions that allow *L. pertusa* community development and provide insights into how its distribution may change with changing climatic conditions.
6) Conducted genetic analysis of several different corals in order to better understand both deep coral phylogeography and the connectivity within coral taxa in the deep GoM.
7) Conducted an in depth study of the geologic history of the most significant new deep-water coral site discovered as part of this program
8) Documented coral communities on artificial substrates and determined depths, densities and growth rates of *L. pertusa*, the key cnidarian foundation taxa on the substrates.

# 2   STUDY SITES AND FIELD ACTIVITY OVERVIEW

The program completed five cruises between 2008 and 2012 to examine specific sites (and what you were looking for). Sites were identified using 3D seismic data initially and additional methodology developed during the program and described below. Cruise overviews are presented in this chapter and much of the cruise details are in appendices.

## 2.1  SITE SELECTION

Most colonial corals require a hard substrate to settle and grow upon. In the deep GoM the majority of the sea floor is soft substrate unsuitable for coral growth, however free-living bacteria at sites of natural oil and gas seepage create conditions favorable for the formation of authigenic carbonates, which form hard-ground areas.  Thus, sites of historic and current hydrocarbon seepage are nearly always associated with some degree of hard-ground development and when these hard grounds are in appropriate locations they may harbor lush deep-sea coral communities. Industry datasets and investigations funded by BOEM and NOAA have shown these sites occur to the deepest parts of the continental slope. Exposed carbonates occur as nodular masses in unconsolidated surface sediments, slabs, boulders-blocks, or mounds of various sizes.  The use of 3D-seismic sea floor amplitude data for finding hard bottom areas associated with hydrocarbon seeps started in the early 1990s. However, during the BOEM Chemo III project we improved on earlier methodologies and developed considerable expertise in the use of 3D-seismic data to locate potential exposed hard grounds through ouranalysis of sea floor reflectivity or surface amplitude derived from 3D-seismic data.  Consistent with earlier research, on hydrocarbon seeps, we followed up on the potential sites identified in this project with remotely sensed seismic data with in-situ verification of the presence of megafaunal communities using cameras and ROVs.

The basic data sets used in this study consisted of 192 3D-seismic surveys acquired over 76,000 mi$^2$ (196.850 km$^2$) across the upper, middle, and lower continental slope of the northern and northwestern GoM.  These are data collected by oil and gas companies as well as speculative acquisitions by survey companies.  The data are held by BOEM in their New Orleans, Louisiana office.

For the 3D-seismic analysis, reflection strength (amplitude) and phase were determined by using a 10 millisecond window from the sediment-water interface into the shallow subsurface.  This window translates into an interval approximately 7.6 m (25 ft) thick.  Phase is a seismic attribute related to amplitude and has a sawtooth appearance resulting from amplitude maxima and minima. Phase can be both positive and negative with values from 180º to -180º depending on the amplitude trace.  A zero phase value corresponds to amplitude maxima, whereas  minimal amplitude values cause a phase reversal.  Phase reversal can indicate the presence of gas bubbles or pockets contained in near-surface sediments.  As applied in the study, phase helps define "fast" (usually hard ) and slow" (usually soft, gas charge ) areas of the seabed and associated shallow subsurface.

The continental slope of the northern GoM is punctuated with seafloor "bright spots," areas of high seismic energy reflectivity or amplitude (Roberts et al., 2006).  At the start of this program numerous sites were selected for further analysis based on their 3D-seismic amplitude character. This work involved accessing the extensive and slope-wide BOEM seismic database.  Selection of

sea floor amplitude anomalies that fit the project requirements was conducted in cooperation with William Shedd of BOEM. For this stage of selection, extensive (and, in many cases overlapping) time data from the 3D seismic surveys was used to generate bathymetry. In most 3D-seismic data sets, the sea floor reflector was strong and well suited to the automatic picking programs on the BOEM New Orleans Office Sun Workstation using Geoquest's "Autopix" and "ASAP" in "IESX". The sea floor horizon was given a unique, consistent name for each survey (wb-survey permit name) to avoid amplitude display problems caused by the wide variation in amplitude scaling between surveys. Due to time and data storage constraints, the sea floor amplitude interpretations were not normalized. Every seafloor horizon was defined as a positive (compressional) event in the horizon settings. As many seed lines were interpreted by hand as was deemed necessary for each survey, depending on the complexity and rugosity of the sea floor bathymetry and the highly variable amplitude response. The automatic picking program was then started and let run overnight. Upon completion, the resulting interpretation was quality checked for bad picks and gaps. This procedure proved to be especially important in some high dip and complex areas to "clean up" the interpretation.

Upon completion of the initial picking process, amplitude interpretation of each survey was posted and potential hard ground sites identified. Those that have high positive amplitudes were outlined with red fault polygons, interpreted as areas with extensive authigenic carbonates and/or hydrates that should have anomalously strong positive reflection coefficients. Those areas with low positive responses or negative responses (phase reversals from peak to trough), often embedded within the high positive areas, were outlined with green fault polygons, interpreted as areas of very high flux rates with gas saturated muds that should have weak positive to negative reflective coefficients. Many sites with abundant chemosynthetic and hard bottom communities have been found using the BOEM seismic database and the techniques described above. During this project, BOEM used this basic methodology to identify over 23,000 potential hard grounds on the northern GoM continental slope (see "wb-anomaly" at http://www.boem.gov/Oil-and-Gas-Energy-Program/Mapping-and-Data/Map-Gallery/Seismic-Water-Bottom-Anomalies-Map-Gallery.aspx) (Figure 2-1).
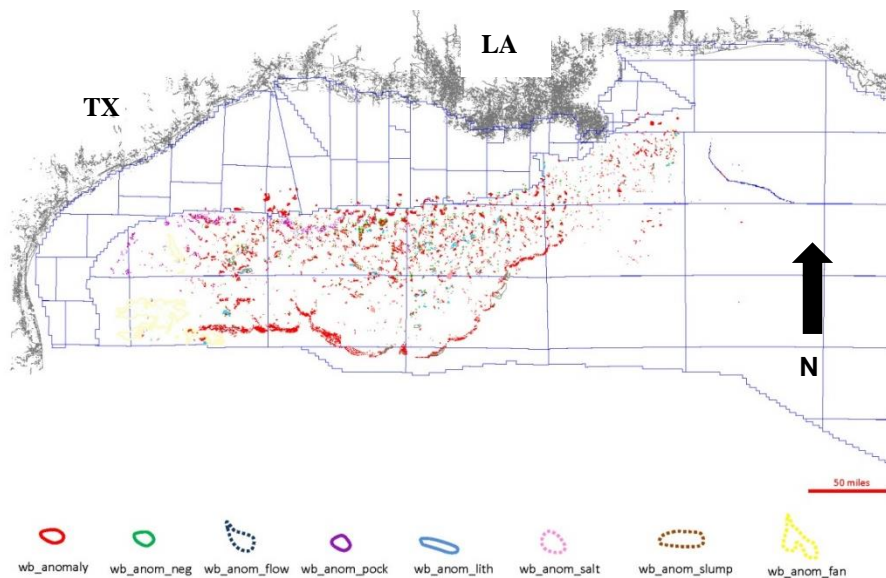


Figure 2-1. Seismic seafloor amplitude anomaly distribution, from BOEM website.
Over 23,000 positive anomalies shown in red are potential hard grounds.

9

For this project, initial site selection was further refined using criteria likely to influence the occurrence of deep-water corals, for the following reasons. The 3D seismic data detect hard bottom conditions in the upper 7-8 m of the shallow subsurface, and is not always a reliable indicator of exposed carbonates.  The hard reflector could be buried by meters of sediment, rendering it inaccessible to corals.  This factor was considered in site selection. In ddition, one of the criteria used during the second stage of site selection was a local topography with potential exposure to bottom currents that would remove sediment accumulation from older hard grounds.  Because currents also deliver food to the corals, local topographic highs, steep slopes, and generally rough topography were also important criteria in addition to recognition of hard-bottom areas in the 3D seismic data sets.

Sites selected for further investigation were normally first surveyed using high quality multibeam sonar from a surface ship and by either a drift camera, a towed camera system, or an autonomous underwater vehicle (AUV).  If any imaging system identified colonial corals in the area, the site was further investigated by ROV. In a few cases later in the program very favorable sites were explored by ROV without previous imaging.   One example, the new sites on the West Florida Slope, were identified based on high quality multibeam maps and known coral occurrence on similar features in the area.  Another example was the 338/294 site discovered by *Jason* based on 3D-seismic data alone.

Over the course of this project a new technique was employed that proved instrumental in the discovery of multiple sites in the vicinity of the Macondo well.  Although a drift or towed camera system can be a very valuable discovery tool, these tools often miss sites because of the relative small areas that are imaged and the possibility of missing exposed carbonates if they are not present in high density.  As a result they are not reliable tools to confirm <u>absence</u> of corals in an area and are likely to miss isolated coral communities. As part of a Natural Resources Damage Assassment (NRDA) program the Principal Investigators (PIs) in collaboration with W. Shedd of BOEM selected a number of sites near the Macondo well using our normal criteria and then used the *Sentry* AUV to first create a very high- (sub-meter) resolution bathymetric map of the area identified from an altitude of 25 m.  From this map, the sub-areas with fine scale rugosity were identified (which often proved to be exposed carbonate boulders or slabs).  These sub-areas were targeted for intensive imaging from an altitude of 5 m on a subsequent AUV dive.  This technique was very successful and is recommended for intense exploration in geographically defined regions where confirmation of both presence and absence is an important consideration.

## 2.2 CRUISE OVERVIEWS

The *Lophelia* II project involved exploration and research of the northern GoM deepwater natural and artificial hard bottom habitats with emphasis on coral communities.  It also included archeological studies of 7 shipwrecks and biological investigations of energy platforms. A total of five dedicated cruises were conducted as part of this program, and piston cores were collected during a sixth cruise primarily dedicated to other programs (see Section 9 of this report). The first *Lophelia* II cruise with a small survey ROV took place in September 2008, and the second cruise using the AUV *Sentry* in June 2009. Cruises 3 and 4, using the *Jason II* ROV were conducted in August–September 2009 and October-November 2010.  A final cruise dedicated to work on energy

platforms was conducted with the Kraken II ROV in July 2012.  Full reports on all of these cruises have been supplied to BOEM.

## 2.2.1  Cruise 1: NOAA Ship *Nancy Foster* and *SeaEye Falcon* ROV

The *Lophelia* II Cruise 1 was conducted on the NOAA Ship *Nancy Foster* from September 2, 2008 to October 2, 2008, and was the first cruise conducted for this contract. The cruise had two legs with a personnel change between the cruise legs. The cruise mobilized and embarked from Galveston, Texas, and returned to Gulfport, Mississippi September 17-19 for the personnel change. Five days were lost to weather on the first leg.  Only a total of thirteen hours of bottom time with the ROV were achieved on the wreck sites over the entire first leg.  Useful data was collected at 3 wreck sites. The *SeaEye Falcon* ROV was used to explore and characterize wreck sites during the first leg and natural reef sites during the second.

The second leg embarked Gulfport Mississippi on September 20 and demobilized in Pascagoula, Mississippi on 2 October 2008.  This leg was somewhat more successful, with only 2 days lost to weather. Of the 10 ROV lowerings, six reached the sea floor and worked for over 2 hours. Manipulator failures and ROV problems limited its usefulness to sites <600 m depth.  Valuable photographic sampling and conductivity-temperature-depth (CTD) data were collected at 5 sites and multibeam data at a total of thirteen sites. Table 2-1 lists sites that were visited during Legs 1 and 2 (Figure 2-2, Figure 2-3).

Table 2-1.

Sites Occupied during Cruise 1

| Leg 1 Sites | Leg 2 Sites |
|---|---|
| EW1008, EW Wreck | AT47 |
| MC497, *Gulfpenn* | EB478 |
| MC796, *Gulfoil* | EW1009 |
| GC245, *Green Lantern* | GB201 |
| | GB535 |
| | GC140 |
| | GC201 |
| | GC234 |
| | GC246 |
| | MC539 |
| | MC751 |
| | MC885 |
| | VK906 |
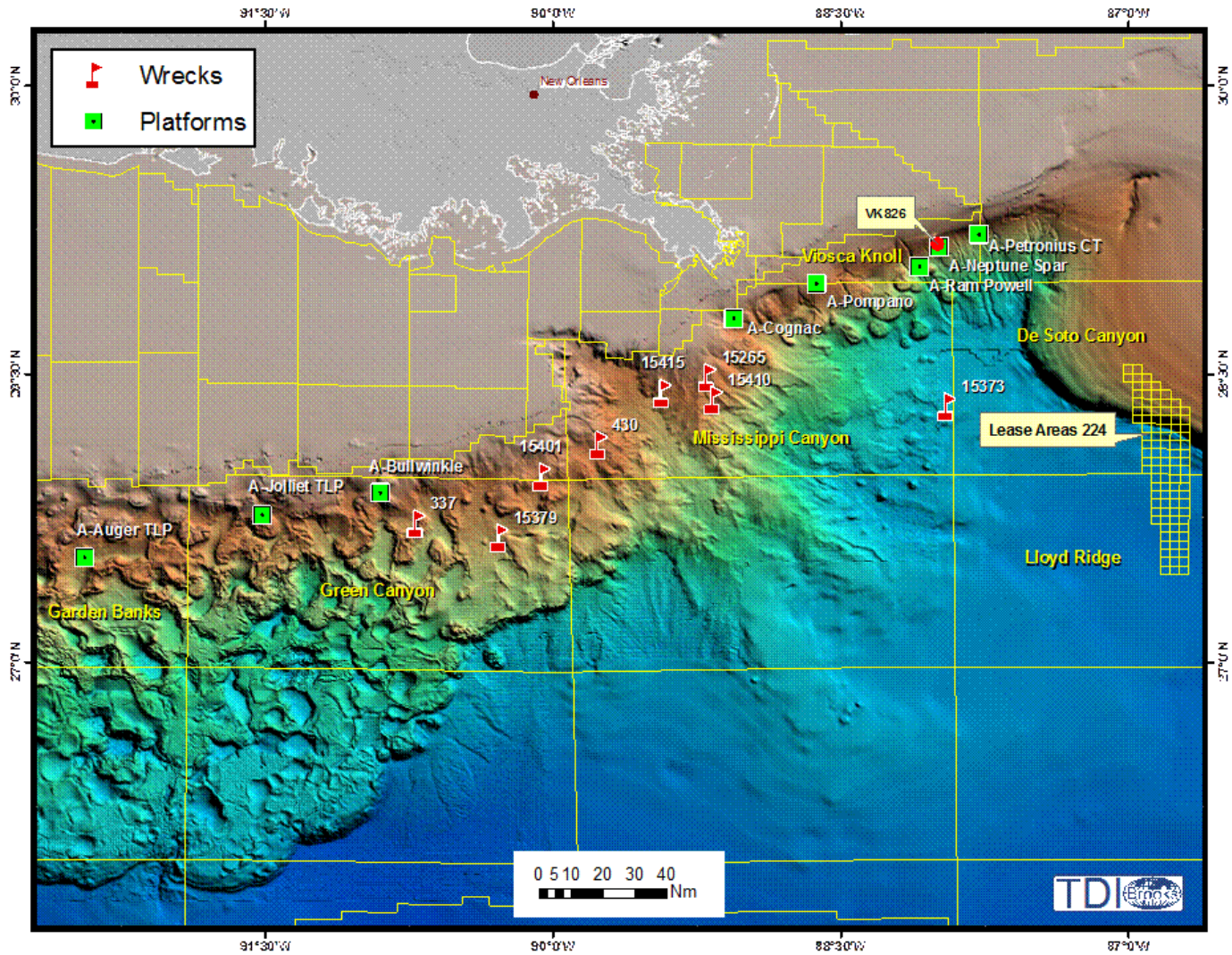
Figure 2-2. Bathymetric map of the northern Gulf of Mexico showing shipwrecks and oil or gas platforms of interest in Cruise 1
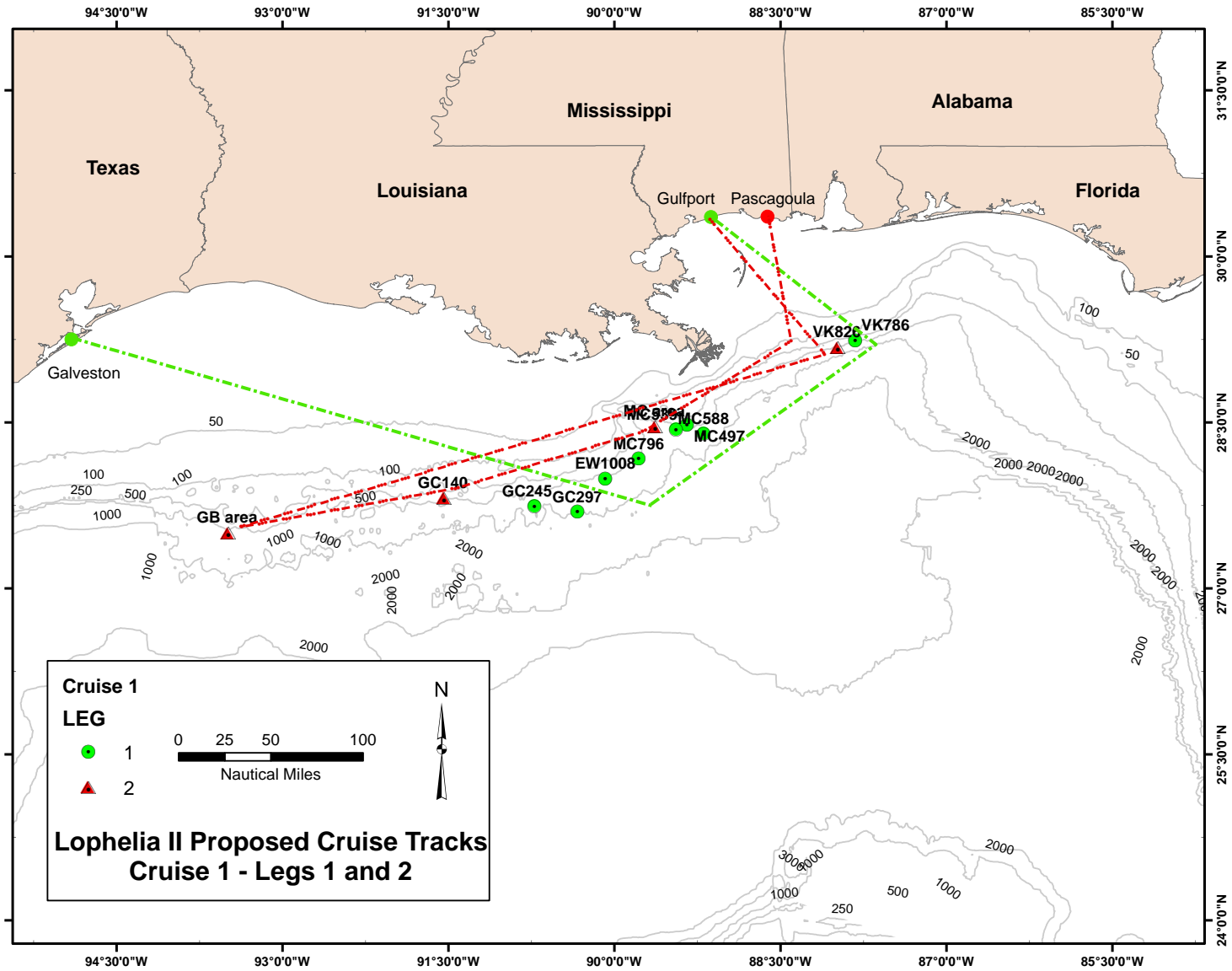
Figure 2-3. Cruise tracks for Leg 1 and Leg 2.

### 2.2.2  Cruise 2: RV *Brooks McCall* and AUV *Sentry*

The *Lophelia* II Cruise 2 was conducted on the TDI-BI Ship *Brooks McCall* from 17 June–1 July, 2009, and was the second cruise conducted for this contract. The cruise mobilized and embarked from Freeport, Texas, and demobilized in Gulfport, Mississippi. The primary objective was to conduct exploratory surveys of suspected deep-sea coral communities with the Woods Hole Oceanographic Institution (WHOI) AUV *Sentry* (Figure 2-4). Although beset with equipment problems for the first half of the cruise, 5 sites were well documented by the end of the cruise, and the final dive at VK826 provided the detailed imaging over detailed bathymetry that forms the basis for most of Section4.1 in this report.
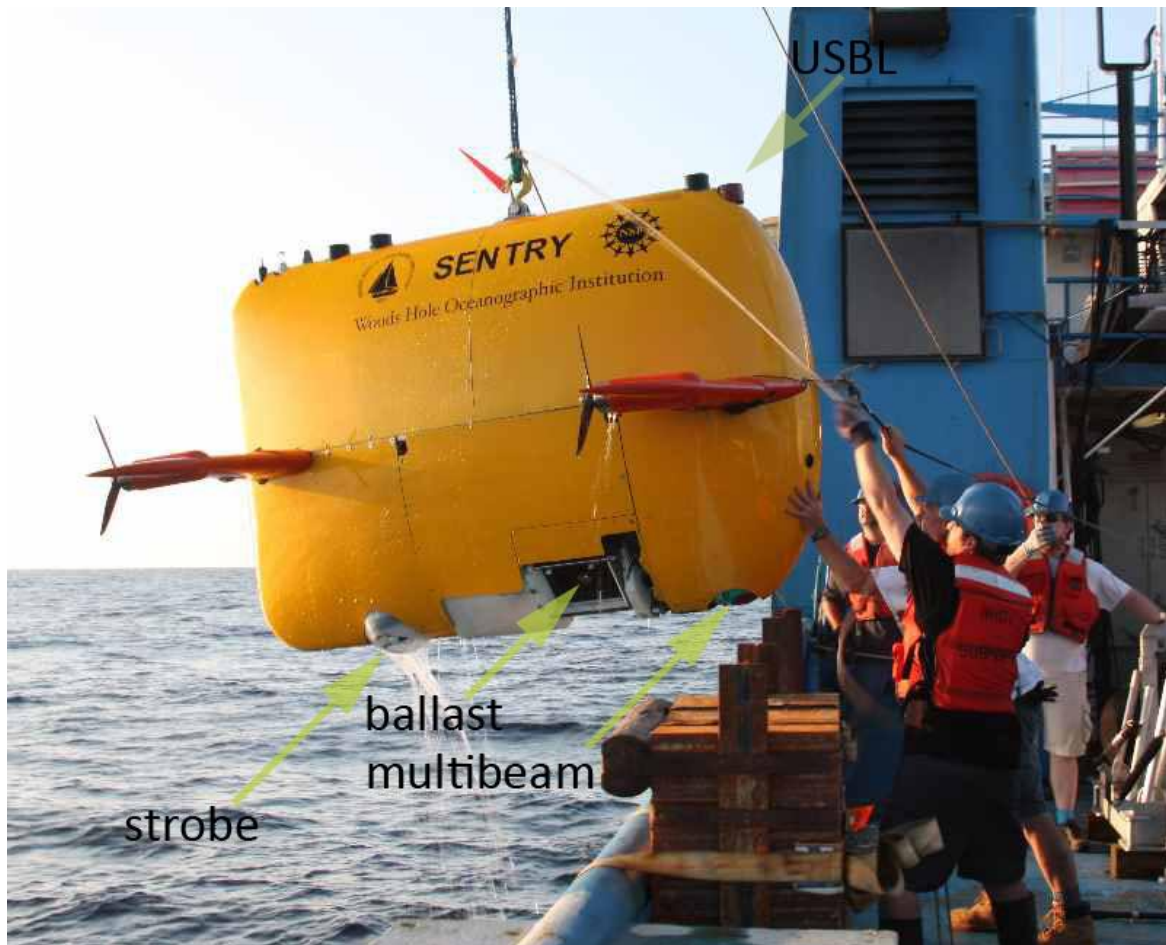


Figure 2-4. The AUV *Sentry* being recovered onto the Research Vessel (R/V) *Brooks McCall* following a successful dive.

Table 2-2 lists sites that were occupied during Cruise 2. The cruise track and site locations are shown in Figure 2-5. The planned AUV surveys were not completed at targeted features in the following lease blocks: GB837, GB535, and GC600.

Table 2-2.

Sites Occupied during Cruise 2

| Dive | Site | Lat | Lon | Depth m | Photographs | Comments |
|------|------|-----|-----|---------|-------------|----------|
| 017 | test | | | | | Self-terminate above bottom |
| 018 | test | | | | 49 | Strobe not synched with camera shallow test West Flower Gardens |
| 019 | GB837 | 27.11967 | 93.89694 | 865.6 | | Weight fell off on 3rd line |
| 020 | GB837 | 27.11967 | 93.89694 | 865.6 | | Camera did not work |
| 021 | GB535 | 27.43115 | 93.59861 | 585.0 | 691 | Phins(INS) inoperable compass substituted |
| 022 | GC600 | 27.36639 | 90.56417 | 1,248.8 | | Self-terminate above bottom 450 m |
| 023 | GC600 | 27.36639 | 90.56417 | 1,248.8 | 163 | Camera stopped after 10 min. |
| 024 | GC246 | 27.71133 | 90.67600 | 755.0 | 570 | Camera took ~800 pics then quit weight fell at start of multibeam |
| 025 | MC885 | 28.08250 | 89.71850 | | 3800 | Photo-survey complete showing gorgonians and small *Lophelia* colonies. Unprogrammed weight drop before multibeam started |
| 026 | MC657 | 28.34364 | 87.93010 | ~2,000 | 5160 | Completed dense mosaic of shipwreck site with multibeam data. Ship was clearly and completely |
| 027 | MC339 | 28.63251 | 88.44917 | 1,398.5 | ~4000 | Completed multibeam and photo survey of mound slopes. No problems or delays with vehicle. No coral or sea fans noted. |
| 028 | VK826 | 29.14200 | 88.03783 | 610.0 | >5000 | Completed multibeam and photo survey of most of knoll area. All systems functional to end of dive. Anticipate good coverage. |
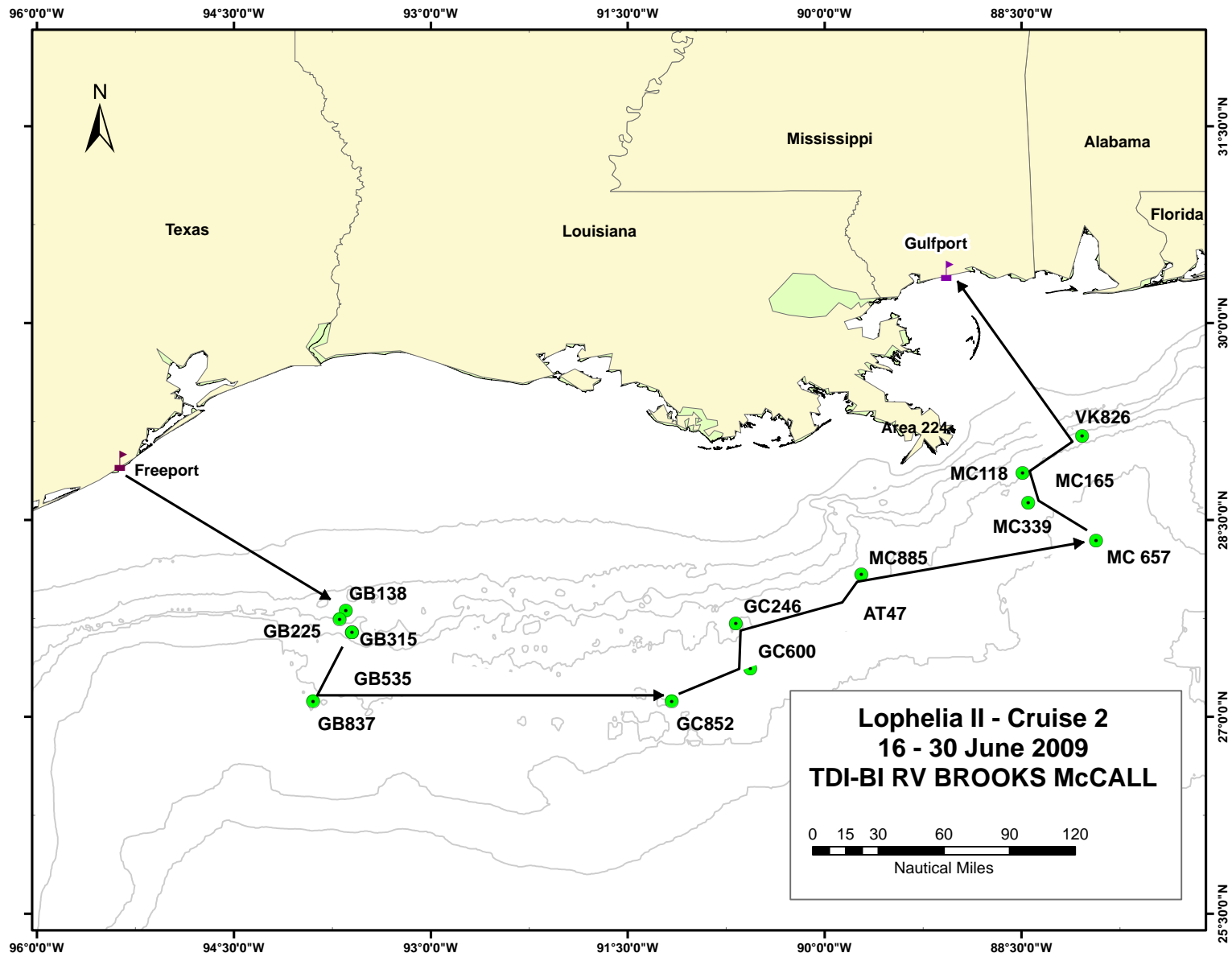
Figure 2-5. Sites visited, Cruise 2.

### 2.2.3 Cruise 3: NOAA Ship *Ronald H. Brown* and the *Jason II* ROV

Cruise 3 was completed on NOAA Ship *Ronald H. Brown* 19 August–12 September 2009. The cruise mobilized in Key West, Florida. One mid-cruise personnel transfer took place on 5 September. The cruise demobilized in Pensacola, Florida, on 12 September 2009.

This cruise employed the ROV *Jason II* to explore new sites, make a variety of deployments and collections, and conduct a variety of studies on natural deep water coral reefs and deep water shipwrecks (Figure 2-6). This was a 25-day cruise with 21 ROV dives and an at-sea personnel transfer.



Figure 2-6. Illustration of the *Jason II/Medea* ROV (WHOI).

*Jason II* was used to: explore 10 new sites (Table 2-3) for the occurrence of deep water coral reefs; make collections of *Lophelia* and other corals for genetic and physiological studies; make collections of communities associated with *Lophelia* and other corals for ecological studies; collect

quantitative digital imagery for characterization of sites and coral communities; collect spatially explicit physical near bottom oceanographic data; deploy cameras and microbial arrays; reposition larval traps and current meters; collect push cores; and conduct a series of linked archeological/ biological investigations on deep water shipwrecks.  In addition to launching and recovering *Jason II*, elevators were deployed and recovered twice, four moorings (two larval traps and two current meters) were deployed, and CTD casts were conducted (Figure 2-7).

Table 2-3.

Sites Characterized Listed in Chronological Order

| Dive | Site | Dates | Times | Depth m | Lat-D | Long-D | Comments |
|---|---|---|---|---|---|---|---|
| J2-453 | Fla Slope-1 | 8/20-8/21 | 2130-1600 | 450 | 26.184100 | -83.292583 | |
| J2-454 | DC583 | 8/22-8/23 | 1720-0745 | 2500 | 28.385493 | -86.611932 | Aborted but dive number unchanged |
| J2-456 | MC294 | 8/23-8/24 | 2140-0745 | 1360 | 28.674300 | -87.518917 | |
| J2-457 | AT047 | 8/24-8/25 | 1630-0730 | 863 | 27.879200 | -88.212217 | |
| J2-458 | GC235 | 25-Aug | 1643-2230 | 530 | 27.737033 | -90.812733 | Aborted: Hydraulic Failure |
| J2-459 | GB299 | 8/26-8/27 | 0830-0740 | 410 | 27.692450 | -91.777100 | |
| J2-460 | GB535 | 8/27-8/28 | 1636-1216 | 600 | 27.422880 | -87.402863 | |
| J2-461 | GC852 | 29-Aug | 0118-2020 | 1400 | 27.124667 | -90.835833 | |
| J2-462 | GC338 | 30-Aug | 0851-2030 | 900 | 27.670000 | -89.520320 | Aborted: OcTan Failure |
| J2-463 | | | | | | | Aborted: jelly |
| J2-464 | MC751 | 8/31-9/1 | 1324-1206 | 460 | 28.189667 | -88.202167 | |
| J2-465 | VK906 | 9/1-9/2 | 2031-2000 | 400 | 29.069000 | -87.622833 | |
| J2-466 | VK826 | 9/3-9/4 | 1119-0805 | 510 | 29.156933 | -87.989333 | |
| J2-467 | VK826 | | | | | | |
| J2-468 | VK786 | 9/5-9/6 | 2030-0810 | 612 | 29.218833 | -86.223667 | *Viosca Knoll* Wreck |
| J2-469 | MC657 | 9/6-9/7 | 1714-0800 | 2256 | 28.343167 | -86.069500 | 7,000 Foot Wreck |
| J2-470 | EW1008 | 9/7-9/8 | 2025-0830 | 610 | 29.142000 | -88.037833 | *Ewing Bank* Wreck |
| J2-471 | GC245 | 9/8-9/9 | 1644-1210 | 627 | 27.389500 | -93.600167 | *Green Lantern Wreck* |
| J2-472 | MC497 | 9/9-9/10 | 2108-0815 | 554 | 28.440333 | -88.680000 | *Gulfpenn* |
| J2-473 | VK906 | 9/10-9/11 | 1633-0815 | 490 | 29.065500 | -87.618333 | |
| J2-474 | VK826 | 11-Sep | 1259-2312 | 510 | 29.156933 | -87.989333 | |
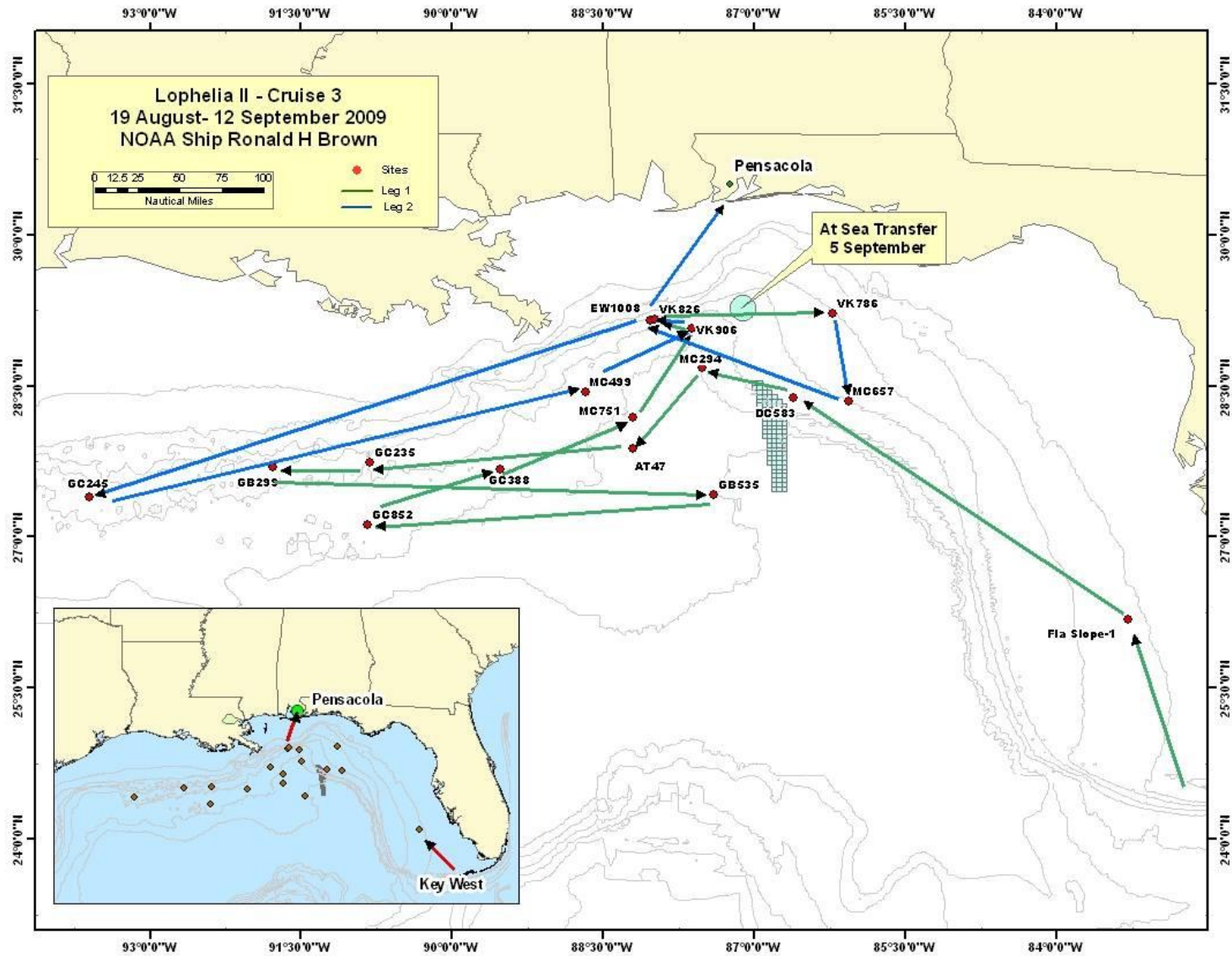
Figure 2-7. *Lophelia* II Cruise 3 track of *Ronald H. Brown*.

### 2.2.4 Cruise 4: NOAA Ship *Ronald H. Brown* and the *Jason II* ROV

This cruise also used the NOAA Ship *Ronald H. Brown* and was conducted from 13 October– 4 November 2010. The cruise mobilized in Pensacola, Florida. One mid-cruise personnel transfer took place on 24 October. The cruise demobilized in Pensacola, Florida on 5 November 2010. This cruise employed the ROV *Jason II* to return to seven of the sites visited with *Jason II* in 2009 and explore eight sites not visited during that cruise, including 5 never visited by ROV (Table 2-4, Figure 2-8). A variety of deployments and collections were made and both natural deep-water coral reefs and deep water shipwrecks. The primary data collected using the ROV included SM2000 multibeam, digital video and still photographic imagery, CTD with dissolved oxygen (DO) and pH sensors, geological samples, biological samples, archaeological material and push cores. Other data streams from the ROVs, such as vehicle attitude, acoustic data, and sonar imagery, were recorded by networked computers in the control van. Navigational data for both the ship and ROV systems were also recorded. While in transit to and from the site, and during times when the ROV is not deployed, Seabeam multibeam bathymetric data were collected. This was a 21-day cruise with 16 ROV dives and an at-sea personnel transfer.

Table 2-4.

Sites Characterized Listed in Chronological Order

| Date | Site | Dive Number | Lat DD | Lon DD |
|------|------|-------------|--------|--------|
| 10/15/2011 | VK826 | J2-526 | 29.158444 | -88.016242 |
| 10/16/2011 | MC885 | J2-527 | 28.066527 | -89.713692 |
| 10/17/2011 | GC246 | J2-528 | 27.689721 | -90.644962 |
| 10/18/2011 | GC354 | J2-529 | 27.597896 | -91.826356 |
| 10/19/2011 | GB299 | J2-530 | 27.684991 | -92.220535 |
| 10/20/2011 | GB535 | J2-531 | 27.421338 | -93.595971 |
| 10/21/2011 | GC140 | J2-532 | 27.811076 | -91.53722 |
| 10/22/2011 | GC249 | J2-533 | 27.737741 | -90.521707 |
| 10/23/2011 | VK906 | J2-534 | 29.068903 | -88.377581 |
| 10/24/2011 | | | | |
| 10/25/2011 | VK906/862 | J2-535 | 29.068996 | -88.376952 |
| 10/26/2011 | MC751 | J2-536 | 28.193494 | -89.798639 |
| 10/27/2011 | MC796 | J2-537 | 28.161336 | -89.752292 |
| 10/28/2011 | | | | |
| 10/29/2011 | MC118 | J2-538 | 28.855867 | -88.493561 |
| 10/30/2011 | DC673 | J2-539 | 28.310634 | -87.307289 |
| 10/31/2011 | VK826 | J2-540 | 29.15462 | -88.022582 |
| 11/1/2011 | | | | |
| 11/2/2011 | MC338 | J2-541 | 28.675076 | -88.481303 |
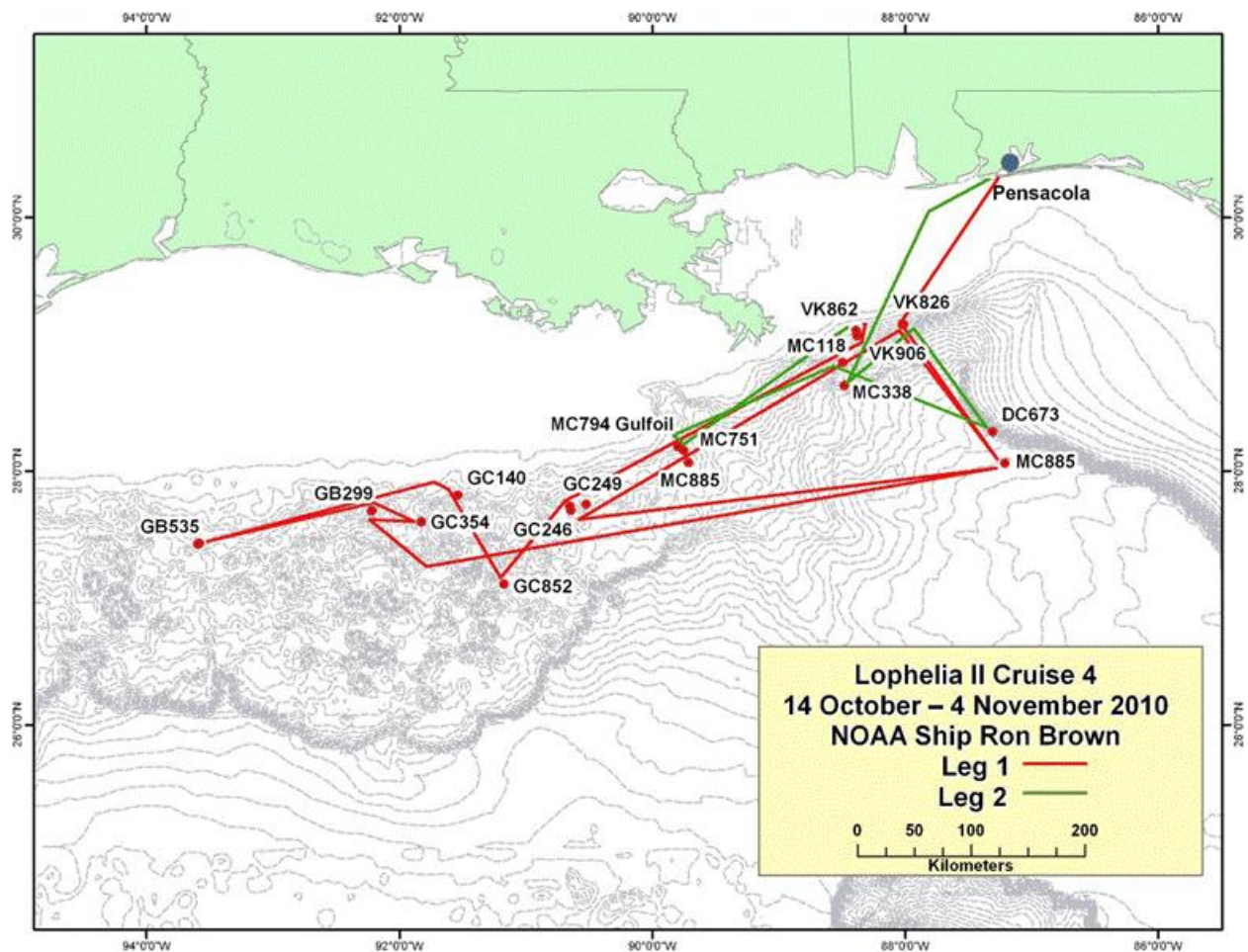
Figure 2-8. Cruise track for Cruise 4 on the NOAA Ship *Ronald H. Brown*.

## 2.2.5  Cruise 5: RV *Brooks McCall* and ROV *Kraken II*

This cruise used the *RV Brooks McCall* and was conducted from 14 July– 24 July 2012. The cruise mobilized in Freeport Texas and demobilized in Pensacola, Florida on 24 July 2012. This cruise employed the ROV *Kraken II*(Figure 2-9) to collect imagery and samples from three energy platforms and one subsea installation (Figure 2-10).  Control box cores were also collected 500 m away from the study platforms when the ROV was not in the water.  A combination of bad weather, problems with the ROV, and eventually entangling and loosing the ROV at one of the platforms prevented achieving all of our objectives during this cruise.  However data collected during the cruise significantly increased the known depth range for *L. pertusa*, demonstrated the presence of colored morphotypes of *L. pertusa* in the GoM for the first time, and provided the best data on growth and settlement patterns with depth for *L. pertusa*, which formed the central pieces of a paper in submission to Deep Sea Research.  At the end of the cruise, after several efforts to obtain permission from the platform operators to initiate rescue operations, the ship returned to port without the *Kraken II* .  It was eventually recovered several weeks later. Appendix A-1 is the Cruise 5 report.

21

Figure 2-9. *Kraken II* ROV being launched at the *Jolliet* Platform.
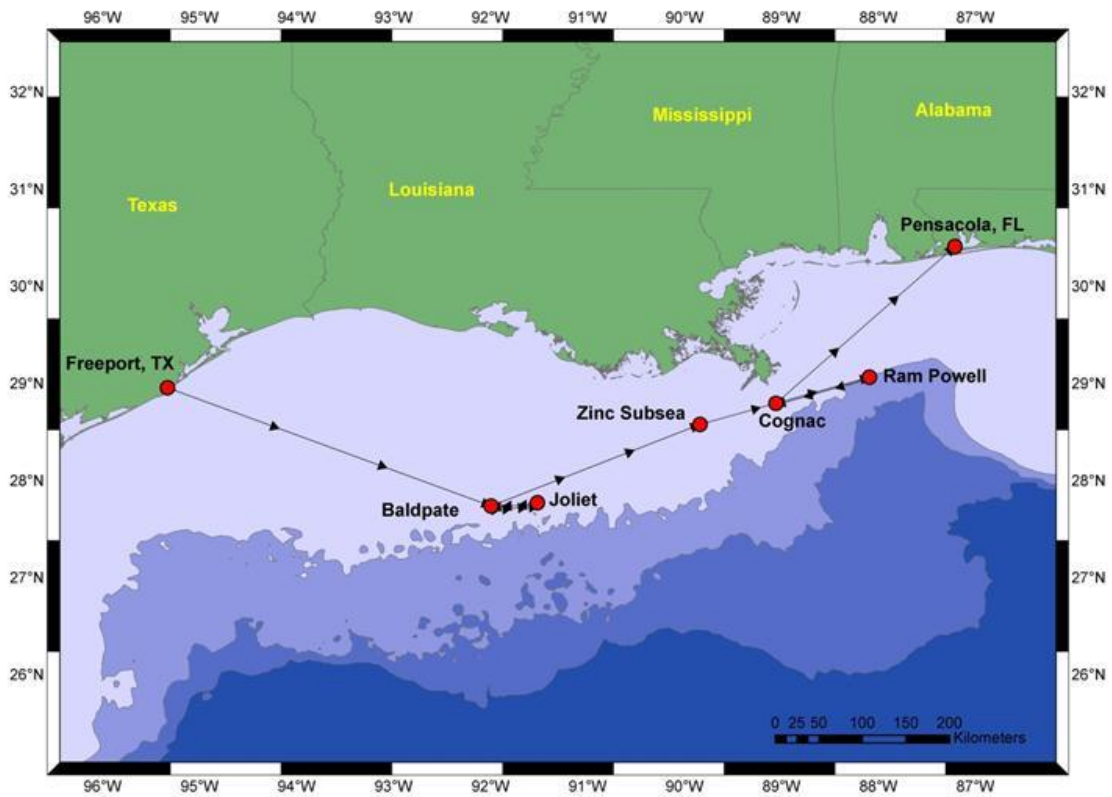


Figure 2-10. Cruise track for Cruise 5.

## 2.3 OVERVIEWS OF SITES VISITED BY ROVS DURING THE TIME PERIOD OF THIS PROJECT

The following section describes site characteristics, biological observations and geological settings of the dive site locations visited over the course of this project as well as some additional newly discovered sites near the site of the Deepwater Horizon spill using techniques developed during this project.

### 2.3.1 Project Study Sites (Sorted by Depth)

### *2.3.1.1 GC140 (250 m depth)*

GC140 site is a large (3 by 4.5 km with 150 m vertical relief) salt-supported bathymetric high centered around 27.81°N, 91.54°W W in about 250 m water depth. This site was dived on twice by the *SeaEye Falcon* ROV and once during the 2010 *Ron Brown* cruise. One area around marker W was mosaicked at this site. Examination of the seismic data revealed several discrete, high positive amplitude anomalies, with the highest amplitudes on the north flank and crest. This site is geologically related to, but older than the well-studied, deeper "Bush Hill" (GC185) close by to the southeast. The subsurface seismic signature at GC140 shows less active migration to the seafloor than is present at GC185, but more high positive amplitudes, suggesting thicker, older authigenic carbonate. The fault that is "feeding" hydrocarbon to GC185 is antithetic to the larger, more deep-seated fault supporting GC140, also suggesting that GC140 is an older seep site. GC140 was visited briefly by Dr. Harry Roberts in the late 1980's and he reported finding corals, but no chemosynthetic communities (aside from a lone tube worm at 280 m).

The top of this very large feature consists of continuous carbonate outcrops and slabs with large furrows between them. Because of the relatively shallow waters of the site (~230 m), there was a high concentration of particulates in the water column and relatively high current velocities. There were few colonial organisms colonizing the very top of the feature, possibly due to the thin veneer of sediment on most of the hard substrata, although anemones and crinoids were occasionally present along with numerous fishes, in particular deepbody boarfish and anthiines. In slightly more sheltered and high relief areas, extremely large (over 2 x 2 m) colonies of *L. glaberrima* were observed, along with the gorgonian *Callogorgia gracilis* with *Asteroschema* sp. (ophiuroid) associates and a few other octocorals, including the soft coral *Anthomstus* sp., which was quite common. Although the general appearance of this site, in terms of both geology and the fauna present, was reminiscent of the shallow VK862 site, many of the octocoral species (including an Atlantic species of *Paramuricea*) and associates (notably the ophiuroids) were observed only at GC140. It should also be noted that *L. pertusa.*, present at VK862, was not observed at GC140.

The eastern flank of the mound was an extremely steep slope, descending to approximately 360 m depth, containing a series of near-vertical cliffs. At the base of many of these sharp features was evidence of seepage, including darkly colored sediments, bacterial mats, and an observation of a methane bubble stream. An oil slick was also noted at the surface during our survey of this site. At 320 m depth, a few isolated tube worms were observed and collected, representing the shallowest collection of a tube worm in the GoM, and confirming the previous record for the shallowest observations of tube worms in the Gulf. The corals *Anthomastus* cf. *grandiflorus*, *Paramuricea* sp. E, *Paramuricea* sp. H, cf. *Echinomuricea* sp., *Scleracis guadalupensis*,

*Callogorgia gracilis*, Keratoisidinae S1a, Keratoisidinae S1b, Keratoisidinae S1c, and *Nicella* sp. were collected from the GC140 site (Appendix A-2).

### 2.3.1.2 VK 906/862 (320 to 400 m depth)

This site is composed of several discrete areas. The first was identified several years ago from BOEM 3D-seismic data and is in the north of VK906 and edge of VK862. The regional area is a complex of mounds and depressions superimposed on a large bathymetric high that generally dips to the south and is the reflection of a tabular salt body in the very shallow subsurface. The area of interest on the top of this regional feature is approximately 4 km X 4 km and ranges in water depth from about 320-400 m. The VK906/862 area between 320 and 350 m depth has been visited multiple times in the past as part of previous MMS (BOEM) and the United States Geologic Survey (USGS) projects. Two areas around markers R and T were mosaicked in this part of the site (in VK862). In this area anemones and white *Leiopathes* sp are very abundant and *L. pertusa* is also present. Large numbers of snowy grouper were present during two previous visits to this area. During the 2008 *Nancy Foster* cruise much more of this site to the south was surveyed by multibeam and a dive was made down the side of a canyon running from 380 to 410 m depth. On this transect both *Callogorgia* and *L. pertusa* were observed, but no large aggregations of either were noted. Other colonial cnidarians present in this area included the bamboo coral *Acanella* and *Muricedes* sp. gorgonians and large numbers of 0.3 m long squid and barrel fish were present in this area during the 2008 dive. At the very end of this dive, a mound that appeared to be composed primarily of coral and carbonate rubble and was capped by a few small colonies of *L. pertusa* was encountered.

At the southern end of the large salt-supported and seaward-dipping bathymetric feature is a series of five small mounds that were identified on a multibeam map constructed from data collected during the 2008 NOAA Ship *Nancy Foster* Cruise. The mounds are roughly 150-300 m in diameter with up to 50 m relief above the surrounding seafloor, distributed in roughly a north-south line with the largest of the mounds at the southern end of the group. On the 3D-seismic surface amplitude maps of the area most of the discrete mounds at the southern end had anomalously low positive signatures. Initially, we thought that this seismic response may be related to bubble-phase gas in the mounds as a product of seepage around the underlying salt mass. However, after the *Jason* dive on the largest of the southern mounds it became apparent that there was no evidence of seepage. A new seismic cross-section through the chain of small mounds clearly indicates that there are no direct migration pathways from the deep subsurface to the mounds. Further, they are sitting on a hard horizontal reflector that appears to be the surface from which the mounds originate. This relationship is unique with regard to all the mounds we have studied on the northern Gulf's continental slope. Seismically, they are similar to the mounds of the pinnacle reef trend of the Mississippi and Alabama Outer Continental Shelf (OCS). No carbonates were found on the crest of the mound, despite a concerted effort to find and collect a sample rock. To test the hypotheses that these mounds in VK906 are *L. pertusa* reefs that started on subtle relief features associated with the hard bottom, a supplemental study was done using gravity cores collected through and near the mounds.

A total of 4 dives were made during the *Ron Brown* cruise in 2009 and 2010 on this southern most mound (nicknamed Roberts Reef) with a summit at about 390 m depth at 29.069°N, 88.377°W. A total of three areas around markers J, L, and Y were mosaicked on Roberts Reef. The bottom of

the trench to the south of the mound was primarily composed of soft sediment with few organisms with a few scattered outcrops that harboring small colonies of *L. pertusa*, antipatharians, and gorgonians (Figure 2-11). The southern-facing base of the main mound structure was confirmed to be primarily carbonate and coral rubble and contained some small colonies of live *L. pertusa*. At the base of the mound on every side surveyed there was a moderately high density of glass sponges, anemones, and assorted crinoids and sea stars.  On the slopes on the E and SW sides of the mound this community is joined first by the red form of *Leiopathes glaberrima* and then later *L. pertusa* at the about 400 m contour.  The density of both are higher near the top of the mound and over the top of the mound at about 390 m depth *L. pertusa* is the dominant coral and the white form of *L. glaberrima* largely replaces the red form and covers extensive portions of the sea floor (Figure 2-12).  The proportion of the substrate covered by live *L. pertusa* is among the highest observed at any site in the Gulf, with the coral forming long swales of standing coral thickets. These *L. pertusa* reefs are apparent on the high-resolution Seabeam multibeam 2000 (SM2K) bathymetry collected during the second *Jason* dive at this site. Most of the *L. pertusa* mounds and swales here are covered with live coral and are often covered with small polyps near their terminal tips suggesting the corals at this mound could be in a quite active growth phase. Anemones and fishes were also very abundant on the top of the mound, including Barrel fish, conger eels, Tinselfish, and *Beryx*.
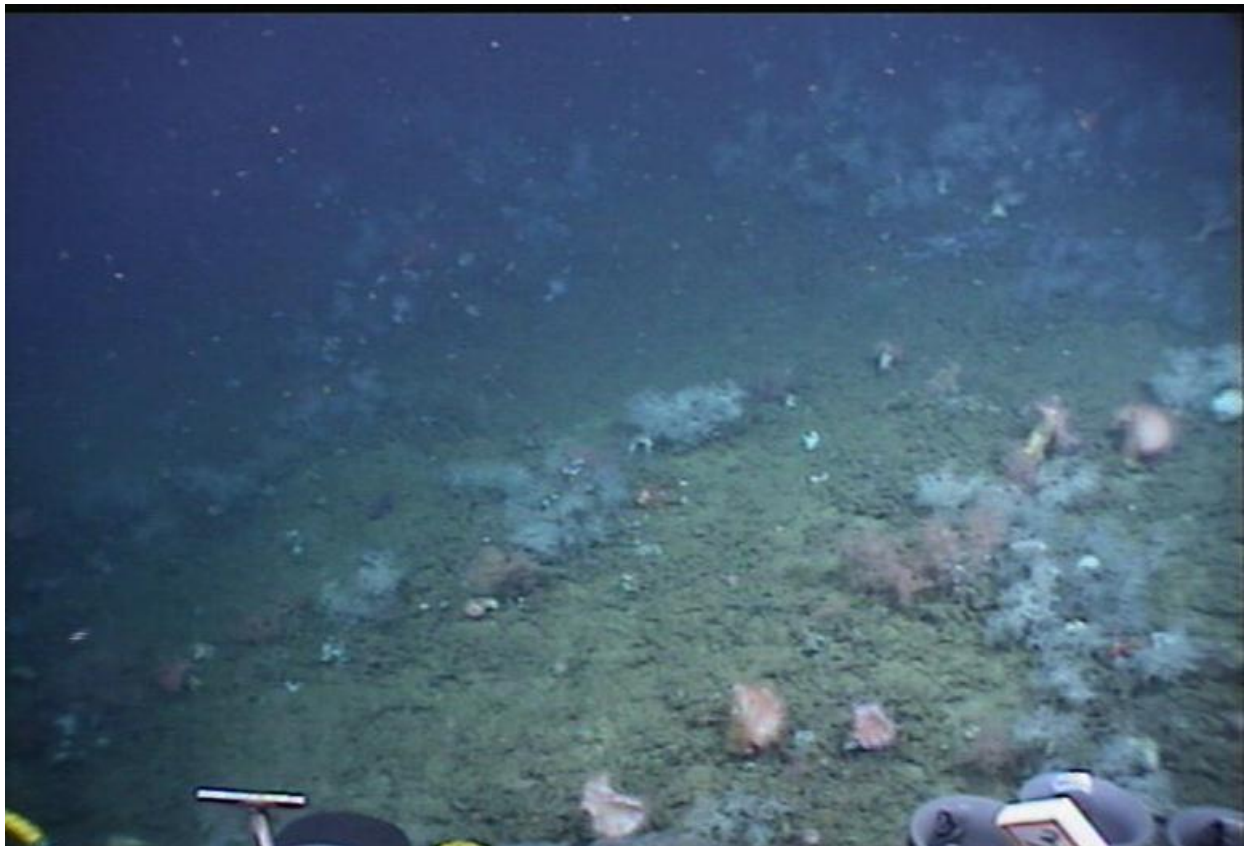


Figure 2-11. Small colonies of *Lophelia*, antipatharians, and gorgonians.
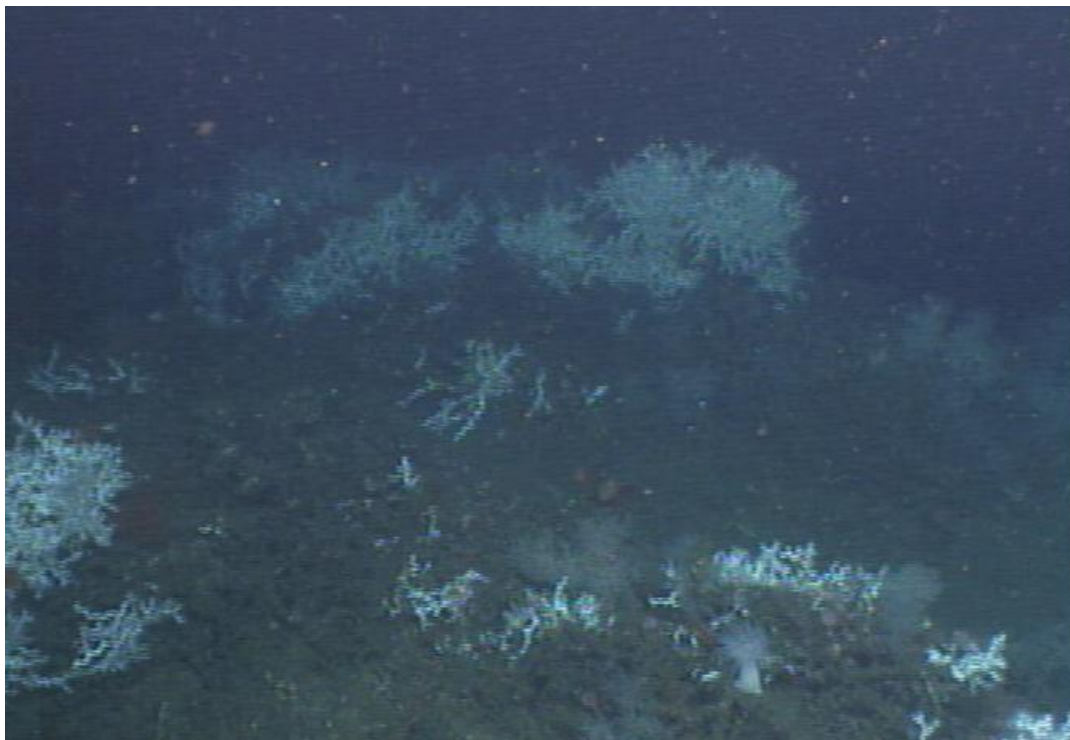
Figure 2-12. *Lophelia* and the white form of *Leiopathes*.

Four other mounds nearby and to the north of Roberts Reef visible on the *Nancy Foster* multibeam maps were also visited. One about 200 m to the SW of Roberts Reef is much smaller and the top is at about 440 m depth. Although the substrate at the base of the mound could not be documented, this mound had very similar fauna as the base of the mound at Roberts Reef, and only a few very small colonies of *L. pertusa*. The next closest mound to the NE of Roberts Reef had lower relief and was colonized by scattered anemones, *L. glaberimma* colonies of a variety of colors, and a few small colonies of *L. pertusa*. Another mound about 600 m to the NNW of Roberts Reef is smaller in diameter but rises from a similar depth to a similar height. Fauna on this mound was in general very similar to that of Roberts Reef, with a similar depth stratification and changes from the base to the crest of the mound. Although overall smaller in size, the percent coverage of *Lophelia* was similar at the crest of this mound. Another mound about 400 m further to the north only rises about 10 m from the sea floor, was actually very hard to identify when on the sea floor with the ROV and did not have a fauna distinctive from that of the surrounding sea floor other than the fact that the density of sea anemones was quite impressive near what was apparently the top of this little bump. The corals *Nidalia dissidens*, *Acanthogorgia aspera*, *Muriceides* cf. *hirta* 1b, *Muriceides* cf. *hirta* 1c, *Paramuricea* sp. E, *Callogorgia am. americana*, and Keratoisidinae S1c were collected from the VK906/862 site (Appendix A-2).

### 2.3.1.3  GB299 (340 – 510 m depth)

The GB299 site was identified on a BOEM 3D-seismic amplitude map with a bathymetry overlay. It is located at 27.692°N, 91.777°W and the areas of interest range in depth from about 340 – 410 m depth. The site was visited both during the 2009 and 2010 *Ron Brown* cruises. Two

areas around markers B and D were mosaicked at this site. This site is situated on NE-SW trending oblong structural high, that is 7-10 km across with variable, but often high positive amplitude response along the top and on the steep southern flank.  The surface of this regional bathymetric high is very irregular with discrete ridges and depressions that generally have the same NE-SW orientation as the overall feature.  The feature is supported by a salt body in the shallow subsurface. Above the top of salt the sedimentary section is highly faulted. Although the subsurface beneath this local seafloor relief is highly faulted and complex, there are few potential migration pathways that show acoustic blanking that could be interpreted as a signature for the presence of gas. However, the high amplitude areas along the southern flank of the overall feature were selected as the first target areas. The top and the southwest flank were also selected as a target for seafloor observations.

Though this site had discrete strong amplitude response coincident with bathymetric highs and steep scarps, no large, continuous areas of carbonate substrate were observed, but small carbonate cobbles and small pavements were typical of the seafloor. There was very little hard-ground fauna on the local topographic high in the area surveyed. The areas of high reflectivity coincided with low relief carbonate rubble and pavements with attached gorgonians and antipatharians which were scattered over much of the area surveyed on the gently sloping northern portion of the site between the depths of 350 and 365 m, and on the ridge to the north between 370 and 390 m. Especially impressive at this site was the diversity and overall high abundance of gorgonians and antipatharians with associated ophiuroids (Figure 2-13, Figure 2-14). Several of the whole coral samples taken that appeared to be growing in mud had authigenic carbonates as their base, buried by the mud (Figure 2-15).



Figure 2-13. Carbonate rubble and pavements with attached gorgonians and
          antipatharians.
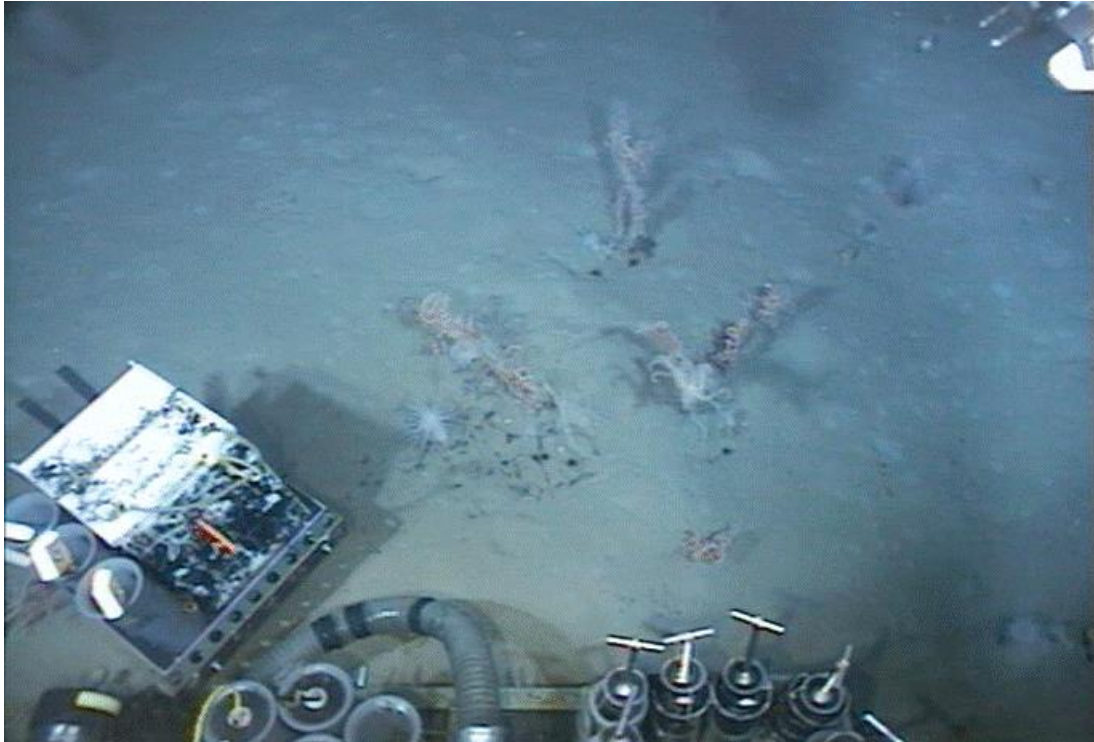
Figure 2-14. Carbonates with corals and sea anemones attached.
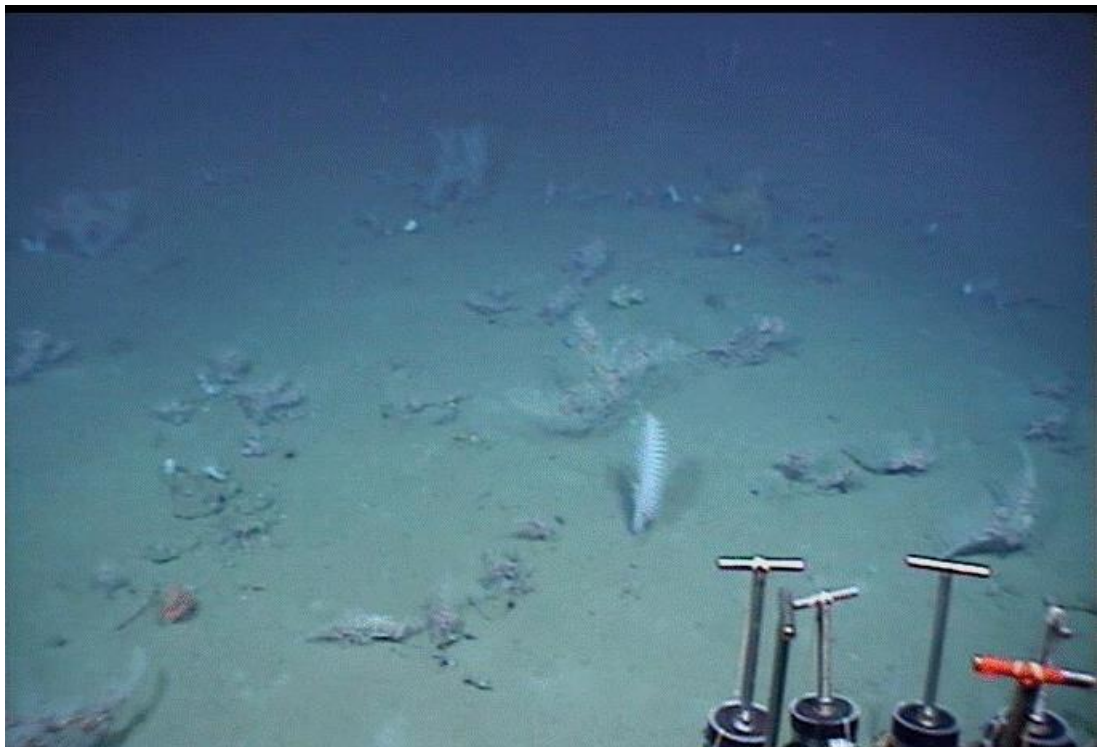


Figure 2-15. Corals growing in what appears to be mud, but with carbonate rubble
        underneath

At least 3 different species of antipatharians and 4 different species of gorgonians were collected along with 5 species of commensal ophiuroids. In addition to the commensal ophiuroids, numerous other echinoderms were present in the hard grounds including several different crinoids and basket stars. Colonial scleractinians were almost completely absent from the areas surveyed, although a single small colony of *Lophelia* was seen along with the occasional cup coral. This is the furthest west site with abundant *Leiopathes* sp and was sampled extensively for genetics work (Figure 2-16).
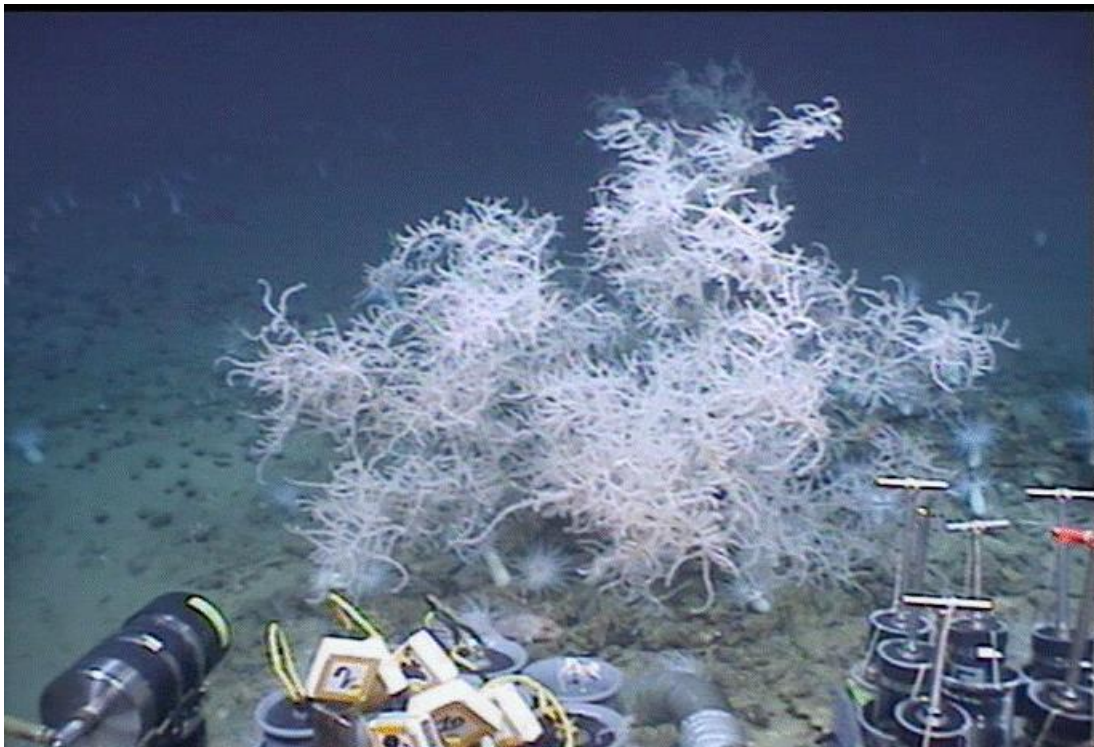


Figure 2-16. A colony of the white color-morph of *Leiopathes*.

The most abundant gorgonian at this site was *Callogorgia* (potentially more than one species), and 1000's of colonies with attached ophioroids were documented. *Callogorgia* occurred virtually all over the site, with the highest density on scattered carbonate rubble along the N facing slope near the 365 m contour line (Figure 2-17).

Figure 2-17. *Callogorgia* spp. colonies with attached ophiuroids.

In one area that was dominated with mottled mud, several half meter wide holes were encountered. The bottom of the holes were indeterminate, but in at least one case appeared to be well over a meter deep, with fish and shrimp living in and around them (Figure 2-18)..  These may have a biological origin or may be gas blowout tubes caused by explosive gas release as interpreted for similar features at GB201 in 2008. The corals *Nidalia dissidens*, *Muriceides* cf. *hirta* 1a, *Paramuricea* sp. E, *Callogorgia am. americana*, Keratoisidinae S1b, and Pennatulacea were collected from the GB299 site (Appendix A-2).

Figure 2-18. Half meter wide holes at GB299.

### 2.3.1.4 West Florida Slope (400 – 450 m depth)

This area was chosen for study because the bathymetry patterns (hummocky bottom and numerous ridges) between about 375 and 500 m depth resembled those of another area 15 km to the north where *L. pertusa* occurrence had been confirmed during *Johnson Sea Link* (JSL) dives in 2003. No 3D-seismic data were available for this area. For this project, the only dive to this area was during the 2009 *Ron Brown* Cruise. This particular site is centered near 26.184°N, 83.292°W and depths between 400 and 450 m.

This site had numerous areas of hard grounds ranging from boulders, pavements, linear ridges, to long, regional scarps formed by outcropping of resistant sedimentary beds, all likely to be exposures of Lower Tertiary carbonates upslope of the Florida Escarpment. At or near the edge of the slope, the top of Cretaceous seismic reflector outcrops everywhere along the extent of the Escarpment, and this site is upslope of this occurrence.

Black corals, *Leiopathes glaberina,* (Figure 2-19) were present in most the areas surveyed, although their density was generally low and their distribution patchy. Much more common were colonies of *Stylaster* sp. (Figure 2-20), which ranged in size from about 10 cm to 50 cm in height. Although there were many areas apparently suitable for *L. pertusa*, it was only found in the deeper areas of the site we visited. Although there are many possibilities for the lack of *L. pertusa* above about 425 m, it was noted that the temperature in these shallower areas ranged up to 13°C, while

in the areas where *L. pertusa* (Figure 2-21 and Figure 2-22) was collected temperatures were in the 9 – 11°C range.
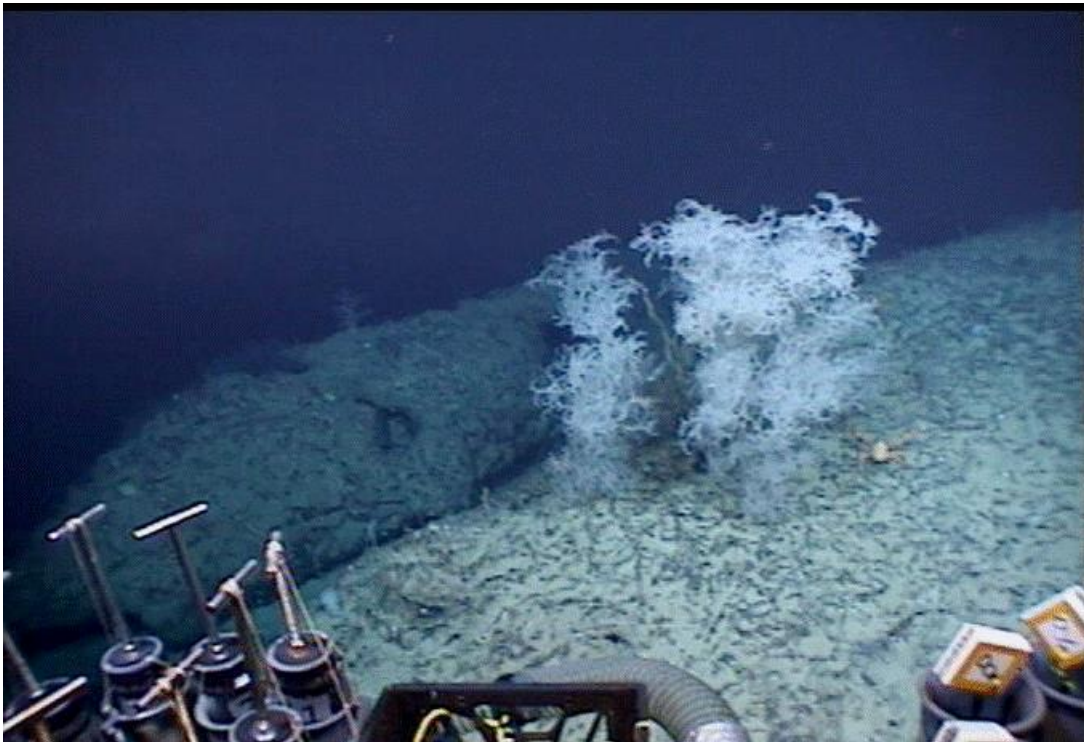


Figure 2-19. Large *Leiopathes* colony.
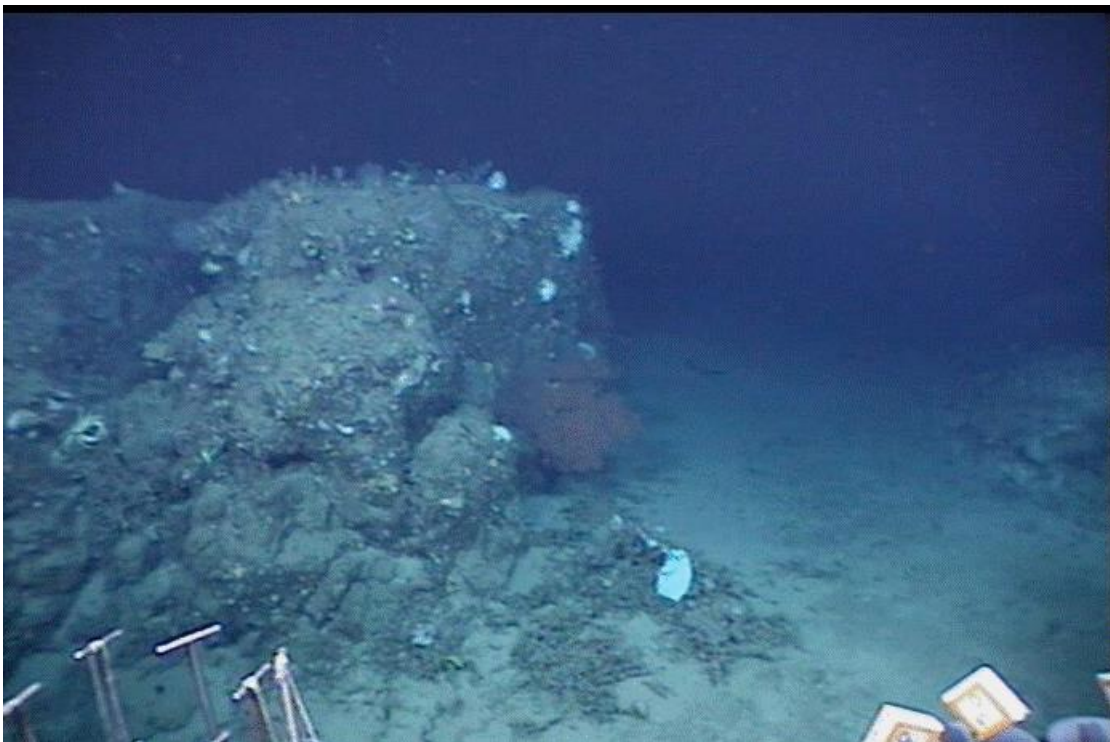


Figure 2-20. Largely unoccupied substrate.
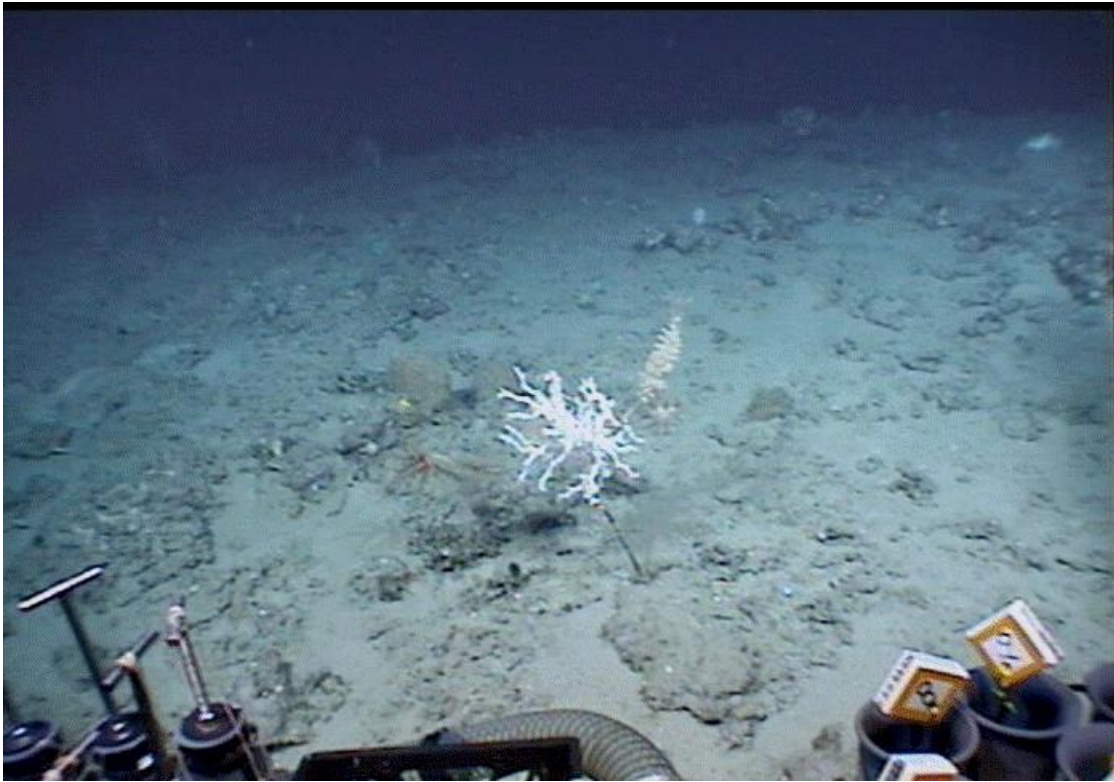
Figure 2-21. *Lophelia* on the West Florida Slope.

The majority of the substantial cnidarian colonies encountered were heavily colonized by crinoids, and many of them by ophiuroids as well. Most of the exposed carbonates were colonized by sponges, although large, potentially habitat forming sponges were rare. Along the shallower ridges were much higher density of fishes, including individual tuna, small sharks, *Beryx* sp., *Hoplostethus occidentalis, Conger oceanicus, Laemonema* spp., and several schools of small unidentified fish. Zooplankton swarms were noted along the edge of one of the shallower ridges. The corals *Anthomastus* cf. *grandiflorus*, *Anthomastus robustus delta*, Aquaumbridae sp. 1a, Aquaumbridae sp. 1b, Aquaumbridae sp., Scleraxonian nov sp. 1, *Anthothela* sp. 2, *Acanthogorgia* sp. 1, *Acanthogorgia aspera*, cf. *Muriceopsis* sp., *Muriceides* cf. *hirta* 1b, *Muriceides* cf. *hirta* 1c, *Muriceides* cf. *hirta* 1d, *Paramuricea* sp. A, Keratoisidinae S1c, and *Plumarella pellucida/dichotoma* were collected from the West Florida Slope (Appendix A-2).
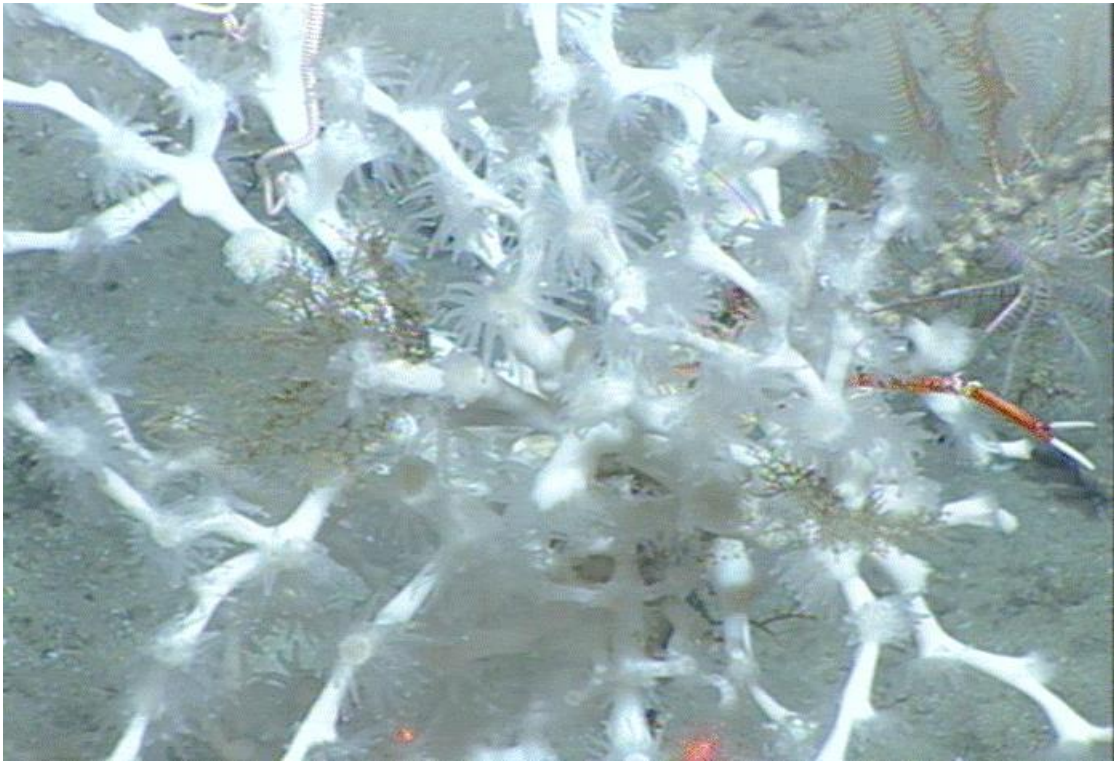
Figure 2-22. *L. pertusa* on the W. Fl. Slope.

### 2.3.1.5 MC751 (450 to 465 m depth)

This site was identified using BOEM 3D-seismic surface amplitude/bathymetry data. This site was dived upon during 3 ROV cruises as part of this project: with the ROV *SeaEye Falcon* in 2008 and on the *Ron Brown* cruises in 2009 and 2010. Three areas around markers G, H1, and H2 were mosaicked at this site.The area of interest is a small oblong feature (about 0.8 to 1.4 km) with moderate (20 m) relief feature and moderate to high seafloor amplitude response on seismic maps. It is located at 28.19°N, 88.202°W on the southernmost end of a south dipping nose at the intersection with a southeast plunging trough created by a down-to-the southwest fault. The fault ends at the site at about 450 – 465 m depth. Seismic cross-sections indicate vertical acoustic blanking of the record beneath the mound suggesting active gas plumbing up to the site and a seafloor environment supportive of chemosynthetic communities and corals.

  There were a few areas of mottled mud, but an area of about 500 by 500 m was dominated by carbonates with relatively clean surfaces. Within this area was an area of about 200 by 200 m with a high-density of authigenic carbonate outcrops, slabs, and boulders colonized by *Lophelia*, *Callogorgia*, and other coral on the tops and *Lamellibrachia luymesi* tube worms around their periphery (Figure 2-23). The abundance of live scleractinian corals in the immediate vicinity of apparent seepage (both tube worms and bacterial mats in some locations) has not been previously observed to the extent that it is found at this site. The other known occurrences of *Lophelia* at relatively active seep sites (such as Bush Hill) consisted of mainly dead coral structure with a few

live polyps at least a few meters away from any tube worms. This site contained live, apparently healthy *Lophelia* growing interspersed with tube worms, and in some cases bacterial mats. A variety of fishes, including blackbelly rosefish and morid cods (*Laemonema* sp.) as well as golden crabs, *Chaceon fenneri*, were relatively abundant at the site.
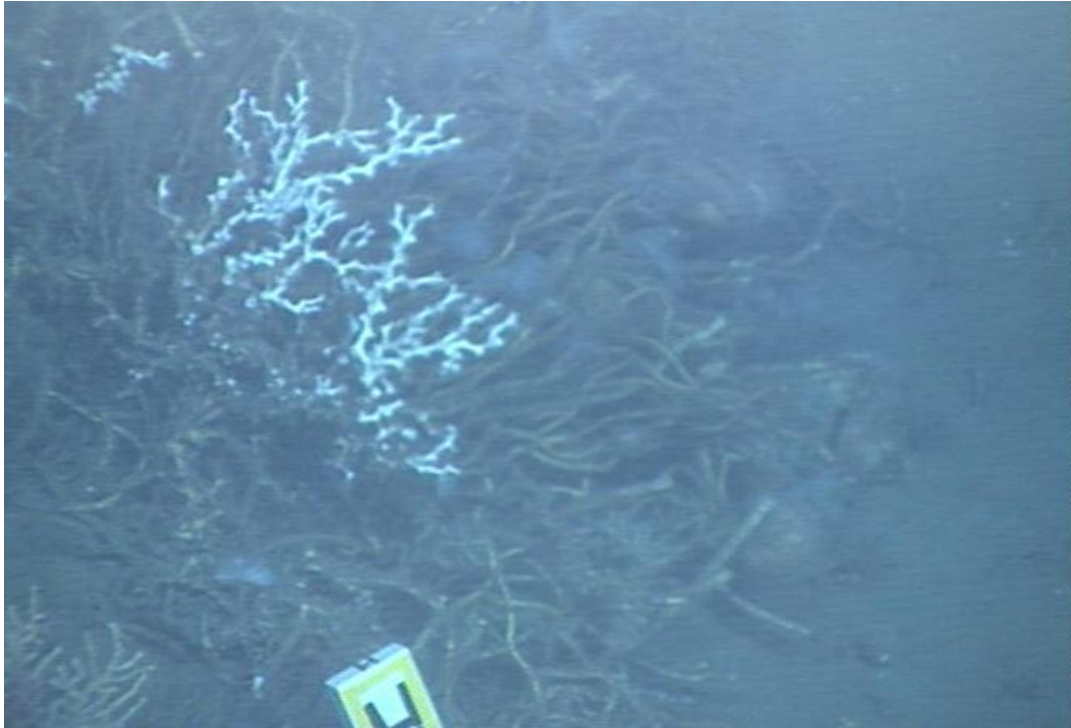


Figure 2-23. *Lophelia pertusa* and *Lamellibrachia luymesi* tube worms.

There was a relatively high diversity of gorgonians at the site as well, including what appeared to be multiple species of *Paramuricea* and a *Paragorgia* sp. (Figure 2-24).  In addition, acesta clams were observed at the proximal end of some tube worm tubes, *Asteroschema* ophiuroids on *Callogrogia* and *Paragorgia*, and *Astrogomphus* ophiuroids and coiled gastropods were visible as associates on *Lophelia*.  Few black corals were observed, but present were *Bathypathes* and *Stichopathes*.  *Icella* corals and a large unknown white octocoral were also observed (Figure 2-25). The corals *Paragorgia* cf. *johnsoni*, *Paragorgia johnsoni*, *Muriceides* cf. *hirta* 1b, *Paramuricea* sp. E, *Swiftia exserta*, *Callogorgia am. delta*, and *Cheliodonisis a. mexicana* were collected from the MC751 site (Appendix A-2).
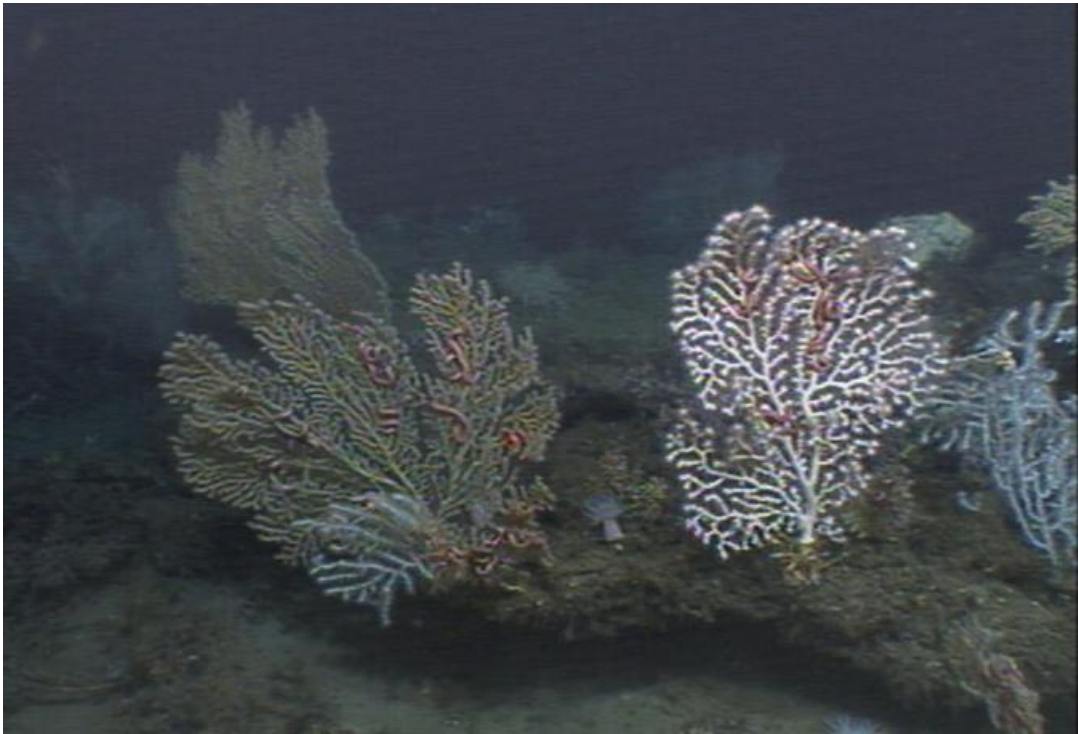
Figure 2-24. *Paragorgia* sp. coral on right side of image with multiple clonies of *Paramuricea* sp.



Figure 2-25. *Lophelia* and *Callogorgia* colonies.

### *2.3.1.6 VK826 (450 – 530 m depth)*

Viosca Knoll 826 is a large and quite complex site from a biological perspective. It is located around 29.2°N, 88.0°W, with corals in water depths from about 450 to 530 m. There has been a great deal of research completed on both the chemosynthetic and deep coral habitats at this site by numerous groups over the past 2 decades. This site was dived on multiple times during both *Ron Brown* cruises in 2009 and 2010 and also mapped and photo-surveyed with *Sentry* during the *Brooks McCall* cruise in 2008. Four areas around markers M, N, O and Q were mosaicked at this site. The chemosynthetic communities are concentrated on the SW flank of the mound. These are dominated by small tube worm aggregations on the edges of carbonate blocks and areas of vesicomyid shell hash. The carbonates are also colonized by a few coral species, mainly *Callogorgia* sp. and a few *L. glaberrima* and *L. pertusa* colonies. The SW facing slope of the mound progresses from this seep area to higher abundances of *L. pertusa* on a similar terrain of carbonate blocks and low-lying areas of shell hash. The E facing slope has more extensive development of *L. pertusa* reef structures accompanied with *L. glaberrima* that tend to be on the steeper slopes on this side of the mound (Figure 2-26). The coverage of authigenic carbonate increases towards to crest of the mound with occasional areas of dense *L. pertusa* coverage, but also an abundance of uncolonized hard substrate. There are also occasional tube worm aggregations down in the cracks in the carbonates as well as shell hash and occasional bacterial mats on soft sediments on the S and W sides of the mound near the crest. Much of the NW corner of the mound remains to be surveyed. The NE corner of the mound is similar to the crest, with abundant carbonates and scattered *L. pertusa* thickets interspersed with a few tube worms.
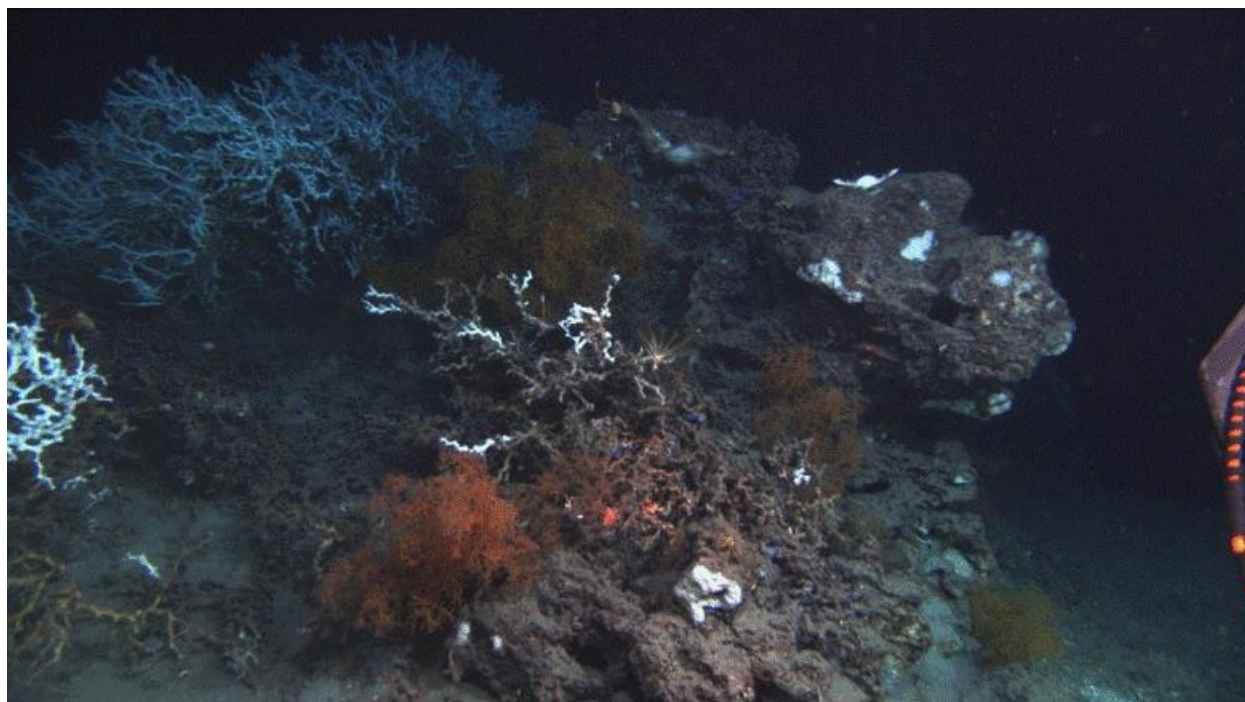


Figure 2-26. A large mound is colonized by red and orange *Leiopathes* sp., *Eumunida picta*, and live and dead *Lophelia pertusa* (VK826).

The newly surveyed peninsula to the E of the main site hosted a very impressive long linear ridge of almost continuous *L. pertusa* colonies over the 500 m surveyed (

Figure 2-27). As we approached this ridge from the west, a large school of *Beryx splendens* surrounded the ROV and followed it for over 6 hours (Figure 2-28). On our second visit to this site, the same fish surrounded the sub again. It is possible that this is a fairly permanent resident population at this site, although future observations are required to confirm this.
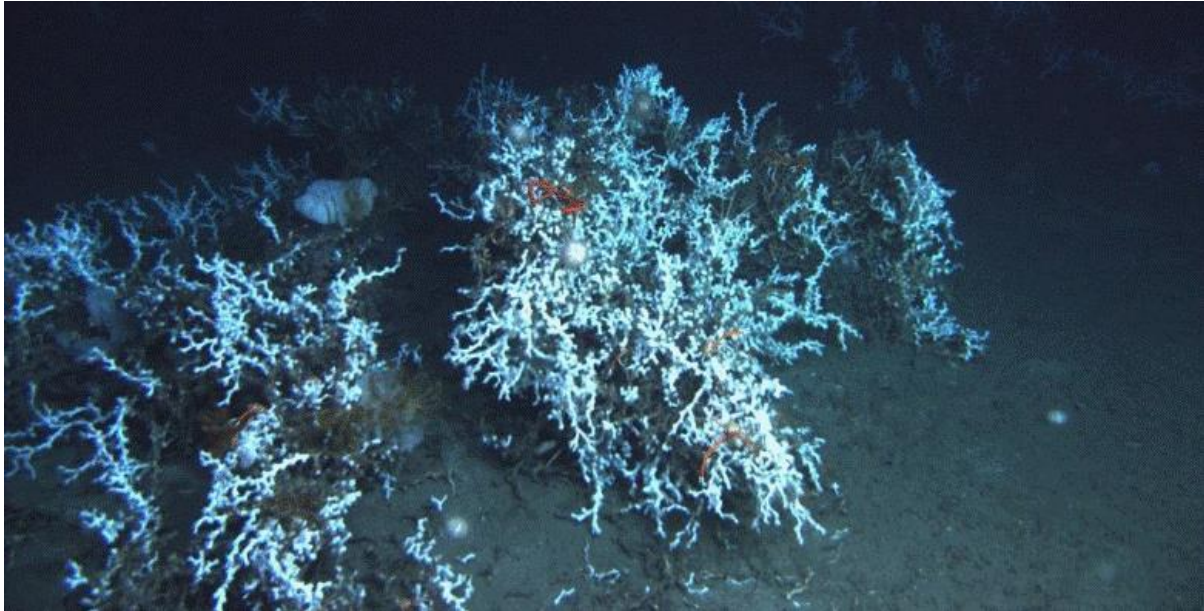


Figure 2-27. Thickets of *Lophelia pertusa* with *Eumunida picta*, *Echinus* urchins, and crinoid associates (VK826).



Figure 2-28. School of *Beryx splendens* over *L. pertusa* with attached crinoid at VK826.

### 2.3.1.7 GC234 (500 – 550 m depth)

GC234 was a primary study site for both the MMS Chemo II and *Lophelia* I projects and portions of the site have been intensively studied in the past. During this project the site was only visited during the 2008 cruise with the ROV *SeaEye Falcon*. This extensive seep and coral site covers several square km and ranges in depth from about 500 to 550 m. The coral area investigated is a roughly linear ridge feature running from 27.747º N, 91.224º W at approximately 500 m depth. During the *Lophelia* I project an area of *Lophelia pertusa* abundance was discovered to the west-northwest of the main seep site studied during Chemo II. It was a roughly north-south ridge colonized by *Lophelia pertusa* most of which was dead standing coral. In between the seep site and the coral ridge is an area of small carbonate boulders colonized by the gorgonians *Callogorgia americana delta*. A multibeam survey revealed an unexplored linear ridge running north from the explored area in the GC234 lease block into the GC190 lease block, and rising from 500 to 450 m. Exploration of this ridge revealed additional carbonate outcrops colonized by *Lophelia pertusa* and *Callogorgia americana*, including some approximately 3 m high and 3-4 m in diameter, consisting of mainly dead *Lophelia* and high abundances of fishes including *Hoplostethus* sp, *Urophycis* sp., Tinsel fish, and conger eels (

Figure 2-29). Other outcrops harbored scattered colonies of a diversity of cnidarians including bamboo corals and gorgonian genera including *Paragorgia*, *Muricea, Scleracis, Thesea ,and Paramuricea* (Figure 2-30). Unfortunately, collections were not possible for most of this dive, so further identification was not possible. The corals Scleraxonian nov sp. 1, *Paragorgia* cf. *johnsoni*, *Acanthogorgia aspera*, *Muriceides* cf. *hirta* 1b, *Paramuricea* sp. A, *Callogorgia am. delta*, and *Cheliodonisis a. mexicana* were collected from the VK826 site (Appendix A-2).
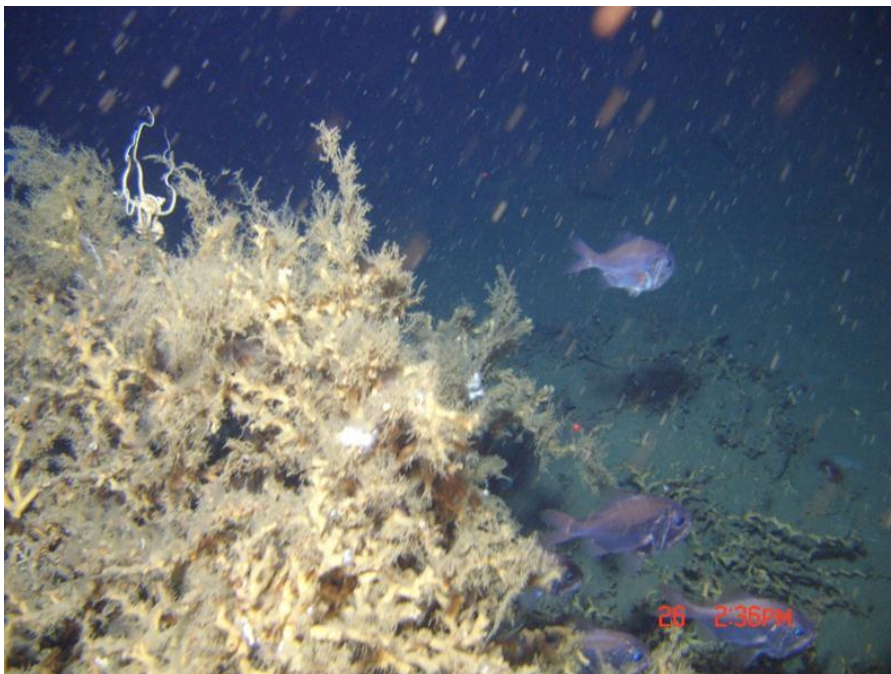


Figure 2-29. Dead *Lophelia* accumulation with *Hoplostethus* sp.
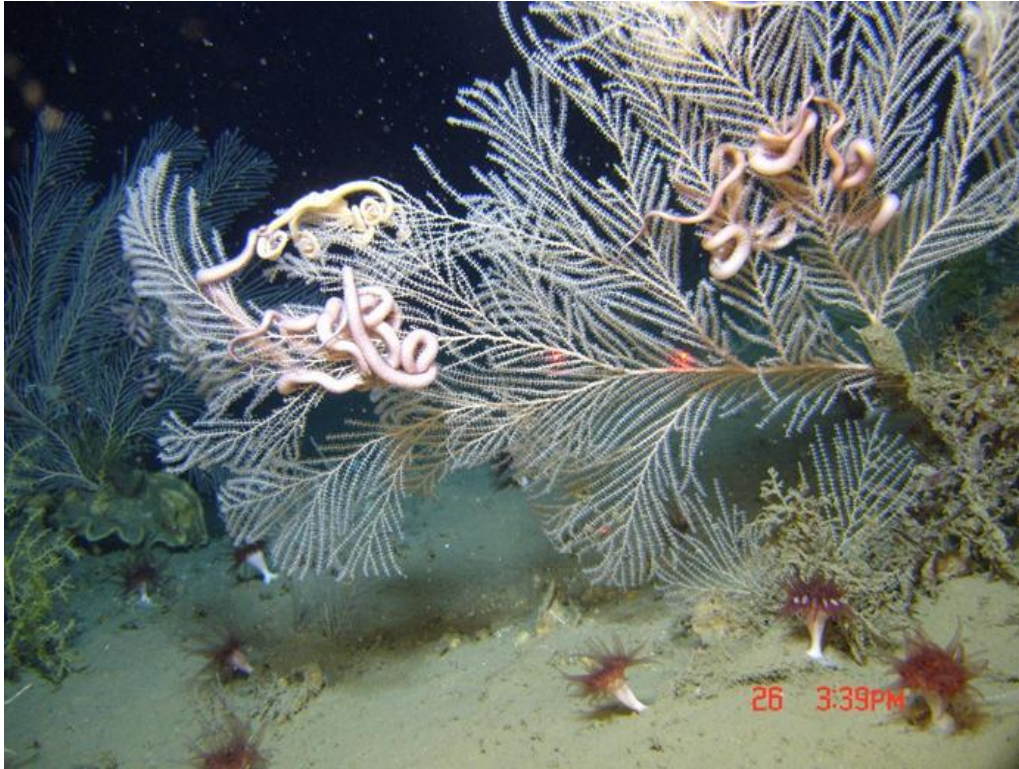
Figure 2-30. *Callogorgia* sp. and *Asteroschema* sp. along with some small cup corals.

### 2.3.1.8 GB535 (515 – 540 m depth)

*L. pertusa* was sighted here during the last few minutes of a JSL dive in 2003 and was dived on during both the 2009 and 2010 *Ron Brown* expeditions as part of this project. Two areas around markers C and E were mosaicked at this site.The site is located at 27.42°N, 93.60°W in between 515 and 540 m water depth. Examination of BOEM 3D-seismic data and bathymetry suggested the presence of hard grounds and the potential for other areas with *Lophelia* in this immediate area. Though the very steep slope of the scarp shows little amplitude variation on the seismic data, high reflectivity on the top of the slope suggested the presence of carbonate hard ground substrates on the top of the slope.

Multibeam bathymetry data acquired during the *Nancy Foster* cruise in 2008 with the *Sentry* AUV identified a large area of fluidized sediment expulsion and several smaller features that also may represent centers for more localized flows. The AUV multibeam data clearly define near-concentric ridges on the surface of this large domal feature, strongly suggesting fluidized sediment expulsion from a point of origin (vent) located toward the southwestern end of this broad area. Photographs from the 2008 *Sentry* survey found no exposed carbonates or corals on the surface of this broad area, but white material interpreted as *Beggiatoa* and evidence of brine seepage were common. Pockmarks, suggesting the rapid release of gas, are typical of the area as well. The data also defined a long ridge of about 50 m relief and small bathymetric features associated with the upper edge of the ridge. Seismic data clearly define this scarp as a fault. The top of this fault with its small mound-like features was the area chosen for investigation.

The substrate near the base of the down-to-the-northwest fault scarp was almost entirely composed of mottled mud with minor carbonate rubble. The steep slope of the fault scarp had a few carbonate cobbles and some areas of rubble, but was primarily mottled mud. The top of the scarp had common carbonate rubble, pavement, and occasional small and large boulders. On the gentle slope past the top of the scarp, seep related features and organisms were observed on pavement and small boulders. These localized communities appear to be responding to seepage along a family of small faults that are "splinters" off the main down-to-the-northwest fault.

Carbonate rubble, pavement and occasional boulders were present close to the ridge crest along the entire length of the ridge surveyed. The most abundant macrofauna on this rubble were white sponges (Figure 2-31).



Figure 2-31. White sponges.

The orange antipatharian whip corals, *Stichopathes* sp, and three octocorals, *Narella* sp. *Nicella* sp., and *Scleracis* sp were patchily distributed on carbonate rubble and on the boulders (Figure 2-32). Additionally, *Lophelia* colonies were present along much of the top of the slope of the ridge and along its crest (Figure 2-33). Colonies of live *Lophelia* ranged from very small colonies consisting of less than 20 polyps to mounds of *Lophelia* framework several meters in diameter and two m high covered with live *Lophelia*. In one area the entire slope below a pair of mounds was scattered with *Lophelia* rubble suggesting a long history of *Lophelia* growth here (Figure 2-34). The corals Stoloniferan sp. 1, *Anthothela* nov sp. 1, *Acanthogorgia aspera*, *Muriceides* cf. *hirta* 1a, *Muriceides* cf. *hirta* 1b, *Muriceides* cf. *hirta* 1d, *Paramuricea* sp. A, *Cheliodonisis a. mexicana*, and *Paracalyptrophora carinata* were collected from the GB535 site (Appendix A-2).

41

Figure 2-32. Patchily distributed fauna on carbonate rubble.
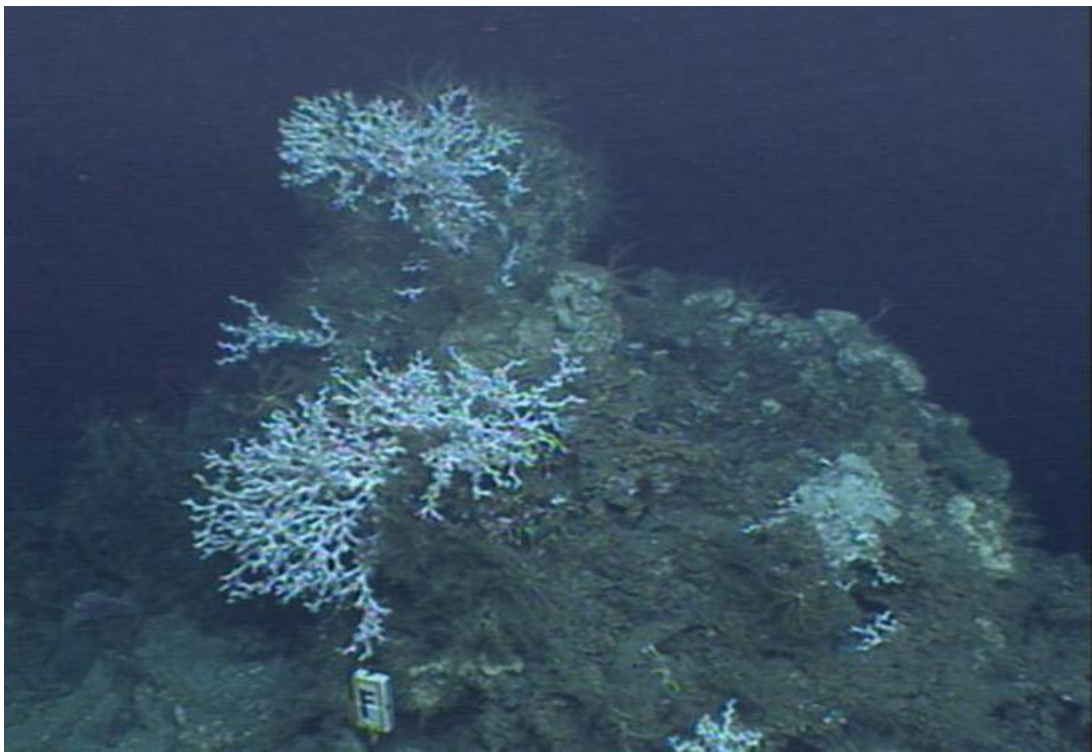


Figure 2-33. *Lophelia* colonies.
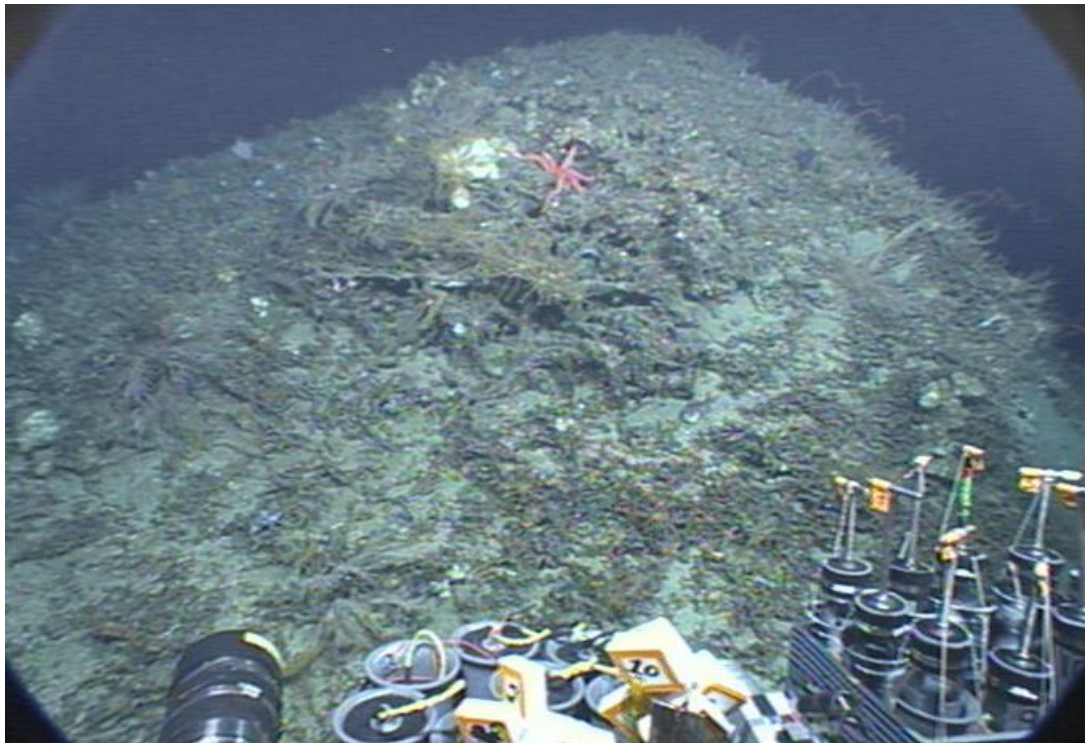
Figure 2-34. *L. pertusa* rubble.

### 2.3.1.9 GC235 (520 m depth)

The GC235 site was identified on BOEM 3D-seismic surface amplitude data superimposed on bathymetry. This site was only visited during a single dive during the 2009 *Ron Brown* cruise. The feature of interest is a roughly circular, low-relief platform with little small-scale relief covered by a "bright spot" of high positive reflectivity on the surface amplitude map. It is located at 27.737°N, 90.813°W in ~520 m of water. Around the northern, western, and southern flanks of the platform very-low-surface-amplitude response and vertical zones of acoustic blanking on seismic cross-sections was interpreted to be related to higher-flux zones of seepage. The seismic data suggested that the top of the platform would have abundant hard-bottom areas and more scattered hard grounds would be characteristic of the apparent higher-flux zones along the northern, western, and southern flanks of the feature.

However, the central area of this site, over the areas of highest reflectivity, consisted of plain sediments, largely uninhabited by visible fauna. No authigenic carbonate hard grounds were encountered associated with top of the platform, which was sediment covered and largely uninhabited by visible fauna. Around the periphery of the area of reflectivity were sediments with limited indications of seepage with occasional bacterial mats and some frenulate siboglinids (pogonophorans). Small boulders were found to the southwest where the amplitude anomalies appear weaker and much smaller, similar to the seismic character at GC234 where corals were found. Some of the exposed authigenic carbonates were colonized by megafauna. One large, 2-3 m high and 2-3 m wide boulder, and a few smaller carbonates were entirely colonized by the vestimentiferans *Lamellibrachia luymesi* and *Seepiophila jonesi* (Figure 2-35). Slightly north and east of this large tube worm aggregation were a number of small, low-lying carbonates colonized

by primnoid gorgonians (some *Callogorgia* spp.), cup corals, and individual tube worms (Figure 2-36). The coral *Callogorgia am. delta* was collected from the GC235 site (Appendix A-2).

Although it is likely that the majority of the exposed carbonates in this area were explored (based on the ROV-mounted sonar), *Jason* developed a hydraulic leak before we could finish a more thorough survey and the dive was terminated.
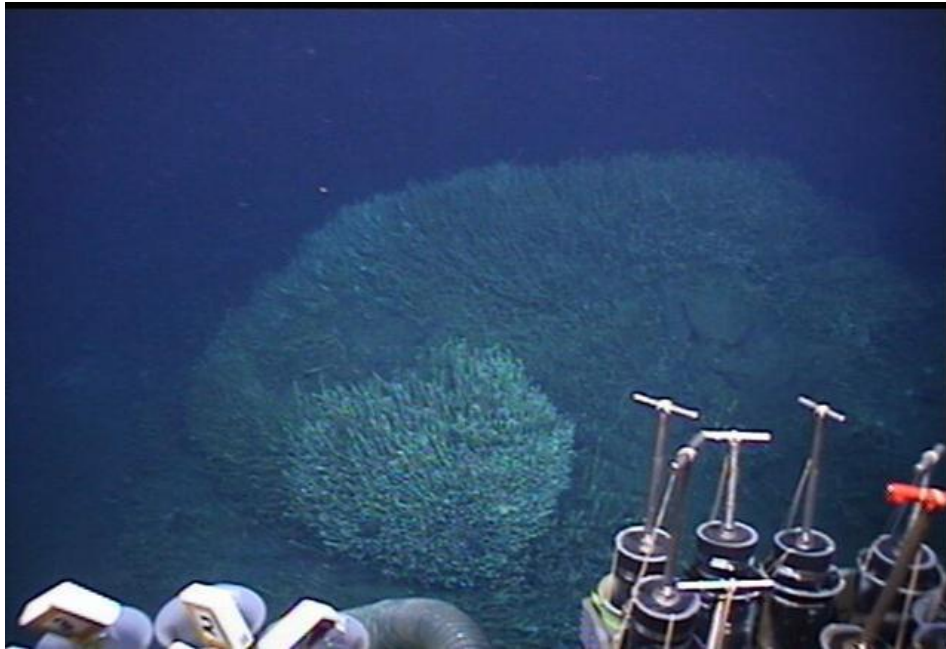


Figure 2-35. Vestimentiferans *Lamellibrachia luymesi* and *Seepiophila jonesi.*



Figure 2-36. Primnoid gorgonians at GC235.

### 2.3.1.10     GC354 (525 m depth)

The GC354 site was one of the primary sites in the *Lophelia* I project, and was explored on a series of dives on both NOAA Office of Ocean Exploration (OER) and National Science Foundation (NSF)-funded seep cruises in the early 2000s. As part of this project it was dived on during the 2010 *Ron Brown* cruise. One area around marker V was mosaicked at this site. The site lies near 27.56°N, 91.82°W on the top and flank of a large mound. The top of the mound, at approximately 525 m depth, contains a series of small *L. pertusa*. coral mounds composed mainly of dead coral framework on large boulders with small accumulations of live coral at the tops. Large sponges are also common on these large boulders, and many of them supported aggregations of *Hoplostethus* fish. On the flank of the mound are boulders and low-lying carbonate outcrops containing a relatively high diversity of octocorals (*Acanthogorgia, Muricedes, Nicella, Paracalptophora*) and antipatharians (*Stichopathes*) with a suite of associates, mainly galatheid crabs. At the base of the slope, approximately 580 m depth, is an area of more active seepage with large flat carbonate blocks and tube worms around the edges where there are seepage conduits. The corals *Acanthogorgia aspera*, *Muriceides* cf. *hirta* 1a, *Muriceides* sp. 3, *Paramuricea* sp. A, *Swiftia exserta*, *Cheliodonisis a. mexicana*, and *Paracalyptrophora carinata* were collected from the GC354 site (Appendix A-2).

### 2.3.1.11     GB201 (525 m depth)

GB201 is a large (~6.5 km by 5.5 km, 250 m high) seafloor structure supported by a shallow salt diapir rising to about 525 m depth located at 27.790ºN, 92.743ºW. This site was first surveyed by Harry Roberts on an exploratory dive in 1997, during which he noted the presence of corals. During this project, this site was only visited during the 2008 cruise with the ROV *SeaEye Falcon*. 3-D seismic amplitude extraction of the seafloor reflector shows several areas with anomalously high positive amplitudes suggesting hard ground development on the seafloor potentially conducive to coral habitat. The northwestern flank and several discreet areas on and near the crest showed the most promise for coral habitat and were chosen for the dive. One characteristic of this feature is the abundance of "pockmarks", circular depressions on the seafloor that are hypothesized to be strong flows of gas without brine or sediment that excavated sediment from the area, as opposed to constructional mud volcanoes and flows that introduce new sediments to the area. There was very limited colonial coral development discovered at this site.  Most of the area surveyed consisted of soft bottom with occasional colonial soft coral or hydroid colonies (Figure 2-37). One area with bacterial mats and methane bubbling from the seafloor immediately adjacent to tube worms was encountered.  In another area a single large black coral (Figure 2-38) and a few *Callorgia* sp. octocorals were observed. Very little megafauna were found in the areas with pockmarks and the low seismic return was consistent with a general absence of hard grounds in these areas of the site. It is possible that the sediment ejected from the numerous pockmarks effectively covered the high-return areas identified in the seismic data with a layer of sediment, thus making them unavailable for coral settlement and growth.

Figure 2-37. A small octocoral colony in GB201. Note the high concentration of particulates in the water.



Figure 2-38. The large black coral at GB201.

### 2.3.1.12    EW1009 (560 m depth)

The EW1009 seep site is ~9 km from the ship wreck in EW1008 at a depth of about 560 m. This site was only visited during the 2008 cruise with the ROV *SeaEye Falcon*. The area of interest is relatively small compared to most the sites targeted for the coral exploration (500 m by 2 km). The primary target at the northern end of the overall site was ~500 m by 600 m, with 20 m vertical relief, and shows moderately high positive amplitude response. The southern two-thirds of the site exhibits low relief and has a prominent pockmark on the eastern side. A single very short dive to EW1009 was conducted without the ultra-short baseline (USBL) navigational system or the compass due to ROV and USBL failures. Additional ROV problems were encountered on the sea floor and only the landing site and a small area immediately around the ROV "garage" was surveyed. The bottom appeared to be soft sediment, but the sediment may have been overlying a thin carbonate crust since there was very little disturbance of the bottom when the ROV landed. No high relief features were seen in a 360° sonar scan of the immediate area.

### 2.3.1.13    MC539  (630 m depth)

The MC539 site is a small mound (~300 by 250 m with ~20 m vertical relief) at 28.413ºN, 89.402ºW in about 630 m depth that was identified using 3-D seismic data. It was selected from the list due to its proximity to the *Gulfpenn* wreck and two production platforms in adjacent lease blocks. This site was only visited during the 2008 cruise with the ROV *SeaEye Falcon*.  The amplitude extraction from the site shows a strong positive response indicating a hard seafloor (authigenic carbonate). The seismic cross-sections across the mound show a vertical acoustic wipeout suggesting active gas migration to the seafloor, providing a source for seepage and therefore authigenic carbonate production. The only dive at this site experienced telemetry and video signal problems and was terminated shortly after reaching the sea floor in the center of the feature identified on the 3-d seismic map.  Only soft bottom was seen during the brief visit to this site.

### 2.3.1.14    MC885  (650 m depth)

The MC885 site was visited during the *Lophelia* I project, and is a known site of chemosynthetic activity that was visited during a series of NOAA OER cruises in the early 2000s (Cordes et al. 2007). The multibeam acquired during the 2008 *Nancy Foster* cruise revealed an additional mound with a very similar appearance to the explored area of the site, and a series of smaller mounds to the south. The mound located approximately 1 km to the east of the known site is a circular bathymetric high (1.3 by 1.3 km, with up to 30 m of vertical relief) with moderately high positive seafloor amplitude response from 3-D sesmic data. The exploratory site and the previously visited site are on a large salt supported bathymetric high (3 by 4 km). This site shows clear indications of vertical gas migration on vertical seismic cross-sections.

Our surveys during the 2010 cruise first relocated some of the markers and areas surveyed during *Lophelia* I on the western mound centered at approximately 28.65ºN 89.71ºW and 620 m depth. This area contained scattered *Lophelia* colonies of fairly small size interspersed with *Callogorgia americana delta*. There were also some larger locations with *Madrepora oculata* growth, making

this the only site in the northern Gulf where these two species of scleractinians are known to co-occur (they also co-occur on the Florida platform). Catshark eggcases were frequently observed on the *Callogorgia americana delta* colonies, as had been observed in previous years. This appears to be a persistent location for the depositing of egg cases on the gorgonian colonies. The eastern mound, centered at approximately 28.62 N, 89.69 W and at 620 m depth, appeared to be more active, exhibiting numerous signs of seepage, including stained sediments and apparently live clams. *Callogorgia americana* delta along with Asteroschema associates were also present on the eastern mound, often interspersed with tube worms (Figure 2-39) but no other corals were observed during our short survey of this area. The coral *Callogorgia* am. delta was collected from the MC885 site (Appendix A-2).



Figure 2-39.  Typical setting at MC885, including small tube worm aggregations and occasional colonies of *Callogorgia americana* delta.

### 2.3.1.15     GC246 (770 – 860 m depth)

This site was targeted for investigation during the first (2008) ROV cruise with the *SeaEye Falcon* DR ROV but problems with ROV prevented a dive during that cruise.  However, bathymetry collected during that cruise was used to plan the single dive accomplished during the 2010 *Ron Brown* cruise. The GC246 site is a large (5 km by 6 km, 100 m vertical relief) salt supported feature with a steep eastern flank and a gradual western flank with the northern edge at 27.6897°N, 90.645°W and features of interest at depth from 770 to 860 m. Five discreet bathymetric highs with positive amplitude responses are aligned roughly north-south along the eastern flank of the top of the feature, all with interpreted sediment flows present down the eastern flank (characterized

by high amplitudes, presumably due to coarse sediment flowing out of the active seep sites and/or lithification of hydrocarbon saturated sediment). The discreet seismic highs located on local bathymetric highs were targeted because of their potential to host hard grounds appropriate for coral settlement. This site was thoroughly explored by *Jason* during a 16 hr dive. Most of the site was soft sediment and several areas of active seepage were found, including a small brine lake, mud volcanoes and areas with mussels and bacterial mats (Figure 2-40). A series of small exposed carbonates harboring *Callogorgia* sp. and symbiotic ophiuroids were present near 27°69°N, 90.645°W at 845 m depth. The corals *Paramuricea* sp. B3 and *Callogorgia am. delta* were collected from the GC246 site (Appendix A-2).



Figure 2-40. A dense field of dead *Bathymodiolus* mussels with disarticulated shells (GC246).

### 2.3.1.16    GC249 (780 - 820 m depth)

GC249 contained a fairly large high-amplitude anomaly that sites at the top of a local bathymetric high. This site, at about 27.72°N, 90.51°W had never been visited before and the multibeam map used to guide the dive was acquired immediately before the single 2010 *Jason* dive. A total of 8 hours was spent surveying this site between 780 and 812 m depth. Most of the site was soft bottom despite the high reflectivity indicated in the seismic maps used to select the site for investigation. Several seep areas were encountered (Figure 2-41). Most common were areas that were dominated by shell hash and bacterial mats with a few *Callogorgia* attached to the consolidated hash. Two areas were encountered with live mussels and one of these also had tube worms associated with small carbonate outcrops. This site is just to the east of the GC246 site, and to the southeast of the known seep site in GC204, and may represent a continuation of these fluid flux features. The coral *Callogorgia am. delta* was collected from the GC246 site (Appendix A-2).
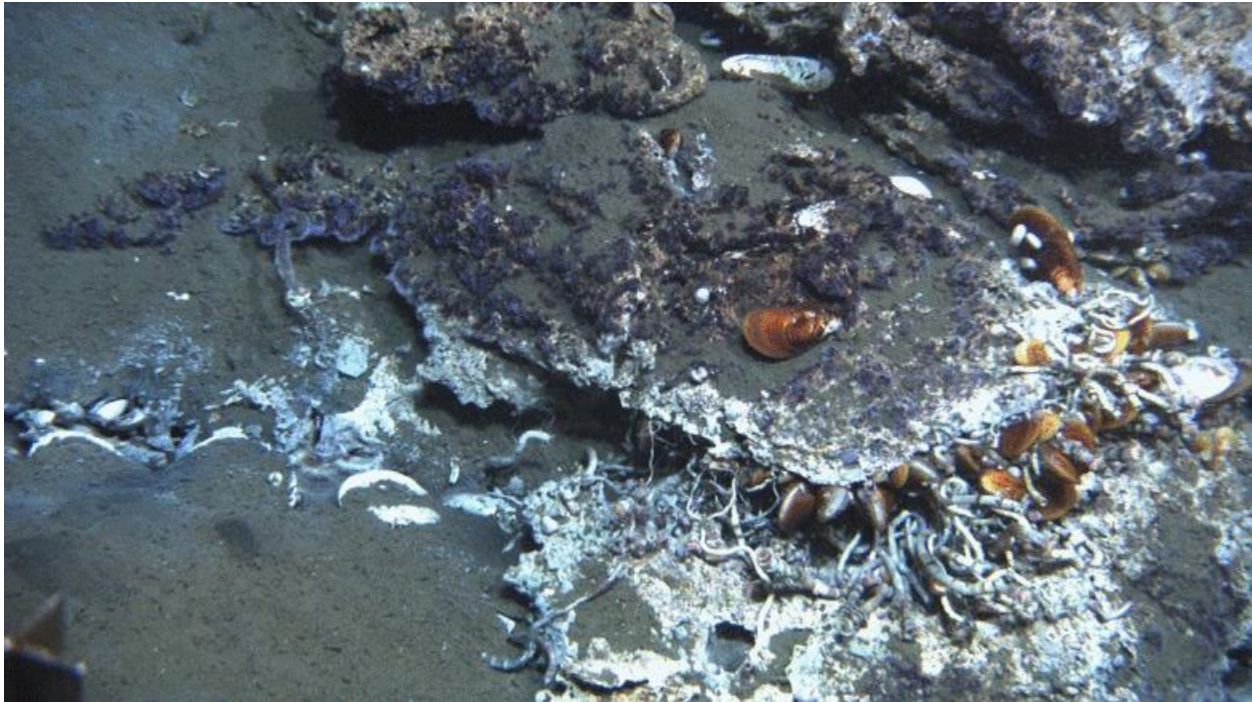
Figure 2-41. Bacterial mats and purple ciliates cover a number of *Lamellibrachia luymesi* tube worms and *Bathymodiolus childressi* mussels (GC249).


### 2.3.1.17    AT47 (835 - 860 m depth)

The feature investigated in AT47 is one of several low relief complexly mounded areas east of the southern end of the Mississippi Canyon where the canyon transitions into the Mississippi Fan. The site is located at 27.88°N, 89.79°W in about 835 - 860 m depth. The only dive to this area was during the 2009 *Ron Brown* Cruise. One area around marker A was mosaicked at this site. Like the productive dive sites in AT 340 visited during the 2006 and 2007 Chemo III cruises, this site is characterized by numerous low relief  mounds and shallow depressions.  The AT47 site was identified on BOEM 3D- seismic data processed to display reflectivity (amplitude) of the seafloor and configuration of the subsurface related to conduits for fluid and gas migration.  Geologically this area constitutes a broad structural nose plunging to the south and supported in the subsurface by salt.  The mounds and shallow depressions defined by bathymetry have distinct high and low positive amplitude signatures, suggesting localized areas of relatively hard and soft bottom.   The areas of high positive amplitude link to faults and other clear migration pathways from the flanks and top of salt as indicated on seismic cross sections. Multibeam bathymetry collected during the first cruise of this project on the NOAA Ship *Nancy Foster* revealed numerous areas with narrow ridges and apparent small mounds of a few meters relief suggestive of possible coral habitat.

Most of the AT47 area that exhibited high positive amplitude on the 3D-seismic data had no carbonate hard grounds exposed at the seafloor.  However, there were clear signs of seepage everywhere, including patches of dark reducing sediment, localized brine flows, and white

50

bacterial mats. The high seismic reflectivity or high positive amplitude of the seafloor reflector appears to be related to the extensive and dense clam beds which covered large areas defined by high surface reflectivity on 3D-seismic data (Figure 2-42). The gross majority of the intact clam-shells that were clearly visible were *Calyptogena ponderosa*. This field identification was confirmed with the collection of a live *C. ponderosa*, one of the only apparently live clams seen during the dive. Brine seeps were scattered throughout the clam beds. Some supported dense, but limited living mussel communities (Figure 2-43). Not only did the shell beds cover large expanses of the sea floor, but on some slopes the beds appeared to be at least several layers thick. There were no colonial corals associated with the clam or mussel beds.
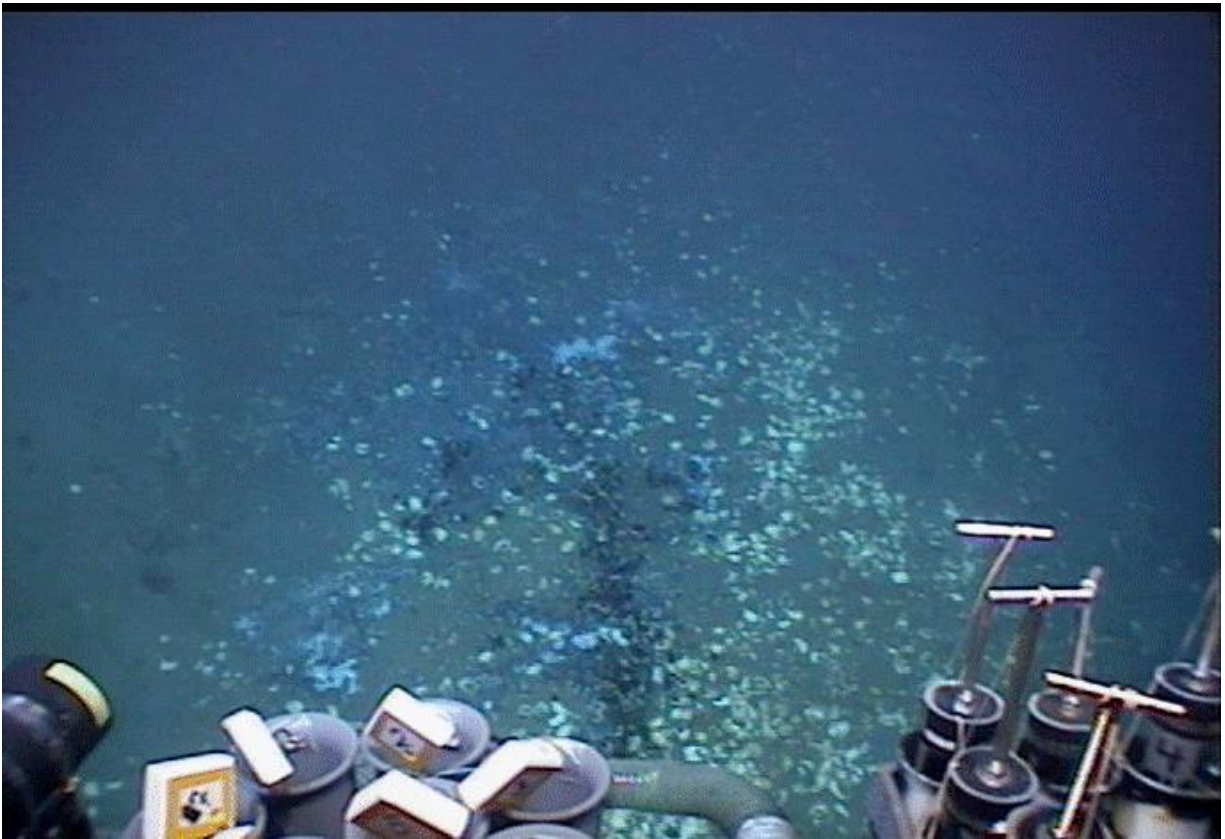


Figure 2-42. Extensive and dense clam beds.

Figure 2-43. Articulated and disarticulated clam shells with some live mussels.

Carbonate pavement may underlie some of the bivalve beds, as the *Jason* was unable to penetrate more a few inches with a pushcore associated with one bed. The highly reflective sites that supported densely populated clam beds occurred on lobate features that extend generally to the south. These may have been old mudflows that have been vertically displaced by the upward movement of shallow subsurface salt. Such movement would have activated local faults that acted as conduits for fluid and gas migration to the modern seafloor supporting a slow seepage environment.

The major exception with respect to coral occurrence was in the southern-most area surveyed, and encountered at the very beginning of the dive. In this area, there was a thin cover of clam shells and live mussels on the lower portions of the slope near a *Madrepora* community, with steadily increasing areas of dead scleractinian coral rubble and small mounds of dead coral as we moved upslope (Figure 2-44). Also notable in this area were numerous golden crabs, often associated with areas of dead coral. Numerous colonies of *Paramuricea* gorgonians were seen attached either to the clam or coral rubble. Even here there was very little if any visible carbonate. Near the apex of this slope, a single large, mini-van size, mound of dead *Madrepora* was encountered (Figure 2-45), with several areas of live coral present on the top and edges of this mound. Also present on the mound were attached gorgonians and at least 4 golden crabs (*Chaceon*). Although this area was impressive for the quantity of dead coral and clam shells, it was apparently of limited extent, less than about 50 m on a side. The abundance of coral rubble and clam shells on the slopes below the *Madrepora* mound suggest this site may have hosted coral and clams for at least hundreds to thousands of years. The corals *Paramuricea* sp. B3 and *Swiftia* cf. *koreni* were collected from the AT047 site (Appendix A-2).

Figure 2-44. Large standing colony of *Madrepora*.
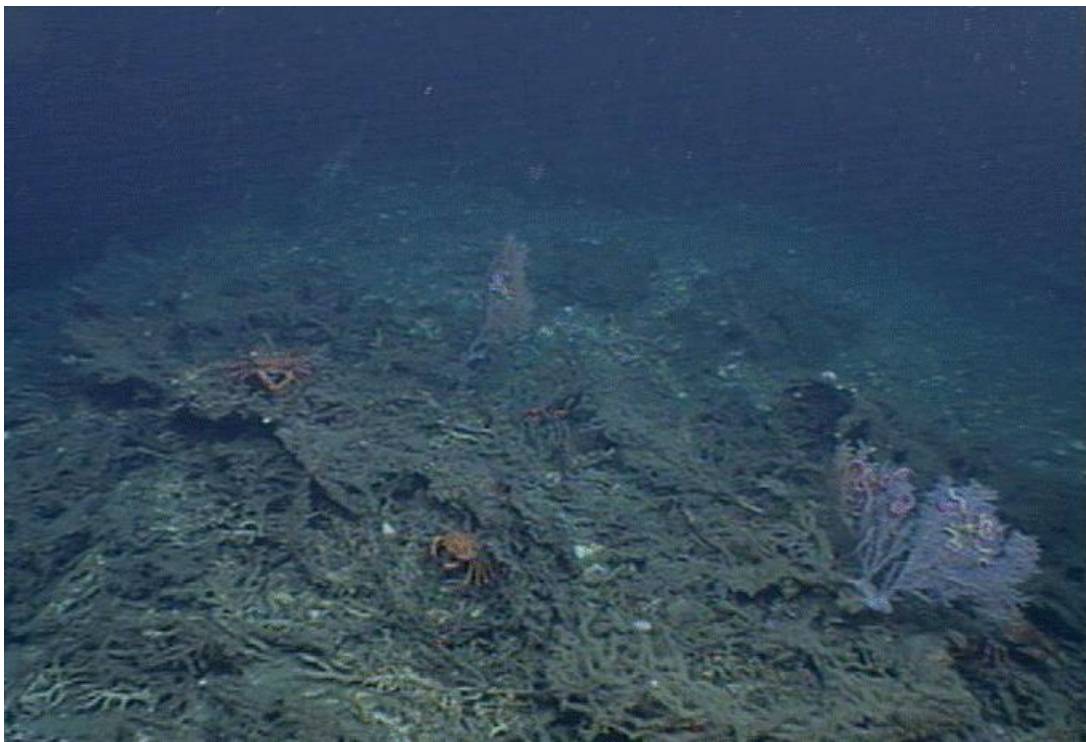


Figure 2-45. Dead *Madrepora*, areas of live coral and golden crabs (*Chaceon*).

### 2.3.1.18    MC118 (880 m depth)

MV118 is also known as the (Ole Miss) Hydrate Observatory Site. The site is clearly visible on 3D seismic maps of the region with the most intense reflectivity within a 100-mile radius. The site is located at 28.85°N, 88.5°W in about 880 m depth. This site has been well mapped by AUV and numerous ROV and *JSL* dives since 2005 and numerous geophysical, geochemical and microbiological instruments are on the sea floor. This site had not been well studied by macrobiologists although in addition to active seeps, hydrates, and seep communities the site hosts several areas with extensive development of colonial corals. We dived on this site one time as part of this project, during the 2010 *Ron Brown* cruise. One area around markers T1 and T2 was mosaicked at this site.

The dominant gorgonian at this site was *Paramuricea* sp. This gorgonian was found attached to carbonate boulders in numerous locations throughout the site, and in some areas was present as quite large (and old) colonies in relatively high densities (Figure 2-46). Most of the colonies of *Paramuricea* encountered hosted commensal ophiuroids. Three areas with live colonies of the hard coral *Madropora* sp. are also present at this site, one of which had more living *Madropora* present than any other site visited as part of this program. *Chrysogorgia* sp. was rare but present at the site and small crabs and anemones were often associated with this coral. Golden crabs (*Chaceon fenneri*) were abundant at this site and present at elevated densities in association with both living and dead *Madropora* thickets. The corals *Paramuricea biscaya* B2, *Paramuricea* sp. B3, and *Chrysogorgia* sp. 1b were collected from the MC118 site (Appendix A-2).
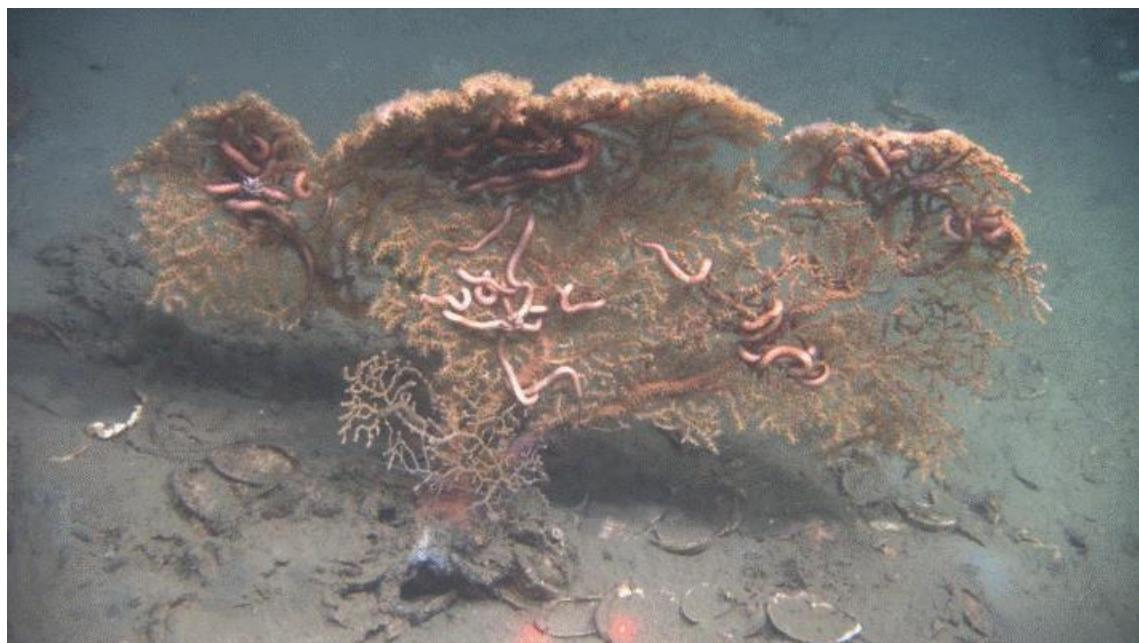


Figure 2-46. A single large colony of *Paramuricea* sp. is seen along with a number of its associated *Astroschema* sp. (MC118).

### 2.3.1.19    GC338 Site Summary (900 m depth)

The GC338 site was chosen because of areas with discrete high positive amplitudes on the seismic interpretation and an east-west trending ridge representing a local bathymetric high.  The site is located at 27.67°N, 89.52°W in about 900 m depth. The site was dived on once during the *Ron Brown* 2009 cruise and the multibeam bathymetry necessary to plan the dive was acquired immediately prior to the dive. The relatively short single dive was aborted prematurely due to an octans failure on the ROV.

The only area visited with significant coverage of colonial cnidarians was on the southern flank of the ridge slightly downslope of the local topographic high.   In this area there were beds of disarticulated vesicomyid shells (primarily *Calyptogena ponderosa*) on the slope with variable amounts of carbonate from scattered rubble (Figure 2-47), to pavement and small boulders.  On the carbonate were scattered colonies of *Callogorgia sp.* with attached ophiuroids and a few colonies of other corals including *Chrysogorgia sp.*, *Bathypathes sp.*, and *Paramuricea sp.* (Figure 2-48 and Figure 2-49).  On the top and N and E flanks of the ridge the seafloor was composed almost entirely of mottled mud and although there were numerous burrows present, very little benthic fauna was noted. Discrete areas of brine seepage and bacterial mat were encountered to the southeast. The corals *Clavularia rudis*, *Muriceides* sp. 2, *Paramuricea* sp. B3, *Callogorgia am. delta*, and *Chrysogorgia* sp. 1b were collected from the GC338 site (Appendix A-2).
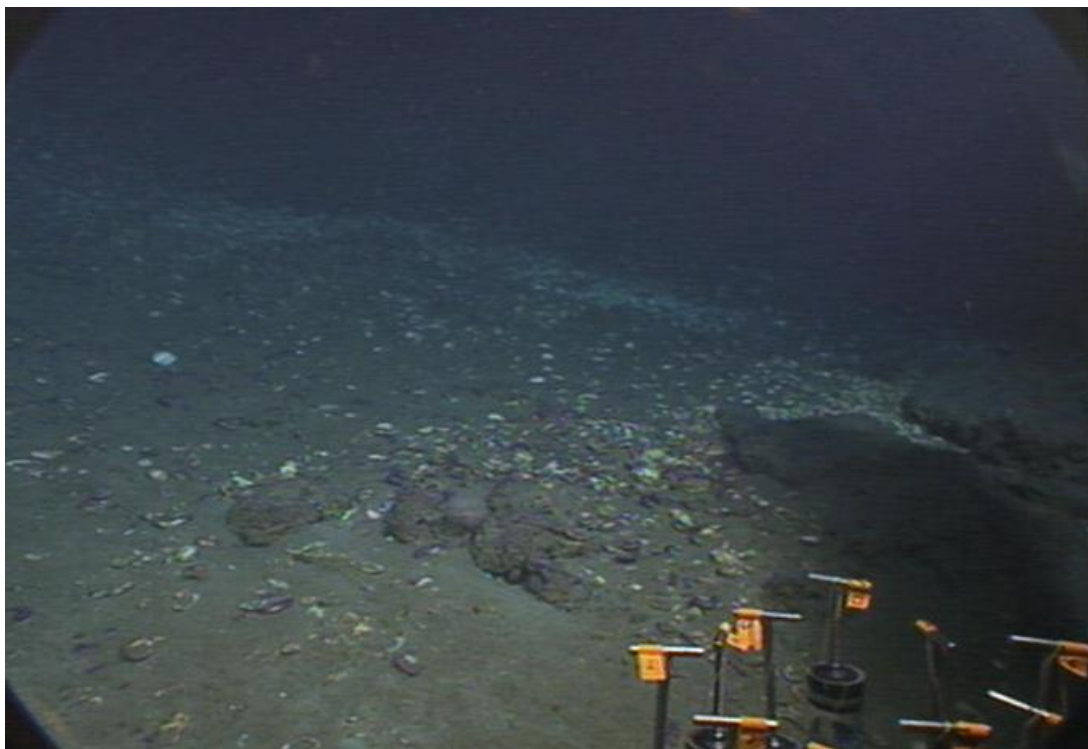


Figure 2-47. Carbonate rubble and clam shells scattered over the seafloor.
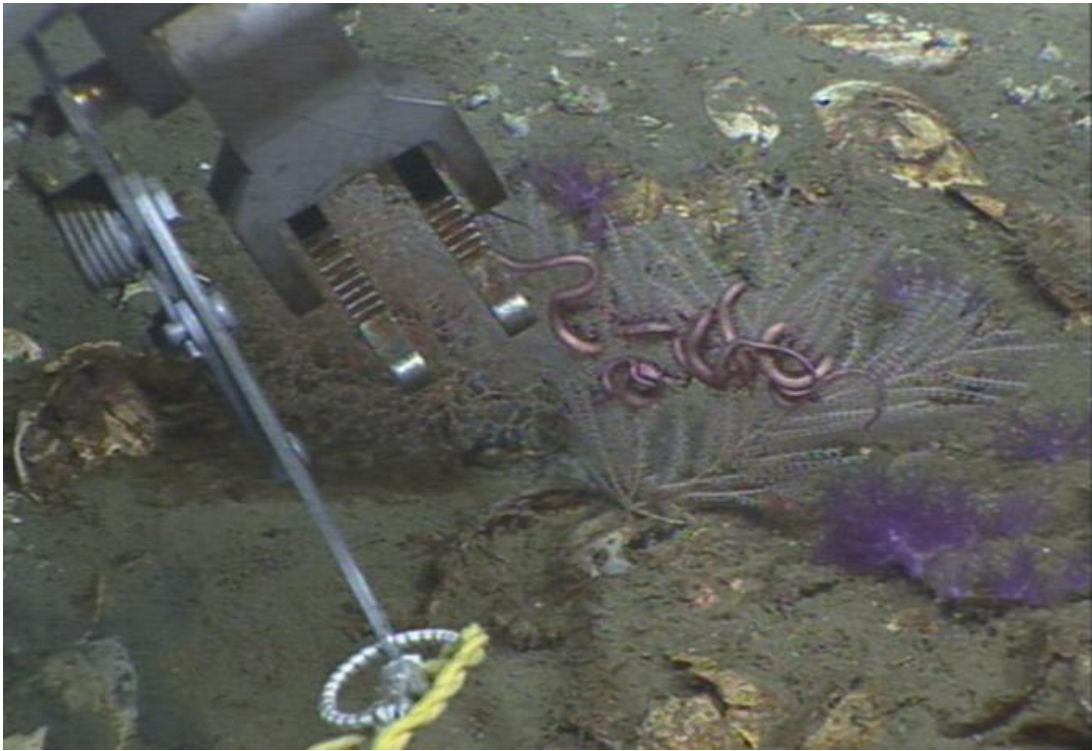
Figure 2-48. *Callogorgia* with attached ophiuroids.



Figure 2-49. *Paramuricea* with attached ophiuroids.

### 2.3.1.20    MC294 Site I (1350 – 1400 m depth)

The MC294 site was discovered and evaluated using BOEM 3D-seismic data. It is characterized by a series of structural highs and lows along a regional northwest-southeast ridge at a depth of approximately 1400 m. Note that this is part of the same feature later investigated as part of the MC338/294 coral sites discovered one year later. The dive to the area described here was made during the 2009 *Ron Brown* cruise. The area chosen for evaluation during the 2009 *Ron Brown* cruise at 28.674°N, 87.519°W and 1360 m depth had anomalously high positive amplitude response on the seismic data.

The high positive reflectivity on the 3D-seismic suggesting the presence of hard grounds on an elevated ridge was confirmed only in one small area where a pavement of authigenic carbonate was encountered covered with a fine layer of mud (Figure 2-50). This site primarily contained relatively featureless sediment, with some evidence for seepage in a few areas. The northern section of the 2 km long ridge contained some isolated patches of stained sediments, bacterial mats, and a few areas of authigenic carbonate pavements. It is likely that carbonate was present at all the seismic anomaly targets, but covered by sediment.



Figure 2-50. Sporadic bacterial mats at MC294.

In some areas where the pavement was fractured, it was colonized by small tube worms and a few small tube worm aggregations (Figure 2-51) along with some seep-related galatheids. There was also one area with dead mussel shells and a small bed of live mussels. There were at least 10 species of fishes encountered at this site as well as a few different species of shrimp and crabs. Overall biological megafaunal density and diversity was quite low, and there were no corals observed at all during the dive. The corals *Clavularia rudis* 1a, Stoloniferan sp. 2, *Paragorgia regalis*, *Acanthogorgia aspera*, *Paramuricea biscaya* B1, *Paramuricea biscaya* B1a, *Paramuricea biscaya* B2, and *Swiftia pallida* were collected from the MC294 site (Appendix A-2).



Figure 2-51. Small tube worm aggregations at MC294.

### 2.3.1.21    *MC388/294  (1370 – 1800 m depth)*

The last dive of the *Ron Brown* 2010 cruise was an exploratory dive to the northern end of MC388 and southern end of MC294. The main coral area around marker AA was mosaicked at this site. The site was chosen because of numerous high reflectance areas along a northward tending ridge in block 338.  Only soft sediment with occasional discolored sediment was seen at the southern end of this ridge near 28.648°N 88.467°W in 1800 m water depth.  No carbonates or significant sonar targets were encountered until about 6 hours into the dive when a single *Madropora* colony on a carbonate boulder at 28.67°N, 88.47°W in 1,370 m depth was discovered.  About 400 m to the north another sonar target led to the discovery of several carbonate boulders colonized by numerous gorgonian corals and other fauna.  Many of the corals at the site were partially or completely covered in a brown flocculent material and the ophiuruids on the corals were exhibiting

abnormal coloration and behavior (White et al. 2012). Analysis of the material on the corals detected hydrocarbons that were later fingerprinted to the Macondo well (White et al., 2012).

This site has subsequently been visited 6 times and the coral colonies in the central portion of the site (Figure 2-52) have been monitored for potential recovery from the initial impact from the spill. The dominant colonial coral at this site is *Paramuricea biscaya* (Grasshoff 1977), a gorgonian with planar arborescence morphology (Figure 2-53). Over the course of all visits we have digitized images of 51 live or recently living *P. biscaya* colonies and categorized the branches of the colonies into three categories: 1) branches with obvious and significant visible impact in the form of coverage by floc (White et al. 2012), excess mucous production, obvious tissue damage, or bare skeleton 2) branches clearly colonized by hydroids; and 3) branches without these forms of obvious visible impact. There were a total of 17 commensal Harmathoid anemones documented on 13 P. biscaya and one *S. palida* at this site. Forty-one of the *P. biscaya* had at least one *Asterschema clavigerum* ophiuroid attached during at least one visit. There were 5 other colonial octocorals at the site in addition to the *P. biscaya*: One large *Paragorgia regalis* (Nutting 1912), two *Swiftia pallida* (Madsen 1970), one *Acanthogorgia aspera* (Pourtalès 1867) and a small area of carbonate encrusted with *Clavularia rudis* (Verrill 1922). A manuscript summarizing the changes through October 2011 was published in Proceedings National Academy of Sciences (PNAS) December 11, 2012:109(50) 20303–20308. (Appendix C-4). The corals *Clavularia rudis* 1a, *Clavularia rudis*, *Stoloniferan sp*. 2, *Paragorgia regalis*, *Acanthogorgia aspera*, *Paramuricea biscaya* B1, *Paramuricea biscaya* B1a, *Paramuricea biscaya* B2*, Swiftia pallida*, and *Keratoisidinae* I2 were collected from the MC388/294 sites (Appendix A-2).
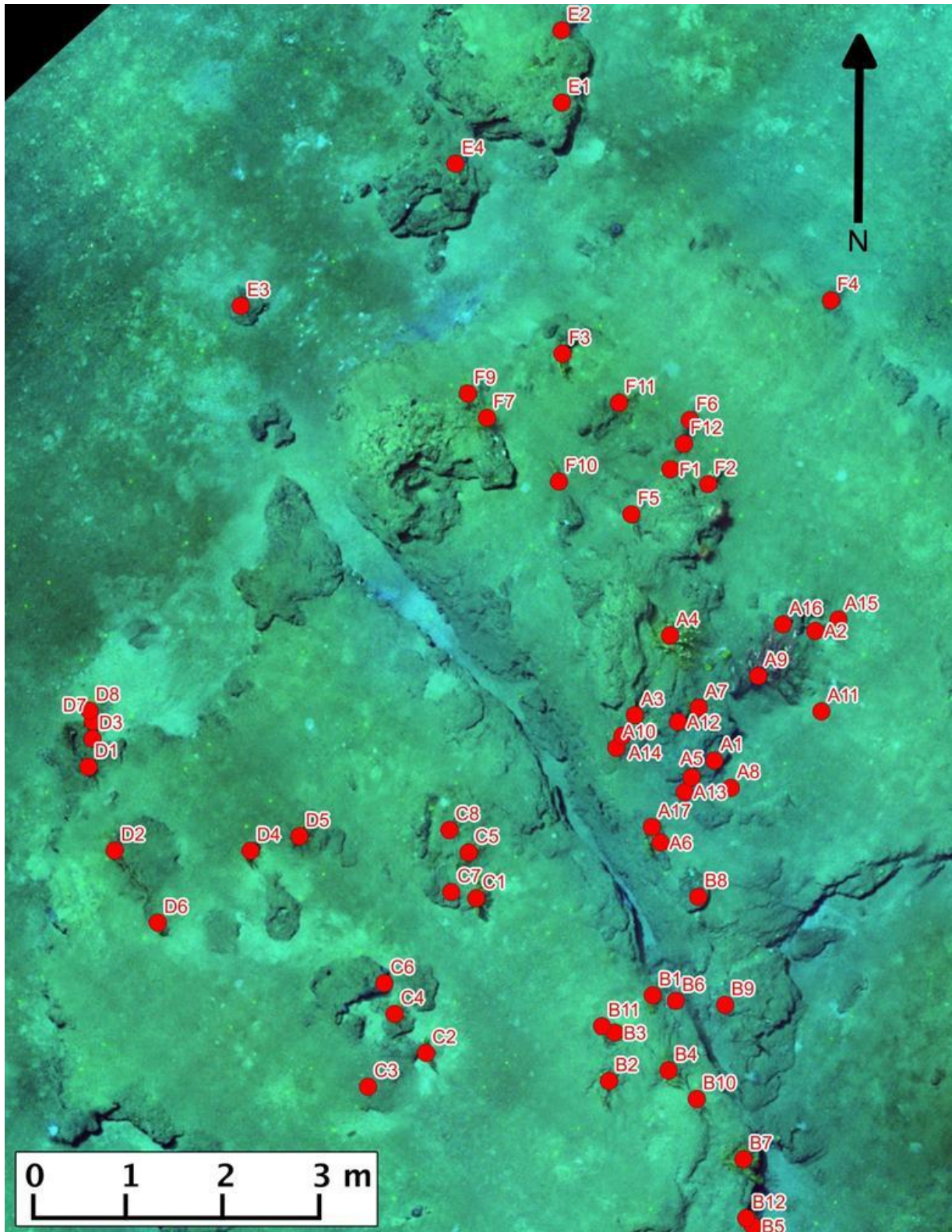
Figure 2-52. Photomosaic of the central area at MC294/338 with each coral identified for
monitoring.
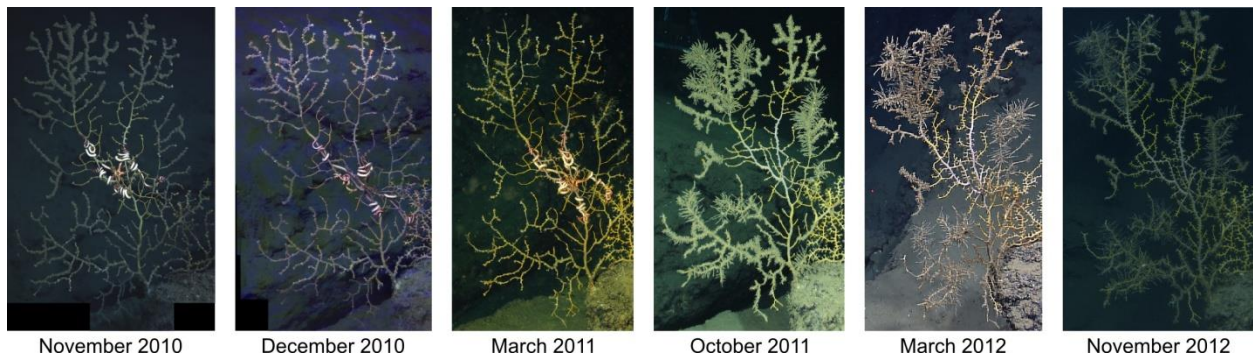
Figure 2-53. Example of a coral (A10) imaged during 6 different visits to the MC338/294 site.

### 2.3.1.22    GC852 (1400 m depth)

The GC852 site was originally identified on BOEM 3D-seismic data which defined it as a prominent N-S trending ridge supported by salt in the shallow subsurface. The ridge is ~15 km long, 5 km wide, with up to 200 m relief, and it resides in ~ 1400 m of water. Discrete strong positive  amplitudes are present along the top and flanks of the feature. This site was chosen for the Chemo III project and extensive seep and hard ground areas were verified during that program using camera sled, *Jason*, and *Alvin.* A high quality bathymetric map of the site was also acquired with C&C Technology's  *Hugin* AUV using an onboard multibeam system. Higher resolution multibeam bathymetry maps were made over selected areas with SM 2000 mounted on *Jason*. The *Hugin* AUV data define the overall site as a elongate ridge with considerable small scale topography on top. During a 2006 *Alvin* dive in support of the Chemo III project, the highest part of the ridge at 27.125°N, 90.836°W and 1400 m deep was found to support a thriving coral community. The southern end and the highest part of the ridge were the focal points of prior visits to GC852 associated with the Chemo III project.

A single dive was made to this site during the 2009 *Ron Brown* cruise as part of the present project. The top of the ridge is covered with large boulders and outcrops of hydrocarbon and seep-related authigenic carbonate. The central part of the top of the ridge is 20-30 m deeper than the shallowest south-central part that supports the coral community discovered during the Chemo III project. This central part is sediment covered and has less exposures of carbonate and fewer corals.

There is a single moderately large area of coral colonization that was nicknamed "Coral Gardens" during the Chemo II project that although dominated by bamboo corals, had a high diversity of colonial corals. Present in this area are *Iridigorgia* sp. colonies as well as *Corallium sp.*, *Paramaruricea sp., Bathypathes sp*. In one area the boulders were extensively colonized by a purple alcyonacean**.** Two portions of this area were colonized by the scleractinian corals *Madrepora oculata*, *Solenosmilia variabilis*, and *Enallopsamia rostrata* (Figure 2-54 and Figure 2-55).
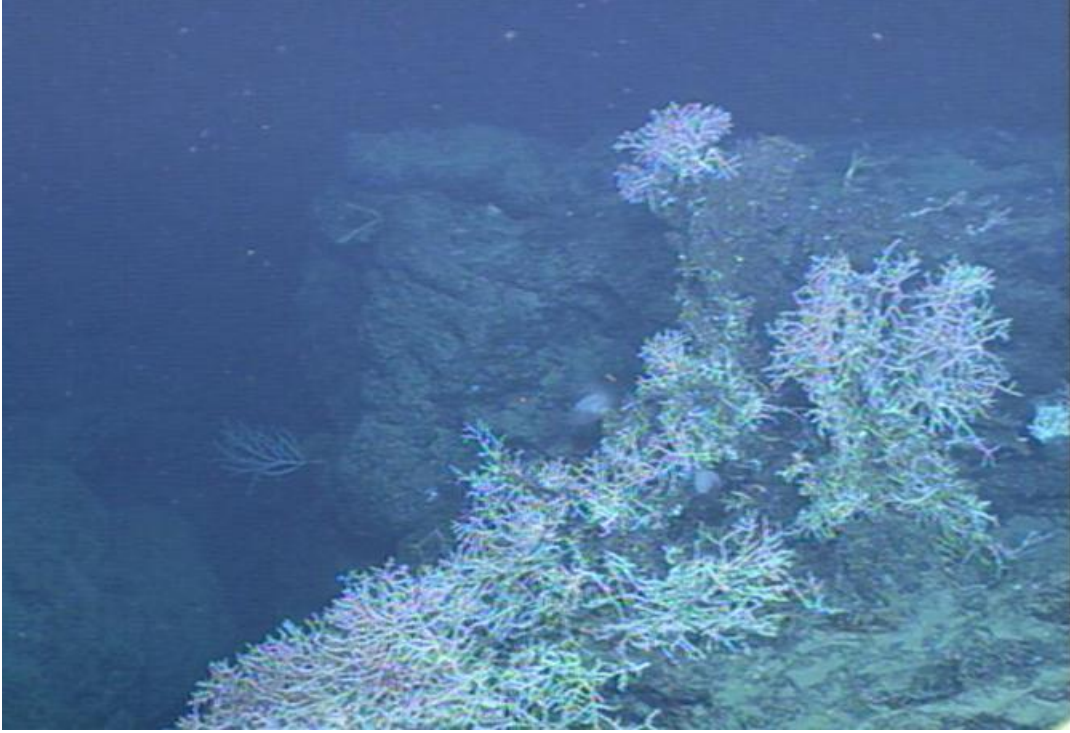
Figure 2-54. Coral colonization at central part of GC852.
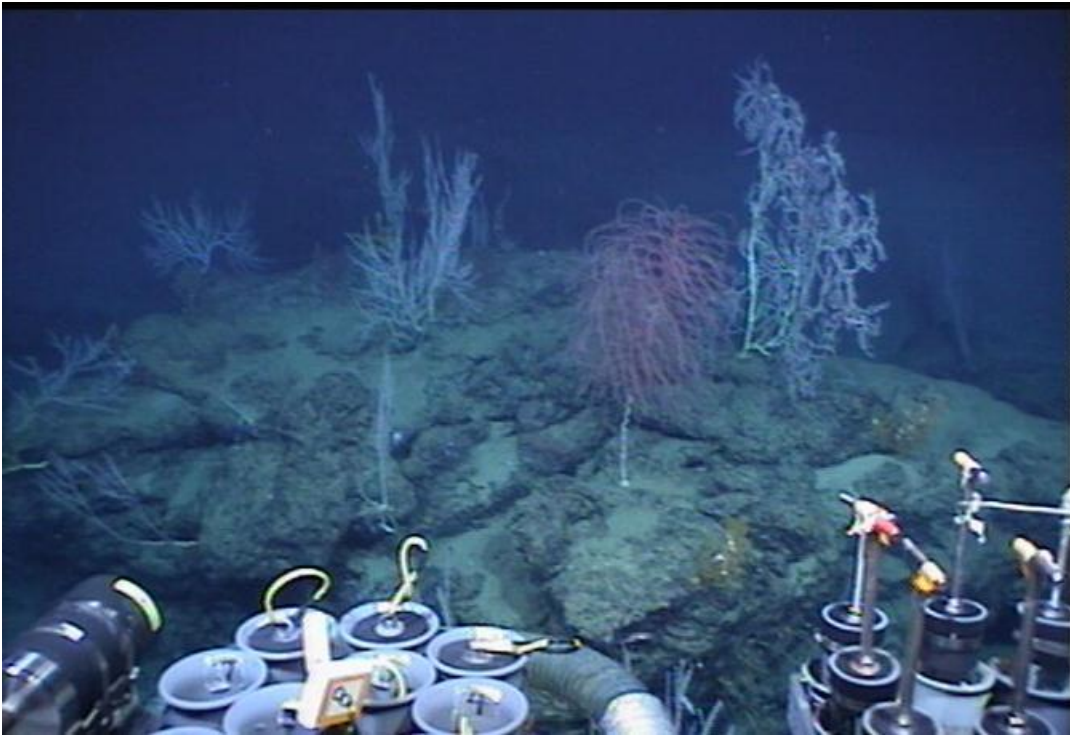


Figure 2-55. *Iridogorgia* and bamboo corals at the central portion of the site.

On the northern end of the ridge are very steep slopes of sediments that appeared to be too unstable to support coral communities (Figure 2-56). At the base of this slope were a few isolated mussel beds. At the tops of the bathymetric highs on the northern end of the ridge were a few isolated octocoral colonies (Figure 2-57). The center of the ridge was also primarily soft sediments and was devoid of corals as well. The corals *Clavularia rudis* 1b, *Corallium* sp. 1, *Paramuricea biscaya* B2, *Swiftia pallida*, *Iridogorgia splendens*, Keratoisidinae I1, Keratoisidinae I2, and *Narellla pauciflora* were collected from the GC852 site (Appendix A-2).
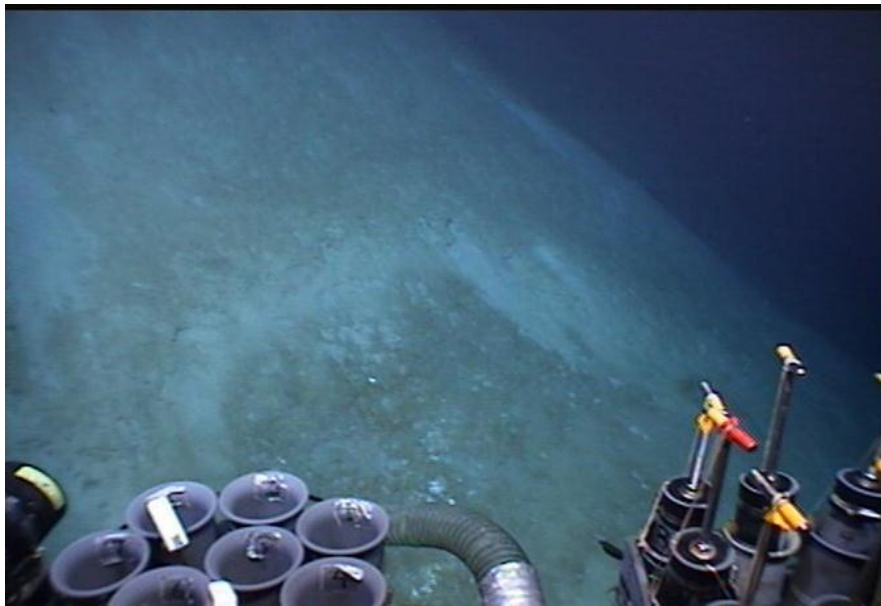


Figure 2-56. Steep slope on the flank of the northern end of the GC852 site.
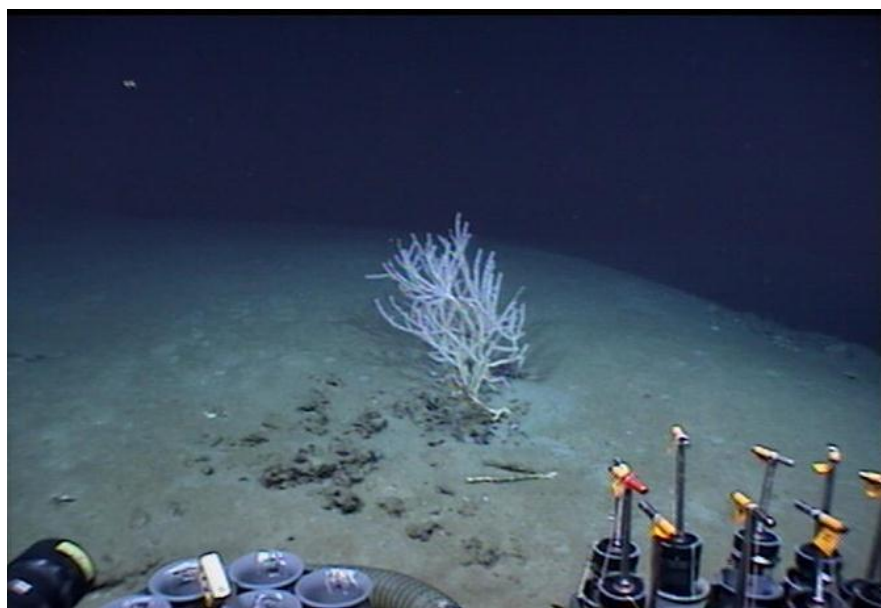


Figure 2-57. Isolated octocoral colonies at northern end of GC852.

### 2.3.1.23 DC583 (2,200 – 2,500 m depth)

The GC852 site was identified on BOEM 3D-seismic data using bathymetric contours with seafloor amplitude underlay. The only dive to this area was during the 2009 *Ron Brown* Cruise. The area of investigated is located at the northwestern end of the Florida Escarpment. Targets near the base of the Escarpment in ~2,500 m of water were investigated followed by a transit up the steep slope, and survey along the break in slope of the Escarpment at a depth of ~2,200 m. The first target at this site was an oval shaped mound at 28°23.11'N, 87°23.28'W bounded on the northwest and southeast by faults, as indicated on seismic cross sections. There was moderately positive amplitude response on the top and upper flanks of the mound. The mound was covered with very light colored sediment on the top (a thin veneer on top of rock?), with two 6-8 m diameter pockmarks with accumulations of pteropod shells at the summit and extensive outcrops of highly indurated rocks on the flanks.

The outcrops were generally massive, non-bedded, and made up of dense, dark brown to black rock – no sedimentary bedding was observed. The surface of several of the outcrops had pillow structures reminiscent of basaltic lava and many had large fissures 10's of m long, 1 meter wide, and 5-10 m deep. There were a few outcrops that appeared to be 2-3 flows stacked on top of each other and extending 10's m. The relief on the fault faces was up to 25 m high and near vertical (in places there were overhangs). These outcrops were colonized by at least two genera of bamboo corals (one branched and one unbranched), one antipatharian and one bubble gum coral (*Paragorgia* sp). These were moderately abundant on the E and N sides of the mound. On the W and S sides of the mound, there were sparse octocoral colonies at the top and scattered tube worm (*Escarpia laminata* and *Lamellibrachia* sp.) aggregations closer to the base (Figure 2-58). *Keratoisis* sp. bamboo corals were common and relatively large, up to 1 m. *Lepidisis* sp. and *Isidella* sp. were present but rare.



Figure 2-58. Tubeworms near the base of the outcrop.

64

The single observation of *Isidella* marks a depth record for this genus in the Gulf, the previously record depth was 1100 m. *Sibogagorgia* sp. was observed repeatedly, another depth record for the genus. On the SW corner of the mound was a very high density seep community with tube worms in the cracks in the rocks and a large bed of mussels (*Bathymodiolus brooksi* and *B. heckerae*) on the cliff face and accumulating at the base of a small platform (Figure 2-59). Associated with the tube worms and mussels were the common species *Munidopsis* sp., *Alvinocaris muricola*, *Ophioctenella acies*, as well as a few additional species awaiting more complete taxonomic identifications.



Figure 2-59. High density seep community.

The area between the mound and the escarpment was covered with plain sediments with occasional holothurians and a few rattail fish. At the base of the escarpment (Figure 2-60) were accumulations of sediments with carbonate crusts and white staining, possibly from outwatering of the escarpment. Above the foot of the wall were near-vertical outcrops and occasional platforms. Though one outcrop did not appear to be sedimentary (lacked any bedding), it did appear to have fossils on the exposed side. Also, there were 2 – 3 cm wide, 20 cm long "tubes" that, in vertical cross-section formed fans and on the rock surface, the tops were rounded and packed together.

This lower portion of the scarp harbored small aggregations of tube worms in vertical cracks and pockets in the rock. Corals were not observed or abundant until the top of the scarp, where paramuricids became remarkably dominant and abundant, each hosting a single *Asteroschema* ophiuroid (Figure 2-61). Bamboo corals, including *Keratoisis* and *Leipidisis* were present, mostly on the east facing outcrops and walls.
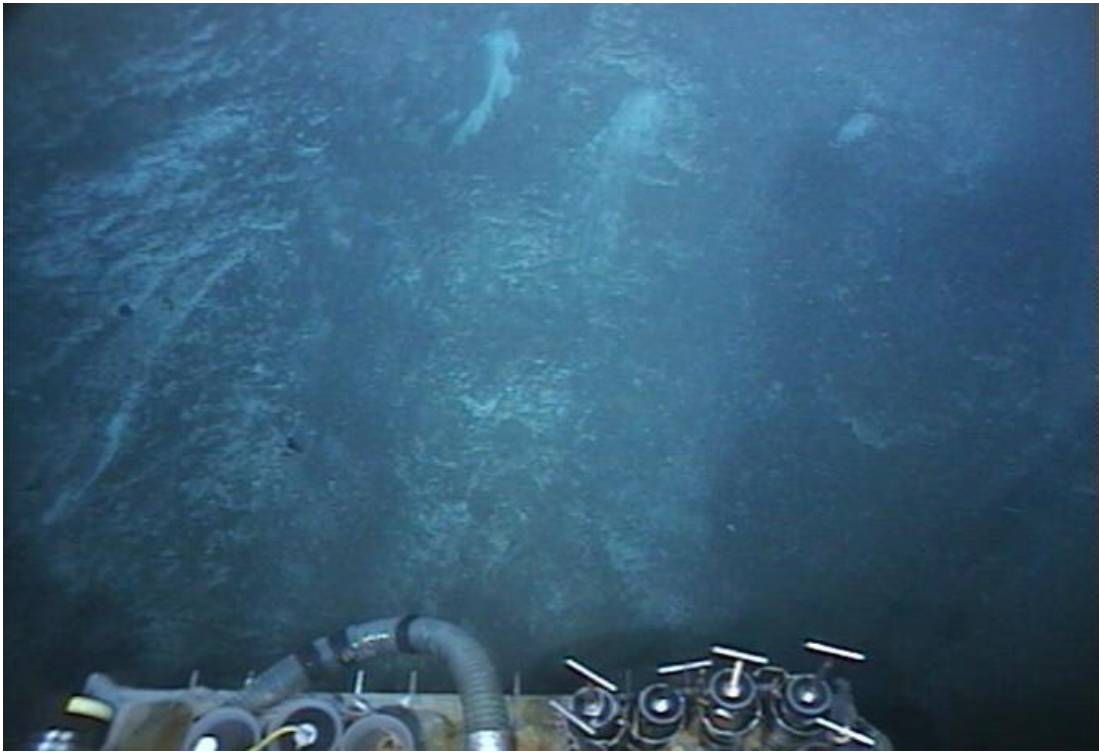
Figure 2-60. The base of the escarpment.
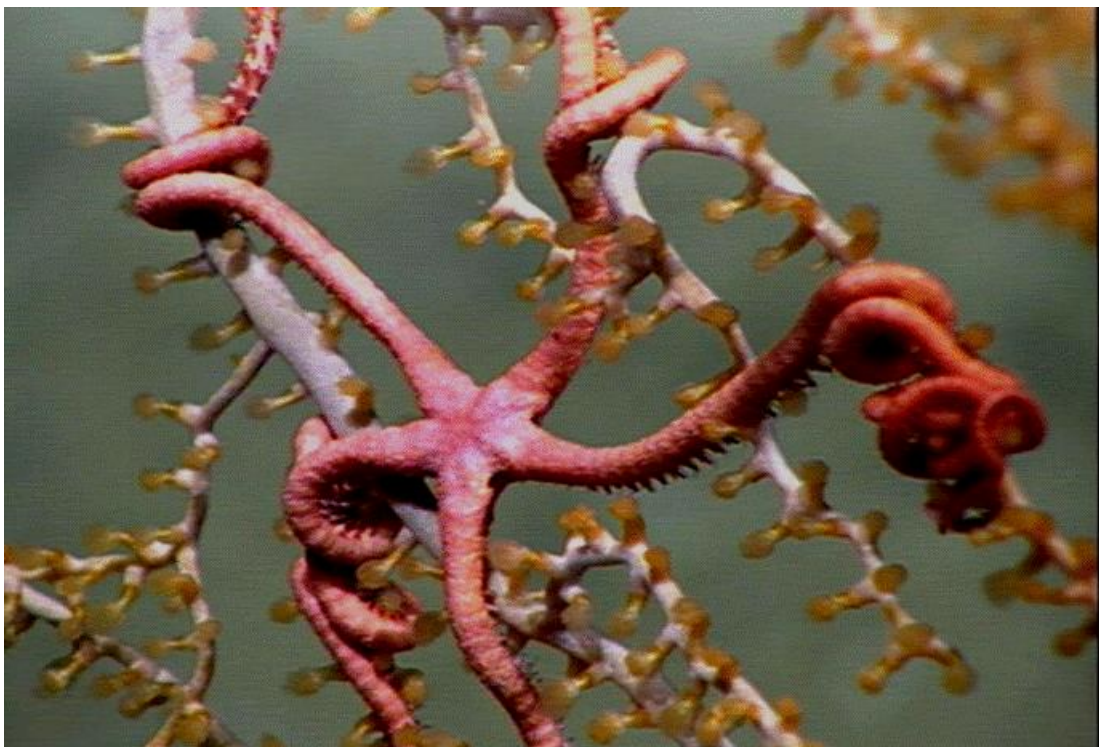


Figure 2-61. Paramuricid hosting a single *Asteroschema* ophiuroid.

At the top of the escarpment a smooth, terraced, "limestone-like" seafloor dominated for at least 75-100 m distance where only holothurians and shrimp were observed. The greatest abundance of *Paramuricea* sp octocorals were at the rim of this "limestone" cap. About 5 m below these octocorals was a ~5 m-tall wall with the densest concentration of bamboo corals, including *Keratoisis* and *Leipidisis,* observed during this project (Figure 2-62). This wall also included a narellid primnoid which may be a new species. Further south along the ridge the carbonate outcrops were largely devoid of colonial cnidarians, although occasional colonies of the octocoral *Iridogorgia*. sp. were encountered along with a large *Bathypathes*- like black coral.

*Asteroschema* sp. brittlestars, shrimp, and isopods were observed on *Paramuricea* sp. and *Chrysogorgia* sp. corals. Overall, 7 octocoral species were observed. Only two fish were observed during the transit to the top and then down the southeast side of the escarpment- a synaphobranchid eel and a *Coryphaenoides* rat tail. The corals *Clavularia rudis*, *Sibogagorgia cauliflora*, *Paramuricea biscaya* B1, *Paramuricea biscaya* B2, *Chrysogorgia averta*, *Iridogorgia magnispiralis*, *Iridogorgia magnispiralis*, Keratoisidihnae I2, Keratoisidinae N1a, Keratoisidinae nr J2a, and Lepidisis sp. D1c were collected from the DC583 site (ch).



Figure 2-62. Bamboo coral colonies.

### 2.3.1.24      DC673 (2,250 to 2,600 m depth)

The DC673 site was identified on BOEM 3D-seismic data using bathymetric contours with seafloor amplitude underlay. Like DC583, the site is located near the northwestern end of the

Florida Escarpment at 28.31°N, 87.144°W where the water depth at the base is about 2,600 m. this site was dived upon one time, during the 2010 *Ron Brown* cruise.

At the base of the Escarpment massive carbonates were often colonized by corals (*Bathypathes*) with seepage around their base hosting chemosynthetic tube worms and mussels. About 100 m up the escarpment there is an impressive feature of live mussels surrounded by a thicket of living tube worms in a crack in the wall (Figure 2-63). Tubeworms at this site were covered with what appeared to be zoanthids. A diversity of corals are present on the wall of the escarpement and up to the top of the escarpment along a ridge including bamboo corals, *Paramuricea* sp. with ophiuroids, *Chrysogorgia* with associated shrimp, *Acanthogorgia, Sibogagorgia* and *Corallium* and at least two black coral species (perhaps *Bathypathes* and *Stauropathes*). Three species of bamboo corals were especially abundant along the wall at ca. 2380-2400 m depth, including a *Lepidisis* whip coral and 2 possible *Keratoisis* spp. The octocoral community here is in general similar to that observed at DC583 in 2009.
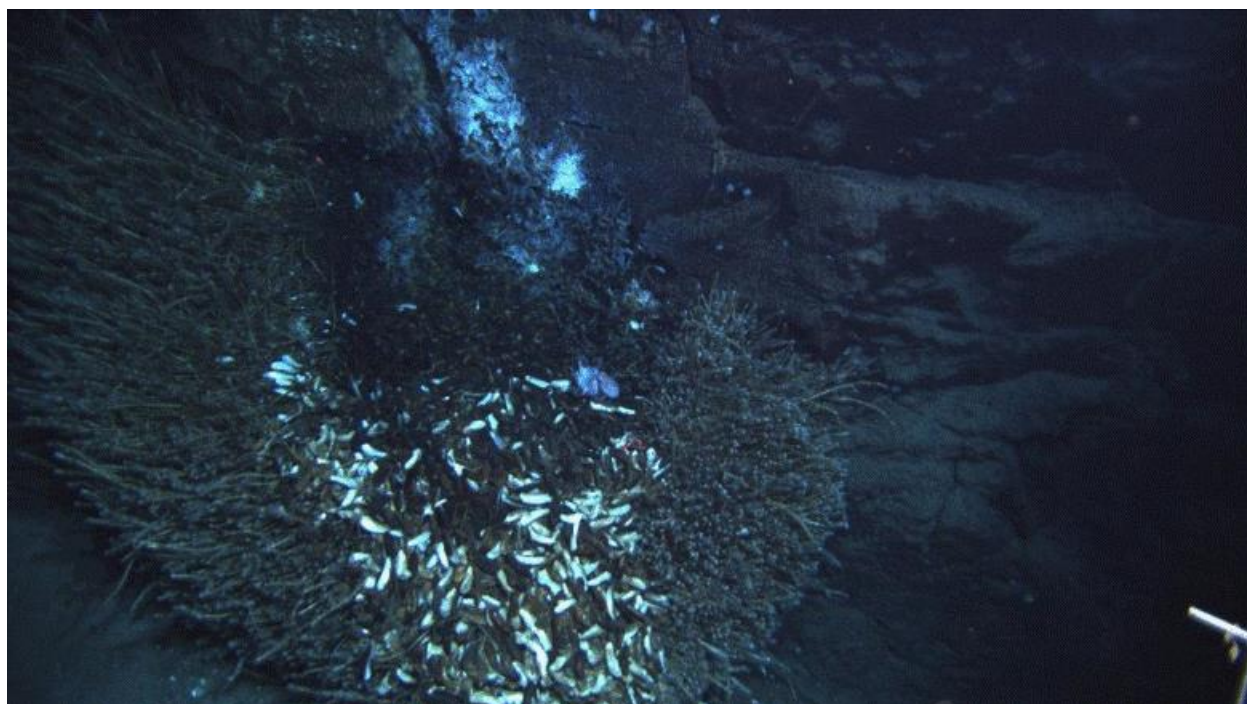


Figure 2-63. An octopus takes refuge in a dense tube worm bush and mussel bed (DC673).

On the top of the escarpment the substrate was mostly sediment with occasional low relief outcrop/boulder with white sediment accumulation around the base. We reached a second ridge at ca. 0330 local time. Another ridge at ~2250 m depth hosted similar coral species in addition to two species of *Iridogorgia* and an additional paragorgid not encountered previously (Figure 2-64). We left the bottom at 0640 local time anticipating an on time recovery on the surface. The corals *Clavularia rudis* 1c, *Anthomastus* sp., *Corallium niobe*, *Sibogagorgia cauliflora*, *Paramuricea biscaya* B1, *Paramuricea biscaya* B2, *Chrysogorgia averta*, *Iridogorgia magnispiralis*, *Iridogorgia splendens*, Keratoisidinae I2, Keratoisidinae N1a, Keratoisidinae nr J2a, and *Lepidisis* sp. D1c were collected from the DC673 site (Appendix A-2).

Figure 2-64. A single *Iridogorgia* sp. is seen settled on a rocky outcrop surrounded by a few small colonies of *Paramuricea biscaya* (DC673).

## 2.3.2  Other Coral Sites Discovered Since the DWH Incident (Sorted by Depth)

The last ROV cruise to natural coral sites of this project occurred in late 2010, about 4 months after the DWH leak was capped.  By the time of that cruise we had examined 3D seismic surveys with BOEM scientists and had chosen several potential hard-ground sites with good potential to host coral communities in the vicinity of the Macondo Well.  On the last dive of the 2010 *Ron Brown* cruise we dove on one of these sites in an unexplored portion of lease blocks MC338 and MC294 and discovered the coral community in lease block MC294 described above.  During a NSF funded cruise in December of 2010 we visited another coral community in MC388 that had been discovered using a drift camera during a cruise designed by C. Fisher, H. Roberts, and W. Shedd (using criteria developed from this project), funded by the NRDA effort and led by W. Shedd of BOEM.  Subsequent to that, an exploration cruise using the AUV *Sentry* and a towed camera system discovered several other coral sites that were subsequently dived on using an ROV. The sites selected for exploration for this effort were also chosen by H. Roberts, W. Shedd, and C. Fisher, and the high success rate of the cruise was a direct reflection of lessons learned during this project and innovative use of the AUV *Sentry* for site exploration. The majority of corals at each of these sites has been individually documented and imaged for ongoing monitoring efforts.    In addition to these sites, another site discovered as part of the NRDA effort in AT 357 was explored by the PIs of this proposal and a subset of the many corals at this site identified and imaged for monitoring.  Below is a short description of each of those sites.

69

### 2.3.2.1 MC159/203 (950 m depth)

The MC159/203 site was discovered first by the AUV *Sentry* and then characterized using an ROV in October of 2011. The site is about 17 nm W-NW of Macondo at 28.8°N, 88.64°W in 950 m water depth. This is another site with heavy colonization of mostly large (old) coral colonies in a small area. A total of twenty coral colonies were found at this site: Two *Acanthogorgia aspera*, Seven *Swiftia* cf. *koreni* (Figure 2-65), and eleven *Paramuricea* sp. B3. Several of the corals at this site were also tangled in longline, and limited damage to the colonies from the longline was noted. Also notable at this site were the relatively high numbers of shark egg cases attached to the corals. The corals *Acanthogorgia aspera*, *Paramuricea* sp. B3, and *Swiftia* cf. *koreni* were collected from the MC159/203 site (Appendix A-2).



Figure 2-65. *Swiftia* cf. *koreni* with longline at MC159/203

### 2.3.2.2 MC036 (1110 – 1120 m depth)

Three-D seismic maps of the MC036 site revealed extensive areas of potential hardground and numerous conduits for seepage over a large area along a SSW to NNE tending ridge. This site was explored by drift camera and although numerous signs of seepage and a few carbonates were observed, no corals were identified. A northern portion was further surveyed by the AUV *Sentry* and numerous carbonates were identified with a few corals associated with one group of boulders.

The first area of corals was surveyed during an ROV cruise in October 2011 and then additional potential targets identified from the *Sentry* survey that were explored by ROV in March 2012 discovered an additional two groups of corals within two hundred m of the first group on the same (SE) edge of the ridge.

The site is about 17 nm N-NE of Macondo at 28.935°N, 88.204°W in about 1,115 m water depth. A total of at least 26 colonies were identified at this site (the exact number cannot be distinguished from the video and photographic records of the dives but several images of "colonies" appear to include 3 or more colonies), in three areas spread over about 200 m of the ridge edge.  It is likely that further exploration would find additional corals at this site.    At least 20 colonies of *Paramuricea* sp (dominated by species B3, Figure 2-66) and 6 colonies of *Chrysogorgia* sp. (Figure 2-67) were imaged for evaluation and long term monitoring.    Two remains of what appeared to be dead *Paramuricea* were present and their condition (lack of small branches) suggests these had been dead for many years.
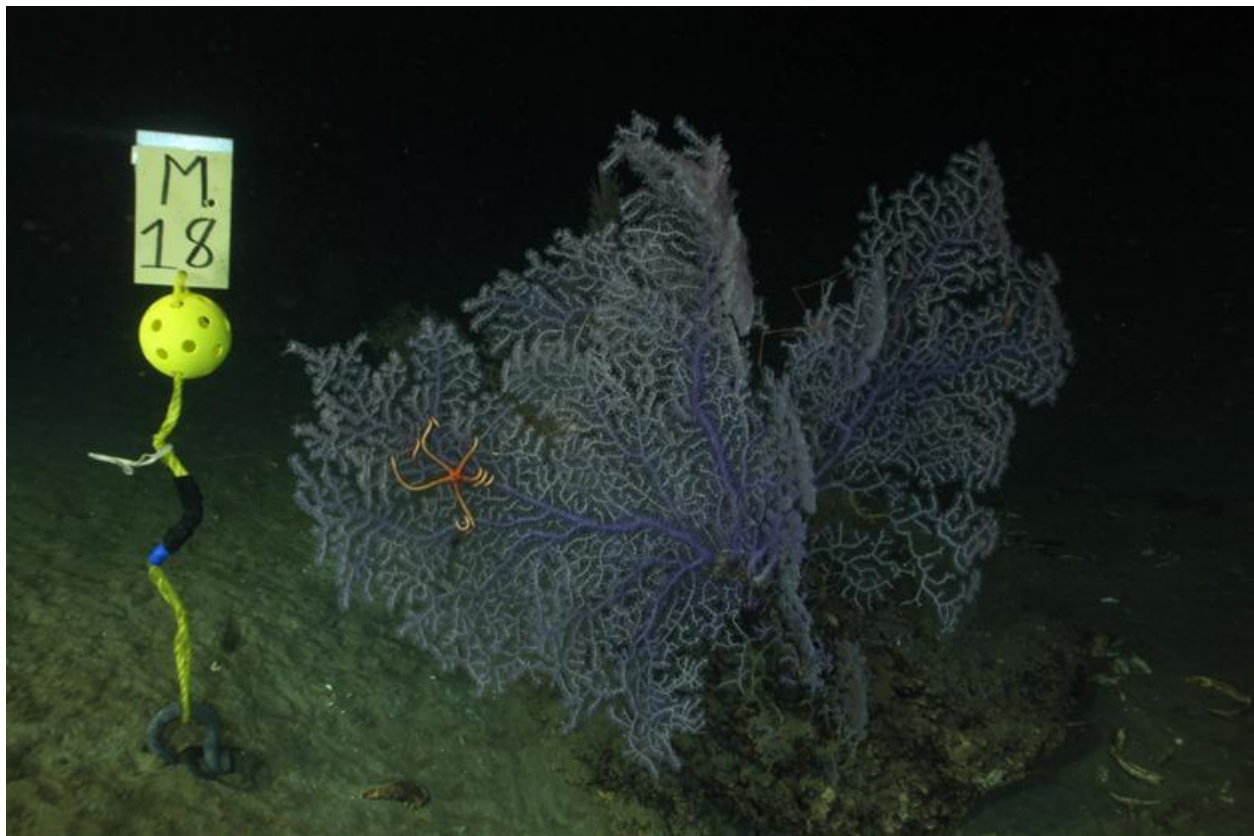


Figure 2-66. *Paramuricea* B3 with attached ophiuroid near marker M18 at MC036.

Figure 2-67. *Chrysogorgia* sp at MC036.

### 2.3.2.3 MC506 (1,040 m depth)

The MC506 site was discovered first by the AUV *Sentry* and then characterized using an ROV in October of 2011.  The site is about 35 nm SW of Macondo at 28.45861°N, 88.85091°W in 1,040 m water depth.  This is a relatively small site with all known coral colonies on 2 large carbonate boulders located in close proximity to each other.  A total of ten coral colonies were found at this site: 9 *Paramuricea* sp B3 and one *Chrysogorgia* sp.  All colonies were large and there was no sign of recent recruitment of colonial corals to this site.  One of the *Paramuricea* was partially tangled in what appears to be longline (Figure 2-68).  Two other colonies had large areas that appeared to have been dead for a long time, with small growing portions on the tip end of a few branches. The corals *Paramuricea* sp. B3 and *Chrysogorgia* sp. 1b were collected from the MC506 site (Appendix A-2).
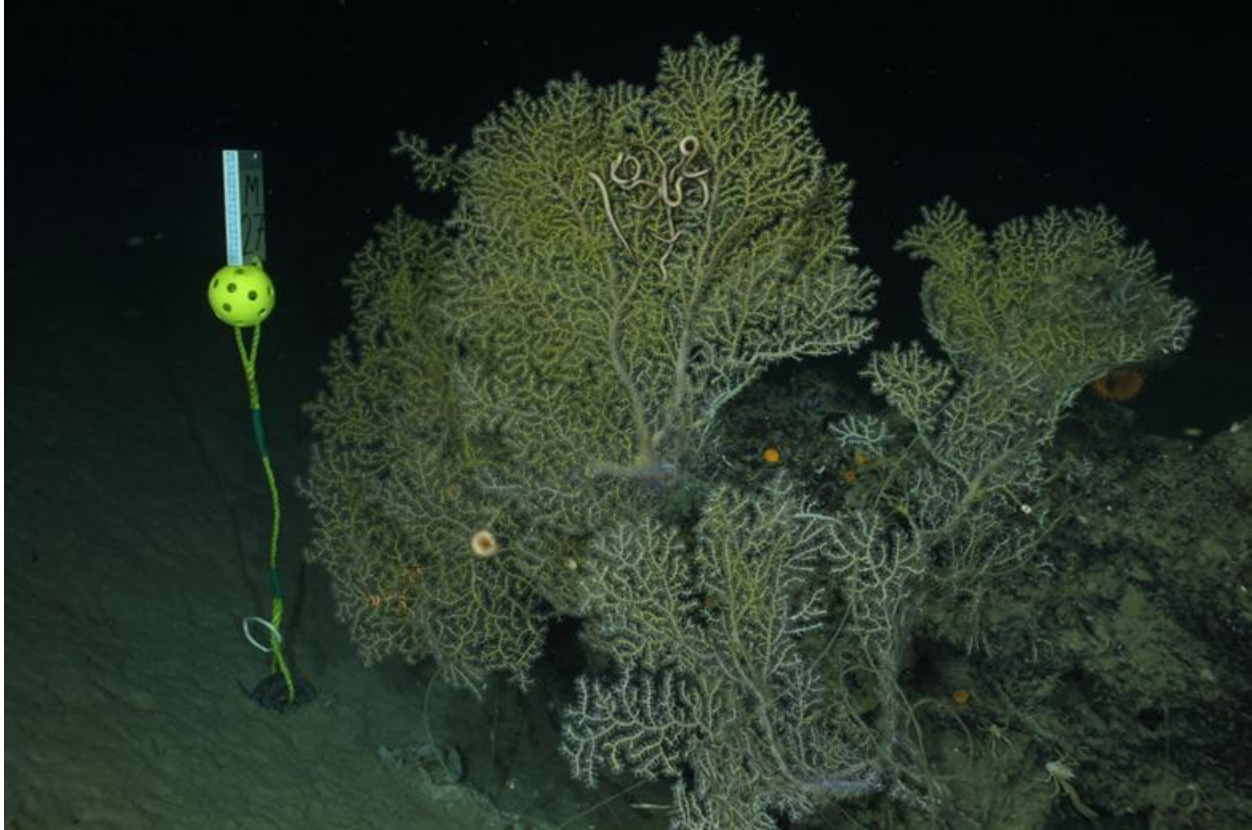
Figure 2-68. *Paramuricea* sp B3 from MC506.  Note long line in lower right and colony in forefront.

### 2.3.2.4  AT357 (1,050 m depth)

The AT357 site is an area of high reflectivity in the 3D seismic that was originally identified by BOEM (then MMS) scientists from a 1997 survey. It is an area of relatively low vertical relief, and therefore did not make the final cut of exploratory sites originally planned for the *Lophelia* II project. This site was originally discovered during a soft-sediment sampling cruise led by Dr. Jim Payne as part of the NRDA effort following the *Deepwater Horizon* incident, and has since been surveyed on three cruise led by PIs of this program.  It is centered near 27.59°N, 89.70°W in about 1,050 m water depth. It has recently been mapped in high resolution using AUVs as part of the GoMRI EcoGig program. This is one of the largest coral communities in the deep GoM, and is several times larger than any currently known in the >1,000 m depth range. The main part of the site is approximately 300 m wide (east-to-west) and 200 m north-to-south and contains numerous outcropping carbonate slabs, platforms, and crusts. There is a large *Madrepora oculata* reef structure in the northern, central part of the site, surrounded by octocoral communities, primarily *Paramuricea* type B3 also including a variety of other gorgonian and black coral species as well as small *Madrepora* (Figure 2-69) colonies. At least 62 coral colonies have been identified and imaged for long term monitoring at this site. It also hosts one of the most diverse arrays of coral-associated fauna seen at any site (e.g., ophiuroids, galatheid crabs, shrimp, and polychaetes). Along the northern edge of the site is a fairly extensive area of seepage with outcropping carbonates, a

mussel bed and occasional methane bubble streams. There are also additional, unexplored areas of potential coral abundance and/or active seepage in the area, which remain ripe for future investigations. The corals *Anthothela* sp. 3, *Paramuricea* sp. B3, and *Chrysogorgia* sp. 1a were collected from the AT357 site (Appendix A-2).



Figure 2-69. *Paramuricea* sp with attached ophiuroid brittle stars at AT 357.
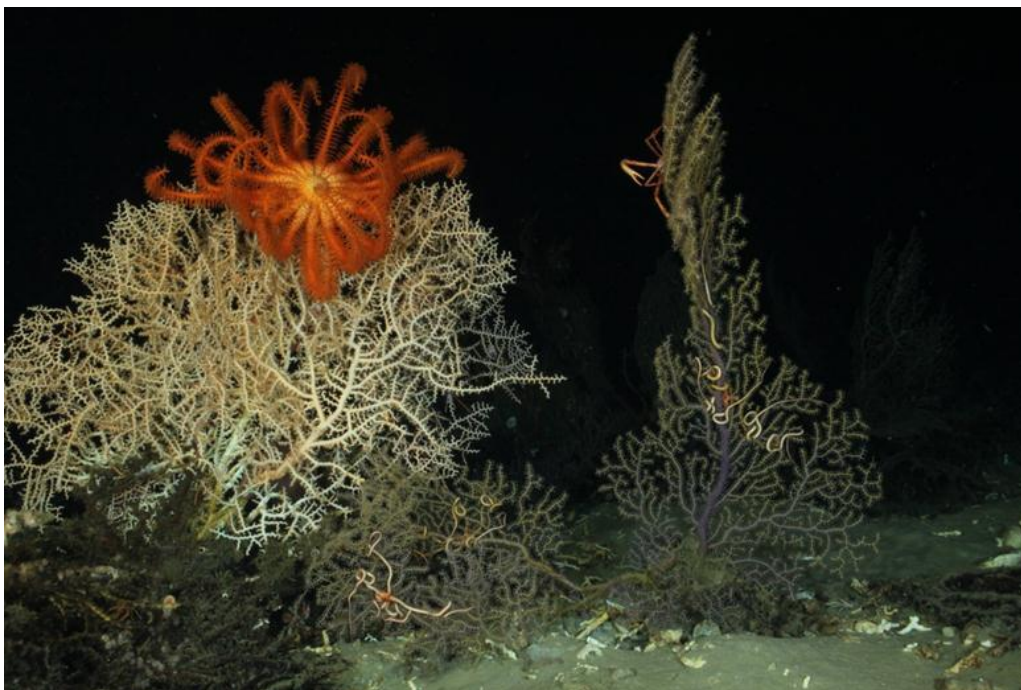


Figure 2-70.  The edge of the large *Madrepora* reef with a Paramuricea type B3 colony. Associates include an orange basket star, galatheid crabs, and ophiuroids.

### 2.3.2.5 MC297 (1,580 m depth)

The MC297 site has the most extensive coral development below 1,000 m within 20 nm around Macando. It is located at 28.68°N, 88.34°W at 1,580 m depth. This site was initially targeted for photo survey by the *Sentry* AUV based on side scan maps provided by BP. The site is composed of two areas separated by about 370 m, each with numerous colonies, and a few scattered boulders and occasional isolated corals in between the two areas with higher density coral development. The site was first visited by an ROV in October of 2011 and at that time hydroid development on many of the corals both areas was very similar to the level of hydroid development on corals at the MC338/294 site discovered during the *Ron Brown* 2010 cruise. It has been visited three times by ROV between October 2011 and October 2012. Most of the corals discovered at this site have been identified (using nearby physical markers) and imaged for continued monitoring. There are at least 80 *Paramuricea* sp (Figure 2-71), three *Bathypathes* sp., two bamboo corals (One Isididae and one Keratoisidinae I2), two other unidentified octocorals (Figure 2-72) and two areas with encrusting *Clavularis rudis*. In addition, two other octocorals overgrown with zoanthids and four apparent *Paramuricea* skeletons that still retained very small branches (and so likely died recently) were present in these two areas. The corals *Clavularia rudis*, *Paramuricea biscaya* B1, *Paramuricea biscaya* B1a, *Paramuricea biscaya* B2, and Keratoisidinae I2 were collect from the MC297 site (Appendix A-2).
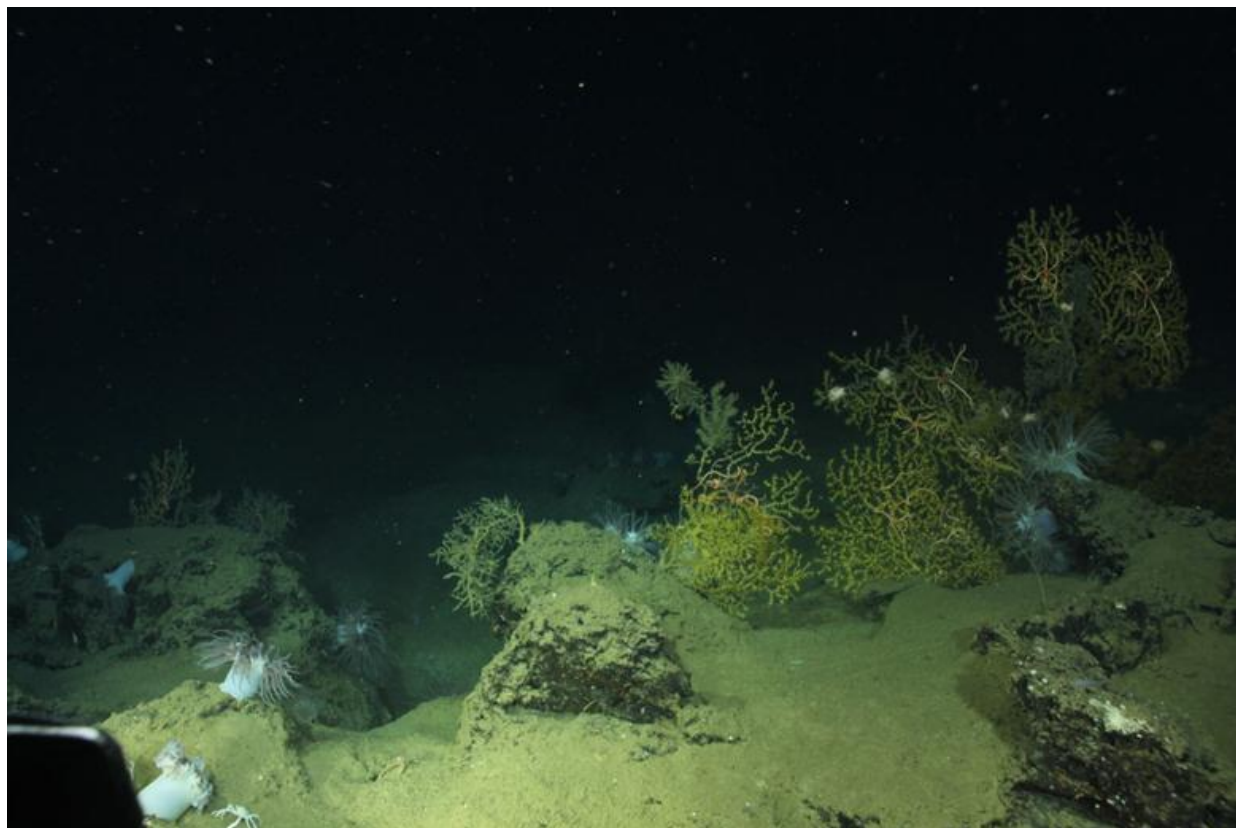


Figure 2-71. *Paramuricea biscaya* at MC297.

Figure 2-72. Unidentified octocoral at MC297.


### 2.3.2.6 MC388 (1,840 – 1,960 m depth)

The presence of coral at the MC388 site was discovered during a drift camera cruise in late 2010. The site was further explored by the AUV *Sentry* and the manned submersible Alvin in December, 2010 during an NSF funded project. Approximately 34 corals at this site were discovered and imaged for monitoring during a NRDA sponsored ROV cruise in October 2011. An additional five corals were discovered and imaged during a cruise with the NOAA OER ship *Okeanos Explorer* in March of 2012. Finally, an additional 27 corals were discovered and imaged during a cruise supported by the Gulf of Mexico Research Initiative (GoMRI) EcoGig project and the Schmidt Ocean Institute. As a result of all of these efforts, numerous carbonate outcrops colonized with coral colonies and tube worms spread over an area of several square km have been documented and imaged for monitoring. The site is about 14.4 nm SE of Macando at 28.63°N, 88.17°W and ranges in depth from about 1,840 to 1,960 m. In addition to whip corals (*Stichopathes* sp.) and encrusting *Clavularis rudis* octocorals, a total of at least 44 *Paramuricea biscaya*, 4 bamboo corals (in the family Keratoisididae), 6 black corals (*Bathypathes* sp.), and an unidentified octocoral are present at this site (Figure 2-73 and Figure 2-74). The corals *Clavularia rudis*, *Paramuricea biscaya* B1, *Paramuricea biscaya* B1a, *Paramuricea biscaya* B2, and Keratoisidinae I2 were collected from the MC388 site (Appendix A-2).
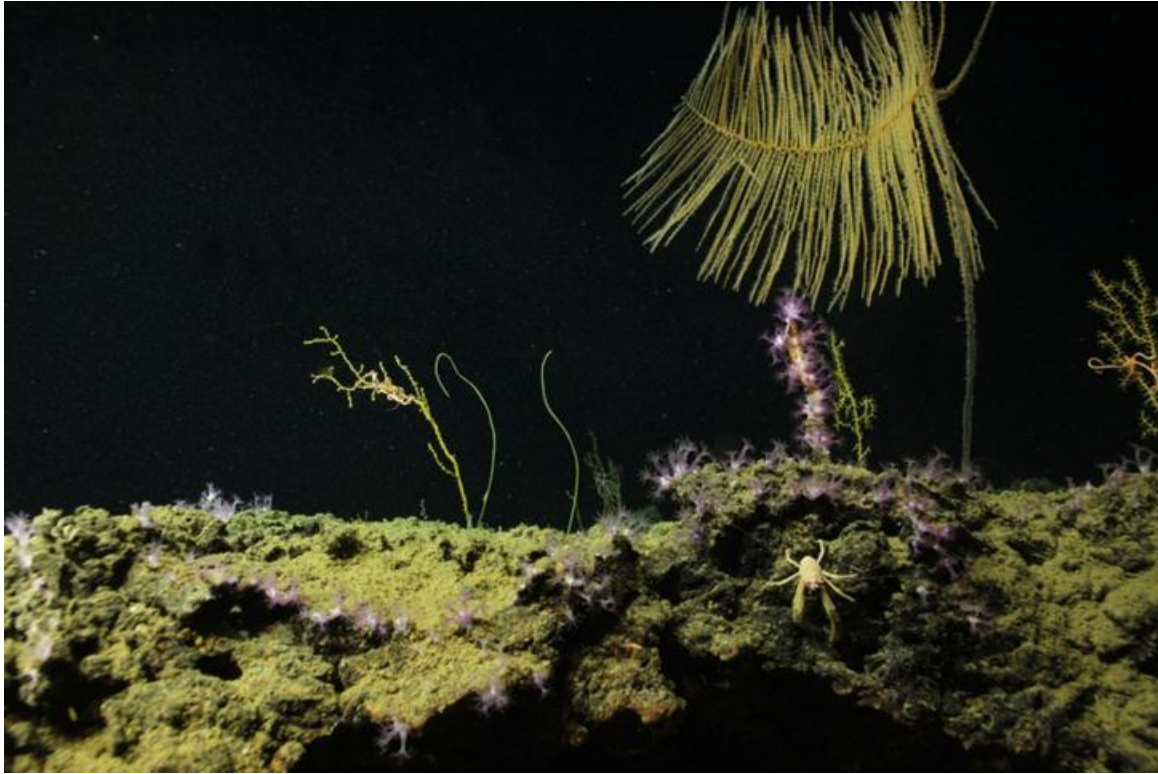
Figure 2-73. Whip coral (*Stichopathes* sp.), *Paramuricea biscaya*, black coral (*Bathypathes* sp.), and encrusting *Clavularis rudis* octocoral in MC388.



Figure 2-74. Unidentified white octocoral in front of *Paramuricea biscaya* at MC388.

# 3  OCEANOGRAPHIC AND GEOLOGIC SETTING

This chapter addresses the carbonate chemistry at multiple sites in the Gulf, the implications of currents at two sites on coral larval dispersal, tests of particulate and sediment dispersal at two sites to estimate biogeochemical fluxes, and testing of biweekly sediment trap samples for the presence of coral larva.

## 3.1  THE CARBONATE SYSTEM AND pH

Portions of this chapter have been published in *Limnology & Oceanography* and should be cited as: Lunden, J.J., S.E. Georgian, and E.E. Cordes. (2013). Aragonite saturation states at cold-water coral reefs structured by *Lophelia pertusa* in the northern Gulf of Mexico. *Limnol. Oceanogr.* 58:354-362.

### 3.1.1  Introduction to Carbonate Testing Performed

In this chapter, we describe the carbonate system from the water column and deep waters of the GoM in an effort to augment the existing global data set of oceanographic carbonate chemistry, particularly in marginal seas such as the GoM. Additionally, we sought to better understand the distribution of the aragonite saturation state ($\Omega_{arag}$) in the context of cold-water coral presence in the GoM. Related to this objective, we tested two hypotheses regarding $\Omega_{arag}$ and *L. pertusa* distribution — that areas of *L. pertusa* presence have higher $\Omega_{arag}$ values than areas lacking *L. pertusa*, and that *L. pertusa* skeletal density positively correlates with $\Omega_{arag}$. With the establishment of baseline values of $\Omega_{arag}$ in deep waters, especially near sensitive biological communities such as cold-water coral reefs, we will be able to detect future changes in carbonate chemistry resulting from ongoing acidification.

### 3.1.2  Methods of Carbonate Sampling and Analysis

#### 3.1.2.1  Sample Collection

All water samples (n = 143) were collected during the *Lophelia* II 2010 expedition using a CTD rosette (water column) and the ROV *Jason II* (bottom water) onboard the NOAA Ship *Ronald H. Brown* (15 October – 5 November 5 2010). Fourteen deep-water stations (depth > 300 m) in the GoM were sampled (Figure 3-1). *Lophelia pertusa* was present at eight of these sites: GC354, GB535, MC751, MC796, VK826, VK862, and VK906). Water column samples ($n$ = 79) were collected using a CTD rosette (SBE-32 submersible array firing assembly, 2.5 L bottle$^{-1}$).  Bottom water samples (n = 64) were collected using a custom-made hydraulically-powered 7-Niskin bottle (1.7 L bottle$^{-1}$) array fitted to the ROV. Upon recovery of the ROV and CTD rosette, water samples were collected from the Niskin bottles and stored in 500 mL polyethylene containers in a cool, dark location until analysis (<2 hours after reaching the surface).

Figure 3-1.  Seven Niskin bottle array fitted to ROV *Jason* during the 2010 *Lophelia* II cruise.

### 3.1.2.2  Analytical Methods

pH (total hydrogen scale) of each sample was measured in duplicate at ~22°C using an Orion 5 Star pH meter with Ross electrode calibrated with Tris-HCl buffer (Dickson Lab, Batch 4, Scripps Institution of Oceanography). Precision for pH analyses was 0.002 units (standard deviation (s.d.)). pH values were corrected for pressure and temperature effects using CO2SYS (Oak Ridge Laboratory, Oak Ridge, TN, Pierrot et al. 2006).  Total alkalinity of each sample was measured in duplicate at 22°C according to SOP3b (Dickson et al. 2007) using a Mettler-Toledo DL15 autotitrator with 0.1 N HCl in 0.6 M NaCl solution and calibrated against certified reference materials (Dickson Lab, Batch 105, Scripps Institution of Oceanography). Precision for total alkalinity analyses was 4.6 $\mu$mol kg$^{-1}$ (s.d.). Temperature (°C), salinity in practical salinity units (PSU), and pressure in decibars (dbar) were obtained in situ using a SBE19 CTD (for bottom water samples on ROV *Jason*) and a SBE 9/11+ CTD (for water column samples).  Total alkalinity was normalized to salinity of 35 parts per thousand (ppt) according to Millero et al. (1998). The aragonite saturation state ($\Omega_{arag}$ and the calcite saturation state ($\Omega_{cal}$), dissolved inorganic carbon (DIC), and carbonate ion ($[CO_3^{2-}]$) concentrations were calculated at *in situ* pressure using CO2SYS. The dissociation constants for carbonic acid ($K_1$ and $K_2$) are from Dickson and Millero (1987) and the aragonite solubility product constant ($K_{sp}$) is from Mucci (1983).

### 3.1.2.3 Statistical Analyses

All statistical analyses were conducted using JMP 8 (SAS). Normality was tested using the Shapiro-Wilk W test, with $p > 0.05$ indicating normally distributed data. When assumptions of normality were not met, non-parametric statistics (Mann-Whitney U test and Kruskal-Wallis analysis of variance (ANOVA)) were employed.

## 3.1.3 Results and Discussion of Carbonate Study

### 3.1.3.1 Total Alkalinity and pH in Surface Waters

Total alkalinity (TA) in surface waters ranged from 2349-2411 $\mu$mol kg$^{-1}$ (mean: 2388). Surface pH$_T$ ranged from 8.08-8.16 (mean 8.11). Total alkalinity measurements from the surface layer agree well with prior work in the GoM. Our TA measurements fall within the range reported by Keul et al. (2010, 2333.0-2411.9 $\mu$mol kg$^{-1}$) in the same region, but do not fit the TA-salinity relationship established by Lee et al. (2006). However, this relationship was nearly significant ($r^2 = 0.225$, $p = 0.0632$) and it is likely that the limited number of surface samples in our study ($n = 16$) impedes this relationship. Salinity-normalized TA in our study (mean: 2375 $\mu$mol kg$^{-1}$) was higher than average salinity-normalized TA (nTA) in sub-tropical Atlantic seawater (2291 $\mu$mol kg$^{-1}$, Millero et al. 1998). However, neither alkalinity relationships calculated from Lee et al. (2006) nor Millero et al. (1998) included data from the GoM.

An additional source of the TA-salinity disparity could be the role of the Mississippi-Atchafalaya system. Riverine input from this system exports high amounts of bicarbonate as a result of rock weathering along the river's track (Suchet et al. 2003). This flux facilitates a delivery of high TA-low salinity water to the northern GoM, potentially distorting the TA-salinity relationship generally observed in oceanic waters. Recently, Guo et al. (2012) described the carbonate chemistry dynamics of the Mississippi River plume in the GoM. They observed elevations in TA due to input from the Mississippi River of up to 400 $\mu$mol kg$^{-1}$ compared to ambient surface seawater (TA $= 2330 - 2700$ $\mu$mol kg$^{-1}$ at S = 0). While our study area was outside of the Mississippi-Atchafalaya river system, the GoM's carbon cycle is strongly influenced by inputs from this plume (Guo et al. 2012).

Recently published results from a 2007 survey of the GoM carbonate system agree well with the surface values from our dataset (Wang et al. 2013). The buffering capacity of seawater may be inferred by the ratio of TA to DIC (TA:DIC). At high TA:DIC, the effects of $CO_2$ influx may be offset by the buffering actions of alkaline species such as bicarbonate and carbonate. The TA:DIC ratio of the surface waters in the GoM is relatively high compared to other coastal systems, including the Gulf of Maine (Wang et al. 2013). According to the Global Ocean Data Analysis Project (GLODAP), open-ocean surface pH typically ranges from 7.95-8.35 (mean: 8.11, Sabine et al. 2005). However, this wide-scale analysis did not include samples from the GoM. Mean surface pH in our study is identical to the global average (8.11) and very close to the North Atlantic Ocean average (8.12) and is consistent with a 0.1 unit decline in pH from pre-Industrial estimates of surface ocean pH (Raven et al. 2005). While this value is expected to further decline over the next century as anthropogenic ocean acidification continues, disparate effects may be observed across different water bodies with different TA:DIC parameters. Establishment of the baseline

carbonate chemistry parameters in the GoM from this study, as well as those of Wang et al. (2013), will permit observation of future changes in pH and associated carbonate variables.

### 3.1.3.2  Total alkalinity and pH in the Deep GoM

In deep waters (> 300 m depth), TA ranged from 2264-2382 $\mu$mol kg$^{-1}$ (mean: 2316) (Figure 3-2, Figure 3-5). TA was significantly different among sites (Kruskal-Wallis test, H = 32.3, p < 0.001). Salinity-normalized TA (nTA) also significantly differed among sites (Table 3-1, Kruskal-Wallis test, H = 36.4, p < 0.001). nTA was lowest at 100-200 m depth and began to increase at 200 m depth (Figure 3-1). At depth, pH ranged from 7.84-8.03 (Figure 3-2) and varied significantly among sites (Table 3-1, one-way ANOVA, $F_{10,49}$ = 4.65, p < 0.001). Highest mean pH was observed at the two deepest sites, DC673 (2500 m) and GC852 (1400 m).  Dissolved inorganic carbon (DIC) at depth ranged from 2135-2231 $\mu$mol kg$^{-1}$ (mean: 2185) and [$CO_3^{2-}$] ranged from 92-123 $\mu$mol kg$^{-1}$ (Figure 3-4).

In addition to the processes described above, the increase in anthropogenic $CO_2$ is likely to contribute to pH declines throughout the water column. Elevated $CO_2$ in the atmosphere leads to direct changes in surface water chemistry, and these changes may be translated to depth relatively quickly if the rate of vertical exchange via vertical mixing and eddy diffusion approaches the rate of lateral exchange by deep-water currents. The Loop Current of the GoM frequently sheds large cyclonic eddies that are propagated westward (Sturges et al. 2010). These eddies, coupled with wind-induced shallow-water currents, combine to produce downwelling along the northern GoM shelf break increasing the rate of vertical exchange (Chang and Oey 2010). There is a relatively low level of lateral exchange of deep water among the GoM, the Caribbean, and the Atlantic Ocean resulting from the relatively shallow sill depths of the two openings to the GoM: the Yucatan Strait at approximately 2000 m and the Florida Strait at approximately 700 m. In a relatively closed oceanographic system subjected to strong anthropogenic forcing such as the GoM, these processes could potentially contribute to our observed decreases in pH and aragonite saturation state with depth.

Several factors are known to influence the inorganic carbon system in deep waters.  One of the primary controls on total alkalinity is the precipitation and dissolution of $CaCO_3$. In the surface ocean, precipitation of $CaCO_3$ by planktonic calcifiers removes bicarbonate, a predominant substrate for calcification (Hofmann et al. 2010). As these organisms die, the shells and tests descend to the seafloor, resulting in a net accumulation of alkaline species with increasing depth (Milliman et al. 1999). This process may increase normalized total alkalinity, which was observed initially at 200 m in the GoM (Figure 3-2); however, other processes such as nitrification, denitrification, and the decomposition of organic matter cannot be excluded (Stumm and Morgan 1981).  The decomposition of organic matter throughout the water column also influences carbonate chemistry dynamics at depth through the release of $CO_2$ resulting in a decline in pH with depth.  In the GoM, lowest pH values were observed within the depth range of the oxygen minimum zone (300-800 m, Guo et al. 1995), reflecting the interaction between organic matter decomposition and pH (Figure 3-3, Figure 3-5).

Progressive ocean acidification will alter the carbonate parameters of the water column of the global ocean. Recently published data show that pH decreased by 0.026-0.043 units from 1991-

2010 in intermediate waters (500-1,100 m) of the Rockall Trough (McGrath et al. 2012). This change was induced by an estimated influx of anthropogenic $CO_2$ of roughly 15 $\mu$mol kg$^{-1}$ over two decades. Like the GoM, the Rockall Trough provides habitat for several species of cold-water corals, including the scleractinians *L. pertusa* and *Madrepora oculata* (White and Dorschel 2010). If similar changes in pH occur in the GoM, $\Omega_{arag}$ would be expected to decrease as much as 0.1 in deep waters. Sustained ocean acidification at this rate could potentially result in undersaturation of aragonite in the deep GoM by the end of this century.
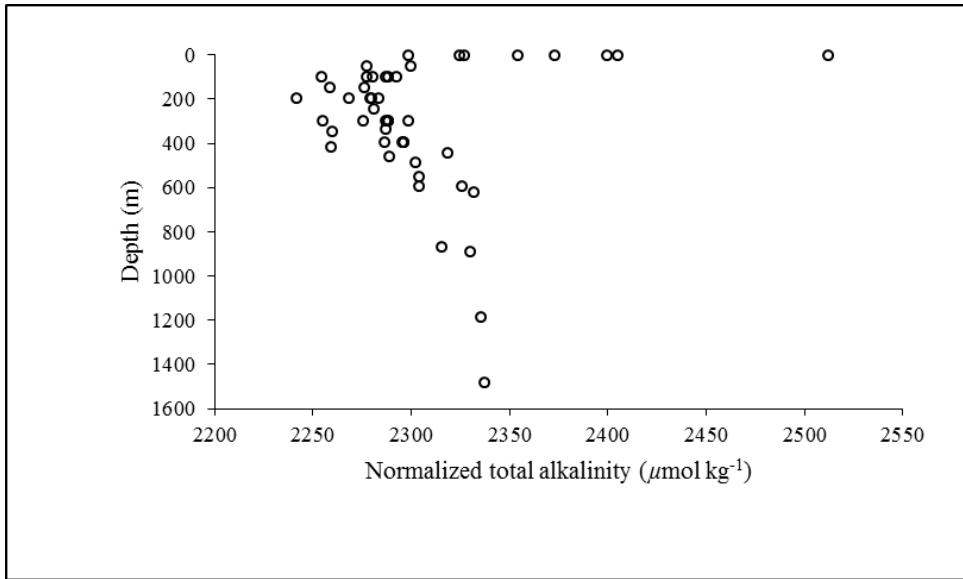


Figure 3-2. Water column profile of normalized total alkalinity (nTA) (µmol kg-1) from 0 to 1600 m.
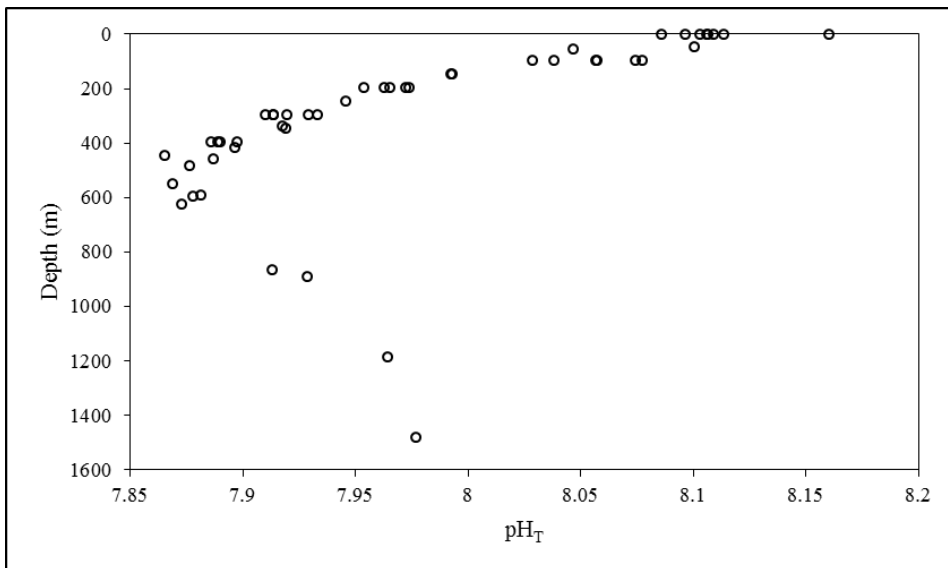


Figure 3-3. Water column profile of pH (total hydrogen scale) from 0 to 1600 m.

Table 3-1.

Carbonate Chemistry Parameters of Deep-water Sites in the Northern GoM

| Site ID | Lease block | Depth (m) | Latitude (°N) | Longitude (°W) | nTA ($\mu$mol kg$^{-1}$) | pH$_T$ | [CO$_3^{2-}$] ($\mu$mol kg$^{-1}$) | $\Omega_{arag}$ |
|---|---|---|---|---|---|---|---|---|
| 1 | DC673 | 2387-2597 | 28.31 | 87.31 | 2312.25-2324.55 | 7.94-7.98 | 105.60-108.79 | 0.98-1.13 |
| 2* | VK826 | 455-526 | 29.15 | 88.01 | 2288.69-2334.74 | 7.89-8.03 | 95.64-123.31 | 1.33-1.69 |
| 3* | VK906 | 390-441 | 29.07 | 88.38 | 2253.82-2332.04 | 7.85-7.95 | 92.49-113.85 | 1.31-1.61 |
| 4* | VK862 | 307 | 29.11 | 88.38 | 2304.13 | 7.92 | 115.5 | 1.66 |
| 5* | MC885 | 620 | 28.06 | 89.72 | 2321.37-2343.03 | 7.87-7.93 | 87.97-98.35 | 1.19-1.33 |
| 6* | MC796 | 530 | 28.14 | 89.76 | 2315.29 | 7.91 | 100.6 | 1.38 |
| 7* | MC751 | 437 | 28.19 | 89.79 | 2304.5 | 7.93 | 105.5 | 1.48 |
| 8 | GC249 | 787-832 | 27.74 | 90.52 | 2326.07-2331.12 | 7.92-7.95 | 96.22-102.33 | 1.26-1.33 |
| 9 | GC246 | 868 | 27.71 | 90.65 | 2315.71-2322.83 | 7.91-7.94 | 93.2-99.7 | 1.20-1.29 |
| 10 | GC852 | 1485 | 27.11 | 91.17 | 2333.86-2341.5 | 7.97 | 105.6-106.4 | 1.20-1.21 |
| 11 | GC140 | 283-320 | 27.81 | 91.54 | 2303-2312.49 | 7.89-7.92 | 107.86-115.61 | 1.55-1.67 |
| 12* | GC354 | 551 | 27.59 | 91.82 | 2297.6-2310.93 | 7.86-7.88 | 89.35-93.17 | 1.22-1.28 |
| 13 | GB299 | 338 | 27.69 | 92.23 | 2285.48-2297.69 | 7.91-7.92 | 108.15-113.26 | 1.54-1.62 |
| 14* | GB535 | 510-534 | 27.43 | 93.58 | 2297.8-2387.45 | 7.87-7.92 | 94.17-102.25 | 1.31-1.41 |

* Denotes presence of *Lophelia pertusa*.

### 3.1.3.3 Aragonite Saturation State

Surface $\Omega_{arag}$ ranged from 4.02-4.36 (mean: 4.18). At depths greater than 300 m, $\Omega_{arag}$ for all stations ranged from 0.98-1.69 (Table 3-1, Figure 3-4, Figure 3-5), with the values under 1.0 measured at 2596 m depth. $\Omega_{arag}$ for *L. pertusa* sites ranged from 1.28-1.69. $\Omega_{arag}$ varied significantly among sites where *L. pertusa* was present (one-way ANOVA, $F_{5,31} = 7.3798$, $p < 0.001$), with highest values found in the eastern-most sites, including the VK bioherms (Figure 3-5).

Within the depth range of *L. pertusa* in the GoM (300-600 m), total alkalinity was lower at sites where *L. pertusa* was present (Kruskal-Wallis test, $H = 5.0905$, $p = 0.0241$); however, this relationship does not hold when total alkalinity is normalized to salinity (Kruskal-Wallis test, $H = 2.7638$, $p = 0.0964$), as salinity is slightly lower at sites where *L. pertusa* is present (presence mean salinity: 35.05, absence mean salinity: 35.38, Kruskal-Wallis test, $H = 17.5330$, $p < 0.001$). Furthermore, there was no significant difference in pH$_T$ where *L. pertusa* was present and absent (Kruskal-Wallis test, $H = 0.2893$, $p = 0.5907$) (Figure 3-5).

Since $\Omega_{arag}$ covaries with depth, an exponential decay function was used to model changes in $\Omega_{arag}$ with depth,

$$\Omega_{arag} = ae^{b \times (depth)} + c \qquad (2)$$

where $a = 3.13122$, $b = -0.00573$, and $c = 1.15589$ (Figure 3-4). Analysis of the residuals between the function and empirically-derived values shows no significant difference in depth-corrected $\Omega_{arag}$ between sites of *L. pertusa* presence and absence (Kruskal-Wallis test, $H = 0.529$, $p = 0.467$).

The aragonite saturation state is increasingly recognized as one of the most important drivers of framework-forming cold-water coral presence (Davies and Guinotte 2011). A key concern for the persistence of cold-water coral reefs and their associated communities is the shoaling of the aragonite saturation horizon as a result of ocean acidification. According to the results presented here for the GoM, the cold-water coral reefs formed by *Lophelia pertusa* presently lie above the aragonite saturation horizon (ASH); however, shoaling of the ASH is expected to continue as a result of ongoing anthropogenic ocean acidification (Guinotte et al. 2006). While it is not known how natural populations of *L. pertusa* will cope with aragonite-undersaturated conditions, experimental evidence suggests a potential for acclimation to $CO_2$-induced acidification. Over the course of six months, *L. pertusa* from the North Atlantic was able to grow under laboratory conditions at $\Omega_{arag}$ of 0.93 (Form and Riebesell 2012). However, this study was limited in its number of genetic replicates ($n = 2$), so it remains unclear if a population of genetically-distinct individuals will respond similarly. Populations from the Porcupine Seabight and Darwin Mounds have been shown to be highly clonal (Waller and Tyler 2005), and these and the rest of the North Atlantic populations are genetically isolated from the GoM (Morrison et al. 2011). Although our findings suggest that *L. pertusa* in the GoM are tolerant of the current saturation states described here, its response to acidification may be different from individuals of the North Atlantic populations. Future work should explore the effects of ocean acidification on *L. pertusa* to determine if acclimation to decreasing pH is possible in populations beyond the North Atlantic.

When comparing sites only within the depth range of *L. pertusa*, $\Omega_{arag}$ was lower at sites where *L. pertusa* was present than at sites where it was absent, conflicting with our hypothesis that high $\Omega_{arag}$ would coincide with *L. pertusa* presence. This result is likely due to the depth constraints on $\Omega_{arag}$ discussed above. *L. pertusa* was absent at sites just below 300 m (GB299 and GC140, 320-340 m depth). This suggests that $\Omega_{arag}$ is unlikely to exclusively control *L. pertusa* presence, and that other environmental factors not accounted for in the present study may significantly contribute to *L. pertusa*'s distribution and abundance in the GoM. Factors other than ocean chemistry shown to limit cold-water coral distribution include temperature, availability of hard substrata for larval settlement, and current speeds adequate to provide sufficient food resources (Roberts et al. 2009).
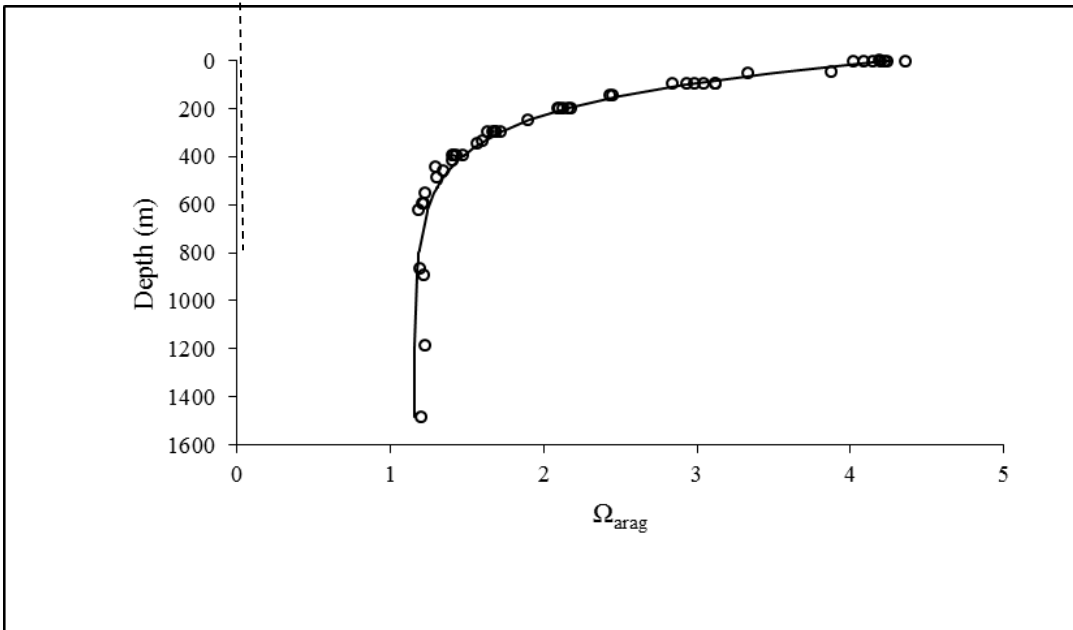
Figure 3-4.  Water column profile of the aragonite saturation state ($\Omega$arag) from 0 to 1600 m. Solid line represents the function $\Omega\text{arag} = ae^{bx(\text{depth})} + c$. Dashed line represents $\Omega\text{arag} = 1.0$.
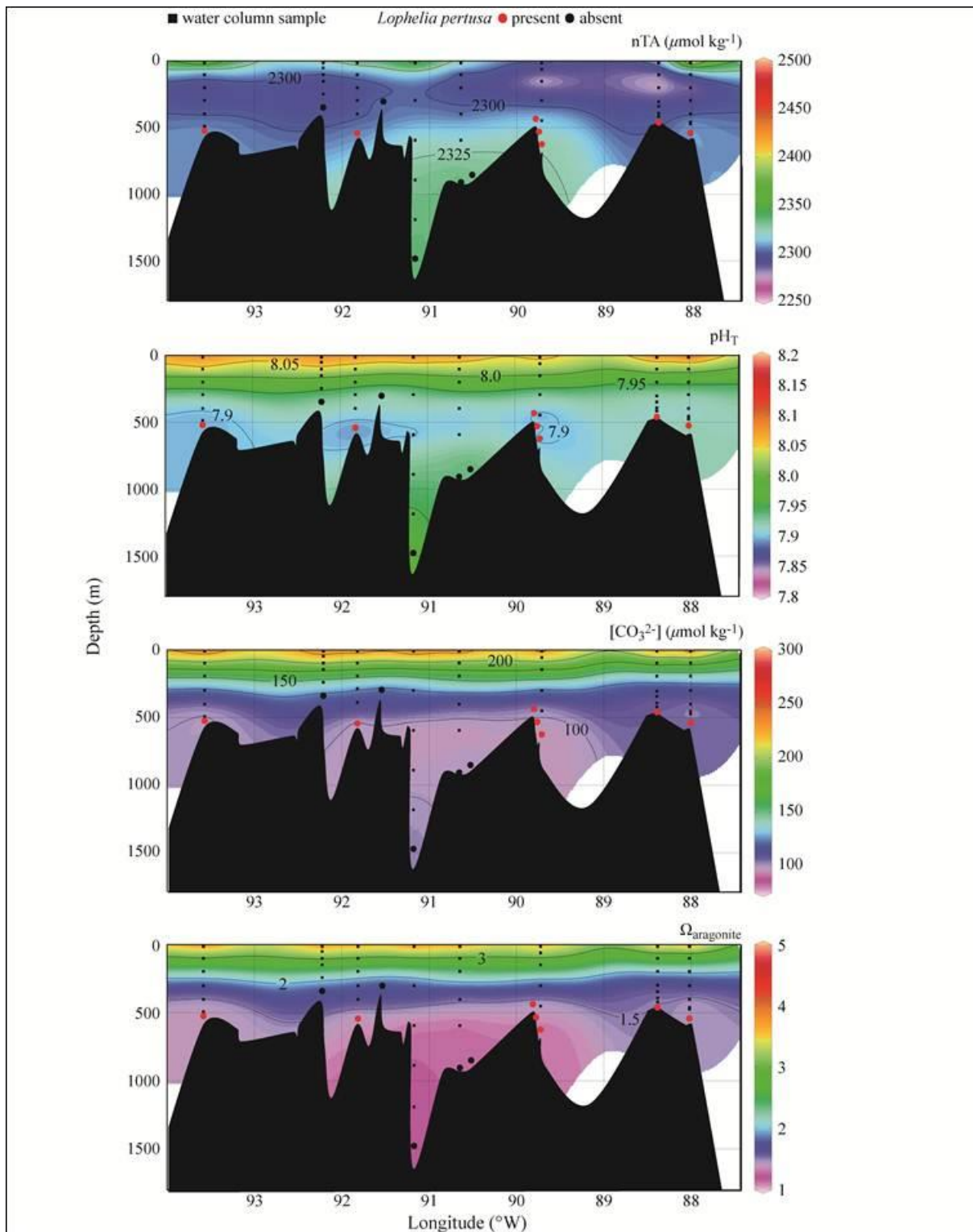
Figure 3-5. Distributions of (A) normalized total alkalinity (nTA) (µmol kg-1), (B) pH (total hydrogen scale), (C) carbonate ion concentration ([CO32-]) (µmol kg-1), and (D) the aragonite saturation state (Ωarag). Areas in white represent no data.

## 3.2 CURRENTS ASSOCIATED WITH VK826 AND GC852 AND IMPLICATIONS FOR LARVAL DISPERSAL

### 3.2.1 Introduction to Current Tests Performed

The dispersal of *Lophelia pertusa* larvae, like the dispersal of the tiny larvae of many marine invertebrates, is subject to the prevailing currents, as tiny larvae are not strong swimmers, but are transported like passive drifters (Morrison, Chap.4). Knowledge of the local circulation is necessary to determine the potential for self-seeding of a reef versus exporting larvae to or recruiting larvae from distant reefs. For this study current meter moorings were deployed for 13 months at two well-developed deep water coral sites that represent different depth ranges and flow regimes. The Vioska Knoll site (VK826) is in 455 m total water depth and the Green Canyon site (GC852) is in 1,424 m total water depth. At VK826 an Aanderaa RCM7 current meter was located 5 m from the bottom and an upward-looking acoustic Doppler current profiler (ADCP) was positioned 9 m above the bottom with an current profiling range of nearly 100 m. Farther west in 1424 m water depth, the mooring at GC852 was equipped with Aanderaa RCM7 current meters at 5 m and 100 m above the bottom. Both moorings were designed to collect data in the near-bottom boundary layer, as well as the prevailing currents in the water column above. For simplicity the VK826 instruments will be referred to as CM03 (lower) and ADCP (upper), while the GC852 instruments will be referred to as CM00 (lower) and CM01 (upper).

The effect of the bottom boundary layer at each site was observed, as well as the linkage between the flow over the mounds and the fluctuations of the Loop Current (LC) and associated eddies. The mooring data exhibit strong motions in the inertial-tidal range, which impact the local circulation and sedimentary environment. *L. pertusa* are filter feeders and typically occur in areas with substantial currents. The observed short-term velocity fluctuations were generally along slope and considerably larger than the mean flow at both locations.

The mooring data was also used to assess the numerical model of deep Gulf circulation which was seeded with inert particles to provide a much broader view of potential larval transport routes, as well as areas of the slope that experience accelerated currents and are therefore favorable to deep coral communities.

### 3.2.2 Deep Mooring Observations at Two *Lophelia pertusa* Sites

#### 3.2.2.1 Overview

Current meter moorings were deployed at the sites of two deep water coral communities in the northern GOM for about13 months. The GC852 mooring was deployed in 1,420 m total water depth in the Green Canyon block to the west of the Mississippi Canyon and the VK826 mooring was located on the western flank of the DeSoto Canyon in 455 m total water depth (Figure 3-6). The moorings were designed to measure currents in both the frictional bottom boundary layer and in the background flow in the water column above. There was 100% data return for both current meters at GC852 and the ADCP at VK826 (

Table 3-2). The minimum threshold for recording current magnitude for the Aanderaas is 1.1 cm/s, below which the vector components of the current aren't resolved. Due to the very weak currents at GC852, slack currents below the 1.1 cm/s threshold accounted for 25.9% of the total record for CM00 and 34.1% of the total record for CM01. These slack currents appear to be real and not the result of fouling. The good data return on current meter CM03 at VK826, which was 5 m off the bottom, was about 83%, which was most likely due to temporary fouling of the instrument. There was strong coherence between CM03 and the lowest bin of the ADCP, indicating that there was likely some fouling of CM03 during the deployment (see Figure 3-7). The correlation coefficients for the current magnitude, u-, and v-components for CM03 and ADCP bin1 are 88%, 97% and 72% respectively.
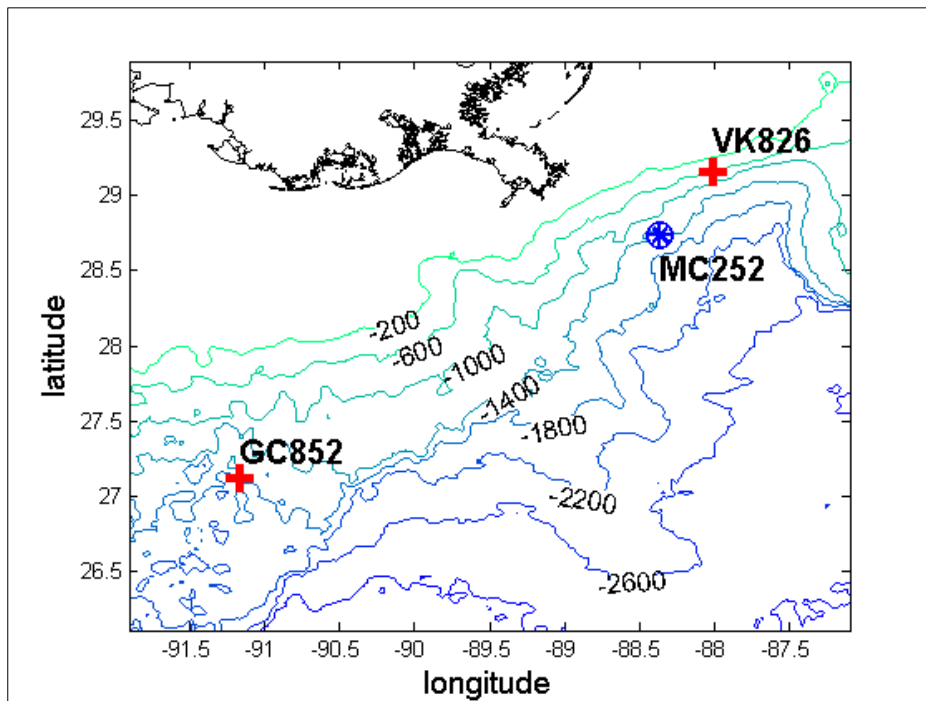


Figure 3-6. Bottom bathymetric contours (meters) in the GoM. The mooring sites are indicated with red crosses. The location of the Macondo 252 well is indicated with a blue circle.
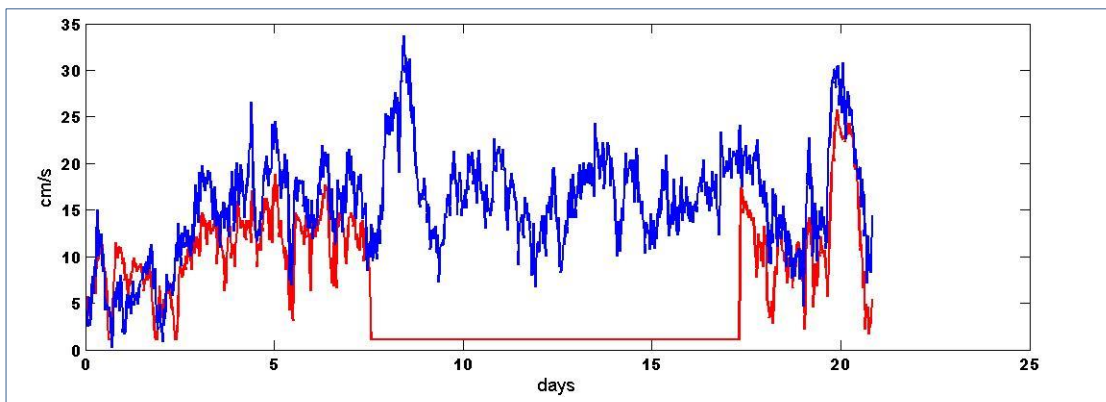


Figure 3-7. Current speed during the first 21 days of the deployment at 450 m (red) and ADCP bin 1 (blue) at 444 m.

Table 3-2.

LSU Deep Coral Study Moorings at Green Canyon 852

| Mooring location; Total depth | Dates of Deployment | Days | Instrument Type (S/N) | Instrument Depth | Percent Data Return |
|---|---|---|---|---|---|
| GC852 27°06.783"N 91°09.874"W 1,420 m | Begin: 8/30/09 02:30 End: 10/22/10 16:56 | 418 | Aanderaa sn#12701 (CM01) | 1320 m | 100% |
| | | | Aanderaa sn#12700 (CM00) | 1415 m | 100% |
| VK826 29°09.690"N 88°01.063"W 455 m | Begin: 9/4/09 14:00 End: 10/15/10 18:29 | 406 | ADCP 300 sn#1219 (ADCP) | 446 m | 100% |
| | | | Aanderaa sn#12703 (CM03) | 450 m | 83% |

### 3.2.2.2 Green Canyon 852

3.2.2.2.1 Historical Observations

Green Canyon 852 (GC852) is the study site for a natural hardground coral community in approximately 1,400 m water depth. This area has been the focus of several BOEM observational and modeling studies. The first long term mooring, FF4, was deployed to the east of GC852 at 26°44.4'N; 91°59.7'W in 1,750 m water depth from April 1987 to September 1988. Hamilton (1990) reported that the currents at 1,650 m below the surface at FF4 were weaker ($\leq 5$cm s^{-1}) than measured at similar depths at other locations along the slope, but the 20-25 day fluctuations were also observed at 1,650 m directly south of FF in 3000 m water depth. These fluctuations are attributed to the westward and upslope propagation of Topographic Rossby Waves (TRWs) (Hamilton, 1990).

Two deep-water moorings were deployed in the Green Canyon area from 1999-2004. Mooring J1 (co-supported by British Petroleum and BOEM) was deployed 102 km to the east of GC852 in the GC782 block (~90°15'W, 27°15'N) at the top of the escarpment in 1,372 m total water depth (Hamilton et al., 2000). J1 was deployed from September 1999 to September 2000 and was equipped with current meters at 10 m, 100 m, and 400 m above the bottom. A very strong event at the beginning of the deployment resulted in a maximum speed at J1 of about 50 cm s^{-1}, but this was considerably less than the maximum of 95 cm s^{-1} observed at 1,600 m at a mooring to the east along the escarpment in nearly 2,000 m total water depth. Mean velocities were calculated from 40-hour low-pass (HLP)-filtered current records for the 100- to120-day intervals that corresponded with large amplitude fluctuations at each mooring. The mean currents at J1 were consistently westward, except for the upper two current meters during the second interval. The mean amplitudes were below 5 cm s^{-1} for all records, except the bottom-most current meter during the first interval. The largest means were observed nearest the bottom. The generally weak currents measured at J1 indicated that deep TRWs were blocked from propagating either westward or into shallower water above the escarpment at this location.

A BOEM-supported observational study of currents near the Sigsbee Escarpment combined data from four deep-water deployments with satellite remote sensing data to look at the relationship between surface eddies and deep currents (McKone et al., 2007). The locations of the first two deployments were south of the GC852 site in approximately 2,200 m total water depth. The first deployment from 2/16/00 – 7/29/00 was located at 26º05.17'N; 29º38.4' and the second deployment was from 7/30/00-5/05/-1 and was located at 26º05.5'N; 29º39.4 N. Maximum current speeds exceeded 140 cm s$^{-1}$ in the surface above 100 m, but were less than 30 cm s$^{-1}$ at the bottom two current meters. The lowest mean speeds were recorded in the transition layer at 1,200 m. The mean direction at the bottom was westward and rotated clockwise with increasing height from the bottommost current meter at 2,213 m to the next current meter at 1,973 m. Spectral analysis of the data supported the presence of TRWs, although it was concluded that the source of the TRWs in the deep layer was non-local and not forced from the surface layer by motions related to the LC and associated eddies.

## 3.2.2.2.2 Mooring Data Analyses

The low frequency current variability was analyzed by removing the tidal and inertial oscillations with a 40-HLP filter. Basic statistics of currents for both raw hourly-sampled data and 40-HLP data are presented in Table 3-3. The daily current vectors are plotted for the 40-HLP data over the entire record in Figure 3-8. The upper panel shows the first 200 days of the deployment for both instruments, followed by the second 200 days of the deployment in the lower panel. The coherence between the upper and lower currents increases during the strong flow events at the beginning of the deployment and from days 280-340 during the latter half of the deployment.

Table 3-3.

Basic Statistics for Green Canyon 252 Mooring Deployment

| Depth(m)/ instrument | Mean Raw | | | Maximum Raw | | | Standard Deviation Raw | | | Standard Deviation 40-HLP | | | Ratio KE40: KEraw (%) | Prin. Axis Dir (True) |
|---|---|---|---|---|---|---|---|---|---|---|---|---|---|---|
| | U | V | Speed | U | V | Speed | U | V | Speed | U | V | Speed | | |
| 1325/ CM01 | -.89 | .-06 | 3.75 | 13.99 | 11.18 | 22.60 | 4.12 | 2.55 | 3.19 | 3.91 | 2.38 | 3.01 | 89.62 | -12.53 |
| 1415/ CM00 | -.63 | .61 | 5.04 | 14.39 | 11.56 | 22.60 | 5.79 | 2.51 | 3.91 | 5.51 | 2.28 | 3.56 | 89.27 | -14.24 |
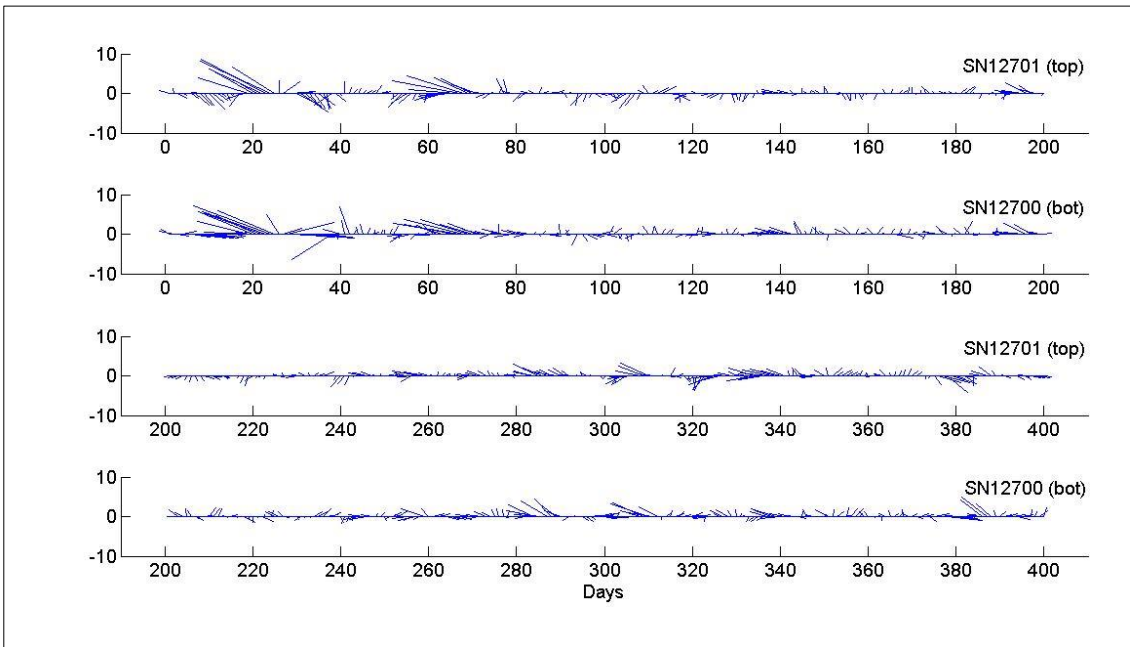
Figure 3-8. Daily averaged 40-hour low-pass filtered  current vectors for CM01 and CM00.

The temperature records at GC852 for top and bottom current meters are highly coherent through most of the deployment, although the extremes are more pronounced in the water column (CM01) than at the bottom (CM00). The large amplitude temperature changes correlate with the strong current events at the beginning of the deployment and mid-way through the second half of the deplyment (Figure 3-9).
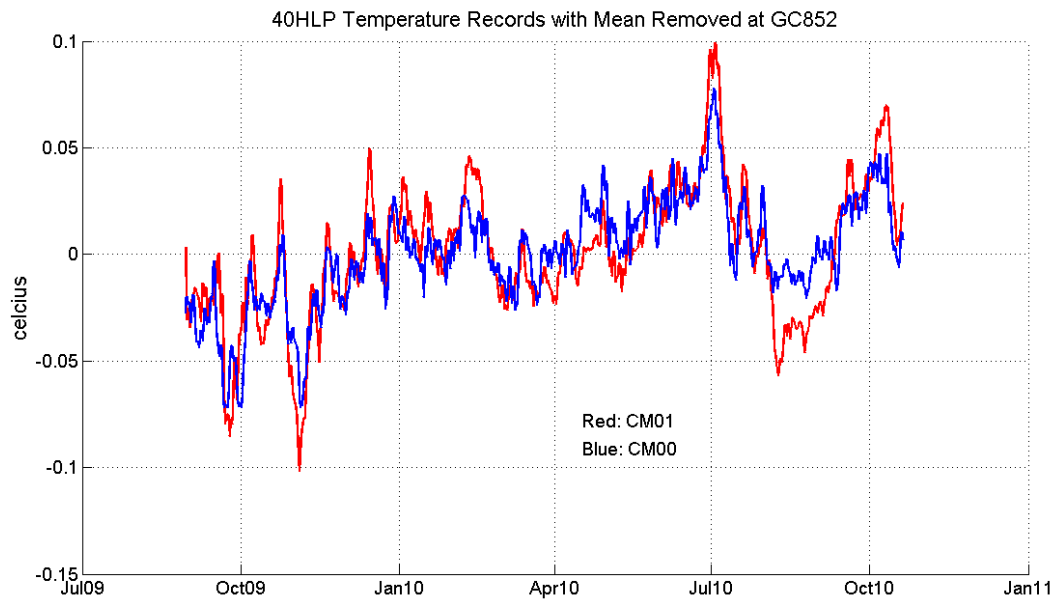


Figure 3-9. 40- hour low-pass filtered  temperature records at CM01 (top) and CM00 (bottom).

91

Figure 3-10 and Figure 3-11 show that the cooler water coincides with a reversal in flow from south to north at both near the bottom and in the water column above. There is also considerable clockwise rotation of the current with height above the bottom as an eddy feature moves over the mooring during the first 37 days. During the latter half of the deployment there was a slight increase in the flow over the mound between days 280 and 340 (Figure 3-12). During this series of events the flow in the water column above the mound was only weakly coupled with the flow at the bottom, when compared to the first 60 days. From closer inspection of the entire record, there appears to be some blocking of the flow to the south in the near bottom, possibly because of the placement of the current meter on the mound.
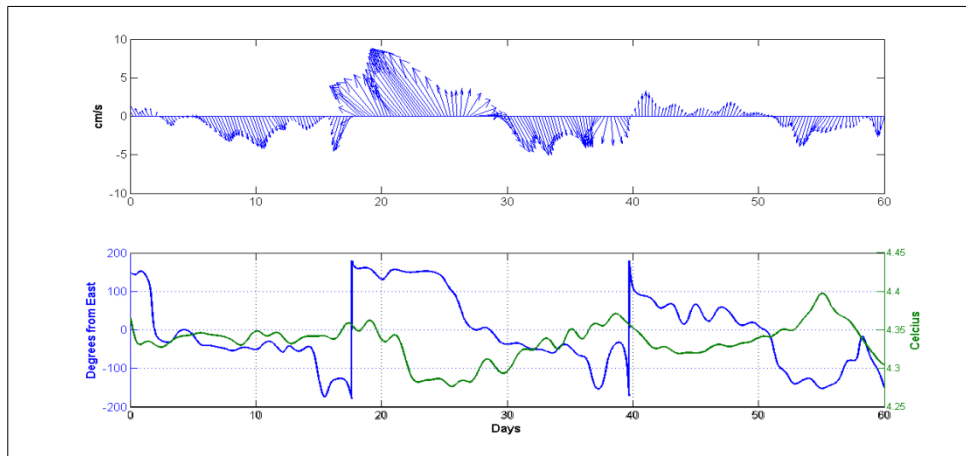


Figure 3-10. Current vectors (top), corresponding current direction (blue), and temperature (green) (bottom) for CM01 days 1-60.
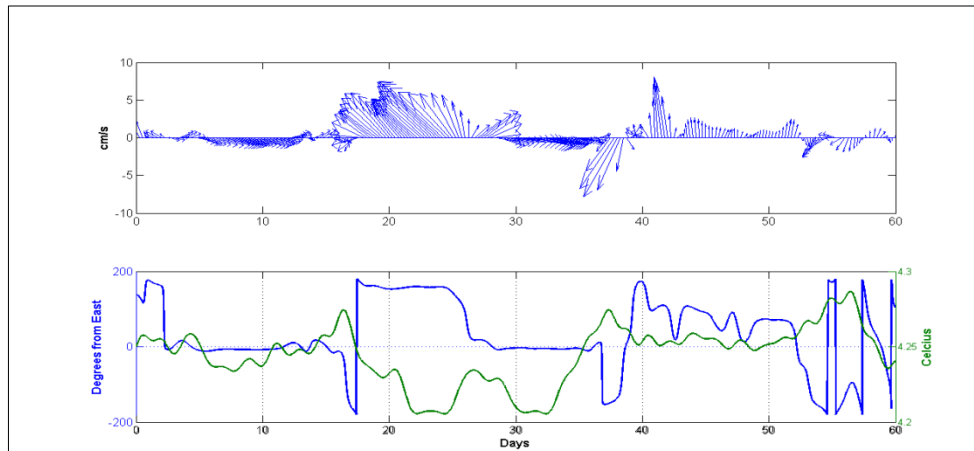


Figure 3-11. Current vectors (top), corresponding current direction (blue), and temperature (green) (bottom) for CM00 days 1-60.
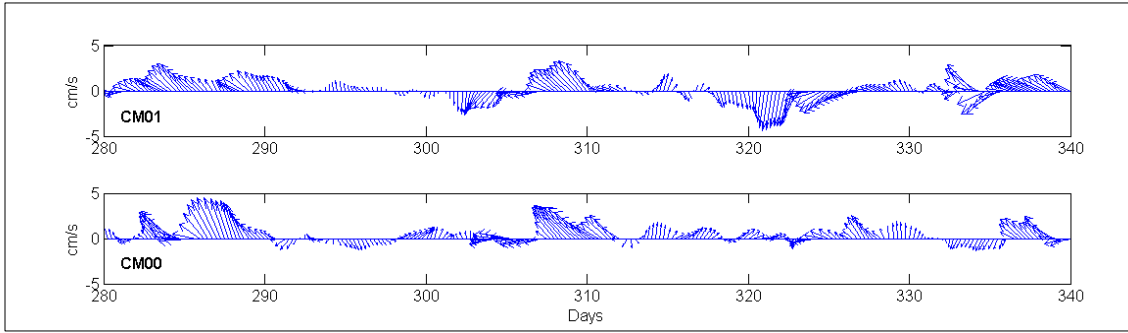
Figure 3-12. Current vectors measured at CM01 (top) and CM00 (bottom) on days 280-340.

The standard deviation ellipse for both depths at GC852 (
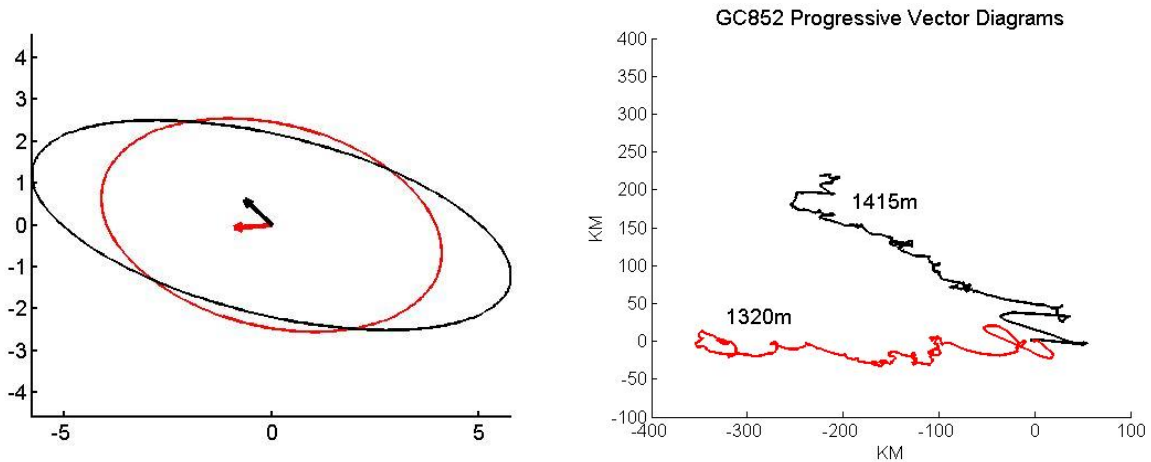


Figure 3-13 left) and the corresponding progressive vector diagrams (Figure 3-13 right) demonstrate a counterclockwise rotation of the mean current direction with height above the bottom. The larger mean for the current meter near the bottom, the magnitude and the direction of the flow for this study are consistent with the historic data in the Green Canyon.
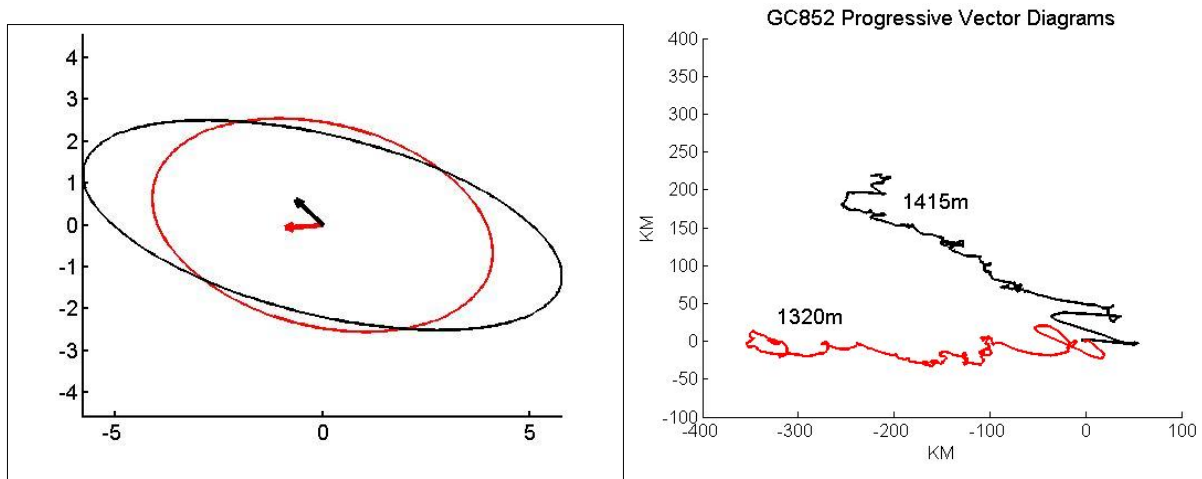


Figure 3-13. Standard deviation ellipses (left) and progressive vector diagrams (right) for CM01 (red) and CM00 (black).

The large velocities observed at the beginning of the record are due to upper level cyclones that move over the mooring during the following intervals: September 20-40 (days 20-40 in Figure 3-8, Figure 3-10, andFigure 3-11) and October 20-November 8 (days 50-70). Both of these events were accompanied by the cooler temperatures at the mooring, and correspond to the pronnouced loops in the progressive vector diagram at the beginning of the record. The southern edge of an anticyclone passed over the mooring in February and resulted in relatively warm water and northwesterly flow. On July 1, 2010, which corresponds to day 300 in Figure 3-9 andFigure 3-12, an anticyclonic (warm core) eddy passed over the mooring resulting in a rise in temperature (Figure 3-9) and a shift from southerly flow to northwesterly.

The largest peaks in the velocity spectrum for both current meters (Figure 3-14) are at 23 and 27-28 days, with smaller peaks at ~20, ~17, ~14, and ~12 days. The peak at 23 days was prominent in the spectra by McKone et al. (2007) at the current meter just off the bottom. McKone et al. (2007) also observed energy peaks at 13 and 16 days. There is significantly more energy in the u-component at both levels, although there is relative more energy in the v-component in the water column. As noted in the discussion above, there is very little flow toward the south and limited north-south fluctuations overall in the bottom layer.

The largest peaks in the rotary spectra (Figure 3-15) are at 12.5 and ~24 hours with smaller peaks between 24 and 27, which correspond to tidal and inertial motions. There is nearly 5-fold increase in the peak clockwise frequency in the bottom layer. The dominant signal in the rotary specta is clockwise for near bottom and up in the water column, which is expected.
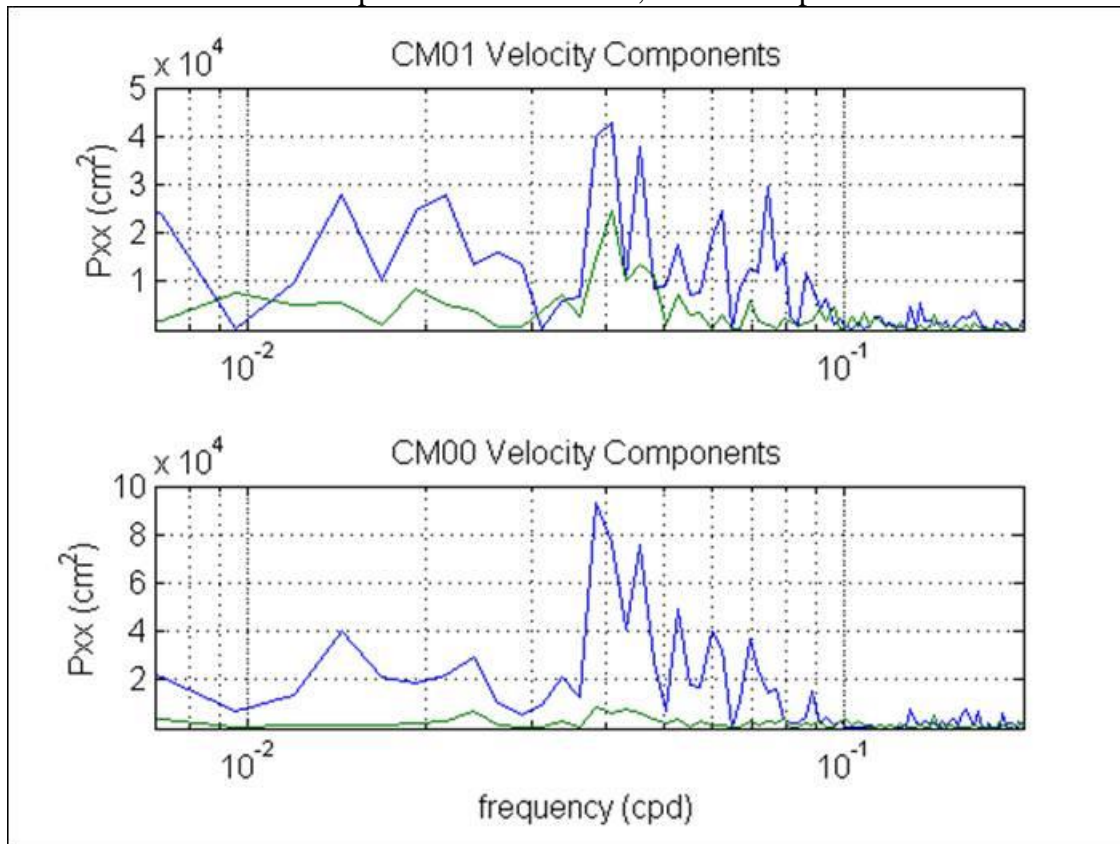


Figure 3-14. Spectra of CM00 (top) and CM01 (bottom) u-velocity (blue) and v-velocity (green) smoothed with a 5 Hanning window.
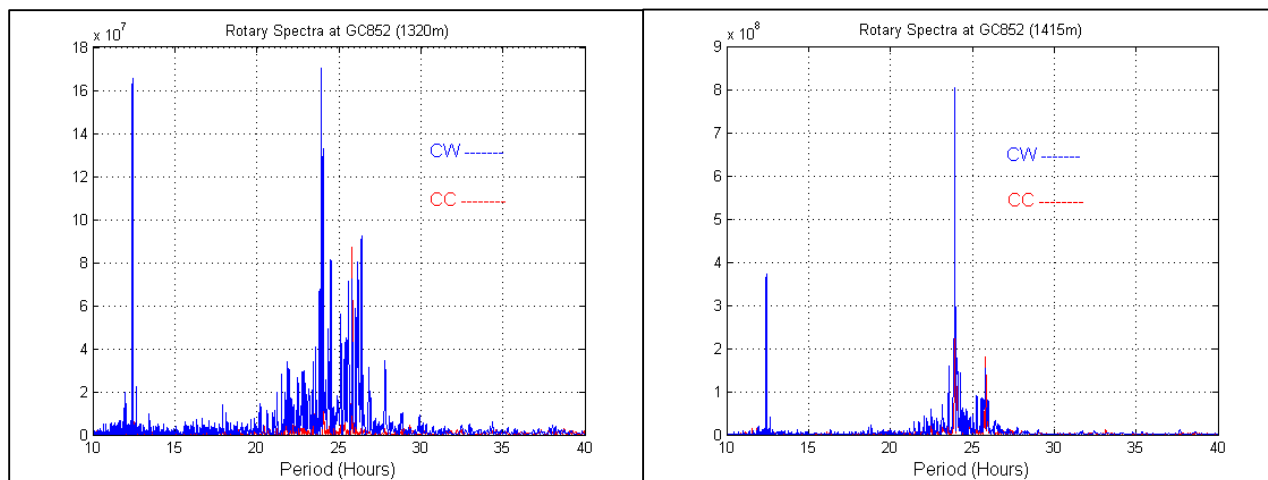
Figure 3-15. Rotary Spectra at CM01 (left) and CM00 (right).

### *3.2.2.3  Vioska Knoll 826*

#### 3.2.2.3.1 Historical Observations

The VK826 current meter mooring was deployed on the western flank of the DeSoto Canyon at 455 m depth at 29º09.69'N, 88º01.063'W. The *L. pertusa* community is situated on exposed carbonate knolls and ridges above a low-relief mound of soft sediments. The mounds are approximately 90 m high and 1-2 km in diameter. The individual *L. pertusa* thickets are 1-15 m high and up to 500 m long. The surficial geology, bathymetry, and coral community distribution in the vicinity of the VK826 mooring were previously described by Schroeder (2002). The center of the low-relief mound observed by Schroeder (2002) had a minimum water depth of 434 m and was centered at 29º09.5'N, 88º01'W, just 370 m to the southeast of the mooring location. The mooring design for this study was intended to provide an understanding of near bottom boundary layer flow over the mounds, which is directly impacted by the topography and the large-scale flow in the water column above the mounds.

The DeSoto Canyon has been the focus of many *in situ* physical oceanography studies over the past 35 years, although the availability of satellite imagery has greatly improved our understanding of the complex circulation with a broad range of horizontal scales of motion. The background flow in the canyon is driven by a combination of the large-scale geostrophic flow, LC eddies and rings, wind-driven currents, upwelling/downwelling, tides, and internal oscillations. The boundary layer flow is influenced by the rough topography associated with the ridges and hummocks, as well as the reflection of internal waves by the sloping bottom topography.

The DeSoto Canyon Eddy Intrusion Study (2000; hereafter referred to as DC2000), funded by BOEM (formerly MMS), was a comprehensive physical oceanographic program designed to understand how the LC and associated eddies exchange momentum and mass between the deep gulf and the shelf within the DeSoto Canyon (Hamilton et al, 2000). The program featured in-situ current measurements, hydrographic data and satellite images to observe and document LC intrusions into the DeSoto Canyon to examine the exchanges of momentum, mass, and vertical vorticity associated the LC-slope interactions over a two-year field season (DC2000). Of specific

relevance to this study were the current and hydrographic measurements at mooring B2, located at 29º12.72'N, 87º52.279'W, which was14.38 km northeast of the VK286 mooring along the 500-m isobath. The DC2000 mooring featured current meters at 200, 300 and 490 m; temperature recorders at 62, 150, and 250 m; and an ADCP at 90 m. The data were subdivided and analyzed according to intervals of sustained flow in the upper 200 m. During the summer of 1997 the northern edge of a deep water cyclone forced anticyclonic flow into the canyon resulting in eastward flow above 200 m with weaker westward currents below. The along-isobath variance was considerably larger at 500 m than the cross-slope variance and the principal direction was along slope toward the southwest with a mean current speed of ~5 cm/s (DC2000). The second interval was characterized by rapid succession of cyclonic LC frontal eddies at a time when the LC was well extended into the northeastern GoM. The circulation in the canyon was cyclonic at all depths except above 100 m in the head of the canyon. The 500-m standard deviation ellipse at B2 exhibited an even larger ratio of along slope to cross-slope variance with a mean velocity of nearly 10 cm/s directed toward the southwest. The third interval was characterized by anticyclonic flow over the central part of the canyon that extended over the water column. The flow on the western flank again exhibited strong topographic rectification with the principal direction toward the southwest and average speed less than 5 cm/s.

### 3.2.2.3.2 Mooring Data Analyses

Basic statistics of currents for both raw hourly-sampled data and 40-HLP are presented in Table 3-4 for both the ADCP data (depths 372-444 m) and the current meter at 450.3 m. There is a counter clockwise rotation of the mean flow with height above the lowest ADCP bin. The means are considerable smaller than the fluctuations due to the back and forth nature of the current which is aligned with the topography. The daily subsampled 40 HLP velocity vectors in ADCP bins 1, 11, 21, and 31 are shown in Figure 3-16 for the entire deployment. The switching back and forth of the current is apparent in the contours of the u-component and occurs through the water column (Figure 3-17). Although the v-component exhibits small fluctuations in time, it varies with height above the bottom. The clockwise rotation of the flow with height above the site is also apparent in the standard deviation ellipses (Figure 3-18) and in the progressive vector diagrams for selected depth records (Figure 3-19). We can also see from the progressive vector diagrams that there was considerably more variation in the direction of the flow during the beginning of the deployment.

The spectra of velocity components for the near-bottom and topmost ADCP bins at VK826 (Figure 3-20) are quite different than the spectra computed for GC852 (Figure 3-14) and the upper and lower spectra are more dissimilar than the upper and lower spectra at VK826. The largest peaks in the spectra for both levels are near 50 days, but it should be noted that the scale for the y-axis is double for the upper bin. The lower bin has relatively large peaks in the 25-33 day and 16-25 day range, but they are actually of the same magnitude as the upper bin. As discussed previously, there is very little energy in the v-component compared to the u-component.

The rotary spectra are compared for the upper most ADCP bin and the current meter just above the bottom (Figure 3-21). The clockwise component is dominant at both levels, as it was at GC852 (Figure 3-15), which is to be expected. The peaks are more concentrated around the tidal-inertial frequencies higher up in the water column than near the bottom. There is not only very little energy at 12.5 hours in the upper record, but the peak at ~12.5 hours is the largest in the near bottom. This

is also quite different from the rotary spectra at GC852, where the energy is more narrowly concentrated in the lower level and the 12.5 hour peak is relatively small.

Empirical orthogonal functions (EOFs) computed from the ADCP velocity components are presented in Figure 3-22. More than 90% of the variability is captured in mode 1 for both components. The greater variation of the v-component than the u-component with depth is apparent in each of the modes, as it is in the contour plots of these components (Figure 3-17). The clockwise rotation from southeasterly to more easterly occurs between 400 m and 410 m, which is apparent in the progressive vector diagrams.

The temperature record from the current meter at 450.3 m for the entire deployment is presented in Figure 3-23 along with the u-component of velocity at 372 m. The temperature and east-west flow are negatively correlated, whereas the u- and v-components are positively correlated. These correlations indicate that southwesterly currents transport relatively warm water from the DeSoto Canyon to the site and when the currents switch direction, northeasterly currents transport relatively cooler water from offshore to the site.

Table 3-4.

Basic Statistics for Vioska Knoll 826 Mooring Deployment

| Depth (m) /SN | Mean Raw | | | Maximum Raw | | | Standard Deviation Raw | | | Standard Deviation 40-HLP | | | Ratio KE40: KEraw (%) | Prin. Axis Dir (True) |
|---|---|---|---|---|---|---|---|---|---|---|---|---|---|---|
| | U | V | Speed | U | V | Speed | U | V | Speed | U | V | Speed | | |
| 372 | -6.0 | -3.9 | 15.3 | 42.5 | 30.1 | 56.2 | 15.7 | 7.1 | 10.6 | 15.1 | 5.5 | 10.4 | 88.6 | 17.9 |
| 374 | -6.0 | -3.8 | 15.2 | 39.4 | 23.5 | 54.8 | 15.6 | 7.0 | 10.6 | 15.0 | 5.4 | 10.4 | 88.7 | 17.8 |
| 376 | -5.9 | -3.8 | 15.1 | 39.8 | 25.3 | 52.9 | 15.6 | 6.9 | 10.6 | 15.0 | 5.3 | 10.4 | 88.8 | 17.8 |
| 378 | -5.8 | -3.7 | 14.9 | 40.5 | 24.4 | 53.3 | 15.5 | 6.9 | 10.6 | 14.9 | 5.3 | 10.4 | 88.9 | 17.9 |
| 380 | -5.8 | -3.7 | 14.8 | 38.6 | 24.4 | 54.3 | 15.4 | 6.8 | 10.6 | 14.8 | 5.2 | 10.4 | 89.1 | 18.1 |
| 382 | -5.8 | -3.6 | 14.6 | 41.0 | 23.5 | 58.5 | 15.3 | 6.7 | 10.6 | 14.8 | 5.2 | 10.4 | 89.3 | 18.0 |
| 384 | -5.8 | -3.5 | 14.5 | 41.7 | 21.1 | 61.6 | 15.3 | 6.7 | 10.6 | 14.7 | 5.1 | 10.4 | 89.4 | 18.1 |
| 386 | -5.8 | -3.4 | 14.3 | 39.4 | 21.3 | 59.0 | 15.1 | 6.6 | 10.6 | 14.6 | 5.1 | 10.4 | 89.5 | 18.0 |
| 388 | -5.7 | -3.3 | 14.2 | 40.6 | 24.7 | 59.3 | 15.1 | 6.4 | 10.5 | 14.5 | 5.0 | 10.3 | 89.7 | 17.7 |
| 390 | -5.7 | -3.2 | 14.1 | 41.9 | 24.7 | 58.1 | 15.0 | 6.3 | 10.4 | 14.5 | 4.8 | 10.2 | 89.8 | 17.3 |
| 392 | -5.7 | -3.0 | 14.0 | 43.4 | 24.5 | 56.9 | 14.9 | 6.1 | 10.4 | 14.4 | 4.7 | 10.2 | 90.0 | 16.9 |
| 394 | -5.7 | -2.9 | 13.9 | 46.5 | 25.7 | 56.4 | 14.9 | 5.9 | 10.3 | 14.4 | 4.5 | 10.1 | 90.2 | 16.3 |
| 396 | -5.7 | -2.7 | 13.7 | 46.1 | 27.7 | 53.6 | 14.8 | 5.7 | 10.2 | 14.4 | 4.2 | 10.0 | 90.4 | 15.5 |
| 398 | -5.7 | -2.6 | 13.6 | 46.1 | 26.3 | 51.2 | 14.8 | 5.5 | 10.1 | 14.3 | 4.0 | 9.9 | 90.6 | 14.6 |
| 400 | -5.7 | -2.4 | 13.5 | 46.2 | 25.4 | 53.3 | 14.8 | 5.3 | 10.0 | 14.3 | 3.8 | 9.9 | 90.9 | 13.8 |
| 402 | -5.7 | -2.2 | 13.5 | 43.5 | 26.2 | 53.9 | 14.7 | 5.0 | 10.0 | 14.3 | 3.6 | 9.8 | 91.2 | 12.8 |
| 404 | -5.8 | -1.9 | 13.4 | 42.9 | 30.9 | 54.0 | 14.7 | 4.8 | 9.9 | 14.3 | 3.4 | 9.8 | 91.6 | 11.8 |
| 406 | -5.8 | -1.7 | 13.3 | 41.5 | 26.4 | 57.1 | 14.7 | 4.6 | 9.8 | 14.3 | 3.2 | 9.7 | 92.0 | 10.7 |
| 408 | -5.8 | -1.5 | 13.2 | 41.0 | 24.5 | 56.8 | 14.6 | 4.3 | 9.7 | 14.2 | 3.0 | 9.6 | 92.4 | 9.7 |
| 410 | -5.8 | -1.3 | 13.1 | 42.5 | 26.6 | 55.8 | 14.6 | 4.2 | 9.7 | 14.2 | 2.9 | 9.6 | 92.6 | 8.8 |
| 412 | -5.8 | -1.2 | 13.1 | 41.5 | 21.8 | 54.9 | 14.5 | 4.0 | 9.6 | 14.2 | 2.8 | 9.5 | 92.9 | 8.1 |
| 414 | -5.8 | -1.1 | 13.0 | 39.5 | 15.1 | 57.3 | 14.4 | 4.0 | 9.5 | 14.0 | 2.7 | 9.4 | 93.0 | 7.5 |
| 416 | -5.8 | -1.0 | 12.9 | 39.2 | 17.4 | 54.1 | 14.3 | 3.9 | 9.3 | 13.9 | 2.7 | 9.3 | 93.0 | 7.1 |
| 418 | -5.7 | -0.9 | 12.8 | 40.9 | 18.2 | 52.8 | 14.1 | 3.9 | 9.2 | 13.8 | 2.6 | 9.1 | 93.1 | 6.6 |
| 420 | -5.6 | -0.9 | 12.7 | 42.1 | 16.4 | 52.4 | 14.0 | 3.8 | 9.1 | 13.7 | 2.6 | 9.0 | 93.1 | 6.3 |
| 422 | -5.5 | -0.9 | 12.5 | 40.1 | 17.7 | 51.0 | 13.8 | 3.8 | 8.9 | 13.5 | 2.5 | 8.9 | 93.0 | 6.1 |
| 424 | -5.3 | -0.9 | 12.3 | 40.4 | 16.6 | 50.9 | 13.6 | 3.7 | 8.7 | 13.3 | 2.5 | 8.7 | 92.8 | 6.1 |
| 426 | -5.0 | -0.9 | 12.2 | 43.6 | 16.2 | 48.2 | 13.4 | 3.7 | 8.5 | 13.1 | 2.5 | 8.5 | 92.7 | 6.0 |
| 428 | -4.8 | -1.0 | 12.0 | 44.8 | 17.2 | 45.9 | 13.2 | 3.7 | 8.3 | 12.9 | 2.5 | 8.3 | 92.5 | 6.1 |
| 430 | -4.7 | -1.0 | 12.0 | 43.1 | 15.7 | 44.8 | 13.2 | 3.7 | 8.2 | 12.9 | 2.5 | 8.2 | 92.4 | 6.0 |
| 432 | -4.6 | -1.0 | 12.1 | 41.9 | 16 | 44.6 | 13.3 | 3.7 | 8.2 | 13.0 | 2.5 | 8.2 | 92.4 | 5.4 |
| 434 | -4.9 | -1.0 | 12.5 | 40.4 | 15.6 | 48.5 | 13.7 | 3.8 | 8.4 | 13.4 | 2.5 | 8.4 | 92.5 | 5.2 |
| 436 | -5.1 | -1.0 | 12.9 | 41.3 | 15.7 | 48.7 | 14.1 | 3.9 | 8.6 | 13.8 | 2.6 | 8.6 | 92.6 | 5.1 |
| 438 | -5.0 | -1.0 | 13.1 | 42.4 | 16.1 | 49.9 | 14.3 | 3.9 | 8.7 | 14.0 | 2.6 | 8.7 | 92.5 | 4.9 |
| 440 | -4.9 | -1.0 | 13.1 | 40.7 | 17.3 | 47.2 | 14.3 | 4.0 | 8.6 | 14.0 | 2.6 | 8.7 | 92.3 | 4.8 |
| 442 | -4.8 | -1.0 | 13.0 | 40.3 | 16.9 | 47.1 | 14.2 | 4.0 | 8.5 | 13.9 | 2.6 | 8.5 | 92.0 | 5.0 |
| 444 | -4.6 | -0.9 | 12.8 | 40.2 | 17.3 | 45.6 | 13.8 | 4.0 | 8.1 | 13.4 | 2.5 | 8.2 | 91.3 | 3.9 |
| 450.3/ Sn12703 | -2.6 | -0.3 | 9.9 | 44.4 | 13.5 | 44.4 | 11.8 | 3.4 | 7.6 | 11.4 | 2.5 | 7.1 | 91.3 | 5.3 |
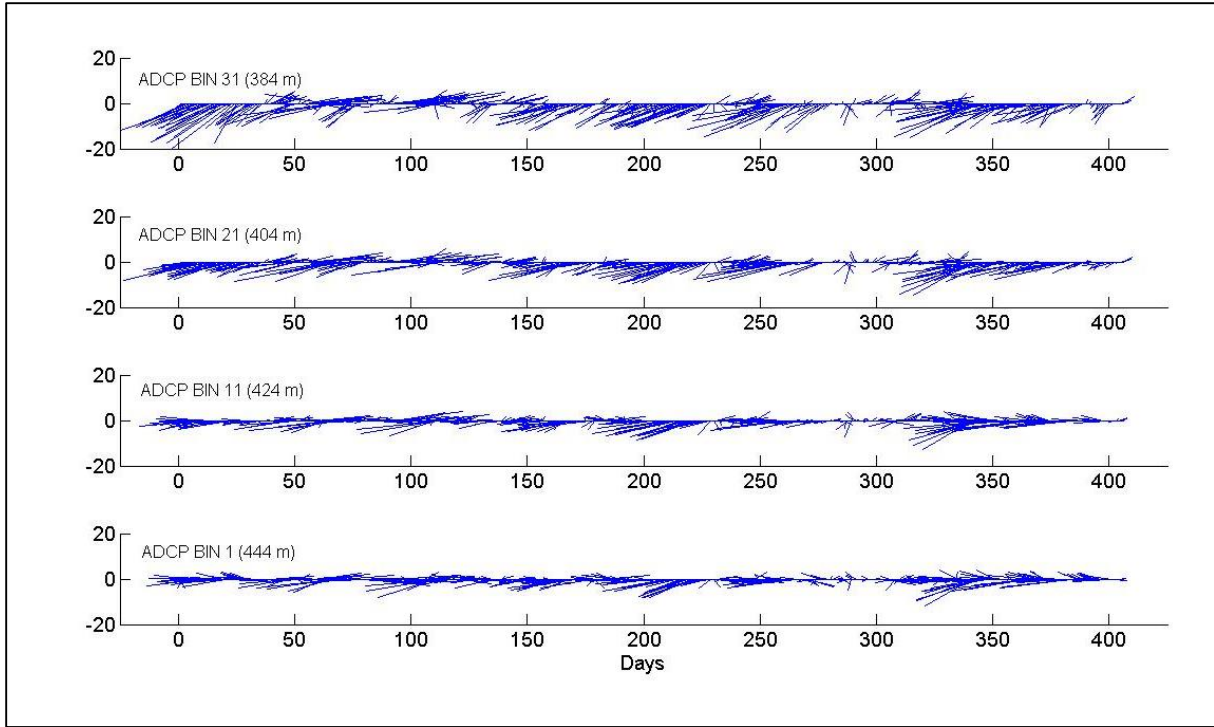
Figure 3-16. Stick plots for ADCP bins 1 (444 m), 11 (424 m), 21 (404 m), and 31 (384 m).
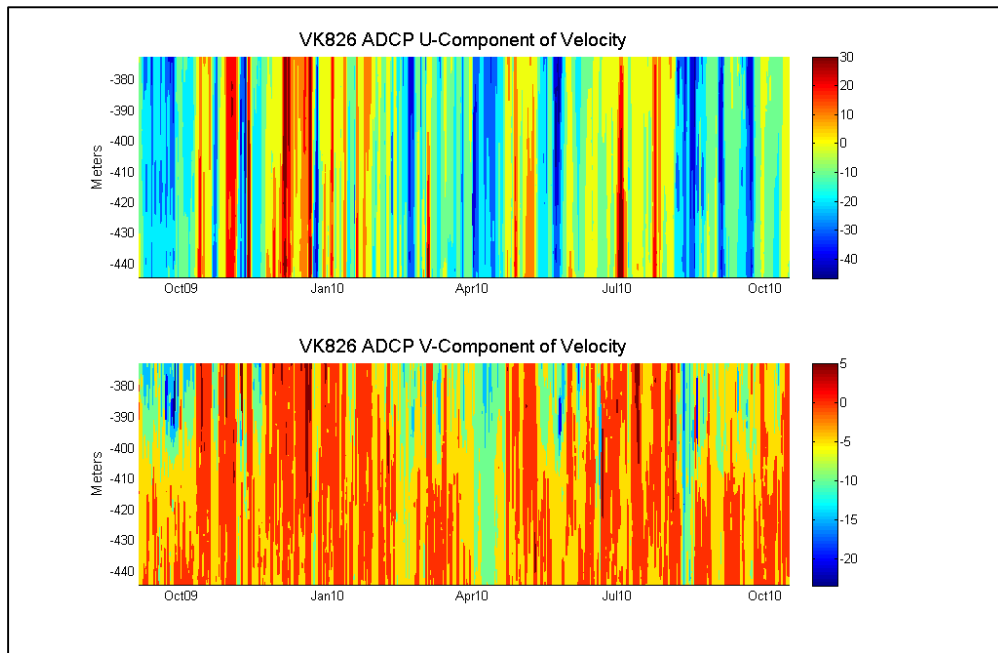


Figure 3-17. Contours of U- and V-components of velocity (cm/s ) for ADCP bins 1-37.
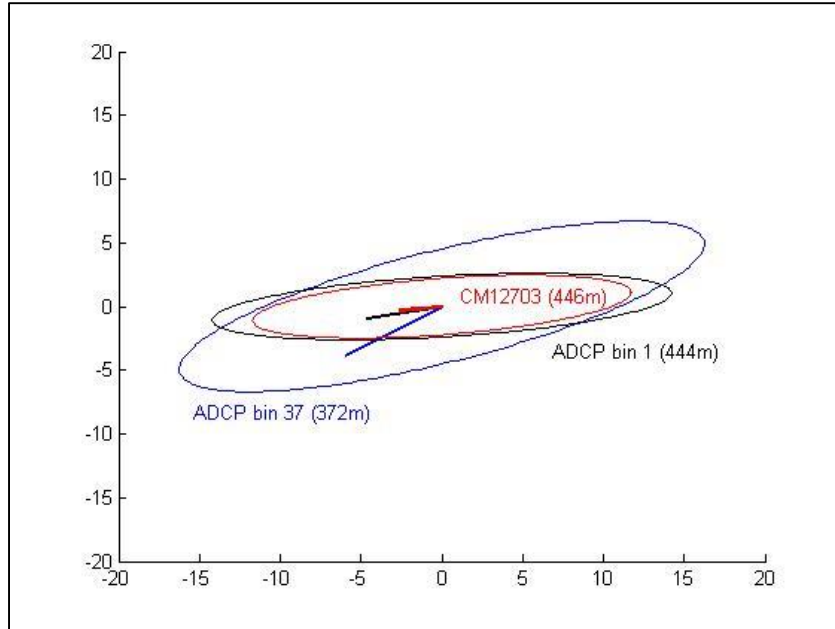
Figure 3-18. Standard deviation ellipses for CM03 (446 m), ADCP bin 1(444 m), and ADCP bin 37 (372 m).
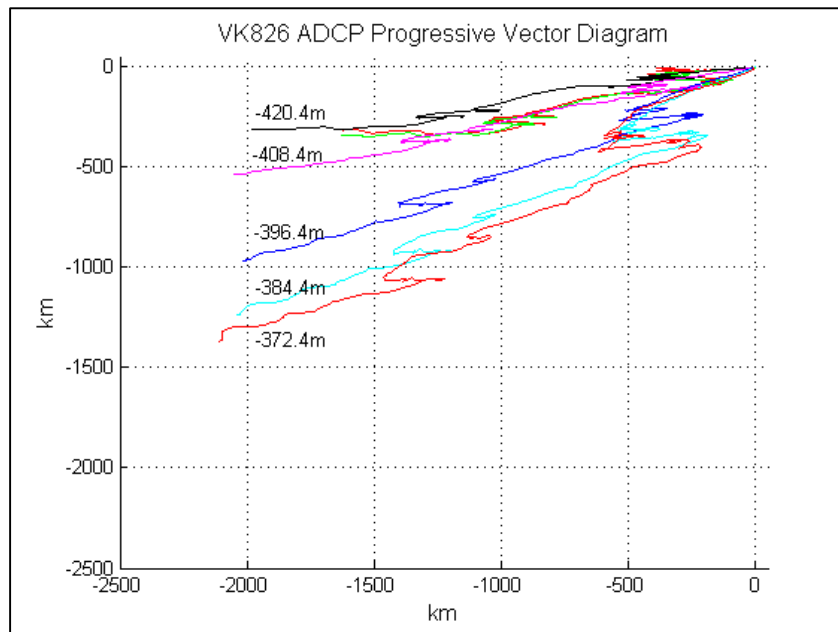


Figure 3-19. Progressive vector diagram for ADCP at 5 depth levels.
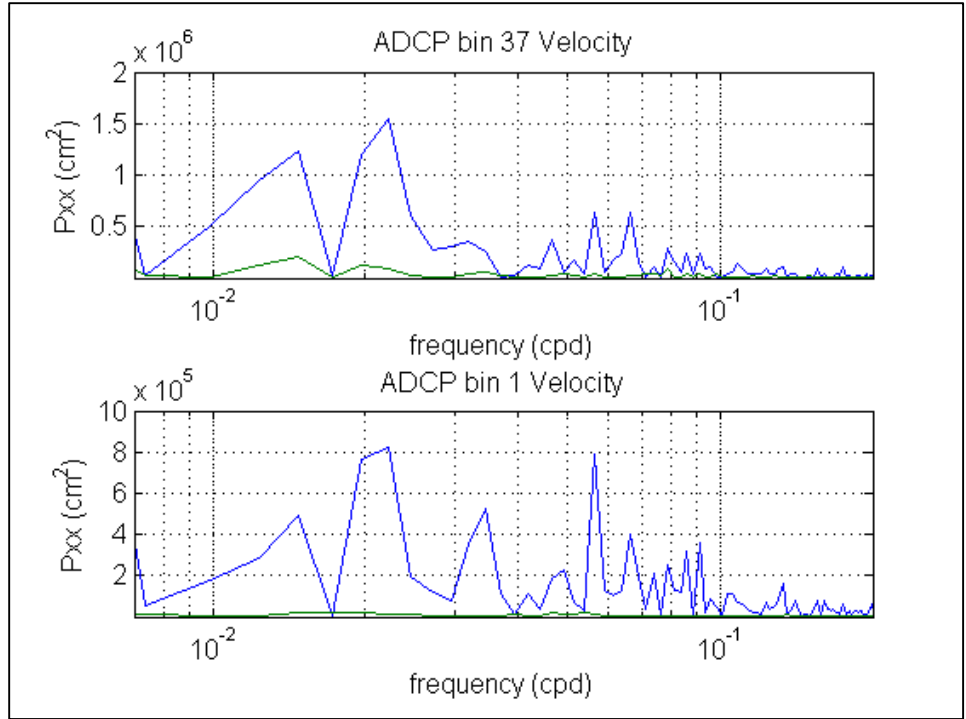
Figure 3-20. Spectra of u-velocity (blue) and v-velocity (green) for bins 1 (446 m) and 37 (372 m) smoothed with a 5 Hanning window.
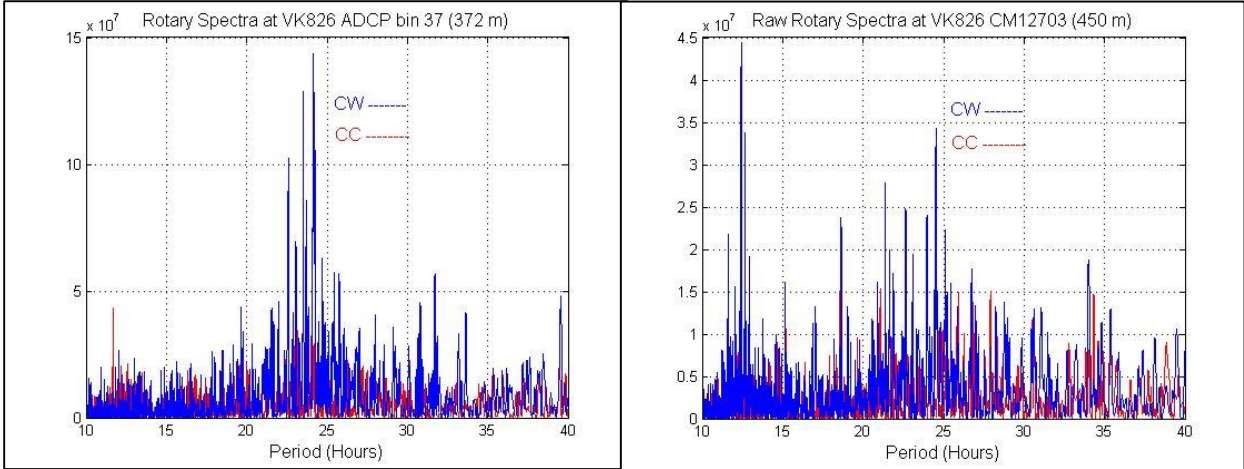


Figure 3-21. Rotary Spectra for the uppermost ADCP bin 37 at 372 m (left) and for the current meter at 450.3 m (right).
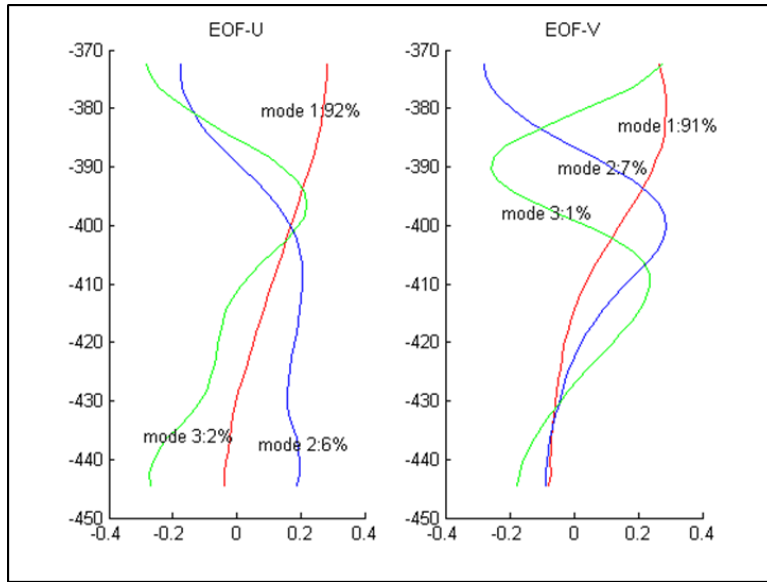
Figure 3-22. EOFs for ADCP bins 1-37 velocity components
at VK826. Modes 1-3 are indicated by red, blue,
and green lines, respectively.
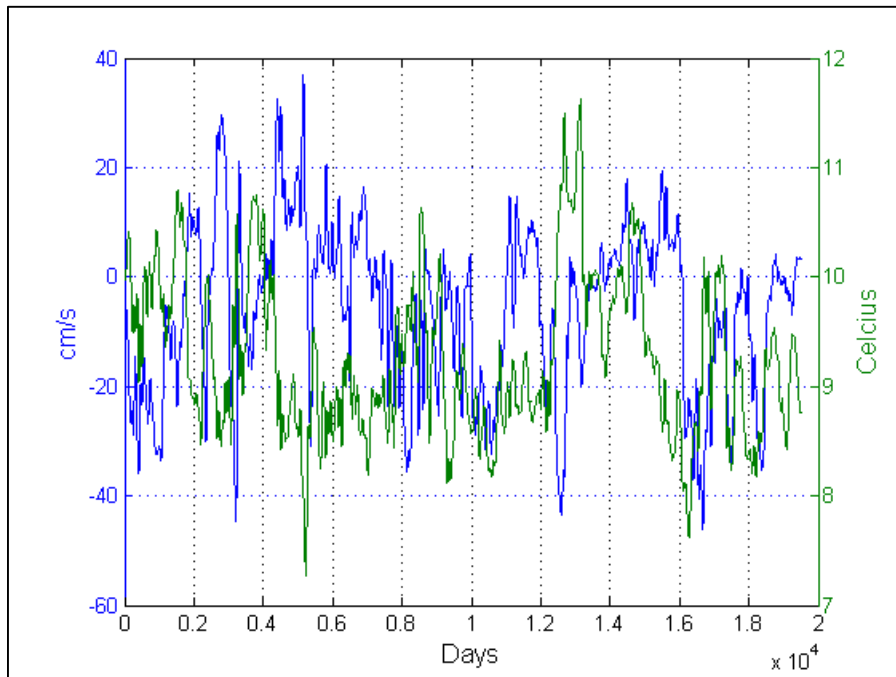


Figure 3-23. 40-HLP temperature from CM03 at 450 m and 40-HLP u-
component of velocity from ADCP bin 37 (372m).

102

### 3.2.3 Summary of Deep Water Currents Analysis

Moorings were deployed at two well-developed *L. pertusa* communites in the northern GoM. The shallower site, VK826, is located to the east of the Mississippi Delta at a depth of 455 m on the western flank of the DeSoto Canyon and the second site, GC852, is located to southwest of the Mississippi Delta at a depth of 1420 m on the northern Gulf slope. The current strength was markedly different between the two sites, although the current direction was along the slope at both locations, which was to be expected. The mean current flow at both locations was also considerably smaller than the magnitude of the fluctuations. The maximum velocity at GC852 peaked at only 22.6 cm/s, whereas the maximum current measured at VK826 was 60 cm/s. The spectra at VK826 was characterized by broad peaks at 80 days and 50 days in both the near bottom and in the water column above. The frequency response centered at 18 days and 30 days in the near bottom at VK826 was not as strong in the water column above. The rotary spectra at VK826 produced a broad frequency response, which was unlike the response at GC852. Both the spectra and the rotary spectra at GC852 indicated very strong inertial-tidal motions, as well as strong frequency response at 12.5 hours. Broad peaks in the frequency response were observed at GC852 centered at 80 days and 50 days, but with reduced magnitude compared to the inertial-tidal response.

The progressive vector diagrams were computed to give an estimate as to how far a drifter could be transported by the currents at a given site over a period of time. The much stronger currents at VK826 resulted in a net vector displacement over the length of the deployment on the order of 2500 km. The net vector displacement at GC852 was on the order of 350 km over the length of the deployment. The mooring data suggest that there is greater potential for transport of coral larvae away from the site at VK826, which is important for establishing new colonies. The currents at both sites exhibited counterclockwise rotation with height above the bottom. The current direction at VK826 was most certainly becoming better aligned with the orientation of the slope upon which the mound is situated.

## 3.3 TIME SERIES ANALYSIS OF PARTICULATE ORGANIC INPUT

### 3.3.1 Objective of Mass Flux Testing

The goal of this sub-project was to investigate settling mass, organic carbon and associated biogeochemical fluxes sinking from the upper water column to deep-water coral sites. To achieve this we deployed and recovered two long-term (~10 month) time-series sediment trap/current meter moorings; one each at two different sites of interest in the GoM.

### 3.3.2 Deployment of Sediment Traps

The instruments used were PARFLUX Mk 78H-21 time series sediment traps (Figure 3-24) each of which was deployed on a 60 m tall mooring (Figure 3-25). One trap was deployed at VK826 (water depth 463 m) and the other at MC751 (water depth 436 m). Each mooring was designed so that the upper surface of the sediment trap was located 6 m above the seafloor and, for each mooring, a current meter was placed 2 m above the surface of the trap to measure current velocities (speed, direction) and water temperature.
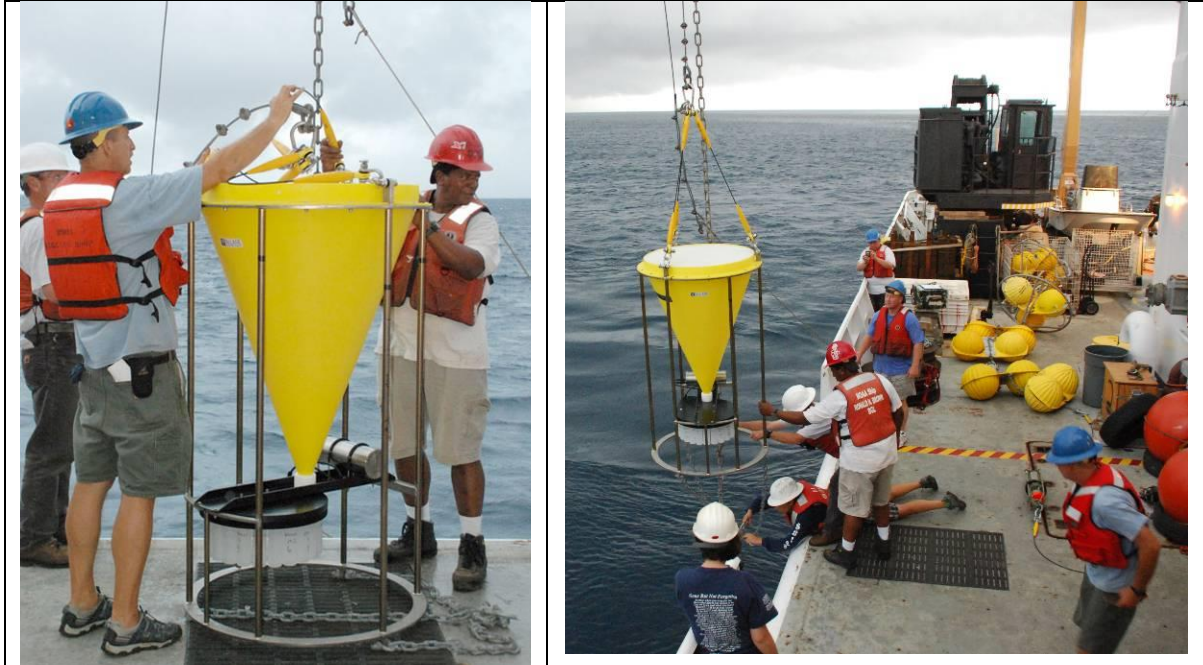
Figure 3-24. PARFLUX sediment traps during deployment.



| | |
|---|---|
| ● | Dualed GLASS BALLS, 17" on2 m, 3/8 chain (4 balls) dry wt. 200 lbs. |
| ● | Dualed GLASS BALLS, 17" on2 m, 3/8 chain (4 balls) dry wt. 200 lbs. |
| | Wire rope, 3/16" |
| | RCM-11 CURRENT METER (S/N: 161) dry wt. 50 lbs. |
| | Bridle (3-1 m wire rope) |
| | SEDIMENT TRAP MK7 (S/N: 12024-3) Dry wt. 100 lbs. |
| | Bridle (3-1 m 1/2" chain) |
| | Chain, 3/8" with swivel |
| | ACOUSTIC RELEASE (Benthos #535 Single) + link Dry wt. 60 lbs. |
| | Chain, 3/8" |
| | ANCHOR |

Figure 3-25. Schematic of 21-cup time-series sediment trap moorings used for this project

Following release to the seafloor, each trap mooring was re-located using the *Jason* ROV and re-positioned precisely, immediately adjacent to the deep-water coral site under investigation (Figure 3-26, Figure 3-27).

Figure 3-26. Sediment Trap Mooring 1 (Site MC751) deployed at 28°11.64'N, 089° 47.90'W on 09/01/09.



Figure 3-27.  Sediment Trap Mooring 2 (Site VK826) deployed at 29° 09.63'N, 088° 01.13'W on 09/04/09.

Each trap was programmed such that the sampling stage would rotate to collect material into a fresh sample cup every 21 days with the first sampling cup being rotated into position to start collecting material on 9/11/2009 and the final sample's collection period ending on 7/2/2010.  Each 250-ml sample cup was filled with DMSO preservative prior to deployment so that, in addition to our planned biogeochemical analyses, splits of the same samples could also be analyzed for microbial, and larval studies (including molecular biological investigations).

### 3.3.3  Recovery of Sediment Traps

The *Ron Brown* cruise in fall 2010 saw the recovery of both time-series traps.  Upon recovery, it was clear that, while the trap from site VK826 had continued collecting samples successfully throughout the sampling period, the invasion of a jellyfish into the sediment trap funnel at the MC751 site had blocked any samples from being collected after 20 Nov 2009.  Accordingly, all 21 anticipated samples from VK826 together with just 5 samples from MC751 (collected contemporaneously with the first 5 samples from VK826) were available for analysis.  In the case of the VK826 site, the samples are of potentially wider significance because the sampling period both preceded and overlapped with the timing of the Deepwater Horizon (DWH) oil spill, which resulted in surface oil slicks that passed directly over the VK826 site.  In separate work, funded by NSF Rapid (2010) and NRDA (2011) we have continued a near-continuous two-year time series from fall 2009 to summer 2011 to investigate whether there is any evidence for seafloor impact related to surface-slicks caused by the DWH accident.  Those later results are not included in this report but archived sample-splits from this project remain stored under NRDA-approved chain of custody protocols.

### 3.3.4  Results of Mass Flux Tests

All samples have now been analyzed for mass flux, together with concentrations of organic and inorganic C, H, N, Al, Ba, Ca, Fe, Mg, Mn, Si, Sr & Ti.  Complete mass and biogeochemical flux data sets are presented in Appendix B-1 and the accompanying current meter records are presented in Appendix B-2.  From the biogeochemical data, relative proportions of biogenic opal, biogenic carbonate, detrital and organic matter fluxes can be calculated.

The mass flux for both traps is directly comparable (Figure 3-28) and the complete record for VK826 shows a pronounced peak in winter 2009-10.  Further, analysis of the contents of the trap samples reveals that they are dominated by lithogenic inputs (Figure 3-28) and the same is true for MC751 (data not shown).

Combining these data with an analysis of the current meter data from the VK826 mooring (Figure 3-29) which shows maximum current speeds in winter 2009-10 and slower velocities in spring-summer 2010, we surmise that the bulk of the flux to the VK826 trap in the northern GoM was related to winter storm activity.  Importantly, however, there are also significant variations in the relative abundance of both biogenic carbonate and organic matter throughout the record (Figure 3-5; *right*), particularly in spring 2010 which coincides with the timing of the DWH Oil Spill.
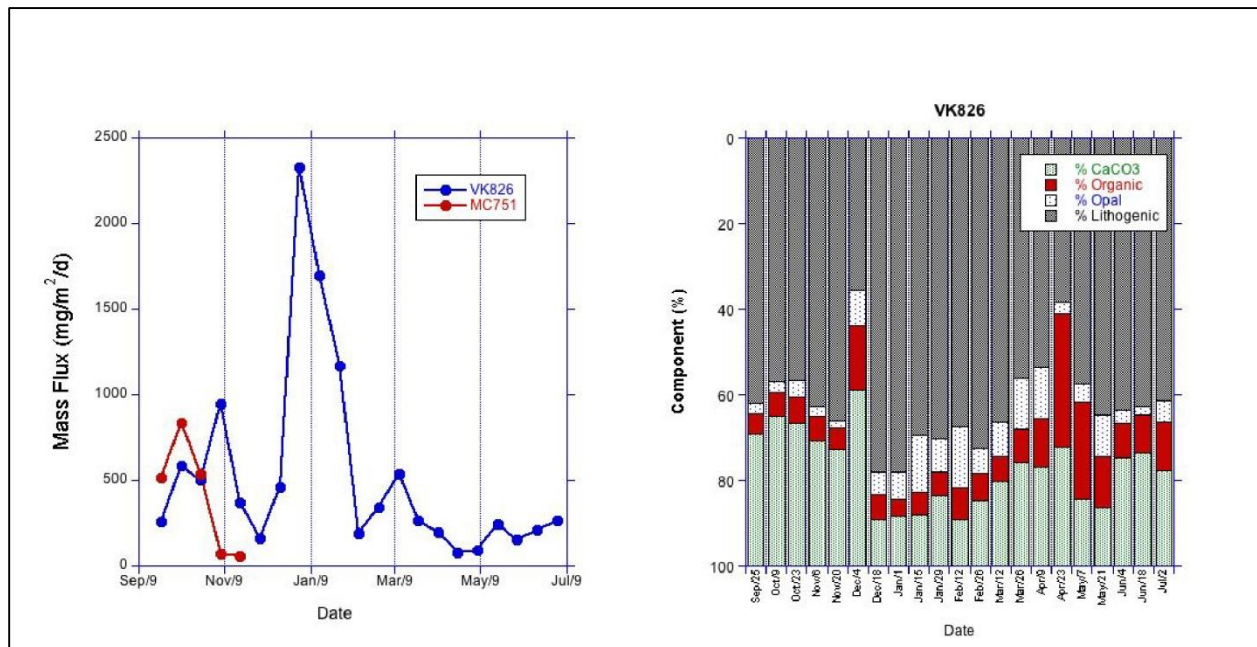


Figure 3-28.  Time-series data, 2009-10.  Left: Mass Flux data (both sites); Right: Four component analysis (VK826).
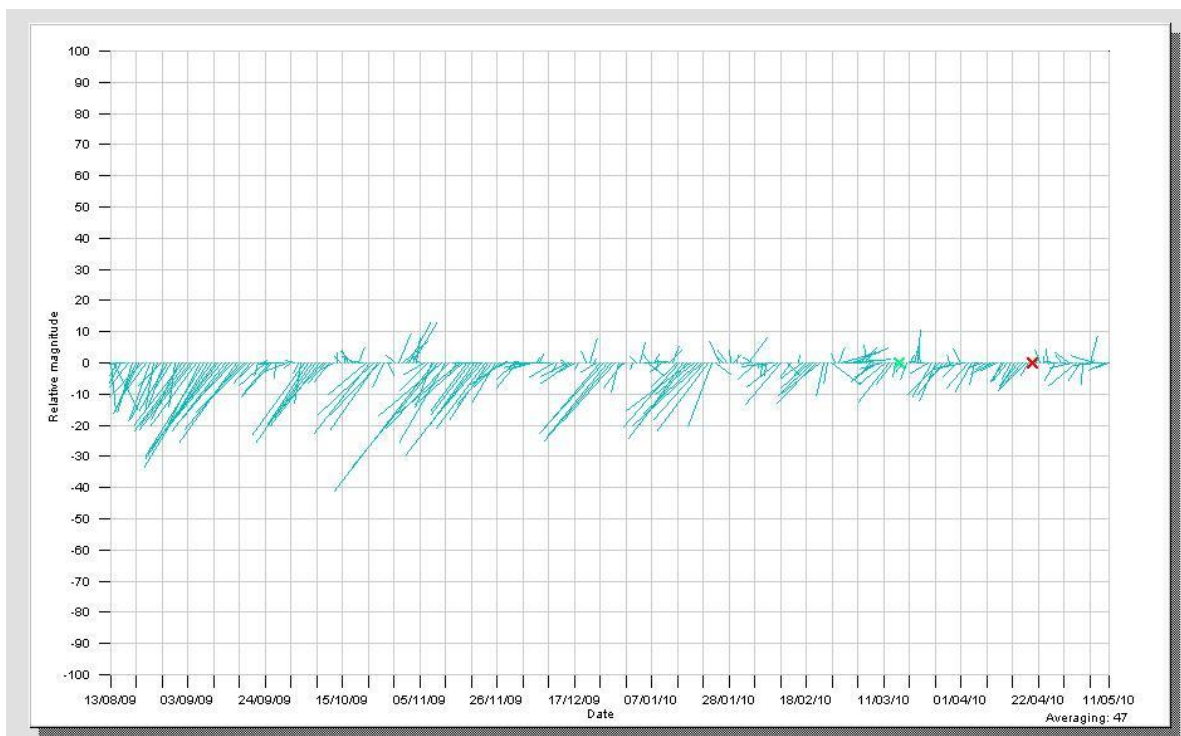
Figure 3-29.  Current meter data displayed as a stick diagram showing direction (stick orientation) and speed (stick length) from the VK826 site.  (Data for MC751 not shown).  Note that maximum velocities occur in winter 2009-10 and much calmer conditions prevailed in spring-summer 2010.


Considering these data in closer detail, the following trends become apparent.  First, the concentration of particulate organic carbon (POC) in the VK826 trap (at a site underlying surface oil slicks within the first week following the April 20, 2010 explosion and fire on the DWH rig) increased to its highest levels in the weeks following the spill (Figure 3-30).  The initial increase in this POC trend, however, pre-dates the DWH accident and may be attributable to spring bloom activity commencing as early as late March/early April of 2010.  Within the period of highest POC concentrations (Figure 3-7a) the concentrations of Ba are also much higher than at any other time in the record.  This, again, could be entirely consistent with a primary productivity signal linked to spring bloom activity.   These time-series data were first reported as part of a presentation at the Association for the Sciences of Limnology and Oceanography (ASLO) aquatic sciences meeting in Puerto Rico in February 2011 and at the Information Transfer Meeting (ITM) meeting held in New Orleans in March 2011.  Resulting from that, our group was subsequently funded by NSF-Rapid and NRDA grants to continue our studies into the Spring and Summer of 2011 to investigate these trends further.  While similar fluxes and POC trends recur in the 2011 spring period, 12 months beyond theDWH spill, the one trend reported here that was not observed again, subsequently, was the increase in carbon/nitrogen (C:N) ratios observed for sediment trap samples at the VK826 site as the discharge from the DWH site progressed (Figure 3-7c).  This is intriguing because high C:N ratios in the natural environment are often interpreted as evidence for more maturated organic matter.  On a like-for-like basis, the high C:N ratios observed for samples collected during the DWH discharge period were not observed at any other time at the same site,

including during the following year's spring bloom, throughout a two-year period, 2009-2011. A working hypothesis, therefore, is that these samples may reflect input of relatively "old" organic carbon that may be related to the DWH accident. While representative (50%) splits of these samples have been transferred to Tim Shank's laboratory for larval analyses, 10% of all these samples have been retained by us under NRDA-approved chain-of-custody protocols for future potential analyses, including hydrocarbon fingerprinting and C-isotope analyses.
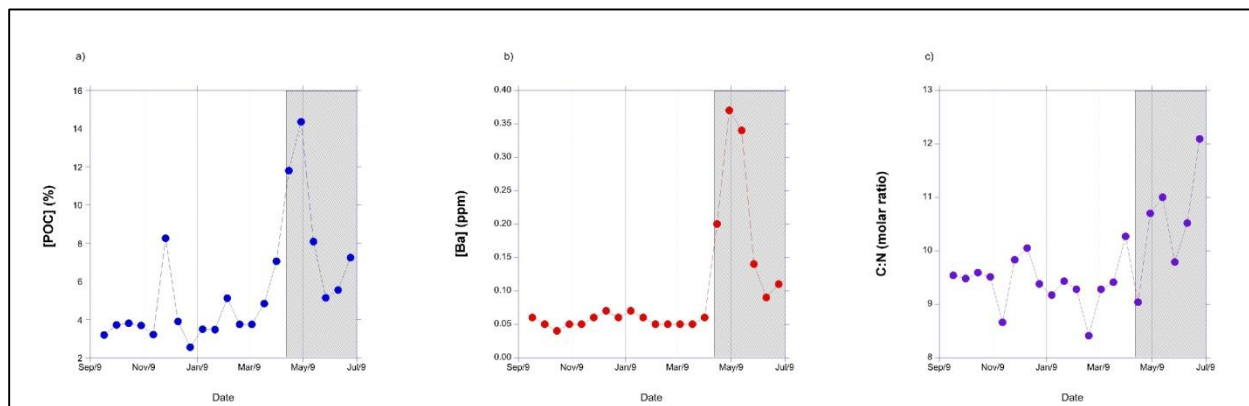


Figure 3-30. Time-series data, 2009-10 for (a) POC concentrations; (b) Ba concentrations; (c) C:N molar ratios at VK826.

## 3.4 LARVAL FLUX TO CORAL SITES - SEDIMENT TRAP RESULTS

Time-series sediment traps (Figure 3-31**a)** were deployed at two sites at ~500 m water depth in the Viosca Knoll 826 and Mississippi Canyon 751 lease blocks to collect the temporal flux of settling particles, including larvae of deep-sea fauna. These traps were operationally defined to autonomously collect biweekly samples in 21 sample bottles (Figure 3-31**b)** from September 2009 through September 2011.

Sediment traps with ID's GOMEX 01 VK01 M2 and RR1 VK02 M2 were deployed at Viosca Knoll 826 site from September 2009 to July 2010 and from June 2010 to January 2011, respectively.
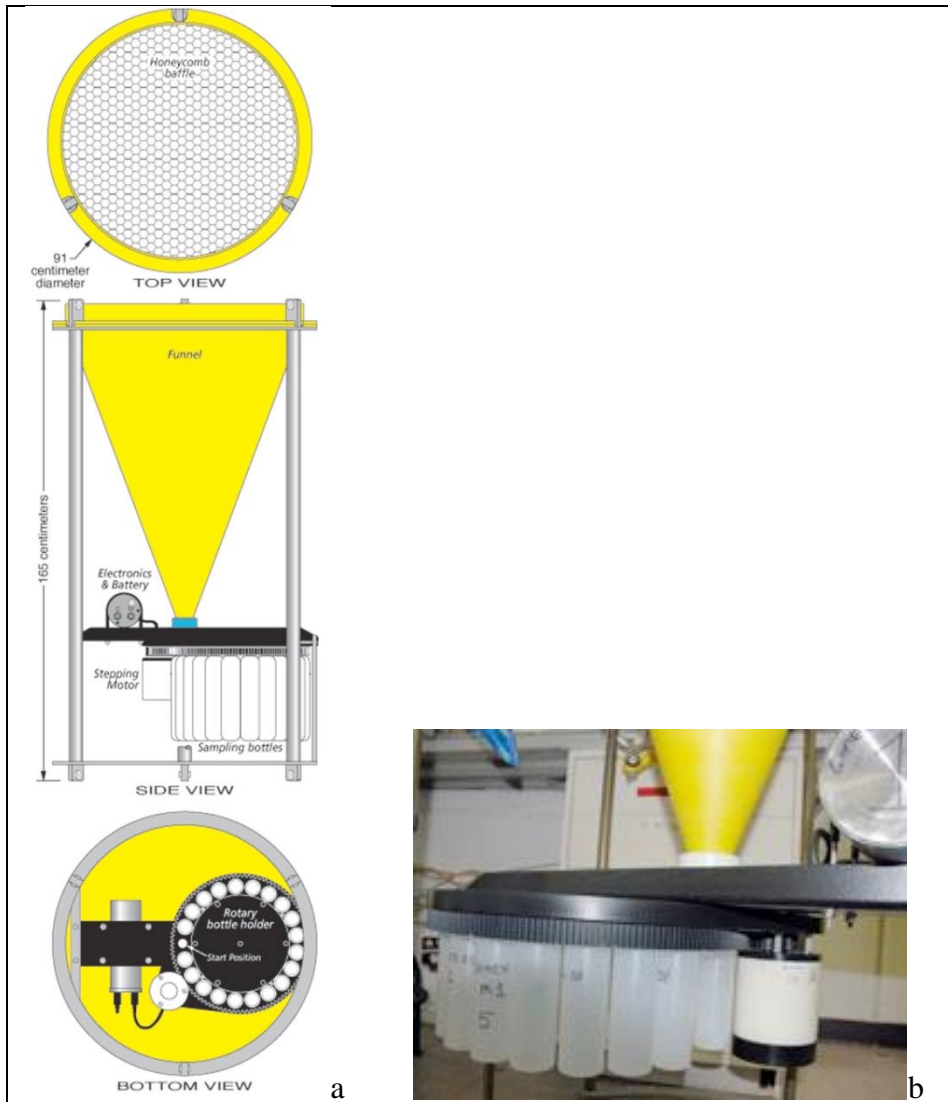
Figure 3-31a,b.  Diagrammatic views of (a) a McLane Parflux sediment
trap and (b) the rosette of 500 ml collection bottles and
autonomously rotated by a motor at the base of the funnel

As standard for deep-sea sediment trap larval collections, the biweekly trap samples were preserved in-situ in the sample bottles in 10% dimethylsulfoxide (DMSO).  Upon retrieval on deck, sediment traps and sample bottles were extensively photographed.   Sample bottles were individually documented via digital imagery, labeled, capped and sealed with tape, and placed in secure refrigerated storage at 4ºC.  Upon reaching port, the samples were shipped in refrigerated storage at the Woods Hole Oceanographic Institution.  Maintained in a 4°C cold room, the samples were run through 5 mm and 1 mm sieves, and divided into splits for biogeochemical, hydrocarbon, and larval recruitment analyses.

All samples were stored in capped and sealed 500 mL plastic vials. The <1mm sediment size fraction was wet-split into 10 parts (relative standard deviation (RSD) of 5%) and the 1mm-5 mm size fraction was wet-split into two parts  (RSD of 10%).  The >5 mm samples were stored without splitting.

The trap deployed at Mississippi Canyon 751 from September 2009 to July 2010 (trap ID: GOMEX 01 MC01 M1) physically did not function after only a few collection sample bottles had rotated (presumably less than 2 months of sampling). As such, parallel temporal analyses of the composition and distribution of organismal material between VK826 and MC751 as originally planned was not possible. We focused our efforts instead on assessing the larval composition and long-term variability in the collections made at VK826 from September 2009 to July 2010 and from June 2010 to January 2011.

### 3.4.1 Biogeochemical Analyses from VK826

The total mass flux shows several peaks throughout our time series (Figure 3-32) that appear to correlate with winter storm deposition from the Mississippi River and is composed primarily of lithogenic material originating from the Mississippi outflow. During the oil release period, total mass flux was low but showed an increase in flux as the sample time period elapsed. Fluctuations in particulate inorganic carbon roughly correspond to total mass flux and was also low but increased during the oil release period (Figure 3-33). Similarly, particulate organic carbon was low, but increased during the oil release period (Figure 3-34). In contrast, C/N increased during the spill period (Figure 3-35). A similar increase was not observed during the following spring.
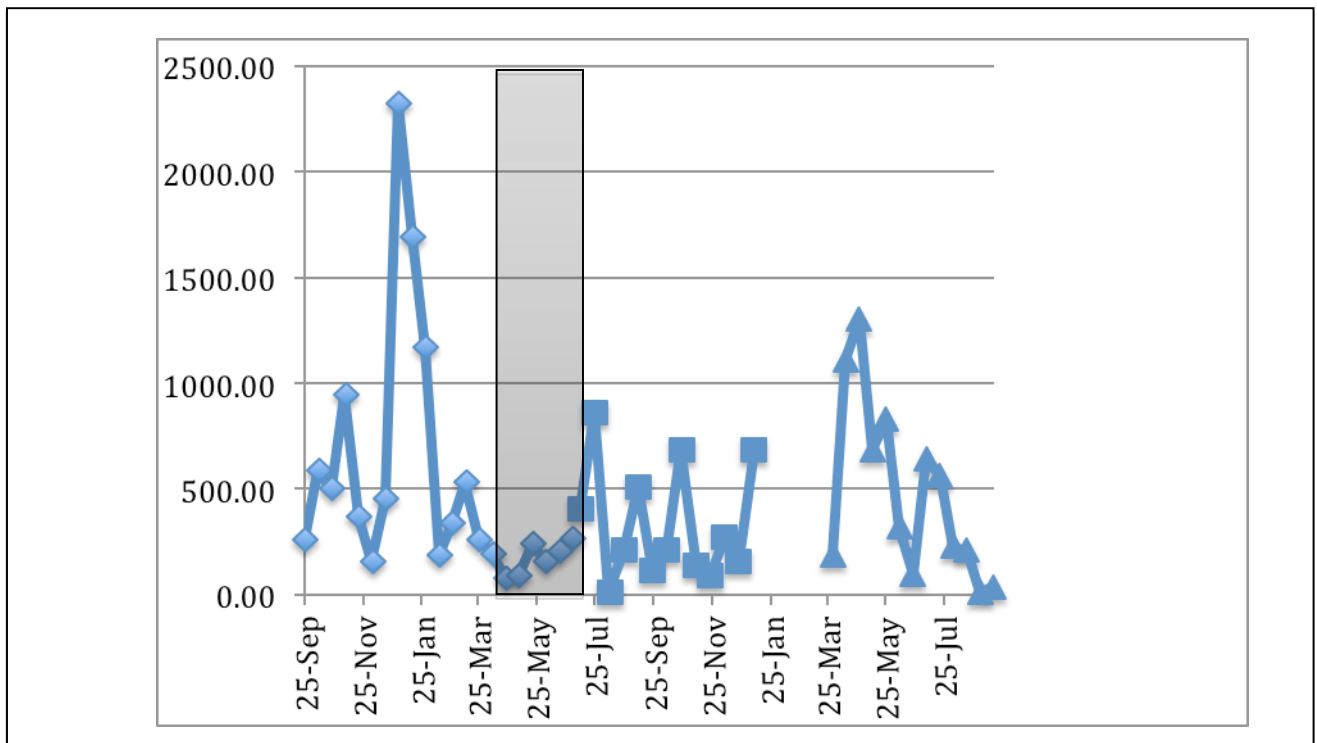


Figure 3-32. Total mass flux (mg/m2/day) from sediment trap series at Viosca Knoll. Shaded area indicates timing and duration of oil spill.
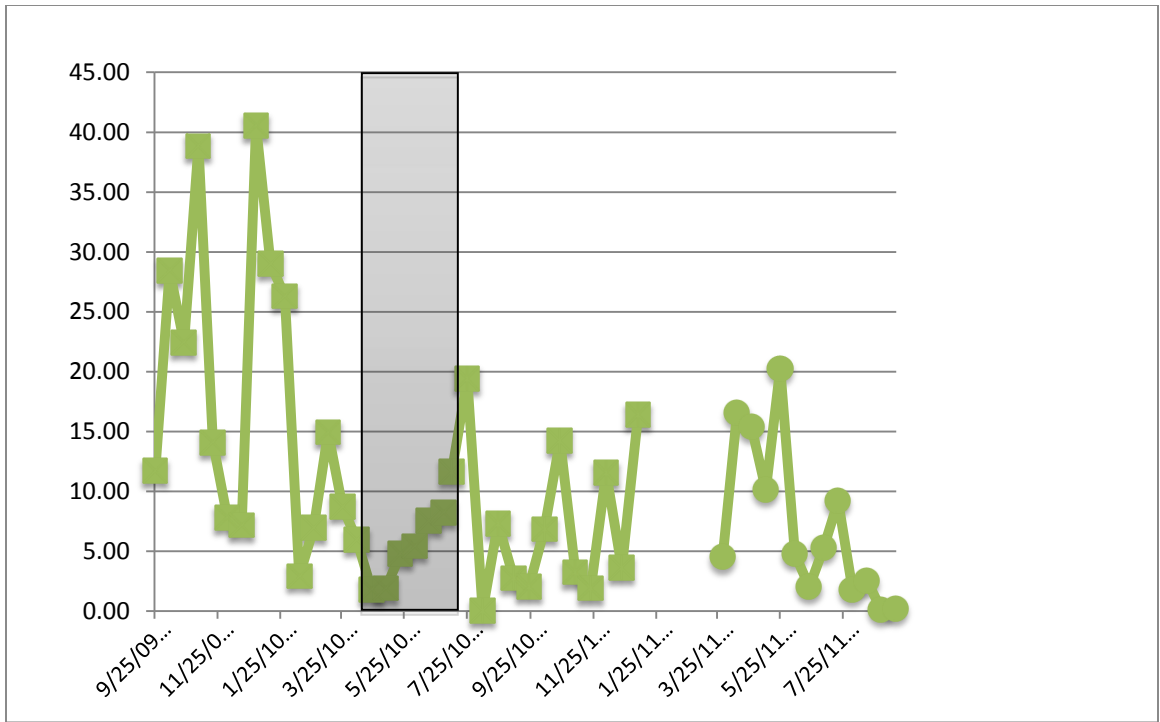
Figure 3-33.  Particulate inorganic carbon (PIC), (mg/m2/day) from sediment trap series at Viosca Knoll.  Shaded area indicates timing and duration of oil spill.
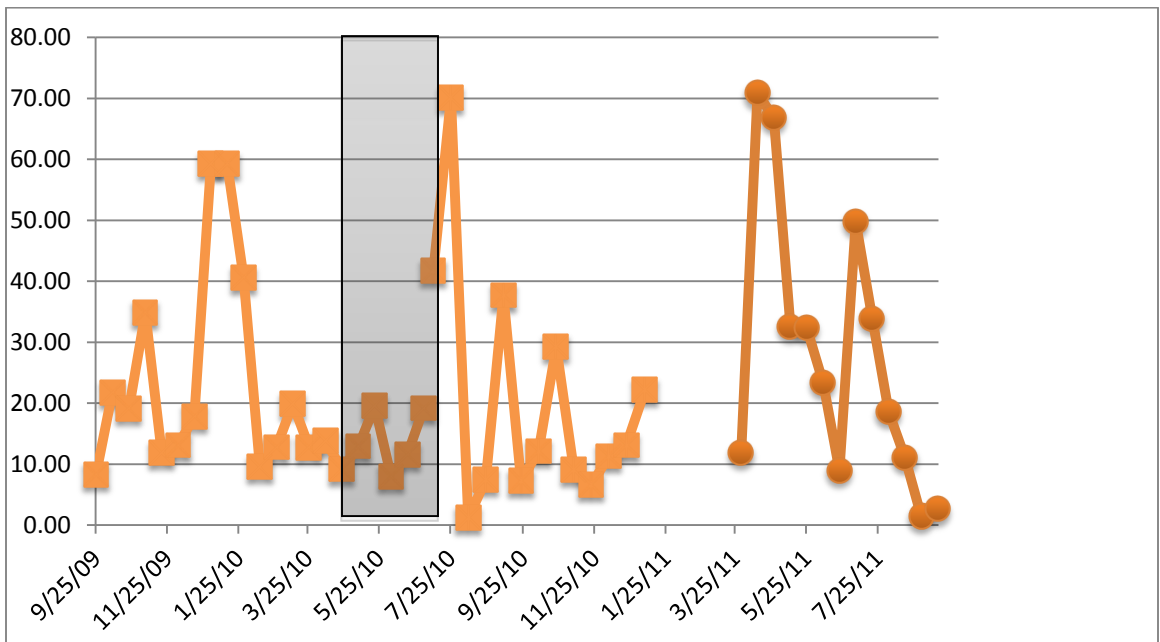


Figure 3-34.  Particulate organic carbon (POC), (mg/m2/day) from sediment trap series at Viosca Knoll.  Shaded area indicates timing and duration of oil spill.
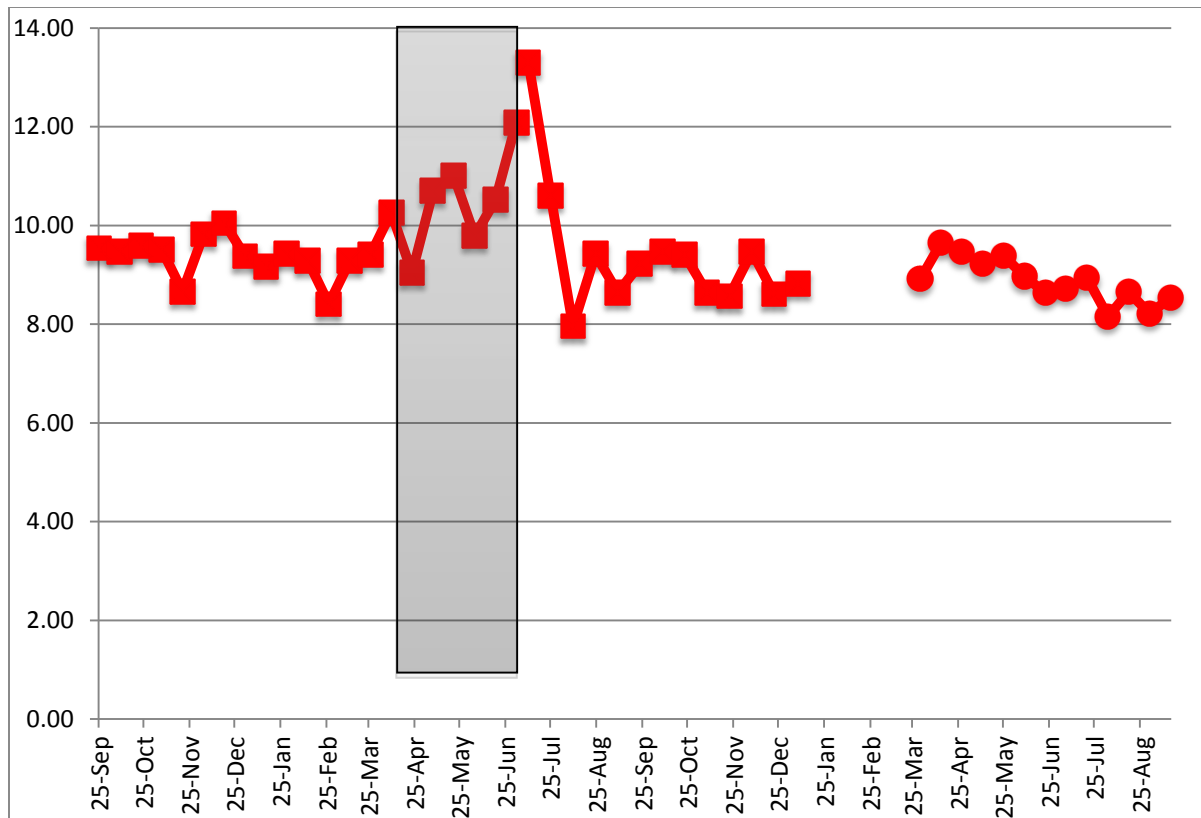
Figure 3-35.  C/N, as calculated using organic carbon from sediment trap series at Viosca Knoll. Shaded area indicates timing and duration of oil spill.

### 3.4.2  Larval Composition and Abundance from VK826

Enumeration of organisms in the different size fractions (>5 mm, 1-5 mm, <1 mm) was conducted using a Leica MZApo microscope. The >5 mm and 1-5 mm sample size fractions were sorted directly in DMSO. Samples from the  <1 mm size fraction were additionally washed with water through 300 μm and 63 μm sieves. Organisms from all samples were removed as they were counted and archived in shell vials with DMSO and stored in a refrigerator at 4° C. Pteropod shells and copepods were the most abundant organisms identified in the >5 mm and 1-5 mm fractions (Figure 3-36). The number of shells from both organisms displayed large peaks during the oil spill period. Gastropod and bivalve shells were most abundant in the <1 mm size fraction in samples collected between August and October 2010. The number of gastropod shells increased through September and peaked in mid-October, while bivalve shells showed a small peak in early September and another small peak in early October (Figure 3-37).  No coral or echinoderm larvae were observed during this period.
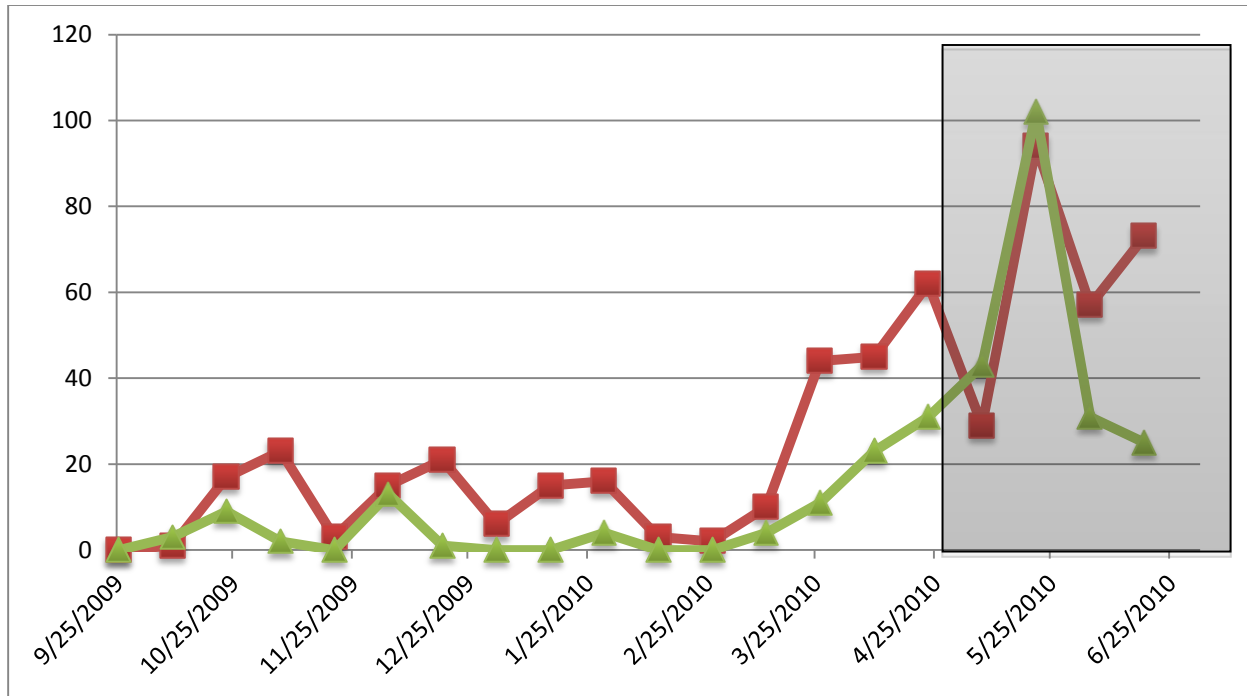
Figure 3-36.  Number of individual specimens collected over time.  The most abundant organisms in the 1-5 mm fraction were pteropod shells (red) and copepods (green). Shaded area indicates timing and duration of oil spill.
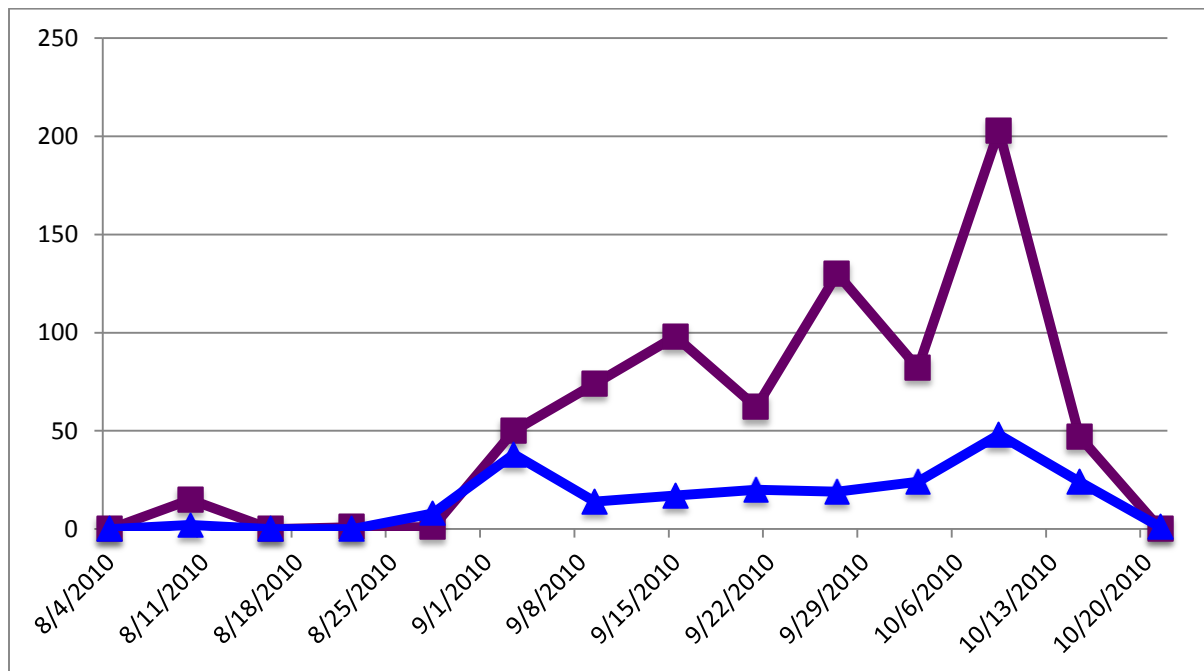


Figure 3-37.  Number of individual specimens collected over time.  The most abundant organisms in the <1 mm fraction are gastropod shells (violet) and bivalve shells (blue). Numbers were pooled from the 300 μm-1mm and 63-300 μm fractions.

The preponderance of shells from various species (e.g., larval bivalves and gastropods) were void of tissue and soft-bodied organisms were rare or absent in these collections. Two possible explanations are that 1) the deployment duration and preservation method resulted in the decomposition of tissue prior to our analyses, and/or that 2) due to the collection time and location, the vast majority of material collected was already dead or decomposing at the time of sampling. If the first explanation is considered most likely, this observation would be counter to all previous trap deployment and larval collections (more than 8), conducted between 2000 m to 2600 m depth for 6 to 10 month deployment intervals. This explanation would provide insight into our inability to extract DNA from sediment trap larvae despite the fact that many of the copepods did contain tissue (this could also suggest an issue with preservation). We conducted over a dozen attempts to extract genomic DNA, utilizing both off-the-shelf Qiagen Extraction Kits for small amounts of tissue (highly successful in the past for obtaining larval DNA from identical sediment traps) and our 10% DMSO recipe. If the second explanation holds true and the sediment trap material was collected at a time and location in which the vast majority was already dead and decomposing, then rationales for this observation would include unknown dynamics associated with nutrient/productivity blooms in this region and potentially some influence of the DWH oil spill. Without additional information, including some MC252 fingerprint analysis on the collected materials, discerning between these two potential options is difficult.

The DWH blowout released hydrocarbons at ~1,500 m depth from April 20, 2010 through July 15 2010. While some of those hydrocarbons persisted in a deep plume, about 15% formed a slick at the surface (Camilli et al 2010). Within a week of the blowout, our Viosca Knoll trap site was underneath this surface slick (Figure 3-38). The Mississippi Canyon 751 trap site was located outside of the area covered by the surface slick. The collection of mostly shelled larval forms without tissue coincident with the Viosca Knoll 826 trap's location under the surface slick suggests a linkage between these two observations.
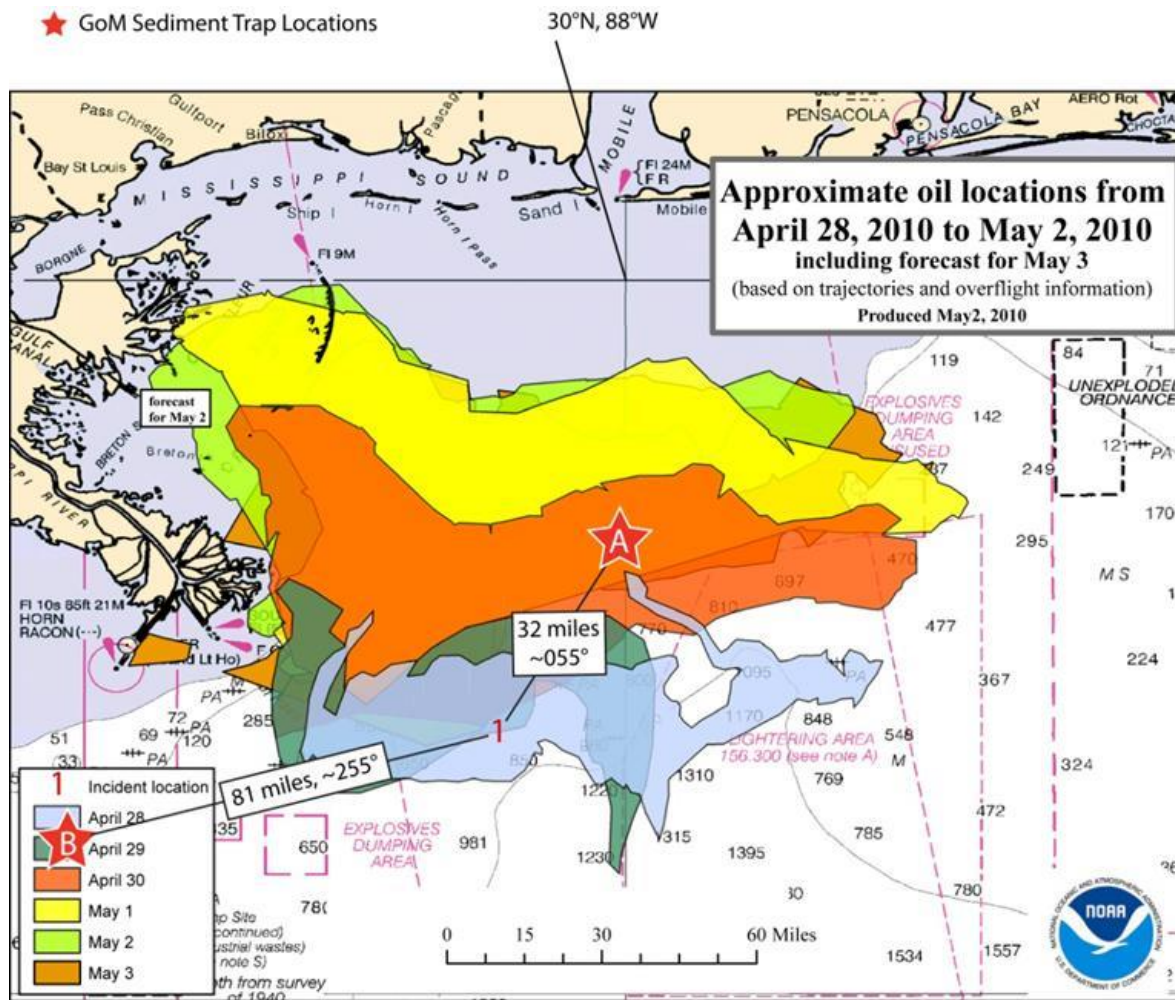
Figure 3-38. The extent of surface slicks on May 2, 2010. Red stars indicate position of
sediment traps.

In parallel with the C/N ratio and prior to the largest increase in concentration of particulate organic carbon in the VK826 trap (underlying surface oil slicks within the first week following the DWH explosion on April 20, 2010), the abundance of pteropods and copepods increased to their highest levels in the weeks during the spill. Larval gastropods and bivalve abundance was maximal in the fall in the samples analyzed to date. As noted previously, the high C/N ratios observed for samples collected during the DWH discharge period were not observed at any other time at this site, including during the following year's spring bloom, throughout the two-year sampling period, 2009-2011. Given that high C/N ratios are considered to derive from more mature organic matter, a working hypothesis is that the observed fluctuations in either organism composition or abundance may correspond directly to the input of relatively "old" organic carbon that may be related to the DWH accident.

These time-series data were first reported as part of a presentation at the ASLO Aquatic Sciences meeting in New Orleans in February 2013, as Govindarajan, A. F., S. Manganini, C. R. German, T. M. Shank (2013) *Effects of the Deepwater Horizon Oil Spill on Biogenic Fluxes and Larval Recruitment*.

115

# 4   COMMUNITY STRUCTURE, BIODIVERSITY, AND BIOGEOGRAPHY

Deep-water corals provide important sources of habitat heterogeneity on continental shelves worldwide. They create habitat for a diverse group of associated fauna that may occur only in association with the corals or in abundances orders of magnitude above that on the surrounding seafloor (Jensen and Frederiksen 1992, Henry and Roberts 2007, Mosher and Watling, 2009). In the Northeast Atlantic alone, over 1,300 species have been recorded living in and on *L. pertusa* habitats in physical and photographic samples (Rogers 1999, Roberts et al. 2006, Henry and Roberts 2007). On two reef structures alone in Norway, 256 species were recorded from recovered coral blocks (Jensen and Frederiksen 1992). In the Porcupine Seabight in the Northeast Atlantic, 313 taxa were collected in 7 box core samples from coral mounds (Henry and Roberts 2007). The diversity of the community on these reefs rivals the diversity of many tropical zooxanthellate coral reefs (Rogers 1999).

However, these studies all involved dredge and box core samples that include species that are likely not intimately associated with coral structure but inhabit the sediments beneath the coral framework and in the case of dredges perhaps as much as 100s of meters away. In the GoM, 68 taxa of large macrofauna and megafauna (> 1 mm sieve size) were found in closely associated with *L. pertusa* in quantitative community collections obtained with custom collection devices deployed from a submersible (Cordes et al. 2008). Photographic surveys indicate that a variety of invertebrate and fish species occur primarily and possibly exclusively in these habitats (Ross and Quattrini 2007, Lessard-Pilon et al. 2010). Some associated species appear to have very specific interactions with *L. pertusa* including the polychaete *Eunice* sp. which may help to assemble coral structure and the coralivorous gastropod *Coralliophila* sp. (Cordes et al. 2008; Becker et al., 2009).

From previous *L. pertusa* community collections in the GoM, it is thought that depth and the relative proportions of live and dead coral are the primary variables that structure *L. pertusa* communities. Depth has been shown to be the most significant variable in numerous community studies in the deep sea, and in the GoM in particular (Cordes et al. 2008, Pequegnat 1990). However, this trend appears to only hold true within a given habitat type, with significant differences found between tube worm and mussel communities at seeps (Cordes et al. 2009) and tube worm and coral communities from the same sites (Cordes et al. 2008). The significance of depth of collection to community structure may be due to a variety of environmental factors that co-vary with depth. These factors, including temperature, pressure, dissolved oxygen concentration, water mass, and aragonite saturation state, may exert a wide variety of effects on the physiology of the species composing the communities at coral sites and may restrict their bathymetric ranges.

In this section we present the results from four approaches based on imagery and physical collections used to gain a better understanding of the community structure, biodiversity and biogeography of deep-water coral communities in the GoM.  The first approach was to use photographic transects (from AUV surveys and randomized parallel ROV transects) to collect data at the largest scale possible within areas of sites supporting coral growth.  This technique provides the best data on density of corals and other fauna within sites with abundant coral growth over large areas, but was not useful to describe coral communities at deep water sites where coral occurrence was very patchy on carbonate boulders and outcrops.  A second approach also used

imagery, but in this case employed construction of photomosaics from imagery taken over haphazardly chosen smaller areas within a site, where numerous coral colonies could be imaged in areas of 10 – 100 m$^2$. A third approach used quantitative collections of the communities associated with the scleractinian corals *L. pertusa* and *M. oculata*. Data collected with this approach was interpreted in conjunction with data from previous studies (Cordes et al., 2008; 2009) using the same equipment and approach. The fourth approach analyzed only the fauna that may be considered symbiotic with corals: the "coral associates" that are attached to or live on the corals.

## 4.1 INSIGHTS INTO COMMUNITY STRUCTURE, BIODIVERSITY AND BIOGEOGRAPHY FROM ANALYSIS OF LARGE-SCALE PHOTOTRANSECTS

### 4.1.1 Introduction

This component of the project examined *Lophelia pertusa* communities at three of the study sites (VK826, VK906, and GB535) on the Northern GoM continental slope. Photographic surveys were used to establish live-to-dead ratios and differences in megafauna for the communities and the community-wide abundance of associated fauna. The sites surveyed had a depth range of 390 to 551 m with a slope range of 0 to 22.8°. GB535 had a slope of 2.8° along the track of the survey and was the deepest of all the sites during the investigation with a depth range of 508 to 551 m. VK906 had the largest range of depth from 490 to 471 m. This also featured the greatest slopes of all the surveyed sites with a range of 12.4 to 22.8°. VK826 had a depth range of 459 to 483 m and a slope that ranged from 0 to 14°.

### 4.1.2 Methods

#### 4.1.2.1 Field Methods

A photographic survey of VK826 (Table 4-1) was collected during August and September of 2009 on the R/V *Brooks McCall*. The survey was completed with the AUV *Sentry* equipped with a Prosilica 1380C camera (pixel dimensions 1360 by 1024, acceptance angles 43° horizontal and vertical) with a Schneider-Kreuznach Cinegon 8 mm lens over a route plotted to collect photos of the *L. pertusa* community below (Figure 4-1A). The photographs were downloaded from the camera to an external hard drive and given file names corresponding to time, date, and photograph number to facilitate geo-reference for the images. The area selected for the AUV survey was located within the Viosca Knoll block 826 (VK826), targeting the major portion of the reef as it was known at that time (Schroeder, 2002). The average altitude for the AUV was 6.68 m.

A second cruise, on R/V *Ronald H. Brown*, during October and November of 2010, used the *Jason II* ROV surveyed coral communities over random transects that targeted known *L. pertusa* communities in VK906, GB535, and a different region at the VK826 site with dense coverage of *L. pertusa* that had been discovered after the 2009 work (Figure 4-1A-C). The average altitude for the ROV survey was 4.74 m. The photographic surveys collected by the *Jason II*, used a Nikon E995 camera (pixel dimensions 2048 by 1536, acceptance angles 54° horizontal, 48° vertical) in a Scorpio underwater housing. Images were stored as jpeg files using the date-time naming convention. The survey regions were rectangular regions of 200 x 200 m or 250 x 250 m positioned

in areas known to contain corals. Prior to beginning the survey, a series of 100-m long transects were chosen at random within the survey area (MacDonald et al., 2010).

Table 4-1.

Summary of photographic samples taken at each site including the number of photographs and total area in meters of the area surveyed.

| Site* | Year | Depth (m) | Latitude | Longitude | Photographs | Photographs with Coral | Total Area (m$^2$) |
|-------|------|-----------|----------|-----------|-------------|------------------------|---------------------|
| VK826 | 2009 | 436-542 | 29 9.5214 N | 88 1.368 W | 1331 | 271 | 33029 |
| VK826 | 2010 | 501-546 | 29 9.2708064 N | 88 1.368 W | 71 | 33 | 851 |
| VK906 | 2010 | 383-465 | 29 4.251 N | 88 23.208 W | 168 | 13 | 2013 |
| GB535 | 2010 | 497-535 | 27 25.6872444 N | 93 34.52 W | 191 | 0 | 2288 |
| * Site names are taken from lease block numbers (See Figure 4-1). | | | | | | | |
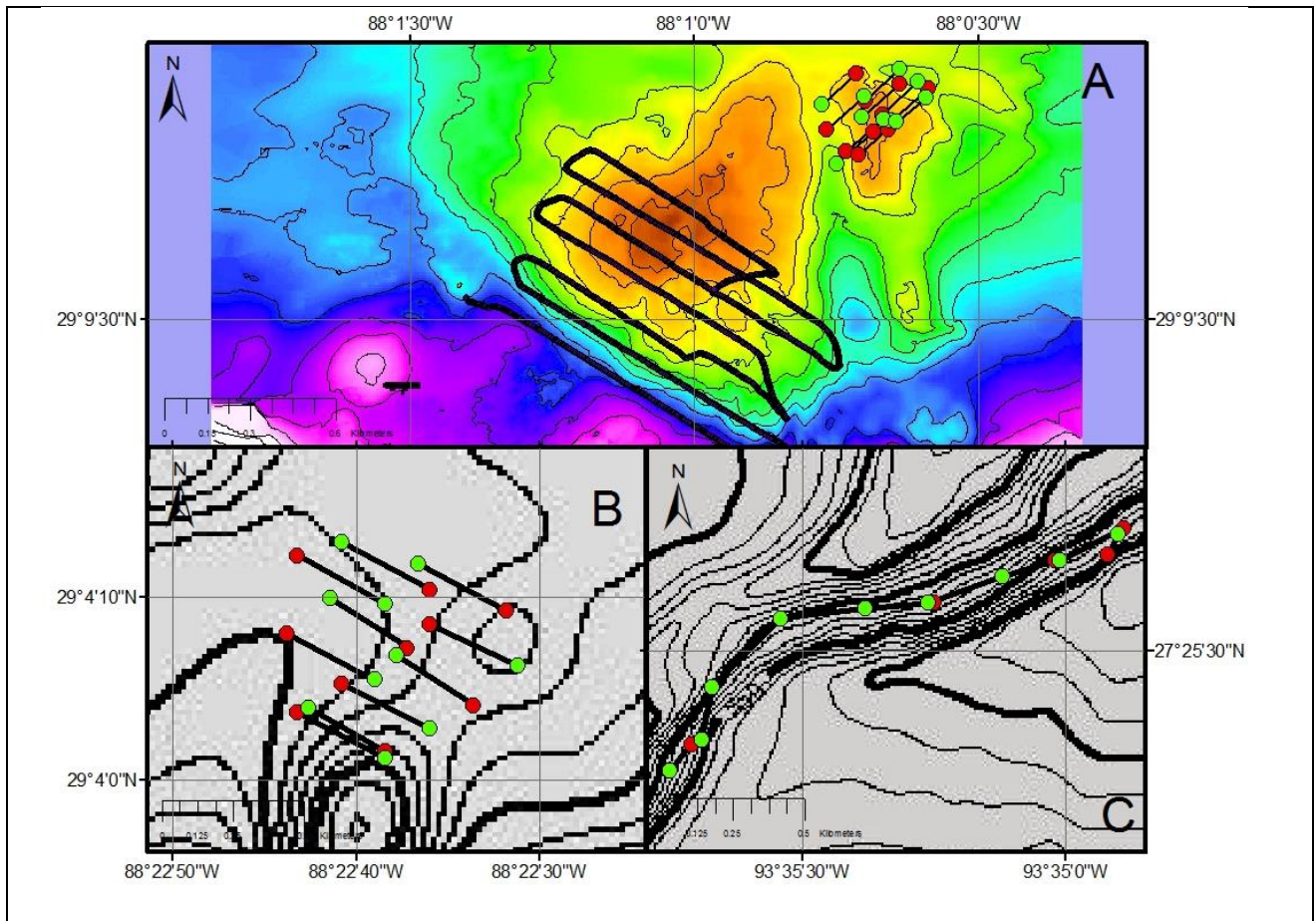


Figure 4-1. Map of regions surveyed using the AUV and ROV. VK826 in 2009 and 2010 (A), VK906 (B), and GB535 (C). Transects from 2010 are denoted by green (starting) and red (stopping) markers.

### 4.1.2.2 Analytical Methods

The photographs were reviewed in detail to determine the presence of *L. pertusa*, other cnidarians and other visible megafauna. When a photograph was found to contain images of *L. pertusa*, the file was analyzed in ImageJ, an image processing program (Burger, 2009), to measure the total area cover of coral, both live and dead. The area of live and dead coral was measured by selecting the perimeter of the coral. The total area of both types of coral was selected and measured, followed by the measurement of the live region of the corals. The dead area was determined by subtracting the live portion of coral from the total amount of coral. These measurements were first collected as the number of image pixels within a perimeter. The scale of the pixels, and the estimated area of coral regions (in $m^2$), was calculated from the horizontal and vertical pixel dimensions of the photographs ($p_h$, $p_v$), horizontal and vertical acceptance angle of the camera lens ($h$, $v$) and the altitude of the camera ($\alpha$) for each photograph (1).

$$horizontal\ pixel\ scale = 2(\tan \alpha \frac{h}{2})/p_h \ \ and \ vertical\ pixel\ scale = 2(\tan \alpha \frac{v}{2})/p_v \ \ (1)$$

The ratio was established by dividing either the live or dead coral by the total amount of coral. Then the percentage was converted to decimals to be used for obtaining the area in $m^2$ of corals in the photographs. Fauna at all sites were identified to the nearest practical taxon (Table 4-2). Unidentified taxa comprised 132 individuals in 9 separate groups and are not listed. Faunal diversity was quantified using the Shannon-Weiner index and all the sites were compared using a Bray-Curtis similarity index based on presence-absence. Total sampling effort for rarefaction was calculated from the area covered in the photographs. Live to dead ratios were compared among surveys by applying a t-test to the mean values in the photographs.

Table 4-2.

Mobile and sessile fauna observed in photographic transects at three study sites.

| Taxa | VK826 (2009) | VK826 (2010) | VK906 (2010) | GB535(2010) |
|---|---|---|---|---|
| Porferia | | | | |
| Porferia spp. | | | 2 | |
| Cnidaria | | | | |
| *Actinoscyphia saginata* | 30 | 3 | 76 | |
| *Actinoscyphia sp. 1* | 13 | 1 | 9 | |
| *Actinoscyphia sp. 2* | | | 24 | |
| *Actinoscyphia sp. 3* | | 17 | | |
| *Actinoscyphia sp. 4* | | | 5 | |
| *Actinoscyphia sp. 5* | 13 | | | |
| Cnidaria: Solitary corals | | | | |
| *Callagorgia americana* | | 4 | | |
| Gorgonacea sp. | 5 | | | |
| *Leiopathes sp.* | 54 | 3 | 26 | |
| *Stichopathes sp.* | | | | 30 |
| Unid coral | 20 | | 1 | |
| Annelida: Polychaeta | | | | |
| Lamellibrachia sp. | 9 | 1 | | |
| Serpulidae sp. | | | 1 | |
| Unid polychaete 1 | 1 | | | |
| Unid polychaete 2 | | | 3 | |
| Mollusca: Cephalopoda | | | | |
| Unid squid | | | 3 | |
| Arthropoda: Crustacea | | | | |
| *Bathynectes longispinia* | 4 | | 1 | 4 |
| *Bathynomous giganteus* | 1 | | | 1 |

Table 4 2. Mobile fauna observed in photographic transects at three study sites. (continued).

| Taxa | VK826 (2009) | VK826 (2010) | VK906 (2010) | GB535(2010) |
|---|---|---|---|---|
| *Chaceon fenneri* | 14 | 1 | 3 | |
| *Eumunida picta* | 41 | 17 | | 6 |
| Eumunida sp. 1 | | | | 1 |
| Eumunida sp. 2 | 2 | | | |
| *Pleoticus robostus* | 1 | | 7 | |
| *Systellaspis pellucida* | 5 | | | |
| *Rochinia crassa* | 1 | | 2 | 1 |
| Arthropoda: Pycnogondia | | | | |
| Pycnogonida sp. 1 | | 4 | | |
| Pycnogonida sp. 2 | 2 | | | |
| Echinodermata | | | | |
| Asterioda spp. 1 | 25 | 3 | 7 | |
| Asterioda spp. 2 | 11 | | | |
| Brisingida sp. | | | | 1 |
| *Centrostephanus longispinus rubricgulus* | | 14 | | |
| *Comactinia meridionalis hartlaubi* | 3 | | | |
| Echinoidea spp. 1 | 82 | | | |
| Echinoidea spp. 2 | | 4 | 1 | |
| Luidia sp. | 7 | | 1 | |
| *Novodinia antellensis* | | | 7 | 4 |
| Ophiuroidea sp. | | 3 | | |
| *Stylocidaris affinis* | 20 | 2 | | |
| *Tethyaster grandis* | 8 | | | 1 |
| Chordata: Actinopterygii | | | | |
| *Cephalopholis cruentata* | 5 | | | |
| *Gephyroberyx darwinii* | 1 | | | |
| *Chaunax suttkusi* | | | | 1 |
| *Hoplpstethus atlanticus* | 39 | | | |
| *Hyperglypha perciformis* | 25 | 3 | 1 | 2 |
| *Prionotus paralatus* | | | 2 | |
| Synodus sp. | 31 | | | |
| *Urophycis cirrata* | 57 | 5 | 19 | 7 |
| *Nezumia aequalis* | | | 1 | |
| Chordata: Chondrichthyes | | | | |
| Unid shark | 1 | | 1 | |
| Chordata: Sirenidae | | | | |
| Psuedobranchus sp. | 16 | | | |

### 4.1.3 Results

### *4.1.3.1 Live-to-Dead Ratios*

Summary results for the live-to-dead ratio of corals observed at the three sites are shown in Figure 4-2. The AUV survey at VK826 in 2009 comprised an area of 33,029 m$^2$; 96% of the area surveyed had no coral cover. The total area of living and dead corals was 1,289 m$^2$. The live-to-dead ratio was 0.241. The average amount of coral framework coverage per photograph containing coral was 4.74 m$^2$ with 0.72 m$^2$ being live coral. The ROV transects at VK826 in 2010 covered 851 m$^2$. The photographs revealed 67% of the area containing no coral coverage. The total area of coral was 280 m$^2$. The live-to-dead ratio was 0.137. The photographs containing coral had an average of 8.48 m$^2$ of coral with 1.64 m$^2$ of the coral being live. The ROV photographic transects at VK906 in 2010 covered an area of 2013 m$^2$. The photographs showed no coral coverage for 97% of the area. Total coral coverage was 53 m$^2$. The live-to-dead ratio was 0.131. The photographs containing coral had an average of 4.41 m$^2$ of coral with 0.30 m$^2$ being live. The live-to-dead ratios observed in the VK826 site in 2009 were significantly greater than observed in another area of VK826 in 2010 (T-test of means, P < 0.05). However there was not a significant difference in the live-to-dead ratio observed during the 2010 surveys of VK826 and VK906, respectively (T-test of means, P > 0.95). The survey transects at GB535 covered an area of 2288 m$^2$. The photographic survey at this site resulted in no coral cover observed.
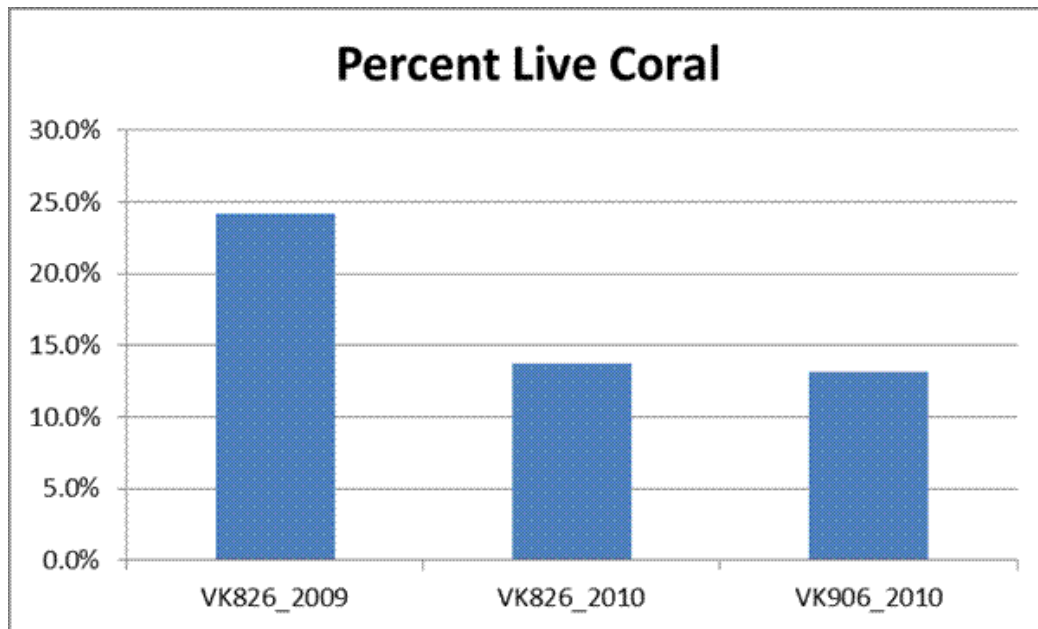


Figure 4-2. Average percentage of live coral cover observed at project sites VK826 and VK906 (None observed at GB535). The 2009 and 2010 results are for surveys of different regions of the VK826 site. See Figure 4-1 for detail.

### 4.1.3.2  Description of Communities

Both areas at Viosca Knoll 826 included large coral mounds that are 5 m wide and a minimum of 1 m tall. These mounds were comprised largely of dead coral matrix that contained sediment and resident mobile fauna. The tips of branches were generally where the living (white) coral was found. The large colonies formed sub-circular terraces across the slope. In the densest areas of mounds, the terraces were almost contiguous. The large mounds were surrounded by coral rubble and small living communities. Most pieces of rubble were just a few centimeters in length. The coral rubble had signs of sediment accumulation in the rubble. Some of the rubble had patches up to 0.5 m in diameter of bacterial mats growing on them; the mats were grey, light brown, and white in color. These mounds had mobile fauna hiding in the dead coral matrix as well as on top of the living material. Crustaceans (*Eumundia picta*) and urchins were seen on top of the living coral, while fish were observed inside the dead coral matrix. Filter-feeding associates were not generally seen on the largest coral banks.

The profile of a typical large carbonate terrace would have a scattering of dead and broken mussel shells at the base than a steep rise of 0.5 to 2.5 m. At the upper edge of the rise, and extending onto flat portion of the outcrop, large, closely spaced colonies of the sea fan *Callagorgia americana* were often seen as were colonies of *Leiopathes glaberimma*.  Mounds smaller in size, 2 m in diameter, were also seen throughout the site. These mounds were similar to the larger mounds with their construction. They were solitary and had rings of coral rubble around them. Unlike the larger mounds, they had filter-feeders attached to the coral matrix along with mobile fauna.

Other areas of the site contained small communities of *Lophelia* of 0.5 m in diameter that were 0.5 to 1 m apart. These communities were attached to visible carbonate substrate and had anemones and serpulidids nearby or attached to the same substrate. These areas were towards the edges of the reef community and had a scattered trail of coral rubble leading to them from the mounds above. Anemones were settled randomly in patches of up to 5 per m$^2$ along this rubble field.  The bottom-most part of the slope surveyed had sediment that consisted mainly of clay that contained tens of burrows per photograph with fauna tracks in every direction and pockmarks throughout. This area contained no coral rubble and very little life was visible, although tracks were all over the area.

Viosca Knoll 906 had coral mounds, up to 2 m in diameter, at the highest point of the survey. These mounds were similar to ones of a similar size at VK826. The mounds were mainly constructed of a dead coral matrix with living tips at the top of the mound. The dead coral matrix was home to filter feeders and soft coral. Crustaceans, fish, and urchins also called the matrix home. The living coral material, which became as large as 0.5 m$^2$ patches, had crustaceans and urchins on it. Around the mounds, areas of high coral rubble fields were colonized by anemones, octocorals, and black corals. The rubble in most cases has sediment, most likely silts and sands, covering it partially. This dense field of coral rubble had many crustaceans, enchinoderms, fish, and urchins throughout. The corals and anemones were seen in densities of up to 5 per m$^2$.

Continuing down the slope, the amount of coral rubble decreased. More of the clay sediment of the seafloor became visible, while the coral rubble appeared to have more coarse sediment on and directly around it. The rubble was colonized by anemones and red *Leiopathes glaberrima*, but in lower abundance than the higher coral rubble area up slope.   At the deepest portion of the survey

123

area, the rubble disappeared and the seafloor sediments were visible. This area contained burrows, pockmarks, and tracks of mobile faunal throughout. This area was sparsely colonized by sea fans and anemones. All the mobile fauna seen in the shallower portion of this site were also observed here with the addition of polychaetes. The Venus flytrap anemone (*Actinoscyphia saginata*) and an unknown species of anemone were observed singly and in groups among the soft sediments of the deeper portion of the VK906 site.

No coral mounds were seen in the Garden Banks 535 random photographic transects. Living corals were, however, observed elsewhere in the overall area. The survey documented several patches of coral rubble among the carbonate outcroppings. The rubble was dead material with little sign of sedimentation unlike the other sites at Viosca Knoll. The patches were around 2 m in diameter and had gorgonians on the rubble.

The majority of the site was stretches of fine sediments with intermittent carbonate outcroppings (>1 m diameter). The sedimented areas feature numerous burrows, pockmarks and lebensspuren like the other sites. Crustaceans and fish were seen throughout the clay areas. The areas containing the carbonate outcroppings generally had octocorals and demosponges, from the family Coralistidae. One of the areas featured a grey bacterial mat with a white outer edge. The demosponges were up to 0.5 m in diameter. A few of demosponges also had crustaceans on or near them.

One large carbonate platform greater than 3 m in width was seen and had several demosponges on its surface. An area containing small, less than one meter carbonate outcroppings had the remnants of a mussel bed scattered throughout. This mussel bed was similar to the one observed at other sites with partially buried and degraded shells, although some of the shells had soft corals attached to them.

### 4.1.3.3 Mobile Fauna

The mobile fauna observed in the photographs presented in a number of different modes. The crustaceans had a tendency to be hidden in or on the coral mounds and by other filter feeders. Some fauna were easily visible resting over the sediment, while under the coral mounds, only the tails of some fish could be seen. Sixty different taxa were observed from the transect photographs (Table 4-2). Each survey contained between 15 and 35 taxa (identified to the lowest practical taxon). A previous study measured species diversity on *Lophelia* reefs offshore Norway and found Shannon-Weiner diversity index value of 5.50 (Jensen and Frederiksen, 1992). Values for the reefs surveyed during the present study ranged from 1.75 to 3.01. The similarity of species for VK826 in 2009 to 2010 was 62.84 using a Bray-Cutis similarity index. VK826 in 2009 and 2010 had similarities to VK906 of 65.03 and 64.21. GB535 had a similarity of 58.86 to VK826 in 2009 and 62.09 in 2010. The similarity to VK906 was 54.75. Rarefaction curves (number of new species per individual sampled at each site) for species richness (Figure 4-3) showed a tendency to level off after 80 to 500 samplings. The VK826 survey in 2009 encountered the most species (35) and individuals (556). The 2010 survey at VK826 found fewer species (18) and individuals (89), and all of the species had been seen in the previous year. VK906 had 27 different species and 302 individuals, while GB535 had 15 species and 62 individuals.
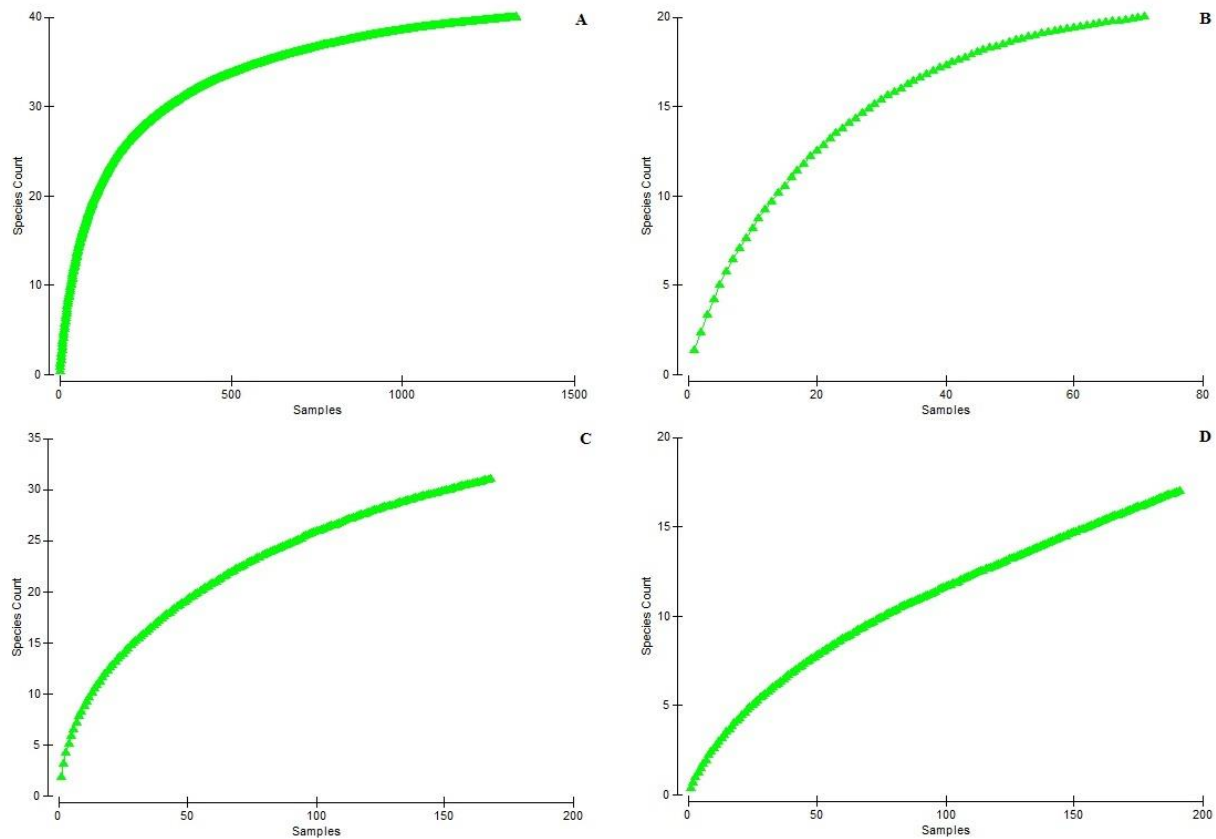
Figure 4-3. Rarefaction curves for photographic sampling of mobile fauna observed in photographic transects at three project sites: A, VK826 (2009); B, VK826 (2010); C, VK906; D, GB535.

### 4.1.4  Discussion

In regions where *Lophelia pertusa* are known to be abundant, *L. pertusa* colonies, including living and dead cover a small fraction of the total bottom area (4.25±15.5%). The *L. pertusa* communities' live-to-dead ratio shows that 1/4 or less of the surface area of coral substrate contains living colonies. These results record the current status of the coral communities surveyed on the Northern GoM continental slope, and can be used as a baseline to study the possible long-term, sub lethal effects from the *DWH* oil spill on the surveyed communities. No immediate damage from the *DWH* oil spill was apparent at VK826 in the live-to-dead ratios from 2009 to 2010.

The difference in live to dead coral cover observed during the different surveys probably reflects the different survey methods and the areas targeted.  The dive tracks for the AUV/ROV are different for the two years. A regular grid, covering a major portion of the reef in that part of the site, was used in 2009, while the 2010 transects were placed randomly over a different 250 X 250 meter area chosen because of high *L. pertusa* density in that area. (MacDonald et al., 2010). Consequently, the 2009 survey found a much smaller fraction of the total survey area with coral cover than any of the 2010 surveys that observed corals.  The fact that the live to dead ratios observed in the 2010 surveys for VK826 and VK906 were significantly lower than in the 2009

survey probably reflects local differences within the larger reef area. Another factor with the potential to affect the live to dead ratio is the age of the reef and time over which dead *L. pertusa* has accumulated or the rate at which local sedimentation buries the non-living coral framework.

The decreasing number of taxa can also be seen comparing VK826 to VK906 and for GB535. Even accounting for sampling differences, increases in depth and proximity, moving away from the Mississippi River outfall, are reflected in decreases in meiofaunal biomass (Baguley et al., 2006). Certain taxa found at Viosca Knoll maybe more adapted for a higher nutrient environment (Cordes et al., 2008), explaining why there is the shift in taxa from Viosca Knoll to the Garden Banks block. The rarefaction curves (Figure 4-3) leveled off between 80 and 500 samplings, which indicate that additional sampling would not have yielded substantially more taxa among the associated fauna. The rarefaction curve for the GB535 site showed the least tendency to reach an asymptote. Taxa richness was lowest at the GB535 site as well, with almost 50% (30) of the individuals captured represented by a single taxon. The difference seen in the taxa at VK826 site between 2009 and 2010 is likely due to the high number of photographs reviewed for the 2009 survey, which covered almost the entire south western portion of the reef while the 2010 transects covered a smaller more concentrated portion of the north east corner of the reef.

## 4.2 INSIGHTS INTO COMMUNITY STRUCTURE, BIODIVERSITY AND BIOGEOGRAPHY FROM ANALYSES OF PHOTOMOSAICS

### 4.2.1 Introduction

A total of 22 photomosaic stations were established in 12 different study sites. Nine of these were only photomosaicked in one year of the project and 13 of them were imaged during cruises on the *Ronald H. Brown* in both 2009 and 2010. These sites were established with three primary goals in mind. The first was to allow comparison between different study areas and across depths using quantitative data of characteristic communities from that site. The second was to begin to investigate temporal change in these communities. Since the images were collected only two years apart, it is too early for robust growth estimates or to see significant changes in the slow growing colonial coral populations; however, comparisons between years provide preliminary information on the stability of the attached fauna and the fidelity of the mobile fauna. The third was to establish baseline stations to follow temporal change over longer time periods and to monitor for anthropogenic impact. BOEM's foresight in establishing these stations was evident after the *DWH* blowout, when the first deepwater megafauna stations chosen for investigation by the NRDAt effort were our study sites at VK906, VK826, and MC751. An attempt was also made to revisit the site first established during the *Lophelia* I project in VK862. Lack of high-quality navigation during the *Lophelia* I project prevented finding and re-occupying that site. However, the stations established during the 2009 *Ron Brown* cruise were re-occupied within weeks of the capping of the Macondo well, and new mosaic stations were established in VK862. All of these and most others established in 2009 were revisited during the 2010 *Ron Brown* cruise for comparison to the pre-spill mosaics.

## 4.2.2 Methods

### 4.2.2.1 Selection of Areas for Mosaics

A total of 22 areas were chosen for mosaics in 12 of the sites selected for this project (Table 4-3). The areas were not chosen randomly, but rather selected because of the presence of corals, usually associated with a single boulder or carbonate outcrop. In order to obtain sufficient resolution in downlooking images to meet the goals for this aspect of the project, it was necessary to collect the images from an altitude of less than 5 m. This limited the total area that could be included in a mosaic, and as a result, a primary criterion in selection of areas for mosaics was a relatively high density of colonial corals. A second first order criterion was practical; local topography had to allow an ROV to maintain a fairly constant altitude over the area. Since a primary focus of the project was the coral *Lophelia pertusa*, we focused on areas that included this coral if it was present at the site being studied. When a site was characterized by the presence of different corals or mixtures of corals, areas with high densities of the corals typical for the site were chosen. After an area was chosen to mosaic, a marker was deployed to facilitate re-occupation of the site and to provide a check for scale calculations from navigation and lasers. Location of the marker was determined using USBL navigation averaged over the time the ROV spent working in this area.

Table 4-3.

Photomosaic designations, locations, visit dates, and areal extents

| Station name | Site | Date imaged (YYYY-MM-DD) | Dive | Area (m²) | Depth (m) | Latitude | Longitude |
|---|---|---|---|---|---|---|---|
| A | AT047 | 2009-08-24 | J2-457 | 39.5 | 839 | 27.8803 | 89.7887 |
| B | GB299 | 2009-08-27 | J2-459 | 55.5 | 360 | 27.6865 | 92.2308 |
| B | GB299 | 2010-10-20 | J2-530 | 39.0 | 360 | 27.6865 | 92.2308 |
| C | GB535 | 2009-08-28 | J2-460 | 39.2 | 516 | 27.4280 | 93.5835 |
| C | GB535 | 2010-10-20 | J2-531 | 53.6 | 516 | 27.4280 | 93.5835 |
| D | GB299 | 2009-08-26 | J2-459 | 75.9 | 359 | 27.6865 | 92.2310 |
| D | GB299 | 2010-10-20 | J2-530 | 57.7 | 359 | 27.6865 | 92.2310 |
| E | GB535 | 2009-08-28 | J2-460 | 8.6 | 520 | 27.4271 | 93.5854 |
| E | GB535 | 2010-10-21 | J2-531 | 41.6 | 520 | 27.4271 | 93.5854 |
| G | MC751 | 2009-09-01 | J2-464 | 34.3 | 441 | 28.1937 | 89.7987 |
| G | MC751 | 2010-10-27 | J2-536 | 77.1 | 441 | 28.1937 | 89.7987 |
| H1 | MC751 | 2009-08-31 | J2-464 | 52.4 | 441 | 28.1940 | 89.7983 |
| H1 | MC751 | 2010-10-26 | J2-536 | 23.8 | 441 | 28.1940 | 89.7983 |
| H2 | MC751 | 2009-09-01 | J2-464 | 29.7 | 441 | 28.1940 | 89.7983 |
| H2 | MC751 | 2010-10-26 | J2-536 | 30.2 | 441 | 28.1940 | 89.7983 |
| J | VK906 | 2009-09-02 | J2-465 | 30.4 | 389 | 29.0697 | 88.3771 |
| J | VK906 | 2010-10-24 | J2-534 | 63.0 | 389 | 29.0697 | 88.3771 |
| L | VK906 | 2009-09-02 | J2-465 | 54.9 | 394 | 29.0693 | 88.3776 |
| L | VK906 | 2010-10-24 | J2-534 | 60.1 | 394 | 29.0693 | 88.3776 |
| M | VK826 | 2009-09-03 | J2-466 | 43.2 | 470 | 29.1581 | 88.0169 |
| M | VK826 | 2010-10-16 | J2-526 | 29.7 | 470 | 29.1581 | 88.0169 |
| N | VK826 | 2009-09-03 | J2-466 | 51.7 | 476 | 29.1578 | 88.0163 |
| N | VK826 | 2010-10-16 | J2-526 | 39.6 | 476 | 29.1578 | 88.0163 |
| O | VK826 | 2009-09-04 | J2-466 | 39.1 | 463 | 29.1648 | 88.0116 |
| O | VK826 | 2010-10-31 | J2-540 | 108.7 | 463 | 29.1648 | 88.0116 |
| Q | VK826 | 2009-09-04 | J2-467 | 48.8 | 479 | 29.1587 | 88.0105 |
| Q | VK826 | 2010-11-01 | J2-540 | 78.3 | 479 | 29.1587 | 88.0105 |
| R | VK862 | 2010-10-26 | J2-535 | 38.5 | 317 | 29.1063 | 88.3842 |
| T | VK862 | 2010-10-26 | J2-535 | 53.0 | 310 | 29.1067 | 88.3843 |
| T1_T2 | MC118 | 2010-10-30 | J2-538 | 25.5 | 884 | 28.8527 | 88.4927 |
| U | MC885 | 2010-10-17 | J2-527 | 26.4 | 633 | 28.4733 | 89.7171 |
| V/M1 | GC354 | 2010-10-19 | J2-529 | 20.9 | 526 | 27.5979 | 91.8264 |
| W | GC140 | 2010-10-22 | J2-532 | 184.9 | 254 | 27.8105 | 91.5370 |
| X | MC118 | 2010-10-30 | J2-538 | 50.2 | 883 | 28.8527 | 88.4925 |
| Y | VK906 | 2010-10-25 | J2-535 | 58.9 | 395 | 29.0690 | 88.3777 |
| AA | MC338 | 2010-11-03 | J2-541 | 307.3 | 1371 | 28.6722 | 88.4765 |
| 5 | GC852 | 2009-08-29 | J2-461 | 38.7 | 1400 | 27.1098 | 91.1661 |

## 4.2.2.2 Image Collection

Downlooking images were acquired with a Nikon E995 digital still camera in a pressure housing mounted on the ROV *Jason II*, operated from the NOAA Ship *Ronald H. Brown*. Illumination was provided with a combination of an hydrargyrum medium-arc iodide lamp light, one or two light-

emitting diode (LED) arrays and a 300 Watt per second strobe, used as appropriate in different terrains, altitudes, and with different color subjects. Down-pointing parallel lasers spaced 30cm apart provided a scale reference internal to each image.

The ROV was maneuvered into one corner of the area to be mosaicked and camera/strobe setting optimized for this location. During collection of the imagery, navigation was accomplished using a closed loop system with a Doppler-velocity navigation stream so the pilot was not flying with the control stick, but rather entering movements digitally. The vehicle heading and altitude was held constant during each mosaic and between years for the same site. The pilot would enter a move (distance) and velocity that allowed collection of a series of overlapping images at the set heading and altitude, and pictures were obtained with approximately 50% overlap between images. At the end of a line, the pilot would enter a lateral move leaving 50% overlap with the previous line and move in reverse an equal distance, ending up with a 50% lateral overlap with the first image. The pilot would again move the ROV laterally and repeat this process until the subject area had been covered with overlapping parallel strips of images. Each image was associated with geographic coordinates from the Doppler velocity navigation stream which normally remained accurate to within a few cm over the course of image collection for an individual mosaic.

Due to variability in conditions at the different monitoring stations, such as turbidity and required altitude to avoid damage to the site, the quality of images varied somewhat between sites and dives. However, images were normally sufficient to identify organisms and objects down to about 1-2 cm in size.
In addition, four stations were established with mosaics imaged from a side-looking perspective. These were analyzed qualitatively and not digitized.


### 4.2.2.3  Creation of Mosaics

Images used in the construction of mosaics were selected for clarity and with a minimum of 20% overlap between subsequent images in a line. The images collected in 2009 were assembled into strips using an algorithm (Pizarro and Singh 2003) implemented as a script in MATLAB version 2010B (Mathworks 2010) and then the strips were manually stitched together into the final mosaic with the Photomerge tool in Adobe Photoshop CS3 (Adobe 200x). Increases in computing power and improvements in the code allowed images collected in 2010 to be assembled into the final mosaics with the Pizarro and Singh (2003) algorithm implemented as a script in MATLAB version 2010B (Mathworks 2010) (See section 4.2.3.1). The resulting mosaic was geo-referenced using coordinates from the center of two images in opposite corners of the mosaic using a geographical information system (GIS) implemented in ArcGIS 10.1 (ESRI 2012) and a projected coordinate system using WGS84 datum.

### 4.2.2.4  Digitizing Mosaics

All fauna in each mosaic were identified to the lowest possible taxonomic level and together with biological substrates were digitized to allow quantitative analysis of the communities and comparisons among the mosaics (See Section 4.2.3.1). Colonial cnidarians, tube worms, encrusting sponges, and areas of dead coral skeletons were digitized as polygons for analysis as potential biological substrates as well as to record presence and location within the mosaic.

Polygon categories included live and dead *Lophelia pertusa*, live and dead *Madrepora oculata*, *Callogorgia* sp. *(*and one dead *Callogorgia* sp*.), Paramuricea spp.*, *Paragorgia* spp., *Antipathes* spp., *Leiopathes* spp., *Stichopathes* spp., *Swiftia pallida*, *Isididae* spp., *Muriceides* cf. *hirta*, *Clavularia rudis*, *Acanthogorgia aspera*, sea pens, other antipatharian corals, unidentified corals, tube worms, encrusting sponges, and hydroids. Solitary fauna were digitized as points, and included five types of crabs, six anemones, four types of sea urchins, whip corals, brittle stars, mussels, clams, giant isopods, individual sponges, crinoids, 11 types of fish, eight types of sea stars, and sea cucumbers. Location-based queries were used to determine the distribution of the solitary fauna across each of the potential substrata (polygons).

### 4.2.2.5 Georeferencing between Years

To compare 2009 and 2010 digitized mosaics, a geographic transformation was applied to the 2009 mosaics to allow the two years to be superimposed upon each other. This was necessary due to slight differences in the altitudes and exact placement of the lines run during image collection in the two years. The geographic transformation used a minimum of 10 coincident control points on each mosaic. The coincident control points were used to "spline" the 2009 mosaic to best match the 2010 mosaic. The geographic "spline" transformation locks the source control points to the target control points, and forces the raster pixels between control points to warp. Since the original digitized "vector polygons" could not be directly transformed, the polygons were rasterized before applying the geographic transformation. The transformed raster was converted back to vector polygons for quantitative analysis with the overlapping 2010 polygons. In most cases this process resulted in minimal warping of the 2009 image; however, in a few cases, obvious warping of the 2009 image was evident after the transformation (i.e., mosaic at marker J in VK906,
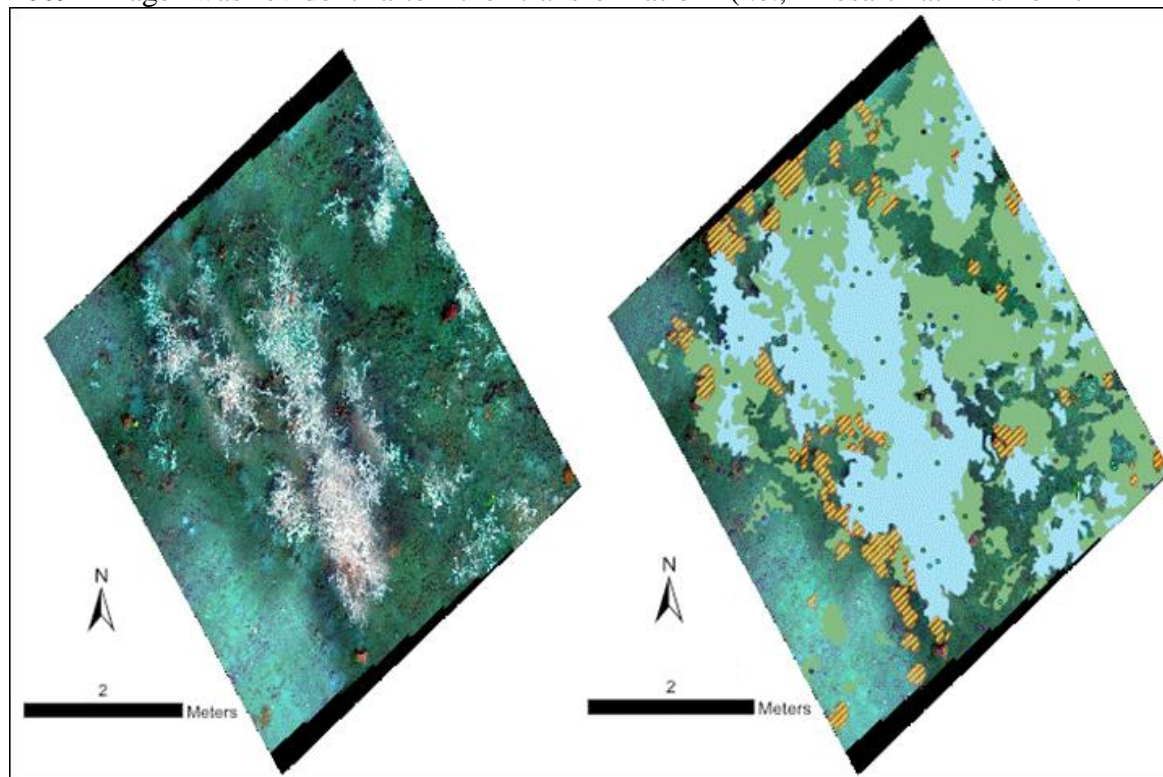
Figure 4-12).  For the comparisons between years, only the overlapping areas of each mosaic that were mosaicked in both years were used, and all differences noted in automated analyses were hand checked to original images.

## 4.2.2.6  GIS and Statistical Comparisons

Diversity was assessed as standardized species richness (calculated as the number of species present within a mosaic divided by the area of the photomosaic), as well as the Shannon diversity index (natural log scale), Simpson's diversity index $(1 - \lambda')$, and Pielou's evenness index, using all organisms that could be enumerated in the images (excluding polygons). The Shannon and Simpson's diversity indices and Pielou's evenness index were calculated using the DIVERSE application in PRIMER 6/ PRIMER-E (Clarke and Warwick 2001).

Similarities in community composition between photomosaic sites and between years were calculated using the Bray-Curtis similarity index in PRIMER 6 (PRIMER-E 2009) after fourth-root transformations. Presence/absence data was also used to analyze both solitary and aggregated fauna (Cordes et al., 2006, and references therein). Non-metric Multi-Dimensional Scaling (nMDS) ordination and average linkage cluster analyses were used to examine similarities among community compositions of the photomosaic sites. Chi-square analyses tested whether there were significant associations between point fauna and substrata within selected photomosaic sites.

## 4.2.3  Results and Discussion

## 4.2.3.1  Summaries of Photomosaics of Coral Communities

Below are summaries of all mosaics constructed from images collected over the course of this project. All are associated with physical markers and their locations are well navigated.  Most have been visited and re-mosaicked at least once.  Below each verbal summary is a low-resolution image of the mosaic and its digitized version.  All digitizations use the same key (Figure 4-4). The full resolution versions of each mosaic, with both the original and re-georeferenced versions of the 2009 mosaics are in Appendix C-2 and C-3.

## Legend

| | | | |
|---|---|---|---|
| ● | Anemone | ▨ *Antipathes* | |
| ● | Brittle star | ▨ *Callogorgia* sp. | |
| ○ | *Cirrhipathes* | ▨ Hydroid | |
| ● | Crab | ▨ Isididae | |
| ● | Crinoid | ▨ *Leiopathes* sp. | |
| ● | Fish | ▨ *Lophelia pertusa* (dead) | |
| ○ | Isopod | ▨ *Lophelia pertusa* (live) | |
| ● | Mussel | ▨ *Madrepora* sp. (dead) | |
| ○ | Pycnogonida | ▨ *Madrepora* sp. (live) | |
| ○ | Sea star | ▨ *Muriceides* sp. | |
| ● | Shrimp | ▨ Other coral | |
| ● | Sponge (individual) | ▨ *Paragorgia* sp. | |
| ● | Squid | ▨ *Paramuricea* sp. | |
| ● | Urchins | ▨ Sponge (encrusting) | |
| ● | Whelk | ▨ *Stichopathes* sp. | |
| | | ▨ Tubeworm | |

Figure 4-4. Key for all digitized photomosaics in this section (4.2.3.1).

## 4.2.3.1.1 GC140: Mosaic Marker W, 2010 (only)

This site is located at 27.81052°N 91.53705°W at a depth of about 254 m. Images for the mosaic were collected on dive J2-532 on 10/22/10. The mosaic covers an area of approximately 185 m$^2$. This mosaic features a large carbonate rock outcropping covered in black and bamboo corals. A few *Stichopathes* sp. and *Paramuricea* sp. are also found at the site along with some unidentified corals. Individual and encrusting sponges can be seen distributed across the site. Mobile fauna include seven anemones, two *Epinephelus niveatus* fish, two *Hoplostethus occidentalis* fish, and 33 ophiuroids.
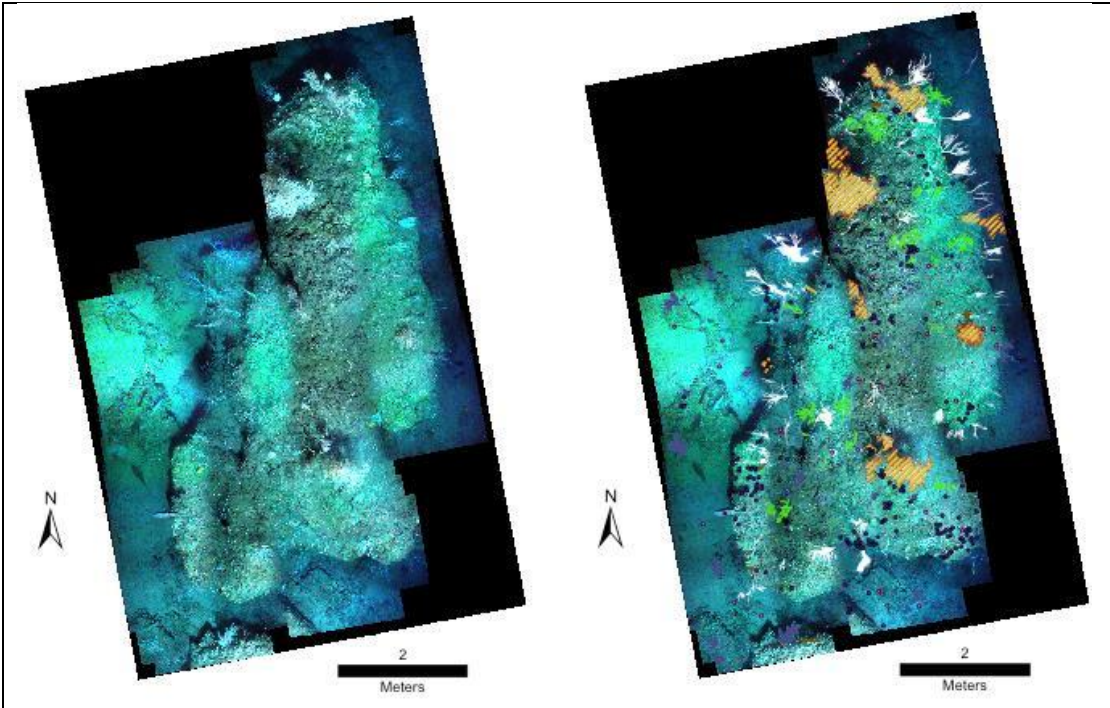
Figure 4-5. Photomosaic of Marker W in 2010 and digitization of this mosaic.

## 4.2.3.1.2 VK862: Mosaic Marker R, 2010 (only)

This site is located at 29.10635˚N 88.38422˚W at a depth of about 317 m. Images for the mosaic were collected on dive J2-535 on 10/26/10. The mosaic covers an area of approximately 38.5 m². The mosaic centers around a raised outcropping covered in sponges, anemones, *Leiopathes* sp., *Callogorgia* sp., and *Lophelia pertusa.* The *Lophelia* is found on the northern half and additional *Callogorgia* sp. are found to the west of the outcropping. To the north there are more colonies of *Leiopathes* sp. and *Callogorgia* sp. present. Anemones and sponges surround the outcropping on the seabed. The southernmost corner of the mosaic features a large *Muriceides* sp. colony. Mobile fauna at this site include six *Hyperoglyphe perciformis* fish, ten crabs, one sea star, and 513 total anemones.

133
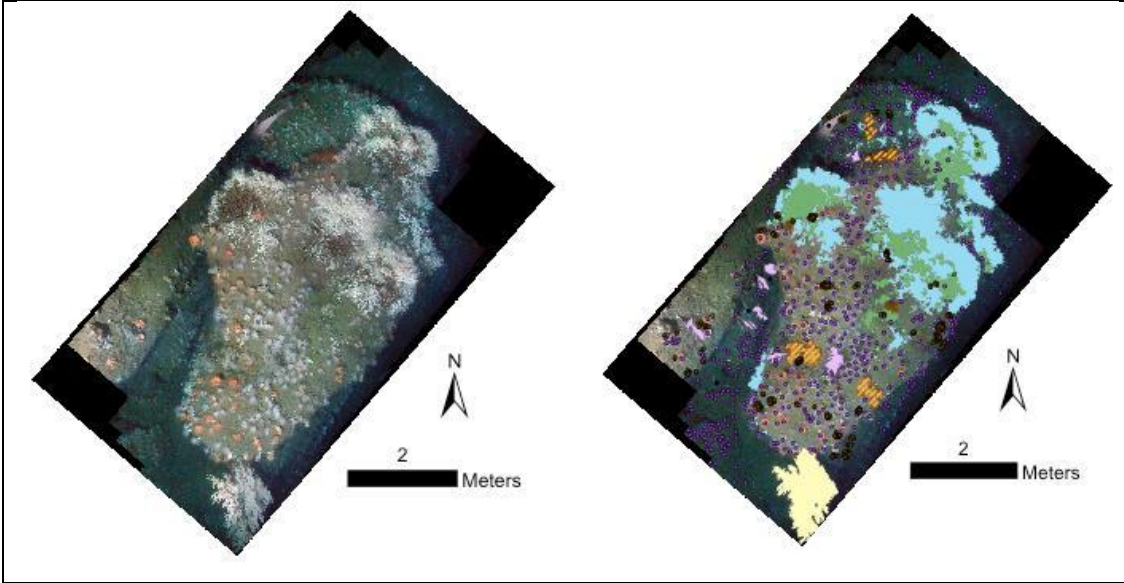
Figure 4-6**.** Photomosaic of Marker R in 2010 and digitization of this mosaic.

## 4.2.3.1.3 VK862: Mosaic Marker T, 2010 (only).

This site is located at 29.10667˚N 88.38426˚W at a depth of about 310 m. Images for the mosaic were collected on dive J2-535 on 10/26/10. The mosaic covers an area of approximately 53.0 m$^2$. Anemones dominant this mosaic and 755 individuals are observed at this site. Isididae and *Leiopathes* sp. are also found here. A shallow cliff is observed going from the western to the northern and then eastern edges of the map. Mobile fauna include one *Hoplostethus occidentalis* fish, one *Hyperoglyphe perciformis* fish, and two urchins.
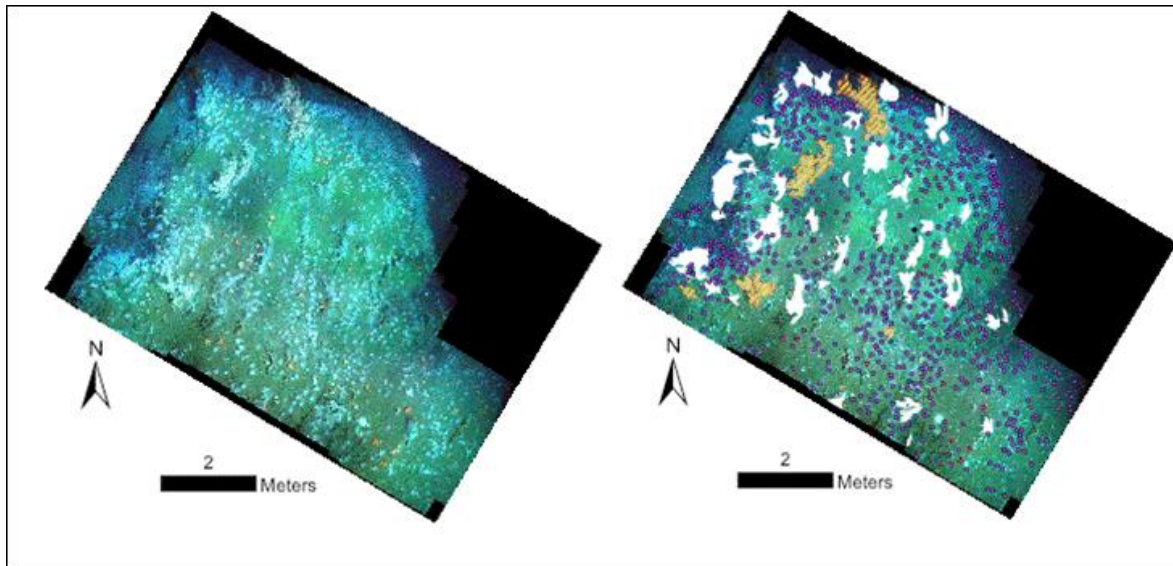


Figure 4-7. Photomosaic of Marker T in 2010 and digitization of this mosaic.

### 4.2.3.1.4 GB299: Mosaic Marker B

This site is located at 27.68648˚N 92.23084˚W at a depth of approximately 360 m.  The substrate in this mosaic is mud and the area is dominated by *Callogorgia* sp. with a few *L. glaberrima*, whip corals, and *Paramuricea* sp.

#### 4.2.3.1.4.1 GB299: Mosaic Marker B, 2009

Images for the mosaic were collected on dive J2-459 on 8/27/09.The mosaic encompasses a roughly rectangular area of about 55.5 m$^2$. *Callogorgia* sp. is the most abundant coral and is observed across the site distributed relatively evenly with slightly less density around the southeast and northwest corners. Four *Paramuricea* sp. and five *Leiopathes* sp. are also located across the site. One hundred sixty-three ophiuroids are observed, the majority of which are in association with the *Callogorgia* sp. Thirteen anemones, seven crinoids, four whip coral, and 60 encrusting sponges are found distributed across the site.
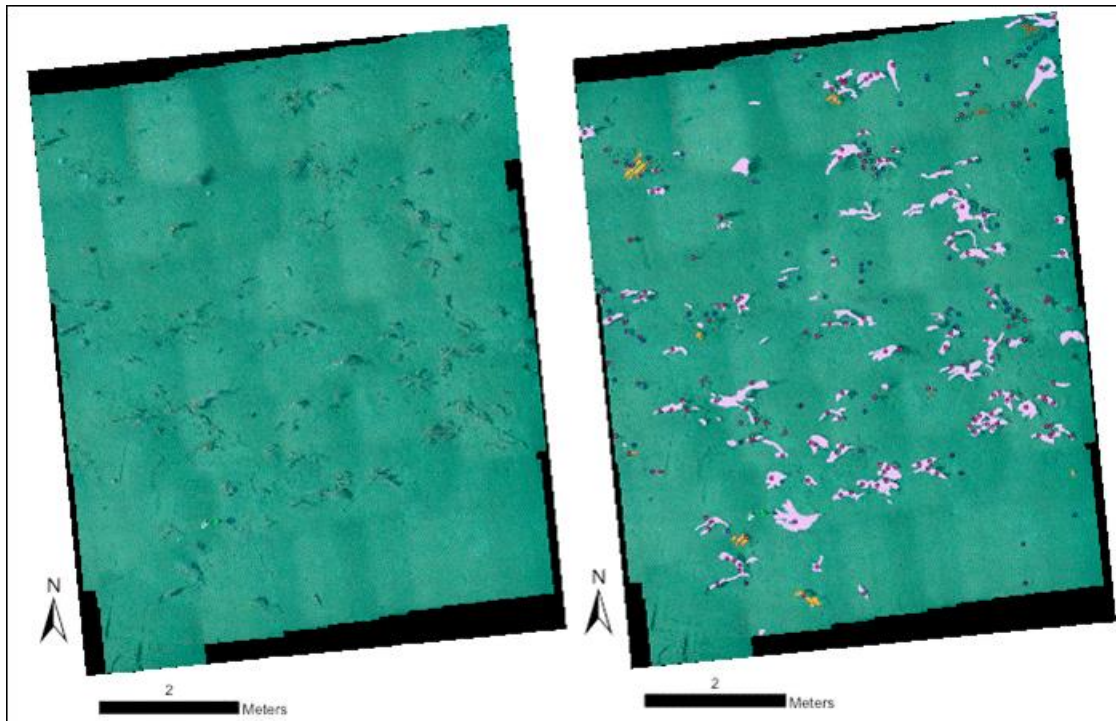


Figure 4-8. Photomosaic of Marker B in 2009  and digitization of this mosaic.

#### 4.2.3.1.4.2 GB299: Mosaic Marker B, 2010.

Images for the mosaic were collected on dive J2-530 on 10/20/10.The mosaic encompasses a roughly square area of about 39.0 m$^2$. *Callogorgia* sp. are observed across the site distributed relatively evenly with less density along the southern edge and northeast corner. One hundred and thirty-five ophiuroids are observed on the *Callogorgia* sp. Four whip coral are also found at this site. Mobile fauna include one crab, 11anemones, one *Helicolenus dactylopterus* fish, 46 urchins, and one crinoid.
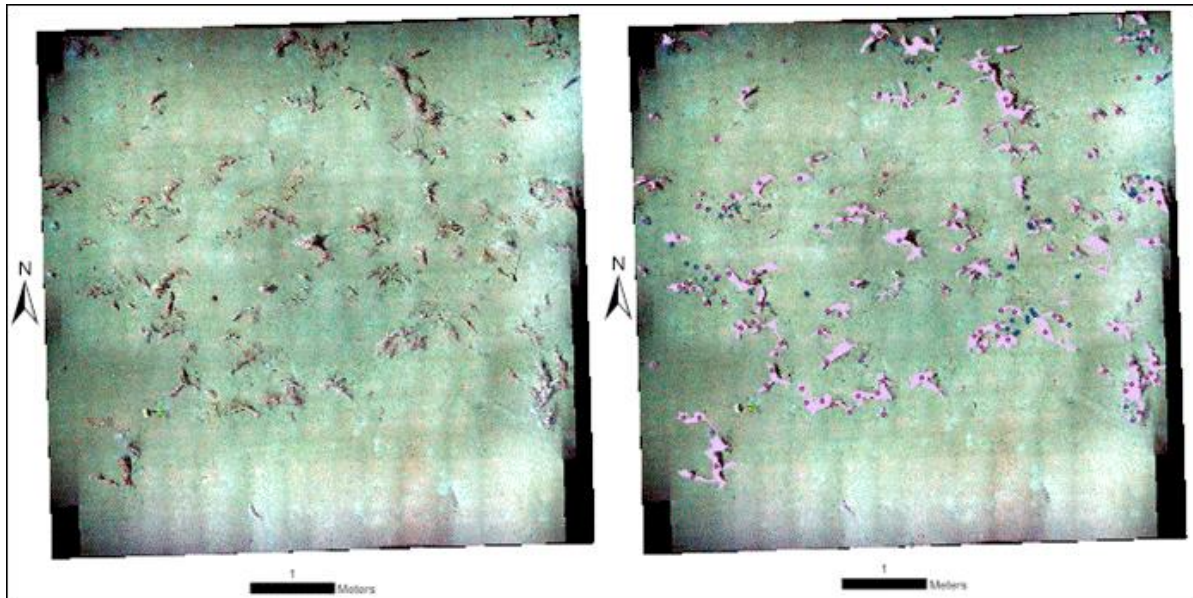
Figure 4-9. Photomosaic of Marker B in 2010 and digitization of this mosaic.

### 4.2.3.1.5 GB299: Mosaic Marker D

This site is located at 27.68647°N 92.23102°W at a depth of about 359 m. *Callogorgia* sp. is the dominant coral at the site with abundant commensal ophiuroids.

#### *4.2.3.1.5.1 GB299: Mosaic Marker D, 2009.*

Images for the mosaic were collected on dive J2-459 on 8/27/09.The mosaic covers an area of approximately 75.9 m². This site is dominated by 82 *Callogorgia* sp. spread across the area. One hundred and thirty-six ophiuroids are found on the *Callogorgia* sp., the seabed, and one *Paramuricea* sp. One Isididae, one whip coral, and one unidentified coral can also be seen. One tube worm, 56 crinoids, 129 anemones, 25 urchins, 26 sea stars, 37 sponges, and one crab are also observed at this site.
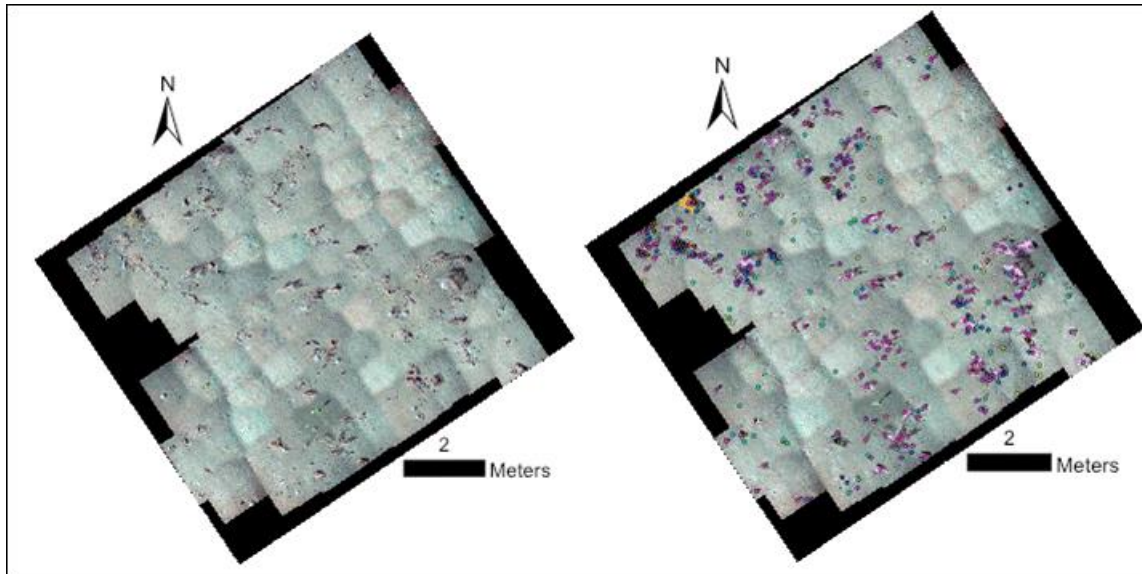
Figure 4-10. Photomosaic of Marker D in 2009 and digitization of this mosaic.

### 4.2.3.1.5.2 GB299: Mosaic Marker D, 2010

Images for the mosaic were collected on dive J2-530 on 10/20/10. The mosaic covers an area of approximately 57.7 m$^2$. This site is dominated by 51 *Callogorgia* sp. spread across the area. Seventy-seven ophiuroids are found on the *Callogorgia* sp., the sea floor, and one *Paramuricea* sp. One sea pen and one whip coral can also be seen. Nineteen urchins, 28 anemones, and one sea star make up the rest of the mobile fauna.
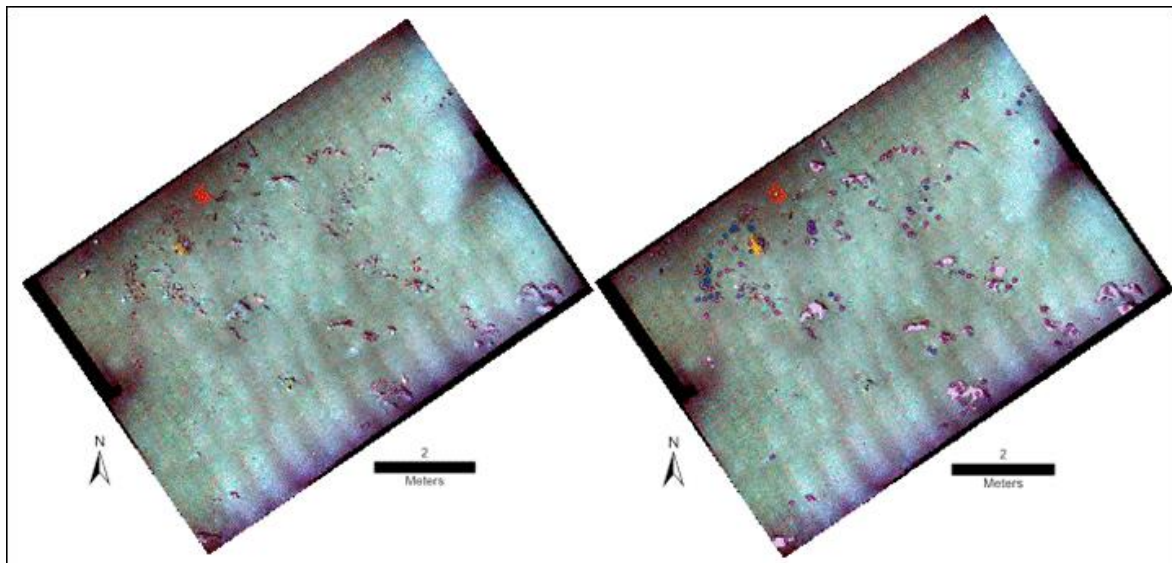


Figure 4-11. Photomosaic of Marker D in 2010 and digitization of this mosaic.

137

## 4.2.3.1.6 VK906: Mosaic Marker J

This site is located at 29.06967˚N 88.37717˚W at a depth of approximately 389 m. Large patches of *Lophelia pertusa* takes up the center of the mosaic and are surrounded by dead *Lophelia* and sediment. Substantial colonies of *Leiopathes glaberrima* are also present at the site.

### 4.2.3.1.6.1 VK906: Mosaic Marker J, 2009

Images for the mosaic were collected on dive J2-465 on 9/2/09. The mosaic encompasses a roughly rectangular area of about 30.4 m$^2$. More living and dead *Lophelia pertusa* are observed along the northeast edge of the mosaic. The southwest edge is relatively barren in comparison. A number of *Leiopathes glaberrima* colonies are seen across the mosaic with many concentrated along the southern edge of the central *Lophelia.* Thirty-six crabs are observed clustered on and around the live *Lophelia.* Other mobile fauna at this site include one *Gephyroberyx darwinii* fish, one Nettastomatidae eel, one sea star, 14crinoids, 20urchins, and 12anemones.
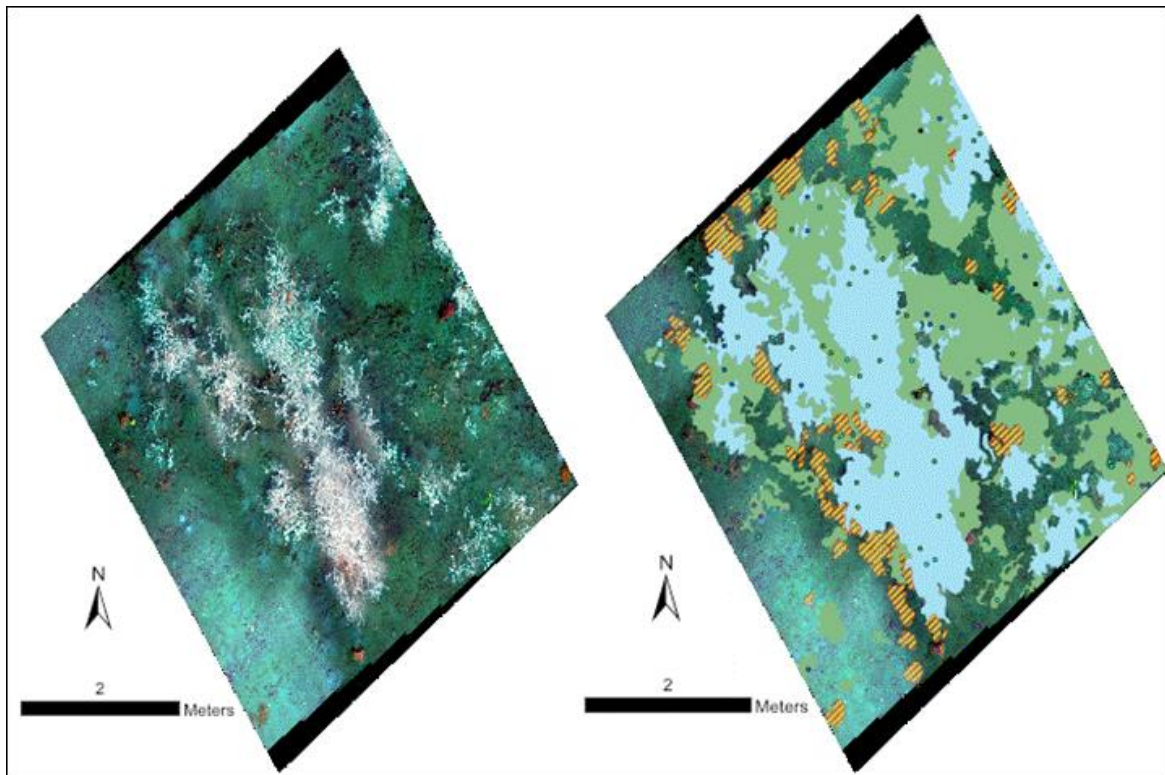


Figure 4-12. Photomosaic of Marker J in 2009 and digitization of this mosaic.

### 4.2.3.1.6.2 VK906: Mosaic Marker J, 2010

Images for the mosaic were collected on dive J2-534 on 10/24/10. The mosaic encompasses a roughly rectangular area of about 62.5 m$^2$. The dead *Lophelia* can be seen across the mosaic. More living and dead *Lophelia pertusa* are observed along the northeast edge of the mosaic. A number

of *Leiopathes glaberrima* colonies are seen distributed across the mosaic. Mobile fauna at this site include 28 crabs, four *Hyperoglyphe perciformis* fish, one unidentified fish, five sea stars, 11crinoids, 20urchins, and 18 anemones.
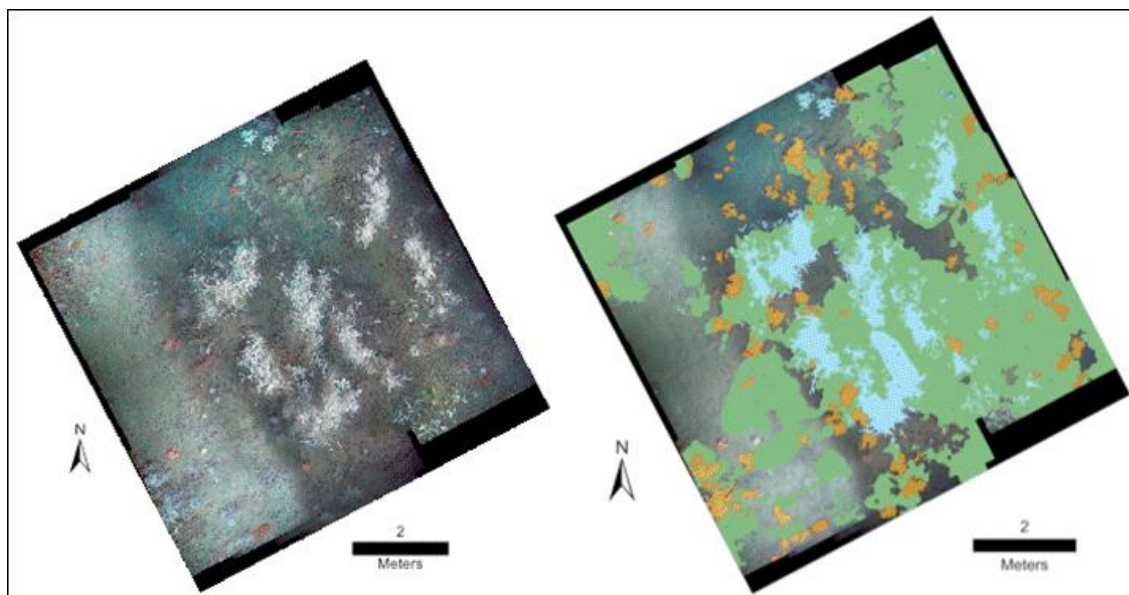


Figure 4-13. Photomosaic of Marker J in 2010 and digitization of this mosaic.

### 4.2.3.1.7 VK906: Mosaic Marker L

This site is located at 29.06933˚N 88.37759˚W at a depth of approximately 394 m. The mosaic areas are dominated with mixed live and dead *L. pertusa*, with numerous colonies of *L. glaberrima*.

#### 4.2.3.1.7.1 VK906: Mosaic Marker L, 2009

Images for the mosaic were collected on dive J2-465 on 9/2/09. The mosaic covers a rectangular area of about 54.9 m$^2$. A patch of *Lophelia pertusa* lies at the center of the mosaic surrounded by dead *Lophelia* and some *Leiopathes* sp. to the north and southeast. The rest of the mosaic is mud that is sporadically covered in sediment and dead *Lophelia pertusa*. Mobile fauna at this site include five crabs, 12anemones and one urchin. An encrusting sponge is also observed at this site.

139
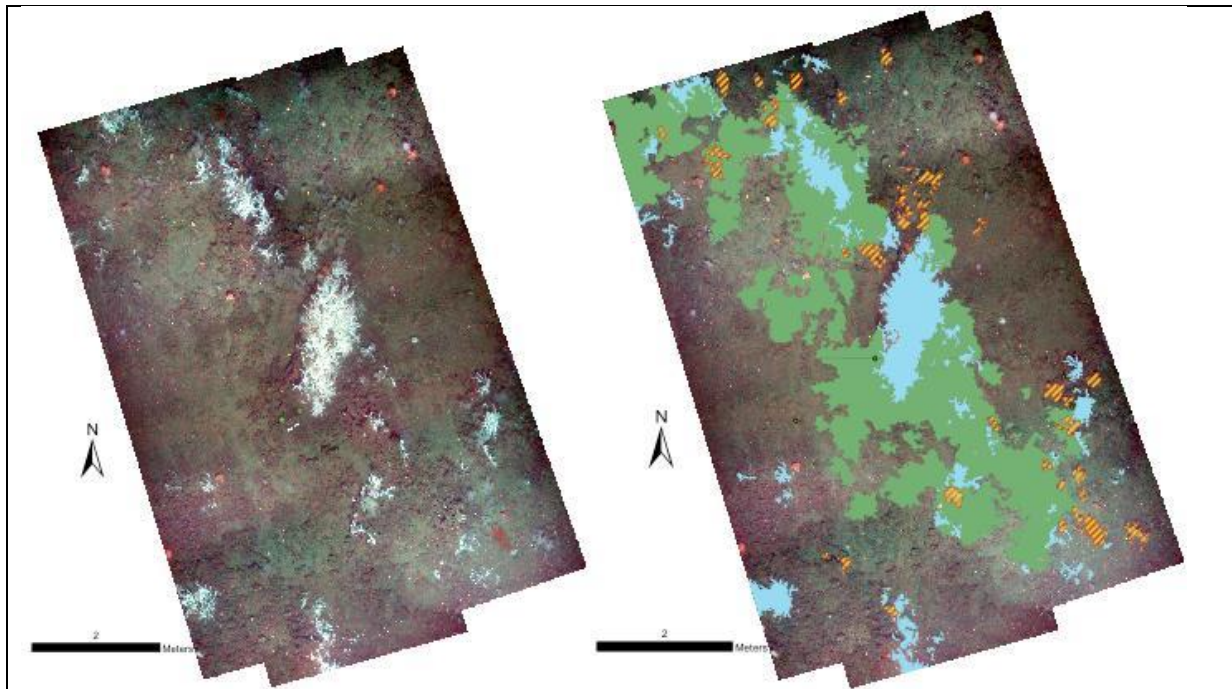
Figure 4-14. Photomosaic of Marker L in 2009 and digitization of this mosaic.

### 4.2.3.1.7.2 VK906: Mosaic Marker L, 2010

Images for the mosaic were collected on dive J2-534 on 10/24/10. The mosaic covers a rectangular area of about 60.1 m$^2$. A patch of *Lophelia pertusa* lies at the center of the mosaic surrounded by dead *Lophelia* and some *Leiopathes* sp. to the north and southeast. The rest of the mosaic is mud that is sporadically covered in sediment and dead *Lophelia pertusa*. Mobile fauna at this site include 16 crabs, 33 anemones and one urchin.
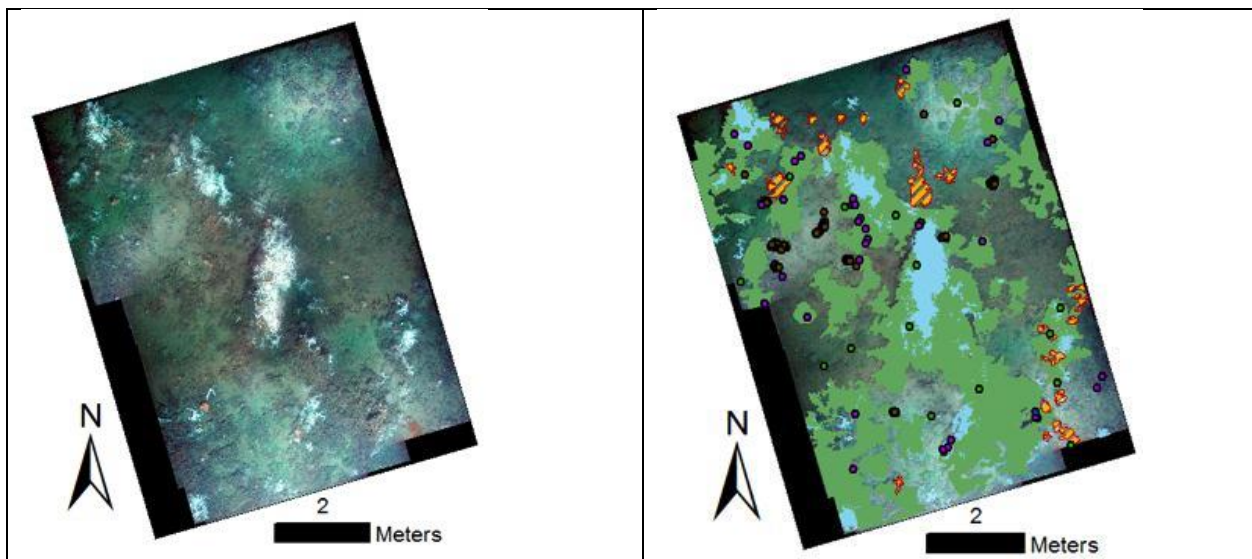


Figure 4-15. Photomosaic of Marker L in 2010 and digitization of this mosaic.

140

### 4.2.3.1.8 VK906: Mosaic Marker Y, 2010 (only)

This site is located at 29.06898˚N 88.37771˚W at a depth of about 395 m. Images for the mosaic were collected on dive J2-535 on 10/25/10. The mosaic covers a long rectangular area of approximately 58.9 m$^2$. This mosaic features a number of large areas of living *Lophelia pertusa* interspersed with dead *L. pertusa*. *Leiopathes* sp. is also abundant across the site with highest density near the northern and southern edges. Forty-two total anemones are found in this mosaic. Other fauna include one *Gephyroberyx darwinii* fish, one *Helicolenus dactylopterus* fish, one *Hyperoglyphe perciformis* fish, 32 crabs, four urchins, 27 sponges, one ophiuroid, and two crinoids.
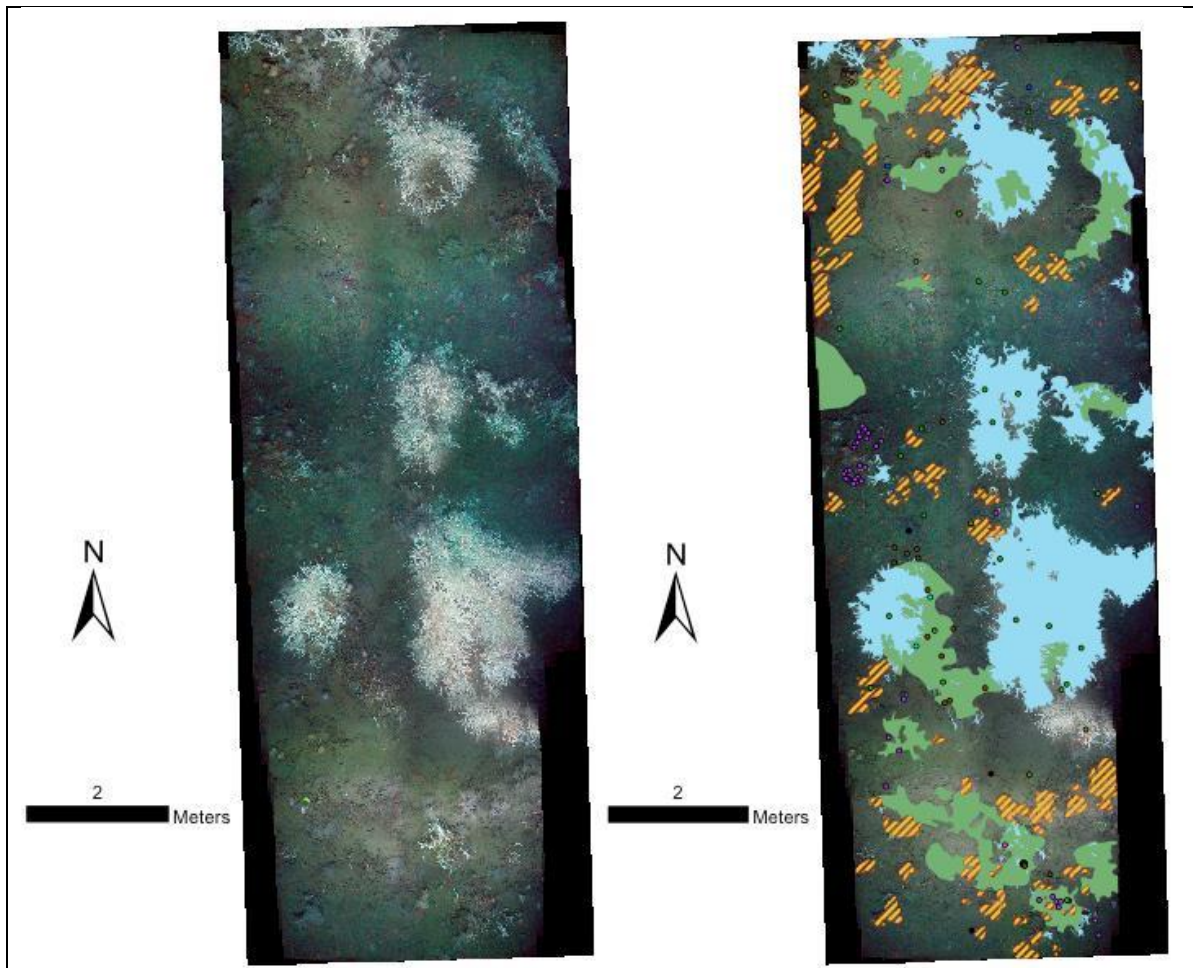


Figure 4-16. Photomosaic of Marker Y in 2010 and digitization of this mosaic.

### 4.2.3.1.9 MC751: Mosaic Marker G

This site is located at 28.19366˚N 89.79871˚W at a depth of approximately 441 m. The primary feature seen in this mosaic is a carbonate rock outcropping covered in dead *Lophelia pertusa*. *Callogorgia* sp colonies are also present. Notable at this site is a large clump of vestimentiferan tube worms.

### 4.2.3.1.9.1 MC751: Mosaic Marker G, 2009.

Images for the mosaic were collected on dive J2-464 on 9/1/09. The mosaic encompasses an area of about 34.3 m$^2$. The dead *Lophelia pertusa* cover about 41% of the total mosaic area. Patches of living *Lophelia pertusa* can be seen in both the center and the North and eastern corners. Six *Callogorgia* sp. are found across the site with 25 associated commensal ophiuroids. Three smaller *Paramuricea* sp. are seen near the center of the mosaic. There are six *Muriceides* sp. and three as yet unidentified corals. The southern corner of the mosaic features a large patch of tube worms. Seven urchins, nine crabs, one Moridae fish, one *Hoplostethus occidentalis* fish, and 45 anemones are also observed.
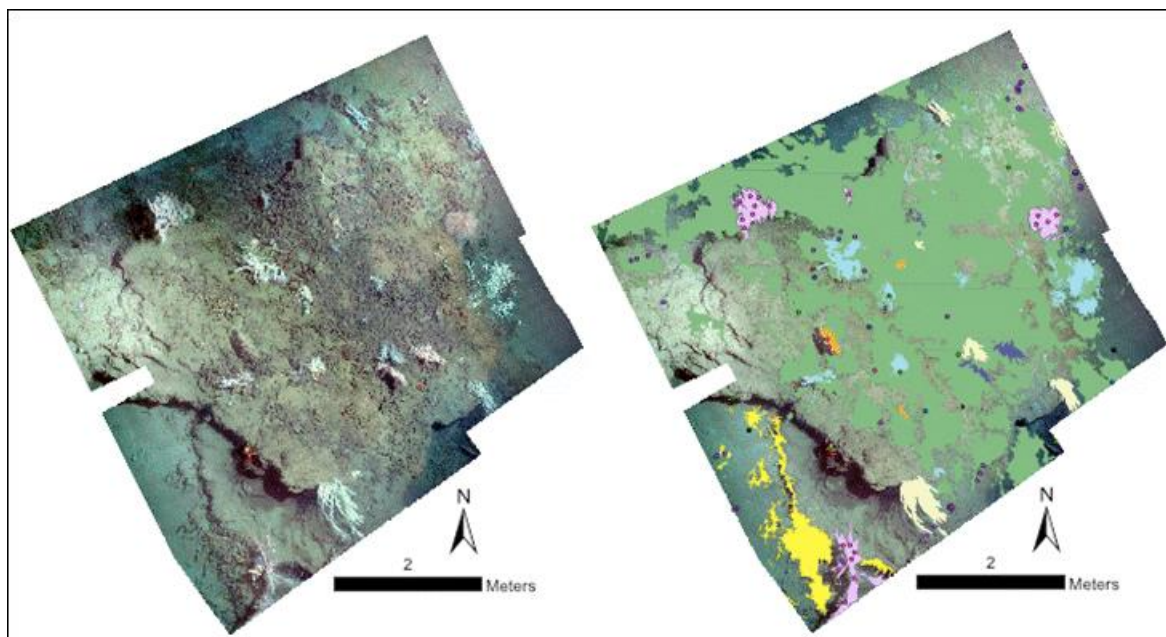


Figure 4-17. Photomosaic of Marker G in 2009 and digitization of this mosaic.

### 4.2.3.1.9.2 MC751: Mosaic Marker G, 2010

Images for the mosaic were collected on dive J2-536 on 10/27/10. The mosaic encompasses an area of about 77.1 m$^2$. Areas of living *Lophelia pertusa* can be seen most notably in the center and eastern corner. *Callogorgia* sp., *Paramuricea* sp., and *Muriceides* sp. are found across the site along with an as yet unidentified coral species. Sponges are also present. Twenty-eight ophiuroids are found on the various corals. The southern corner of the mosaic features a large patch of tube worms. Four urchins, ten crabs, and 17anemones are also observed.
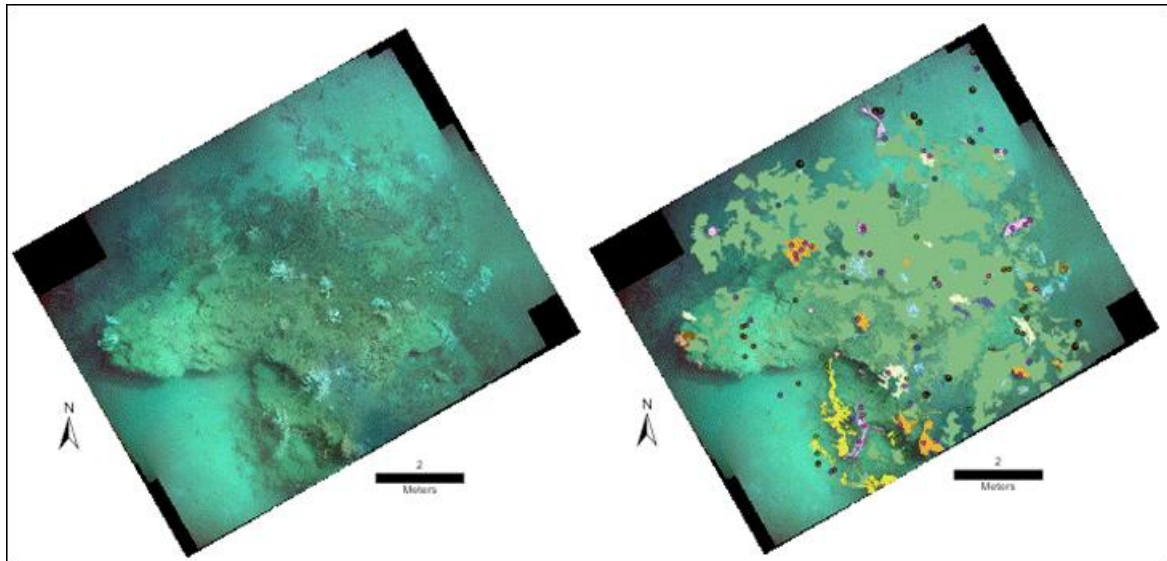
Figure 4-18. Photomosaic of Marker G in 2010 and digitization of this mosaic.

### 4.2.3.1.10    MC751: Mosaic Marker H1

This site is located at 28.19404˚N 89.79831˚W at a depth of approximately 441 m. An elevated outcropping is in the center of the mosaic surrounded by tube worms and mixed dead and live *Lophelia pertusa*.  In some cases the *L. pertusa* is very closely intermingled with the tube worms.

#### *4.2.3.1.10.1 MC751: Mosaic Marker H1, 2009*

Images for the mosaic were collected on dive J2-464 on 9/1/09. The mosaic encompasses an area of about 52.4 m$^2$. In addition to the carbonate outcropping dominating the center of the mosaic, part of another outcropping can be seen in the northwest corner of the mosaic. Live *Lophelia pertusa* is found among the dead *Lophelia pertusa. Paramuricea* sp. and *Callogorgia* sp. are also found at this site.  Forty sponges, one sea star, 42 mussels, eight crabs, two *Helicolenus dactylopterus* fish, 13brittle stars, and four anemones are also observed. The vast majority of all fauna at this site is clustered around the outcroppings with the exception of the *Callogorgia* sp. and their associated ophiuroids.
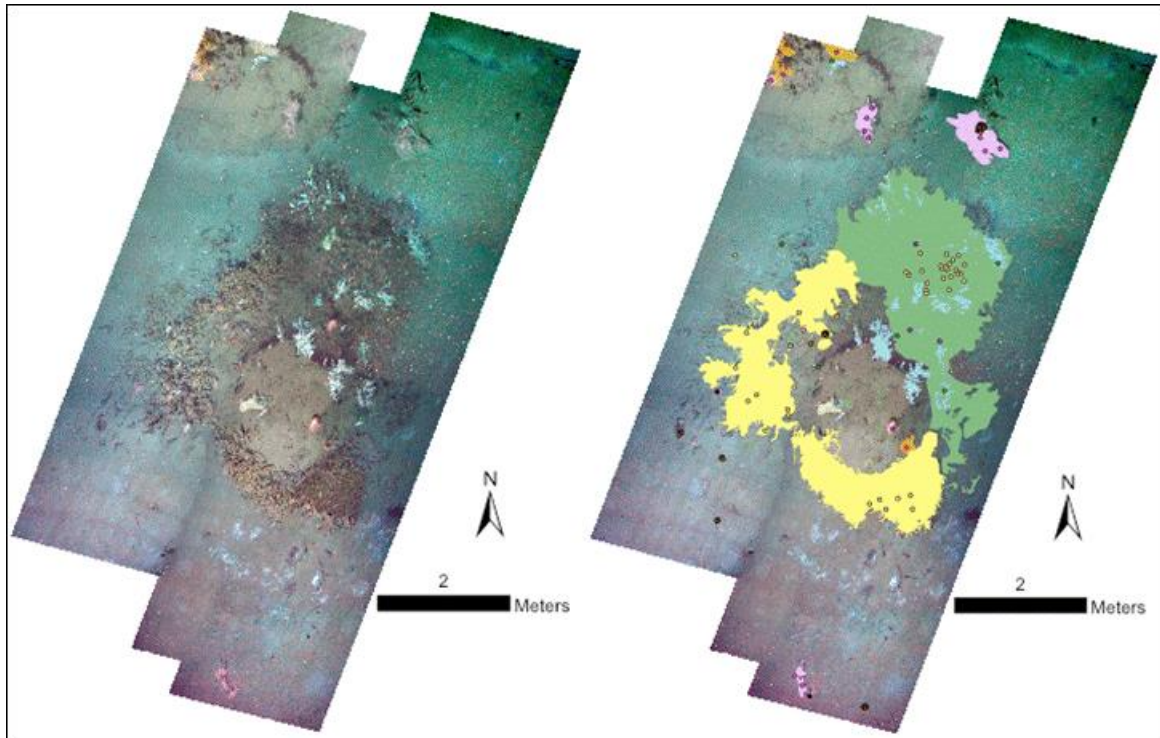
Figure 4-19. Photomosaic of Marker H1 in 2009 and digitization of this mosaic.

### 4.2.3.1.10.2 MC751: Mosaic Marker H1, 2010

Images for the mosaic were collected on dive J2-536 on 10/26/10. The mosaic encompasses an area of about 23.8 m$^2$. Another outcropping can be seen in the northern corner of the mosaic. Live *Lophelia pertusa* is found among the dead *Lophelia pertusa. Paramuricea* sp. and *Callogorgia* sp. are also found at this site. Sponges, 34 mussels, five crabs, one *Helicolenus dactylopterus* fish, one *Hoplostethus occidentalis* fish, 33 brittle stars, and 28 anemones are also observed. The vast majority of all fauna at this site is clustered on the outcroppings with the exception of one large colony of *Callogorgia* sp. near some tube worms and sponges and with associated commensal ophiuroids found northeast of the central outcropping.
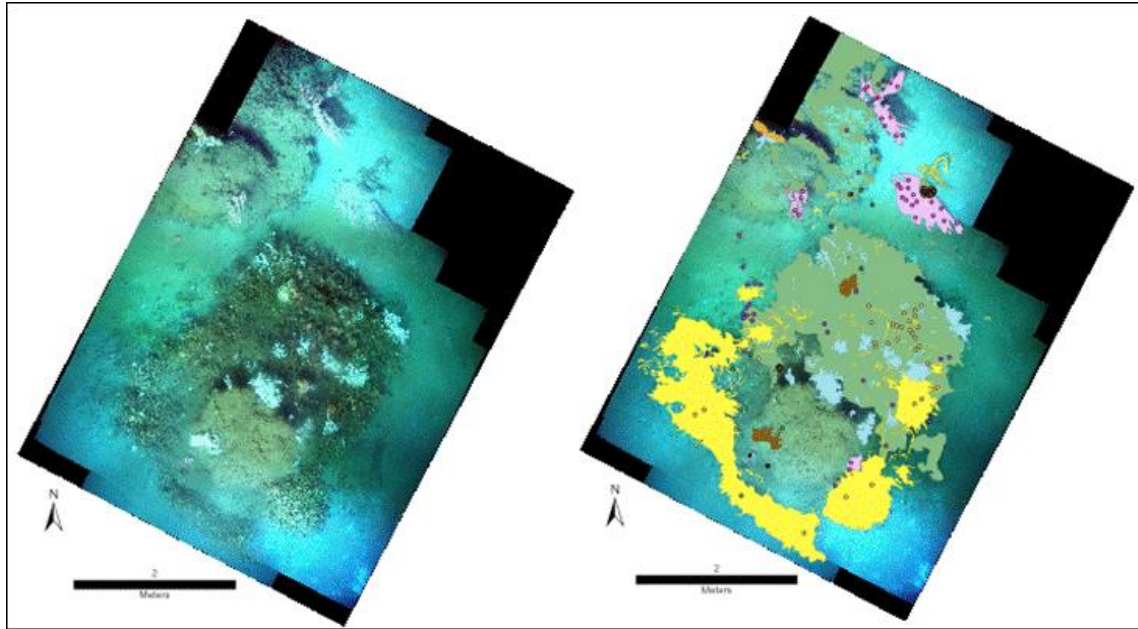
Figure 4-20. Photomosaic of Marker H1 in 2010 and digitization of this mosaic.


## 4.2.3.1.11    MC751: Mosaic Marker H2

This site is located at 28.19404˚N 89.79831˚W at a depth of approximately 441 m. The most notable topographical feature of this mosaic is an elevated area covered in sediment in the southwest corner of the mosaic. Much of the fauna is concentrated in and around this area. *Callogorgia* sp. is quite abundant.  *L. pertusa*, *Paramuricea* sp. and vestimentiferan tube worms are also present at the site.


### *4.2.3.1.11.1 MC751: Mosaic Marker H2, 2009*

This site is located at 28.19404˚N 89.79831˚W at a depth of approximately 441 m. Images for the mosaic were collected on dive J2-464 on 9/1/09. The mosaic encompasses an area of about 29.7 m$^2$. A patch of dead *Lophelia pertusa* lies in the middle of the mosaic and the edge of another patch can be seen at the bottom with some live *Lophelia pertusa.* The most prolific coral at this site is *Callogorgia* sp. Both the *Callogorgia* sp. and *Paramuricea* sp. at this location are covered in ophiuroids. An individual *Muriceides* sp. colony is present on the west side of the mosaic. Tubeworms are found in the southeast corner of the site. Sponges and hydroids are also present. Eleven crabs, one urchin, 65 anemones, and one sea star make up the mobile fauna present at this site.
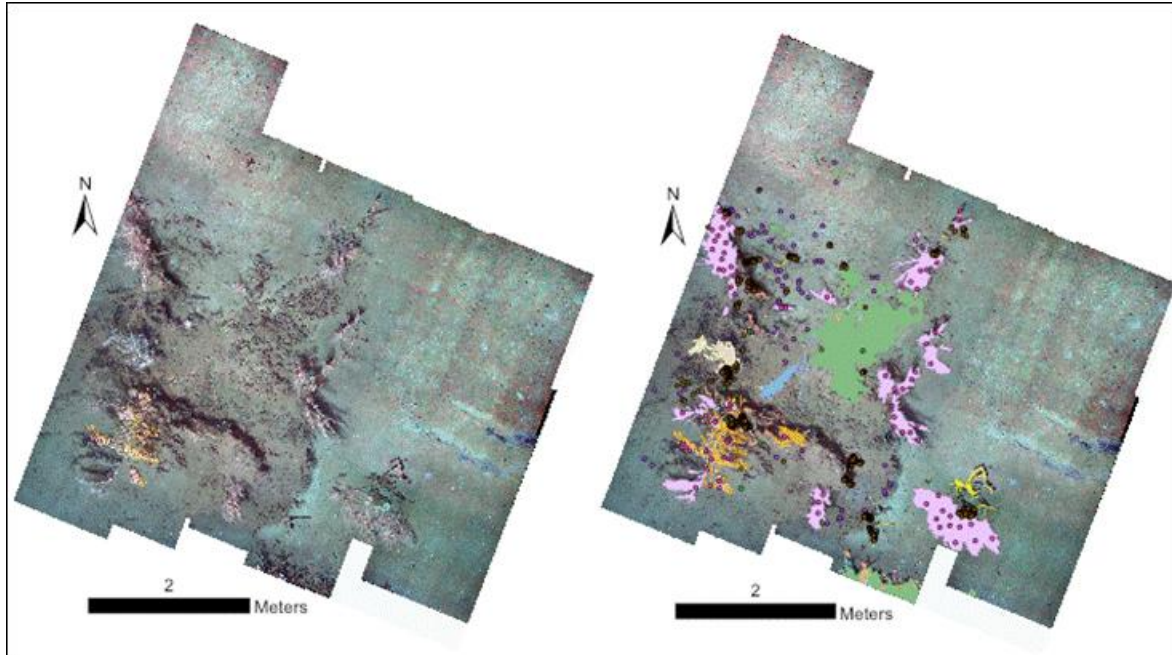
Figure 4-21. Photomosaic of Marker H2 in 2009 and digitization of this mosaic.

### 4.2.3.1.11.2 MC751: Mosaic Marker H2, 2010.

This site is located at 28.19404˚N 89.79831˚W at a depth of approximately 441 m. Images for the mosaic were collected on dive J2-536 on 10/26/10. The mosaic encompasses an area of about 30.2 m$^2$. A patch of dead *Lophelia pertusa* lies in the middle of the mosaic and the edge of another patch can be seen at the bottom with some live *Lophelia pertusa*. The most prolific coral at this site is *Callogorgia* sp. Both the *Callogorgia* sp. and *Paramuricea* sp. at this location are covered in ophiuroids. Tubeworms are found at the southern edge of the outcropping. A large number of encrusting and individual sponges, four crabs, one urchin, seven anemones, and one *Hoplostethus occidentalis* fish are observed.
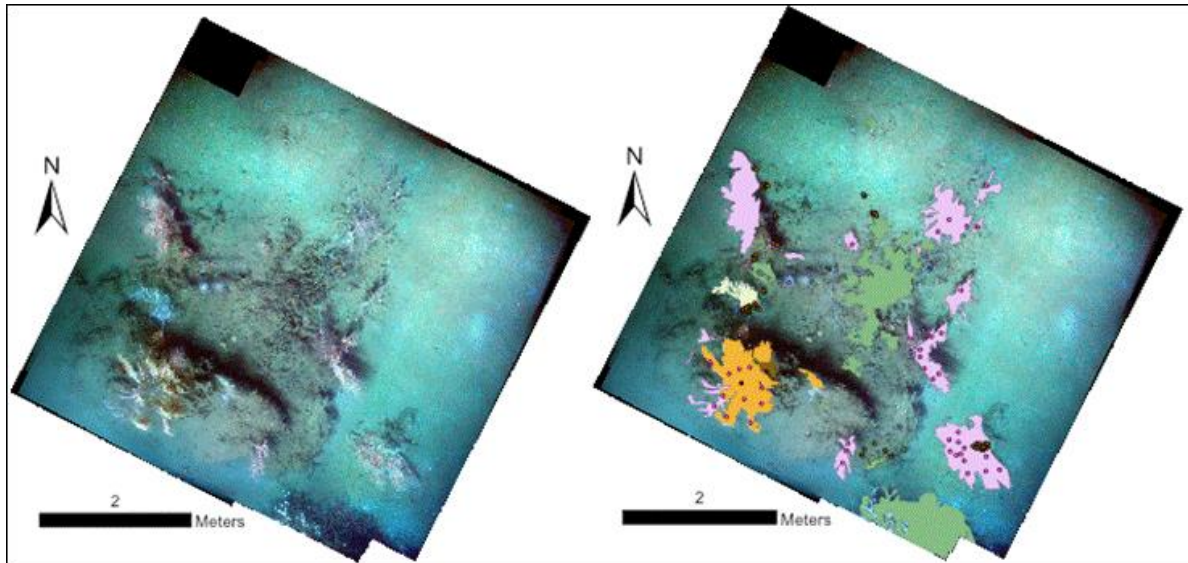
Figure 4-22. Photomosaic of Marker H2 in 2010 and digitization of this mosaic.

## 4.2.3.1.12    VK826: Mosaic Marker M

This site is located at 29.15807°N 88.01685°W at a depth of approximately 470 m. The mosaics are dominated by a single large clump of mixed living and dead *L. pertusa*. Several *L. glaberrima* are also present around the periphery of the main clump of *L. pertusa*.

### 4.2.3.1.12.1 VK826: Mosaic Marker M, 2009

Images for the mosaic were collected on dive J2-466 on 9/3/09. The mosaic has an area of about 43.2 m². The central area of mixed living and dead *L. pertusa* is surrounded by sea floor composed of mud. Four *L. glaberrima* are also found at this site. Mobile fauna include one urchin, 17 crabs, one sea star, one Nettastomatidae eel, and one *Helicolenus dactylopterus* fish. These fauna are found in highest density on and around the *L. pertusa*.
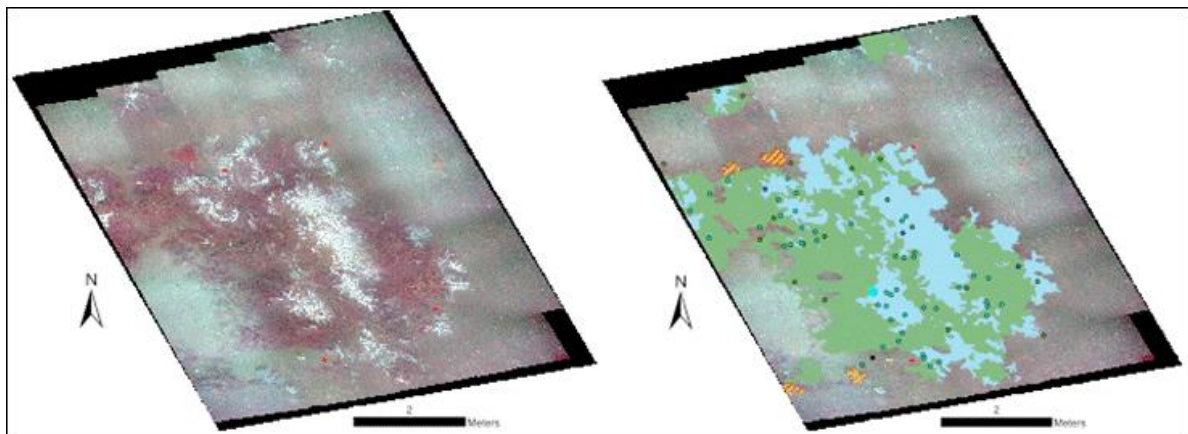


Figure 4-23. Photomosaic of Marker M in 2009 and digitization of this mosaic.

### 4.2.3.1.12.2 VK826: Mosaic Marker M, 2010

Images for the mosaic were collected on dive J2-526 on 10/16/10. The mosaic has an area of about 29.7 m². The *Lophelia* is surrounded by sea floor composed of mud. *Leiopathes* sp. coral colonies are also found at this site. Mobile fauna include 11urchins, 13 crabs, one sea star, one *Hoplostethus occidentalis* fish, and 38 crinoids. These fauna are found in highest density on and around the *Lophelia.*
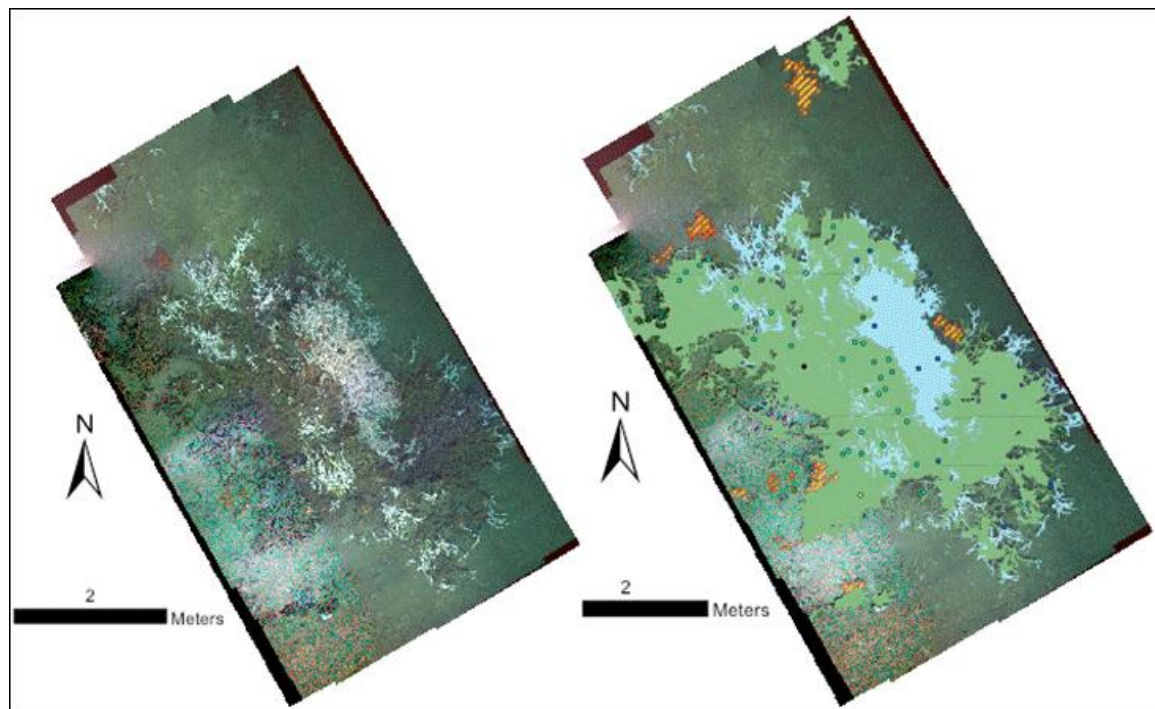


Figure 4-24. Photomosaic of Marker M in 2010 and digitization of this mosaic.

## 4.2.3.1.13    VK826: Mosaic Marker N

This site is located at 29.15807°N 88.01685°W at a depth of about 476 m. The mosaics are dominated by a mixed clump of living and dead *L. pertusa*.  Two isolated vestimentiferan tube worms are surrounded by the *L. pertusa* clump.

### 4.2.3.1.13.1 VK826: Mosaic Marker N, 2009.

Images for the mosaic were collected on dive J2-466 on 9/3/09. The mosaic covers an area of approximately 51.7 m². The middle of the mosaic features both living and dead *Lophelia pertusa*. The dead area spreads from the center of the mosaic to the northeast corner. More *Lophelia* are visible at the south and west edges of the mosaic. The primary substrate is mud and to the south it is covered with some sediment and dead coral. Two tube worms and three sponges are found near the center of the mosaic. Seven urchins, 12crabs, and 21 crinoids are observed concentrated around the *Lophelia.* Other mobile fauna consist of one Nettastomatidae eel, one *Helicolenus dactylopterus* fish, and two sea stars.
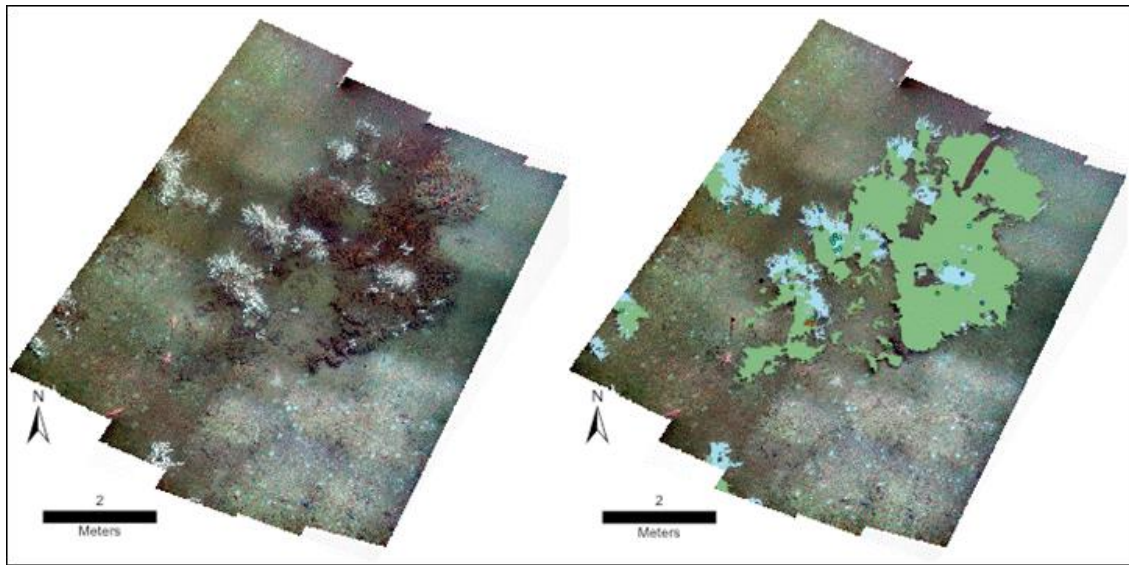
Figure 4-25. Photomosaic of Marker N in 2009 and digitization of this mosaic.

### 4.2.3.1.13.2 VK826: Mosaic Marker N, 2010

Images for the mosaic were collected on dive J2-526 on 10/16/10. The mosaic covers an area of approximately 39.6 m$^2$. The middle of the mosaic features *Lophelia pertusa* both living and dead. The dead area is larger and extends from the center of the mosaic to the northeast corner. More *Lophelia* are visible at the south and west edges of the mosaic. The primary substrate is mud and to the south it is covered with some sediment and dead coral. Two tube worms and three sponges are found near the center of the mosaic, and nine urchins, one crab, one sea star, and nine crinoids are observed concentrated around the *Lophelia.* Other mobile fauna consist of two *Hoplostethus occidentalis* fish and one *Helicolenus dactylopterus* fish, and two sea stars.
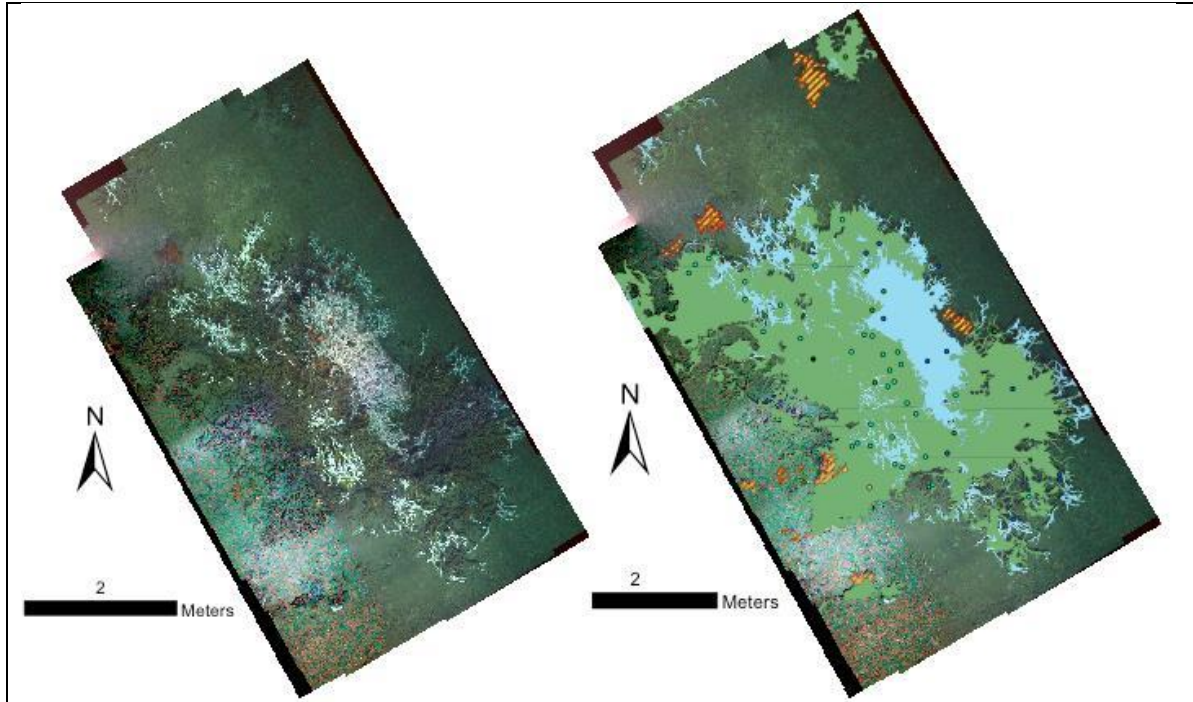
Figure 4-26. Photomosaic of Marker N in 2010 and digitization of this mosaic.

### 4.2.3.1.14    VK826: Mosaic Marker O

This site is located at 29.16484°N 88.01156°W at a depth of about 463 m.  Both mosaics are dominated by large areas of living and dead *L. pertusa* although the 2010 mosaic includes a substantial area not included in the 2009 mosaic.

#### *4.2.3.1.14.1 VK826: Mosaic Marker O, 2009*

Images for the mosaic were collected on dive J2-466 on 9/4/09. The mosaic is roughly square shaped with an area of approximately 39.1 m$^2$. Dead and living *Lophelia pertusa* cover the southwestern half of the mosaic with living *Lophelia* concentrated in the center and the southern corner of the map. One sea star, 22 crabs, three urchins, and 32 crinoids are found around the *Lophelia.* Four *Helicolenus dactylopterus* fish and three Nettastomatidae eels are observed along with one squid swimming over the site.
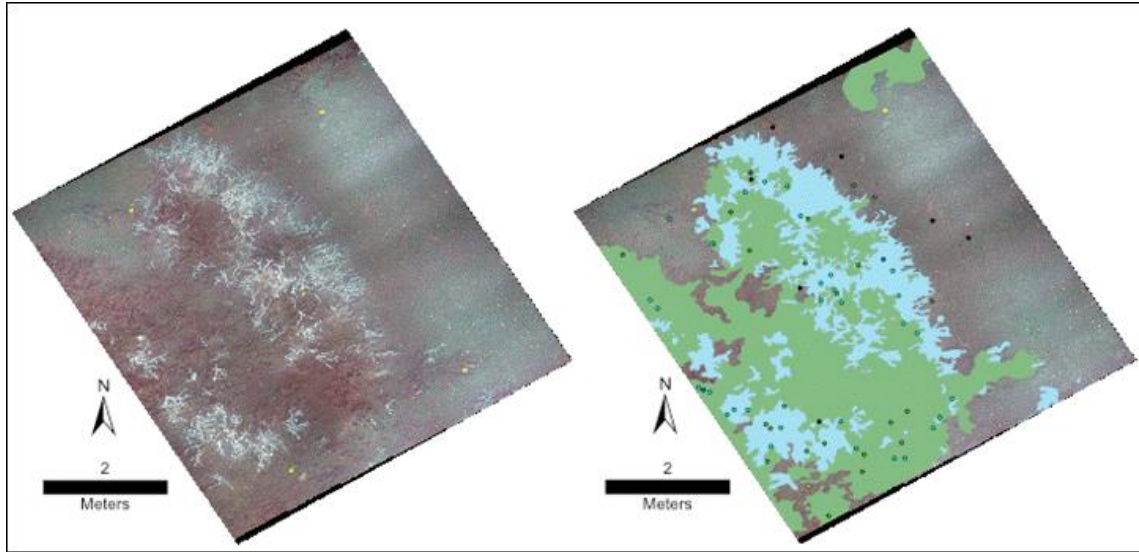
Figure 4-27. Photomosaic of Marker O in 2009 and digitization of this mosaic.

### 4.2.3.1.14.2 VK826: Mosaic Marker O, 2010

Images for the mosaic were collected on dive J2-540 on 10/31/10. The mosaic is roughly rectangular and covers an area of approximately 108.7 m$^2$. Dead and living *Lophelia pertusa* cover the southwestern and northern portions of the mosaic. Areas not covered in *Lophelia* appear to be barren sea floor. Fourteen crabs, four anemones, and 24 crinoids are found around the *Lophelia.* Two Nettastomatidae eels are also observed in the north.
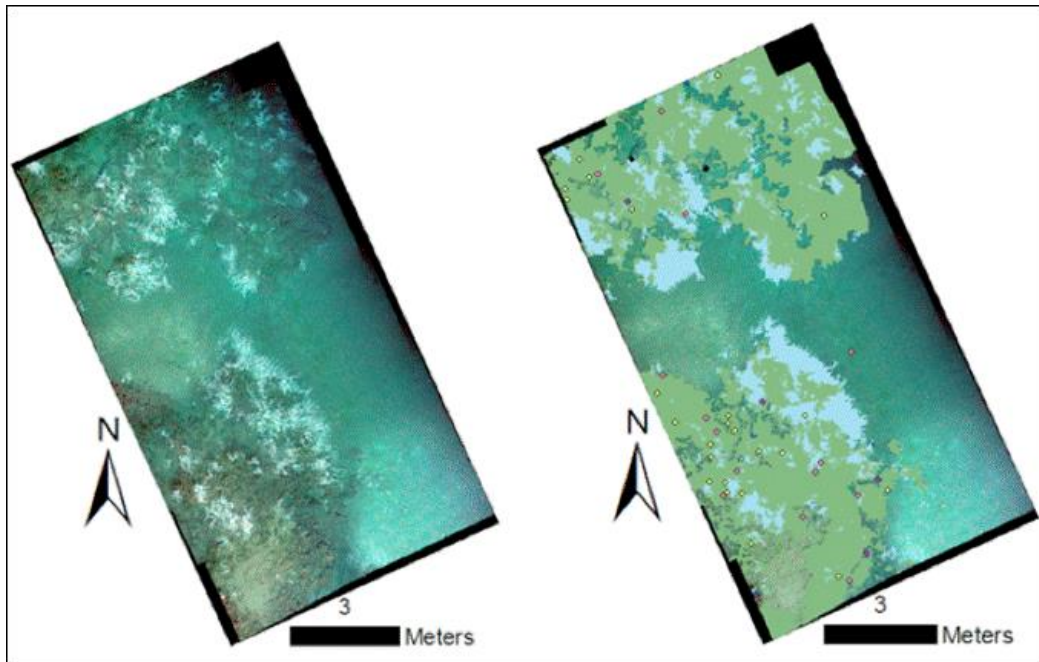


Figure 4-28. Photomosaic of Marker O in 2010 and digitization of this mosaic.

## 4.2.3.1.15    VK826: Mosaic Marker Q

This site is located at 29.15873°N 88.01053°W at a depth of approximately 479 m. The mosaics are dominated by several clumps of living and dead *L. pertusa*.

### 4.2.3.1.15.1 VK826: Mosaic Marker Q, 2009

Images for the mosaic were collected on dive J2-467 on 9/4/09. The mosaic encompasses a roughly rectangular area of about 48.5 m$^2$. Live and dead *Lophelia pertusa* cover about 83% of this mosaic. Tubeworms are found in the western corner and near the center of the map. One encrusting sponge is also observed. Mobile fauna including one crinoid, three Nettastomatidae eels, two *Hoplostethus occidentalis* fish, one Moridae fish, eight sea stars, 59 crabs, one shrimp, and 18 urchins are also found at this site. Much of the mobile fauna is found around the center of the mosaic.
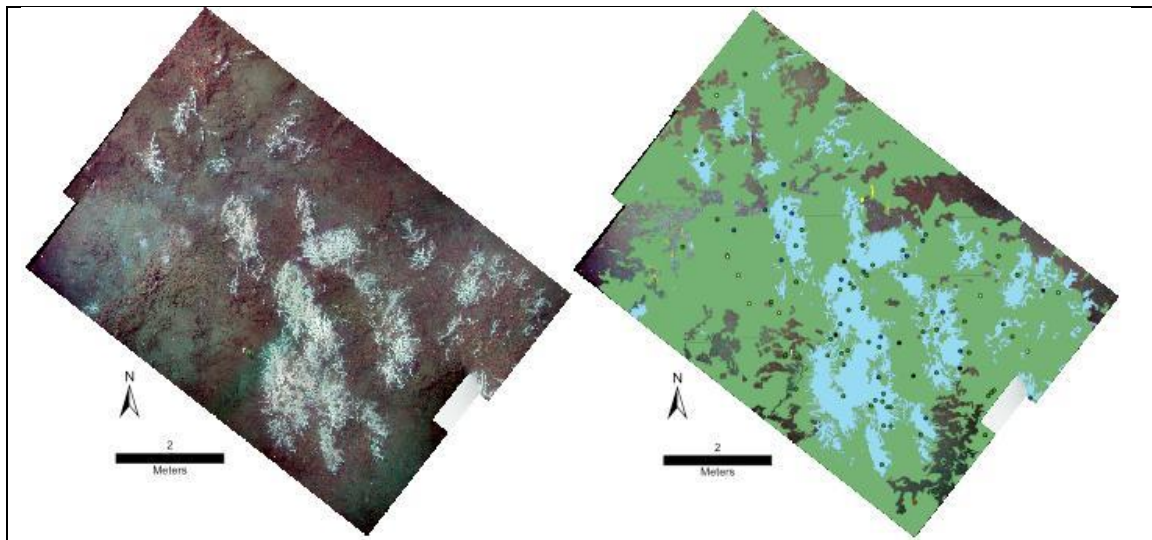


Figure 4-29. Photomosaic of Marker Q in 2009 and digitization of this mosaic.

### 4.2.3.1.15.2 VK826: Mosaic Marker Q, 2010

Images for the mosaic were collected on dive J2-540 on 11/1/10. The mosaic encompasses a long rectangular area of about 78.3 m$^2$. Live and dead *Lophelia pertusa* cover about 64% of the mosaic's total area. Encrusting sponges are observed near the middle of the mosaic. Mobile fauna including three *Hoplostethus occidentalis* fish, one *Laemonema goodebeanorum* fish, 24 crabs, and six urchins are also found at this site. Much of the mobile fauna is found around the center of the mosaic near the living *Lophelia*.
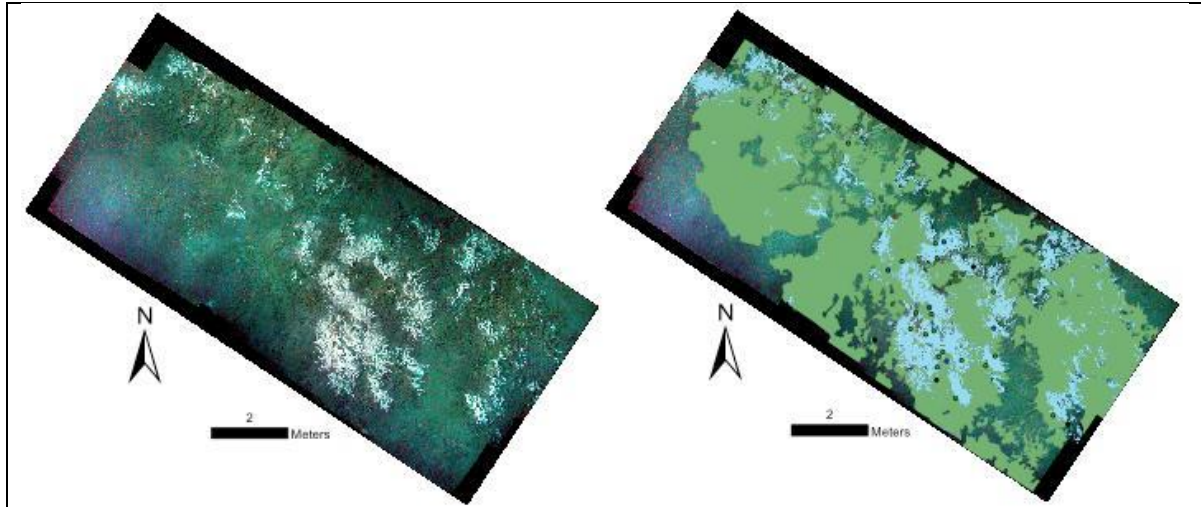
Figure 4-30. Photomosaic of Marker Q in 2010 and digitization of this mosaic.

## 4.2.3.1.16    GB535: Mosaic Marker C

This site is located at 27.42798°N 93.58346°W at a depth of about 516 m. The mosaic is centered on three carbonate rock outcroppings with some sediment and mud between and around them. Some areas of the rock and sediment are covered in mussel shells. Sponges and whip corals are abundant in this mosaic, *L. pertusa, Paramuricea* sp. and *Antipathes* sp. are also present.

### *4.2.3.1.16.1 GB535: Mosaic Marker C, 2009*

Images for the mosaic were collected on dive J2-460 on 8/28/09.The mosaic encompasses an area of approximately 39.2 m$^2$. The dominant fauna at this location are whip corals, of which 197 are observed. Some living and dead *Lophelia pertusa colonies are* seen on the northernmost outcropping.  Fifteen *Paramuricea* sp. and 27 *Antipathes* sp. can also be seen across the site. A number of mobile fauna were also observed. Five fish including two Moridae, two *Hyperoglyphe perciformis*, and one *Hoplostethus occidentalis* are present along with 25 crabs and 71 crinoids.
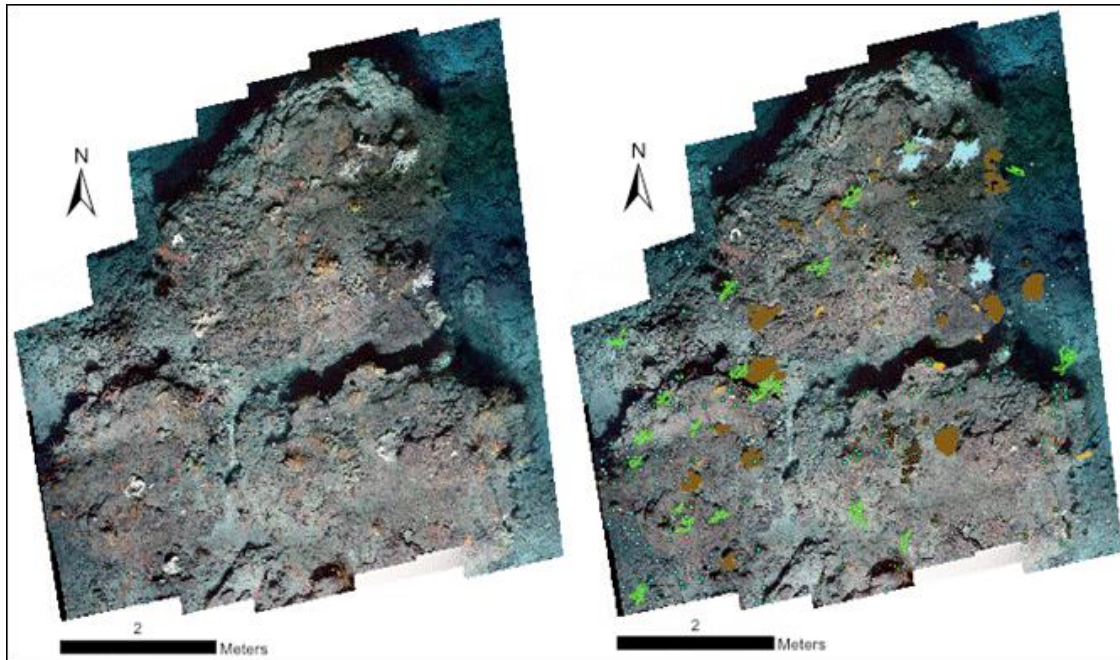
Figure 4-31. Photomosaic of Marker C in 2009 and digitization of this mosaic.

### 4.2.3.1.16.2 GB535: Mosaic Marker C, 2010

Images for the mosaic were collected on dive J2-531 on 10/20/10. The mosaic encompasses an area of about 40 m$^2$. Sponges are found across the mosaic on the outcroppings along with 65 whip corals. A colony of *Lophelia pertusa* with some dead regions is seen on the northernmost outcropping. Mobile fauna at this site include three crabs, one unidentified fish, and 39 crinoids.
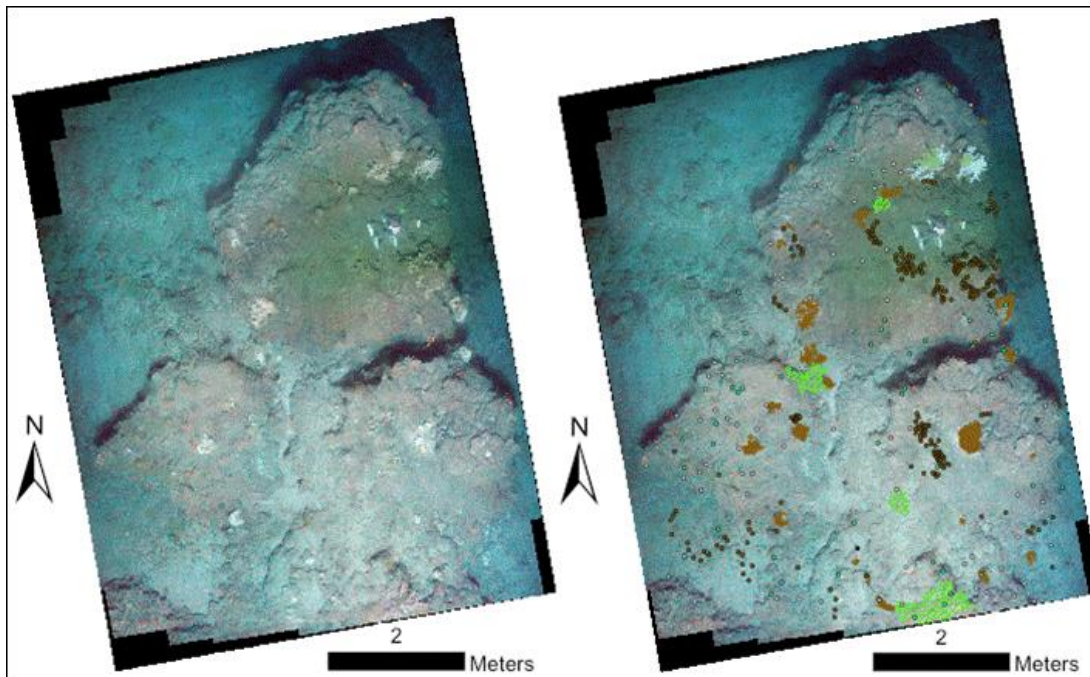


Figure 4-32. Photomosaic of Marker C in 2010 and digitization of this mosaic.

154

## 4.2.3.1.17　GB535: Mosaic Marker E

This site is located at 27.42714°N 93.58539°W at a depth of approximately 520 m. The site is covered almost entirely in dead *Lophelia pertusa* with small areas of live *L. pertusa. Callorgia* sp. and whip corals are also abundant at the site.

### 4.2.3.1.17.1 GB535: Mosaic Marker E, 2009

Images for the mosaic were collected on dive J2-460 on 8/28/09. The mosaic encompasses a roughly square area of about 8.6 m$^2$. Twenty-two *Callogorgia* sp. are concentrated across the northern half of the mosaic. Forty three whip coral, one *Muriceides* sp. coral colony, and one *Antipathes* sp. coral colony are also observed along with 93 small areas of living *Lophelia pertusa* interspersed among the dead coral regions. Encrusting sponges, one tube worm, two anemones, six crabs, two urchins and 94 crinoids are also seen.
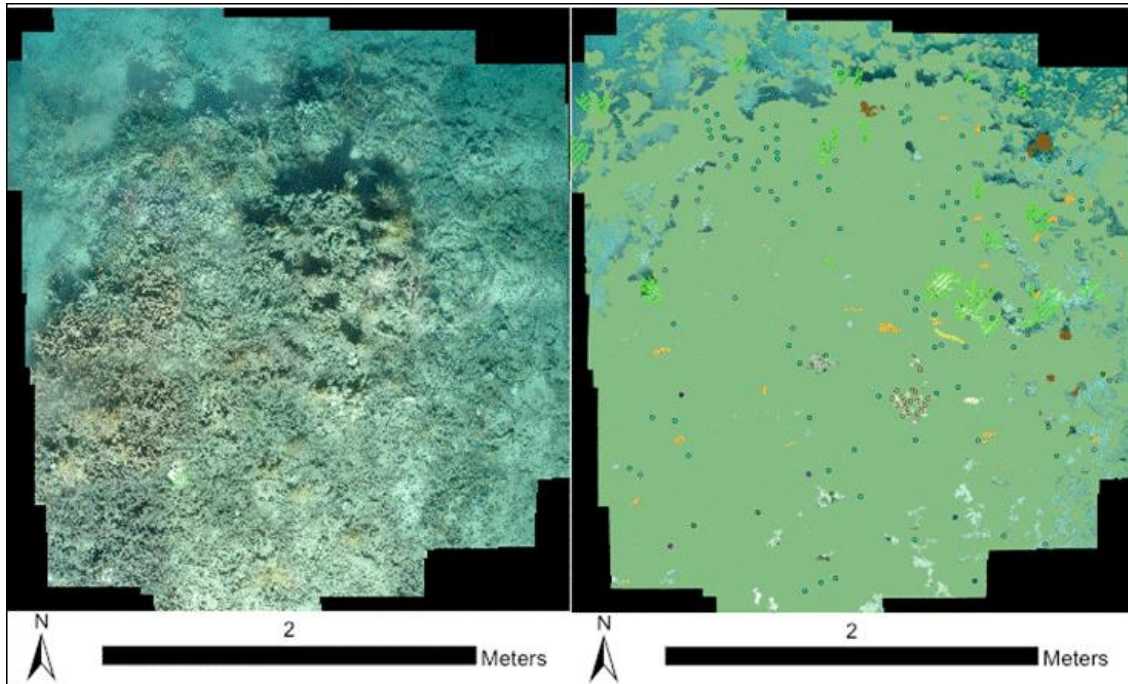


Figure 4-33. Photomosaic of Marker E in 2009 and digitization of this mosaic.

### 4.2.3.1.17.2 GB535: Mosaic Marker E, 2010

Images for the mosaic were collected on dive J2-531 on 10/21/10. The mosaic encompasses a roughly square area of about 19.3 m$^2$. *Antipathes* sp., are found around the center of the mosaic. Twenty-four whip coral, and some encrusting sponges are also observed at this site. Twenty-eight mussels, 68 crinoids, one Hoplostethus occidentalis fish, four crabs, and one anemone are also found here.

155
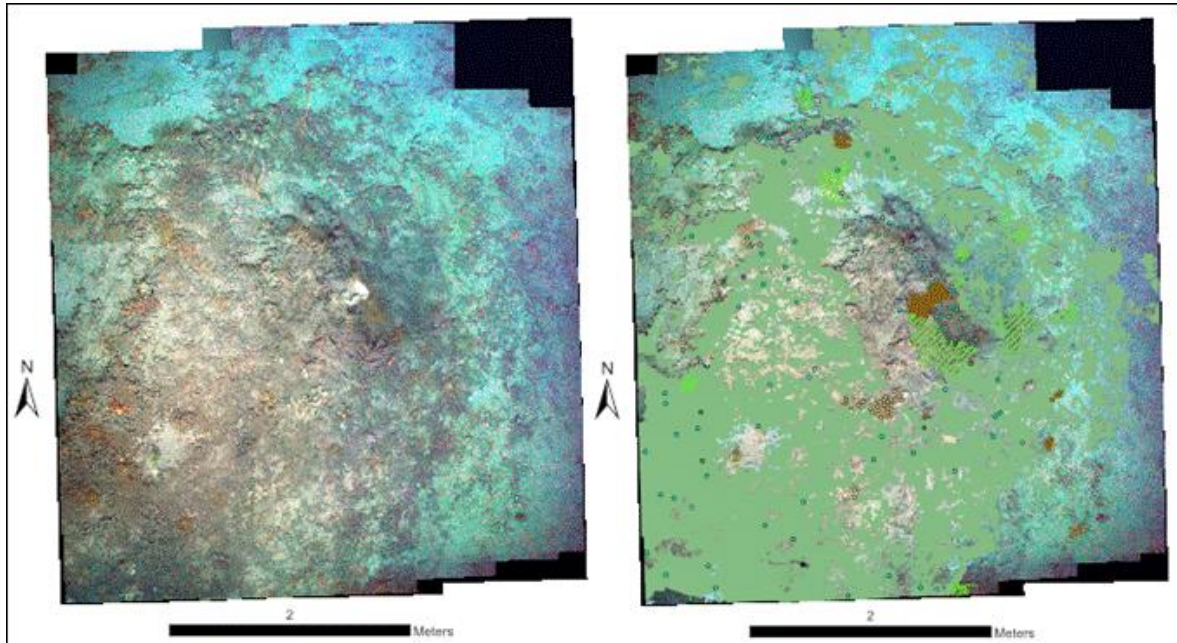
Figure 4-34. Photomosaic of Marker E in 2010 and digitization of this mosaic.

## 4.2.3.1.18    GC354: Mosaic Marker V, 2010 (only)

This site is located at 91.82641˚N 91.82641˚W at a depth of about 526 m. Images for the mosaic were collected on dive J2-529 on 10/19/10. The mosaic covers an area of approximately 21 m². The mosaic features a raised carbonate rock outcropping in the center of the image. Dead *Lophelia pertusa* coral extends from this rock to the north and east with a few interspersed areas of living *Lophelia*. Three sponges, 27 anemones, 36 crabs, and one *Hoplostethus occidentalis* fish are found at this site concentrated on and around dead *Lophelia* on the northern half of the site.
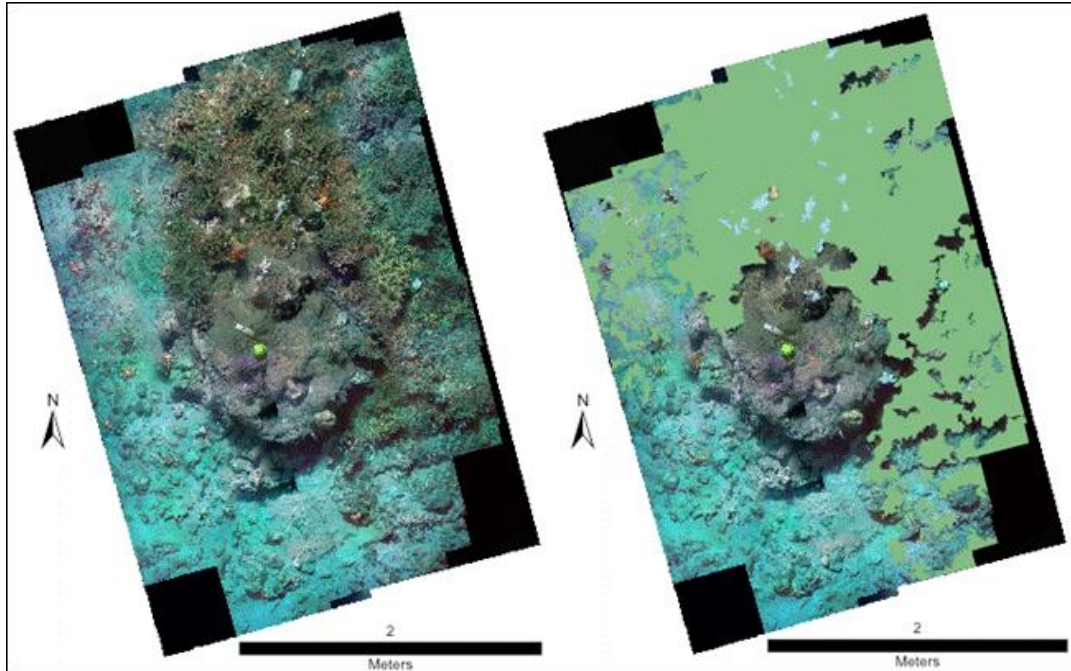
Figure 4-35. Photomosaic of Marker V in 2010 and digitization of this mosaic.

### 4.2.3.1.19    MC885: Mosaic Marker U, 2010 (only)

This site is located at 28.47330˚N 89.71707˚W at a depth of about 633 m. Images for the mosaic were collected on dive J2-527 on 10/16/10. The mosaic covers an area of approximately 26.4 m². Most of the surface is mud but a few exposed carbonate rocks are visible with attached corals. Live and dead *Madrepora* sp. are observed on the central outcroppings. A number of *Callogorgia* sp. colonies can be seen on the seabed and other rocks. Eight ophiuroids are found on these *Callogorgia* sp. One isopod, one Moridae fish, and two urchins compose the rest of the visible mobile fauna.
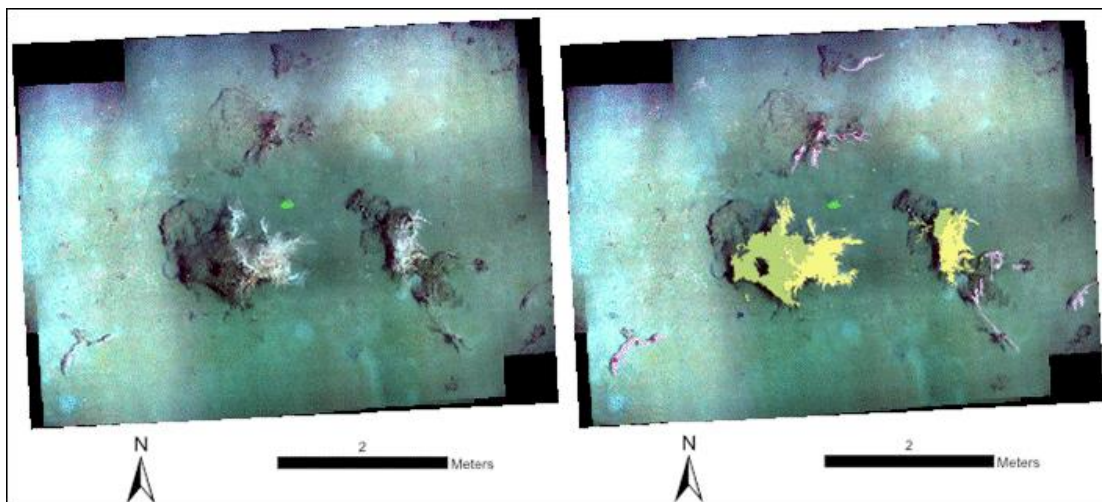


Figure 4-36. Photomosaic of Marker U in 2010 and digitization of this mosaic.

### 4.2.3.1.20   AT047: Mosaic Marker A, 2009 (only)

This site is located at 27.88028°N 89.78869°W at a depth of approximately 834 m. Images for the mosaic were collected on dive J2-457 on 8/24/09. The mosaic encompasses a roughly square area of about 39.5 m². The southern half and part of the northwest portions of the mosaic are covered in dead *Madrepora* sp. and the center of the northern mass features some living *Madrepora* sp. The rest of the mosaic is covered in sediment littered with clam shells and coral rubble with a few small outcroppings of carbonate rock. *Paramuricea* sp. is observed on the eastern and western corners covered in 21 ophiuroids. Thirty crabs, one sea star, five urchins, one pycnogonida, six shrimp, three whelks, and an anemone are also found at this site with the crabs concentrated on and around the patches of dead *Madrepora* sp.
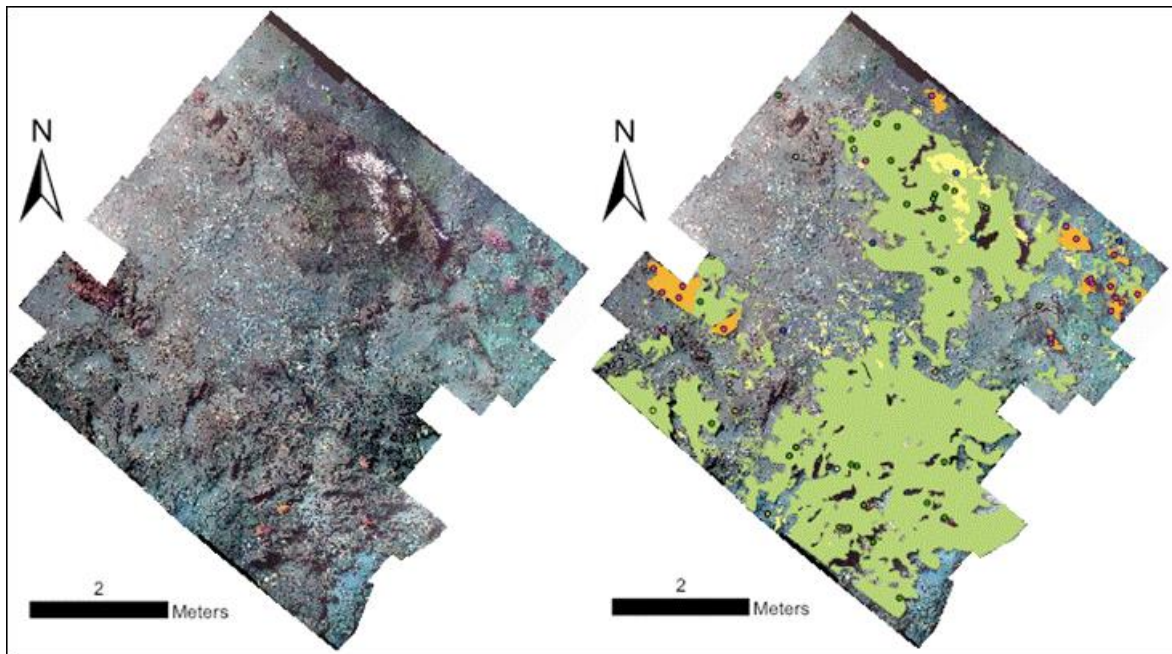


Figure 4-37. Photomosaic of Marker A in 2009 and digitization of this mosaic.

### 4.2.3.1.21   MC118: Mosaic Markers T1 and T2, 2010 (only)

This site is located at 28.85275°N 88.49270°W at a depth of about 884 m. Images for the mosaic were collected on dive J2-538 on 10/30/10. The mosaic covers an area of approximately 25.5 m². The primary substrate is mud with some dead coral. A carbonate rock outcropping is visible in the southwest corner. The sole coral found in this mosaic is the deep sea scleractinian *Madrepora oculata.* Living colonies are found at the center of the map growing on and surrounded by dead coral. Eighteen red crabs, *Chaceon quinquedens,* are visible among the coral.
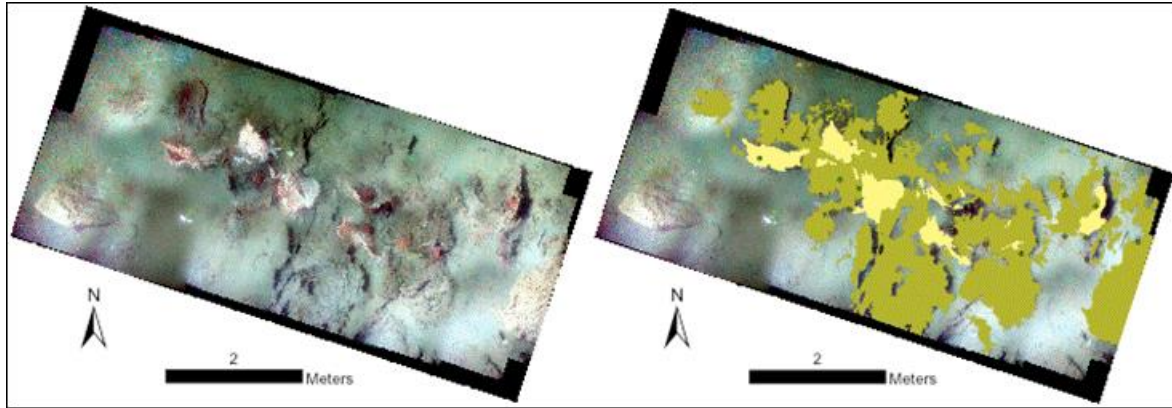
Figure 4-38. Photomosaic of Markers T1/T2 in 2010 and digitization of this mosaic.

## 4.2.3.1.22    MC118: Mosaic Marker X, 2010 (only)

This site is located at 28.85271°N 88.49253°W at a depth of about 883 m. Images for the mosaic were collected on dive J2-538 on 10/30/10. The mosaic covers an area of approximately 50.2 m². The primary substrate is mud with some dead coral. Some carbonate rock outcropping is visible in the northeast corner and near the center. The sole coral found in this mosaic is the deep sea scleractinian *Madrepora oculata.* Living colonies are found along the center of the map growing on and surrounded by dead coral. Twenty-two red crabs, *Chaceon quinquedens*, and six as yet unidentified crabs are visible among the coral. One hundred fifty-two  mussels are also present, concentrated mainly at the south corner of the mosaic but with smaller patches found along the center of the mosaic's length.
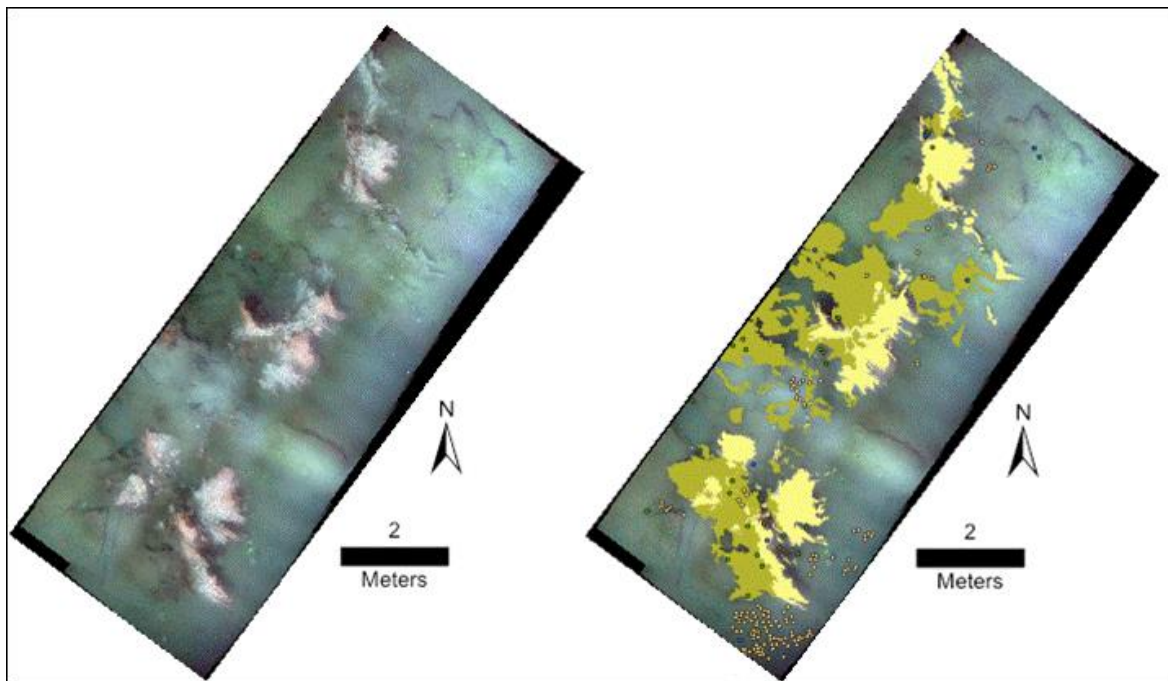


Figure 4-39. Photomosaic of Marker X in 2010 and digitization of this mosaic.

### 4.2.3.1.23    MC294/338: Mosaic Marker AA, 2010 (only)

This site is located at 28.67224°N 88.47652°W at a depth of about 1,371 m. Images for the mosaic were collected on dive J2-541 on 11/3/10. The mosaic covers a large area of approximately 307.3 m$^2$. A rocky outcropping lies at the center of this mosaic with a shallow trough running down its center northwest to southeast dividing it in two. *Paramuricea* sp. is the most abundant coral at this site, of which there are 45 observed colonies.   Thirty-nine ophiuroids are found on the *Paramuricea* sp. Three single colonies of *Paragorgia* sp., *Clavaluria rudis,* and *Acanthogorgia aspera* are also observed. Mobile fauna at this site include six anemones, 20 crabs, and one Nettastomatidae eel. The vast majority of fauna lies on the outcroppings.
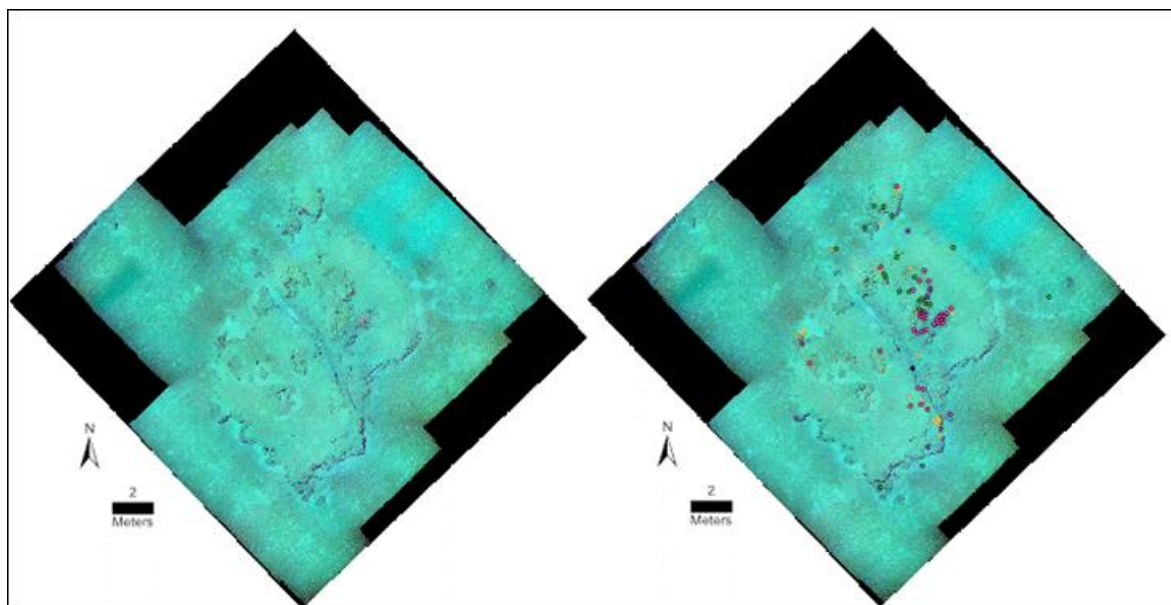


Figure 4-40. Photomosaic of Marker AA in 2010 and with each coral located on the mosaic.

### 4.2.3.1.24    GC852: Mosaic Marker 5, 2009 (only)

This site is located at 27.10978°N 91.16614°W at a depth of about 1,400 m. Images for the mosaic were collected on dive J2-461 on 8/29/09. The mosaic covers a rectangular area of approximately 38.7 m$^2$. This mosaic is centered on a rocky outcropping populated by a diversity of corals including *Leiopathes* sp., *Antipathes* sp., *Paramuricea* sp., *Madrepora* sp., Isididae, and the encrusting octocoral *Clavaluria rudis*. Some small crabs are found on and around the coral and five ophiuroids are observed on a *Paramuricea* in the southeastern corner of the mosaic. Three anemones and one Moridae fish are also found in this mosaic.
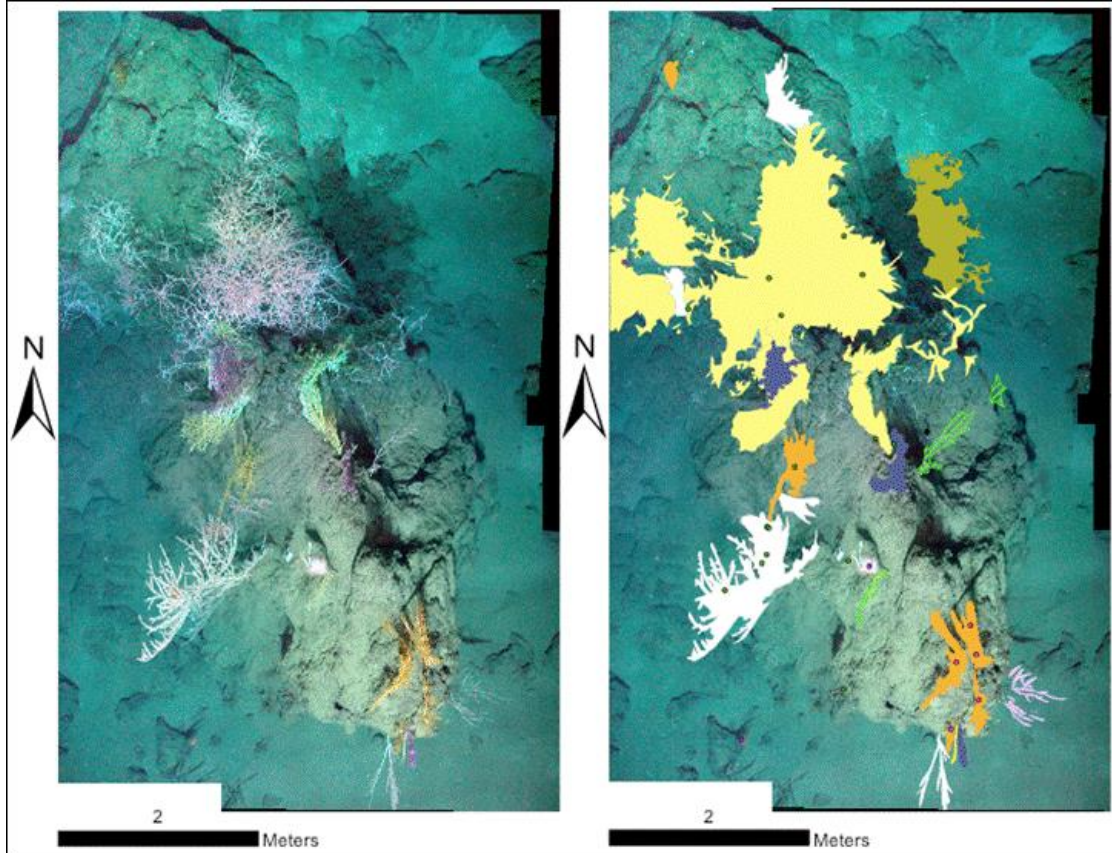
Figure 4-41. Photomosaic of Marker 5 in 2009 and digitization of this mosaic.

### 4.2.3.2 Mosaics Imaged from a Vertical Perspective:

4.2.3.2.1 Vertical Mosaic F - J2-460 - GB535 - Heading 309˚ (8/28/09)

This site is located at 27.4273˚N 93.5852˚W at a depth of approximately 520 m. The mosaic is a profile of a carbonate rock outcropping (approximately 1.5 m height) with several colonies of *Lophelia pertusa,* occupying the uppermost portions of the outcrop and a smaller one near the base. Three whip corals are around the base, and about 15 crinoids are scattered across the mound. Eight *Galatheid* sp. are present, mainly on the live *Lophelia pertusa* colonies. A solitary anemone, *Callogorgia* sp.*,* and *Paramuricea* sp.*,* are also present.
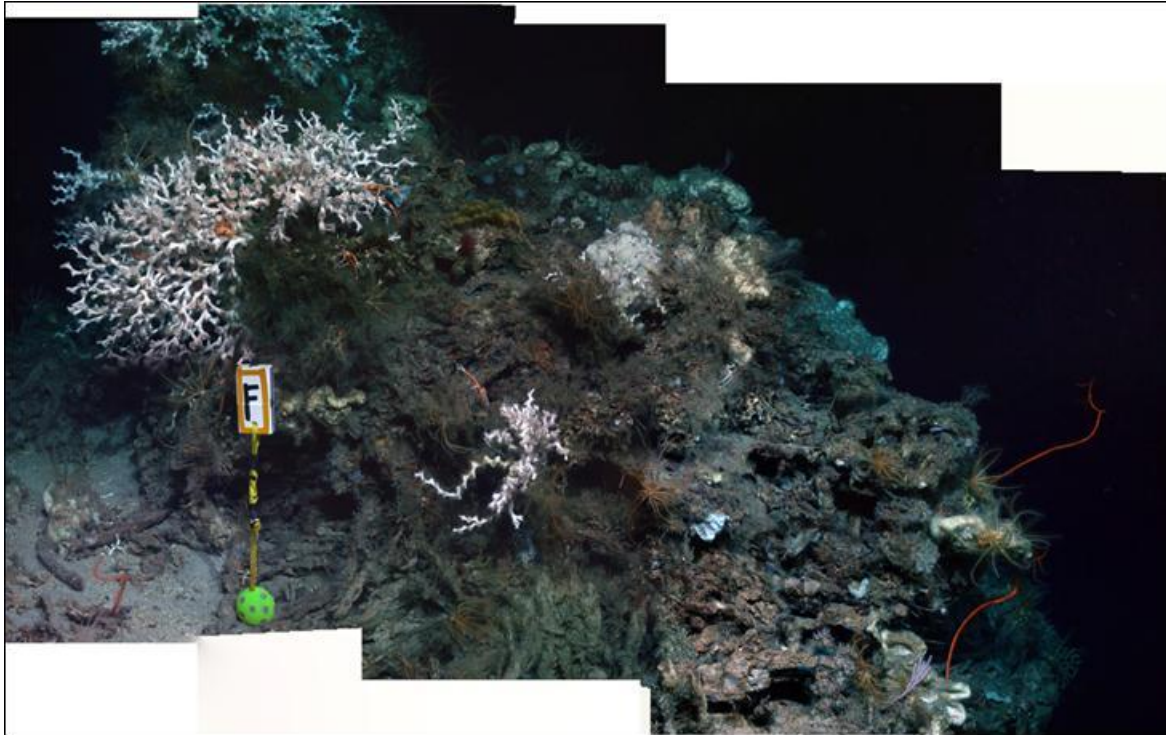
Figure 4-42. Vertical Mosaic F.

## 4.2.3.2.2 Vertical Mosaic 39 - J2-532 - GC140 - Heading 272˚ (10/22/10)

This site is located at 27.81112˚N 91.5372˚W at a depth of approximately 270 m. The mosaic is a profile of carbonate boulders; the uppermost boulder is densely populated with large *Leiopathes* sp.*,* with several *Callogorgis* sp. lower on the boulder. The lower portion of the boulder is covered in encrusting sponges, with whip corals flanking the boulder.
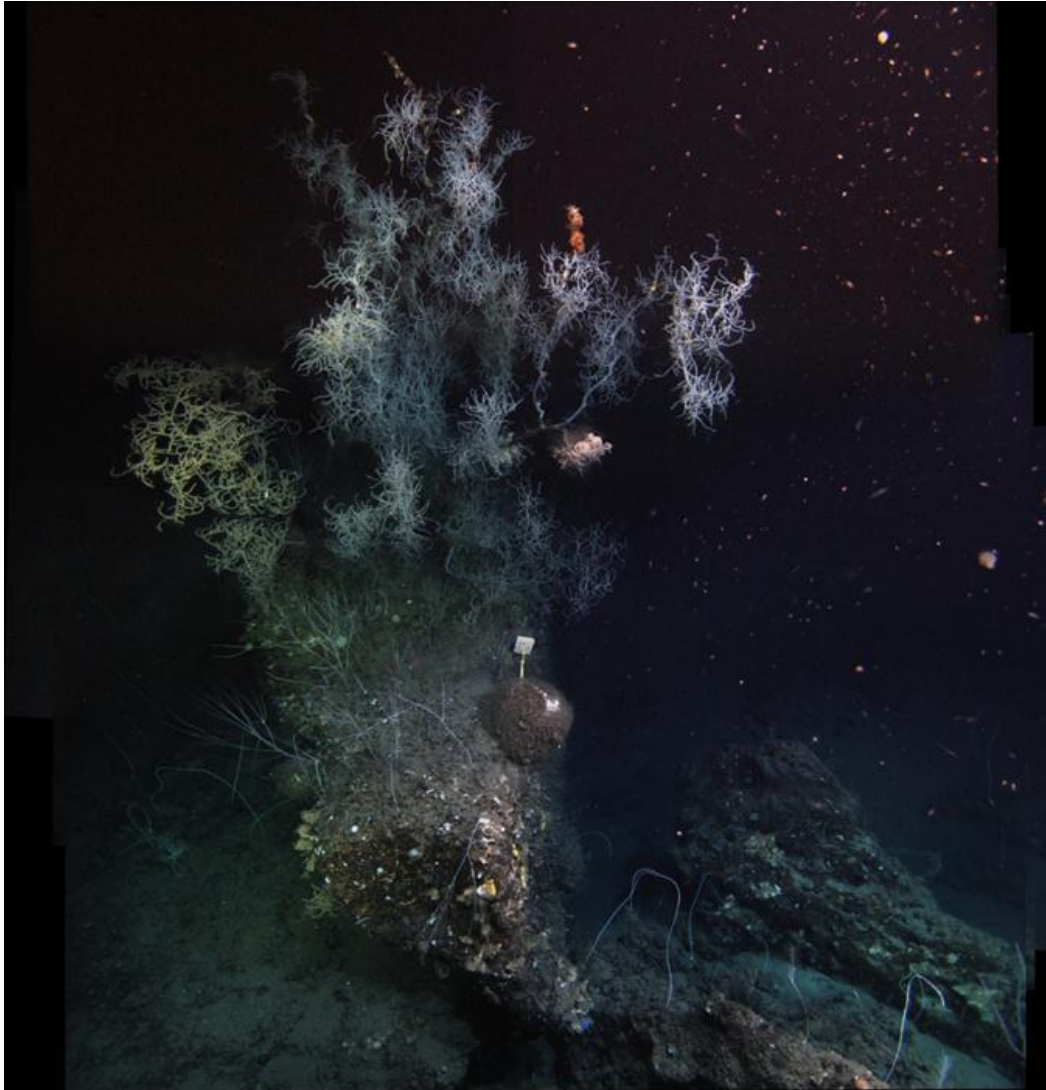
Figure 4-43. Vertical Mosaic 39.

## 4.2.3.2.3 Vertical Mosaic T1-T2 - J2-538 – MC118 - Heading 108˚ (10/30/10)

This site is located at 28.8527˚N 88.4927˚W at a depth of approximately 885 m. This mosaic is a profile of a low-elevation carbonate outcropping dominated by live *Madrepora oculata* growing on dead coral rubble. There are eight *Chaceon quinquedens* scattered about the *Madrepora* reef. There is one shrimp and *Galatheid* sp. crab in the middle of the image. There are no other coral species present.
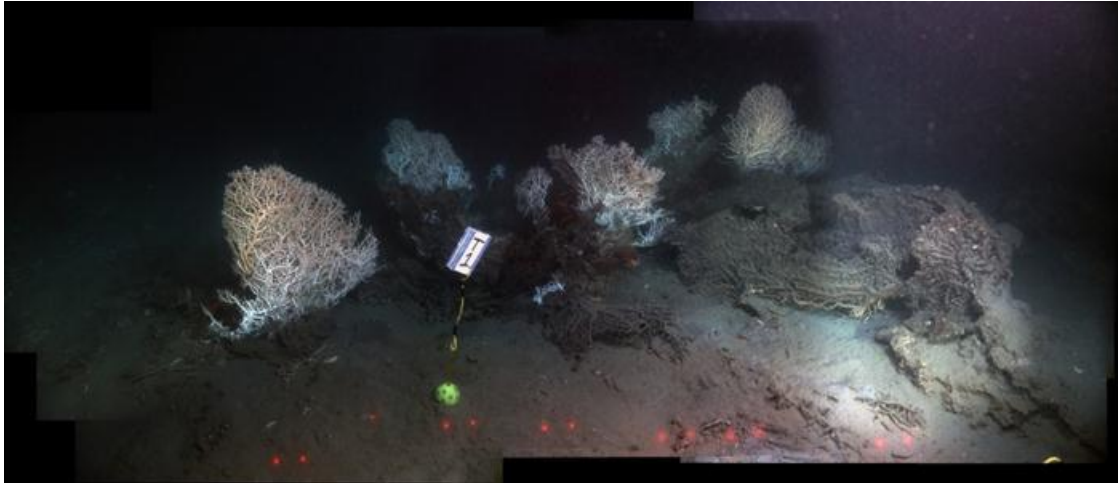
Figure 4-44. Vertical Mosaic T1-T2.

## 4.2.3.2.4 Vertical Mosaic X - J2-538 - MC118 – Heading 34˚ (10/28/10)

This site is located at 28.8527°N and 88.49257°W at a depth of approximately 880 m. Mosaic X is dominated by live *Madrepora oculata*, with some dead coral rubble scattered around the base. There is a solitary white sea urchin at the top of a *Madrepora* colony. There are approximately 10 *Chanceon quinquedens* swarming the reef.
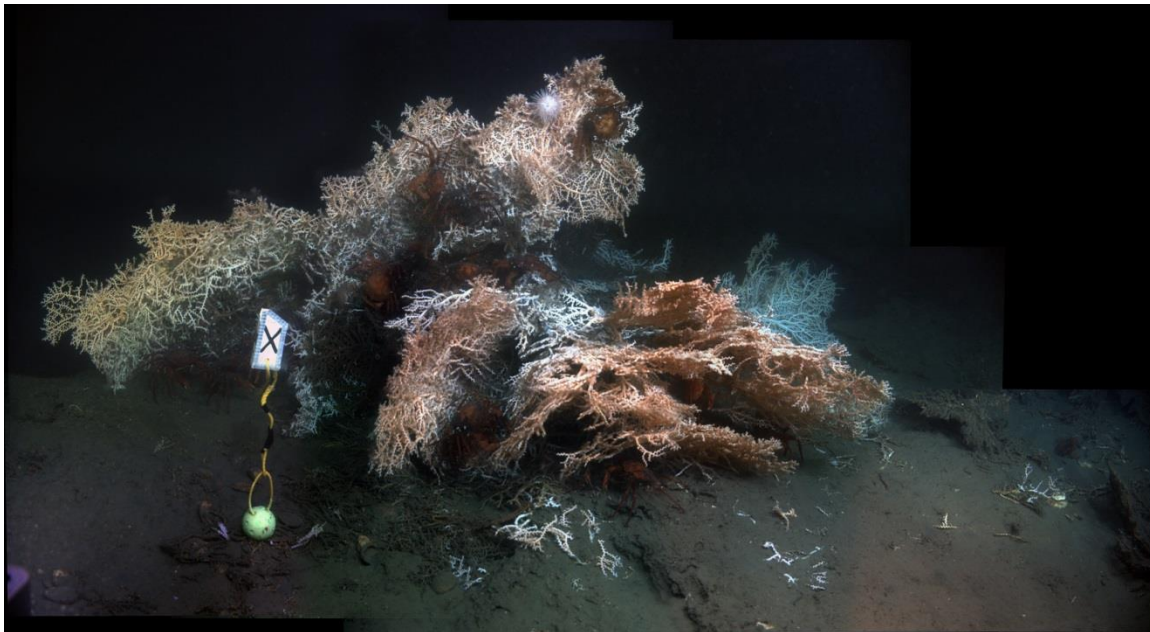


Figure 4-45. Vertical Mosaic X.

### 4.2.3.3 Comparison among Sites

To compare among sites, only one mosaic from each site was used in the analyses. The 2010 mosaic was used if the site was mosaicked in both years, but if it was only imaged in 2009, then the mosaic from that year was used. The mosaics can be compared in three ways using Bray-Curtis dissimilarity values, and the figures shown here each reflect one of these comparisons: 1) One can compare the "substrata" (dominated by living and dead corals) present in each by comparing the relative polygon areas, where the relative area reflects the proportion of total polygon area occupied by each substratum type. This approach compensates for different total areas mosaicked. 2) The solitary fauna (usually dominated by mobile fauna) can be compared between mosaics using the density of each faunal type, which again compensates for the different total sizes of the mosaics. 3) To compare the communities as a whole, the presence/absence of each type of fauna is compared. This is more sensitive to the size of the mosaics because none are capturing near the total diversity for the sites or regions: the larger the mosaic, the more of the total diversity likely to be sampled. This is one reason for the significant variation among mosaics and clearly indicates a high level of beta diversity within and among sites.

The two GB535 mosaics and the three mosaics from MC751 were the only ones greater than 80% similar to each other, and in some cases, mosaics from one site were less than 60% similar based on Bray-Curtis dissimilarity values calculated from species presence/absence (Figure 4-46). In Figure 4-47, the similarities in substrate types within a site/area are evidenced by the high level of similarity among most of the VK906 and VK826 sites and the generally tight grouping between pairs of mosaics within a site. On the other hand, the high ß diversity between mosaics within sites like VK862 and overall within a region are also evident in this figure. Similarities among areas within a site and also the high level of ß diversity within sites and among regions are also evident in the solitary fauna (Figure 4-48). The role of different corals in influencing the structure of the different communities can be seen quite clearly when the same data is coded by the dominant coral found within the mosaic (Figure 4-49).
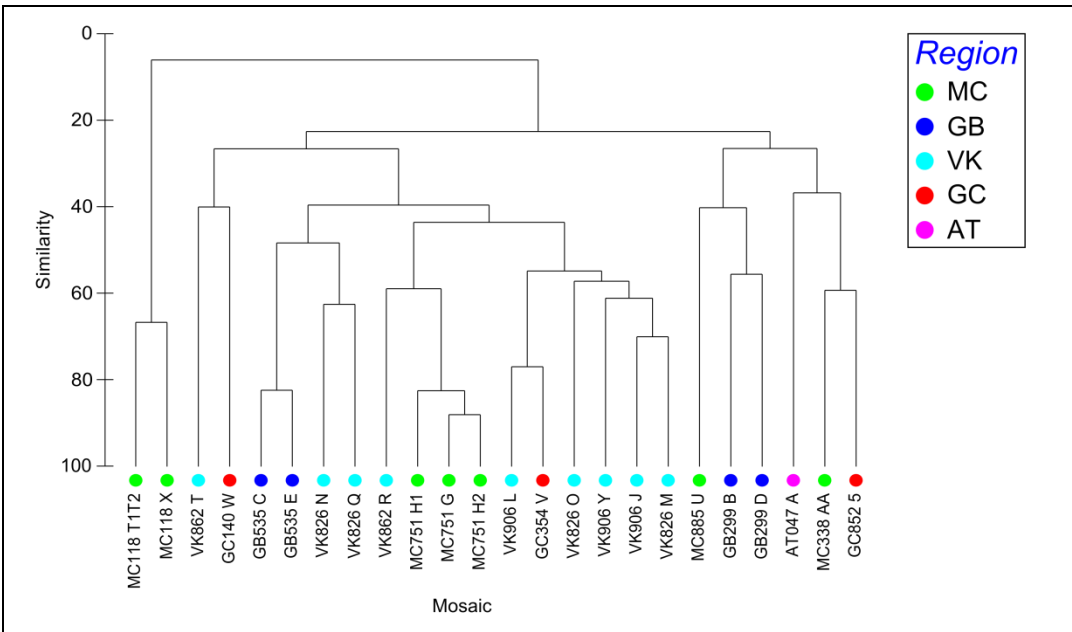
Figure 4-46. Hierarchical cluster dendrogram based on Bray-Curtis Index values of total faunal presence/absence showing the relationship between mosaic sites. If the site was imaged twice (in both 2009 and 2010), only the 2010 mosaic was used in this analysis. The mosaic sites are color-coded by lease block region.
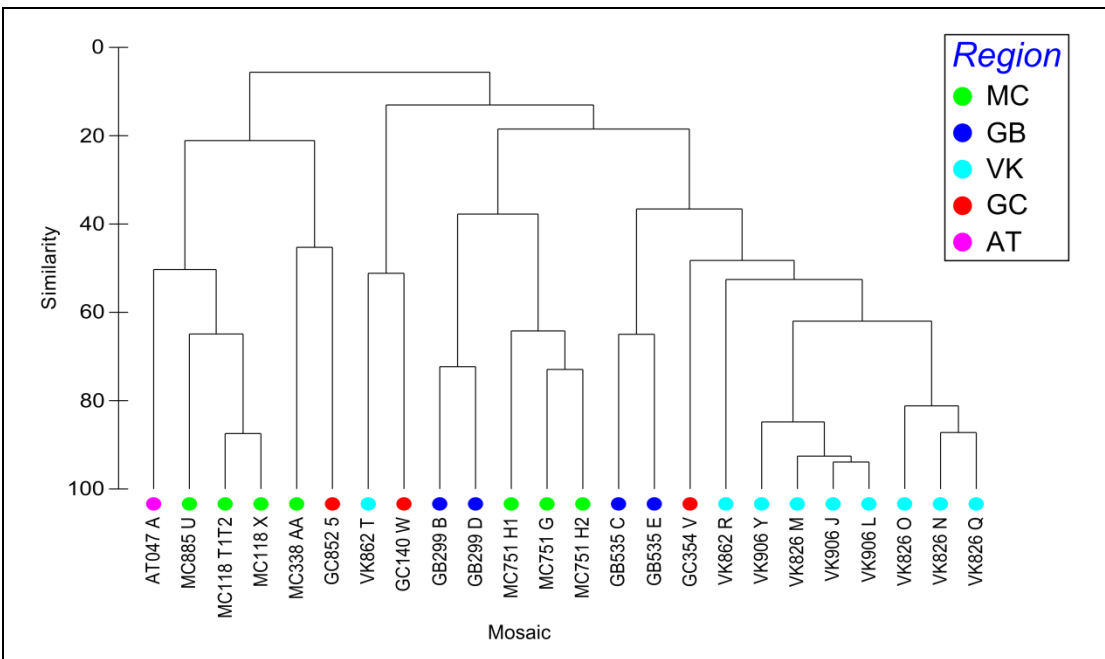


Figure 4-47. Hierarchical cluster dendrogram based on Bray-Curtis Index values of relative polygon coverage showing the relationship between mosaic sites. If the site was imaged twice (in both 2009 and 2010), only the 2010 mosaic was used in this analysis. The mosaic sites are color-coded by lease block region.

166
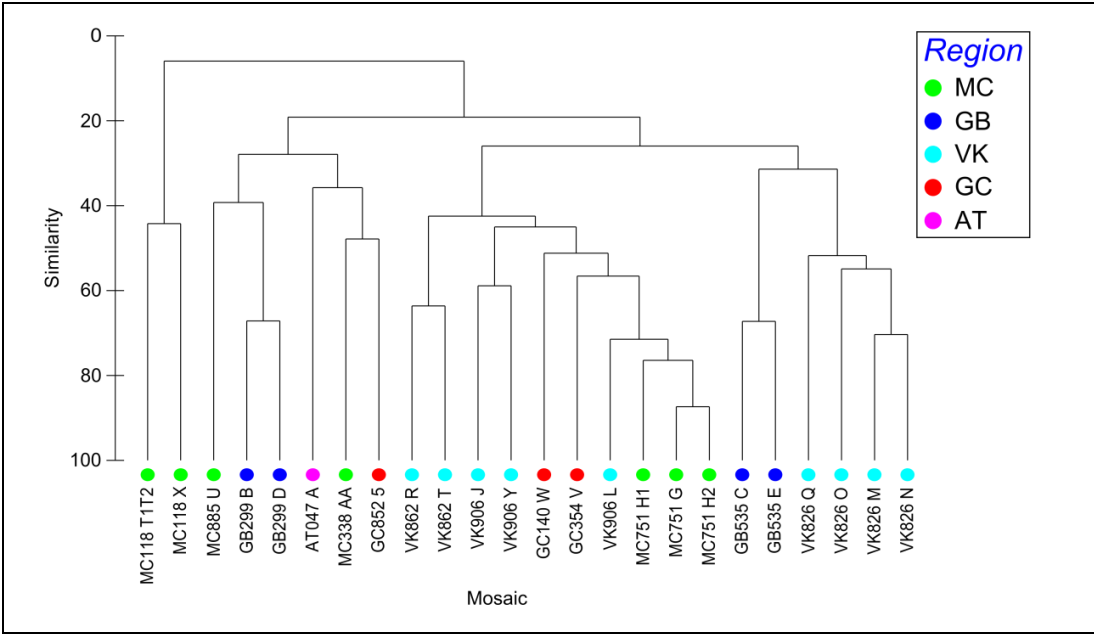
Figure 4-48. Hierarchical cluster dendrogram based on Bray-Curtis Index values of solitary fauna density showing the relationship between mosaic sites. The mosaic sites are color-coded by lease block region.
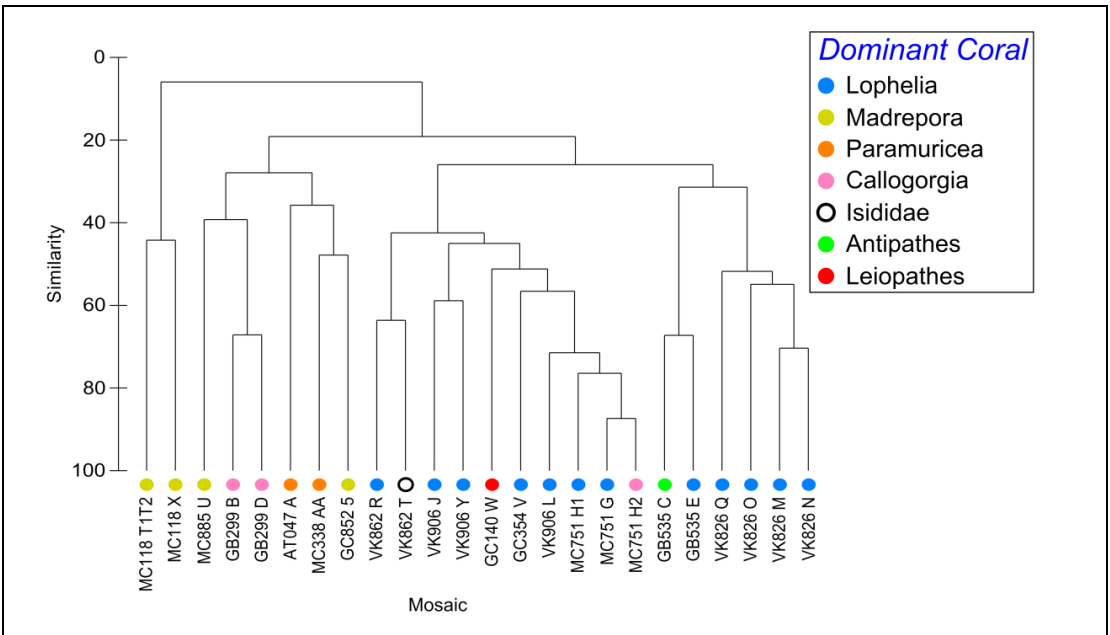


Figure 4-49. Hierarchical cluster dendrogram based on Bray-Curtis Index values of solitary fauna density showing the relationship between mosaic sites. If the site was imaged twice (in both 2009 and 2010), only the 2010 mosaic was used in this analysis. The mosaic sites are color-coded by the dominant coral present at that mosaic site.

When the same data is viewed in a multidimensional scaling ordination further insights into the patterns of solitary fauna biogeography become evident. Figure 4-50 shows the mosaics coded by region, and although there is some grouping by site, no clear discrimination by site is evident. In Figure 4-51, the mosaics are coded by dominant coral (data from Figure 4-49), and there is clear grouping of the communities associated with *L. pertusa,* and some evidence of grouping for other dominant corals. When the mosaics are coded by depth, the reason that some non- *L. pertusa* communities grouped with the *L. pertusa* communities is evident, as is the primary role of depth as a determinant of community structure (Figure 4-52). The same factors and the primary role of depth are evident in analysis of the fauna coded as polygons ("substrata") (Figure 4-53) and all fauna are analyzed as taxon presence/absence (Figure 4-54 with mosaics coded by depth).
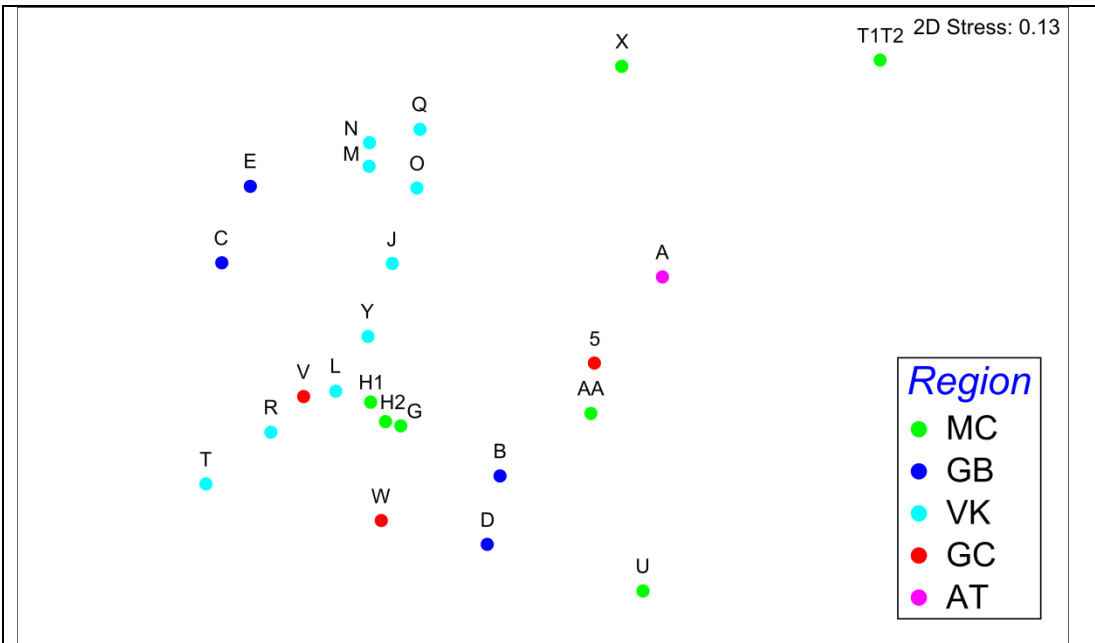


Figure 4-50. Non-metric multidimensional scaling ordination plot based on Bray-Curtis Index values of solitary fauna density. Each point represents a mosaic site color-coded by lease block region. If the site was imaged twice (in both 2009 and 2010), only the 2010 mosaic was used in this analysis.
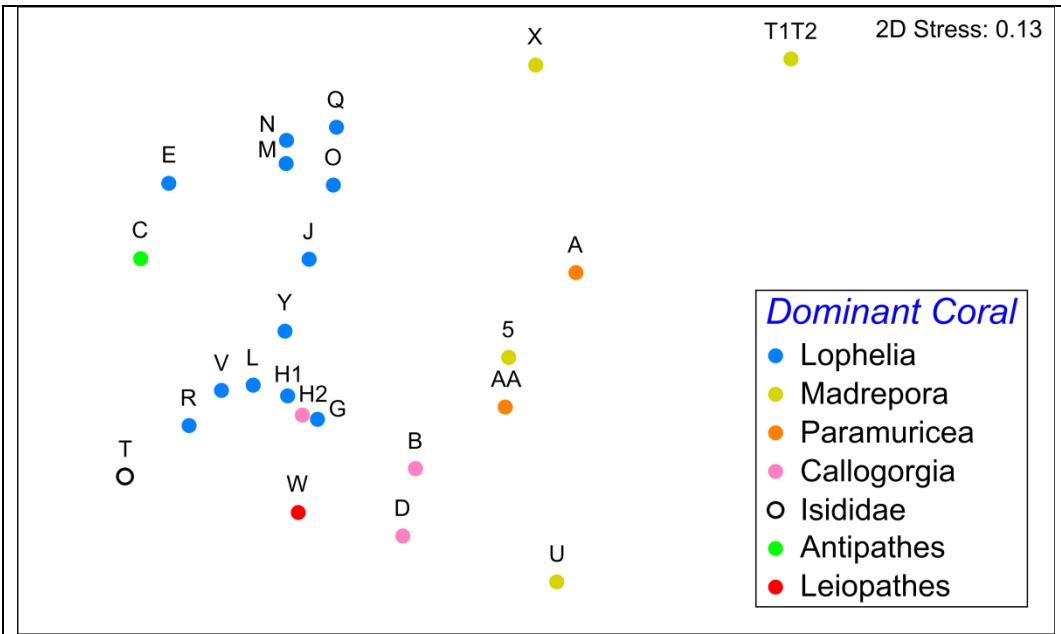
Figure 4-51. Non-metric multidimensional scaling ordination plot based on Bray-Curtis Index values of solitary fauna density. Each point represents a mosaic site color-coded by the dominant coral present at that mosaic site. If the site was imaged twice (in both 2009 and 2010), only the 2010 mosaic was used in this analysis.
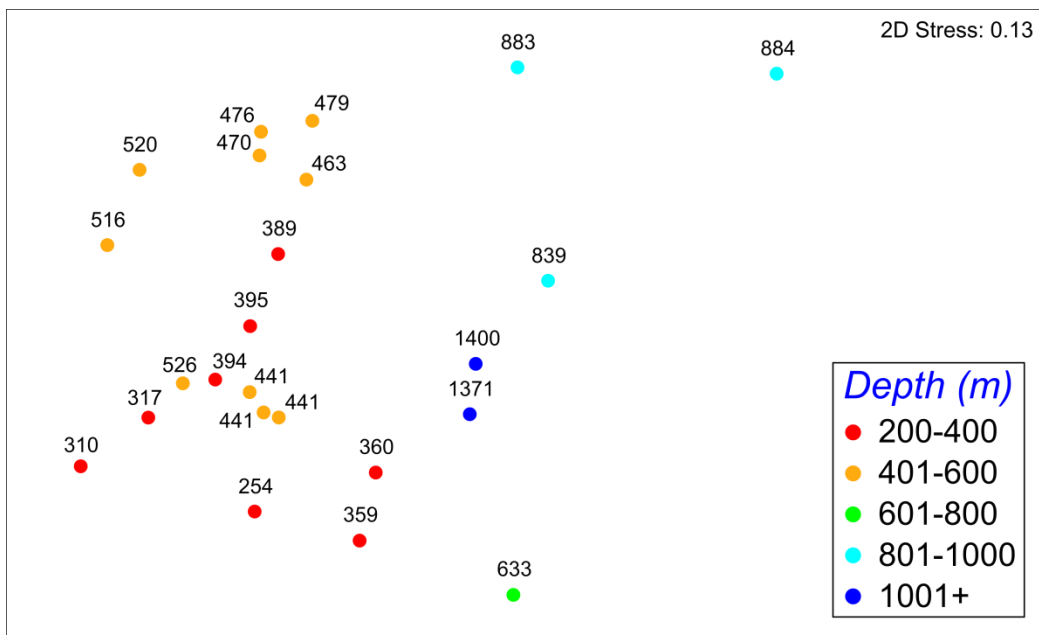


Figure 4-52. Non-metric multidimensional scaling ordination plot based on Bray-Curtis Index values of solitary fauna density. Each point represents a mosaic site color-coded hotto cold by depth and labeled with the site depth in meters. If the site was imaged twice (in both 2009 and 2010), only the 2010 mosaic was used in this analysis.
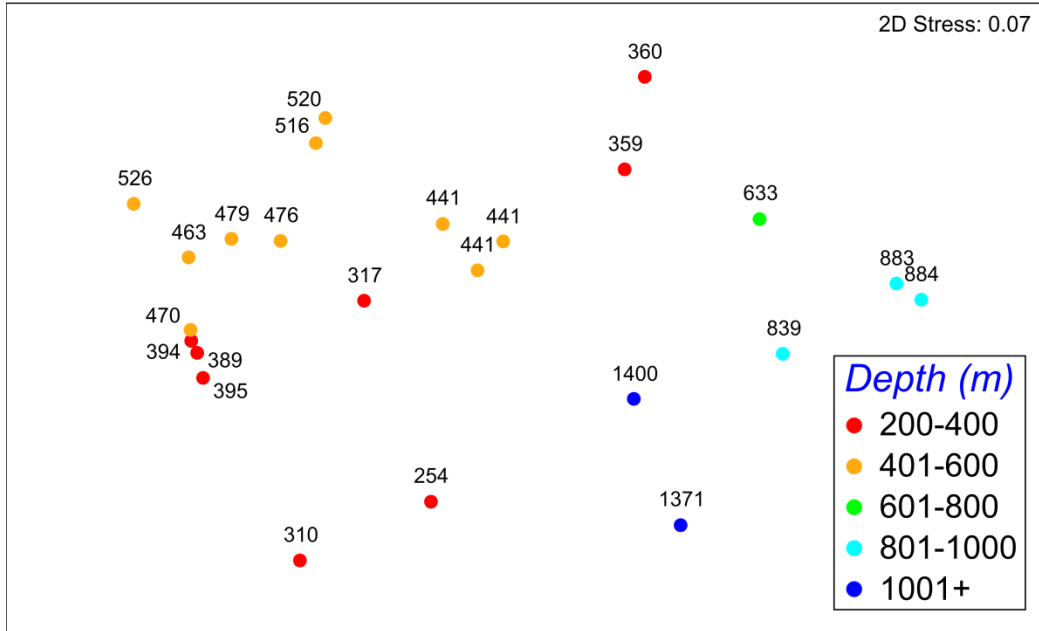
Figure 4-53. Non-metric multidimensional scaling ordination plot based on Bray-Curtis Index values of relative polygon coverage. Each point represents a mosaic site color-coded hot to cold by depth and labeled with the site depth in meters. If the site was imaged twice (in both 2009 and 2010), only the 2010 mosaic was used in this analysis.
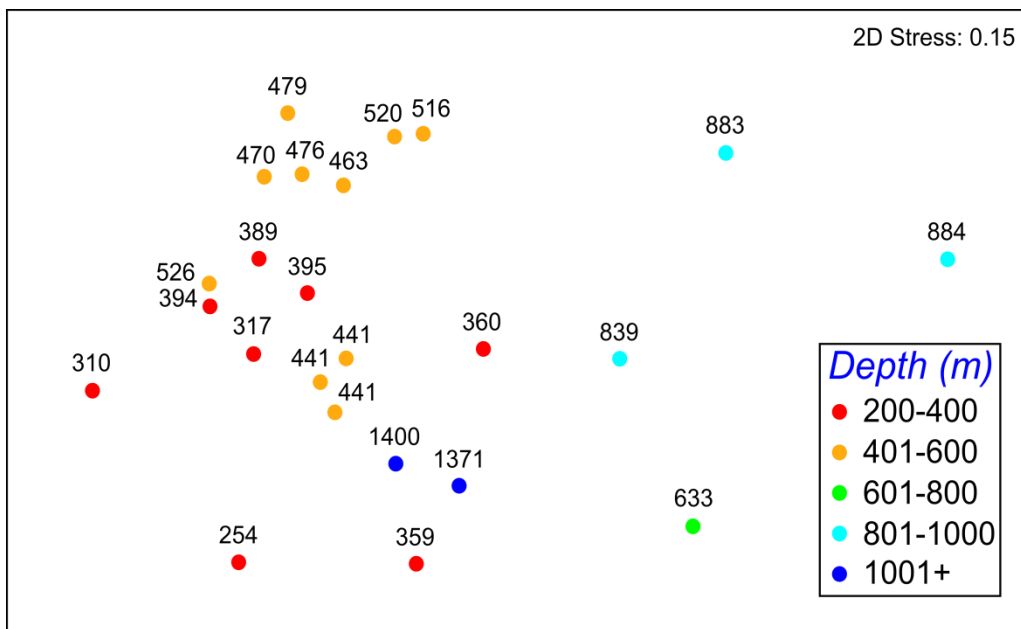


Figure 4-54. Non-metric multidimensional scaling ordination plot based on Bray-Curtis Index values of faunal presence/absence. Each point represents a mosaic site color-coded hot to cold by depth and labeled with the site depth in meters. If the site was imaged twice (in both 2009 and 2010), only the 2010 mosaic was used in this analysis.

Further insights into the role of region in the structure of the communities can be seen if much of the variation caused by depth and dominant coral is removed, and only the communities in the depth range where natural *L. pertusa* reefs are known to occur are included. Ordinations of both solitary fauna density and taxon presence/absence over this range clearly show mosaics grouping by site (Figure 4-55 and Figure 4-56). In these figures, the colors indicate the relative longitude with east to west going from hot to cold colors, and the communities seem to segregate by east and west of the Mississippi outflow as well (the Mississippi Canyon region being the dividing point).
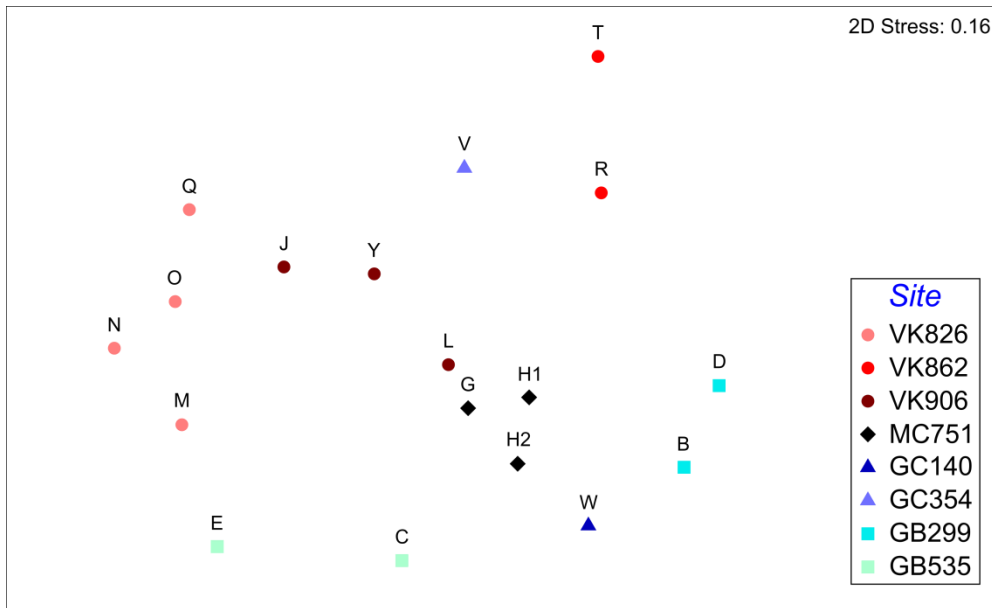


Figure 4-55. Non-metric multidimensional scaling ordination plot based on Bray-Curtis Index values of solitary fauna density. Each point represents a mosaic site within the range of *Lophelia pertusa* (200-600 m) labeled by mosaic site. The points are color coded longitudinally east to west by a red to blue gradient. Mississippi Canyon locations are colored black with sites west of the Mississippi Canyon colored blue and those east colored red. The shapes of the points are grouped by lease block region. If the site was imaged twice (in both 2009 and 2010), only the 2010 mosaic was used in this analysis.
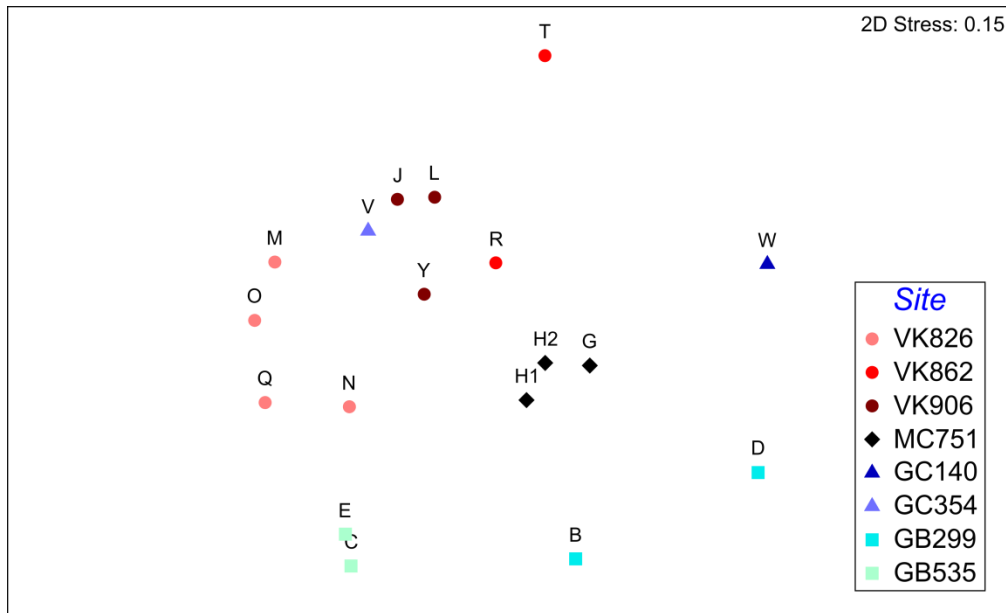
Figure 4-56. Non-metric multidimensional scaling ordination plot based on Bray-Curtis Index values of faunal presence absence of mosaic sites within the depth range of *Lophelia pertusa* (200-600 m) labeled by mosaic site. The points are color coded longitudinally east to west by a red-to-blue gradient. Mississippi Canyon locations are colored black with sites west of the Mississippi Canyon colored blue and those east colored red. The shapes of the points are grouped by lease block region. If the site was imaged twice (in both 2009 and 2010), only the 2010 mosaic was used in this analysis.

### 4.2.3.4 Fidelity of Solitary and Mobile Fauna to Substratum Types

By comparing the distribution of the solitary fauna across substrata to the availability of these substrata, one can determine if particular species are found on specific substrata more often than would be expected by chance alone and therefore detect preferences of the solitary fauna for particular substrata or conditions (Podowski et al., 2010). The results of this comparison are presented in Figure 4-57 to Figure 4-61 for those species that were observed at least 10 times in the 2010 mosaics. In extreme cases, this analysis can provide strong evidence for the fidelity of particular solitary species for particular corals. This was apparent with ophiuroids showing a preference for gorgonian corals at most sites, (gorgonians are included in the "other biological substrata" in the figures) (Figure 4-57). . Sites are arranged from west to east. $\chi^2$ analyses tested the null hypothesis that fauna are randomly distributed across all substratum types (*$p < 0.05$, **$p < 0.01$, ***$p < 0.0001$).

 The "other biological substrata" category include several different species, which very likely explains the different pattern seen at GC140 W for ophiuroids. The deep sea golden crab *Chaceon* sp. was only seen at three sites and was only abundant when *Madropora* sp. was present (Figure 4-57). Crinoids, on the other hand, while sometimes showing a preference for dead *L. pertusa* (sites VK826 M and VK826 O for example), more often show a distribution mimicking that of available substrata (Figure 4-57).

172

Two morphotypes of urchins were identified separately for this analysis and have similar distribution on available substrata. Statistical comparison is hampered by the low numbers of the *Cidaris* sp urchin; however, the absence of the other morphotype at all three MC751 sites where it occurs is notable and may reflect the integration of corals and tube worms at this site (Figure 4-58). Both were sometimes present at the same site and were often found on living or dead scleractinian coral when it was present.

The only colonial cnidarian treated in the solitary fauna class (as a point rather than a polygon) were the whip corals. They were only present on the western most sites. There is no evidence that these colonial corals have a substratum preference, although their presence on dead *L. pertusa* is notable (Figure 4-58). Two of the morphotypes of anemones (*Actinia* sp. and *Actinoscyphia* cf. *saginata*) have very similar distributions among sites, with both species present whenever either is abundant (Figure 4-59). Both are only rarely found on living biological substratum. The third morphotype is a type that burrows in sediment and as expected was never found on biological substrates and often present at sites without the other two morphotypes (Figure 4-59).

In many cases, the total number of individuals at a site is simply too small to draw conclusions about distribution patterns (Figure 4-60). Low numbers of observations were typical for several taxa of the most mobile fauna, and patterns should emerge if this database is increased with future visits and additional sites. In one case, a morphospecies of galatheid crab, "crab type 5", only 15 individuals were seen, but all were found at a single site, MC294, which is both the most easterly of the mosaic sites and also the deepest. Another galatheid, *Eumunida picta*, was found at most of the sites visited, and although it is found more often on hard substrata in the areas mosaicked than the surrounding sedimented seafloor, there was no strong indication of a preference among the substratum types in the mosaics (Figure 4-61). The taxon category "individual sponges" is polyphyletic. Close examination of this data set by sponge taxonomists might provide new information on distributions of different taxa, particularly at the two sites in MC751 (H1 and H2), where sponges were very often found associated with biological substrata other than scleractinian corals (Figure 4-61).
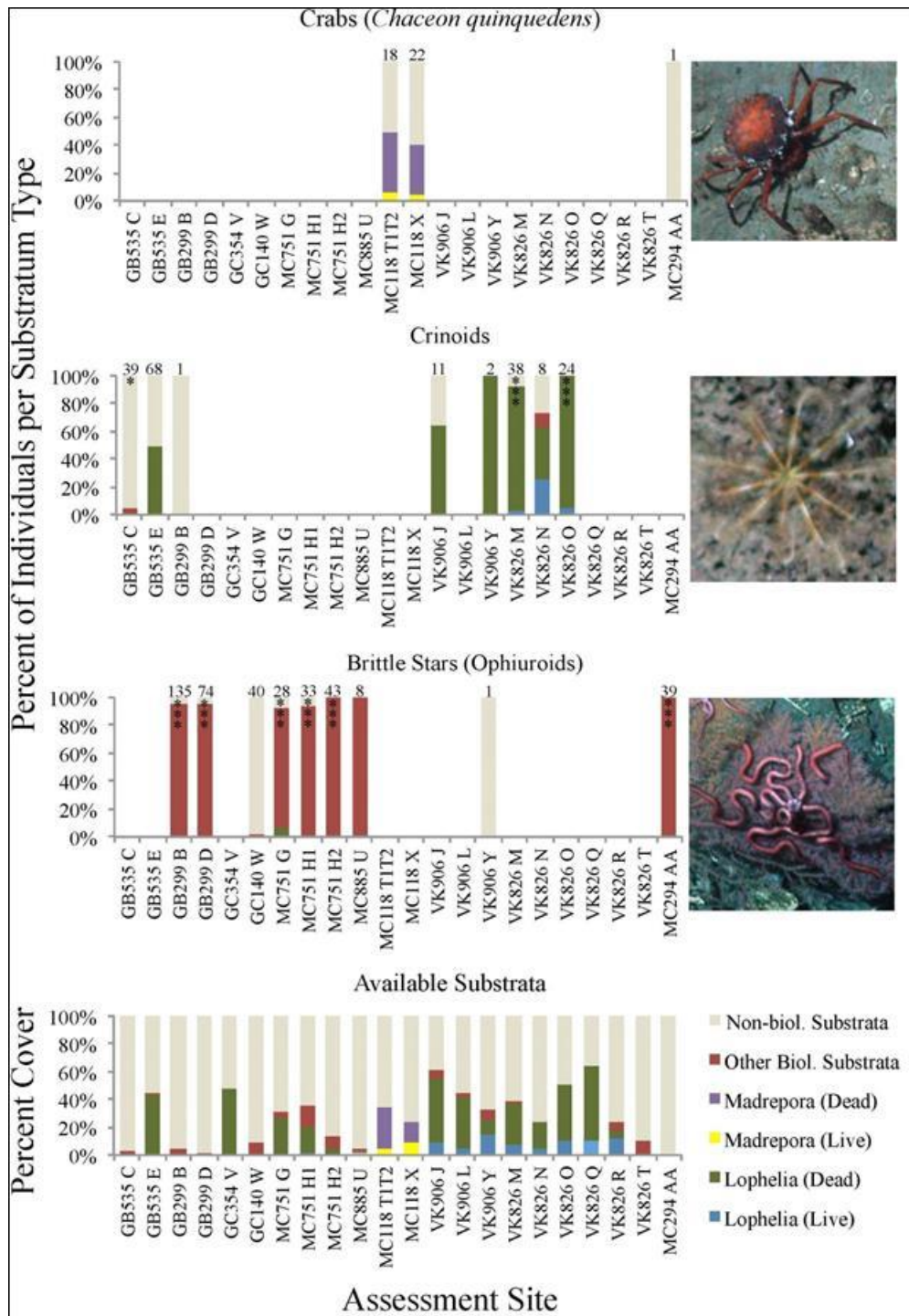
Figure 4-57. The top three graphs show the percent of the total population of the taxon (crabs, crinoids, brittle stars) that occurred on each substratum type at each site. Population size (n) at each site is shown over the columns. The bottom graph shows the percentage of each substratum type available at each site.
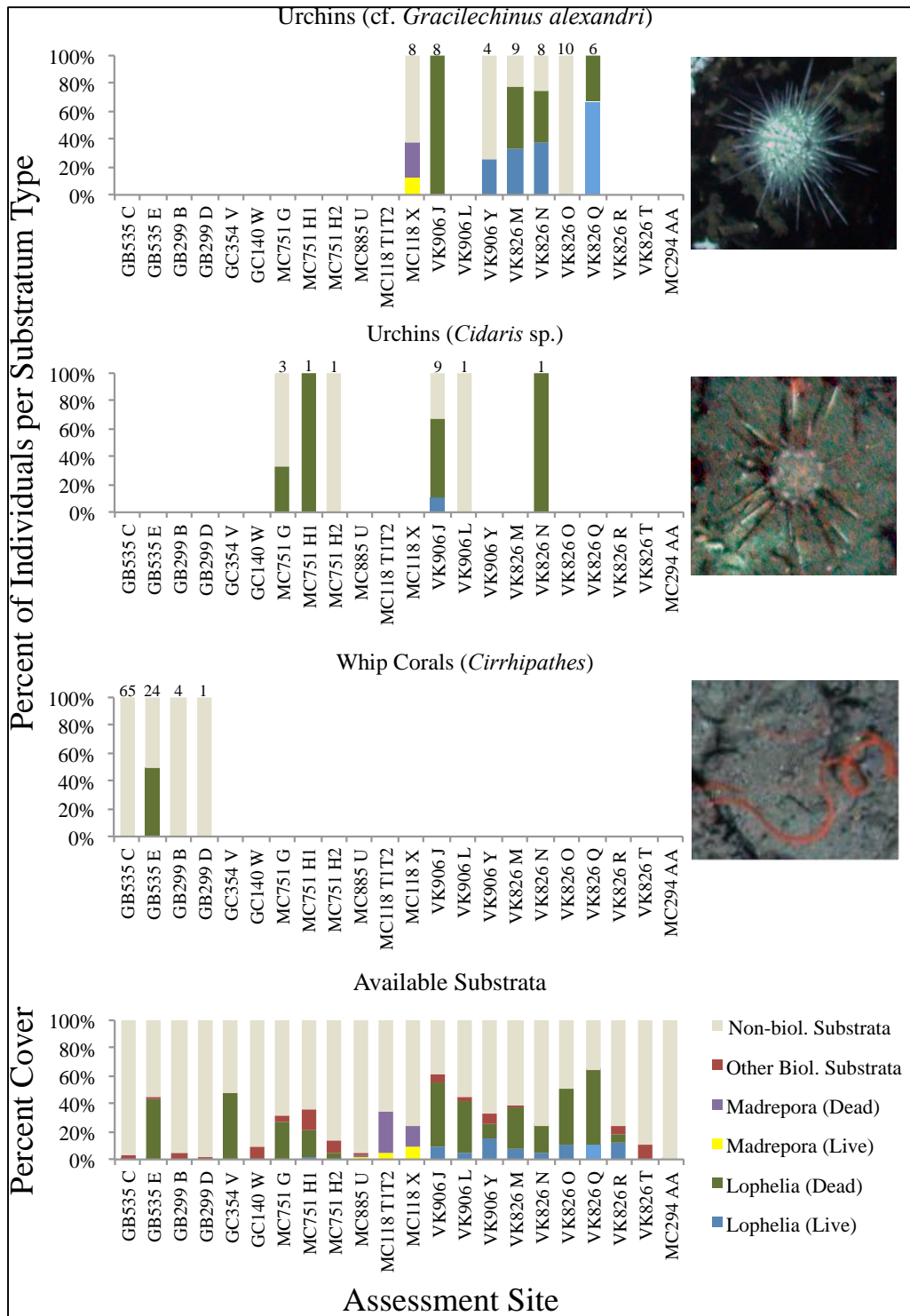
Figure 4-58. The top three graphs show the percent of the total population of the taxon (urchins, whip corals) that occurred on each substratum type at each site. Population size (n) at each site is shown over the columns. The bottom graph shows the percentage of each substratum type available at each site.
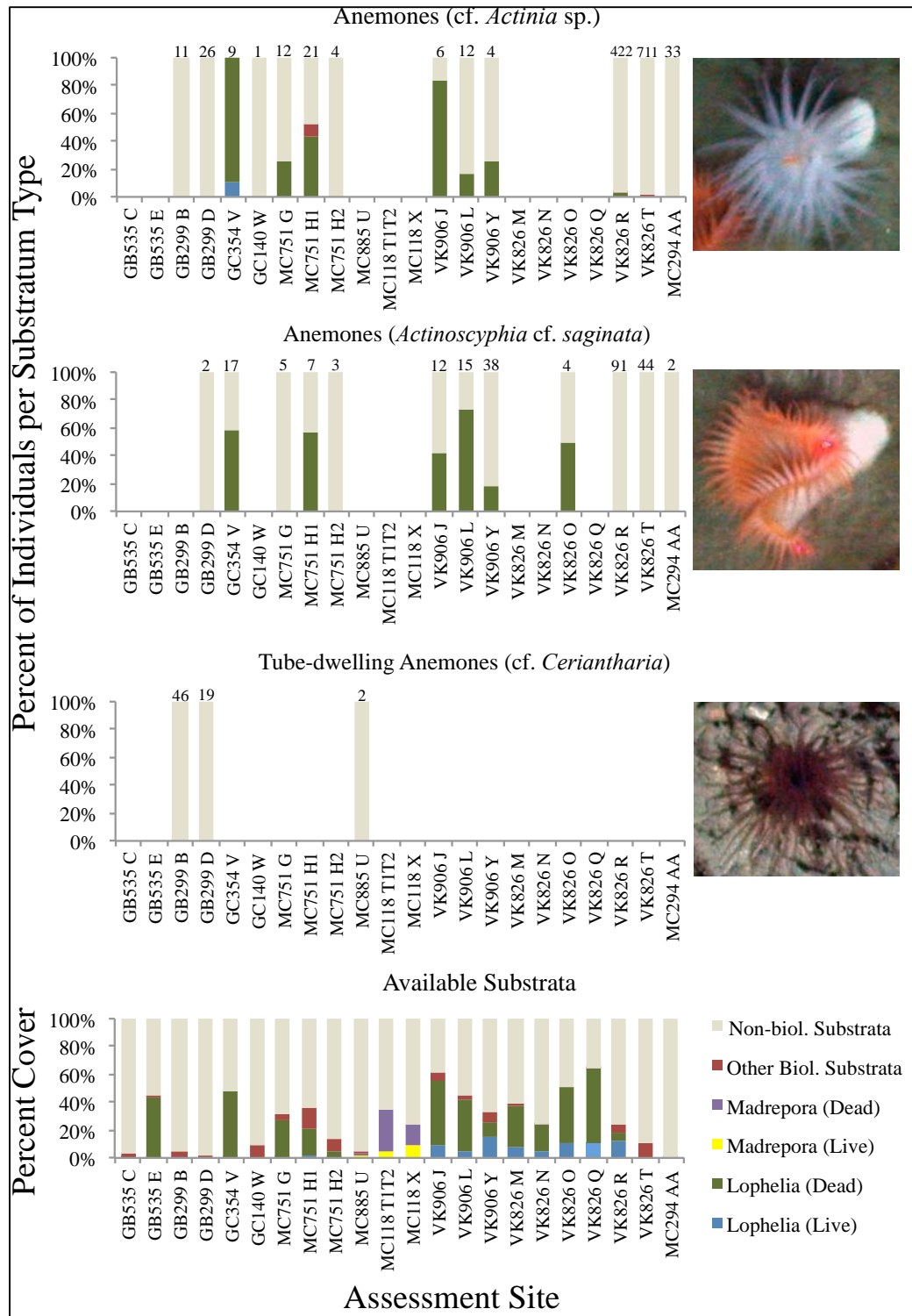
Figure 4-59. The top three graphs show the percent of the total population of the taxon (anemones) that occurred on each substratum type at each site. Population size (n) at each site is shown over the columns. The bottom graph shows the percentage of each substratum type available at each site.

176
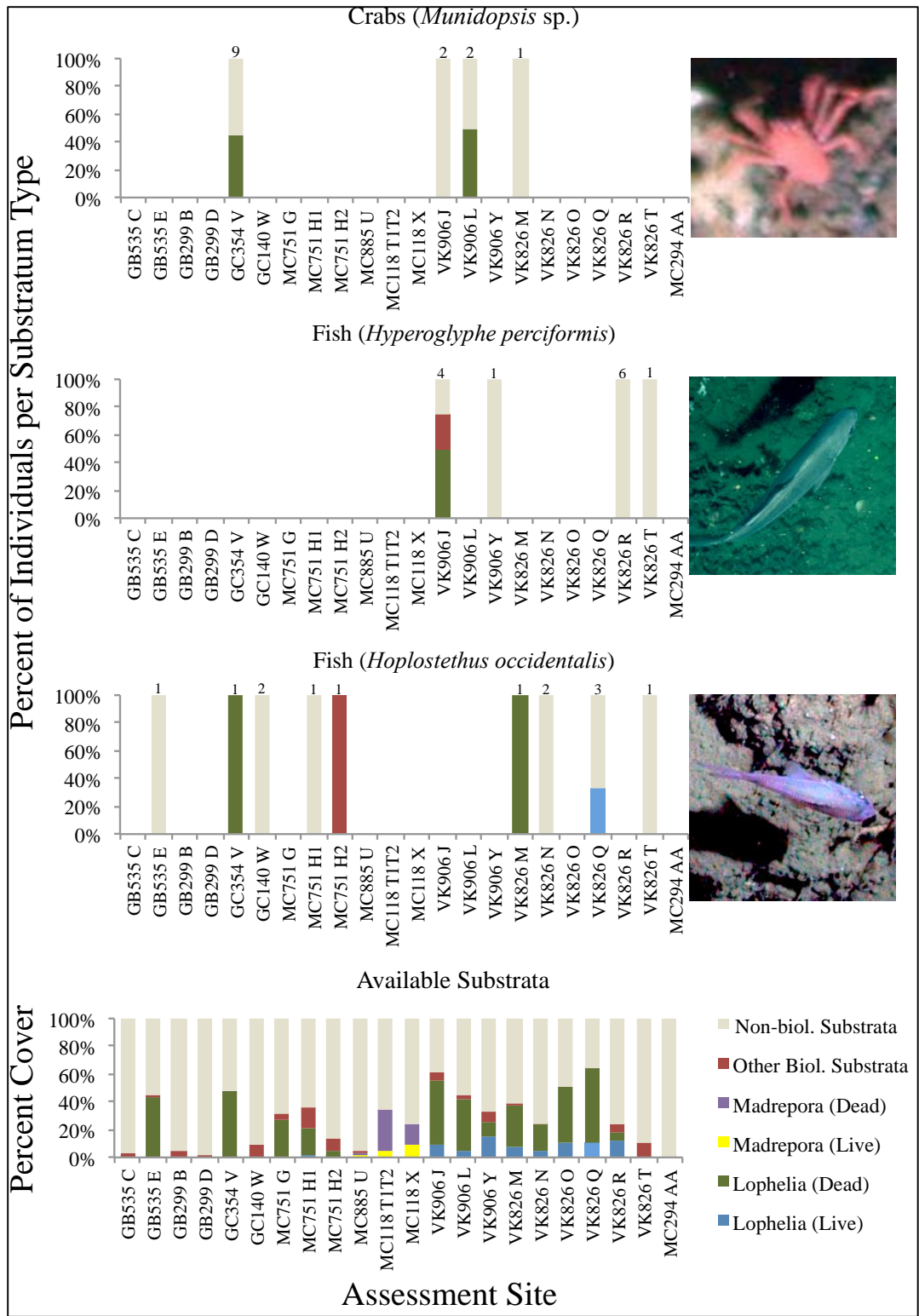
Figure 4-60. The top three graphs show the percent of the total population of the taxon (crabs, fish) that occurred on each substratum type at each site. Population size (n) at each site is shown over the columns. The bottom graph shows the percentage of each substratum type available at each site.
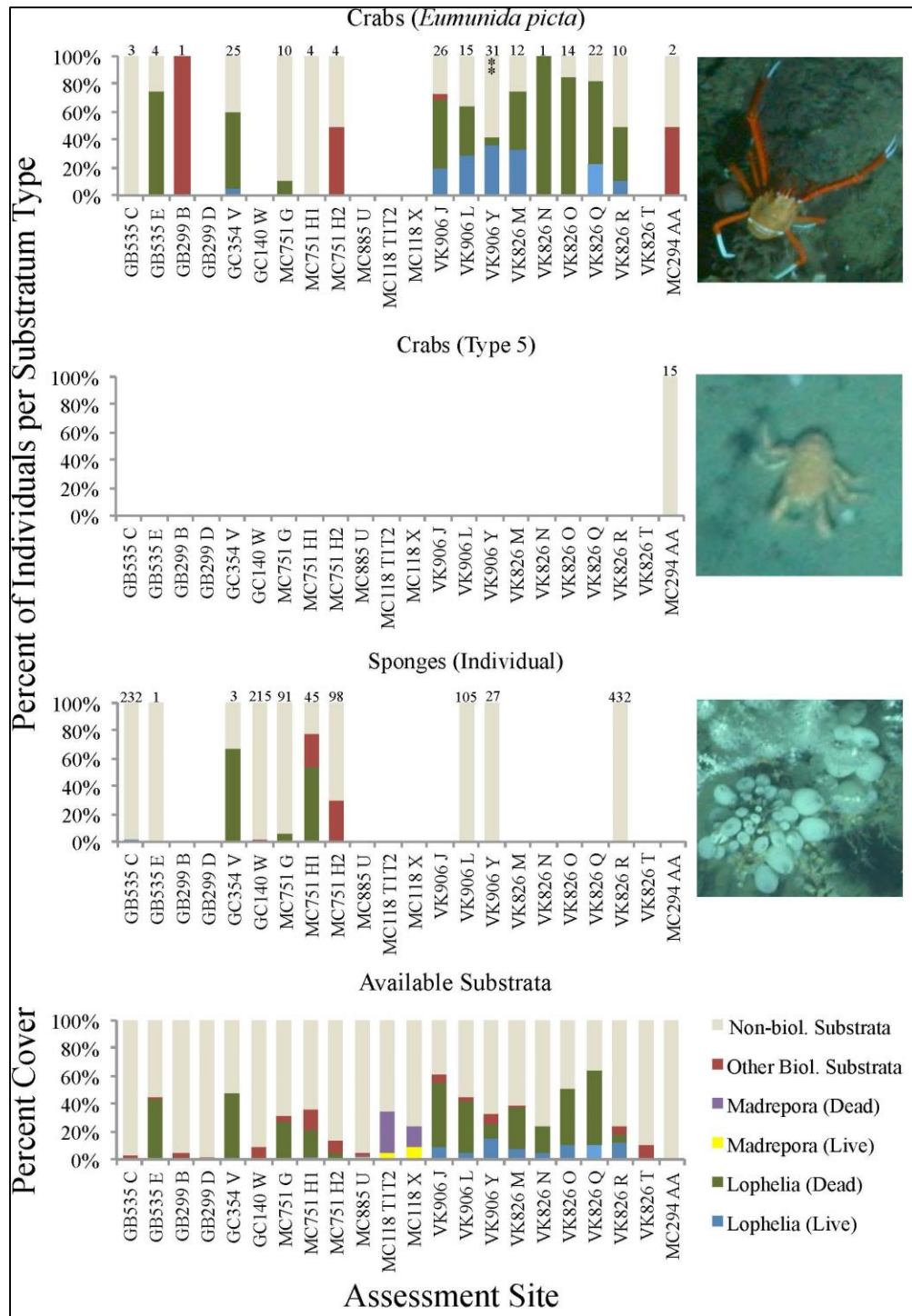
Figure 4-61. The top three graphs show the percent of the total population of the taxon (crabs, sponges) that occurred on each substratum type at each site. Population size (n) at each site is shown over the columns. The bottom graph shows the percentage of each substratum type available at each site.

### 4.2.3.5 Temporal Change in Communities between Years

Comparison of sites between years provides insights about both the coral community fauna and about the strengths and limitations of the technique. When the similarity between mosaics is compared based on presence absence of all species, all but three sites are more different between years than they are to other sites, and even those three pairs are less than 80% similar (Figure 4-62 and Figure 4-63). This is clearly due to the solitary fauna (which includes the most mobile fauna) and not the fauna/biological substrata digitized as polygons (which is dominated by corals). When only the relative areas occupied by different categories digitized as polygons are compared, most pairs are quite similar between years (>80%), despite being digitized by different individuals in different years (Figure 4-64)). All mosaics were examined manually to determine if there were real changes in the corals between years. In most cases the differences appear to be do to differences in the altitude and lines between surveys (which leads to some distortion when the two are georeferenced to each other) and in some cases differences in digitization technique between years (and digitizers). In one case a loss of a *L. pertusa* colony was found to have been caused by ROV operations during deployment of a camera system. Another apparent difference was tracked to displacement of the marker by about 1 meter between visits. The biggest difference in the digitized polygon data set between years was found in the two mosaics from GB299, where the polygons are dominated by upright gorgonian corals, and relative size of polygons is highly dependent on the angles of the imaging (Figure 4-8 and Figure 4-9). Even these show over 65% Bray-Curtis similarity, and inspection of the original mosaics did not identify real changes in the populations or individuals. In no case was an unexplained significant difference in the corals supported by re-inspection of the mosaics. This suggests that despite the profound acute impacts of the *Deepwater Horizon* spill on coral communities in the vicinity of the Macondo well, the other communities surveyed as part of this study, including *L. pertusa* reefs 38 to 60 km to the North and 150 km to the west, were not acutely impacted by the spill in ways that were visually apparent four months after the well was capped.
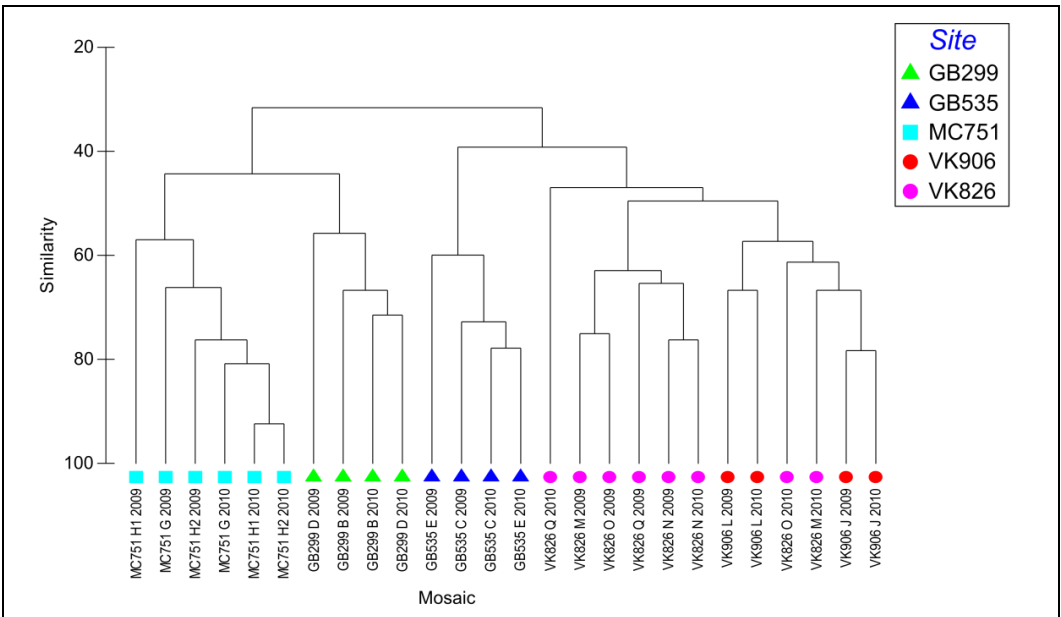
Figure 4-62. Hierarchical cluster dendrogram based on Bray-Curtis Index values of total faunal presence absence showing the relationship between the overlapping portions of mosaic sites imaged in both 2009 and 2010. The mosaic is color-coded by site and the shapes are grouped by lease block region.
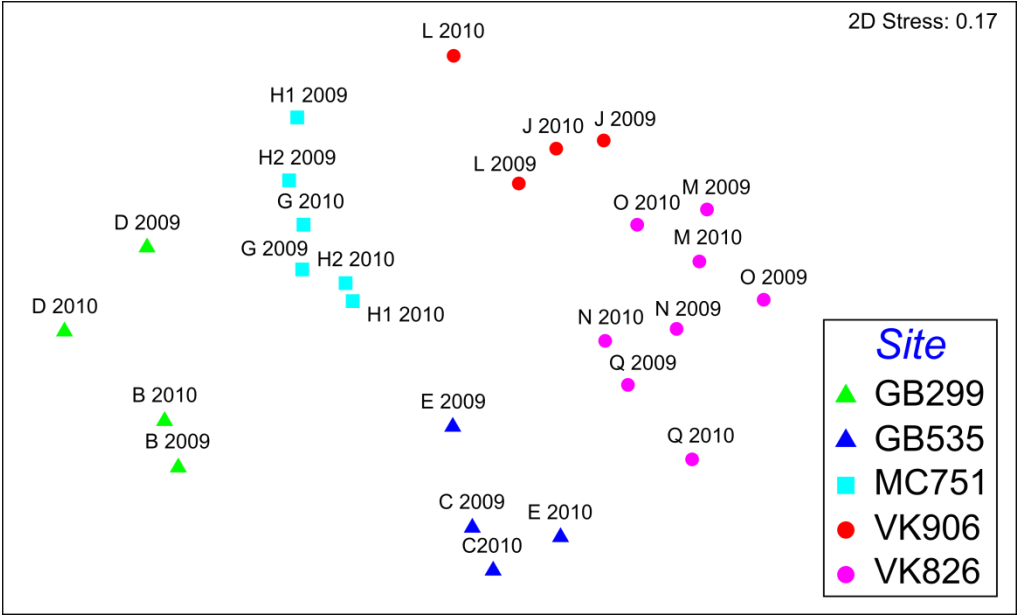


Figure 4-63. Non-metric multidimensional scaling ordination plot based on Bray-Curtis Index values of faunal presence absence showing the distance between the overlapping portions of mosaic sites imaged in both 2009 and 2010. Each point represents a mosaic color coded by site and grouped by shape according to lease block region.
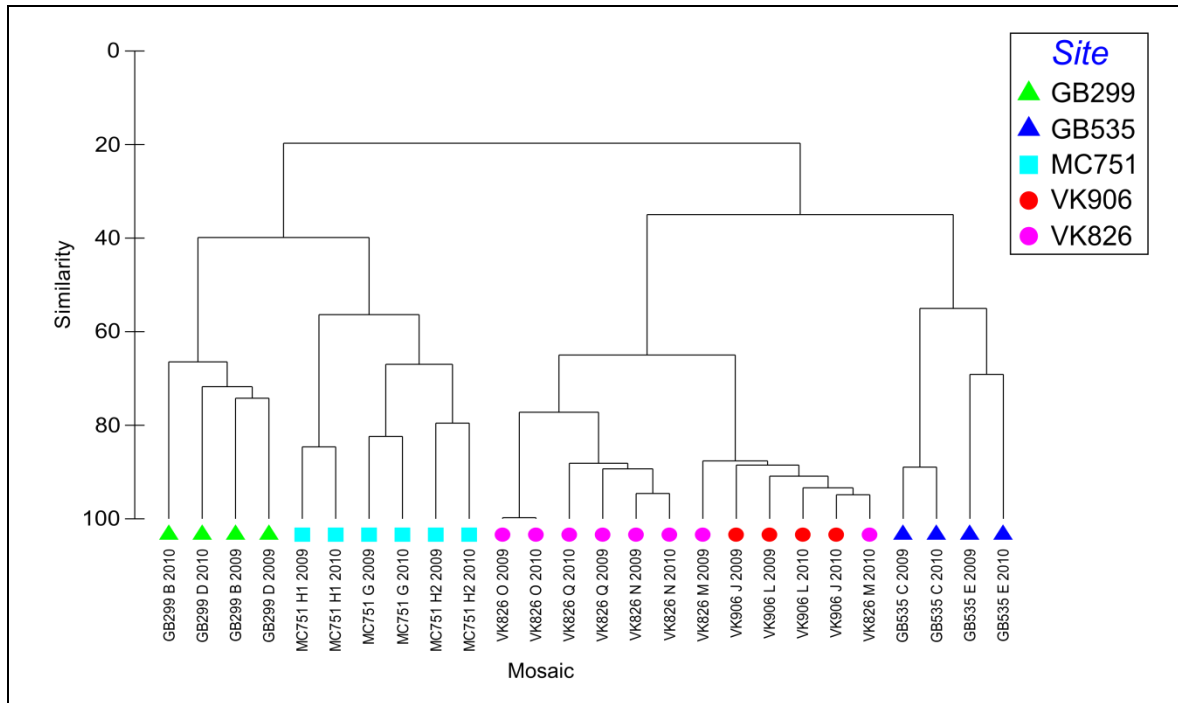
Figure 4-64. Hierarchical cluster dendrogram based on Bray-Curtis Index values of relative polygon coverage showing the relationship between the overlapping portions of mosaic sites imaged in both 2009 and 2010. The mosaics are color-coded by site and the shapes are grouped by lease block region.

On the other hand, there were often very large and real differences between years with respect to solitary fauna. This faunal group is dominated by mobile fauna including crustaceans, fishes and echinoderms. Five of the sites showed less than 50% similarity (Figure 4-65). Although some of the differences between years are certainly a result of differences in resolution, different digitizers, and what fauna were visible during a survey (the 3-dimensional framework of the site allows plenty of places for fauna to hide from the camera), another component of the differences will be the fact that the mobile fauna are free to leave and return to the sites at will. Real variation in the presence of visible mobile fauna between years at the same sites was confirmed by re-inspection of the original mosaics. This suggests that a substantial amount of data will need to be acquired to accumulate the baseline information about this faunal group that will allow real changes to be detected over time.
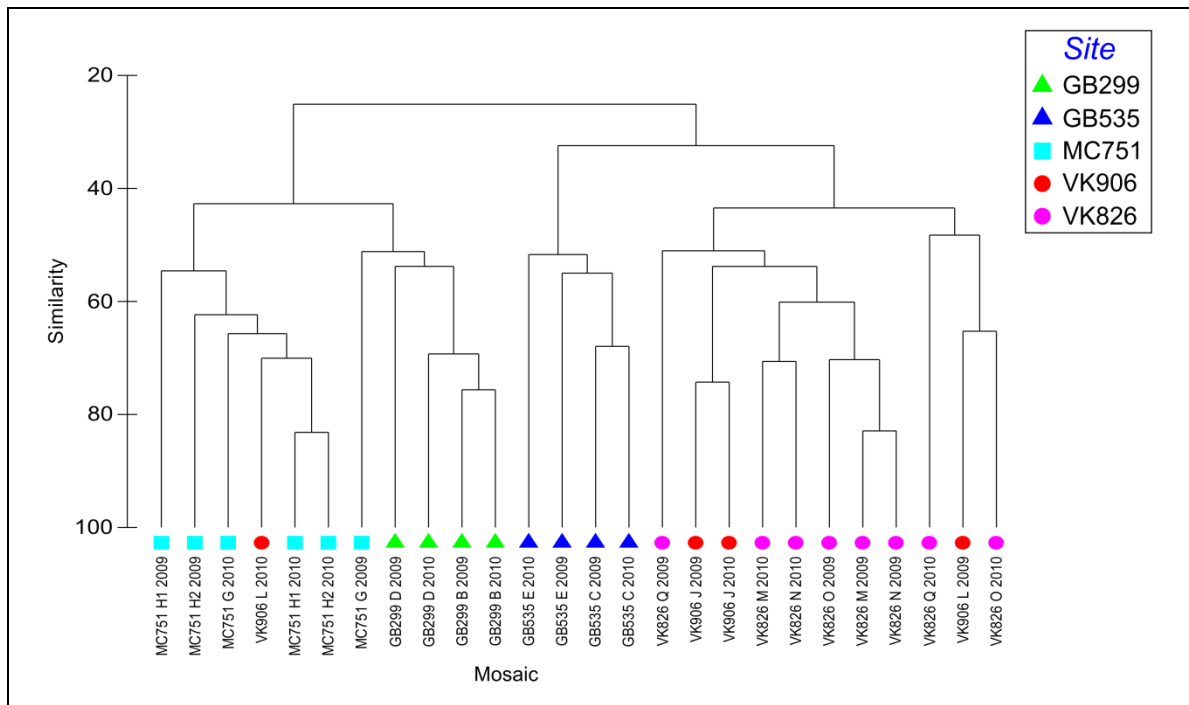
Figure 4-65. Hierarchical cluster dendrogram based on Bray-Curtis Index values of solitary fauna density showing the relationship between the overlapping portions of mosaic sites imaged in both 2009 and 2010. The mosaics are color-coded by site and the shapes are grouped by lease block region.

## 4.2.4 Strengths and Weaknesses of Mosaics for the Study of Deep-sea Corals and Communities

Digitizing the mosaics for quantitative analyses is currently very time-intensive, and the benefits of using this approach must be weighed against the costs. There are clear advantages for general quantitative descriptions of the sites that allow evaluation of biogeographic patterns. Similarly, this approach is well suited to inventory both attached resident fauna and the mobile fauna that visit a site, and to investigate preferred substrata for mobile fauna and fidelity of fauna to particular geological and biological substrata. However, comparing the quantitative data from the digitized mosaics is of limited use for quantitative comparisons between years to detect small changes. This is because small differences in altitudes and the exact lines run during image collection will produce images with different two-dimensional projections of the three-dimensional corals. Also, artifacts are compounded when mosaics are digitized by different people, even with extensive cross-training and oversight.

However, the original mosaics can be used to detect change through manual re-inspection when the analysis of the quantitative data suggests it is warranted. Because the two years of mosaics bracketed the *DWH* incident, all mosaics were rechecked manually, and this provided hard data confirming a lack of acute effects of the incident on most of the known deepwater coral communities in the GoM.

This technique should provide considerable insight into *in situ* growth rates and patterns for the scleractinian corals imaged. However, the slow growth rates of deep sea scleractinians result in very small increments of growth over a single year, and this amount of growth is at the limit of detection for the images used in the down looking mosaics. The best imagery collected for this analysis was in 2010, and a repeat visit to some of these sites after 2013 will allow documentation of growth patterns and rates over this interval. As part of this study, four coral community monitoring stations were established with photographs taken from the side using a forward-looking camera (Figure 4-42 to Figure 4-45). These stations and precisely navigated horizontal-perspective images of individual coral colonies will most likely prove to be more useful for growth studies in deep-sea corals.

The mosaic created for the site in MC338 was used in a very different way than the others. This site was found to have been impacted from the *DWH* incident (White et al., 2012). Analyses to determine the extent of the impact and ultimate fate of the impacted corals required that all corals at the site be identified and then followed as individuals over time (Appendix C-4 ). To accomplish this, the mosaic was used as a map (Figure 4-40). The map allowed us to plan and execute ROV dives to collect the images without impacting corals, to unambiguously identify specific individual coral colonies during each of 5 subsequent visits, and to unambiguously document the disappearance of a coral from the site between two of the visits. We have utilized this technique at several other sites investigated separately from this BOEM project, in the wake of the DWH incident.

## 4.3 INSIGHTS INTO COMMUNITY STRUCTURE, BIODIVERSITY AND BIOGEOGRAPHY FROM ANALYSES OF QUANTITATIVE COLLECTIONS

As part of the *Lophelia* II studies, quantitative sampling of coral, and a few mussel-bed communities was carried out in order to accomplish a number of the primary objectives of the larger project. At a first order, we set out to characterize newly discovered sites and examine patterns of community connectivity  so the communities could be placed in the larger biogeographical context. Further, we set out to test whether natural and artificial substrates harbored distinct communities, and determine what were the specific factors governing community structure and diversity.

### 4.3.1  Quantitative Collection Methods

Quantitative sampling of *Lophelia* communities, as well as any other appropriate communities encountered on natural or artificial substrates, was accomplished using the "mussel pot" collection devices. The coral pot samples will combine the advantages of quantitative sampling found with camera-guided grab samples with the precision and replication afforded by a submersible to provide the most comprehensive samples of specific habitat types while significantly minimizing our impact on the coral structures over the use of other sampling methodologies. These coral pot devices consist of a 'pot' made of 1/8" thick rolled aluminum. The interior diameter is 26 cm and the height of the pot is 29 cm. A Kevlar bag was attached to the pot and cinched closed by rotating a handle on the top of the pot connected to a draw string.

On board ship, the coral pot collections were transferred to the cold room where large attached and unattached fauna were removed. The coral skeleton was rinsed and loose small fauna, sediment and other material was sorted through a series of sieves (1 mm, 250 µm, 63 µm), and material passing through a 1mm sieve but caught on the 250 µm and 63 µm sieve was preserved for meiofaunal analyses by Amanda Demopoulos (USGS). Associated macrofauna (>1 mm) were separated based on morphology and preliminary identifications were carried out. Prior to sub-sampling, associated fauna were identified to the lowest possible taxonomic level and enumerated. The average diameter, volume, and proportion of live coral were determined for the *Lophelia* skeleton in each collection. Fragments containing live coral polyps were removed and sub-sampled for genetics for Cheryl Morrison (USGS). Sub-samples of foundation species and associated fauna were formalin-fixed and ethanol preserved (for morphological taxonomic studies and voucher collections), frozen (for stable isotope and molecular genetics studies), preserved in ethanol (for molecular systematic and phylogeographic analyses). See Chapter 6 for stable isotope studies and Chapter 5 for molecular genetics results.

Diversity of associated fauna was assessed using a combination of statistics. Alpha diversity was estimated as species richness (number of species), using the Shannon-Weaver diversity statistic (an information content statistic measuring the apportioning of individuals among taxonomic units), and in rarefaction curves (number of new species per individual sampled at each site). Beta diversity was estimated as the similarity in community structure (presence and density of taxa) between pairs of samples using the Bray-Curtis statistic. Patterns in beta diversity were examined using cluster analysis to determine groupings of increasing numbers of samples based on the Bray-Curtis statistic, and multidimensional scaling, a non-parametric ordination technique also based on the Bray-Curtis similarity metric. All analyses were carried out in Primer V 6.0.

### 4.3.2 Quantitative Collection Results and Discussion

There were 22 collections made at 12 different sites ranging in depth from 388 m to 2445 m (Table 4-4). There were 17 collections of *L. pertusa*-associated communities, three of *Bathymodiolus* mussel-associated communities, and two of *Madrepora oculata* communities. There were between 1 and 183 individuals of associated fauna in each collection, and between 1 and 15 species in each collection (Table 4-5). In all collections together, there were 64 species; 50 species associated with *L. pertusa*, 8 species associated with *M. oculata*, and 17 species associated with *Bathymodiolus* sp. Of the species associated with *L. pertusa*, 26 of these were collected in this study for the first time. This brings the total number of macrofauna species known to be associated with *L. pertusa* to at least 90, although this number could be even higher considering that the taxonomy of some of these species remains unresolved.

Table 4-4.

Collection information for all coral pot samples taken during this study

| Dive | Date | Site | Latitude | Longitude | Depth (m) | Collection Device | Foundation Species | Name |
|------|------|------|----------|-----------|-----------|-------------------|--------------------|------|
| J2-453 | 2009/08/21 | WFla Slope | 26°10.84 | 84°42.32 | 443 | MP-D | *Lophelia pertusa* | Wfla |
| J2-454 | 2009/08/23 | DC583 | 28°23.09 | 87°23.30 | 2445 | MP-D | *Bathymodiolus* sp. | DC583 |
| J2-457 | 2009/08/24 | AT047 | 27°52.79 | 89°47.30 | 853 | MP-D | *Bathymodiolus* sp. | AT047-1 |
| J2-457 | 2009/08/24 | AT047 | 27°52.81 | 89°47.33 | 839 | MP-B | *Madrepora oculata* | AT047-2 |
| J2-460 | 2009/08/28 | GB535 | 27°25.68 | 93°35.03 | 515 | MP-D | *Lophelia pertusa* | GB535-1 |
| J2-460 | 2009/08/28 | GB535 | 27°25.81 | 93°34.65 | 511 | MP-F | *Lophelia pertusa* | GB535-2 |
| J2-460 | 2009/08/28 | GB535 | 27°25.64 | 93°35.13 | 515 | MP-B | *Lophelia pertusa* | GB535-3 |
| J2-464 | 2009/09/01 | MC751 | 28°11.63 | 89°47.93 | 441 | MP-B | *Lophelia pertusa* | MC751-1 |
| J2-464 | 2009/09/01 | MC751 | 28°11.63 | 89°47.90 | 439 | MP-D | *Lophelia pertusa* | MC751-2 |
| J2-465 | 2009/09/02 | VK906 | 29°4.18 | 88°22.62 | 388 | MP-F | *Lophelia pertusa* | VK906-1 |
| J2-465 | 2009/09/02 | VK906 | 29°4.16 | 88°22.65 | 393 | MP-D | *Lophelia pertusa* | VK906-2 |
| J2-466 | 2009/09/03 | VK826 | 29°9.89 | 88°0.70 | 463 | MP-B | *Lophelia pertusa* | VK826-8 |
| J2-466 | 2009/09/03 | VK826 | 29°9.46 | 88°0.97 | 475 | MP-D | *Lophelia pertusa* | VK826-9 |
| J2-467 | 2009/09/03 | VK826 | 29°9.52 | 88°0.63 | 469 | MP-F | *Lophelia pertusa* | VK826-10 |
| J2-472 | 2009/09/10 | *Gulfpenn* | 28°26.47 | 89°19.09 | 557 | MP-D | *Lophelia pertusa* | *Gulfpenn* |
| J2-473 | 2009/09/11 | VK906 | 29°4.14 | 88°19.09 | 393 | MP-D | *Lophelia pertusa* | VK906-3 |
| J2-528 | 2010/10/17 | GC246 | 27°42.10 | 91°38.91 | 834 | MP-B | *Bathymodiolus* sp. | GC246 |
| J2-529 | 2010/10/18 | GC354 | 27°35.87 | 91°49.58 | 526 | MP-B | *Lophelia pertusa* | GC354-4 |
| J2-531 | 2010/10/20 | GB535 | 27°25.68 | 93°35.01 | 518 | MP-B | *Lophelia pertusa* | GB535-4 |
| J2-536 | 2010/10/26 | MC751 | 28°11.61 | 89°47.92 | 440 | MP-B | *Lophelia pertusa* | MC751-3 |
| J2-537 | 2010/10/27 | *Gulfoil* | 28°9.68 | 89°45.15 | 532 | MP-B | *Lophelia pertusa* | *Gulfoil* |
| J2-538 | 2010/10/29 | MC118 | 28°51.16 | 88°29.55 | 884 | MP-B | *Madrepora oculata* | MC118 |

Table 4-5.

Summary statistics from community collections

| .Name | Volume (mL) | | avg diam (cm) | | surface area | | | | | Diversity | | |
|---|---|---|---|---|---|---|---|---|---|---|---|---|
| | Live | Dead | Live | dead | (cm²) | %live | #sp | #ind | H' | J' | Es(10) | Es(20) |
| Wfla | 77 | 330 | 0.48 | 0.72 | 2472 | 18.9 | 8 | 13 | 1.93 | 0.926 | 6.8 | 8.0 |
| DC583 | - | - | - | - | - | - | 7 | 51 | 1.19 | 0.610 | 3.6 | 5.2 |
| AT047-1 | - | - | - | - | - | - | 7 | 127 | 1.24 | 0.639 | 3.7 | 5.0 |
| AT047-2 | - | - | - | - | - | - | 2 | 2 | 0.69 | 1.000 | 2.0 | 2.0 |
| GB535-1 | - | 310 | - | 0.73 | 1701 | 0.0 | 3 | 3 | 1.10 | 1.000 | 3.0 | 3.0 |
| GB535-2 | - | 240 | - | 0.71 | 1345 | 0.0 | 3 | 10 | 0.64 | 0.582 | 3.0 | 3.0 |
| GB535-3 | - | 1490 | - | 0.91 | 6542 | 0.0 | 8 | 19 | 1.99 | 0.955 | 6.3 | 8.0 |
| MC751-1 | 290 | 770 | 0.82 | 0.75 | 5552 | 27.4 | 8 | 17 | 1.69 | 0.814 | 5.6 | 8.0 |
| MC751-2 | 5 | 110 | 0.70 | 0.68 | 677 | 4.3 | 2 | 4 | 0.56 | 0.811 | 2.0 | 2.0 |
| VK906-1 | 165 | 1320 | 0.93 | 1.37 | 4564 | 11.1 | 10 | 43 | 1.74 | 0.754 | 4.9 | 7.0 |
| VK906-2 | 40 | 300 | 1.15 | 1.10 | 1230 | 11.8 | 5 | 19 | 1.19 | 0.740 | 3.8 | 5.0 |
| VK826-8 | 40 | 740 | 0.72 | 1.12 | 2865 | 5.1 | 7 | 14 | 1.73 | 0.889 | 5.8 | 7.0 |
| VK826-9 | - | 470 | - | 0.78 | 2410 | 0.0 | 4 | 4 | 1.39 | 1.000 | 4.0 | 4.0 |
| VK826-10 | 370 | 95 | 1.18 | 0.62 | 1870 | 79.6 | 1 | 1 | 0.00 | - | 1.0 | 1.0 |
| *Gulfpenn* | 260 | 342 | 0.78 | 0.91 | 2828 | 43.2 | 9 | 183 | 0.73 | 0.332 | 2.4 | 3.5 |
| VK906-3 | 5 | 390 | 0.66 | 0.96 | 1664 | 1.3 | 3 | 4 | 1.04 | 0.946 | 3.0 | 3.0 |
| GC246 | - | - | - | - | - | - | 5 | 11 | 1.41 | 0.879 | 4.8 | 5.0 |
| GC354-4 | 9 | 1586 | 0.31 | 0.80 | 8046 | 0.6 | 15 | 20 | 2.52 | 0.932 | 8.2 | 15.0 |
| GB535-4 | 9 | 102 | 0.50 | 0.71 | 647 | 8.1 | 12 | 17 | 2.40 | 0.964 | 8.2 | 12.0 |
| MC751-3 | | 247 | | 0.74 | 1335 | 0.0 | 4 | 4 | 1.39 | 1.000 | 4.0 | 4.0 |
| *Gulfoil* | 77 | 493 | 0.66 | 0.97 | 2500 | 13.5 | 4 | 30 | 0.43 | 0.314 | 2.0 | 3.0 |
| MC118 | - | - | - | - | - | - | 6 | 9 | 1.68 | 0.936 | 6.0 | 6.0 |

The most common species were polychaetes (Appendix C-1). These included *Euratella* sp., a tube-dwelling, suspension-feeding sabellid worm; *Glycera tesselata*, a small predatory polychaete; and *Eunice* sp., the larger, tube-dwelling, predatory polychaete that was part of the laboratory time-lapse study (Chapter 7). Following these species, were sessile epifaunal and encrusting species including unidentified species of small anemones and sponges. Other common mobile fauna included *Coralliophila* sp., the corallivorous gastropod, a few different species of *Munidopsis*, and unidentified species of amphipods.

Diversity ranged from one species and a Shannon-Weaver H' value of 0 in one of the collections from VK826 to 15 species in 20 individuals collected H' = 2.52) in GC354-4. Diversity of all *L. pertusa*-associated communities collected to date (including those from *Lophelia* I, Cordes et al. 2008) was most related to the surface area of coral in the collection (Figure 4-66). This was evident for both the total number of species ($r^2 = 0.583$, $p < 0.0001$) and for the Shannon-Weaver diversity index ($r^2 = 0.241$, $p = 0.0044$). In the *Lophelia* I study, the Bushmaster junior device was used for coral collections, while in this study, the mussel pot collection device was used. While the mussel pots had numerous advantages, including multiple collections per dive and smaller size on the ROV basket, the Bushmaster samples were more likely to provide a comprehensive survey of community composition. Secondarily, diversity was inversely related to the proportion of live

coral in the collection in terms of Shannon-Weaver diversity ($r^2 = 0.171$, $p = 0.0188$), but not number of species ($r^2 = 0.040$, $p = 0.2721$), with dead coral framework supporting higher diversity levels. This pattern has been observed repeatedly in *L. pertusa* habitats in a variety of locations including the GoM (Cordes et al. 2008, Lessard-Pilon et al. 2010) and Norway (Mortensen et al. 1995), and using a variety of sampling methods.
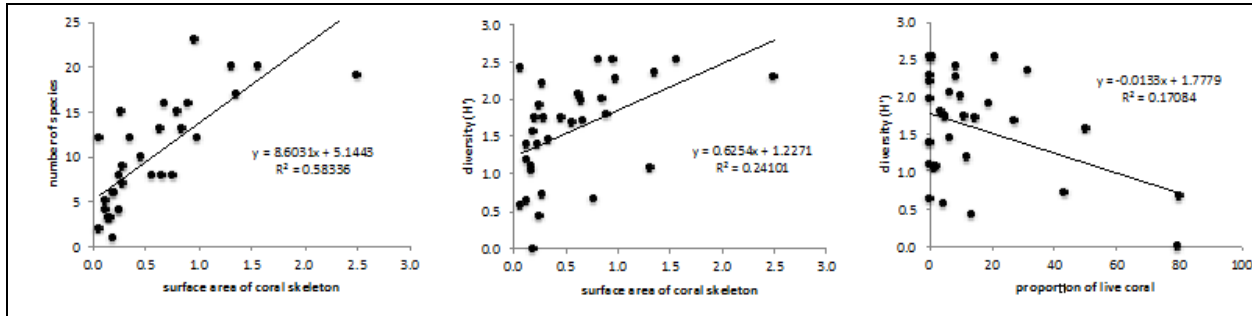


Figure 4-66. Diversity of coral communities collected during *Lophelia* I and II related to characteristics of the coral skeleton in the collections. Only significant regression relationships are shown.

Diversity did not show any significant trends with either depth or longitude (east-west patterns). The lack of a trend with depth is likely to be a result of the narrow range of depths sampled (313 to 557 m), with the majority of the collections were between 400 and 525 m due to the restricted range of *L. pertusa* on natural substrata in the Gulf. The lack of a trend in diversity from east to west is similar to the lack of a trend in the diversity of octocoral communities (see section 5.1). This is also consistent with a lack of a trend in the diversity and community composition of seep communities (Cordes et al. 2007).

When all communities were analyzed together, there was a very high level of beta diversity, with low similarities shown among large groups of collections. The two *M. oculata* community collections did not have any species in common. It is clear that the macrofaunal communities associated with this deep-living scleractinian species require further investigation. The *Bathymodiolus* sp. communities sampled in this study only shared one species in common, the chiton that was present at both AT047 and MC118. Species that were associated with *L. pertusa* that also appeared in one or more of these collections include *Glycera tesselata* from the seep at GC246, *Munidopsis* sp. 1 in both mussel and coral habitats at AT047, and *Phascolosoma turnerae* at GC246. All of these species are very common in the GoM and had previously been reported from both seep and coral habitats. Because of the low numbers of shared species among all foundation species, additional community analyses focused on the *L. pertusa* collections from this study supplemented with those from the *Lophelia* I study (Cordes et al. 2008; CSA, 2007).

The ordination plot (Figure 4-67) reveals the high beta diversity (low overall community similarity) at the large, heterogeneous site of VK826, with lower levels of diversity at most of the other sites. The western sites of GB535, GC354, and GC234 appear to be clustered in the ordination, suggesting lower beta diversity and an overall similarity in community composition within those sites. However, the overall level of community similarity between the sites is fairly low, particularly between GB535 and the two Green Canyon sites. The MC751 and VK906 sites,

although fairly small in extent, represent larger areas of the ordination, suggesting higher beta diversity within these sites than the western sites. Interestingly, the two wreck sites, *Gulfpenn* and *Gulfoil* were most similar to one another, with a Bray-Curtis similarity value of 35.5, driven by the high abundance of anemones in both collections. Depth and distance between collections did not appear to influence the patterns in community similarity, with collections from different sites at different depths clustering among one another, for example GB535-1 was most similar to VK906-2 and GC234-1 was most similar to VK826-1.  The lack of an effect of depth in this data set likely represents the limited depth range of the collections, and of the known *L. pertusa* distribution on natural reefs.
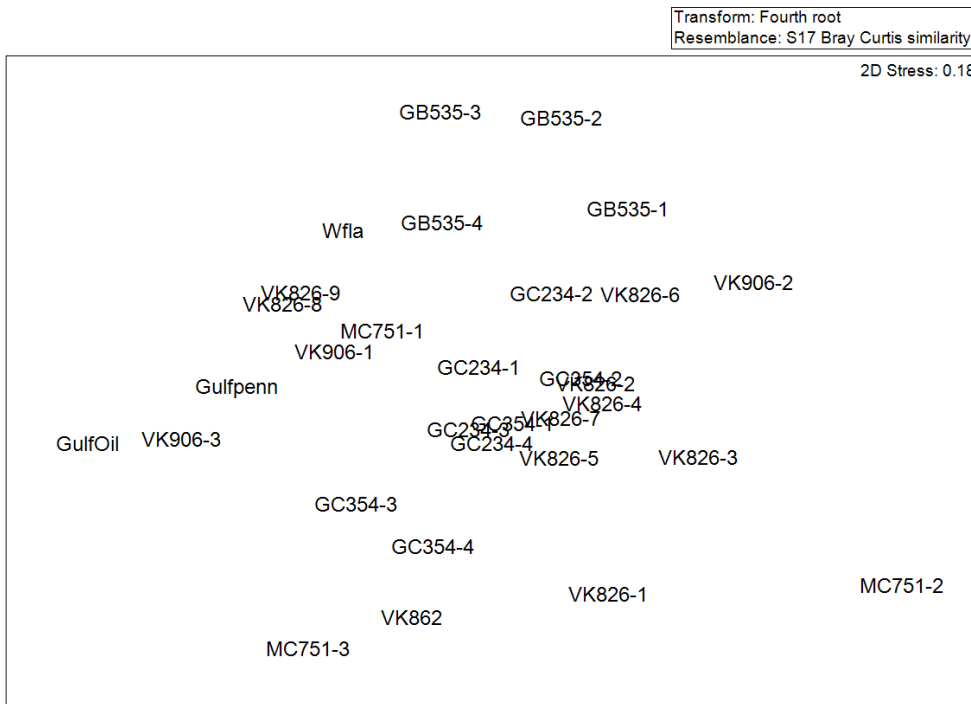


Figure 4-67. Multidimensional scaling ordination plot of community similarity (based on Bray-Curtis similarity), where collections that appear closer together have higher community similarity.

## 4.4  BIODIVERSITY AND FIDELITY OF CORAL ASSOCIATES

### 4.4.1  Introduction

Deep-sea corals provide habitat structure for an array of species that have developed diverse symbiotic relationships with relative specificities to their host corals (Watling et al. 2011). Corals provide complex structures that can host other organisms and their importance as biotic substrate increases with depth as the complexity of geological substrate declines (Buhl-Mortensen et al. 2010).  To date, 5 of the 32 known Phyla occur as symbionts on deep-water corals.  These include Cnidaria, Annelida, Mollusca, Arthropoda (Crustacea) and Echinodermata. Several studies have shown specific relationships between corals and associated symbiont living on these corals and have alluded to the importance of understanding these relationships to understand the evolution of diversity in the deep ocean (Shank 2010).  Diverse invertebrate fauna, from attached forms such as anemones and hydroids to mobile crustaceans, particularly anomuran and palaemonid shrimp,

and ophiuroids are now known to exist as "associates" on deep-sea corals. However, very little is known about the ecological requirements of these interactions and strategies maintaining the relationships among hosts and associated epibiotic symbiont (Buhl-Mortensen and Mortensen 2004a; Buhl-Mortensen and Mortensen 2004b). The few specific examples include the Atlantic shrimp *Pandalus propinquus* and *Caridion gorgoni* that are considered to be facultative commensals on the deep-sea corals *Paragorgia arborea* and *Lophelia pertusa,* and the shrimp *Synalpheus townsendi* reported to be a facultative commensal on *Oculina* reefs. In the Pacific Ocean, the shrimp *Periclimenes franklini* and *P. propinquus* are considered to be facultative symbionts of the cold-water corals in the Coral Sea.

Mutualism is an interaction in which both individuals benefit from the interaction. Obligate mutualisms are those in which both partners require the presence of the other to survive and/or grow and/or reproduce. Facultative mutualisms are those in which the participating species can survive/grow/reproduce without each other, but generally do better if the partner is present. For example, in the plant world, some aphids cannot survive unless they are tended by ants. Thus they have an obligate interaction with ants. However, the ants often do not require the aphids to survive. Their interaction with the aphids is considered facultative. For deepwater corals and their epibiotic symbionts, these two categories represent end points on a continuum. For example, interactions can also be specialized or generalized. Specialists are organisms that only interact with one or a few species. Generalists interact with many species. Thus obligate and specialized would be considered when an organism interacts with only one or a few species, and they must interact to survive, while facultative and specialized would be considered when an organism does not require the interaction, but if they do, it is with only one or a few other species. Historically, invertebrate symbionts of corals have been routinely classified as commensalistic, parasitic or mutualistic according to the relationship of the 'guest' to the 'host'. This is typically categorized as +/0 for commensals, +/- for parasites and +/+ for mutualists, among the various relationships along the symbiotic continuum, the symbols indicating the effect of the association on the fitness of the guest and the host. In all cases, the fitness of the guest is enhanced by the association, but the fitness of the host may be unaffected, negatively impacted or improved (Watling et al., 2011).

Determining the types of relationships for deepwater corals and their associated fauna, is extremely difficult, and thus rarely done. The "fidelity" of these relationships is largely if not entirely unknown. Fidelity refers to not only the species composition of the specificity of the coral and associate relationship, but the strength of that relationship. In general, most deepwater coral symbionts live on a narrow range of host species. Multiple host species may be in the same geographical area, on the same seamount perhaps, but may not be closely related phylogenetically (Watling et al., 2012). One of the few examples of a well documented case of high host fidelity is the ophiuroid, *Ophiocreas oedipus*, who lives only on the chrysogorgiid coral, *Metallogorgia melanotrichos*, and somehow no other symbionts appear to be allowed to take up residence (Mosher and Watling, 2009). Indeed, among >200 observations from both the Atlantic and Pacific, no living *M. melanotrichos* has been observed without its *O. oedipus* symbiont or with more than one symbiont. However, examples like this are few.

During the present study, it was our first-tier goal to identify x coral and associated symbionts taxonomically, in order to identify the composition and distribution of coral-associate partnerships that exist in the deep GoM. Then, to utilize high-resolution imagery as possible to conduct

sufficient observations of deepwater corals and their symbionts to detect patterns in the distribution of coral and associated symbiont composition that might shed light on both the symbiotic nature of the relationship (facultative vs. obligate) as well as host symbiont fidelity.

The GoM is considered to be part of the western Atlantic and Caribbean biogeographic area (Neigel 2009). It is divided into a northern area, which is part of the warm-temperate Carolinian Marine Province and a southern area that is part of the Tropical Northwestern Atlantic Province. There is a further subdivision of the northern GoM into a northeastern and a northwestern region separated by the mouth of the Mississippi River or Mobile Bay, AL. These two northern areas differ geologically and in physical conditions often reinforced by the outflow of the Mississippi and Atchafalaya rivers (Neigel 2009).

We examined more than fifteen stations with deep sea coral (DSC) communities in the deep GoM and additional sites ranging from 5 to about 100 miles from the wellhead in the wake of the *DWH* incident. In addition to assessing the composition of coral associates via taxonomy (see associate genetic section), we documented putative patterns of associative relationships between particular invertebrates and their host corals via high-resolution imaging and sampling of representative taxa.

## 4.4.2 Methods

### 4.4.2.1 Coral Associate Sample Collection for Image Reference

Samples of DSCsand their invertebrate associates in the GoM were collected by the ROV *SeaEye Falcon* DR during the TDI-Brooks R/V *Nancy Foster*/*SeaEye Falcon* expedition (September 20 to October 2, 2008), the ROV *Jason II* during the TDI-Brooks R/V *Ron Brown*/*Jason II* expeditions (August 6 to September 12, 2009 and October 15 to November 1, 2010), and using an industrial ROV on board the R/V *Holiday Chouest* during a non-*Lophelia* II research expedition (October 1 – 24, 2011) (Figure 4-68). Collection depths were between 249 m and 2600 m.
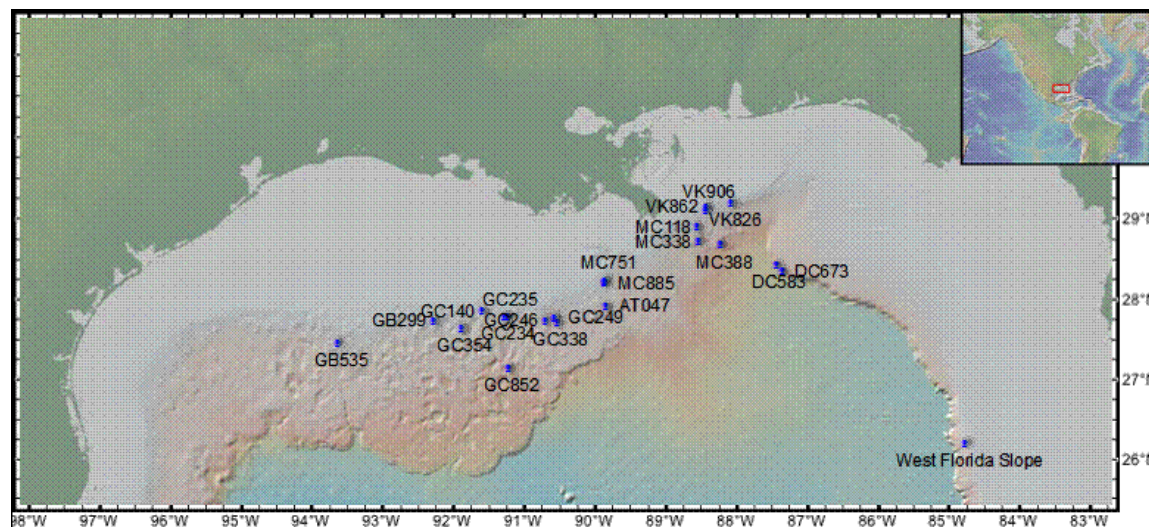


Figure 4-68. *Lophelia* II coral associate sampling sites in the GoM. GB = Garden Banks, GC = Green Canyon, MC = Mississippi Canyon, VK = Vioska Knoll, and DC = DeSoto Canyon.

The biological samples were processed immediately after recovery of the ROV. For each sample, tissue was either frozen at -80°C or preserved in 70% ethanol for subsequent genetic analyses. Images of the colonies were taken during the collection; additional images were taken in the wet laboratory on board the ship.

### 4.4.2.2 Analysis of Reference Sample Collections

We compiled and analyzed the collection records from the *Lophelia* II 2008, 2009, and 2010 cruises to the GoM to study patterns of association and fidelity between coral hosts and their invertebrate associates. Collected samples of invertebrate associates were identified to the lowest taxonomic level possible and as discrete morphospecies and correlated to the coral hosts from which they were collected.

### 4.4.2.3 Lophelia II 2009 Video Analysis

We analyzed 178 hours of high-resolution video footage collected with the ROV *Jason II* during the cruise *Lophelia* II in 2009 in the GoM. The video was subsampled collecting discrete frame-grabs of well-imaged (i.e., the identity of the coral and associate were observable in the image with reference to the collected samples) coral communities and their invertebrate associates. These images were then reviewed to quantify corals and invertebrate coral associates which were identified to the lowest taxonomic level possible.

### 4.4.2.4 Multivariate Analysis

To assess the compositional distribution of coral associates, image data subsampled from the *Lophelia* II 2009 cruise was standardized by total observations made in a sample bin. Relative abundances were used rather than abundances calculated from area because of the high degree of variability in the altitude of the ROV and in the magnification of the camera throughout the dives. Correlation matrices using the Bray-Curtis similarity index on fourth-root transformed data were generated and cluster analysis and multidimensional scaling (MDS) were used to determine similarity of biological assemblages based on species composition. In addition, an analysis of similarity (ANOSIM) was performed to test for differences between these biological assemblages. The analyses were performed at several scales by grouping the observations into different sample bins:
1. By geographic region, examining regional differences between
   a. The northeastern GoM (east of the Mississippi River mouth)
   b. The northwestern GoM (west of the Mississippi River mouth)
2. By 500 m depth bins, examining differences in community structure by depth
   a. 0-500 m
   b. 500-1000 m
   c. 1000-1500 m
   d. >1500 m

These analyses were performed with the statistical package PRIMER v6 (Clarke and Gorley 2006; Clarke and Warwick 2001) and the results presented below.

### 4.4.3  Results

### *4.4.3.1  Coral-Associate Composition and Distribution*

More than 720 coral-associated invertebrate individuals (including species of brittle stars, shrimp, amphipods, anemones, barnacles, and crabs) were sampled for species and coral-relationship determination (Appendix C-1).

A total of 123 coral colonies were imaged and analyzed from nine different sites in the GoM (Table 4-6). Coral hosts are listed at left column and the associated invertebrate fauna are listed along the top row, by groups within phyla. Each letter represents a unique associate morphospecies within a particular phylum. The total number of morphospecies found either on a host coral or within an associate group is listed at right and bottom. We have identified more than a total of 120 invertebrate morphospecies from 6 phyla living on >18 host coral substrates, including octocorals, black corals, and scleractinian corals from the 3 *Lophelia* II cruises between 2008-2010 (Figure 4-69, Table 4-6). Of these 120 morphospecies of coral associates, the most common and diverse associates were from the phyla Arthropoda (38 distinct morphospecies, dominated by galatheid/chriostylid crabs) and Echinodermata (30 different morphospecies, primarily ophiuroid brittle stars). While species of crustaceans were the most diverse on corals, the most abundant taxa observed by site were anemones (Table 4-7; WFS = W. Fl. Slope, DC = DeSoto Canyon, AT = Atwater, GB = Garden Banks, GC = Green Canyon, MC = Mississippi Canyon, VK = Vioska Knoll.). Coral-associated species hosted only by dead coral skeleton (e.g., specific barnacles and polychaetes) were also observed. The corals with the greatest diversity of associates were the live scleractinian *Lophelia pertusa* and the paramuriceid species. At least 7 species of sponges (previously not identified as being important or abundant associates living on deep-water corals, Watling et al. 2012) were observed on *L. pertusa*. Interestingly, sponges and polychaetes were not observed on any other live host coral taxa (Table 4-6). Aploacophorans (along with gastropods) are the one of the few known molluscan groups considered as coral associated symbionts. This was also observed to be true in our sample collection, with 4 aplacophoran species living commensally on *Muriceides*, a plexaurid, and paramuriceid corals. . While Crustaceans are the most speciose among Gulf coral associates, the most abundant associates on Gulf corals are anemones and ophiuroids (Table 4-7).

Table 4-6.

Composition and distribution of coral associated symbionts by coral host type.

| PHYLUM: | ANNELIDA | ARTHROPODA | CNIDARIA | | | ECHINODERMATA | MOLLUSCA | | PORIFERA | Total |
|---|---|---|---|---|---|---|---|---|---|---|
| | Polychaeta | Crustacea | Anemones | Hydroids | Zoanthids | Ophiuroidea | Aplacophora | Gastropoda | Sponges | Species |
| Alcyonacea | | | | | | | | | | |
| Bamboo coral | | | D | | | D | | | | 2 |
| Callogorgia | | T | F, G | | | A, C, D, F, K, L, M | | | B, C, E | 13 |
| Chrysogorgia | | E, M | | | | | | | | 2 |
| Corallium | | F | | B | | | | | | 2 |
| Keratoisis | | D, J, P, S, X | | | | D, L | | | | 7 |
| Muriceides? | | C | | B | | D | A | | | 4 |
| Nicella white | | | A | | | C | | | | 2 |
| Paragorgia | | | | | | C, G | | | | 2 |
| Paramuriceid | | A, G, I, L | B, H | B | B, C | B, C, D, G, M | A, B | B | | 17 |
| Plexaurid | | | | | | | A | | | 1 |
| Primnoid | | | | | | C, K | | | | 2 |
| Purple gorgonian | | | | | | C, G | | | | 2 |
| Antipatharia | | | | | | | | | | |
| Antipatharian | | G, I, J, L, AA | | | | H, I, N | | | | 8 |
| Dead Antipatharian | A | H | | | C | | | | | 3 |
| Leiopathes | | G, I, J, K, M, AA | C, F | B | C | E | | | | 11 |
| Tanacetipathes | | D, O, Q | | B | | | | | | 4 |
| Scleractinia | | | | | | | | | | |
| Dead *Lophelia* | B, C, E | | | A | | J | | | | 5 |
| *Lophelia* | D, F, G, H, I | B, D, O, R, U, V, W, Y, Z | A, C, E | B | A, F | D, O | | A, B, C, D, | A, B, C, D, E, F, G | 33 |
| **Total Species** | **9** | **38** | **11** | **7** | **6** | **30** | **4** | **8** | **7** | **120** |
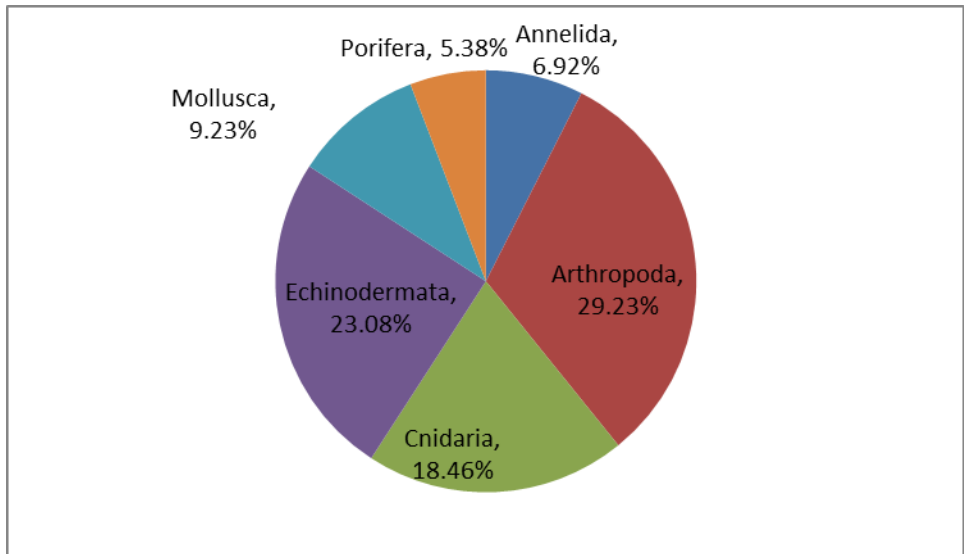
Figure 4-69. Coral associate taxonomic composition by phyla over three *Lophelia* II cruises.

Table 4-7.

Abundance of coral associates across five different phyla observed in a subset of coral colonies imaged during the 2009 cruise.

| Site | Coral Colonies | Cnidarians | Echinoderms | Porifera | Crustaceans | Annelids |
|---|---|---|---|---|---|---|
| WFS | 16 | 178 | 11 | 54 | 3 | 0 |
| DC583 | 20 | 147 | 18 | 0 | 0 | 0 |
| AT047 | 9 | 57 | 36 | 0 | 0 | 0 |
| GB299 | 17 | 498 | 210 | 1 | 1 | 0 |
| GB535 | 16 | 564 | 39 | 36 | 5 | 0 |
| GC852 | 21 | 374 | 13 | 1 | 1 | 0 |
| GC338 | 1 | 25 | 1 | 0 | 1 | 0 |
| MC751 | 15 | 238 | 152 | 1 | 5 | 15 |
| VK826 | 8 | 139 | 3 | 0 | 0 | 0 |
| **Total** | **123** | **2220** | **483** | **96** | **16** | **15** |

### 4.4.3.2 Multivariate Analysis

Similarities between the associated faunal communities on coral colonies were determined using multivariate statistical analyses. Cluster analysis and MDS indicate that there is a distinct difference between the coral colony associates found in the northeastern GoM and those found in the northwestern GoM, which was found to be highly significant by ANOSIM analyses (p=0.001) (Figure 4-70). When observations were binned across the GoM into 500 m depth bins, cluster analysis and MDS indicated distinct differences between different depth regions, which were found to be highly significant by ANOSIM analyses (p=0.001) (Figure 4-71).
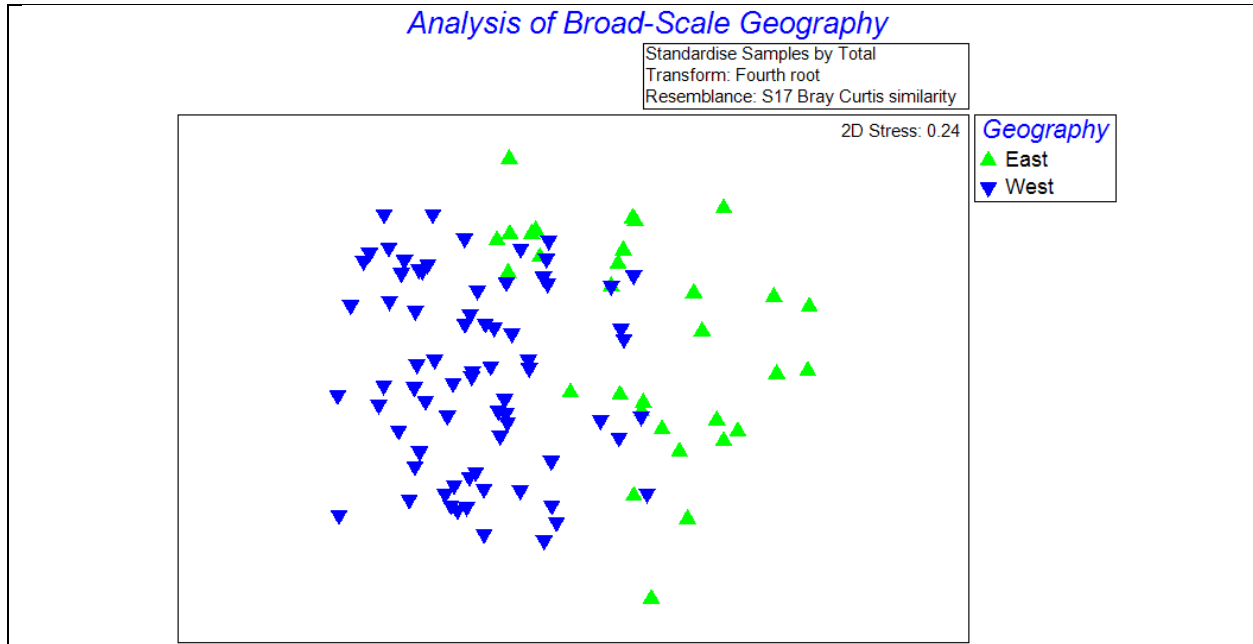


Figure 4-70. Multidimensional scaling plot of coral associates located in the northeastern GoM (East, green triangles) and the northwestern GoM (West, blue triangles) using the Bray-Curtis similarity index. The distinction of east and west is delineated by the location of the entrance of the Mississippi River into the Gulf. Ordination points superimposed by geographic area.
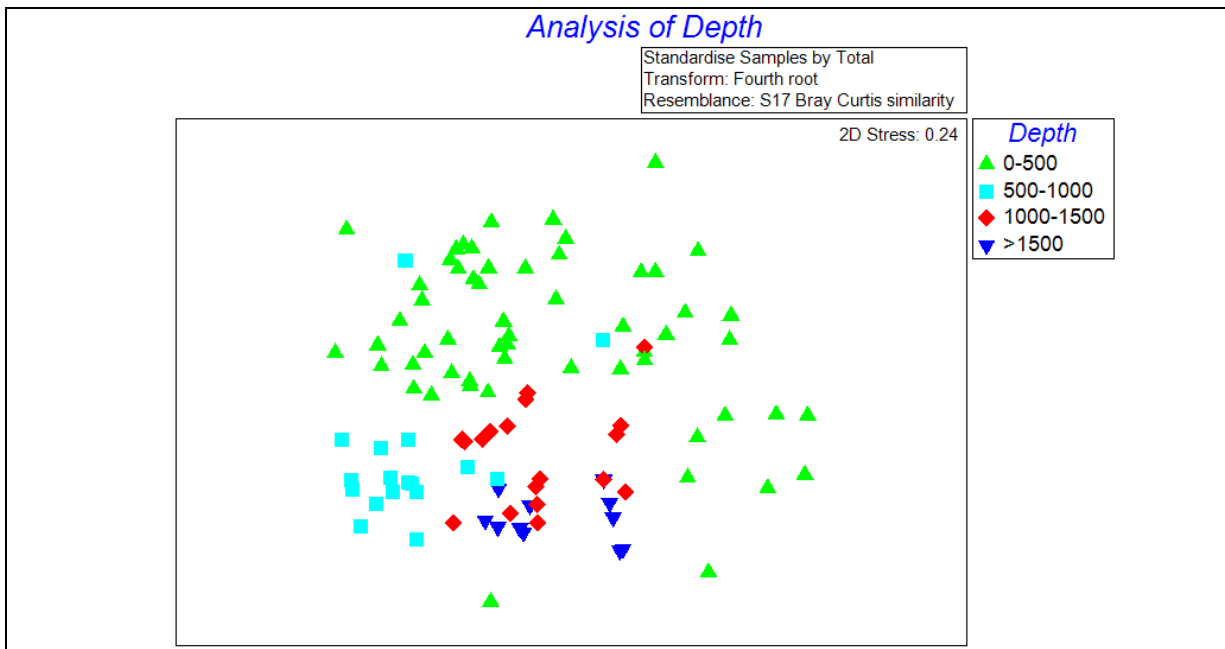
Figure 4-71. Multidimensional scaling plot of coral associates for 500 m depth bins using the Bray-Curtis similarity index. Ordination points superimposed by depth region: Green = 0-500 m, Cyan = 500-1,000 m, Red = 1000-1500 m, Blue > 1,500 m.

## 4.4.3.2.1 Assessing associates as indicators of coral ecosystem health

The *Lophelia* II program provided critical observations and baselines that enabled an unintended outcome of comparative studies of a coral community located approximately 11 km southwest of the *DWH* oil spillat a depth of 1370 m. This site was observed over the course of 5 ROV and submersible Alvin dives from November to December 2010 in conjunction with *Lophelia* II expeditions. The ophiuroid associates of 52 corals within this impacted community were imaged over the course of 5 five ROV and submersible Alvin dives from November to December 2010. The time series of images were analyzed for changes in color, movement, and posture, (White et al., 2012).

Of the 52 coral hosts examined at the coral community at MC294, 2% hosted actinarian anemones, 73% hosted the ophiuroids *Asteroschema clavigerum*, and 25% had no associates. *A. clavigerum* is normally tan to red in color (Figure 4-72), but 44% had distinctly white arms and 9% were almost entirely bleached. *A. clavigerum* typically have arms tightly-coiled around their coral hosts, but 27% had abnormal posturing with loosely coiled arms. Between two visits to the site approximately one month apart, 13% of ophiuroids transitioned from the tighly-coiled to loosely coiled posture and two individuals sent a completely splayed-out posture with their arms hardly coiled around the corals, a previously undocumented behavior (Figure 4-72) (White et al. 2012).
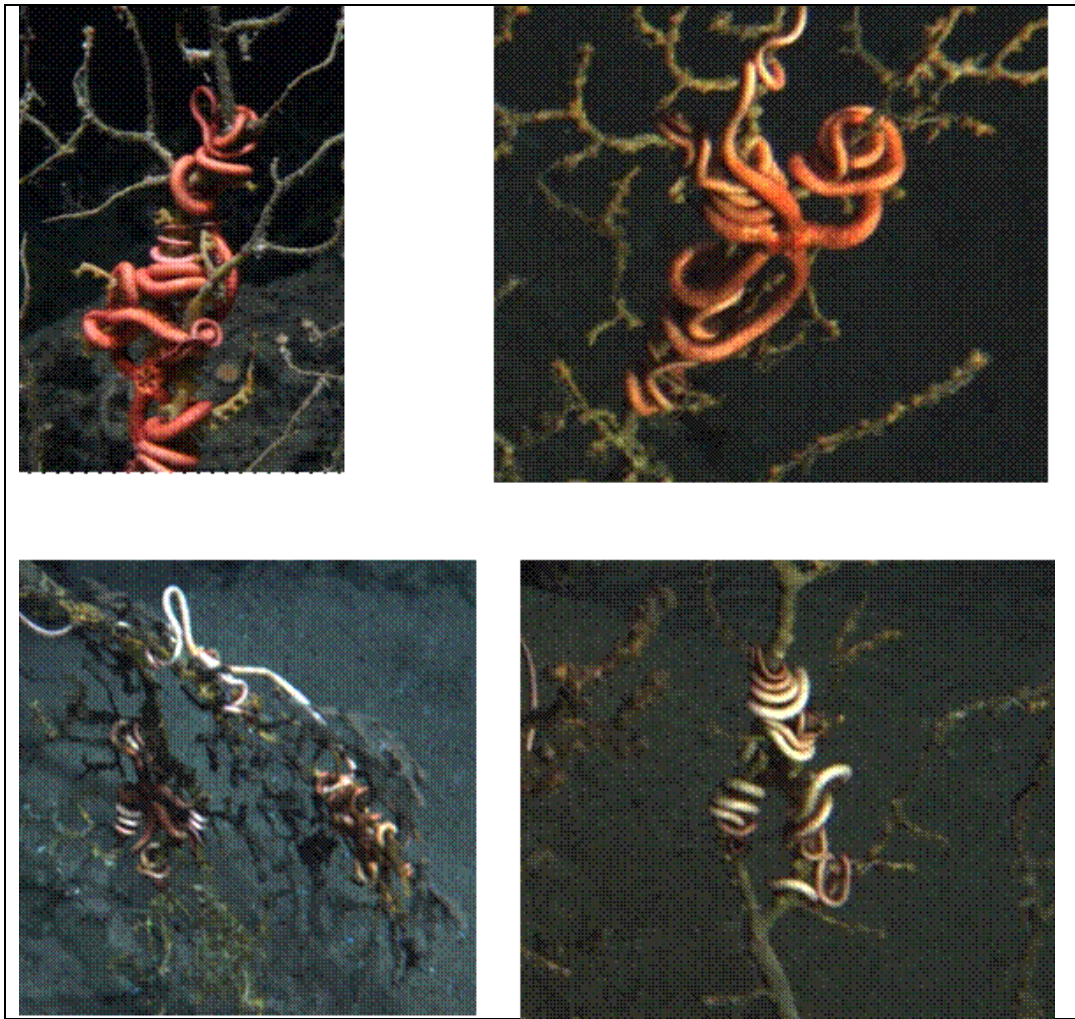
Figure 4-73.  Images of Asteroschema clavigerum from MC294.  The top two images show the typical tan to red coloration and tightly-coiled arm posture observed in this species. The bottom two images show the white armed and completely bleached coloration as well.

### 4.4.4  Discussion

#### 4.4.4.1 Taxonomic Composition and Associations

The most abundant phyla of invertebrate associates of corals observed in this study were the Arthropoda (mainly crustaceans), the Echinodermata (mainly ophiuroids), and the Cnidaria (hydroids and anemones).  The crustacea are often abundant where benthic biomass is often dominated by suspension feeders that provide important habitat for smaller invertebrates (Metaxas and Davis 2005; Rogers 1994; Samadi et al. 2007; Stocks 2004).  The patterns of associate fidelity to coral hosts correspond with previous studies of corals and their associates.  The reef-forming scleractinian *Lophelia pertusa* hosted the largest number of morphospecies of associates based on the 2008-2010 cruise observations, perhaps owing to the frequent mixture of living and dead *L.*

197

*pertusa* material and the specific fauna associated with both types of material. Comparison of the associates found on dead *L. pertusa* to those on live *L. pertusa* associates found 5 distinct species, including polychaetes, barnacles, hydroids, and ophiuroids that were observed only on dead *L. pertusa*. In addition, the observation of associates with higher fidelity occurring on gorgonians is similar to previous studies that found facultative and highly specialized relationships between corals and associated fauna (Buhl-Mortensen and Mortensen 2004a; Buhl-Mortensen and Mortensen 2004b; Buhl-Mortensen and Mortensen 2005; Buhl-Mortensen et al. 2010).

Associative relationships were identified from video and sampling to yield more than 110 coral-associate partnerships. When we observed a particular associate living on any coral on 20 or more occurrences, we regarded this as a association pair candidate. If an association with a single species of coral occurred 100% of these observations, we considered this to be an association of "obligate" mutualism. Any percentage less than 100%, would place the candidate association in a "facultative" category. We noted few findings of having "obligate" associations by this definition, in fact there were only a few (e.g., *Asterschema clavigerum* on *Paramuricea biscaya*), with more with multiple host corals –for example, the shrimp *Bathypalaemonella serratipalma* observed only on *Chrysogorgia* spp. and *Iridogorgia* spp. (a similar relationship was observed in deep-sea coral communities on the New England and Corner Rise Seamounts, Cho 2008). We noted that if we were to lower the required percentage to 80% (from "obligate" to "high fidelity) or allow for multiple hosts ("obligate general"), many taxa, particularly almost all ophiuroid species (e.g., *Asteroschema* spp and *Astrogomphus* sp.) and crab species (chriostylid and galatheid spp.) immediately fall into this category. Assigning any of these to obligate, facultative, mutualistic or even fidelity in many cases, would require greater observations and sampling to be certain of associate taxonomic identity. While we note that many (120 morphospecies of associates) of coral-symbiont associations exist in the Gulf (the extent of which was clearly not known prior to this study) with the observation that similar patterns exist in the Atlantic (Shank 2010), the work to appropriately designate and assess the fidelity of host and associate corals is ongoing.

### 4.4.4.2  Regional Patterns

In the comparison of coral associates within the study area, the coral associate communities of the northeastern and northwestern GoM were found to be significantly different. This regional difference was observed in the multivariate analyses of coral associate community composition performed on the regional scale. A similar pattern of regional differences was observed in megafauna assemblages associated with deep-water gorgonian corals in different sites in the Northeast Channel in Canada (Metaxas and Davis 2005).

These regional differences may be caused by a variety of factors (Neigel 2009). Geologically, the northwestern GoM is characterized by terrigenous sediment while the northeastern GoM is characterized by carbonate. In addition, the outflows of the Mississippi and Atchafalya rivers may also serve as a barrier for dispersal for coastal organisms. In support of this observation, genetic differences have been observed between northeastern and northwestern populations of the thalassinidean *Callichirus islagrande* (Staton and Felder 1995), although we did not detect this regional barrier to dispersal in our genetic studies or the overall structure of the coral commnities.

### 4.4.4.3 Depth Patterns

Cluster analysis and multivariate analyses of community composition suggest distinct faunal assemblages based on depth when observations are binned into 500 m depth intervals. Many factors co-vary with depth, which may determine the vertical distribution of fauna. In the Northeast Atlantic, for example, maximum depths of deep-water corals often reflect changes in the depths of water masses that have temperatures suitable for the corals. This was seen for deep-water gorgonian corals in the Northeast Channel of Canada (Mortensen and Buhl-Mortensen 2004).

Similar faunal zonation by depth has been seen in other studies. Distinct faunal assemblages based on depth have been observed in various seamount communities (Hoff and Stevens 2005; Samadi et al. 2007). Important faunal boundaries are thought to occur globally around 1000-1400 m depth (Howell et al. 2002), coinciding with the differences observed in this study. Similar faunal boundaries have been seen in asteroids in the North Atlantic at ~1,100 m (Howell et al. 2002), 1,200-1,300 m for decapod crustaceans (Cartes and Sarda 1993), and 1,000 m for cerianthid anemones (Shepard et al. 1986). This boundary has been attributed to slope gradient, which is related to the formation of enhanced bottom currents through internal tides and can effect sediment transport and substratum type (Howell et al. 2002). A study of the deep-sea megabenthic fauna south of New England also showed similar breaks separating two distinct faunal assemblages between 1,290 m and 1,380 m and 1947 m – 2116 m (Haedrich et al. 1980). There is a peak in diversity for invertebrate megafauna in the northwest Atlantic between 1900 – 2,300 m (Howell et al. 2002; Rex 1981) and also a bathymetric boundary of a well-defined intermediate region of 2,500-3,500 m where bathyal fauna meet, and overlap with, abyssal fauna (Haedrich et al. 1980; Howell et al. 2002). This depth zonation pattern is probably the result of a complex combination of physical factors and biological interactions (Gage and Tyler 1991).

Within the Gulf, differences in coral associate composition varied markedly with depth and biogeographic location. Yet while these differences exist, remarkable similarities in coral-associate taxonomic composition and relationships (e.g., ophiuroids on paramuricids and chirostylid crabs on antipatharian black corals) exist in deepwater coral ecosystems around the world.

## 4.5 USE OF IMAGERY AS BASELINE DATA FOR STUDY OF TEMPORAL CHANGE IN CORAL COMMUNITIES

One of the goals of using imagery in the way we did for this program was to establish study sites where one could study natural temporal changes in deep sea coral communities and also to establish baseline observation stations that could be used if needed in the future to evaluate potential anthropogenic-induced changes. When working in an environment as remote as the deep sea, one must consider the tradeoffs between many different approaches to monitoring corals and their communities. To best follow the health of entire marine communities, repeated surveys of randomly established transects has been the method of choice for many shallow benthic environments. These are most often established using scuba in relatively accessible habitats where the organisms of interest are present at relatively high density and where the established transect can be marked and relocated with relative ease. We successfully used the approach of large-scale transects for coral surveys in two of the sites we investigated, VK826 and VK906, where corals are present over fairly large areas and at moderate density (Section 4.1). This approach may also be fruitful at the deeper water site in AT 357 where gorgonians and *Madropora* are widespread over an area several hundred meters on each side. However, at all of the other sites surveyed below 400 m depth the coral distribution is very patchy and random transects flown with an ROV most often missed the corals completely. Although these transects would be impossible to repeat exactly with current technology, additional random transects could be flown in the future at some sites and could detect large scale and/or significant changes in the communities (see section 4.1). This is one of the approaches that should be used for sites where it is appropriate.

To allow collection of photographic data at the community scale and to establish study sites for repeated monitoring in areas with very patchy coral development, we deployed markers and collected imagery for photomosaics over haphazardly chosen study sites of between 8 to 100 square meters with high coral density (Section 4.2). A repeat visit to thirteen of the stations after one year indicated that the stations are quite easy to relocate and are generally very stable. We found that detecting and quantifying coral growth after a single year is often problematic because of the very slow growth rate of the corals. However, at most stations this should be possible after a time period of 3 to 5 years. Documenting and understanding the patterns of natural temporal change in deep water coral communities will likely require decades of intermittent visits and study. These stations will be appropriate for monitoring natural change in the corals over decades and for quickly detecting abrupt change as might occur from potentially deleterious anthropogenic activities or accidents. Although there is considerable variation in the presence of mobile fauna between visits, after a few years of study a database will accumulate enough data to allow robust monitoring of these populations as well.

One disadvantage of monitoring corals using down-looking imagery (either from transects or mosaics) is that many of the octocorals that can dominate some deep-sea coral communities are largely planar ("sea fans" and their allies). These types of corals are best visualized from a horizontal ("side-looking") perspective. Four horizontal monitoring stations were established during the *Lophelia* II project (Figure 4-42 to Figure 4-45) prior

to the discovery of the impacted corals during the last dive of the last cruise to the natural coral site reported in White et al., 2012. This site is dominated by *Paramuricea* sp. and numerous horizontal monitoring stations of individual corals were established at this site.

A lesson learned through the study of the impacted corals near the Macondo well was the value of using individual coral colonies as monitoring stations. Since corals are attached to the sea floor and "sample" the water column for food and gas exchange, they are well suited to act as biological monitors for water quality in the normally quite stable deep-sea environment. Large deep-sea coral colonies are often many hundreds of years old, and thus natural mortality is a rare event. Because they are attached, when impacted they remain at the site of impact and provide a long lasting record of that impact. We have now returned six times to the corals discovered during the last dive of the 2010 *Ron Brown* cruise and have re-imaged most of the corals there to better understand the pathway and time course of recovery (orlack of recovery) after exposure to toxic hydrocarbons or dispersants (Appendix C-4). This methodology can also be used to provide direct measures of in-situ growth as the resolution of the images and branching patterns of the corals allow terminal branch growth (or loss) to be easily quantified. Similarly, the high resolution images allow quantification and monitoring of the entire assemblage of coral associates on each colony. A total of over 250 individual corals have been marked and imaged for monitoring in the deep GoM in connection with studies of the impact from the DWH spill.

A combination of both photomosaics and individual colony monitoring has proven to be a powerful tool for study of temporal change in coral communities. The mosaics allow precise identification and localization of all colonies imaged as well as a record of mobile fauna at the site. When the site is revisited, re-imaging of the constituent coral colonies can be done very quickly and efficiently, and should any corals "disappear" this can be confirmed unequivocally. When working remotely in the deep sea, the combination of these monitoring strategies is very powerful and is recommended for future establishment of deep-sea coral monitoring stations.

# 5 PHYLOGENETIC DIVERSITY AND CONNECTIVITY

## 5.1 OCTOCORAL COMMUNITY STRUCTURE AND PHYLOGENETIC DIVERSITY

### 5.1.1 Background

The GoM harbors a diversity of octocorals occurring from shallow waters to depths of at least 3000 m. Octocoral diversity has been documented in taxonomic keys (museum records), two PhD dissertations (Giammona, 1978; Etnoyer, 2009) and a comprehensive checklist of GoM octocorals (Cairns and Bayer, 2009). From these accounts, it is known that at least 162 octocoral species occur in the entire GoM, but only 48% of these species are found in waters > 200 m (Cairns and Bayer, 2009). Despite these efforts to characterize the regional species pool in the GoM, the deep GoM remains poorly explored. Furthermore, whether octocorals assemble into distinct biogeographic provinces in the deep region largely remains unknown, but various biogeographic provinces have been proposed (Giammona, 1978; Cairns et al., 1993; Etnoyer, 2009). Faunal zonation with depth has been observed in the GoM across numerous taxonomic groups such as fishes (Powell et al., 2003), macrofauna (Wei et al., 2010), and chemosynthetic communities (Cordes et al., 2007; 2010). Whether these same zonation patterns extend to a hard bottom associated fauna such as corals is unclear. Discerning the distributions of octocorals in the deep GoM would help to elucidate deep-water biogeographic provinces, provide estimates of local diversity, and illustrate meta-community patterns; thus, providing critical data for the effective conservation of deep-water coral habitat.

Molecular barcoding combined with morphology is a useful approach to guide species identifications, while contributing to the growing efforts to discern the phylogenetic relationships of octocorals. Proper delineation of both population and species boundaries are also important when elucidating patterns in community structure. Testing hypotheses of coral community assembly in the deep sea first requires knowledge of the regional species pool from which coral assemblages are derived. Moreover, merging genetics into biodiversity estimates and community ecology enables conservation efforts to consider preserving genetic diversity and the evolutionary processes that generate this diversification (Moritz et al., 2002).

*Lophelia* II cruises enabled targeted collections of octocorals on the local scale using remotely operated vehicles and submersibles. We used a combination of molecular barcoding with morphological taxonomy to 1) identify a deep-water regional species pool, 2) provide estimates of diversity on both taxonomic and phylogenetic scales, and 3) add to the growing efforts of characterizing the phylogenetic relationships of octocorals. With this dataset, we were able to determine whether the community structure of octocorals is structured by 1) depth such that similar communities occur at sites in similar depths or by 2) location, such that similar communities occur in nearby sites. Furthermore, we were able to examine how phylogenetic diversity shifts with depth in the GoM and compare this diversity to sites beyond the GoM.

## 5.1.2 Methods

### 5.1.2.1 Sample Collections

Specimens were collected at depths of 250-2,500 m during seven cruises in 2008-2011 from 31 hard-bottom sites and 2 shipwrecks in the northern and eastern GoM during the *Lophelia* II project and additional projects using remotely operated vehicles [ROVs *Jason, Seaview, Mohican Schilling UHD, (NRDA)]* and human-occupied vehicles [HOVs *Alvin* (NSF RAPID) and *Johnson-Sea-Link (*USGS)] (Figure 5-1 ). Although a few genera (*Callogorgia* and *Paramuricea)* were targeted for population genetics, we attempted to collect at least one individual of every species of octocoral observed during each dive. We did not, however, target pennatulaceans (sea pens) as these species are associated with soft substrata; a habitat that was not the focus of the present study. One sea pen was, however, collected from GB299.  Coral colonies were first imaged and then branches from each colony were snipped.

All specimens were preserved onboard. Approximately 2-3 cm tissue samples per specimen were frozen at -80ºC and preserved in both 95% ethanol (ETOH) (stored at -20 ºC) and a high-salt EDTA preservative (stored at -80 ºC). Voucher specimens of each individual were also obtained and either preserved in 95% ETOH or dried. Specimens were identified following numerous taxonomic keys (e.g., Deichmann, 1936; Grasshoff, 1977; Madsen, 1970; Bayer, 1961, 1981; Sanchez, 2005; Cairns and Bayer, 2002, 2004) and many were sent to taxonomic experts (J Sanchez, S Cairns, J Thoma, B Horvath, L van Ofwegen) for confirmation. Species were identified to the lowest possible taxon (see Appendices A-2, D-1 – D-2); many genera and families are currently undergoing taxonomic revision.  Morphological identifications using Scanning Electron Microscopy (see Appendix D-2) were facilitated with molecular barcoding.  Representatives of all species will be deposited in the Smithsonian Institution, DC.
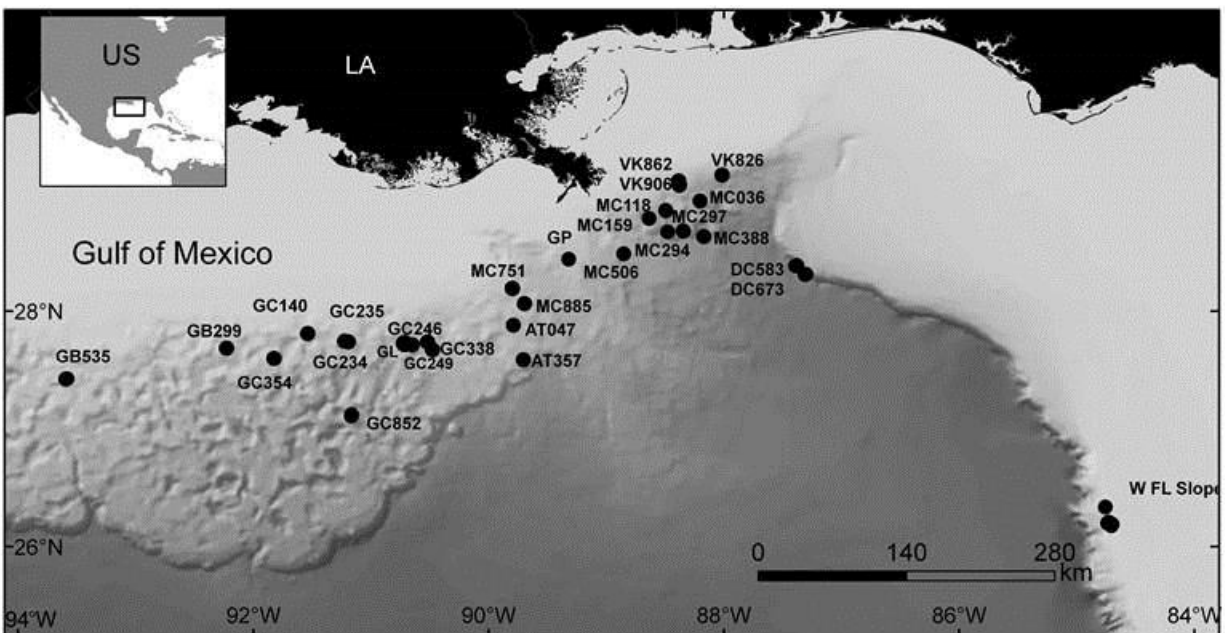


Figure 5-1.  Sites where octocorals (soft corals, stoloniferan corals, and gorgonians) were collected during surveys.

### *5.1.2.2  Molecular Barcoding Methods*

DNA was extracted using a Qiagen DNeasy kit. The extended mitochondrial barcode (*COI+igr1+MutS*) was sequenced for phylogenetic inference, as these gene regions are the most useful for species delimitation  (McFadden et al., 2011). Approximately 850 base pairs (bp) from the 5' end of the mitochondrial *MutS* gene and ~1000 bp of the *COI+igr1* region were polymerase chain reaction PCR amplified (Table 5-1), following McFadden et al., 2006, 2011) and sequenced (Genewiz, Inc and UW-HtSeq). The sequences were edited, aligned by ClustalW and adjusted by eye by viewing amino acid alignments (BioEdit, MEGA). The gene regions were concatenated into a 2153 bp extended barcode and Bayesian (mrBayes) and Maximum Likelihood (GARLI, Zwickl, 2006) analyses were performed. Using JModelTest (Guindon and Gascuel, 2003; Posada, 2008), the General-Time-Reversible model plus the gamma distribution (GTR+G) was chosen as the most appropriate nucleotide substitution model for *MutS* (813 bp; AICc=8492.87); the transversion model plus invariable sites with a gamma distribution (TVM+I+G) was chosen for *COI* (752 bp, AICc=7342.72), and the transition model with a gamma distribution (TIM+G) was chosen for *igr1* (AICc=5446.99).

Table 5-1.

PCR primers and protocols used to amplify targeted gene regions

| Gene | | Sequence (5' to 3') | PCR Profile [a] |
|---|---|---|---|
| *COI+igr1* | COII8068F[1] | CCA TAACAGGACTAGCAGCATC | 94°:30 s, 60°:90 s, 72°:60 s |
| | COII8068xF[1] | CCATAACAGGRCTWGCAGCATC | 94°:30 s, 60°:90 s, 72°:60 s |
| | SIRONAD6R1[b, 2] | ATTGCCCCTATGTTAGTTCTAG | 94°:30 s, 54°:45 s, 72°:60 s |
| | COIOCTR[3] | ATCATAGCATAGACCATACC | |
| *MutS* | ND4L2475F[4] | TAGTTTTACTGGCCTCTAC | 94°:30 s, 51°:45 s, 72°:60 s |
| | ND42599F[3] | GCCATTATGGTTAACTATTAC | 94°:30 s, 51°:45 s, 72°:60 s |
| | CO3BAM5657F[c, 4] | GCTGCTAGTTGGTATTGGCAT | 94°:30 s, 53°:45 s, 72°:60 s |
| | ANTHOCORMSH[b, 5] | AGGAGAATTATTCTAAGTATGG | 94°:30 s, 50°:45 s, 72°:60 s |
| | MUT3458R[6] | TSGAGCAAAAGCCACTCC | |

[a]PCRs began with 5 min denaturing step at 94°C and ended with 10 min elongation at 72°C. 32 cycles were conducted for each
[b]Forward primer for scleraxonians (with the exception of *Sibogagorgia*).
[c]Forward primer for bamboo corals (with the exception of Keratoisidinae clade S1)
[1]McFadden et al., 2004, [2]Uda et al., 2011, [3]France and Hoover, 2002, [4]Brugler and France, 2007, [5]Herrera et al., 2010, [6]Sanchez et al., 2003

Data were partitioned so that the appropriate models could be applied to each gene region in Bayesian and likelihood analyses. In MrBayes, the number of generations was set to 7,000,000, with a sampling frequency of every 100 generations followed by a burnin of 10,000 trees. The consensus tree was rooted at the midpoint and displayed in FigTree. Both posterior probabilities and bootstrap frequencies from likelihood analyses (calculated in the Sumtrees of the DendroPy

v3 package, Sukumaran and Holder, 2010) are indicated on the consensus tree. We also created a phylogeny (as described above) of 199 *MutS* sequences (731 bp) to gain a more thorough picture of the relationships of the GoM haplotypes within the larger octocoral phylogeny. This analysis was restricted to *MutS* only because this gene region has been most often sequenced in previous studies. The most similar sequences to GoM haplotypes were downloaded from GenBank (National Center for Biotechnology Information [NCBI]) and included in the analysis as well as many representatives across the octocoral sub-orders. Pairwise p-distances were calculated between all haplotypes for the extended barcode and the more inclusive *MutS* only (MEGA).

### 5.1.2.3 Community Structure Analyses

We first constructed a species accumulation curve to estimate how well the deep-water regional species pool was sampled. (EstimateS; Colwell, 2005). The resampling based self-organizing background subtraction (SOBS) method was used to generate the expected number of species per sample and 95% confidence intervals (Gotelli and Colwell, 2001; Colwell et al., 2004). Multivariate analyses were used to determine differences in octocoral assemblages across sites (Primer 6, Clarke and Warwick, 2001; Clarke and Gorley, 2006). We delineated species boundaries between taxa by morphological characteristics and a criterion of 0.5% p-distance between putative species (see McFadden et al., 2011). Similarities between sites (B-Diversity) were calculated using the Sorensen Index on presence-absence data. A non-metric multidimensional scaling (MDS) ordination plot and a dendrogram based on hierarchical clustering of group average linking were created from the similarity matrix; similarity clusters defined by the dendrogram were overlain onto the MDS plot. In addition, because we did not incorporate any *a priori* knowledge of depth zonation, a SIMPROF test was used to determine whether any of the clusters were significantly dissimilar from one another.

### 5.1.2.4 Phylogenetic Diversity Analyses

We calculated phylogenetic diversity at each site (Phylocom v4.2, Webb et al., 2008) using Faith's index (FI) of diversity (Faith, 1992). FI is the sum of the branch lengths that connect all species occurring at a particular site within the phylogenetic tree. Both the GoM regional phylogeny (including all haplotypes) and the whole phylogeny based on *MutS* only were used for phylogenetic diversity calculations. Calculations were based on topology following Faith, 1992. Phylogenetic distance shared by species at a site was substituted for number of species in the Sorensen's Index to obtain a measure of phylogenetic betadiversity. Phylobetadiversity estimates between pairs of sites were then input into PRIMER and a MDS plot was created.

## 5.1.3 Results and Discussion

### 5.1.3.1 Overview

435 specimens representing at least 52 species were collected from 33 sites in the GoM (Appendices A-2 through D-1). The species-accumulation curve indicated that the regional deep-water species pool was well sampled; however it appears that a few more species (~ 1 species per site) would be discovered with additionally surveyed sites (Figure 5-2).
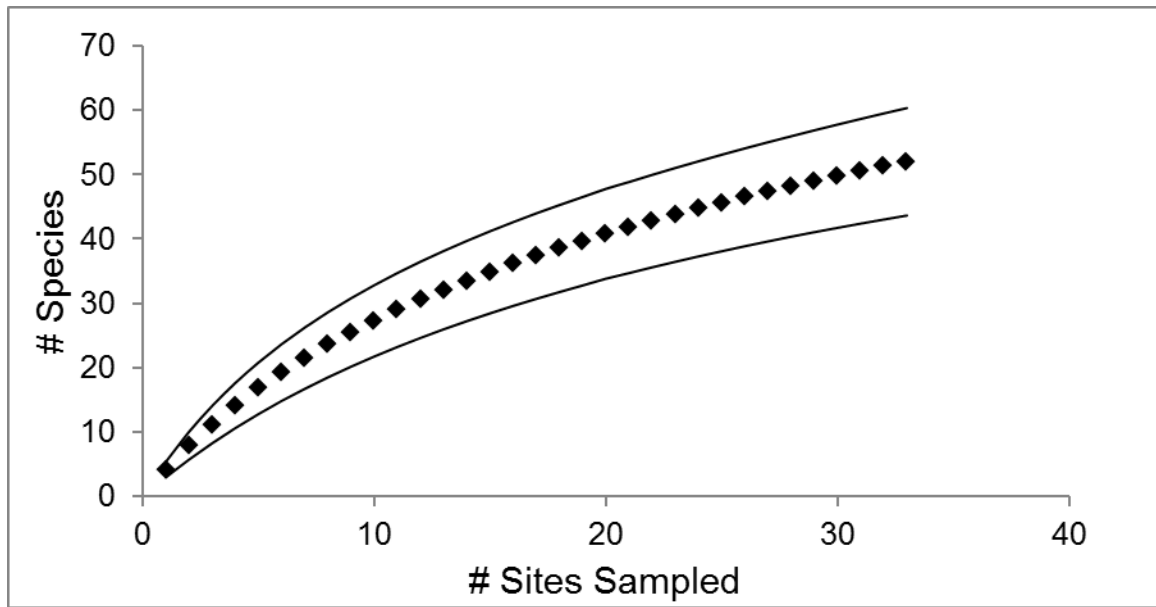
Figure 5-2. Species-accumulation curve (dotted line) and 95% confidence intervals (solid lines).

Five of the six sub-orders of Alcyonacea (sensu McFadden et al., 2010) were represented in collections. Although one pennatulacean was collected, we excluded this soft-substrate associated species from analyses because of the focus on hard-bottom areas in this study. Holaxonians and calcaxonians were the most diverse groups of octocorals collected, representing at least 16 and 17 species, respectively. The genera *Callogorgia* and *Paramuricea* were the most widespread and abundant octocorals observed in the GoM. *Callogorgia* was limited to the upper to middle slope, while *Paramuricea* was more abundant at deeper sites along the middle to lower slope (~1,000-2,500 m). Bamboo corals (Isididae) were also common and occurred in shallow and deep waters (250-2,500 m); however, colonies were lacking from most mid-slope depths (~500-1,000 m). Scleraxonians were well represented in collections with eleven species, including the genera *Corallium, Paragorgia,* and *Sibogagorgia*. An additional three sub-species collected appear to be endemic to the GoM: *Chelidonisis aurantiaca mexicana* (Isididae)*, Callogorgia americana delta* (Primnoidae)*,* and *Anthomastus robustus delta* (Alcyoniidae).

### 5.1.3.2 New Records and New Species

A total of 12 species collected were previously not known to occur in the GoM (Cairns and Bayer, 2009), thus the geographic ranges of several taxa were extended (AppendicesA-2 to D-1). These new records include: one stoloniferan (*Clavularia rudis),* at least 4 scleraxonians *(Corallium niobe, Paragorgia regalis, P. johnsoni, Sibogagorgia cauliflora)*, two holaxonians (*Paramuricea biscaya, Swiftia pallida),* and three chrysogorgiids (*Chrysogorgia averta, Iridogorgia splendens, I. magnispiralis)*. Further, during the *Okeanos* cruise in the GoM in 2012, *Metallogorgia melanotrichos* was observed in DC673. Many of these octocorals appear to have worldwide distributions; for instance, several have been collected off New Zealand (Sanchez 2005) and the North Atlantic Seamounts (Thoma et al. 2009; Pante et al., 2012).

206

At the very least, 4 new species of octocorals were collected; however, there may be up to 4 additional new species (*Anthothela* sp. 2-3, Stoloniferan sp. 1 and 2; Appendix D-1). One new scleraxonian species was collected from the Gulf Penn wreck, where it was blanketing portions of the wreck (Figure 5-3). This species was also collected at VK826, VK906, and the West Florida Slope and was subsequently found in collections from *Lophelia* I.



Figure 5-3. New species of scleraxonian growing on the *Gulf Penn* wreck.

One new species of *Anthothela* was collected at GB535 (Figure 5-4). Further, potentially two additional *Anthothela* spp. represent new species. *Anthothela* and the un-described species of scleraxonia are being described by Kirrily Moore (CSIRO, Univ. Tasmania) as part of her PhD Dissertation.
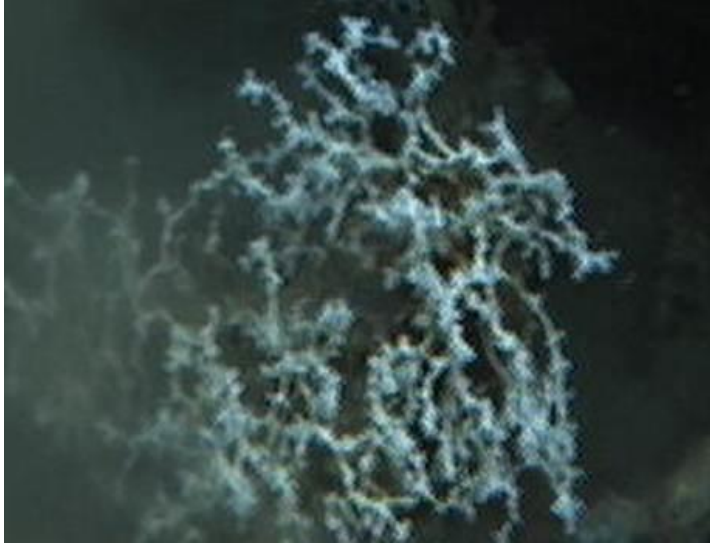
Figure 5-4.  Photo of Anthothela nov. sp. 1 at GB535.

Two individuals representing a newly described family of soft coral were collected from the West FL Slope (Figure 5-5). These species represent two new species of Aquaumbridae. Aquaumbridae is a family of soft coral (Alcyoniina) that was first described from the Pacific, off of Isla de Coco, Costa Rica in 300 m depth (Breedy et al., 2012). This family groups in the Holaxonia-Alcyoniina clade, and its closest known relative appears to be a holaxonian, *Alaskagorgia.*


Figure 5-5.  Photo of Aquaumbridae from the W FL Slope.

One unidentified stoloniferan was collected from GB535, and potentially represents a new species. This species was found growing on a hexactinellid sponge (Figure 5-6).

Figure 5-6.  Unidentified stoloniferan growing on a glass sponge.

### 5.1.3.3 Molecular Barcoding

We used a molecular barcoding approach combined with morphology to delimit species boundaries and to obtain an estimate of the phylogenetic diversity of corals in the GoM.  Further, barcoding octocorals from the GoM allowed us to contribute to the growing efforts of octocoral phylogenetics, including adding sequence data on new, rare, and poorly sampled taxa. Many sequences that we obtained were not in GenBank nor were any close relatives in GenBank. Of the 435 specimens collected, 422 were successfully barcoded, resulting in 64 unique *COI+igr1+MutS* haplotypes; which now represent 20% of the octocoral barcodes in the entire NCBI GenBank database (Figure 5-7). We were successful in amplifying the extended barcode with different primer pairs (Table 4-1) for 420 specimens; however, *COI+igr1* could not be amplified for species in the genus *Anthomastus. MutS* alone differentiated 59 haplotypes and *COI+igr1* distinguished only 56. For the majority of species, the same haplotype was observed among all individuals, although there are a few exceptions (Figure 5-7). Although genetic distances of >1% most often indicate different species, those with genetic distances of 0.5-1% warrant additional attention (McFadden et al., 2010). In most cases, species delineations between sister taxa were achieved by coupling the minimum p-distance of 0.5% with distinguishable morphological characteristics; however a few problematic sister taxa are still unresolved. In fact, many of the genera collected in this study are currently undergoing taxonomic revision.

Bayesian and maximum likelihood analyses recovered similar topologies, and the majority of nodes were strongly supported (>90% posterior probabilities and bootstrap values). However, maximum likelihood analysis was unable to resolve a few polytomies that were situated toward the base of the tree. Two clades consisting of Holaxonia-Alcyoniina-Stolonifera (with *Anthothela)* (Clade 1) and Scleraxonia-Calcaxonia (with *Anthomastus)* (Clade 2) were strongly supported (100% posterior probability) (Figure 5-7).

These recovered clades are consistent with previous phylogenetic analyses (McFadden et al., 2006). We also recovered interesting and new patterns within the phylogeny including: 1) the polyphyly of the Isididae with *Chelidonisis a. mexicana* occurring basal to the calcaxonians, 2) the basal position of the shallower occurring, *Scleracis guadalupensis* relative to the deep-water *Swiftia* clade, and 3) the close relationship of *Swiftia* with shallow water gorgoniids.
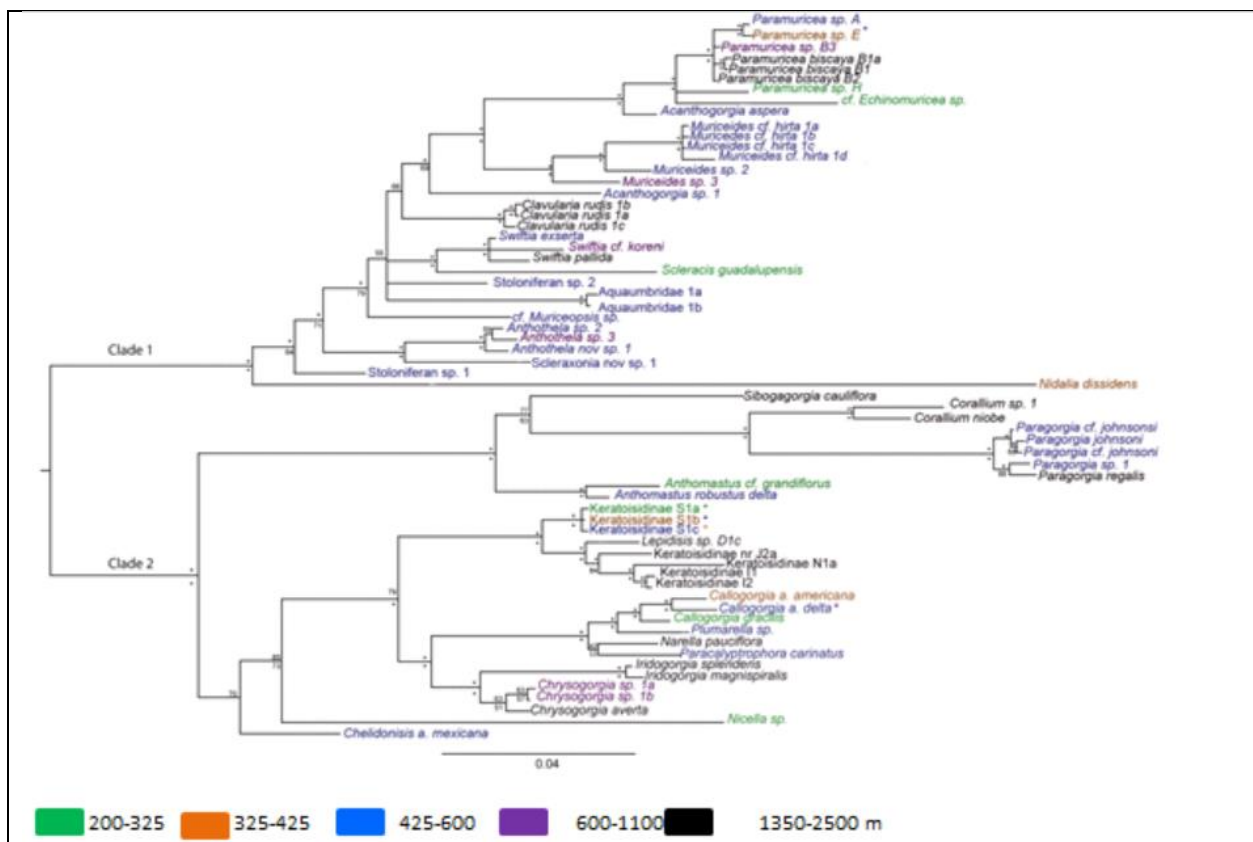


Figure 5-7.  Phylogenetic inference of the extended barcode (COI+igr1+MutS) of GoM deep-water octocorals. Consensus tree based on Bayesian analysis with posterior probabilities (above nodes) and bootstrap values (below nodes) indicated on tree. Posterior probabilities are >90% (*) unless indicated. Tree was rooted at the midpoint.

### *5.1.3.4 Diversity and Community Structure*

5.1.3.4.1 α-Diversity

Overall, species richness at sites in the deep GoM was fairly low, with 1-12 species occurring at each site (Figure 5-8).
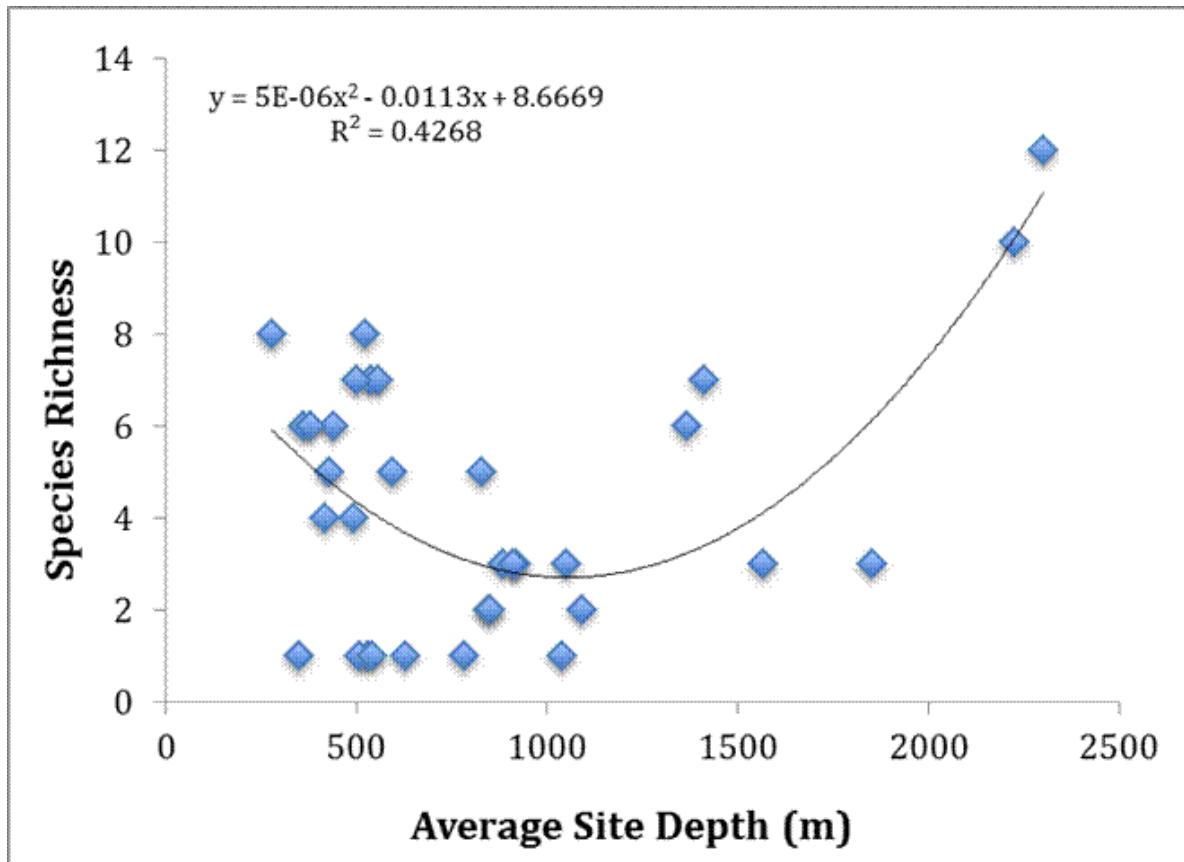
Figure 5-8 The deepest sites (2100-2500 m) contained the most number of species, with 12 species at DC673 and 10 species at DC583, followed by the shallowest (<325 m) site, GC140, with 8 species and a site on the W Fl Slope (525 m) with 8 species. Peaks in species richness at the shallowest (< 325 m) and deepest (> 2100 m) sites sampled contrasts with other faunal diversity patterns in the GoM. In chemosynthetic tube worm and mussel communities, diversity peaks were evident at ~1,400 m and 500-600 m with a marked decrease at 2000 m (Cordes et al., 2010). Diversity peaks were also evident at 1400 m in soft sediment macrofaunal communities (Pequegnat, 1983), whereas in fishes, species richness steadily decreased with increasing depth (Pequegnat et al., 1990; Powell and Haedrich, 2003). The observed peak at the shelf-slope transition at GC140 for octocorals likely represents a merging of fauna, and may be attributed to mid-domain effects (Colwell and Lees, 2000). Some of the species collected at the shallow GC140 site are also known to occur on the continental shelf (*C. gracilis, S. guadalupensis*). The octocoral species richness peak at ~2,000 m is similar to other diversity patterns in the deep North Atlantic (see Rex and Etter, 2010). For octocorals, this diversity peak may be due in part to evolutionary processes. The majority of species occurring at these depths were from two closely related families, the Isididae and Chrysogorgiidae, the latter of which diversified in the deep-sea (Pante et al., 2012).
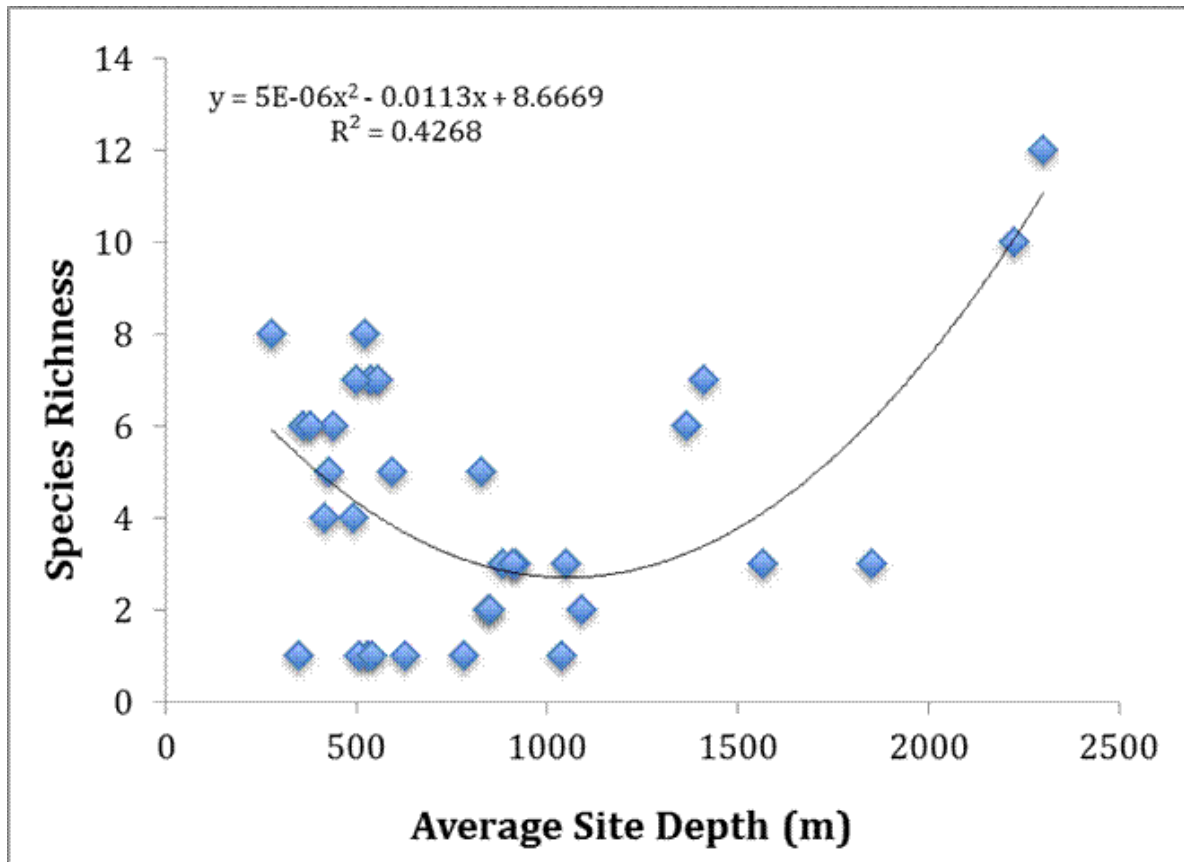
Figure 5-8. Species richness by average site depth.

Combining phylogenetic information into diversity estimates has advantages over taxonomic diversity alone, including allowing for the consideration of evolutionary history into local or regional comparisons of biodiversity, instead of conventional species richness (Faith and Baker, 2006). Faith's index of phylogenetic diversity also indicated high phylogenetic diversity at the DC sites, with the addition of GC852 (1400 m) and the upper slope sites (~450 m), VK906, VK826 and MC751. In contrast, most mid-slope sites, (600-1,100 m) harbored the fewest species (1-3 species), but had varying phylogenetic diversity (10-26). The few species at these sites were from genetically distant clades. Furthermore, although species richness was lower at MC751 and VK826 compared with that of the shallower GC140 site, phylogenetic diversity was higher at these sites compared to GC140 based on the extended barcode. Interestingly, most of the species present at GC140 appear to occupy basal positions within clades compared to species from MC751 and VK826. This suggests that the shelf-slope transition may be an area of early divergence in octocorals, with only a subset of these species able to colonize the deep sea.

### 5.1.3.4.2 β-diversity

Sorensen's Index of taxonomic β-diversity revealed seven distinct species assemblages that were 80-95% dissimilar from one another (Figure 5-9). Five of these assemblages were associated with five depth zones: <325 m, 325-425 m, 425-600 m, 600-1,100 m, and 1350-2400 m. Significant

212

differences between these depth zones were evident (SIMPROF, <0.05), with a few exceptions. First, two GC sites, GC234 (493 m) and GC235 (530 m), grouped with sites occurring at 600-1100 m depth at the 80% similarity level. This was likely due to *C. a. delta* occurring at GC234 and being the only species at GC235 (530 m), GC249 (777-790 m), and MC885 (623-637 m); *Paramuricea* sp. type B3 and *Chrysogorgia* sp. type 1 were also common at sites in depths of 600-1100 m. Second, although occurring within the 400-600 m depth zone, assemblages at the Gulf Penn (541 m) and WFL4 (507 m) were significantly different from the other sites (SIMPROF, p=0.002) because only one species, scleraxonian nov. sp., occurred at these two sites.

Further assemblage structure was evident within three of the depth zones, and some within-depth groupings were significantly different (Figure 5-9). Within 325-425 m, the octocoral assemblage at VK862 was significantly different from GB299 and VK906 (SIMPROF, p=0.006). All three sites shared one species, *C. a. americana,* but no other octocorals were present at VK862. The species assemblage at GB299 and VK906 also included *N. dissidens, M.* cf. *hirta, Paramuricea* sp. type E, and Keratoisidinae S1. Within 425-600 m, the assemblage structure at the West Florida slope (WFS) differed from sites to the west at a dissimilarity (Sorensen's Index) of 70%; however, this pattern in assemblage structure was not significantly different (SIMPROF, p>0.05). Species assemblages within this depth zone of 425-600 m included *Muriceides* cf. *hirta,* cf. *Muriceopsis* sp*., Paramuricea* sp. type A and *C. a. mexicana,* but *Plumarella dichotoma/pellucida* (two morphological species with identical haplotypes) occurred only at the WFS whereas *C. a. delta* occurred to the west. Within 1,350-2,400 m, assemblage differences were evident with two distinct assemblages at 60% dissimilarity. DC sites 583 and 673 were significantly different from MC294, GC852, MC297 and MC388 (SIMPROF, p=0.04). Although *P. biscaya* and *C. rudis* occurred at all deep (>1300 m) sites, the presence of *S. cauliflora, C. averta, Iridogorgia* spp., and several isidids at the DC sites influenced assemblage patterns. This reveals the presence of an additional depth break at 2,100 m.
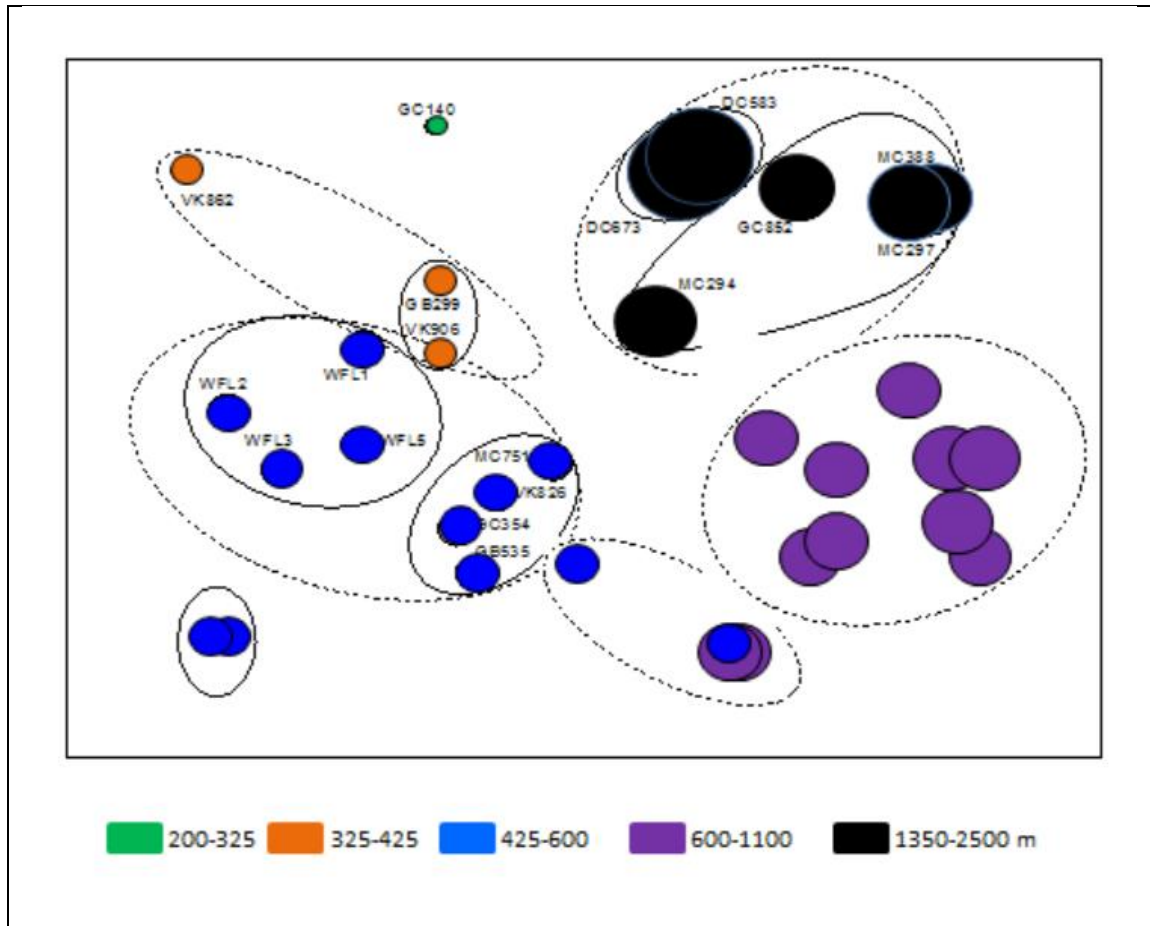
Figure 5-9. MDS plot with distance between points representing Sorensen's
Index of Similarity. Assemblage similarity at > 20 (dotted line) and
35% (solid line) are indicated. Circle size denotes average site depth.
Stress=0.06.

Biogeographic provinces have been previously proposed for numerous taxonomic groups in the GoM, and some of these boundaries can be confirmed or expanded upon for deep-sea octocorals. Giammona (1978) suggested that octocorals assemble into six zones: sub-tropical, western Florida, northern, western, southeast Mexican coast, and an oceanic or deep-sea assemblage. Increased diversity at some stations in the northern GoM suggested an additional east-west boundary across the Mississippi River Delta. Although we did not observe the east-west break in coral community structure in the northern GoM, perhaps due to limited sampling west of the Green Canyon sites, we did find that mid-slope octocoral communities differed between the West Florida Slope and the remaining mid-slope communities in the northern GOM. The GoM Loop Current may serve as an oceanographic barrier to dispersal of larvae originating in the northern GoM, but also as a conduit of exchange between the GoM and the Caribbean Sea.

Bathymetry, or the variables associated with bathymetry, is the primary factor responsible for patterns observed in octocoral community structure. Expanding on Giammona (1978) who proposed one, extensive deep-sea coral assemblage, Etnoyer (2009) used museum records to demonstrate that the deep-water assemblage can be divided into at least three provinces that range

214

from 200-800 m, 800-1,600 m, and > 1,600 m. The assemblage patterns observed in the present study further refine the proposed depth provinces, with additional breaks on the upper to lower slope at 300, 400, 600, 1,000, 1,350, and 2,100 m. These zones are more similar to depth zones noted for other taxa in the GoM, such as soft sediment macrofauna (Wei et al., 2010), chemosynthetic communities (Cordes et al., 2007, 2010), and megafaunal invertebrates and fishes (Pequegnat, 1983; Pequegnat et al., 1990; Powell and Haedrich, 2003). However, the additional depth breaks observed across the upper to middle slope, particularly < 1,000 m, appear to be unique to deep-water octocorals in the GoM. The refined community boundaries are likely the result of targeted exploration of deep GoM hard substrates. Soft substrate species may be less specialized, and possibly have broader depth distributions than those species associated with hard substrates, as observed in sea pens off of Newfoundland (Baker et al., 2012). The question of whether these depth breaks are ubiquitous throughout the entire GoM awaits further exploration along the Texas and the Mexican coasts as well as through the Yucatan and Florida Straits. Regardless, depth zonation is apparent and predictable in the deep-water octocoral assemblage and plays a more important role than geographic distance in structuring octocoral communities, a pattern also observed in GoM chemosynthetic communities (Cordes et al., 2007).

We further expanded our analyses to examine the phylogenetic differences of species among sites. Preliminary estimates of phylo-betadiversity indicated that larger depth differences between pairs of sites had higher dissimilarity in phylogenetic structure (Figure 5-10). Furthermore, patterns in phylo-betadiversity illustrated that the relatedness of species shifts with increasing depth in the GoM, and the deepest sites harbor a greater number of closely related species compared to the shallower sites. *In situ* diversification of isidids and chrysogorgiids at the deepest sites appear to be driving these patterns.
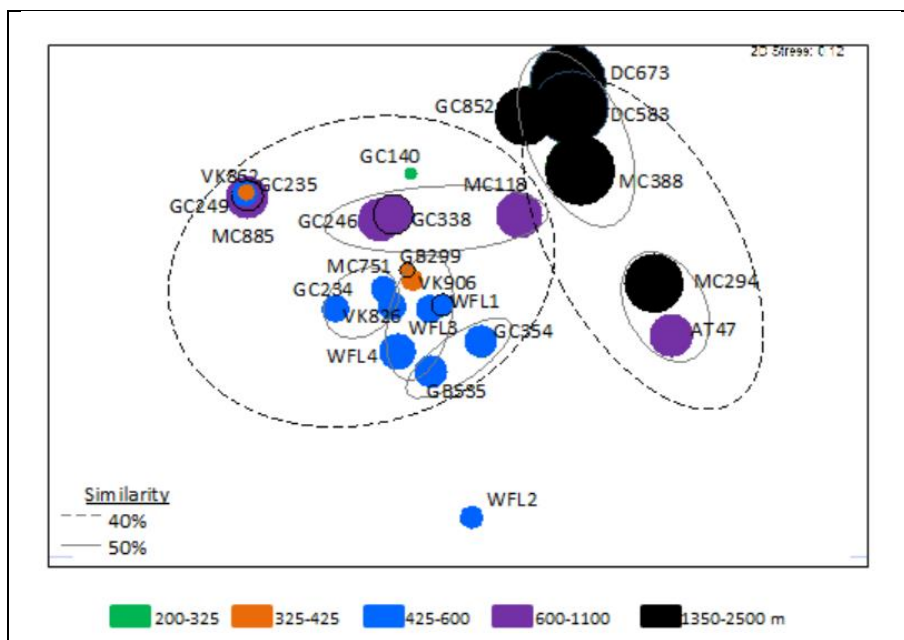


Figure 5-10. . MDS plot with distance between points representing Sorensen's Index of Phylogenetic Similarity (mean branch length substituted for species in Sorensen's Index). Assemblage similarity at > 20 (dotted line) and 35% (solid line) are indicated. Circle size denotes average site depth.

### 5.1.3.5 Regional Comparisons of Communities

Limited samples collected during a 2009 USGS cruise off the southeastern US allowed us to examine the similarity in phylogenetic diversity between octocorals collected in the GoM with octocorals collected off of Cape Canaveral (CC) FL in two depth zones (400-500 m, and 600-800 m). Although further sampling off of CC will likely yield additional data, these results provide a first glimpse into biogeographic differences between the Atlantic and the GoM. Using only *mtMutS,* seven haplotypes were amplified from off CC from 15 samples (Figure 5-11). In general, each haplotype represented a unique species; however, *mtMutS* haplotypes were identical within two species of *Plumarella* (*P. aculeata P. laxiramosa;* identified by S. Cairns); additional sequencing is needed to resolve whether this *Plumarella* complex contains 1 or 2 species. *Plumarella* spp. was the only coral sequenced in the shallower depth zone off CC (400-600 m), and this is an abundant genus in this depth range off eastern FL.

The differences in phylogenetic diversity between the CC and GoM sites were apparent, with novel haplotypes collected off CC; only two haplotypes were shared between the GoM and the CC sites (*P. pellucida/dichotoma, Muriceides* cf. *hirta). Plumarella aculeata* and *P. laxiramosa* were collected off CC and did not occur on the WFS, where *Plumarella dichotoma/pellucida* (two morphological species with identical haplotypes) were abundant. However, *P. aculeata/laxiramosa* were collected in slightly shallower depths at the CC site (~400-440 m) than the WFS, indicating that this species may prefer shallower depths compared to its congeners. This is further supported with the collection of *Plumarella pellucida/dichotoma* off CC, at a depth of 491 m. This depth range is similar to the depth range on the WFS where *Plumarella* occurred (488-595 m), indicating that these differences may be a result of depth. The remaining species sequenced from CC were collected at depths of ~750 m: *Lepidisis* sp. D1b, cf. *Muriceopsis* sp. type B, *Muriceides* cf. *hirta* 1d, and *Placogorgia cf. placomus. Muriceides* cf. *hirta* appears to have a wide distribution, both geographically and bathymetrically. This species was collected throughout the GoM-from GB535 to WFS -at depths ranging from ~410-540 m. Furthermore, increased genetic diversity within this species is apparent (four haplotypes), and the *Muriceides* cf. *hirta* type 1d haplotype occurred at both CC and in the GoM. The other three haplotypes (*Lepidisis* D1b, *cf. Muriceopsis* type B, and *P.* cf. *placomus)* collected were not found in the GoM, although genetically similar haplotypes occurred. In general, differences in genetic diversity occurring between these regions suggests a biogeographic break between the continental slope of the GoM and the southewast US however, additional sampling off the southewast US and particularly on the WFS are needed to gain a more thorough picture of 1) whether differences in genetic diversity and community structure are due to biogeographical or bathymetric breaks and 2) where these breaks occur.
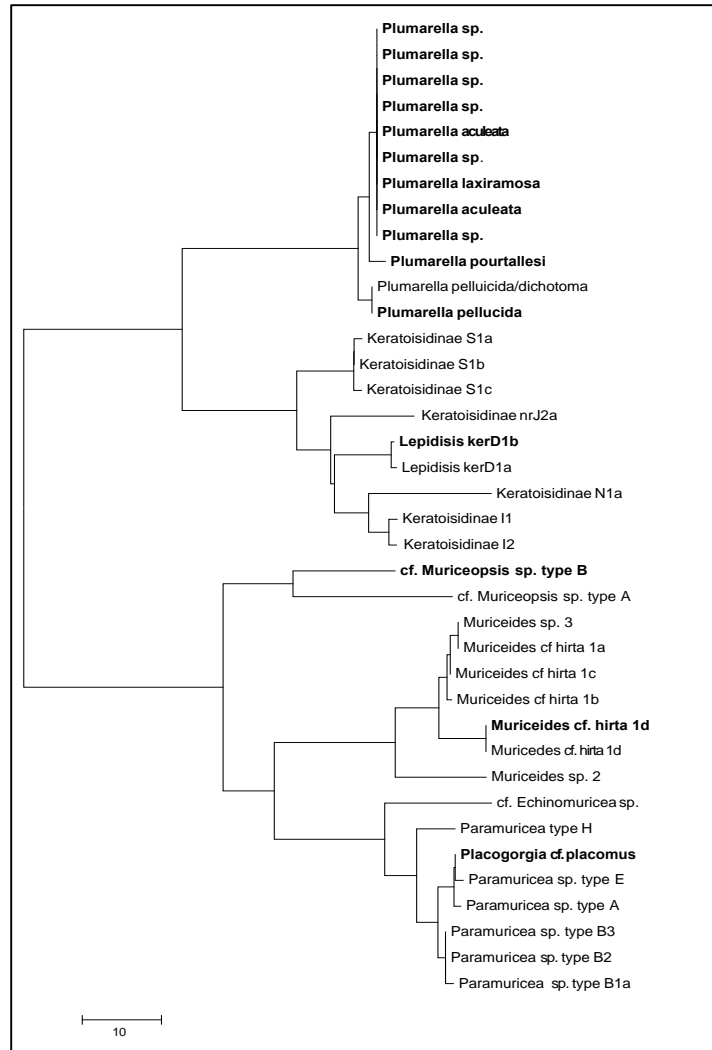
Figure 5-11.  Neighbor-joining tree of mtMutS haplotypes
sequenced from collections off Cape Canaveral,
FL (in bold) and genetically-similar haplotypes
sequenced from the Gulf.

## 5.1.4  Conclusions

The molecular barcoding approach allowed us to identify distinct species associated with hard substrates.  Further, a considerable number of species that were not known to occur in the region were documented. Because cryptic species are often revealed and morphological characteristics of species are still being resolved, it is important to continue incorporating genetic techniques into identifying species boundaries, and thus community boundaries, of deep-sea species. The species-accumulation curve did not quite reach an asymptote, indicating that additional species will likely be collected with additional sampling. Moreover, our results indicated that octocoral communities assemble primarily into distinct bathymetric provinces in the deep GoM, followed secondarily by location as the WFS sites differed from the sites in the northern GoM. Our data also indicate that phylogenetic history plays an obvious and primary role in octocoral community assembly in the deep sea.

## 5.2 Genetic Diversity of Two Common Octocorals

### 5.2.1 Background

*Lophelia* II surveys indicated that two common octocoral genera occur along the continental slope in the GoM. *Callogorgia* is common at depths ranging up to 1,000 m whereas *Paramuricea* occurs at depths up to 2,400 m, but is most common at deeper sites (>1,000 m). These two genera increase habitat heterogeneity on the continental slope and have potentially symbiotic relationships with ophiuroid brittle stars. *Callogorgia* also serves as egg-laying substrate for scyliorhinid catsharks (Etnoyer and Warrenchuk 2008). Because of their abundance and ecosystem importance in the GoM, it is imperative to understand species boundaries within these two genera, as well as their genetic connectivity across the GoM. Therefore, mitochondrial (mtMutS, cox1+igr), nuclear rDNA (28S), and microsatellite loci coupled with morphological data are being used to understand the boundaries of populations and species within these genera. Genetic data will provide insight into whether populations are structured by depth and/or by distance, while enabling the determination of migration pathways and source populations.

### 5.2.2 Methods

#### 5.2.2.1 Morphological Identification

Approximately 2-3 cm tissue samples were obtained from each specimen (165 *Callogorgia, 103 Paramuricea)*, frozen at -80ºC and preserved in both 95% ETOH (stored at -20 ºC) and a high-salt EDTA preservative (stored at -80 ºC). Voucher specimens of each individual were preserved in 95% ETOH or dried. Species were identified using morphological characteristics (Bayer 1982; Cairns & Bayer 2002; Cairns 2010; Grasshoff 1977). Scanning election microscopy (Quanta 600 FEG at the Penn Nanotechnology Regional Center) was used to identify morphological differences between haplotypes.

#### 5.2.2.2 Phylogenetics

##### 5.2.2.2.1 Callogorgia

DNA was extracted using a Qiagen DNeasy kit. The extended mitochondrial barcode (*cox1+igr1+mtMutS*) was sequenced for 159 individuals; 6 individuals could not be barcoded because of tissue preservation issues. Approximately 850 bp from the 5' end of the mitochondrial *mtMutS* gene and ~1000 bp of the *cox1+igr1* region were amplified through PCR (following McFadden *et al.* 2006, 2011) and sequenced (Genewiz Inc and UW-HtSeq). We also amplified and sequenced an ~810 bp fragment of the nuclear *28S* ribosomal gene in each species following McFadden and van Ofwegen (2012). All sequences were edited, aligned by ClustalW (gap opening penalty= 25, extension penalty=15) and visually adjusted by viewing amino acid alignments in MEGA v5 *28S* was aligned using the L-INSi method (gap opening penalty=1.53; extension penalty=0.07) in MAFFT and amino acid alignments were visually adjusted. The mitochondrial gene regions were concatenated into a 1708 bp extended barcode and *28S* resulted in a 799 bp alignment. Uncorrected p-distances were calculated for both mitochondrial and nuclear loci

(MEGA v5). Bayesian analysis (BEAST) was used to determine the phylogenetic relationships of *Callogorgia,* including two species collected from outside the GoM: *C. verticillata* and *C. gilberti.* Data were partitioned so that the appropriate nucleotide models could be applied to gene regions. The maximum clade tree was rooted with the outgroup *Plumarella* sp. and displayed in Figtree.

### 5.2.2.2.2 Paramuricea

DNA extractions were performed using the Qiagen DNeasy Blood and Tissue Kit. The extended mitochondrial barcode (*COI+igr1+MutS*) was sequenced following McFadden et al. (2006, 2011). Approximately 850 bp from the 5' end of the mitochondrial *MutS* gene and ~1000 bp of the *COI+igr1* region were PCR amplified and the resulting sequences were edited, aligned by ClustalW and adjusted by eye by viewing amino acid alignments (BioEdit, MEGA). The gene regions were concatenated into a 1602 bp extended barcode. Pairwise p-distances were calculated between all haplotypes (MEGA v5). A median joining network of haplotypes was created (Network v 4.6, http://www.fluxus-engineering.com/).

## 5.2.2.3 Microsatellite Marker Development

Two individuals each of *Paramuricea* and *Callogorgia* were sequenced on a full plate on Roche-454 (Engencore, Colombia SC), resulting in ~1 million reads (Table 5-2). A greater number (~2X) of reads were obtained for *Callogorgia* compared with *Paramuricea.* Average lengths of reads ranged from 340-348 ±147-148 (s.d.) bp. Reads were input into the QDD2 (Meglecz and Martin 2011) program, which is a program that enables microsatellite selection and subsequent primer design (PRIMER 3). Table 5-2 illustrates the results from QDD2. 556 to 1,438 unique reads and contigs were obtained for each individual that had optimal primers and microsatellites that repeated at least 5 times and had motifs ≥3 (e.g., AGT). Reads containing microsatellites were BLASTed against one another and these reads were then searched for polymorphic microsatellites. From a list of 114 potential loci that had good primers, 39 primer pairs were ordered and tested for amplification across *C. a. americana and C. a. delta*. Forward primers were ordered with unlabeled tails (T1-T4), and these same tails were ordered with fluorescent labels. All loci were amplified using the following PCR profile: initial denaturation: 94 ˳C at 5 min, followed by 32 cycles of 94 ˳C 20 s, 54 ˳C at 20 s, 72 ˳C at 30 s, followed by a final elongation of 72 ˳C at 30 min. After locus testing across populations, cycle number was increased to 45 for reactions and annealing temperatures are in progress of being optimized for ideal amplification of selected loci. The following final concentrations are used in 10ul PCR reactions: 10-20 ng DNA template, 1uM dNTPs, 1X Buffer, 0.15 uM Reverse Primer, 0.15 uM fluorescent-labeled tag (PET, 6FAM, NED, VIC), 0.04 uM Forward Primer, 2.5 mM $MgCl_2$, and 0.1 units Taq. Forward primers with fluorescent tags (PET, NED, VIC, 6FAM) were ordered for the selected loci (see Results) for multiplexing. PCR products were pooled and analyzed on an ABI 3130XL Genetic Analyzer at the University of Pennsylvania. Fragments were sized using the microsatellite plug-in for Geneious with GS500LZ size standards (Applied Biosystems, Inc.). The Microsoft Excel add-on GenALEx was used to determine departures from Hardy Weinberg, and observed and expected heterozygosity at each locus. Genetic distances between pairs of individuals were calculated and plotted in a Principal Coordinate Analysis. An Analysis of Molecular Variance (AMOVA) was used to determine whether $F_{ST}$ values were significant. $F_{ST}$ is the proportion of the total genetic

variance contained in a subpopulation (the S subscript) relative to the total genetic variance (the T subscript). Values range from 0 to 1, with High $F_{ST}$ indicating a considerable degree of differentiation among populations. Pairwise $F_{ST}$ values were coupled with pairwise geographic distances and depth differences between sties to test whether populations are isolated by depth and/or by distance in the GoM. Using the IDB on the Web program, a Mantel test was used to test for significant correlation between depth and geographic distance with genetic distance ($F_{ST}$).

Although efforts have been primarily focused on *Callogorgia*, we also tested population differentiation in *Paramuricea*. For *Paramuricea*, 45 potential loci were discovered and 29 were subsequently ordered and weretested for amplification in *Paramuricea* type B3 and *P. biscaya*.

Table 5-2.

Reads obtained from 454 sequencing and subsequent results from a microsatellite discovery program (QDD2, Meglecz and Martin 2011)

| Individual | Total # Reads | Size Range | Unique Reads (>80 bp) with $MSAT_{5+}$ | Unique Reads (>80 bp) with Primers | Unique Reads (>80 bp) with Primers & MSAT Motif >3 |
|---|---|---|---|---|---|
| C. am delta (MC751) | 430,346 | 24-743 (347±147) | 12,306 | 7,680 | 1,438 |
| C. am delta (VK826) | 293,081 | 24-708 (348±148) | 10,056 | 6,240 | 1,290 |
| P. biscaya B1 (MC294) | 258,590 | 24-1086 (347±148) | 3,938 | 2,619 | 569 |
| P. biscaya B2 (GC852) | 184,264 | 26-896 (340±149) | 3,181 | 2,188 | 556 |

## 5.2.3 Results and Discussion

### 5.2.3.1 Taxonomic Status and Phylogenetic Relationships

#### 5.2.3.1.1 Callogorgia

Extensive GoM collections (n=165 individuals) yielded three *Callogorgia* taxa: *C. americana americana* (n=31), *C. americana delta* (n=122), and *C. gracilis* (n=12). Sclerite counts and structures were useful in species identification (Figure 5-12). Taxonomic designations based on morphology were further confirmed with the occurrence of a unique mitochondrial molecular barcode (*cox1+igr1+mtMutS)* obtained for each taxon; no haplotype variability was observed among individuals within a taxon. Of all *Callogorgia* spp. sequenced in this study, putative species were 0.4-1.6% genetically divergent (p-distance) at the extended mitochondrial barcode (Table 5-3). P-distances obtained at *28S* were generally higher, ranging from 0.38-4.53% (Table 5-3). Total genetic divergences at both mitochondrial and nuclear loci ranged from 0.40-2.45% (Table 5-3). The USNM1116119 voucher specimen of *C. gracilis* was identical to the GoM *C. gracilis*.
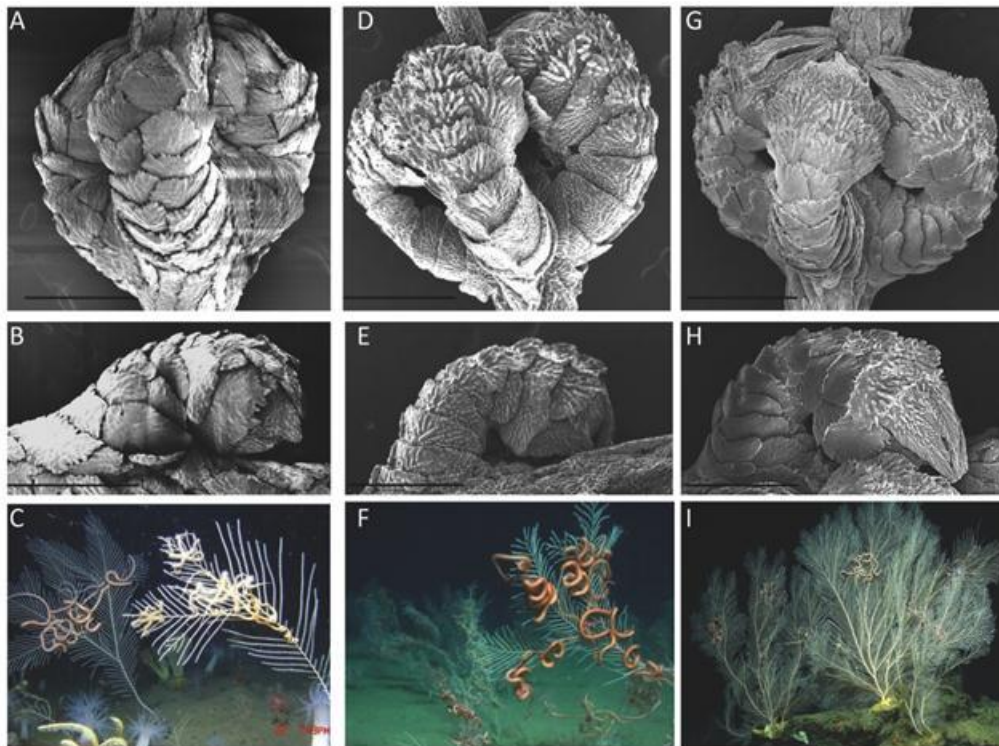


Figure 5-12.  Morphology of GoM *Callogorgia* spp. Scanning electron microscopy images of polyps and whole colony images for (A-C) *Callogorgia gracilis*, (D-F) C. a. americana, and (G-I) C. a. delta. 500 um scale bar indicated.

Resolving the taxonomic status of the sub-species *C. americana delta* and *C. a. americana* was in part the impetus for this study, as these sub-species are among the most commonly occurring octocoral species in the deep GoM. In 2002, Cairns and Bayer delineated these two sub-species

221

based primarily on differences in sclerite structure and distribution. *Callogorgia a. americana* was previously thought to be restricted to the Caribbean Sea, Florida Straits, and southern GoM while *C. a. delta* was a northern GoM endemic. The extensive records provided in this study demonstrated that both taxa are present in the northern GoM and they differ genetically and morphologically. Further, these two species inhabited different depth zones (*C. a. americana*: <425 and *C. a. delta*: 425-1,000 m), at least in the GoM. This depth differentiation is possibly the result of parapatric speciation along an environmental gradient in depth, a pattern seen in other corals (Prada and Hellberg 2013). Alternatively, niche differences in *Callogorgia* could have accrued after speciation, and the observed distributions could either be due to historical colonization of *C. a delta* into deeper areas of the GoM followed by adaptation to depth-related variables or the result of competitive exclusion (e.g. for limited space) of one taxon from their congener's respective preferred habitat.

Table 5-3.

Pairwise uncorrected p-distances (%) for *Callogorgia* species at (A) mitochondrial cox1+igr1+mtMutS, (B) nuclear 28S, and (C) both mitochondrial and nuclear loci

| A | *C. gracilis* | *C. verticillata* | *C. a. americana* | *C. a. delta* |
|---|---|---|---|---|
| *C. gracilis* | | | | |
| *C. verticillata* | 0.35 | | | |
| *C. a. americana* | 1.47 | 1.41 | | |
| *C. a. delta* | 1.59 | 1.47 | 1.24 | |
| *C. gilberti* | 1.18 | 1.06 | 0.82 | 0.41 |

| B | *C. gracilis* | *C. verticillata* | *C. a. americana* | *C. a. delta* |
|---|---|---|---|---|
| *C. gracilis* | | | | |
| *C. verticillata* | 1.25 | | | |
| *C. a. americana* | 4.53 | 4.40 | | |
| *C. a. delta* | 3.78 | 3.65 | 1.63 | |
| *C. gilberti* | 3.90 | 3.77 | 1.76 | 0.38 |

| C | *C. gracilis* | *C. verticillata* | *C. a. americana* | *C. a. delta* |
|---|---|---|---|---|
| *C. gracilis* | | | | |
| *C. verticillata* | 0.64 | | | |
| *C. a. americana* | 2.45 | 2.36 | | |
| *C. a. delta* | 2.29 | 2.17 | 1.36 | |
| *C. gilberti* | 2.05 | 1.92 | 1.12 | 0.40 |

Two pairs of sister taxa with allopatric distributions were recovered from the phylogeny: 1) *C. a. delta* with *C. gilberti* and 2) *C. gracilis* with *C. verticillata* (Figure 5-13). Sister taxa in both clades were only ~0.4-0.6% genetically divergent, just around the threshold (0.5% p-distance) provided by McFadden et al. (2011) for delimiting species boundaries. However, morphology combined with allopatric distributions suggests that these taxa are most likely distinct species. In 2010, Cairns synonymized *C. gilberti* with *C. americana,* noting that these two taxa were morphologically indistinguishable. Although sclerite counts overlap, it appears that counts in *C.*

*gilberti* range somewhat higher, with 10-12 abaxial, 4-5 outer lateral and 2-3 inner lateral compared with 9-11 abaxial, 3-4 outer lateral, and 1-2 inner lateral in *C. a delta.* In addition, *Callogorgia gilberti* is known from off the Hawaiian Islands and Cross Seamount in 326-965 m (Cairns 2010) whereas *C. a. delta* had been described only from the GoM (Cairns and Bayer 2002). The sister species *C. gracilis* and *C. verticillata* also have allopatric distributions. *Callogorgia gracilis* has been previously documented from the GoM and throughout the Caribbean (Cairns and Bayer 2002) whereas *C. verticillata* is only known from the eastern Atlantic and Mediterranean Sea. The presence of inner lateral sclerites and a greater number of outer later sclerites are characters distinguishing between *C. gracilis* and *C. verticillata* (Cairns and Bayer 2002).
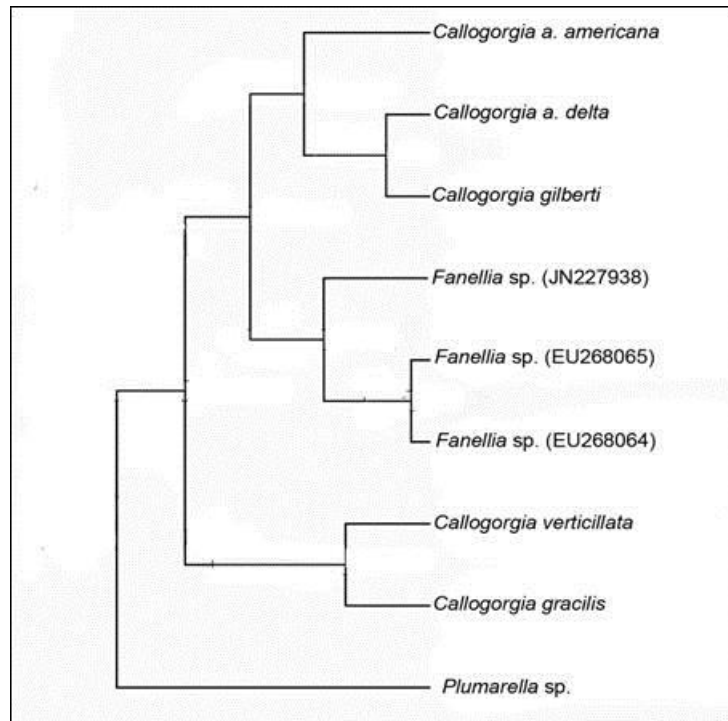


Figure 5-13. Maximum clade credibility tree of *Callogorgia*
at combined loci (cox1+mtMutS+28S) Posterior
probabilities were all >90%. Numbers designate
genbank sequences.

### 5.2.3.1.2 Paramuricea

Samples of 103 colonies of *Paramuricea* were collected for genetic and morphological analyses. Molecular barcoding techniques combined with morphology enabled identification of likely five species of *Paramuricea* in the northern GoM. Seven haplotypes of the extended barcode emerged within the *Paramuricea* genus and were 0.1-2.2 % divergent from each other (Table 5-4). *Paramuricea* type H was 1.7-1.8% divergent from the other *Paramuricea* haplotypes. *Paramuricea* types A and E were genetically quite similar (0.2% divergent), but morphological differences indicated that these likely represent different species (Figure 5-14). *Paramuricea* type A had thorny spindle-shaped coenenchymal sclerites (some bent) and elongated thornscales. In contrast, sclerites observed in *Paramuricea* type E were irregularly shaped and sized, and contained spindles and branched spindles. Four *Paramuricea* type B haplotypes were identical at

223

*MutS,* but they differed in 1-2 bp polymorphisms at *COI;* B1a had an additional polymorphism in *igr1* (0.1-0.2% p-distance). Although p-distances were low, morphological differences between type B3 and *P. biscaya* types B1, B1a, and B2 were identifiable (Figure 5-15).
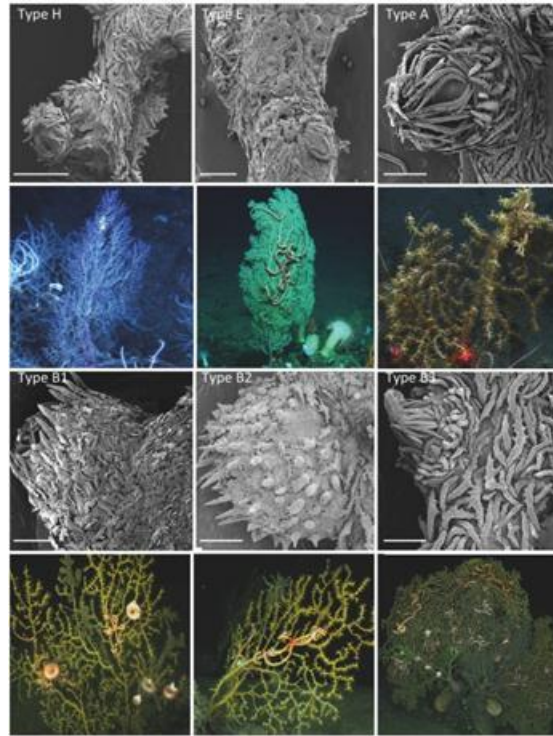


Figure 5-14.  Scanning electron microscopy of sclerite composition and structure of six haplotypes of Paramuricea with photos of colony morphology.  Scale bar indicates 500 um.

Table 5-4.

Pairwise uncorrected p-distances (%) for Paramuricea spp. at  mt cox1+igr1+mtMutS

|  | Type A | Type E | *P. biscaya* B1 | *P. biscaya* B1a | *P. biscaya* B2 | *Type* B3 |
|---|---|---|---|---|---|---|
| Type E | 0.19 |  |  |  |  |  |
| *P. biscaya* B1 | 0.62 | 0.69 |  |  |  |  |
| *P. biscaya* B1a | 0.69 | 0.75 | 0.06 |  |  |  |
| *P. biscaya* B2 | 0.50 | 0.56 | 0.12 | 0.19 |  |  |
| Type B3 | 0.56 | 0.62 | 0.19 | 0.25 | 0.06 |  |
| Type H | 2.10 | 2.25 | 1.87 | 1.94 | 1.75 | 1.81 |
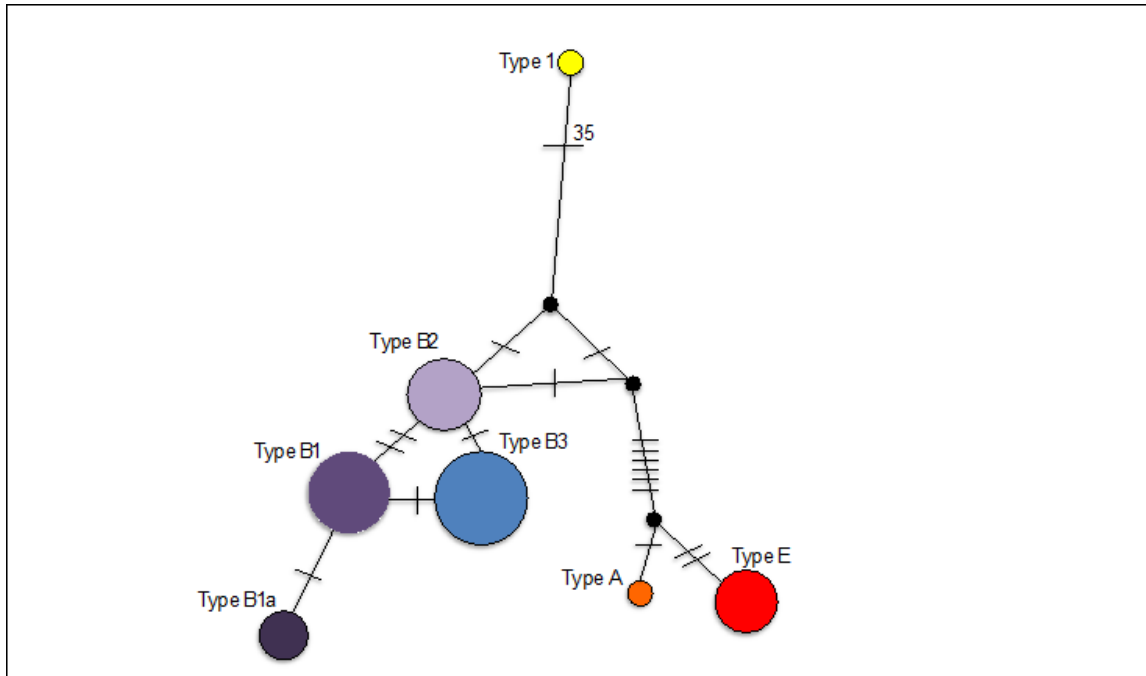
Figure 5-15. Median joining network of haplotypes collected in the GoM. Size of circle corresponds to total number collected. Number of substitutions is indicated by slash marks (except Type 1 to the remaining is indicated by a number 35).

*Paramuricea* type B3 differed by having bent spindle-shaped, coenenchymal sclerites and blunt thornscales whereas plate-shaped sclerites were found in *P. biscaya* and thornscales were more elongated compared with type B3.

Although there was low genetic divergence in the extended mitochondrial barcode between *Paramuricea* types A and E and between *Paramuricea* types B3 and *P. biscaya,* there were consistent differences in sclerite morphology between the haplotypes, suggesting that these likely represent different species. Although additional genetic markers or genomic data are needed to confirm the species boundaries within this genus, the molecular barcodes used in this study allowed us to identify independent, phylogenetic lineages of *Paramuricea.* Furthermore, each putative species appears to inhabit specific depth zones in the northern GoM, with *Paramuricea* Type H at < 260 m, type E at 280-400 m, type A at 443-550 m, type B3 at 837-1,040 m, and *P. biscaya* at 1,370-2,400 m.

The *mtMutS* haplotypes of *Paramuricea* found in the GoM appear to be geographically widespread throughout the North Atlantic. Our haplotype designations correspond to those identified from the North Atlantic seamounts and along the continental margin off the northeast US coast, Norway, and in the Caribbean Sea (Thoma et al., 2009). The widespread distribution of these haplotypes suggests that, at the very least, historical dispersal of this genus occurred throughout the deep sea, which has been noted in other species of cold-water corals. Our population genetics studies using microsatellites are needed to examine further population differentiation within the GoM and beyond.

### 5.2.3.2 *Microsatellite Analyses*

#### 5.2.3.2.1 *Callogorgia*

Of 39 primer pairs that were tested for amplification across individuals, 12 loci were polymorphic and consistently amplified in both *C. a. delta* and *C. a. americana* (Table 5-5)*.* The number of alleles per locus ranged from 1-13, and the majority were private alleles within a species. Overall, there was low allelic diversity (mean $3.55 \pm 3.08$ s.d.) at most loci within a species, with the exception of GIR, GD1, EFD, and CYO. The low allelic diversity at both microsatellite and mitochondrial loci in both *Callogorgia* spp. in the GoM suggests that these species underwent a recent population bottleneck and/or the GoM was colonized by a few number of individuals. Severe reduction in population size can influence the genetic variation within and among populations, often resulting in reduced genetic diversity (e.g., Bouzat et al. 1998). In addition, five out of the 12 loci in *C. a. delta* showed either heterozygote excess (GIR, A50, EME, EFD) or deficiency (B3S) *(*Table 5-5)**.** Heterozygote deficiency (low frequency of heterozygotes) is often indicative of small populations and/or inbreeding. However, more data are needed to confirm this as the lack of heterozygotes at B3S could also be to the presence of null alleles, which occur when mutations in the primer region prevent primer binding (Callen et al. 1993). The excess in heterozygosity (higher frequency of heterozygotes) at the four loci (GIR, A50, EME, EFD) is often indicative of higher genetic diversity; however, some studies have suggested that heterozygosity can increase at a few number of loci after a founder event or population bottleneck due to chance (Leberg 1992, Cornuet and Luikart 1996). More data are needed to test whether *Callogorgia* spp. in the GoM were established from just a few individuals (founder effect) or whether these species have undergone a recent population bottleneck.

Using a population genetic approach, *Callogorgia americana americana* and *C. a. delta* were clearly delimited based only on four loci (GD1, EME, DAV, JKM). Analysis of molecular variance (AMOVA) of the two species of *Callogorgia* revealed an $F_{ST}$ value (genetic distance) of 0.374 (*P*<0.001), demonstrating significant genetic differentiation between these two species. A principal coordinate analysis based on pairwise genetic distances (calculated in GenALEx) of 40 *Callogorgia* spp. also revealed clear separation of the two species, as indicated by two separate clusters in Figure 5-16. Few of the same alleles were found in both species across the four loci. No alleles were shared at GD1 or DAV; 1 allele was shared at EME, and 1 allele was shared at JKM. Further data are needed to assess whether there are any hybrids of the two species of *Callogorgia.*

Table 5-5.

Locus name, primer sequences, type of fluorescent label on each forward primer, repeat motif, size range in base pairs. For each species, N=number of individuals genotyped, NA=number of alleles, HO =observed heterozygosity, HE=expected heterozygosity and pHWE =p-value indicating departure from Hardy Weinberg equilibrium per locus using a Chi-Square Test. A Bonferroni adjustment was made to α. Significance (*) = p<0.004

| Locus | Motif | Allele Sizes | Primers (5'-3') | Fluorescent Label/Tail | Species | N | $N_A$ | $N_{PA}$ | $H_E$ | $H_O$ | $P_{HWE}$ |
|---|---|---|---|---|---|---|---|---|---|---|---|
| *Ca*C3L | AAGT | 217-229 | F: AGGTGTTGCCTATAGACGTG R: ACTAATTTGATAAATTGACAGT | PET-T1 | C. a. amer | 3 | 1 | 1 | - | - | - |
| | | | | | C. a. delta | 22 | 2 | 2 | 0.136 | 0.127 | 0.731 |
| *Ca*B3S | AAT | 228-243 | F: CTGCAGCAATCTGGACTTAC R: ATGATGCCGTTATTTTATCA | 6FAM-T2 | C. a. amer | 4 | 2 | 1 | 0.278 | 0.333 | 0.729 |
| | | | | | C. a. delta | 21 | 2 | 1 | 0.245 | 0.095 | * |
| *Ca*GIR | AAAC | 256-332 | F: ATTTCGAAGACGAGGAACTC R: ACTAGGGCTTAACATCCCTG | VIC-T4 | C. a. amer | 4 | 5 | 2 | 0.750 | 1.000 | 0.285 |
| | | | | | C. a. delta | 27 | 13 | 10 | 0.444 | 0.896 | * |
| *Ca*DAV | ACG | 164-179 | F: CGATAACCGTTTGCATACTC R: TGCGTAGTTATCGTAGTGGG | NED-T3 | C. a. amer | 18 | 4 | 3 | 0.560 | 0.667 | 0.322 |
| | | | | | C. a. delta | 83 | 2 | 1 | 0.353 | 0.361 | 0.828 |
| *Ca*A50 | AAC | 245-260 | F: AACCCTGCCACTTCTAGTTT R: CGCATCATTAACCTACATGG | NED-T3 | C. a. amer | 6 | 2 | 2 | 0.375 | 0.500 | 0.414 |
| | | | | | C. a. delta | 33 | 3 | 3 | 0.579 | 0.970 | * |
| *Ca*JWL | AAAT | 271-279 | F: TTTTATCTGTATAGTTGAATTAAG R: GAAGAGGGGACTACGCTAA | NED-T3 | C. a. amer | 15 | 1 | 0 | - | - | - |
| | | | | | C. a. delta | 64 | 4 | 2 | 0.283 | 0.266 | 0.960 |
| *Ca*FHM | AAT | 221-227 | F: CTTTTACCAAACCAAGTCCC R: CCTGCAAACTATCCTGATGA | 6FAM-T2 | C. a. amer | 11 | 2 | 1 | 0.351 | 0.273 | 0.458 |
| | | | | | C. a. delta | 33 | 2 | 1 | 0.485 | 0.500 | 0.866 |
| *Ca*GD1 | ACAGCT | 116-212 | F: AAATTACTCCTTTTCCAAACT R: TCTCATTACCGCTGTTTTGT | VIC-T4 | C. a. amer | 18 | 3 | 3 | 0.364 | 0.444 | 0.689 |
| | | | | | C. a. delta | 45 | 11 | 11 | 0.854 | 0.733 | 0.243 |
| *Ca*JKM | AAC | 255-264 | F: CGATGGTTGGTCCATTAGTA R: GCTAGCGGAGTATGACAATG | 6FAM-T2 | C. a. amer | 24 | 3 | 2 | 0.570 | 0.583 | 0.955 |
| | | | | | C. a. delta | 106 | 2 | 1 | 0.496 | 0.462 | 0.479 |
| *Ca*EME | AGT | 226-244 | F: TTTCGTAGTTACCGTGCATC R: CCATTTAAAACCACAGGTCA | NED-T3 | C. a. amer | 27 | 4 | 2 | 0.533 | 0.593 | 0.895 |
| | | | | | C. a. delta | 110 | 3 | 1 | 0.485 | 0.682 | * |
| *Ca*EFD | AAT | 159-216 | F: TGCCTTTTACAGCAGAGCTA R: TACACCGGTTACACCAGAAC | VIC-T4 | C. a. amer | 15 | 9 | 8 | 0.651 | 0.600 | 1.00 |
| | | | | | C. a. delta | 112 | 4 | 3 | 0.211 | 0.232 | * |
| *Ca*CYO | AACT | 154-190 | F: CTTGTCGCATGTAATCCAAT R: CCCGTTTAGATGTCAAACTT | NED-T3 | C. a. amer | 1 | 2 | 1 | - | - | - |
| | | | | | C. a. delta | 13 | 8 | 7 | 0.462 | 0.740 | 0.028 |

*Tails were added to the 5' ends of forward primers as follows: T1: GGCTAGGAAAGGTTAGTG, T2: TCATACATGTCTCTCAGCGTAAAC, T3: ACCAACCTAGGAAACACAG, T4: GACTATGGGCGTGAGTGCAT
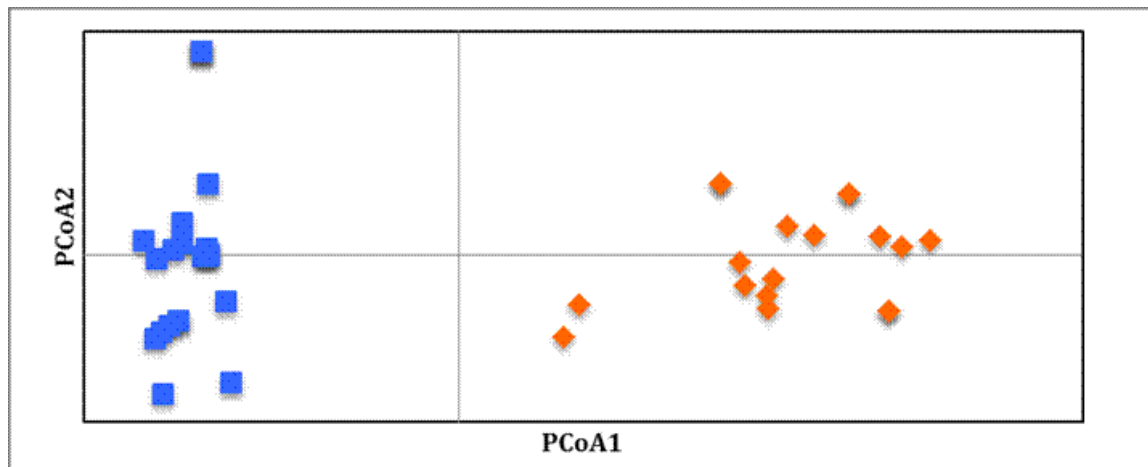
Figure 5-16. Principal coordinate analysis of *Callogorgia americana americana* (orange diamonds) and *Callogorgia americana* delta (blue squares).

To further examine whether *Callogorgia americana delta* is isolated by depth and/or by distance in the GoM, population differentiation was examined across seven sites. Five loci (GDI, EME, DAV, JKM, JWL) from 94 individuals were used for these preliminary analyses. The principal coordinate analysis based on pairwise genotypic distances (calculated in GenALEx) of 94 *Callogorgia a. delta* revealed no clear separation of populations (Figure 5-17); however, most individuals from the deeper sites (>600 m) clustered together, with some individuals, particularly from MC885 and MC751, clustering with individuals in both deeper and shallower depths. The average pairwise $F_{ST}$ value (genetic distance) was 0.091 (*P*=0.001) in *Callogorgia a. delta* across the entire GoM, suggesting overall, low population differentiation among sites in the northern GoM. Upon further examination of pairwise $F_{ST}$ values, some genetic differentiation was apparent and significant between certain sties (Table 5-6), particularly GC246.and GC249 with the shallower GC235, MC751 and VK826; however, GC249 was also significantly different from GC338 and GC246, which are in approximately the same depth range (~800 m). This is likely due to the combination of few individuals genotyped at GC249, GC338, and GC246 and missing data at the GD1 locus for most of the individuals at GC249.
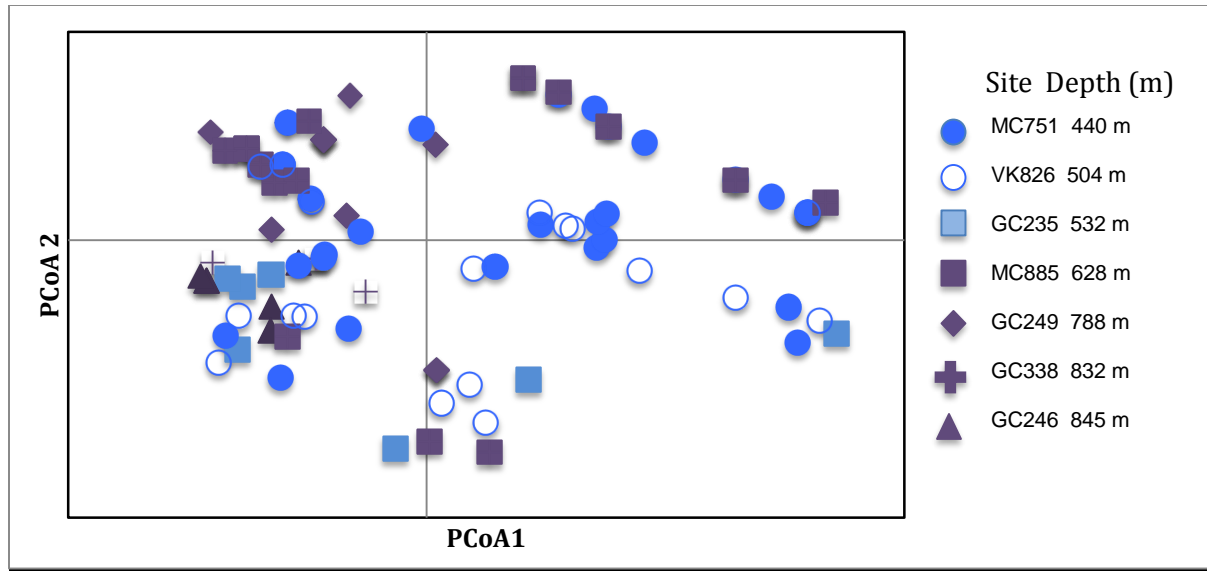
Figure 5-17. Principal coordinate analysis based on genotypic distances of *Callogorgia americana* delta across seven sites. Sites are color coded by mean depth (blue< 600 m, purple > 600 m).

Table 5-6.

Pairwise FST values among sites arranged by increasing depth. FST values in bold are significant (AMOVA, Bonferroni adjustment, p<0.003).

|        | MC751 (440 m) n=27 | VK826 (504 m) n=18 | GC235 (532 m) n=7 | MC885 (628 m) n=16 | GC249 (788 m) n=16 | GC338 (832 m) n=4 | GC246 (845 m) n=6 |
|--------|------|------|------|------|------|------|------|
| VK826  | 0.023 | | | | | | |
| GC235  | **0.113** | 0.000 | | | | | |
| MC885  | 0.051 | 0.051 | **0.114** | | | | |
| GC249  | **0.090** | **0.102** | **0.165** | 0.056 | | | |
| GC338  | **0.152** | 0.088 | 0.056 | **0.181** | **0.164** | | |
| GC246  | **0.223** | **0.119** | 0.057 | **0.182** | **0.192** | **0.160** | |
| Values closer to 1 indicate greater population differentiation. n=number of individuals genotyped and used in analyses. Average site depth of collections is noted in parentheses | | | | | | | |

Because of missing data at GC249, we removed this site from further tests of isolation by depth and distance. Isolation by depth tests indicated a trend for greater genetic differentiation with increasing depth differences between sites (Z = 380.7760, r = 0.3508 , p = 0.0760, Figure 5-18A). In contrast, no significant correlation was found with genetic distance and geographic distance (Z = 229.2670, r = -0.3034, p = 0.2490, Figure 5-18B). These results indicate that populations are likely structured by depth rather than distance in the northern GoM. These results contrast patterns observed in other foundation species in the deep GoM, such as those from chemosynthetic

communities. *Bathymodiolus childressi* showed no population differentiation across a large depth range (~500-2,000 m) (Carney et al 2006) and *Lamellibrachia luymesi* showed weak, but significant population differentiation across the northern GoM (McMullin et al. 2010). However, collections of *Callogorgia* further to the west of Green Canyon might reveal population differentiation across the northern GoM. Nevertheless, isolation by depth within *Callogorgia a. delta* upholds the overall pattern that bathymetry is important in the evolution and ecology of octocorals in the GoM.
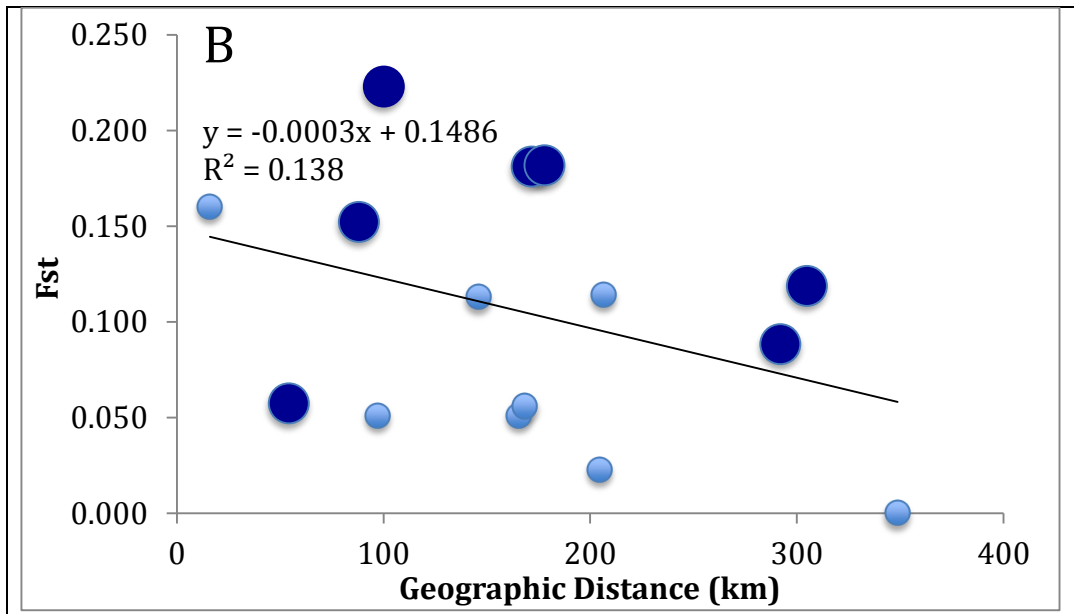


Figure 5-18. Pairwise genetic differentiation patterns with respect to a) depth and b) geographic distance in *Callogorgia americana* delta. Large, dark blue circles indicate depth differences of >200 m between sites.

## 5.2.4 Conclusions

The combined molecular and morphological approach used allowed us to successfully delimit closely related species of two genera that are common in the GoM. Three species of *Callogorgia* are present in the GoM, *C. gracilis, C. americana americana,* and *C. americana delta.* Furthermore, mitochondrial and nuclear data indicated that the sub-species of *C. americana* are clearly distinct, and full species status is warranted, although there may be a few hybrids within sampled populations. *Callogorgia* spp. also clearly differentiate by depth, with further structure in *C. a. delta* across 400-1,000 m depth. Preliminary results suggest that *Callogorgia* either underwent a severe population bottleneck or the GoM was founded by relatively few individuals, but further analyses are needed to test this hypothesis. Our results to date also indicate that species of *Paramuricea* segregate by depth, with at least five species inhabiting specific depth zones in the GoM. Bathymetry, rather then geography, is important in population structure within both genera in the northern GoM.

## 5.3 BLACK CORAL GENETICS AND CONNECTIVITY

### 5.3.1 Introduction

The scale over which coral communities in general, and deep-sea communities in particular, should be managed is not readily apparent. Many marine organisms have planktonic larvae and it is not clear how far these larvae travel. Do they connect sites, regions or even entire ocean basins? Estimates of connectivity through larval exchange are needed to understand the scale at which populations are regulated, estimate the risk of extinction of locally devastated populations and understand the nature of barriers to dispersal in the ocean (e.g. depth, currents). In order to answer these questions, we utilize a combination of modern molecular and classical cladistic approaches to determine relations among communities in the GoM. This requires a nested analysis of first determining species status to exclude cryptic species, followed by a sub-species level analysis of population structure and geneflow.

Here, we focus on the dispersal capabilities of the black coral, *Leiopathes glaberrima* in the GoM. Three biogeographic regions have been described for the GoM based on species distribution and food availability (Cairns, Figure 5-19). Most of the deep GoM is soft sediment, however hard grounds occur as a result of authigenic carbonate deposition associated with current or historical hydrocarbon seepage. When the hard grounds occur in areas where hydrological conditions are appropriate for sediment removal, gas exchange and food delivery, colonial corals may occur. Previous connectivity studies of organisms associated with these hard grounds, including the deep sea scleractinian coral *Lophelia pertusa*, and hydrocarbon seep vestimentiferan worms *Lamellibranchia luymesi* and *Seepiophila jonesi*, and the seep mussel *Bathymodiolus childressi* suggested panmixia among sites within the northern GoM (Carney, et al. 2006; McMullinet al. 2010; Morrisonet al. 2011). However, no study has addressed population connectivity in any of the approximately 30 species of black corals (antipatharians) found in the GoM (Opresko 2009).

*L. glaberrima* is one of the most abundant corals on carbonate outcrops between about 200 and 600 m (Brooke and Schroeder 2007) in the GoM and occurs world-wide including the North Pacific (Hawaiian islands), Mediterranean Sea, the Caribbean and Western and Eastern Atlantic (Cairns and Opresko 1993). It is a foundation species whose three-dimensional structure provides habitat for many cold-water reef organisms (Brooke and Schroeder 2007). Multiple color morphs of *L. glaberrima* co-occur in the GoM and the Atlantic and polyp size also varies within colonies (D. Opresko, per. comm.) but their species status is unclear (Opresko 2009). Many corals have the capacity to change colony shape, form and color in response to the environment, but these morphological differences are sometimes attributable to genetic variation (Todd 2008). In the antipatharia, differentiation at the species level is complicated by morphological simplicity and high plasticity (Opresko 2009). According to Opresko (2009), collections of black corals from the GoM suggest the possibility of un-described species of *Leiopathes*, which are indistinguishable by classic taxonomy. Therefore, in order to perform population genetics, analyses the species status of the color morphotypes had to be determined.
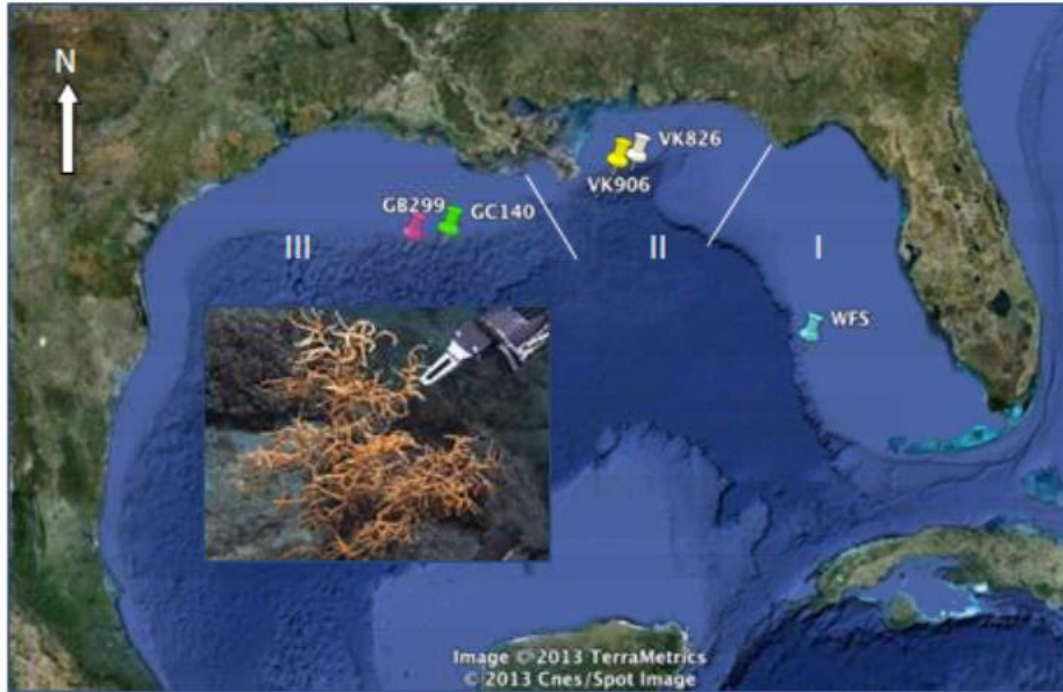
Figure 5-19. Sampling sites for *Leiopathes glabberima* (inset) in the GoM.
GB = Garden Banks, GC = Green Canyon, VK = Vioska Knoll,
WFS = West Florida Slope. GB and GC are in biogeographic
region I, VK is in biogeographic region II and WFS is within
biogeographic region III (Cairns and Opresko 1993). Map from
Google Earth.

In marine benthic organisms, population subdivision is influenced by timing of reproduction, larval duration, circulation patterns and availability of substrate (Miller 1998; Palumbi 2003; Morrison, Ross et al. 2011). The life history of *Leiopathes glaberrima* is unknown, but studies in other antipatharians suggest annual reproduction, with larvae that are negatively buoyant, non-feeding and short lived (10 days) (Miller 1997; Miller 1998). Asexual larvae have also been observed (Miller 1997). Therefore, the lack of population structure in *L. pertusa* with relatively long larval duration or of the vestimentiferans with long-lived and positively buoyant larvae, might not be representative of the population structure of *L. glaberrima*.

Here, we used mitochondrial and nuclear markers to test the hypothesis that color morphs of *Leiopathes glaberrima* constitute one biological species. We then developed ten novel microsatellite loci for *L. glaberrima* and applied them to samples from the GoM to determine population genetic structure, reproductive characteristics and gene flow patterns in this important foundation species.

Molecular markers are still sparse for the Cnidaria. Mitochondrial markers have low levels of variation in some cnidarian groups making species identification difficult (Hellberg 2006), and hence microsatellite markers have been the marker of choice for population genetic studies. Yet, previous work had indicated that in corals unusual microsatellite motives might be common

(Baums et al. 2005). To facilitate development of microsatellite markers in the Cnidaria in general and generate markers for *L. glaberrima*, we studied characteristics of microsatellite markers in 9 species of Cnidaria and have submitted this work for publication (Appendix D-3).

## 5.3.2 Methods

### 5.3.2.1 Sample Collection, DNA Extraction, Sequencing and Genotyping

222 samples from different morphotypes of *Leiopathes glaberrima* from five sites in the GoM (Figure 5-19) were collected by the ROV *Jason II* during the TDI-Brooks R/V *Ron Brown*/*Jason II Lophelia* II expedition (August 6 to September 12, 2009 and October 15 to November 1, 2010), and by the USGS R/V *Seward Johnson/JSL* cruise (September 16 to 23, 2009 and Sept 22 to October 2, 2010). Collection depths were between 248 m and 674 m depths. The samples show a range of color patterns from white to red (Table 5-7). For each sample, tissue was frozen at -80°C, preserved in 70% ethanol and in RNA later. Images of the colonies were taken during the collection; additional images were taken in the wet laboratory on board of the ship. Depth and locations were obtained from the ROVs logs.

Table 5-7.

*Leiopathes glaberrima* samples from the GoM. Two lineages (L1 and L2) were identified with microsatellite (Msat) loci. The total number of samples (N) and number of distinct multilocus genotypes, Ng, as identified by microsatellite genotyping is indicated. Samples were categorized by sampling depth (in 50 m intervals) and colony color when available

| Sites | N | Msat | | Depth (m) | | | | | | | Color | | | | |
|---|---|---|---|---|---|---|---|---|---|---|---|---|---|---|---|
| | | L1 | L2 | 200-250 | 251-300 | 301-350 | 351-400 | 401-450 | 451-500 | 501-550 | orange | pink | red | white | yellow |
| GB299 | 30 | 28 | . | . | . | 11 | 17 | . | . | . | 1 | 3 | . | 15 | 1 |
| GC140 | 23 | 20 | 2 | 8 | 15 | . | . | . | . | . | 4 | 9 | . | 7 | . |
| VK826 | 75 | 8 | 46 | . | . | . | . | 4 | 55 | 3 | 14 | 13 | 19 | 9 | 4 |
| VK862 | 2 | . | . | . | . | . | 1 | . | . | . | 1 | . | . | . | . |
| VK906 | 74 | 5 | 29 | . | . | 1 | 9 | 18 | . | . | 4 | 4 | 10 | 10 | |
| WFL Slope | 6 | . | 1 | . | . | . | 1 | 2 | . | 3 | 3 | . | . | 1 | . |
| N | 210 | 64 | 136 | 8 | 15 | 12 | 28 | 24 | 55 | 6 | 27 | 29 | 29 | 42 | 5 |
| Ng | 150 | 61 | 79 | . | . | . | . | . | . | . | . | . | . | . | . |
| Ng/N | 0.71 | 0.95 | 0.58 | . | . | . | . | . | . | . | . | . | . | . | . |

To test the species identity of the samples, different color morphotypes of *L. glaberrima* from five sites (

Table 5-8) were compared using *Leiopathes*-specific primers to three mitochondrial genes: COI, ND5 and Trp (partial TrnW-ITS-NADH) using published methods (Brugler and France 2007; Sinniger and Pawlowski 2009). Amplification products were treated with Exo-Sap reaction (GE Healthcare) and sequenced at the Genomic Core Facility at University Park.

Table 5-8.

Samples (N) of *Leiopathes glaberrima* were sequenced at three mitochondrial loci (COI, ND and TRP) from five sites in the GoM

| Marker | N GB299 | GC140 | VK826 | VK906 | WFLSlope | Total |
|---|---|---|---|---|---|---|
| COI | | 1 | 27 | 12 | | 40 |
| ND | 1 | 1 | 25 | 25 | 3 | 55 |
| TRP | 2 | 1 | 22 | 16 | 1 | 42 |
| **Total** | **3** | **3** | **74** | **53** | **4** | **137** |

Microsatellites (Simple Sequence Repeats SSRs) for population connectivity analyses of *L. glaberrima* were designed using sequence data from a single plate of *454* sequencing. Contigs and singletons were imported to the Tandem Repeat Finder (TRF) database and processed using the default values of Match: 2, Mismatch: 7, Indels: 7 as alignment parameters (Benson 1999). Sequences were annotated for perfect motifs and flanking regions of at least 100 bases using Geneious (Drummond, Ashton et al. 2010) and imported to Primer 3 for primer design (Rozen and Skaletsky 2000). Primers were realigned to the sequences with Codon Code Aligner (CodonCode Corporation, Dedham, Massachusetts). Candidate loci were tested for polymorphism and reliable amplification on samples from the most geographically distant sites in the GoM (VK906, GB535 and West Florida Slope) resulting in polymorphic 10 loci (Table 5-9). 210 samples yielded complete multilocus genotypes for all 10 loci (Table 5-8).

### 5.3.2.2 *Phylogenetic and Population Genetic Analyses*

Sequences were edited and aligned using Codon Code Aligner (CodonCode Corporation, Dedham, Massachusetts). Bayesian phylogenetic trees were constructed in MrBayes (Ronquist and Huelsenbeck 2003), the parameters used were 4 heated chains (temp= 0.2) with 1100000 MCMC generations and random seed of 1063, sample frequency was 200 generations. The burn in for the consensus 50% majority rule tree was 500.

Population genetic analyses were performed using the program GenAlEx vers 6.5 (Peakall and Smouse 2006). First, exact matches at all loci were identified. Samples that shared the exact multilocus genotype (MLG) at all 10 loci were considered to be clonemates of the same genet. GenAlEx estimated the probability of identity (or the probability that two samples share the same multilocus genotype even though they are not clones) as $10^{-7}$ across populations when using all 10 loci. Subsequent population genetic analyses were performed on the unique MLGs only. Loci were then tested for adherence to Hardy-Weinberg Equilibrium when considering all unique MLGs and when analyzing microsatellite lineage 1 and 2 (see below) separately. Principal Coordinate analysis was performed on a pairwise genetic distance matrix ($F_{st}$) among all samples in GenAlEx. The program Structure (Pritchard, Stephens et al. 2000) was further used to detect the number of genetically distinct clusters, K, in the dataset and was run with $10^6$ steps. 10% of the MCMC chain was discarded as burnin and each K was repeated three times. We assumed admixture and did not specify a location prior as we suspected the presence of multiple lineages per location. Structure results were analyzed with the program Structure Harvester (Earl and vonHoldt 2012) to find the

most likely number of population, K. Indeed, Structure identified the presence of two co-occurring lineages.

Table 5-9.

Microsatellite loci developed for L. glaberrima. The ten microsatellite loci developed for *L. glaberrima* were amplified in two multiplexes (plex 1-2) and three singleplex reaction. Given is the locus name, primer sequences, repeat type followed by the number of repeats and the size range of the alleles amplified in base pairs (bp). Annealing temperature was 54°C for Multiplex 1 and BC19, 57°C for Multiplex 2, and 55°C for singleplexes 34 and 36. Forward primers were fluorescently labeled with one of four dyes (6FAM, VIC, PET or NED)

| Locus | Primer sequence (5'-3') | STR motif | Size (bp) | Plex |
|---|---|---|---|---|
| BC1 | F: PET-TAG TAC CCT CGC AGC AGG GTG | (ACT)6 | 182-185 | 2 |
| | R: GAA TTC CGC TCG TCC TCC A | | | |
| BC5 | F: 6FAM-TGA AGA GTG AGC ACT CGT T | (TTG)8.6 | 193-235 | 2 |
| | R: CAG TAT GTC CGC GTC ATC TT | | | |
| BC8 | F: NED-CAC AGT AAG CTG ACC GTC TGC | (TTA)11 | 119-147 | 2 |
| | R: TAC CGT ATG CCC ACG AAG AGC | | | |
| BC11 | F: PET-GAG ACA TGA CTT TCC AGA TCC GCT | (AAC)14 Y (TGTAA)4 | 123-183 | 1 |
| | R: CGT AAA TCA GCA CAC ATT TCC GGT | | | |
| BC22 | F: NED- GCA ACA GAG AGC TTG GTT CAA | (GTT)10 | 142-163 | 1 |
| | R: CTT CCT GTC CCA ACA CCC T | | | |
| BC43 | F: VIC-ATC CTC TGT GGT GTA TGT T | (CCA)5 | 141-147 | 1 |
| | R: AGT GAT CTC CCA TTC GAC C | | | |
| BC67 | F: 6FAM-TCC CTT TCA AGA TCC GTA | (ATT)10 | 133-172 | 1 |
| | R: CGA CTA CAA TTC GAT CAA CA | | | |
| BC19 | F: 6FAM-GCC AAT ATT GCT GCG GTT AC | (GTTGGC)10.5 | 198-309 | single |
| | R: AAG AGA CAG GTC CGG TTG AA | | | |
| BC34 | F: T1-GGC TAG GAA AGG TTA GTG GCC ACA TGT CGT CCT GGA TAC G<br>R: GCC TAA CTT TTA CTT TAT TTA TTG CAT | (AACAAG)9 | 168-204 | single |
| BC36 | F: T3-ACC AAC CTA GGA AAC ACA GGA GCC CTG AAG GAT CAG AGA<br>R: AAA AGC ATC TAC GGG TGG TG | (ACA)4 ATAG (TAA)9 | 174-207 | single |

## 5.3.3  Results

Mitochondrial markers have low levels of variation in some cnidarian groups making species identification difficult (Hellberg 2006). This was observed in our data as two of the three markers used (COI and ND5 fragments) had no resolution to distinguish between the samples of *L. glaberrima* from throughout the GoM (Table 5-7, Figure 5-20). In contrast, two lineages of *L. glaberrima* were recovered from Trp sequencing, but those lineages were unrelated to color morph (white, red and orange were mixed within both groups) (Figure 5-21). Other the Trp clades were unrelated to geography as samples from VK906 (n = 16) and VK826 (n = 22) were intermixed (Figure 5-21). The distinction between the two lineages was due to a single amino acid change. More genes are needed to determine if the two lineages are distinct enough to be considered 2

species. To accomplish this, we developed and employed highly polymorphic microsatellite markers.

Microsatellite loci amplified reliably and had on average 6.28 (+/- 0.53 Standard error [SE]) alleles per locus (Figure 5-22). Expected heterozygosity ranged from 0.26 to 0.90 (average = 0.61 +/- 0.03 SE). Probability of identity ranged from $2.8 * 10^{-3}$ to $1 * 10^{-9}$ per population when considering all loci indicating high power to distinguish between asexually produced individuals and those that are closely related (Figure 5-22). When analyzing only unique multi-locus genotypes (MLGs), departures from Hardy-Weinberg equilibrium were significant in 23 out of 50 comparisons, mostly involving the two VK populations that harbor both microsatellite lineages (see below). When analyzing the two lineages separately, only 2 out of 38 tests and were significant for L1 (Figure 5-22). Ho ever, half of the 34 tests in L2 remained significant (Figure 5-21).
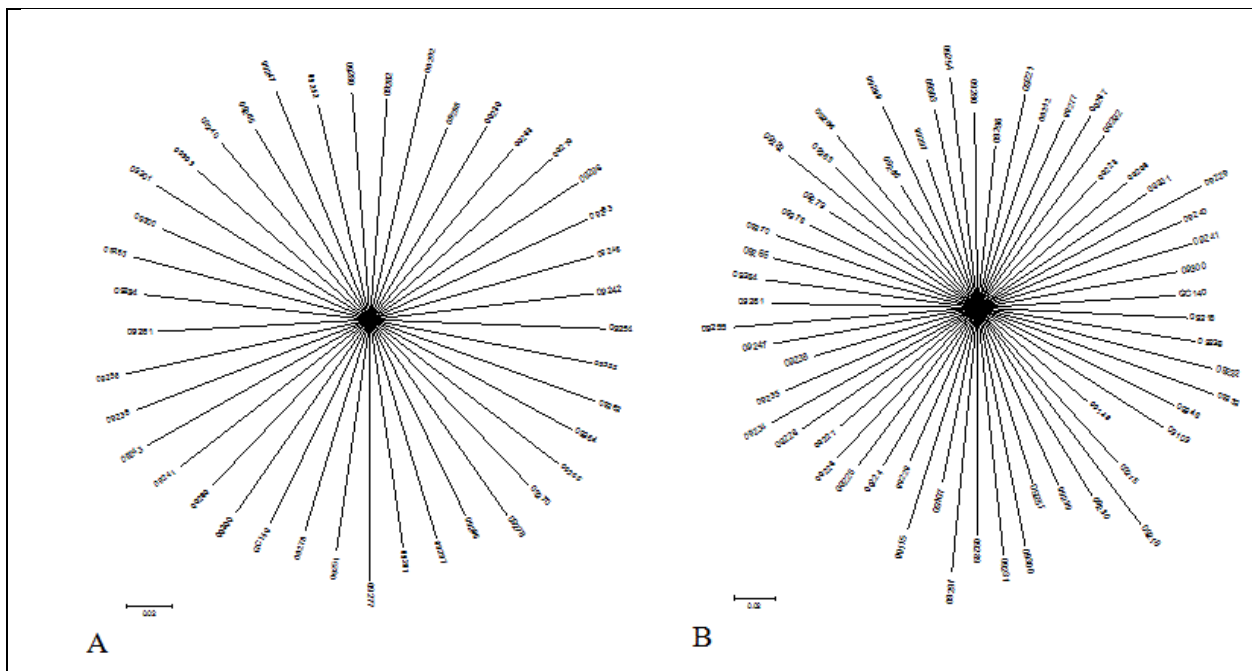


Figure 5-20. Bayesian phylogenies of two mitochondrial markers COI (A, 740bp; GenBank Accession numbers: KF013048 - KF013088) and ND5 (B, 660 bp, GenBank Accession numbers: KF012993 - KF013047). There was very little sequences diversity in *L. glaberrima* samples from throughout the GoM resulting in star-shaped phylogenies.

Structure (Figure 5-23) and principal coordinate analysis ( Figure 5-24) indicated the presence of two divergent lineages in the dataset. GC140, GB299 and WFS each were dominated by lineage 1 whereas VK906, the deepest of the sites, was dominated by lineage 2. VK826 harbored both lineages and 10 samples showed evidence of hybridization between them (assignment probability of <0.8). The most parsimonious explanation for this co-occurrence is the presence of cryptic species. And while the lineages do not correspond with color or depth (Figure 5-25); they do occupy different areas at VK826, the site where both occur (Figure 5-26). Lineage 1 is mostly restricted to the northern edge of the site (Figure 5-26). New datasets were created, each containing MLGs with >0.8 probability of belonging to one of the two lineages (Lineage 1: n = 61, Lineage

2: N = 78, unassigned N: 10). When analyzing each lineage separately, geographic differentiation was small and significant only for lineage 2 (Table 5-11), perhaps due to the now small sample sizes.

Table 5-10

*Leiopathes glaberrima* microsatellite loci. Given are: N = number of samples genotyped at that locus, Na = No. of Different Alleles, Ho = Observed Heterozygosity, He = Expected Heterozygosity, Ht = Total Expected Heterozygosity, F = Fixation Index. Fis = (Mean He - Mean Ho) / Mean He, Fit = (Ht - Mean Ho) / Ht, Fst = (Ht - Mean He) / Ht. SE = standard error. Calculated by GenAlEx vers. 6.5

|  |  | BC1 | BC5 | BC8 | BC11 | BC19 | BC22 | BC34 | BC36 | BC43 | BC67 | Total |
|---|---|---|---|---|---|---|---|---|---|---|---|---|
| $N$ | Mean | 29.60 | 29.20 | 29.40 | 29.60 | 29.40 | 29.80 | 29.80 | 29.20 | 29.60 | 29.60 | 29.52 |
|  | SE | 9.13 | 8.74 | 8.74 | 9.10 | 8.91 | 9.09 | 9.09 | 8.74 | 8.91 | 9.22 | 2.56 |
| $N_a$ | Mean | 2.00 | 6.00 | 5.80 | 11.60 | 12.20 | 4.20 | 5.80 | 4.60 | 2.40 | 8.20 | 6.28 |
|  | SE | 0.00 | 0.71 | 0.58 | 1.33 | 1.07 | 0.73 | 0.80 | 0.93 | 0.24 | 1.24 | 0.53 |
| $H_o$ | Mean | 0.29 | 0.76 | 0.49 | 0.87 | 0.90 | 0.26 | 0.57 | 0.56 | 0.30 | 0.69 | 0.57 |
|  | SE | 0.09 | 0.09 | 0.07 | 0.04 | 0.03 | 0.04 | 0.08 | 0.03 | 0.11 | 0.10 | 0.04 |
| $H_e$ | Mean | 0.23 | 0.66 | 0.69 | 0.87 | 0.87 | 0.38 | 0.62 | 0.62 | 0.34 | 0.77 | 0.61 |
|  | SE | 0.06 | 0.02 | 0.02 | 0.01 | 0.01 | 0.07 | 0.04 | 0.06 | 0.08 | 0.06 | 0.03 |
| $F$ | Mean | -0.19 | -0.15 | 0.29 | -0.01 | -0.04 | 0.27 | 0.09 | 0.05 | 0.22 | 0.12 | 0.07 |
|  | SE | 0.07 | 0.11 | 0.10 | 0.06 | 0.04 | 0.10 | 0.09 | 0.13 | 0.19 | 0.10 | 0.04 |
| $F_{is}$ |  | -0.26 | -0.16 | 0.29 | 0.00 | -0.04 | 0.32 | 0.08 | 0.10 | 0.10 | 0.10 | 0.05 |
|  | SE |  |  |  |  |  |  |  |  |  |  | 0.06 |
| $F_{it}$ |  | -0.17 | -0.13 | 0.34 | 0.04 | 0.00 | 0.56 | 0.14 | 0.22 | 0.38 | 0.20 | 0.16 |
|  | SE |  |  |  |  |  |  |  |  |  |  | 0.07 |
| $F_{st}$ |  | 0.07 | 0.02 | 0.06 | 0.04 | 0.04 | 0.36 | 0.07 | 0.13 | 0.31 | 0.11 | 0.12 |
|  | SE |  |  |  |  |  |  |  |  |  |  | 0.04 |

Table 5-11.

Analysis of molecular variance (AMOVA) among sites and lineages (L1 and L2). Within individual analysis was suppressed and significance evaluated based on 999 permutations across the whole dataset.  % = percent of the estimated total variance. Df = de

| All | Source | df | SS | MS | % | $F_{st}$ | $F_{st}$ max | $F'_{st}$ |
|---|---|---|---|---|---|---|---|---|
|  | **Among Pops** | 4 | 103.49 | 25.87 | 12% | 0.12** | 0.38 | 0.32 |
|  | **Within Pops** | 293 | 915.98 | 3.13 | 88% |  |  |  |
|  | **Total** | 297 | 1019.48 |  | 100% |  |  |  |
|  |  |  |  |  |  |  |  |  |
| **L1** | **Among Pops** | 3 | 10.33 | 3.44 | 1% | 0.01 | 0.40 | 0.01 |
|  | **Within Pops** | 118 | 352.11 | 2.98 | 99% |  |  |  |
|  | **Total** | 121 | 362.44 |  | 100% |  |  |  |
|  |  |  |  |  |  |  |  |  |
| **L2** | **Among Pops** | 1 | 10.84 | 10.84 | 4% | 0.04** | 0.41 | 0.09 |
|  | **Within Pops** | 148 | 436.00 | 2.95 | 96% |  |  |  |
|  | **Total** | 149 | 446.84 |  | 100% |  |  |  |

237
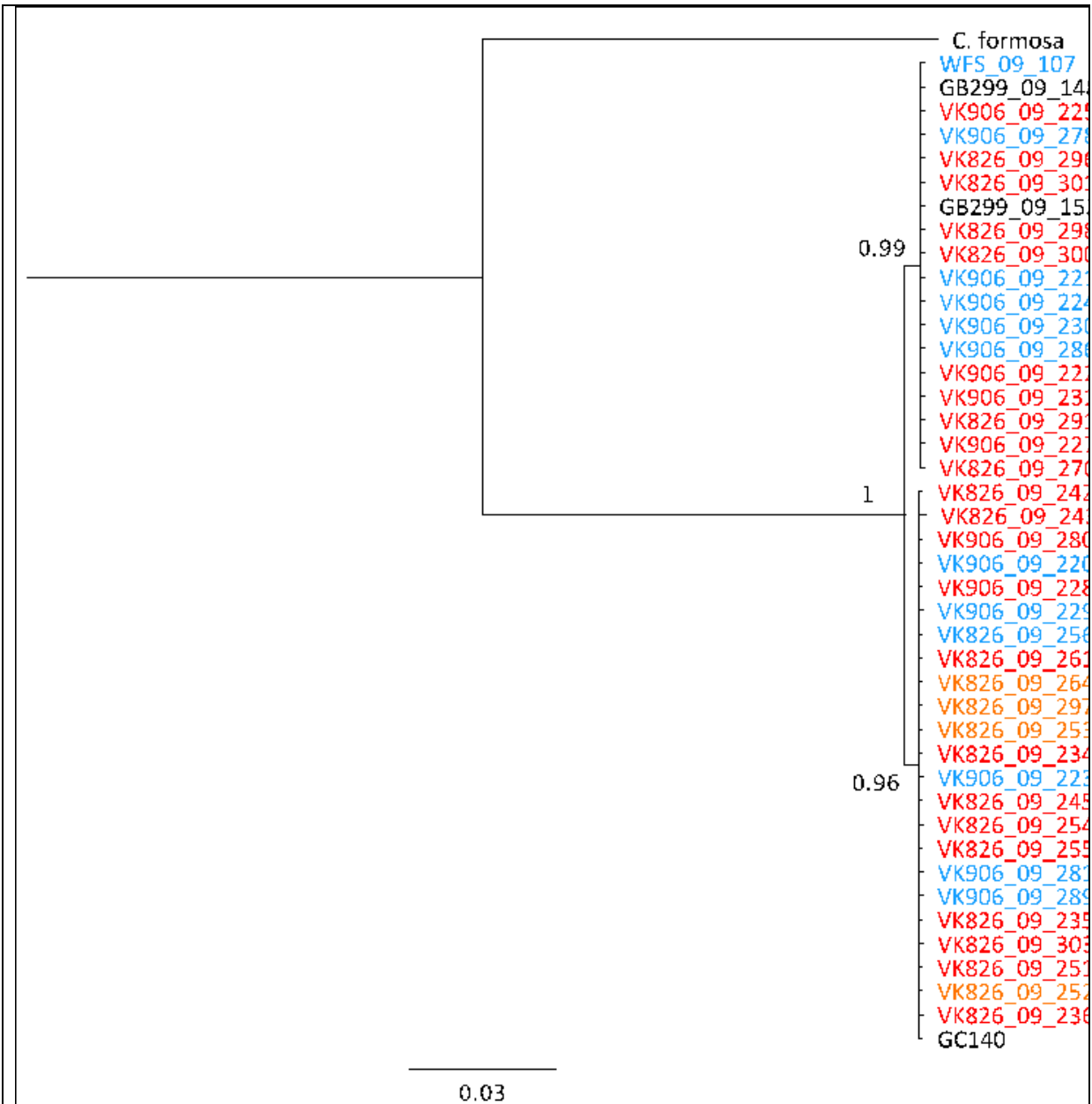
Figure 5-21. Phylogeny (Bayesian Inference) of a portion of the mitochondrial TRP gene (730 bp GenBank Accession numbers: KF013089 - KF013130). Two lineages within *L. glaberrima* from the GoM are revealed by the TRP gene, distinct by one amino acid change. Numbers represent posterior probabilities. Note that the two lineages are unrelated to color of the colonies (Red labels indicate red colonies, orange labels orange colonies, blue labels white colonies and black labels are colonies with no associated color information), sampling site (VK906, VK826) or microsatellite lineage designation (see next section).

Of the 210 samples genotyped, 20 had MLGs that occurred more than once in the dataset. The ratio of the number of unique MLGs over the number of samples was 0.95 in Lineage 1 ($N_g = 61$, N = 64) and 0.57 in Lineage 2 ($N_g = 78$, N = 136). Most of the potential clones were found in lineage 2 at VK906, where the two largest genets had 15 and 21 members (Figure 5-27). In contrast, the largest number of clonemates per genet was just 3 in lineage 1 (GB299). Studies are still needed to determine the mode of clonal reproduction (ameiotic larval production, fragmentation or polyp bail-out). However, so far clones appear to be restricted to specific sites as no MLGs were shared between sites. The largest distance between clonemates was 610 m in lineage 2 (Table 5-12, only colonies were included in this table for which geographical location was recorded with accuracy of < 10 m). Clonemates of the same genets sometimes (n = 6 or 5%) showed different shades of orange to red but not white and red (Figure 5-28).
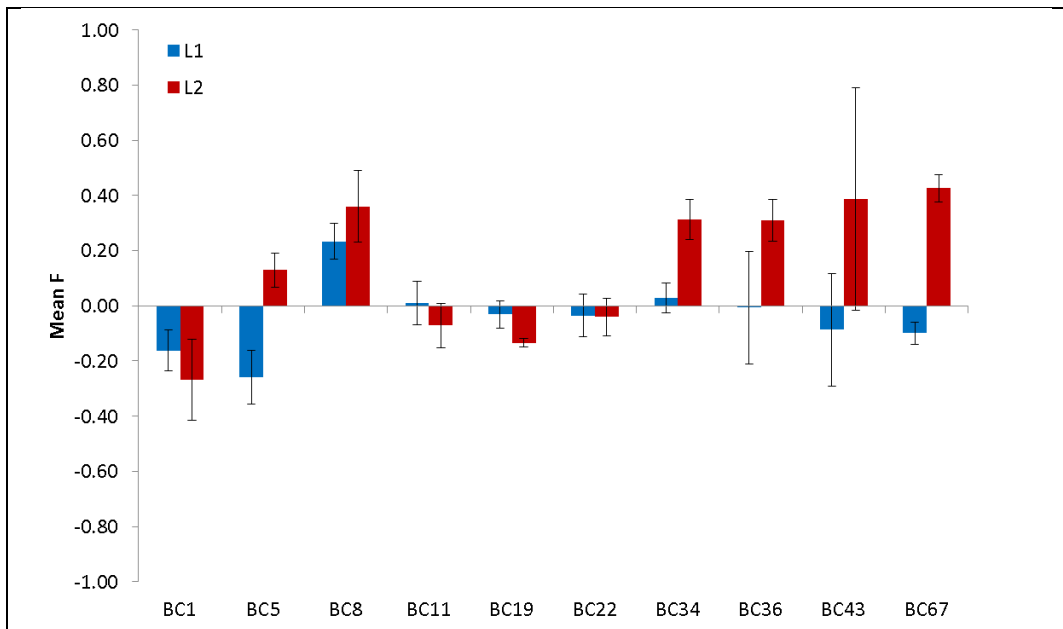


Figure 5-22. Mean F values for microsatellite loci. Mean F values were not significantly different from zero for most loci (BC 1 – BC 67) in lineage 1 (L1) but in lineage 2 (L2), F-values consistently deviated from expectations. Given are means across loci and their standard errors.
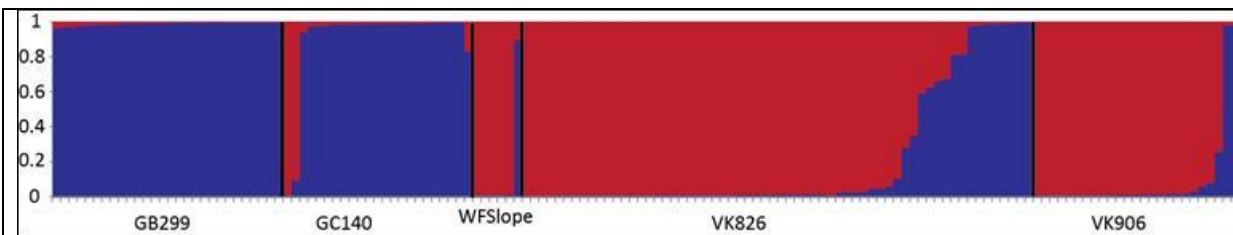


Figure 5-23. Population genetic analysis of 148 *L. glaberrima* genotypes from the GoM. The STRUCTURE plot shows the probability of membership of each of the samples in K=2 clusters (the optimal number of clusters for this dataset). VK826 harbors colonies with ancestry in both lineages (hybrids). VK862 excluded (n=2).

239
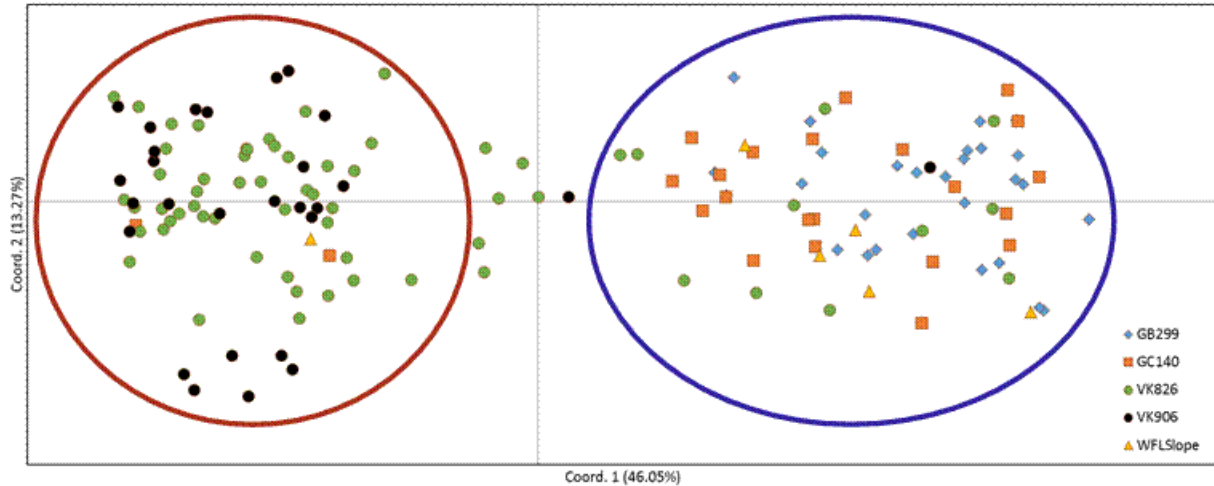
Figure 5-24. Principal coordinates analysis of 148 *L. glaberrima* genotypes from the GoM. For comparison with Fig 3, the two lineages identified via STRUCTURE analysis are indicated here by the blue and red circle. Shown are the first two axes, explaining 46.05% and 13.27% of the variation, respectively. VK862 excluded (n=2).

Table 5-12.

Spatial spread of genets (m) for collections with good navigational data. Navigational accuracy within a single cruise is generally about +/- 5 m at this depth using USBL alone and about twice that (+/- 10 m) when data from independent visits are combined. In many cases distances between corals were determined using doppler velocity navigation streams during a single dive and this can result in paired distance estimates accurate to about 0.5 m. N = number of ramets per genet. SD = standard deviation, * only a single clone pair was identified.

| Site | Clone ID | Mean (m) | SD | Max (m) | N | Msat Lineage |
|---|---|---|---|---|---|---|
| VK826 | BC1054 | 104 | 84 | 155 | 3 | 2 |
| | BC1055 | 72 | 40 | 108 | 3 | 2 |
| | BC1064 | 2* | | 2 | 2 | 2 |
| | BC1073 | 2* | | 2 | 2 | 2 |
| | BC1122 | 2* | | 33 | 2 | 2 |
| | Mean (SD)* | 43 (45) | | 60 (69) | | |
| VK906 | BC1093 | 60 | 32 | 131 | 19 | 2 |
| | BC1094 | 37 | 21 | 75 | 13 | 2 |
| | BC1098 | 65 | 35 | 106 | 4 | 2 |
| | BC1110 | 80 | 61 | 117 | 3 | 2 |
| | BC1117 | 610* | | 610 | 2 | 2 |
| | BC1099 | 144* | | 144 | 2 | 2 |
| | BC1097 | 45* | | 45 | 2 | 2 |
| | BC1096 | 42* | | 42 | 2 | 2 |
| | Mean (SD)* | 135 (195) | | 159 (186) | | |
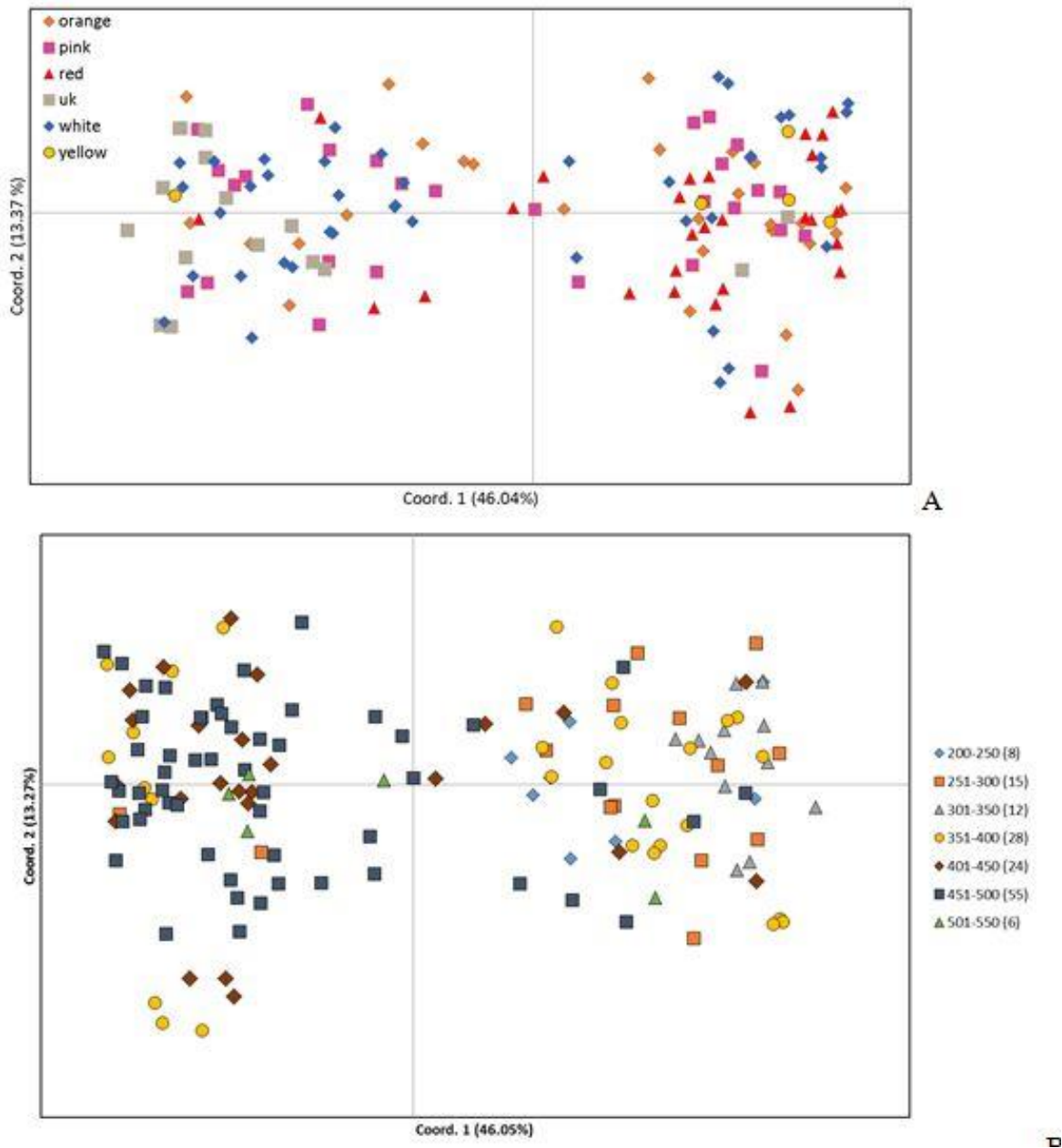
Figure 5-25. Principal coordinates analysis of 148 *L. glaberrima* genotypes from the GoM. No structuring by color of the colony (A) or by depth (B) is evident. Shown are the first two axes, explaining 46% and 13% of the variation, respectively. Depth is in 50 m increments. Samples sizes per depth given in parentheses. uk = color unknown.
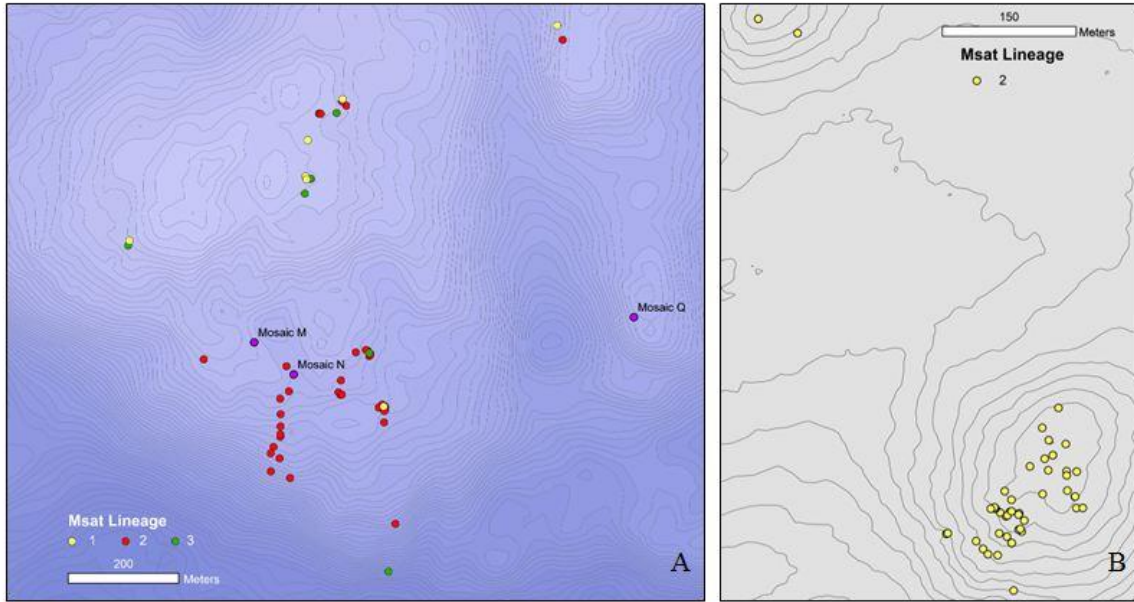
Figure 5-26.  Geographical distribution of *Leiopathes glaberrima* lineages.  Vioska Knoll 826 (A) harbors two lineages of L glaberrima (Msat Lineage 1, 2). Lineage 1 is mostly restricted to the northern edge of the site. Lineage 2 and hybrids between lineages 1 and 2 (designated as Lineage 3) occur throughout the site.  Permanent markers (Mosaic N – Q) are indicated. Vioska Knoll 906 (B) harbors only one lineage of *L. glaberrima* (Msat 2). Two meter contours created by Miles Saunders from R/V *Falkor* Shipboard Multibeam 11/2012. Maps oriented towards North.
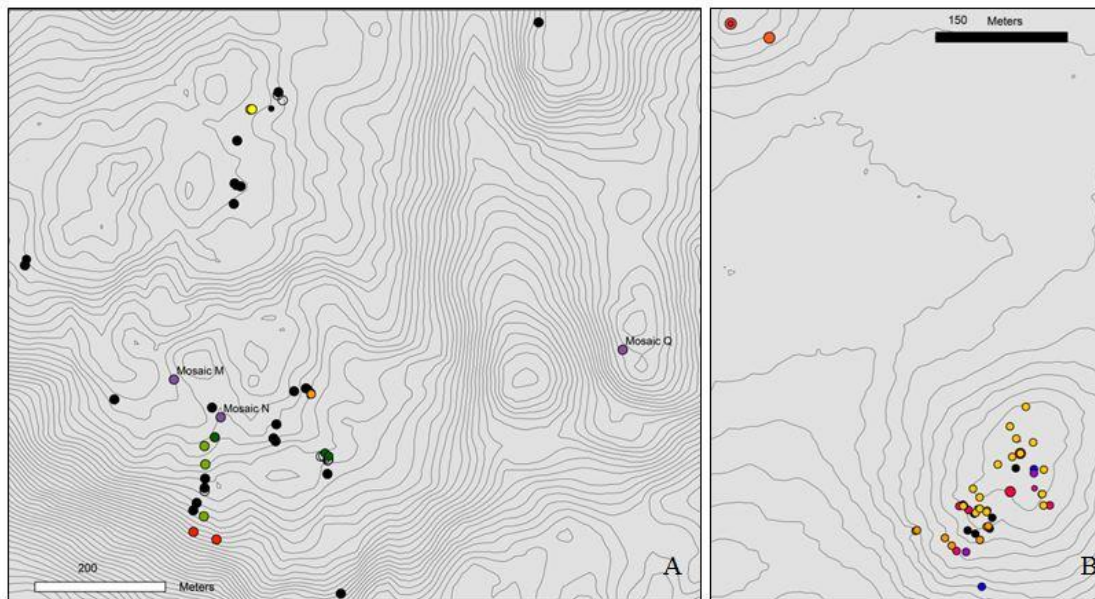


Figure 5-27.  Geographic distribution of clone mates of *Leiopathes glaberrima* at VK826 and VK906. Msat lineage 2 of *Leiopathes glaberrima* frequently reproduces asexually at Vioska Knoll 826 (A) and VK906 (B) while lineage 1 does so rarely. Same fill

242

indicates that two colonies are clonemates. Black fill indicates colonies with unique genotype, represented only once at the site. No clones were shared between sites. Two meter contours created by Miles Saunders from R/V *Falkor* Shipboard Multibeam 11/2012. Map oriented towards North.
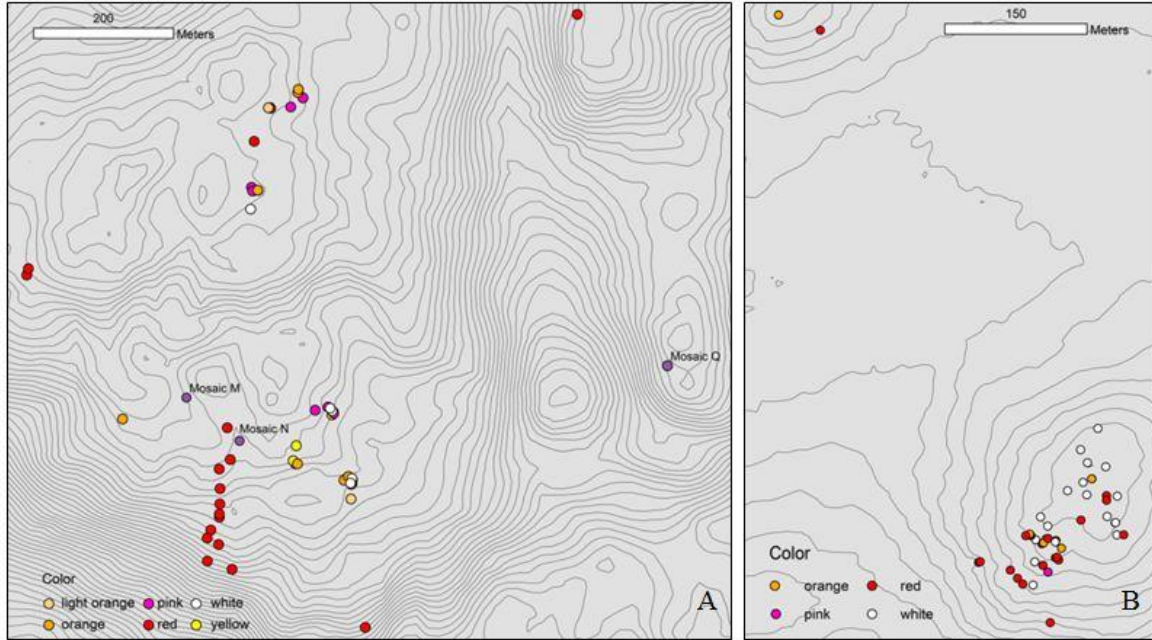


Figure 5-28.  Geographic distribution of *Leiopathes glaberrima* color morphs in VK826 and VK906. A) VK826, B) VK906. Two meter contours created by Miles Saunders from R/V *Falkor* Shipboard Multibeam 11/2012. Map oriented towards North.

### 5.3.4  Discussion

The black coral, *Leiopathes glaberrima*, is an important foundation species in the deep GoM and elsewhere. Here, we developed new microsatellite loci and applied them to samples from three biogeographic regions in the GoM. We discovered the presence of two lineages. Lineage 1 is wide-spread throughout the Gulf, dominating Green Canyon, GB and the West Florida Shelf site. One Vioska Knoll site, VK906, almost exclusively harbors lineage 2. VK826, 25 nm from VK906, contains both lineages and a few of the colonies appear to be of mixed ancestry indicating hybridization between the lineages at this site. It is unclear at this point what taxonomic status the lineages have as neither color pattern nor mitochondrial DNA patterns coincide with the lineages defined via microsatellite genotyping. Nevertheless, reproductive patterns appear to differ between the lineages. Lineage 2 has much higher levels of clonal reproduction than Lineage 1 (Table 5-12). However, because sampling effort was not constant among sites, this finding will have to be confirmed in future studies. VK906 is a much smaller site than VK826 and thus samples were taken closer together, increasing the chance of sampling clonemates. When analyzed separately, lineage 1 does not show further geographic differentiation among sites in the GoM, similar to findings for *L. pertusa* (Morrison, Ross et al. 2011). Increased sample sizes and geographic coverage might discover more subtle signs of population structure in the future. Interestingly, the

two lineages also differed in their adherence to Hardy-Weinberg equilibrium assumptions (Figure 5-22).

The wider spread lineage 1 conforms to the expectations of an outbred species (once clones are removed from the dataset). In contrast, lineage 2 is highly inbred. Recall that lineage 2 dominated at VK906, where samples came from two isolated mounds, each about 200 m in diameter rising 40 m from the ocean floor. The top of each mound is densely settled with corals, including *L. pertusa* and *L. glaberrima*. The combination of limited habitat and relative isolation of this site might explain the increased inbreeding found in lineage 2.

Repeated multilocus genotypes were only found within sites and were never shared among sites (largest distance between two clonemates was 611 m, Table 5-12) indicating that asexual reproduction is a local process. The two principal modes of asexual reproduction in corals are fragmentation and production of asexual (ameiotic) larvae. Often, planktonic larvae have a broader dispersal potential than large fragments, but not so in black corals, which are thought to have short-lived, crawl away larvae (Miller 1998; Wagner et al 2011, Waller and Tyler 2005). In addition, we have at times observed that polyps will "bail-out" (Sammarco 1982), dropping from the skeleton of the colonies to the floor of aquaria when stressed, which may provide yet another form of asexual reproduction. We cannot at present distinguish between these potential modes of asexual reproduction, and this will not be an easy task due to the cost and difficulty of working with deep sea species.

Cryptic species are common in the marine environment (Knowlton 1993). Recent advances in genetic tools have led to the discovery of several cryptic lineages within morphologically similar collections of corals (Pinzón, Sampayo et al. 2013; Boulay, Hellberg et al. 2014). Mitochondrial DNA has poor resolution power in the Cnidaria (Shearer, Van Oppen et al. 2002; Hellberg 2006), and nuclear ITS markers are multi-copy, which complicates their interpretation (Ridgway 2002; Álvarez and Wendel 2003; Forsman, Hunter et al. 2006). Therefore, microsatellite markers have become increasingly popular for detection of cryptic lineage (Souter 2010; Nakajima, Nishikawa et al. 2012). Similar to the findings for *L. glaberrima*, the wide-spread shallow-water reef builder *Porites lobata*, actually consists of two morphologically similar species in the Eastern Pacific (Boulay, Hellberg et al. 2014). The two *Porites* species differ in the amount of asexual reproduction. *P. evermanni*, the species with higher frequency of asexual reproduction is able to persist in more marginal environments, perhaps because locally well adapted genotypes do not require the presence of a sexual partner to proliferate and dominate local communities (Boulay, Hellberg et al. 2014). If true for the two lineages of *L. glaberrima*, they might occupy different niches in the deep GoM. Corroborating evidence for this interpretation comes from the distribution of *L. glaberrima* at VK826 where lineage 1 appears mostly restricted to the northern edge of the site (Figure 5-26).

Because of the discovery of cryptic lineages within the dataset, sample sizes and geographic coverage were not sufficient to test dispersal and gene flow hypotheses rigorously for the two lineages. Additional sampling will be necessary to accomplish that goal. However, our preliminary evidence indicates that lineage 1 is wide-spread with high connectivity among populations whereas lineage 2 is restricted and shows limited gene flow even between the nearby sites of VK826 and VK906. Bio-physical modeling of dispersal pathways would allow us to test the hypothesis that

the isolation and shape of VK906 contributes to increased self-recruitment at that site (Baums, Paris et al. 2006). Additionally, the data suggests that the two lineages differ in their sexual and asexual reproductive strategies. This hypothesis could be tested with histological investigations of the two lineages.

It is important to note that because of the restricted distribution and high amount of inbreeding observed, lineage 2 deserves particular attention with respect to management and oversight of deep living corals in the GoM.

# 6 TROPHIC STUDIES

## 6.1 BACKGROUND

Octocorals (soft corals) in the GoM add heterogeneity to the seafloor and provide important habitat to other species (Buhl-Moretensen et al. 2010), but the nutritional sources for these corals, especially those occurring on the deeper portion of the continental slope below 1000 m are not well understood. Previous studies have noted that deepwater corals often occur in areas of past or current hydrocarbon seepage and some have suggested a nutritional link between the corals and local chemoautotrophic primary production from the seep environment. In the *Lophelia* I project, Becker et al. (2009) analyzed the stable isotope compositions of the reef-forming coral *Lophelia pertusa* and its associated fauna, as well as a few samples of octocroals from deeper sites, and found no evidence of significant incorporation of seep-derived nutrition by deepwater corals. In the *Lophelia* II project, we expanded our sampling of deepwater corals, especially octocorals occurring at deeper sites, to discern spatial and interspecific patterns in coral tissue stable isotope contents and infer nutritional sources.

Some octocorals, especially the genera *Callogorgia* and *Paramuicea*, may form symbiotic relationships with ophiuroid brittle stars (Figure 6-1). Researchers that have observed similar associations in other deep sea environments have suggested that the brittle stars are suspension feeders and use the structure of the gorgonians to escape the benthic boundary layer and increase their contact with food particles carried by bottom currents or resuspended from the sediment (Buhl-Moretensen et al. 2010) or that they consume a product of the corals such as mucus or feces (Emson and Woodley 1987). Tissue was sampled from 37 octocoral and ophiuroid pairs to examine whether there is evidence of a trophic relationship between the corals and their epizoic ophiuroids.

Tissues were also sampled for stable isotope analysis from the associated macrofauna in two of the quantitative *L. pertusa* coral pot collections. In the *Lophelia* I project, *L. pertusa* was often observed growing intermixed with senescent seep tube worms, but these communities were not targeted for collection and stable isotope analysis to determine the importance of seep primary production to this community. This previous work showed seep-derived nutrition is not a requirement for the corals or their associated communities (Becker 2009), but it remains to be determined whether the animals associated with *L. pertusa* utilize this source when it is in very close proximity to the corals. One of the two coral pot collections used for stable isotope analysis targeted a community of intermixed *L. pertusa* and seep tube worms.

Figure 6-1. *Callogorgia americana* and commensal ophiuroids.

## 6.2 METHODS

### 6.2.1 Sampling

Tissue samples for stable isotope analysis were obtained from corals and ophiuroids collected for genetic analyses into collection quivers and the biobox by removing coral tissue from the skeleton or, for ophiuroids, dissecting a piece of leg muscle tissue. Stable isotope samples were also taken from two of the coral pot collections that targeted *Lophelia pertusa* and its associated community. For these collections, up to three individuals of each species were sampled by dissecting a piece of muscle tissue from large animals or using whole individuals for smaller animals. The samples were rinsed with deionized water to remove any residual seawater and frozen at -70°C.

### 6.2.2 Stable Isotope Analysis

Samples were dried at 60°C, homogenized, and acidified with 5% (2 normal) phosphoric acid to remove inorganic carbonate. Samples were redried and subsamples were analyzed for stable carbon and nitrogen isotope compositions at the Stable Isotope Facility at the University of California, Davis, using an Integra elemental analyzer coupled with a PDZ Europa 20-20 isotope ratio mass spectrometer (Sercon Ltd., Cheshire, United Kingdom). Data are calibrated to National Institute of Standards and Technology (NIST) reference materials.

Values are expressed using δ (delta) notation and reported in units of permil (‰), where

$\delta X = [(R_{sample}/R_{standard}) - 1] \times 10^3$,
$X = {}^{13}C$ or ${}^{15}N$ and $R = {}^{13}C/{}^{12}C$ or ${}^{15}N/{}^{14}N$.

Values are reported relative to Pee Dee Belemnite (PDB) for carbon and air $N_2$ for nitrogen. Samples were sometimes too small to obtain the $\delta^{15}N$ composition and only the $\delta^{13}C$ is reported.

### 6.2.3 Statistical Analysis

Simple linear regression was used to test for a relationship between the $\delta^{13}C$ values of corals and their commensal ophiuroids. For $\delta^{15}N$ values, a nonparametric Spearman Rank correlation analysis was performed, because $\delta^{15}N$ data were not normally distributed.

## 6.3 RESULTS

### 6.3.1 Interspecific and Spatial Variation in Coral Tissue Stable Isotope Compositions

The majority of the corals had tissue stable isotope $\delta^{13}C$ values between -24‰ and -17‰ and $\delta^{15}N$ values from 6‰ to 12‰ (Table 6-1, Figure 6-2). *Callogorgia americana delta* had the broadest range in stable isotope values ($\delta^{13}C$ = -33.3 to -20.2‰ and $\delta^{15}N$ = 2.1‰ to 11.5‰). Higher $\delta^{15}N$ values were found in one *Paramuricea biscaya* B1 individual (14.9‰) and some *Callogorgia americana americana* individuals (14.9‰, 15.3‰, 18.0‰) (Figure 6-2).

Table 6-1.

$\delta^{13}C$ and $\delta^{15}N$ compositions for all soft corals sampled in this study

| Coral taxon | $\delta^{13}C$ | $\delta^{15}N$ | Site | Dive | Depth |
|---|---|---|---|---|---|
| *Callogorgia americana americana* | -21.3 | 8.5 | GB299 | J2-530 | 361 |
| *Callogorgia americana americana* | -19.9 | 10.5 | GB299 | J2-530 | 358 |
| *Callogorgia americana americana* | -20.9 | 10.3 | GB299 | J2-530 | 358 |
| *Callogorgia americana americana* | -21.8 | 10.5 | GB299 | J2-530 | 359 |
| *Callogorgia americana americana* | -21.9 | 9.0 | GB299 | J2-530 | 360 |
| *Callogorgia americana americana* | -19.5 | 15.3 | VK862 | J2-535 | 352 |
| *Callogorgia americana americana* | -19.7 | 14.9 | VK862 | J2-535 | 352 |
| *Callogorgia americana americana* | -20.3 | 18.0 | VK862 | J2-535 | 357 |
| *Callogorgia americana delta* | -24.6 | 5.6 | GC246 | J2-528 | 845 |
| *Callogorgia americana delta* | -23.9 | | GC246 | J2-528 | 845 |
| *Callogorgia americana delta* | -25.4 | | GC246 | J2-528 | 847 |
| *Callogorgia americana delta* | -25.0 | 5.2 | GC246 | J2-528 | 848 |
| *Callogorgia americana delta* | -27.1 | | GC246 | J2-528 | 846 |
| *Callogorgia americana delta* | -25.1 | 6.6 | GC249 | J2-533 | 778 |
| *Callogorgia americana delta* | -33.1 | 2.1 | GC249 | J2-533 | 789 |
| *Callogorgia americana delta* | -32.3 | 2.8 | GC249 | J2-533 | 790 |
| *Callogorgia americana delta* | -33.3 | 3.0 | GC249 | J2-533 | 790 |
| *Callogorgia americana delta* | -21.1 | 8.4 | GC249 | J2-533 | 790 |
| *Callogorgia americana delta* | -22.1 | 9.5 | MC751 | J2-536 | 442 |
| *Callogorgia americana delta* | -22.1 | 9.5 | MC751 | J2-536 | 442 |
| *Callogorgia americana delta* | -22.4 | 9.9 | MC751 | J2-536 | 441 |
| *Callogorgia americana delta* | -21.9 | 10.8 | MC751 | J2-536 | 443 |
| *Callogorgia americana delta* | -22.9 | 9.7 | MC885 | J2-527 | 627 |
| *Callogorgia americana delta* | -23.8 | 9.4 | MC885 | J2-527 | 631 |
| *Callogorgia americana delta* | -23.8 | 8.5 | MC885 | J2-527 | 630 |
| *Callogorgia americana delta* | -28.8 | 4.4 | MC885 | J2-527 | 625 |
| *Callogorgia americana delta* | -23.3 | 8.8 | MC885 | J2-527 | 631 |
| *Callogorgia americana delta* | -27.7 | 5.4 | MC885 | J2-527 | 625 |
| *Callogorgia americana delta* | -21.2 | | VK826 | J2-540 | 543 |
| *Callogorgia americana delta* | -21.1 | 10.2 | VK826 | J2-540 | 543 |
| *Callogorgia americana delta* | -21.4 | | VK826 | J2-540 | 543 |
| *Callogorgia americana delta* | -21.0 | 11.1 | VK826 | J2-540 | 541 |
| *Callogorgia americana delta* | -20.2 | 11.5 | VK826 | J2-540 | 541 |
| *Callogorgia americana delta* | -21.3 | | VK826 | J2-540 | 540 |
| Cup Coral | -20.5 | | MC118 | J2-538 | 887 |
| *Leiopathes* | -20.7 | 7.4 | GB299 | J2-530 | NA |
| *Leiopathes* | -20.6 | 8.2 | GB299 | J2-530 | 342 |
| *Leiopathes* | -21.0 | 9.2 | GB299 | J2-530 | 342 |
| *Leiopathes* | -21.0 | 9.3 | GB299 | J2-530 | 358 |
| *Leiopathes* | -20.5 | 9.2 | GB299 | J2-530 | 361 |
| *Leiopathes* | -19.3 | 9.8 | VK906 | J2-534 | 403 |
| *Leiopathes* | -19.6 | 10.6 | VK906 | J2-534 | 403 |
| *Leiopathes* | -20.8 | 9.9 | VK906 | J2-534 | 391 |
| *Leiopathes* | -19.5 | 9.3 | VK906 | J2-534 | 403 |
| *Leiopathes* | -19.0 | 9.7 | VK906 | J2-534 | 401 |

Table 6-1. $\delta^{13}$C and $\delta^{15}$N compositions for all soft corals sampled in this study (continued)

| Coral taxon | $\delta^{13}$C | $\delta^{15}$N | Site | Dive | Depth |
|---|---|---|---|---|---|
| *Leiopathes* sp. | -19.9 | 9.6 | VK906 | J2-534 | 401 |
| *Leiopathes* sp. | -19.5 | 9.4 | VK906 | J2-534 | 409 |
| *Leiopathes* sp. | -19.6 | 10.1 | VK906 | J2-534 | 403 |
| *Leiopathes* sp. | -19.0 | 9.4 | VK906 | J2-534 | 403 |
| *Leiopathes* sp. | -19.1 | 9.9 | VK906 | J2-534 | 403 |
| *Leiopathes* sp. | -19.2 | 10.8 | VK906 | J2-534 | 402 |
| *Lophelia pertusa* | -19.5 | 10.3 | MC751 | J2-536 | 441 |
| *Lophelia pertusa* | -22.3 | | GC354 | J2-529 | 526 |
| *Lophelia pertusa* | -19.6 | 8.7 | GB535 | J2-531 | 517 |
| *Lophelia pertusa* | -21.0 | | VK906 | J2-534 | 403 |
| *Lophelia pertusa* | -19.3 | 10.8 | VK906 | J2-534 | 393 |
| *Lophelia pertusa* | -18.5 | 10.4 | VK906 | J2-534 | 401 |
| *Lophelia pertusa* | -18.2 | 10.6 | VK906 | J2-534 | 399 |
| *Lophelia pertusa* | -19.1 | 9.9 | VK906 | J2-534 | 402 |
| *Lophelia pertusa* | -19.9 | 10.8 | MC751 | J2-536 | 441 |
| *Lophelia pertusa* | -19.2 | 10.4 | MC751 | J2-536 | 440 |
| *Lophelia pertusa* | -18.4 | 10.4 | MC751 | J2-536 | 439 |
| *Lophelia pertusa* | -18.0 | 9.6 | MC751 | J2-536 | 441 |
| *Lophelia pertusa* | -20.0 | 9.8 | MC794 Gulfoil | J2-537 | 532 |
| *Madrepora* | -25.5 | | MC338 | J2-541 | 1373 |
| *Muriceides cf. hirta* 1a | -18.9 | 11.0 | VK906 | J2-534 | 432 |
| Octocoral | -16.6 | 10.8 | MC751 | J2-536 | 440 |
| Octocoral | -23.0 | 5.5 | MC751 | J2-536 | 440 |
| *Paramuricea biscaya* B1 | -20.8 | 10.2 | DC673 | J2-539 | 2160 |
| *Paramuricea biscaya* B1 | -18.3 | 11.3 | DC673 | J2-539 | 2203 |
| *Paramuricea biscaya* B1 | -18.5 | 10.9 | DC673 | J2-539 | 2398 |
| *Paramuricea biscaya* B1 | -21.1 | 14.9 | DC673 | J2-539 | 2207 |
| *Paramuricea biscaya* B1 | -20.0 | 11.6 | DC673 | J2-539 | 2313 |
| *Paramuricea biscaya* B2 | -20.9 | 10.6 | DC673 | J2-539 | 2400 |
| *Paramuricea* sp. | -19.1 | 9.6 | MC338 | J2-541 | 1373 |
| *Paramuricea* sp. B3 | -22.6 | 7.1 | GC246 | J2-528 | 845 |
| *Paramuricea* sp. B3 | -20.0 | 9.7 | MC118 | J2-538 | 885 |
| *Paramuricea* sp. B3 | -20.0 | 10.7 | MC118 | J2-538 | 889 |
| *Paramuricea* sp. B3 | -19.4 | 8.3 | MC118 | J2-538 | 884 |
| *Paramuricea* sp. B3 | -20.6 | 9.3 | MC118 | J2-538 | 887 |
| *Paramuricea* sp. B3 | -21.5 | 10.5 | MC118 | J2-538 | 884 |
| *Paramuricea* sp. E | -20.0 | 9.7 | GB299 | J2-530 | 342 |
| *Paramuricea* sp. E | -20.5 | 9.2 | GB299 | J2-530 | 361 |
| *Paramuricea* sp. E | -20.5 | 9.2 | GB299 | J2-530 | 361 |
| *Paramuricea* sp. E | -20.1 | 9.0 | GB299 | J2-530 | 361 |
| *Paramuricea* sp. E | -20.2 | 10.3 | MC751 | J2-536 | 441 |
| *Paramuricea* sp. E | -20.5 | 6.6 | MC751 | J2-536 | 441 |
| *Paramuricea* sp. E | -20.7 | 11.9 | MC751 | J2-536 | 440 |
| *Paramuricea* sp. E | -20.7 | 10.2 | MC751 | J2-536 | 440 |
| *Paramuricea* sp. E | -19.3 | 10.0 | MC751 | J2-536 | 441 |
| *Swiftia exserta* | -20.9 | 6.6 | MC751 | J2-536 | 440 |
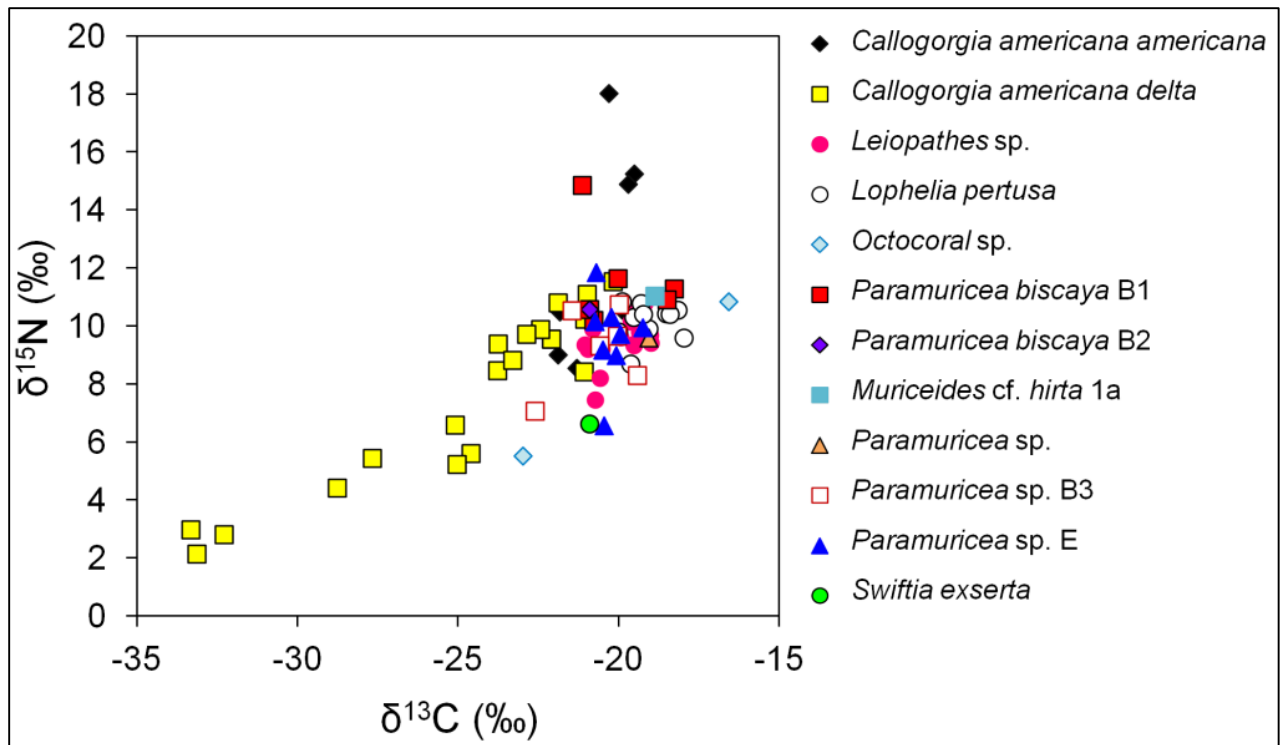
Figure 6-2. $\delta^{15}N$ vs. $\delta^{13}C$ for all soft corals sampled for stable isotope analysis.

The $\delta^{13}C$ and $\delta^{15}N$ values of *Paramuricea* sp. E and *Leiopathes* sp. did not differ substantially between sites (Figure 6-3c,d). *Callogorgia americana americana* $\delta^{15}N$ values differed between VK862 ($\delta^{15}N$ = 14.9 to 18.0‰) and GB299 ($\delta^{15}N$ = 8.5 to 10.5‰, Figure 6-3c), while $\delta^{13}C$ values were similar between VK862 (-19.5 to -20.3‰) and GB299 (-19.9‰ to -21.9‰, Figure 6-3c). Stable isotope values of *Callogorgia americana delta* did not differ between VK826 and MC751 (Figure 6-3a). The stable isotope values of samples from GC246 clustered together and were markedly different from the $\delta^{13}C$ and $\delta^{15}N$ compositions of samples from MC751 and VK826 (Figure 6-3a). There was a large range of both $\delta^{13}C$ and $\delta^{15}N$ values in *Callogorgia americana delta* sampled from GC249 ($\delta^{13}C$ = -33.3 to -21.1‰; $\delta^{15}N$ = 2.1 to 8.4‰: Figure 6-3a) and MC885 ($\delta^{13}C$ = -28.8 to -22.9‰; $\delta^{15}N$ = 4.4 to 9.7‰ $\delta^{15}N$, Figure 6-3).
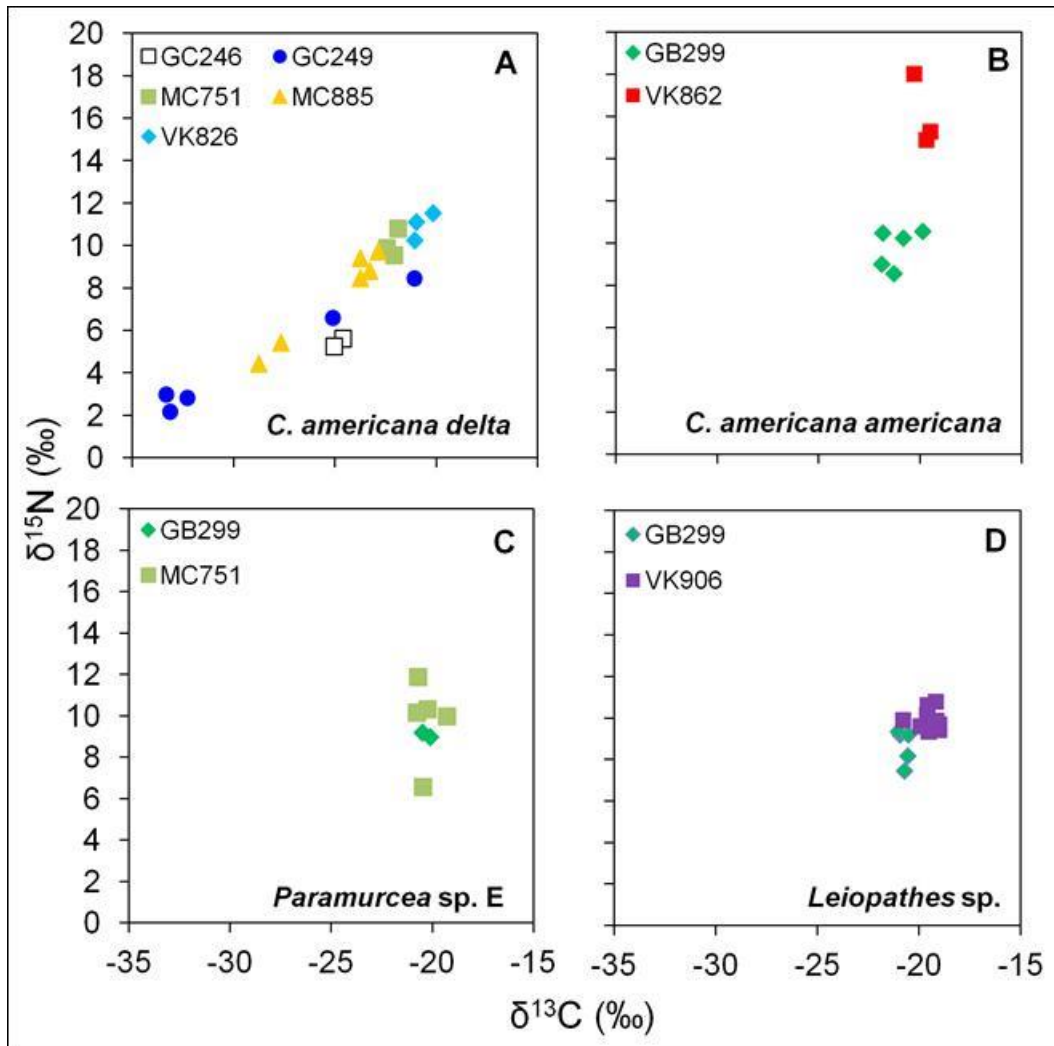
Figure 6-3.  $\delta^{15}N$ vs. $\delta^{13}C$ of (A) *Calligorgia americana delta*, (B) *Callogorgia americana americana*, (C) *Paramuricea* sp. E, and (D) *Leiopathes* sp., with difference symbols representing different sampling sites.

## 6.3.2  Corals with Paired Commensal Ophiuroids

There was a significant linear relationship between tissue $\delta^{13}C$ composition of corals and the commensal ophiuroids that were associated with them (simple linear regression: $R^2 = 0.51$, $p < 0.0001$; Figure 6-4a), but the relationship was not significant for $\delta^{15}N$ (Spearman rank correlation for non-normally distributed data: $p=0.076$; Figure 6-4b). Qualitatively, the $\delta^{15}N$ values of ophiuroids and their paired coral appear similar, except for the *C. americana americana* individuals with anomalously high $\delta^{15}N$ values, whose paired ophiuroids had tissue $\delta^{15}N$ values within the lower end of the ophiuroid $\delta^{15}N$ range ( Figure 6-4b, Figure 6-5b).

# Table 6-2.

$\delta^{13}$C and $\delta^{15}$N values of octocorals and their epizoic ophiuroids (oph.). Where more than one ophiuroid was present on the same coral, the coral stable isotope data are repeated on a separate line

| | | $\delta^{13}$C | | $\delta^{15}$N | | | | |
|---|---|---|---|---|---|---|---|---|
| **Coral taxon** | **Paired oph. taxon** | **Coral** | **Oph.** | **Coral** | **Oph.** | **Site** | **Dive** | **Depth (m)** |
| *Callogorgia americana americana* | *Asteroschema* sp. 1 | -21.3 | -16.4 | 8.5 | 9.4 | GB299 | J2-530 | 361 |
| *Callogorgia americana americana* | *Asteroschema* sp. 1 | -19.9 | -16.8 | 10.5 | 10.2 | GB299 | J2-530 | 358 |
| *Callogorgia americana americana* | *Asteroschema* sp. 1 | -20.9 | -16.0 | 10.3 | 11.4 | GB299 | J2-530 | 358 |
| *Callogorgia americana americana* | *Asteroschema* sp. 1 | -19.5 | -16.7 | 15.3 | 8.4 | VK862 | J2-535 | 352 |
| *Callogorgia americana americana* | *Asteroschema* sp. 1 | -19.7 | -16.7 | 14.9 | 8.4 | VK862 | J2-535 | 352 |
| *Callogorgia americana americana* | *Asteroschema* sp. 1 | -20.3 | -16.6 | 18.0 | 6.3 | VK862 | J2-535 | 357 |
| *Callogorgia americana delta* | *Asteroschema* sp. 1 | -27.1 | -24.6 | -- | 5.6 | GC246 | J2-528 | 846 |
| *Callogorgia americana delta* | *Asteroschema* sp. 1 | -25.4 | -20.5 | -- | 8.3 | GC246 | J2-528 | 847 |
| *Callogorgia americana delta* | *Asteroschema* sp. 1 | -25.0 | -20.6 | 5.2 | -- | GC246 | J2-528 | 848 |
| *Callogorgia americana delta* | *Asteroschema* sp. 1 | -23.9 | -21.1 | -- | 8.7 | GC246 | J2-528 | 845 |
| *Callogorgia americana delta* | *Asteroschema* sp. 1 | -24.6 | -20.2 | 5.6 | 7.8 | GC246 | J2-528 | 845 |
| *Callogorgia americana delta* | *Asteroschema* sp. 1 | -21.1 | -22.9 | 8.4 | 5.8 | GC249 | J2-533 | 790 |
| *Callogorgia americana delta* | *Asteroschema* sp. 1 | -21.9 | -19.1 | 10.8 | 11.0 | MC751 | J2-536 | 443 |
| *Callogorgia americana delta* | *Asteroschema* sp. 1 | -22.1 | -16.9 | 9.5 | 11.2 | MC751 | J2-536 | 442 |
| *Callogorgia americana delta* | *Asteroschema* sp. 1 | -22.1 | -16.9 | 9.5 | 11.2 | MC751 | J2-536 | 442 |
| *Callogorgia americana delta* | *Asteroschema* sp. 1 | -22.4 | -18.0 | 9.9 | 9.1 | MC751 | J2-536 | 441 |
| *Callogorgia americana delta* | *Asteroschema* sp. 1 | -22.9 | -18.7 | 9.7 | 10.4 | MC885 | J2-527 | 627 |
| *Callogorgia americana delta* | *Asteroschema* sp. 1 | -23.3 | -17.5 | 8.8 | 10.7 | MC885 | J2-527 | 631 |
| *Callogorgia americana delta* | *Asteroschema* sp. 1 | -20.2 | -17.8 | 11.5 | 9.6 | VK826 | J2-540 | 541 |
| *Callogorgia americana delta* | *Asteroschema* sp. 1 | -21.4 | -16.9 | -- | 10.8 | VK826 | J2-540 | 543 |
| *Callogorgia americana delta* | *Asteroschema* sp. 1 | -21.2 | -16.8 | -- | 9.9 | VK826 | J2-540 | 543 |
| *Callogorgia americana delta* | *Asteroschema* sp. 1 | -21.1 | -16.9 | 10.2 | 10.8 | VK826 | J2-540 | 543 |
| *Callogorgia americana delta* | *Asteroschema* sp. 1 | -21.0 | -16.3 | 11.1 | 11.5 | VK826 | J2-540 | 541 |
| *Callogorgia americana delta* | *Asteroschema* sp. 1 | -21.3 | -15.4 | -- | 11.4 | VK826 | J2-540 | 540 |
| *Muriceides* cf. *hirta* 1a | *Astrogomphus* sp. | -18.9 | -17.2 | 11.0 | 11.4 | VK906 | J2-534 | 432 |
| *Muriceides* cf. *hirta* 1a | *Astrogomphus* sp. | -18.9 | -17.3 | 11.0 | 11.9 | VK906 | J2-534 | 432 |
| *Paramuricea biscaya* B1 | *Asteroschema clavigerum* | -20.8 | -17.8 | 10.2 | 12.2 | DC673 | J2-539 | 2160 |
| *Paramuricea biscaya* B1 | *Asteroschema clavigerum* | -21.1 | -16.9 | 14.9 | 13.0 | DC673 | J2-539 | 2207 |
| *Paramuricea biscaya* B1 | *Asteroschema clavigerum* | -18.5 | -14.6 | 10.9 | 14.1 | DC673 | J2-539 | 2398 |
| *Paramuricea biscaya* B1 | *Asteroschema clavigerum* | -18.3 | -14.9 | 11.3 | 12.8 | DC673 | J2-539 | 2203 |
| *Paramuricea biscaya* B2 | *Asteroschema clavigerum* | -20.9 | -15.4 | 10.6 | 13.1 | DC673 | J2-539 | 2400 |
| *Paramuricea* sp. B3 | *Asteroschema* sp. 1 | -22.6 | -21.1 | 7.1 | -- | GC246 | J2-528 | 845 |
| *Paramuricea* sp. B3 | *Asteroschema* sp. 1 | -21.5 | -17.0 | 10.5 | 11.1 | MC118 | J2-538 | 884 |
| *Paramuricea* sp. B3 | *Asteroschema* sp. 1 | -21.5 | -16.2 | 10.5 | 12.0 | MC118 | J2-538 | 884 |
| *Paramuricea* sp. B3 | *Asteroschema* sp. 1 | -20.6 | -17.7 | 9.3 | 11.1 | MC118 | J2-538 | 887 |
| *Paramuricea* sp. E | *Asteroschema* sp. 1 | -20.0 | -16.8 | 9.7 | 10.4 | GB299 | J2-530 | 342 |
| *Paramuricea* sp. E | *Asteroschema* sp. 1 | -20.1 | -16.7 | 9.0 | 10.4 | GB299 | J2-530 | 361 |
| *Paramuricea* sp. E | *Asteroschema* sp. 1 | -20.2 | -17.4 | 10.3 | 11.3 | MC751 | J2-536 | 441 |
| *Paramuricea* sp. E | *Asteroschema* sp. 1 | -20.5 | -17.6 | 6.6 | 10.8 | MC751 | J2-536 | 441 |
| *Swiftia exserta* | *Astrogomphus* | -20.9 | -15.7 | 6.6 | 8.2 | MC751 | J2-536 | 440 |
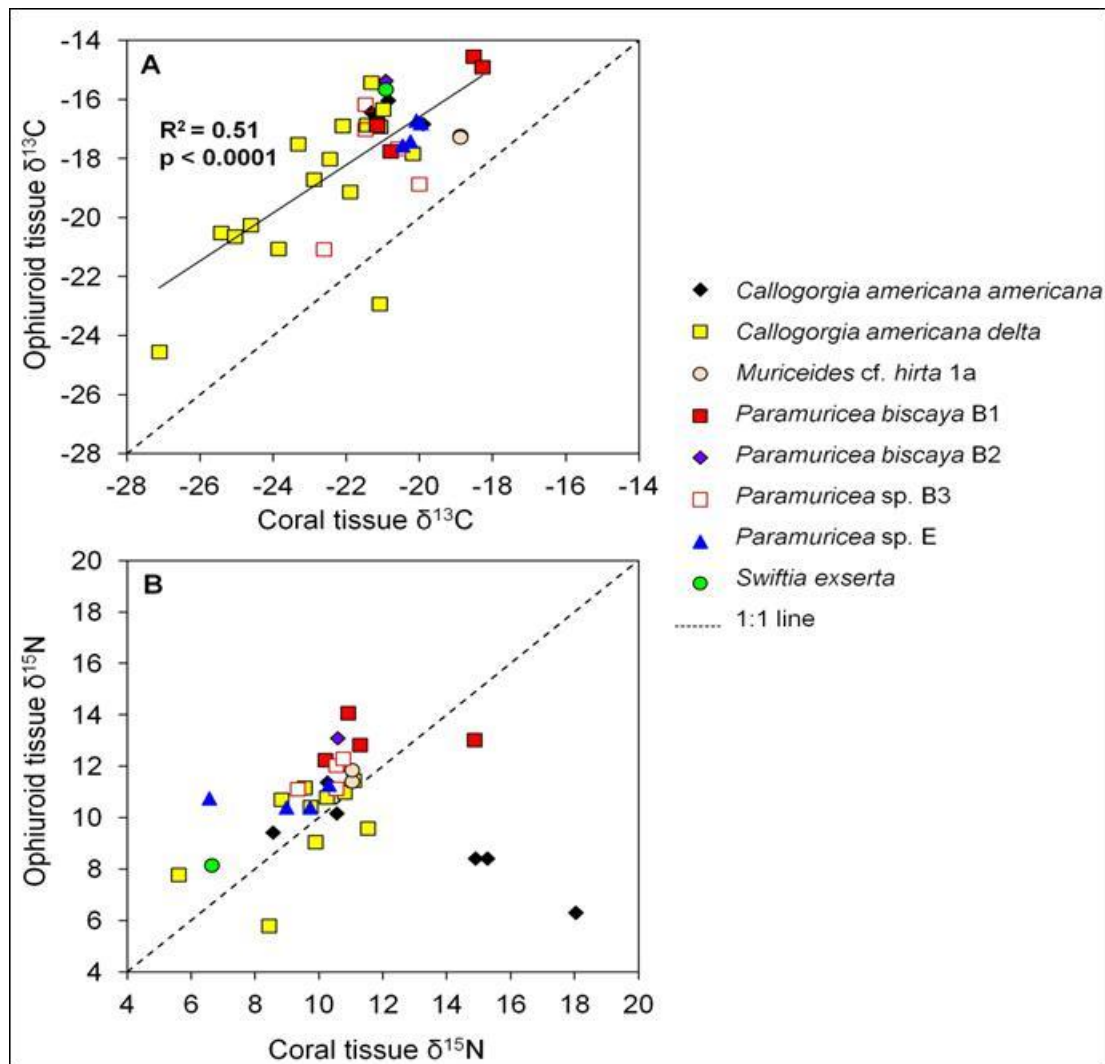
Figure 6-4. (A) $\delta^{13}C$ of epizoic ophiuroids vs. $\delta^{13}C$ of their host corals. (B) $\delta^{15}N$ of epizoic ophiuroids vs. $\delta^{15}N$ of their host corals. The solid line in (A) represents a simple linear regression and the broken line in both panels represents equal values on the x- and y-axes.

*C. a. delta* and their paired ophiuriods *Asteroschema* sp. 1 had the most variability in carbon and nitrogen stable isotope values, but also showed a significant linear relationship between all sampled pairs for $\delta^{13}C$ (p=0.0014; Figure 6-5c). The tissue $\delta^{13}C$ values of ophiuroids associated with *C. a. delta* clustered by site similarly to their paired corals, while spatial variation in the $\delta^{15}N$ values is hard to discern because of small sample sizes and a small range overall of $\delta^{15}N$ values (Figure 6-5c,d).

Tissue $\delta^{13}C$ values were similar between sites for *C. a. americana* and their paired ophiuroids *Asteroschema* sp.1 (Figure 6-5a). The tissue $\delta^{15}N$ values of the *C. a. americana* differed markedly by site since the three anomalous values were from one site, but their paired ophiuroids *Asteroschema* sp. 1 had similar $\delta^{15}N$ values between sites (Figure 6-5b).
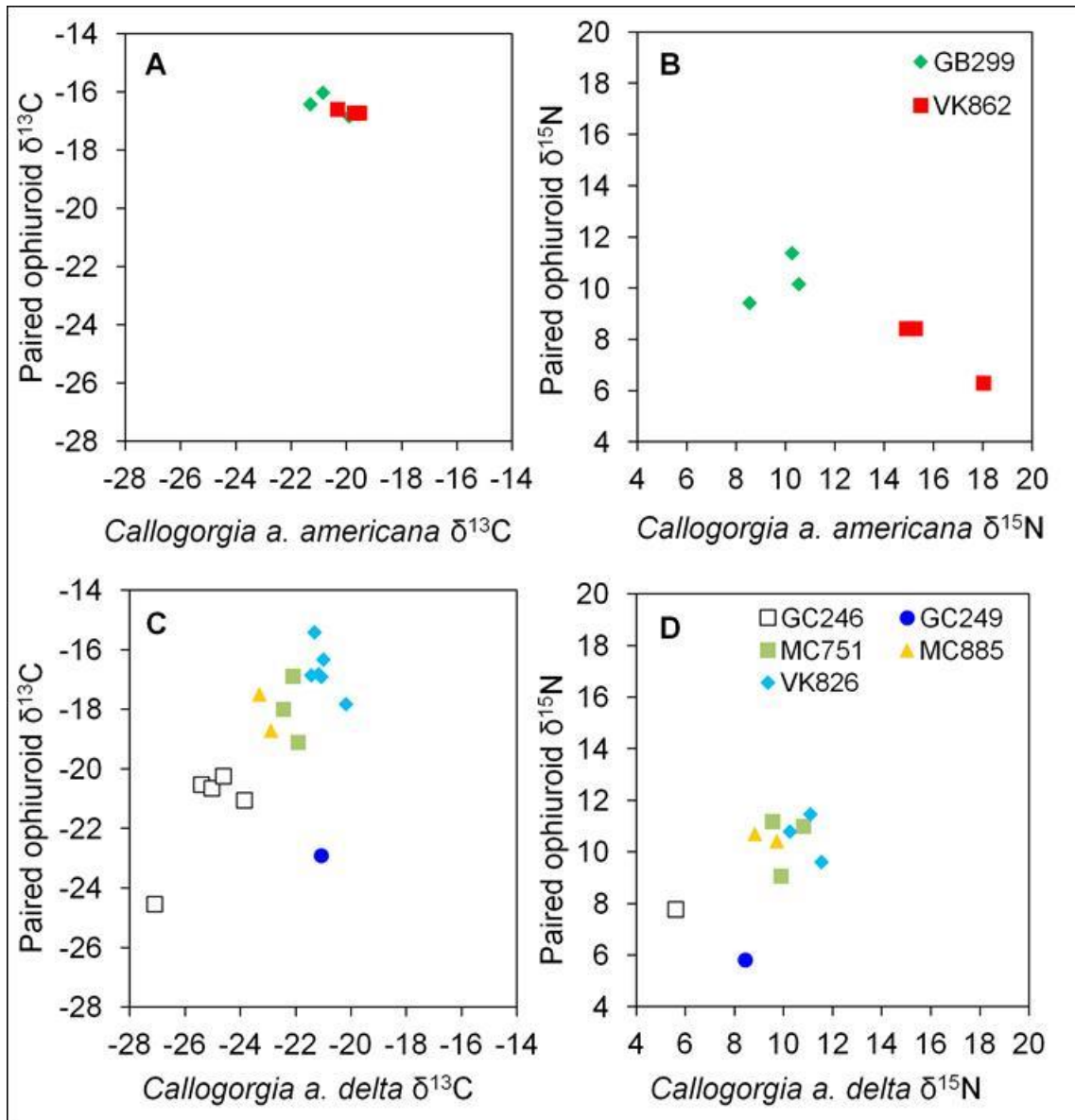
Figure 6-5. (A) $\delta^{13}C$ of associated ophiuroid vs. $\delta^{13}C$ of *Callogorgia americana americana*, (B) $\delta^{15}N$ of associated ophiuroid vs. $\delta^{15}N$ of *Callogorgia americana americana*, (C) $\delta^{13}C$ of associated ophiuroid vs. $\delta^{13}C$ of *Callogorgia americana delta*, (D) $\delta^{15}N$ of associated ophiuroid vs. $\delta^{15}N$ of *Callgorgia americana delta*.

*Paramuricea biscaya* B1 and B2 samples were paired with *Asteroschema clavigerum* individuals and had a narrower range of stable isotope values compared to *Callogorgia* samples, with coral $\delta^{13}C$ values ranging from -21‰ to -18‰ and coral $\delta^{15}N$ values ranging from 10‰ to 15‰. Corresponding ophiuroids had tissue $\delta^{13}C$ values ranging from -18‰ to -15‰ and $\delta^{15}N$ values ranging from 12‰ to 14‰. *Paramuricea biscaya* B1 and B2 pairs have $\delta^{15}N$ values at the high end of the overall $\delta^{15}N$ distribution (Figure 6-4b), and two *P. biscaya* B1 pairs had the highest $\delta^{13}C$ values of all coral-ophiuroid pairs (Figure 6-4a). There is less variability in $\delta^{13}C$ and $\delta^{15}N$ values in *Paramuricea* sp. B3 and E pairs, and they tended to group close to the center of the overall distribution.

*Muriceides* cf. *hirta* 1a and paired *Astrogomphus* sp. individuals had $\delta^{13}C$ and $\delta^{15}N$ values near the densest areas in the overall distributions (Figure 6-4). The pair of *Swiftia exserta* and *Astrogomphus* sp. had tissue $\delta^{13}C$ values of -21‰ for the coral and -15‰ for the ophiuroid, and $\delta^{15}N$ values of 7‰ for the coral and 8‰ for the ophiuroid (Figure 6-4), putting this pair at the very high end of the $\delta^{13}C$ range, and very low end of the $\delta^{15}N$ range.

### 6.3.3 Macrofaunal Community Associated with *Lophelia pertusa*

In the coral pot collection from the MC751 study site, the associated macrofauna had tissue $\delta^{13}C$ values ranging from -28.5 to -16.6‰ and $\delta^{15}N$ values ranging from 5.3 to 10.8‰ (Figure 6-6a). In the collection from GB535, the associated fauna had $\delta^{13}C$ values ranging from -22.8 to -17.6‰ and $\delta^{15}N$ values from 7.5 to 13.8‰ (Figure 6-6b).
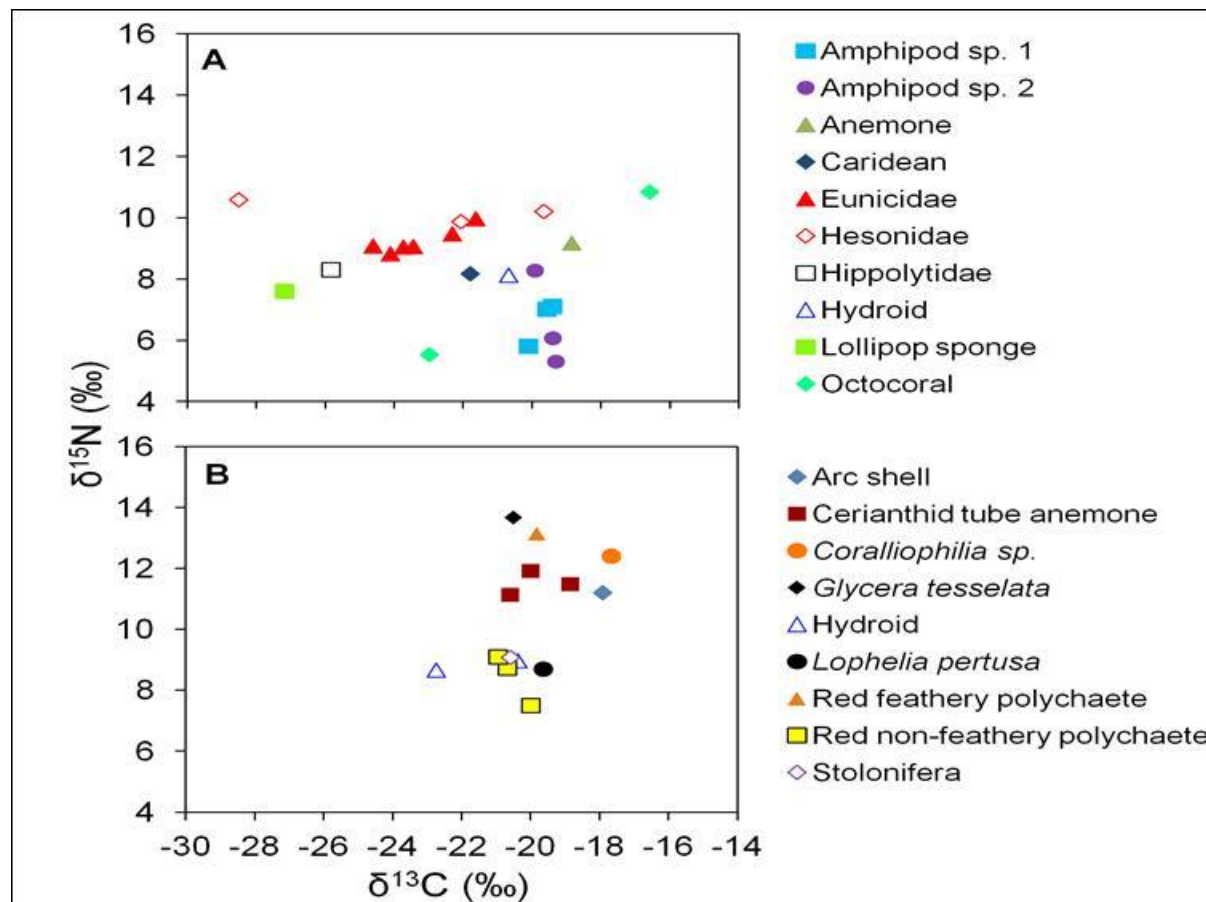


Figure 6-6. (A) $\delta^{15}N$ vs. $\delta^{13}C$ of *Lophelia pertusa* and associated macrofauna from quantitative coral pot collections from MC751 (dive J2-436) and (B) GB535 (dive J2-531).

## 6.4 DISCUSSION

### 6.4.1 Nutrition of deepwater corals

The majority of coral species had tissue $\delta^{13}C$ and $\delta^{15}N$ values consistent with nutrition primarily derived from surface primary productivity, but the more variable and more negative $\delta^{13}C$ values

and $\delta^{15}N$ values in *Callogorgia americana delta* provide the strongest evidence to date of a nutritional link between a deepwater coral species and hydrocarbon seep primary production (Table 6-1, Figure 6-2). Other authors have suggested such a link based on the tendency of corals to occur in close proximity to seeps (Hovland and Risk 2003). However, previous stable isotope analysis of coral tissue and skeleton suggested that, at least in the GoM, the association between corals and seeps is driven more by the availability of hard substrate in the form of authigenic carbonate, a feature unique to past or present seeps on the Gulf's otherwise muddy seafloor, and that corals settle after seepage has become mostly inactive (Becker et al. 2009).

Recent work incorporating phylogenetic and ecological niche modeling that was part of the current project showed that the occurrence of *C. a. delta* was positively correlated with the presence of active seepage and was able to settle and grow even on small pieces of hard substrate such as coral rubble or clam shells (Quattrini et al. 2013; Section 9.2 of this report). The ability of this species to tolerate chemical conditions of the seep environment (exposure to hydrocarbons and sulfides and low oxygen concentration) and take advantage of a local source of primary production may release it from competition, since other corals relying on surface production are limited to areas with flow regimes producing sufficient food delivery, such as local topographic highs which accelerate currents and interact with internal waves to resuspend sediment organic matter and increase feeding opportunities (Genin et al. 1986, Davies et al. 2009, Duineveld et al. 2012). Indeed, the distribution of *Paramuricea* spp. in the GoM, whose stable isotope values are indicative of photosynthesis-based nutrition, is most commonly observed on local topographic highs (Doughty et al. in press).



Figure 6-7. Small tube worm aggregations interspersed with colonies of *Callogorgia americana* delta at MC885.

### 6.4.2   Nutritional Associations Between Corals and their Epizoic Ophiuroids

The significant correlation between $\delta^{13}C$ values in epizoic ophiuroids and their host gorgonian corals, indicates either a direct trophic interaction between the two organisms or that they share a food source (Figure 6-4a). The latter is more likely based on the results of other studies that observed the behavior and gut contents of epizoic ophiuroids from other regions (Emson and Woodley 1987, Fujita and Ohta 1988). In these studies, the authors concluded that the ophiuroids are suspension feeders and are not predating the corals, since ophiuroids were observed capturing suspended particles from the water column, host corals were not damaged, and no coral polyps were found in the gut contents of the ophiuroids. The $\delta^{15}N$ values, although not significantly correlated, are also similar between ophiuroids and host corals (excepting the corals with anomalously high $\delta^{15}N$ values), and the $\delta^{15}N$ of ophiuroids do not show a consistent trophic enrichment (+3.4‰; (Minagawa and Wada 1984), further supporting that the ophiuroids are not preying upon the coral, but rather share a common food source.

Together, the previous observations and the current stable isotope data indicate that the ophiuroid-gorgonian association benefits the ophiuroid by providing access to a food source that is similar to the food source of the coral, but the effect of the association on the coral is not known. The association could be parasitic (e.g. ophiuroids stealing food from polyps), mutualistic (e.g. ophiuroids help to prevent sedimentation by removing particles from polyps), or commensal (e.g. ophiuroids simply use the vertical structure of the coral to surmount the benthic boundary layer and capture particulate matter and prey from the water column, or they eat a byproduct of the coral such as mucus or feces).

### 6.4.3   Nutritional Sources for Fauna Associated with *Lophelia pertusa*

In the two coral pot collections of *Lophelia pertusa* and its associated community, the majority of fauna had tissue stable isotope values indicative of primarily photosynthesis-derived nutrition (Gearing et al. 1984) ( Figure 6-4). Although, in the collection from MC751, the $\delta^{15}N$ values of some organisms were lighter than the GB535 collection, and the four lollipop sponges had $\delta^{13}C$ values in between -27.6 and -26.1‰ and one hesionid polychaete had a tissue $\delta^{13}C$ value of -28.5‰, indicating that these animals may derive some nutrition from seep primary production (Table 6-1, Figure 6-6). This is quite possible, since the coral pot collection from MC751 was made in an area with *L. pertusa* attached to tube worms and contained vestimentiferan tube worms (Figure 6-8).

Figure 6-8.  *Lophelia pertusa* growing on vestimentiferan tube worms with *Acesta sp* at MC751.

# 7  *LOPHELIA PERTUSA* LABORATORY EXPERIMENTS

## 7.1  INTRODUCTION

Ocean change is expected to manifest itself in a variety of ways. Due to the high density and specific heat of seawater, the oceans store a large portion of the heat produced by the greenhouse effect and global warming (Levitus et al. 2000). Since the 1950s, most of this storage has occurred within the upper 700 m of the Atlantic Ocean (Levitus and Boyer 2005), with observed temperature increases ranging from 0.1 to 0.2ºC (Barnett et al. 2005).  Increasing seawater temperature decreases the solubility of oxygen and enhances thermal stratification of the water column (Keeling et al. 2010). Finally, the increased flux of anthropogenic $CO_2$ to the surface ocean results in ocean acidification (Raven et al. 2005). These changes, acting both independently and collectively, may challenge the persistence of marine organisms and their associated communities in the future global ocean.

Maximal performance of physiological functions in a number of marine organisms occurs within a relatively narrow range of environmental conditions. Temperature is perhaps the primary physical driver of the limits to species distribution and abundance (Gaston 2003). The stability of both proteins and cell membranes are dependent on temperature (reviewed in Hofmann and Todgham 2010), thereby exerting considerable effects on organismal survivorship. Dissolved oxygen concentrations are critical to the maintenance of respiration, and the energetic requirements of most eukaryotes are sustained by aerobic respiration. pH is of similar significance to physiological functioning, particularly with respect to acid-base balance (Pörtner et al. 2005), and the regulation of this balance is often correlated to an organisms' metabolic rate (e.g. Goffredi and Childress 2001, Pane and Barry 2007). As a result of ocean acidification, changing seawater pH will distort the carbonate chemistry of seawater with particularly negative effects on the growth of calcareous species.

Given the relatively narrow range of physical conditions associated with the habitat of *L. pertusa*, changes in these variables may alter its current distribution via negative effects on survivorship and growth. Temperature likely controls both the upper and lower bathymetric limits of *L. pertusa* worldwide (Frederiksen et al. 1992, Roberts et al. 2006). Recent long-term data from the Viosca Knoll *L. pertusa* reefs show ranges of 6.5-11.6ºC with seasonal fluctuations of up to 5ºC  (Mienis et al. 2012); furthermore, daily fluctuations of up to 1ºC have also been reported within the area (Davies et al. 2010). Dissolved oxygen is relevant to *L. pertusa* persistence because the corals appear to be near their lower limits in the GoM. Near *L. pertusa* habitats on Viosca Knoll, DO was measured between 2.6 and 3.2 mL·L$^{-1}$ (Schroeder 2002), while in the North Atlantic it is commonly between 3 and 6 mL·L$^{-1}$ (Dodds et al. 2007). pH is widely considered to be one of the most important factors related to coral calcification (Doney et al. 2009), and data from the *L. pertusa* reefs in the GoM show pH ranging from 7.86-8.03, with a mean around 7.90 (Lunden et al. 2013). The purpose of the present study was therefore to employ short-term experiments in the laboratory to investigate *L. pertusa*'s responses to changes in temperature, dissolved oxygen, and pH (and aragonite saturation state).

Despite the above-referenced changes to the marine environment, research has predominately focused on easily-accessible, tractable, nearshore systems such as rocky intertidal communities

(e.g. Helmuth et al. 2006), coral reefs (e.g. Hughes et al. 2003), seagrass beds (e.g. Orth et al. 2006), and kelp forests (e.g. Henkel et al. 2009), among others. Investigations of climate change impacts in extreme environments are considerably less common, particularly due to the logistical and financial constraints associated with collection and maintenance of target species. In the past several years, investigations of climate change effects in remote environments (e.g. high-latitude regions and deep-sea communities) have emerged as new priorities for study (Hofmann et al. 2010), as well as presently poorly-understood biological impacts of ocean acidification (Garrard et al. 2012).

Physiological investigations of deep-sea organisms in the laboratory typically require sophisticated holding aquaria that replicate the natural environments of the study species. This has primarily been manifested in the form of flow-through aquaria that receive high-quality and presumably uncontaminated natural seawater from offshore areas (e.g. Mortensen 2001, Olariaga et al. 2009, Naumann et al. 2011). However, flow-through systems require close proximity to a natural seawater source, restricting most research to coastal research facilities. Furthermore, flow-through systems may be compromised in the event of an unforeseen disturbance to the seawater supply, such as an oil spill, pathogen outbreak, or changing seawater chemistry due to ocean acidification. An alternative to the flow-through system is a recirculating, or "closed" system, which functions independently of an offshore seawater supply and remains under the complete autonomy of the facility or researchers maintaining it.

Recirculating aquaria require efficient and vigorous filtration to prevent the accumulation of toxic waste products and detritus within the system. Three primary modes of filtration are generally used for recirculating aquaria: biological, chemical, and mechanical. Biological filtration refers to the decomposition of organic and inorganic wastes produced by the aquarium inhabitants, and relies heavily on microbial processes such as nitrification (the oxidation of ammonium to nitrite then nitrate by aerobic bacteria) and denitrification (the reduction of nitrate to nitrite by anaerobic bacteria). Both aerobic and anaerobic bacteria proliferate within sediments and on complex structures with high surface area, thus necessitating platforms such as sand, gravel, or convoluted surfaces as substrata within the system. Chemical filtration involves the removal of organic compounds lacking nitrogen, such as dissolved organic carbon (Delbeek and Sprung, 2005), and can be accomplished via granular activated carbon (GAC), phosphate adsorption media, and protein skimming. While any of these methods are commonly used, protein skimming is considered to be the most effective as it removes intact organic molecules prior to decomposition (Delbeek and Sprung, 2005). Finally, mechanical filtration is the physical removal of particulate matter within the aquarium, and relies heavily on sponge pads and other fibrous, screened materials that can trap particulate matter. Mechanical filtration can also be supplemented by an ultraviolet light sterilizer, which kills pathogenic bacteria that can accumulate and harm the aquarium livestock.

In order to manipulate variables relevant to climate change, several methods are available. To simulate changes in seawater pH, common perturbations include $CO_2$ bubbling and strong acid addition. However, only bubbling of $CO_2$ accurately replicates the effects of ocean acidification via increases in $pCO_2$ and dissolved inorganic carbon. Addition of strong acids to reduce pH results in a decrease in total alkalinity, a parameter that is not expected to change as a result of ocean acidification. Therefore, the recommended method for simulating ocean acidification in the

laboratory is bubbling of pure or pre-mixed $CO_2$ into aquaria (Gattuso et al. 2010). However, one caveat of using synthetic seawater in recirculating aquaria is the high buffering capacity characteristic of synthetic sea salts. Artificial salt manufacturers intentionally augment the buffering capacity of artificial salts primarily via bicarbonate additions to prevent the pH crashes that occur frequently in recirculating aquaria with high livestock loads, particularly due to the release of hydrogen ions during denitrification (Delbeek and Sprung, 2005). This excess buffering capacity results in an abnormally high total alkalinity of the seawater (around 3600 $\mu mol \cdot kg^{-1}$ compared to 2300 $\mu mol \cdot kg^{-1}$ of natural seawater at a salinity of 35 ppt), therefore limiting the environmental relevance of acidification experiments using synthetic sea salts.

Manipulating dissolved oxygen in the laboratory is primarily accomplished by degasification, which involves bubbling an inert gas, such as nitrogen, into the seawater. This method has been used previously in several laboratory studies of aquatic organisms (e.g. Breitburg et al. 1997, Geist et al. 2006), including cold-water corals (Dodds et al. 2007). However, methods for maintaining targeted concentrations of dissolved oxygen in the absence of mass-flow controllers are largely absent from the literature.

Here we describe the development and maintenance of recirculating aquaria for maintaining deep-sea corals and associated fauna independent of a natural seawater supply. We also describe the development, maintenance, and manipulation of smaller, recirculating aquaria used for short-term experiments on the cold-water coral *Lophelia pertusa*. We share our findings and experiences from this work with the goal of promoting experimental investigations on traditionally under-studied organisms, particularly with respect to new directions in climate change research.

## 7.2 DEVELOPMENT OF RECIRCULATING AQUARIA FOR EXPERIMENTATION WITH DEEP-SEA CORALS

### 7.2.1 Methods

#### 7.2.1.1 Maintenance Aquaria Design and Setup

Two replicated aquaria systems were constructed as primary holding tanks for the animals (Figure 7-1) shows a representative example of these systems). The two systems were maintained in different locations in the laboratory: one system was constructed in a constant-temperature room, and the other was constructed in the laboratory. Temperature of the laboratory system was controlled by a flow-through chiller (TECO®), and a drop-in coil chiller (Aqua Logic®) was installed in the constant-temperature room system to prevent temperature fluctuations in the event of thermostat failures in the room. Each system consisted of a 100 gallon holding tank and a 50 gallon sump tank – the constant-temperature room system consisted of all-glass aquaria and the laboratory system consisted of fiberglass insulated tanks (Aquatic EcoSystems) to achieve temperature stability. The sump tank was divided into three compartments using ½" plexiglass baffles for the different filtration applications (biological, chemical, mechanical). Circulation was controlled by a Quiet One 6000 submersible pump, with a flow rate of 1000 gallons per hour and a turnover rate of ~seven times per hour. A Koralia® Hydor™ powerhead (1050 gallons per hour) interfaced with an OceanPulse® Duo™ wavemaker provided water movement within the holding tank in 90-second cycles.

Tank filtration was identical in each system, and was accomplished via several methods. Biological filtration in the sump was accomplished via a Jaubert plenum (Jaubert, 1989). The plenum itself was constructed using 0.3" plastic egg crate lighting panel wrapped in fiberglass window screen. The plenum was positioned 1" from the bottom of the sump by ¾" inner diameter poly-vinyl chloride (PVC) pipes. Florida crushed coral (20 pounds) was placed directly above the plenum, and sand (90 pounds, sieved at 250 µm) collected from the New Jersey shore was placed directly above the crushed coral. Two small rocks (2-3 pounds each, 3" in diameter) with macroalgal growth, also collected from the New Jersey shore, were added to the sand bed. Lighting of the sump was provided by a 40 watt incandescent bulb operating on 12-hour light/dark cycles. A small 50 watt submersible heater (Tetra®) was added beneath the plenum to facilitate water diffusion through the sand bed. Mechanical and chemical filtration was accomplished using a protein skimmer/foam fractionator (Coralife® Super Skimmer™ 125G), which was cleaned weekly. Two sponge filters placed in the holding tank provided supplementary mechanical filtration. Finally, an untra-violet (UV) sterilizer (Coralife® Turbo Twist 3X™ with 9 watt UV bulb) was placed immediately before the submersible return pump to control algal growth and water-borne pathogens. Biweekly water changes (15-20% system volume) were also performed to limit nitrogenous and organic waste buildup and replace micronutrients and trace metals.



Figure 7-1. Representative example of maintenance aquarium setup. The upper aquarium is the display tank and held the corals and associates. Below the aquarium is the sump tank and requisite filtration compartments.

### 7.2.1.2 Experimental Aquaria Design and Setup

In order to maintain stability and consistency within the maintenance tanks, three smaller, all-glass aquaria were used for experimental testing. This design provided tight control and manipulation of environmental parameters, as well as a cost-effective means to perform replicated experiments. The experimental aquaria used were 20 gallon all-glass aquaria (24" x 13" x 17") covered with ¼" plexiglass and fitted with individual filtration units (AquaClear® 30) in a constant-temperature

room. Each filtration unit contained components for the three primary filtration types: a foam insert to remove debris and particulates (mechanical filtration), a granular-activated carbon insert (chemical filtration), and ceramic porous "bio-balls" to foster growth and proliferation of beneficial bacterial communities (biological filtration). To supplement water circulation provided by the filter, each aquarium was fitted with a circuit of Tygon® tubing powered by a submersible pump (Maxi-Jet).

### 7.2.1.3 Animal Collection, Maintenance, and Processing

All animals were collected from the Viosca Knoll leasing area in the northern GoM using the remotely-operated vehicle *Jason II* on two separate cruises in 2009 and 2010 with the necessary permits from the U.S. Department of Interior and NOAA National Marine Fisheries Service. The primary sampling locations within the area were lease blocks VK906 and VK826 (390-550 m depth). The VK826 *L. pertusa* reef is one of the most well-studied in the GoM (e.g. Cordes et al. 2008, Davies et al. 2010), and long-term data (11 months) show temperatures ranging from 6.5-11.6°C, salinity from 34.9-35.4, and mean current speed to be 8 cm s$^{-1}$ (with peaks at 38 cm s$^{-1}$, Mienes et al. 2012). At VK906, long-term (8 months) data show temperature ranging from 8-12.4°C and short-term data (12 hours) show salinity ranging from 34.9-35.5 (TDI-Brooks Intl. unpublished). To reflect these *in situ* conditions, the aquaria were maintained at a temperature of 8°C and a salinity of 35 ppt. Seawater was prepared regularly using distilled water and Instant Ocean® sea salt. Temperature was measured daily using a glass thermometer and salinity was measured daily using a refractometer (VitalSine®) that was calibrated daily.

Animals were transported to the laboratory in 4 liter screw-top polypropylene containers on ice via overnight air and ground transportation (total transit time was less than 24 hours). Upon return to the laboratory, each container was bubbled for 3 minutes with air and received 250 mL of maintenance aquaria seawater every hour for four hours. After transfer to the maintenance aquaria, corals were broadcast-fed MarineSnow® plankton diet three times weekly. MarineSnow® is a commercially-available mixture of zooplankton and phytoplankton that replicates the naturally-occurring particulate organic matter (typically known as "marine snow") that is found suspended throughout the water column, and is frequently observed at cold-water coral habitats (Frederiksen et al. 1992; Brooke et al. 2009). Mechanical filtration was suspended for one hour following each feeding. Galatheoid crabs in the aquaria were target-fed crushed frozen Mysis shrimp (Hikari Sales U.S.A., Inc.).

### 7.2.1.4 Carbonate Chemistry Manipulations

To reduce the elevated total alkalinity characteristic of synthetic seawater, 12.1 N HCl was added to seawater used in acidification experiments in order to reach a total alkalinity of 2,300 µmol·kg$^{-1}$, the mean total alkalinity of natural cold-water coral reefs in the GoM (Lunden et al. 2013). The amount of HCl added was determined by the following equation

$$V_{HCl} = \frac{[TA_i - TA_f] * m_{sw}}{N_{HCl}}$$

where

$V_{HCl}$ is the volume of HCl to be added in mL

264

$TA_i$ is the initial total alkalinity of Instant Ocean at salinity 35 ppt in $\mu mol \cdot kg^{-1}$
$TA_f$ is the final (desired) total alkalinity of 2,300 $\mu mol \cdot kg^{-1}$
$m_{sw}$ is the mass of seawater to be acidified in kg
$N_{HCl}$ is the normality (molarity) of HCl in $\mu mol \cdot mL^{-1}$

To acidify a given volume of seawater in gallons, one would first determine the mass of seawater by:
$$m_{sw} = 3.785 V_{sw} * D_{sw}$$
where
$m_{sw}$ is the mass of seawater
$V_{sw}$ is the volume of seawater in gallons
$D_{sw}$ is the density of seawater, 1.029 $kg \cdot L^{-1}$
3.785 is a conversion factor to convert gallons to liters

As an example, to acidify 20 gallons of Instant Ocean seawater at salinity 35 ppt and a total alkalinity of 3,600 $\mu mol \cdot kg^{-1}$ with hydrochloric acid at a concentration of 12,100 $\mu mol \cdot mL^{-1}$,
$$m_{sw} = (3.785*20)*1.029$$

$$m_{sw} = 77.895 \text{ kg}$$

and

$$V_{HCl} = \frac{[3600-2300]*77.895}{12100}$$

$$V_{HCl} = 4.51 \text{ mL}$$

Therefore, 4.51 mL of 12.1 N HCl would bring 20 gallons of 35 ppt Instant Ocean seawater to a total alkalinity of 2300 $\mu mol \cdot kg^{-1}$.

Total alkalinity was measured at 22°C according to SOP3b (Dickson et al. 2007) using a Mettler-Toledo DL15 autotitrator with 0.1 mol $L^{-1}$ HCl in 0.6 mol $L^{-1}$ NaCl solution and calibrated against certified reference materials (Dickson Lab, Scripps Institution of Oceanography). After seawater was brought to the target total alkalinity of 2,300 $\mu mol \cdot kg^{-1}$, it was aerated overnight with an air pump and air stone to drive off excess $CO_2$ from the acid addition step. After 48 hours of aeration, the seawater reached an ambient pH of 7.90 and was ready to be used for the experimental trials.

The recommended pH scale for ocean acidification experiments is the total hydrogen scale, which accounts for both free hydrogen ions as well as hydrogen ions complexed with water ($H_2O$) and sulfate ($SO_4^{2-}$) (Dickson 2010). In order to control pH on the total scale, Tris/HCl buffers of a similar ionic strength of seawater (0.7 M) can be used. For these purposes, all pH electrodes were calibrated weekly with Tris/HCl buffers using the recipes of Nemzer and Dickson (2005).

Manipulation of pH was accomplished via bubbling of pure $CO_2$ gas into the aquarium. $CO_2$, purchased from Airgas, was delivered from a five-pound cylinder to the aquaria through a $CO_2$ dosing system purchased from Drs. Foster and Smith. Bubbling of $CO_2$ was controlled by a pH

monitor (Pinpoint, American Marine Inc.) interfaced with a pH electrode in the aquarium and a solenoid valve on the gas regulator. When pH rose above a pre-determined setpoint appropriate for the experiment, the solenoid valve would open, releasing $CO_2$. $CO_2$ would then dissolve into the aquarium seawater through a $CO_2$ reactor. The flow rate of $CO_2$ was adjusted by a needle valve on the solenoid regulator, and monitored with a bubble counter. Using this system, we sought to control pH at 7.90, 7.75, and 7.60 for a period of two weeks. pH was recorded daily over the course of each experimental trial.

### 7.2.1.5 Dissolved Oxygen Manipulations

Dissolved oxygen concentrations were controlled via bubbling with oxygen-free nitrogen gas independently into each aquarium. Control of nitrogen flow was accomplished via CGA 580 dual-stage gas regulators with output valve controls (Airgas). First, the output valve was opened slightly to release a slow bleed of nitrogen into the aquarium, followed by adjusting the output pressure to 4 psi. Since the experimental aquaria were open systems (i.e. not closed off from atmospheric gas exchange), oxygen was able to re-enter the aquarium through surface diffusion. To achieve targeted dissolved oxygen concentrations, the output valve was carefully positioned to allow the bleed of nitrogen (and subsequent removal of oxygen) to equilibrate with the surface diffusion of oxygen and achieve the desired dissolved oxygen concentration. Using this system, we sought to control dissolved oxygen at 5, 3, and 1 mL·$L^{-1}$ for a period of two weeks.

### 7.2.2 Results

### 7.2.2.1 Maintenance Aquaria

The maintenance aquaria described above provide a stable setting that closely resembles the physical conditions (with the exception of pressure) experienced by cold-water corals and associated fauna in the GoM. Temperature has remained constant (8ºC) in both recirculating aquaria, partially due to the back-up support of aquarium chillers on emergency power in the event of malfunctions. Salinity has remained stable at 35 ppt through daily checks and occasional additions of distilled water. Nutrients (ammonia, nitrate, nitrite) have remained undetectable for several years, and have been controlled primarily via our filtration setup with supplemental partial water changes.

### 7.2.2.2 Experimental Aquaria

The experimental aquaria described above also provided a stable setting for experiments on *L. pertusa*. Temperature remained constant throughout all experiments, and the ¼" plexiglass lids effectively reduced evaporation and thus changes in salinity. Furthermore, the filtration units described above were effective in keeping ammonia, nitrate, and nitrite levels below 1.0 ppm at all times. The Tygon® tubing circuit powered by the Maxi-Jet pump facilitated complete circulation of the water and prevented accumulation of "dead zones" within each experimental aquarium.

### 7.2.2.3 Animal Collection, Maintenance, and Processing

Based on our observations, animals collected within 48 hours of shipping had the lowest mortality rates upon return to the laboratory. There was also a noticeable effect of transportation mode, with

animals shipped via air having significantly higher survivorship (100%) than animals shipped via ground (30-40%). Corals began expanding their polyps approximately three days after the initial transfer to the maintenance aquaria, and were fully expanded within seven days of transfer. When transferred to experimental aquaria, corals began expanding their polyps within one hour and all polyps were fully expanded within twelve hours.

Several species of deep-water invertebrates have survived continuously since 2009 in our holding tanks, supporting their efficacy. Time-lapse imagery of the aquaria shows episodic opening and closing of *Lophelia pertusa* polyps, although this was not periodic and aligned closely with feeding intervals. Time-lapse imagery also showed movement of the associated gastropod *Coralliophila* sp. and the crustacean *Eumunida picta*, opening and closing of serpulid worms, and construction of parchment tubes on coral skeletons and aquarium glass by the polychaete *Eunice* sp. We also observed several molting events of the crustacean *E. picta*, suggesting it received sufficient nutrition to maintain growth in the aquarium. While *in situ* behavioral analyses of cold-water coral communities are currently lacking, these observations agree with prior aquarium observations of these fauna in flow-through systems (Mortensen 2001, Mueller et al. 2013). No spawning of gametes or settling of larvae was apparent; however, spawning of *L. pertusa* in the field is attributed to seasonal environmental cues in the North Atlantic (Waller and Tyler 2005) and the GoM (Morrison et al. 2011).

### 7.2.2.4 Carbonate Chemistry Manipulations

The addition of hydrochloric acid to synthetic seawater effectively reduced the total alkalinity to the targeted value of 2300 $\mu mol \cdot kg^{-1}$. Because the method used to measure total alkalinity generally applies to the typical oceanic range of 2,000 to 2,500 $\mu mol \cdot kg^{-1}$ (Dickson et al. 2007), our initial measurements of total alkalinity in synthetic seawater were often underestimated by up to 400 $\mu mol \cdot kg^{-1}$. This often necessitated a second addition of a smaller volume of HCl to reach 2,300 $\mu mol \cdot kg^{-1}$. Once the target total alkalinity was reached, it did not change significantly over the course of our experimental trials (Figure 7-2).
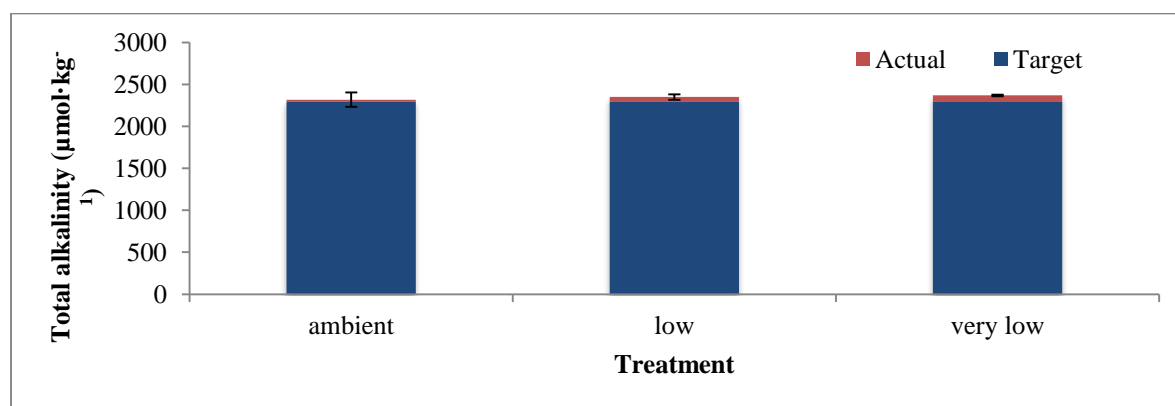


Figure 7-2.  Actual and target values of total alkalinity in carbonate chemistry manipulations. Error bars represent standard deviation of mean actual (observed) total alkalinity.

The off-the-shelf CO2 systems used here were primarily designed to control CO2 levels for plants in freshwater aquaria; however, they provided an effective means to reach the targeted pH values

267

within the scope of this study. One five-pound cylinder of CO2 per aquarium was sufficient to complete all pH experiments over the course of our experimental trials, which lasted over several months. Measured pH for each trial was $7.90 \pm 0.08$, $7.78 \pm 0.04$, and $7.67 \pm 0.10$ (mean $\pm$ s.d.,Figure 7-3). The variance in pH from our experimental trials is of a similar order to other recent ocean acidification studies using CO2 bubbling (e.g. Rodolfo-Metalpa et al. 2011; Edmunds 2012; Form and Riebesell 2012). We observed the greatest variance in pH in the lowest treatment (pH 7.60), where CO2 bubbling was most active. In rare, isolated occasions during the pH 7.60 trial, CO2 bubbling was temporarily disrupted due to faults with the CO2 controller. However, daily checks of the systems were sufficient to identify deficient controllers in our trials and maintain our targeted pH values.
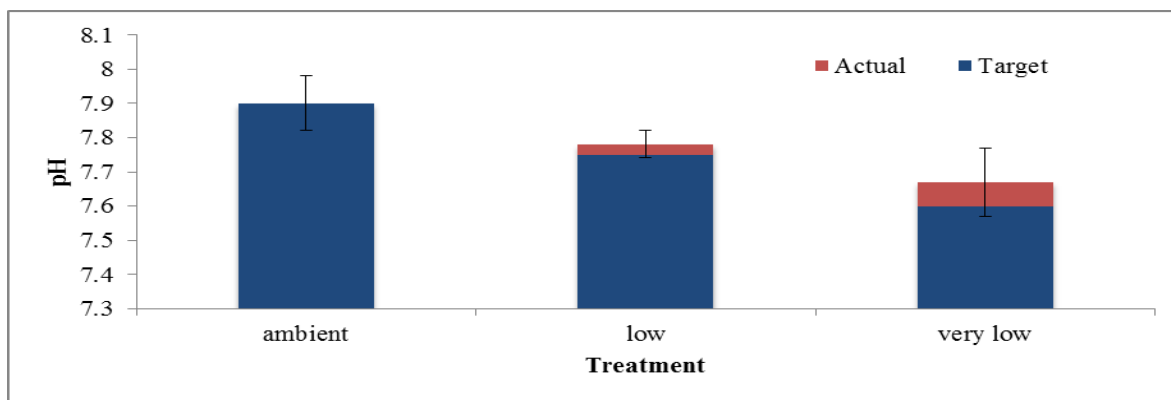


Figure 7-3.  Actual and target values of pH in carbonate chemistry manipulations. Error bars represent standard deviation of mean actual (observed) pH values.

### 7.2.2.5  Dissolved Oxygen Manipulations

Dissolved oxygen was maintained at target levels for each treatment. Measured DO for each trial was $5.32 \pm 0.28$ mL$\cdot$L$^{-1}$, $2.92 \pm 0.21$ mL$\cdot$L$^{-1}$, and $1.57 \pm 0.28$ mL$\cdot$L$^{-1}$ (mean $\pm$ s.d., Figure 7-4). Although we sought to reach 1 mL$\cdot$L$^{-1}$, the minimum oxygen concentration that we were able to achieve was 1.57 mL$\cdot$L$^{-1}$. It is likely that the diffusion of atmospheric oxygen back into the aquarium restricted reaching our minimum target DO. Nevertheless, our methods provided an effective way to manipulate and control DO values without the use of a mass-flow controller.
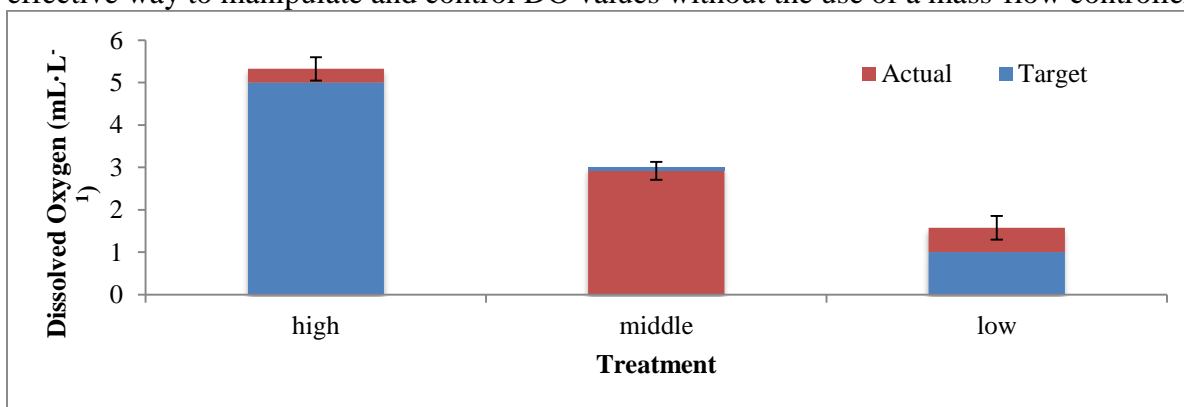


Figure 7-4. Actual and target values of dissolved oxygen in oxygen manipulations. Error bars represent standard deviation of mean actual (observed) dissolved oxygen values.

### 7.2.3 Discussion

This study describes an effective and practical means to maintain deep-water invertebrates for multiple years in the laboratory, independent of a natural seawater supply, including the ecologically relevant cold-water coral *L. pertusa*. In addition, our trials testing the manipulation of variables related to climate change (pH, dissolved oxygen) were effective at reaching and sustaining target treatment conditions for several weeks. Future work will include trials to assess longer-term control of these manipulations.

Because of the logistical challenges associated with collecting and maintaining deep-water corals, much of the research on them has been limited to ship-board experiments, and consequently lags behind related work on easily accessible shallow-water taxa. To date, only six laboratory-based manipulative studies of climate change variables exist for deep-water corals (Brooke et al. 2013, Dodds et al. 2007, Form and Riebesell 2012, Maier et al. 2012, Maier et al. 2013a, b), compared to the greater than twenty related studies of tropical and sub-tropical corals (as reviewed in Andersson et al. 2011). While several factors are responsible for this incongruity – including financial and logistical limits to the access of deep-water sites - it is our hope that improvements and developments in the husbandry of deep-water corals, including this work, will lead to greater insight into their responses to variables relevant to global climate change.

It is well-known that experiments in the laboratory cannot fully replicate the consortium of physical and biological variables observed in the field (e.g. pressure, alterations in current regimes and associated pulses of particulate material, interspecific interactions, etc.). However, laboratory studies are useful in characterizing responses to discrete perturbations and can help generate new avenues of investigation for future studies. Additionally, it is our hope that laboratory experiments such as those described here will aid in identifying potential thresholds of tolerance or mechanisms of resilience for important taxa in order to inform the management of sensitive deep-sea habitats.

One of the pivotal variables we found to affect cold-water coral endurance in the maintenance aquaria was water flow. We initially utilized two powerheads running simultaneously in the maintenance aquaria, but observed very few expanded coral polyps with this setup. We observed increased polyp expansion after installing a wavemaker to cycle power between the two powerheads, which clearly reduced the turbulence experienced by the corals. However, we observed maximal polyp expansion after removing one of the powerheads altogether, resulting in oscillations of turbulence and rest on 90-second cycles. On a related note, we also observed maximal polyp expansion when the sump outlets were positioned horizontally to distribute water across the surface layer of the aquarium. This positioning resulted in weakened water turbulence as opposed to vigorous turbulence when the outlets were positioned vertically, and the corals in our system appeared to be sensitive to this arrangement. Investigators seeking to utilize similar systems may need to modify one or both of these controls on water flow to simulate the natural environment or needs of species acclimatized to different flow regimes.

During the course of our studies, we tested several shipping methods for transporting animals to our laboratory in 2009 and 2010. We found that shipping via next-day air resulted in 100% survivorship of animals. While often more economical, ground transportation generally exposes the animals to greater disturbance during transit. We recommend air travel whenever appropriate and possible.

## 7.3 OBSERVATIONS OF FAUNA IN LABORATORY AQUARIA

Behavioral observations were recorded by time-lapse photography in the maintenance aquaria. Still photographs were taken hourly with a Canon® EOS 50 digital camera controlled by a Canon® TC-80N3 remote timer. The camera was positioned approximately one (1) meter from the aquarium. Animal movement rates were quantified using a scale bar in the frame of the camera and distance was standardized by the diameter of PVC pipes (5 cm).

### 7.3.1  *Lophelia pertusa*

For each frame with sufficient photo quality, the number of extended polyps on each nubbin was counted and recorded.  The percentage of visible polyps per nubbin was then correlated against a continuous time cycle divided into twenty-four-hour resolution periods.  No significant pattern of coral activity was observed, though a higher than average percentage of extended coral polyps was observed in the period immediately after a feeding event (Marine Snow®).  The corals did not show evidence of anticipating food delivery, despite maintaining a regular feeding schedule.

During the early experimental trials, very few polyps were visible by researchers entering the cold room.  It was later determined that the vibrations from opening the door induced retraction. Although a causal relationship could be not evaluated, the corals were often retracted when the squat lobster was visible in close proximity to the nubbins.  It is possible that this coral retraction is a distinct, interspecific response, though it may be that source-nonspecific vicinal vibrations induce instinctual retraction.

### 7.3.2  *Coralliophila* sp.

The aquarium observations included *Coralliophila* sp., a genus of coral eating snail commonly found in association with *Lophelia* reefs.  Although the snails are known to be corallivorous (Brawley and Adey 1982) no photographs from the time-lapse directly recorded this feeding behavior.  Snails were observed on the corallium, but never on the skeleton immediately surrounding the calyx. It was not uncommon that snails would remain stationary for several days between relocating, then expend significant effort to reposition over the course of a few hours. Minor adjustments, such as changing orientation or displacement of less than 5 cm, were frequent. During a ten hour period on November 15th, 2011, one specimen of *Coralliophila* sp. changed its position at a maximum rate of 10 to 15 cm per hour, the highest rate observed during time-lapse recordings. It is not known what motivated such a significant displacement as its final destination was beyond the scope of the camera.

### 7.3.3  *Eunice* sp.

Previous studies have detailed the mutualism between *Lophelia pertusa* and the polychaete worm, *Eunice norvegica* (Roberts 2005, Mueller et al. 2013).  Using a similar time-lapse technique, Roberts (2005) observed the polychaete worm transplant a smaller coral fragment and join the two via the secretion of the parchment tube in which the worm resides. The fragment transplant required slightly more than one minute to complete, while the parchment tube developed over a four month period.  It is believed that these parchment tubes form a substrate between branches across which the polyps can anastomize.

Over the course of this time-lapse study, coral fragments lying directly on the glass bottom of the aquarium would inexplicably shift between photographs. Several frames suggest the squat lobster or *Eunice* worms may disturb smaller fragments not epoxied to PVC base. However, due to the 1-hour lapse between photographs, it was difficult to conclusively attribute fragment movement to the *Eunice* polychaete worm. The best example of worm aggregation appeared in the lapse between 2:58AM and 3:58AM on February 18th, 2012 (Figure 7-5). Although no visible parchment tubes were formed during the study period, the previous study (Roberts 2005) consisted of long-term observations starting in October 1998, with parchment tube formation not observed until October 2004.
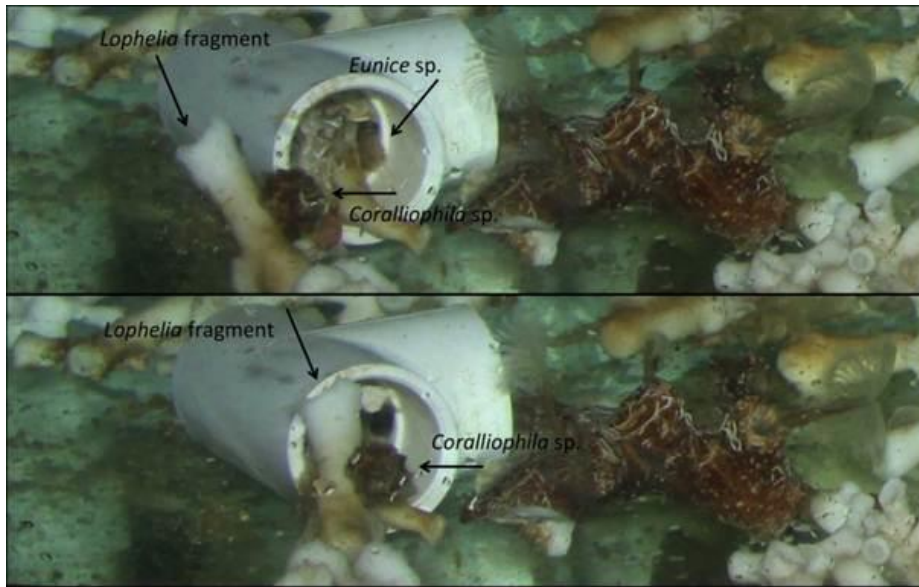


Figure 7-5. Example of consecutive time-lapse photographs showing movement of *Lophelia pertusa* fragment, likely caused by the activity of *Eunice sp.* inhabiting a small PVC coral mount. Also shown is the typical position of the *Coralliophila sp.* gastropod on the *Lophelia* fragment.

## 7.4 pH EXPERIMENTS

### 7.4.1 Methods

#### 7.4.1.1 Experimental Design and Setup

Each experiment was conducted in a constant-temperature room at Temple University (TU). Three 20 gallon aquaria ("tall" type: 24" x 13" x 17") with individual filtration units (AquaClear 30) and pH controllers (Pinpoint®, American Marine Inc.) were used for each experiment (Figure 7-6). Three individual coral nubbins of unique genotype were randomly assigned to each tank for a total of nine nubbins per treatment. Each experiment lasted for a total of fifteen days, with an initial eight-day conditioning period to allow the corals to acclimate to the tank conditions. Growth was measured between days eight and fifteen to obtain a daily growth rate. Mortality was measured daily and at the conclusion of each treatment.

The following experiments were conducted:
  1. pH: ambient (7.90), low (7.75), very low (7.60)
  2.
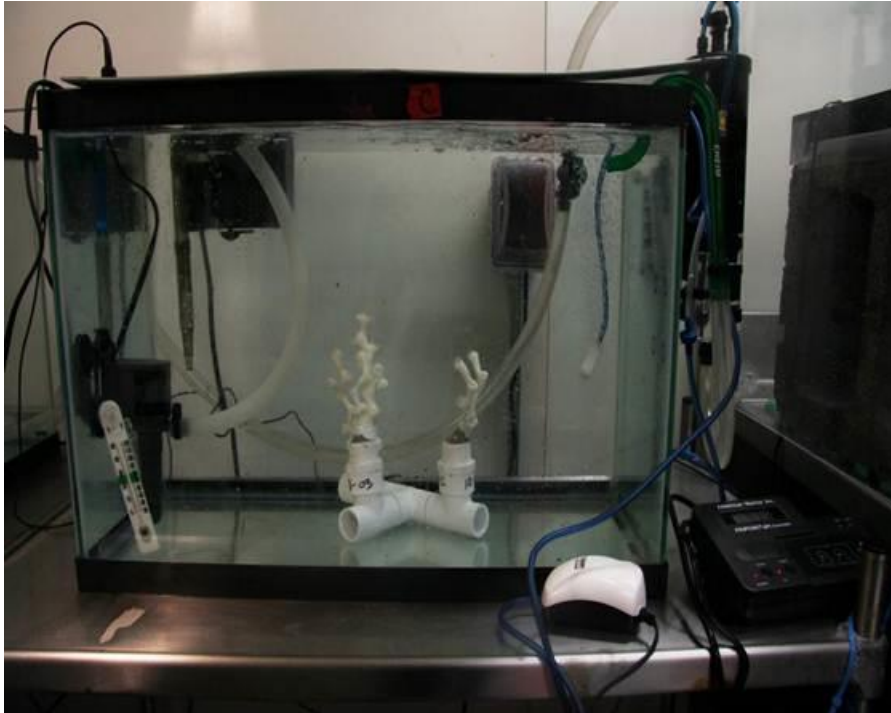


Figure 7-6.  Experimental aquarium (20 gallons) with pH controller setup.

### 7.4.1.2  Sample Collection, Preparation, and Maintenance

Colonies of *Lophelia pertusa* were collected during the 2010 *Lophelia* II cruise using ROV *Jason II*. Coral branches were placed in temperature-insulated bioboxes (volume = ~20 L) at depth.  Upon return to the surface, corals were kept alive in 5 gallon aquaria in the ship's constant-temperature room.  Upon return to port, coral samples were immediately transported overnight to TU.

At TU, corals were maintained in one of two holding tanks (recirculating, 120 gallons and 90 gallons) at temperature 8°C and salinity 35 ppt. Regular partial water changes (15-20%) were performed with seawater made using Instant Ocean® sea salt. Submersible power heads were placed in each holding tank to ensure water movement and turbulence sufficient to cause swaying of coral polyps.  Corals were fed three times weekly using a combination of MarineSnow® Plankton Diet (Two Little Fishies, Miami Gardens, FL) and freshly hatched *Artemia* nauplii.

Prior to experimental manipulations, coral branches were fixed to 1" PVC male adapters using HoldFast epoxy to minimize handling (Figure 7-7).  Monofilament line (diameter = 0.30 mm) was looped through each PVC adapter to allow for buoyant weighing of the coral branch (see growth measurements below).  All coral branches weighed less than 60 g in water.  For the experiments, corals were first fragmented into nubbins using bone cutters. The nubbins were then fixed to ¾" PVC male adapters with HoldFast® epoxy resin and secured to a PVC support base. All nubbins were subsequently swabbed for genotypic analyses; no mortality resulted from swabbing of

nubbins. After accounting for differences in genotype, nubbins were randomly assigned to one of three tanks for each experimental treatment.



Figure 7-7. *Lophelia pertusa* attached to 1" PVC male adapter pieces in the maintenance aquarium.

The pH experiment consisted of three treatments to compare growth of *L. pertusa* at ambient pH (7.90), low pH (7.75), and very low pH (7.60). Each treatment was conducted on two separate groups (henceforth "group 1" and "group 2") of coral nubbins. Experimental incubations were maintained at temperature 8°C and salinity 35 ppt. pH was controlled by injection of $CO_2$ using a Pinpoint® pH controller (American Marine Inc., Ridgefield, CT). pH electrodes were calibrated weekly using Tris-HCl and AMP-HCl buffers (Dickson et al. 2007).

The temperature experiment consisted of five treatments to compare growth and mortality of *L. pertusa* at 8°C, 10°C, 12°C, 14°C, and 16°C. Experimental incubations were maintained at pH 7.90 and salinity 35 ppt. The experimental aquaria were maintained in a constant-temperature room, and the temperature of the room was adjusted as appropriate for each treatment.

The dissolved oxygen experiment consisted of three treatments to compare mortality of *L. pertusa* under low-level dissolved oxygen (1 mL·L$^{-1}$), middle-level dissolved oxygen (3 mL·L$^{-1}$), and high-level dissolved oxygen (5 mL·L$^{-1}$). Experimental incubations were maintained at temperature 8°C and salinity 35 ppt. To manipulate dissolved oxygen concentrations, oxygen-free nitroge gas was bubbled into each tank through a $CO_2$ reactor (Aqua Medic 1000). Flow of nitrogen was controlled with CGA 580 regulators (Airgas). Dissolved oxygen concentration in each aquarium was recorded each day with an Orion 5 Star DO/pH meter (calibrated daily).

### 7.4.1.3  Seawater Preparation and Analyses

Experimental seawater was prepared using Instant Ocean® sea salt at a salinity of 35 ppt.  Since Instant Ocean® produces seawater with a total alkalinity of approximately 3600 $\mu mol \cdot kg^{-1}$ (1.5X that of natural oceanic values), 12.1 N HCl was added to reduce the total alkalinity to 2300 $\mu mol \cdot kg^{-1}$ (mean total alkalinity at GoM *L. pertusa* reefs, Lunden et al. 2013). The seawater was then bubbled with oxygen for ~24 hours to drive off excess $CO_2$ and to restore pH to ambient conditions (7.90).

Total alkalinity was measured twice weekly in each aquarium by potentiometric open-cell titration using a Mettler-Toledo DL15 automatic titrator according to SOP3b (Dickson et al. 2007) with certified reference materials courtesy of A. Dickson (Scripps). pH (total hydrogen scale) was recorded daily using the Pinpoint® pH controller.  The aragonite saturation state was calculated using CO2SYS (Pierrot et al. 2006) with total alkalinity, pH, temperature, and salinity as input variables. Nutrient concentrations (ammonia [$NH_3$], nitrate [$NO_3^-$], and nitrite [$NO_2^-$]) were measured weekly using API® aquarium test kits.

### 7.4.1.4  Survivorship Measurements

Survivorship was assessed by daily observations of polyp tissue presence and behavior. Final survivorship counts were taken 3 to 4 days following the end of an experiment after transfer to the maintenance tank, as in Brooke et al. (2013). Survivorship is reported as cumulative survivorship, the percentage of live polyps at the end of each treatment compared to the original number of live polyps at the beginning of the experimental series.

### 7.4.1.5  Growth Measurements

Each coral nubbin was weighed at the start and end of the experimental period (seven days) by the buoyant weight technique (Davies et al. 1989) using a Denver Instruments SI-64 analytical balance (d = 0.1 mg).  A weighing chamber was constructed using ½" plexiglass to prevent air movement from disturbing the balance.  Each coral was transported from its respective aquarium to the weighing chamber in a four liter Pyrex® beaker and suspended from the balance.  The buoyant weight was recorded only after the coral nubbin stabilized (typically after 2 minutes).  Each coral nubbin was weighed three times to determine measurement precision (~2-3 mg). Seawater density was determined by buoyantly weighing a 2.5 $cm^2$ aluminum block with known density (2.7 $g \cdot cm^{-3}$).

Coral weight in air (i.e. dry weight) was calculated by the following equation:
$$W_a = \frac{W_w}{1 - \frac{D_w}{SD}}$$

Where
$W_a$ = coral weight in air (dry weight)
$W_w$ = coral weight in water (buoyant weight)
$D_w$ = density of seawater
$SD$ = coral skeletal density (= 2.82 $g \cdot cm^{-3}$, taken from Lunden et al. 2013)

Coral growth rate is reported as percent growth per day ($\% \cdot d^{-1}$), which was calculated by the equation:

$$G_t = 100 \times \frac{M_{t2} - M_{t1}}{M_{t1}(T_2 - T_1)}$$

Where

$G_t$ = growth rate as $\% \cdot d^{-1}$
$M_{t2}$ = mass (mg, dry weight) at time 2 (end of experimental period, day fifteen)
$M_{t1}$ = mass (mg, dry weight) at time 1 (start of experimental period, day eight)
$T_2$ = time 2 (end of experimental period, day fifteen)
$T_1$ = time 1 (start of experimental period, day eight)

### 7.4.1.6 Statistical Analyses

We used one-way ANOVA and Tukey's honestly significant differences (HSD) to test for significances in survivorship and growth rates across experimental treatments where assumptions for parametric tests were met. When parametric assumptions were not met, we used the nonparametric Mann-Whitney and Kruskal-Wallis tests. All statistical analyses were performed using JMP10® statistical software.

### 7.4.2 Results

pH was maintained at target levels for each treatment (see Table 7-1 and Figure 7-8). For the group 1 coral experiments, pH varied significantly across all three treatments (Kruskal-Wallis test, H = 19.7481, p < 0.001). pH was 7.90 ± 0.05 for the ambient pH treatment, 7.79 ± 0.06 for the low pH treatment, and 7.67 ± 0.15 for the very low pH treatment. Pairwise comparisons reveal significant differences in pH between each treatment (see Table 7-2). For the group 2 coral experiments, pH varied significantly across all three treatments (Kruskal-Wallis test, H = 30.1405, p < 0.001). pH was 7.90 ± 0.08 for the ambient pH treatment, 7.78 ± 0.04 for the low pH treatment, and 7.67 ± 0.10 for the very low pH treatment. Pairwise comparisons reveal significant differences in pH between each treatment (see Table 7-3).

Table 7-1.

Experimental conditions (mean ± S.D.) of pH experiment

| Treatment | pH | | $\Omega_{arag}$ | |
| --- | --- | --- | --- | --- |
| | Group 1 | Group 2 | Group 1 | Group 2 |
| Ambient | 7.90 ± 0.05 | 7.90 ± 0.08 | 1.47 ± 0.17 | 1.47 ± 0.23 |
| Low | 7.79 ± 0.06 | 7.78 ± 0.04 | 1.18 ± 0.18 | 1.11 ± 0.10 |
| Very low | 7.67 ± 0.15 | 7.67 ± 0.10 | 0.97 ± 0.39 | 0.92 ± 0.23 |
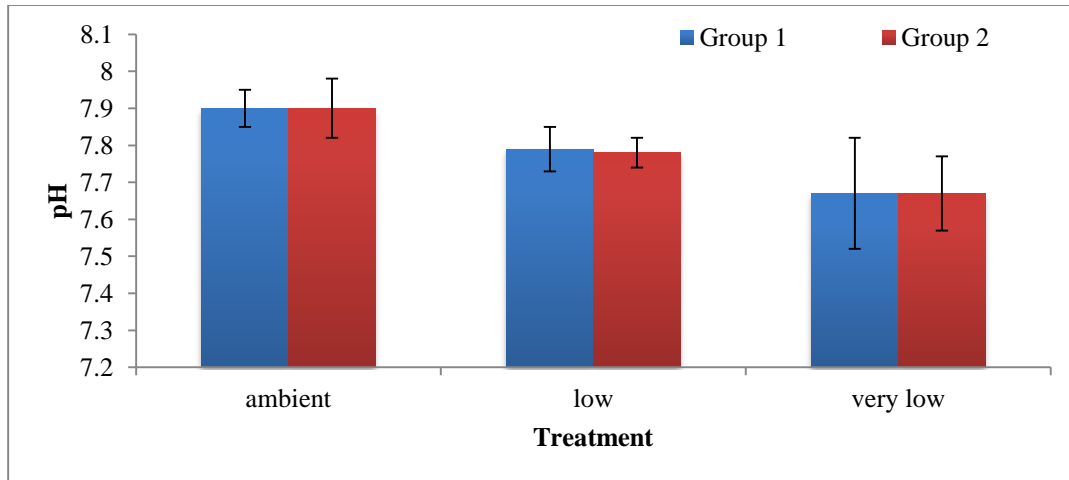
Figure 7-8. pH conditions (mean ± S.D.) for groups 1 and 2 for the pH experiments.


Table 7-2.

Pairwise comparisons ($\alpha = 0.05$) of pH among treatments in group 1 pH experiment

|  | Ambient | Low | Very low |
|---|---|---|---|
| Ambient |  |  |  |
| Low | 0.0004 |  |  |
| Very low | 0.0007 | 0.0034 |  |


Table 7-3.

Pairwise comparisons ($\alpha = 0.05$) of pH among treatments in group 2 pH experiment

|  | Ambient | Low | Very low |
|---|---|---|---|
| Ambient |  |  |  |
| Low | <0.0001 |  |  |
| Very low | <0.0001 | 0.0004 |  |


The target aragonite saturation state ($\Omega_{arag}$) was maintained for each treatment (see Figure 7-8 and Figure 7-9). For the group 1 coral experiments, $\Omega_{arag}$ varied significantly across all three treatments (Kruskal-Wallis test, H = 20.4448, p < 0.001). $\Omega_{arag}$ was 1.47 ± 0.17 in the ambient pH treatment, 1.18 ± 0.18 in the low pH treatment, and 0.97 ± 0.39 in the very low pH treatment. Pairwise comparisons reveal significant differences in $\Omega_{arag}$ between each treatment (see Table 7-4). For the group 2 coral experiments, $\Omega_{arag}$ varied significantly across all three treatments (Kruskal-Wallis test, H = 30.859, p < 0.001). $\Omega_{arag}$ was 1.47 ± 0.23 in the ambient pH treatment, 1.11 ± 0.10 in the low pH treatment, and 0.92 ± 0.23 in the very low pH treatment. Pairwise comparisons reveal significant differences in $\Omega_{arag}$ between each treatment (see Table 7-5).

276
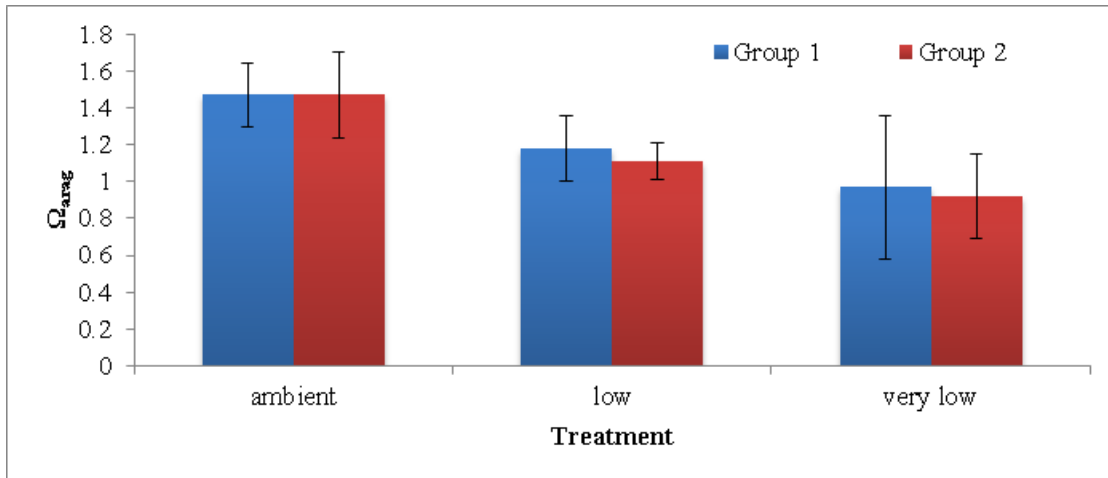
Figure 7-9. Ωarag conditions (mean ± S.D.) for groups 1 and 2 for the pH experiments.


Table 7-4.

Pairwise comparisons ($\alpha = 0.05$) of $\Omega_{arag}$ among treatments in group 1 pH experiment

|  | Ambient | Low | Very low |
|---|---|---|---|
| Ambient |  |  |  |
| Low | 0.0002 |  |  |
| Very low | 0.0007 | 0.0036 |  |


Table 7-5.

Pairwise comparisons ($\alpha = 0.05$) of $\Omega_{arag}$ among treatments in group 2 pH experiment

|  | Ambient | Low | Very low |
|---|---|---|---|
| Ambient |  |  |  |
| Low | <0.0001 |  |  |
| Very low | <0.0001 | 0.0007 |  |


Average growth rates for *L. pertusa* group 1 corals were $0.011 \pm 0.003$, $0.006 \pm 0.002$, and $-0.008 \pm 0.03$ %·d$^{-1}$ for ambient, low, and very low pH treatments, respectively (mean ± SE, Figure 7-10). Growth rate was not significantly different between the ambient and low pH treatments (Mann-Whitney U test, U = -1.31276, p = 0.1893). Growth rate was significantly affected (relative to ambient) in the very low pH treatment, where net dissolution was observed. Survivorship was 100% across all treatments.
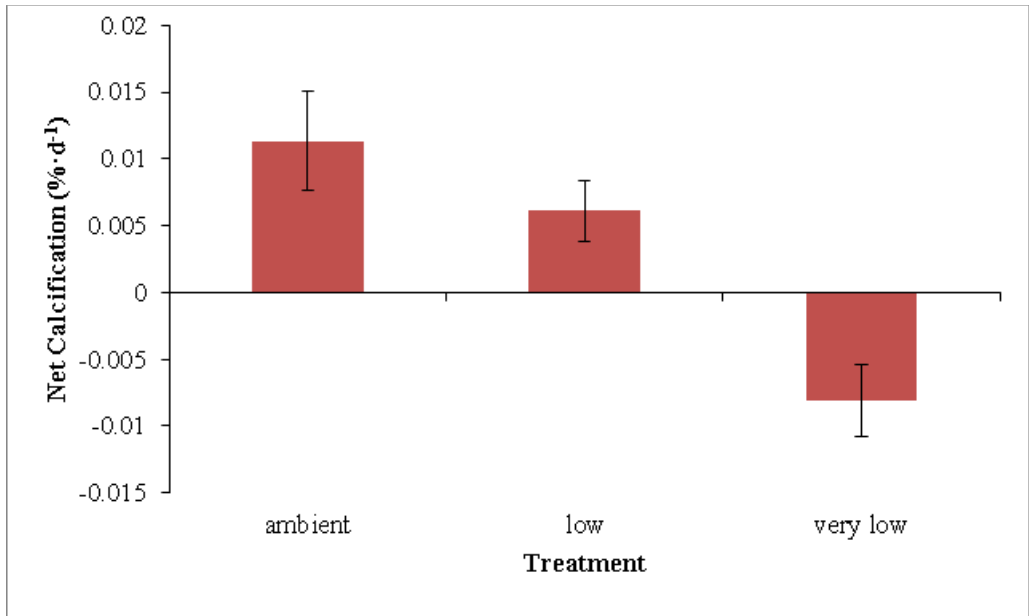
Figure 7-10.  Growth of *L. pertusa* (over 7 days, mean ± S.E.) from the group 1 pH experiments.

Average growth rates for *L. pertusa* group 2 corals were $0.039 \pm 0.01$, $-0.012 \pm 0.004$, and $-0.005 \pm 0.003$ %·d$^{-1}$ for ambient, low, and very low pH treatments, respectively (mean ± SE, Figure 7-11). Growth rate was significantly affected (relative to ambient) in both the low and very low pH treatments, where net dissolution was observed. Growth rate was not significantly different between the low and very low pH treatments (Mann-Whitney U test, $U = -0.9977$, $p = 0.3184$). Survivorship was 100% across all treatments.
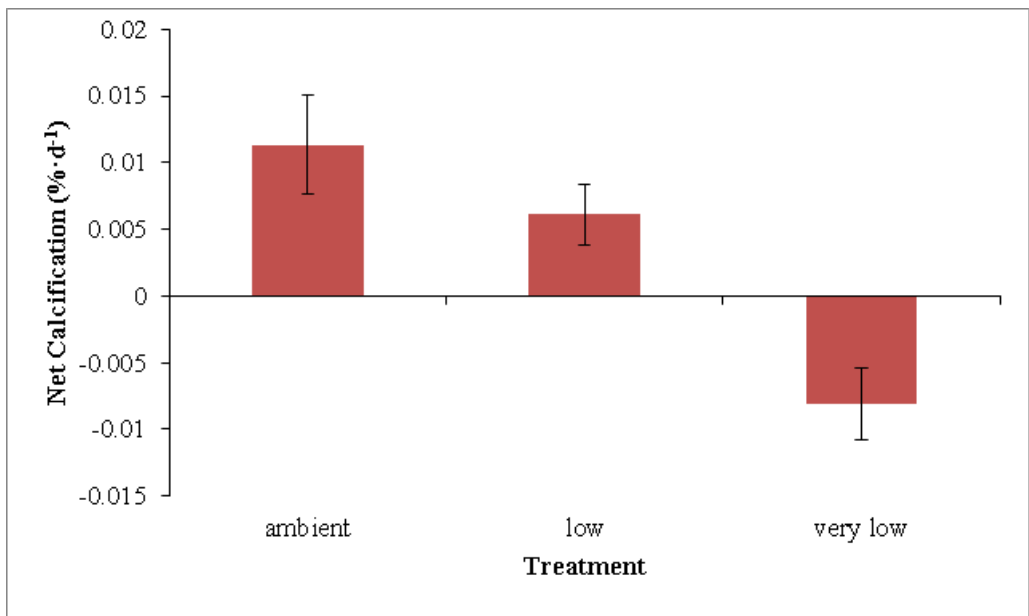


Figure 7-11.  Growth of *L. pertusa* (over 7 days, mean ± S.E.) from the group 2 pH experiments.

Coral growth rates differed significantly between group 1 and group 2 in the ambient treatment (Mann-Whitney U test, U = -2.4679, p = 0.0136) and the low treatment (Mann-Whitney U test, U = 3.3082, p = 0.0009). In the very low treatment, both experimental groups responded similarly (Mann-Whitney U test, U = -0.4726, p = 0.6365) by undergoing net dissolution (Figure 7-12). No tank effects were observed in any treatment (see Table 7-6). To constrain the critical threshold for calcification to occur beyond the *a priori* observations from the pH treatments, a linear regression of calcification of each coral to the measured pH and aragonite saturation state of each tank was performed. Results from this analysis show a critical pH of 7.73 (Figure 7-13) and aragonite saturation state of 1.06 (Figure 7-14) for net calcification to occur.
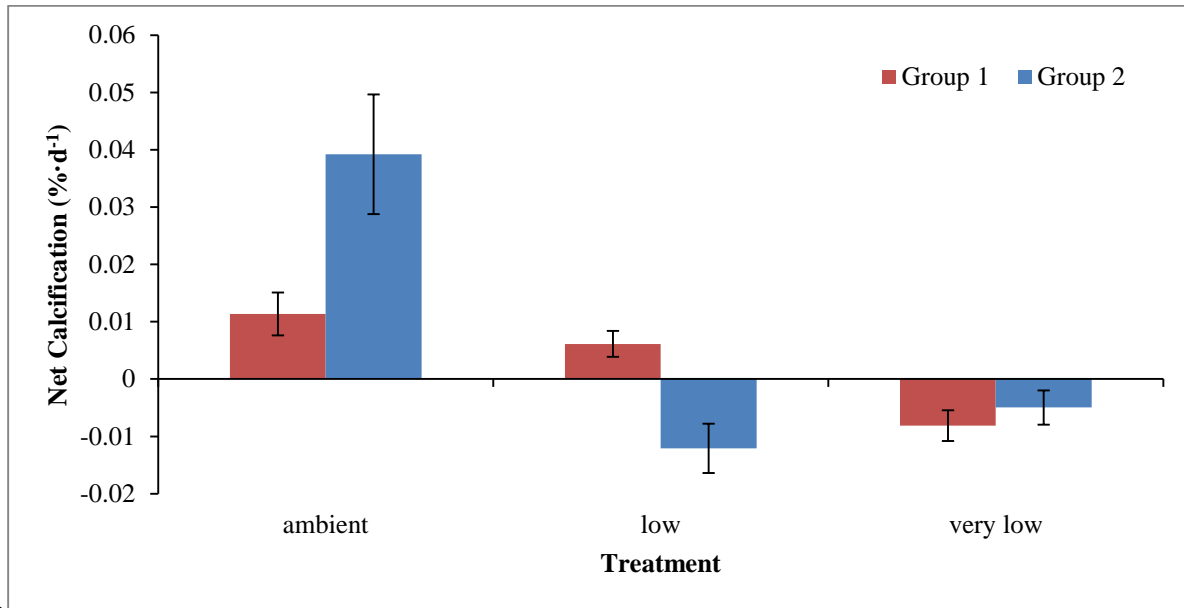


Figure 7-12.  Growth of *L. pertusa* (over 7 days, mean ± S.E.) from both groups 1 and 2 for the pH experiment.

Table 7-6.

Results from Kruskal-Wallis tests (α = 0.05) on tank effects (differences in growth rate among tanks) in pH experiment

| Treatment | H | | p | |
|---|---|---|---|---|
| | Group 1 | Group 2 | Group 1 | Group 2 |
| Ambient | 0.6944 | 0.5556 | 0.7066 | 0.7575 |
| Low | 0.2222 | 0.0278 | 0.8948 | 0.9862 |
| Very low | 5.1389 | 0.2222 | 0.0766 | 0.8948 |
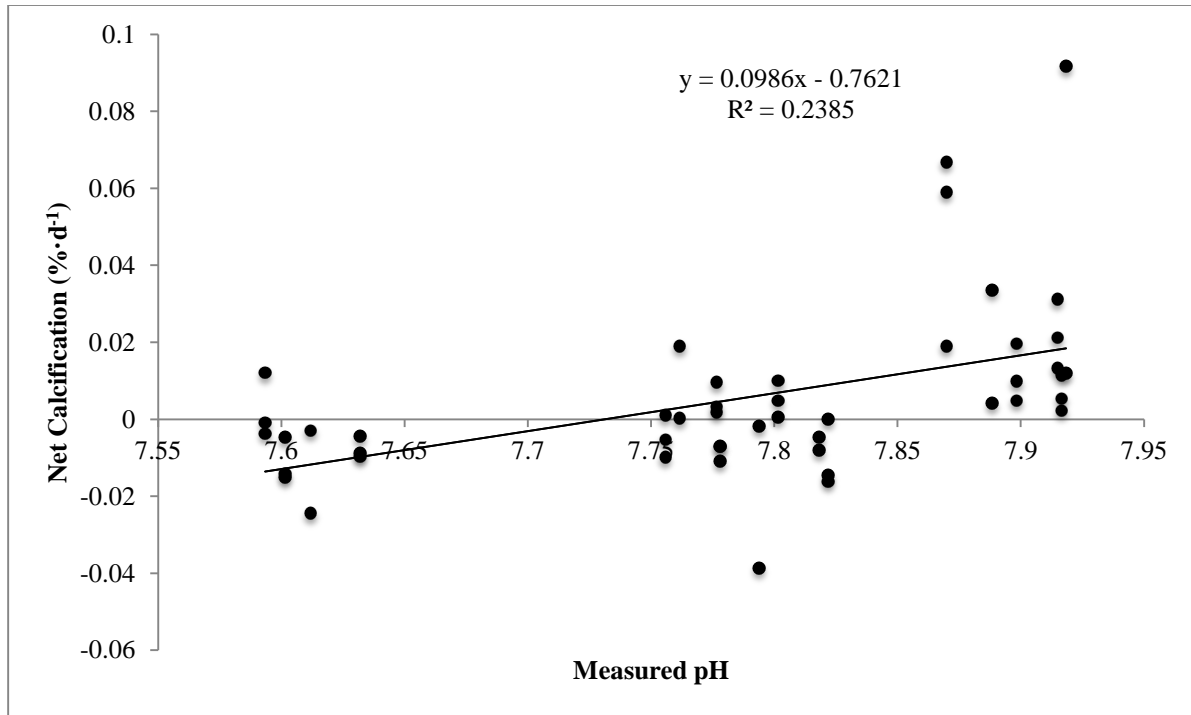
Figure 7-13.  Linear regression of *L. pertusa* growth to measured pH (over 7 days, mean ± S.E.) from both groups 1 and 2 for the pH experiment.
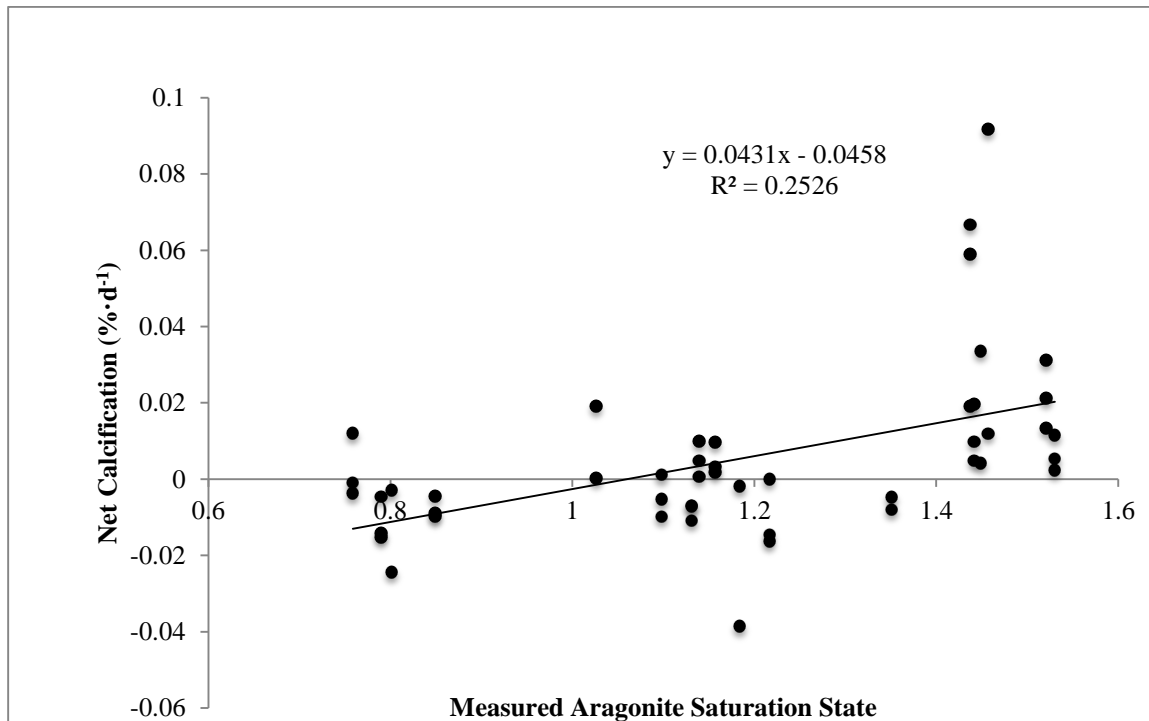


Figure 7-14.  Linear regression of *L. pertusa* growth to measured aragonite saturation states (over 7 days, mean ± S.E.) from both groups 1 and 2 for the pH experiment.

## 7.4.3 Discussion

Mortality due to pH stress has not been reported in the literature. In fact, acidification experiments over 12 months resulted in no mortality in the scleractinian species *Oculina patagonica* and *Madracis pharencis*; however, complete dissolution of the skeleton was observed in both species (Fine and Tchernov 2007). This implies that low pH may not necessarily contribute directly to mortality in scleractinian corals including *L. pertusa*, but may subject the corals to increased exposure to predators such as the gastropod *Coralliophila* sp.

Our growth rate results from the ambient pH treatments agree well with published data for *L. pertusa* from the North Atlantic Ocean (Maier et al. 2009) and the Mediterranean Sea (Orejas et al. 2011, Form and Riebesell 2012, Maier et al. 2012). The growth rates between the two groups were significantly different at ambient conditions, and this difference may be attributed to the biological variation between the two groups. Furthermore, variability in *L. pertusa* growth rate has been reported in recent papers (Maier et al. 2009, Form andRiebesell 2012, Maier et al. 2012). Factors such as polyp rank (i.e. age) and size are recognized as major contributors to coral growth rate, with younger, higher ranked polyps growing faster than older polyps (Mortensen 2001, Brooke and Young 2009). While both groups in our experiment consisted of similarly-sized coral nubbins, no data is available on polyp age.

The results from this set of experiments suggest a complex set of responses to ocean acidification in *L. pertusa* from the GoM. Perhaps the most striking result in this set of experiments is the disparate response of the two groups in the low pH (7.75) treatment. While the two groups did not experience statistically significant different conditions in pH or aragonite saturation state, mean pH and mean $\Omega_{arag}$ were slightly lower (by 0.1 pH units and 0.08 in $\Omega_{arag}$) in the group 2 treatments (Figure 7-11 and Figure 7-12, Table 7-1). These slight differences, though not statistically significant, may be biologically relevant to calcification in *L. pertusa*.

The difference in responses may also be attributed to the genotypic variation of the two experimental groups. Variation among responses to ocean acidification with respect to genotype has also been observed in bryozoans (Pistevos et al. 2011), oysters (Parker et al. 2012), and coccolithophores (Langer et al. 2009). Recently, Schaum et al. (2013) found that geographic location and life history (i.e. ecotype) are vital contributors to plastic responses to ocean acidification in picoplankton. Since all coral specimens used in our pH treatments were from the same geographic location (VK906), it is likely that genotype played a larger role than ecotype in this experiment.

Thresholds for calcification in a variety of calcifying species often do not often coincide with an aragonite saturation state equal to 1.0. For example, various studies in shallow-water corals identify the threshold for calcification to occur at 2.0 (reviewed in Doney et al. 2009). Because *L. pertusa* is most often observed at *in situ* aragonite saturation states significantly below 2.0 (Form and Riebesell 2012, Lunden et al. 2013), its threshold for calcification must fall under its observed environmental range. The present study identifies a calcification threshold of 1.06, significantly lower than the threshold observed in shallow-water taxa. Form and Riebesell (2012) observed positive net calcification at an aragonite saturation state of 0.93 in a long-term study, suggesting acclimation to reductions in aragonite saturation state; however, the samples used in this study come from only two biological replicates. In the present study, one *L. pertusa* genet sustained net

positive calcification at an aragonite saturation state of 0.75. While *L. pertusa* may in fact be able to acclimate to ocean acidification, it is not clear if the results obtained in Form and Riebesell (2012) are due entirely to acclimation or to an as-yet-unidentified mechanism, potentially under genetic control, that confers resistance to ocean acidification. Results from a boron systematics study show *L. pertusa*'s capability to up-regulate pH and aragonite saturation state at the calcification site (McCulloch et al. 2012); however, it is unclear if this mechanism applies universally to *L. pertusa* individuals across a range of populations. Future work should further investigate the role of genetic variability to ocean acidification responses.

## 7.5 TEMPERATURE EXPERIMENTS

### 7.5.1 Methods

#### 7.5.1.1 Experimental Design and Setup

Each experiment was conducted in a constant-temperature room at TU. Three 20 gallon aquaria ("tall" type: 24" x 13" x 17") with individual filtration units (AquaClear 30) and pH controllers (Pinpoint®, American Marine Inc.) were used for each experiment (Figure 7-6). Three individual coral nubbins of unique genotype were randomly assigned to each tank for a total of nine nubbins per treatment. Each experiment lasted for a total of fifteen days, with an initial eight-day conditioning period to allow the corals to acclimate to the tank conditions. Growth was measured between days eight and fifteen to obtain a daily growth rate. Mortality was measured daily and at the conclusion of each treatment.

The following temperature experiments were conducted: 8, 10, 12, 14, 16°C

Methods for seawater analyses, survivorship, and growth measurements are identical to those described above for the pH experiments.

### 7.5.2 Results and Discussion

Temperature was maintained at target levels for each treatment (see Table 7-7 and Figure 7-15). Temperature was significantly different across all treatments (Kruskal-Wallis test, H = 92.1309, p < 0.001). Pairwise comparisons revealed significant differences in temperature between each treatment (see Table 7-8). In the 16°C experiment, pH was significantly higher than all other temperature treatments (Figure 7-15, Kruskal-Wallis test, H = 10.6864, p = 0.0303). $\Omega_{arag}$ varied significantly among treatments (Figure 7-17, Kruskal-Wallis test, H = 63.5289, p < 0.0001) but was statistically similar between the 8°C and 10°C experiments (Mann-Whitney test, U = 0.02819, p = 0.9775).

Table 7-7.

Experimental conditions (mean ± s.d.) of temperature experiment

| Treatment (°C) | Temperature (°C) | pH | $\Omega_{arag}$ |
|---|---|---|---|
| 8 | 8.36 ± 0.23 | 7.92 ± 0.04 | 1.53 ± 0.14 |
| 10 | 9.91 ± 0.52 | 7.92 ± 0.04 | 1.54 ± 0.12 |
| 12 | 11.93 ± 0.28 | 7.89 ± 0.07 | 1.68 ± 0.21 |
| 14 | 14.02 ± 0.29 | 7.93 ± 0.03 | 1.92 ± 0.14 |
| 16 | 16.03 ± 0.48 | 7.95 ± 0.04 | 2.08 ± 0.18 |
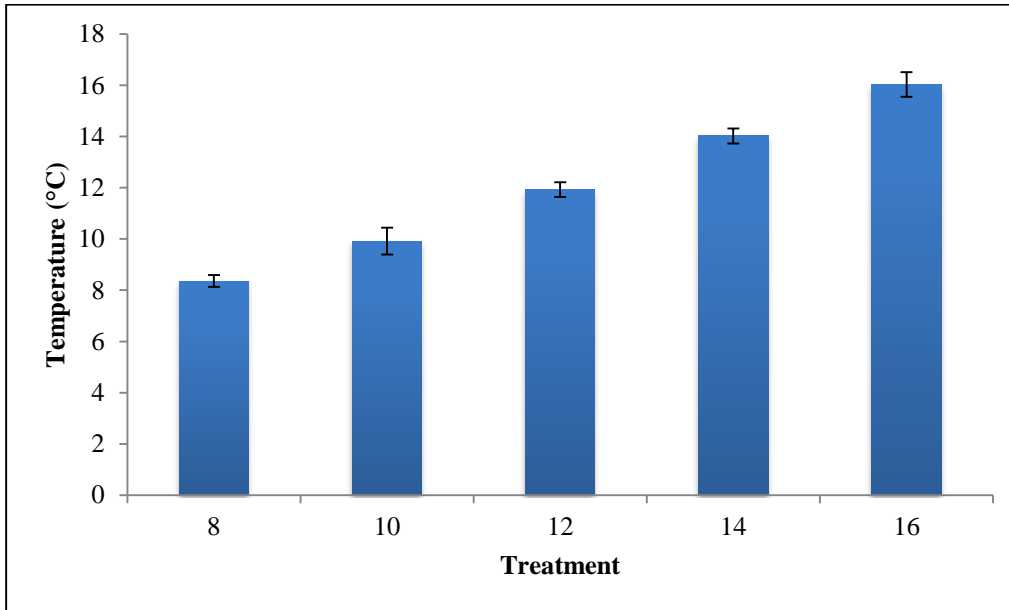


Figure 7-15.  Temperature conditions (mean ± s.d.) for the temperature experiments.

Table 7-8.

Pairwise comparisons ($\alpha = 0.05$) of temperature among treatments in the temperature experiment

|  | 8 | 10 | 12 | 14 | 16 |
|---|---|---|---|---|---|
| 8 |  |  |  |  |  |
| 10 | <0.0001 |  |  |  |  |
| 12 | <0.0001 | <0.0001 |  |  |  |
| 14 | <0.0001 | <0.0001 | <0.0001 |  |  |
| 16 | <0.0001 | <0.0001 | <0.0001 | <0.0001 |  |
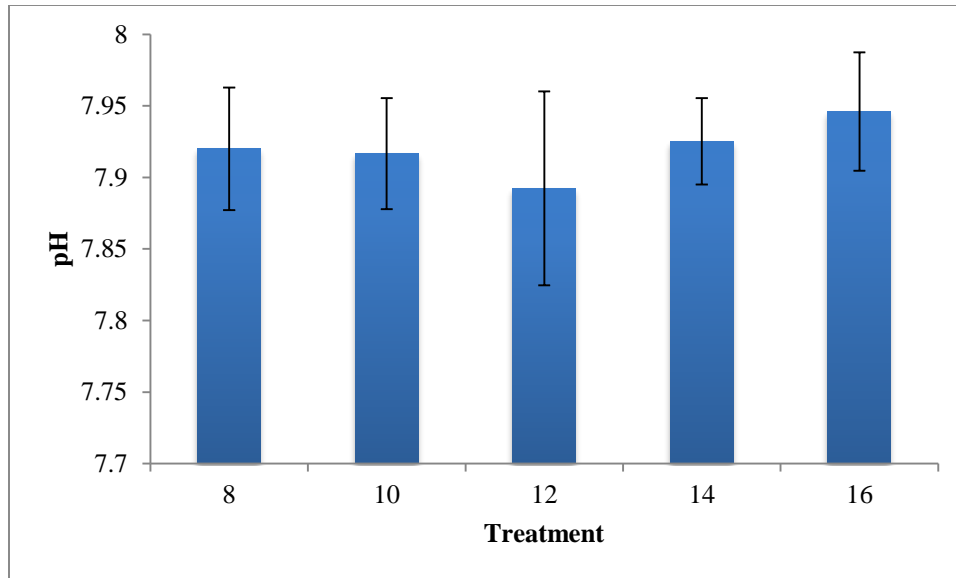
Figure 7-16. pH conditions (mean ± s.d.) for the temperature experiments.
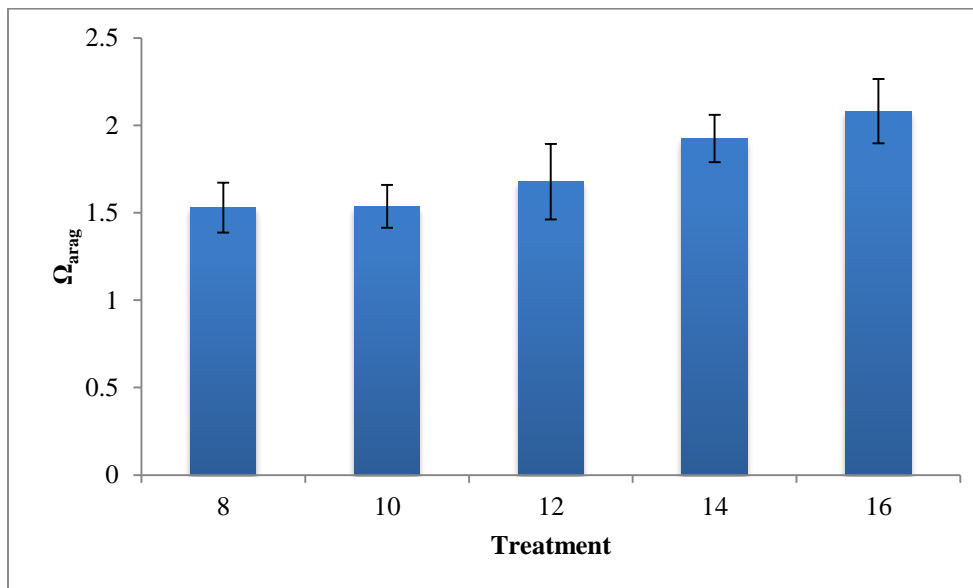


Figure 7-17. Ωarag conditions (mean ± s.d.) for the temperature experiments.

Cumulative survivorship of *L. pertusa* differed significantly among temperature regimes (Figure 7-18, Kruskal-Wallis test, H = 33.9737, p < 0.0001) after 8 days at each treatment. Cumulative survivorship was 100% in the control treatment (8°C) and decreased in each successive treatment. At 10°C, cumulative survivorship was 86.73 ± 6.21% (mean ± SE, n = 9). At 12°C, cumulative survivorship was 69.88 ± 6.13% (mean ± SE, n = 9). At 14°C, cumulative survivorship was 53.58 ± 8.52% (mean ± SE, n = 9). All corals experienced 100% mortality during the recovery period between the 14°C and 16°C experiments. Because of this, a new set of experimental corals was used for the 16°C experiment. Percent survivorship was 0% in the 16°C treatment.
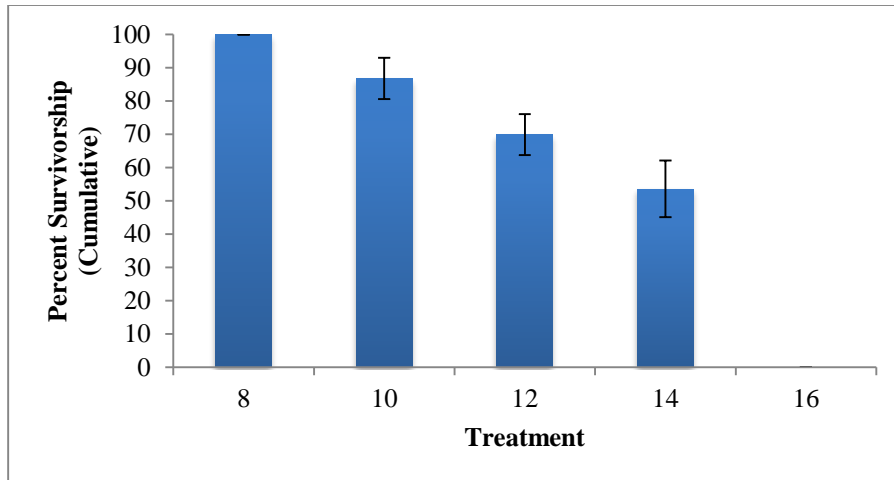
Figure 7-18. Cumulative survivorship of *L. pertusa* (over 7 days,
        mean ± S.E.) from the temperature experiments.

Average *L. pertusa* growth rates were $0.002 \pm 0.002$, $-0.012 \pm 0.009$, $0.0002 \pm 0.007$, $0.002 \pm 0.003$, and $-0.006 \pm 0.005$ %·d$^{-1}$ for the 8°C, 10°C, 12°C, 14°C, and 16°C experiment, respectively. Relative to the control (8°C), growth rate was significantly decreased at 10°C (Mann-Whitney test, $U = -2.1529$, $p = 0.0313$) and 16°C (Mann-Whitney test, $U = -1.9726$, $p = 0.0485$). No tank effects were observed in any treatment (see Table 7-9).

Table 7-9.

Results from Kruskal-Wallis tests ($\alpha = 0.05$) on tank effects (differences in growth rate among tanks) in temperature experiment

| Treatment (°C) | H | p |
|---|---|---|
| 8 | 1.444 | 0.4857 |
| 10 | 0.4722 | 0.7897 |
| 12 | 1.1111 | 0.5738 |
| 14 | 2.25 | 0.3247 |
| 16 | 1.0667 | 0.5866 |

*H = variance of the ranks among groups; p = probability of getting a particular value of H by chance*

Previous work in *L. pertusa* from the GoM shows that the upper mortality limit is approximately 15°C (Brooke et al. 2013), and our data support these findings. While Brooke et al. (2013) found that exposure at 15°C resulted in ~20% mortality in *L. pertusa*, our data show that prolonged exposure at 10°C, 12°C, and 14°C results in pronounced mortality (see Figure 7-18). These effects may be due to the corals prolonged exposure to 8°C in the maintenance tanks, and these observations may be an effect of short-term thermal stress in animals acclimated to relatively stable conditions. However, all corals suffered complete mortality during the recovery period between the 14°C and 16°C experiments, resulting in a completely new set of corals being used for the 16°C experiment.

As of this study, results showing temperature effects on cold-water coral growth are completely absent from the literature. Our data show that *L. pertusa* significantly decreases its growth rate

when exposed to temperature stress at 10°C and 16°C. However, growth rate gradually approaches the control (8°C) at 12°C and at 14°C. It is possible that an initial stress of 10°C was sufficient to induce the drastic reduction in growth rate observed here; however, increases in temperature are related to increases in $\Omega_{arag}$ (Figure 7-17), and the growth observed at 12°C and 14°C may reflect these increases. Since all corals subsequently died during the recovery between the 14°C and 16°C experiments (described above), a new set of corals was used for the 16°C experiment, all of which exhibited net dissolution (Figure 7-19) and 0% survivorship at the conclusion of the experiment (Figure 7-18). The decrease in calcification may be attributed to an initial stress response by the corals, similar to the response observed at 10°C (Figure 7-19).
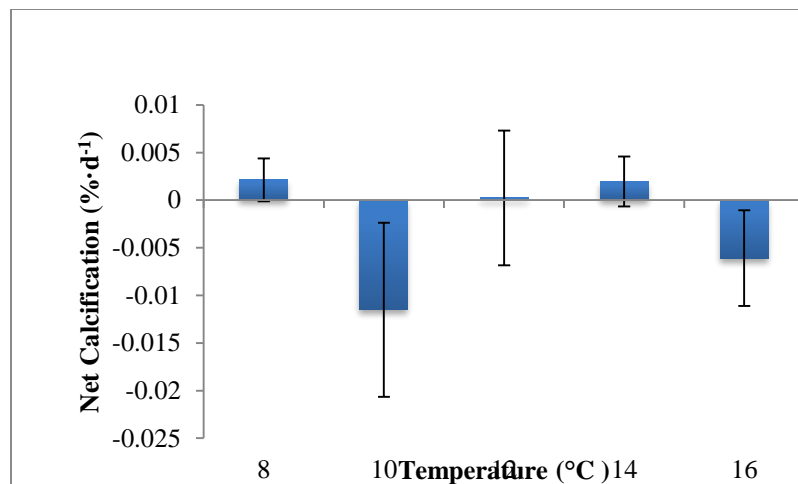


Figure 7-19.  Growth of *L. pertusa* (over 7 days, mean ± S.E.)
            from the temperature experiment.

## 7.6  DISSOLVED OXYGEN EXPERIMENTS

### 7.6.1  Methods

#### 7.6.1.1 Experimental Design and Setup

Each experiment was conducted in a constant-temperature room at TU. Three 20 gallon aquaria ("tall" type: 24" x 13" x 17") with individual filtration units (AquaClear 30) and pH controllers (Pinpoint®, American Marine Inc.) were used for each experiment (Figure 7-6). Three individual coral nubbins of unique genotype were randomly assigned to each tank for a total of nine nubbins per treatment. Each experiment lasted for a total of fifteen days, with an initial eight-day conditioning period to allow the corals to acclimate to the tank conditions. Growth was measured between days eight and fifteen to obtain a daily growth rate. Mortality was measured daily and at the conclusion of each treatment.

The following dissolved oxygen experiments were conducted: high (5 mL·L$^{-1}$), middle (3 mL·L$^{-1}$), low (1 mL·L$^{-1}$).
Methods for seawater analyses and survivorship measurements are identical to those described above in the pH experiments.

## 7.6.2 Results and Discussion

Dissolved oxygen was maintained at target levels for each treatment. Average DO concentration was $5.32 \pm 0.28$ mL·L$^{-1}$, $2.92 \pm 0.21$ mL·L$^{-1}$, and $1.57 \pm 0.28$ mL·L$^{-1}$ for the hyperoxic, normoxic, and hypoxic treatments, respectively (Figure 7-20). DO was significantly different across all treatments (Kruskal-Wallis test, $H = 474.75$, $p < 0.001$). Pairwise comparisons revealed significant differences in DO between each treatment (see Table 7-10).
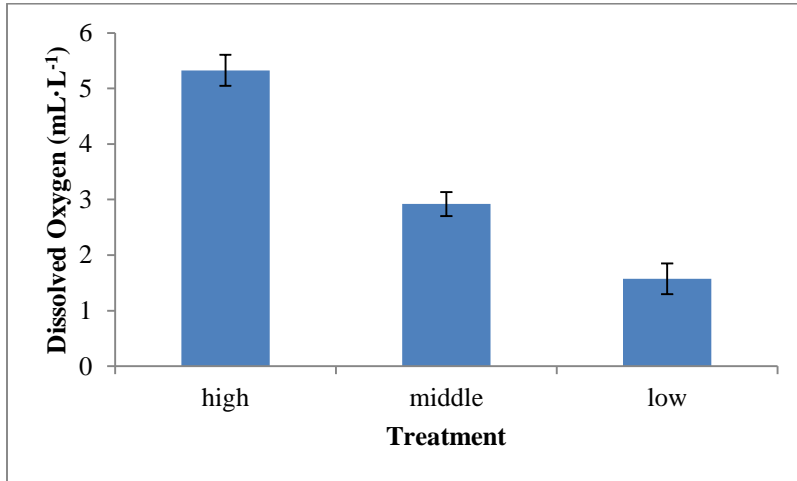


Figure 7-20. Dissolved oxygen conditions (mean ± S.D.) for the dissolved oxygen experiments.

Table 7-10.

Pairwise comparisons ($\alpha = 0.05$) of dissolved oxygen among treatments in the dissolved oxygen experiment

|  | Hyperoxic | Normoxic | Hypoxic |
|---|---|---|---|
| Hyperoxic |  |  |  |
| Normoxic | <0.0001 |  |  |
| Hypoxic | <0.0001 | <0.0001 |  |

Survivorship of *L. pertusa* was 100% at both the hyperoxic and normoxic treatments. However, survivorship decreased to 0% in the hypoxic treatment (DO = $1.57 \pm 0.28$ mL·L$^{-1}$, Figure 7-21). No mortality was observed in between treatments.
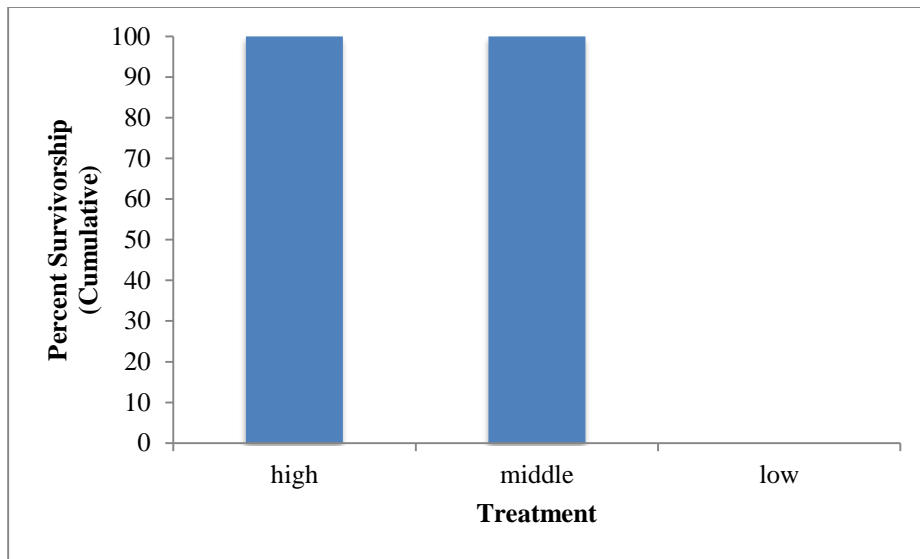
Figure 7-21.  Percent survivorship of *L. pertusa* (over 7 days, mean ±
            S.E.) from the dissolved oxygen experiments.

Results from 2008, 2009, and 2010 cruises show spatial and temporal variability in dissolved oxygen at *L. pertusa* sites in the GoM, with a minimum oxygen concentration of 1.5 mL·L$^{-1}$ observed at VK906 in 2009. This suggests that, at a minimum, *L. pertusa* at VK906 is episodically exposed to hypoxic conditions; however, these exposures likely do not last long enough to inflict significant mortality. Previous work has explored the metabolic tolerance of *L. pertusa* to various oxygen concentrations, and found that *L. pertusa* is unable to maintain aerobic respiration at oxygen concentrations less than 3.26 mL·L$^{-1}$ at 9°C (Dodds et al. 2007).  However, this work was performed on samples from the Northeast Atlantic, where the mean local oxygen concentration was 6.10 mL·L$^{-1}$.  Oxygen concentrations ranging from 2.6-3.2 mL·L$^{-1}$ have been reported from the GoM surrounding *L. pertusa* mounds (Schroeder 2002, Davies et al. 2010), and field results from this project show dissolved oxygen reaching a minimum of 1.5 mL·L$^{-1}$ near *L. pertusa* mounds. These results suggest a lower oxygen threshold for *L. pertusa* aerobic respiration in the GoM; however, our mortality data show that long-term exposure (8 days) to sustained hypoxic conditions near 1.57 mL·L$^{-1}$ results in complete mortality. While *L. pertusa* is able to employ anaerobic respiration for periods up to 96 hours (Dodds et al. 2007), our data suggest that this strategy is not sufficient to maintain energetic requirements over longer periods. Future experiments should utilize respirometry to study the oxygen demands of GoM *L. pertusa*, and potentially will be able to resolve the maximum timeframe that *L. pertusa* is able to utilize anaerobic respiration to maintain physiological processes.

Growth studies under the dissolved oxygen regimes were complicated by the elevation in pH and aragonite saturation state due to the injection of nitrogen gas (Figure 7-22). Nitrogen gas is commonly employed in dissolved oxygen manipulations as it removes oxygen from the seawater; however, nitrogen also removes dissolved carbon dioxide, resulting in an elevation in pH and aragonite saturation state. At elevated saturation states, abiogenic calcium carbonate can precipitate onto the coral skeleton. In fact, Holcomb et al. (2009) observed precipitation of abiogenic calcium carbonate at $\Omega_{arag}$ near 5.0. The $\Omega_{arag}$ of the dissolved oxygen experiments ranged from 3.23-4.88 (Figure 7-22), with the highest $\Omega_{arag}$ observed in the low dissolved oxygen

treatment where nitrogen injection was most pronounced. The abiogenic formation of calcium carbonate due to the elevation in $\Omega_{arag}$ inhibited our interpretation of the effects of dissolved oxygen changes on growth in *L. pertusa*.
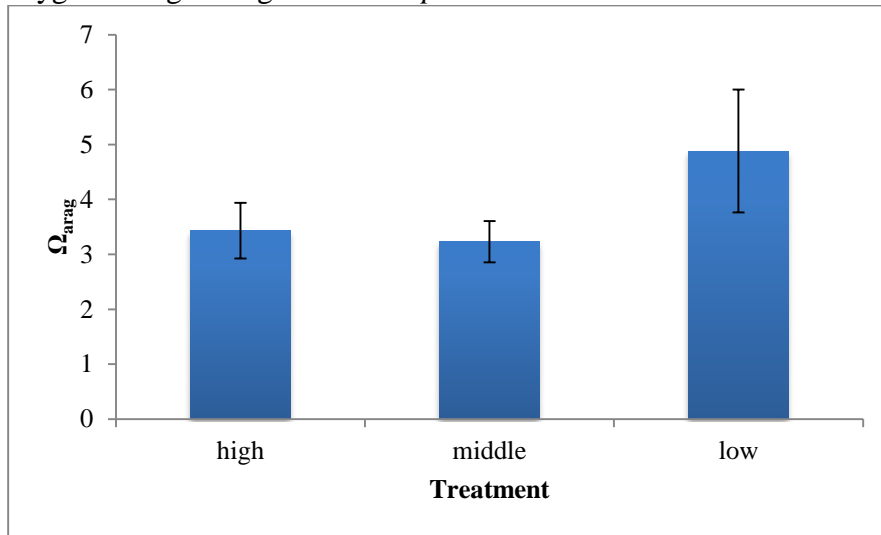


Figure 7-22. $\Omega_{arag}$ conditions (mean ± S.D.) for the dissolved oxygen experiments.

# 8   BIOLOGICAL COMMUNITIES ON ARTIFICIAL SUBSTRATES, WITH EMPHASIS ON *LOPHELIA PERTUSA*.

## 8.1   INTRODUCTION:

This component of the project was fine tuned to an emphasis on *Lophelia pertusa* occurrence and growth rates on artificial substrates due to a number of factors that limited our access to appropriate imagery and samples for a more comprehensive study of all of the platforms.

Images from a total of seven platforms and one subsea installation were utilized for this aspect of the project.  The data that could be derived from the imagery varied greatly depending on the quality of the imagery and the associated data we were able to obtain for that imagery. In many cases, the imagery supplied by the platform operators was not of sufficient quality to identify most species with certainty, and in some cases even identifying "coral" was problematic.  However, the bright white color of *L. pertusa* and the fact that it was usually the only moderate-sized colonial coral on the platforms facilitated aspects such as determination of the density of colonies. Imagery that was appropriate for fish surveys was extremely limited and was not appropriate for collection of data on coral sizes and densities on the platforms because fish surveys required a wide field of view while coral surveys required close-up imagery of the structural members of the platform. Because much of the imagery was collected without the use of parallel lasers for scale, it was critical to know the diameter of the members in the images and this data was often not possible to obtain from the operators of the platforms, because the exact member being surveyed was not always known.  In these cases, we were able to constrain the diameters of the structural members in question to within an error of about 50%.   We received platform inspection videos from platform operators for Pompano, Petronius, and Neptune that included portions of video of sufficient quality and with accompanying data appropriate for this study. We also obtained inspection video from the Baldpate platform, which was not appropriate for most of our work on *Lophelia pertusa*. This was appropriate for a qualitative fish survey, however, and that data are reported below.

From July 12 – 24, 2012 the *Kracken* ROV was used from the *RV Brooks McCall* specifically to survey and sample platforms for this study.  A combination of weather, ROV capabilities and problems, and concerns with entanglement due to incomplete information from platform operators combined to compromise this research effort.  As a result, only a few collections were made, and no community collections were accomplished.  When it became apparent that the amount of imagery we could collect would be quite limited, the decision was made to concentrate on imagery appropriate to quantify *L. pertusa* and other colonial coral occurrence and growth rates, recognizing that this would preclude collection of data on fish occurrence.  Imagery was collected from Jolliet, Cognac, and Ram Powell, as well as the Zinc subsea installation before the cruise was terminated due to loss of the ROV.

Although we have limited data above about 150 m depth, it was noted that in general all platforms had a zone of extensive biological coverage near the air-water interface that gradually transitions into a zone of relatively sparse large fauna at around 100 m depth.  This zone transitions back to a zone of encrustation with larger attached fauna starting with anemones and progressing to *L.*

*pertusa* growth at about 200 m.  Near the sea floor (or below the depth of occurrence of *L. pertusa*), there is a transition to a zone with no *L pertusa* but abundant anemones.  The depth of these zones shifts slightly with each platform and may be related to the age and water depth of the platform. Though *L. pertusa* and large anemones do co-exist at the upper and lower ends of *L. pertusa* depth range, they do not co-exist in abundance where either taxa is present at high densities. Very few non-*L. pertusa* corals were observed on the platforms within the depth range focused on for this study (below 175 m) with the exception of Cognac.

## 8.2  OVERVIEW OF EACH PLATFORM STUDIED:

### 8.2.1  Neptune

Water depth – 1,952 ft (595 m)
Installation date – 1996
Complex ID 24235
Lease block – VK826
Structure type – Spar

We received video from a rig inspection conducted from May 9-12, 2011 that contained 168 ½-hour video files, 28 of which were of suitable quality for our use.  Each file was a scan at constant heading of one structural member, or two parallel members, from varying distances.  Potentially usable scanned structural members included wires, pile chains, risers, export risers and umbilicals.

Video observations began at 153 m depth.  There were no large attached cnidarians between 150 and 300 m, although small solitary orange cnidarians and what appeared to be small hydroid colonies were present in this depth range.  *L. pertusa* was the only colonial coral seen on Neptune and was present from 262 to 614 m depth.  Fly trap and other large anemones were present on many structural members below approximately 300 m depth and became abundant below 550 m depth as *L. pertusa* density decreased.

### 8.2.2  Pompano

Water depth – 1,312 ft (400 m)
Installation date – 1994
Complex ID 24130
Lease Block – VK989
Structure Type – Solid

Three separate video collections were received and used for analyses of Pompano communities: an inspection video collection taken November 8, 2008; a video collection obtained at our request during an inspection survey on July 14, 2009; and an inspection video collection from June 2-6, 2011.  Coral samples collected in 2009 were also supplied to USGS collaborator, Cheryl Morrison. The first two video collections were standard definition videos and the 2011 video was high definition (HD).

Eight digital versatile discs (DVDs) were supplied by the platform operators from the 2008 survey and 5 of these included video suitable for this study. Each DVD contained approximately 1 hour 45 minutes of video and there was a total of 5 hours of useable footage from this set. This inspection video was of the riser array which was a 5-pipe-by-8-pipe grid of evenly spaced 76.2 cm (30 in.) and 91.4 cm (36 in.) diameter structures running vertically from the sea floor to the surface. This grid was periodically intersected by horizontal members and other support structures. The video collection included interrupted vertical scans of single risers from shallow to deep water as well as horizontal scans of one side of the array where the video moves from one riser to another while maintaining the same depth and heading. Because of the intersecting horizontal members, and limitations of the ROV due to its umbilical, there are no continuous scans of a single riser from 152 m (500 ft) to the sea floor 400 m (1,312 ft). Density estimates reported below were calculated by "piecing" together data from numerous scans of various risers.

The video collection from 2009 looked specifically at *L. pertusa* occurrence on the structure. The primary focus of the video is continuous scans at constant heading of two ~320 cm diameter legs with a few minutes of additional structure visible. Total video time for this collection is 2.5 hours.

The most recent video collection was from a 2011 HD video inspection of the entire jacket of Pompano from the surface to the sea floor, but does not include scans of risers. Large leg structures and smaller vertical, horizontal, and diagonal members of varying sizes and at different headings were inspected. This collection of video was organized by scans of individual structural components and contained 338 video files that ranged from 1-15 min in length and each contained a complete scan of one to four structural components. Components are units of structure defined by the dive company operating the inspection; most often, these components are either structure nodes or lengths of structure between nodes. Components other than members are not used in this analysis. Scans are pieced together for an analysis of coral density with increasing depth.

Data collection began at 122 m depth. Small anemones and hydroids are visible but scarce until they become more abundant through the interval to 183 m where fly-trap and other large anemones begin to appear. Four non-*L. pertusa* (unidentified) colonial corals (Figure 8-1) were observed in the 2008 video collection between 183 m and 366 m; these corals were not near each other. Orange *L. pertusa* were present on Pompano. In the 2011 video, numerous white globular shaped corals or sponges (Figure 8-2) were found at approximately 137 – 183 m (450-600 ft). A small school of amberjacks, *Seriola dumerili,* was present at 170 m depth (Figure 8-3). Fly-trap anemones were abundant and constituted the most predominate, large identifiable fauna on the base of the structure.

Figure 8-1. An apparent colonial coral that is not *L. pertusa* is visible on the left edge of this structural member on Pompano at 336 m depth. Four "corals" resembling this were seen at Pompano.



Figure 8-2. White globular coral or sponge from Pompano 5/24/2011 survey at a depth of 180 m (590 ft).

Figure 8-3. Small school of amberjacks, *Seriola dumerili*, seen on the 2011 survey of Pompano at 178 m depth.

## 8.2.3 Petronius

Water depth – 1,771 ft (540 m)
Installation date – late 1998 (top and bottom sections), June 2000 (24 inch risers)
Complex ID -  70012
Lease block – VK786
Structure type – Compliant Tower

We received an inspection video collection taken October 10 to 12, 2008 for the Petronius platform. Approximately 41 hours of video on 6 disks were screened, yielding approximately 20 hours of usable video. The videos contain broken scans of various structures at multiple headings, including large ~335 cm (132 inch) legs; smaller vertical, horizontal, and diagonal jacket members, and risers from the surface to the sea floor (540 m). The videos contain short scans of member or riser segments interrupted by other members or by breaks in camera focus on the structure that are "pieced" together for analysis of density with increasing depth.

The faunal progression for Petronius is very similar to that of Pompano, where there is a zone of little to no large fauna from about 60 m to 180 m depth. Large fauna, dominated by anemones,

become gradually more abundant below this depth. The first *L. pertusa* was seen at 248 m and increased in abundance until approximately 450 m then persisted until about 10 m above the sea floor. Below this depth was a zone with extensive coverage of fly-trap anemones.

The fallen South Platform, which resides on the sea floor nearby, is covered with anemones, but no visible *L. pertusa* or other colonial corals were present on this structure.

## 8.2.4  Baldpate

Water depth – 1,650 ft (503 m)
Installation date – 1998
Complex ID - 33039
Lease block – GB260
Structure type – Compliant Tower

We received one inspection video totaling 4.5 hours taken on September 27, 2008. An attempt to dive on Baldpate was made during the *Brooks McCall* cruise in 2012, but the dive was aborted soon after approaching the structure due to unanticipated obstructions on the platform. The presence of *L. pertusa* on the structure was confirmed but no other usable data were collected.

The 2008 Baldpate survey was not adequate for *L. pertusa* density or growth analysis but did allow better survey of fish populations than other platform surveys even though the depth gauge only functioned intermittently. The survey started at 67 m depth and noted numerous reef-type fish associated with small sea fans and tubastraea colonies. Fish present above 125 m depth included french angelfish, rock hind, graysby, blue tang, gray triggerfish, bermuda chub, squirrelfish and reef butterfly fish. Fish density abundance decreased markedly and was almost absent by 126 m depth, although a squirrelfish, a reef butterfly, and a small roughtongue bass were noted at this depth. Sea fans were absent by 137 m and fish were very sparse below this depth. A few Anthiines were noted between 140 m and 240 m depth, but large attached inverts were very rare. A single roughtongue bass was seen at 241 m depth. The first *L. pertusa* were seen at 282 m and the first fly trap anemone at 308 m. *L. pertusa* remained relatively rare to 333 m and fish were almost completely absent. Brisingid starfish were first sighted at 310 m and became abundant down to about 360 m. Small *L. pertusa* appeared to become more abundant from this depth and were present until 5-10 m from the sea floor (about 500 m).

## 8.2.5  Jolliet

Water depth – 1,781 ft (543 m)
Installation date – 1989
Complex ID 23583
Protraction Area – Green Canyon
Lease block – GC184
Operator name – MC Offshore
Structure type – Tension Leg Platform (TLP)/Template

The Jolliet platform was surveyed on July 17, 2012 using the *Kraken* ROV on the *RV Brooks McCall*. One and a half hours of usable video footage were collected during a single pass down one tendon of the structure from 35 m to 437 m depth. No biota clearly identifiable while colonial corals were observed from 35 m to 75 m, though small flora and fauna, and numerous fish, including schools of jack and chub, were present at this depth (Figure 8-4, Figure 8-5). Larger fauna, including some unidentifiable potential coral colonies and smaller unidentified cnidarians, were present between 75 m and 110 m. From 110 m down to 235 m the faunal coverage decreased steadily; only small attached fauna was present and no identifiable corals were observed in this depth range. Starting at 235 m, anemones, zooanthids and hydroids began to increase in abundance until about 275 m. Attached fauna was again sparse between 275 and 300 m depth. The first *L. pertusa* colony was seen at 294 m and *L. pertusa*, larger anemones and other solitary cnidarians increased in abundance from about 300 m to 437 m where *L. pertusa* and fly-trap anemones were abundant. The base of this structure was not imaged. No identifiable corals other than *L. pertusa* were observed on this structure. Non-white *L. pertusa* were observed on this structure.



Figure 8-4. School of jacks (species level ID not possible from image) imaged at 37 m depth on platform Jolliet.

Figure 8-5. School of chub, *Kyphosus sectatrix*, at 38 m depth on platform Jolliet.

## 8.2.6 Ram-Powell

Water depth – 3,264 ft (995 m)
Installation date – 1997
Complex ID 24229
Lease block – VK956
Structure type – TLP/Template

Ram Powell was surveyed on July 20, 2012 using the *Kraken* ROV on the *RV Brooks McCall*. Almost five and a half hours of video footage, including 3 hours of footage suitable for analysis, were collected during a single pass up one tendon of the structure from the sea floor at 995 m to 200 m, when the survey was terminated because of time constraints. Ram Powell was the only structure surveyed that extended past the known depth range for *L. pertusa*, so was the only structure where robust data on deepest depth of occurrence, and relations between depth and density and growth rate were obtained. Large attached fauna were almost completely absent from 200 m to 275 m depth. Large anemones were first seen at 275 m depth and were sparse down to about 350 m. Below this depth, both anemones and *L. pertusa* became increasingly abundant, along with smaller solitary cnidarians. Below 600 m, *L. pertusa* and the larger anemones persisted but abundance decreased with depth, and smaller cnidarians became quite rare. The last *L. pertusa* was noted at 801 m, and below this depth visible attached megafauna were very sparse. One *L. pertusa* colony was found on the sea floor near the base of the structure (Figure 8-6); however this colony had dead or dying polyps on the ends of several branches and was interpreted as most likely

297

representing a dying fragment that had been dislodged from the structure above.   No fish were observed during the scan of the tendon.



Figure 8-6.  *L. pertusa* on the sea floor under Platform Ram Powell at a depth of 1,010 m.

### 8.2.7  Cognac

Water depth – 1,033 ft (315 m)
Installation date – 1978
Complex ID 22178
Lease block – MC194
Structure type – Solid

Cognac was surveyed on July 21, 2012 using the *Kraken* ROV on the *RV Brooks McCall*.  One hour and 45 min of video footage suitable for analysis was collected during a single pass up one leg of the structure from the sea floor to 165 m depth. Cognac was the oldest structure surveyed, and several aspects of the coral communities there  probably reflect this:

There were several areas on Cognac where the *L. pertusa* growth had reached the thicket stage, and it was not possible to differentiate individual colonies.

Although, like the other structures, there was no *L. pertusa* attached to the basal 5-10 m of this structure, there were abundant living (and apparently healthy) *L. pertusa* on the sea floor near the

base (Figure 8-7).  This likely reflects survival of some fragments that have been dislodged from the structure above.

Another reflection of the age of this structure was the significantly increased presence of what appear to be non-*L. pertusa* colonial corals (Figure 8-8 and Figure 8-9), similar in appearance to the few seen on Pompano.

Finally, unlike the other structures surveyed, no large anemones were present in areas of highest *L. pertusa* abundance, perhaps reflecting out-competition by *L. pertusa*.

No data was collected at depths above 165 m.   No large attached fauna was present between 165 m and 180 m.  Between 180 m  and 250 m, a non *L. pertusa* colonial coral was present with a peak in abundance near the bottom of this range. *L. pertusa* was present between 218 m and 320 m.  No large anemones were present above 280 m nor were they present at peak *L. pertusa* depths (260 m to 325 m). There was no *L. pertusa* on the base of Cognac (within about 5-8 m of the sea floor), but unlike like other structures,  *L. pertusa* were observed on the sea floor near the base of the structure (Figure 8-7). Non- white *L. pertusa* were observed on this structure.



Figure 8-7.  *L. pertusa* colonies growing on the sea floor near the base of Platform Cognac at depth of 322 m.
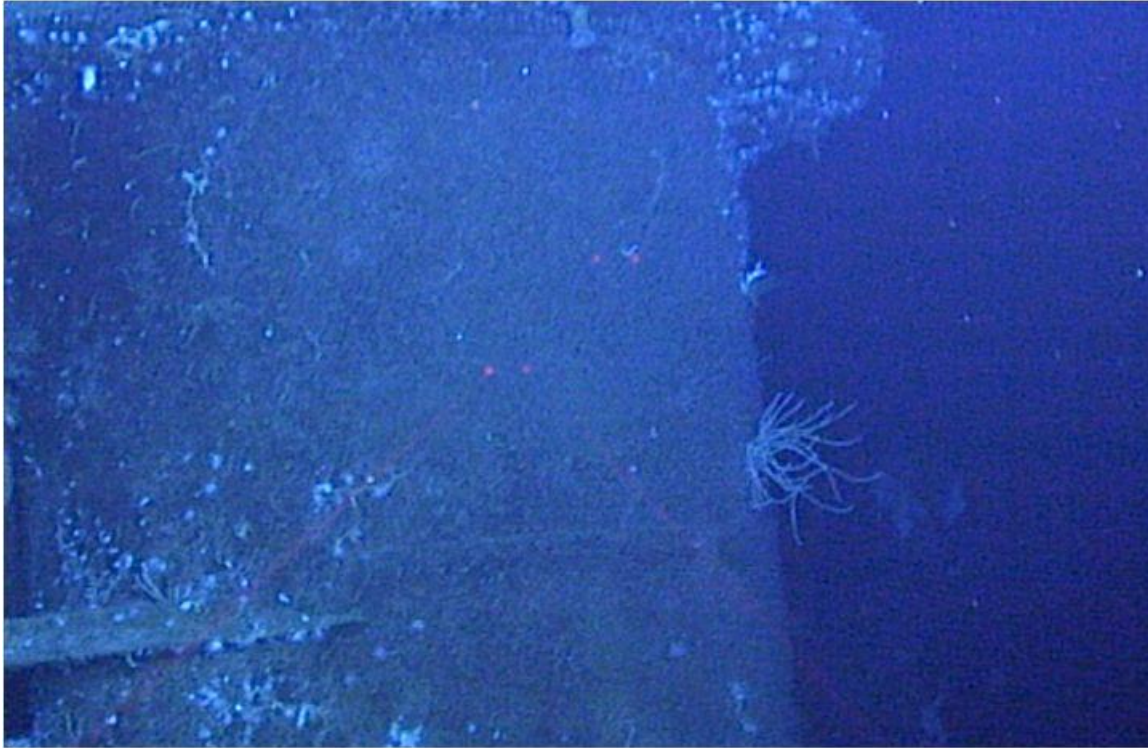
Figure 8-8.  Close-up of what appears to be a non-*L. pertusa* colonial coral on Platform
Cognac at a depth 234 m.



Figure 8-9.  Numerous "non-*L. pertusa* colonial corals" on Platform Cognac at a depth of 328 m.

## 8.2.8  Zinc Subsea Installation

Water depth – approximately 1,500 ft (450 m)
Installation date - 1991
Protraction Area – Mississippi Canyon
Lease block – MC355
Operator name- Exxon Mobil
Structure type – Subsea

The Zinc subsea installation was surveyed on July 19, 2012 using the *Kraken* ROV on the *RV Brooks McCall*.  No observable megafauna was found at the base of this installation.  There was heavy sedimentation around the base of the main installation and bare steel was often visible on basal parts of the main installation. About 7 m above the sea floor, on turrets near the top of the main installation there were scattered small *L. pertusa* colonies, zoanthids and small anemones (Figure 8-10, Figure 8-11).  Most imagery was collected from an abandoned flow-tube test pile located several meters away from the main installation.  Similar to the other installations, anemones, but no *L. pertusa*, were present on the basal parts of the test pile (Figure 8-12). However, *L. pertusa* were abundant higher up on this structure. This test pile was approximately 15 m in height, including four corner protrusions from the elevated flow-tube platform. Fish, including numerous Atlantic roughy, were observed around and inside of the platform area of the abandoned test pile (Figure 8-13).  Large fly-trap and other anemones were also visible on this test pile, but no corals other than *L. pertusa* were observed.   Squat lobsters, crabs, ctenophores, and copepods were numerous as well at the test pile.
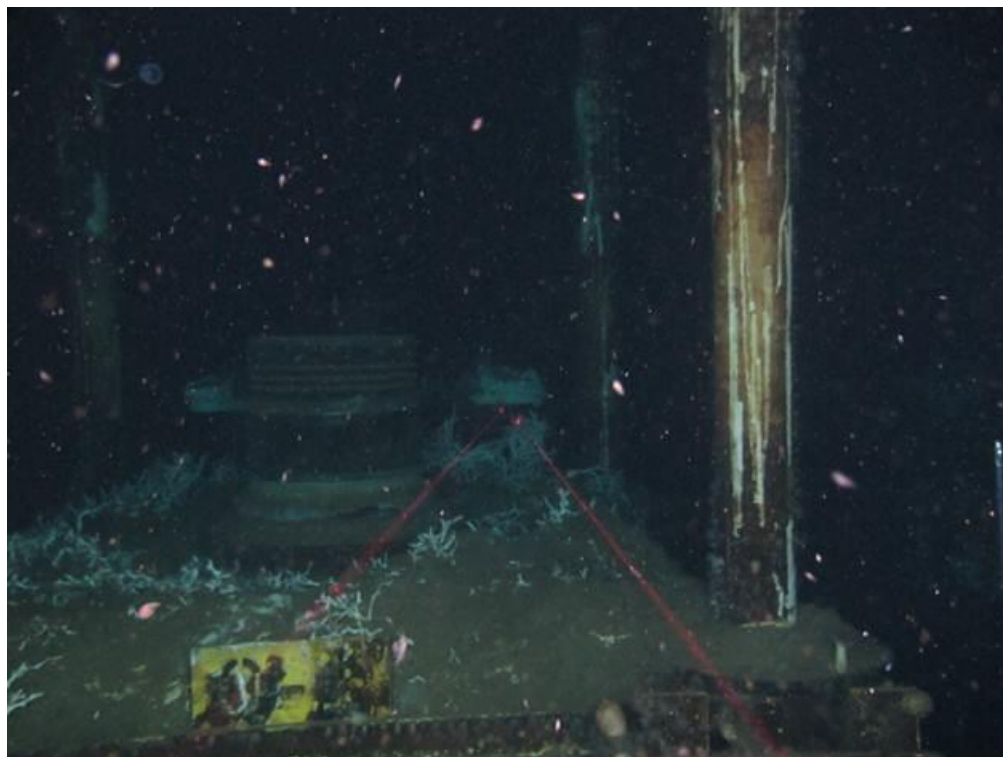


Figure 8-10.  Flow-tube connection at Zinc installation with broken *L. pertusa* approximately 7 m above the sea floor.

301

Figure 8-11.  Fauna incrusted flow-tube connection about 7 m above the sea floor at the  Zinc installation.



Figure 8-12.  Light cnidarian encrustation with no *L. pertusa* on base of the abandoned test pile near the Zinc installation (within 5 m of the sea floor).

Figure 8-13. Atlantic roughy, *Hoplostethus occidentalis*, among *L. pertusa* around the abandoned test-pile near the Zinc installation at 450 m depth.

## 8.3 GROWTH RATES, DENSITIES, AND DISTRIBUTION OF *LOPHELIA* PERTUSA ON ARTIFICIAL STRUCTURES IN THE GULF OF MEXICO

(Excerpted from a manuscript of the same title authored by Elizabeth A. Larcom, Danielle McKean, and Charles Fisher, submitted to Deep Sea Research in April 2013)

### 8.3.1 Abstract

Using industry inspection video and ROV imaging, we examined *Lophelia pertusa* (*Linnaeus* 1758) on 10 artificial structures of known ages (9 to 103 years) in the northern GoM (GoM). Five different types of deep-water hydrocarbon installations with depths ranging from 320 m to 995 m, and three shipwrecks with depths ranging from approximately 530 m to 615 m were examined. Density, depth ranges, and growth rates of *L. pertusa* colonies were calculated from video and image analysis. *L. pertusa* colonies were present on all structures examined. Minimum calculated growth rates for the largest colonies ranged from 0.32 to 3.23 cm/year on the different structures. Colony density varied with structure type, age, and depth, with of the highest density between 503-518 m on the single structure that spanned the entire depth range of occurrence of *L. pertusa*. *L. pertusa* on thinner and deeper, hydrocarbon structure types (spar and tension leg platforms) appear

303

to have higher colonization rates as they support higher densities in less time. However, on average, colonies have slower growth rates on these structures than colonies on more massive, shallower hydrocarbon structure types (compliant and solid platforms). In general, the calculated minimum growth rates were higher on the hydrocarbon installations than on the shipwrecks, which were substantially older. A continuum of colony sizes was documented on all installations, suggesting multiple settlement events. *L. pertusa* thickets were observed on the oldest structures with most structural components covered by colonies of *L. pertusa*. The shallowest depth of *L. pertusa* observed was at 201 m and the deepest at 801 m, considerably expanding the known depth range of the species in the northern GoM. Brown, orange, and mottled morphotypes were documented for the first time in the GoM. All energy platforms examined for this study were colonized by *L. pertusa* and it is likely that most artificial surfaces in appropriate depths in the GoM will be as well.

## 8.3.2  Introduction

Though most recent literature has focused on natural *L. pertusa* reefs (Brooke and Schroeder, 2007; Freiwald, 2002; Freiwald and Henrich, 1997; Roberts, et al., 2010; Rogers, 1999; Schroeder, 2002; Sulak, 2008; Willson, 1979), *L. pertusa* growth on anthropogenic substrates such as sub-sea cables (Duncan, 1877; Wilson, 1979), oil and gas platforms (Bell and Smith, 1999; Gass and Roberts, 2006; Schroeder et al., 2005) and ship wrecks (Church et al., 2007; Roberts et al., 2003), is well documented.

There are numerous types of hydrocarbon drilling, production, and storage structures in the GoM that either have a surface component supported by long rigid members, buoyancy, or a combination of the two. Other types of installations are entirely sub-sea. All of these structures, as well as shipwrecks, can provide a substrate favorable for the settlement of a variety of invertebrate taxa and have the potential to provide habitat for *L. pertusa* settlement and growth.

Growth rates previously reported for *L. pertusa* vary widely. Growth rates determined for North Sea *L. pertusa* from depths < 300 m range from measurements of 2.6 mm/yr under laboratory conditions to *in situ* estimates of 20 – 25 mm/yr using stable and radio isotopic techniques (Freiwald and Henrich, 1997; Mikkelsen, et al., 1982; Mortensen and Rapp, 1998). Direct measurements of *L. pertusa* from the Mediterranean kept in aquaria had linear extension rates ranging from 15-17 mm/year (Orejas et al., 2007). *In situ* measurements using pieces of *L. pertusa* stained on the surface with Alizarian Red and then deployed in their natural habitat in the GoM found average linear growth rates of 2.4 to 3.8 mm/year (Brooke and Young, 2009). The highest growth rates measured for *L. pertusa* are in the range of slower growing massive shallow-water scleractinian corals (Orejas et al., 2011) yet are considerably greater than most deep water antipatharian or gorgonian coral growth rates (Prouty et al., 2011; Roark et al., 2009).

Growth rates for colonial corals on anthropogenic substrates can be constrained by dividing colony size by the amount of time the substrate has been available for colonization. Growth rates determined using this method for *L. pertusa* in the North Sea, where its maximum depth of occurrence is 132 m, range from 5 mm/year to 36 mm/year (Bell and Smith, 1999; Gass and Roberts, 2006; Roberts, 2002; Wilson, 1979). This method assumes the coral larvae settled and started growing immediately after the substrate was first available and therefore provides a

minimum growth rate, as settlement is unlikely to occur instantly and will continue to occur as long as suitable substrate is available to competent larvae. Here we determine occurrence, growth rates, densities and distributions of *L. pertusa* colonies on oil and gas platforms, and on several ship wrecks, and examine how these parameters vary with depth and structure type in the GoM.

### 8.3.3 Methods

We examined *Lophelia pertusa* distribution and growth on 6 energy platforms of four different types, one sub-sea installation, and three shipwrecks in the Northern GoM (Table 8-1.

Structure characteristics. and *L. pertusa* occurrence and growth rates, Figure 8-14). The data used in this study was acquired from a combination of inspection videos provided by platform operators and imagery acquired specifically for this study. Industry supplied inspection video from three different platforms was used in this study: Platforms Pompano, Petronius, and Neptune, including video from two different years for Pompano and two different member types installed in different years for Petronius. In July 2012, we conducted a cruise specifically to acquire data on *L. pertusa* distribution on energy platforms using the Research Vessel *Brooks McCall* and the ROV *Kraken 2* . Imagery was collected using a Kongsberg HD Video Camera and Canon PowerShot G11 10 m pixel Digital Still camera. The shipwrecks were imaged in 2009 and 2010 from the ROV *Jason II*, using an HD video camera. Both frame grabs from video and digital still images were used in our analyses.

Table 8-1.

Structure characteristics. and *L. pertusa* occurrence and growth rates

| Structure | Location (Lat., Long.) | Structure Type/ Structure Member(s) Surveyed | Age of Structure at Time of Imaging (years) | Approximate Water Depth of Structure (m) | Depth of Range of Occurrence (m) | Depth Interval of Highest Averaged Density (m) | Highest Averaged Density (colonies/m$^2$) | Number of Colonies Measured for Growth Rate | Min. Growth Rate of top 10% of Corals (cm/year) Ave. ± 1 SD | Minimum Growth Rate (cm/year) |
|---|---|---|---|---|---|---|---|---|---|---|
| **Petronius** | -87.8, 29.2 | Compliant Tower/Risers | **9** | 532 | 248 - 530 | 442-457 | **0.93** | 36 | **3.23** ± 0.18 (n=4) | **3.47** |
| **Petronius** | -87.8, 29.2 | Compliant Tower/Legs | 10 | 532 | 248 -530 | 411-427 | 1.31 | N/A | N/A | N/A |
| **Pompano 2008**[a] | -88.6, 29.0 | Solid /Risers | 14 | 400 | 218- 378 | 351-367 | 1.03 | 71 | 2.12 ± 0.14 (n=7) | 2.32 |
| **Ram Powell** | -88.1, 29.0 | Tension Leg/Leg | 15 | **995** | 288-**801** | **503-518** | **10.69** | 317 | 1.45 ± 0.16 (n=32) | 1.86 |
| **Neptune** | -88.0, 29.2 | Spar/Risers | 15 | 614 | 262-614 | **503-518** | 8.54 | **632** | 1.23 ± 0.19 (n=63) | 1.78 |
| **Pompano 2011**[a] | -88.6, 29.0 | Solid/Legs and Support Members | 17 | 400 | **201**-394 | 351-367 | 2.73 | 503 | 2.20 ± 0.20 (n= 50) | 2.93 |
| **Jolliet**[b] | -91.5, 27.8 | Tension Leg/Leg | 23 | 524 | 294-unknown | 411-427 | N/A | 239 | 1.22 ± 0.09 (n=24) | 1.53 |
| **Zinc** | -89.9, 28.6 | Subsea Installation/ Conductor Support | 21 | 447 | N/A | N/A | N/A | 38 | 2.48 ± 0.35 (n=4) | 3.00 |
| **Cognac** | -89.1, 28.8 | Solid/Leg and Support Members | 34 | **320** | 218 – 320 (seafloor)[c] | **325-260** | **Thickets** | 50 | 2.06 ± 0.15 (n=5) | 2.30 |
| *GulfPenn* | -89.3, 28.5 | Ship Wreck | 66 | ~550 | N/A | N/A | **Thickets** | 42 | 1.25 ± 0.08 (n=4) | 1.36 |
| *GulfOil* | -89.8, 28.1 | Ship Wreck | 67 | ~535 | N/A | N/A | **Thickets** | 9 | 1.12 ± 0.32 (n=9)[e] | 1.60 |
| *Green Lantern* | -90.1, 28.0 | Ship Wreck | **103-86**[d] | ~615 | N/A | N/A | **Thickets** | 7 | 0.36 ± 1.1 (89 years) (n =7)[e] **0.32** ± 0.9 (103 years) | 0.53 (89 years) **0.45** (103 years) |
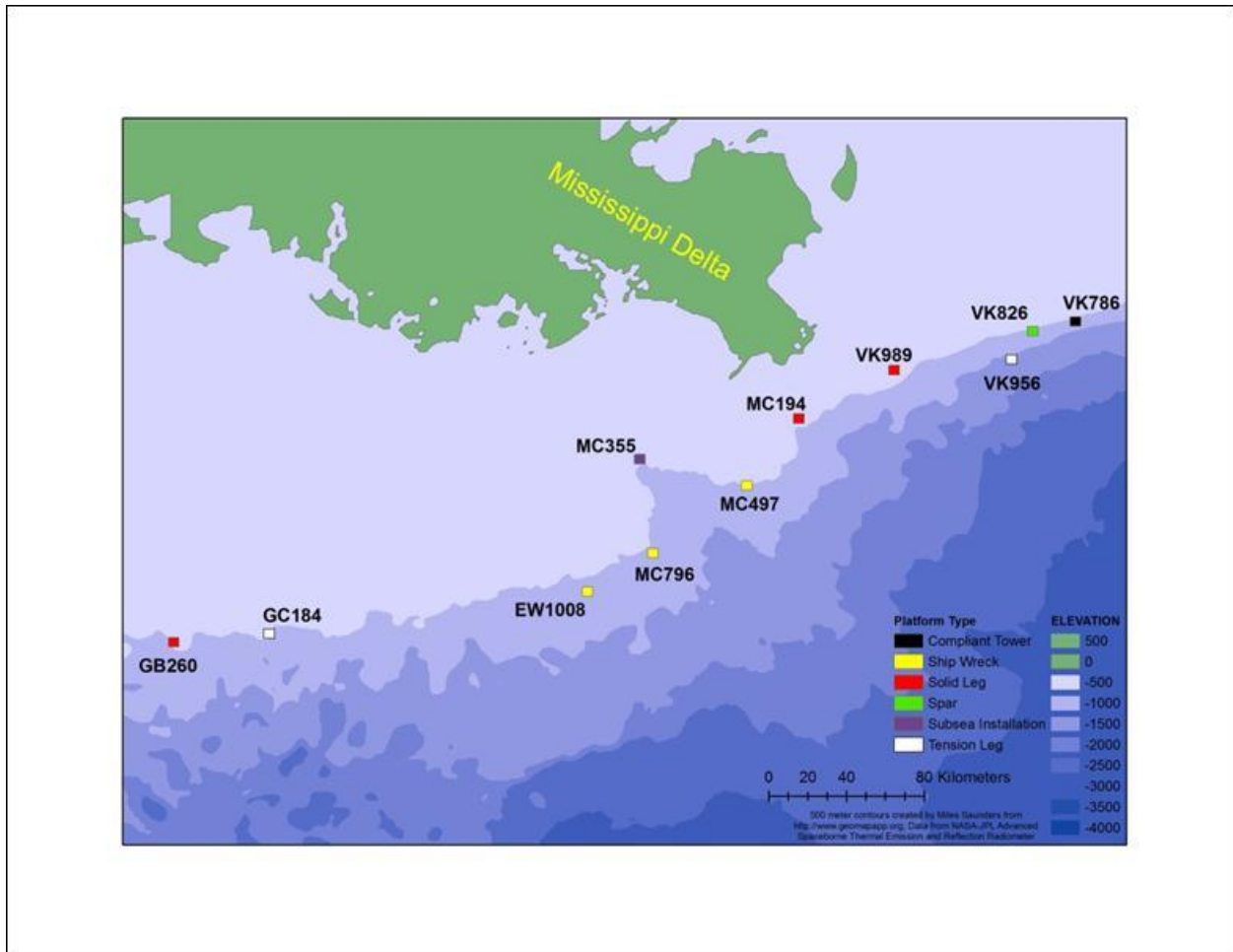
Figure 8-14. Location of platforms, shipwrecks, and sub-sea installation by lease block.

The video analysis software Studiocode 4.5.1 was used to log and classify the data acquired from the video survey. Studiocode allows the user to create unique, customizable "codes" (such as "*L. pertusa* present," "horizontal structure," "depth interval," etc.) that are synced via a timeline to the video and frame grabs from the video, and can be accessed through an interactive database. Although only subsets of the entire video record were suitable for most measurements, the shallowest and deepest unambiguous depth of occurrence of *L. pertusa* was recorded for each structure.

Two different methods were used to estimate scale in the images. For the quantitative analyses from the industry supplied inspection video, only images with both sides of the structure member in the frame were used for analysis because the structure diameter was used for scale in these images. Scale for the images acquired during the July 2012 cruise and from the ship wrecks was acquired from a pair of forward-facing parallel lasers spaced 10 cm apart mounted in the plane of the video and aimed at the center of the structure member. Only colonies clearly attached to a vertical or horizontal structure member, where colony attachment point could be reasonably inferred, were used for measurements; colonies growing near pipe junctions, on projecting or

307

irregular structures, or on closely adjoining structures were not used for any quantitative analyses. Colony area and growth rate measurements were taken from video screen shots or digital images using Adobe Photoshop CS3 or PixelStick 2.3 and converted from pixels to cm using scale determined as described above.

In order to avoid overestimating growth rates, all measurements for growth determinations were taken from a clear attachment point on the anthropogenic structure to the furthest apparent extension of that colony from that attachment surface ($d_f$ in Figure 8-15a).  This method always provided a conservative measure for the maximum extension of the colony from its point of attachment, even if the colony was partially obscured by the structure or had fused with other colonies.  Growth rate (cm/year) was calculated by dividing $d_f$ by the time that the anthropogenic substrate had been available for colonization. Coral measurements that yielded the highest growth rates in each data set were re-measured and checked by an independent observer.

Two sets of data that could be obtained from all corals present in suitable quality video of the energy platforms were used for analysis of *L. pertusa* depth distribution patterns; density of colonies and colony area.  For density measurements, only *L. pertusa* with attachment points on the side of a vertical structural member facing the ROV were used; *L. pertusa,* where portions of a colony were seen "peeking" out from the far side of the structure, were not counted for density. Density was calculated by dividing the number of colonies within a 15.25 m (50 ft) depth interval by the surface area of half the face of a cylindrical structure ($\pi rh$) where r is the radius of the structure and h is the length of the structure member or usable video within a given depth interval. Some portions of video unsuitable for colony size or measurements for calculation of growth rate due to video quality were still used for density calculations when *L. pertusa* colonies could be clearly identified.

For colony area measurements, only colonies that were clearly visible and appeared to be single colonies were used.  Colonies with shapes that suggested two or more colonies had grown together were not measured.  For colonies on the face of a structural member, area was estimated from measurement of two diameters: one along the colony's longest axis ($d_1$) and one perpendicular to this ($d_2$) using the equation for an ellipse where area $=(d_1/2)*(d_2/2)*\pi$ (Figure 8-15). Colony area for *L. pertusa* visible in profile on the edge of the structures was calculated using the equation for a circle, where area $= (d_1/2) 2 * \pi$, and $d_1$ was the colony diameter parallel to the structure (Figure 8-15).
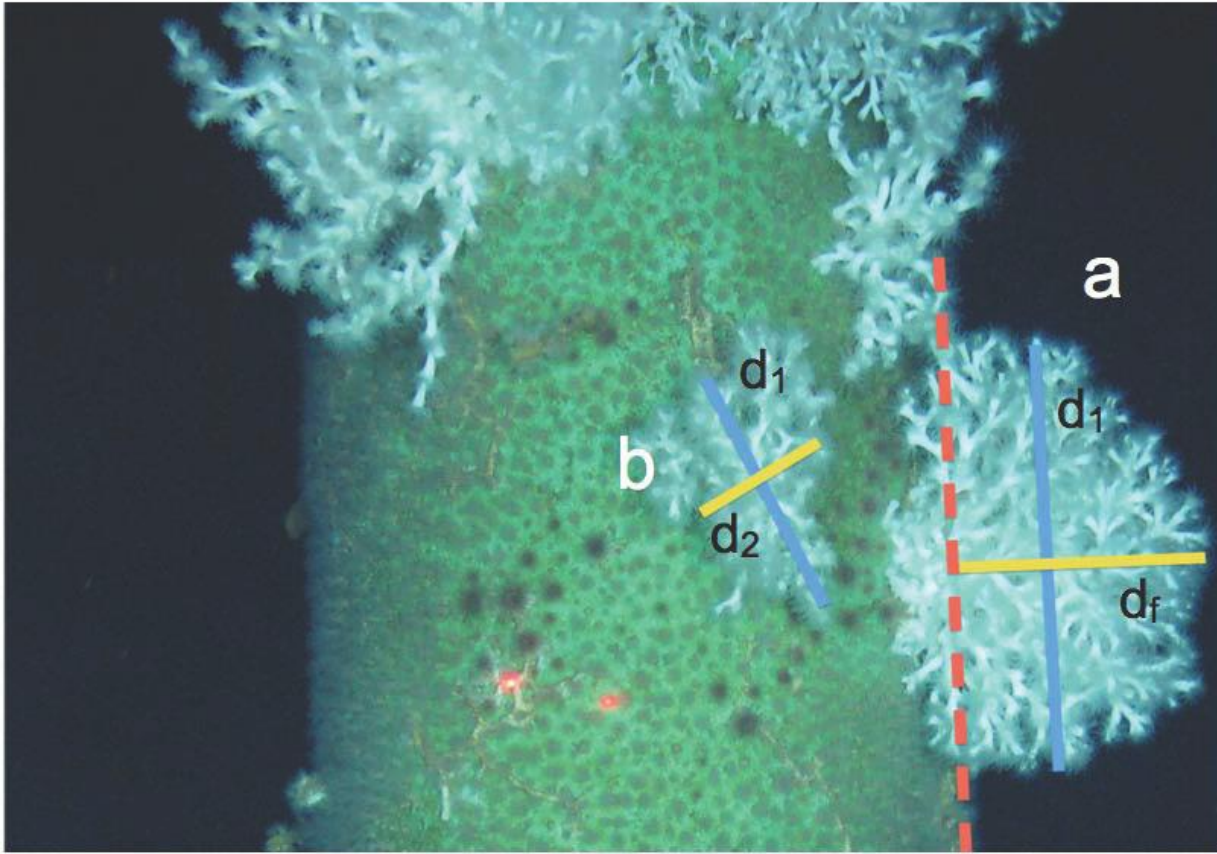
Figure 8-15. Diagram of the measuring protocol for *L. pertusa* colonies. For the determination of growth rates, maximum extension from an attachment point, such as shown for colony "a", is used. The dashed line is used to establish a point of colony contact with the structure. The light line ($d_f$) represents the distance used to estimate minimum linear colony growth rates. The dark line ($d_1$) represents the measurement of colony diameter, which, in conjunction with the linear extension measurement, is used to calculate minimum colony area for corals captured in profile. To determine colony area for corals on the surface of the structures, two diameters are measured (see coral "b"); one at the widest point of the colony (dark line, $d_1$) and another perpendicular to the other, mid point on line $d_1$ (light line, $d_2$). The two lasers in the image are 10 cm apart and used for scale.

To estimate the maximum percent coverage of *L. pertusa* on a given structure, non-overlapping screen shots were taken of each rig at the middle of the 10 m depth interval of maximum colony density and at 5 m above and below this depth. Inkscape 0.48.2 was used to outline the structure and *L. pertusa* colonies over the surface of the structure and percent coverage calculated from the areas of each (Figure 8-16). This method will overestimate percent coverage as it assumes the structural member is flat so structure surface is underestimated and colonies towards the edge of the column will obscure a disproportionate area of the actual surface. However, these data were only used for relative comparisons between platforms and over time.

309

Figure 8-16.  Example of screen shot used for percent coverage analysis.  Structure G at 304 m with 57% of the structure covered with *L. pertusa*.  The structure is outlined in red and the *L. pertusa* covering the platform surface are outlined in black.

## 8.3.4  Results

The growth rates calculated from the largest colonies ranged from 1.5 to 3.5 cm/yr on the various platforms and 0.45 to 1.6 cm/yr on the wrecks.  Using the average of the largest 10% of the corals measured for this analysis on each structure, the calculated rates ranged from 1.2 to 3.2 cm/yr on the platforms and from 0.4 to 1.1 cm/yr on the wrecks.  There was a significant linear correlation between the age of the structure and the calculated growth rate, with the lower growth rates calculated from the older structures ($R^2$ adj. =54.8%, p =0.009, Table 8-2).  There was not a significant correlation between age and growth rate with individual structure types, all rigs, or only wrecks.  Using a two-sample T-test, solid/compliant platforms had significantly higher growth rates than spar/tension leg platforms (p=0.04) and all rigs combined had a significantly higher growth rate than wrecks (p=0.025).

The shallowest occurrence of *L. pertusa* on the platforms ranged from 201 m on Pompano to 294 m on Joliet (Table 8-1).  Only one platform examined spanned the entire potential depth range of *L. pertusa* and the deepest occurrence noted on that platform was 801 m (Ram Powell, Table 8-1). On all platforms that we were able to survey from above the first occurrence of *L. pertusa* to the sea floor, the density of *L. pertusa* colonies peaked at some intermediate depth (Figure 8-17).  For the shallower water platforms, this peak depth was constrained by the platform water depth.  On the deeper water platforms, the peak in colony density occurred at about 500 m (Table 8-1, Figure 8-17).

Table 8-2.

Regression statistics for: Growth rate vs. maximum age of corals (Figure 8-23)

| Structure Type(s) | Regression Equation (Minimum growth Rate =) | $R^2$ adj. (%) | p-value of constant |
|---|---|---|---|
| All Rigs and Wrecks | – 0.0225 Structure Age[a,b] + 2.74 | 54.8 | **0.009** |
| All Rigs | – 0.0308 Structure Age[a] + 2.87 | 0.0 | 0.42 |
| Compliant/Solid | – 0.0344 Structure Age[a] + 3.39 | 16.9 | 0.33 |
| Spar/Tension Leg | – 0.0362 Structure Age[a] + 2.36 | 89.2 | 0.15 |
| Wrecks | – 0.0285 Structure Age[a,b] + 3.23 | 89.4 | 0.15 |

[1]*Structure age at the time of imaging. [b] An average of the earliest and latest possible dates of sinking (96 years) was used for the shipwreck Green Lantern.*
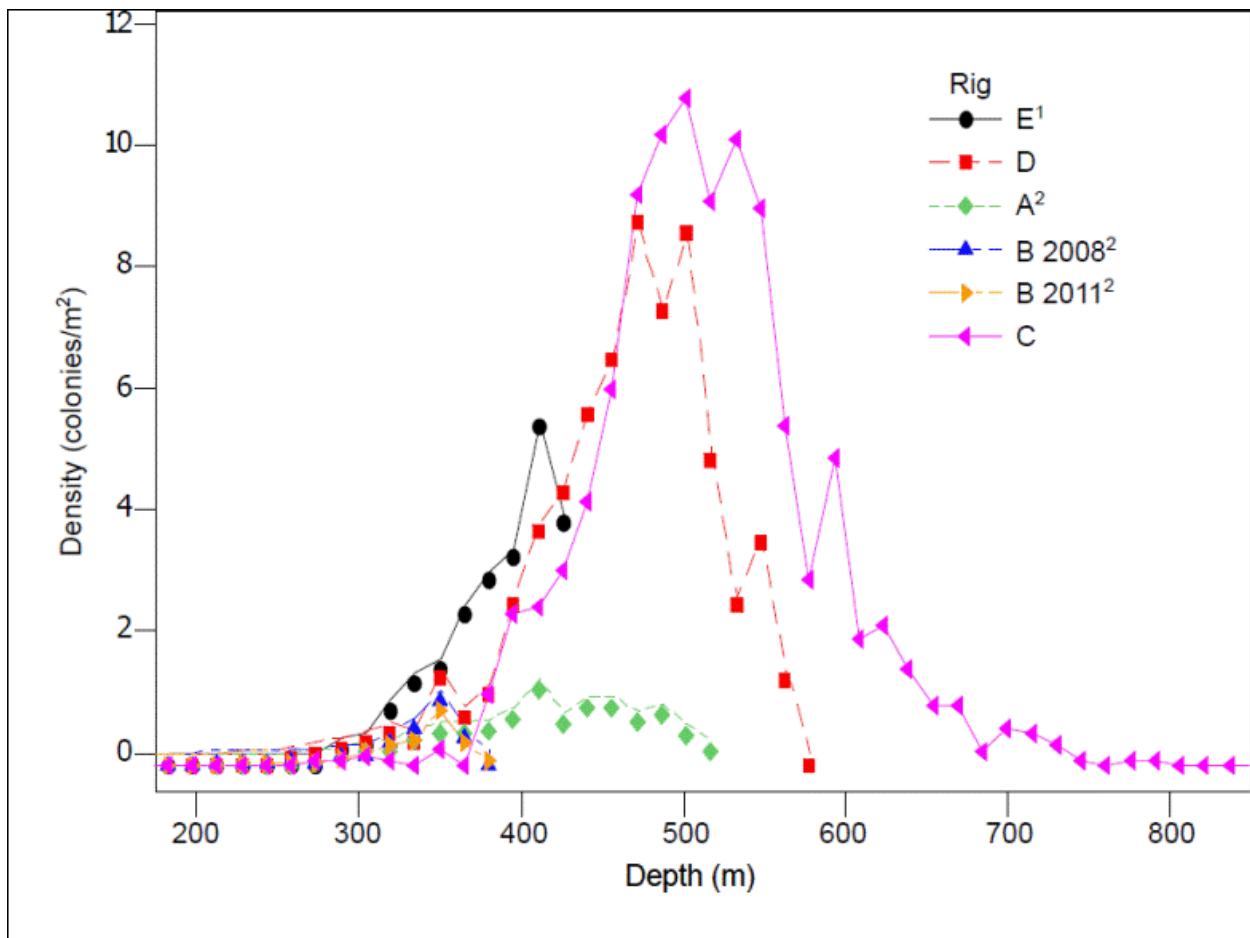


Figure 8-17. Colony density vs. depth  Scatter plot of colony density vs. depth. Petronius=A, Pompano=B, Ram Powell=C, Neptune=D, Jolliet=E, Zinc=F. Cognac was not included in this analysis because portions of the structure were covered in "thickets" of *L. pertusa* and thus colony density could not be determined.  [1]Measurements only obtained to 437 m.  Structure depth is 524 m.[2] Solid or compliant type structures.  The other platforms are spar or tension leg type structures.

The maximum densities on the different platforms ranged from about 1 to 10.8 colonies /m$^2$ and on the older platforms and some wrecks the colonies had merged into thickets (Table 8-1, Figure 8-17). In general, the highest densities of colonies were observed on the deeper platforms and the solid and compliant tower type structures had lower peak and average densities then the spar and tension leg type structures (Table 8-1, Figure 8-17).

Another measure of the density of *L. pertusa* on the artificial structures is the percent coverage. Using a one-way ANOVA with post-hoc Tukey's analysis, there was no significant difference ($\alpha$= 0.05) in the percent coverage of areas with maximum colony density on any platforms except the oldest platform which had the highest percent coverage (average 65.65%, SD 8.9%). However, the lowest maximum coverage occurred on the youngest platform imaged (average 1.67% SD, 1.13%). All wrecks at appropriate depths had *L. pertusa* growth at the thicket stage (Figure 8-18) and on the two World War II wrecks with extensive relief, coverage was 100% on many portions of the ship.
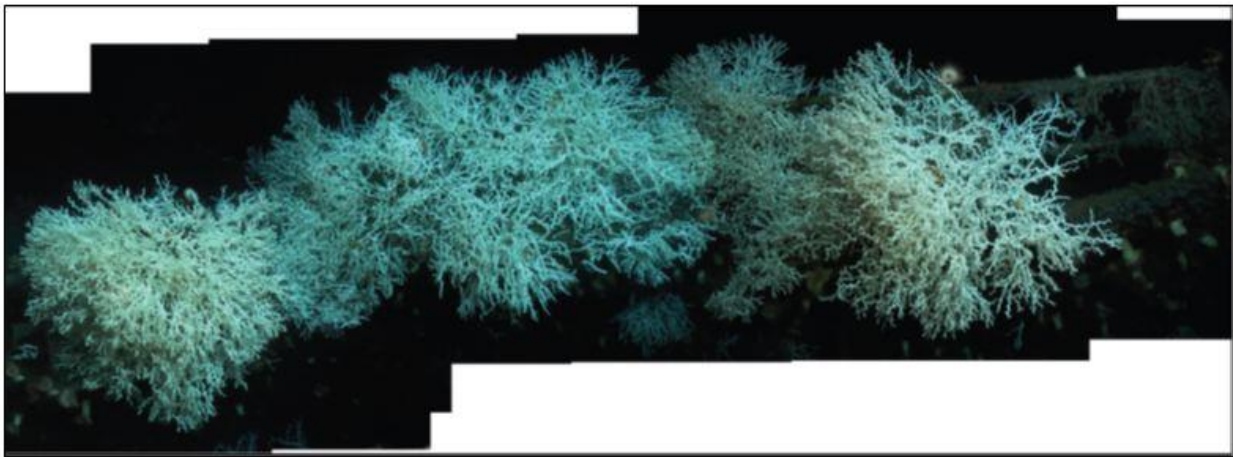


Figure 8-18. Mosaic of *L. pertusa* thickets growing on the bow of the *Gulfoil* shipwreck.

Although only colonies where growth away from the attachment substrate could be measured were used for the age calculations, the sizes of all colonies were estimated from the photographs. The largest colony on a platform with shape consistent with it arising from a single settlement event was 5,660 cm$^2$. In general, colony size was least in the depth intervals near the edges of the observed depth range and peaked at the same depth as colony density and maximum growth (Figure 8-19). On the one platform that spanned the full depth of occurrence of *L. pertusa*, the calculated growth rate of the largest colonies found per 15.25 m (50 ft) depth interval was significantly and positively correlated with the density of *L. pertusa* (R$^2$ adj.= 52.2%, p-value < 0.0001) (Figure 8-20).
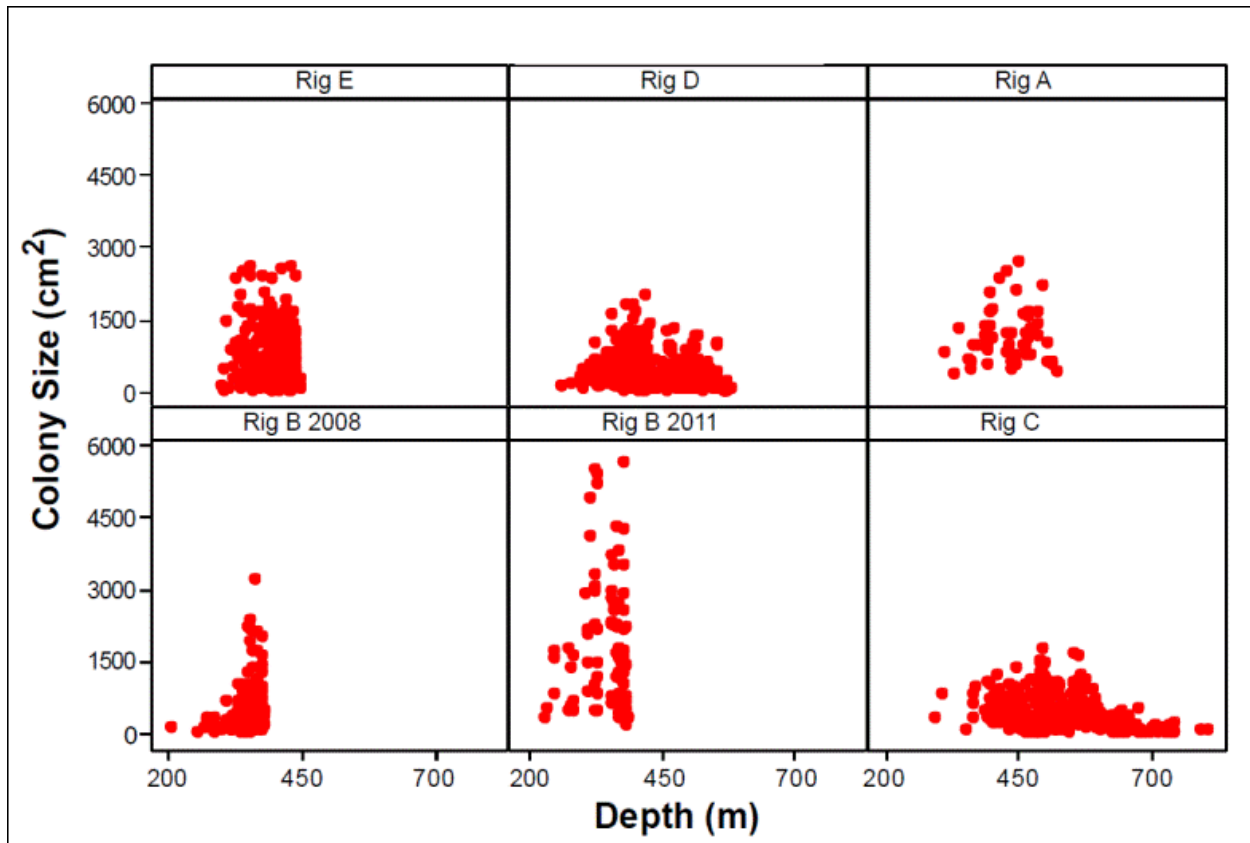
Figure 8-19. Scatter plots of colony area (size) vs. depth. Petronius=A, Pompano=B, Ram Powell=C, Neptune=D, Jolliet=E. Only Ram Powell is in a water depth that exceeds the known depth range of *L. pertusa*. Colony measurements are biased against smaller colonies that may not have shown up on poorer quality video and against very large colonies at high densities where individual colonies were difficult to distinguish from one another.
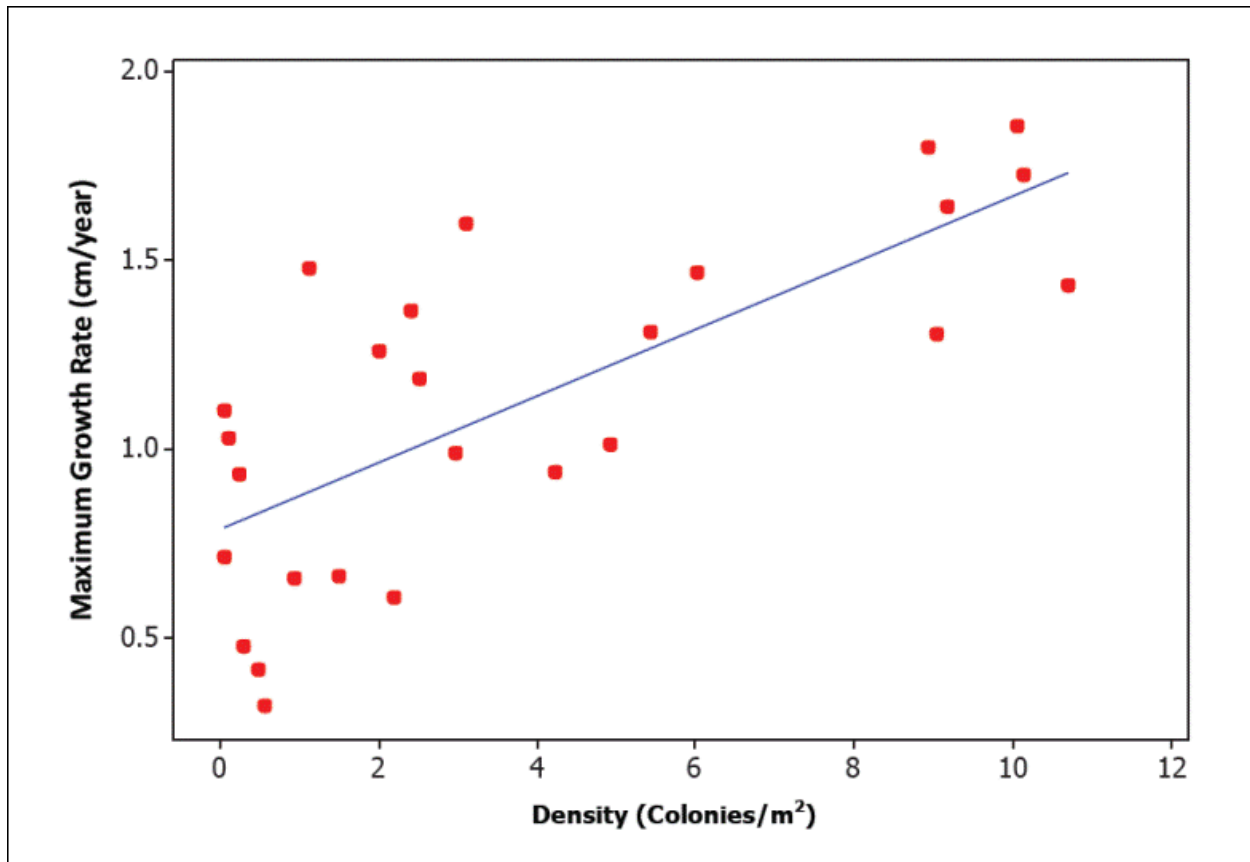
Figure 8-20.  Relationship between highest growth rate and density on different depth segments of Ram Powell. The highest growth rate measured in a 12.25 m (50 ft) section of the structure plotted against the density of colonies in that section.  Ram Powell was used for this analysis because it is the only platform in our data set that spans the entire depth range of *L. pertusa*.  The regression equation for this data set is.  $y = 0.088 + 0.79$.  $R^2$adj.$= 52.2\%$, p-value $< 0.0001$.

No *L. pertusa* growth was observed between the sea floor and 5-10 m above the sea floor on any structure, although one had *L. pertusa* growing on the sea floor near the base (Structure G) and a colony was found on a mostly buried flowline near another (Structure D). While *L. pertusa* colonies are absent on the base of these structures, anemones and other fauna are often present and abundant (Figure 8-21).

Of 4,383 *L. pertusa* colonies measured for this study, fourteen were not white.  The non-white *L. pertusa* colonies were observed on four platforms between 276 and 497 m depth. Colors ranged from bright orange, various shades of brownish-orange (Figure 8-22a) to one mottled brown/orange and white colony (Figure 8-22b).  Though non-white colonies on the same rig occurred within 50 m of each other, non-white colonies were never observed adjacent to one another.
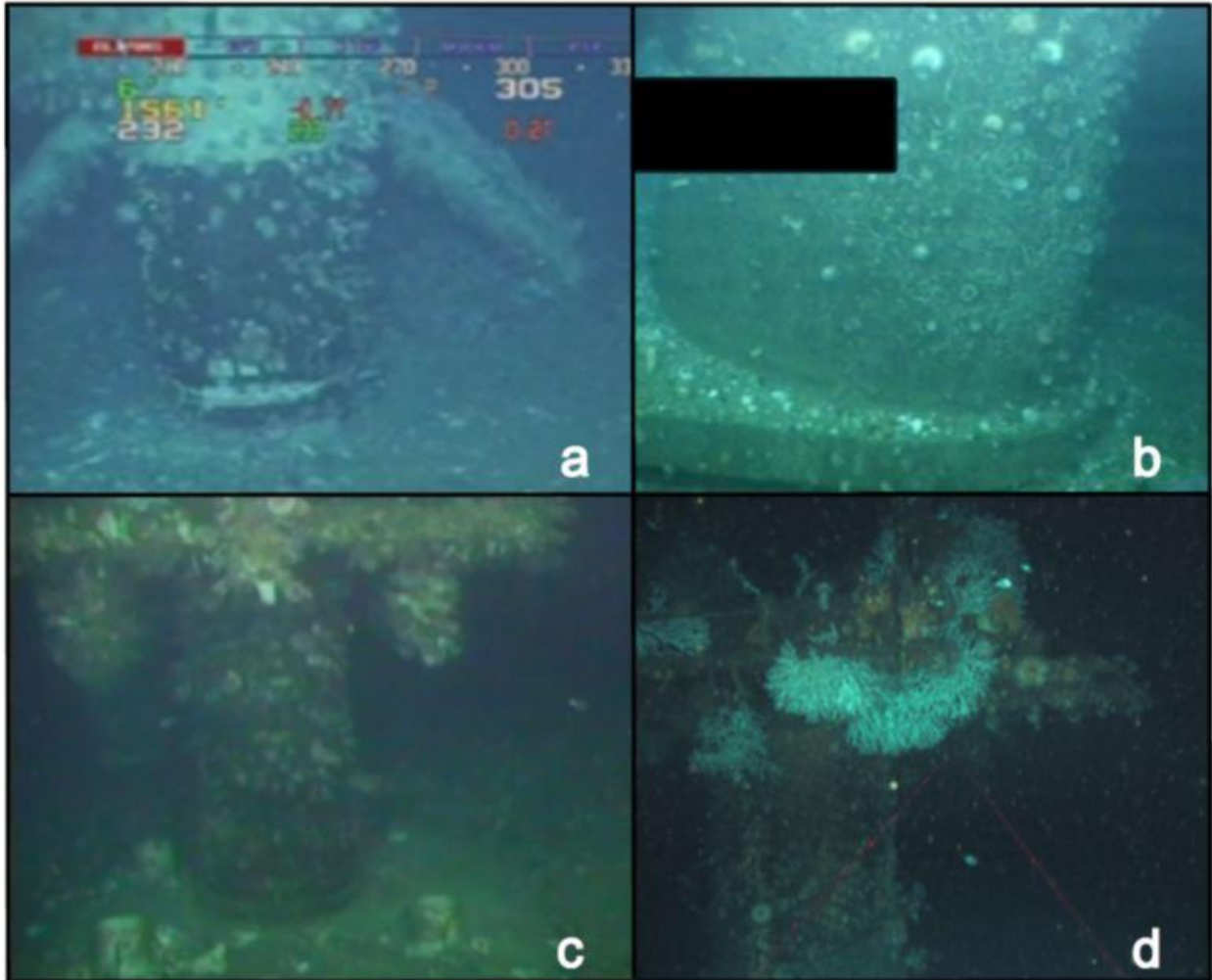
Figure 8-21. Example images of structure bases showing absence of *L. pertusa* below 5-10 m above the sea floor. Approximately 2.5-3 m of structure are visible in each image. a) leg of Petronius; b) leg of Pompano; c) riser connection on Neptune; d) abandoned flow tube connection at Zinc showing the beginning of *L. pertusa* colonization approximately 8 m off the sea floor.
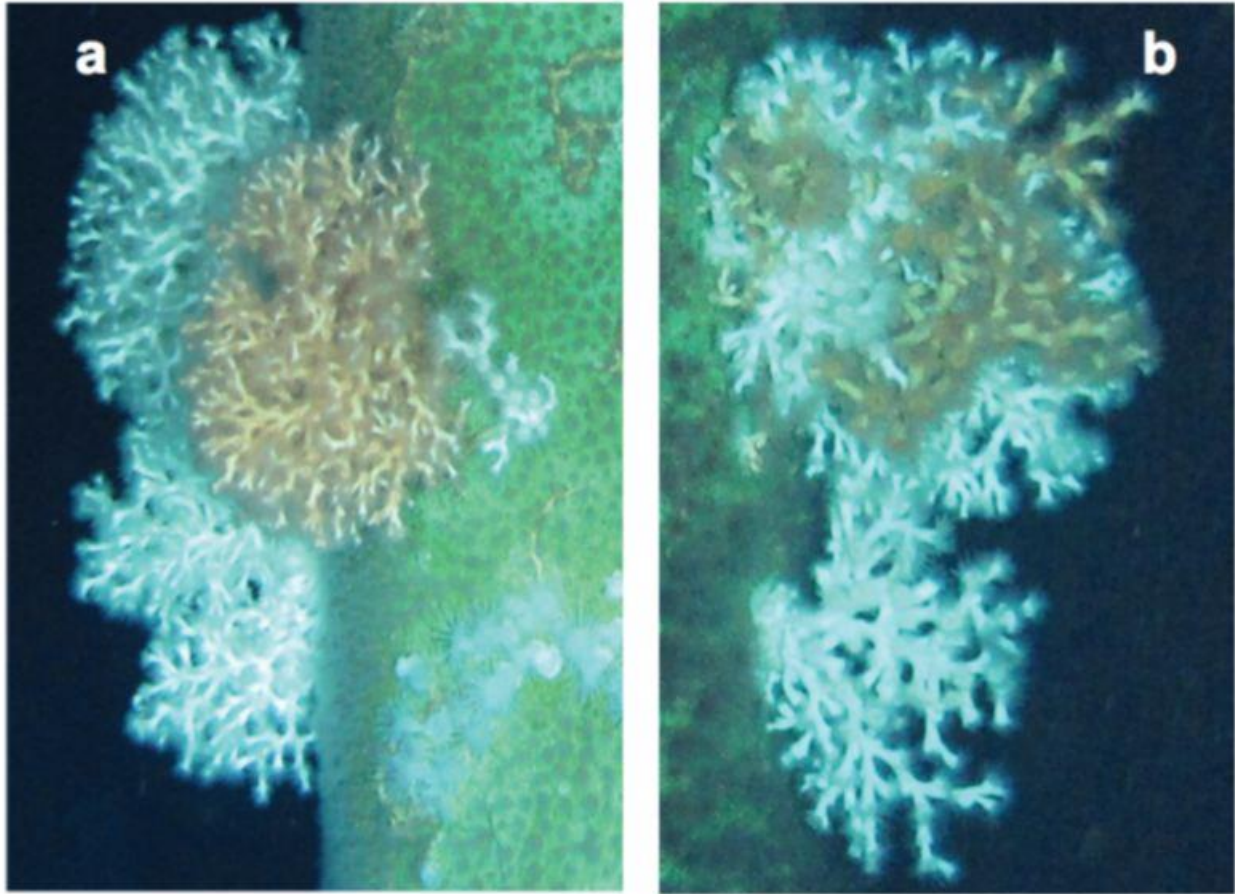
Figure 8-22.  Colored *L. pertusa* colonies - a) An orange *L. pertusa* colony at ~300 m on  Jolliet.
b) A colony of mixed colored *L. pertusa* at ~400 m on Jolliet.

### 8.3.5  Discussion

In this study we examined the growth rates of *L. pertusa* along with their density and depth distribution on artificial structures in the GoM.  The highest growth rates reported here (3.47 cm/yr)are similar to the highest published rates for *L. pertusa* measured on artificial structures in shallower water (Gass and Roberts, 2006). These rates are higher than those reported for deep water *L. pertusa* in the GoM using other techniques such as *in situ* staining (Brooke and Young, 2009).  Although it has been suggested that corals may have higher growth rates on metal structures due to electrical currents generated on those structures (Sabater and Yap, 2002), more recent studies found no significant gain in growth rate due to electrical currents, although it has positive effects on coral survival (Strömberg, et al., 2010) We consider that this non-invasive method for determining growth rate perturbs the coral less and more likely reflects natural rates at the depths measured.

Though growth rates are variable between structures (Table 8-1), overall, growth rates are negatively correlated with the age of a structure (Figure 8-23, Table 8-2). This may reflect faster growth or younger colonies, and/or the more linear branch growth inherent in early colony growth vs. the increased zig-zagging morphology of branches on older colonies.
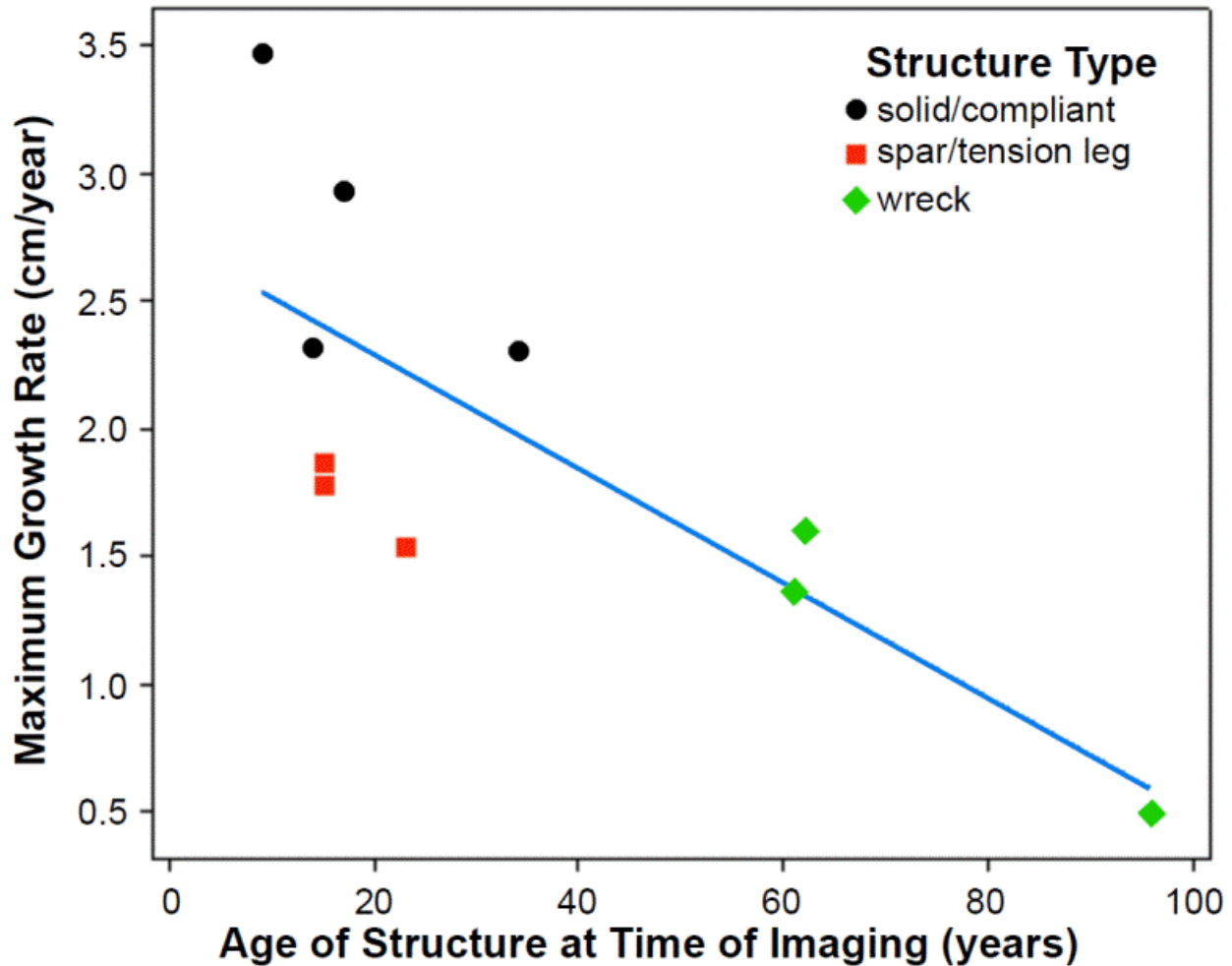
Figure 8-23.  Minimum growth rate vs. age of structure (maximum possible age of coral colony). There was no significant relation between growth rate and age of the structure within any subgroup and the line shown is for all structures (R2 sdj = 54.8, p = 0.009). See Table 8-2for regression statistics.

It is difficult to compare solid/compliant and spar/tension leg structures because no solid/compliant structure reached optimal *L. pertusa* settlement depth. (Table 8-1, Figure 8-17). Possibly because of the increased depth available for settlement, the maximum colony densities on spar/tension leg structures was approximately four times greater than on solid/compliant structures (Table 8-1). Conversely solid/compliant structures have significantly higher growth rates in comparison to spar/tension leg structures of similar ages even though all solid/compliant structures are at sub-optimal depth for *L. pertusa* settlement.   This may reflect the more massive, cross-braced compliant/solid structures affecting currents and facilitating food or oxygen delivery to the corals. Despite initial colony densities, percent coverage of *L. pertusa* on solid/compliant towers and ship wrecks is often quite significant (Figure 8-16, Figure 8-18), with large colonies reaching thicket stage by 34 years (Figure 8-16, Figure 8-19).

There are numerous natural potential source populations, both east and west of the structures studied here (Morrison et al., 2011), to provide larva that may settle on deep water installations. Because we found *L. pertusa* on every artificial structure examined (including shipwrecks at appropriate depths) (Table 8-1, Figure 8-18), there are likely numerous other structures harboring substantial *L. pertusa* growth in the northern GoM.

This study expands the known depth limit for *L. pertusa* in the GoM from 640 m (Schroeder et al., 2005) to 801 m (Table 8-1). Ram Powell provided the first opportunity to look at areas suitable for *L. pertusa* settlement throughout a continuous 995 m depth range at a single location. As expected, *L. pertusa* were not present above the thermocline, and it is likely that temperature defines its upper depth range in the GoM. Temperatures of 6° C were recorded at the maximum depth of occurrence during this study; whether *L. pertusa's* depth range is limited by physiological considerations, food supply, or lack of propagules cannot be determined from this study. In addition, using Ram Powell as a model, there appears to be a favorable depth range for *L. pertusa* settlement at 500-520 m (Table 8-1, Figure 8-17) and there is a strong positive correlation ($R^2$ adj.= 52.2%, p< 0.0001) between the growth rate of *L. pertusa* and colony density on this structure. For all structures, the continuum and variation in *L. pertusa* colony size throughout the majority of its depth range (Figure 8-19) is indicative of regular, reoccurring and ongoing colony settlement as opposed to rare settlement events.

In addition to expanding the depth range of *L. pertusa*, this study is the first to document the presence of non-white *L. pertusa* morphotypes in the GoM (Figure 8-22), though non-white *L. pertusa* are common in the North Atlantic. The rarity and distance separating these non-white colonies suggests that they are not clones, but the result of individual larval settlement. The absence of non-white *L. pertusa* on natural substrates in the GoM might indicate that the platforms are serving as "stepping stones" for invasion of these colored morphotypes into the Gulf. Though it is unknown whether *L. pertusa* color morphs are linked to genetic differences (Mortensen, 2001), it has been suggested that each may harbor different bacteria consortia (Neulinger et al., 2008).

For structures shallower than 800 m, there appears to be some type of "bottom effect" that renders the base of structures unsuitable for *L. pertusa.* (Figure 8-21, Figure 8-17, Table 8-1) even when the structure is no longer producing or handling hydrocarbons (i.e., Structure F). Although *L. pertusa* were absent on the bottom 5-10 m of all energy installations examined, other fauna were present on this portion of the installations, most notably, fly-trap anemones, suggesting that this effect is not the result of anti-fouling agents. The reason for this "bottom effect" is unknown and may be due to competition from fauna better equipped to utilize food that falls from upper levels on the platforms or some type of unfavorable sediment and/or current condition.

Despite the potential for new and continued *L. pertusa* habitat on artificial structures in the GoM, these are not normal substrates for *L. pertusa*. On natural substrates, *L. pertusa* growth can progress from single colonies, to thickets, then mature coppices (Wilson, 1979) which provide habitat for a variety of species on live, dead, and live/dead mixtures of *L. pertusa* (Cordes et al., 2008; Jensen and Frederiksen, 1992; Lessard-Pilon et al., 2010; Mortensen et al., 1995). Community biodiversity on and around *L. pertusa* reefs can be comparable to that of shallow-water reefs (Jensen and Frederiksen, 1992; Rogers, 1999) and can provide habitat for commercial deep-sea fish (Ross and Quattrini, 2007). Though artificial structures will provide habitat for

numerous other species, this live/dead mixture of *L. pertusa* cannot form on vertical or steep diagonal structures where dead-bioeroded *L. pertusa* will be swept away and fall to the sea floor. As a result, the communities closely associated with *L. pertusa* on platforms are not as species rich as those associated with natural *L. pertusa* reefs.

Energy platforms, sub-sea installations, and shipwrecks afford a unique and valuable opportunity to study many aspects of *L. pertusa* biology because of: 1) the known date of installation for growth rate and population studies, 2) the large depth range of potential substrate in a single location represented by the deeper water platforms, and 3) wide distribution and large numbers of potential substrates in known locations of the deep GoM. Here we reported on a relatively small number of artificial structures, at very limited points in time. Repeat visits to these and additional structures will allow researchers to understand more fully *L. pertusa* settlement and growth patterns, physiological requirements, and the connectivity of populations throughout the GoM.

# 9   VK906 *LOPHELIA* MOUND PISTON CORE ANALYSIS

While evaluating 3-D seismic sea floor amplitude data for hard bottom areas that could support deepwater coral communities, Dr. Harry Roberts of Louisiana State University's Coastal Studies Institute and BOEM colleague Bill Shedd identified some unusual mounds in the Visoca Knoll lease area, block 906.  These mounds occur on the upper continental slope south of the late Pleistocene "Lagniappe" shelf-edge delta (Roberts et al., 2004) and southeast of the modern Mississippi River delta (Figure 9-1).  Unlike the acoustically reflective areas (high positive sea floor amplitude) that develop primarily because of authigenic carbonate precipitation in association with microbial oxidation of hydrocarbons that have migrated to the seabed, the VK906 mounds exhibited low acoustic reflectivity (low positive sea floor amplitudes) and a nonstratified or acoustically transparent interior.  The morphology and seismic character of the mounds is similar to *Halimeda* bioherms discovered in the eastern Java Sea and opposite the Mahakam Delta of Borneo (Roberts et al., 1987) which suggested they may be organically built features and therefore made them a focal point of scientific interest.

Azooxanthellate corals of the dark, cold-water environments of the northern GoM continental slope are known to have wide geographical and depth ranges.  Of these deep-water corals, *Lophelia pertusa* is known to build impressive colonies and low-relief mounds  (Sulak, 2008).  However in the Atlantic off the eastern coast of the United States (Newton et al., 1987, Paull et al., 2000, Messing et al., 1990; and others), along the north Atlantic-European margins (White et al., 2005; Freiwald, 1997, Mortensen et al., 2001; and others), and recently off the coast of Mauritania and Angola (Colman et al., 2005, Eisele et al. 2011, Le Gilloux et al. 2009) large lithoherms and mounds composed largely of *Lophelia* coral debris have been recognized and studied.  Where age-dated, some of these mounds represent developmental time scales of thousands of years.

However, until large deep-water *Lophelia* mounds were discovered during the present BOEM-NOAA funded project,  *Lophelia* mounds of such magnitude had not been discovered in the GoM.  In fact, Sulak (2008) indicates that known *Lophelia* colonies and low-relief mounds in the GoM, such as the impressive coverage of *Lophelia* on the hard substrates of authigenic carbonate in VK826 (Schroeder et al., 2005), do not have extensive rubble cones around them or build large mounds like the Atlantic examples.  The coral-covered mounds found in VK906 are different from other *Lophelia* build-ups so far recognized from the GoM.  They are much larger, cone-shaped, and from initial surface observations appear to have been constructed of significant accumulations of coral rubble.Figure 9-2 A illustrates a 3-D seismic surface amplitude map of the ocean bottom area supporting the mounds and an associated North-South oriented seismic profile through several mounds.  The mounds are located above a shallow subsurface salt body that impacts the bathymetry of the area, creating a well-defined low-relief tabular structure with a distinct gully-like depression along the western and southern margins.  The sea floor above the salt and in the gully-like areas is highly reflective, especially above the edges of the subsurface salt body.  By contrast, the small mounds have a 3-D seismic surface amplitude that is lower than the general background for the area (a very low positive 3-D seismic amplitude).
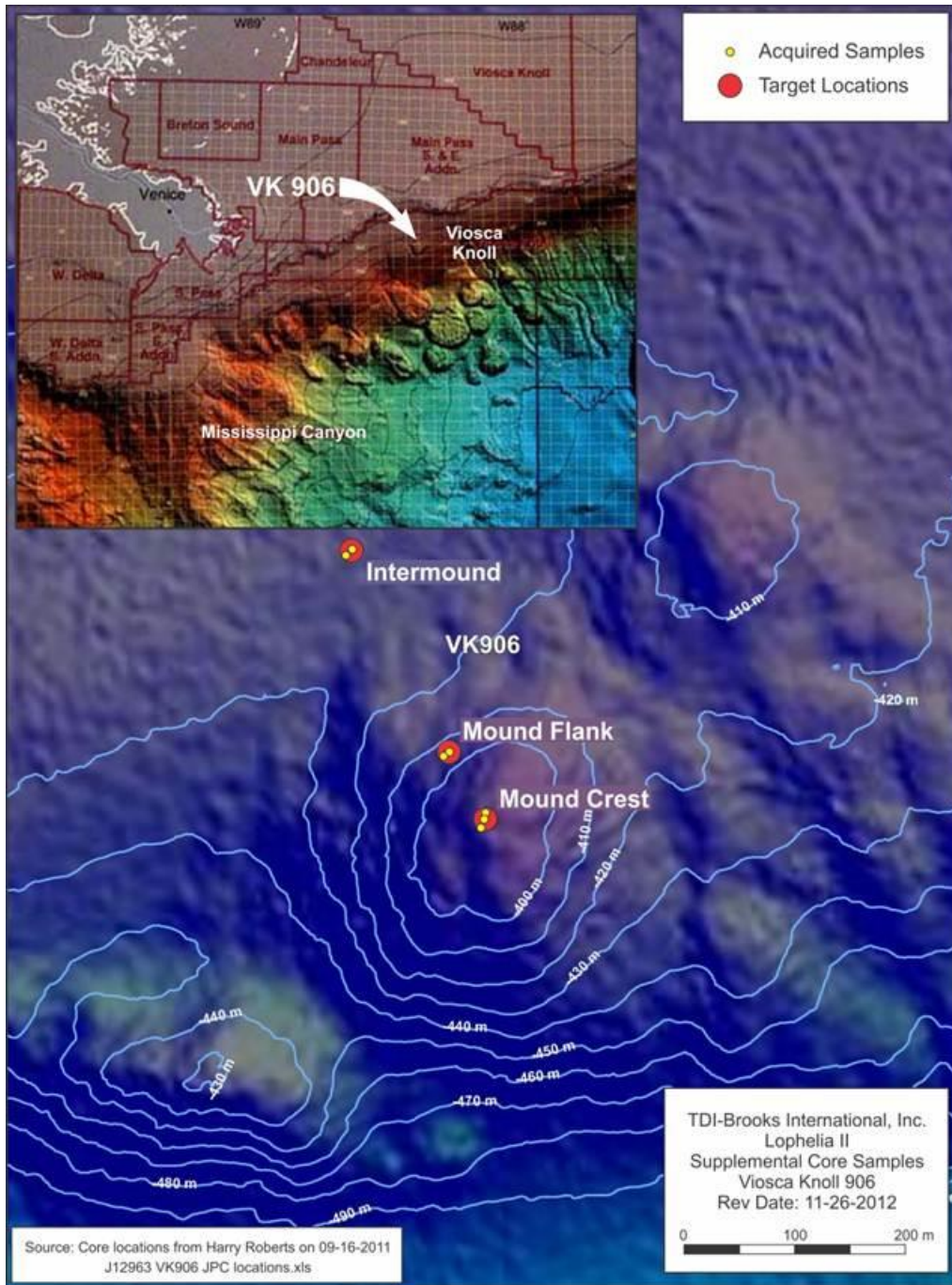
Figure 9-1. The inset in this figure illustrates the location of VK906 on the background of computer-shaded multibeam bathymetry of the OCS and upper continental slope. The mound identified on this map was cored at the crest and flank. Note that the water depth of the mound crest is less than 400 m (1,312 ft.) and the base is between 420 m (1,378 ft.) and 430 m (1,410 ft.). Core locations are shown at the mound crest, mound, flank, and an intermound site.

The seismic profile of Figure 9-2 B indicates that the mounds have apparently built on a highly reflective surface that is clearly displayed outside and lateral to the mounds. This surface is also imaged through the largest mound and it appears that the mounds built on this surface. At first, a hydrocarbon seep origin was considered for these features. However, as the seismic profile of Figure 9-2 B and other profiles not presented in this report illustrate, clear migration pathways from the subsurface to the mounds are not easily defined. Later, ROV dives made on the largest of the mounds (Figure 9-2 B), as part of the *Lophelia* II Project, confirmed a lack of hydrocarbon seep-related characteristics on the surface of the mound and around it. However, we found that the mound crest and upper flanks were densely populated by "thickets" of the deep-water coral *Lophelia pertusa* (Figure 9-3).

These coral "thickets" are defined by the surface roughness on the multibeam bathymetry image acquired by the Woods Hole Oceanographic Institution's *Jason II* ROV (Figure 9-2 B). These observations plus the unique seismic characteristics of this mound generated questions concerning whether *L. pertusa* was actually responsible for constructing the mound or that the present coral cover was simply the product of a convenient mounded substrate. In addition, higher total alkalinity levels were observed adjacent to the mound at VK906 as compared to the background water column. Although broad trends in water column carbonate chemistry could result from the complex current structure of the GoM, these highly localized elevations in concentration are not likely to be related to large-scale oceanographic patterns. The largest mound and its associated subsurface geology does not have characteristics that would lead to an interpretation that it was initially built by fluidized sediment extrusion at the seabed. So, how did the mound form, what is its developmental history and age? From other studies of deep-water corals and the structures they build, mostly concentrated in the northeastern Atlantic, we know that *L. pertusa* is capable of building sizeable mounded features (Freiwald, et al., 1997; Mortensen et al., 2001; White et al., 2005 and others).

To answer important scientific questions about the VK906 mounds, samples were needed from a mound interior. With a modest addition to the *Lophelia* II Project budget, TDI-Brooks International, Inc. was employed to take Jumbo Piston Cores (JPCs) in the largest of the VK906 mounds and in the intermound area where the reflective surface on which the mounds appear to have developed could be encountered. On May 28, 2012 cores were acquired using the R/V *Brooks McCall*. The core sites are shown on Figure 9-1. Both Standard Piston Cores (PCs) and Jumbo Piston Cores were acquired. The mound crest and flank were cored with the Jumbo Piston Corer. A sheared piston bolt prevented a Jumbo Piston Core from being taken at the intermound site. Statistics associated with the coring program are given in Table 9-1.
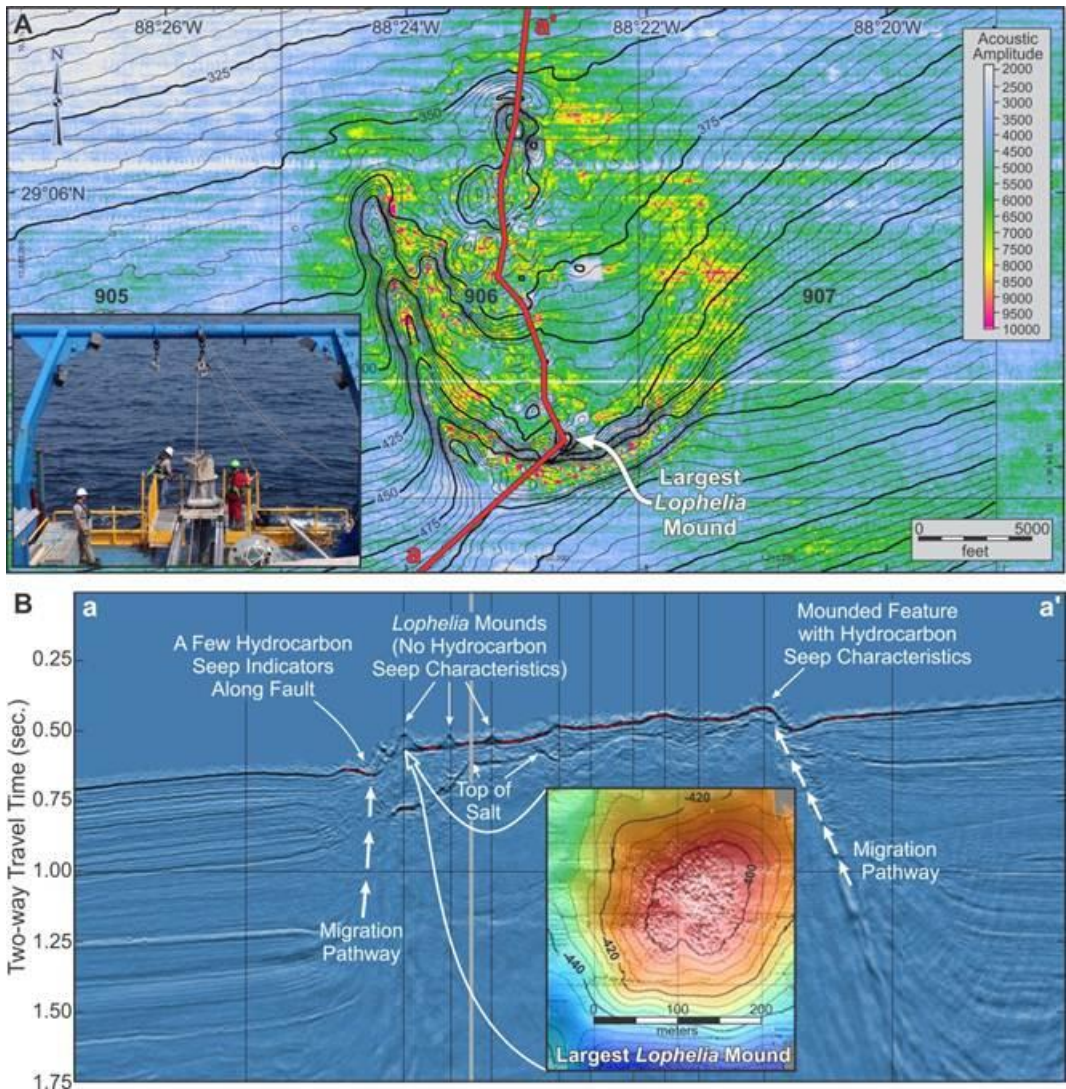
Figure 9-2.  (A) This combined 3-D seismic sea floor acoustic amplitude and bathymetry map generally defines a shallow subsurface and tabular salt body with a gully-like sea floor depression along its western and southern flanks.  Note that the scattered patterns of high surface amplitude generally occur around the flanks of the salt body, but high amplitudes are not exclusive to the flanks.  The bathymetry defines several mounds above the salt body.  Seismic line a-a´ cuts through three of these mounds near the southern end of the salt body and is the location of the profile illustrated below.  The inset is the aft deck of the R/V *Brooks McCall* on site to collect a Jumbo Piston Core from the largest *Lophelia* mound shown on the seismic profile below. (B) This seismic profile is oriented roughly N-S across the shallow tabular salt body over which small mounded features occur on the sea floor.  The inset is a high resolution bathymetric image of the largest *Lophelia* mound located at the southern edge of the salt body. This multibeam bathymetry image was acquired by the ROV *Jason II*.  The "roughness" at the mound crest and upper flanks is a reflection of living *Lophelia* thickets currently growing on the mound surface.

323
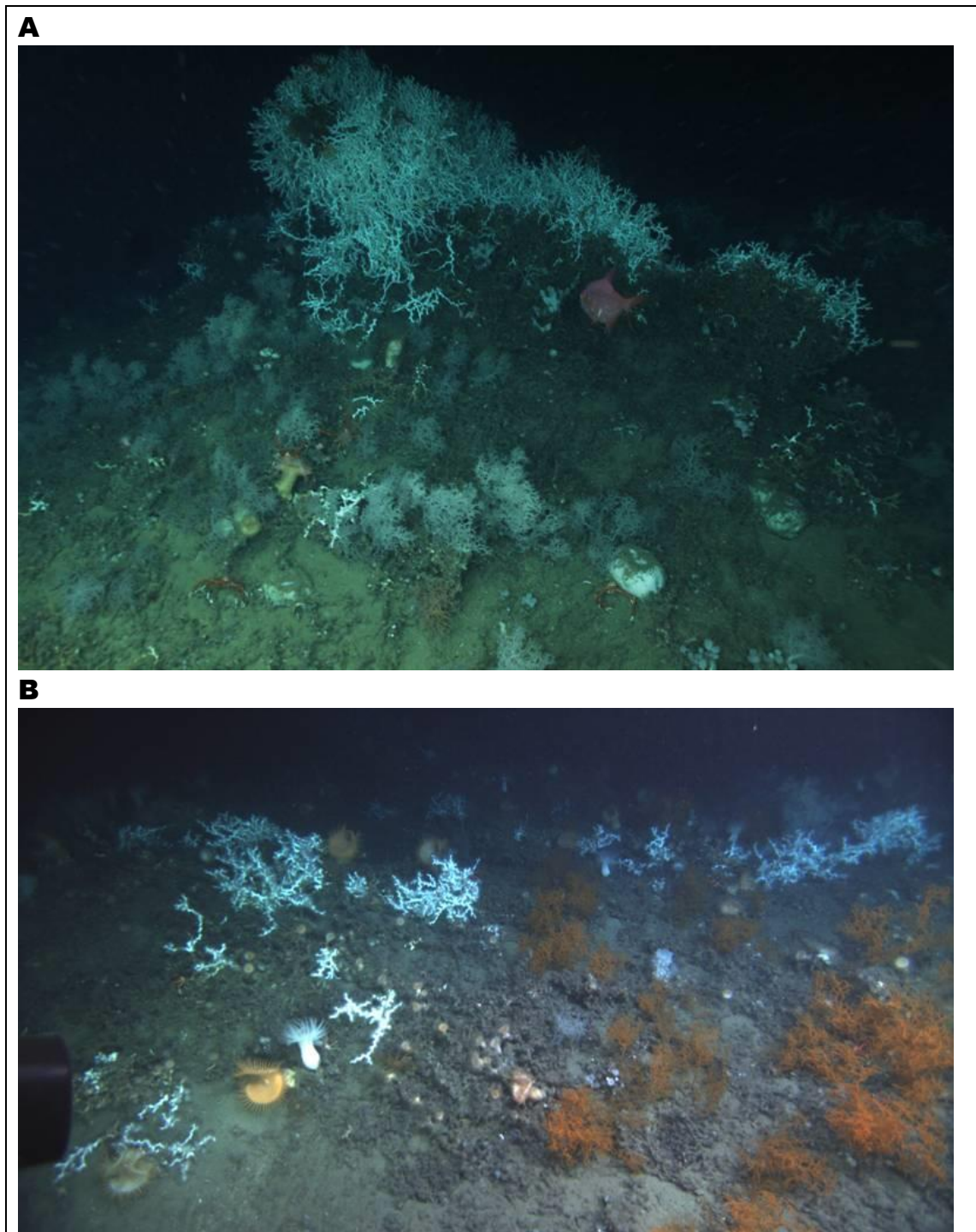
Figure 9-3. (A) A living *Lophelia* "thicket" on top of a small mounded structure near the crest of the *Lophelia* mound of Figure 9-2B. (B) Living *Lophelia* and coral rubble on the surface of the largest mound seismically imaged in Figure 9-2B.

Table 9-1.

Core acquisition data

| Site | Type | Recovery | Data-Time | USBL Lat | USBL Lon | USBL Depth (m) |
|------|------|----------|-----------|----------|----------|----------------|
| Intermound | PC | 14'02" (4.2 m) | 5/18/12 7:27 | N29 04.3020 | W088 22.7054 | -428 |
| Mound Flank | PC | 15'10" (4.8 m) | 5/28/12 8:10 | N29 04.2028 | W088 22.6496 | -407 |
| Mound Crest | PC | 17'08" (5.3 m) | 5/28/12 8:49 | N29 04.1700 | W088 22.6293 | -393 |
| Mound Crest 44 JPC | JPC | 40'05" (12. 3) | 5/28/12 10:35 | N29 04.1731 | W088 22.6287 | -379 |
| Mound Crest 2 64ft JPC | JPC | 53'08" (16.4 m) | 5/28/12 13:07 | N29 04.1657 | W088 22.6316 | -377 |
| Mound Flank 64ft JPC | JPC | 54'09" (16.7 m) | 5/28/12 14:58 | N29 04.2005 | W088 22.6529 | -389 |
| **Intermound 64ft JPC | JPC | 0' | 5/28/12 16:48 | N29 04.2994 | W088 22.7087 | -409 |

Coordinates are WGS84 UTM 16N M. PC is piston core.**Piston bolt sheared during Jumbo PC deployment at Intermound site; no recovery

## 9.1 METHODS OF INVESTIGATION

### 9.1.1 Mound Discovery

The database used to analyze the continental slope sea floor and shallow subsurface potential coral community sites consisted of over 190 time-migrated 3-D seismic volumes acquired over the northern GoM continental slope. These data acquired for the oil and gas industry housed at the BOEM office in New Orleans and can be accessed for BOEM-sponsored environmental studies under proprietary conditions. Sites for data collection using a submersible or ROV were selected based on 3-D seismic sea floor amplitude (or acoustic reflectivity) analysis. The details of the site selection process are presented in a separate section of this report. The methodology of sea floor evaluation for identifying hard bottoms associated with hydrocarbon seeps that may be the sites of deep-water coral communities is also presented in Roberts et al. (2010). These methods of analyzing BOEM-held 3-D seismic data were used in identifying potential coral community sites in support of the *Lophelia* II Project. The *Lophelia* mound discussed in this section of the final report was discovered by analyzing 3-D seismic data from the continental slope southeast of the modern Mississippi River delta, the Visoca Knoll Lease area.

### 9.1.1.1 Core Acquisition

As previously stated, both Standard Piston Cores with a 7.6 cm (3 in) diameter and larger Jumbo Piston Cores (JPC) with a 12.7 cm (5 in) diameter were acquired from the largest and most southern mound of the mounds in VK906. The standard piston cores were taken first to test the penetrability of the mound prior to risking a bent core barrel with the much longer JPC. Table 9-1 shows that two JPCs were acquired from the mound crest, the longest of which was 16 m (53 ft.). The longest JPC was acquired from the mound flank. This core was 16.4 m (54 ft.) long. A JPC was not taken as planned in the intermound area because of a malfunction of the coring equipment. However, a 4.2 m (14 ft.) long Standard Piston Core was acquired at the predetermined intermound site.

### 9.1.1.2  Core Analyses

Prior to cutting the cores and sampling the sediments for a variety of analyses, the cores were analyzed using a remote sensing multisensor core logger, a non-destructive method of testing. Multisensor logger profiles are presented for the Mound Crest 2 Core (Figure 9-4), the Mound Flank Core (Figure 9-5), and the Intermound Core (Figure 9-6).

### 9.1.1.2.1    Multisensor Core Logger

This relatively new system for logging the geophysical properties of sediment cores allows both whole cores and split cores to be measured in a nondestructive fashion (Schultheiss and Weaver, 1992; Schultheiss and McPhail, 1989). The current sensor configuration measures (a) bulk density (using gamma-ray attenuation), (b) magnetic susceptibility at user-defined sample intervals down the core, (c) electrical resistivity, and (d) compressional (P) wave velocity (500 kHz). Split-core logging may provide slightly more reliable results than whole core logging as it mostly eliminates core-slumping effects that can lead to spurious results; it also gives higher resolution magnetic susceptibility readings. However, in most cases splitting the core may not be practical because of other demands such as geotechnical work. Only bulk density, magnetic susceptibility, and resistivity were acquired on the mound cores.

**Bulk Density:**  Density is determined by measuring the attenuation of gamma rays through the core. A $^{137}$Cs gamma source in a lead shield, with optional 2.5 mm or 5 mm collimators, provides a thin gamma beam which passes through the core. An integrated gamma detector measures the intensity of the beam relative to standards providing the gamma density of the core material. Density can be measured with an accuracy better than 1% depending upon count time used and cores condition. Calibration standards are machined from a standard aluminum billet and stepped to enable calibration equations to be determined. Separate calibration samples are matched to each type of core liner used.
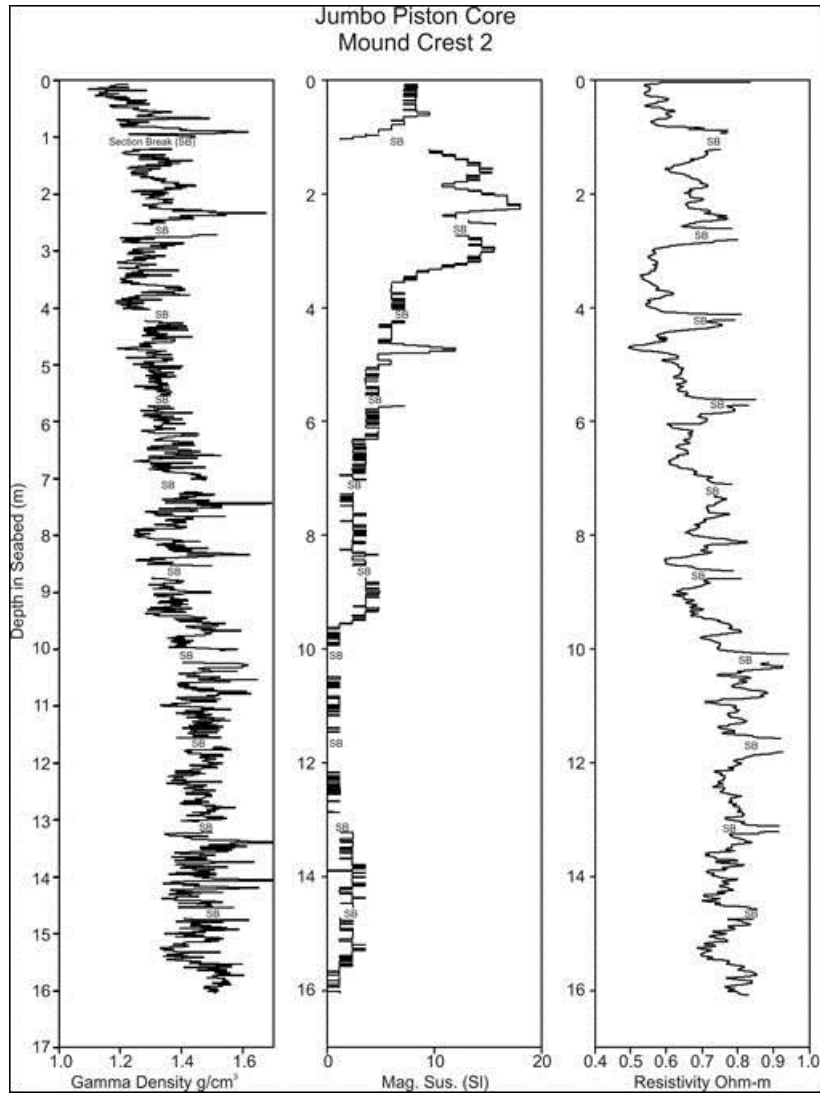
Figure 9-4.  Multisensor core logger profiles of Gamma Density,
Magnetic Susceptibility, and Resistivity for the Mound Crest
2 JPC.
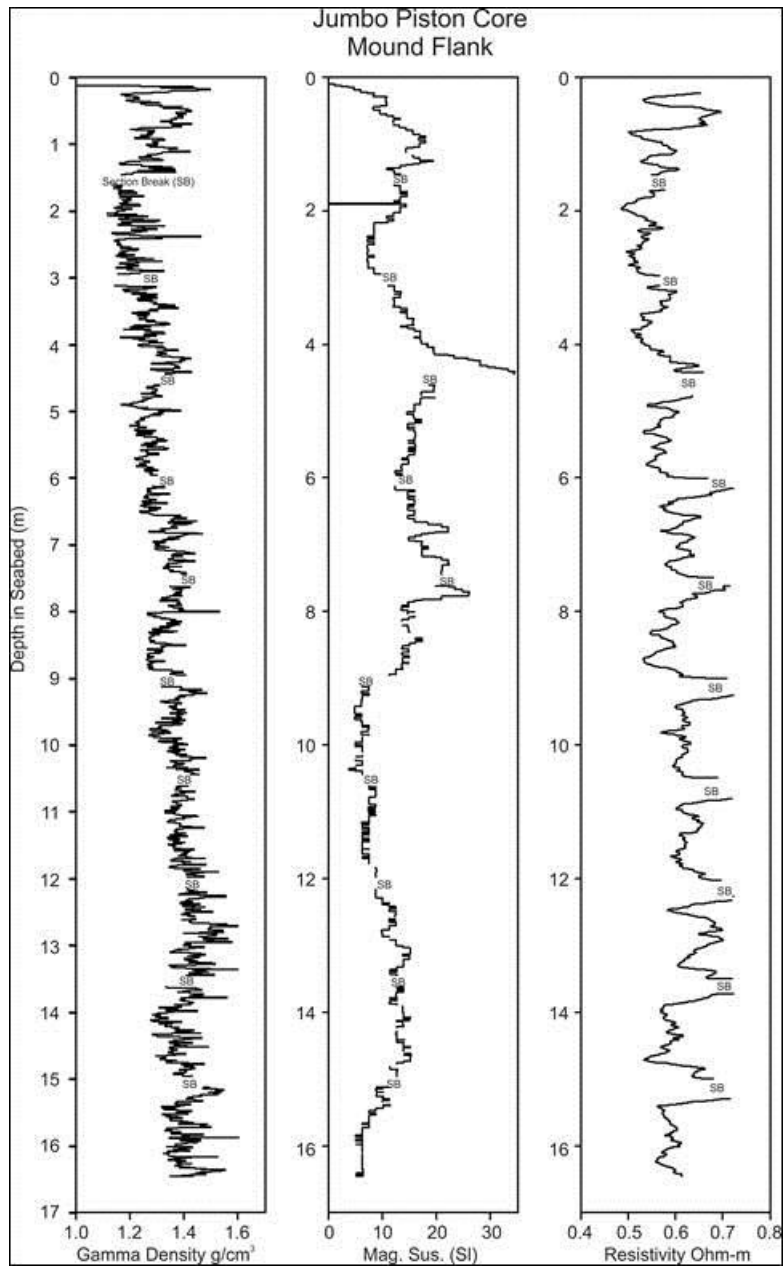
Figure 9-5.  Multisensor core logger profiles of Gamma Density,
          Magnetic Susceptibility, and Resistivity for the
          Mound Flank JPC.
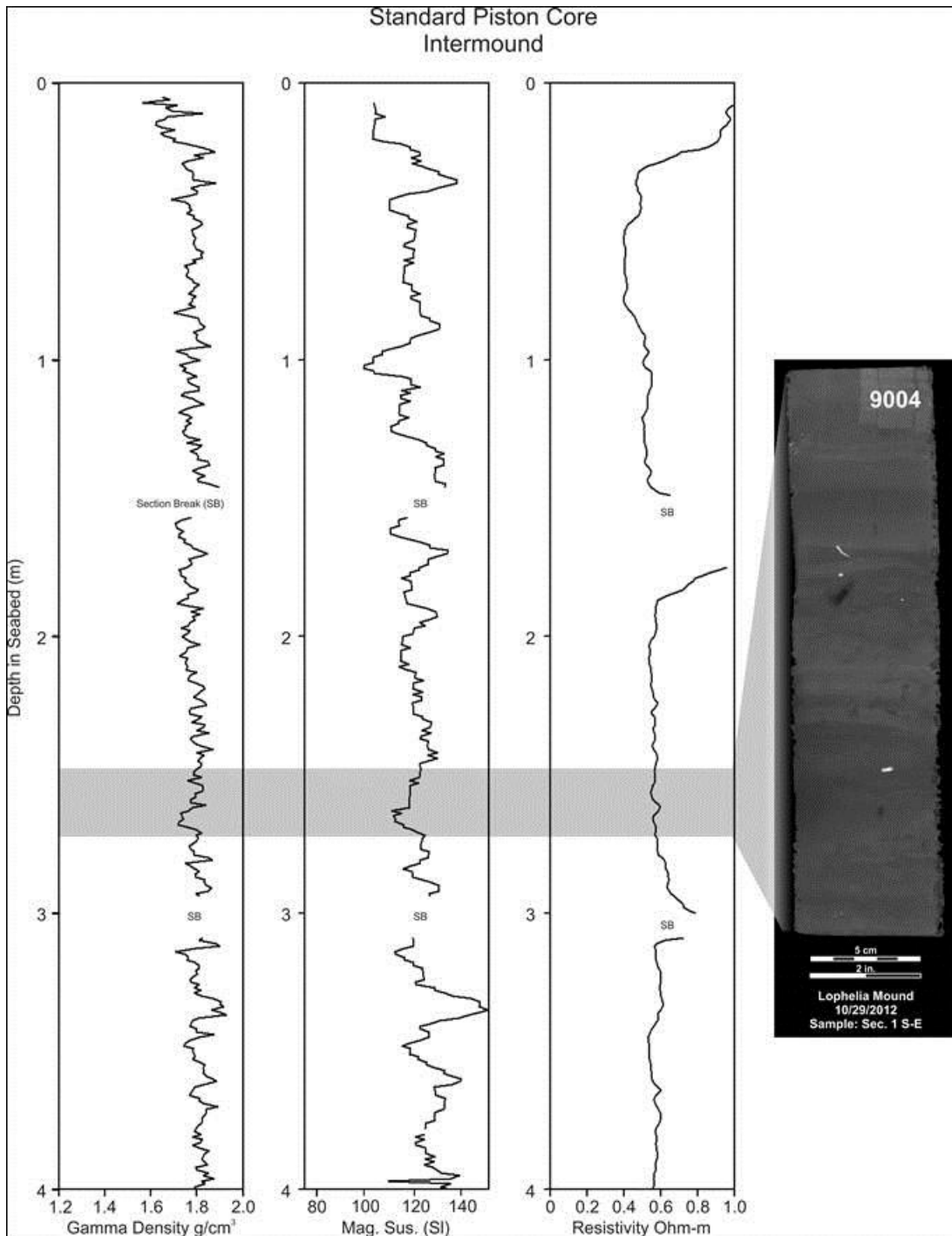
Figure 9-6. Multisensor core logger profiles of Gamma Density, Magnetic Susceptibility, and Resistivity as well as an example X-ray radiograph for the Intermound Standard Piston Core. Note the subtle clay-to-silty clay layering revealed in the X-ray radiograph.

**Magnetic Susceptibility**:  Two sensor systems are available: a loop sensor for use with whole cores and a point sensor for use with horizontally split cores.  The new point sensor enables down-core spatial resolutions of better than 5 mm to be achieved.  Accuracy is typically within 5% depending on core quality and type of material.  Calibration/check samples are provided with each sensor.

**Electrical Resistivity:**  The multisensor core logger is equipped with a non-contact resistivity sensor, the newest sensor developed by GeoTek.  The non-contact resistivity sensor technique operates by inducing a high-frequency magnetic field in the core, from a transmitter coil, which in turn induces electrical currents in the core which are inversely proportional to the resistivity.  Very small magnetic fields regenerated by the electrical current are measured by a receiver coil.  To measure these very small magnetic fields accurately, a difference technique has been developed which compares the readings generated from the measuring coils to the readings from an identical set of coils operating in air.  This technique provides the requisite accuracy and stability required.  Resistivities between 0.1 and 10 ohm-meters can be measured at spatial resolutions along the core of approximately 2 cm.

**Multi-Sensor Core Logger Data Editing**:  Raw sensor data were processed using calibration parameters to provide measurements in standard units of measurement for each sensor.  For presentation purposes, the words "section break" were included on the multisensor core logger profiles for those areas influenced by proximity of core endcaps, and obvious gaps in sediment visible through core liner.  This influence is most significant for magnetic susceptibility, resistivity sensors, and p-wave sensors which have lower spatial resolution ($> 1$ cm) than do sensors for sound speed and gamma density ($< 1$ cm).

### 9.1.1.3  Digital Core Photography

Each core section was split longitudinally and the surface of one core half prepared for photography.  The other core half was placed in plastic sleeving to preserve the core for future analyses and then placed in a cold storage locker.  All sections of each core designated for photography were assembled in stratigraphic order and fed into the GeoTek Multisensor Core Logger equipped with a high resolution scanning digital camera and data recorded on the system's computer.

### 9.1.1.4  Age Dating (Radiocarbon and U/Th)

Coral samples were selected for radiocarbon dating from two living *Lophelia* corals at the surface of the mound and at five sites within the Mound Crest 2 core (JPC) ranging from the mound surface to a depth down-core of 490 cm (16 ft.).  The samples were ultrasonically cleaned before shipping to Beta Analytic Inc. of Miami, Florida where they were acid etched and analyzed according to standard methodology for producing radiometric dates.  After applying a $^{13}C/^{12}C$ correction, conventional age dates were calculated.  The Conventional Radiocarbon Age is cited with the units "BP" (Before Present).  Present is defined as AD 1950 for the purposes of radiocarbon dating.

A total of five coral samples were selected for U/Th dating over the entire sedimentary sequence sampled in the Mound Crest 2 Core (JPC). These samples were ultrasonically cleaned prior to shipment to the U/Th dating laboratory at the University of Minnesota. Methods similar to those applied to *Lophelia* corals of the North Atlantic by Schroder-Ritzrau et al. (2005) were being applied to the samples collected from VK906.

### 9.1.1.5 Clay Mineralogy

Selected samples of matrix sediment spanning the entire length of the Mound Crest 2 (JPC) were submitted to the X-Ray Diffraction Laboratory in the Department of Geology and Geophysics at Lousiana State University for clay mineral analysis. The clay-size (<2μm) fraction from each sample was extracted by dispersion in a 0.1% $Na_3PO_4$ solution followed by removal of the top 5 cm of the water column after 3.5 hours of settling. High-speed centrifugation separated the solids from the slurry. The extraction was repeated several times. Oriented films were produced by combining clay pastes and smearing onto glass slides. X-ray diffraction patterns were collected after each sample had been air-dried, exposed to an ethylene-glycol saturated atmosphere, and heated to 300°C and 550°C for an hour, respectively. The X-ray diffraction patterns were produced with CuKα radiation in a Bruker/Siemens D5000 diffractometer at 40 kV and 30 mA between 2-36°2θ at an interval of 0.02°2θ per second using a rotating sample holder. A second run will be made with the carbonates removed using a buffer pH5 Sodium Acetate-Acetic acid solution in a 95° oven. Then, the clay-size fraction will be extracted and the resulting smear sample run on theX-ray diffractions.

### 9.1.1.6 Elemental Analyses

Coral samples were selected from the entire stratigraphic interval sampled by Mound Crest Core 2 (MC-2), a Jumbo Piston Core. The samples were washed in distilled water and ultrasonically cleaned to remove matrix sediment from the sample exteriors and within the corallites. The samples were dried for 24 hours at 105 °C, then ground to a powder. About 1 g (weighed to four decimal places) of ground dry coral skeletal materal was placed in a 75 ml glass digestion tube and extracted with 5 ml of concentrated trace-metal-grade nitric acid at ~ 120 °C for 8 h. The mixture was diluted to 50 ml with deionized water. Metal analyses were performed on the clear supernatant using a Varian model MPX ICP-OES.

### 9.1.1.7 Skeletal Density

Density of *L. pertusa* skeletons was measured from Mound Crest Core 2 according to the methods in Section 3.1.

## 9.2 INITIAL RESULTS

The data collection on samples from the VK906 *Lophelia* mound is on-going and only a preliminary appraisal of this unusual feature is presently available. Although long cores were taken both from the mound crest and mound flank (Figure 9-1) most of the sampling so far has

been concentrated on the Mound Crest 2 JPC which was 16.4 m (53 ft. 8 m) long.  A JPC was also planned for the Intermound site (Figure 9-1), but technical problems during field acquisition prevented a long stratigraphic section from being sampled.  The point of this Intermound core was to sample and date the stratigraphic horizon with high acoustic reflectivity characteristics on which the *Lophelia* mounds above the southern end of the tabular salt body seemed to have developed. A Standard Piston Core 4.2 m (14 ft.) long was taken at the site, but preliminary results suggest that the highly reflective horizon was not encountered (Figure 9-2).

## 9.2.1  Lithostratigraphy

Prior to cutting the cores and sampling for a variety of analyses, the cores were logged using a multisensor core logger.  All cores were logged.  The Mound Crest 2 JPC, the Mound Flank JPC, and the Intermound Standard Piston Core logging results are presented in this report (Figure 9-4, Figure 9-5 and Figure 9-6).  Of the two cores acquired from the *Lophelia* mound, the Mound Crest 2 core (Figure 9-4) exhibits the most variability in all three logger profiles (Gamma Density, Magnetic Susceptibility, and Resistivity).  Down-core variability in these properties suggests that the mound is not a homogeneous geologic-biologic feature, but that the interior of the mound has a definable lithostratigraphy.  Although the Mound Flank Core logger profiles exhibit a similar variability, the variations are not as pronounced, which probably means a degradation of the stratigraphic signal by slumping and other forms of sediment redistribution.

Once special techniques were developed to cut these cores, they were photographed with a high-resolution digital camera associated with the multisensor core logger.  The entire Mound Crest 2 core is presented in Figure 9-7 and a close-up of a selected core section is shown in Figure 9-8. Several observations can be made about the lithostratigraphy and overall character of the mound interior from the combined multisensor core logger data sets and the core photograph.  First, coral fragments are certainly a major component of mound construction to a depth of 16.4 m (53 ft. 8 in), the maximum depth of penetration (Mound Crest 2 JPC) at the mound crest.  Second, concentrations of coral "rubble", smaller coral fragments, and voids alternate with zones of relatively coral-free matrix sediment containing few voids.  Although most voids are interpreted as being natural structures of the mound interior, some were caused or enhanced by the core-cutting process.  Third, the matrix sediment is primarily hemipelagic in origin, composed of clay minerals and a high proportion of calcareous microfossil tests.  A typical X-ray diffraction scan (0-36°, 2G) of the mound's matrix sediment (heated, glycolated, and air dried) indicates the presence of dominant clay minerals (smectite, chlorite, illite, and kaolinite) as well as quartz and calcite (Figure 9-9).  The quartz and calcite (microfossil tests) are found in the clay-size fraction but occur mostly in the silt and fine sand fraction.  The Mound Crest 2 core photograph, Figure 9-7, as well as the core logger profiles of Figure 9-4 suggest that the mound has an internal stratigraphy.  Color variations in the core photography clearly indicate different stratigraphic layers.  A dark clay layer in Section 4 and a very light gray-to-white unit at the base of the Mound Crest 2 core (Section 11) are two dramatic examples.  Preliminary results from X-ray diffraction data (Figure 9-10) indicate down-core variations in clay mineral composition suggesting different sediment sources for the clay fraction of the hemipelagic matrix sediment.  Data collection is on-going on the Mound Crest 2 core.
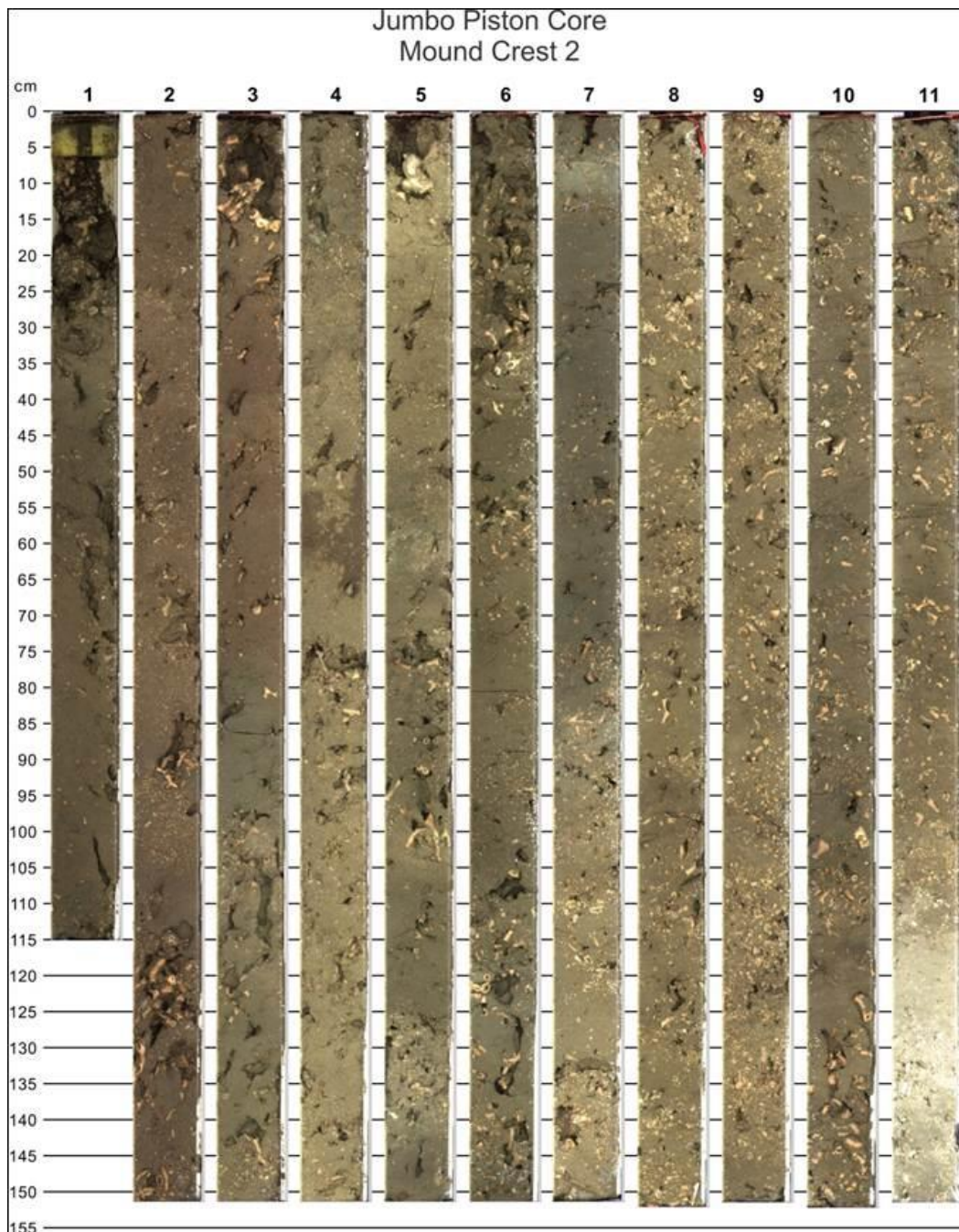
Figure 9-7.  This high resolution digital image of the Mound Crest 2 JPC illustrates that corals occur throughout the mound which was sampled to a depth below the mound surface of ~ 16 m (53 ft.).  The JPC was cut into eleven sections, as shown in this photograph.

Samples of the matrix sediment spanning the entire sedimentary sequence sampled by this core are currently being analyzed for variations in clay minerals and a similar suite of coral samples are being analyzed for trace metals.  These data sets will be combined with age dating, results of

biostratigraphy, and coral density measurements to derive a developmental history for the mound. The Mound Flank and Intermound cores are currently being sampled for similar analyses as described above in order to compile a more complete depositional history for the VK906 mound.



Figure 9-8. This photograph is a close-up of the middle of Section 4 of the Mound Crest 2 JPC illustrated in the previous figure. Note the densely packed coral "sticks" and smaller fragments. The matrix sediment is rich in clay minerals and calcareous microfossil tests. The width of the core photograph is ~ 12 cm (5 in).

## 9.2.2  Biostratigraphy and Age Dating

Biostratigraphy of the VK906 mound is being developed by long-time colleague on continental slope studies, Dr. Barry Kohl, formerly with Chevron and now an adjunct professor at Tulane

University. In addition to biostratigraphy, age dating by carbon-14 (C-14) and uranium/thorium (U/Th) was accomplished on selected samples sent to Beta Analytic Labs and the University of Minnesota's U/Th dating lab, respectively. Two of the fundamental questions about the VK906 mound concerns its age. When did the mound start growing? What was its developmental history? Because of the intensive paleontological and sedimentological work conducted in support of the oil and gas industry, the northern GoM has a well-developed biostratigraphic framework. Figure 9-11 is a stratigraphic chart for the GoM illustrating oxygen isotope stages and biostratigraphic zones. Initial results of the biostratigraphic analysis are summarized in the depositional rate curve for the Mound Crest 2 core (Figure 9-12). One of the initial surprises came from the dating of microfossils from matrix sediments at the top of the core as well as C-14 dating of a coral fragment near the core top. Both data-points indicate that beneath the "thickets" of *Lophelia* corals living on the surface of the mound, the sediments and coral fragments suggest the mound surface may be as old as 40 ka BP (thousand years Before Present). Table 9-2 presents C-14 dates from two samples of living coral from *Lophelia* communities at the crest of the mound and coral samples collected from the Mound Crest 2 core. It is not unexpected that a sample from a living coral colony could be as old as 700 BP. Surprisingly, dates from samples beneath the top sample from the mound sediments are beyond the range of C-14 dating. Biostratigraphically, the top sample from the Mound Crest 2 core was in the Pleistocene with the absence of *Gl. menardi(i),* abundant *Globorotalia crassaformis* and common *Gl. inflata* (interpreted as Zone Y, Figure 9-11). This assemblage of planktonic foraminifera suggests that the mound surface is older than 12 ka BP. The microfossil data coupled with the C-14 age of over 40 ka BP, for surface coral debris, indicates a long period of nondeposition or erosion (Figure 9-12). Previous slope studies indicate that in some areas of the Viosca Knoll lease area, Holocene hemipelagic sediments are over 3 m (9.8 ft.) thick. These sediments are completely absent from the *Lophelia* Mound Crest 2 core.

Table 9-2.

Radiocarbon Dating

| SAMPLE NUMBER | ESTIMATED AGE |
|---|---|
| CONVENTIONAL RADIOCARBON | |
| MC 2 (Living) | 360 $^+/_-$ 30 BP |
| MC 2 (Living) | 710 $^+/_-$ 30 BP |
| MC 2 – (Surface) | 40,710 $^+/_-$ 670 BP |
| MC 2 – 75 cm | Dead Date |
| MC 2 – 230 cm | Dead Date |
| MC 2 – 405 cm | Dead Date |
| MC 2 – 490 | Dead Date |
| U/Th DATING | |
| MC 2 – 18 cm | 1,391 ± 6 |
| MC 2 – 371 cm | 74,924 ± 225 |
| MC 2 – 410 cm | 69,496 ± 185 |
| MC 2 – 1125 cm | 202,618 ± 1216 |
| MC 2 – 1620 cm | 281, 184 ± 2796 |
| MC= mound crest ; BP = before present | |

Section 3 of the Mound Crest 2, core photograph (Figure 9-7) contains *Gl. flexuosa* (Zone X, Figure 9-11) indicating a warm period during the Pleistocene, ≥ 89 ka BP. Thirteen samples collected between 4.1 m (13.5 ft.) and 15.6 m (51.3 ft) below the sea floor all had consistent occurrences of *Gl. flexuosa*. However, as Figure 9-12 indicates, there is another prominent unconformity at approximately 4 m below the sea floor in the Mound Crest 2 core. It is estimated from the biostratigraphy that sedimentary section between 65-89 ka BP is missing from the mound at this horizon.

At the bottom of the core (~ 16 m or 52 ft. below the sea floor) a distinctive "light grey-to-white" unit occurs (see the Mound Crest 2 core photography, Figure 9-7). This unit contains abundant *Gl. inflata* and no *Gl. flexuosa* indicating a cool water period, below the 5e highstand, which is interpreted to be in Zone W, (Figure 9-11) ≥ 130 ka BP. However, U/Th dates from this horizon suggest that it is much older.

Table 9-2 presents both radiocarbon and U/Th age dates for the Mound Crest 2 core. The top U/Th date puts the mound surface in the Holocene while the radiocarbon data places the surface at ~ 40 ka BP (Pleistocene). The U/Th date at 18 cm (7 in) below the mound surface may have resulted from a fragment of very young coral being buried by bioturbation and subsequently captured in the JPC. In the test Standard Piston Core taken from the Mound Crest, abundant *Gl. menardii,* indicating younger Holocene were found along with rare occurrences of *Gl. inflata* and common *Gl. crassaformis* indicating a microfossil assemblage of mixed Holocene and Pleistocene age(s). The U/Th date of 74.9 ka BP, at 371 cm (146 in), is just above the unconformity identified biostratigraphically (Figure 9-12) and in the same basic age range interpreted from planktonic foraminifera.

The sample dated by U/Th just below the unconformity, 410 cm (161.4 in), is slightly younger (69 ka BP, Table 2) than the sample above it. This sample appears to be in the *Gl. flexuosa* zone which has a minimum date of 89 ka BP. The planktonic foraminifera suggest that there may be a transition zone between the 371 cm (146 in) and 410 cm (161.4 in) horizons. Mixing of sediments and resulting dates from this zone are highly probable.

The remaining two U/Th dates are not easily resolved with biostratigraphy data. Five new U/Th dates are now being processed and more samples are being taken to refine the biostratigraphic analyses of the Mound Crest 2 core as well as the Mound Flank and Intermound cores.
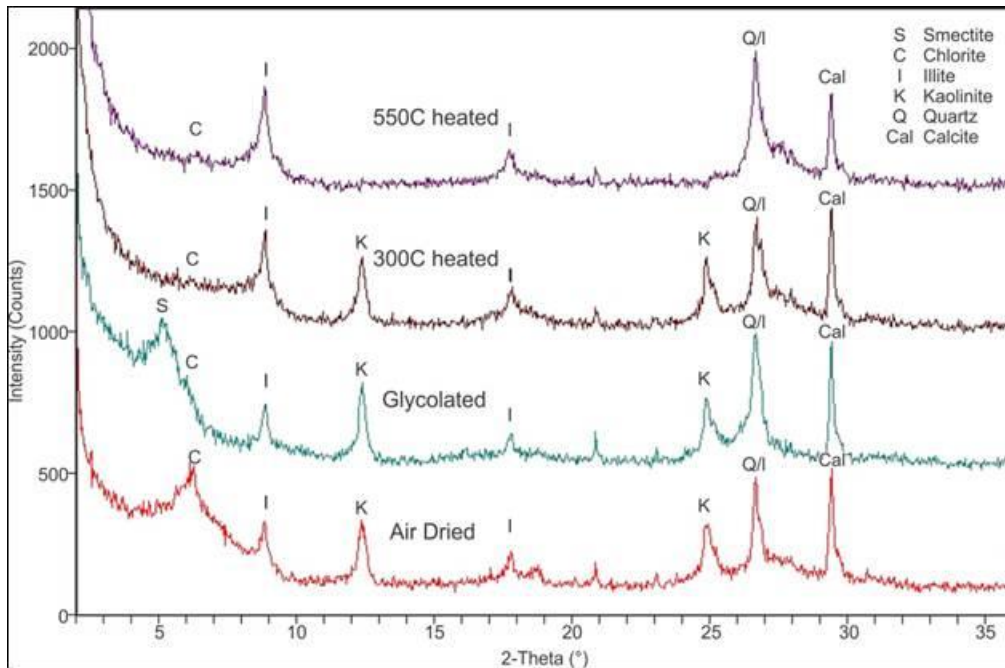
Figure 9-9. X-ray diffraction data (0-36° 2ɵ) of the matrix sediment (depth of 15 m below the sea floor in the Mound Crest 2 core) illustrating the presence of smectite, chlorite, illite, and kaolinite on heated, glycolated, and air-dried scans. Quartz and calcite (microfossil tests) are also present, but mostly in the silt and fine sand fraction.
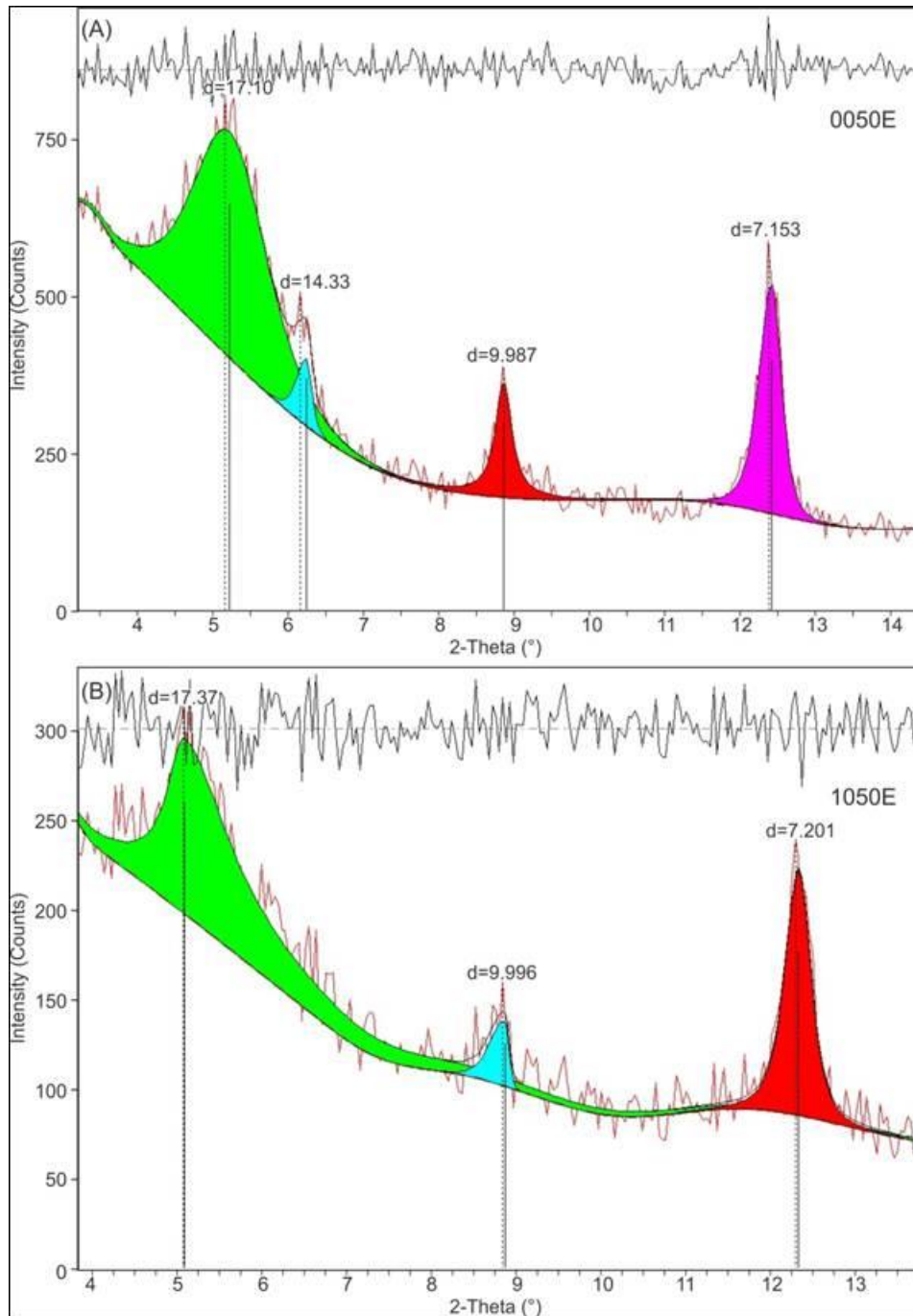
Figure 9-10. (A) Clay minerals in the Mound Crest 2 core matrix
sediment at the 0.5 m (1.6 ft.) level. (B) Clay minerals in the
Mound Crest 2 core matrix sediment at the 10.5 m (34.4 ft.)
level.

338
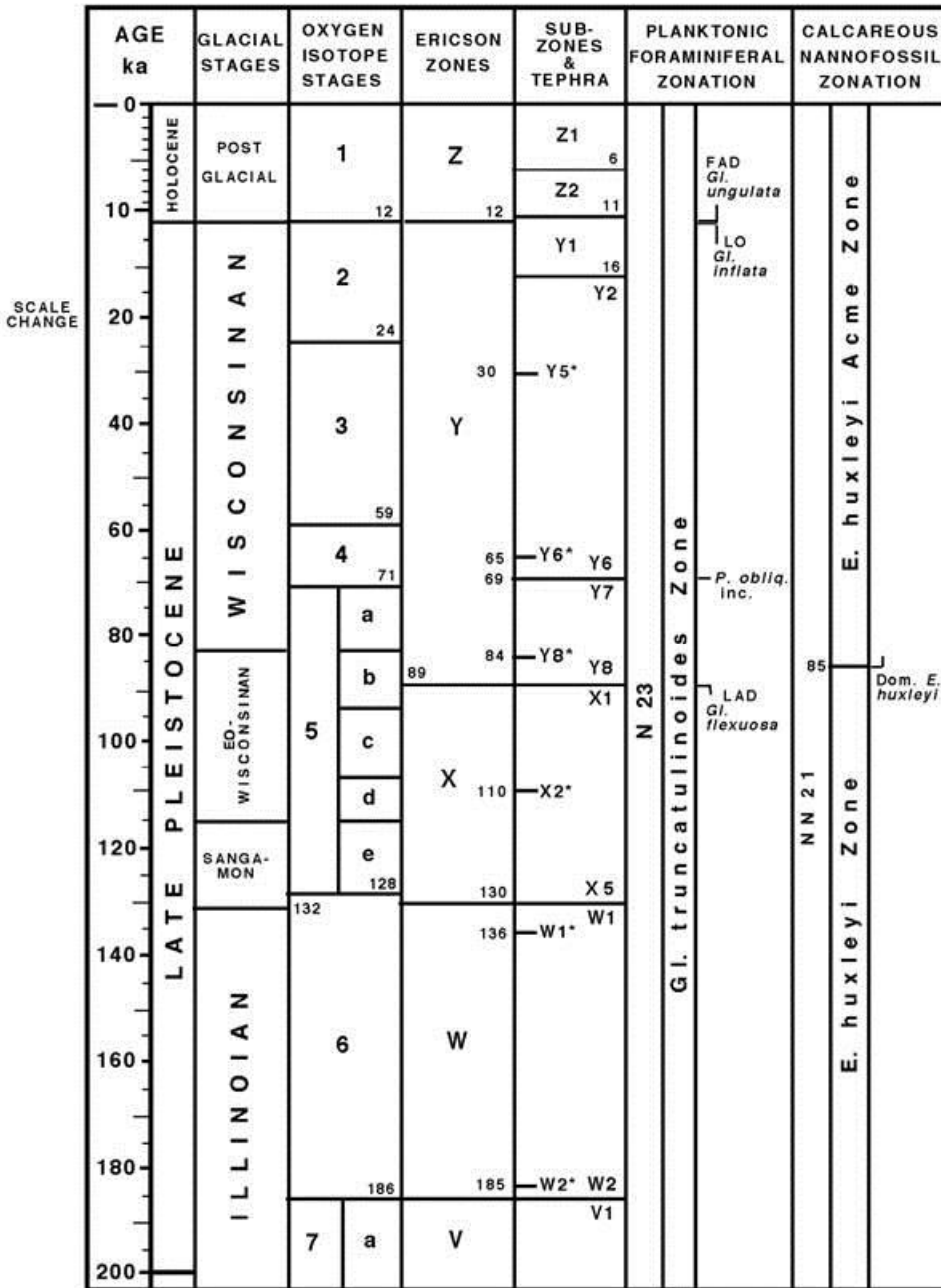
Figure 9-11.  A stratigraphic chart for the GoM showing the oxygen isotope
stages, biostratigraphic zones and subzones, and tephra (after Kohl et
al., 2004).  All dates are in conventional years BP.
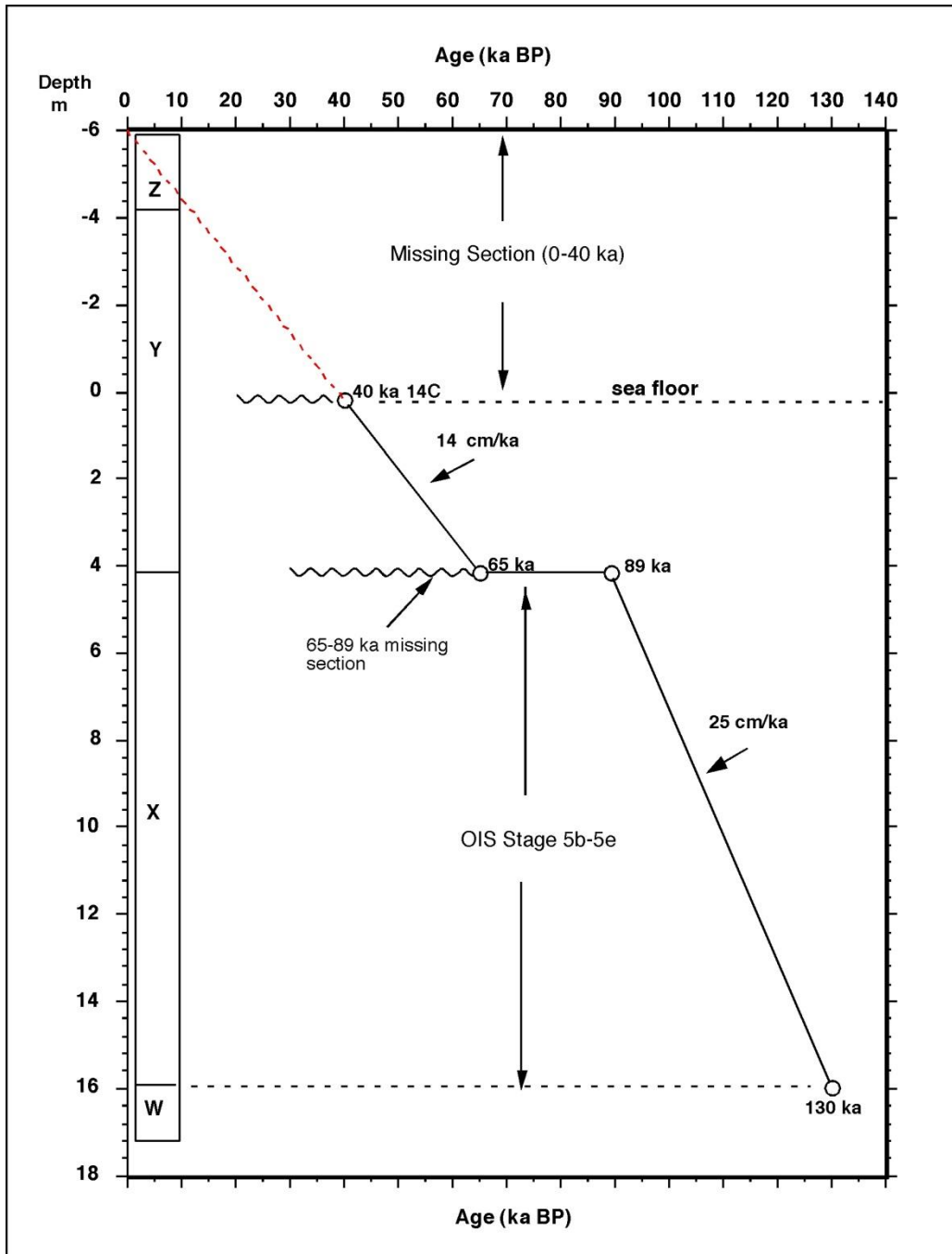
Figure 9-12. A depositional rate curve for the Mound Crest 2 core (MC-2), Viosca Knoll Block 906. The graph illustrates two unconformities encountered in the core. The first is at the sea floor with an age of 40 ka BP, based on a 14C date from a *Lophelia pertusa* coral sampled from top of core. The second unconformity is based on foraminiferal biostratigraphic datums and represents 24 ka of missing section. The left hand column shows the boundaries of the foraminiferal Ericson zones interpreted by Kennett et al. (1972). A projection based on the sedimentation rate shows that approximately six m of core may be missing from the top. The X/W boundary was reached at 16 meters below sea floor. All dates are in conventional years BP.

### 9.2.3  Skeletal Density

Skeletal density of *Lophelia* (Figure 9-13) throughout the mound may provide information concerning aragonite saturation state at this site over the time course of mound formation. Initial investigation of skeletal density does not show a clear trend over time, but does show a series of discontinuities that may correspond to the trends observed in the stratigraphy. The skeletal densities of living corals from the site show the same range as the entire core section. This suggests that, if there is an effect of alkalinity on skeletal density, that the present day range of alkalinity experienced at the site is similar to the range of conditions that have occurred throughout the history of coral growth at VK906. In the top section of the core, down to approximately 4 m, the density of the coral skeleton is relatively high, from 2.7 to 2.9 g cm$^{-3}$. Below this section, from 4.5 to 7 m, average density is lower, and the lowest values recorded were present. From 7 to 9 m, skeletal density was relatively high. Below this point in the core, most of the data fall into the 2.7 to 2.9 g cm$^{-3}$ range, with some low values also recorded.

Low densities could either represent a change in the aragonite saturation state under which the corals are laying down their skeleton, or a change in growth rate. High skeletal density would result from high omega values, or relatively low growth rates. A boron proxy for calculating pH from *Lophelia* skeletal samples is currently under development as part of a collaboration between the Cordes lab and the Prouty lab at USGS. Once this proxy has been calibrated, it will be used to determine the oceanographic conditions under which the coral skeleton formed, and will elucidate the factors that have resulted in the densities measured.
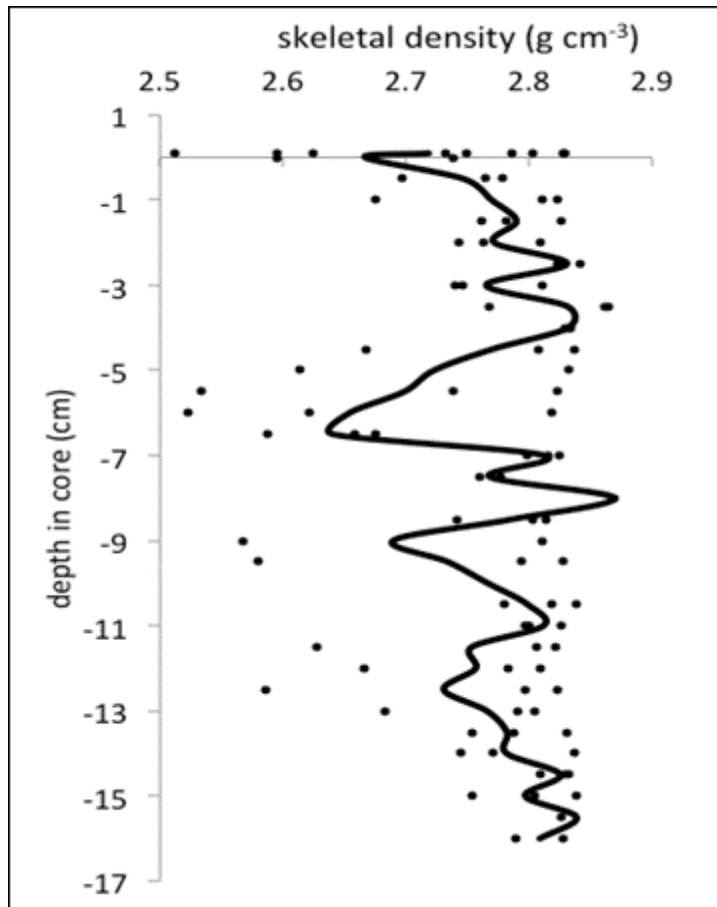
Figure 9-13.  Skeletal density of *Lophelia pertusa* samples from the Mound Crest 2 core.

# 10 ARCHAEOLOGY

## 10.1 INTRODUCTION

### 10.1.1 Overview

The historic shipwreck component of the *Lophelia* II Study was planned around a four-year timeline and details investigations of six historic shipwrecks. Years one through three of the project was dedicated to fieldwork, historical research, data collection, and data analysis. The fourth year of the project involved additional research, data analysis, and reporting.

The shipwreck component is an important continuation of the MMS's 2004 Deep Wrecks I Study (OCS Study MMS 2007-015). It will expand our knowledge base of how shipwrecks function as artificial reefs and allow scientists to compare findings and test hypotheses put forth in the first study findings. The inclusion of wooden hull shipwrecks in this study provides new information on deepwater reef processes since these wrecks represent long-standing areas of composite and hard substrate in a mostly barren seafloor environment. These studies and others like them will continue to help researchers understand the processes and importance of deep-water shipwrecks as significant archaeological site, but also as artificial reef environments.

Archaeologically, the documentation, identification, and analysis of additional deepwater shipwreck sites increases our understanding of deepwater wreck site formation processes, wreck deterioration rates, and the role of the GoM shipping in both regional and global maritime history. The study of these deepwater wrecks will allow theBOEM, formerly the MMS, to refine their avoidance criteria predictive model developed during the Deep Wrecks I Project. This predictive model is another tool that government agencies, such as the BOEM and other archaeological researchers can use to accurately assess the potential limits of a wreck sites, establish adequate avoidance areas around them, and develop comprehensive research designs.

### 10.1.2 Archaeological Component Objectives

1. To record each vessel through detailed imagery to establish its type, date of construction and positive identification if possible.
2. To establish nationality, ownership (past and present), use history, cause of loss, mission and cargo at time of loss through fieldwork and historical research.
3. To determine the extent and condition of the artifact assemblage on each vessel and the presence of diagnostic artifacts.
4. To determine potential eligibility to the National Register of Historic Places through archival research and the analysis of imagery and to prepare a National Register nomination form for potentially eligible vessels.
5. To assess impacts of biofouling communities to these shipwrecks to determine the stability of these sites and rate of deterioration.

This multidisciplinary study focuses on the biological and archaeological aspects of seven GoM shipwrecks in the north-central portion of the GoM. Four of these wrecks represent wooden sailing vessels of unknown age and origin, while the remaining three (*Gulfpenn*, *Gulfoil*, and *U-166)* were

lost to wartime activity between early April and late July 1942.  All seven shipwrecks were discovered during oil and gas surveys and were reported to the MMS as required by Federal regulations.  Water depth at the investigation sites ranges from 534 to 2,270 m.  Each shipwreck was investigated to determine site boundaries, National Register eligibility, preservation state and stability, and the potential for man-made structures or objects to function as artificial reefs in deepwater (Figure 10-1).

### 10.1.3 Project Organization

The BOEM and NOAA''s Office of Ocean Exploration (NOAA OE) organized the study under the auspices of the National Oceanographic Partnership Program (NOPP). TDI Brooks, Inc., the primary contractor for this study, contracted C & C Technologies, Inc. (C&C), to oversee the archaeological analysis.  C&C contracted the PAST Foundation (PAST) to assist in the archaeological component of the study.  TDI Brooks, Inc. contracted Droycon Bioconcepts, Inc. (DBI) to undertake the micro-biological   assessments related to the archaeological component. The Key Personnel for the project are listed in the following table (Table 10-1).

Table 10-1

Key Archaeological Component Personnel

| Personnel | Title | Organization |
|---|---|---|
| Daniel Warren, MA | Marine Archaeology Principle Investigator | C&C |
| Robert Church, MA | Marine Archaeology Co-Principle Investigator | C&C |
| Robert Westrick, MA | Marine Archaeologist | C&C |
| Shawn Arnold | Marine Archaeologist | C&C |
| Sheli Smith | Marine Archaeologist | PAST |
| Anne Corscadden Knox | Marine Archaeologist | PAST |
| Roy Cullimore | Microbiologist | DBI |
| Lori Johnston | Microbiologist | DBI |

## 10.2 GEOGRAPHIC OVERVIEW

The GoM is a semi-enclosed small ocean basin that formed by Late Triassic to Early Jurassic rifting followed by Late Jurassic to Early Cretaceous seafloor spreading.  The Gulf has been receiving sediment influx dominated by the Mississippi River since Late Jurassic.  Sediments accumulated along the GoM's northern margin during the Mesozoic and the Cenozoic have attained a thickness in excess of 14.9 km.  Rapid deposition along the northern margin of the GoM during the Tertiary and the Quaternary resulted in the accumulation of particularly thick

sedimentary sequences and an up to 296 km basinward migration of shelf edge since the Cretaceous at an exceptionally high rate of 4.8 to 5.9 mm/year (Coleman et al. 1991).
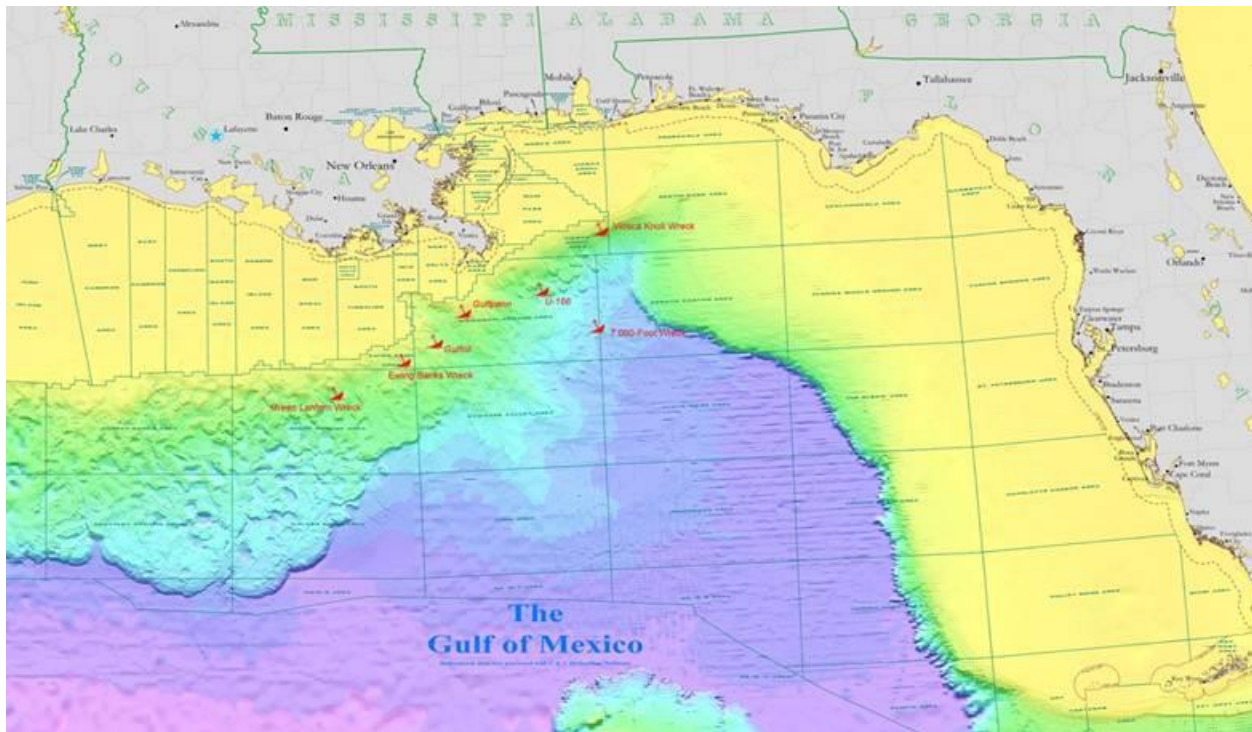


Figure 10-1. Overview map with locations of shipwrecks examined in this study.

The Mississippi Canyon is the conduit for source materials moving seaward into the Mississippi Fan. Bouma et al (1985) describes the Mississippi Canyon as a major erosional and partially filled structure. Initial development of this canyon is suggested to have begun about 50,000 to 55,000 years ago in the middle continental slope and retrogressed onto the shelf 25,000 to 27,000 years before present. Retrogressive large-scale slumping on an unstable shelf-slope areas during a sea level low stand or during the initial sea level rise are believed to have caused the canyon to widen and lengthen further up-shelf. Several other smaller-scale canyons create fans by similar processes east and west of the Mississippi Canyon on the shelf-slope area (Bouma et al. 1985).

In the east-central GoM, a large regional, deep-water feature exists that is identified as the Mississippi Fan. This feature was the subject of the Deep Sea Drilling Project Leg 96 in 1983 and was interpreted as a channel-levee-overbank complex. The Mississippi Fan is approximately 560 km long and up to 600 km wide. It extends southeast from the base of the continental slope at a depth of approximately 300 m, across the continental rise and onto the abyssal plain, to a point roughly halfway between the Campeche Escarpment and the Florida Escarpment. The Mississippi Fan is bounded by the Texas-Louisiana Slope region to the west and the Florida Escarpment to the east. Water depths for the Mississippi Fan range from approximately 300 m at the base of the slope to 3,200 m on the abyssal plain. The fan has been described as a broad arcuate submarine fan comprised of a number of fan lobes separated by pelagic oozes or muddy sediment (Bouma et al. 1985).

In 1989, following an examination of the most recently deposited fan lobe, Bouma and others suggested a sea-level-driven model which effectively divided the Mississippi Fan into three sections for descriptive purposes: upper fan, middle fan, and lower fan. The upper Fan has a slightly convex shaped surface with a wide channel at its apex flanked by laterally discontinuous reflectors believed to be overbank deposits. The middle fan holds the greatest accumulation of sediment and is imaged on sonar data as a leveed, sinuous channel complex that averages 1.2 to 2.5 km in width. Less prominent channel complexes that undergo rapid channel abandonment define the lower fan. It can be assumed similar fans have been active during the geologic past in the entire Mississippi Canyon, Atwater Valley, and Lund Areas. Channel deposits consist of fining upward turbidite sequences (gravel to clay size) with the base of the gravel representing the time of the episodic event (Bouma et al. 1989).

## 10.3 HISTORICAL BACKGROUND

### 10.3.1 Maritime Activity in the Northern Gulf of Mexico 1800-1820

At the beginning of the nineteenth century, the GoM was an arena of commerce, political unrest, and piracy, each one intertwined with the other. In 1800, newly elected President Thomas Jefferson appointed Robert Livingston as the United States' minister to Spain. Jefferson immediately sent him to purchase the city of New Orleans and the surrounding area from the Spanish Crown. After his arrival in Spain, Livingston discovered Spain had secretly traded the Louisiana territory to Napoleon Bonaparte of France. Thomas Jefferson feared French control of the Mississippi River would cause serious trouble for American shipping in the GoM. Jefferson, therefore, dispatched Livingston and James Monroe to Paris in 1803 to negotiate the sale of New Orleans to the United States. Napoleon was initially unreceptive to the offer. He was, however, at war with Britain and became apprehensive that Britain, already with a naval presence in the GoM, would take Louisiana from him before he could secure the region. Eventually, Napoleon's concern over the ongoing war with Britain and the need of money to finance the war led him to make a surprising offer. Instead of just New Orleans, Napoleon offered up the entire Louisiana Territory to Livingston and Monroe. Although authorized only to buy New Orleans, Livingston and Monroe returned home having negotiated the purchase of the entire Louisiana Territory, nearly doubling the size of the United States (Tindall 1988; and Bradshaw 2002).

During negotiations for the purchase of the Louisiana Territories, the territorial boundaries were only vaguely defined. When Livingston asked the French foreign minister about the boundaries, the minister replied that Livingston had "made a noble bargain" and America would no doubt "make the most of it." The vague boundaries gave the United States a strong claim to parts of Texas and Florida in addition to Louisiana. The Spanish were furious when the sale was made public, claiming that Napoleon had no right to agree to sell the territory before he actually took possession of it. By 1806, clashes between Spain and America over disputed territory led to a lawless no-mans-land for several miles east of the Sabine River that became a haven for thieves, smugglers, and pirates (Figure 10-2) (Tindall 1988; and Bradshaw 2002).

Figure 10-2. North-central Gulf Coast in 1806.

The first two decades of the nineteenth century were a heyday for privateering, piracy, and other illicit activities in the Caribbean and the GoM as the war between France and Britain wore on and Spanish influence in the new world waned. During this period, warring countries bolstered their sea power by issuing *Letters of Marque* to private men-of-war to attack enemy ships for profit. The value of these captured ships, referred to as prizes, was to be split between the privateer and the government. In the words of author William C. Davis, "The English preyed on the French, the French upon the English, and everyone went after the Spaniards' vessels." The line between privateering and piracy was often blurred as many privateers also engaged in smuggling and were, at times, indiscriminate in their attacks on merchant shipping. In 1803, the United States outlawed the importation of foreign slaves, making slave smuggling a profitable enterprise and Spanish slave ships attractive targets for privateers and pirates. The high demand for cotton production spurred on the slave trade and the availability of new land allowed cotton and sugarcane plantations to boom in the Louisiana Territory. The market for slave labor continued to rise and New Orleans was the doorway for this commerce, legal and illegal alike (Davis 2005; and Bradshaw 2002).

On April 30, 1812, barely a month after Louisiana became a state; the United States declared war on England in response to the British practice of illegally impressing American sailors into the Royal Navy. The Gulf Coast was ill prepared for the war and the impending British invasion. In December 1814, British forces invaded the Lower Mississippi Valley, entering Lake Borgne to the east of New Orleans. The British arrived with a fleet of fifty naval vessels including several 74-gun ships of the line. These included *Tonnant*, *Ramillies*, and *RoyalOak* along with various frigates, brigs, and armed transports. The Americans met the opposing force with a small defensive navy composed of the 22-gun sloop *Louisiana*, the 14-gun schooner *Carolina*, several lightly armed gunboats, and a few other small vessels. The Americans lost the majority of their gunboat flotilla near Lake Borgne and the British destroyed *Carolina* in the Mississippi River south of New Orleans (Eller et al. 1965; Dudley 1992). Despite heavy naval losses, Jackson's forces, comprised of mostly militia, repelled the British Army's advance on New Orleans (Davis 2005).

Before 1812, most waterborne commerce in the central part of the Gulf was centered on New Orleans. On January 10, 1812, the first steamboat arrived at New Orleans from Pittsburgh. Soon after the introduction of steam vessels, maritime commerce in the GoM increased dramatically (Pearson et al., 1989). This increase in commerce resulted in cities growing rapidly which led to outbreaks of diseases such as cholera and yellow fever. The first outbreak of cholera in New Orleans is documented as having arrived by steamboat in late October 1832, shortly after an outbreak of yellow fever. The outbreak lasted just over three weeks and left nearly 5,000 people dead. In 1848, cholera was again brought to New Orleans by merchant vessel and killed 1,641 people in two weeks. Despite the disease being linked to bowel discharge around 1866, cholera returned almost every year until 1875. The threat of disease was so great that cities began forcing vessels to quarantine (Figure 10-3) before any unloading operations (Duffy 1971).



Figure 10-3.   Illustration depicting New York Harbor quarantine of immigrant vessels (Graetz, 1883).

During the Civil War, the GoM was a theater of conflict for Union blockaders, daring blockade-runners, and Confederate "commerce raiders" or privateers. Early in the war, U.S. President Abraham Lincoln proclaimed a blockade of Southern ports. Confederate President Jefferson Davis responded to this action by issuing *letters of marque* to Confederate privateers allowing them to attack U.S. shipping. By January 1862, the converted mail steamer CSS *Sumter* had captured or destroyed eighteen U.S. merchant ships on her cruise from New Orleans to Gibraltar. The CSS *Alabama* sank the steamer USS *Hatteras* off the coast of Galveston, Texas in the summer of 1862. CSS *Alabama* sank a record seventy-six vessels before being sunk herself off the coast of Cherbourg, France by the USS *Kearsarge* (Watts, 1988).

348

After the Civil War, the presence of stern-wheelers began to increase in frequency. A variety of sailing craft such as schooners, clippers, and "New Orleans" luggers were, however, still in demand along the northern Gulf coast. These vessels carried merchant goods such as lumber, naval stores, and cotton to major ports such as Pensacola, Mobile, and New Orleans, as well as ports along inland waterways and foreign destinations. Although most histories focus on steam vessels in the last half of the 19th century, the amount of traditional sailing vessels outnumbered steam ships nearly 2 to 1. Between 1868 and 1897 the total number of sailing vessels built and documented in the U.S. equaled 18,344 with a combined tonnage of 2,916,470.88 compared to 10,231 steam vessels with a combined tonnage of 2,903,226.62 (Commissioner of Navigation 1897). The overall tonnage of steam vessels increased as a greater number of large screw-driven vessels started being produced in 1879. Screw-driven vessels provided the means to increase trans-oceanic commerce.

The need for steam propulsion decreased with the beginning of oil production in Louisiana and Texas at the onset of the twentieth century. By around 1915, steam engines began to fade away as diesel engines emerged (Pearson et al. 1989). Although oil production in this region led to increasingly larger vessels being constructed with experimental designs to transport this new commodity with greater profitability, the need for wooden sailing vessels never ceased (Flodin 1919). Wooden vessels continued to be used for fishing, transportation and commercial shipping. The naval stores and timber industries were rapidly spreading across the southern states and smaller wooden vessels were used to move the products from inland waterways to the Gulf Coast's major ports. Wares would then be transferred to larger sailing vessels and shipped around the globe (Bloomster 1940).

### 10.3.1.1    Wooden Vessel Types

Between 1770 and 1830, the common types of sailing vessels in the GoM included ships, barques, sloops, schooners, brigs, brigantines, luggers, and clippers and others, as described below.

. The largest class of sailing vessel, called a ship contained at least three masts, square-rigged on each mast, and included a bowsprit.

Barques were similarly rigged to ships, but had only fore-and-aft sails on the mizzenmast. Ships and barques were generally employed as merchantmen for transoceanic voyages (U.S. Dept. of the Treasury, Bureau of Statistics 1886; and Swanson 1991). Sloops were quite common globally and one of the oldest styles of vessels utilized for trade in the Americas. They were small vessels, often less than 50 ft in length. They carried a single mast with a bowsprit and rigged with fore-and-aft mainsail, and jib or foresail. Sloops could sail close to the wind and were highly maneuverable in narrow waters. Their seaworthiness and sailing characteristics made them popular vessels to both merchants and privateers (U.S. Dept. of the Treasury, Bureau of Statistics 1886; and Swanson 1991).

Fore-and-aft rigs include schooners, brigs and brigantines. This type of rig was prominent in the Caribbean and, over the course of the eighteenth century, adopted into shipbuilding in North America. The brig, brigantine, and schooner are examples of the impact of the Caribbean Bermuda-rig (Smith 2007).

Small coastal schooners were introduced in American waters during the early eighteenth century. Schooners are typically two-masted, fore-and-aft rigged vessels, often with light square topsails. They are fast and relatively easy to handle. The early coastal schooners were typically 20 to 90 tons and 50 to 90 ft in length. By the late nineteenth century, larger schooners of over 300 tons and greater than 100 ft in length became common. These larger vessels often carried more than two masts (Swanson 1991; and U.S. Dept. of the Treasury, Bureau of Statistics 1886).

Brigs and brigantines were popular vessels for coastal trade by the last quarter of the eighteenth-century. The terms brigs and brigantines are often used synonymously in historical documents, but the rig and period of introduction are slightly different. Brigs, common in the Americas by the mid-eighteenth century, are two-masted, square-rigged vessels with a fore-and-aft sail (or gaff) on the main mast, which aided maneuverability (Figure 10-4). Brigantines are a later adaptation of the brig. They have a brig foremast, but with a main mast similar to a schooner except they carry a light topsail on the main mast. It is impossible to tell the difference between the two vessels archaeologically unless the masts and sparring are present. Brigs/brigantines could take advantage of light winds and easily navigate coastal waters. Their intermediate size, approximately 100 to 130 ft in length, and rig versatility made them well suited for the coasting trade (Smith 2005; U.S. Dept. of the Treasury, Bureau of Statistics 1886).

The lugger derives its name from the dipping lugsail. The lugsail is a modification of the square sail which allows one corner of the sail to rise above the mast. Luggers may have one to three masts and were used for coastal fishing (U.S. Dept. of the Treasury, Bureau of Statistics 1886).

Clipper ships were modeled after French luggers that visited American ports during the revolutionary war. Clippers were designed by lengthening the lines of swift sailing coastal vessels to incorporate a ships rigging. They are characterized by a curving stem that lengthens the bow above the water, concave waterlines that draw out and sharpen the forward body of the ship creating the widest breadth of the vessel further aft than traditional ships, and a rounding up of the transom causing the stern to be lighter (Figure 10-5). The name clipper is thought to be derived from the term clip, which was used at the time to describe something that runs or flys smoothly. The fast sailing clipper ships were said to clip over the waves and not through them. Until the advent of screw-driven diesel vessels, clippers were the fastest vessels on the water (Clark 1910).
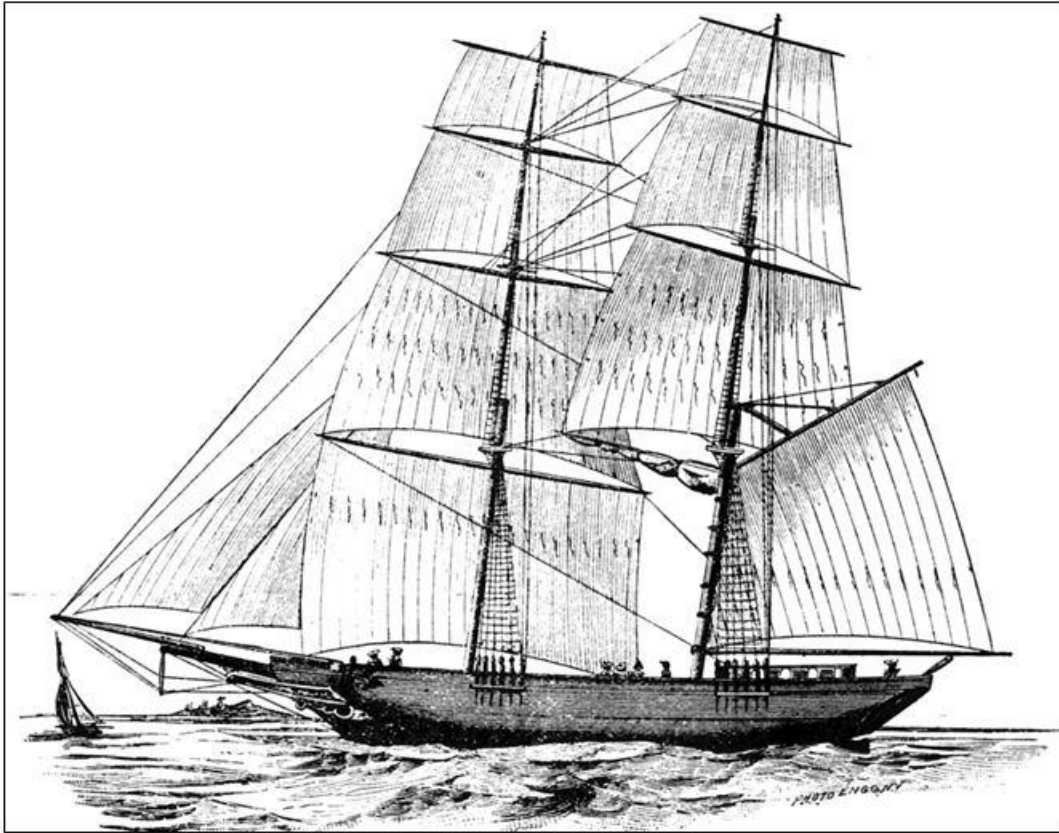
Figure 10-4. Typical nineteenth-century brig (U.S. Dept. of the Treasury, Bureau of Statistics 1886).
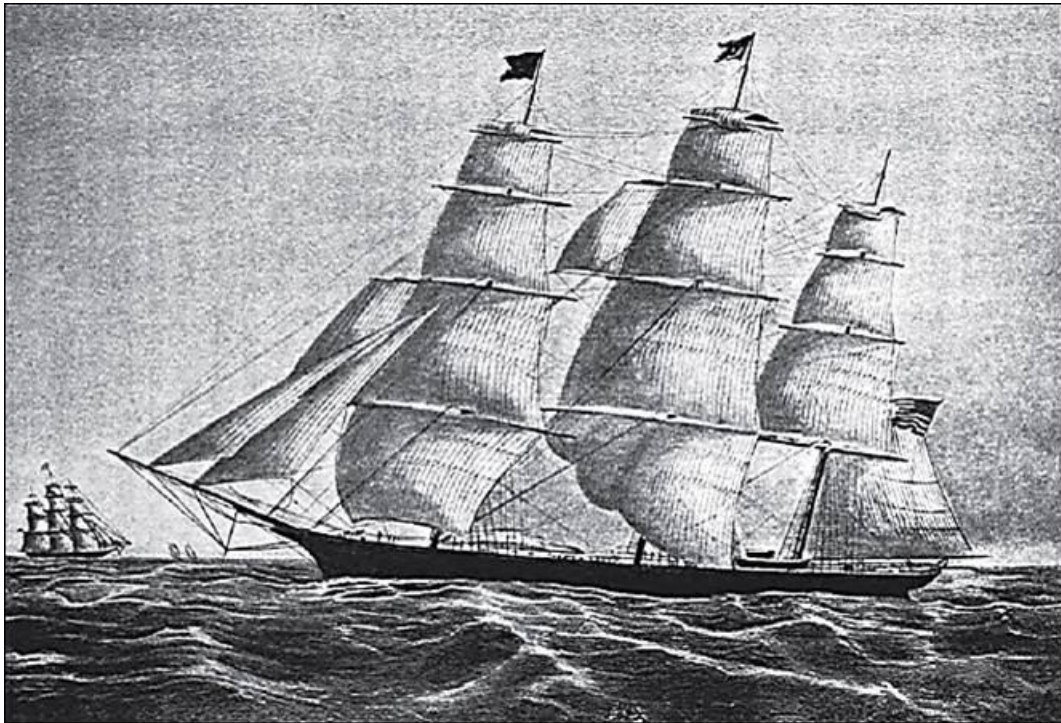


Figure 10-5. Clipper ship Young American (Clark 1910).

### 10.3.1.2    Sheathing

Adding to the hazards of tropical weather and political instability, the warm waters of the Caribbean and GoM were home to a distinctive biological combatant: the shipworm (Teredinidae). Proportionally more vessels were lost to shipworm damage than to war and weather. Christopher Columbus and other explorers left vessels in the Caribbean because by the time they were ready to return to Europe, the ships were unseaworthy due to shipworm damage to the hulls (Smith 2007). The most common shipworm type is *Teredonavalis*. *Teredos* are actually highly specialized wood-eating marine bivalves (mollusks). They can be found throughout the world, but are more densely concentrated in the Caribbean Sea than most other bodies of seawater. Adult *Teredos* can survive freezing temperatures and varying salinity after boring inside of a wooden hull, which allowed Caribbean species to spread through the world's oceans during the age of exploration. Shipworms earned the name "termites of the sea" because they could destroy the interior part of a wooden structure before the damage was noticed externally (Turner 1966). Shipwrights used various methods over the centuries to protect ship hulls from these marine borers, including lead sheathing and sacrificial planking. Global expansion following the fifteenth and sixteenth centuries made voyages to tropical waters commonplace and increased the need for better hull sheathing technology (Jones 2004).

The search for a better sheathing material led to the suggestion of copper as early as 1708, but it was considered too expensive to develop (Jones 2004). By the 1750s, the British Royal Navy reconsidered the use of copper sheathing. Despite galvanic corrosion problems during experiments with copper sheathing on warships during the 1750s to 1770s, the Navy adopted copper sheathing in the 1780s (Lavery 2000; Jones 2004). The advantages of copper sheathing on naval vessels led to increased usage on merchant vessels. Merchants sailing in tropical waters found the sheathing increased the ship's life and the widespread use of copper sheathing led to standardization of copper sheathing nail patterns during the latter part of the eighteenth and early nineteenth centuries (McCarthy 2005; Smith 2007). The rise in the number of coppered hulls is reflected in British ship registries. During the 1780s, only 3 percent of registered British shipping was sheathed, but by 1816, this number increased to 18 percent (McCarthy 2005). The sheathing of merchant ships appears to have been trade dependent. Slavers, East Indiamen, and post office packets were the most commonly coppered vessels. However, any ship in a high-return trade that voyaged to the southern hemisphere or to tropical waters was likely to be coppered (McCarthy 2005).

Manufacturing techniques for rolling copper sheathing changed very little until the 1830s. In 1832, George Frederick Muntz formulated an alloy of 40 percent zinc and 60 percent copper that he called Muntz metal. Throughout the mid- to later nineteenth century, Muntz metal became the sheathing standard and led to the introduction of standard sheathing sizes (approximately 18 in by 24 in) and gauges (18, 20, and 22) (Lavery 2000).

### 10.3.2 World War II in the Gulf of Mexico

Three factors have influenced the GoM's role in trade, economic development, and maritime commerce: exploration, warfare, and natural resources. Deep canyons mark the Gulf region's submerged bottomlands. Natural resources around the GoM including cotton, tobacco, and petroleum products have driven the Gulf's economy and shipping since the sixteenth century. Shipping routes follow traditional patterns, and shipwrecks are often found near those trade routes.

The GoM is no exception, and shipwrecks from the age of exploration through modern day have been located near traditional shipping lanes (Garrison et al. 1989).

World War I saw an increase in GoM tanker traffic as petroleum products became more important to American industry. Although Atlantic coast shipping was threatened during WWI, the Gulf's maritime community was affected little during the First World War. The situation was different in World War II. During World War II, several German U-boats operated in the GoM, using shipping lanes and navigational beacons to locate and torpedo unsuspecting prey (Blair 2000:467, 498).

In 1942, the world was at war and Germany controlled most of Europe. Hitler launched Operation Drumbeat under Admiral Karl Dönitz's command. Using Germany's *Unterseebootes* (U-boats), Operation Drumbeat brought the war to United States coastlines. The U-boat mission was simple: disrupt Allied supply lines. World War II U-boats struck shipping along the Atlantic coast, and infiltrated the United States' undefended backyard - the GoM. U-boat's specifically targeted tankers carrying valuable petroleum products from the Gulf coast to American refineries and abroad. During the early war years, Americans had a false sense of security created by the vast oceans that kept the war at a distance. When U-boats entered the GoM, many German commanders noted that coastal lights burned as in peacetime.

The spring of 1942 was an opportune time for U-boats in the GoM. The Commander of the Gulf Sea Frontier had not yet ordered mandatory convoys and naval escorts. Likewise, many merchantmen sailing Gulf waters were unarmed and unaware of the U-boat threat. Until July 1942, the Gulf remained a German pond where the U-boats hunted and attacked at will (Blair 2000: 588).

*U-507,* under Korvettenkapitän Harro Schacht's command, torpedoed the first vessel in Gulf waters on May 4, 1942 when she sankthe freighter *Norlindo* off Key West, Florida (Wiggins, 1995). *Norlindo*'s sinking unleashed a wave of destruction in the GoM. Korvettenkapitän Harro Schacht's crew aboard *U-507* sank eight vessels in the GoM, making it one of the most successful U-boats in this theater of war. *U-507*'s fourth victim was the cargo freighter, *Alcoa Puritan*. *U-507* also sank the tanker, *Virginia* on May 12 (Schacht 1942: 13, 32, 52). In May 1942, a second U-boat *U-506* joined the Gulf campaign, sinking the tankers, *Gulfpenn* on May 13 and *Halo* on May 20*,* and six other merchant vessels (Würdemann 1942: 12, 22, 30).

By July 1942, the United States increased efforts to protect shipping in southern waters. Coastal lights were shut off, lighthouse beacons were dimmed, and strict information blackouts enacted. Aerial reconnaissance and radio listening posts helped American naval and Coast Guard units track the U-boat threat. Merchant vessels were ordered to travel in convoys with naval escorts. These efforts diminished the number of vessels sunk by U-boats by August 1942 and turned the tide of the U-boat threat in American coastal waters.

*U-166*, commanded by Kapitänleutnant Hans-GüntherKühlmann, joined the fray in July, 1942. *U-166* took position off the Mississippi River's mouth in operational area DA-90. The U-boat's mission was to lay mines and attack merchant shipping (War Diary 1942: 36, 53, 92; and Blair 2000: 633). Although the nine TMB mines were successfully laid only a few hundred yards off

the jetties in the Southwest Pass of the Mississippi River, none detonated. TMB mines were shallow-water German torpedo-launched mines that sat on the seabed and were activated by the magnetic or acoustic signature of a passive ship. Kühlmann sank the passenger freighter SS *Robert E. Lee* approximately 45 miles southeast of the Mississippi River on July 30, 1942. PC-*566*, the naval vessel escorting the freighter, then sank *U-166* (Blair 2000: 633; and USS PC-566 1942). Deep water and conflicting first-hand accounts from 1942 hid *U-166*'s actual location for nearly 60 years. Although 75 percent of all U-boats were sunk by the war's end, only one (*U-166*) was lost in the GoM.(Blair 2000:704).

The German U-boat freely hunted these waters until late 1942, when American antisubmarine measures improved and helped turn the tide (Blair 2000: 696). By May of 1943, twenty-four German U-boats had entered the Gulf. Seventeen U-boats sent 56 merchant vessels to the bottom and badly damaged 14 others (Church et al. 2002). For those 56 ships, the American response to German U-boat attacks in the GoM came too late. Hundreds of merchant mariners lost their lives and ships to German torpedoes. Many tankers became floating bombs when torpedoes ignited the petroleum products in the holding tanks, leaving the crews either entombed in a fiery hull, or afloat in the blaze. The GoM war zone was a submerged and surface war front for military and non-military vessels alike.

## 10.3.3 Oil and Gas Development and Shipwreck Discovery

The oil and gas industry supports the largest percentage of commercial marine surveys in the GoM by far. The increased interest in developing deepwater oil and gas prospects has also led to significant advances in marine survey technology and equipment such as sophisticated deep-tow survey systems, improved Remote Operated Vehicle (ROV) technology, Autonomous Underwater Vehicles (AUV), and precision acoustic positioning systems. The development and use of these systems has facilitatedthe identification of potentially significant shipwrecks, biological life forms, and geological formations. The increased deepwater oil and gas exploration in the Gulf's deepwater areas has also increased shipwreck discoveries. The shipwrecks investigated for this study were found on oil and gas related surveys. Further significant discoveries can be expected as the search for natural resources moves into increasingly deeper waters.

## 10.3.4 Regulatory Role of the BOEM and BSEE

Increases in deepwater oil and gas exploration, development, and production coexist with the development of new technologies that reduce the operational costs and risks associated withthe discovery of high-volume oil and gas reserves.

Expanding deepwater commercial development brings increasing challenges for managing Submerged Cultural Resources on the OCS and shelf slope. The BOEM requires a clearer understanding of the size of debris fields that can be expected around deepwater wrecks, as well as their state of preservation and research potential to fulfill obligations stipulated by Section 106 of the National Historic Preservation Act of 1966 (36 CFR 800). This information is critical for determining disturbance avoidance areas. Part 36 CFR 800.4(c) states that "the Agency Official

shall make a reasonable and good faith effort to identify historic properties that may be affected by (an) undertaking and gather sufficient information to evaluate the eligibility of these properties for the National Register." Sufficient documentation must be provided to the BOEM on each site to carry out an adequate evaluation of National Register of Historic Places (NRHP) criteria (USDI MMS 2004).

The former MMS played an instrumental role in the development of the Rigs-to Reefs program in the GoM. The Agency's efforts led to the National Fishing Enhancement Act of 1984 and publication of the National Artificial Reef Plan in 1985. Converting offshore oil and gas structures is well accepted as beneficial to fisheries on the continental shelf of the entire GoM (Ekins P., et al, 2006). Forty-nine (49) structures have been converted to artificial reefs from a total of 383 structure removals between 1999 and June 2002. In the near future, decisions will be required for the removal of structures located in waters beyond the continental shelf. Current guidelines outlined in 30 CFR Part 250.1728 allow the BOEM Regional Supervisor to approve alternate plans for removal of structures when the water depth is greater than 800 m (2,624 ft). Removal options for shallower depths have previously relied on the concept that the structure left behind serves a positive fisheries enhancement or other beneficial environmental function. The BOEM now requires information that will help describe the ecological role (if any) man-made structures may have in the deepwaters of the GoM (in this case, greater than 91.4 m (300 ft) (USDI MMS 2004).

## 10.4 METHODS

### 10.4.1 Survey Methodology

Each site was systematically investigated using an acoustically positioned ROV following a pre-established survey plan (See Section 10.4.2.1 Archaeological Methods). The ROV survey was designed to maximize the efforts and time for both the archaeological and biological studies. It carried the necessary equipment (See Section 4.1.2) to obtain high-quality imagery, accurately measure artifacts and biological organisms, and document seafloor conditions or features. Detailed visual inspections provided needed data to document each wreck's cultural and biological characteristics. Although different specific elements were of interest to the biologists and the archaeologists, the video footage collected was used for both the biological and archaeological studies undertaken.

A minimum of one archaeologist and one biologist were available at all times to ensure important features were not missed. Video footage was recorded continuously during ROV operations at each site and digital still photographs or screen captures were taken of pertinent archaeological and biological features.

### 10.4.2 Archaeological Methods

#### 10.4.2.1    Field Methods

Standardized investigation methods were used at each study site. The archaeologist's priorities varied depending on whether previous inspections had positively identified the shipwreck. At previously un-investigated shipwreck sites, the first priority was determining the historic potential

of the site, mapping the site boundaries/extent, and producing an accurate site plan. At previously identified shipwreck sites, the priority was mapping the site boundaries/extent and producing an accurate site plan. Site maps were produced using real-world coordinates to allow importation into a GIS database.

The investigation methodology used all available information and survey data for each site to plan field operations. The survey data included side-scan sonar, magnetometer, subbottom profiler, bathymetric data, AUV camera footage, and video footage. Previously acquired survey data was essential for determining the "expected" boundaries of each site and for developing an efficient survey plan. At each shipwreck site, the investigations followed the same pattern of reconnaissance, mosaic photography, biological sampling, close-up photography, and artifact recovery.

### 10.4.2.1.1  Reconnaissance Transects

After the ROV was deployed, a reconnaissance survey of the main wreckage was conducted. The reconnaissance allowed the science team to assess the current conditions of the wreck site and aided them in determining where to collect samples and place the microbial experiments. For the reconnaissance survey, the ROV slowly moved down each side of the hull (outboard of the gunwale) to inspect the outer hull (where applicable) and the material on the seafloor near, but outside of the hull. Then the ROV moved inboard to view the inner hull and contents (at some sites it was necessary to only make one pass along the side). Time was also spent thoroughly inspecting the bow and stern areas.

### 10.4.2.1.2  Mosaic Transects

The mosaic transects were comprised of a series of closely spaced parallel ROV lines. They were designed to allow *Jason II*'s downward looking digital still camera to capture overlapping images of the wreck site. A mosaic of these images was produced to form a single image encompassing the entire wreck site. If mosaics from previous surveys, such as an AUV camera survey, were available, the ROV mosaics were limited in scope to significant areas of the wreck as determined by the archaeological team.

### 10.4.2.1.3  Biology Transects

Biology transects documented the sea life near and away from the wreck site. The survey consists of two sets of predetermined survey lines consisting of three parallel transects, 50 m long, and spaced 10 m apart (line spacing depended on conditions at each site). One set of transects ran over the long axis of the wreck at an altitude that allowed good visual documentation of the wreck. The second set was run in the same pattern 100 m away from the wreck.

Core samples were taken near the wreck site and away (100 m) from the wreck. The cores were taken in pairs for collection consistency and to expedite this task.

Microbial platforms were placed at each site. These are long-term experiments to analyze the microbial activity and rate of hull deterioration at each site.

### 10.4.2.1.4   Close-Up Transects

Close-up inspections included detailed photography and documentation of specific corals or other areas of biological interest (e.g., rusticle formations), and specific areas of archaeological interest (e.g., specific artifacts or areas of hull construction.).  The archaeologists and biologists conducted these operations in conjunction with each other or split the time, depending on the varying interests at each site.

### 10.4.2.1.5   Artifact Recovery

Limited diagnostic artifacts were recovered at each site upon instructions of the principal archaeologist and in consultation with the BOEM archaeologist.  The materials recovered from the wreck sites for identification and dating purposes included: copper sheathing, wood, ceramics, and shipboard equipment.


### *10.4.2.2   Post-Field Operations Archaeological Data Assessment*

Following each period of field operations, all the digital data was brought to the C&C's Lafayette or Houston offices.  Once at C&C, a backup copy of the data was produced for the data archive, then additional copies of each dataset were provided to C&C's archaeological staff.  The data was then assessed by the archaeologist assigned to each shipwreck site.  Assessment of the collected data included review of video and still footage to document the pertinent construction attributes, ship components, artifacts, etc., followed by examination of field notes and historical research.

For each shipwreck assessment, standard descriptions and definitions related to ship construction (Figure 10-6) and documentation were used.  Overall site dimensions and distances are discussed using metric measurements.  Specific construction details of each of the vessels are described using the measurement units most likely used during construction.  In the case of the *Gulfpenn*, *Gulfoil*, and the four wooden shipwrecks, this was assumed to be English measurements.  In the case of the *U-166*, metric measurements were used based the location and date of its construction.
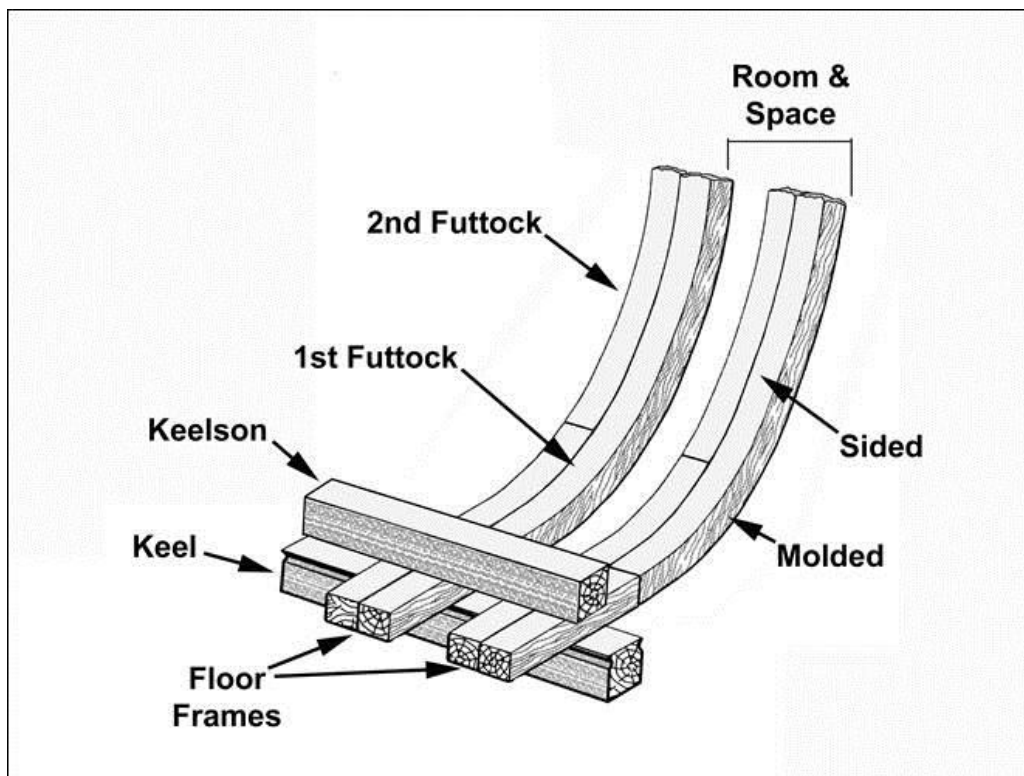
Figure 10-6. An example of double-framed construction illustrating ship construction terminologies used in this report.

## 10.4.3 Conservation Methods

### 10.4.3.1    Field Conservation

The recovered artifacts were placed in plastic containers filled with seawater, and kept submerged in an environment similar to where they were recovered.  Some field photos were taken, but with the movement of the ship, most details were blurry.  Current photos of each artifact were taken in the lab.  Any of the objects that may have been light sensitive, such as the paper in the compass, were kept covered as much as possible to reduce damage.  Artifacts were protected with foam mattress padding during transport from the ship to the University of West Florida Conservation Laboratory.

### 10.4.3.2    Laboratory Conservation

For every artifact, the first step of the conservation process was to photograph and document the artifact.  The next step was the removal of chlorides from the artifact.  An object immersed in salt water absorbs salt chlorides from the water.  If the chlorides are still in the artifact as it dries, serious damage can occur.  Chlorides are removed by soaking artifacts in successive tap water baths until the chloride level has been lowered to below 100 parts per million.  Once the chlorides have been removed, the conservation process, which is dictated by artifact type, can proceed.

358

A detailed description of the conservation methods employed in stabilizing and conserving the artifacts recovered during the project is provided in the University of West Florida Conservation Report found in Appendix E-2

## 10.5 SHIPWRECK SITE ASSESSMENTS

### 10.5.1 *Viosca Knoll* Wreck Site

#### 10.5.1.1 Historical Background of the Viosca Knoll Wreck

The *Viosca Knoll* Wreck Site is the remains of a wooden sailing vessel dating from the latter nineteenth century. Discovered in 2003 during an archaeological, engineering and hazard pipeline survey, the wreck was named for the lease block area where it was found. Archival research has failed to identify the name or nationality to this shipwreck. Since its discovery, a deep-tow and AUV survey and two government sponsored ROV investigations have been conducted at the site.

#### 10.5.1.2 Field Investigations

##### 10.5.1.2.1 Discovery and Exploration

In 2003, a pipeline survey for Mariner Energy discovered the unidentified shipwreck south of the Petronius platform. The survey used a deep-tow AMS 120 Sonar Mapping System, which included 120 kilohertz (kHz) side-scan sonar. The wreck was outside the pipeline survey corridor, but was imaged during a line turn. Several additional investigation lines were run over the site to obtain additional geophysical data (Church 2003). In May 2004, C&C conducted an AUV survey of the shipwreck site using *C-Surveyor I*. High-resolution multibeam bathymetry and side-scan sonar data were collected on 27 survey lines crisscrossing the site. The side-scan sonar showed debris scattered west and southwest of the shipwreck (Figure 10-7). Numerous drag scars, characteristic of those caused by large anchor chain and cable, were also noted in this sonar data. One drag scar crosses the wreck's northern end (Figure 10-8). An elongated seafloor depression or large drag scar exists east of the wreck (Figure 10-9 and Figure 10-10). The southeast portion of the wreck (port side) exhibits an average of 2 m of relief with the stem post standing approximately 3.3 m high (Church and Warren 2008).
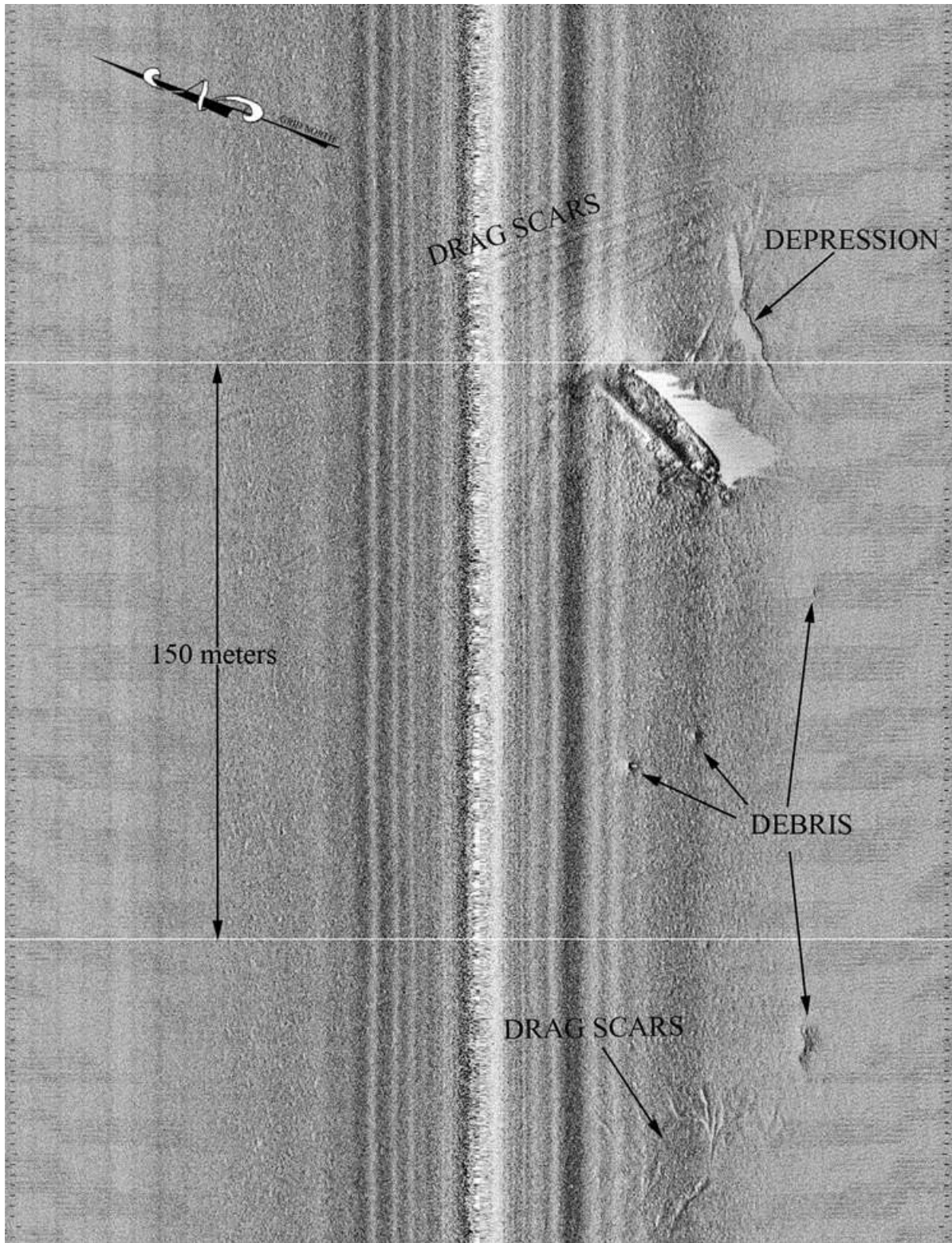
Figure 10-7.  Side scan sonar image of the VK Wreck and surrounding area (courtesy of C & C Technologies, Inc.).
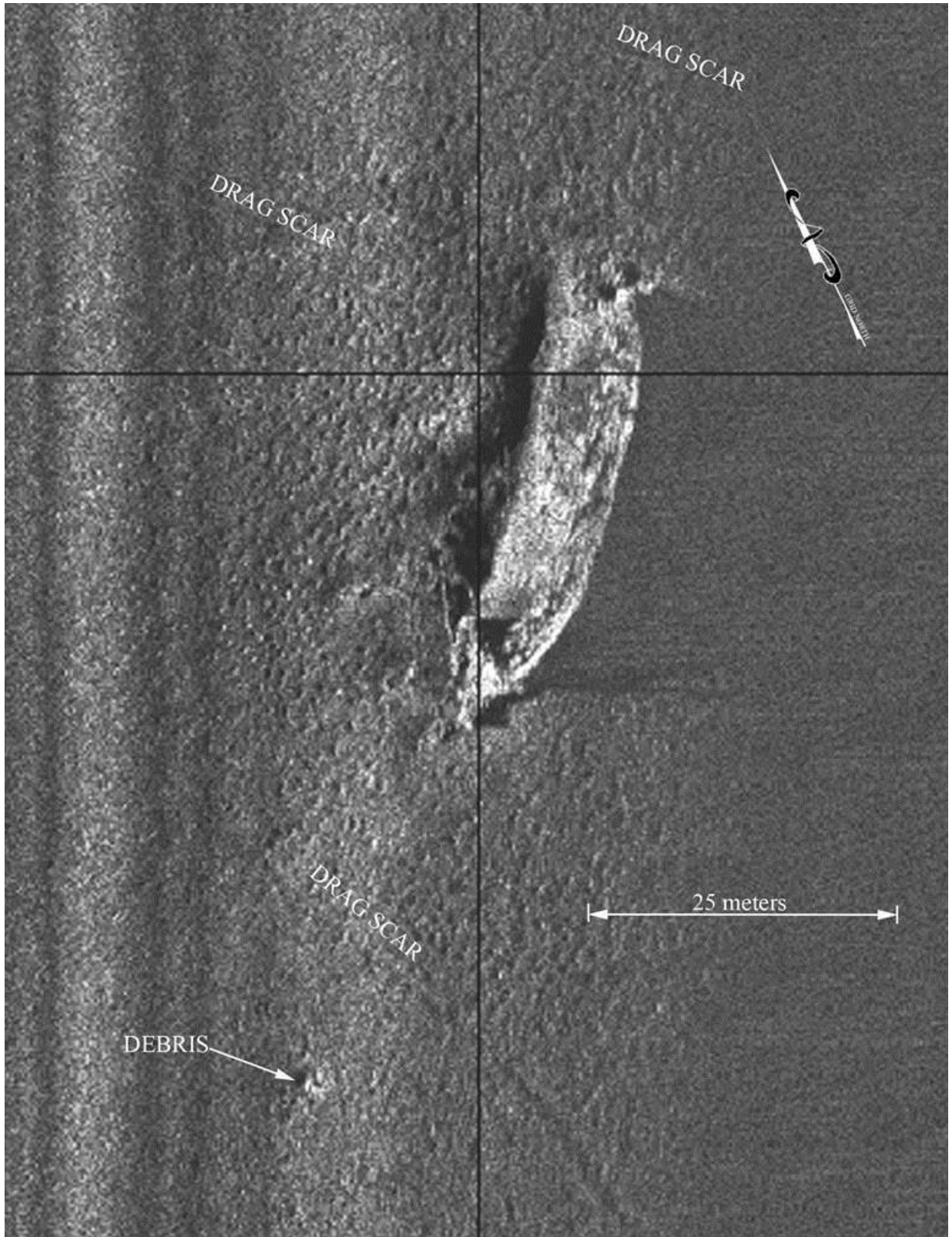
Figure 10-8.  Side scan sonar image, close-up of the VK Wreck (courtesy of C & C
Technologies, Inc.).
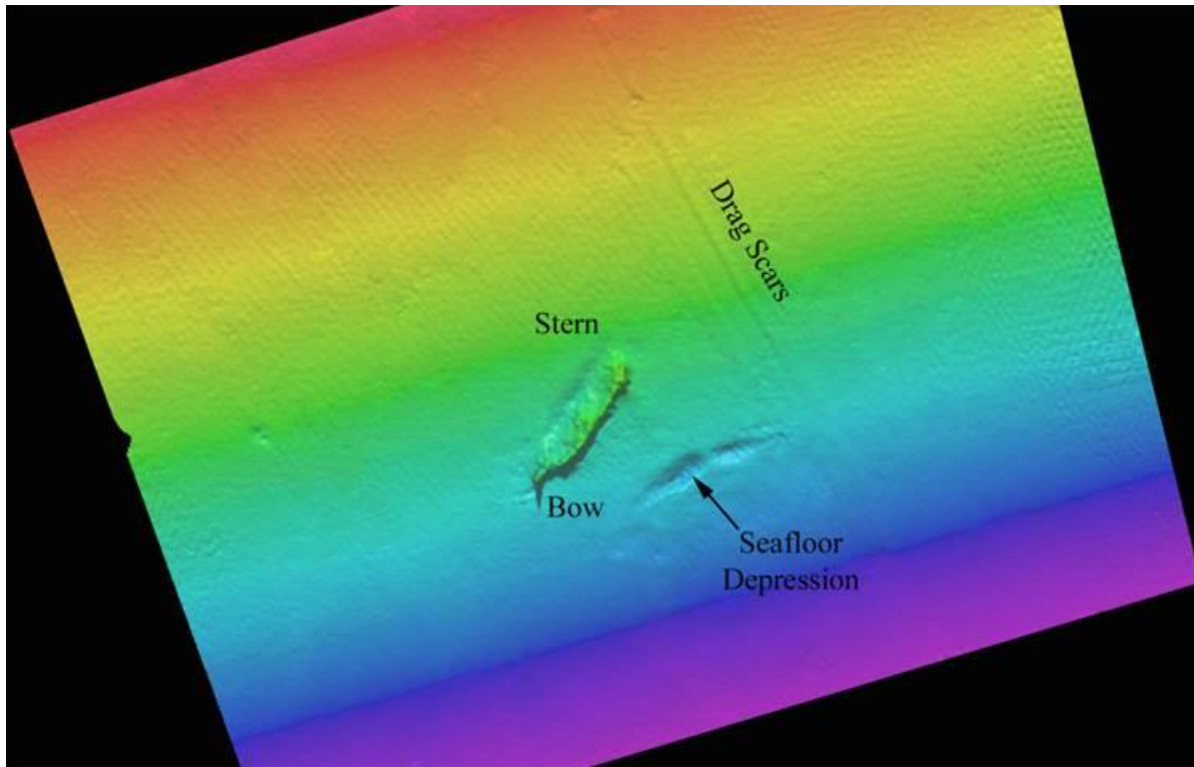
Figure 10-9.  North-up plan view of the VK Wreck. Processed multibeam image at 1.5-foot bin size (Courtesy of C & C Technologies, Inc.).
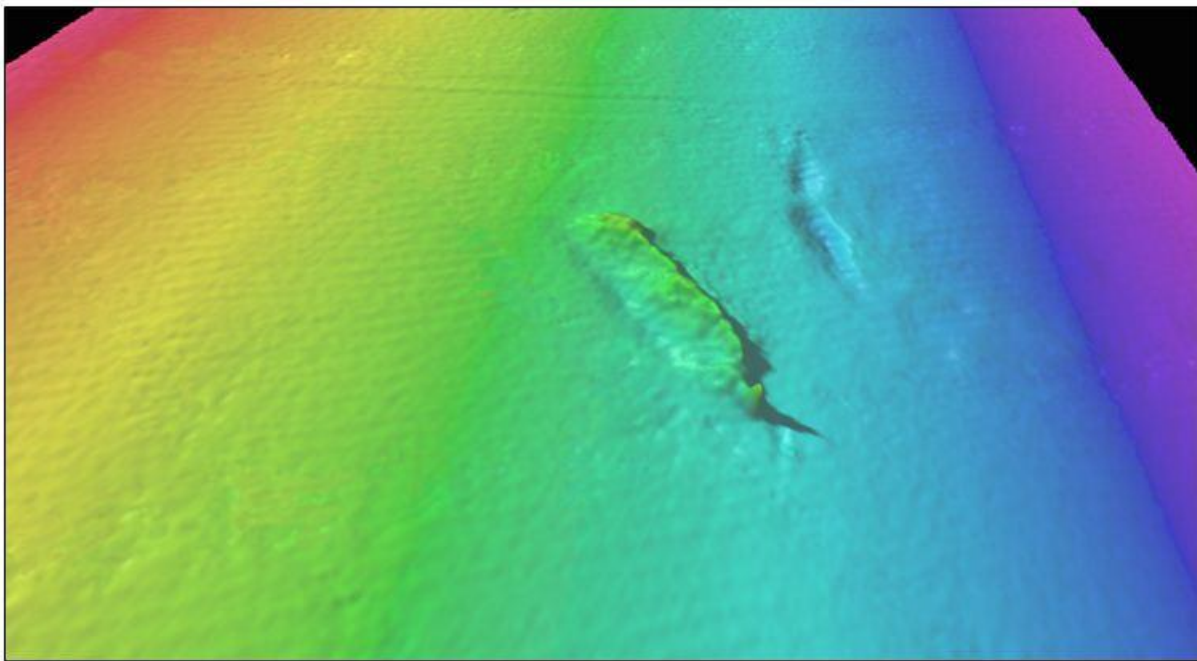


Figure 10-10.  A 3-D perspective view of the VK Wreck. Processed multibeam image at 1.5-foot bin size (courtesy of C & C Technologies, Inc.).

### 10.5.1.2.2    *Viosca Knoll* Wreck 2006 ROV Investigation (OCS Study MMS 2008-018)

A site investigation was planned during the 2004 fieldwork for the MMS's *Archaeological and Biological Analysis of World War II Shipwrecks in the Gulf of Mexico* (OCS Study MMS 2007-015), but adverse weather made investigating the site impossible at that time (Church et al. 2007). The MMS later sponsored a site investigation in July 2006 (OCS-Study MMS 2008-018). The site was visually inspected used a Saipem American Innovator Class ROV deployed from the HOS *Innovator*. The investigation was conducted under the direction of C&C marine archaeologist Robert Church and BOEM marine archaeologists Jack Irion and David Ball (Church and Warren 2008). Visibility on-site was poor during the 2006 investigation, averaging only 2.4 to 3.6 m. The ROV position was continually recorded (at 6 second intervals) using a Sonardyne USBL System.

The entire investigation was conducted in approximately 6 hours and began with a site reconnaissance followed by photo mosaic transect lines. A photo mosaic was produced using screen captures from the ROV's video camera. The mosaic lines consisted of eight transects run over the wreck site on a heading of 35 degrees and an equal number of reciprocal lines run on a heading of 215 degrees. Line spacing was less than 2 m to ensure visual overlap. Detailed visual inspections of specific areas of interest were conducted upon completion of the mosaic lines. The final part of the survey was the visual inspection of outlying debris noted from the geophysical data and/or detected with the ROV's scanning sonar during the site investigation.

### 10.5.1.2.3    *Lophelia* II: Reefs, Rigs, and Wrecks 2009 Field Cruise

In September 2009, the second ROV investigation of the *Viosca Knoll* Wreck was conducted as part of the *Lophelia* II: Reefs, Rigs, and Wrecks Study. Over an approximate 12-hour period (10.5 hours on the wreck site) on September 5 and 6, 2009, the *Lophelia* II team used Woods Hole Oceanographic Institution's *Jason II* ROV launched from the NOAA Research Vessel *Ronald H. Brown* to document the shipwreck site. Visibility on-site was fair during the 2009 investigation, averaging 6 to 7 m. Limited material was collected during the project to help better understand the wreck site.

The 2009 investigation consisted of an initial reconnaissance survey, site mosaic transects, detailed inspection of significant features (both biological and archeological), deploying biological experiments, and artifact collection. The one hour reconnaissance consisted of a preliminary examination around the full perimeter of the main hull to assess its current condition and to prioritize areas for additional investigation and material collection. The reconnaissance began on the port side at the bow and moved slowly along the port side toward the stern. After an examination of the stern, the ROV moved along the starboard side towards the bow. The ROV then moved inboard with a starboard view and slowly transited back toward the stern, videoing the interior of the hull.

Following the reconnaissance, 19 parallel track-lines at 1 meter spacing were flown over the main hull, taking a series of evenly spaced still photographs for mosaic purposes. The digital still camera was mounted in a vertical viewing position and the ROV was flown at a 6-m altitude during transects. Approximately three hours were spent conducting the photo mosaic transects.

Biological operations were conducted over the next three and a half hours, including biological transects, collecting sediment cores, deploying microbiological experiments, and detailed biological documentation. Three biological transects were run 100 m southeast of the wreck site. Sediment core samples were collected at distances varying from 100 m away to 10 m from the wreck site. Short-term and long-term microbiological experiments were placed on the aft portion of the wreck to assess microbial activity and preservation potential. Detailed photographs and measurements were taken of coral and other features of biological interest at the bow and along the port side of the wreck.

Following the biological investigation, close-up examination was conducted of archaeological features in conjunction with limited artifact recovery and recovery of the short-term microbiological experiment. Approximately one and one-half hours was allocated for those tasks. The remaining 2 hours of the dive included investigation of outlying artifacts and preparations for ROV recovery. The archeologists and biologists concurrently conducted the detailed examination of the outlying artifacts.

### 10.5.1.3    Geographic Settings

The *Viosca Knoll* Wreck is in the southeastern portion of the Viosca Knoll Area of the GoM (Figure 2-2). The project area is located south-southeast of Mobile, Alabama on the upper continental slope. The seafloor dips south-southeast across the site at a gradient of 5 degrees. Very soft clays are the predominate near-seafloor soils at the site. The Alabama River provided sediment input into this area prior to and subsequent to the sea level low stand, which occured about 18,000 years BP. Sediment input into this area was highest when the St. Bernard delta was active between 1,500 and 4,000 years BP (Frazier, 1967). Sedimentation rates for the area became much lower as the Mississippi River deltas and lobes migrated southwest. The deeper stratigraphy in the region is influenced by the upper eastern Mississippi Fan which was fed through submarine canyons or channels originating on the upper slope (Dixon and Weimer, 1998).

### 10.5.1.4    Discussion of Archaeological Findings at the VK Wreck

10.5.1.4.1    Physical Site

The vessel is oriented with the bow pointing southwest and the stern northeast (Figure 10-11). Average water depth at the site is 612 m Below Sea Level (BSL). The vessel measures between 121.3 to 141 ft (37 to 43 m) long and approximately 26 ft (8 m) at the beam. It is estimated the vessel had an approximate 5:1 length-to-beam ratio. It is not possible to get an exact measurement with the currently available data because the stern is not intact and the vessel is listing to starboard. Individual artifacts, rigging and other hull material are scattered primarily out from the stern, bow, and starboard side making the overall measurement of this portion of the site 47×19 m. A few additional outlining artifacts are located as much as 143 m west-southwest of the hull making the overall site dimensions 188 × 67 m.
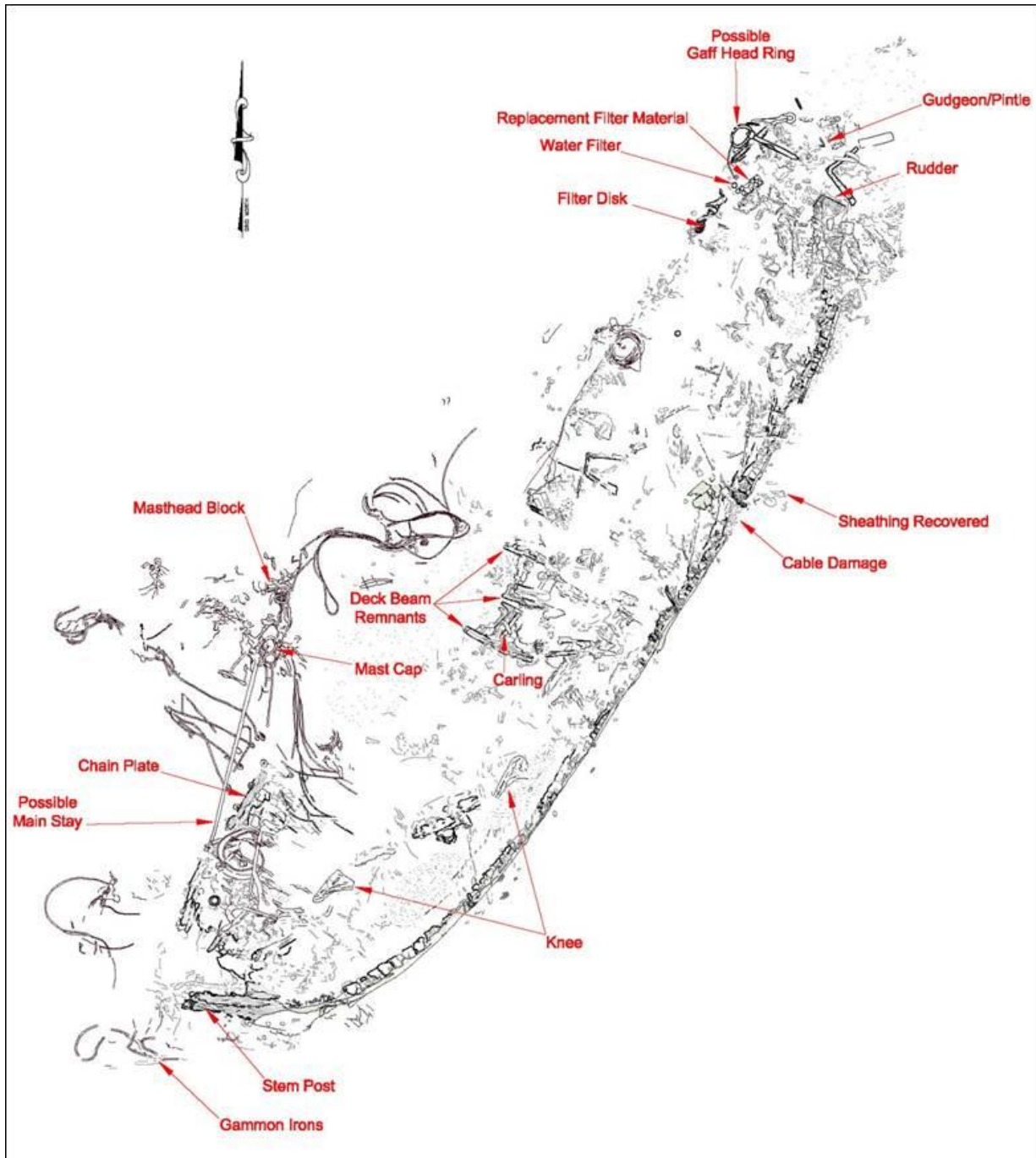
Figure 10-11. *Viosca Knoll* Wreck Site Drawing based on ROV investigation findings.

The wreck's starboard side is mostly flush with the seafloor, while the port side exhibits between 3.3 and 6.6 ft (1 to 2 m) relief, exposing the turn of the bilge. The hull is listing approximately 41 degrees to starboard, based on the angle of the stempost (Figure 10-12). Marine sediments and biofouling obscure much of the construction details, but some inferences can be made regarding hull construction. Remnants of the frames, and possibly the wale, and clamp are visible at some locations along the port side. The construction appears to be double framing. The frames, at what

is believed to be the second and third futtocks, are approximately 7.5 in (19 cm) sided and 6.5 in (16 cm) molded. The room and space is approximately 8 to 9 in (20 to 23 cm). The hull planking measures approximately 8.6 in (22 cm) wide and 1.5 to 3.5 in (4 to 8.9 cm) thick where discernible on the starboard side.



Figure 10-12. Front view of stem post showing list to starboard.

### 10.5.1.4.2   Sheathing

The hull of the *Viosca Knoll* Wreck is sheathed primarily in Muntz metal and although some non-uniform lengths may have been used, the majority of sheathing appears to be standard $48 \times 14$ inch ($121.9 \times 35.5$ cm) sheets with 1 to 1.5 in (2.5 to 3.8 cm) overlap between sheets (Figure 10-13). The sheathing is held to the hull by copper or copper alloy fasteners, which are staggered between rows forming a typical diamond nail pattern. The fasteners spacing is 5.25 in (13.3 cm) between nails horizontally and 3.5 in (8.9 cm) diagonally. Diagonal foiling (buckling) is observed along the copper or copper alloy sheathing, which is typical for copper-sheathed vessels found in deep-water (Figure 10-14). The reason the sheathing becomes buckled is not fully known, but is possibly related to either compression of the wood at depth or anaerobic bacteria activity. DBI tested a section of new copper sheathing in a laboratory experiment and observed buckling of the sheathing after six months. (Appendix E-1). The foiling likely occurs in a diagonal pattern on the shipwreck because of the diagonal nail pattern holding the sheathing to the hull.
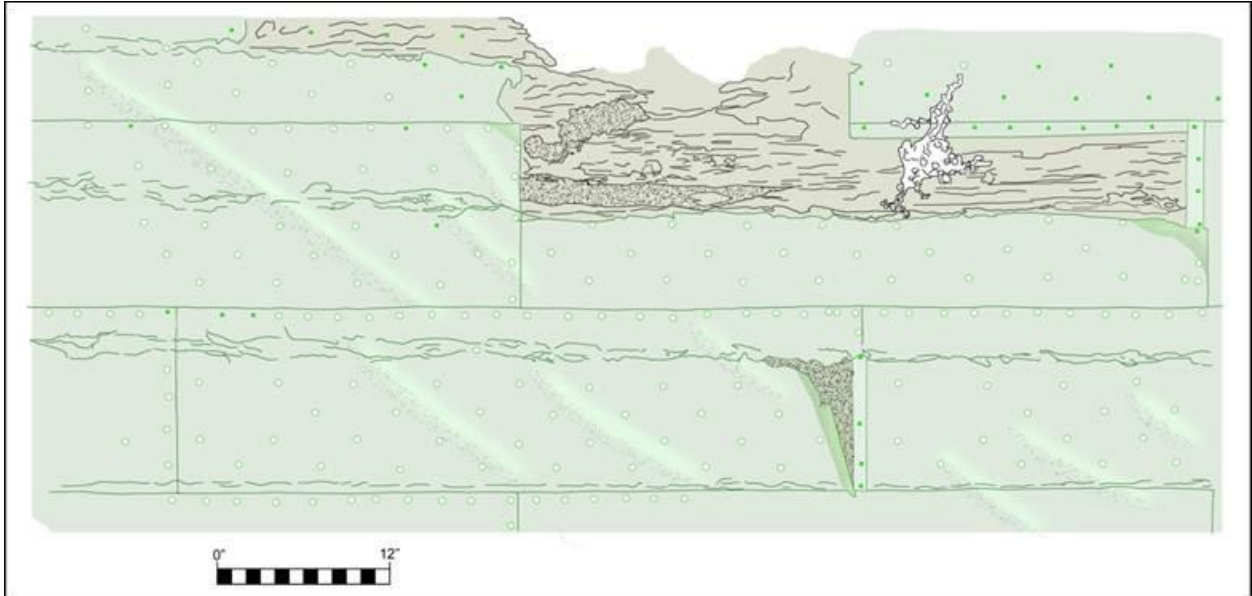
Figure 10-13.  Sheathing detail from starboard side.



Figure 10-14.  Diagonal foiling observed in sheathing (Starboard side).

## 10.5.1.4.3    Bow

The stempost remnant stands approximately 10.8 ft (3.3 m) proud of the seafloor (Figure 10-15). The upper remnants of the stem measure 10 in (25.5 cm) molded and 6 in (15.2 cm) sided.  A portion of apron or inter-stem is visible (Figure 10-16).  The rabbet appears to be visible on the stempost exposing the juncture of the hull strakes.  It was not possible to accurately measure the lower portions of the stem (above the sheathing) because of substantial biological growth.  The front edge of the sheathed cutwater measures 4 in (10.1 cm) wide.  The bow appears to gently round from the keel to the apparent water line.  Possible remains of the gammon irons and head rigging lie beneath the stempost (Figure 10-17).  A small section of thin net is visible on the seafloor forward of the bow (Figure 10-18).  The net is likely intrusive to the site.  Various other construction features were observed including disarticulated knees and possible cant frames.  No windlass or anchor chain was observed at the wreck site.



Figure 10-15.  Mosaic of the bow (view from port side).
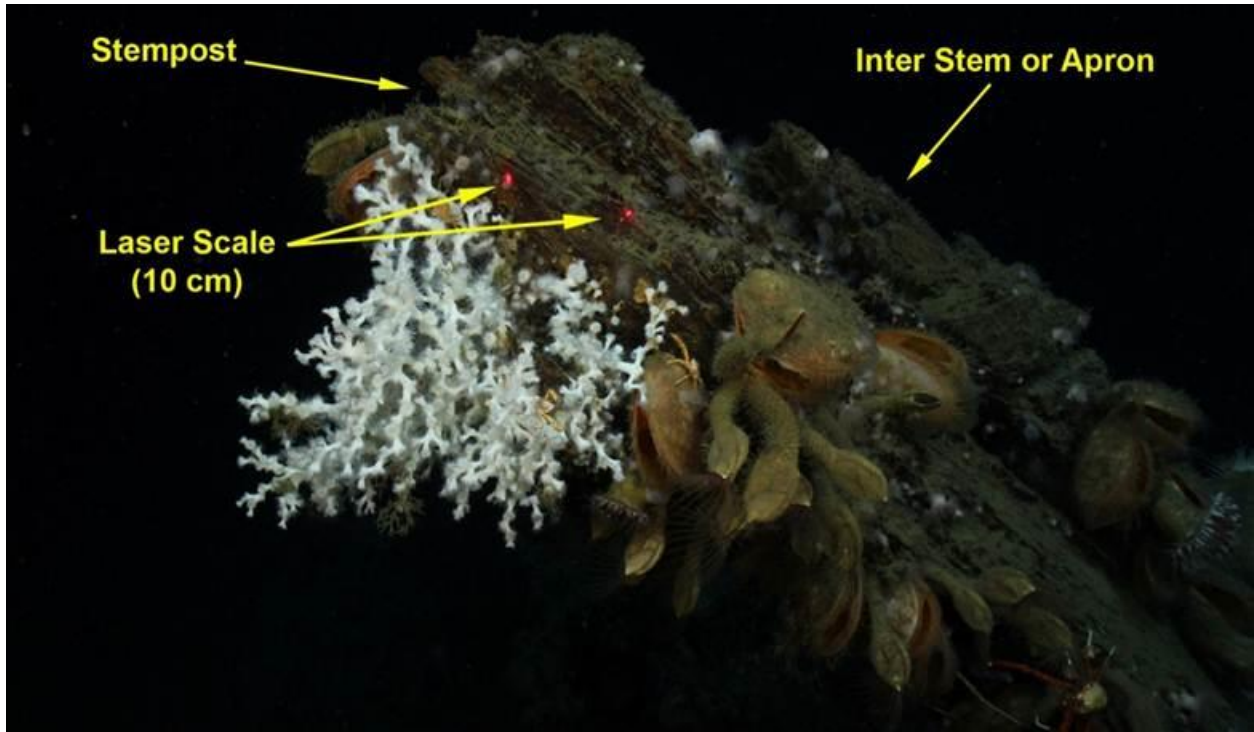
Figure 10-16. Close up profile of upper stem remains.
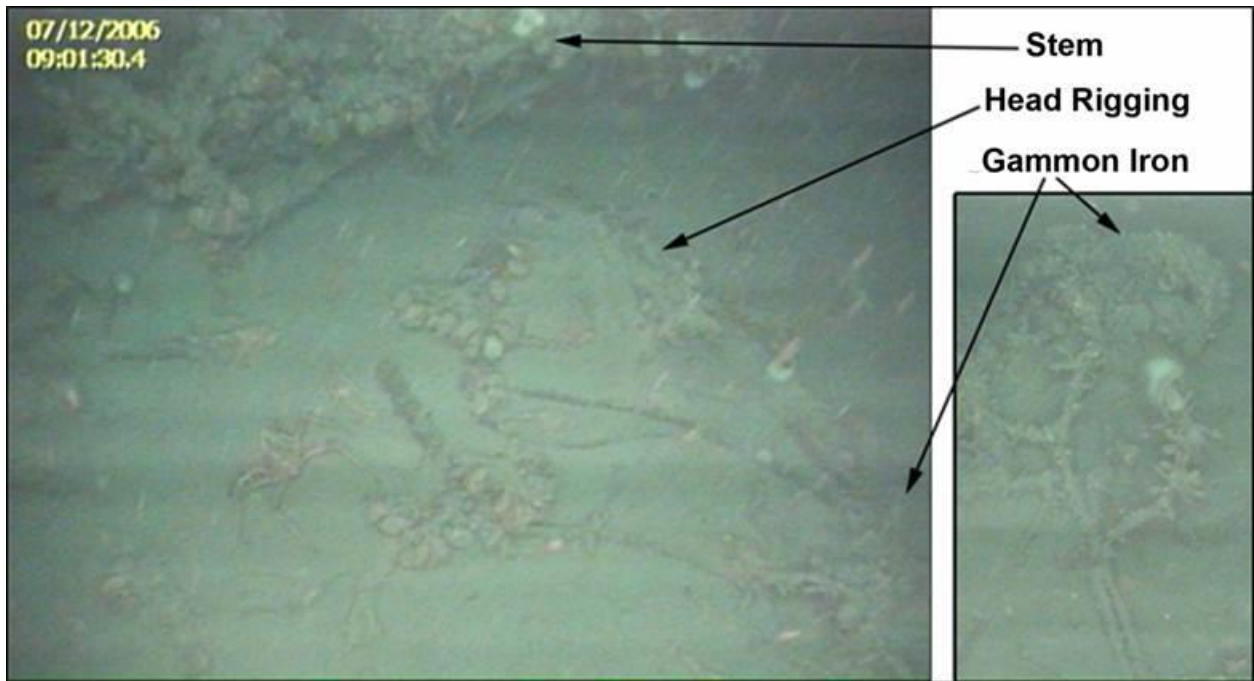


Figure 10-17. Gammon irons and head rigging.
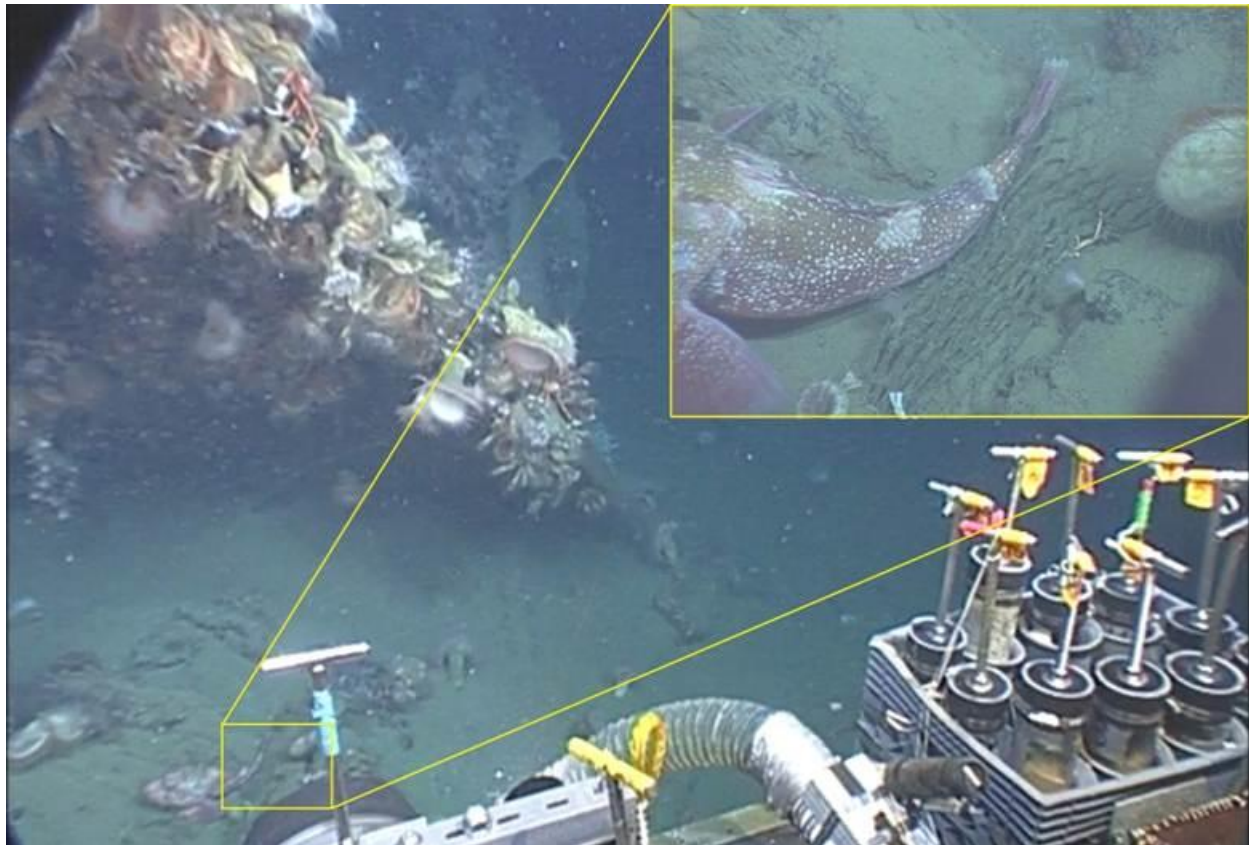
Figure 10-18. Image of net remnants on the seafloor near the *Viosca Knoll* Wreck's bow.

### 10.5.1.4.4　Stern

The aft portion of the wreck is badly deteriorated and shows damage consistent with possible cable impact to the hull. A 0.5-to-1-meter tear in the hull's starboard side is visible approximately 14 m forward of the stern and 26 m aft of the stem (Figure 10-19). This damage correlates to a seafloor drag scar recorded on the geophysical survey data. The drag scar crosses the wreck at an approximate 29-degree angle. The location where the drag scar crosses the hull likely corresponds with the possible mainmast position. Aft of the drag scar, most of the stern is missing or damaged. Some of the exposed wood structure in the stern exhibited much less deterioration than the other wood material at the site, indicating possible recent exposure.

A portion of the rudder appears to remain in place with a possible loose gudgeon laying exposed on the seafloor less than 2 m away (Figure 10-20 and Figure 10-21). The rudder measures 7.5 in wide (19 cm). Only one meter of the rudder is exposed above the seabed and the upper portion is broken away. It is not known how much of the upper portion of the rudder is missing. The width of the possible gudgeon is also approximately 7.5 in (19 cm).
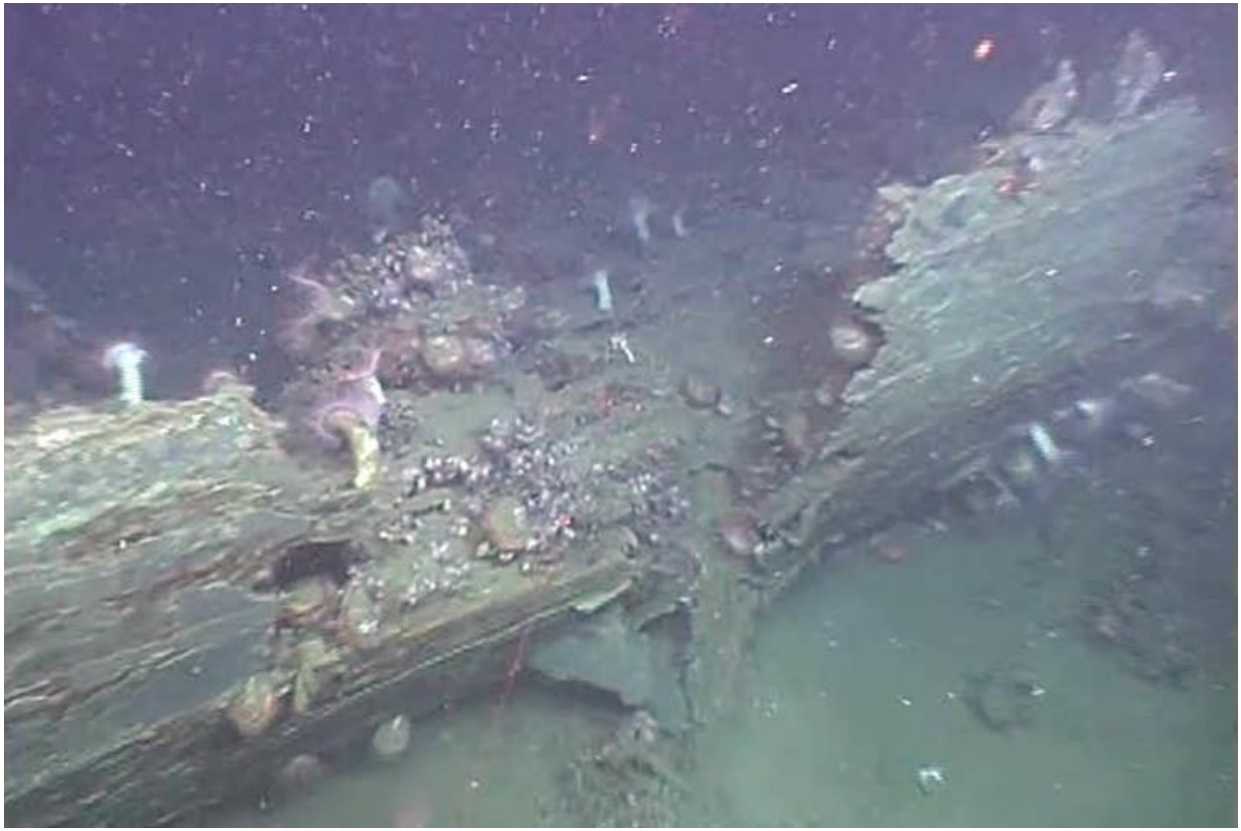
Figure 10-19.  Image of the *Viosca Knoll* Wreck showing the tear in the port hull.

Figure 10-20. Copper-sheathed rudder of the VK Wreck with close-up inset showing a portion of the pintle (10 cm laser scale shown at bottom of inset).



Figure 10-21. Possible Gudgeon strap lying on the seafloor at the stern of the VK Wreck.

Two ingots of possible lead, based on its whitish color, are laying on the seafloor at the stern, as are numerous other unidentified ship parts and objects. The ingots measure 14 in (36 cm) long and 2 in (5 cm) wide. One is at the end of the stern and the other is near a large metal ring on the starboard side of the stern remains. The metal ring is possibly brass, copper, or copper-alloy and is lying on top of the other stern debris (Figure 10-22). The interior diameter of the ring is 29.5 in (75 cm) and it is 4.3 in (11 cm) thick. A 6.5 foot (2m)section of metal shaft appears to be attached to the top of the ring. The function of the ring is not known, but may be associated with a mast such as a gaff head-ring.
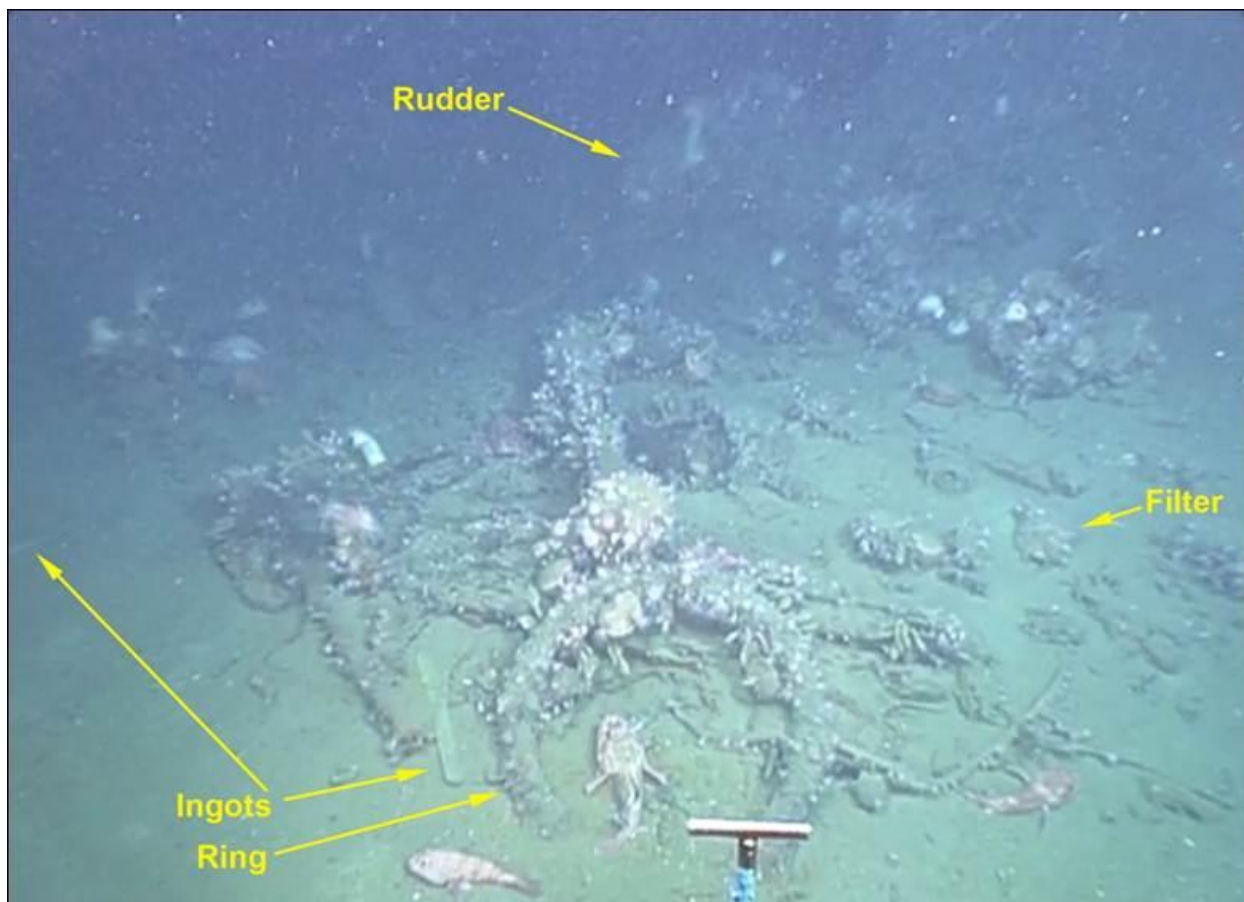


Figure 10-22. Starboard side view of the VK Wreck's stern showing possible gaff head-ring, ingots, water filter on the right side of the image, and rudder in the background.

Approximately 1.5 m forward of the ring and shaft was the lower portion of a ceramic water filter (Figure 10-23). The filter was originally thought to be an earthenware crock until it was recovered. Nearby are what appear to be eight or more charcoal replacement filters. They are arranged side-by-side in two rows as if once in a box or bound together. The packaging of the replacement filters have mostly disintegrated. A ceramic disk with holes sits on it's edge less than two m forward of the filter along the starboard side (Figure 10-24). The ceramic disk appears to be the disk that once separated the chambers in the filter.
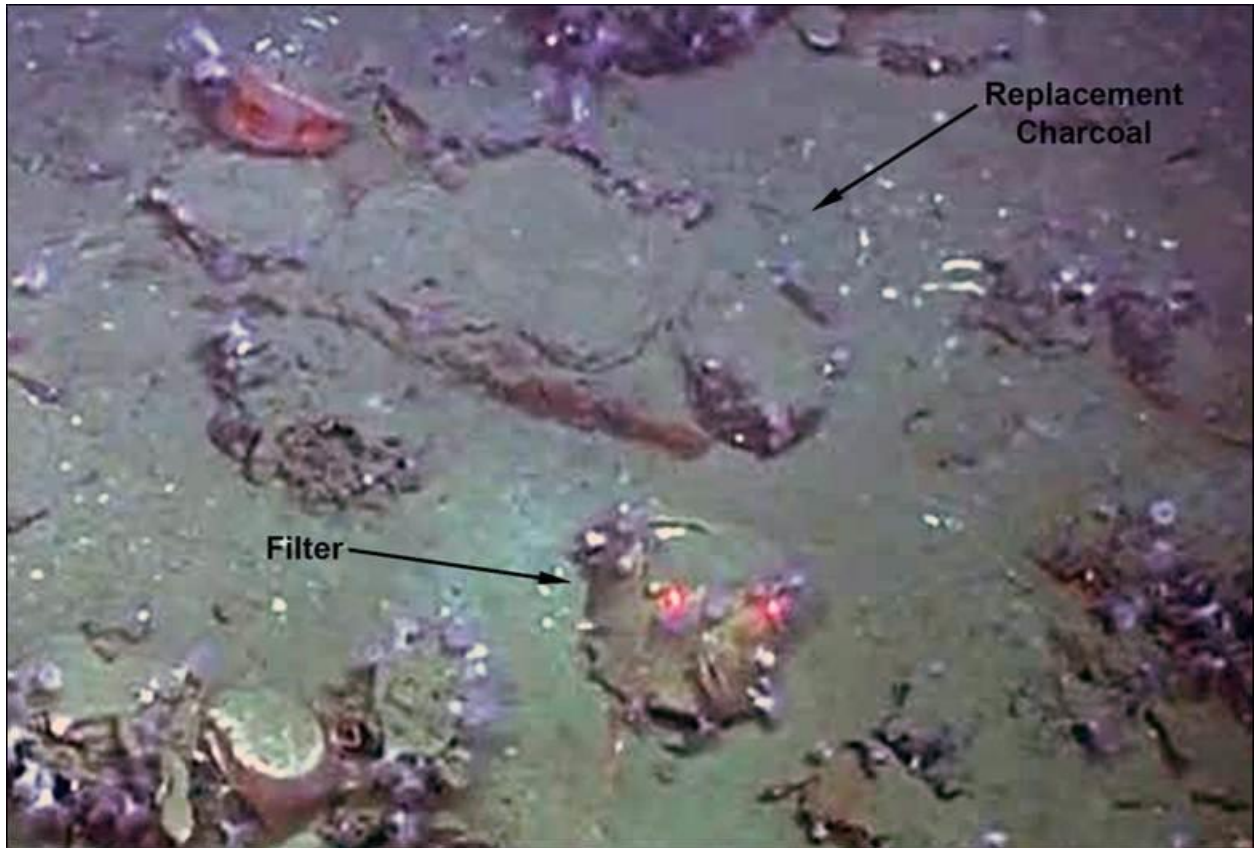
Figure 10-23. Water filter and replacement charcoal.



Figure 10-24. Ceramic disk, which is likely part of the water filter.

## 10.5.1.4.5    Rigging

A coil of line or wire rope is located along the starboard side 8 to 9 m forward of the stern (8.6 m forward of the ring and shaft).  The drag scar that crosses the wreck missed the coil of line by approximately 4 m.  No other rigging is visible near this portion of the hull although rigging from the main mast should be present near this location.

A substantial amount of apparent foremast rigging is present along the starboard side of the hull. A 24.6 foot (7.5 m) section of large standing rigging (possibly a main stay) lies along the seafloor adjacent to a portion of chainplate (Figure 10-25).  The standing rigging is approximately 4 in (10.1 cm) in diameter.  A broken section of rigging also lies inside the hull at a 47-degree angle to that lying on the seafloor and may represent another section of the same standing rigging.  The rigging within the hull passes through several large rigging eyes.  A mast cap is visible as well as a possible masthead block within the rigging lying on the seafloor.  The chainplate remains and visible portions of standing rigging are possibly from the vessel's port side.  As the mast eventually fell to starboard with the list of the vessel, the port side rigging would have pulled away from the deteriorating hull and fallen to the seafloor landing on the starboard side of the hull.  When the ship's mast deteriorated, only the rigging remained to mark its location.  The rigging in this area of the site does not appear to have been disturbed after settling to the seafloor.  The location and orientation of the rigging indicates it is the foremast rigging, which fell back and to the starboard side.
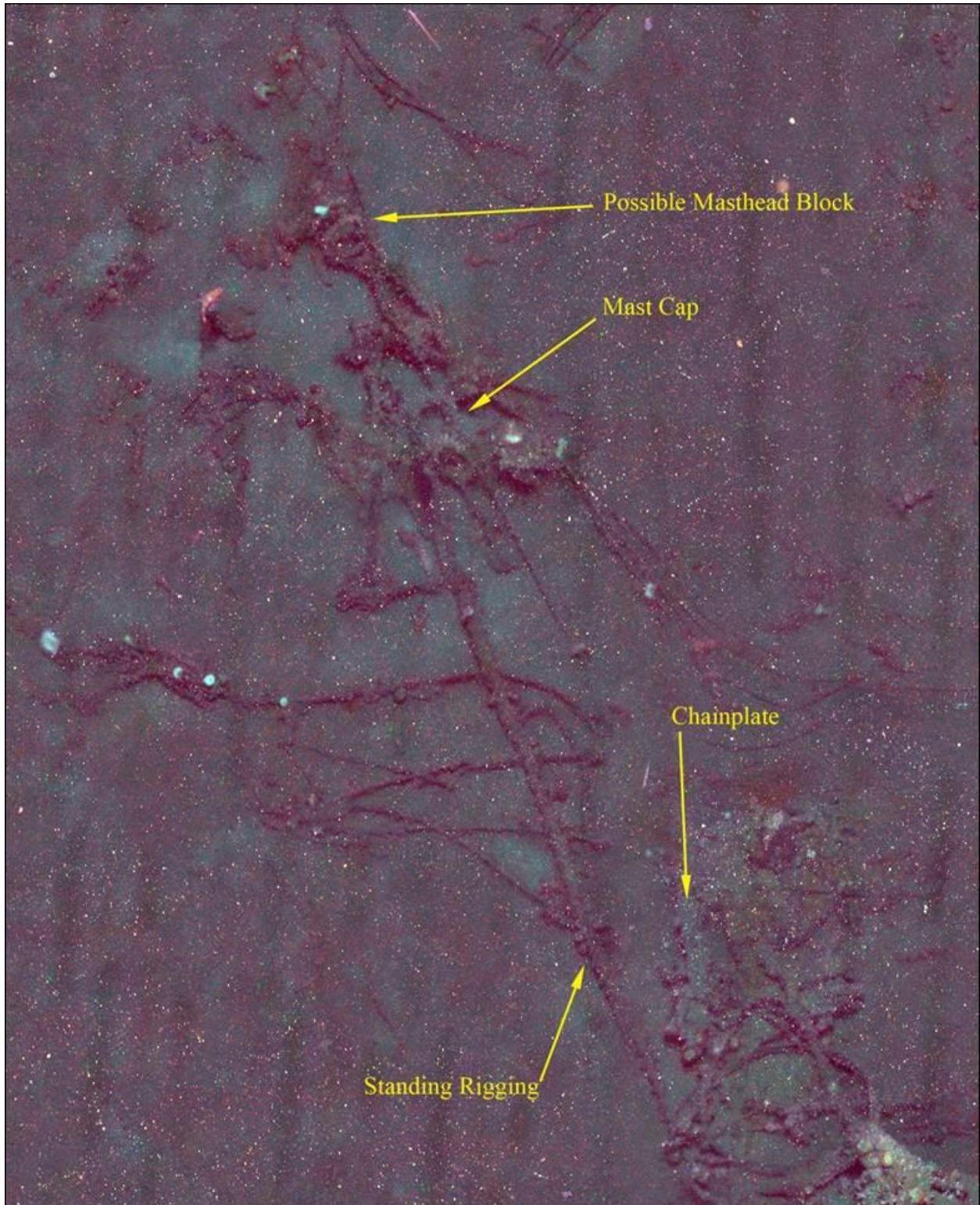
Figure 10-25. Mosaic of the VKE Wreck's foremast rigging, showing mast cap, chain plate, and possible masthead block.

Based on the amount of extant rigging, and the placement and the size of the rigging, the vessel appears to have been two-masted. The most likely vessel types for a two-masted vessel of this size are either a brig or schooner. Typical proportions for a brig or two-masted schooner places the foremast 1/4 or less of the total length from the stem and the main mast approximately 3/5 of the total hull length from the stem. These are the typical proportions; however, these dimensions are not set in stone. The foremast in both brigs and schooners were often less than a 1/4 of the of the hull's total length from the stem. The main mast, though less common, may be less than 3/5 of the hull's total length from the stem (Smith 2005, Chapman 2006, Steffy 1994, and Rybka and Moreland 1994).1 If the 40-meter long *Viosca Knoll* Wreck followed the traditional layout, the foremast would have been approximately 10 m aft of the stempost and the main mast approximately 24 m aft of the stempost.

### 10.5.1.4.6    Deck Beams Other Construction features

Numerous deck beam remnants are visible within the hull. The deck beams appear to be on 4-foot centers, but are spreading apart at various locations. Lodge knees and hanging knees are visible at various locations within the hull. Near amidships are the remains of deck beams associated with intact carling and lodging knees (Figure 10-26 and Figure 10-27), which are visible on the starboard side of the vessel. This extant deck structure indicated the lower hull is likely intact below the silt covered deck. If the lower hull is intact, cargo and other contents may have survived in this area.



Figure 10-26.  VK Wreck's deck structure from starboard view showing deck beams and lodging knees.

---

1 Ship dimensions and construction information were compiled from documentation on the Brig *Frolic*; the U.S. Navy Brigs *Jefferson*, *Eagle*, and *Niagara*; and Fredrik Henrikaf Chapman's substantial drawings of brigantines and schooners.
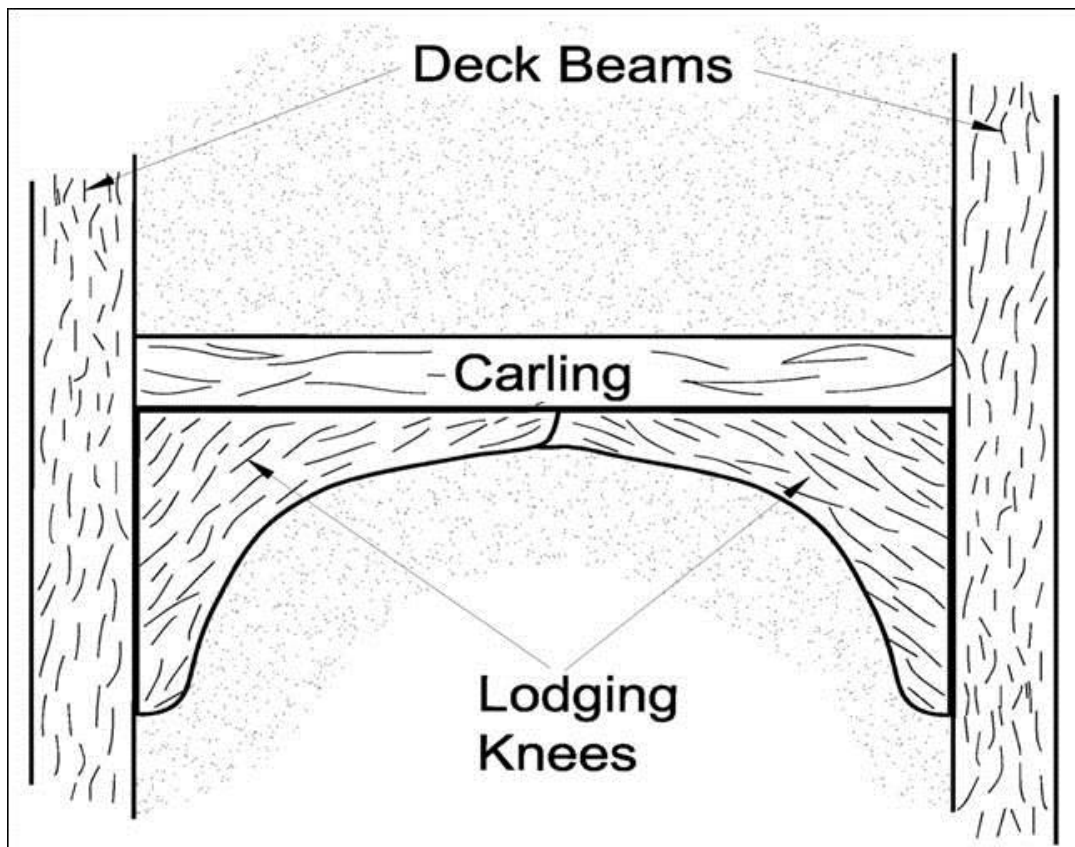
Figure 10-27. Deck structure detail in plan view (drawing by Robert A. Church).

## 10.5.1.4.7    Scattered Artifacts - Outlying Material

A mass of rigging, including a mast cap, is located 142 m west-southwest of the hull. This may be rigging from the main mast, which is notably absent at the hull. The rigging covers an area measuring 11 × 6 m. A section of possible quarter-inch polypropylene rope appears to be tangled in the rigging. It is not known whether the "polypropylene" became associated with the rigging at the time it was displaced or if it was intrusive to the site. A possible ceramic cup or insulator is lying beside the mast cap and a section of possible standing rigging chain (the chain links measure approximately 1.5 in (4 cm) long). The object is white in color, concaved in the middle, and measures 3.5 in(9 cm) tall. It is approximately 3 in in diameter on the ends, narrowing to 2.4 in in the middle (7.5 cm in diameter, narrowing to 6 cm in the middle) (Figure 10-28).
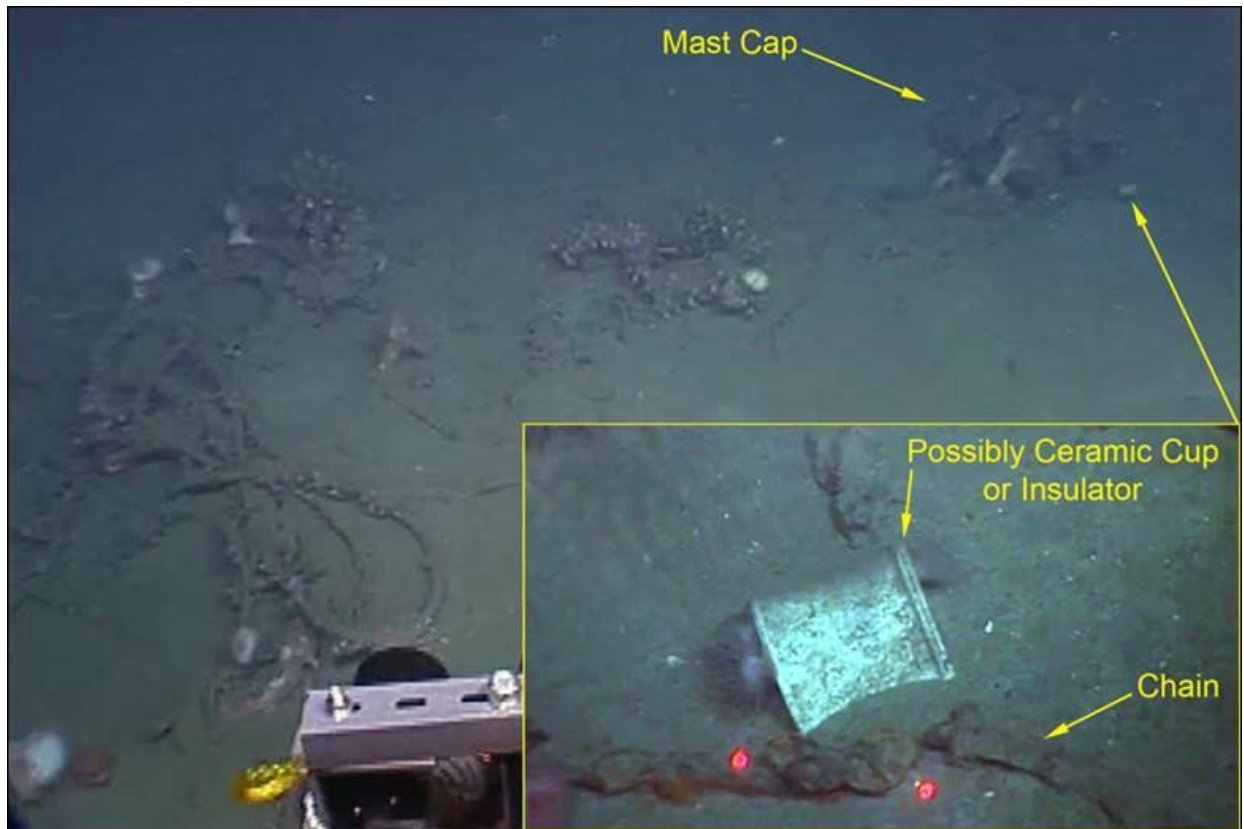
Figure 10-28. Rigging away from VK Wreck's main hull and possible ceramic cup or insulator located near mast cap.

A line of other debris was observed between the hull and this rigging. The largest outlying artifact observed is a patent stove standing upright in a seafloor depression (Figure 10-29). It measures approximately 30 in (77 cm) wide and 26 in (65 cm) deep. Although the details are obscured by sediment and biofouling, a raised lip is visible around the edge. Marine stoves often had a raised lip or band around the top edge to keep pans from sliding off the surface while at sea. Accurately estimating the stove's height was not possible because of the angle of view and the fact that the feet are partly embedded in the seafloor, but it stands at least half a meter above the sediment. The stove is located 74 m west-southwest of the hull.

A possible lantern (Figure 10-30) and an unidentified object (Figure 10-31) were also documented 63 m west-southwest and 38 m south of the hull, respectively. The lantern is lying on its side. It measures approximately 18 in (45 cm) in height and 12 in (30 cm) in width. The viewing glass is not visible and may have fallen inside the body or is missing. The unidentified object measures approximately 18 in (45 cm) in diameter and is covered with biofouling.
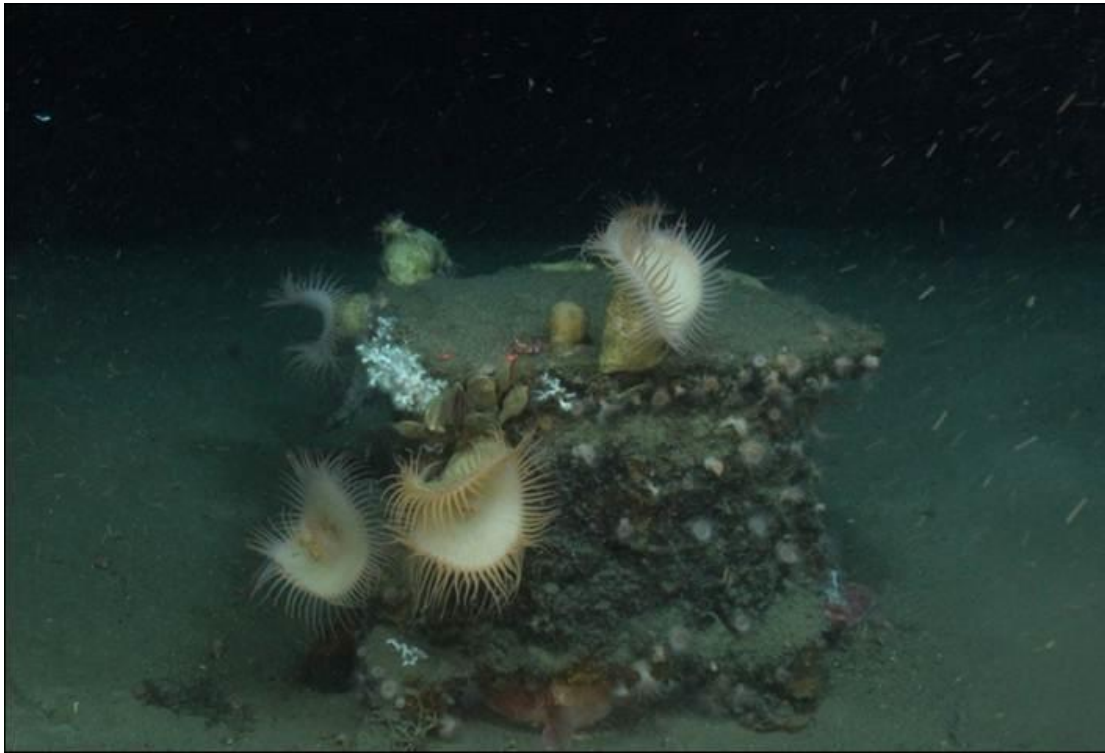
Figure 10-29.  Patent stove found away from main hull.
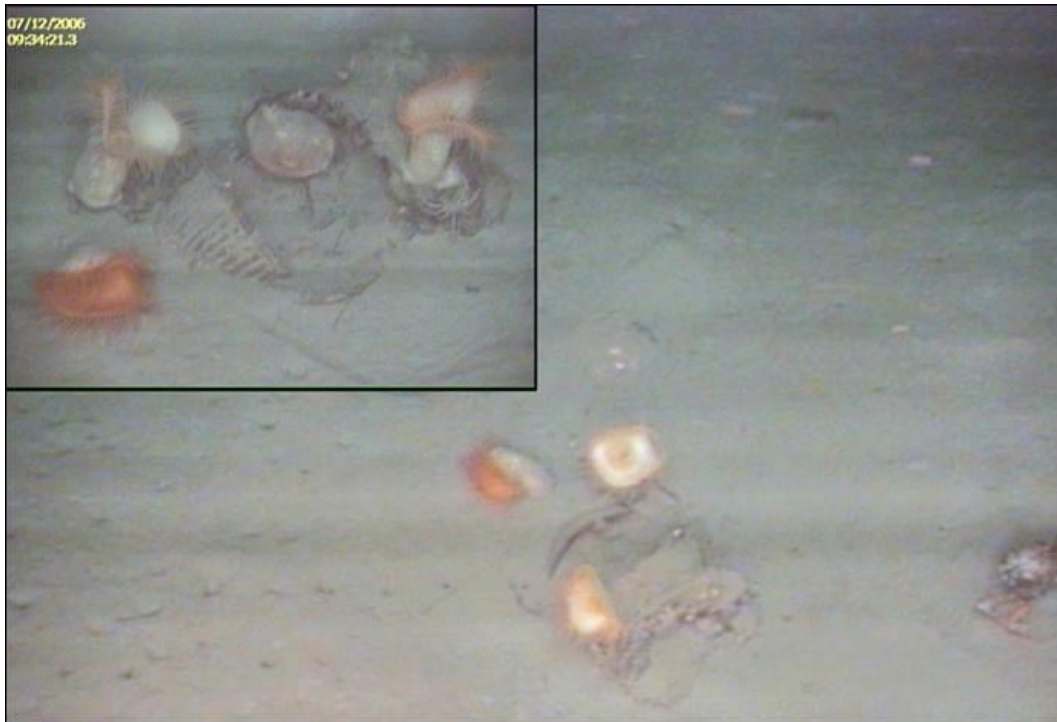


Figure 10-30.  Lantern away from main hull at VK Wreck site  (2006 image, MMS 2008-018).

Figure 10-31.  Unidentified object away from main hull at VK Wreck site  (2006 image, MMS 2008-018).

### 10.5.1.5    *Recovered Artifacts*

Two artifacts, a ceramic water filter and sample of metal sheathing, were recovered from the *Viosca Knoll* Wreck site during the 2009 investigation.  The artifacts were conserved at the University of West Florida (UWF) Archaeology Institute's conservation lab in Pensacola, Florida and the conservation report can be found in Appendix E-2

The water filter (Artifact: MMS09.15303.C.001) is salt glazed stoneware and only consists of the lower portion of the filter.  The upper portion of the filter was not found during the investigation. The filter was recovered from the aft starboard side of the shipwreck.  The recovered portion of the filter measures 21 cm in diameter and 15 cm in height.  It features a decorative fern leaf motif to each side of the spout opening at the bottom.  The words "Water Filter," "Corporation St.," and "Manchester" are written above the spout (Figure 10-32).  The spout was separated during recovery and rejoined in the conservation lab.

Figure 10-32.  VK Wreck's Water filter after conservation.

Such filters were common in the later nineteenth century because diseases like cholera and typhoid were linked to impure water supplies.  By 1863, Slack & Brownlow was manufacturing charcoal filters in Manchester England and by 1876 had competition from William M. Jowett & Co.  The filter recovered from the *Viosca Knoll* Wreck matches the style and design of portable filters manufactured by William M. Jowett & Co., located at 75 Corporation Street in Manchester between 1876 and 1884 (Figure 10-33).  They produced and sold compressed charcoal filters for ships and steamboats.  An 1876 advertisement lists the company as the successor to the Messrs. G. Busse and Co. and the "sole manufacture of their Improved Royal Patent Prize Medal Charcoal Block and Loose Charcoal Rapid Water Filters; manufacturers to the Admiralty…" (Slater's 1863-1884).  The water filter recovered from the *Viosca Knoll* Wreck is likely the lower quarter of a Jowett & Co. filter providing a possible *terminus post quem* of 1876 for the shipwreck.

Figure 10-33. An 1882 advertisement in Export Merchant Shippers showing a Jowett & Co. Water Filter.

The sample of metal sheathing (Artifact: MMS09.15303.M.002) was recovered from the seafloor near the damaged area on the aft port side of the wreck. It is a single strip of sheathing measuring 44.5 cm long and 11.5 cm wide (Figure 10-34). Field observation indicated the metal is copper or copper alloy. A portable X-Ray Fluorescence analyzer was used at the UWF conservation lab to identify the exact metal type. The results of the X-Ray Fluorescence analysis showed the metal is composed of 65.57% copper, 28.61% zinc, 2.68% lead, 1.95% iron, 1.09 tin, and 0.1% other

metals. The X-Ray Fluorescence results indicate a copper: zinc ratio of 1:44. A sample of the metal sheathing was also sent to DBI's lab in Saskatchewan, Canada and the full microbiology wreck report can be found in Appendix E-1. The sample was tested at the Saskatchewan Research Council laboratory using Inductively Coupled Plasma Atomic Emission Spectroscopy. The test indicated a copper: zinc ratio of 1:59. Although the test at UWF and DBI resulted in slightly different ratios, they both indicate the sample is likely Muntz Metal and is consistent with late nineteenth century sheathing.



Figure 10-34. Muntz Metal Sheathing from the Viosca Knoll Wreck.

### 10.5.1.6    Site Preservation

The VK Wreck site is currently in a moderate state of preservation. The hull is partially intact where it is sheathed. The sheathing's anti-biofouling properties likely offer some protection to the hull sections in direct contact with it. This is consistent with other GoM deep-water discoveries, where wooden hull remains are present in conjunction with copper sheathing and is largely absent above the line of sheathing. The bow is partly intact, but the stern is heavily damaged, most likely from post sinking and anthropogenic disturbance. The vessel is heeled over to starboard, leaving much of the deck area and port side exposed. Since the starboard side is mostly buried, an accurate assessment of its preservation state cannot be made, but it is likely that it has been protected by the seafloor sediments and remains relatively intact.

In an effort to monitor the wreck's preservation, a short-term etching microbial tester and long-term Wooden Wrecks  General Underwater Corrosion Coupon Instruments (WW-GUCCI) platform were deployed at the site to test microbial activity and monitor deterioration rates (Figure 10-35). The etching tester was not left in place long enough for a reaction to occur and to provide information on the level of microbial activity at the site. The WW-GUCCI platform, deployed near the stern of the wreck, is designed to provide a long-term indication of site deterioration rates from microbial and chemical deterioration. Reexamination of the test platform in the future will be invaluable in assessing long-term preservation of the *Viosca Knoll* Wreck site.
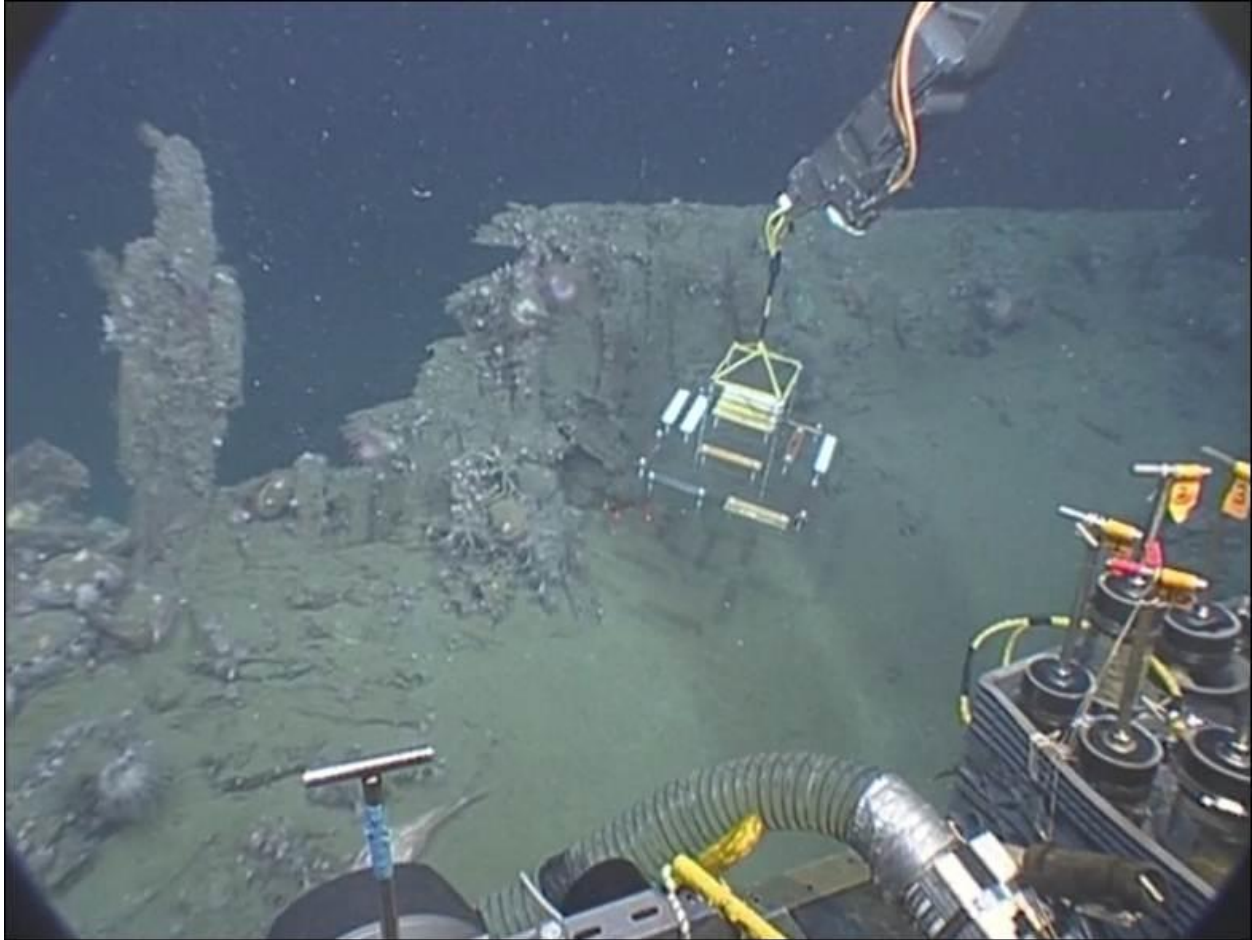
Figure 10-35.  WW-GUCCI Microbial Test Platform being deployed near the port stern.

## 10.5.2    7,000 Foot Wreck Site

### *10.5.2.1     Historical Background of the 7,000 Foot Wreck*

The 7,000 Foot Wreck is the remains of a sheathed wooden hull sailing vessel.  The wreck was discovered during an oil and gas exploration of the Mississippi Canyon Area in 1986.  The wreck is named for the major bathymetric contour nearby.  The original name and nationality of this vessel remain unknown.  Since its discovery in 1986, there have been two AUV surveys and one ROV investigation of this site.

### *10.5.2.2     Field Investigations*

#### 10.5.2.2.1    Discovery and Exploration

In 1986 a deep tow survey being undertaken as part of an oil and gas exploration program documented a possible target in the Mississippi Canyon area.  The target was described as an "elongated, apparently solid, oval sonar contact 27 m in length and 11 m in width" (Pearson, et. al).  In 2005, when the entire Mississippi Canyon area was designated an archaeological high-probability region, the wreck site was reported to the MMS Social Sciences Unit and was

determined to be a potential shipwreck site. A 2,000-foot radius archaeological avoidance zone was established around the wreck site by the MMS.

In 2006, Shell Exploration and Production Inc. (Shell) was exploring the deep waters of the Mississippi Canyon area for potential oil and gas exploration in the same region as the 1986 survey. Shell contacted C & C Technologies, Inc. to conduct a geophysical survey of the area using C&C's *C-Surveyor II*<sup>TM</sup> AUV system. Since the entire Mississippi Canyon area had been designated as an archaeological high-probability area in 2005, the survey included an archaeological assessment.

The planned survey covered the area of the potential shipwreck located on the 1986 deep tow data. Because of the presence of a previously discovered shipwreck in the area, a series of high-frequency (430 kHz) side-scan sonar investigation lines were planned as part of the overall survey. A review of the geophysical data by a C&C marine archaeologist confirmed that the target was a shipwreck site. The AUV side-scan data indicated the wreck site is 23 m long and 6 m wide, with 1 meter of seafloor relief (Warren, 2006).

The high-frequency geophysical data from the 2006 AUV survey indicated that the 7,000 Foot Wreck was likely a wooden sailing vessel (Figure 10-36). The intact nature of the wreck suggested it was copper sheathed. An area of lighter reflectivity noted in the geophysical data along the starboard side of the vessel was interpreted as resettled sediments that were disturbed during the wrecking process. No debris trails were noted extending out from the wreck. A linear feature extending off the bow area of the wreck was thought to be mast or rigging remains. The subbottom data indicates that as much as 1.8 m of the wreck could be buried beneath the seafloor.
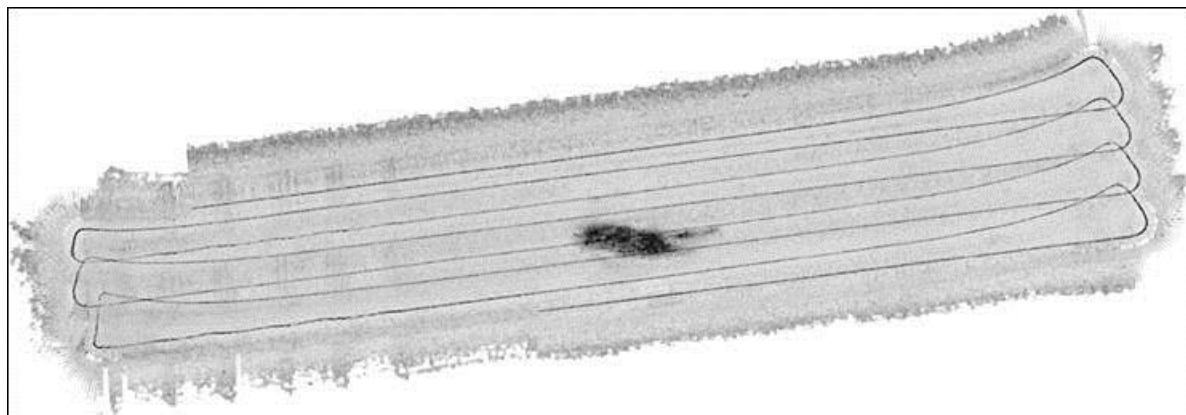


Figure 10-36.  Multibeam backscatter mosaic image of 7,000 Foot Wreck from data collected by the ABE *Sentry* AUV (Woods Hole Oceanographic Institution).


## 10.5.2.2.2    Woods Hole Oceanographic Institution 2009 AUV Survey

WHOI conducted an AUV survey of the site with the Autonomous Benthic Explorer (ABE) *Sentry* ROV system in July 2009. The *Sentry* AUV system incorporated a multibeam sonar system and camera for this survey. The *Sentry* survey collected approximately 21 images of the site, providing the first visual evidence that is was an historic shipwreck (Figure 10-37). These images were

compiled into the first digital site map of the wreck that was used to plan and undertake the 2009 ROV investigation of the site.
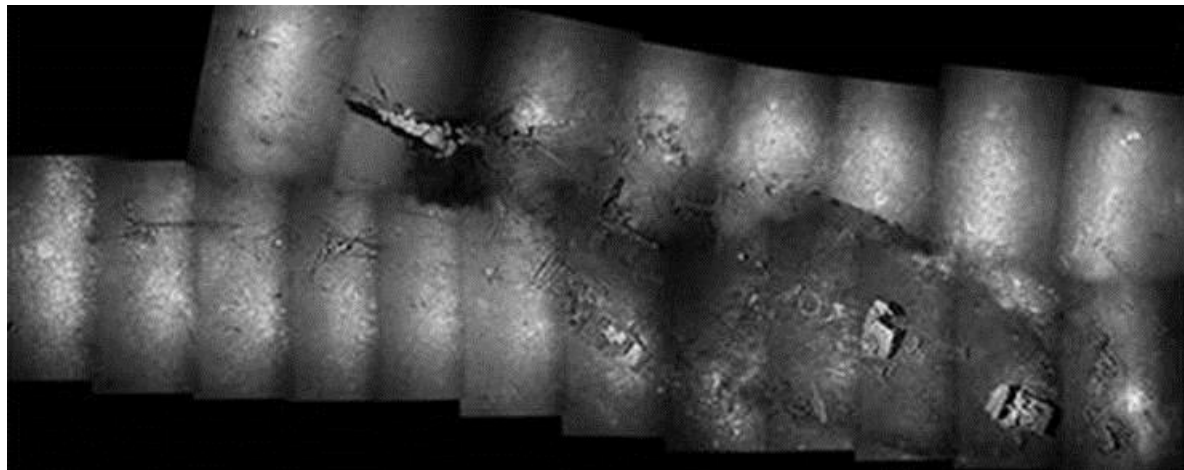


Figure 10-37.  Photomosaic of the 7,000 Foot Wreck comprised of images taken from the ABE *Sentry* AUV (Image Woods Hole Oceanographic Institution).

### 10.5.2.2.3  *Lophelia* II: Rigs, Reefs, and Wrecks 2009 Field Cruise

In September 2009, the first ROV investigation of the 7,000 Foot Wreck was conducted as part of the *Lophelia* II: Rigs, Reefs, and Wrecks Study.  Over a roughly 15.5-hour period during September 6 and 7, 2009, the *Lophelia* II team used WHOI's *Jason* II ROV launched from the NOAA Research Vessel *Ronald H. Brown* to document the shipwreck site.

The 2009 ROV exploration of the 7,000 Foot Wreck began with a standard reconnaissance survey around the wreck site.  The project team began the reconnaissance at the bow of the wreck, moved aft down the starboard side around the stern and up the port side before ending again at the bow. During the 2.5 hour reconnaissance dive, the project team documented aspects of the wreck site including construction details, rigging remnants, machinery, and artifact assemblages, as well as biota found on the wreck site.

After completing the initial reconnaissance survey, the team set up to mosaic the wreck site with the ROV cameras.  For the next 2 hours the ROV crew flew 12 lines over the wreck.  Each line was run approximately 1 meter apart at an altitude of 6 m above the seafloor.

Once the mosaic survey was completed, the project team began investigation of the wreck's biology.  For the next 3 hour,s the team gathered biological samples (including rusticles) collected push cores, and deployed both long-term and short-term microbiological experiments.

With the biological and core sampling finished, the *Lophelia* II team spent the next 6 hours doing detailed documentation.  During this phase of the dive, digital imagery and detailed still photographs were taken of key wreck features and artifacts noted during the reconnaissance survey.  Once the documentation was completed, the recovery of potentially diagnostic artifacts from the site was undertaken.  The recovery of the ship's compass, a section of copper sheathing and the short-term microbiological experiment took up the last 2 hours of the investigation.

### 10.5.2.3    Geographic Settings

The 7,000 foot wreck is located in the northern GoM in the eastern portion of the Mississippi Canyon area. It actually lies in 7,450-ft of water.  At the time, the discovery represented the deepest historic shipwreck ever found in the GoM.  The Mississippi Canyon is the outlet for sediment materials that transgress seaward into the Mississippi Fan.  The Mississippi Fan is a submarine fan in the deepwater region of the GOM.  Bouma and Coleman (1985) describe the canyon as a major erosional and partially filled structure.  Initial development of this canyon is suggested to have begun around 50,000 to 55,000 years ago in the middle continental slope and retrogressed onto the shelf by 25,000 to 27,000 years before present.  A pronounced eastward migration of the ancestral Mississippi River depocenter occurred depositing progradational sediments east of the present-day Mississippi River delta during the Middle Miocene period.  The seafloor in this region gently slopes toward the south with local variations (Lee and George, 2002).

### 10.5.2.4    Discussion of Archaeological Findings

#### 10.5.2.4.1    Physical Site

The following description of the 7,000 Foot Wreck site (Figure 10-38) is compiled from data collected during the 2009 WHOI *Sentry* AUV survey and the 2009 *Lophelia* II ROV investigation.

The 7,000 Foot Wreck represents the remains a copper-sheathed wooden sailing vessel.  The wreck is oriented with the bow pointing in a southerly direction and is lying upright on the bottom.  The overall site size is approximately 27 m × 6.4 m.  The hull remains of the 7,000 Foot Wreck are approximately 50 ft (15 m) × 15 ft (4.5 m) and is nearly flush with the seafloor, giving the vessel a 3:1 length-to-beam ratio

The 7,000 Foot Wreck site is composed of the main hull and associated remains (Figure 10-38 and Figure 10-39).  The stem post and head knee, windlass, steering wheel and gear housing and three anchors are the most prominent features on the site.  There are no identifiable debris trails or areas of isolated scattered debris associated with the wreck site.  The wreck site is confined to a fairly well-defined area with only a section of foremast rigging observed extending outside the immediate vicinity.
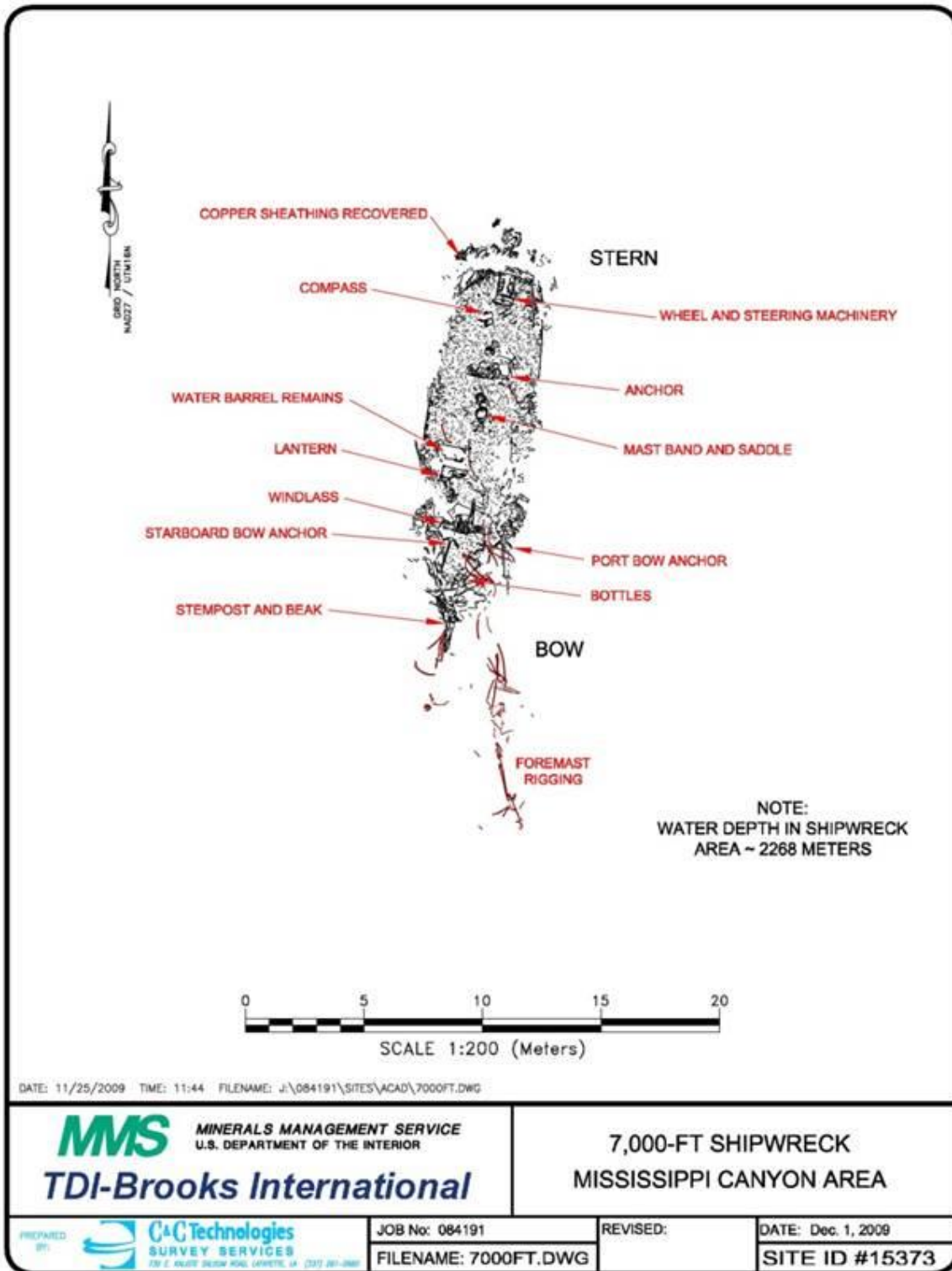
Figure 10-38. Site map of the 7,000 FT Wreck based on ROV investigations.

Figure 10-39.  Color photomosaic showing the 7,000 Foot Wreck site layout (Image Woods Hole Oceanographic Institution).

The head knee and stem post are relatively intact at the bow and are two of the most prominent features on the site.  Along the vessel's starboard side, various debris and artifacts were noted including wood and metal fragments, two bow anchors, and the vessel's upside down windlass. Proceeding aft near amidships, other components were encountered including part of the ship's water barrel, a galley stove, main mast remnants, decking, and another anchor.  Further towards the stern, the ship's compass was observed near a hatchway.  To the rear of the hatchway, the remains of the ship's patent steering stands proud of the seafloor and appears remarkably well-intact.

### 10.5.2.4.2    Bow and Hull

The 7,000 Foot Wreck has a sharp clipper-shaped bow and an elliptical stern or transom.  The bow is similar to the bow found on the *Lettie G. Howard*, a two-masted schooner built at Essex, Massachusetts in 1893 (Figure 10-40).  This type of vessel was commonly used by American offshore fishermen.  The elliptical stern design was popularized during the 1840s and remained a quite prevalent construction characteristic in sailing vessels even into the 1920s.

Figure 10-40.  American schooner Lettie G. Howard was built at Essex, Massachusetts in 1893 (Image from South Street Seaport Museum, New York).

### 10.5.2.4.3    Stem and Head Knee

The remains of the bow include the remnants of the head knee (Figure 10-41).  In older vessels this is often referred to as a beak.  The head knee is attached to the stem post and served to the support the bow sprit.  The stem post remains largely intact complete with two bobstay fittings and partially intact bobstay rigging.  The stem post has a molded dimension of approximately 12 in (30 cm) and a sided dimension of 8 in (20 cm).  It extends approximately 6 ft (1.8 m) above the seafloor.  The bobstay fittings are composed of iron and appear to be forged as single pieces. Bobstays were an integral part of the ship's head rig and were important because they applied downward pressure to counteract the force affected on the bowsprit by the jib sails.
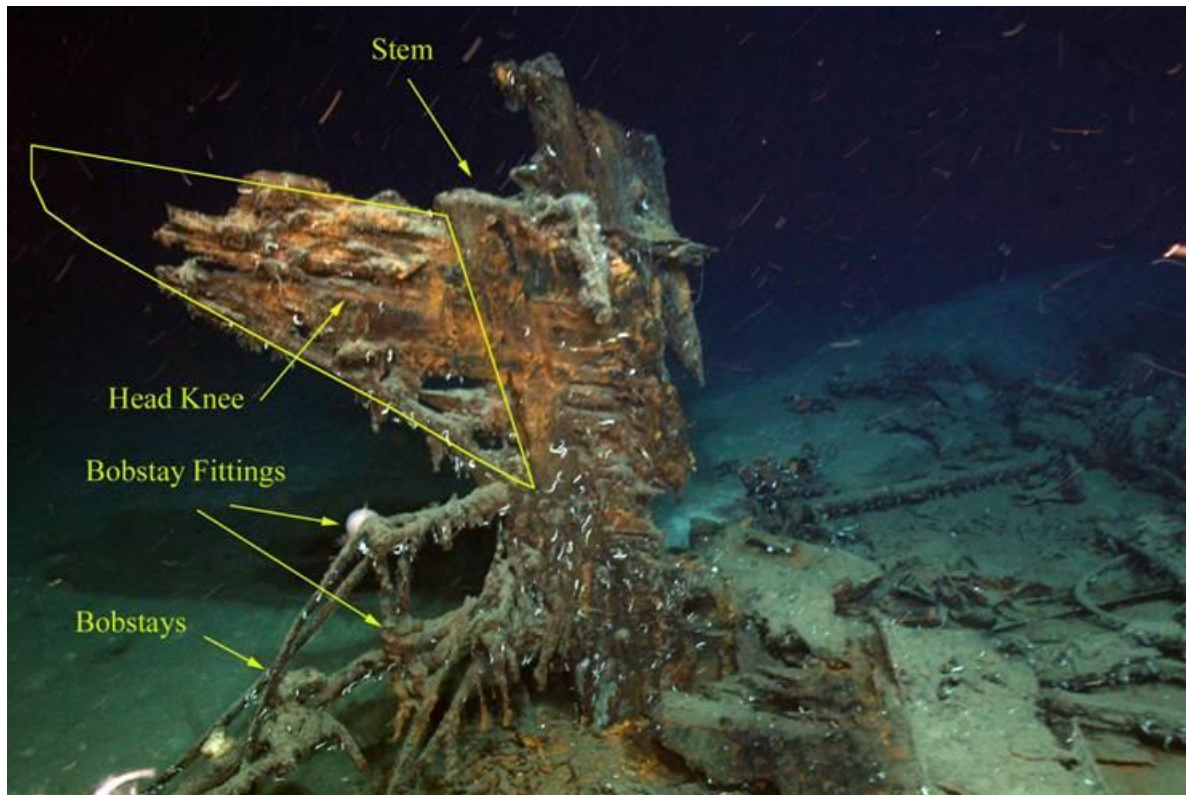
Figure 10-41. Stem post remains on the 7,000 Foot Wreck.

## 10.5.2.4.4 Windlass

An anchor windlass is a device that restrains and manipulates the anchor chain and/or rope, allowing the anchor to be raised and lowered. Typically speaking, the term "windlass" refers only to horizontal winches. Vertical designs are referred to as capstans. Smaller vessels in general and merchant vessels in particular utilized horizontal winches or windlasses. The windlass consisted primarily of a barrel. Either hexagonal or octagonal in section, which included the bar holes, and which was supported at the end in the carrick bit. The pump-break type windlass was a further development of the concept. A column was mounted ahead of the windlass supporting a cross head into which bar could be inserted. The up and down pumping action of the cross head was converted into rotary movement by means of connecting rods and gearwheels positioned on the spindle. The ratchet-type action would engage the vertical links forward of the Samson post, providing considerable leverage as the arms were pumped up and down to turn the windlass barrel. By the late 19th century many manually operated windlasses had been replaced by ones driven by small steam engines (Davis 1988; Mondfeld2005).

The windlass found on the 7,000 Foot Wreck was mounted crosswise on the foredeck of the vessel (Figure 10-42, Figure 10-43 and Figure 10-44). It measures nearly 7 ft (2.1 m) in length. The warping drum, warping head and side bits remain relatively intact. One of the wooden side bit knees remains intact but the other has deteriorated. The windlass has flipped upside down from its original position. This may have occurred during the wrecking event or possibly over time as the wooden deck deteriorated. Remnants of deck planking can still be seen at the base of the knee.

Figure 10-42. Image showing the over-turned windlass in bow of 7,000 Foot Wreck.



Figure 10-43. Overhead view of the over-turned windlass on 7,000 Foot
Wreck, bow is toward upper left corner of image.
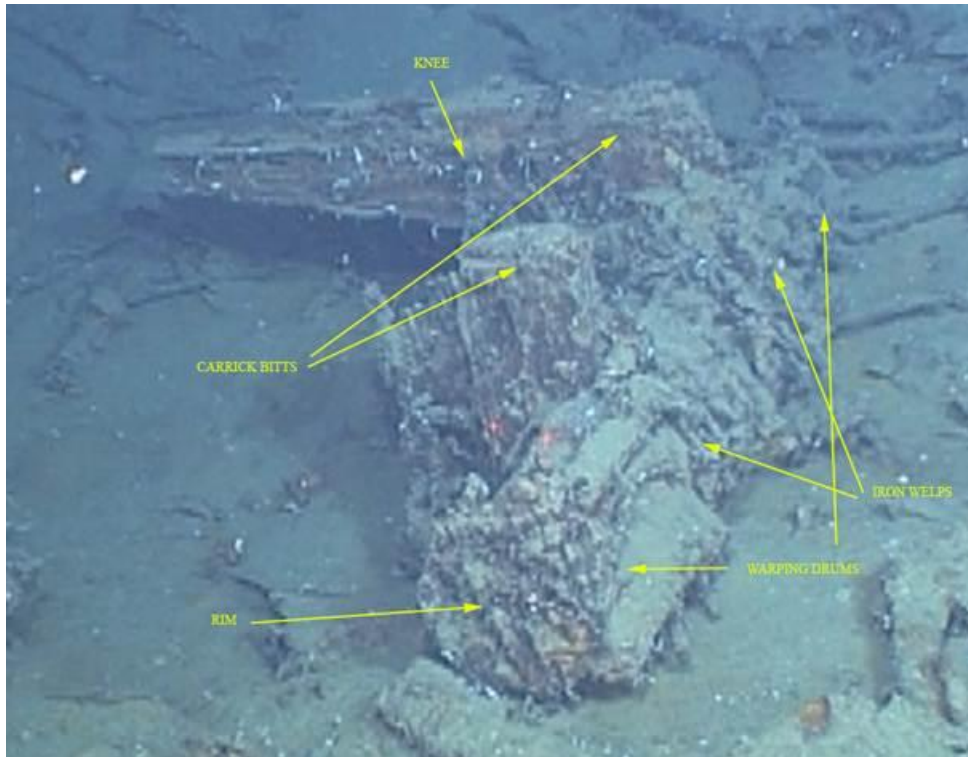
Figure 10-44. Windlass on 7,000 Foot Wreck with individual components identified.

### 10.5.2.4.5 Rigging and Mast Components

A substantial amount of rigging remains present on the 7,000 Foot Wreck site. The observed rigging appears to be comprised entirely of wire rope. It is difficult to differentiate between standing and running rigging on the site because of the orientation of the rigging as well as the accumulation of sediments. The remaining wire rope may denote the heavier standing rigging and it is possible the more lightly constructed running rigging, if made out of hemp, sisal or similarly perishable natural fiber, has not survived over time.

According to historical evidence, the development of a twisted (helical) rope formed from helical strands dates back to approximately 500 B.C. Examples of rope consisting of three strands twisted together; with each strand in turn, consisting of several bronze wires twisted together were unearthed during excavations at Pompeii (Worchester 1946).

There were relatively little technological advancements in the development of wire rope for the next 2,300 years. The invention of the steam plough in England around 1830 provided an increased demand for wire rope, but it was the Bessemer process that really provided a great technological leap forward. The Bessemer process was the first inexpensive process developed for the mass-production of steel from molten pig iron. Henry Bessemer patented the process in 1855. The process had a tremendous impact on both the quantity and quality of steel production (Bodsworth 1998).

394

The invention of the first usable modern wire rope is credited to Wilhelm Albert, a German mining engineer between 1831 and 1834. The invention was not complicated and consisted of three lengths of all the same size wrought-iron wire twisted around each other by hand to make a strand. Next, three or four identical strands were twisted around one another in similar manner to make the rope. The wire rope was employed as hoisting cables in the vertical shafts of the Harz Mountain silver mines in Germany from 1834 to 1854 (Sayenga 1998).

While the Germans were achieving success using wire rope in the mining operations, Andrew Smith, a London inventor, was experimenting with various methods of applying wire ropes to ship's rigging. Smith manufactured several kinds of wire rope for maritime applications, using the ropewalk techniques from the hemp cordage industry. Around the same time, another Englishman named Robert Newall devised a way to make wire ropes in a factory using machinery to replace the hand-twisted method (Sayenga 1998).

Wire rope is composed of three parts: wires, strands and a core. The basic unit is the wire and a predetermined number of wires of the proper size are fabricated in a uniform geometric arrangement called the "pitch" of "lay" to form a strand (Figure 10-45). The completed strands are identical in diameter. The required number of strands are then laid together symmetrically around a core to form the rope.

All of the wire rope observed on the 7,000 Foot Wreck displays a "Regular Lay" or "Right Lay" (also known as a "Right-Hand Helix.") or a "Lang Lay - Right Lay") configuration. That is, the strands in the wire rope are laid to form a helix about the core similar to the threads of a typical screw. The strands, when viewed lengthwise, are wound helically away from the observer in a clockwise direction. However, from viewing video alone, it is nearly impossible to differentiate which of these two types of methods were employed as it is difficult to discern if the individual wires within the strands are laid in opposite directions.
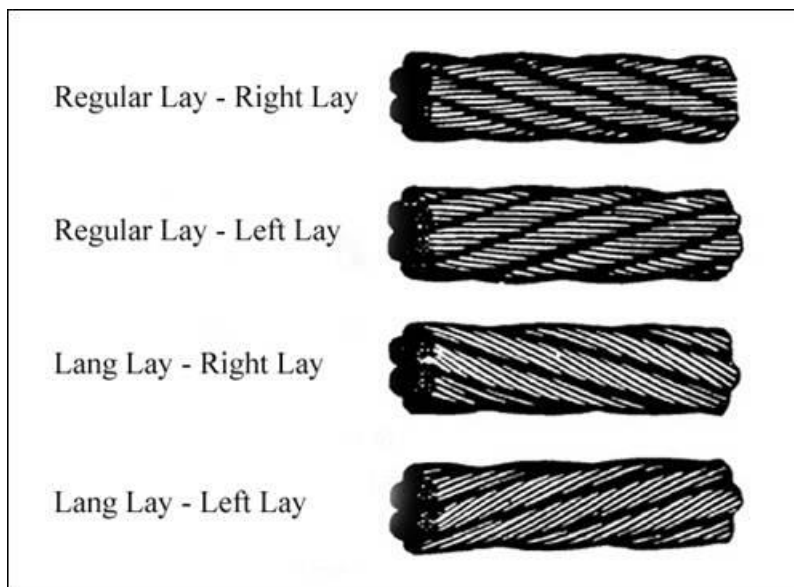


Figure 10-45. Wire Rope Lays (Wire Rope and Fiber Rigging
Navy Ships' Technical Manuel Chapter 613).

395

## 10.5.2.4.6    Foremast Rigging

Several sections of rigging are visible at the wreck site (Figure 10-46 and Figure 10-47).  One large section of rigging extends south away from the bow section.  This rigging begins in the area near the over-turned windlass and extends out from the bow approximately 13.4 m.  This rigging is likely from the foremast which would have been near the vicinity of the overturned windlass.  The wooden mast deteriorated, leaving the rigging to mark its location.



Figure 10-46.  Remnants of foremast rigging and mast cap from the 7,000 Foot Wreck.



Figure 10-47.  Close-up view of foremast rigging and possible mast cap from the 7,000 Foot Wreck.

396

## 10.5.2.4.7 Mainmast Rigging

The rigging from the mainmast and foremast appear to be along the same alignment lying forward and 15 degrees to port. The mainmast fell in a forward direction and apparently ended up either directly on top of or alongside the foremast. This could have occurred during the initial wrecking event, but more than likely the masts remained partially held in place by the rigging following the sinking. These components would have been under stress and as the structural elements lost their integrity and began to deteriorate and fail, the mast would have toppled forward. Other than where the rigging originates and terminates, it is difficult to ascertain which rigging is associated with each mast (Figure 10-48). The location of the rigging depicted in Figure 10-49 probably denotes rigging associated with the main mast. A ring, approximately 6 in (15 cm) in diameter lies nearby and probably represents some type of rigging hardware. Several mast caps are visible on the site as well as the yoke for the gaff jaw that would have supported to boom on the mainmast. The purpose of the cap was to provide support for the topmasts. Mast caps were made of wood and iron in the 19th century. The rectangular hole in the rear was mounted over the mast head cap tenon while the topmast heel fit into the round hole.



Figure 10-48. Miscellaneous rigging in the bow of the 7,000 Foot Wreck.

Figure 10-49.  Mainmast rigging and components on the 7,000 Foot Wreck.

## 10.5.2.4.8    Mast Band and Yoke

A mast band and yoke lies amidships approximately 21.53 ft from the stern and 31.9 ft from the bow (Figure 10-50). The mast band measures 1.5 ft (0.46 m) inside diameter.  The mast band or hoop attached to the fore edge of a boom sail, which slipped on the mast as the sail was raised or lowered.  The spars, boom, gaff, job, bowsprit, etc. had standard ratios and proportions.  Mast hoops were fitted around the masts to hold the component timbers, they were originally made of wood fixed in place with rope but by the end of the 19th century iron hoops had taken their place.
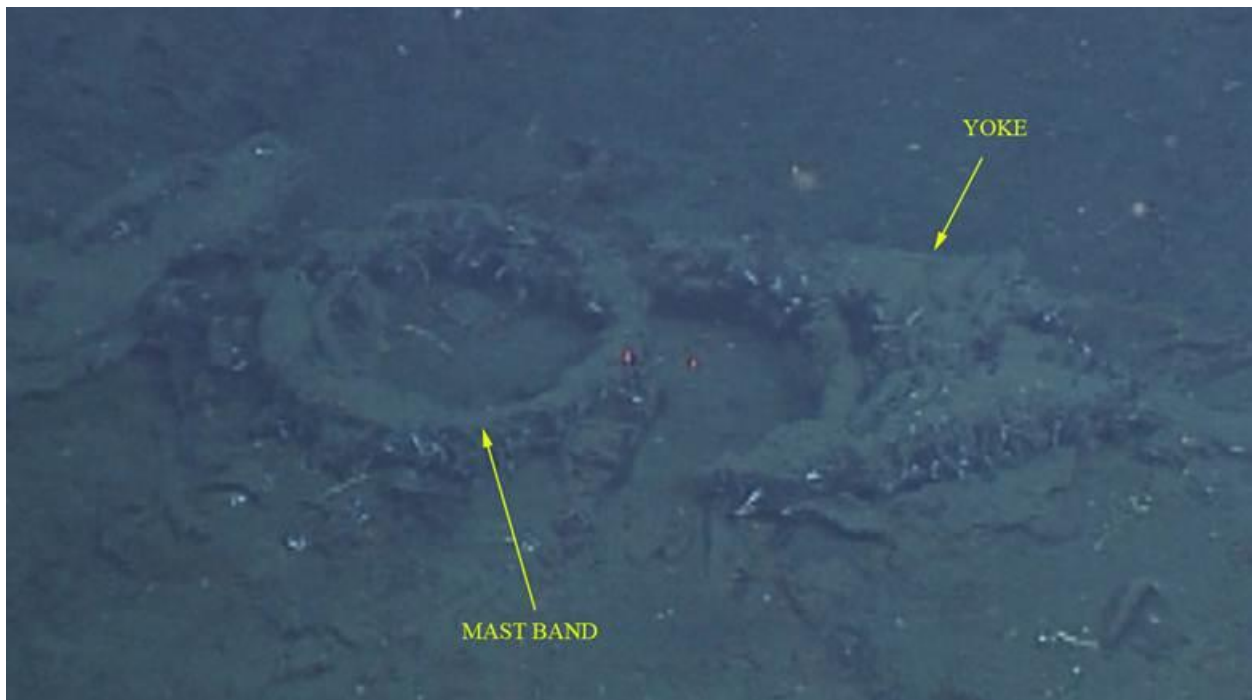


Figure 10-50.  Mast band and yoke in the interior of the 7,000 Foot Wreck.

## 10.5.2.4.9  Sheathing

The 7000 Foot Wreck's hull is constructed of wood that has been sheathed in copper or a copper alloy. A large section of sheathing was observed near the bow and appears largely intact. Twenty-two sheathing nails or tacks protrude up from the section (Figure 10-51 and Figure 10-52). The nails are approximately 1 inch (2.5 cm) long and are spaced approximately 3 in (7.6 cm) apart. The ROV attempted to recover what appeared loose sample of the sheathing, but this effort was abandoned when it became obvious the sheathing was still attached to the larger section. Another sheathing sample, however, was successfully recovered from another section of the wreck.
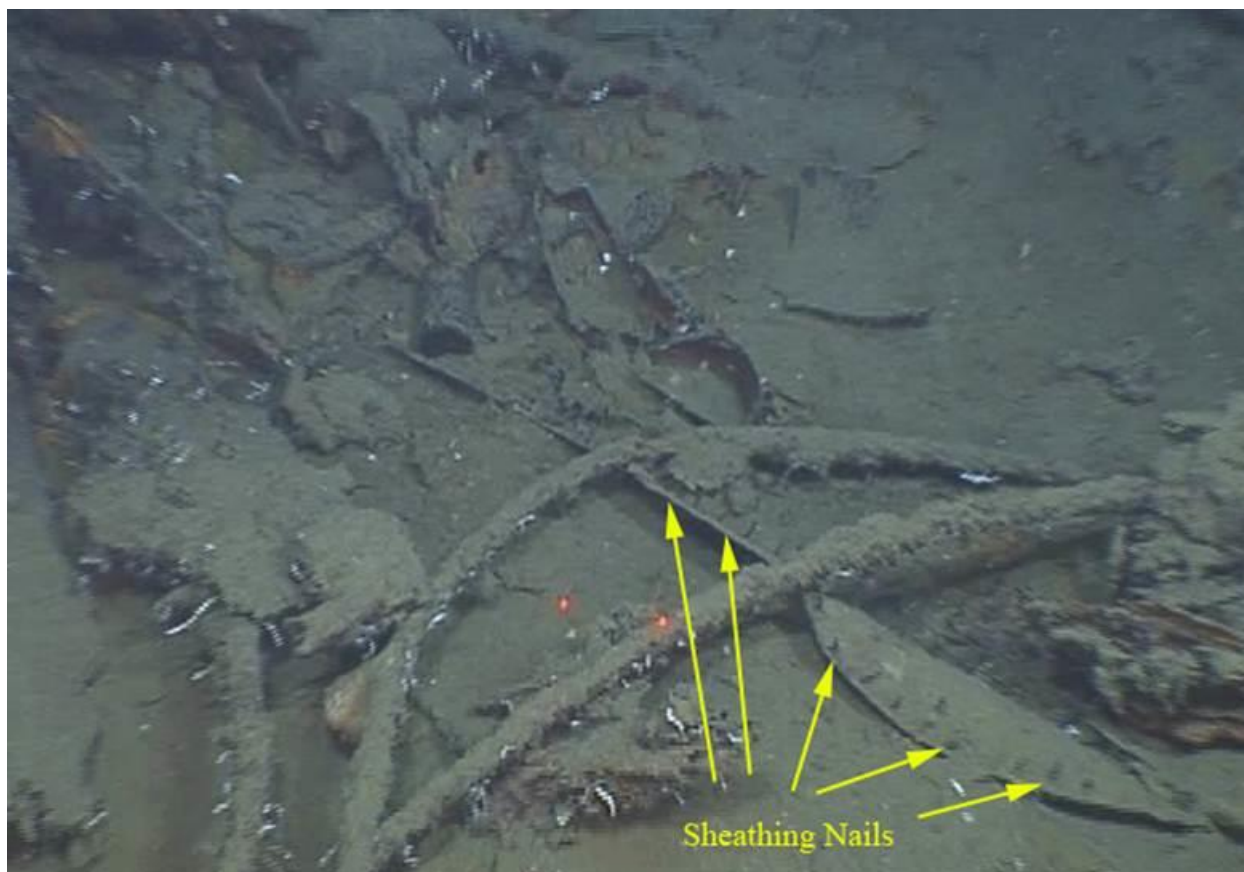


Figure 10-51. Copper sheathing with sheathing nails intact near bow of 7,000 Foot Wreck.

Figure 10-52. Close-up of a section of sheathing with sheathing nails intact in the 7,000 Foot Wreck.

### 10.5.2.4.10   Anchors

Three anchors have been identified on the 7,000 Foot Wreck. Two of these anchors are located on the bow (Figure 10-53 and Figure 10-54), the third is located amidships (Figure 10-55 and Figure 10-56). Their wooden stocks have long since deteriorated. The starboard anchor measures approximately 8 ft (2.4 m) in length, while to port anchor appears slightly smaller and measures about 6.5 ft (2 m) in length. The distance between the arms on the anchors measured approximately 2.67 and 2.40 ft (0.81 and 0.73 m), respectively. The slightly larger size of the starboard anchor is not an unusual characteristic because sailing vessels often carried anchors of various sizes and weight. An anchor, as with any piece of equipment, was utilized as long as it remained in working order. As anchors were lost or damaged, they would be replaced with what was available. It is also possible that the use of different sized anchors at the bow was intentional to give the crew a choice of anchors to deploy, depending on conditions. The various measurements that were able to be ascertained from studying ROV video for each anchor are listed in Table 10-2.

Figure 10-53. Anchor at starboard bow of 7,000 Foot Wreck.

As the 7,000 Foot Wreck deteriorated, the starboard anchor was deposited inside the hull and the port side anchor was deposited outside the hull. The flukes of both anchors are pointing towards the stern, suggesting they were still secured at their "ready" position on the bow at the time of the loss.



Figure 10-54. Anchor at port bow of 7,000 Foot Wreck.

A third auxiliary anchor lies amidships.  The iron from the anchor has defused into the surrounding wood and preserved a small section of decking it had once been contacting.  The rest of the deck has collapsed and deteriorated, leaving the anchor leaning at an upright angle on the bottom.  The third anchor would have been more than likely been used as a spare anchor in the event the vessel lost one of its primary anchors or could have been deployed during an emergency.   It was impossible to accurately determine the anchor's size from the overall data, due to its orientation and angle in which it is sitting (Figure 10-57).
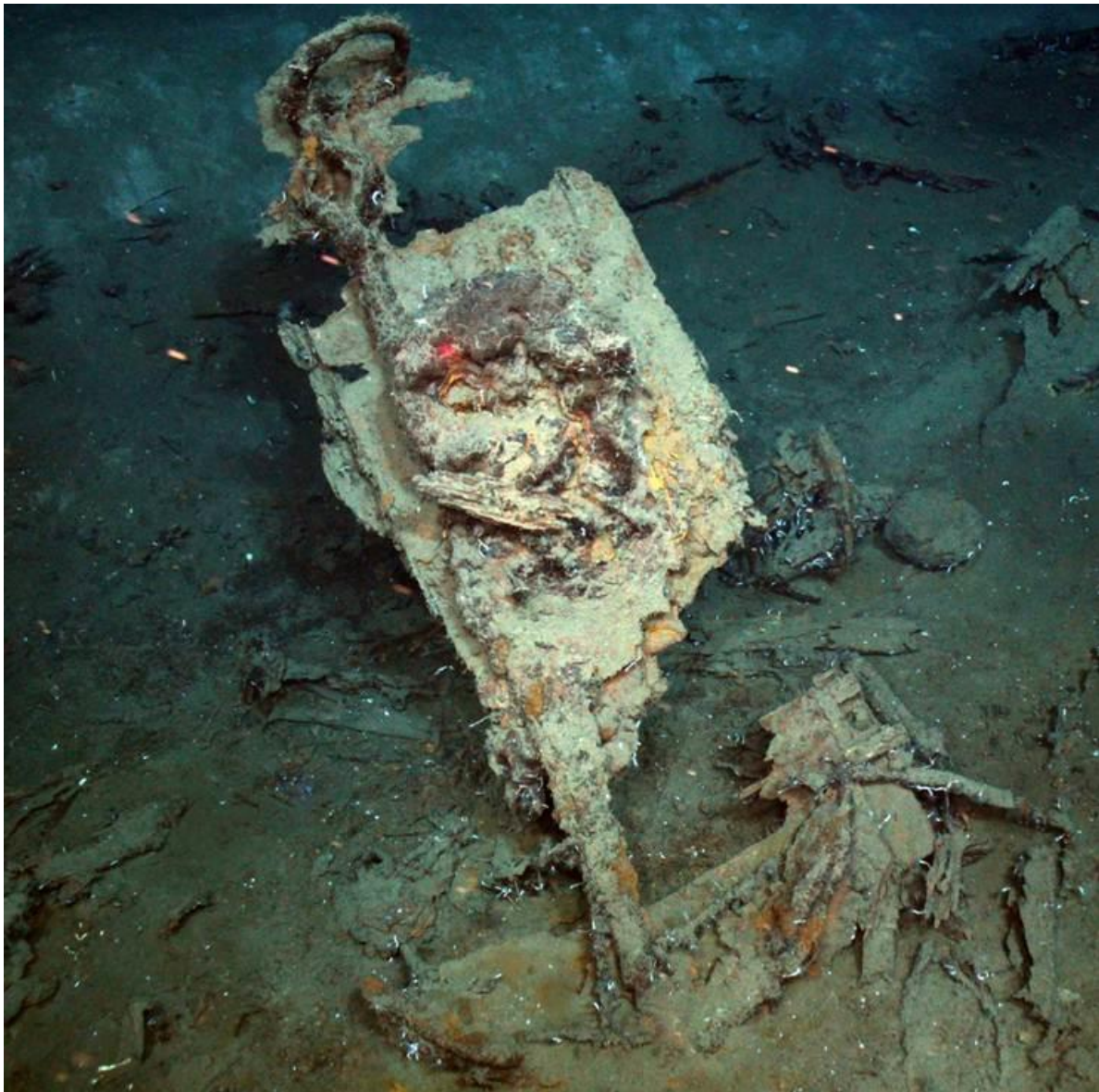


Figure 10-55.  Auxiliary anchor amidships on the 7,000 Foot Wreck (view to starboard).

Figure 10-56.  Auxiliary anchor amidships on the 7,000 Foot Wreck (view to starboard).
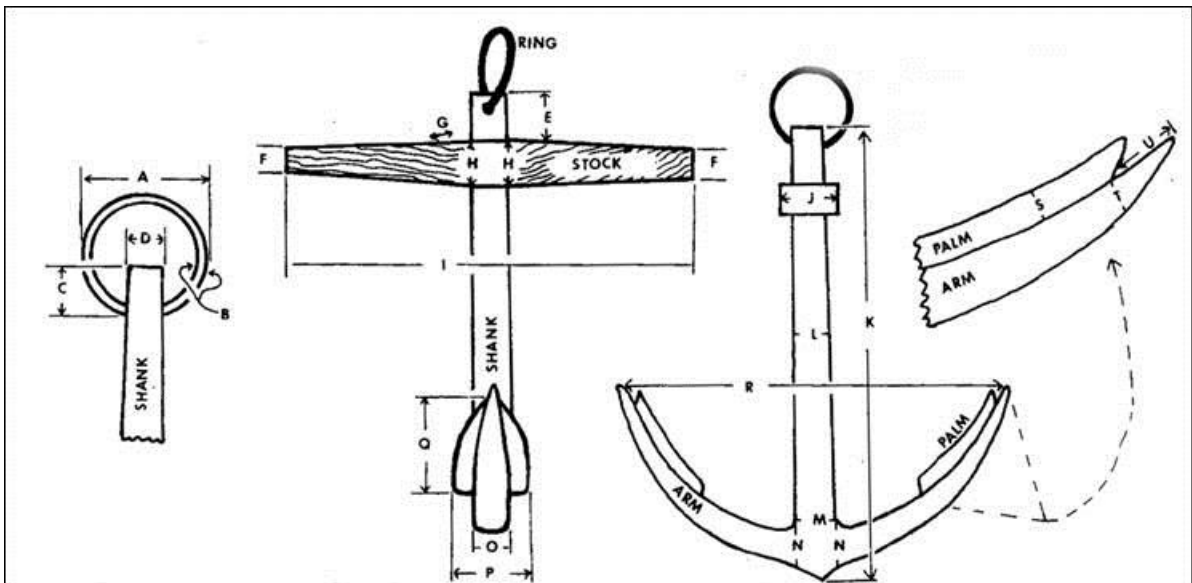


Figure 10-57.  Image showing standard measurement points for anchor documentation.

Table 10-2.

7,000 Foot Wreck Anchor Data Information

| Measurement Point (Fig 10-57) | Standard Measurement Point Description | Bow (Port) | Bow (Starboard) | Third Anchor |
|---|---|---|---|---|
| A | Ring diameter | .51' | N/A | .83' |
| B | Ring thickness | N/A | N/A | .125' |
| C | Top of shank to base ring | N/A | N/A | .135' |
| D | Top shank diameter | .19' | .25' | .25' |
| E | Distance from top stock to top of shank | N/A | N/A | |
| F | Stock width on each end – right | N/A | N/A | |
| F | Stock width on each end – left | N/A | N/A | |
| G | Stock thickness next to shaft | N/A | N/A | |
| H | Stock width each end of shank – right | N/A | N/A | |
| H | Stock width each end of shank – left | N/A | N/A | |
| I | Stock length | N/A | N/A | |
| J | Stock thickness at ends – right | N/A | N/A | |
| J | Stock thickness at ends – left | N/A | N/A | |
| K | Length of shaft | 6.54' | 8.00' | 5.83' |
| L | Mid-shank diameter | .18' | .26' | .30' |
| M | Basal shank diameter | .20' | .33' | .33' |
| N | Arm diameter – right | .34' | .40' | .36' |
| N | Arm diameter – left | .33' | .39' | .36' |
| O | Thickness of arm | N/A | N/A | |
| P | Width of palms – right | N/A | N/A | |
| P | Width of palms – left | N/A | N/A | |
| Q | Length of palms – right | N/A | N/A | |
| Q | Length of palms - left | N/A | N/A | |
| R | Distance between arm tips | 2.40' | 2.67' | 2.50' |
| S | Palm thickness – right | N/A | N/A | .160' |
| S | Palm thickness – left | N/A | N/A | .160' |
| T | Arm thickness at end of palm – right | N/A | N/A | .167' |
| T | Arm thickness at end of palm – left | N/A | N/A | .167' |
| U | Distance from end of palm to arm – right | N/A | N/A | |
| U | Distance from end of palm to arm – left | N/A | N/A | |

## 10.5.2.4.11 Wheel and Steering Machinery

One of the most impressive components of the 7,000 Foot Wreck is the ship's wheel and steering machinery (Figure 10-58). The amazingly intact feature is located at the stern of the vessel. The wheel appears to be iron. The wooden handles have mostly deteriorated, except for a partial remnant of one handle. At least one quarter of late 19th century sailing vessels were fitted with steering mechanisms that included patented double worm steering gears (Gordon P. Watts. Jr., personal communication), however, in the case of the 7,000-Foot Wreck, it is nearly impossible to match this machinery with a patented model from just a visual inspection. Even if the steering machinery found on the 7,000-Foot Wreck featured a patented worm steering gear, it would be difficult to determine whether it was fitted with this equipment initially, or it was adapted at a later point in the vessel's career.
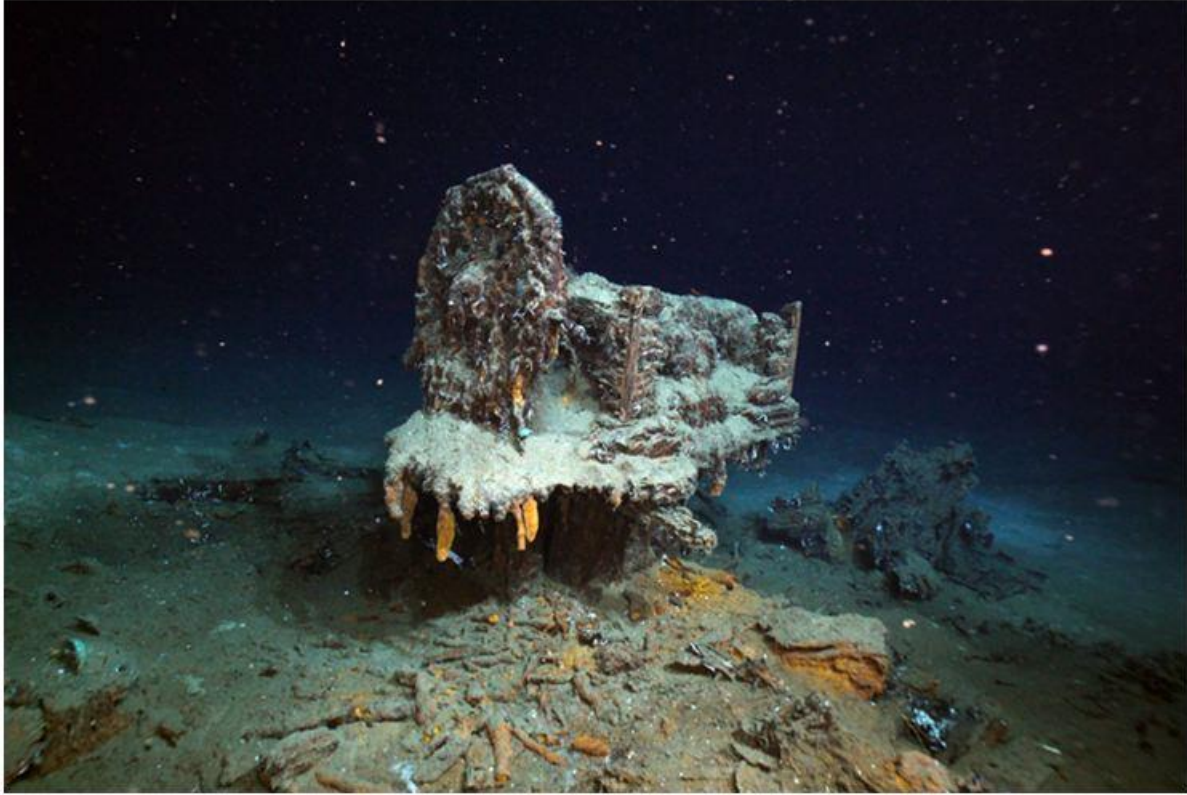
Figure 10-58.  The 7,000 Foot Wreck's helm, showing the wheel, exposed wheel-box, and
rudder case.

The steering gear housing encountered on the 7,000 Foot Wreck is much more reminiscent of American-built vessels of the late 19th century.  Figure 10-59 and Figure 10-60 depict the differences between typical European steering gear housings and American steering gear housings from the same time period.  The steering gear housing is also known as a wheel-box.  The gear housing box measures approximately 4 ft (1.2 m) long $\times$ 2.8 ft (0.85 m) wide $\times$ 2 ft (0.60 m) high based upon all the available data.  The wheel itself measures approximately 2.65 ft (0.80 m) in diameter (Figure 10-61).  The entire structure stands about 4 ft (1.21 m) off the bottom.  Based on Chapelle (1973), the design and angle at which the wheel shaft on the 7,000 Foot Wreck goes into the box suggests it is a style of wheel-box that was very common on vessels built between 1860 and 1885.
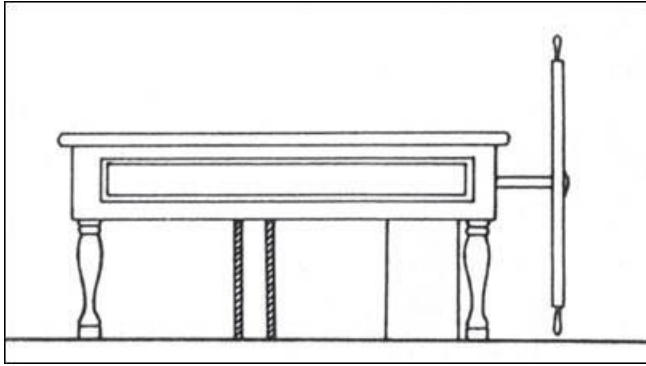
Figure 10-59.  Steering gear housing European type,
late 19th century (Mondfeld).
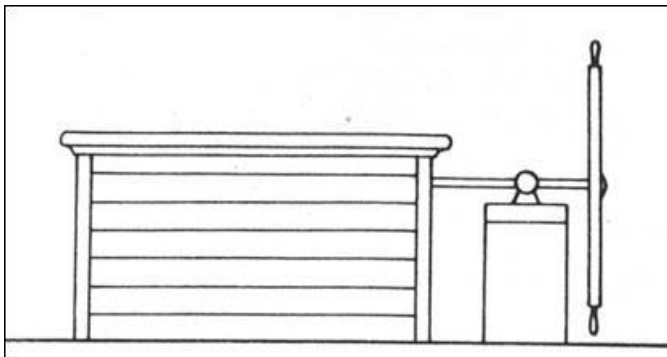


Figure 10-60.  Steering gear housing American type,
late 19th century (Mondfeld).
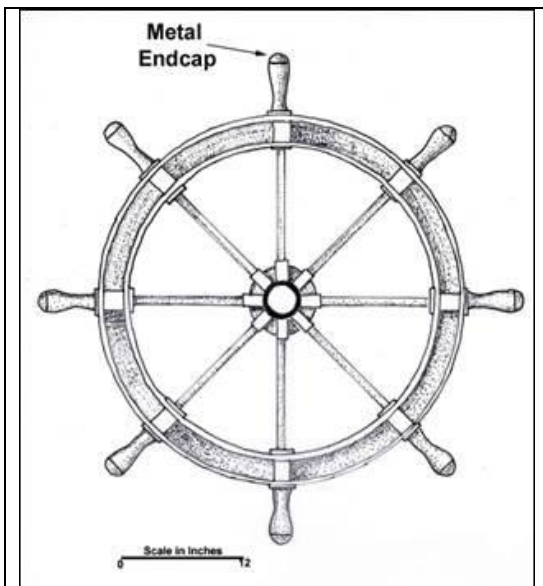


Figure 10-61.  Ship's wheel similar to that on
the 7,000 Foot Wreck (Drawing by
Daniel Warren, Image modified from
Chapelle, Fishing Schooners).

### 10.5.2.5    *Artifacts*

10.5.2.5.1    Stove

An object tentatively identified as the ship's stove was observed on the starboard side amidships approximately 27.50 ft aft of the stem post (Figure 10-62). The stove measures approximately 4.54 (1.4 m) × 1.86 (0.57 m) ft. The ship's stove aboard late 19$^{th}$ and early 20$^{th}$ century vessels was an important feature. It provided dual functionality, as it provided a both a heat source for cooking and warmth to the crew during times of cold weather.
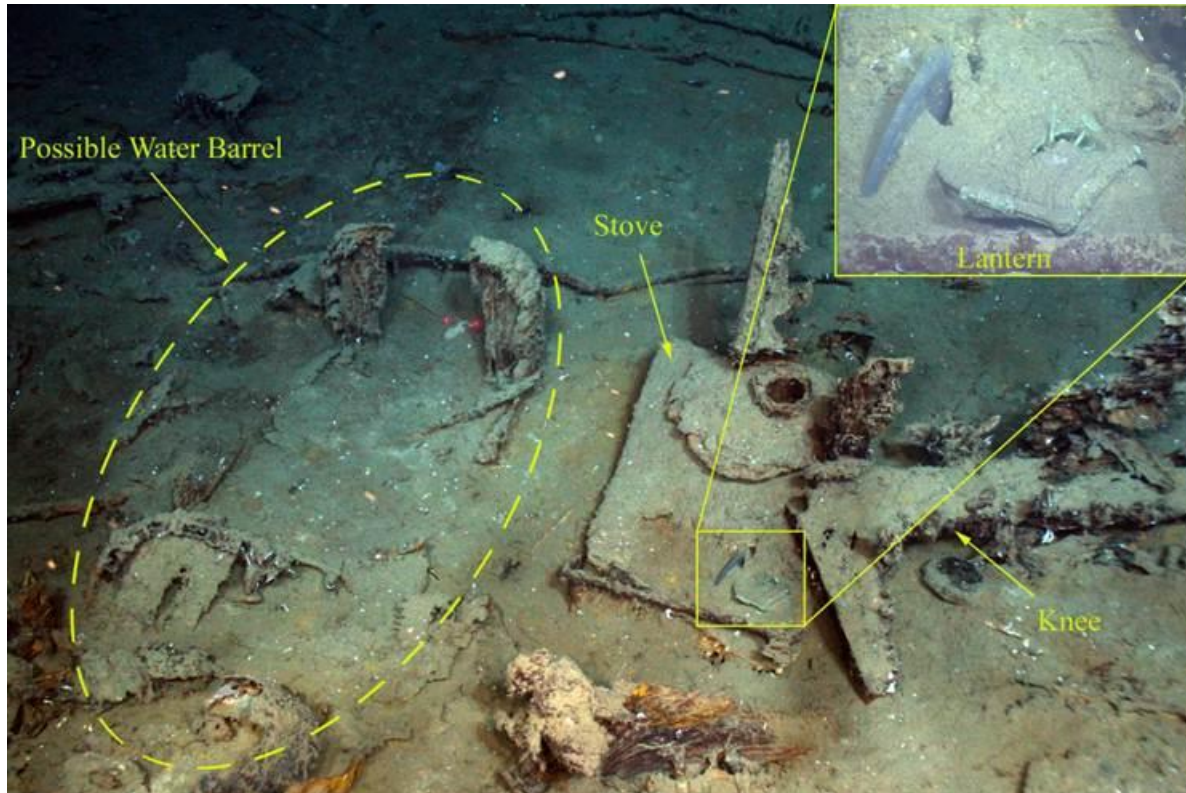


Figure 10-62. Image from the 7,000 Foot Wreck showing a possible galley stove (center) and a possible water barrels (center left and bottom left).

10.5.2.5.2    Water Barrel

The deteriorated remains of what may represent a wooden water barrel was noted just aft of the stove (Figure 10-62). Two edges of the barrel are protruding upright from one end, while the opposite edges have collapsed inward. The fact that various items identified as a stove, lantern and possible water barrel lie in close approximation to one another suggest this area may have contained the ship's galley.

### 10.5.2.5.3    Bottles and Containers

At least one possibly intact bottle was observed near the bow section. One intact jug, possibly a demijohn was also visible (Figure 10-63). Other bottle fragments were observed clustered in the same area but the exact number could not be ascertained since most of the fragments were partially buried or obscured by silt and debris. The bottle is manufactured of dark, possibly green, glass. The jug appears to possibly be brown slipped stoneware, but it is difficult to determine based on the video data. The presence and number of the containers indicate they are associated with daily shipboard activities rather than cargo. Their location in association with other artifacts, such as the nearby stove suggests this portion of the wreck contained a crew area, most likely the galley.
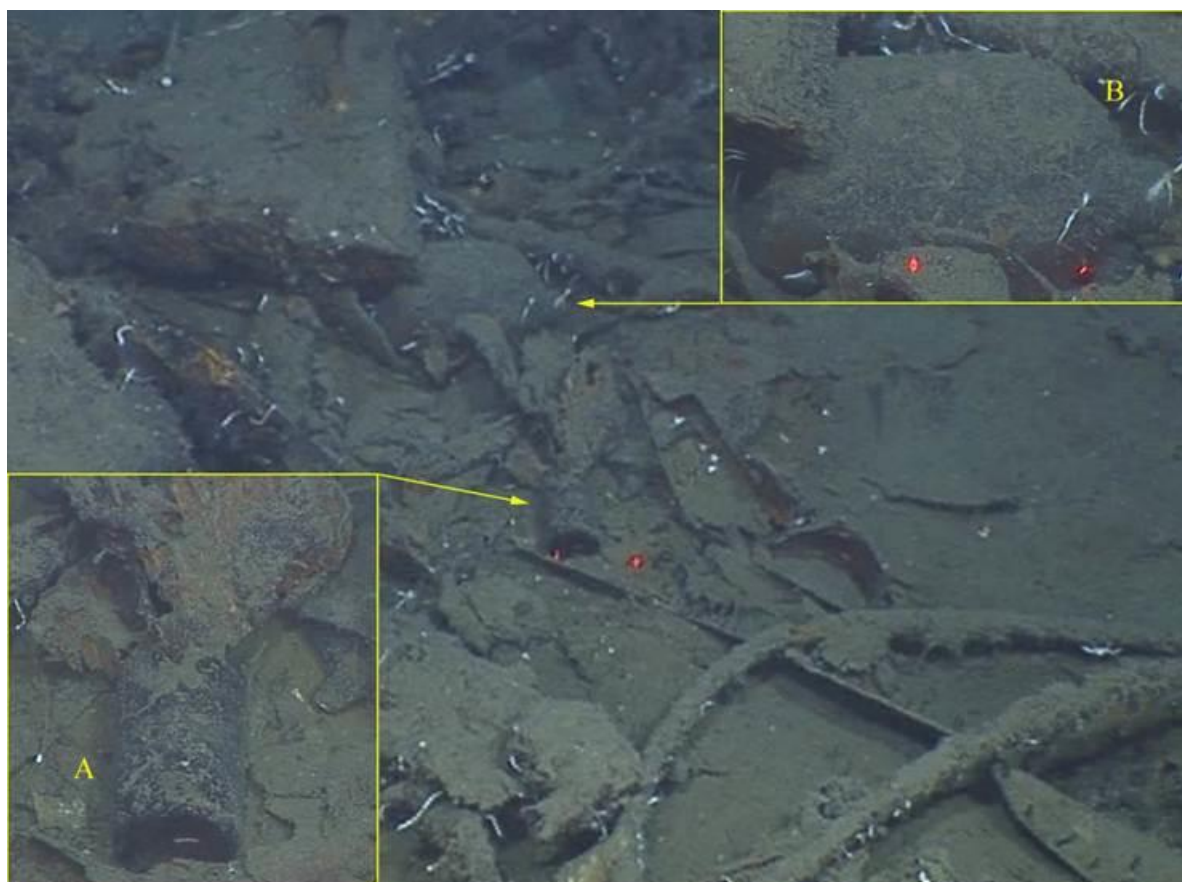


Figure 10-63. A bottle (A) and Jug (B) in the forward area of the 7,000 Foot Wreck.

### 10.5.2.5.4    Hanging Knee:

A hanging knee possibly from the deck above has fallen onto the stove (Figure 10-64). The knee measures approximately 3.92 (1.19 m) × 1.90 (0.58 m) ft. This tentative identification is based on the size and shape of the object. Hanging knees were a vertical angular timber shaped into a right angle. They were used to reinforce and support the ends of the deck beams where they came into contact with the sides of a vessel (Steffy 1994).

10.5.2.5.5    Lantern

The deteriorated remains of what appears to be a lantern are located on the stove (Figure 10-64). The round base measures approximately 6 in (15 cm) in diameter and is made of a grayish, apparently non-corrosive metal. Part of the frame and two possibly brass adjustment screws were observed protruding from the sediment. Since no glass was observed, it is either missing or dislodged and buried.



Figure 10-64.  Image of a lantern resting on top of the ship's stove in the forward area of the 7,000 Foot Wreck.


### 10.5.2.6    Recovered Artifacts

Three artifacts, the ship's compass, a sample of metal sheathing, and a wood sample were recovered from the 7,000 Foot Wreck site during the 2009 investigation. The artifacts were conserved at the UWF Archaeology Institute's conservation lab in Pensacola, Florida and the conservation report can be found in Appendix E-2.

One of the most potentially diagnostic artifacts selected for recovery was a ship's compass (Artifact MMS09.15373.CO.001.) *Jason II* successfully retrieved the compass at 9:12 on September 7, 2009 (Figure 10-65). The compass was located in an area just forward of the wheel box, which is consistent with historical data for ships of the period. Originally, compasses such as

this would have been mounted in a box, on a pedestal, or housed in a binnacle in the vessel's bridge or steering cockpit.
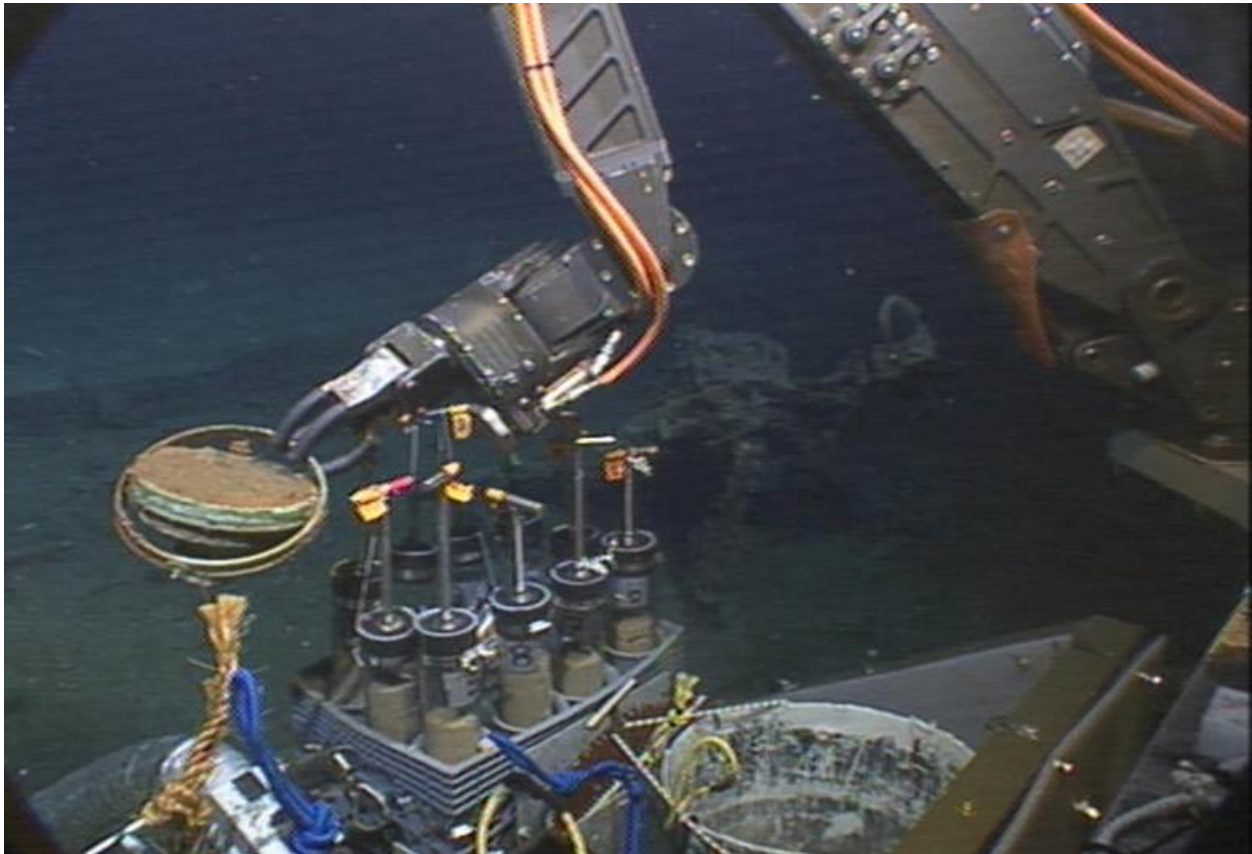


Figure 10-65.  The 7,000 Foot Wreck's compass being recovered during the 2009 site investigation.

The compass is circular, with an outer ring attached at two opposite points, a glass cover on the face, and a hollow center filled with liquid and the compass card.  The outer circle of the compass rotates around the main body of the compass itself, and has two prongs that stick out from opposite sides. The compass is marked "D.Baker & Company – Boston" (Figure 10-66).  The floating wet compass card has a patent date "PAT'D NOV 3, 1874-JUNE 1, 1875.  The card is divided into eight Cardinal Points, each of 45 degrees, and then into 1/8 and 1/16th points.  Each subtends an arc of 11¼ degrees comprising in total 360 degrees of the compass.

Figure 10-66.  The 7,000 Foot Wreck's compass following
        conservation.

According to historical research and interviews with a descendant, David Baker was born on November 7, 1817 in Harwich, Massachusetts on Cape Cod and was a seaman and then a ship's captain for many years until he retired from that and started his company making compasses. He moved off the Cape to Boston.  The 1860 census has his residence still in Harwich. The 1860, 1870, and 1880 census has his residence in Boston.  The 1890 census has his residence in Melrose, Massachusetts.  David died August 26, 1895 and his sons George and Howard Bakertook over the company and ran it for some unknown amount of years.  According to Paul Baker, the company may have been bought out by Star Compass around 1915, but he has been unable to locate any historical documents to confirm that information (Personal correspondence, 2012 and 2013).

David Baker held many U.S.patents in his compass design, one of which was the use of oil instead of the standard alcohol and water mix in use at that time. His patent for using oil was actually very revolutionary and that type of oil is still used in modern compasses today.  Some of David Baker's patents are shown in Table 10-3.

Table 10-3.

Patents awarded to David Baker

| U.S. Patent # | Description | Date |
|---|---|---|
| 7,837 | Design for Compass Card | November 3, 1874 |
| 163,838 | Improvement in Mariner's Compass | June 1, 1875 |
| 568,227 | Mariner's Compass | September 22, 1896 |

The compass recovered from the 7,000 Foot Wreck has a serial #3883 stamped on both the compass and gimbal ring (Figure 10-67). The compass comes from a period when makers were experimenting with different innovations for flotation compasses. The Baker compass was a popular instrument from its first appearance on ships in the 1870's and 1880's.

According to Howard Maglathlin of Viking Instruments, Inc. located in Kingston, Massachusetts, the Baker Company was actually located in Melrose, Massachusetts, just north of Boston. Later David Baker worked with a partner, Thomas Hooper at 54 Ann Street in Boston. It appears the earlier examples were marked "BOSTON" while the ones bearing the later 5-digit serial numbers were marked MELROSE MASS. This indicates that the compass found on the 7,000-Foot Wreck is an earlier production model Baker compass (Maglathlin, personal communication).



Figure 10-67. Serial numbers located on the outer edge of the 7,000 Foot Wreck's compass.

The compass provides a *"terminus post quem"* of 1875 for the 7,000 Foot Wreck, but is not an indicator of a loss date. According to marine archaeologist Gordon Watts, "a compass that works is a working compass" and as such it would have been a prized possession of mariners from any era and utilized as long as it was in good working order (Watts, personal communication). So it is not inconceivable that the compass could be much older than the vessel represented by the 7,000 Foot Wreck.

The sample of metal sheathing (Artifact: MMS09.15373.M.002) consists of three small sections of sheathing attached to wood with tacks (Figure 10-68). The wood is flat on the external side, yet the opposite side is riddled with damage from marine organisms. Many *Teredo navalis* tubes were pulled from the artifacts before conservation. The wood is colored green and black, presumably stains from the oxidation that occurred to the cuprous sheathing during its time underwater. The wood is soft and spongy, and flakes at the slightest touch. A series of cuprous metal tacks line the corners of the sheathing.



Figure 10-68. Cuprous metal sheathing and wood recovered from the 7,000 Foot Wreck.

Table 10-4.

Dimensions of Copper Sheathing from the 7,000 Foot Wreck

|  | Piece 1 | Piece 2 | Piece 3 |
|---|---|---|---|
| Length | 29cm | 22cm | 18.5cm |
| Width | 18cm | 9.5cm | 7cm |
| Thickness | 3cm | 3cm | 3cm |
| Weight | 203.5g | 182.6g | 112.7g |

Subsequent conservation revealed the wood itself was a light brown under the metal, indicating that it had been well protected by the sheathing; while the rest of its exposed surface was a dark brownish green color. Dr. Amy Mitchell-Cook, an underwater archaeologist and history professor at UWF who specializes in wood identification examined the sample and determined that the wooden planks beneath the sheathing were either white or red oak, due to the strong, single rays running out from the center/ heart of the wood.

This artifact was originally intended as a wood sample thought to contain copper sheathing at the time of recovery (Figure 10-69). Subsequent conservation revealed the sample contained no sheathing. The object consisted of eight small fragments of wood and calcareous marine growth.



Figure 10-69. Wood Sample from 7,000 Foot Wreck.

### 10.5.2.7 Site Preservation

The wreck site is currently in a moderate state of preservation. The hull is partially intact where it is sheathed. The sheathing's anti-biofouling properties likely offer some protection to the hull sections in direct contact with it. This is consistent with other GoM deep-water discoveries, where wooden hull remains are present in conjunction with copper sheathing and largely absent above the line of sheathing. The stem post and head knee remains partially intact. The ship's wheel and steering gear housing are also remarkably intact. Since the wreck is mostly buried, an accurate assessment of its preservation state cannot be made, but it is likely that it has been protected by the seafloor sediments and remains relatively intact.

In an effort to monitor the wreck's preservation and rate of deterioration, a short-term etching microbial tester and long-term WW-GUCCI platform were deployed at the 7,000 Foot Wreck site to study microbial activity and monitor deterioration rates. The etching tester was not left in place long enough for a reaction to occur and provide information on the level of microbial activity at the site. The WW-GUCCI platform, deployed near the ship's steering gear housing, is designed to provide a long-term indication of site deterioration rates from microbial and chemical deterioration. Reexamination of the test platform in the future will be invaluable in assessing long-term preservation of the 7,000 Foot Wreck site.

## 10.5.3 *Ewing Bank* Wreck Site

### 10.5.3.1 Historical Background of the Ewing Bank Wreck

The *Ewing Bank* Wreck is the remains of a wooden sailing vessel that may date from the latter half of the 19th century. Discovered in 2006 during an oil and gas exploration survey, the wreck was named for the lease block area where it was found. Archival research undertaken since 2006 has failed to identify the name or nationality to this shipwreck. Since its discovery in 2006 there have been two AUV and two ROV investigations of this site.

### 10.5.3.2 Field Investigations

#### 10.5.3.2.1 Discovery and Exploration

In 2006, Remington Oil and Gas Corporation wasconducting explorations of the deep waters of the Ewing Bank region in the GoM for potential oil and gas development. Remington contacted C&C Technologies, Inc. (C&C) to conduct a geophysical survey of the area using C&C's *C-Surveyor II* AUV system. Since the Ewing Bank Lease Area had recently been designated an archaeological high-probability zone, the survey included an archaeological assessment.

During the assessment of the geophysical survey data, a C&C marine geologist identified a target that looked ship-like in shape (Figure 10-70). Side scan sonar data showed an ovoid area of moderate reflectivity enclosing an area of high reflectivity. Measurements taken from the sonar and multibeam data indicated the target was approximately 45 m long, 12 m wide, with 2.5 m of relief.

The target was brought to the attention of C&C marine archaeologists who confirmed it was a likely shipwreck site. A check of available shipwreck databases found that no wreck had been previously noted in the area. Since this was a new discovery, the then MMS Social Sciences Unit was notified as stipulated under Notice-to-Lessees (NTL) 2005-G07. The MMS concurred that it was likely a shipwreck site and established a 1,000-foot radius avoidance zone around the wreck area.

In November 2006, a following survey for ATP Oil and Gas, Inc. (which had recently purchased Remingtion Oil and Gas) was conducted on several anchor placement locations in the Ewing Bank area. As part of this survey, a series of lines were also flown over the *Ewing Bank* Wreck site using the *C-Surveyor* AUV at an altitude of approximately 20 m. Data from the AUV's 430 kHz side scan sonar, subbottom profiler, and multibeam systems confirmed it was a shipwreck.

Based on the details from the side-scan sonar, the wreck appeared to be the remnants of a wooden sailing vessel. The intact nature of the wreck indicated that it could be copper sheathed. A linear feature, running down the center of the wreck was speculated to be keelson remains. An area of disturbed seafloor to the port side was thought to be ballast. The side-scan data did not show any debris trails outlying from the wreck. Subbottom data indicated the hull was partially buried in the seafloor. Despite the high-frequency data, the determination of bow and stern could not be made, nor could a determination of age.

Figure 10-70.  A 2006 210p- kHz side scan sonar image of the *Ewing Bank* Wreck (ATP Oil and Gas).

## 10.5.3.2.2    C&C Technologies, Inc. 2007 AUV Survey

In 2007, C&C's *C-Surveyor II* AUV underwent sea trials and testing following a system upgrade. One of the test locations was the *Ewing Bank* Wreck.  During a single dive, several test lines were flown over the wreck at an altitude of approximately 20 m to image it with the AUV's 430 kHz side-scan sonar, subbottom profiler, and multibeam systems (Figure 10-71).  Review of the data reconfirmed the findings of the 2006 surveys.  Despite the additional data, scientists were still unable to discern the bow and stern or determine an accurate age for the vessel.
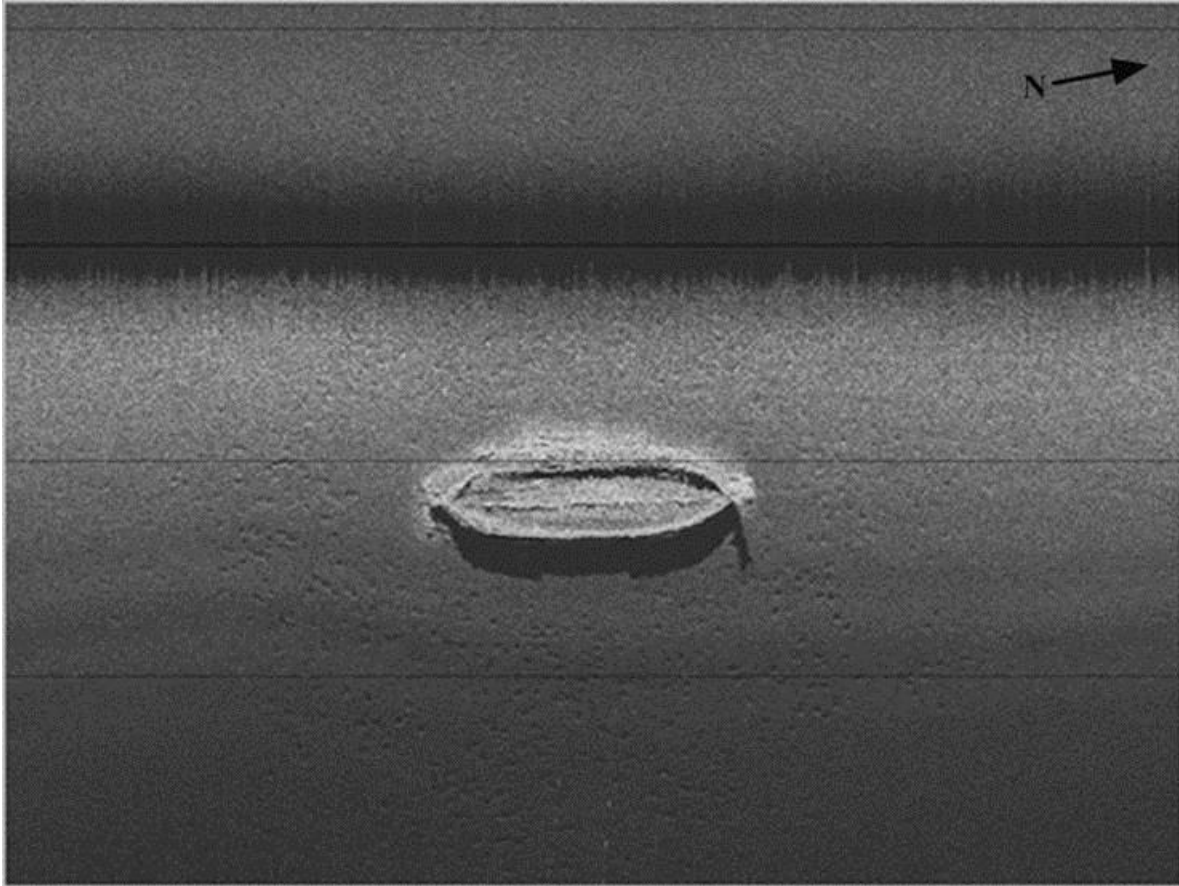
Figure 10-71.  A 410-kHz side scan sonar image of the *Ewing Bank* Wreck (C & C
        Technologies, Inc.)

### 10.5.3.2.3   *Lophelia* II: Rigs, Reefs, and Wrecks 2008 Field Cruise

In September 2008, the first ROV investigation of the *Ewing Bank* Shipwreck was conducted as
part of the *Lophelia* II: Rigs, Reefs, and Wrecks Study.  Over September 6 and 7, 2008, the
*Lophelia* II team used a *SeaEye Falcon* ROV launched from the NOAA Research Vessel *Nancy
Foster* to explore the shipwreck site.

Despite ROV and equipment issues, the team explored the wreck site for just under 8 hours over
the two-day period.  During this time the ROV completed a reconnaissance survey of the wreck
collecting both video and still imagery.  Archaeologists confirmed the wreck was historic and
completed a preliminary map of the wreck site, determining that the bow was at the northern end
of the wreck, and that what was originally thought to be ballast on the port side was actually a
sediment berm.  During the investigation, biologists also documented coral colonies and took core
samples from around the wreck for later analysis.

### 10.5.3.2.4   2009 C&C Technologies, Inc. AUV Survey

In June 2009, C&C conducted a second AUV survey over the *Ewing Bank* Wreck.  This survey
was part of an internal testing program for C&C's new AUV underwater photographic system on

the *C-Surveyor III* AUV.  Launched from the support vessel M/V *Miss Ginger*, *C-Surveyor III* ran five camera transects over the wreck at 5-meter intervals between lines.  The AUV's camera system collected 64 images of the wreck site and surrounding area.  A photomosaic compiled of these images by C&C gave scientists there first complete site photograph of the *Ewing Bank* Wreck.  This photographic mosaic assisted scientists in planning and conducting the September 2009 ROV investigation of the site.

### 10.5.3.2.5    *Lophelia* II: Rigs, Reefs, and Wrecks 2009 Field Cruise

In September 2009, the second ROV investigation of the *Ewing Bank* Shipwreck was conducted as part of the *Lophelia* II: Rigs, Reefs, and Wrecks Study.  Over a roughly 12-hour period during September 7 and 8, 2009, the *Lophelia* II team used Woods Hole Oceanographic Institution's *Jason II* ROV launched from the NOAA Research Vessel *Ronald H. Brown* to document the shipwreck site.

The 2009 ROV exploration of the *Ewing Bank* Wreck began with a standard reconnaissance survey around the wreck site. The wreck reconnaissance started at the stern, moved up the starboard side, around the bow, and down the port side before ending again at the stern.  During the roughly 2-hour reconnaissance dive, the project team documented aspects of the shipwreck including sheathing, fastener, and framing details, as well as sessile, invertebrate, and vertebrate fauna found on the wreck (Figure 10-72).

For approximately the next 1 ½ hours following the reconnaissance survey, a series of mosaic lines were run over the wreck.  Since a detailed mosaic of the *Ewing Bank* wreck was made previously using high-resolution AUV camera images, only 6 mosaic lines were flown with the *Jason II* ROV system.  During the mosaic survey, *Jason II* flew 1 meter transects at an altitude between 5.5 and 6.5 m above the seafloor.

Once the mosaic survey was finished, the next 2 ½  hours were spent collecting biological samples and deploying both long-term and short-term microbiological experiments. During this time span, 9 push cores were collected and a long-term microbiological test platform was placed forward of the stern along the wreck's centerline.

After completing the biological and core sampling, the project team conducted detailed inspection of areas of the wreck noted during the reconnaissance survey. Investigating and capturing still imagery of key features of the wreck, along with the recovery of 4 diagnostic artifacts took approximately 4 ½ hours to complete.  Once the detailed inspections were finished, the next hour was spent gathering rustle samples and retrieving the short-term biological experiments before terminating the investigation and returning the ROV to the surface
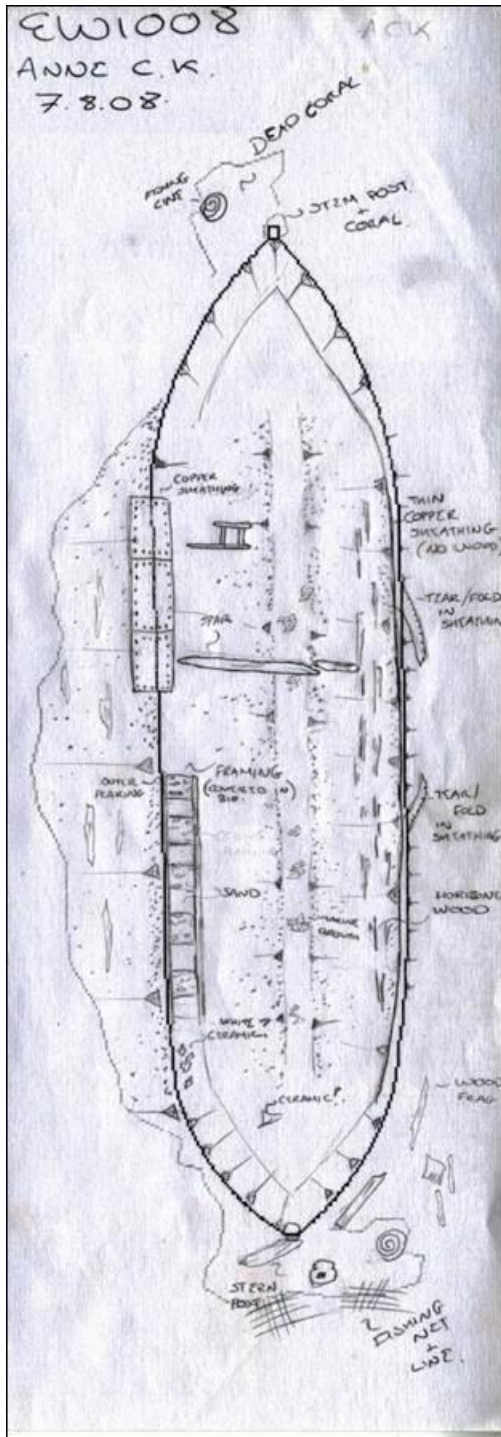
Figure 10-72.  The 2008 field drawing of the *Ewing Bank* Wreck
(Anne Corscadden Knox and PAST Foundation).

## 10.5.3.2.6    2012 C&C Technologies, Inc. AUV Survey

In September 2012, C&C conducted a third AUV survey over the *Ewing Bank* Wreck.  This survey was part of an internal testing program related to C&C's AUV underwater photographic system on the *C-Surveyor III* AUV.  Launched from the support vessel M/V *Miss Ginger*, *C-Surveyor III* ran 40 camera transects over the wreck and a large area around it at 4-meter intervals between lines.  During this survey, over 6,700 images of the wreck site and surrounding seafloor were obtained.

### 10.5.3.3    *Geographical Setting*

The *Ewing Bank* shipwreck site is located on the upper Louisiana continental slope in a water depth of 2,040 ft Mean Sea Level (MSL).  The shelf break is oriented northeast to southwest 15 miles to the north-northwest of the site, and the Mississippi Canyon is found 35 miles to the northeast.  A broad, low-relief submarine ridge of overbank deposits occurs between the shipwreck site and Mississippi Canyon (R. George, personal communication 3/16/2012).

The shipwreck is located on the eastern flank of a bathymetric trough oriented north-northwest to south-southeast.  The seabed slopes southwest at 2.3 degrees.  The bathymetric trough is 4,000 ft across with 50 ft of relief. It feeds into a basin extending across the southern half of portions of the Ewing Bank area (R. George, personal communication 3/16/2012).

Recent sedimentation in the area is primarily hemipelagic clay which has a very soft consistency. Turbidity flows originating upslope from the site are presumed to occur periodically and are a source of silt and clay.  Landslide or debris flow units which formed during the last marine transgression underlie the site.  The seabed irregularities found across the area are the topographic expression of these underlying debris flows (R. George, personal communication 3/16/2012).

The *Ewing Bank* wreck is resting on a south-trending slope.  The average seafloor gradient at the wreck site is 1 degree (Figure 10-73).  Seafloor sediments around the wreck are characterized as soft silty clays or mud (Warren, 2006).
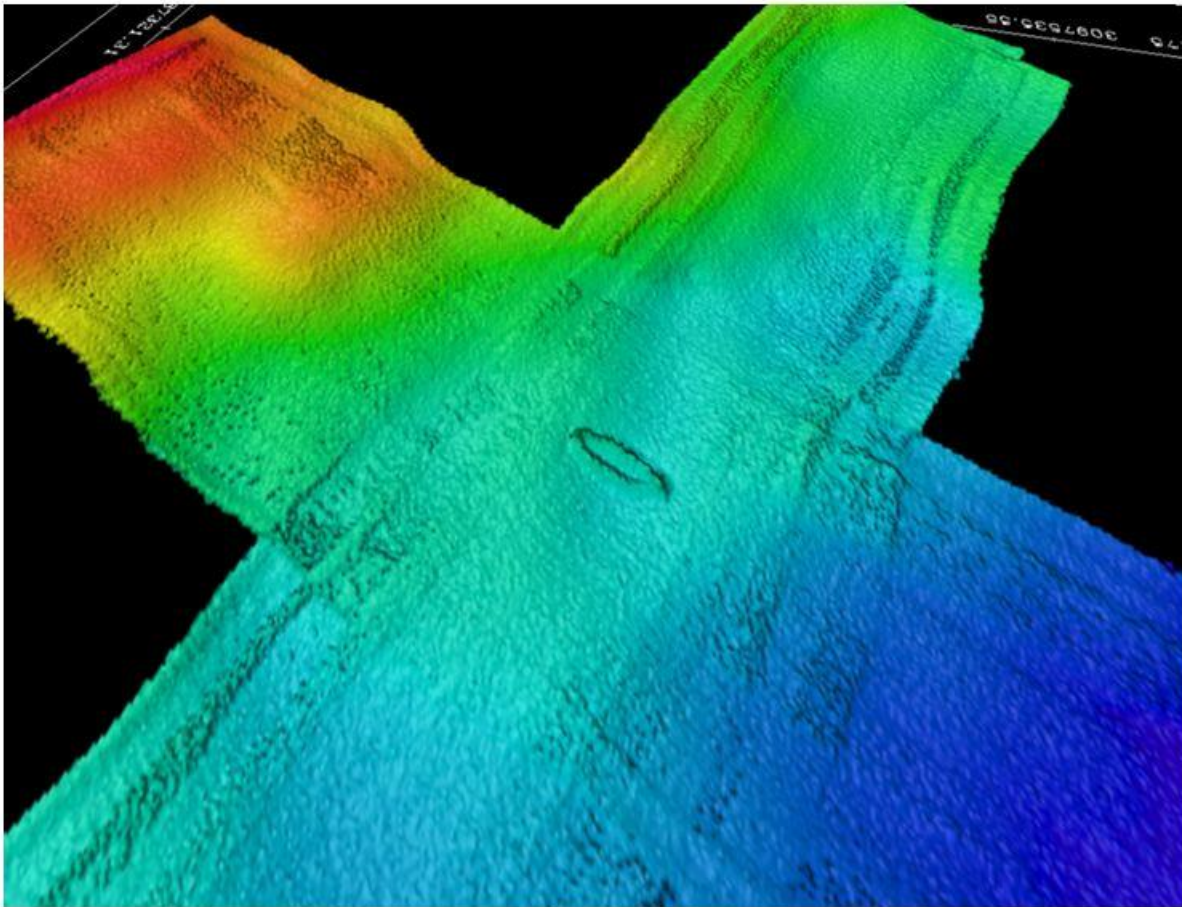
Figure 10-73. Multibeam bathymetry image of the *Ewing Bank* Wreck (C & C Technologies, Inc.).

### *10.5.3.4      Discussion of Archaeological Findings*

10.5.3.4.1    Physical Site

The following description of the *Ewing Bank* Wreck site is compiled from data collected during the 2009 and 2012 C&C AUV camera surveys and the 2008 and 2009 *Lophelia* II ROV investigations.

The *Ewing Bank* Wreck represents the remains of a sheathed wooden sailing vessel. The wreck is oriented with the bow facing a north-northeasterly direction (Figure 10-74). Average water depth at the site is 621 m BSL. There are no discernible debris scatters outside the immediate area of the wreck. The overall site size is roughly 40 m × 13 m.

The *Ewing Bank* Wreck site is composed of only the main hull and associated remains. There are no observed debris trails or areas of isolated scattered debris associated with the wreck site. The wreck is resting upright on its keel but appears to have a port list (west). The wreck site is confined

to a small area and consists of three distinct components: the main hull remains (Figure 10-75, Area 1); the exterior port debris zone (Figure 10-75, Area 2); and exterior stern debris area, inclusive of associated materials along the port and starboard stern quarters (Figure 10-75 Area 3).
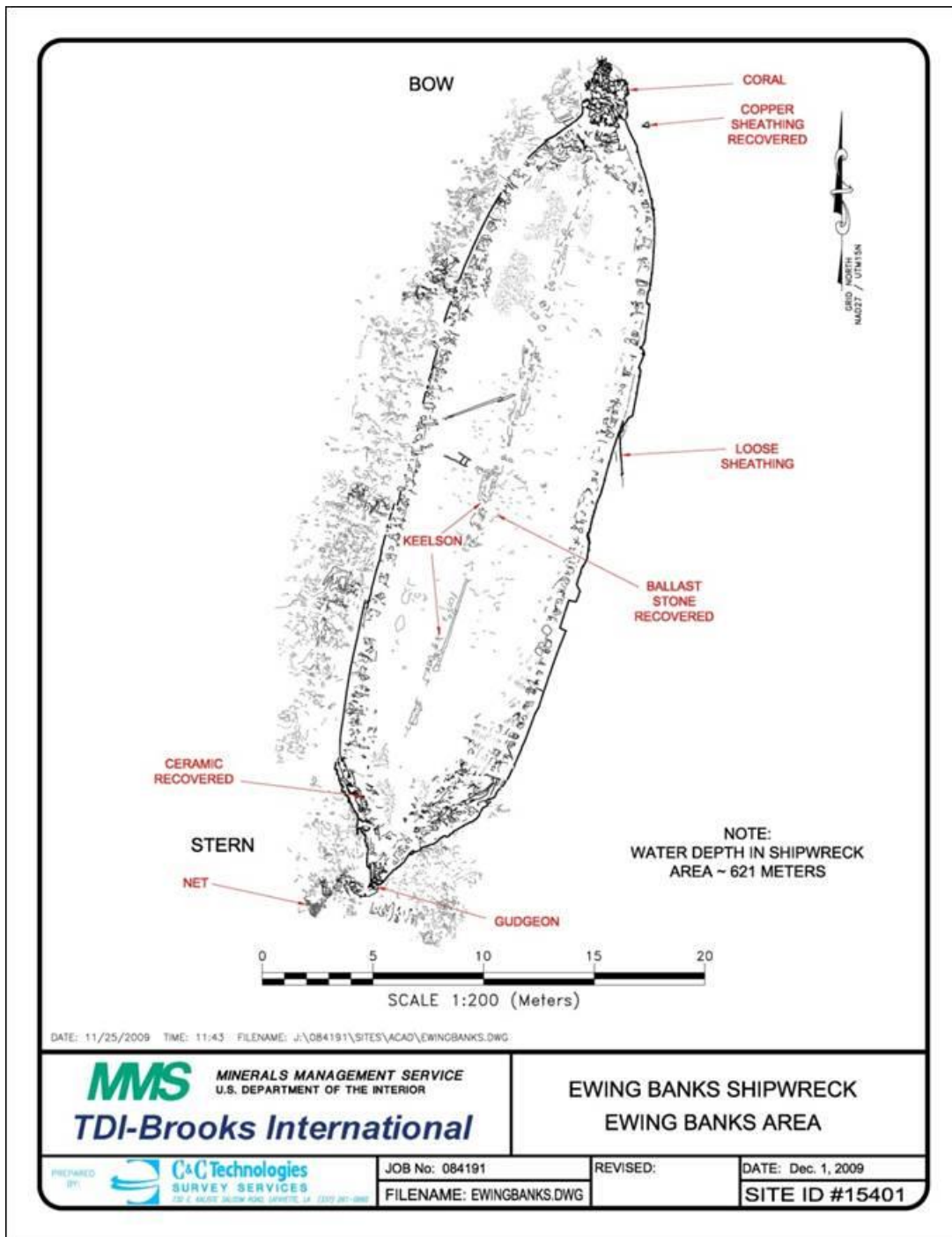


Figure 10-74. Site map of the *Ewing Bank* Wreck based on ROV investigations.
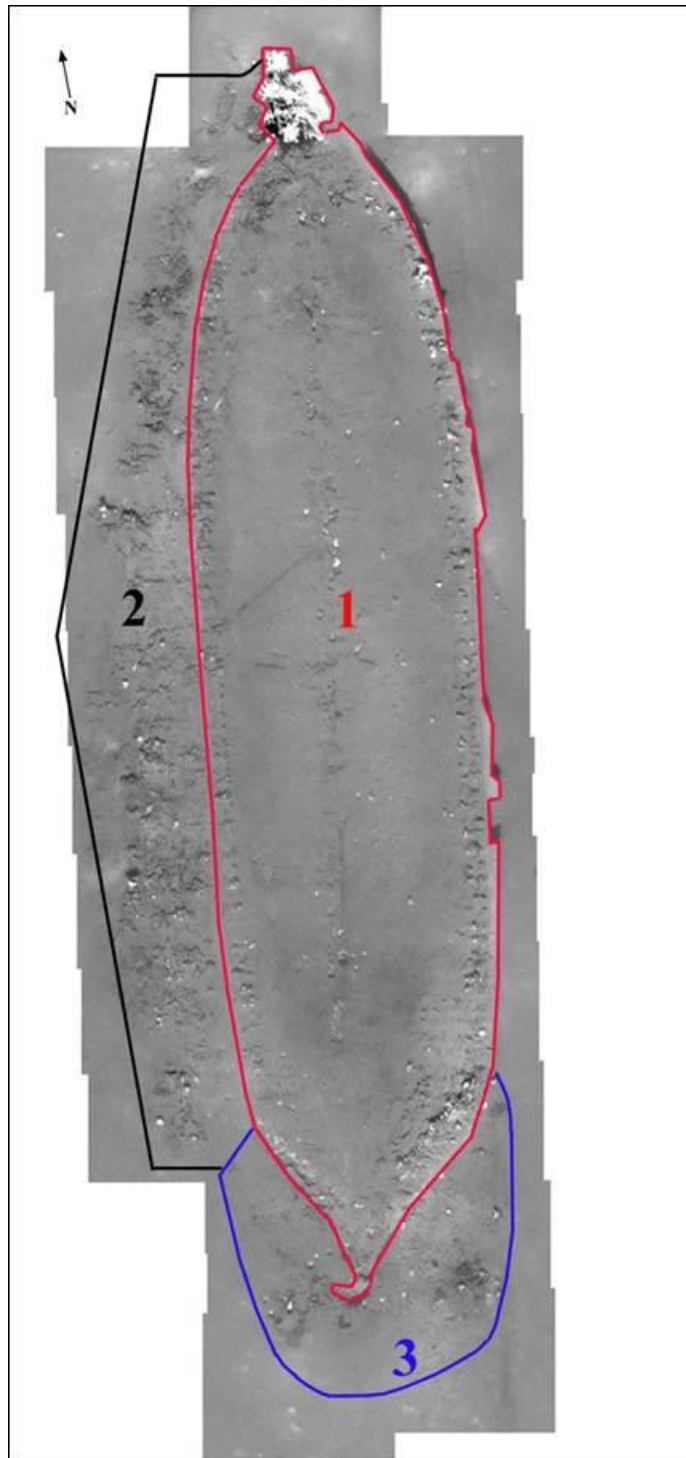
Figure 10-75. Photomosaic of the *Ewing Bank* Wreck showing the three main areas of the wreck site: Area 1 (red outline) is the main hull; Area 2 (black outline) is the port debris zone; and Area 3 (blue outline) is the stern debris area (Image C &C Technologies, Inc.)

The dominant feature at the site is the *Ewing Bank* Wreck's hull (Figure 10-75, Area 1). The hull is extant from just below the water line to the keel and is sheathed in a cuprous metal (Figure 10-76). Portions of both the stempost and sternpost remain intact. It is oriented with the bow to the north-northeast. The wreck sits on the seafloor with a 7 to 10 degree port list based on the angle of the hull. The hull remains of the *Ewing Bank* Wreck are approximately 120 ft (36.5 m) × 33 ft (10 m) with 10 ft (3 m) of the hull extending above the seafloor, giving the vessel a 4:1 length-to-beam ratio. The hull is moderately sharp at the bow, with rounded turn-of-the-bilge, and broad beam.

Because of the port list, a portion of the starboard hull is exposed (Figure 10-77). The sheathed portion of the stem post is intact and still attached at the bow. Aft of the stem, silt covers much of the forward hull's interior. Along the port and starboard interior hull edges, cant frames protrude from the silt. Ceiling planking remnants overlay portions of the port frames. Throughout this area, vestiges of possible decking remnants are scattered about.

Within the waist, the vessel's stone ballast is obscured by a thin veil of silt (Figure 10-78). The ballast covers the width of the lower hull and extends from just aft of the forecastle region of the bow to just forward of where the stern tuck begins. Fragments of piping and possible structural components are strewn over the top of the ballast. On either side of the ballast, the deteriorated tops of frames or futtocks are visible just above the silt line as they extend up the side of the hull from beneath the ballast.

Aft of the ballast pile, in the stern area, a possible keelson remnant and a stern frame are visible. To the starboard of the possible keelson remnant, caulking remnants that lie up the side of the hull serve to outline the location of long-deteriorated ceiling planking. To the port and slightly aft of the potential keelson piece is a concentration of ceramics. Within the hull, sediments cover much of this material, but numerous fragments of vessels are exposed near the edge of the hull. Intermixed with the ceramics are two sections of metal pipe, possibly lead, connected by a metal flange. Continuing aft from keelson area, the stern post is partially intact and still attached to the hull. The stern post is also sheathed in copper or copper alloy. The rudder is missing, but a single gudgeon strap is still intact with a partial pintle attached to it.
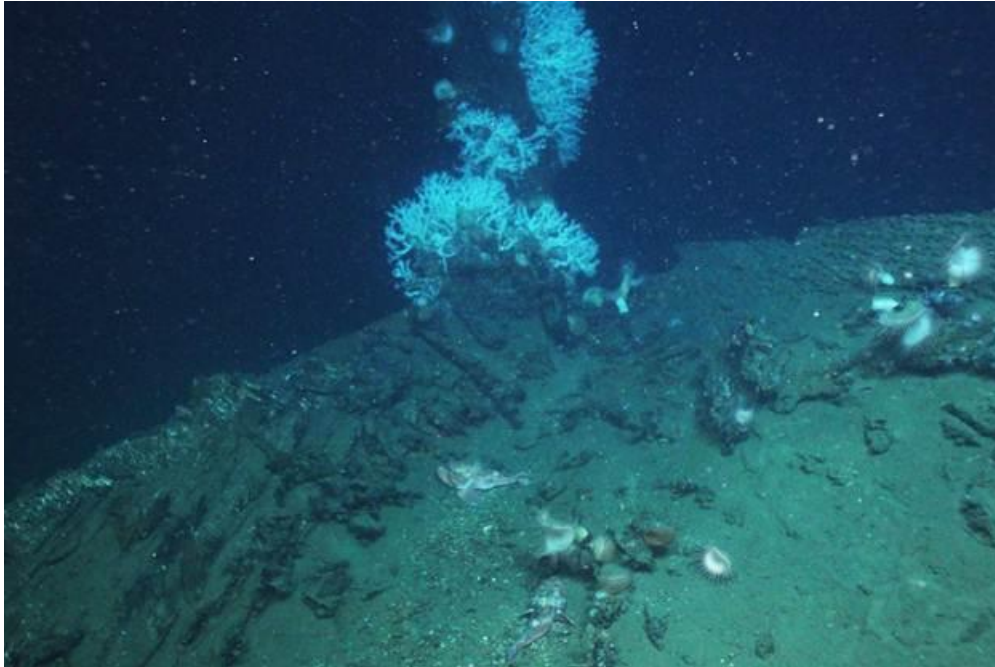
Figure 10-76.  View of bow and stempost of *Ewing Bank* Wreck (Aquapix
        Camera Image, *Lophelia* II, 2009: Deepwater Coral Expedition:
        Rigs, Reefs, and Wrecks).



Figure 10-77.  ROV video image capture of exposed hull remains at the *Ewing
        Bank* Wreck's starboard bow.
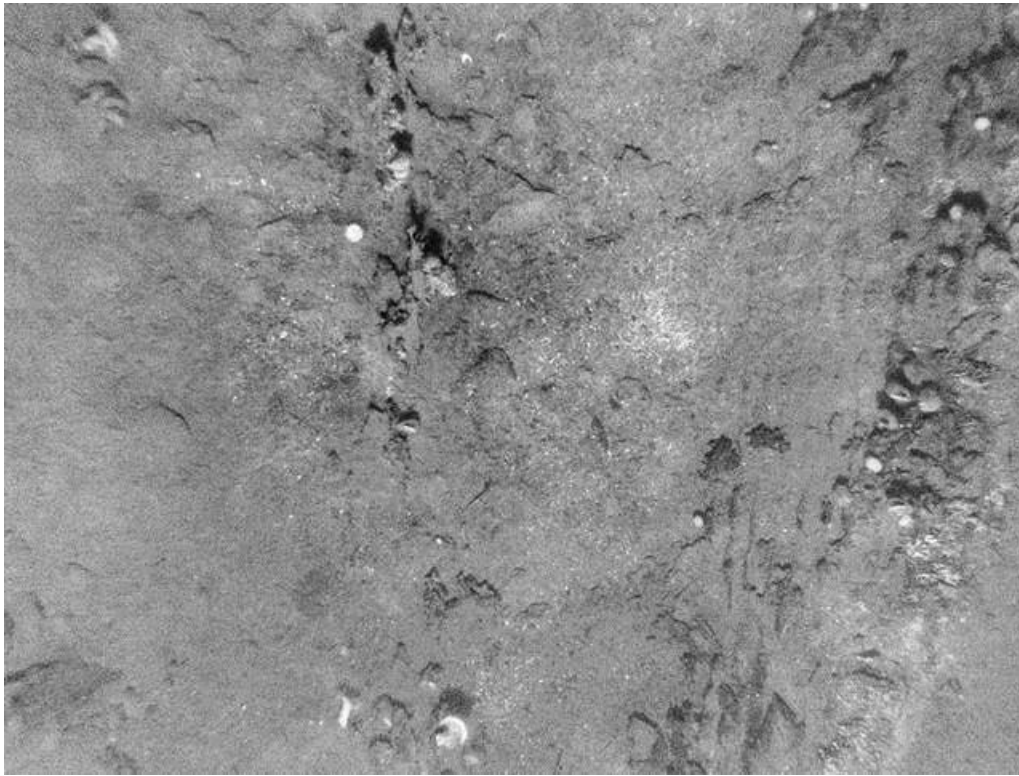
Figure 10-78.  AUV Camera photograph showing a portion of the *Ewing Bank* Wreck's ballast pile. (C & C Technologies, Inc.)

On the port (western) exterior of the hull, a low-relief sediment berm has built up, obscuring much of the exterior port hull (Figure 10-79).  The berm appears to have built up over time around remnants of the upper hull that collapsed onto the seafloor.  The apparent stratified remains within this berm make up the "port debris zone" (Area 2 on overall mosaic).  At its greatest width, this debris zone is approximately 3 m wide.  Although much of the deposits are buried within the silt, a myriad of partially decayed wooden hull components, copper fasteners, and unknown conglomerates are exposed on the berm's surface.  The density of materials is highest along the midship area, but diminishes rapidly at the bow and stern.

The edge of the exterior stern debris zone is just aft of where the hull turns toward the stern post on the port side (Figure 10-80 and Figure 10-81).  This debris area is demarcated by an irregular sediment stain, seen in the AUV imagery, encompassing the stern area.  This stain, which may represent the only remnants of the upper stern overhang, extends approximately 6 m across the stern and 2.4 m aft of the stern post.  Within this debris area are hull remnants, including the possible remnants of the rudder, corroded and unidentifiable iron conglomerates, and intrusive material, which include a modern fishing net.  This debris area ends abruptly on either side of the hull at the point where the hull turns toward the bow.

Moving up the starboard side of the hull, there is very little debris on the seafloor.  Because of the port list, the starboard hull is exposed.  In some areas the side of the hull is exposed from the turn-of-the-bilge to the edge of the remaining sheathing, a distance of up to 76 cm.  Along this side of

427

the vessel, there is a noticeable absence of material remains equivalent to those on the port side. The seabed here is free of materials, other than intermittent sections of sheathing that have fallen off the hull.
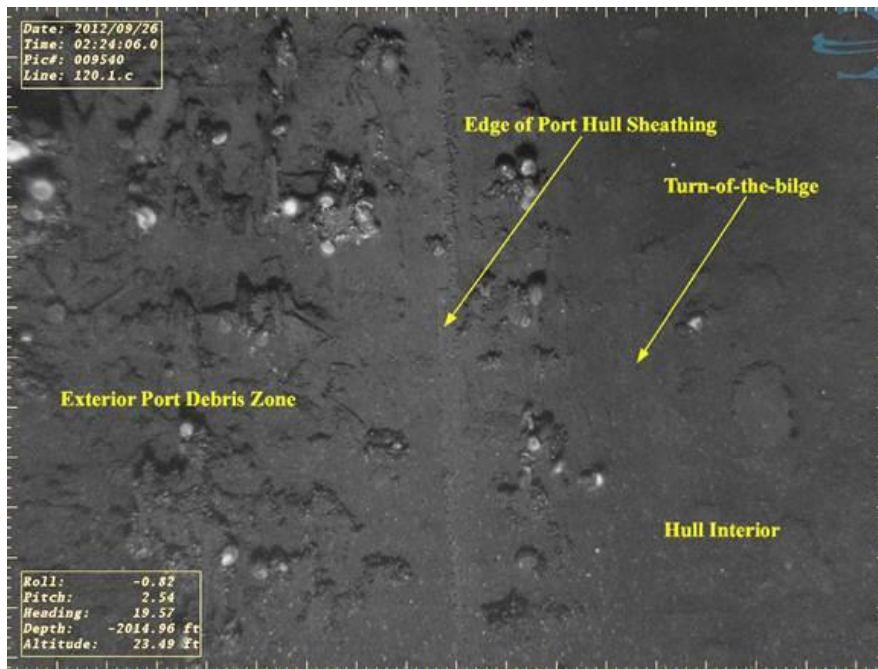


Figure 10-79.  AUV camera photograph showing portions of the exterior port debris zone and the *Ewing Bank* Wreck's interior hull (C & C Technologies, Inc.).
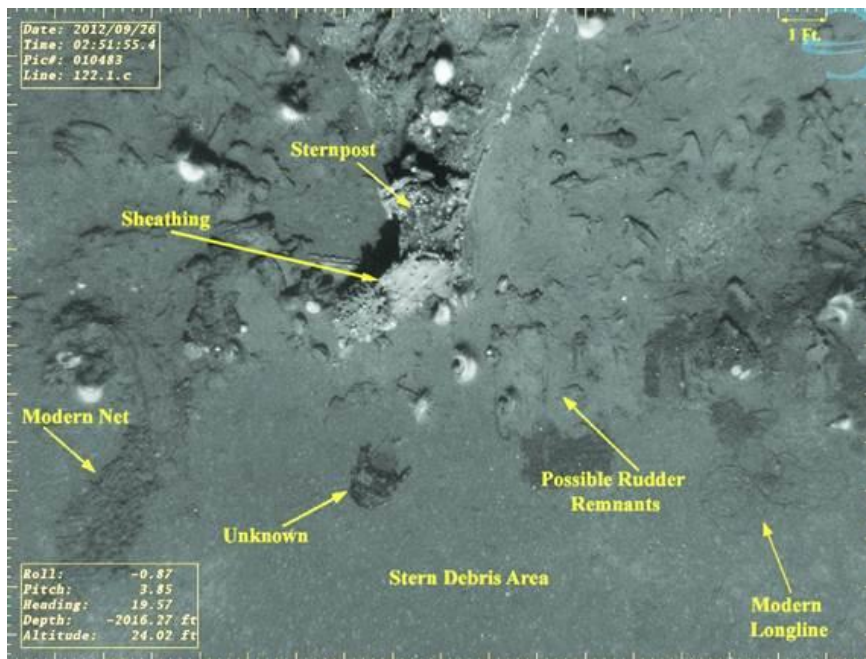


Figure 10-80.  AUV camera photograph of the stern and stern debris area of the *Ewing Bank* Wreck (C & C Technologies, Inc.).

Figure 10-81. ROV video capture image looking north towards stern and stern debris area of the *Ewing Bank* Wreck

### 10.5.3.4.2 Bow

The bow area of the hull is identified by the partially intact stempost (Figure 10-82). The stempost is wood and has a large colony of *Lophelia pertusa* coral growing on its upper sections. The stem is the highest point of relief on the wreck sites. It extends approximately 12 ft (3.6 m) above the seafloor and has sided and molded dimensions of 6 in (15 cm) and 12 in (30 cm), respectively. The stem assembly appears to show the stempost, apron, and possible breast hook. The stem deadwood and lower stempost are not visible. The stem flares out slightly from the hull near the keel. This flare increases near the top of the stem.

The outer portion of the stem is sheathed with copper or copper alloy (Figure 10-83). The sheathing on the stem extends 2 ft (0.61 cm) higher than the top of the existing copper on the hull. This suggests the waterline was higher than represented by the remaining hull sheathing. There is also a significant amount of iron and corrosion product on the stem. Using the current data, it is difficult to ascertain whether this is a result of iron plate that has been added to the stem as a repair or re-enforcement, or corrosion from numerous iron fasteners.
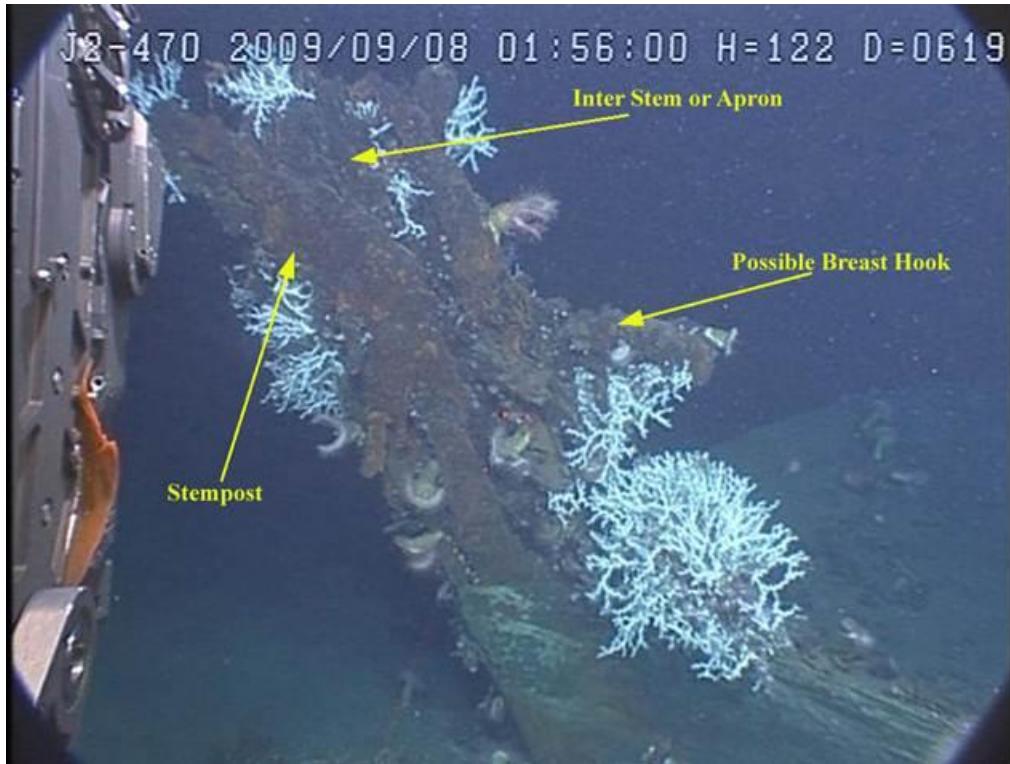
Figure 10-82.  ROV video capture image of the *Ewing Bank* Wreck's stempost (port view) with major components identified.



Figure 10-83.  Photograph of copper sheathing on the *Ewing Bank* Wreck's stempost (Aquapix Camera Image, *Lophelia* II, 2009: Deepwater Coral Expedition: Rigs, Reefs, and Wrecks).

## 10.5.3.4.3    Frames and Outer Planking

Sediment and ballast obscure much of the *Ewing Bank* Wreck's construction details.  The assessment of framing and outer planking details is based on examination of exposed or partially exposed timbers near the hull edges.

Overall, the *Ewing Bank* Wreck is a stoutly built vessel.  Cant frames are visible in the bow (Figure 10-84).  Several of these are partially exposed on the starboard bow just below the edge of the extant sheathing.  The cant frames in the bow are approximately 12 in (30 cm) sided (molded dimension measurements could not be taken) and set at an approximate angle of 20° to the assumed centerline keel location.

In several areas along the interior edge of the hull, portions of main timbers are exposed.  Only a few of these are intact enough to show edges.  Based on the limited scope of the video data, the *Ewing Bank* Wreck appears to have paired frames, with a room and space averaging 14 in (35.6 cm).  The deteriorated condition of many of the frames and the build-up of silt hampers detailed measurements of the frame timbers.

Near the port bow, a section of the interior hull between the outer planking or strakes and the interior ceiling planking is intact (Figure 10-85).  The space between the strakes and the ceiling planking is approximately 4 in (10 cm).  From this information, it can be surmised that frames in this section of the hull could have had a molded dimension of up to 4 in (10 cm). This image also indicates that the outer planking was approximately 3 in (7.6 cm) thick.
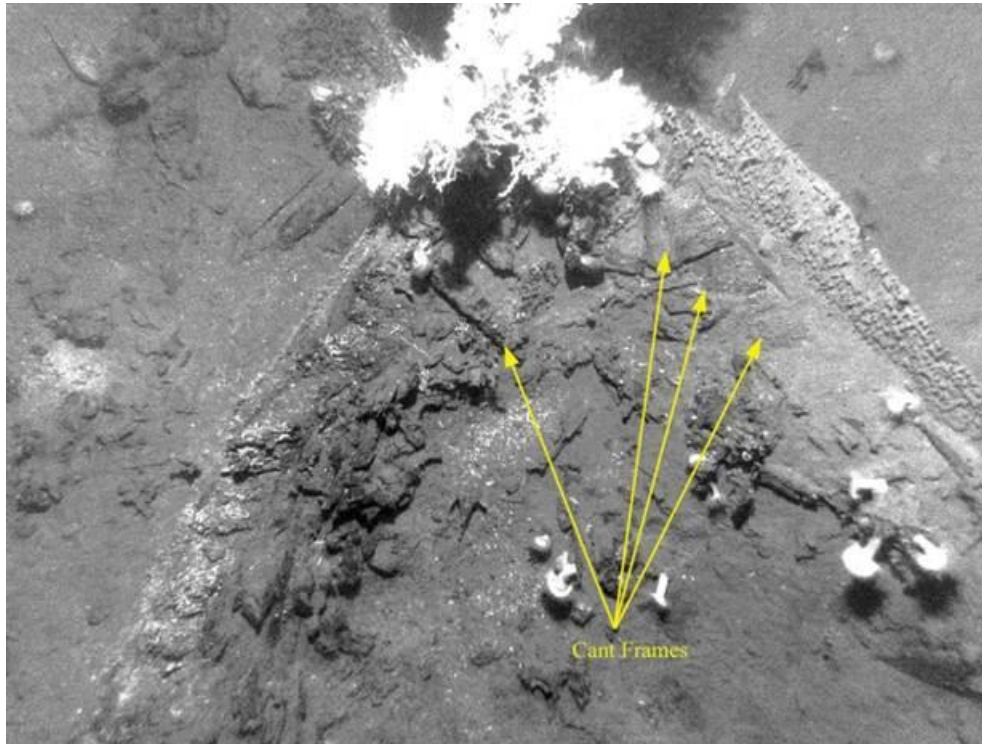
Figure 10-84. AUV camera photograph of the *Ewing Bank* Wreck's bow interior showing cant frames (C & C Technologies, Inc.).



Figure 10-85. ROV video capture image showing the *Ewing Bank* Wreck's outer hull planking, hull framing, and interior ceiling planking.

## 10.5.3.4.4    Ceiling Planking

In several locations on the wreck, vestiges of the *Ewing Bank* vessel's interior ceiling planking is visible. In some cases, planks are partially intact, while in other places, only the caulking remains to outline the shape of the now-disintegrated ceiling planks. Figure 10-86 shows one of the few partially intact ceiling planks on the wreck. Near the beginning of the starboard stern tuck, a section of ceiling planking is visible at the edge of the hull. This piece of planking is approximately 3 in (7.6 cm) thick.Near the same area, but further down in the hull's interior, Figure 10-87 shows an area where the ceiling planking has deteriorated, but the caulking remnants outline individual planks. Measurements of the caulking indicate the ceiling planking was approximately 4 in (10 cm) wide.



Figure 10-86.  ROV video capture image showing ceiling planking on the *Ewing Bank* Wreck's starboard stern.

Figure 10-87. ROV video capture image of caulking remnants outlining disintegrated ceiling planking in the *Ewing Bank* Wreck's starboard stern.

### 10.5.3.4.5    Stern

The stern post is still partially intact and attached the hull (Figure 10-88).  The remaining section is nearly vertical, measuring approximately 4 ft (1.2 m) high, 12 in (30 cm) sided, and 12 in (30 cm) molded.  A section of sheathing that once protected the missing upper section of stern post is folded over onto the seafloor.  This piece, approximately 3 ft (0.91 m), indicates that the stern post was sheathed to at least a height of roughly 7 ft (2.1 m).

Attached to the sternpost are a gudgeon and a portion of a pintle. The sternpost gudgeon measures 12 in (30 cm) in length, 12 in (30 cm) in width, and 2.5 in (6.4 cm) deep.  It has a circular opening on its after edge to allow the pintle's vertical pin to attach to the gudgeon.  Both the gudgeon and the pintle appear to be manufactured as single pieces. The pintle is broken near the edge nearest the gudgeon. It is a clean break and there does not appear to be any evidence of twisting that would indicate a forced break. The pintle, like the gudgeon, is 12 in (30 cm) wide, 2.5 in (6.4 cm) deep, and, although broken, its length is likely 12 in (30 cm), the same as the gudgeon. The pintle and gudgeon appear to set flush, indicating the vertical pin fitting into the gudgeon is, at most, 2.5 in (6.4 cm) long. The diameter of the pintle's vertical pin could not be assessed from the current data. No other gudgeon braces or traces of the rudder have been positively identified, although debris that could be related to the rudder mechanism is present near the starboard side of the sternpost.

434
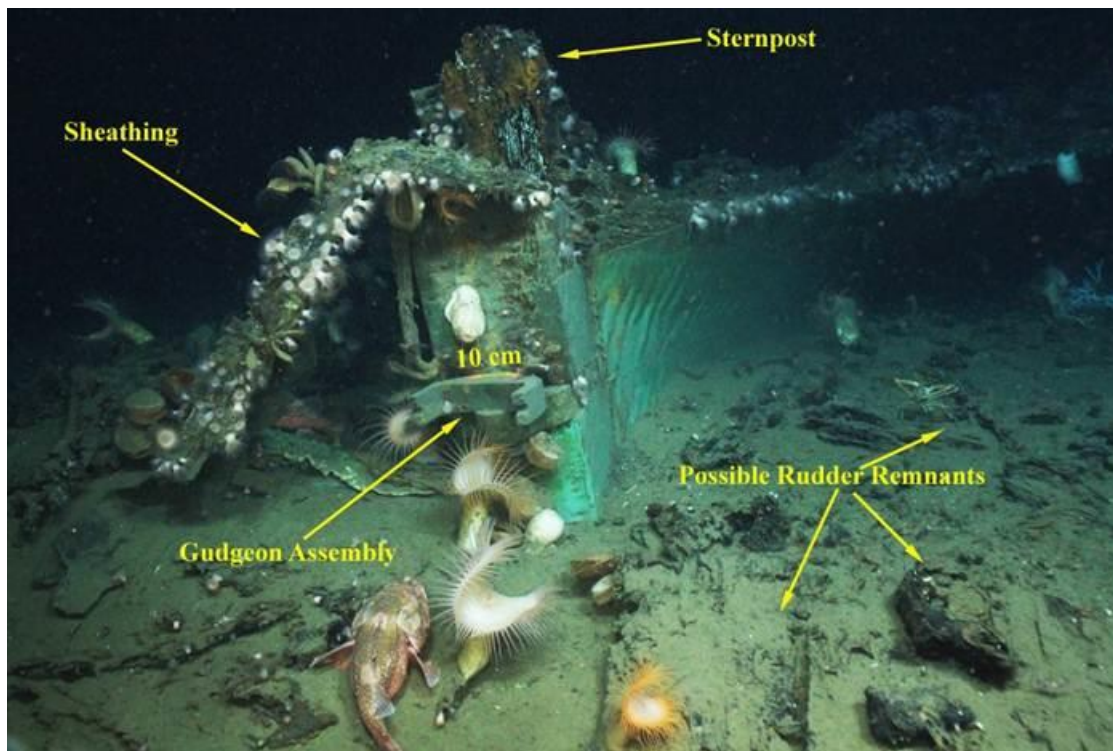
Figure 10-88.  Photograph showing details of the *Ewing Bank* Wreck's stern (Aquapix Camera Image, *Lophelia* II, 2009: Deepwater Coral Expedition: Rigs, Reefs, and Wrecks).

### 10.5.3.4.6    Fasteners

Several varieties of fasteners are present at the *Ewing Bank* Wreck.  These fasteners range from small sheathing nails to large spikes and bolts, called drift pens.  All of the fasteners appear to be hardened copper or copper alloy.  Although iron fasteners have not been located, rusticles and unidentifiable conglomerates noted at several locations are likely remnants from deteriorating iron fasteners.

The smallest fasteners at the site are sheathing nails.  These appear to be hardened copper.  They are approximately 1 inch (2.54 cm) in length with a flat head and tapering shank.  These fasteners are spaced on the sheathing approximately 4 inch (10 cm) apart (Figure 10-89 and Figure 10-90).

Five types of larger fasteners have been found and noted on the site.  All of these are non-threaded spikes or bolts.  These types of fasteners are typically used for fastening planking or framing components below the waterline.  Table 10-5 provides a description of each large fastener type, while images of each type are shown in Figure 10-91 to Figure 10-95.

The average shank or shaft diameter of the larger fasteners is 0.75 inch (1.9 cm) with lengths between 14-16 in (36.6 to 40.6 cm).  The only variation is the Type 4 fastener that has a shank diameter of 1 inch (2.54 cm).  Desmond (1998) indicates that the 0.75 inch (1.9 cm) diameter bolts were used to fasten 3 to 5.5 inch (7.6 to 13.97 cm) thick planking.  Bolts having a 1 inch (2.54 cm)

435

diameter were used to fasten planking or timbers with a thickness of 6 in (15 cm) or greater.  The bolts with 0.75 inch (1.9 cm) diameter shanks are likely through bolts for attaching the outer planking.   The larger diameter of the Type 4 bolt suggests it may be a frame or timber bolt rather than a through bolt for attaching planking.



Figure 10-89.  ROV video capture image of *in situ* sheathing nails on the
Ewing Bank Wreck's starboard hull sheathing.



Figure 10-90.  Photograph of sheathing nail from the *Ewing Bank* Wreck
(University of West Florida).

Table 10-5.

Large fasteners identified at the *Ewing Bank* Wreck site

| Name | Type | Shank Length (inches) | Description | Figure No. | Notes |
|---|---|---|---|---|---|
| Type 1 | Bolt | 16 | Rounded shaft non-threaded bolt. Rounded head w/square underside. Washer attached to end of shank. 3/4" shaft diameter | 10-91 | Similar to modern carriage bolt/coach bolt. Presence of washer could indicate a type of forelock bolt. |
| Type 2 | Spike | 16 | Tapering shaft spike like fastener with squarish head. Shaft tapers from 3/4" near head to 1/2" at point. | 10-92 | |
| Type 3 | Bolt | 14 | Rounded shaft non-threaded bolt with flared head. 3/4" shaft diameter. | 10-93 | Possible evidence of clenching noted on some examples. |
| Type 4 | Bolt | 16 | Rounded shaft non-threaded bolt. Flat round head. 1" shaft diameter. | 10-94 | |
| Type 5 | Bolt | Unknown | Rounded shaft non-threaded bolt. 2" flat round head. 3/4" shaft diameter. | 10-95 | |



Figure 10-91. ROV video capture image of a Type 1 fastener on the *Ewing Bank* Wreck.

437
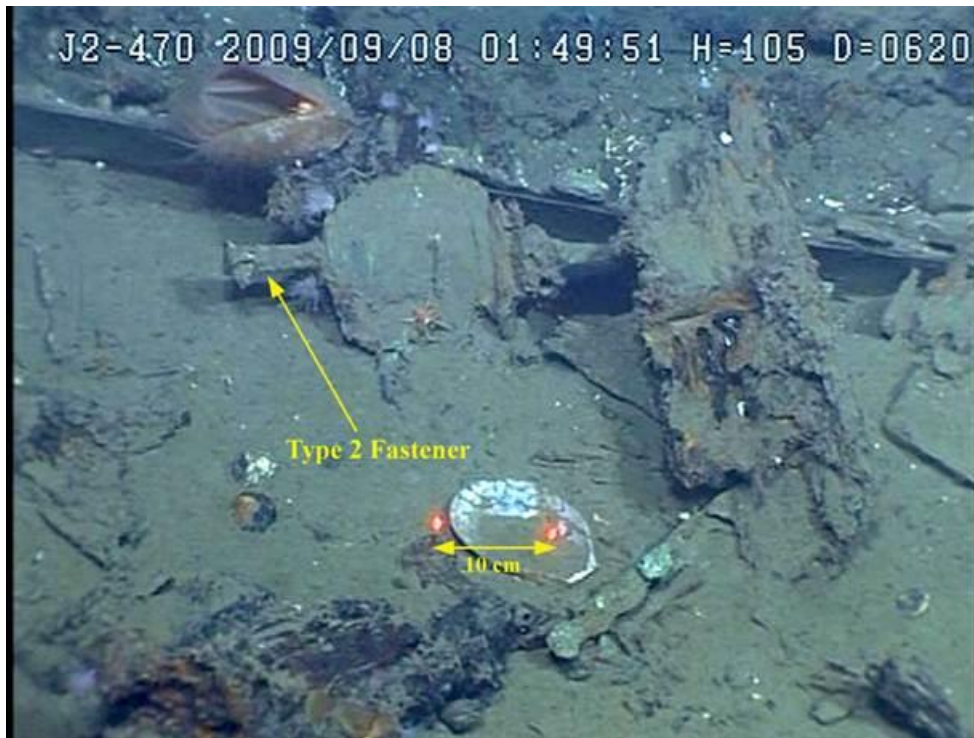
Figure 10-92.  ROV video capture image of a Type 2 fastener on *Ewing Bank* Wreck.



Figure 10-93.  ROV video capture image of a Type 3 fastener on the *Ewing Bank* Wreck.

Figure 10-94.  ROV video capture image of a Type 4 fastener on the *Ewing Bank* Wreck.



Figure 10-95.  ROV video capture image of a Type 5 fastener on the *Ewing Bank* Wreck.

## 10.5.3.4.7    Sheathing

The hull of the *Ewing Bank* Wreck is sheathed with a cuprous metal.  A recovered sample was identified as Muntz metal.  Other than some irregular stealer pieces near the bow, the sheathing appear to be standard rectangular sheets varying in length from approximately 3.3 to 3.94 ft (1 to 1.2 m) and approximately 11.8 in (30 cm) wide.  The majority of sheets have the same dark green patina coloration.  However, there are several areas on the exposed starboard hull that have lighter colored sheets.  The difference in sheet coloration suggests that these areas may represent where worn out or damage sheathing has been repaired (Figure 10-96).

There is roughly a 2-inch (5 cm) overlap between sheets for fastening. Fasteners on the overlapping edges are spaced roughly 2 in (5 cm) apart.  The sheathing is held to the outer planking by hardened copper fasteners, which are staggered between rows forming a typical diamond nail pattern.  The fastener spacing is 4 in (10 cm) between nails.  Fasteners on the overlapping edges are spaced 2 in (5 cm) apart.

Diagonal foiling (buckling) occurs on the sheathing (Figure 10-97).  This foiling has been observed on other deepwater wrecks with sheathed hulls.  Why the sheathing buckles is not fully understood, but it may result from compression of the wood at depth or the activity of anaerobic bacteria.  The foiling likely occurs in a diagonal line because it follows the pattern of the nails holding the sheathing to the hull planking.



Figure 10-96. ROV video capture image showing Muntz metal copper
sheathing and possible repair areas on the *Ewing Bank* Wreck's
starboard hull.

Figure 10-97. ROV video capture showing diagonal foiling of sheathing on
the *Ewing Bank* Wreck's starboard stern.

### 10.5.3.4.8 Miscellaneous Ship Components

Although most of the materials on the *Ewing Bank* Wreck are related directly to the vessel's construction, there are miscellaneous ship components or remnants of them visible at the site. These include the ballast pile, sections of pipe, a ladder-like remnant, and a flange assembly.

The ballast pile is the largest of these non-construction components (Figure 10-98). The pile extends across the width of the wreck from the forecastle area to just forward of the stern tuck. The video data suggests the ballast pile maybe 11.8 to 24 in (30 to 60 cm)deep. The ballast stones appear to be irregular in shape. The size of the ballast stones, based on those visible in the video data, ranges from less than 11.8 in (30 cm) up to as much as 3.2 ft (1 m) in length.
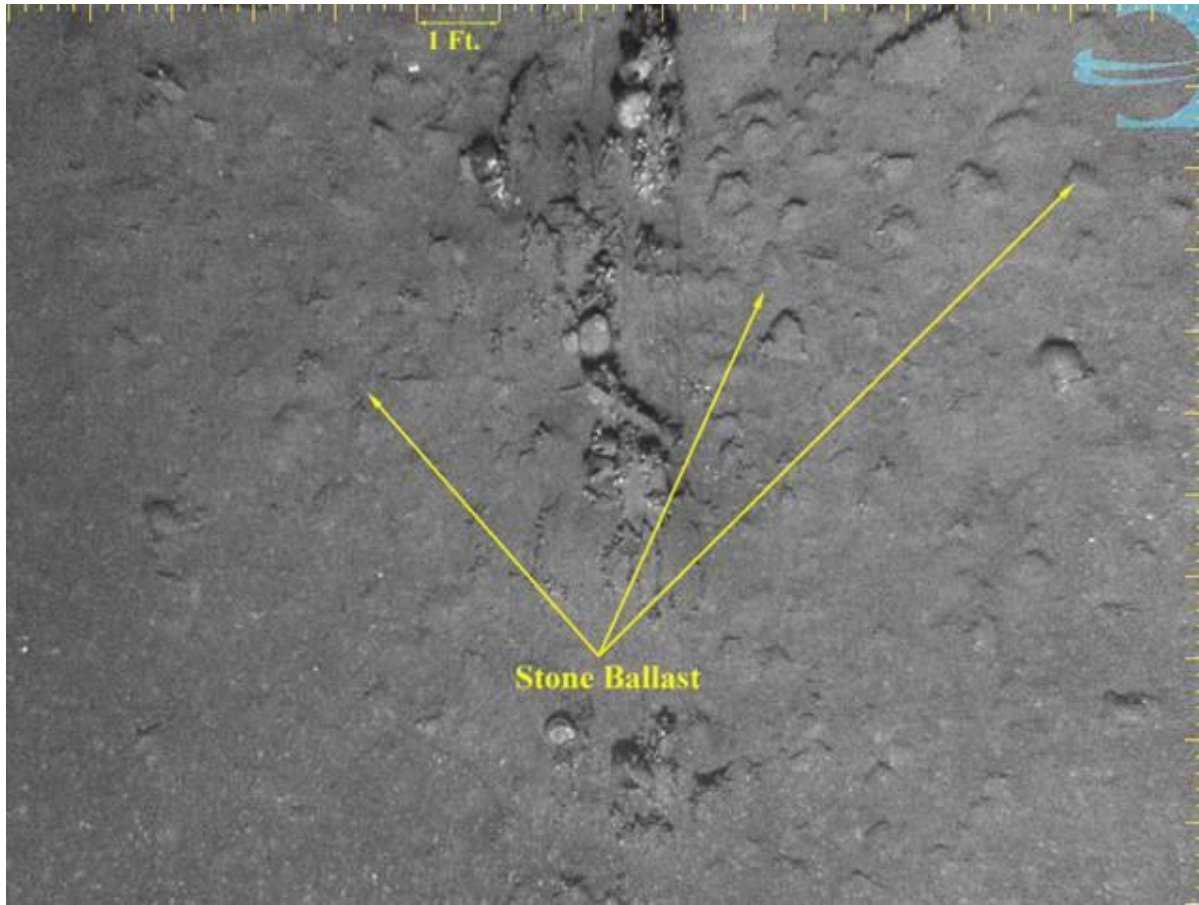
Figure 10-98.  AUV photograph of the *Ewing Bank* Wreck's stone ballast
        partially covered in silt (C & C Technologies, Inc.).

Other non-construction components include sections of pipe on the interior of the vessel.  One section of pipe overlays the ballast pile along the centerline near the middle of the wreck (Figure 10-99 and Figure 10-100).  This pipe is approximately 16.4 ft (5 m) long and has a curved section at the end nearest the stern that protrudes 11.8 in (30 cm) up from the top of the ballast pile. The second segment of pipe is near the forward end of the ballast pile extending diagonally from the centerline aft to the wreck's port side (Figure 10-101). It is broken into three pieces that have a combined length of 11.8 ft (3.6 m). Both sections of pipe have about a 4 inch (10 cm) outside diameter and appear to be made of ferrous material. The total length of both pipe segments is 28.2 ft (8.6 m).  The proximity of pipe segments of the same diameter in proximity to each other indicates that they were likely connected at one time.  Although the exact purpose of these pipes it is not known, it is speculated that they may be related to the ship's bilge pump system.

Figure 10-99. ROV video capture image of pipe remnant in *Ewing Bank* Wrecks interior hull (view to port).
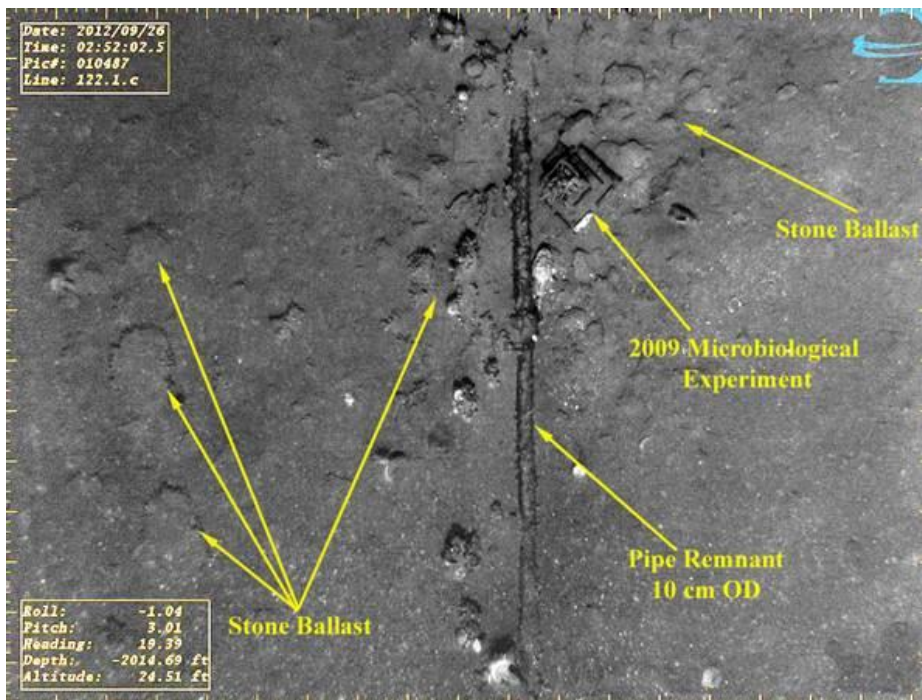


Figure 10-100. AUV camera photograph off pipe remnant, ballast, and 2009 microbiological experiment in the *Ewing Bank* Wreck's interior aft hull (Image C & C Technologies, Inc.).
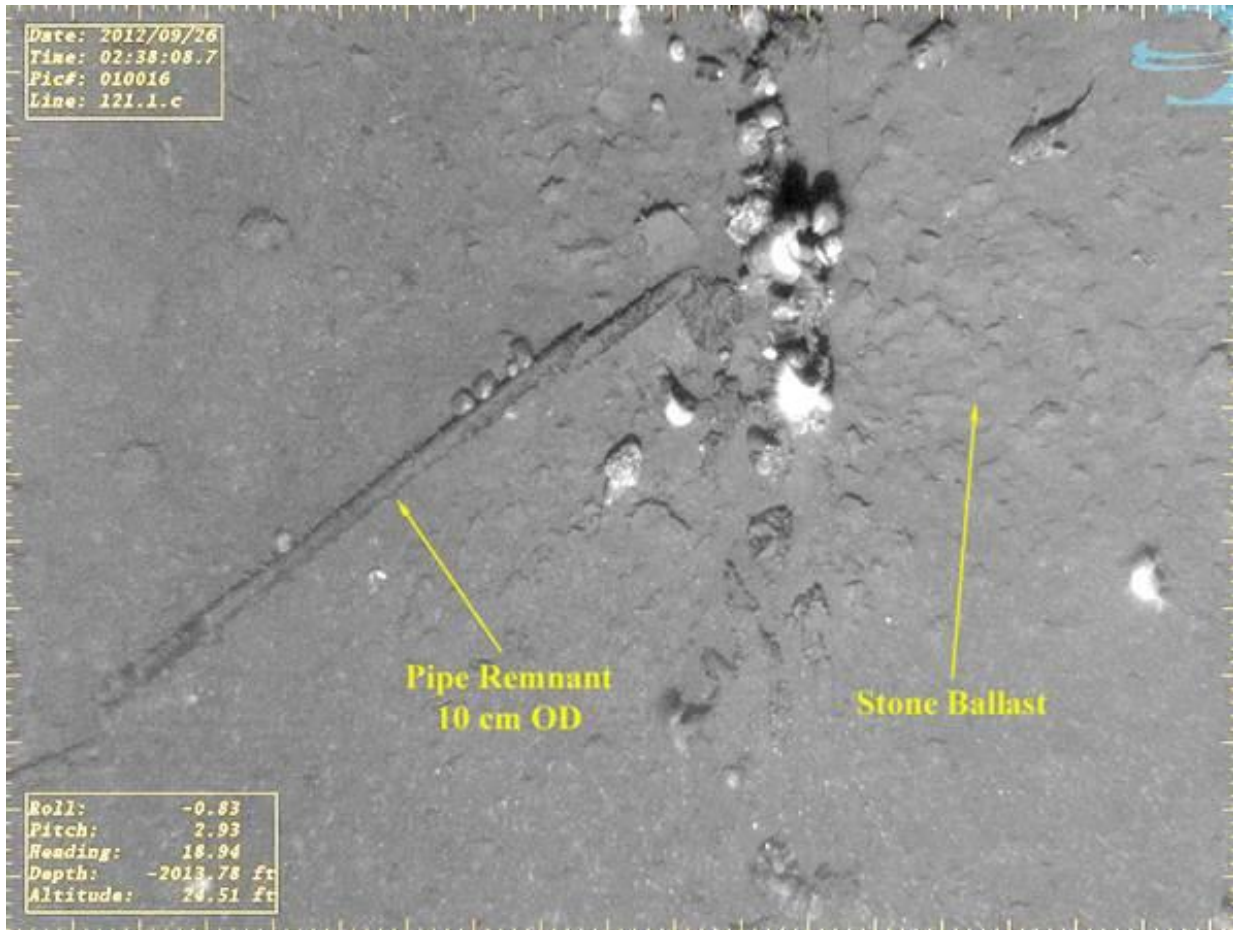
Figure 10-101.  AUV camera photograph of pipe remnant in the *Ewing Bank*
       Wreck's forward hull (Image C & C Technologies, Inc.).


Between the two larger sections of pipe, is a wooden remnant that resembles a ladder (Figure 10-102).  It has two parallel slats of wood 1.9 to 2.3 ft (0.60 to 0.70 m) in length connect by two extant rungs 11.8 to 13.8 in (30 to 35 cm) in length.  The rungs are spaced about 11.8 in (30 cm) apart.  No similar structure has been found on the wreck site and its actual role on the ship remains unknown.  This could represent the remnants of a bulkhead structure or possibly a hatch ladder.

Figure 10-102. AUV camera photograph of ladder-like object in the *Ewing Bank* Wreck's interior hull (C & C Technologies, Inc.).

The last and most intriguing ship components on the *Ewing Bank* Wreck are two flange assemblies (Figure 10-103). The flange assemblies rest on the interior port stern quarter just past where the hull turns inward towards the stern. Each flange has a section of lead pipe attached to it. The flanges have an outside diameter of 5.9 in(15 cm). The attached segments of lead pipe are approximately 4 inch (10 cm) outside diameter. The overall length of the assembly is difficult to determine because the leg piping is folded and flattened, but conservative estimates based on the ROV footage indicate the assembly is a least 2.5 ft (0.75 m) long. It is interesting to note that the estimated diameter of the lead piping is similar to that of the ferrous pipes discussed previously. It is possible that both those pipe segments and the flange assembly represent the last vestiges of the *Ewing Bank* Wreck's bilge pump system.

Figure 10-103.  ROV video capture image of flange assemblies and pipe remnants on the *Ewing Bank* Wreck's port stern.

## 10.5.3.4.9    Artifacts

There is a noticeable dearth of material culture remains on the *Ewing Bank* Wreck.  The only artifacts documented on the wreck related to daily activities of passengers and crew is a concentration of ceramics near the port stern interior (Figure 10-104).  The data suggests the concentration consists of 12 to 15 fragmented vessels of various forms, including cups, plates, and at least one platter.  Most of the ceramics appear to be undecorated white paste wares, but some fragments of molded-and-flow blue or transfer-print-decorated wares were also noted on the site (Figure 10-105).  The condition, location, and variety of materials in the concentration indicate that the materials were likely discarded in the bilge area before the vessel sank.
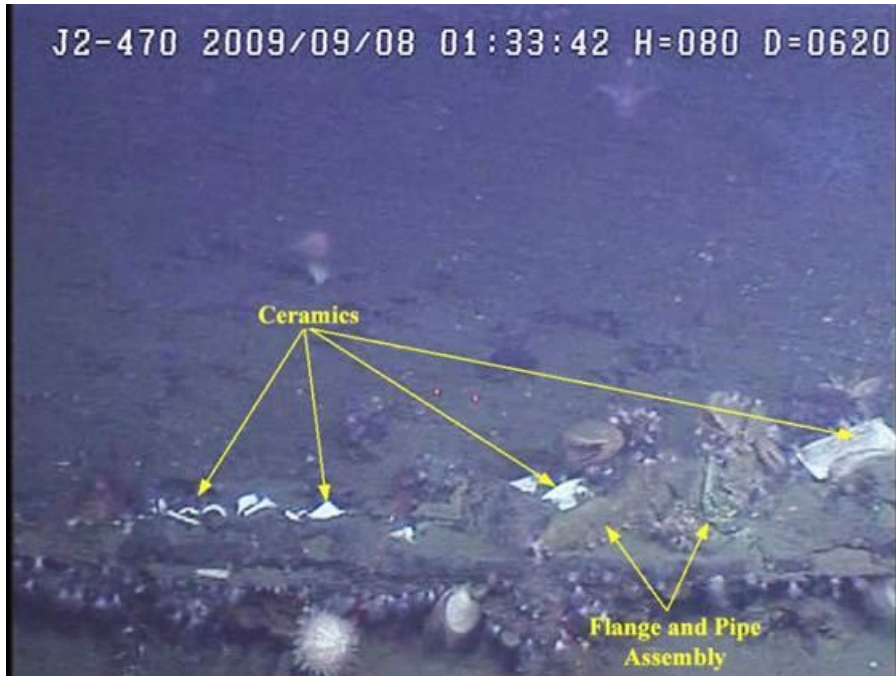
Figure 10-104. ROV video capture image of ceramic concentration at the *Ewing Bank* Wreck's port stern.



Figure 10-105. ROV video capture image of ceramic container and flow blue decorated plate fragmenton the *Ewing Bank* Wreck.

### 10.5.3.5    Recovered Artifacts

Four artifacts—a partial ceramic vessel, a ballast stone, a net sample, and sample of metal sheathing and fastener—were recovered from the *Ewing Bank* Wreck site during the 2009 investigation.  The artifacts were conserved at the UWF Archaeology Institute's conservation lab in Pensacola, Florida and the conservation report can be found in Appendix E-2.

A single ceramic vessel recovered from the port stern interior of the *Ewing Bank* Wreck was only partially intact (Figure 10-106). The recovered portion measures 3.8 in (9.76 cm) in length, 3.8 in (9.76 cm) in diameter, and represents approximately two-thirds of the whole vessel.  It is round in shape, tapers slightly towards its base, and has a cameo-decorated ear or lug handle.  There are no marks indicating the maker or date of manufacture on the cup.
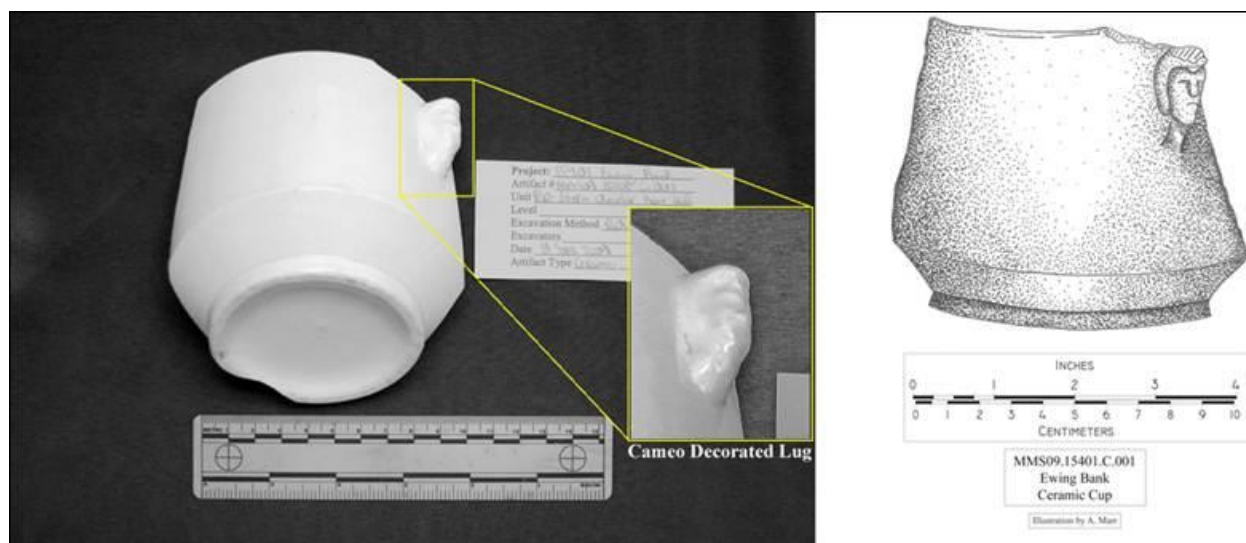


Figure 10-106.  Photograph and drawing of ceramic piece recovered from the *Ewing Bank* Wreck showing cameo design on lug handle (University of West Florida).

The ceramic piece recovered from the *Ewing Bank* Wreck is molded utilitarian white ironstone, often referred to in the vernacular as "hotel ware".  White ironstones were introduced in the 1840s but by the 1870s and 1880s ironstone production was mainly the heavy utilitarian wares.  The shape of the piece indicates a Gothic Period (1850-1870) influence, while the presence of ears or lugs on the sides suggest it may be a sugar bowl or a toilet ware such as a shaving mug (Wetherbee, 1996; Mansberger, 2011).  No maker's mark or date are on the piece, however, the cameo design on the lug handle appears to be a molded decoration known as "Pharaoh Cameo".  The Pharaoh Cameo design (Figure 10-107) was introduced by J & G Meakin in the 1870s and 1880s (White Ironstone Society, 2011), but like most ware designs from the period, may have been copied by other manufacturers.

Figure 10-107. A J & G Meakin "Pharaoh" cameo decorated sugar bowl (Image courtesy of the White Ironstone Society).

One ballast stone sample was recovered from the starboard amidships area of the *Ewing Bank* site for analysis. The ballast stone was bisected to examine the interior (Figure 10-108). The ballast stone is yellowish in color with some darker staining on the portion that was buried in the sediment. An acid test using a hydrochloric acid mixture, carried out at the C&C Houston office, on a section of recovered ballast stone determined it is a calcareous stone most likely limestone. On the interior of the stone are several small cracks with what appears to be crystalline deposits (Figure 10-109). To date, the origin of the ballast has not been determined.
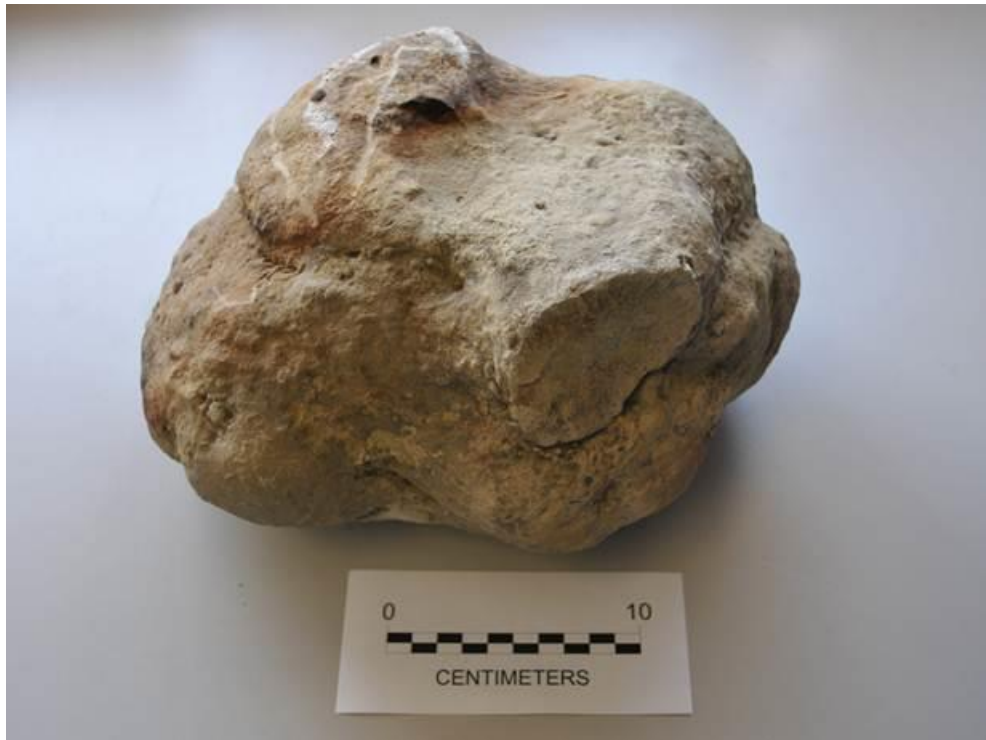
Figure 10-108.  Photograph of ballast stone recovered from *Ewing Bank*
Wreck (University of West Florida).



Figure 10-109.  Photograph showing crystalline structure on interior of
ballast stone from the *Ewing Bank* Wreck.

There is evidence of intrusive anthropogenic material on the *Ewing Bank* Wreck Site. Most of the material is a long line that likely drifted into the wreck. One piece of intrusive material, a section of net, does not appear to have drifted into the wreck. The net, located off the wreck's port stern, is partially covered by a section of hull lying on the seafloor. A piece of this net was recovered during 2009 (Figure 10-110 and Figure 10-111). The net was analyzed at UWF, unfortunately a miscommunication between field personnel led to the net being discarded. The UWF analysis indicated that this is a modern section of netting. The net fragment had a brownish to yellowish brown color and, according to the UWF Conservation report (2011); microscopic examination determined it was made of "modern plastic" material. This suggests a braided monofilament or polypropylene material. It is thought that the net is a remnant of a deepwater trawl net that snagged on a piece of the stern that once extended higher above the seafloor than it does today.
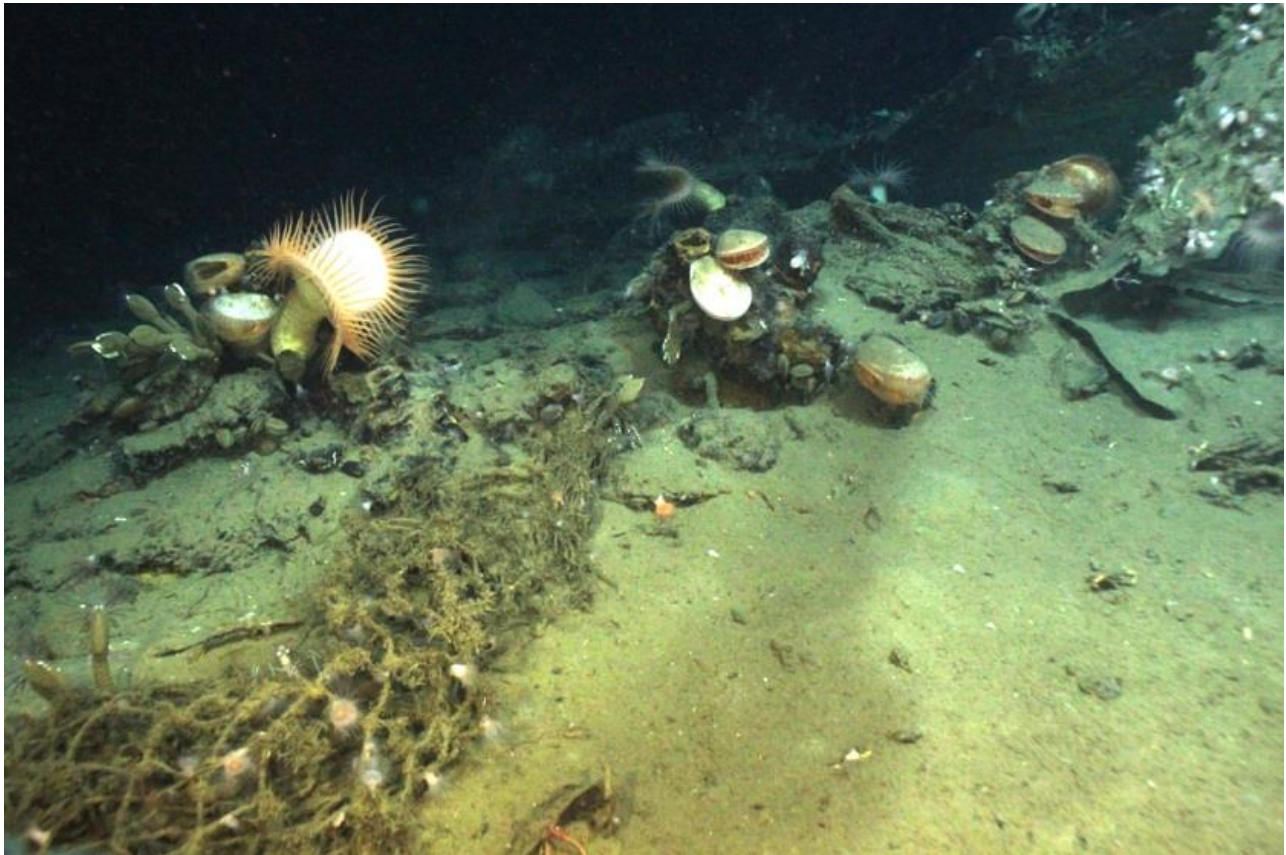


Figure 10-110. Photograph of net in *Ewing Bank* Wreck's stern debris zone (Aquapix Camera Image, *Lophelia* II, 2009: Deepwater Coral Expedition: Rigs, Reefs, and Wrecks).

Figure 10-111. Photograph of net recovered from *Ewing Bank* Wreck (University of West Florida).

The *Ewing Bank* Wreck's hull is sheathed in a cuprous metal. During the 2009 investigation a sample of sheathing including a fastener and wood was recovered near the starboard bow of the wreck (Figure 10-112 and Figure 10-113). The sample underwent conservation and analysis at the UWF Conservation lab. Post-conservation examination of the sheathing confirmed the fastener spacing of 4 in (10 cm) observed on the video, except in the overlap areas where the spacing is approximately 2 in (5 cm) (Figure 10-112). Post-conservation examination of the sheathing also revealed a maker's stamp on the copper (Figure 10-113). The maker's stamp is composed of a large ovoid circle around a smaller ovoid circle. Between the inner and outer circles, the word "MUNTZ" is clearly visible, but the remaining text is undecipherable. The inner circle contains images of 3 crowns with the number "18" beneath them. The presence of the maker's stamp identifies the sheathing as Muntz Metal. This identification was confirmed using a hand-held portable X-Ray Fluorescence device which determined the percentage of metals in the sheathing were consistent with the 60/40 copper-to-zinc ratios used in Muntz metal.
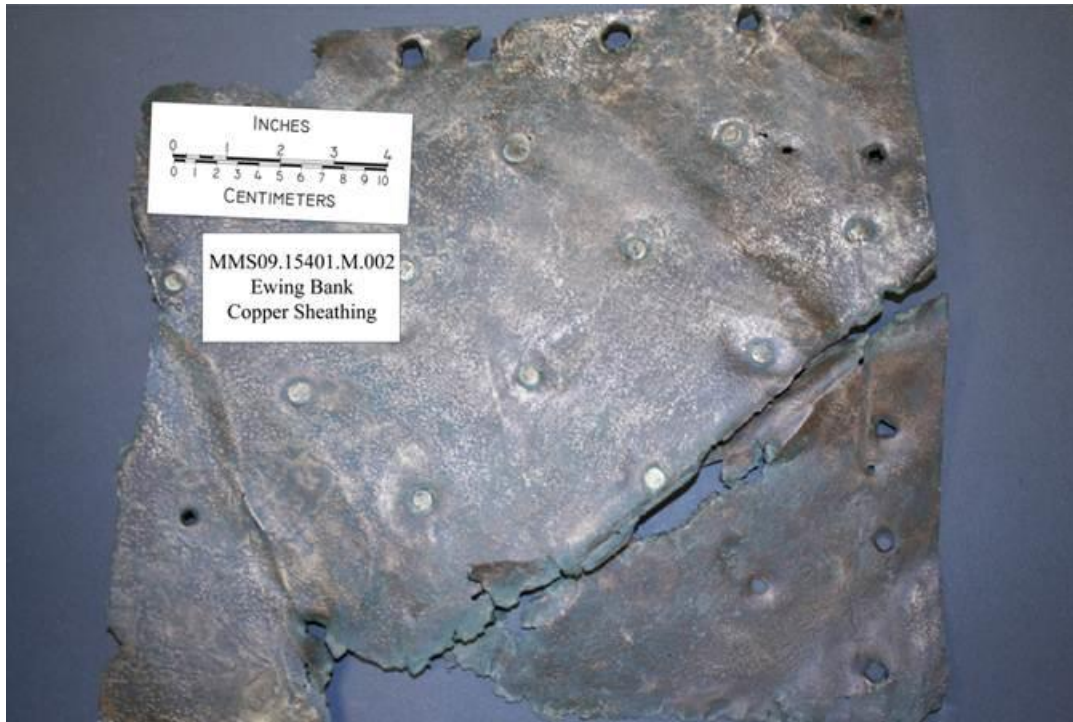
Figure 10-112. Photograph of Muntz Metal sheathing recovered from
*Ewing Bank* Wreck Site (University of West Florida).



Figure 10-113. Close-up of Muntz Metal maker's stamp on sheathing sample
recovered from *Ewing Bank* Wreck (University of West Florida).

### 10.5.3.6      Site Preservation

The wreck site is currently in a low to moderate state of preservation.  The hull is partially intact where it is sheathed from just below the waterline to the keel.  Although the sheathing's anti-biofouling properties have provided some protection to the hull sections that are in direct contact with it, much of the wood structure on the interior highly is degraded and there are no extant hull remains above the copper sheathing. This is consistent with other GoM deep-water discoveries, where remains of wooden hull are present in conjunction with copper sheathing and largely absent above the line of sheathing.  The bow and stern are both partly intact, however, the stern does exhibit some damage, most likely anthropogenic disturbance to the wreck caused by trawling activities.  The vessel is heeled over to port, leaving the outer starboard hull partially exposed down to the turn-of-the-bilge.  Some damage to the copper sheathing was observed on this part of the wreck, but the sheathing appears to be mostly intact.  The port side is partially buried by a berm of sediment that formed after the ship sank.  This berm, which likely contains stratified hull remains, obscures much of the port hull exterior, so an accurate preservation assessment of this section was not possible.  It is likely, however, that this section of the hull, protected by the sediments, remains relatively intact.

In an effort to monitor the wreck's preservation, a short-term etching microbial tester and a long - erm WW-GUCCI platform were deployed at the site to test microbial activity and to monitor deterioration rates.  The etching tester was not left in place long enough for a reaction to occur or provide information on the level of microbial activity at the site.  The WW-GUCCI platform was deployed amidships near a section of pipe along the keelson, and will provide long term indications of site deterioration rates from microbial and chemical deterioration.  Reexamination of the test platform in the future will be invaluable in assessing long-term preservation of the *Ewing Bank* Wreck site.

## 10.5.4 *Green Lantern* Wreck Site

### 10.5.4.1      Historical Background of the Green Lantern Wreck

The *Green Lantern* Wreck Site is the remains of a wooden sailing vessel dating from the late nineteenth to early twentieth century.  Since its discovery in 1996, there have been a deep-tow and an AUV survey of the site, several industry sponsored ROV investigations, and two government sponsored ROV investigations. Archival research has failed to identify the name or nationality of this shipwreck.

### 10.5.4.2      Field Investigations

10.5.4.2.1     Discovery and Exploration

C&C and William & Associates discovered the shipwreck in 1996 while conducting a pipeline survey for BP Exploration Inc.  The survey used a deep-tow AMS 120 Sonar Mapping System, which included 120 kHz side-scan sonar (George 1996). In March 2004, C&C conducted an archaeological, engineering and hazard survey for a proposed pipeline route for GulfTerra Energy Partners, L.P. (GulfTerra) using the C-*Surveyor I* AUV, which imaged the shipwreck.  In September 2004, GulfTerra sponsored the first ROV investigation of the wreck site led by a

professional marine archaeologist. A reconnaissance of the site and surrounding area revealed a copper-clad sailing vessel that appeared to date from the nineteenth century. Several features and artifacts were documented during the ROV survey, including a navigation lantern found lying on the seafloor near the aft starboard side of the wreckage (Figure 10-114). The word "ESTRIBOR," which is Spanish for "starboard," is stamped on the face of the lantern. Thereafter the site was referred to as the *Green Lantern* Wreck in reference to the green/starboard lantern (Church et al 2004).



Figure 10-114. Starboard Signal Lantern near the Stern.

Subsequently, two more oil and gas industry ROV investigations of the site took place in July 2007 and April 2010. These investigations were required by the BOEM/BSEE (MMS at the time) as monitoring efforts associated with infrastructure installation near the area.

### 10.5.4.2.2    *Lophelia* II: Reefs, Rigs, and Wrecks 2008 Field Cruise

A site investigation was planned during the *Lophelia* II: Reefs, Rigs, Wrecks 2008 Field Cruise. Poor visibility and strong current at the seafloor, however, made investigating the site impossible at that time. The 2008 research team deployed an ROV at the site and made visual contact with the stern of the shipwreck. Several attempts were made to fly over the site, but the dive was aborted because of adverse conditions.

### 10.5.4.2.3    *Lophelia* II: Reefs, Rigs, and Wrecks 2009 Field Cruise

In September 2009, an ROV investigation of the *Green Lantern* Wreck was conducted as part of the *Lophelia* II: Reefs, Rigs, and Wrecks Study. Over an approximate 20-hour period (17.5 hours on the wreck site) on September 8 and 9, 2009, the *Lophelia* II team used Woods Hole Oceanographic Institution's *Jason II* ROV launched from the NOAA Research Vessel *Ronald H. Brown* to document the shipwreck site. Visibility on-site was good during the 2009 investigation,

455

equaling or exceeding 8 m. Limited cultural material was collected during the project to help better understand the wreck site.

The 2009 investigation consisted of an initial reconnaissance survey, site mosaic transects, detailed inspection of significant features (both biological and archeological), deploying biological experiments, and artifact collection. The one-and-half hour reconnaissance consisted of a preliminary examination around the full perimeter of the main hull to assess its current condition and to prioritize areas for additional investigation and material collection. The reconnaissance began at the stern and proceeded up the starboard side, moving slowly toward the bow. After an examination of the bow, the ROV moved along the port side towards the stern. The ROV then moved up the centerline of the vessel from stern to bow imaging the interior of the hull.

Following the reconnaissance, 14 parallel track-lines at 1 meter spacing were flown over the main hull taking, a serious of evenly spaced still photographs for mosaic purposes. The digital still camera was mounted in a vertical viewing position and the ROV flown between 4.9 and 5.3 m altitude during transects. Approximately three hours were spent conducting the photo mosaic transects.

Biological operations were conducted over the next six and a half hours, including biological transects, collecting sediment cores, and detailed biological documentation. Three parallel biological transects were run 100 m east of the wreck site. Sediment core samples were collected at distances varying from 100 m away to 10 m from the wreck site. Detailed photographs and measurements were taken of coral and other features of biological interest at various areas of the wreck.

Following the biological investigation, close-up examination was conducted of archaeological features along with the deployment of short-term and long-term microbiological experiments near the starboard bow (approximately 6.5 m aft of the stem). Approximately two hours were allocated for those tasks. The next approximately seven hours included rusticle collection, retrieval of the short-term microbiology experiment, and artifact recovery. Six artifacts were recovered, which are described the artifact recovery section below.

### 10.5.4.3    Geographical Setting

The *Green Lantern* Wreck is in the north-central portion of the Green Canyon area of the GoM (Figure 10-115). The project area is located south-southwest of New Orleans, Louisiana on the upper continental slope. The topography of the region is characterized by diapiric highs and basin-like topography. The seafloor across the site, however, dips southward at a gradient of less than 1 degree.

The geologic setting of the northern GoM is the result of extensive sediment loading and buoyant salt movement. Diapirs, ridges, domes, and anticlines of Mid-Jurassic age (Mann, 1987) underlay the entire Texas-Louisiana slope. Salt intrusions have dramatically influenced the regional geology of the outer shelf and upper slope Gulf Coast areas. Many of these mobile salt bodies protrude through the thick Pleistocene deposits and exist very near the seafloor. These salt bodies have uplifted, deformed, and faulted the overlying deposits and have created bathymetric highs on the seafloor. Authigenic carbonates, which are derived from bacterial reduction of hydrocarbons

escaping through the seafloor, can be found in the deeper portions of the continental shelf and continental slope. The diapiric salt of the upper slope has migrated downslope, evolving into ridges, massifs, and lobes or tongues in the lower slope (Lee et al., 1989).

### 10.5.4.4

### 10.5.4.5    *Discussion of Archaeological Findings*
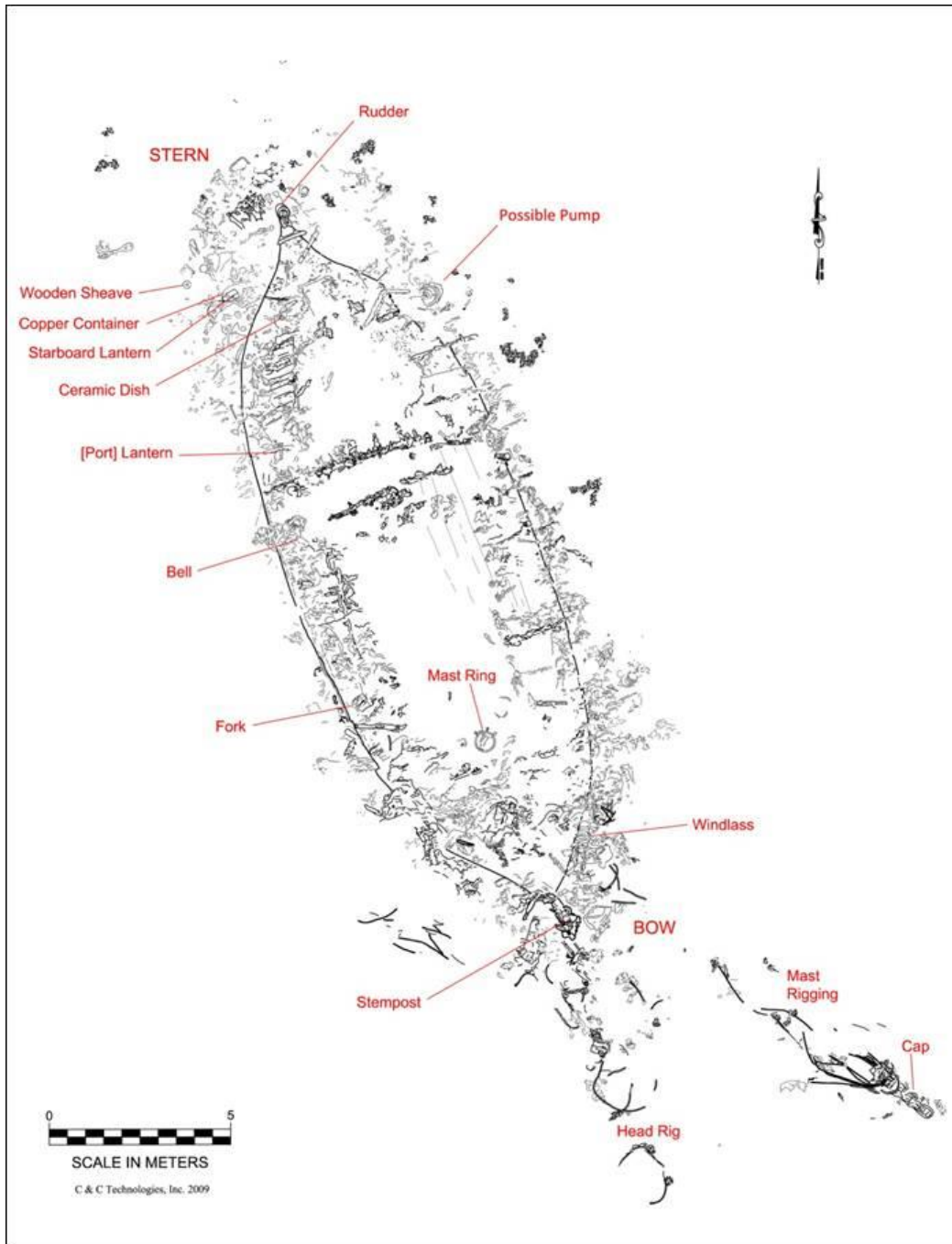


Figure 10-115. *Green Lantern* Wreck Site drawing based on ROV investigations.

## 10.5.4.5.1   Physical Site

The vessel is oriented with the bow pointing southeast and the stern northwest (Figure 10-115). Average water depth at the site is 915 m Below Sea Level (BSL). The vessel measures 69 ft (21 m) length and approximately 23 ft (7 m) in width at beam indicating a 3:1 length-to-beam ratio. Individual artifacts, rigging, and other hull material are scattered out from the hull making the overall measurement of the site 108 × 33 ft (33 × 10 m). A dark -olored glass bottle was documented in 2004 lying approximately 23 m west of the bow (no photograph available). Other than the one bottle, no additional artifacts have been observed away from the main site.

The wreck is sitting on an even keel with 3 to 5 ft (1 to 1.5 m) of relief along the starboard gunwale and 1 meter or less along the port side. Remnants of the double frames are visible along the aft starboard side (Figure 10-116). The exposed frames, at what is believed to be the first and second futtock, have a room and space of 20 in (50 cm) (the room is approximately 11 in (29 cm) and the space is approximately 8 in (21 cm)). The sided dimension of each frame in the pair is from 5.5 to 6 in (14 to 15 cm). The molded dimension could not be measured because of the angle of view and buildup of sediment between the frames.
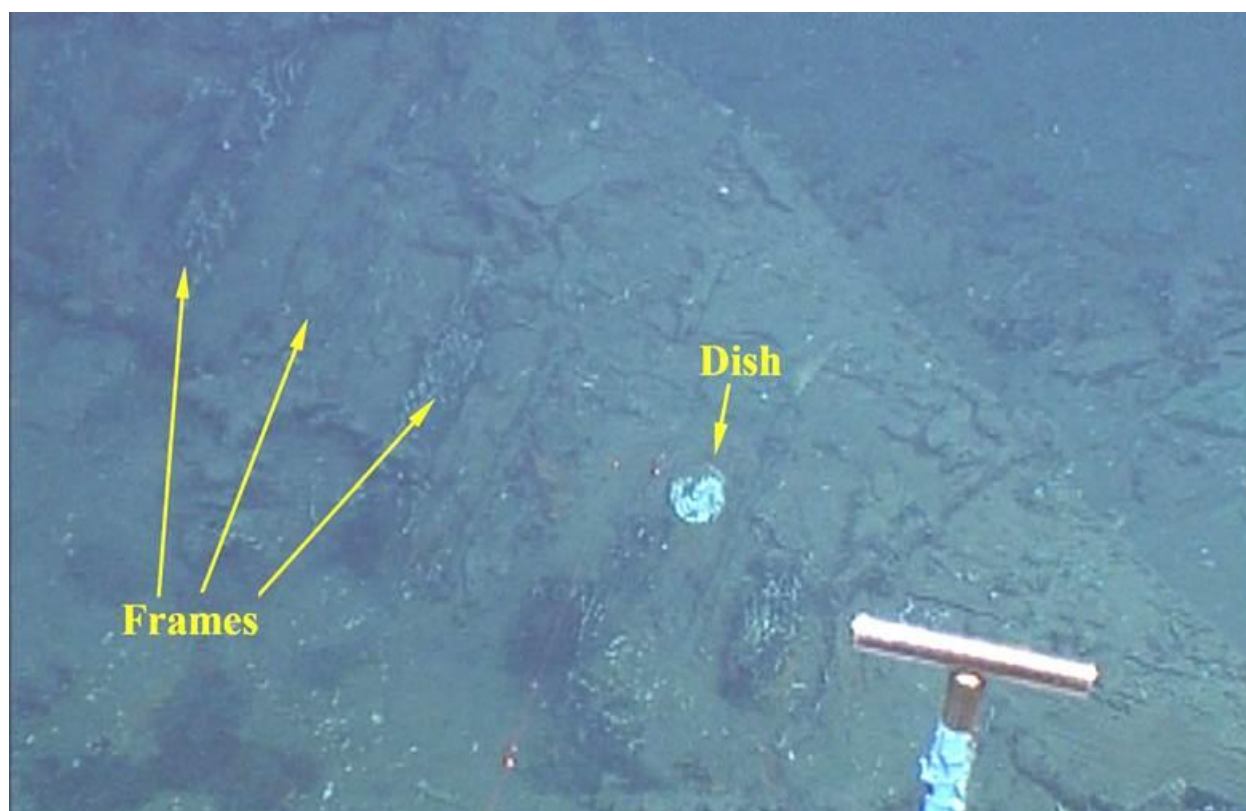


Figure 10-116.  View of aft starboard frames and ceramic dish at the *Green Lantern* Wreck.

## 10.5.4.5.2   Sheathing

The hull is sheathed in copper or a copper alloy such as Muntz metal, but a sheathing sample was not collected for analysis at this site. The sheathing appears to be standard 48×14 inch (121.9 × 35.5 cm) sheets with 1 to 1.5 in (2.5 to 3.8 cm) overlap between sheets. The sheathing is held to

the hull by copper or copper alloy fasteners, which are staggered between rows forming a typical diamond nail pattern. The fasteners spacing is 5.25 in (13.3 cm) between nails horizontally and 3.5 in (8.9 cm) diagonally. Diagonal foiling (buckling) is observed along the copper or copper alloy sheathing, which is typical of copper-sheathed vessels found in deep-water (Figure 10-117). The reason the sheathing becomes buckled is not fully known, but is possibly related to either compression of the wood at depth or the activity of anaerobic bacteria (See Viosca Knoll Site analysis in Section 4.1 and the DBI microbial report in Appendix E-1).
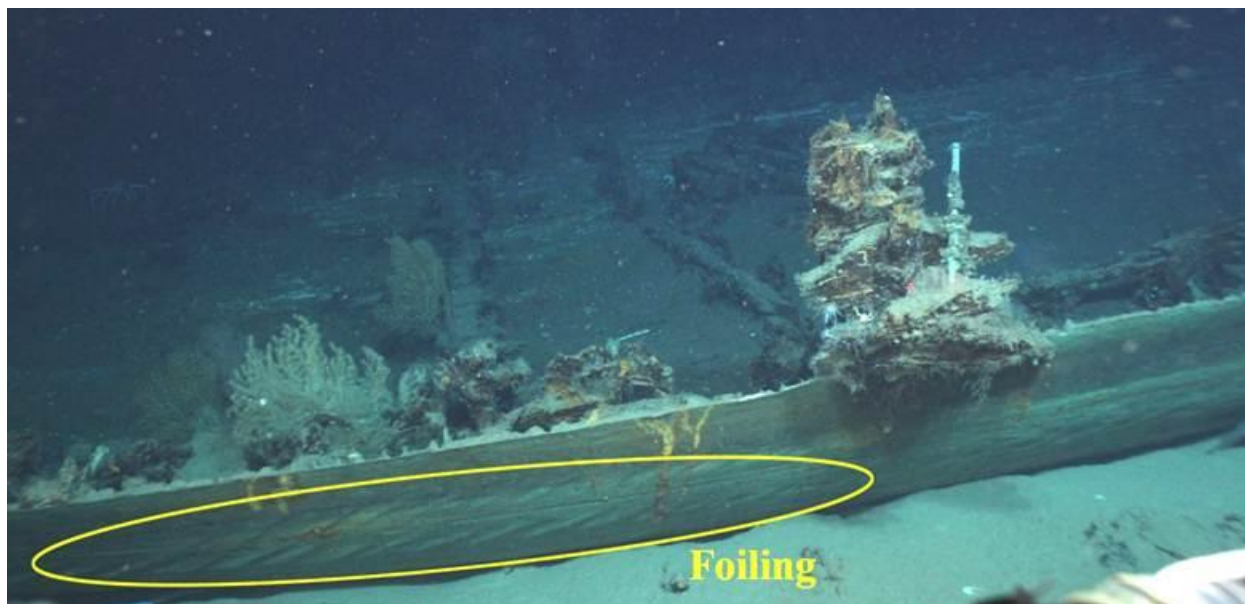


Figure 10-117. Diagonal foiling observed in sheathing (tarboard side) on the *Green Lantern* Wreck.

### 10.5.4.5.3    The Bow

The stempost (remnants of the post and apron) stands approximately 9 ft (2.7 m) proud of the seafloor and 7 ft (2 m) beyond the top edge of the copper sheathing (Figure 10-118). The upper remnants of the stem measure 20 in (50 cm) molded (approximately 22 in (57 cm) just above the sheathing) and 11 in (28 cm) sided (upper and lower). Three bobstays fittings are present. The two lower fittings have four-sided nuts and bolts fastening the hardware together, but the upper fitting has a six-sided nut and bolt, which may represent a repair (Figure 10-119). The gripe or cutwater piece is missing above the bobstays fittings, but two iron drift pins outline where the edge of the gripe would have been. The missing section may also be where the gripe transitioned into the head knee.

Two draft marks are visible on the starboard side of the stem (Figure 10-118 and Figure 10-119). The marks are one foot apart. The lower is the 5-foot mark represented by Roman numeral "V" and the upper is the 6-foot mark represented by Roman numeral "VI." Part of the upper mark is nearly obscured by rusticle growth. The 5-foot mark is approximately 60 cm above the mud line. No draft mark or nail pattern indicating another draft mark are visible below the 5-foot mark.
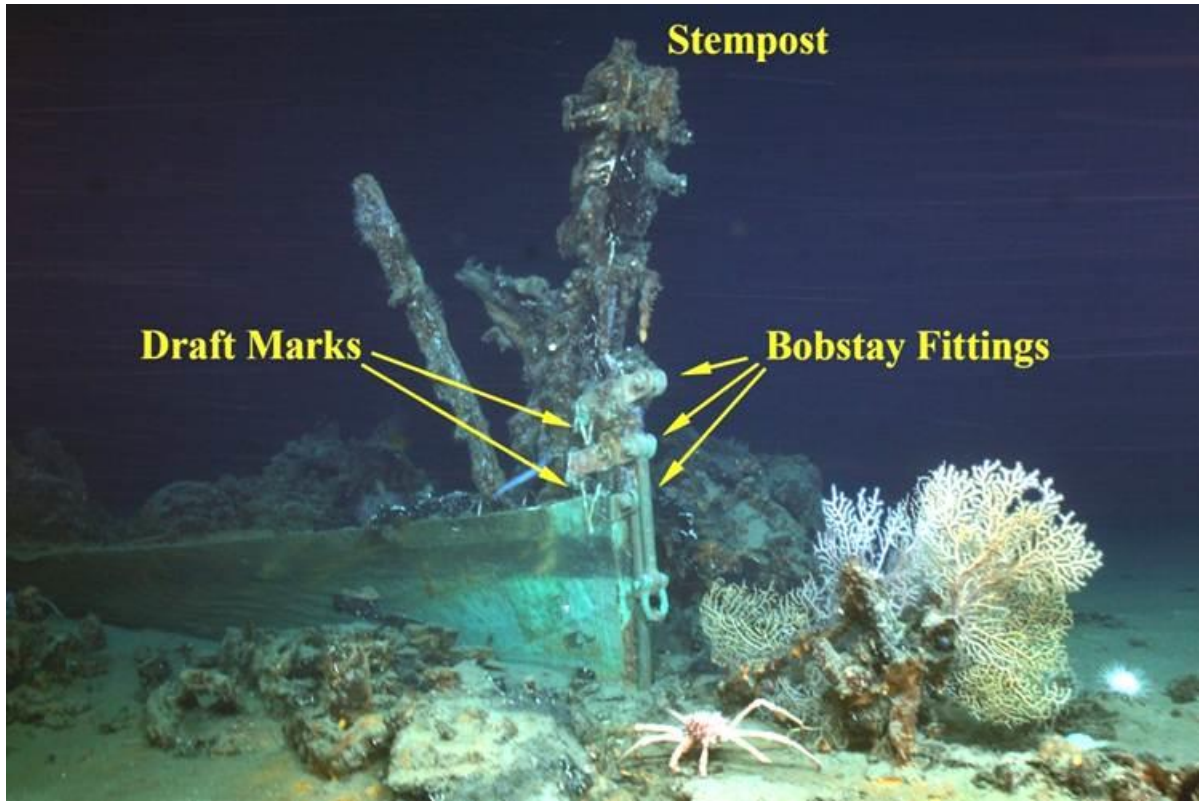
Figure 10-118.  Bow of the *Green Lantern* Wreck (view from starboard side).
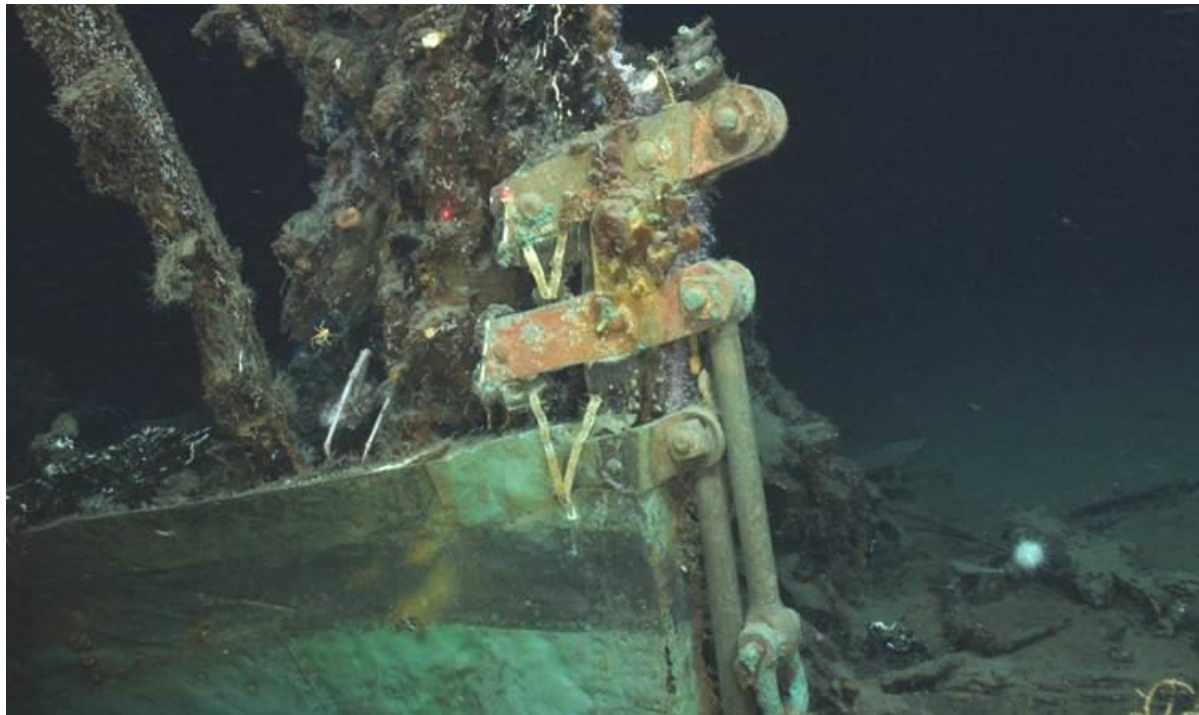


Figure 10-119.  Close-up of bobstay fittings and draft marks on the *Green Lantern* Wreck

The ship's windlass is lying on the seafloor against the port side of the bow (Figure 10-120). It appears to be an iron patent windlass. Portions of the warping ends and driving wheel are visible through the rusticles, other biological growth, and entangled rigging. Chain is visible around the forward edge, which is likely the port side end of the windlass. Chain is also present among the seafloor debris on the starboard side opposite the windlass. The chain links measure approximately 5 in (13 cm) each.



Figure 10-120. Windlass lying to the port bow of the *Green Lantern* Wreck.

## 10.5.4.5.4    Rigging

The head rigging is visible on the seafloor forward of the stem. Visible portions of this rigging extend approximately 8.5 m forward of the bow. Possible gammon irons covered with biofouling are partially visible just forward of the stem. The bow sprit cap is present 4 m from the stem.

Rigging for a single mast is visible to the port side of the head rig. The visible portion of the mast rigging extends approximately 12 m from the hull. The furthest visible portion of the rigging includes the mast cap. This rigging runs across the windlass and back towards a mast rig lying on the hull at midship. The mast ring is located 4.7 m aft of the stem post. The distance from the mast cap to the mast ring is 15 m.

During the initial investigation of the site in 2004, a faint line of shell hash was noted running in a line from the mast cap towards the hull. That line of shell hash likely denoted the location where the mast was laying as it slowly disintegrated or was consumed by microbes and invertebrates. The shell remnants have become obscured by sediment and were not visible during the 2009 investigation.

10.5.4.5.5    Between the Bow and Stern

Most of the port hull and sheathing is flush with the seafloor aft of the windlass. The starboard side, however, exhibits approximately a meter of relief from the bow to the stern. Many of the loose artifacts were observed along the starboard side near the gunwale or lying on the seafloor near the stern, with some material also located on the seafloor near the bow.

A mass of various remains and internal components are present along the starboard side between the stem and mast ring. Most are unidentifiable due to deterioration and biofouling. Some recognizable parts include chain, rigging, and a coil of possible copper tubing (Figure 10-121). Ferrous material is present within these remains, as is evident from reddish-orange rust and rusticle formations. Some of these components could be part of the windlass bitt and anchor chain. Approximately 1 meter aft of this "mass," a single fork was found lying near the starboard gunnel. The fork is one of the artifacts recovered and is discussed in Section 10.5.4.5 and the Artifact Conservation Report (Appendix E-2).
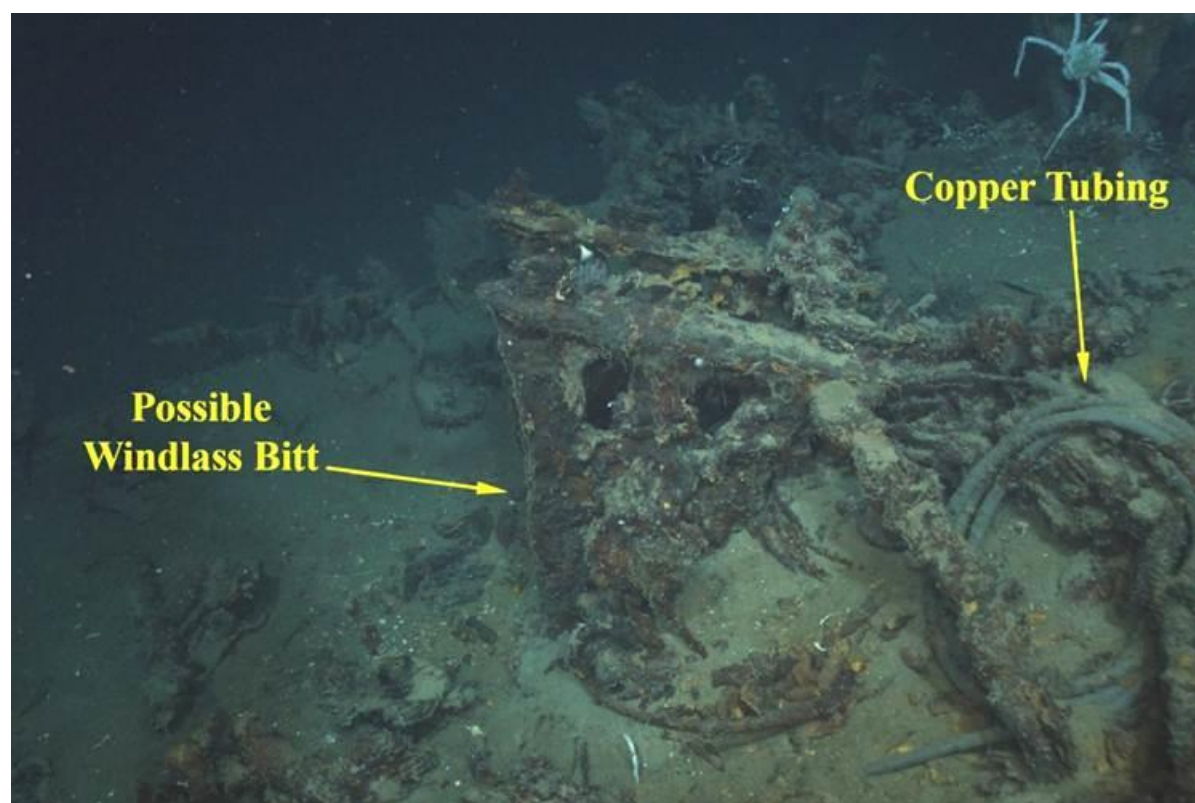


Figure 10-121.  Copper tubing and possible windlass bitt (upside down) at the *Green Lantern* Wreck site.

A bell was located approximate 5.5 m aft of the fork (11.5 m from the bow and 9 m from the stern). It is located 1 meter inboard and partially covered with other material. It is a small bell measuring 6 in (15 cm) in diameter and 6 in (15 cm) tall. The bell is one of the artifacts recovered and is discussed in Section 10.5.4.5 and the Artifact Conservation Report (Appendix E-2). A round sheet of glass stands on end against the hull just outboard of the bell (Figure 10-122). The glass is

approximately 11 in (28 cm) in diameter with at least 4 in (10 cm) extending above the height of the copper sheathing.
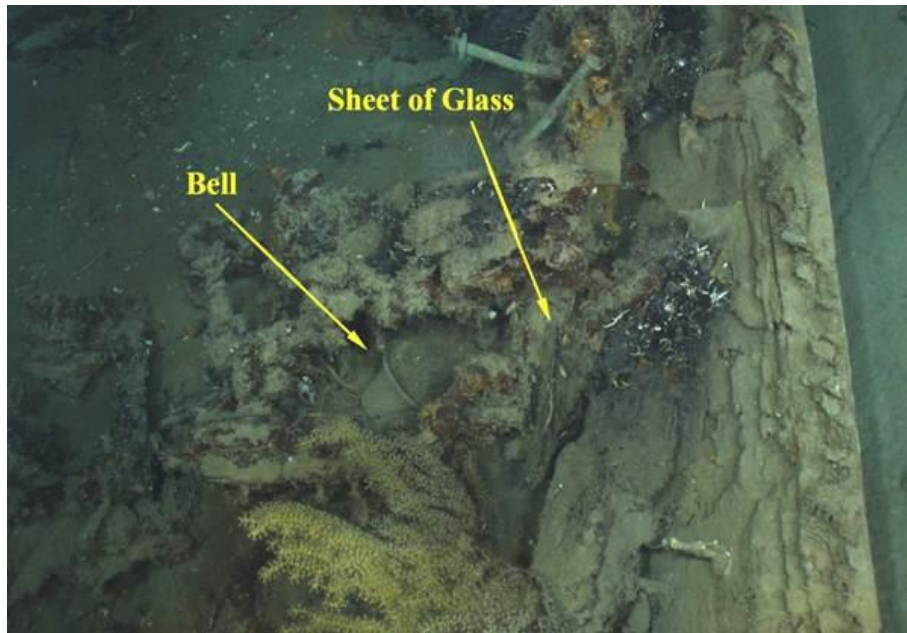


Figure 10-122.  Small bell and round sheet of glass (setting on edge) at the *Green Lantern* Wreck site.

One of the vessel's signal lanterns (Figure 10-123) is located approximately 2.5 m aft of the bell and approximately 6 m forward of the stern.  It is located 0.7 m inboard along the starboard side. This lantern is thought to be the port signal lamp because the starboard lantern is located on the seafloor near the stern (4.5 m away).



Figure 10-123.  Port signal lantern of the *Green Lantern* Wreck.

## 10.5.4.5.6    The Stern

Four frame pairs are exposed near the stern.  As previously mentioned the exposed sections are believed to be at the first and second futtock.  A ceramic dish was located on the starboard side just aft of the exposed frames (Figure 10-116).  The dish was face down approximately 0.7 m inboard and 2.5 m from the sternpost.  The dish is one of the artifacts recovered and is discussed in Section 10.5.4.5 and the Artifact Conservation Report (Appendix E-2).  Directly opposite the dish on the port side, is a 6.5 foot (2 m) section of bent pipe.  It is bent where it crosses the edge of the sheathing.  The possible remains of a bilge pump or other machinery is laying on the seafloor near the end of the pipe and the two appear to be associated (Figure 10-124).  The possible pump head is located at the edge of the gunwale remains, just outside of the sheathing.

The rudder and rudder post are mostly intact.  The majority of the rudder is buried, but the upper gudgeon and pintle is visible (Figure 10-125).  The vessel appears to have been steered by a tiller and the remnants are visible of the hardware that would have attached the tiller to the rudder post.  The sternpost is gone above the copper sheathing.  There is, however, a structural component forward of the sternpost that helps indicate the shape and dimensions of the sternpost.  The molded dimension of the sternpost was approximately 15 in (38 cm) and forward-sided dimension was 18 in (45 cm) with the aft-sided dimension measuring approximately 8 in (20 cm).
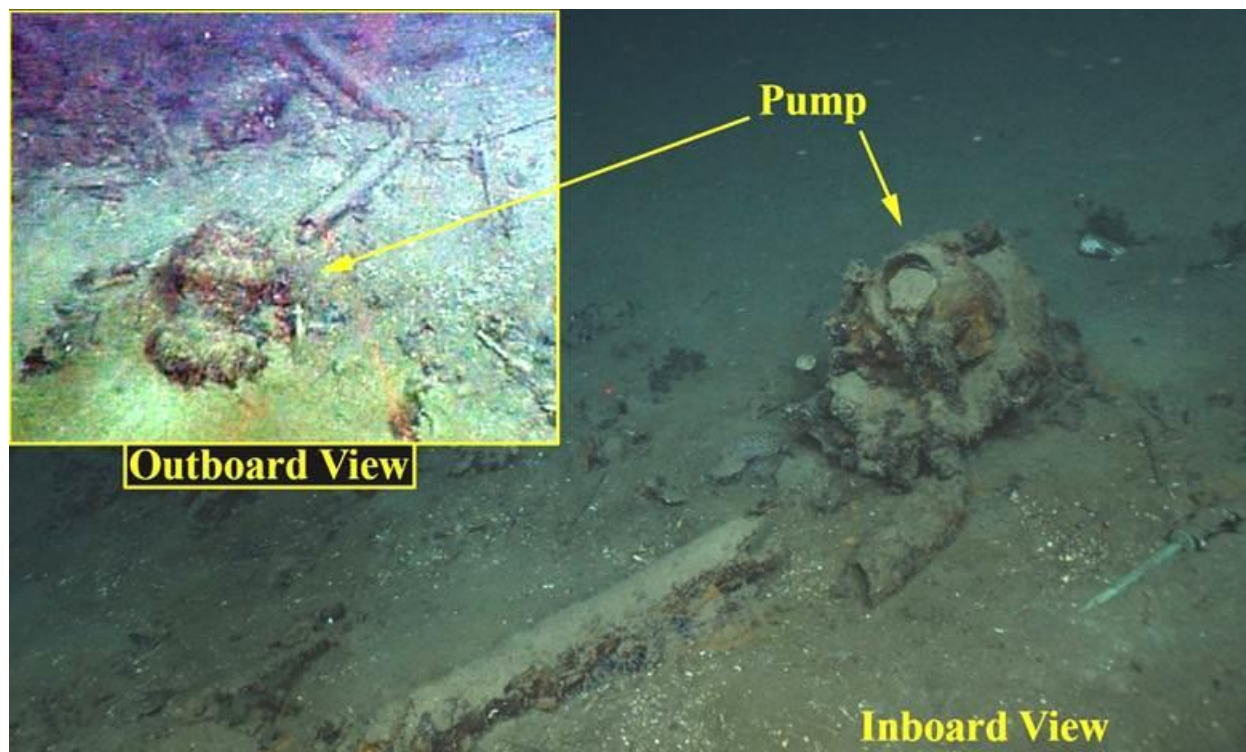


Figure 10-124.  Possible bilge pump and pipe at the *Green Lantern* Wreck site.
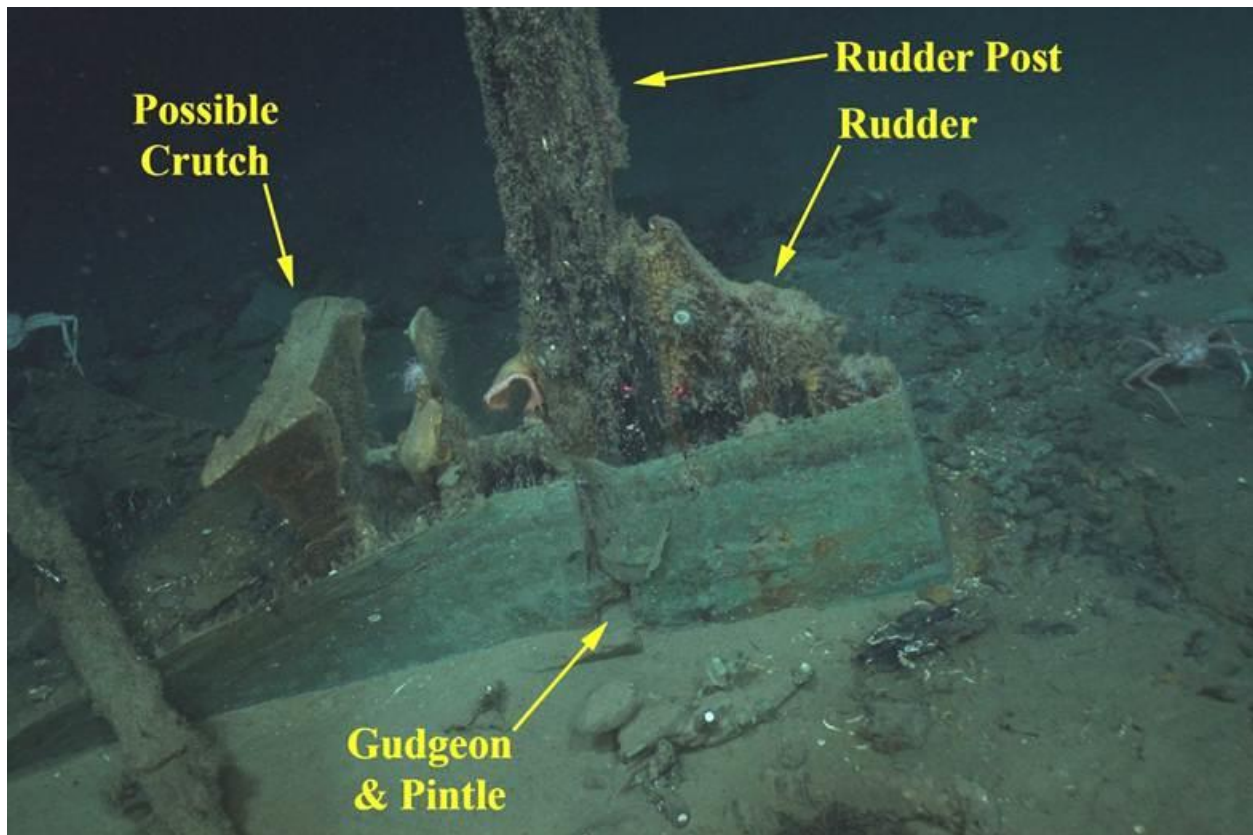
Figure 10-125. Port side view of the rudder, and gudgeon and pintle at the *Green Lantern* Wreck site.

The structural component forward of the sternpost is notably more intact than other structural components of the stern (Figure 10-125). This piece may be metal or of a different wood type than the other parts of the hull, which has allowed it to survive longer. The exact function is not certain, but it can best be described as a crutch. The possible crutch stands approximately 12 in (30 cm) above the copper sheathing. It measures 33 in (84 cm) wide at it widest point and 5 in (12 cm) thick at the middle of the top surface. It is notched to fit around the forward edge of the sternpost and shaped to fit into the port and starboard sides where they begin to come together at the stern similar to a transom piece.

A copious amount of wreck material and individual artifacts are concentrated on the seafloor at the stern, particularly to the starboard side. The various objects include several wooden sheaves, copper or brass drift pins, glassware, the starboard signal lantern, and numerous other unidentified artifacts. Among these items, the starboard lantern, a sheave, and round cap orplug suspected to be associated with the lantern were part of the artifacts recovered. They are discussed in Section 10.5.4.5 and the Artifact Conservation Report (Appendix E-2).

### 10.5.4.6    Recovered Artifacts

Six artifacts were recovered from the *Green Lantern* Wreck site during the 2009 investigation including a bell, wooden sheave, metal fork, ceramic dish, starboard signal lantern, and copper cap or plug.  The artifacts were conserved at the UWF Archaeology Institute's conservation lab in Pensacola, Florida and the conservation report can be found in Appendix E-2.

The bell (Artifact: MMS09.373.C.005) is a small bronze bell measuring 6 in (15 cm) in diameter (Figure 10-126).  There are no discernible maker's marks on the bell.  Likewise, the wooden sheave is a typical block sheave, which measures 8 in (20 cm) in diameter and 13.5 in (34 cm) thick (Figure 10-127).  It was thought that it might be a patent sheave prior to recovery and was only discovered to be an indistinct wooden sheave after recovery.



Figure 10-126.  Bell recovered from the *Green Lantern* Wreck (post-conservation).

Figure 10-127. Wooden sheave recovered from the *Green Lantern* Wreck
(pre-conservation).

The metal fork (Artifact: MMS09.373.M.002) has four prongs and measures 7 in (17.5 cm) long (Figure 10-128). It is made of a metal alloyed composed primarily of copper, zinc, nickel, iron, and tin. "SIM… GEORGE H. ROGERS" is engraved on the back indicating it was made by the Simeon L. & George H. Rogers Co. The Simeon L. & George H. Rogers Co. began manufactured silver flatware in Hartford, Connecticut in 1901. The company was acquired by Wm. A. Rogers Limited in 1918 (Goodwin, et al. 1901; and Silver, 2013).

Figure 10-128.  Fork recovered from the *Green Lantern* Wreck

The small white ceramic dish (Artifact: MMS09.373.C.006) measures 5.5 in (14 cm) in diameter (Figure 10-129).  It bears the makers mark of Wood and Sons Ltd. on the underside.  The mark consists of the Royal Arms with "IRONSTONE CHINA" above and "WOOD AND SON LTD, ENGLAND" below.  Wood and Sons was established as an earthenware manufacturer in Burslem, England in 1865.  The company was incorporated in 1910 as Wood and Sons Ltd. and began using this maker's maker at that time (Perry, 2010).



Figure 10-129.  Ironstone plate recovered from the *Green Lantern* Wreck.

The lantern measures 17 in (43 cm) tall and 9 in (23 cm) wide.  As previously mentioned, the word ""ESTRIBOR," (Spanish for starboard) is written on the lantern's door (Figure 10-130).  The body

468

of the lantern is made primarily of copper. A small "Broad Arrow" made of copper was attached to the body, but became separated during conservation. The lens is made of two sections of green glass. One says "London" and the other says "Miller's Patent."



Figure 10-130. Navigation lantern recovered from the *Green Lantern* Wreck.

The small round cap or plug measures 4.5 in (11.6 cm) in diameter and 1.7 in (4.3 cm) thick (Figure 10-131). It is composed primarily of copper lead and zinc. Originally thought to be a container, it was discovered during conservation that it is not meant to open and possibly serves as some type of plug. It was recovered directly adjacent to the lantern and may be associated.



Figure 10-131. Copper plug from the *Green Lantern* Wreck (post-conservation).

### 10.5.4.7    Site Preservation

The wreck site is currently in a moderate state of preservation.  The hull is partially intact where it is sheathed with copper or Muntz metal.  The sheathing's anti-biofouling properties likely offer some protection to the hull sections in direct contact with it.  This is consistent with other GoM deep-water discoveries, where remnants of the wooden hull are present in conjunction with copper sheathing and largely absent above the line of sheathing.  The bow is partly intact as is the stern.  Based on the draft marks, approximately 4 ft (1.2 m) of the lower hull is buried beneath the sediment.

A short-term etching microbial tester and la ong-term WW-GUCCI platform were deployed just forward of midship along the starboard side to test microbial activity and to monitor deterioration rates (Figure 10-132).  The etching tester deployed at this site was the only shortterm tester left in place long enough for a reaction to occur.  The etching tester remained on the site for 27 hours and revealed a high level of microbial activity.  The preliminary results indicate a high rate of biological determination can be expected at the site.  The WW-GUCCI platform is designed to provide a long-term indication of site deterioration rates from microbial and chemical deterioration.  Reexamination of the test platform in the future will be invaluable in assessing long-term preservation of the *Green Lantern* Wreck site.
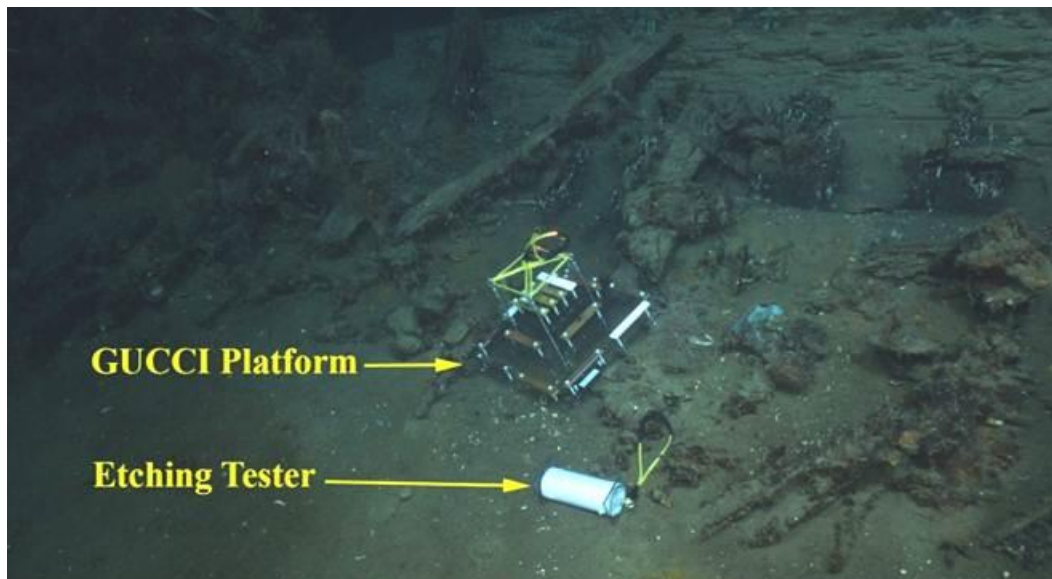


Figure 10-132.  GUCCI Microbial Test Platform deployed along the starboard side of the *Green Lantern* Wreck site.

## 10.5.5 *Gulfoil* wreck site

### 10.5.5.1    Historical Background of the Gulfoil

Built by New York Shipbuilding Company in Camden, New Jersey, *Gulfoil's* keel was laid on February 22, 1912 and was completed on August 29, 1912 (Figure 10-133 and Figure 10-134).  The ship had a length of 406 ft (123.8 m), a breadth of 51 ft (15.5 m), a depth of 30 ft (9.1 m), and

was 5,188 gross tons (New York Shipbuilding Company 1911). Henry G. Morse established The New York Shipbuilding Company in 1900. He chose Camden, New Jersey as the site for his yard because of the availability of good land, its proximity to railroad lines, and a large labor force of experienced shipyard workers. Morse employed a five-principal business plan at the New York Shipbuilding Company. Morse's plan incorporated a mold-lift template system for hull steel, prefabrication of relatively large structural components, the use of overhead cranes to move prefabricated structures, covered ship-building ways and outfitting basins to allow year-round work, and the installation of heavy machinery using overhead cranes before launching (New York Shipbuilding Company 1911).



Figure 10-133. *Gulfoil* circa 1912.(Independence Seaport Museum).

Utilization of these five principles at the New York Shipbuilding Company allowed faster production of all vessel types. The efficiency of Morse's five principled process led New York Shipbuilding Company to become the third largest shipbuilding firm in the world by World War I. By World War II, the New York Shipbuilding Company had built 44 active-duty naval ships and over the course of the war supplied another 26 combat vessels to the United States Navy. To meet increased wartime manufacturing demand, the New York Shipbuilding Company employed 30,000 workers. During World War II, the Camden Yard produced a variety of vessels for the allied forces including three seaplane tenders, two destroyer tenders, eight light cruisers, nine light aircraft carriers, one repair ship, two battle cruisers, and one battleship (New York Shipbuilding 1949). After WWII, the company built a few nuclear submarines, but these efforts were not enough to keep the company financially solvent. In 1967, New York Shipbuilding, unable to compete in the industry, closed for business (Kube-McDowell 2009).
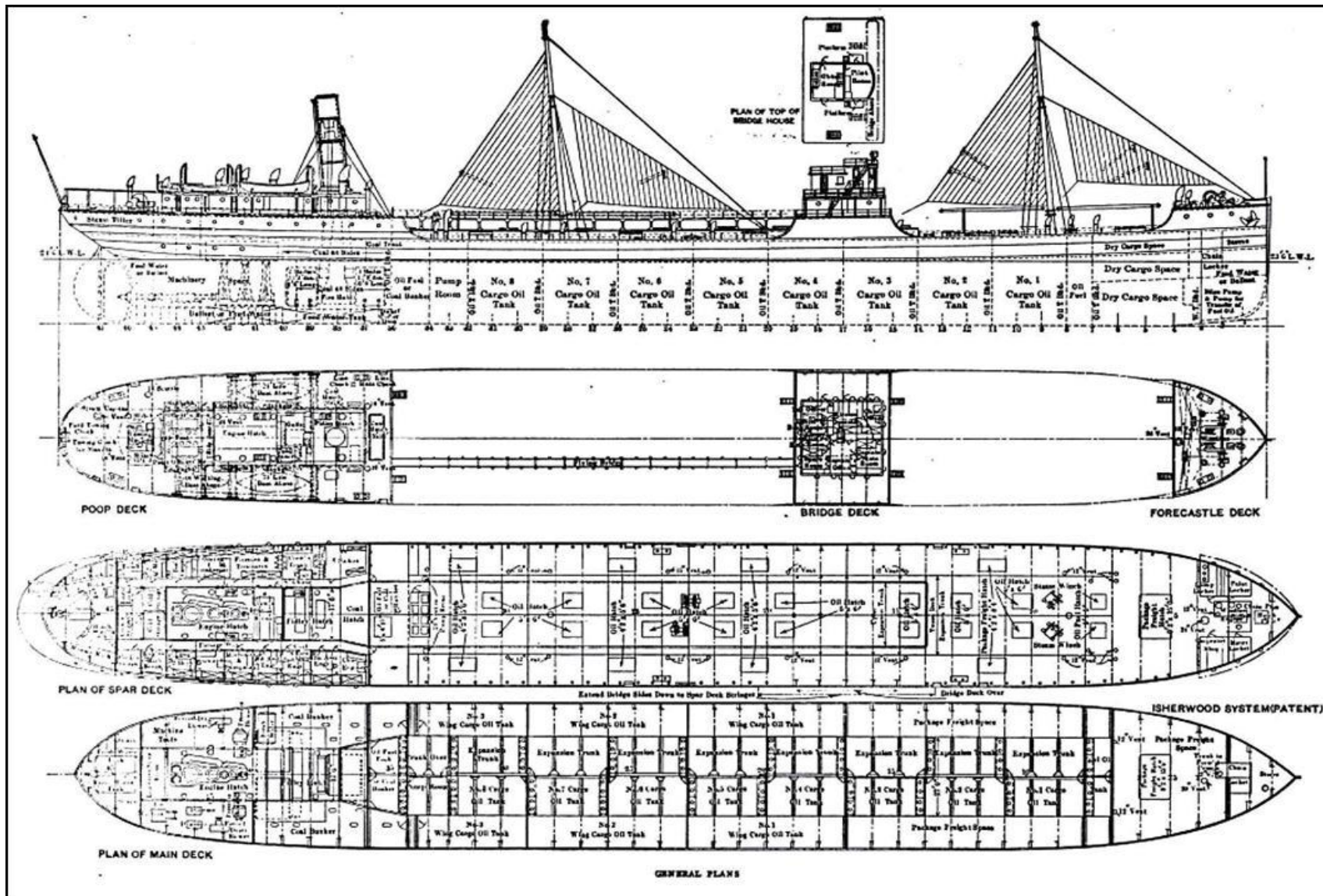
Figure 10-134. Architectural drawing of the *Gulfoil*.(International Marine Engineering 1912).

Among the many ships built by the New York Shipbuilding Company at Camden before World War I, was a series of tankers for the Gulf Oil Corporation. The Gulf Oil Corporation was an expansion of the J. M. Guffey Petroleum Company. It was founded in 1901 after oil was discovered at Spindletop, Texas. Gulf Oil promoted the idea of branded product sales by selling fuel from pumps marked with the distinctive Orange Disk logo. Gulf Oil grew steadily in the inter-war years with the company being characterized by its vertically integrated business activities. The company supported multiple undertakings including exploration, production, transportation, refining, and marketing. One of Gulf's initial visionary steps was the introduction of the first drive-in service station in 1911 (Gulf Oil International 2011; Clark and Odintz 2012 ).

Today, Gulf Oil International (GOI) holds operations in over 70 countries. In the U.S., Gulf Oil is owned by Cumberland Farms Inc, which has licensing agreements with various independent distributors to use the "Gulf" brand to sell oil products (Gulf Oil International 2011).

The ships built for the Gulf Oil Corporation by the New York Shipbuilding Company included the tanker *Gulfoil*. *Gulfoil* was the first American-built oil tanker to incorporate the Isherwood system of ship construction (International Marine Engineering 1912, (Figure 10-135). This method of construction, developed by British naval architect Joseph Isherwood, uses longitudinal framing instead of the traditional transverse framing carried over from wooden ship construction. Isherwood obtained a British patent in 1906 and an American patent on June 11, 1912 (U.S. Patent Office 1912; Groner 1922) for the system of using a series of longitudinal frames in large vessels to prevent buckling (hogging/sagging). The longitudinal frames traverse the length of the vessel bottom, sides, and beneath the decks. They are connected to transverse bulkheads via brackets essentially making the transverse frame a single continuous piece. Isherwood's system creates 70.6 percent more strength at the bilge connection which is constantly subjected to severe stress. (Flodin 1919).
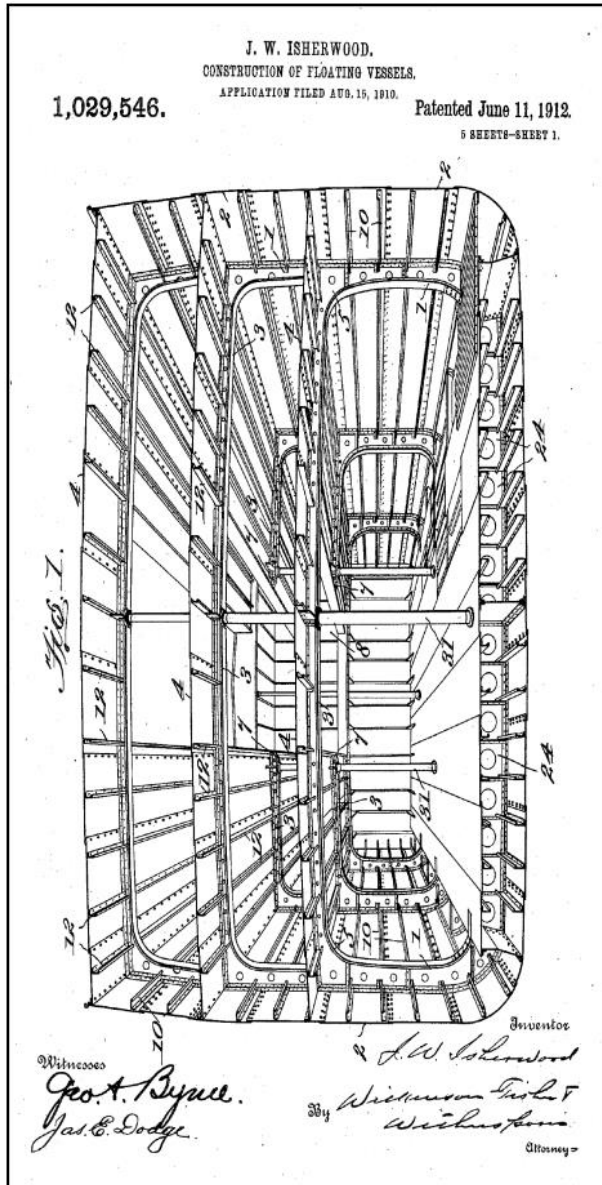
Figure 10-135.  Figure of Isherwood System of Ship
          Construction. (U.S. patent 1,029,546
          1912).

The method of using longitudinal frames has many advantages beyond the added strength.  A ship built on the Isherwood system uses 7 percent less steel than a ship of the same type built using transverse framing.  This 7 percent savings in steel equates to the ship possessing less dead weight which means the longitudinally framed vessel has a greater carrying capacity.  Longitudinal frames allow for more space between transverse bulkheads by fitting the longitudinal frames directly to the decks and hull plating.  This increase in space creates better ventilation and easier below-deck maintenance access.  Longitudinal frames also reduce vibration. The reduction in vibration increases the longevity of the vessel because it reduces friction on connecting parts such as rivets and welds (Flodin 1919).

474

The *Gulfoil* was initially employed to transport refined oil, crude oil, and asphalt from The Gulf Refining Company's docks in Port Arthur, TX to ports along the U.S. Eastern Seaboard. During U.S. involvement in World War I, ship movements were blocked from public record. As a result, *Gulfoil*'s movements from March 13, 1917 until August 24, 1920 have not been located (Fuel Oil 1914, 1915, 1916; Oil and Gas 1917). During the inter-war years, *Gulfoil* was involved in the Mexico oil trade, transporting oil from Tampico, Mexico to Port Arthur, TX (Oil Trade 1918, 1919, 1920). The *Gulfoil's* movements prior to America's entry into World War II have not been located. It is known, however, that *Gulfoil* was en route from Port Arthur to New York when it was sunk by *U-506* (Wiggins 1995).

When Grossadmiral Karl Dönitz sent his U-boats to American waters in the winter of 1942, he tasked several with patrolling the GoM. Among these vessels was *U-506* under the command of Kapitänleutnant Erich Würdemann. Würdemann and his crew were the second U-boat ordered to the GoM (Tent 2003). There were only four U-boats operating in the GoM in May 1942. Those four U-boats however, sank 41 ship,s equaling 220,000 tons of lost cargo. These sinkings were an all-time high (until June 1942) for U-boat operations anywhere in the world. On average, seventy-five merchant vessels operated in the GoM at any given time. This sinking rate equates to the average life span of a ship in the GoM in 1942, being less than two months (Sternhell and Thorndike 1946).

At 2200 hrs. on May 16, 1942, *U-506* spotted a fully loaded tanker, *Gulfoil*, traveling on a course of 110 degrees in the GoM. Seizing the opportunity to inflict damage to allied shipping, *U-506* launched torpedoes from tubes two and three. It took only 34 seconds for the torpedoes to travel 634 m before impacting the starboard side of *Gulfoil.* The first torpedo is reported to have struck amidships and the second torpedo struck the engine room. The mate on watch in *Gulfoil's* wheelhouse at the time of the attack reported the first torpedo struck near tank No. 4. And the second torpedo struck the engine room 15 seconds later, killing three men. The first impact caused the vessel to list 40 degrees before the second impact partially righted the vessel. The ship sank stern first with a heavy list so rapidly that the crew did not have time to launch the life boats. *Gulfoil* sank in approximately 2 minutes with only 19 of the 40 crewman surviving (Würdemann 1942; Wiggins 1995; Browning 1996).

### 10.5.5.2    Field Investigations

#### 10.5.5.2.1    Discovery and Exploration

The site was first discovered in September 2005, when Diamond Offshore Drilling, Inc. contracted Oceaneering International, Inc. to conduct sonar and ROV video documentation of approximately 670.6 m of 20-inch pipe lost from the *Ocean Voyager* oil rig during hurricane Katrina. During the investigation, sonar revealed a potential shipwreck. In October 2005, Fugro Chance Inc. conducted a geophysical survey of the area, which produced another image of the shipwreck. Fugro Chance notified the MMS and provided a data reproduction of the side-scan sonar image of the vessel. No further investigation was conducted until the first leg of the 2008 *Lophelia* II Study.

## 10.5.5.2.2 *Lophelia* II: Reefs, Rigs, and Wrecks 2008 Field Cruise

A reconnaissance survey was carried out on the site suspected to be *Gulfoil* on September 15, 2008 during the *Lophelia* II study using the *Falcon SeaEye* ROV launched from the NOAA Research Vessel *Nancy Foster*.

The ROV was in the water and nearing bottom, when a generator on the *Nancy Foster* broke down, sending the vessel adrift.  Once propulsion was regained, the *Nancy Foster* was back on location and the ROV launched within an hour.  Strong subsurface currents and low visibility, a result of Hurricane Ike, hampered operations and resulted in the loss of the microbial experiment intend to be placed on the wreck site. The ROV reached the wreck in approximately half an hour and began the reconnaissance survey.  Despite conditions, the ROV successfully surveyed a portion of the wreck's port side for an hour.  Although the wreck was covered with colonies of *Lophelia* corals, it was positively identified by the word "*Gulfoil*" emblazoned on the stern. Continuing equipment issues and poor site conditions allowed only 48 m of the port hull to be investigated  (deck level from the stern to just forward of the after cabin) before the dive was terminated when the ROV lost power.

## 10.5.5.2.3 *C-Surveyor III* 2009 AUV Survey

Field investigations at the *Gulfoil* were not undertaken in 2009 as part of the *Lophelia* II study; however, C & C Technologies, Inc., conducedt an AUV survey of the shipwreck in May 2009. This AUV investigation was part of an equipment upgrade test comparing the AUV's 230 kHz dynamically focused and 410 kHz side-scan sonar systems on C&C's *C-Surveyor III* AUV. During this survey, *C-Surveyor III* ran eight transects over *Gulfoil* at 75-m line spacing to image the main hull wreckage and associated debris fields. The sonar images revealed the vessel to be mostly intact with a debris trail extending approximately 230 m to the south and a separate debris field approximately 300 m west of the site (Figure 10-136).
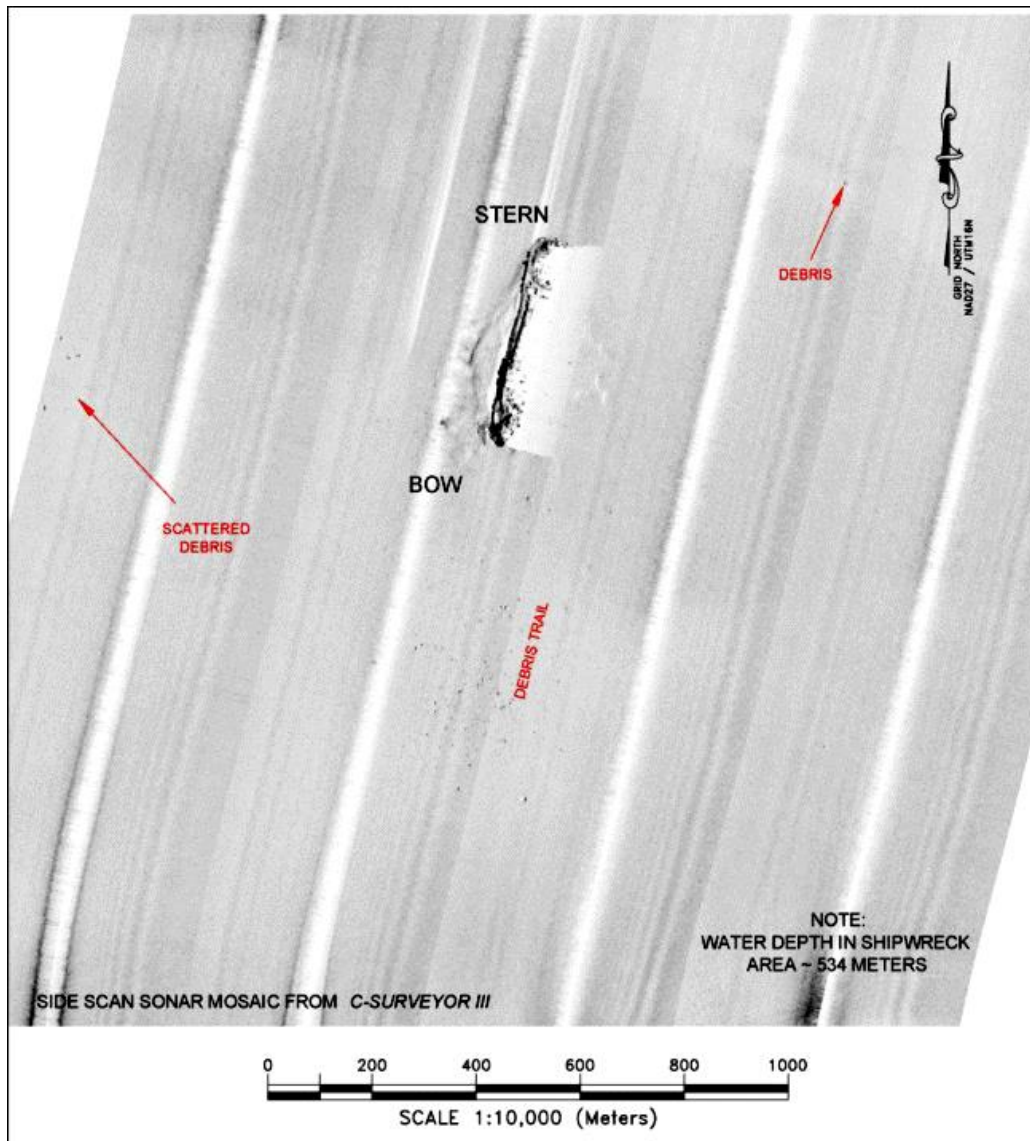
Figure 10-136. 2009 Side scan sonar mosaic of the *Gulfoil* site (C & C Technologies, Inc.).

### 10.5.5.2.4    *Lophelia* II: Reefs, Rigs, and Wrecks 2010 Field Cruise

A second ROV investigation of *Gulfoil* occurred on October 27 and 28, 2010, from the NOAA Research Vessel *Ronald H. Brown*. The ROV *Jason II* from the Woods Hole Oceanographic Institution took high-definition video and photographs, as well as biological samples. The 2010 investigation began at a debris field to the west of the wreck site. Investigations over a 1.5 hour period confirmed the debris field wreckage was related to the sunken tanker. The ROV then transited to the wreck site and approached the starboard side of *Gulfoil's* bow. From this point, they worked their way around the bow and began moving aft along the port side. The ROV then returned to the bow and began investigating the wreck from top to bottom along the starboard side to the port stern. The ROV remained on site for approximately 19 hours conducting archaeological and biological investigations.

### 10.5.5.3    Geographical Setting

*Gulfoil* is located in the northern GoM in the western portion of the Mississippi Canyon area. The site is south of the Mississippi River's mouth along the northern edge of the Upper Mississippi Fan. The wreck site rests on the canyon's western slope and is likely influenced by material flowing down the canyon. The seafloor in this region gently slopes toward the south, with local variations.

### 10.5.5.4    Discussion of Archaeological findings

#### 10.5.5.4.1    Physical Site

The following description is compiled from data collected during the 2008 and 2010 *Lophelia* II field expeditions and the 2009 C&C AUV tests. Visibility at the site was approximately 10 m during both ROV investigations. The *Gulfoil* lies upright on the seafloor with the bow down slope. The wreck is oriented with the bow pointing south-southwest and stern north-northeast. Water depth at the site is approximately 534 m BSL. The wreck has a relief of approximately 16.8 m above the seabed.

Three primary components characterize the *Gulfoil* site: the main hull with bow pointing south-southwest, a debris trail extending 230 m south-southwestward from the hull, and separate debris field approximately 300 m to the west of the hull. The debris areas contain miscellaneous ship components. Debris in the western debris field includes items such as ventilator hoods, deck grating from the engine or boiler rooms, and unidentifiable debris. The builder's specifications list the only areas on the ship to utilize removable deck grating as the engine and boiler rooms. Removable deck grating allows easy access to engine and boiler components for maintenance purposes. Figure 10-137 displays deck grating from the debris field with deck grating from the liberty ship Jeremiah O'Brian. The presence of the deck grating in the western debris field is significant because it correlates with the location the second torpedo struck the engine room.



Figure 10-137.  Deck grating from *Gulfoil* (left) and deck grating from Jeremiah O'Brien (right) (*Jason II* ROV camera; William M. Briggs, 1012).

Overall, the site appears relatively intact. The ship is resting with a slight list to starboard. The superstructure is almost entirely obscured by abundant coral formations. These coral formations cover almost every part of the vessel that extends from the main deck into the water column.

The ship's bow displays a large hull buckle in the middle of the cutwater (Figure 10-138). This damage appears to be caused by the ship's impact with the seafloor. The folding of steel plates and beams in what is one of the most structurally sound areas of a vessel may indicate the force with which the ship struck the seafloor or it could be evidence of a previously undocumented mishap in the ship's life. The ship's bow anchors are still in the stowed position with their chains leading to the intact windless. Portions of the masts and cargo booms lay on the main deck roughly pointing bow-to-stern next to their cargo winches.
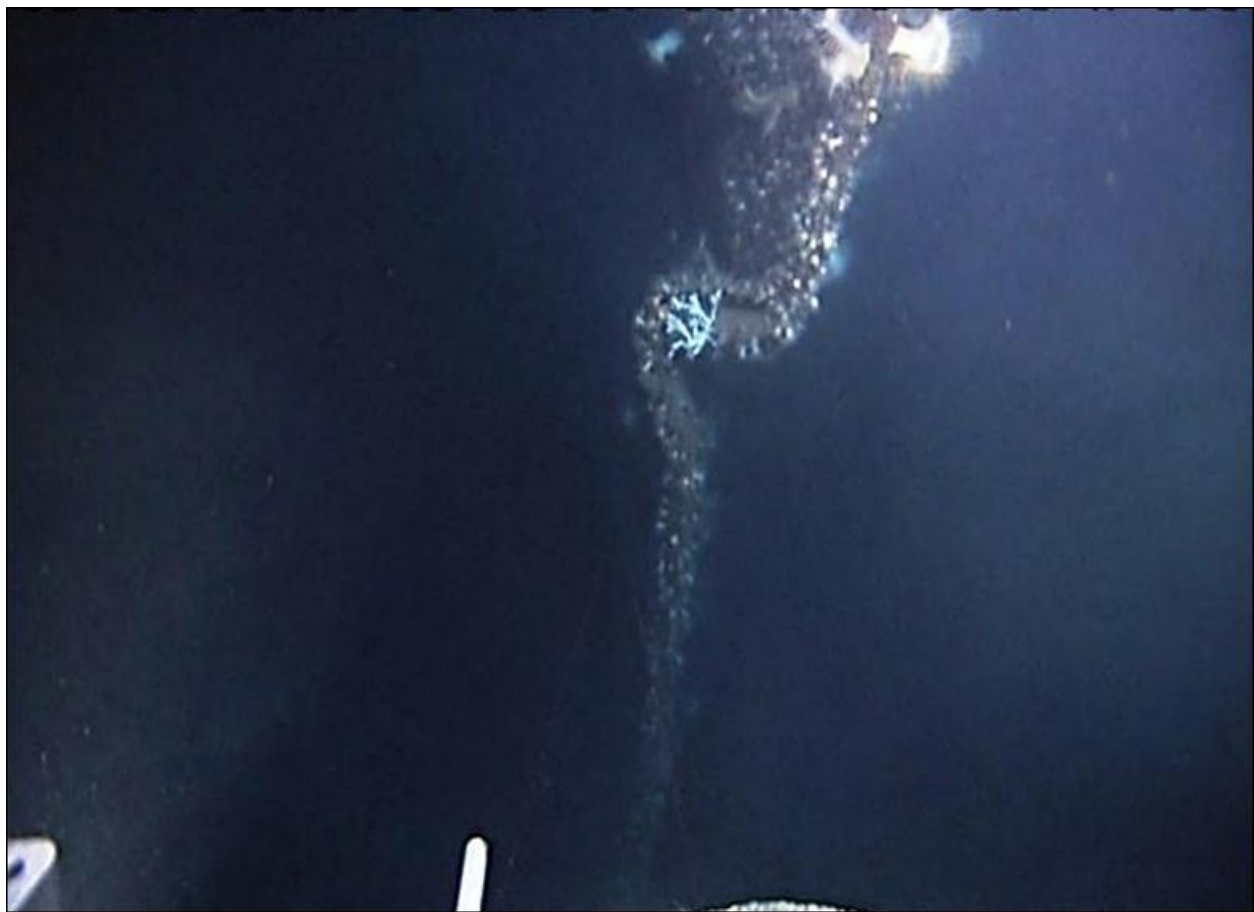


Figure 10-138. Buckle in bow of the *Gulfoil*.

Forward of the wheelhouse, in the oil fuel and dry cargo storage areas on the starboard side of the hull, is a large hole with an accompanying gash extending from just above the waterline to below the mud line and from just aft of the forecastle nearly to the wheel house (Figure 10-139). The hull plating in the area of the hole is bent inwards and the cargo hatches and some of the deck plating above this damage are bent upwards almost in half, indicating a violent explosion (

Figure 10-140).  This damage contradicts historic accounts from the crews of *Gulfoil* and *U-506* identification of the first torpedo impact (Würdemann 1942; Wiggins 1995; and browning 1996).
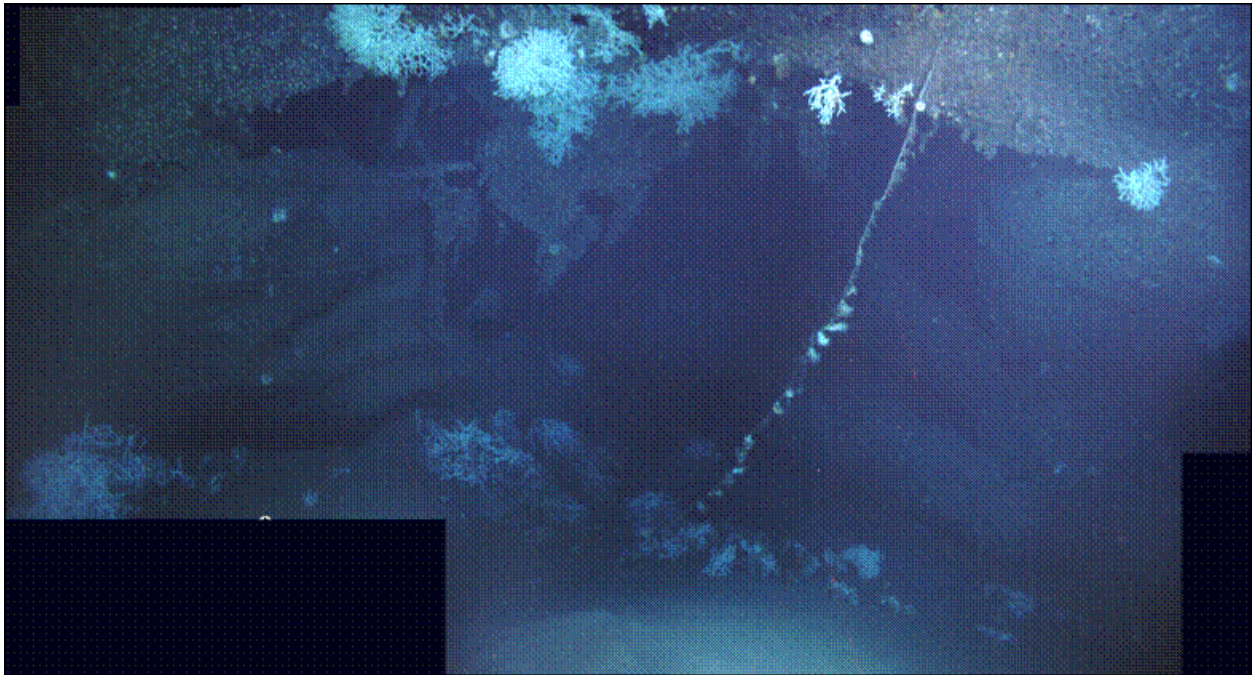


Figure 10-139.  Forward hull damage in the *Guloil* (C&C Photo mosaic).

Figure 10-140.  Deck plate/cargo hatches from the *Gulfoil* associated with hull damage.

The stack with ship's whistle still attached is located on the seafloor adjacent to the forward structural damage (Figure 10-141).  The stack was originally located on the stern of the vessel extending above the after cabin.  Its presence on the seafloor near the bow of the ship indicates that the stack may have come loose as *Gulfoil* plunged stern-first through the water column.



Figure 10-141.  *Gulfoil's* stack and ship's whistle.

The wheelhouse is almost entirely covered in the deep-water coral *Lophelia pertusa* (Figure 10-142). The architecture seems to be intact, with ladders still present on the weather decks. The hull in this area appears structurally sound with no sign of torpedo damage near starboard Tank 4, where the first torpedo is reported to have struck.
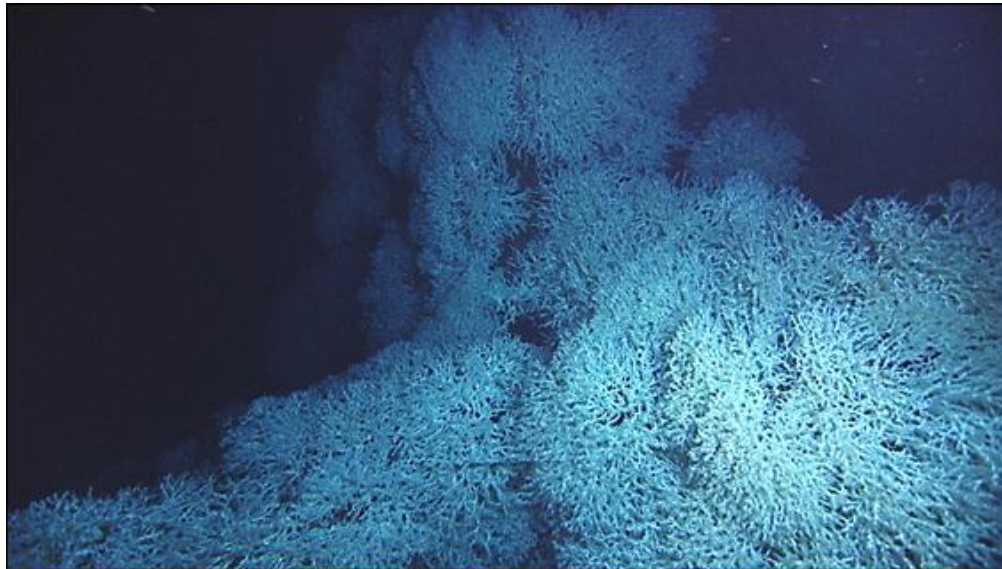


Figure 10-142. Wheelhouse coral growth on the *Gulfoil*.

The amidships area is relatively intact, with abundant coral growth covering the catwalk, main deck structures and entire after cabin. An ammunition box with shell casings for the ship's 4-inch naval gun rests on the port side deck near the after cabin (Figure 10-143).
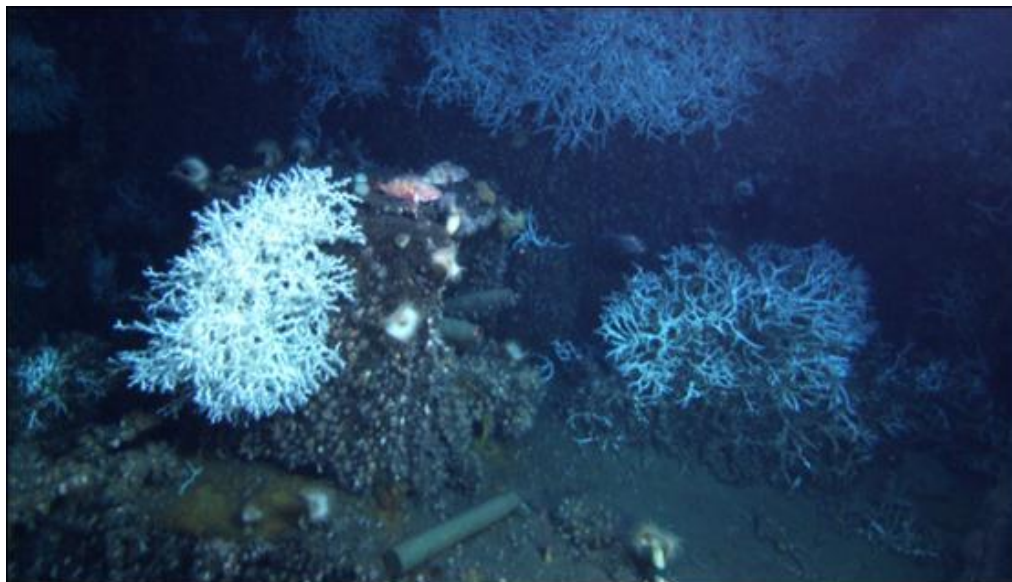


Figure 10-143. Ammunition box with shell casings on the *Gulfoil*.

The location of where the second torpedo struck the starboard side is visible beneath the after cabin from the main deck to below the mud line (Figure 10-144). One of *Gulfoil's* three Scotch boilers is visible through the after portion of the hole. This damage is consistent with historic reports that state the second torpedo struck the engine room causing the vessel to sink stern-first at a very rapid rate (Würdemann 1942; Wiggins 1995; Browning 1996). Interestingly, there is still glass present in the portholes just above this area.



Figure 10-144. Hole from the second torpedo.

Visible on the fantail is the auxiliary steering helm which stands in its original position near the aft bulkhead of the after cabin with no coral growth and the ship's defensive 4-inch gun, which is covered in coral (Figure 10-145). The vessel's name is still visible across the stern in raised letters (Figure 10-146).
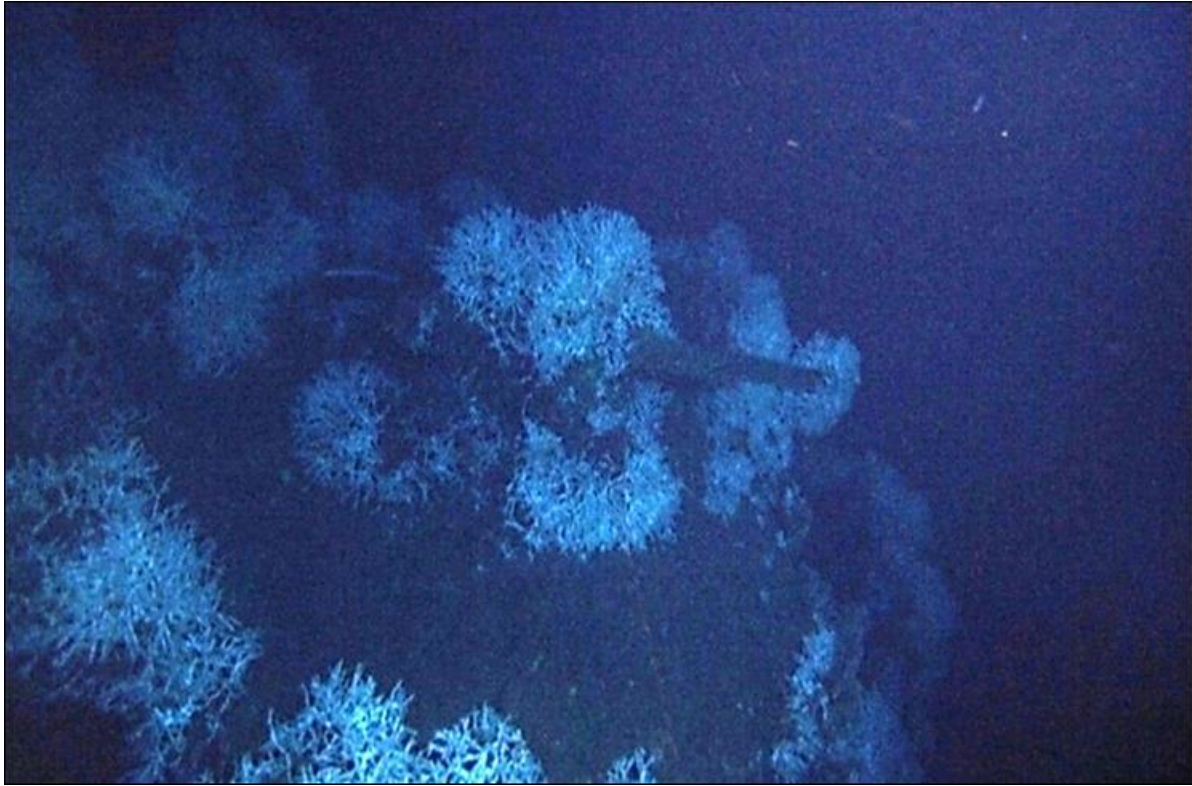
Figure 10-145. *Gulfoil's* 4-inch gun with auxiliary steering on the left side of the photo.



Figure 10-146. *Gulfoil*'s transom with a portion of the name visible.

### 10.5.5.5 Site Formation and Distribution

The features observed during the investigation, combined with the historical record provide clues to understanding the *Gulfoil* site formation processes and a possible sinking scenario. The logs of *U-506* state that the *Gulfoil* was on a heading of 110 degrees at the time of the attack. *U-506* fired two torpedoes, which hit the tanker 15 seconds apart. Survivor accounts indicate that *Gulfoil* sank in approximately 2 minutes after the attack (Würdemann 1942; Wiggins 1995; Browning 1996). The tanker now sits on the seafloor on a heading of 193 degrees with a debris trail extending 230 meters toward the south-southwest.

In 2007, a Debris Distribution Model was developed based on data from deep-water World War II wreck sites as part of the *Archaeological and Biological Analysis of World War II Shipwrecks in the Gulf of Mexico* (OCS Study MMS 2007-015). The distribution formula was conceived as a preliminary first step in developing a predictive model for shipwreck site distribution in deep-water. As such, it was based on a small sample of World War II era ships that met with catastrophic ends. The Distribution Model provides a method to estimate the potential distance debris will spread out as a steel hull vessel sinks with regards to water depth (Church et al. 2009). The formula for that distribution is 20 percent of water depth plus the length of the hull and is listed below. Comparing the *Gulfoil* site with other wreck sites using the Deep Wrecks Debris Distribution Model shows that a vessel the size of *Gulfoil* at the site depth of 534 m BSL could have an artifact distribution of 231 m extending from the main hull of the wreckage.

$$0.20wd + vl \geq \text{site boundary}$$

Where:  wd = water depth
vl = vessel length

This estimate corresponds to the length of the debris trail associated with *Gulfoil* extending to the south-southwest of the main hull, but fails to account for the separate debris field to the west. It was initially hypothesized during the field investigation that these two debris fields represented the two separate torpedo impacts. Further examination of the geophysical data showed, however, that the center of the western debris field is over 300 m from the end of the debris trail. Based on available historical records, *Gulfoil* was traveling at 11 knots (11 knots equals 5.6589 m/second) when the torpedoes struck the ship. The torpedoes hit 15 seconds apart and at that speed, *Gulfoil* could not have traveled more than 85 m ($15 \times 5.689$) between the first and second torpedo strikes.

The assessment of data further shows that the near-parallel paths of both torpedoes would have been much closer together than 85 m. The first torpedo hit near the bridge and the second torpedo exploded in the engine room. The distance along the ship from the first to the second hit location is approximately 80 m apart. With the tanker moving forward at 11 knots and covering a distance of 85 m, the spatial separation between the two torpedoe's parallel paths just prior to impact would have been only 5 m (Figure 10-147). The data shows, with a high degree of certainty, that the observed artifact scatter to the west of the main wreck site represents the location of both torpedo impacts on the *Gulfoil*.
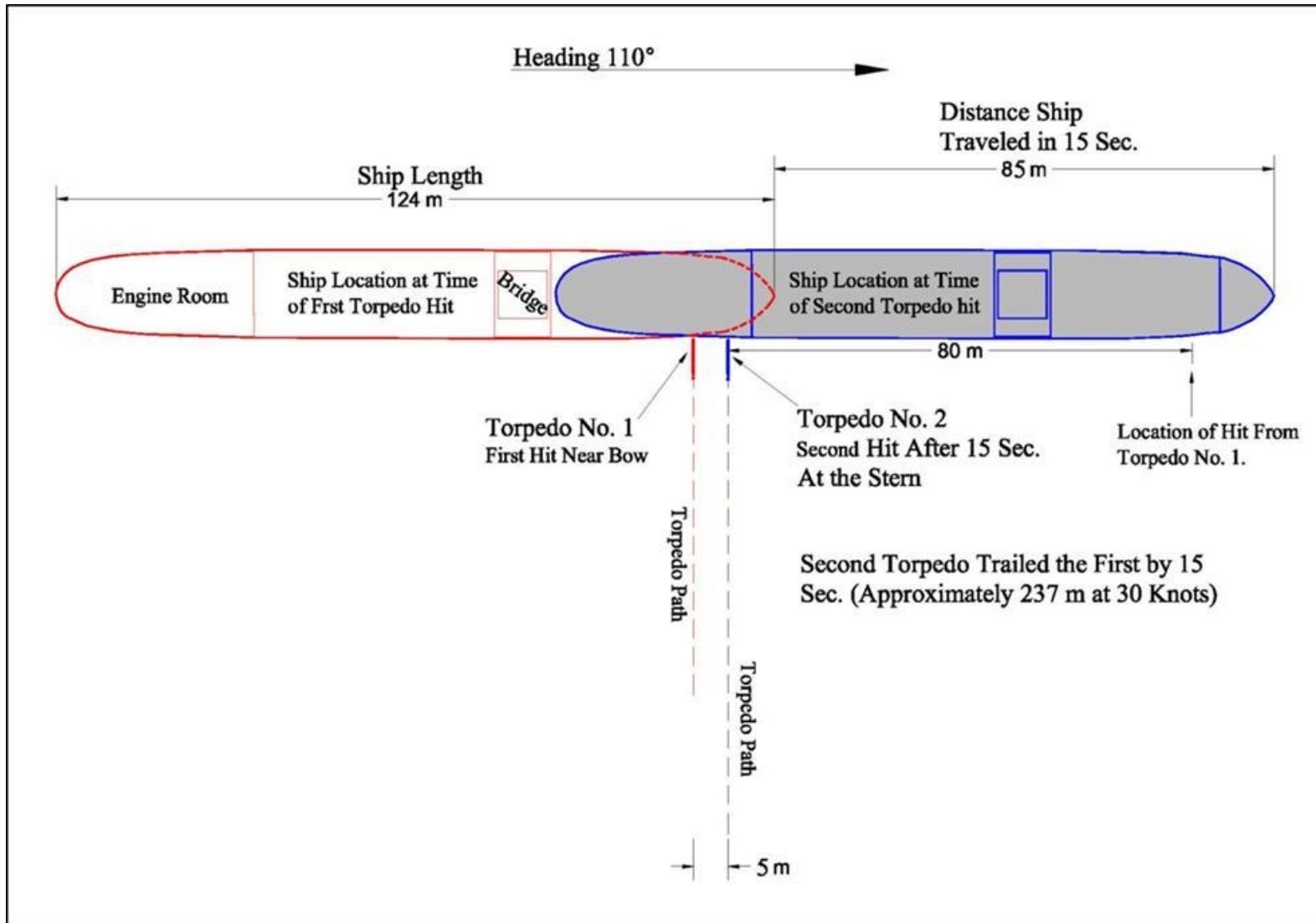
Figure 10-147. Estimated attack scenario on *Gulfoil* based on torpedoes approaching perpendicular to the tanker. Red shows the first torpedo hit and blues shows the second.

Identification of the torpedo impact location to the west of the main wreckage raises two questions: How far could the tanker have theoretically traveled in two minutes after the torpedoes hit and will the theoretical calculations match what is found at the site? To answer these questions, the events following the second torpedo impact must be examined mathematically. The second torpedo struck the engine room, presumably stopping the engines at the time of the torpedo's detonation. Historical and archaeological evidence indicate the *Gulfoil* sank-stern first within 2 minutes after the torpedo impacts. In order for this to occur, the *Gulfoil* must have slowed during that time span from 11 knots to a near stop before it plunged beneath the surface stern-first, but could it have traveled far enough in 2 minutes to account for the distance between the two debris fields? To determine this, standard acceleration (or in this case deceleration) formulas were used to mathematically calculate the rate of deceleration (represented as a negative number) and the distance travelled by *Gulfoil*.

The first step in this calculation was determining *Gulfoil's* rate of deceleration. This was calculated using the formula:

$$\mathbf{a = (V_f - V_i)/t}$$

Where:  a = acceleration in m/second (m/s)
$V_f$= Final Velocity in m/s
$V_i$= Initial Velocity in m/s
t = time in seconds

Using a final velocity of 0 m/s, an initial velocity of 5.65884 m/s, and a time of 120 seconds, *Gulfoil's* deceleration after the second torpedo impact would be −0.04716 m/s. With a known deceleration rate, the distance *Gulfoil* travelled before sinking was determined using the formula:

$$\mathbf{d = (V_f+V_i)t + (1/2)at^2}$$

Where:  d = distance in m (m)
$V_f$= Final Velocity in m/s
$V_i$= Initial Velocity in m/s
t = time in seconds
a = deceleration rate in m/s

Using the calculated deceleration (−0.04716 m/s) to solve the equation shows the *Gulfoil* would have covered a distance of approximately 340 m in the 2 minutes following the second torpedo impact. Additionally, the torpedo damage to the starboard side reportedly gave *Gulfoil* a starboard list and may have created additional drag. This additional drag would have possibly resulted in the vessel slowly turning to a southerly course. Applying a constant 3° estimated turn to starboard (south) for a distance of 340 m from the approximate torpedo impact location, places the *Gulfoil* very near the southern end of the debris trail before sinking.[2] As the *Gulfoil* sank, it plunged stern-first in a north-northeast direction towards the seafloor, leaving a trail of debris in its wake (Figure 10-148).

---

2 The product (340 m) was a calculated distance resulting solely from the data entered. The estimate of 3°, however, is an uncalculated adjustment to the ship's course based on where the end of the debris trail starts, knowing that the ship did not likely continue on a heading of 110°.
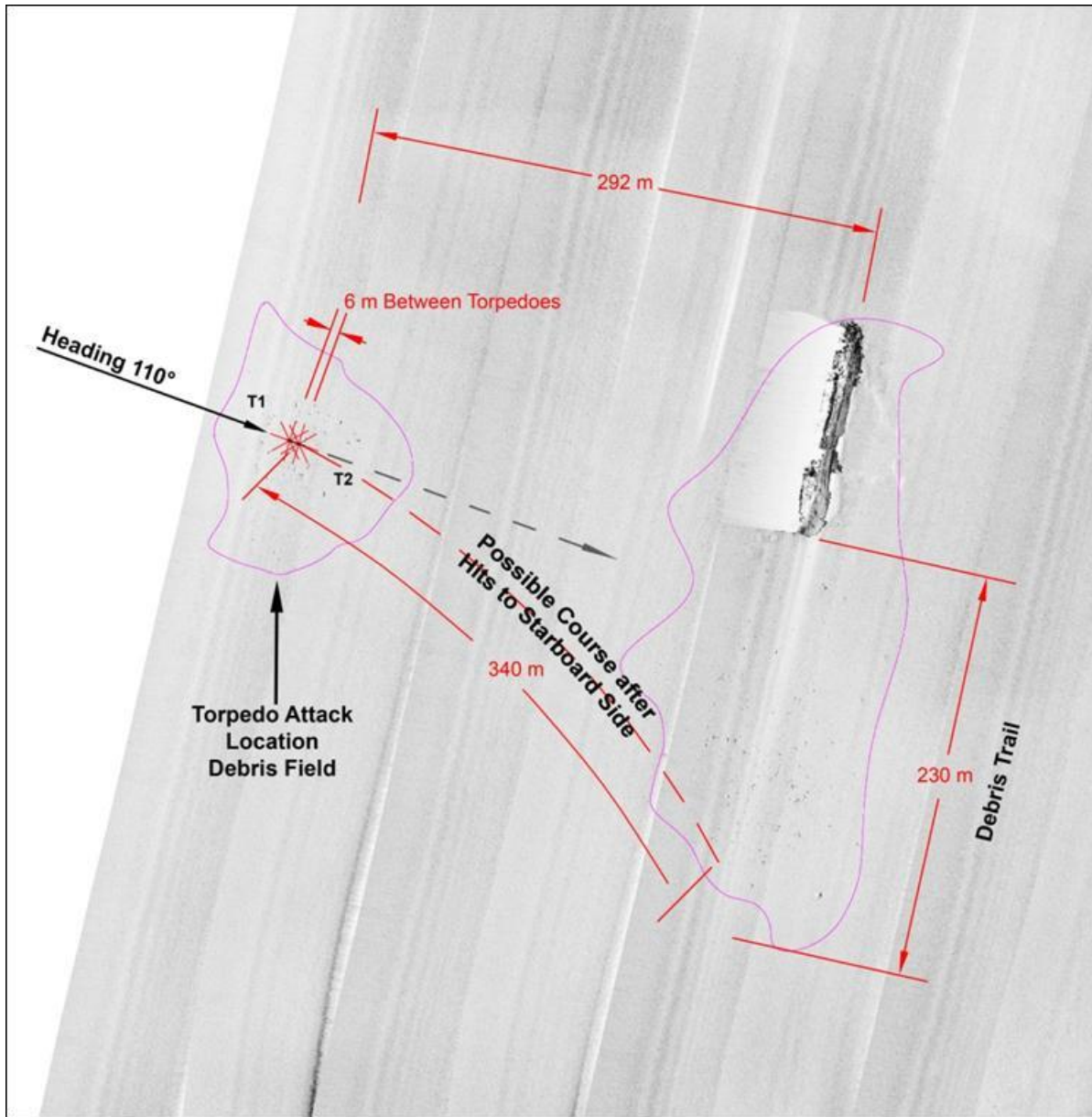
Figure 10-148. Sonar mosaic image with estimated *Gulfoil* surface attack and sinking scenario (Sonar data courtesy of C & C Technologies, Inc.).

Therefore, the substantial distance between the two debris areas can be accounted for by the decelerated movement of *Gulfoil* during the 2 minutes following the U-boat attack. The distance covered also explains the initial miscalculation of the site size using the shipwreck distribution model formula, which could only account for the distribution of debris after the vessel left the surface sinking to the seafloor. The debris from the torpedo hits and debris trail from the hull are then taken as two sinking events for the purpose of modeling the distribution of debris. Initial debris fell from *Gulfoil* when the torpedoes struck the hull. The debris would spread out from that point leaving a scattered "shotgun" pattern of artifacts on the seafloor. The observed debris field west of *Gulfoil* is scattered approximately 82 m from the estimated center. That places the debris

field well within the projected distribution estimate of 106 m using the Debris Distribution Model. When the vessel itself left the surface two minutes later, wreckage began trailing away from the tanker as air was forced out of the hull and hydrodynamic shear acted on the hull as it fell toward the seafloor. The debris trail and hull remains also fit into the distribution model as previously discussed.

Combining the shipwreck Debris Distribution Model with estimated distance traveled based on deceleration and time following the torpedo attack proved invaluable in understanding the site formation processes at the *Gulfoil*. The ability to more accurately predict site distributions should also aid investigations of other shipwreck sites lost through catastrophic sinking events related to warfare or accident. If the necessary information is available, researchers will be able to better calculate projected search areas, determine the location of the initial sinking event, and better understand the site formation processes at work on deep-water wreck sites.

### 10.5.5.6    Site Preservation

The *Gulfoil* is in a good state of preservation. The starboard (western) side of the wreck has extensive damage from torpedo impacts just forward of the central bridge area and near the stern. This damage does not appear to have destabilized the hull which appears to still be sound. Other than the visible torpedo damage, the wreck is mostly intact. Rusticles are visible on the anchors and hanging from hull plating around the damaged areas on the starboard side. The vessel's superstructures and most of the other ship's components extending into the water column are covered with extensive growths of coral, making accurate assessment of structural integrity nearly impossible. Currently no microbiological or corrosion test platforms are in place on the site.

### 10.5.6 *Gulfpenn* Wreck Site

### 10.5.6.1    Historical Background of the Gulfpenn

In 1916, the Sun Shipbuilding Company was formed in Chester, Pennsylvania, as an affiliate to the Sun Oil Company to bolster tanker construction, which was in great demand because of World War I. After the war, the Sun Shipbuilding Company continued constructing tankers, including *Agwihavre*, later renamed *Gulfpenn* (Figure 10-149 and Figure 10-150). *Agwihavre*'s keel was laid on April 2, 1920, and was launched June 16, 1921 (Kavanagh et al. 2001). She was built for the Atlantic, Gulf, and West Indies Steamship Line of New York. The vessel was a screw steamer powered by a quadruple expansion engine, located in the aft portion of the vessel. She had a length of 480.6 ft (146.5 m), a beam of 65.6 ft (20 m), a 36.7 ft (11.2-m) depth of hold, and was 8,862 gross tons. The tanker had a plain stem with forecastle head, elliptical stern, and two masts. The Gulf Oil Corporation of Philadelphia, Pennsylvania acquired the vessel in 1942. Ownership of *Agwihavre* was transferred to the Gulf Oil Corporation of Philadelphia, Pennsylvania, and the vessel was renamed *Gulfpenn*. On March 11, 1942, the *Gulfpenn* (Official Number 221244) was registered in the Port of Philadelphia, Pennsylvania under license to Arthur S. Hodges, as a coasting trade vessel (*Gulfpenn* 1921; and *Gulfpenn* 1942).

Figure 10-149. Tanker *Gulfpenn*, photograph taken by the United States Coast Guard (Courtesy of Mariner's Museum, Newport News, Virginia).

On February 28, 1942, *Gulfpenn* had its first exposure to U-boat activity when the crew received word that the unarmed oil tanker SS *Oregon* was attacked north of Cape Engano, Dominican Republic. *Oregon* was en route from Aruba to New York with a cargo of fuel oil when *U-156* (Hartenstein), which was out of torpedoes, caught and sank the tanker with its deck guns. *U-156* killed several of *Oregon*'s crew with machine-gun fire while they launched lifeboats. The following day, *Gulfpenn* rescued a group of survivors from *Oregon* (Hughes 2004; and Hocking 1969: 528).

On May 13, 1942, the unarmed *Gulfpenn* was transporting 90,000 barrels of gasoline from Port Arthur, Texas, to Philadelphia, Pennsylvania. *Gulfpenn* was steaming about eight km ahead of another tanker, *Gulfprince*. At dawn *Gulfprince* was attacked by *U-507*. The first two torpedoes fired by *U-507* were spotted by *Gulfprince*'s lookouts and successfully evaded. The third glanced off the tanker's hull, but did not explode. The impact caused some damage, but both tankers escaped. *Gulfprince* sent a radio alert of the attack. Captain Harro Schacht of *U-507* stated in his logs that it was useless to pursue the tanker on the surface because his deck guns were secured, it was getting light, and the area had been alerted to his presence (Schacht 1942; and SeaWaves 2005).

At 1450 hours (CT) on May 13th, *Gulfpenn*'s luck ran out when she crossed paths with *U-506*. The tanker had been traveling at 11 to 12 knots and zigzagging in irregular patterns. They were running radio-silent with four lookouts on duty, one on the forecastle, one on the bridge, and two on the aft deck. The weather was clear with moderate seas and light winds. Visibility was good and one other ship could be seen approximately 8.8 km astern. The U-boat's torpedo struck the engine room, destroying that section of the ship, immediately stopping the engines, and killing all of the personnel in the engine room. The tanker sank stern first, taking only five minutes to slip beneath the waves. Out of the 38 crewmen, 26 made it into lifeboats. Of these 26, one man died in a lifeboat while the Honduran vessel *Telde* rescued the remaining 25 survivors less than three hours after the attack (Burch 1942a).

Figure 10-150.  Architectural drawing of the tanker Agwihavre or "*Gulfpenn*," by the Sun Shipbuilding Company, July 8, 1920 (From the Independence Seaport Museum collection).

### 10.5.6.2    Field Investigations

10.5.6.2.1    Discovery and Exploration

In 1994, the shipwreck, *Gulfpenn,* was discovered during a deepwater survey in Mississippi Canyon conducted for Shell International Exploration and Production Inc. John E. Chance and Associates using the Texas A&M University deep-tow system conducted the survey. The wreck was detected at the edge of the survey swath by side scan sonar, which was set at a range of 750 m per channel (Figure 10-151). The large sonar target was within 13 km of the historical location of *Gulfpenn*. Marine archaeologist Laura Landry conducted an archaeological assessment of the survey and tentatively identified the shipwreck as *Gulfpenn* (Landry 1994).
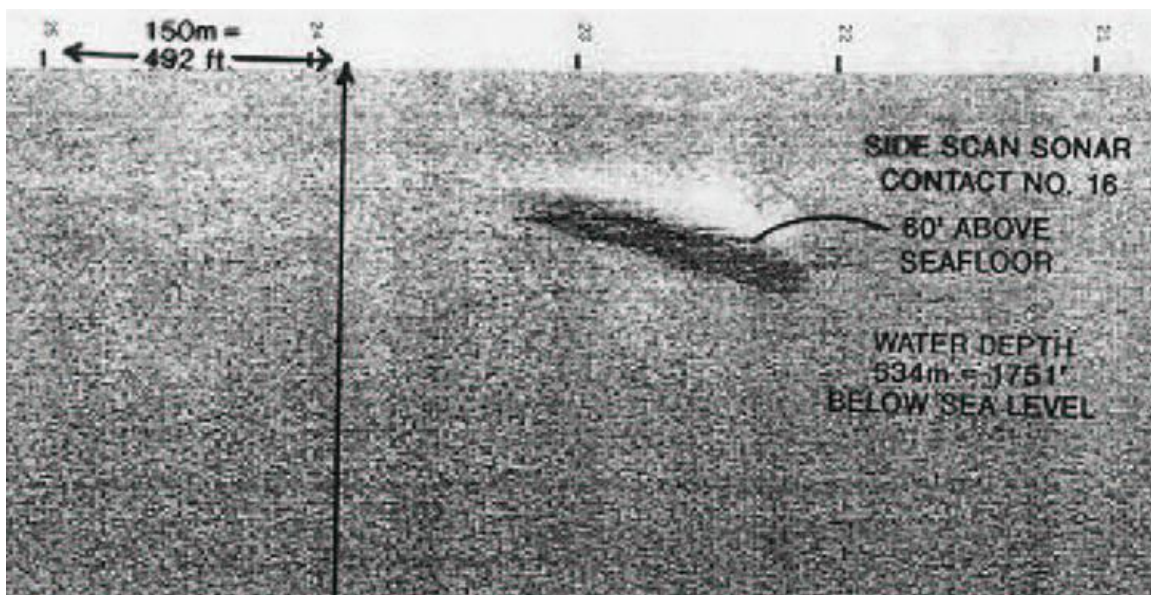


Figure 10-151. Side scan sonar image of *Gulfpenn* from the Texas A&M University deep-tow system (Courtesy of Shell International Exploration and Production Inc.).

10.5.6.2.2    2004 DeepWrecks I ROV Investigation

The *Gulfpenn* shipwreck site was investigated in 2004 as part of the Deep Wrecks I Project. Investigations at the site were carried out using a Triton XL11 ROV from August 4 to 5 and August 11 to 13, 2004 operated from the M/V HOS *Dominator*. As part of this project, the main hull and the surrounding area were investigated in detail. The examinations found the bow and forward sections of the main hull relatively intact, but with extensive deterioration of the superstructure. The aft section of the vessel was severely damaged and the stern had detached from the main hull. The missing stern section was found approximately 27 m northwest of the bow. Debris fields surround the main hull structure, with the largest field extending out nearly 161 m northwest of the remaining hull. The investigation concluded that the damage noted on the *Gulfpenn* was consistent with the historic accounts and surmised that, following the torpedo attack, the stern tore away from the main hull.

The 2004 investigations also determined the site is in a moderate state of preservation. It is speculated that the aft section is deteriorating at a higher rate than the rest of the vessel as a result of the damaged sustained at the time of wrecking.

### 10.5.6.2.3    *Lophelia* II: Reefs, Rigs, and Wrecks 2008 Field Cruise

Archaeological investigations at the *Gulfpenn* were undertaken on September 8, 2008 from the R/V *Nancy Foster*. At 1041 hours, the ROV was put in the water to check the trim after the camera changes (The macro-camera was added to the ROV to replace the WesTech SDS3030). Unfortunately, during the trim check the ROV was pulled under *Nancy Foster* and the tether fouled between the ship's rudder and port Z-drive. At 1105 hours, the cage was launched in an effort to pull the ROV down and unfoul the tether, which was successful and at 1110 hours, the tether cable was pulled free. The ROV was safely on the deck of *Nancy Foster* at 1220 hours. The ROV was back in the water at 1315 hours. Between 1315 and 1358 hours, the ROV descended to the *Gulfpenn* site. After a forty-three minute descent, the ROV was on the bottom. Progress across the seafloor was slow, because of strong current and poor visibility. At 1439 hours, the team began ROV investigations of the suspected stern section. They observed what appears to be the vessel's rear flagpole, still standing after more than a half century on the seafloor. At 1500 hours, the ROV was moved to the cage for a brief inspection. At 1505, the ROV headed to the wreck's main section. The ROV maneuvered to inspect the abundant coral colonies on the bow. Significant amounts of coral, which had broken off and fallen from the hull above, were observed on the seafloor. From 1520 to 1600 hours, the team inspected the *Gulfpenn*'s leeward (port) side where working conditions were more favorable. At the forward edge of the aft deckhouse, a large *Lophelia* colony, once attached to the lifeboat davit was found in pieces scattered across the ship's hull and a the surrounding seafloor. Following the port side investigations, the ROV moved to the starboard side to inspect a microbial platform placed in 2004, but strong currents hampered ROV operations. Between 1757 and 1803 hours a temperature logger was placed on the starboard bow. At 1805 hours, the main LED light on the ROV malfunctioned and the vehicle was recovered without collecting biological samples.

During the ROV recovery, the tether was fouled in the port Z-drive and severed. The damaged tether forced the termination of further investigations on the *Gulfpenn.*

### 10.5.6.2.4    *Lophelia* II: Reefs, Rigs, and Wrecks 2009 Field Cruise

The 2009 investigation of the *Gulfpenn* took place on September 10, 2009. This investigation focused on documenting the *Lophelia* colonies and biologic activity on the wreck, so archaeological investigations were limited. For a complete description of the 2009 investigations at *Gulfpenn*, please refer to the biological section of this report. The limited archaeological investigations at the site focused on the superstructure near the middle of the wreck and on the previously placed microbiological platform. *Jason II* was used to image areas of the bridge and to photograph the engine order telegraph that was used to communicate between the bridge and the engine room. Near the aft deckhouse, the microbial experiment deployed in 2004 was relocated. It had fallen over on its side, so the team picked it up with *Jason II* and stood it against one of the structures on the deck. An additional long-term microbiological experiment was set on the

*Gulfpenn*'s port bow, along with a short-term experiment. The short-term experiment was unfortunately not recovered at the end of the dive. At 11:37, the investigations on the *Gulfpenn* were finished and *Jason II* returned to the surface.

### 10.5.6.3     *Geographical Setting*

The *Gulfpenn* wrecksite area is located in the central portion of the Mississippi Canyon area of the northern GoM. The site is south of the mouth of the Mississippi River along the Upper Mississippi Fan's northern edge. The Mississippi Fan is a bow-shaped fan made up of several fan-lobes and separated into three major regions: Upper, Middle, and Lower. The Mississippi Canyon is the conduit for the source material that comprises the Mississippi Fan (Bouma et al. 1985). The wreck site rests on the canyon's eastern slope and is likely influenced by the material flowing down the canyon. The seafloor in this area gently slopes at approximately three degrees toward the south with local variations in the seafloor slope. The seafloor trend at the wreck site is to the south-southwest (Figure 10-152). This area's sedimentation rate is relatively low in this area, approximately 2.13 mm per year.

### 10.5.6.4     *Discussion of Archaeological Finding*

#### 10.5.6.4.1     Physical Site

The following description of the wreck site is compiled from data collected during the 2004 DeepWrecks field expedition and the 2008 and 2009 *Lophelia* II field seasons.
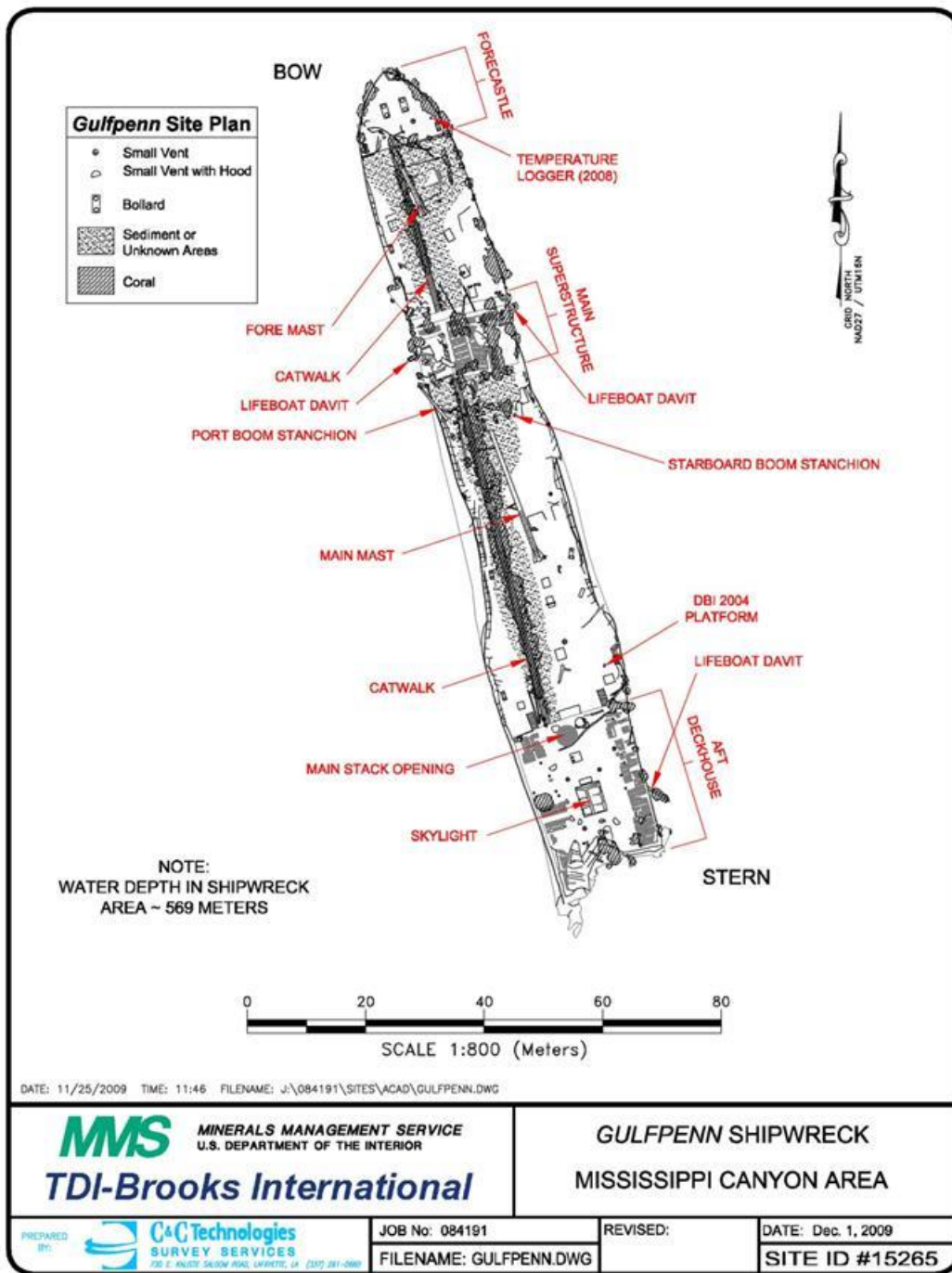
Figure 10-152. Site Map of the *Gulfpenn* Wreck Site base on ROV investigations.

The wreck is oriented with the bow pointing north-northwest and stern to south-southeast (Figure 4–146). Water depths range from approximately 553 m at the bow to 555 m at the stern. The vessel's bow extends into the water column more than the stern. The deck of the forecastle stands

495

about 18 m above the ambient seafloor as opposed to the aft deckhouse, which rises approximately 5.5 m above the ambient seafloor.

The bow and forward section are relatively intact (Figure 10-153). The catwalk and piping are extant from the forecastle to the bridge structure. Coral covers the catwalk and railing, particularly along the starboard side of the vessel, obscuring much of the structural detail. The foremast has separated from the deck and fallen forward. The foot of the mast lies on the deck and the mid-portion lies across the forecastle near the end of the catwalk. The mast's upper parts appear to have broken away and are gone. Figure 10-154 shows a site map of the shipwreck's main structure.



Figure 10-153. Bow of the *Gulfpenn.*
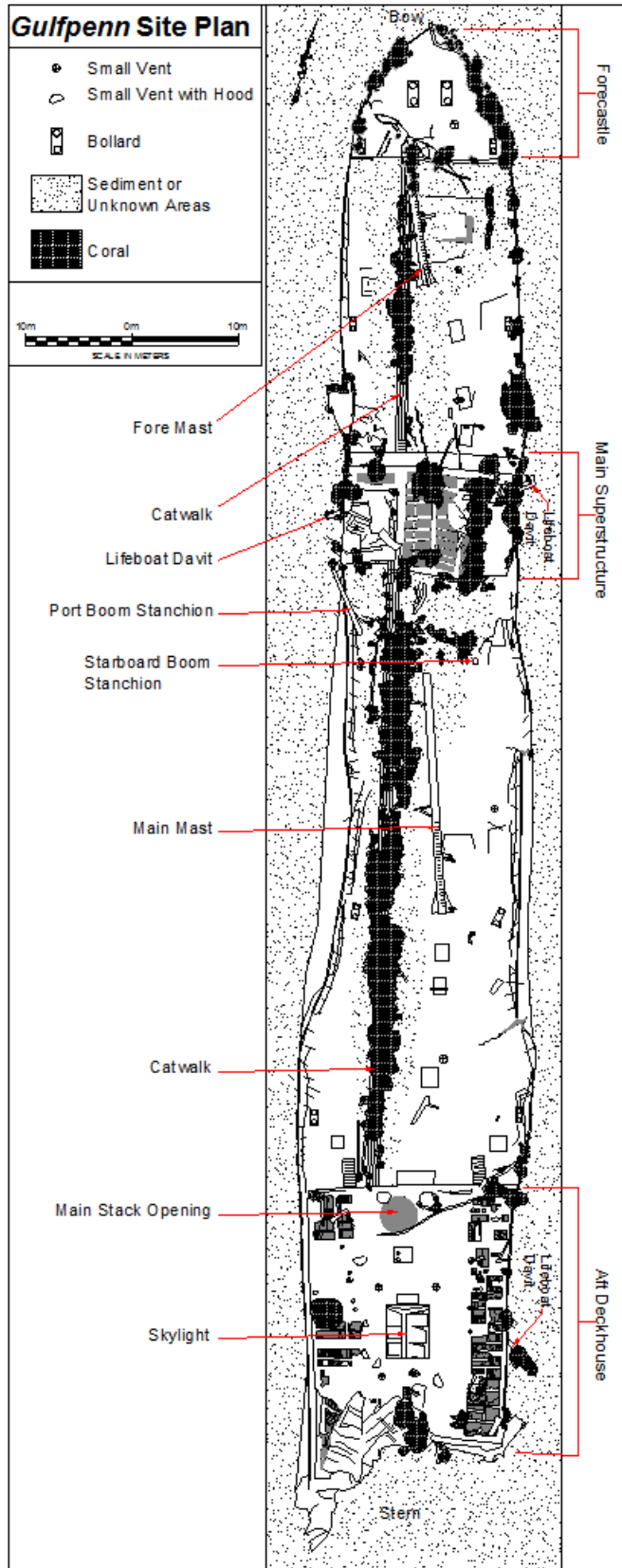
Figure 10-154. Site drawing of *Gulfpenn*'s main structure (Drawn by Robert A. Church).

497

The superstructure's upper works show a considerable deterioration. The pilothouse is gone and the bridge's deck is disintegrating. The remaining superstructure, mainly on the port side, is collapsing with sections of metal plating partially suspended from the vessel. The ship's telegraph has fallen over and spans part of the metal framework of the bridge (Figure 10-155). The superstructure's starboard side is almost entirely obscured by prolific coral formations.
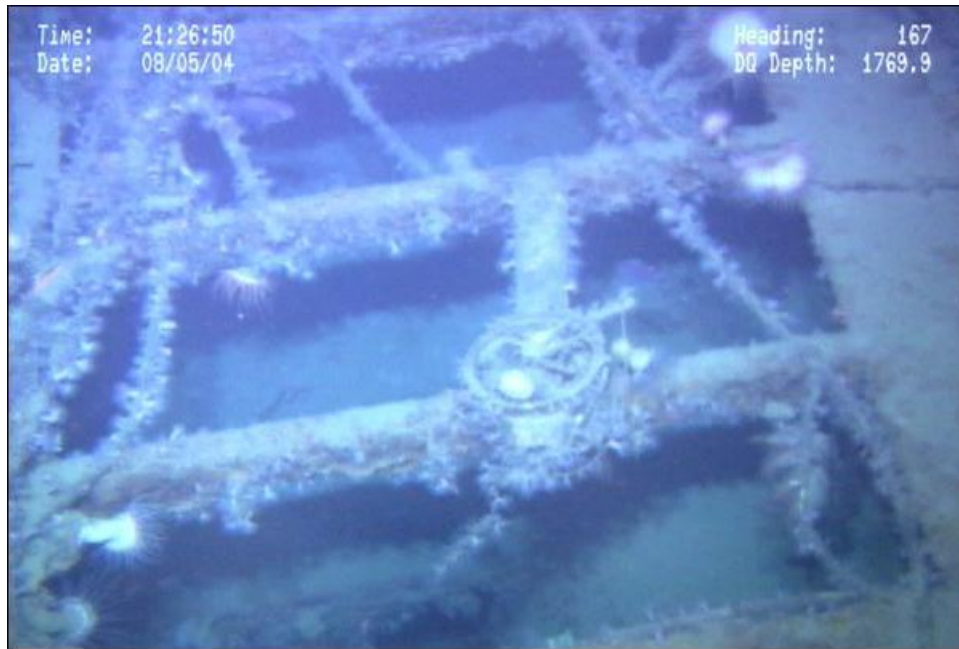


Figure 10-155. Top of *Gulfpenn*'s superstructure showing the bridge
           telegraph lying across the exposed deck frame supports.

Extensive damage is also present aft of the vessel's main superstructure. Although the catwalk and piping from the main structure to the aft deckhouse are intact, the hull amidships has partially collapsed. Sections of the railing and gunwales are lying nearly flat against the deck and the deck is buckled inward in places. There are two hull breaches on the starboard side. The first is approximately 16.7 m aft of the main superstructure and the second is approximately 25.5 m further aft than the first rupture (Figure 10-156). On deck, the starboard stanchion (small mast) remains upright approximately 8.3 m aft of the main superstructure, but the port stanchion has fallen forward with the upper part extending beyond the side of the ship. The main mast has fallen forward and lies on the deck (Figure 10-157). Corals cover the catwalk along this section of the wreck.

Figure 10-156. Breach in the *Gulfpenn's* hull along the vessel's starboard side.



Figure 10-157. Foot of the *Gulfpenn's* main mast lying on the deck.

*Gulfpenn*'s aft portion exhibits the most severe damage. The deck of the aft deckhouse is deteriorating and has partially collapsed inward exposing the interior. The main smokestack is gone, leaving behind a gaping hole where it once stood. Two vent pipes were originally located directly forward of the main stack. The starboard vent pipe still stands, albeit missing a vent hood. The port vent has been destroyed with only fragments visible where it should be. A skylight or air vent at the deckhouse's center is relatively intact. Roughly nine m aft of the skylight the hull ends abruptly in a contortion of mangled metal plating. Almost 11 m of the stern has been ripped away.

Only partial remains of the aft helm controls, used for docking, are visible forward of this severely damaged area (Figure 10-158).  Coral partly covers the wreck's aft section, and is more prevalent on the vessel's starboard side.  Coral growth obscures much of the vessel's structural details on the starboard side, making them difficult to distinguish.



Figure 10-158.  Remains of the *Gulfpenn's* docking helm control on the aft deckhouse.

An extensive artifact scatter surrounds the wreck site.  The main debris zone extends nearly 161 m northwest from the vessel.  An area of light debris extends 130 m southwest of the main hull. Smaller debris extends 65 m to 70 m east and west of the primary wreckage.  A large section of the ship, which appears to be the stern's missing section (Figure 10-159), lies within the main debris field 27 m northwest of the bow.  Other material within this dense debris field includes vent hoods and pipe (Figure 10-160(a,b)), railing, twisted metal, and a lifeboat (Figure 4–155).  The vent shown in Figure 10-160a lies within a few meters of the suspected stern section.  The vent hood shown in Figure 10-160b lies 133.6 m northwest of the bow.  The lifeboat shown in Figure 10-161 is 73 m northwest of the bow.  The missing stack lies 25 m east of the aft deckhouse's starboard side, nearly perpendicular to its original deck location (Figure 10-162).  The funnel is almost completely flattened, with the top pointing away from the vessel.  The ladder and steam whistle running up the stack's forward edge are still intact.

Figure 10-159.  Possible section of the *Gulfpenn's* detached stern.
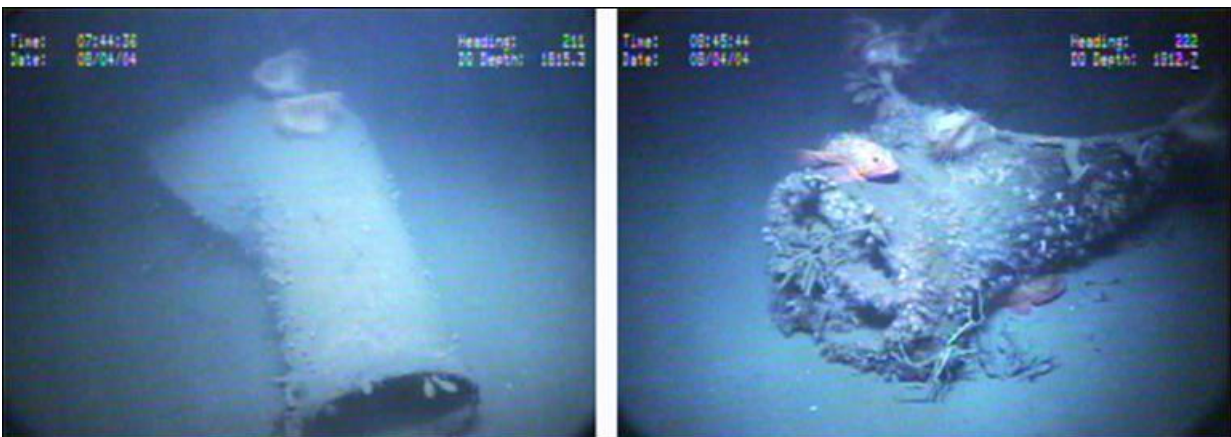


Figure 10-160.  a) Vent hood (left) lying near the separated stern section.  b) Vent hood (right) lying near the northern extent of the *Gulfpenn's* debris field.

Figure 10-161.  Lifeboat from *Gulfpenn* in the debris field (Photo mosaic).



Figure 10-162.  *Gulfpenn*'s main stack, lying to the vessel's starboard side (Photo mosaic).

*Gulfpenn*'s stern damage is consistent with the historical accounts of the U-boat attack.  The evidence suggests the torpedo attack ripped the stern from the main hull.  As the disarticulated stern plunged to the seafloor spilling debris, the remainder of *Gulfpenn*'s hull sank near the after most section.  As the hull planed downward it, crossed over the fragmented stern section and debris trail impacting the seafloor behind it.  *Gulfpenn*'s main hull impacted the seafloor aft section first, collapsing the torpedo-damaged aft hull and leaving the bow extending proud off the seafloor.  The masts' standing rigging possibly parted as a result of explosions during the attack.  Drag encountered through the water column as the vessel sank likely caused forward stress on the masts before the ship impacted the seafloor.  The fore and aft masts have both fallen forward, at a similar angle of four to nine degrees to port with their foot lying near the base, indicating they likely collapsed as a result of uniform stress experienced on impact.  It is possible that both masts fell before impact, but if the bolts holding the base had already given way, the masts would likely have slid aft on impact, which is not indicated from their present orientation.

### 10.5.6.5    Site Preservation

The wreck site is in a moderate state of preservation.  The bow section is in good condition, but the aft section has considerable damage from the wrecking event.  Some decking is still intact, but is rapidly deteriorating.  The severe damage to the hull's aft section indicates the aft section likely will collapse before the bow and main superstructure.

## 10.5.7 *Deustche Kreigsmarine* (DKM) *U-166* Site

*U-166* site was not initially one of the wreck sites scheduled for investigation during the *Lophelia* II; Rigs, Reefs, and Wrecks project.  However, the 2010 field investigations of nearby biological sites provided an unanticipated opportunity to visit the wreck.  Due to project time constraints, no detailed archaeological documentation was undertaken.  Operations on the site during the 2010 visit were limited to brief visual examination of the two hull sections and the long-term microbiological experiment deployed during the 2003 investigations, sediment core sampling, and biologic sampling.  The historical background and discussion of previous work are provided here for reference.  For in-depth discussions of this site, see "Archaeological and biological analysis of World War II shipwrecks in the GoM:  Artificial reef effect in deep water" (OCS Study MMS 2007-015).

### 10.5.7.1    Historical Background of DKM U-166

During the early months of 1942, the war seemed far away to most Americans, but in reality an ominous threat lurked in the waters off the Eastern and Gulf Coasts.  America's entry into World War II, provided Hitler the opportunity to extend U-boat attacks to America's shores just as the Kaiser had in World War I.  This time, however, Hitler's U-boats would not limit attacks to America's East Coast.  They would strike deeply into America's backyard, the GoM.  In just over a year's time, beginning in May 1942, twenty-four German U-boats entered the GoM.  Seventeen of these U-boats, including *U-166*, sank fifty-six merchant ships and damaged several others (Wiggins, 1995).

*U-166* (Figure 10-163 and Figure 10-164) was built at the Seebeck Shipyard in Bremen, Germany between December 6, 1940 and March 23, 1942 (Morgan and Christ 2003).  *U-166* was 76.8 m long, had a beam of 6.8 m, and a draft of 4.7 m.  It was one of 54 type IXC U-boats constructed by Germany during World War II.  The IXCs were long-range fast-attack submarines.  They were built to carry the war to foreign shores using two supercharged nine-cylinder MAN diesel engines that generated 2,200 horsepower each, and 208 tons of fuel.  On the surface, a IXC could make 18.3 knots, and 7.3 knots submerged.  Larger diesel bunkers than previous designs allowed the IXCs a surface range of 11,000 nautical miles at 12 knots, and a submerged range of 63 nautical miles at 4 knots.  Like most type IXs, *U-166* had a full double hull with the outer hull extended nearly down to the keel (Miller 2000; and Rössler 2001).  According to Rössler (2001), IXCs had a pressure hull composed of 10 sections with each section constructed of 4 to 6 steel plates welded on circular frames to form short cylinders.  The plates had a thickness of 18.5 mm everywhere on the hull, except the conning tower where the plate thickness was increased to 22 mm (Rössler 2001).  The deck was wide and flat leaving room for ten torpedoes stored in pressure-tight containers.  A IXC U-boat typically carried a complement of at least four officers and forty-four crew during wartime (Blair 2000; and Miller 2000).  The class IXs were based on earlier Type IA

U-boats but had substantial improvements to engines, fuel capacity, and armament. The Type IXs and its short-range counterpart, the Type VII, formed the backbone of the German U-boat fleet (Miller 2000).



Figure 10-163. *U-166* at sea in early 1942 (Kuhlmann Collection courtesy of the PAST Foundation and the National D-day Museum).
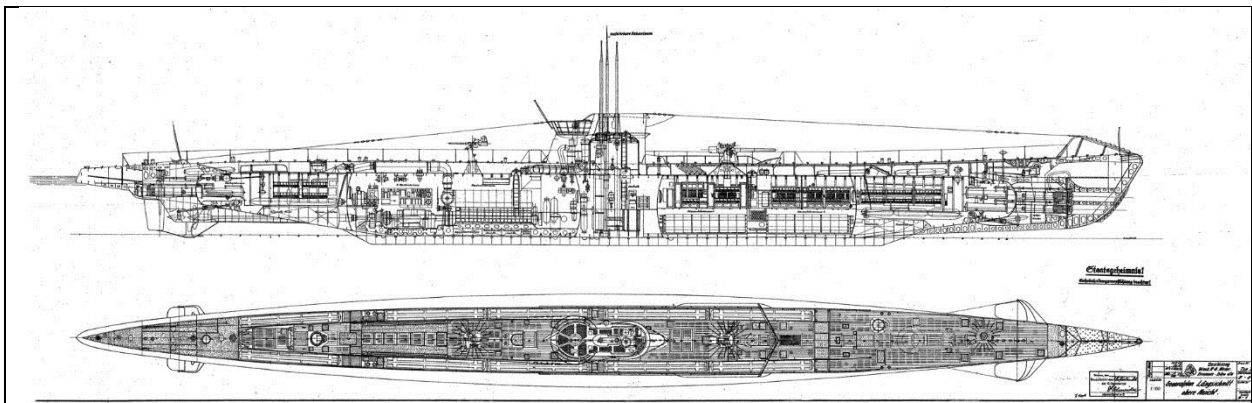


Figure 10-164. Schematic of a Type IXC U-boat (Courtesy of National Park Service and PAST Foundation).

*U-166* was armed with twenty-two torpedoes that could be fired through four forward or two aft tubes. For surface actions, a 105-millimeter deck gun was mounted forward of the conning tower. Other armaments included a 20-millimeter machine-gun mounted on the single *wintergarten* and a 37-millimeter anti-aircraft gun on the aft deck for defense against aircraft or surface vessels.

According to Miller (2000), later IXCs were constructed with an extended *wintergarten* for mounting additional anti-aircraft weaponry.

*U-166* was constructed under the auspices of the man who eventually commanded her, Oberleutnantzur See Hans-GüntherKuhlmann (Figure 10-165).  Kuhlmann, who was born in Cologne in 1913, served in the German Merchant Marine until joining the Kriegsmarine in January 1937.  At the start of the war in 1939, he served as the No. 2 Torpedo Officer on the German heavy cruiser *Blücher* until January 1940 when he transferred to the U-boat arm.  Kuhlmann was assigned to *U-37* as a third watch officer and over the next 13 months, he rose to the rank of first watch officer before leaving the boat for U-boat commander training.  After successfully completing the commander's course Kuhlmann was assigned to the 24th U-boat Flotilla and in March 1941 was given command of the training boat, *U-7*.  In July 1941, he took command of the *U-580*, remaining on that boat until it was lost off Norway during a training exercise.  Kuhlmann survived and took command of *U*-166 in March 1942.  He then took his new boat and crew for a sixty-nine day shakedown cruise (Busch and Röll 1999).  It would be one of only two cruises made by the *U-166* (Morgan and Christ 2003).

Kuhlmann brought *U-166* back into port on May 31, 1942.  Seventeen days later *U-166* left port on its first war cruise.  The destination was the GoM.  There Kuhlmann and his crew would mine enemy ports and attack allied shipping.  Three days into the voyage, the crew of the new U-boat barely escaped a night attack by allied aircraft.  The remainder of the crossing was uneventful and *U-166* and her crew entered the Caribbean in mid-July.  Kuhlmann and his crew did not claim a victory for several days after reaching the Caribbean.  Then on July 13, 1942, they sank the 84-ton schooner *Carmen*.  This success was followed in relatively quick succession by sinking of the 2,309-ton freighter *Oneida*, and the 16-ton trawler *Gertrude*.  Finding only small vessels in this area, Kuhlmann continued towards the GoM and the area off the mouth of the Mississippi River (Morgan and Christ 2003).



Figure 10-165.  Oberleutnantzur See Hans-Günther
Kuhlmann (Kuhlmann Collection courtesy of the
PAST Foundation and the National D-day Museum).

*U-166* entered the GoM in mid-July 1942 and proceeded to lay mines off the southwest pass of the Mississippi River (Morgan and Christ 2003). On July 27, 1942, Kuhlmann radioed German Naval Command reporting completion of mine-laying activities and that he was proceeding to hunt shipping (War Diary 1942: 36,53,92). It would be the final message from *U-166*.

While *U-166* sailed to its assigned operation area, the passenger freighter *Robert E. Lee* left Port-of-Spain, Trinidad bound for New Orleans, Louisiana on July 20, 1942 carrying 270 passengers, six merchant marine officers, and 131 general crewmembers. *Robert E. Lee* transited the Caribbean with a heavily escorted convoy, but during the morning hours of July 29, it rendezvoused with United States Navy Patrol Craft *566* (Figure 10-166) near Key West, Florida.



Figure 10-166. An undated photograph of PC-566 (Courtesy of Mariner's Museum).

Built in Houston, Texas, PC-*566* was a 461 class patrol craft. It was 178 ft (54.3 m) long, had a 23-foot (7 meter) beam, and could cruise at 20 knots. Constructed to defeat the enemy submarine threat, PC-*566* was heavily armed with deck guns, rockets, and depth charges. Escorting *Robert E. Lee* was the naval vessel's first mission and Lt. Commander Herbert C. Claudius' first command. Under orders from the Commander of the Gulf Sea Frontier, PC-*566* was to escort *Robert E. Lee* to Tampa, Florida where the steamer would re-provision (Charlton 2003; Henderson 1942; and USS PC-*566* 1942).

*U-166* prowled shipping lanes near the Mississippi River mouth at the same time *Robert E. Lee* and PC-*566* arrived at Egmont Key Light, Tampa Bay, on July 29, 1942 around 2145 hrs. When no pilots were available, the steamer used Morse code and signal lights to communicate with PC-*566*. *Robert E. Lee* stated they would proceed to New Orleans rather than wait. At 2325 hrs, PC-*566* broke radio silence to notify the Commander of the Gulf Sea Frontier that *Robert E. Lee* was

continuing to New Orleans and to request orders. PC-*566* was ordered to escort *Robert E. Lee* and the two vessels were immediately underway (Church et al 2002; Henderson 1942; and USS PC-*566* 1942).

*Robert E. Lee* and PC-*566* transited across the Gulf through the night and into the next day, drawing closer to *U-166*. July 30 was a clear, calm day. PC-*566* was running half-mile ahead and to port of *Robert E. Lee*. The freighter and her naval escort were approximately 45 nautical miles southeast of the Southwest Pass of the Mississippi River when *U-166* spotted the freighter. At 1637 hrs, *U-166* fired a torpedo at the freighter's starboard side. Passengers and crew on *Robert E. Lee* noticed an elongated shape 150 m to starboard (Henderson 1942). The single torpedo fired by *U-166* struck *Robert E. Lee*'s starboard side. The resulting explosion tore through C and B decks destroying the engines. Lookouts aboard PC-*566* spotted the U-boat's periscope and the patrol craft moved to attack.

PC-*566*'s radio operator had been transmitting their estimated arrival time to the Port Director of New Orleans when *U-166* attacked. The transmission was cancelled and an SOS for *Robert E. Lee* sent instead. Six lifeboats and sixteen life rafts were launched from *Robert E. Lee* as passengers and crew frantically abandoned ship. *Robert E. Lee*'s bow rose out of the water until it reached a precariously steep angle, and the vessel suddenly plunged to the bottom. *Robert E. Lee* sank between six and ten minutes after the torpedo attack according to survivors and naval witnesses. The disaster resulted in the deaths of ten crewmembers and 15 passengers (Church et al 2002; Henderson 1942; USS PC-*566* 1942; and Winnier 2003). As the freighter sank, Kuhlmann made a fatal error. Evidently not noticing the patrol craft, he kept *U-166* at periscope depth, and PC-*566* moved in for the kill.

*U-166*'s first indication that they were under attack was probably when PC-*566*'s active sonar rang against the U-boat's hull from just 230 m away. The U-boat immediately submerged, but PC-*566* maintained the contact for another 120 m. Once PC-*566* lost contact, it returned to the point where *U-166* was last detected and a depth charge pattern of five charges was laid with settings for 76.2 m (250 ft), 45.7 m (150 ft), and 30.5 m (100 ft). Following the first set of depth charges, PC-*566* reversed course for 1000 m to re-establish sonar contact. At that time Captain Claudius noted *Robert E. Lee* was gone, and only lifeboats and rafts remained where the vessel had once been. PC-*566* again detected *U-166* with sonar only 550 m away. The contact was maintained as *PC-566* closed to within 350 m, and dropped a second pattern of five depth charges. Soon the first airplane from New Orleans arrived on the scene and Claudius instructed the pilot to perform an aerial search for the U-boat. Commander Claudius circled the area cautiously, using *PC-566*'s sonar to search for the U-boat. When the second plane arrived Claudius speculated the U-boat was either sunk or disabled and it was safe to begin rescue operations. While conducting the sonar search, PC-*566*'s crew noted a large oil sick on the surface. The brownish-gray slick was 60 m in diameter, and smelled of diesel oil. No other debris floated to the surface, but Claudius believed the U-boat was either sunk by the attack, or was "so mortally wounded that she would never return to her base" (USS PC-566 1942).

Aside from the fatal torpedo that sank *Robert E. Lee*, the only evidence of *U-166*'s presence on July 30, 1942 was the periscope that had been spotted and the oil slick that appeared after PC-*566* dropped its second set of depth charges. The submarine, believed by Naval Command to be only

slightly damaged by PC-*566* during its attack, would turn out to have been sunk during the battle, but the location of the only U-boat lost in the GoM during World War II would not be identified for half a century.

Two days after the attack on *Robert E. Lee,* two U.S. Coast Guardsmen, Pilot Henry White and Radio Operator George Boggs, were patrolling in a J4F amphibious aircraft roughly 160 km south of Houma, Louisiana, when they spotted a U-boat on the surface. As the U-boat crash-dived towards deeper water, White and Boggs attacked with their only weapon, a single depth charge. White and Boggs reported the depth charge exploded near the submarine and an oil slick appeared on the surface. When they returned to base, they were informed the incident was classified. White and Boggs were later told they destroyed *U-166* and were decorated for their actions.

For the next 59 years, history recorded *U-166* sank 160 km south of Houma, Louisiana by two U.S. Coast Guard Aviators, Pilot Henry White and Radio Operator George Boggs on August 1, 1942. Despite numerous regional oil and gas surveys and expeditions seeking *U-166*, the sub was not found until 1986. Then it remained incorrectly identified until 2001. *U-166*'s location near *Robert E. Lee* proves PC-*566* destroyed *U-166* on July 30, 1942. Historical records regarding U-boat actions in the GoM indicate White and Boggs attacked *U-171*. Although White and Boggs did not sink *U-171*, they did drive it from the coast and temporarily prevent it from sinking Allied vessels. Unfortunately, the commanding officer of *PC-566* H. G. Claudius died in 1981 before learning that his attack on the U-boat that day in July 1942 had succeeded. Most of the surviving members of *PC-566* have been informed of the discovery and history has been corrected.

### 10.5.7.2 Field Investigations

#### 10.5.7.2.1 Discovery and Exploration

In 1986, Shell Offshore, Inc. was exploring the deep waters of the Mississippi Canyon area in the GoM for potential oil and gas prospects. Shell contracted John E. Chance and Associates to conduct a survey of the region using a 4075 EDO deep-tow system. During the survey, they detected two shipwrecks. The only shipwrecks that the MMS listed in the vicinity were two World War II casualties, *Robert E. Lee* and *Alcoa Puritan*. At the time, no archaeological assessments were required in deepwater lease blocks and it was not until 1994 that an archaeologist reviewed the data and prepared an assessment. Given the information at the time, it was realistic to assume *Robert E. Lee* and *Alcoa Puritan* had been found. No further investigations were undertaken because of the time and expense involved in conducting deep-tow surveys.

#### 10.5.7.2.2 2001 Autonomous Underwater Vehicle (AUV) Survey

In January 2001, C&C conducted a survey for BP and Shell International in the Mississippi Canyon area near *Robert E. Lee*'s reported location. C&C performed the survey utilizing *C-Surveyor I*, its new AUV, a completely untethered survey platform. During this survey, a large wreck was detected near the edge of the survey swath. C&C marine archaeologists Robert Church and Daniel Warren verified with the MMS that this was *Robert E. Lee*. *Alcoa Puritan*'s reported proximity to *Robert E. Lee*, prompted BP and Shell to agree that additional survey investigation with the AUV be conducted to locate any wreckage in relation to the proposed pipeline route.

In March 2001, the additional survey work was completed. C&C archaeologists reviewed the data and noted *Robert E. Lee*'s wreckage and a new area of wreckage, less than a mile to the east, where the 1986 survey had placed the wreck of *Alcoa Puritan*. During analysis, it became apparent that the wreckage thought to be *Alcoa Puritan* was inconsistent with that size freighter. The wreckage, however, matched the dimensions of a Type IXC German U-boat (76.8 m in length and 6.7 m wide), the same class as *U-166*.

Based on the geophysical evidence, a new hypothesis was developed to explain why *U-166* was 225.3 km east of its recorded position. The hypothesis proposed that *U-166* was destroyed on July 30, 1942, by Patrol Craft *566*'s depth charge attack, and that Coast Guard aviators White and Boggs bombed a different submarine that escaped. An examination of *U-171*'s reconstructed logs, the only other U-boat in the area at the time, lends credence to this hypothesis. These logs stated that *U-171*, around early August 1942, while off the Louisiana coast, was bombed by a "flying boat" (a good description of an amphibious aircraft) but sustained no damage. The attack's exact date could not be determined since the original logbooks were lost when *U-171* was destroyed by a mine in the Bay of Biscay when returning from its GoM patrol.

The hypothesis that the second area of wreckage could be *U-166* led BP and Shell to sponsor site-specific investigations of the suspected *U-166* and *Robert E. Lee* sites using the *C-Surveyor I* AUV. The results of this data (Figure 10-167) provided additional support to the *U-166* hypothesis and stressed the need for verifying the wreck's identity through visual inspection.
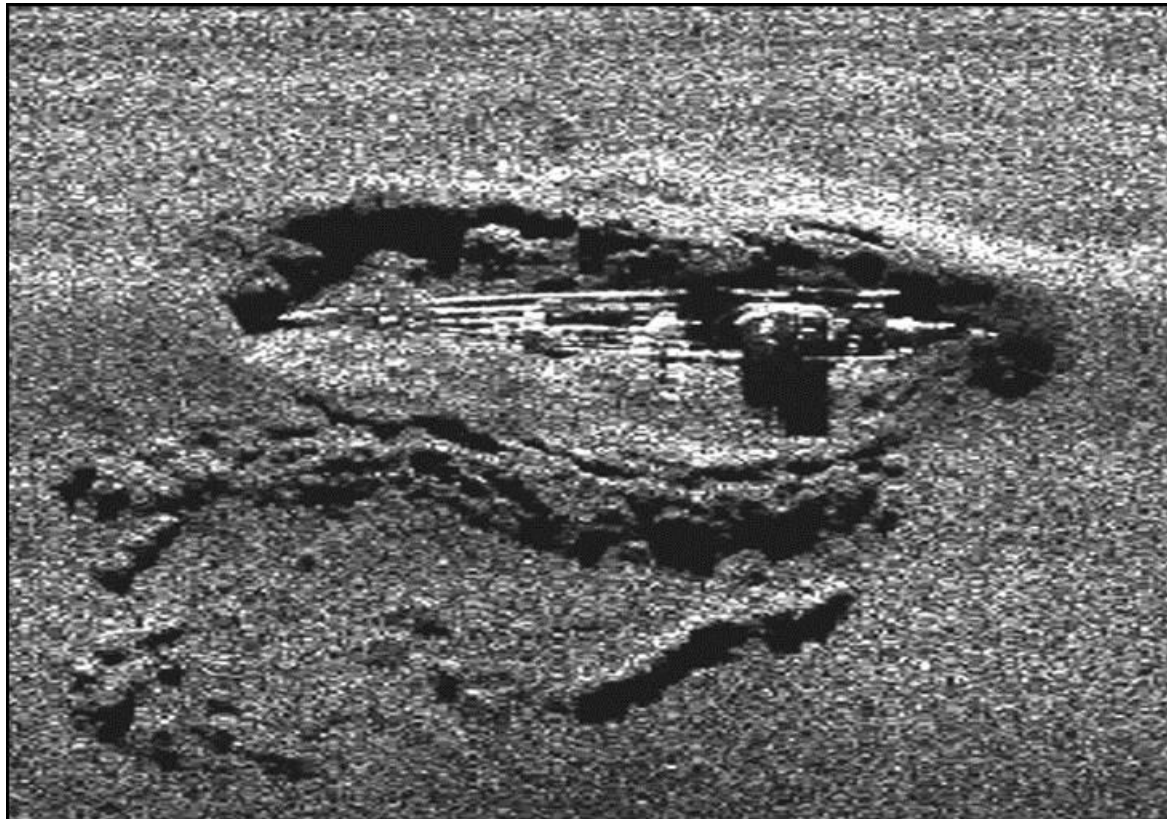


Figure 10-167. High-resolution side scan sonar image of *U-166*, 2001 (Courtesy of BP, Shell, and the National D-Day Museum).

Between May 31 and June 1, 2001, a research team comprised of representatives from BP, Shell, C&C, and the MMS traveled to the Mississippi Canyon Area to determine if the German U-boat, *U-166* had been located. The research team used *Gary Chouest*, an anchor-handling vessel under contract to Shell and equipped with an Oceaneering Millennium VI ROV.

The first glimpse of the vessel was the unmistakable conning tower of a German U-boat. The 105-mm deck gun, 37-mm, and 20-mm antiaircraft guns were clearly visible. Post-field analysis and research revealed that each feature matched that of *U-166*.

Three distinct areas of wreckage were noted during the 2001 investigations of the *U-166* wreck site: the stern, the bow, and a debris field. The site is oriented roughly north to south (Figure 10-168). The stern remains are located near the site's eastern limits and consist of an approximately 55-meter hull section including the deck guns and conning tower. The bow remains are located near the site's western extent approximately 140 m west of the stern section. The bow section consists of approximately a 20-meter hull section extending from the prow aft to just past the forward torpedo hatch. Debris is scattered throughout the site, but the main scatter is between the bow and stern sections. The debris consists of various materials dislodged or ripped from the U-boat as it plunged to the seafloor.
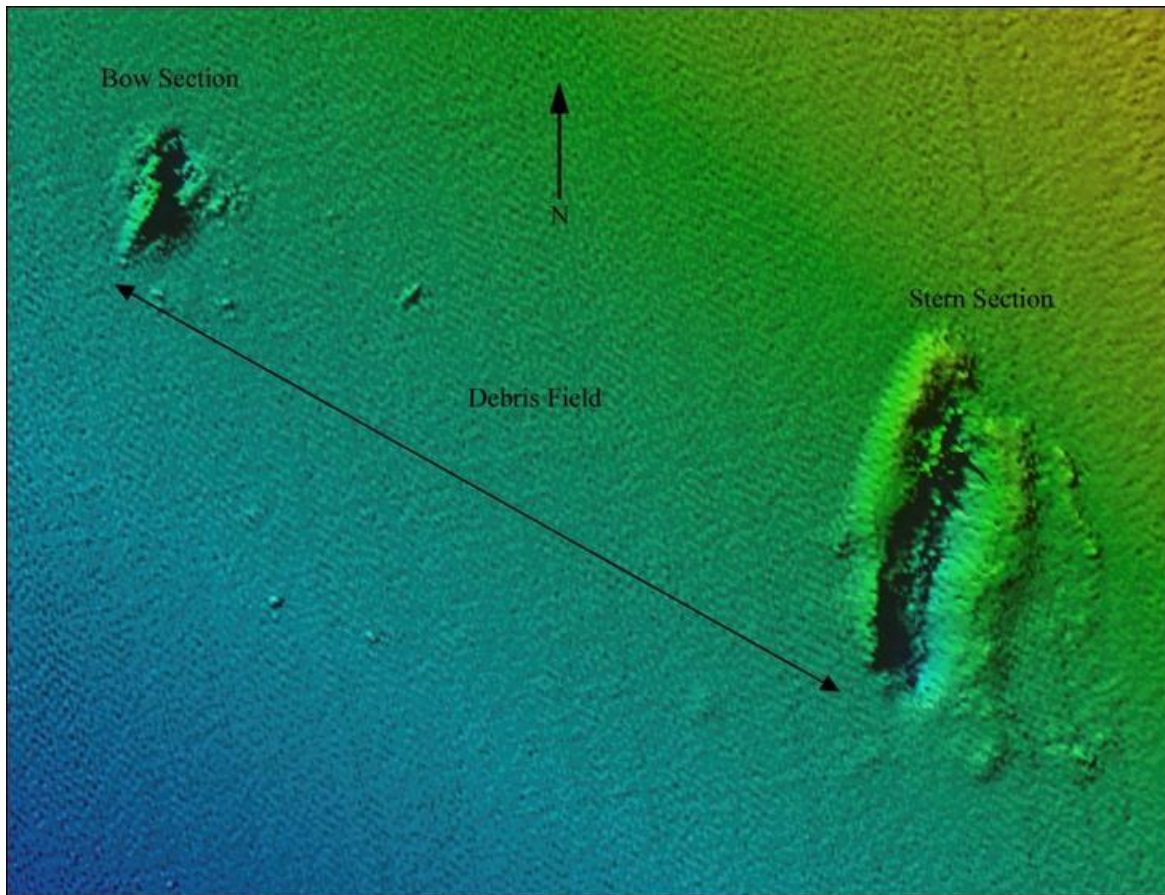


Figure 10-168. Bathymetric data collected in 2001 showing the *U-166* wreck site (Courtesy of BP, Shell, and the National D-day Museum).

The investigation of the bow section provided a revealing look at a possible cause of the U-boat's demise. A large indentation in the deck may be the result of a depth charge explosion. Just aft of this feature, the bow was torn from the rest of the hull and the serrated metal flares outward as if caused by an internal explosion. It is possible that a depth charge exploded very near the deck, ruptured the pressure hull, which in turn caused an internal explosion. It was speculated that salt water rushing into the battery room, which is located in this area of the U-boat, could have caused the batteries to explode.

The expedition successfully identified the long-sought-after U-boat and its last victim. Unfortunately, only cursory wreck site examinations were carried out because of the ROV's limited availability and capabilities. Time constraints with the ROV allowed only approximately 4 hours of investigation time at the wreck.


### 10.5.7.2.3    2003 C & C Technologies, Inc./NOAA OE Site Investigations

In October 2003, C&C Technologies, Inc., in conjunction with the NOAA Office of Ocean Exploration, Droycon Bioconcepts, Inc., and the PAST Foundation conducted a more thorough investigation of *U-166* (Warren et al. 2004; and Church et al. 2004). The project's purpose was to document in detail the *U-166* wreck site. Over five days in October 2003, archaeologists and other scientists successfully recorded *U-166*'s remains.

To conduct the fieldwork, scientists used Sonsub's Innovator Class ROV from NOAA's Research Vessel *Ronald H. Brown*. The ROV surveyed the wreck site following a pre-determined survey grid. The grid consisted of sixty-three lines oriented north-to-south and spaced 4.57 m apart to provide overlapping coverage. During the survey, the ROV flew between 1.83 and 4.57 m above the seafloor to minimize the chance of missing wreck pieces.

During the 2003 mapping project, 307 artifacts, and/or groups of artifacts were documented at the *U-166* site. Over 50 hours of high-resolution digital video and approximately 1,800 digital still images were taken. No artifact materials were recovered because of the wreck's status as an international war grave.

In addition to the archaeological investigations, the microbiological communities (rusticles) growing on *U-166* were documented. Assessment of the rusticles at the *U-166* site was accomplished with the placement of long and short-term experiments, and rusticle sampling from different wreck sections. Short-term experiments, called BARTS and etch tests, were placed on the wreck site at various locations and left in place for approximately 48 hours. The experiments helped biologists determine the types and level of bacterial activity present at the wreck site. The long-term experiments utilized test platforms containing a variety of materials such as wood, iron, and aluminum. The long-term experiments were left on the wreck and checked during the 2004 site visit (Figure 10-169).
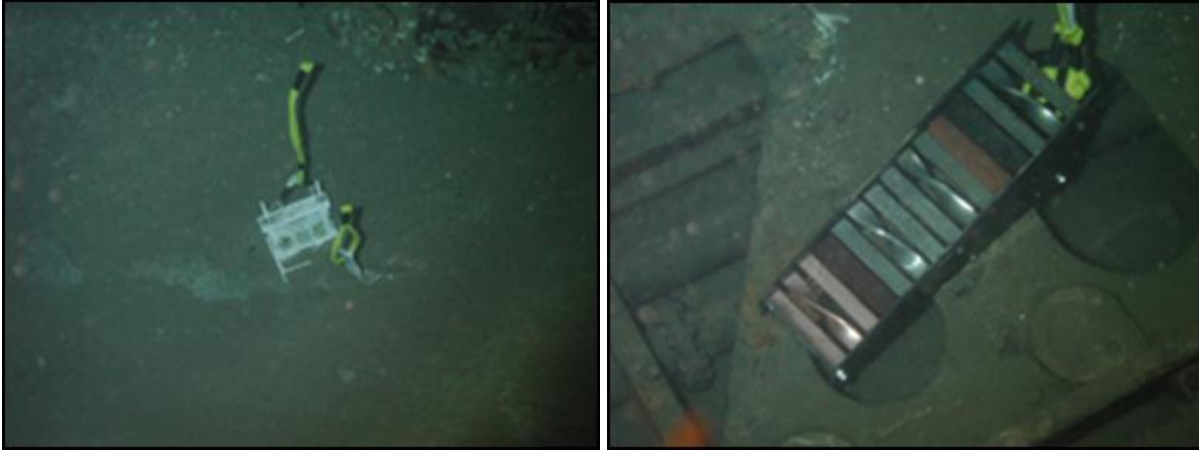
Figure 10-169. Microbiological experiments with BARTS and etch tests (left) and test platforms (right).

## 10.5.7.2.4    2004 Deepwrecks I Site Investigation

The 2004 Deepwrecks I archaeological investigations undertaken at *U-166* continued the 2003 fieldwork. The site's southern extent was not established during 2003, and the 2004 work focused on locating this boundary. During the 2004 project, the science team surveyed seven additional lines south of where the 2003 investigations ended. The lines were approximately 330 m long, spaced 20 m apart, and covered an area approximately 100 m wide. The survey was terminated when the investigation of two successive lines found no further artifacts.

The seafloor covered by the 2004 survey is relatively flat and composed of the same sediment found throughout the *U-166* wreck site. The 2004 investigations located twenty-three additional artifacts associated with the wreck site. These were mainly hull fragments, most with more extensive impact craters than those to the north. Other artifacts documented during this field season included possible clothing.

## 10.5.7.2.5    *Lophelia* II: Reefs, Rigs, and Wrecks 2010 Field Cruise

In November 2010 the wreck of the German U-boat, *U-166* was visited as part of the *Lophelia* II 2010 field investigations. Over a 2.5 hour period on November 3, 2010 visual investigations of the stern and bow hull sections, core sampling, and biological sampling were undertaken using the *Jason II* ROV from on board the NOAA Research Vessel *Ronald H. Brown*. The examination of the *U-166* began with photo documentation of the stern hull remains. Starting from the forward deck, the *Jason II* ROV was flown down the starboard side to the stern of the wreck as video and still imagery were acquired of the deck areas, conning tower, and guns. Once at the stern, *Jason II*'s course was reversed and the ROV headed back to the area of the conning tower. At the after side of the conning tower, the long-term microbiological experiment platform deployed during the 2003 investigation was relocated and visually documented (Figure 10-170). Once examination of the test platform was completed, a single biological sample was acquired from the starboard after rail followed by the recovery of a single core sample at the stern. After collecting the core sample, *Jason II*, transited to the bow section of the *U-166*, approximately 140 m to the west of the stern. Once at

the bow section, a 360 visual survey of the bow was conducted, including the relocation and visual inspection of the long-term microbiological experiment platform placed on the bow in 2003. Before leaving the bow section, a single core sample was taken just forward of the prow. Following the recovery of the core sample, *Jason II* began a transit to the nearby wreck of the *Robert E. Lee*. During the transit, an electrical problem forced the termination of the dive and the recovery of the ROV. Cruise time constraints prevented an additional ROV dive.
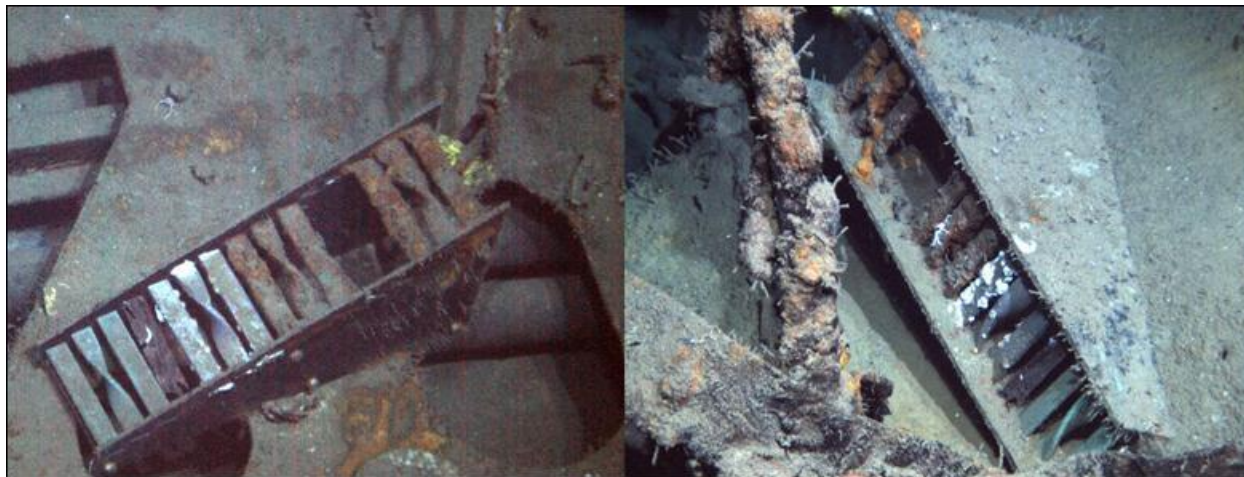


Figure 10-170. Images of the long term microbiological experiments on the *U-166*'s stern (left) and bow (right) taken during the *Lophelia* II 2010 field cruise.

## 10.6 CONCLUSIONS

The historic shipwreck component of the *Lophelia* II: Rigs, Reefs, and Wrecks Study investigated six shipwreck sites in detail and visited one additional shipwreck site to monitor experiment platforms placed during previous investigations. Of the six primary vessels in this study, two are World War II era vessels (*Gulfoil* and *Gulfpenn*) and four are wooden shipwrecks of unknown date and identity. During the project's three consecutive field seasons, details of these six sites were recorded using *in situ* documentation methods. From this data, the identities of the two World War II era vessels were reconfirmed. Study of the four wooden shipwrecks provided insights into their construction styles, when they were likely built, and when they may have been lost. However, despite extensive historical research, the identities of these four vessels remain a mystery. The data acquired using *in situ* documentation methods did not contain details specific enough to associate any of the study wrecks with any one candidate out of the hundreds of sailing vessels lost in the GoM in the nineteenth century. Conclusions regarding each of the six primary study wreck sites, their eligibility to the National Register of Historic Places, and discussions of the site distribution model equations are provided below.

### 10.6.1 *Viosca Knoll* Wreck

The *Viosca Knoll* Wreck Site is an unidentified wooden sailing vessel located 612 m Below Sea Level in the Viosca Knoll Area of the GoM. It was likely two-masted vessel, although the exact rig type could not be positively discerned from the current data. The Muntz Metal Sheathing, abundance of wire rope rigging, and hull construction components indicate a mid- to late-nineteenth century construction date. The artifact assemblage, such as the patent stove and the

William M. Jowett & Co. water filter indicates the vessel was lost sometime after the mi- 1870's. The *Viosca Knoll* Wreck Site is eligible for nomination to the National Register of Historic Places under Criterion D based on archaeology and the site's potential association with a transitional period of maritime commerce in the GoM. Further archaeological investigations of the site are likely to yield valuable data on the construction characteristics of merchant sailing vessels and shipboard life in the mid- to late- nineteenth century.

## 10.6.2 7,000 Ft Wreck

The 7,000 Foot Wreck site represents the remains of a small wooden two-masted sailing vessel and was probably fore-and-aft rigged. Vessels with this style of rig required only small crews and were common in the coastal and fishing trades. The steering gear housing on the 7,000 Foot Wreck indicates it was probably an American-built vessel and the deck layout is similar to that of New England fishing vessels of the same period. The vessel's wire rope rigging, hull construction, and ship components indicate a mid- to late- nineteenth century construction date. The recovered compass indicates the vessel was lost sometime post 1874. The *Viosca Knoll* Wreck Site is eligible for nomination to the National Register of Historic Places under Criterion D based on archaeology and the site's potential association with a transitional period of maritime commerce in the GoM. Further archaeological investigations of the site are likely to yield valuable data on the construction characteristics of merchant sailing vessels and shipboard life in the mid to late nineteenth century.

## 10.6.3 *Ewing Bank* Wreck

The *Ewing Bank* Wreck Site is an unidentified wooden sailing vessel located 621 m BSL in the Ewing Bank area of the GoM. The limited artifact assemblage, and lack of ship components and rigging make analysis of the *Ewing Bank* Wreck challenging.The Muntz Metal Sheathing, ceramic assemblage, and hardened copper fasteners indicate a mid-nineteenth century construction date. The ironstone ceramic designed with the"Pharaoh Cameo" stylehandle suggests a post-1870 sinking date. The moderately sharp bow, rounded turn-of-the-bilge, and broad beam suggest that the *Ewing Bank* Wreck was a sailing merchant vessel. The *Ewing Bank* Wreck Site is eligible for nomination to the National Register of Historic Places under Criterion D based on archaeology and the site's potential association with a transitional period of maritime commerce in the GoM. Further archaeological investigations of the site are likely to yield valuable data on the construction characteristics of merchant sailing vessels from the mid nineteenth century.

## 10.6.4 *Green Lantern* Wreck

The *Green Lantern* Wreck Site is an unidentified wooden sailing vessel located 915 m BSL in the Green Canyon area of the GoM. The possible Muntz metal sheathing, patent iron windlass, and hull construction components indicate a likely late nineteenth century construction date. The artifact assemblage, particularly the Simeon L. & George H. Rogers Co. fork and Wood and Sons Ltd. ceramic dish conclude the vessel had to have sunk after 1910 and likely within the first quarter of the twentieth century. The *Green Lantern* Wreck Site is eligible for nomination to the National Register of Historic Places under Criteria C and D. It is eligible under Criterion C because it exhibits unique naval architecture characteristics in its construction, particularly at the stern. It is eligible under Criterion D based on archaeology and the sites potential association with a

transitional period of maritime commerce in the GoM. Further archaeological investigations of the site are likely to yield valuable data on the construction characteristics of merchant sailing vessels and shipboard life in the mid to late nineteenth century.

### 10.6.5 *Gulfoil* Wreck

*Gulfoil* was registered as a "407 foot class" tanker built of steel construction. The ship was constructed at New York Shipbuilding in Camden, New Jersey in 1912. *Gulfoil* was the first U.S. tanker to incorporate the British tradition of longitudinal frames in its construction. *Gulfoil* was sunk by the German U-boat 506 on 16 May 1942. The ship rests upright, relatively intact in on the seafloor, site supports a great deal of marine life, and is an excellent example of pre-WWII U.S. ship construction. *Gulfoil* displays 1912 U.S. oil tanker construction with a bridge amidships, 2 masts/cranes and catwalks connecting the bridge to the engine room located aft. The ship design is a plain head with a rounded stern typical of oil tankers of the period. It is constructed of steel and incorporates longitudinal framing introduced as the Isherwood system of ship construction.

The U.S. tanker SS *Gulfoil* is eligible for nomination to the National Register of Historic Places under Criteria A, C, and D. It is eligible for nomination under Criterion A for its role in U.S. commerce during WWII. Additionally, the wreck of *Gulfoil* denotes a significant period in American history as a casualty of WWII in the GoM and demonstrates the effectiveness of German submarine operations in U.S. waters. Under Criterion C, it is eligible for nomination as it demonstrates a period of national significance in transitional naval architecture by being the first U.S. tanker to utilize longitudinal framing in its construction. Longitudinal framing continues to be a tradition in building modern vessels. Under Criterion D, it is eligible for nomination because its continued study will allow researchers the opportunity to further develop formulas to predict and describe artifact scatters on deepwater wreck sites.

### 10.6.6 Gulfpenn Wreck

*Gulfpenn* was built in 1920 by Sun Shipbuilding and Dry Dock Company, an affiliate of Sun Oil Company, Chester, Pennsylvania. The Atlantic, Gulf, and West Indies Steamship Line owned Hull No. 40, originally christened *Agvihavre*, until being sold to the Gulf Oil Corporation. *Agvihavre*, was one of many steel tankers built by the Sun Oil Company's yard to compensate for WWI shipbuilding shortages. The vessel's keel was laid on April 2, 1920, and the ship launched June 16, 1921 (Kavanagh et al. 2001). The steel hull had a plain head and an elliptical stern. *Gulfpenn* was sunk by the German U-boat 506 on 13 May 1942. The ship rests upright on the seafloor but is broken into two sections and has a large associated debris field. The site supports a great deal of marine life and is an excellent example of pre-WWII U.S. ship construction.

The *Gulfpenn* archaeological site is eligible for nomination to the National Register under Criteria A and D. It is eligible for nomination under Criterion A for its role in U.S. commerce during WWII, a time in world history when the industrial power of Germany was in direct opposition to the industrial might of the United States. Additionally, the wreck of *Gulfpenn* denotes a significant period in American history as a casualty of WWII in the GoM and demonstrates the effectiveness of German submarine operations in U.S. waters. Under Criterion D, it is eligible for nomination because its continued study will allow researchers the opportunity to further develop formulas to predict and describe artifact scatters on deepwater wreck sites.

515

## 10.6.7 Site distribution equations

The Deep-Wreck I (OCS Study MMS 2007-015) Debris Distribution Model was used to help understand how the tankers *Gulfoil* and *Gulfpenn* sank, based on the distribution of artifacts on the seafloor. Combining that information with deceleration formulas to estimate the distances the tankers traveled after being torpedoed proved invaluable in understanding the full wrecking event and site formation processes at those wreck sites. If the actual location of such an attack or other catastrophic event leading to a sinking is not known, but the necessary data are available, researchers should also be able to use the same methodology to calculate projected search areas and work back from the wreck location to determine the location of the initial attack/event. The same methodology could then be used to find additional material (scattered artifact fields) related to a wreck site that may be a good distance away and possibly even outside the original survey area for a site. Locating such material would not only help document the remains on the seafloor, but also aid in understanding the events on the surface that led to the sinking. This would not be limited to only battle field scenarios, but any event such as an explosion, collision, etc. that led to a ship sinking. The authors are now applying these methods to wrecks such as the *Robert E. Lee* and *U-166* sites, other World War II casualties, andother wrecks sites found in deep water.

# 11 EDUCATION AND OUTREACH

## 11.1 *LOPHELIA* II CURRICULUM: UNDERSTANDING DEEP-SEA CORAL ECOLOGY

Recognizing the value of helping students understand the mission, importance and challenges of energy management, we developed a curriculum based on the real-life practices of prioritizing exploratory energy drilling sites while minimizing ecosystem impact. The curriculum was inspired by the mission of the *Lophelia* II scientific research project, and was developed with significant contributions from several members of the project team (see Acknowledgements section in Teachers Guide in Appendix F-1. The curriculum targets high school level students in biology and environmental science and references cruise logs, seafloor video and relevant multimedia modules to provide an authentic context for students.

Our approach in developing the curriculum follows the principles of Problem Based Learning (PBL). According to Barrows and Kelson (1993), PBL is a *curriculum* and a *process*. A PBL *curriculum* typically consists of carefully selected problems that demand from the learner acquisition of critical knowledge and problem-solving proficiency, and the PBL *process* typically replicates the commonly used approach to resolving problems or meeting challenges encountered in life and career. The *Lophelia* II curriculum is designed around a real-life based Challenge Scenario – an activity in which students adopt the role of marine scientist to address the challenge of prioritizing potential drilling sites while minimizing ecosystem impacts. To address the challenge, students work through six instructional lessons to obtain the necessary background knowledge to determine which exploratory sites represent the least impact to deep-sea coral communities.

The curriculum's six lessons introduce students to: 1) the organisms typically found in deep-sea coral communities, 2) the basic biology of corals, 3) the requirement for hard-bottom substrate for coral development, 4) the impact of ocean acidification on corals, 5) the importance of currents for dispersal and food delivery, and 6) the food web supported in a coral ecosystem. Through these lessons, students learn what *Lophelia* needs to survive and where these conditions may be found on the seafloor, so that students can then identify which areas may be considered sensitive habitat. Techniques for how scientists approach studying such ecosystems are also embedded in the lessons. In the challenge scenario, students learn about trade-offs in resource and ecosystem management, and develop an understanding of the processes and information used in making decisions around resource management as they prepare their "Environmental Impact Assessment and Prioritization" Reports. Each of the lessons incorporate links to specific NOAA OceanExplorer content, primarily from the *Lophelia* II signature cruises as well as other relevant GoM cruises and learning modules, providing real-world context and background information to students as they work through the unit.

## 11.2 OCEAN LITERACY PRINCIPLES AND FUNDAMENTAL CONCEPTS

This curriculum was developed in accordance with National Science Education Standards and Ocean Literacy Principles. Ocean literacy is defined by seven essential principles supported by detailed fundamental concepts. The fundamental concepts are comparable to those underlying the

National Science Education Standards. Each lesson in the curriculum touches on one or more ocean literacy essential principles and fundamental concepts. These principles and concepts are identified within each lesson.

## 11.3 TEACHER GUIDE AND SUPPORT MATERIALS

A 90-page Teachers Guide was prepared to help teachers implement the curriculum and is included in Appendix F-1. For each lesson in the Teachers Guide, teacher notes contain focus questions, learning objectives, ocean literacy principles addressed, appropriate background information, and links to appropriate reference material available on the NOAA OceanExplorer website. Lessons also come with support materials necessary for the particular lesson. The Challenge Scenario includes 5 seafloor maps, map notes and a student handout in the form of a Memo describing the challenge. Lesson 1 includes three photomosaics, each with six high-resolution images, a dichotomous key of seafloor organisms, and a teacher's key to the organisms in each photomosaic. Lessons 3, 4 and 6 include PowerPoint presentations along with slide notes to help teachers present new material to students. All lessons include reproducible student handouts. All support materials are found either within the Teachers' Guide or on the accompanying files on the DVD.

## 11.4 CURRICULUM TESTING

The curriculum was tested with four high school teachers and their students in the Seattle Public School district in the Spring of 2011. Teachers were provided notebooks with all materials in printed form and online training before using the curriculum. They were asked to keep records of how long each lesson took, what worked well and what did not, and suggestions for modification. Feedback was obtained both in written form and through interviews, and suggestions were incorporated into the final version. Teachers received a small honorarium for their efforts.

## 11.5 DISSEMINATION

The final curriculum was released at the National Science Teachers Associationconference in Phoenix, Arizona in December 2012. Twenty-five teachers attended a short workshop on the project and received a DVD with all support materials included. Feedback from conference workshop attendees was highly positive, including one teacher's comment expressing appreciation that the DVD included all the materials (e.g., maps, student handouts, videos, PowerPoint presentations, website links) necessary to instruct students.

The curriculum was designed to be disseminated online. The Teachers Guide and support materials including maps are formatted to be easily downloaded and printed on standard size paper, for ease of use in classroom settings. Videos and PowerPoints may also be downloaded for classroom use.

## 11.6 VIDEO PRODUCTION

### 11.6.1 Video Production Summary

A massive amount of video was collected aboard the *Lophelia* II Expeditions. In total, about 50 hours of video were collected and archived in 2008, with 1200 hours of video in 2009, and 885 hours in 2010. The ROV *Jason II* is equipped with four video cameras, and each recorded compressed video (.mpeg format) on DVD media. A total of 24 hours of broadcast quality "Best of" video was collected on DVCam tape media from the three-chip camera on *Jason II* in 2009. Additional broadcast quality footage of ship operations (three hours) was recorded to Mini-DV tape format using a Sony three-chip camera shooting standard definition. Video recording in 2009 was standard definition, but recording in 2010 was upgraded to high-definition format.

The "Best of" video from 2009 was edited (or reduced) into two different output products: 1) moderate resolution (360 x 240) videos in .mov format (240 minutes) showing highlights from all sites, suitable for public lectures and presentations and 2) broadcast resolution (720 x 480) highlight videos (16 minutes) from 10 select sites, suitable for broadcast media. The 10 selected sites were: West Florida Shelf, DeSoto Canyon, Viosca Knoll 826, Viosca Knoll 906, Mississippi Canyon 751, Green Canyon 852, and Garden Banks 535, the *Gulfpenn* wreck, a 7,000-ft wreck, and the *Green Lantern* wreck. Durations range from 1–3 minutes, depending on the site. Videos include title cards, rights-free music, and logos from NOAA and BOEM.

The broadcast quality highlights from 2009 were ultimately intended for the 20-minute documentary about the *Lophelia* II project, but the short format also helped to accomplish interim tasks, such as public outreach and education. Currently, 12 videos are uploaded to YouTube with text and metadata approved by project Principal Investigators. The clips may be searched using the term '*Lophelia* II'. The videos have proven popular online. The median *Lophelia* II video was viewed 7,500 times. Videos from West Florida, Garden Banks, VK826, and VK906 were each viewed more than 7,500 times since March 2010. Two clips hosted by NOAA Office of Ocean Exploration ranked very highly. "Extraordinary Redeye Gaper" had 88,313 views and "Seafloor Walking: Graneledone Octopus" had 16,837 views.

The YouTube format has also proven useful in other ways. For example, clips were previewed online by Dan Rather's news team for a June 22, 2010, broadcast on HDNet featuring Dr. Erik Cordes. The production quality and popularity of the highlight videos also gained an invitation for the collection to appear in Google Earth's new Ocean layer. A Google Earth tour has been rendered from the highlights with text, metadata, and web links relevant to our research (Figure 11-1). (The tour can be downloaded from: http://db.tt/IwvW2d). The *Lophelia* II tour in Google Earth is a narrative progression (with a beginning, middle, and end) that tells the story of *Lophelia* II using approved text with the best available footage from 2008 and 2009 (see Table 11-1 for text and links). Essentially, the Google Earth tour functioned as a storyboard for the final intended 20-minute documentary of the three-year expedition.

The final 20-minute documentary was designed to incorporate new elements, such as personal interviews with project scientists, more music, more institutional logos, new graphic illustrations, title cards, and multi-lingual closed-captioning for foreign language speakers and the hearing impaired. Interviews with scientists captured overarching themes of geology, biology, archeology,

management, and technology. Researchers were able to explain their science in their own words, relaying a palpable sense of passion and excitement for ocean exploration. A full transcript of the documentary is available in Appendix F-2. The total running time for the documentary was 23 minutes, including logos and credits.

Currently, the documentary can be streamed online, viewed on smartphones, and/or downloaded at full resolution from NOAA's Ocean Explorer website and Bureau of Ocean Energy and Management on YouTube. NOAA's website offers a variety of file formats and file sizes for download, while the BOEM YouTube site offers state-of-the-art spatial and temporal tracking and unprecedented access for interested viewers from all over the world.

NOAA's Ocean Explorer website:
http://oceanexplorer.noaa.gov/explorations/12*Lophelia*/media/movies_2/*Lophelia*_video.html

BOEM YouTube website:
http://www.youtube.com/watch?v=MZG_qPKEvAk
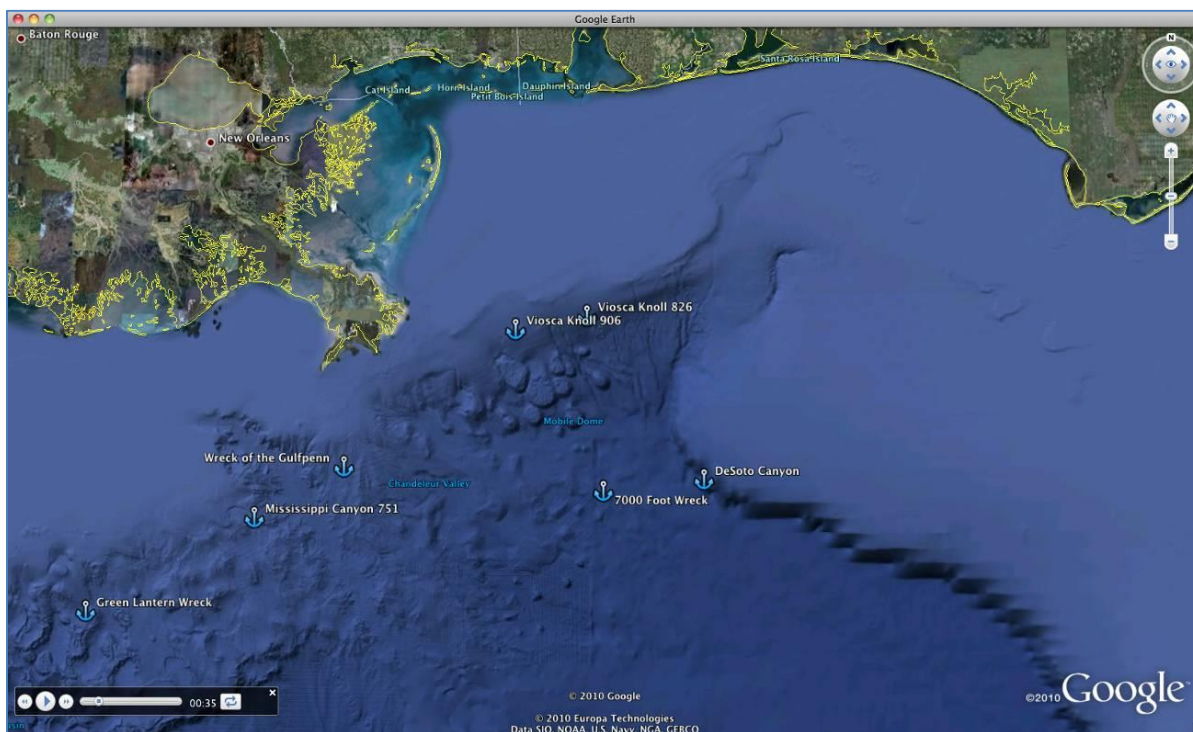


Figure 11-1.  Video tour on Google Earth.

Additional venues may become available for the *Lophelia* II videos in the near future. There is potential for the 23-minute documentary or the short highlights to appear in the Sant Hall of the Oceans at Smithsonian Institution's National Museum of Natural History in Washington, DC. Other venues include the Blue Ocean Film Festival in San Francisco, CA or the Beneath the Waves Film Festival, which tours around the world. These venues would make the *Lophelia* II video widely available for perpetuity, for public viewing and download to computers and smartphones around the world.

520

Table 11-1.

*Lophelia* II Tour in Google Earth

| Location | Lat | Lon | Depth | RunT | Description |
|---|---|---|---|---|---|
| West Florida Slope | 26.20467 | -84.7225 | 459 | 1:47 | Submerged ridges near 500 m depth on the West Florida slope were the first targets for the *Lophelia* II: Reefs, Rigs, and Wrecks 2009 Expedition. Many animals were seen, including the deep-sea coral *Lophelia pertusa*, our flagship species (white with zig-zag branches). Fish included a shark, silver dollar, sea robin, and an Atlantic roughy. Small *Lophelia* colonies grew on the twig-like skeletal axis of a black coral. *Jason II* collected *Lophelia*, and a yellow sea fan with a brittle star attached. |
| | | | | | http://www.youtube.com/watch?v=aa9yoUZYQp8 |
| DeSoto Canyon 583 | 28.38602 | -87.3873 | 2455 | 1:49 | Scientists peer through the lens of *Jason II* at 2,500 m (8,200 ft) depth near DeSoto Canyon. Submarine canyons are steep-sided features that cut through the continental slope. At this site, an exposed rock bed juts from the abyssal plain, providing substrate for bamboo and black corals, a chemosynthetic mussel community, and a deep-sea octopus. This was the deepest dive of *Lophelia* II 2009 expedition. |
| | | | | | http://www.youtube.com/watch?v=r2Q-a-nNoTI |
| Viosca Knoll (VK) 826 | 29.15636 | -88.01608 | 496 | 1:24 | A school of alfonsino fish swims over Viosca Knoll 826 (VK826), a natural deep reef, and an example of the kind of habitat scientists will study aboard the *Lophelia* II expeditions. VK826 refers to a BOEMRE leasing system for oil and gas. BOEMRE sponsored researchers aboard *Lophelia* II will compare the biota of natural reefs to biota on artificial reefs, like oil rigs and shipwrecks. Ocean chemistry is measured using a rosette of Niskin bottles and a Conductivity-Temperature-Depth (CTD) deployed over the side of the boat. |
| | | | | | http://www.youtube.com/watch?v=J6dAS1ScmbA |
| *Gulfpenn* Wreck | 28.44 | -89.32 | 561 | 1:05 | The USS *Gulfpenn* was transporting 90,000 barrels of gasoline when it was torpedoed by German submarine U-506 on May 13, 1942. Twenty-five crewmembers survived the attack, but thirteen died. The ship now lies at 550 m in the GoM, encrusted by an amazing community of *Lophelia pertusa* coral, fish, and invertebrates. |
| | | | | | http://www.youtube.com/watch?v=8Ir6uJfvYwQ |
| Mississippi Canyon (MC) 751 | 28.19072 | -89.79861 | 455 | 2:52 | The Mississippi River continues below the sea surface in the GoM to 4000 m depth as a submarine canyon called the Mississippi Canyon. Nutrients from the river support abundant deep-sea coral communities. *Callogorgia* and *Lophelia* corals settle and grow on carbonate outcrops, feeding on suspended matter. Brittlestars, squat lobsters, and urchins occur on most colonies. Active methane seeps are in the immediate vicinity. The "infaunal" community is observed using sediment push-cores. |
| | | | | | http://www.youtube.com/watch?v=CyMSvhx_r0A |
| 7,000-ft Wreck | 28.33 | -87.93 | 2256 | 1:14 | A 7,000-ft wreck is the deepest known shipwreck in the GoM. The original name is unknown, but archaeologists suspect the wooden-hulled vessel was a two-masted schooner. The bow and ships wheel are encrusted with rusticles and other signs of life. A date inscribed on the compass recovered from the wreck indicates the ship sank after June 1, 1875. The ship's wheel is prominent on the wreck. |

## Table 11-1. *Lophelia* II tour in Google Earth (continued)

| Location | Lat | Lon | Depth | RunT | Description |
|---|---|---|---|---|---|
| | | | | | http://www.youtube.com/watch?v=5kYOIBCbeVk |
| Viosca Knoll 906 | 29.09839 | -88.40345 | 300 | 1:15 | Viosca Knoll 906 is home to a *Leiopathes* black coral community. The number "906" identifies the oil and gas lease block that encompasses area. Black corals can be incredibly long lived. Living colonies are white, salmon, or orange. Only the skeleton is black. The branches are habitat for fishes and crustaceans. Barrelfish were one type of commercial fish that was present in the area. Geneticists aboard *Lophelia* II will decode the black coral DNA to determine whether we see one species or many. |
| | | | | | http://www.youtube.com/watch?v=U6IqiLHT7nU |
| Garden Banks (GB) 535 | 27.42292 | -93.59727 | 600 | 1:30 | The westernmost aggregation of *Lophelia pertusa* coral in the North Atlantic was discovered in an oil and gas lease block called Garden Banks 535 during *Lophelia* II 2009 Expedition. *Lophelia* colonies occurred on large carbonate outcrops near 500 m depth. Many squat lobsters and fishes were seen in and around the coral colonies, including slimeheads, tinselfish, and a chain catshark. |
| | | | | | http://www.youtube.com/watch?v=85YtHgRAV3I |
| *Green Lantern* Wreck | 27.71667 | -90.71667 | 915 | 1:13 | C&C Technologies, Inc. found the *Green Lantern* wreck during a deep-tow survey in 1996, and their archeologists investigated in 2004. The wreck is an unidentified copper-clad sailing vessel that measures approximately 20 m in length. The wreck is named for one of the ships lanterns found lying just outside the stern. The lantern caught the attention of the archeologists. It was embossed with the word Estribor, Spanish for "starboard." Just like modern ships, historic vessels ran a green light on the starboard side and a red lantern on the port side. |
| | | | | | http://www.youtube.com/watch?v=6BermqpuVis |
| Green Canyon (GC) 852 | | | | 3:08 | Green Canyon is a submerged ridge at 1410 m (4625 ft) depth in the GoM with high diversity of deep-sea corals. The ridge was explored by the science party of the *Lophelia* II 2009 Expedition in August, 2009 using the *Jason II* ROV. The research was part of an ongoing initiative by Bureau of Ocean Energy Management, Regulation and Enforcement (now BOEM) and National Oceanic Atmospheric Administration to understand deep-sea habitat in the Gulf. The project now provides important baseline information to the Natural Resource Damage Assessment resulting from the *Deepwater Horizon* oil spill. |
| | | | | | http://www.youtube.com/watch?v=1Lii6f5cd2M |
| Attribution: | | | | | Videos by Aquanautix. Music is by Kevin MacLeod, www.incompetech.com. *Lophelia* II 2009: Reefs, Rigs, and Wrecks Expedition was sponsored by the Minerals Management Service (later BOEMRE, now BOEM) and National Oceanic and Atmospheric Administration (NOAA). |
| Total | | | | 15:57 | |

# 12 IMPROVED PREDICTION OF COLD-WATER CORALS OCCURRENCE IN THE GULF OF MEXICO

## 12.1 BACKGROUND

Understanding the environmental and geographic distribution of species is an ongoing challenge in deep-sea ecology. Distribution patterns in the deep-sea are generally poorly resolved, in part due to the difficulty and expense of surveying deep water regions, and the vast area of unexplored seafloor (e.g., Gage 2004). It has been estimated that only 0.0001% of the deep-sea has been surveyed (Gjerde 2006) and much of this past work has focused on a few relatively well studied areas (e.g., North Atlantic seamounts). A better understanding of species' biogeographical distributions is fundamental for designing and implementing management plans, shaping future research efforts, and assessing anthropogenic impacts. Given the recent increase in the rate and scale of anthropogenic disturbance to the deep-sea, it is imperative to more fully characterize the distribution and niche of deep-sea species before these ecosystems are irrevocably altered or lost.

Cold-water corals comprise the majority of the world's known coral species and support biodiversity hotspots in the deep-sea by providing structurally complex habitats. They fill vital ecological roles in the deep-sea through nutrient cycling, habitat creation, and carbon sequestration. Due in part to their importance in structuring deep-sea communities, it is increasingly important to understand how ecological factors interplay with species' traits to influence observed distributions. Currently, the factors that are primarily responsible for controlling cold-water coral distributions are only partially understood. Previous work has shown that corals cluster on elevated seafloor features where the current regime and topography combine to generate locally accelerated flows, which increases food availability, larval dispersal, and sediment and waste removal (Frederiksen et al. 1992; Mortenson et al. 2001; Masson et al. 2003; White et al. 2005; Guinotte et al. 2006). The availability of hard substrata is generally thought to be necessary for larval recruitment (e.g., Freiwald et al. 1999), however, settlement may also occur on mixed bottoms, small substrata including shells, cobbles, or boulders, and man-made objects (Wilson 1979; Gass and Roberts 2006). The success of cold-water corals also appears to be influenced by the aragonite or calcite saturation state, with numerous field reports that most cold-water coral aggregations occur at higher saturation states (Guinotte et al. 2006; Lunden et al. 2013), as well as experimental results that suggest an energetic cost associated with calcification at low saturation states (e.g., Turley et al. 2007; Maier et al. 2009, but see Thresher et al. 2011). Finally, cold-water corals are heterotrophic filter feeders that are reliant on the transfer of energy from surface primary production of which only 1-3% reaches the deep-sea (Deuser 1986). Therefore, high surface productivity and nutrient availability are expected to be positively linked with cold-water occurrence (e.g., Tittensor et al. 2009).

Ecological niche models are being increasingly used to characterize the distribution of both terrestrial and marine organisms by statistically coupling occurrence records with environmental parameters. This approach has recently gained traction in the deep-sea, where extensive direct observations are logistically difficult, and occurrence data are often sparse. A number of deep-sea species distributions have been recently characterized using a variety of modeling techniques, including squat lobsters (Wilson et al.2007), echinoids (Pierrat et al. 2012), and several species of

cold-water gorgonians (Leverette and Metaxas 2005; Bryan and Metaxas 2006, 2007; Tong et al. 2012; Yesson et al. 2012; Quattrini et al. in press). In addition, North Atlantic and global populations of *L. pertusa* have been modeled using a variety of techniques (Dolan et al. 2008; Guinan et al. 2009; Tittensor et al. 2009; Howell et al. 2011; Davies et al. 2008; Davies and Guinotte 2011). However, these studies generally used low-resolution environmental data (30 m$^2$ - 1°; but see Dolan et al. 2008) and did not include the GoM. Populations in the GoM are genetically isolated (Morrison et al. 2011) and *L. pertusa* may occupy a different niche space in other biogeographical areas than in the GoM.

There is an immediate need to better establish the baseline niche of cold-water corals in the GoM and to develop quantitative methodology for locating novel coral sites. We built ecological niche models for five species of cold-water corals in the GoM: *Lophelia pertusa*, *Leiopathes glaberrima*, *Callogorgia gracilis*, and *C. americana delta* and *C. a. americana*. Our specific goals were to: 1) develop high-resolution, local-scale models at commonly studied sites in the GoM to quantify niche and predict novel occurrences at each site, 2) generate a lower-resolution, large-scale model for each species to allow for the inclusion of additional environmental data and to facilitate discovery of novel cold-water coral sites in unexplored regions of the GoM, and 3) evaluate and compare the niche space occupied by each species in the GoM.

## 12.2 METHODS

### 12.2.1 Occurrence Data

Video data collected during ROV and human-operated vehicle (HOV) dives spanning from 2005 – 2011 were reviewed to extract cold-water coral occurrences, which were linked to USBL navigational data (slant error of 1%) to yield a set of georeferenced occurrence points for each site. Occurrences observed on video were supplemented with observation and collection logs; however, we found that observations recorded during dives generally underreported occurrences. Additional occurrences were obtained from Schroeder et al. (2005) and the Smithsonian National Museum of Natural History database. Only occurrence records obtained from submersible or ROV dives were included from the Smithsonian National Museum of Natural History database to avoid potential inaccuracies in the recorded location of samples collected by trawling or unknown sources. To ensure that only spatially explicit presence points were included in analyses, we removed duplicate points that occurred within the same multibeam grid cell. *L. pertusa* and *L. glaberrima* were generally highly visible and easily distinguishable from other species, making the probability of detection extremely high in surveyed areas, eliminating a common source of modeling error. *Callogorgia spp.* were not visually distinguishable but were identified to species level both genetically and morphologically (Quattrini et al. in press; see Section 4.3.1).

### 12.2.2 Environmental Data

*Loca- scale models:* Bathymetric data were acquired in 2008 using a Kongsberg-Simrad EM1002 multibeam echosounder (95 kHz, 111 beams, 150° coverage) mounted on the *R/V Nancy Foster*. This yielded high quality bathymetric data, which were gridded at either 5 or 8 m and used to derive subsequent environmental layers using ArcGIS 10.1 (ESRI). Aspect, curvature, rugosity, and slope, believed *a priori* to structure coral distribution, were calculated using the Digital Elevation Map Surface Tool (v. 2.1.292, Jennes 2011). Aspect, which measures the directionality

of the steepest slope, has an inherent circularity when measured in radians so a cosign transformation was applied to create an index of northness on a continuous scale from -1 (facing south) to +1 (facing north), and a sine transformation to create an index of eastness, on a scale from -1 (facing west) to +1 (facing east). Curvature assigns more positive values to more convex seafloor surfaces, and more negative values to more concave surfaces. Slope was measured in degrees using the 4-cell method (Fleming and Hoffer 1979) which has been shown to marginally outperform Horn's method (Horn 1981), the default in ArcGIS (see Jones 1998). Rugosity is a measure of seafloor complexity, calculated as the ratio of surface area to planar area (Jenness 2004). We calculated bathymetric position index (BPI) using the Land Facet Corridor Designer (v.1.2.848, Jenness et al. 2013). BPI quantifies the relative position of points to their surrounding features. Depressions are assigned a negative value and positive features are assigned positive values. Values of zero indicate either a flat surface or a continuous slope. Importantly, this measure is inherently scale dependent (see Lunblad et al. 2006), so we calculated BPI at a number of scales: 5, 25, 100, and 500 m. Seismic data were obtained at a relatively high resolution (generally <10 m$^2$) for most sites (excluding GC140 and GC246) from BOEM 3D seismic surface reflectivity images. Each image was georeferenced and then reclassified using a histogram equalized scheme to classify areas of each site by dividing the initial image values into four categories according to their intensity values: very high, high, low, and very low.

*Callogorgia mosaic models* – To ecologically distinguish closely related sister taxa in the *Callogorgia* genus, additional environmental variables believed *a priori* to structure gorgonian populations were included in a separate set of *Callogorgia spp.* models: seep activity, temperature, salinity, dissolved oxygen, and calcite saturation state ($\Omega_{calcite}$). This necessitated a modified data processing method, in which variables were restricted to a 50 m buffer around dive tracks to allow for the inclusion of data that lacked site-wide coverage. Temperature, salinity, $\Omega_{calcite}$, and dissolved oxygen data were interpolated to the same resolution as the available bathymetry data using the inverse distance weighted technique in ArcGIS. Points identified from video as seep habitat were buffered to a 25 m radius, and regions within buffers were considered to be seep environments and regions outside of buffers were considered to lack seep activity. Other topographical variables were derived from bathymetry as described above. In order to standardize models to the same study area, all sites containing any of the *Callogorgia* species were mosaicked together to form a single raster layer for model generation and subsequent niche evaluation (GC140, GC234, GC246, MC751, MC885, VK826, and VK862/906).

*Large-scale models*: Bathymetry data were obtained at a 25 m$^2$ resolution from the Texas Sea Grant College Program for an area in the northern GoM covering over 67,000 km$^2$. Aspect, BPI, curvature, rugosity, and slope were derived as described above, except that BPI was calculated at scales of 25, 100, and 1000 m. Hard bottom locations were available as a polygon layer from BOEM and were converted to a 50 m$^2$ resolution binomial raster (1=hard bottom, 0=soft bottom). Student's t-tests were used to determine if model predictions varied significantly with substrate type. Phosphorus and nitrate surface data were obtained from the National Oceanographic Data Center. Chlorophyll *a* surface data (a proxy for primary productivity) were obtained from Moderate Resolution Imaging Spectroradiometer data via the Giovanni online data system maintained by the NASA GES DISC. Aragonite saturation states ($\Omega_{arag}$) were obtained at depth from a 2010 cruise on the R/V *Ronald Brown* (Lunden et al. 2013; see Section 3.2) and the 2007 Gulf of Mexico and East Coast Carbon cruise (Wang et al. 2013). Although *L. glaberrima* and

*Callogorgia spp.* utilize the calcite form of calcium carbonate instead of the aragonite form, we included only aragonite because the two datasets were calculated from the same carbonate data. Surface nutrient and aragonite saturation state data were interpolated to a 25 m$^2$ resolution using the inverse distance weighted technique in ArcGIS. A consensus model was created by training a model using the occurrence points for all species.

## 12.2.3 Model Generation and Evaluation

Numerous niche modeling approaches exist, ranging from relatively simple regression, linear, or additive models (see Pearce and Ferrier 2000), more complex genetic algorithms and neural networks (Stockwell and Noble 1991; Recknagel 2001), and sophisticated machine-learning algorithms (Hirzel et al. 2002, 2006; Phillips et al. 2006). Most traditional methods for modeling species' distributions require both presence and absence data. However, obtaining accurate absence data in the deep-sea is usually impossible due to the prohibitive amount of time and expense required. Therefore, datasets on the absence of deep-sea species are typically sparse and biased due to the limited field of view of the ROV and lack of systematic observations across all of the potentially occupied substrata. Regardless of the environment, habitat suitability predictions from absence data may be inaccurate or misleading due to dispersal limitation, biotic interactions, detection error, or historical reasons (see Hirzel et al. 2002). Therefore, we used the machine-learning MAXENT algorithm (v3.3.3k, Phillips et al. 2006) because it utilizes pseudoabsence (background) data rather than true absence data, and has consistently outperformed other presence-only techniques (Elith et al. 2006; Tittensor et al. 2009). Models were created using default MAXENT parameters (convergent threshold = 10-5, regularization=1, number of background points = 10,000, default prevalence = 0.5; see Phillips and Dudik 2008), however, we increased the number of maximum iterations to 5,000 to ensure model convergence. During model training, 10% of occurrences were withheld and used to test each model, a process known as k-fold cross validation (k=10) that outperforms other commonly used validation techniques (Kohavi 1995). A jackknifing procedure, in which models are constructed using different combinations of variables, was used to determine the percent contribution of each variable to final models. To further assess variable contributions, we generated response curves that show how model predictions change as a function of the range of values for the variables that contributed the most information to models. To assess whether predictions were significantly different among seismic classes (very high, high, low, very low), we employed a one-way ANOVA followed by pair-wise Holm-Sidak post-hoc tests, or a Kruskal-Wallis ANOVA with a Tukey post-hoc test if the data violated either the normalcy or equal variance test (SigmaPlot 12.3). Since correlations between variables confound interpretation of variable importance, we assessed the Pearson-product movement correlation between each variable in JMP (v.9.0.0, SAS Institute). However, even highly correlated variables were not removed from models (with the exception of calcite, see above) because MAXENT has been shown to be robust with regards to correlated inputs (Phillips et al. 2006). Each model produced two continuous outputs, a raw output for subsequent statistical analysis (see below), and a more intuitive logistic output ranging from 0-1. Commonly referred to as the habitat suitability index, the logistic output indicates the probability of occurrence at each locality, visualized as a habitat suitability map.

The predictive ability of models was assessed by comparison to a random model using a threshold-dependent exact binomial test, with the null hypothesis stating that the model predicts test points no more accurately than a random model. The ability of models to accurately predict test data was

also assessed using a threshold-independent receiver operating characteristic curve, which tests the ability of the model to correctly rank both presences and absences. The true positive rate (sensitivity) of the model is plotted against the false positive rate (1 – specificity). Receiver operating characteristic curves are evaluated by the area under the curve (AUC) metric that indicates the probability that the model will rank true occurrences over negative occurrences. The maximum theoretical AUC is 1.0 and a random model has a theoretical AUC of 0.5. Values greater than 0.7 are indicative of 'good' model performance, while values above 0.9 are considered 'excellent' (Swets 1988; Fielding and Bell 1997).

As a final test of model accuracy, a model was generated from an independently collected dataset of *L. pertusa* occurrences from photographic transects conducted at VK826 by the autonomous vehicle *Sentry* (WHOI) in 2009 (see Section 4.1).  Seven transects averaging 885±123 m in length were conducted in the area covering the large knoll at the center of the site in an ordered, predetermined fashion and were therefore subject to less bias than occurrences observed from ROV and HOV dives. Georeferenced photographs were taken at regular, overlapping intervals and analyzed for living or dead *L. pertusa* cover. A single MAXENT model was trained using only these occurrences with identical environmental layers and parameters as the original VK826 model. The resulting model was compared to the originally calculated model.

### 12.2.4 Niche Evaluation

To determine the niche breath of each species, we used the statistical package ENM Tools (v1.3, Warren et al. 2008, 2010). ENM Tools measures niche breath in accordance to the inverse concentration (B1) metric developed by Levins (1968) and reintroduced by Nakazato et al. (2010). A larger index value indicates that the species occupies a wider niche space, and a smaller value indicates that the species occupies a more specialized niche; given by the following equation where *p* equals the proportion of occurrences found in the environment *i*:

### 12.2.5  Niche Breadth:   $1/B = \Sigma pi2$

To determine the extent to which each species' niche overlaps, we calculated the *I* metric for each pair of niche models (Warren et al. 2008). The *I* metric is a modified Hellinger distance (van der Vaart 1998) ranging from 0-1, where x and y are the two species being compared and *p* is the probability of each species occurring in the geographic space *i*:

$$\textbf{Niche overlap (\textit{I}):} \quad I\,(p_X, p_Y) = 1 - \frac{1}{2}\sqrt{\Sigma_i(\sqrt{p_{X,i}} - \sqrt{p_{Y,i}})^2}$$

A value of 0 indicates that niches are completely discordant and a value of 1 indicates that niches are identical. We followed the guidelines established by Rödder and Engler (2011) for interpreting the *I* metric: values below 0.2 indicate no or limited niche overlap, values between 0.2 – 0.4 indicate low overlap, values 0.4 – 0.6 indicate moderate overlap, and values greater than 0.6 indicate high overlap. To determine if each species' niche was more or less similar than expected by chance, we employed the identity test in ENM Tools. The identity test measures niche overlap (*I*) between a null distribution of random models. If the actual value of *I* between two species' niches is significantly lower than the null distribution, the niches are considered to be divergent. If the environmental conditions available to each species are considerably different (e. g., species

occupy separate depth zones), it is possible to observe significant divergence under the identity test, even if the species occupy similar niches in reality. Therefore, we also employed the background test in ENM Tools for the *Callogorgia spp.* mosaic models, because the species do not coexist at any site and it is therefore likely that that they occupy different conditions. The background test compares the actual niche overlap (*I*) between species to two null distributions of models generated in the environment available to each species. If the observed overlap between species' niches is significantly lower than both of these null distributions, than the niches are considered to be significantly divergent.

We generated a rough estimate of the geographic range of each species by buffering occurrences by 20 km and dissolving overlapping areas in ArcGIS (*sensu* Nakazato et al. 2010). While this method is unlikely to be representative of the true range of the species in the GoM, it provides a uniform method to compare the relative range of each species within the study area. We then estimated niche filling, the proportion of suitable area that was actually occupied, by comparing the geographic range to a binary prediction of suitability where 'suitable' habitat was defined by the sensitivity-specificity sum maximization approach (Liu et al. 2005).

### 12.2.6 Predictive Modeling Program

To allow researchers who are unfamiliar with modeling techniques to apply our model to their own data to predict cold-water coral locations, we incorporated models for each species into the downloadable program 'Cold-water Coral Modeler', freely available along with a user's manual on the Cordes website. The program was constructed in C# using Microsoft Visual Studio 2012. It utilizes the lambda file created by MAXENT during model generation to project a predictive model onto bathymetric data input by the user, generating a habitat suitability map in a novel geographic region. Input data can be gridded at any resolution using any spatial reference but must match the input layers used in our original models.

## 12.3 RESULTS AND DISCUSSION

### 12.3.1 Local Scale Models

MAXENT models were constructed for *L. pertusa* at seven sites in the GoM: VK826, VK862/906, MC751, MC885, GB535, GC234, and GC354 (Table 12-1), visualized as habitat suitability maps (Figure 12-1). Evaluation of models with test data showed that all models were robust. The average test AUC for all sites was 0.967±0.02, with a lowest AUC value of 0.934 at VK826. All models significantly outperformed a random model (exact binomial test, $|p|<0.01$; Table 12-1). Niche breadth (inverse concentration) averaged $77.9±67.8 \times 10^{-3}$ across all sites and ranged from 13.47 at GB535 to 153.17 at GC234. VK862/906, MC751, and GC354 all had intermediate niche breadths of 31.70, 30.94, and 30.98 respectively. AUC was significantly correlated with niche breadth (Pearson's correlation, $r = -0.86$, $p<0.05$), indicating that models performed better when *L. pertusa* occupied a narrower niche space. The number of occurrences used to train models was not correlated with either AUC (Pearson's correlation, $r = -0.11$, $p=0.82$) or with niche breadth (Pearson's correlation, $r = -0.32$, $p=0.48$).

Table 12-1.

Input data and model evaluation for *L. pertusa* local scale models. The number of spatially explicit occurrences and the average AUC±s.d. are shown with significance marked (exact binomial test, *=p<0.01, ** p<0.001). The two primary explanatory variables for each model are listed along with the percentage of information contributed by each variable, as determined by jackknifing

| Site | No. of occurrences | Average AUC ± s.d. | Niche breadth (x 10$^{-3}$) | Variable 1 | Variable 2 |
|---|---|---|---|---|---|
| VK826 | 1242 | 0.934±0.004[**] | 104.47 | BPI-500 m (57.6%) | Depth (40.2%) |
| VK826 (*Sentry*) | 454 | 0.956±0.012[**] | 86.02 | BPI-500 m (65.9%) | Depth (30.0%) |
| VK862/906 | 425 | 0.975±0.006[**] | 31.70 | BPI-500 m (96.4%) | BPI-100 m (1.1%) |
| MC751 | 166 | 0.986±0.007[**] | 30.94 | Depth (51.9%) | BPI-500 m (29.4%) |
| MC885 | 11 | 0.952±0.045[*] | 180.61 | BPI-500 m (38.9%) | Hard bottom (23.8%) |
| GB535 | 26 | 0.996±0.002[**] | 13.47 | BPI-500 m (60.1%) | Rugosity (19.6%) |
| GC354 | 29 | 0.979±0.037[**] | 30.98 | Depth (42.5%) | Hard bottom (27.5%) |
| GC234 | 15 | 0.947±0.073[*] | 153.17 | Depth (42.7%) | Hard bottom (41.3%) |

In all models, suitability indices for *L. pertusa* were higher at positive BPI values, indicating that elevated seafloor features provided better habitat than depressions or flat areas (Figure 12-2). BPI calculated at a large scale (500 m) was the primary or secondary explanatory variable in five out of seven models, contributing an average of 56.5% of information in those models (Table 12-1). While rugosity was among the top two explanatory variables only at GB535 (percent contribution of 19.6%), suitability indices increased with greater rugosity at all sites, plateauing at a rugosity value of approximately 1.2. The higher suitability indices observed at positive BPI and rugosity values demonstrated that *L. pertusa* has a clear preference for more complex, elevated topography, and indicated that depressions and flat areas were generally sub-standard habitat. Elevated regions have been shown to increase local current speeds, boosting the transport of food and nutrients (Thiem et al. 2006), increasing larval supply (Piepenburg and Müller 2004) and reducing sediment deposition (Rogers 1994). These results were not surprising, because previous work has often associated the presence of *L. pertusa* and other cold-water corals with steep, elevated, and complex topography even at large scales (e.g., Bryan and Metaxes 2006; Davies et al. 2008, but see Tittensor et al. 2009), an association known as the 'enhanced current hypothesis' (see Masson et al. 2003). The high-resolution bathymetry used here would only further reveal the ability of relatively small features to affect local current regimes. In addition, since established colonies increase sedimentation rates by acting as a barrier to current flow, the presence of large *L. pertusa* structures may have facilitated historical mound growth, creating a feedback loop that further elevated successful colonies (Paull et al. 2000).
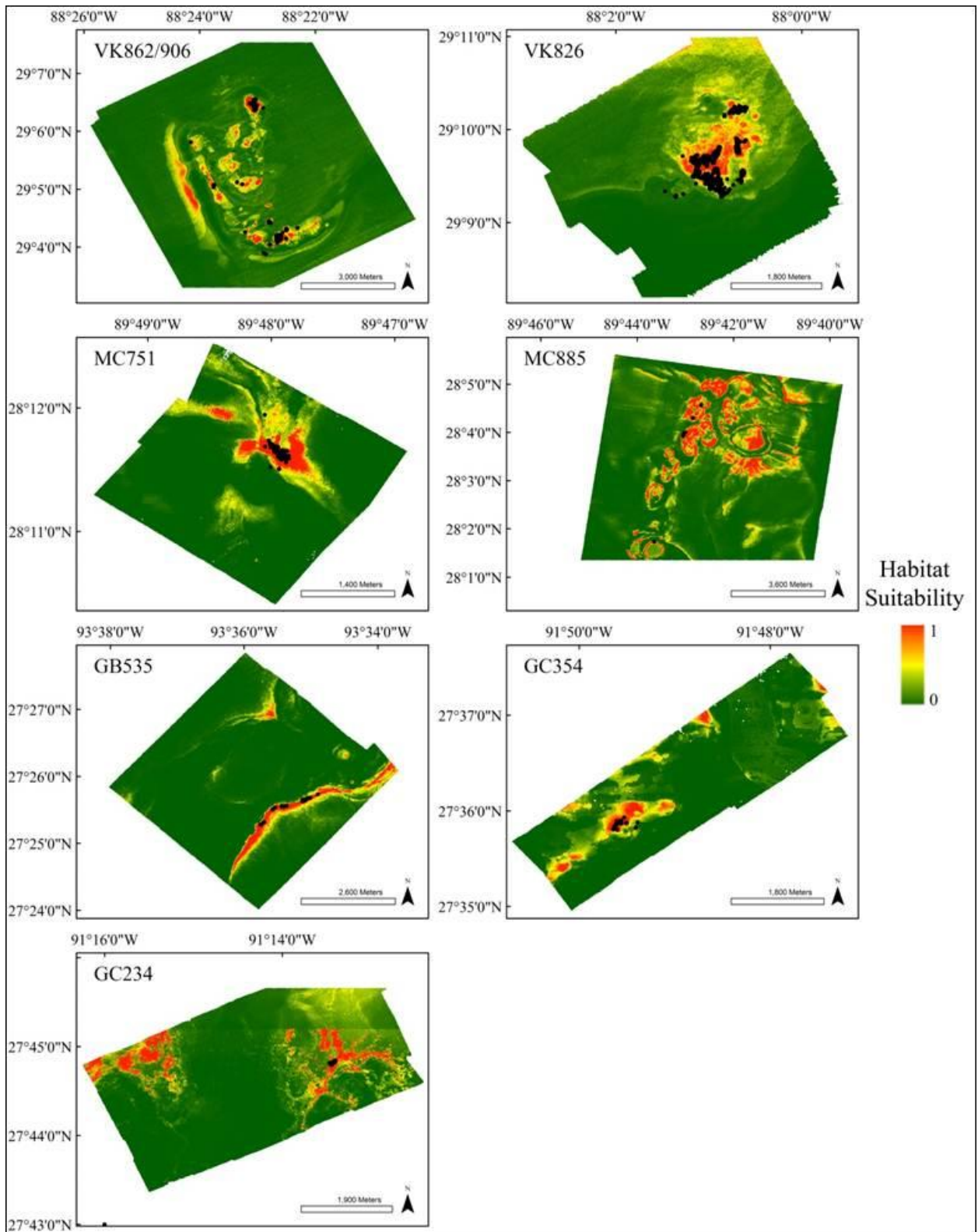
Figure 12-1.  Local-scale habitat suitability models for *L. pertusa*. Warmer colors indicate locations that are predicted to be more suitable. Black points indicate occurrences used to train and test the models. Note differences in scale.
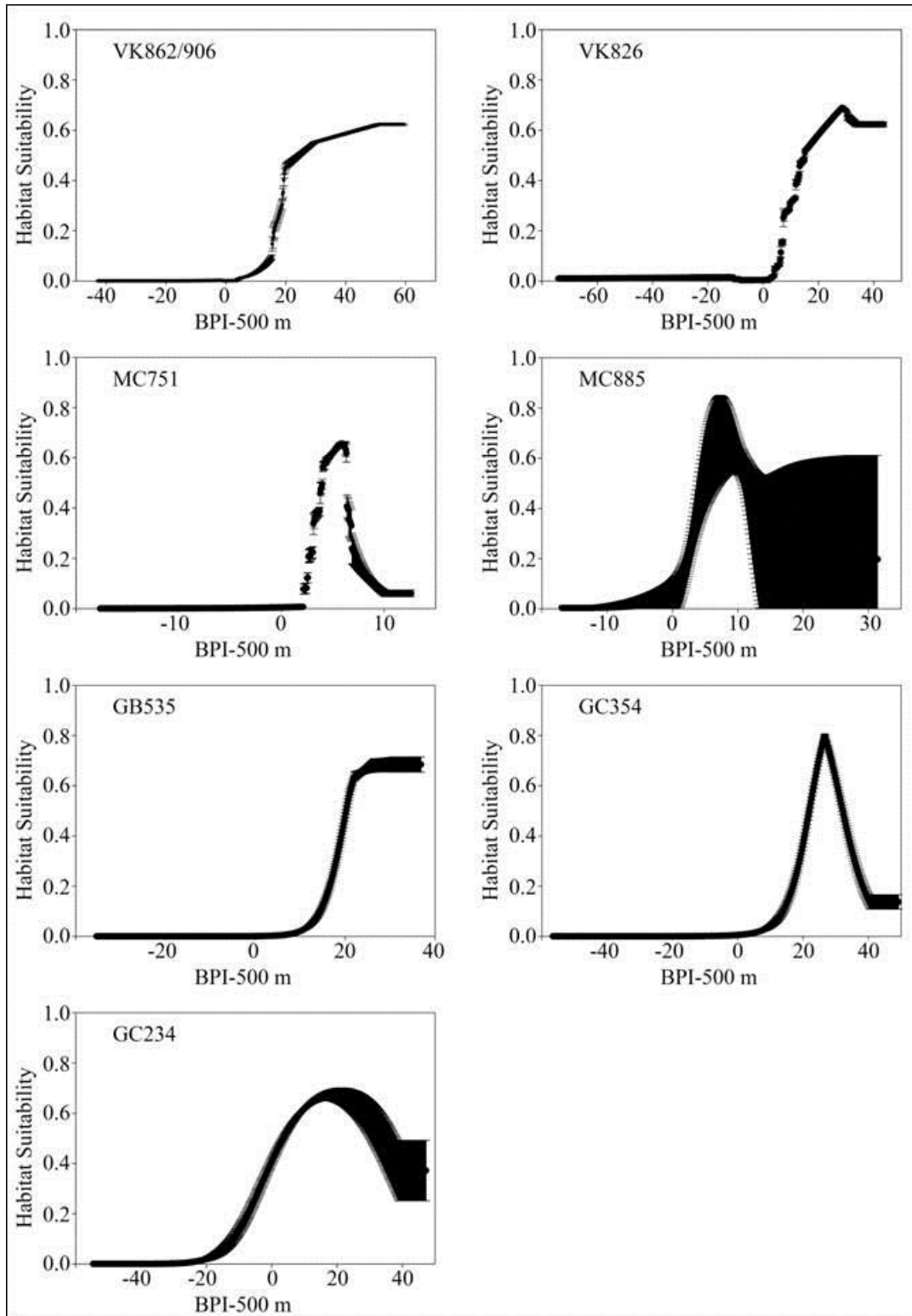
Figure 12-2. Response of the predicted habitat suitability for *L. pertusa* to changes in bathymetric position index (BPI) calculated at the 500 m scale for local scale models. Error bars indicate standard deviation. In general, locations with higher BPI values were predicted to be more suitable for *L. pertusa*.

531

However, at VK826, MC751, MC885, GC354, and GC234, suitability indices peaked before the maximum BPI values at each site, indicating that there may be an obstacle to colonization or survival at the shallowest features of a site. This finding is consistent with recent studies that recorded reduced diversity on the summits of seamounts relative to the surrounding slopes, thought be influenced in part by extreme hydrological forces, exposure to oxygen-minimum zones, or fine-scale topography of the summit (see review by Clark et al. 2010). At sites with large mound structures (e.g., VK826), the summits may experience dramatically accelerated currents that have been shown to prevent the recruitment of other invertebrate larva (e.g., Mullineaux and Garland 1993) and negatively affect *L. pertusa* feeding rates (Purser et al. 2010). Alternatively, it is plausible that since locations with extremely high BPI values were not as common at most sites, they were less likely to be inhabited simply by chance.

Depth was the primary or secondary explanatory variable in four out of seven *L. pertusa* models, contributing an average of 35.5% of information in those models (Table 12-1). Suitability indices tended to be higher in the shallower regions of each site, with highest index values between depths of approximately 300-600 m (Figure 12-3), within the known depth range for *L. pertusa* in the GoM. The presence of hard bottom (measured as relative surface seismic reflectivity) was the secondary explanatory variable in three models (MC885, GC354, and GC234), contributing an average of 30.9% of information. At all sites, the suitability index was significantly higher when seismic reflectivity was very high or high (Kruskal- Wallis, $p<0.01$, post-hoc Tukey $p<0.05$; Figure 12-4). This finding confirms previous work suggesting that *L. pertusa* and other coral species require hard substrate for the initial attachment and recruitment of larva (Wilson 1979), and may largely explain the absence of corals at locations that are otherwise suitable.
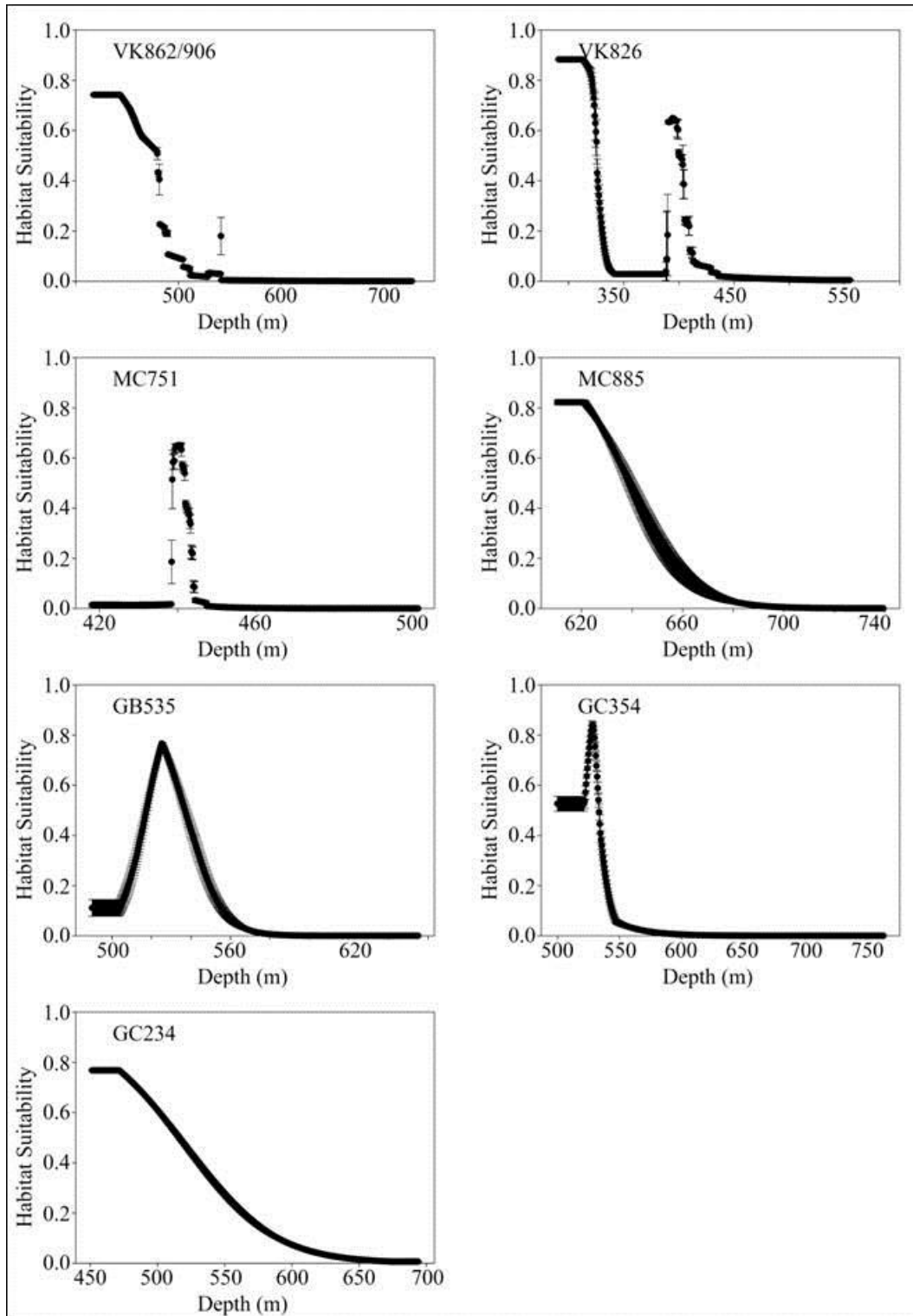
Figure 12-3. Response of the predicted habitat suitability for *L. pertusa* to changes in depth (m) in local scale models. Error bars indicate standard deviation. In general, *L. pertusa* had the highest suitability indices between depths of approximately 300-500 m.
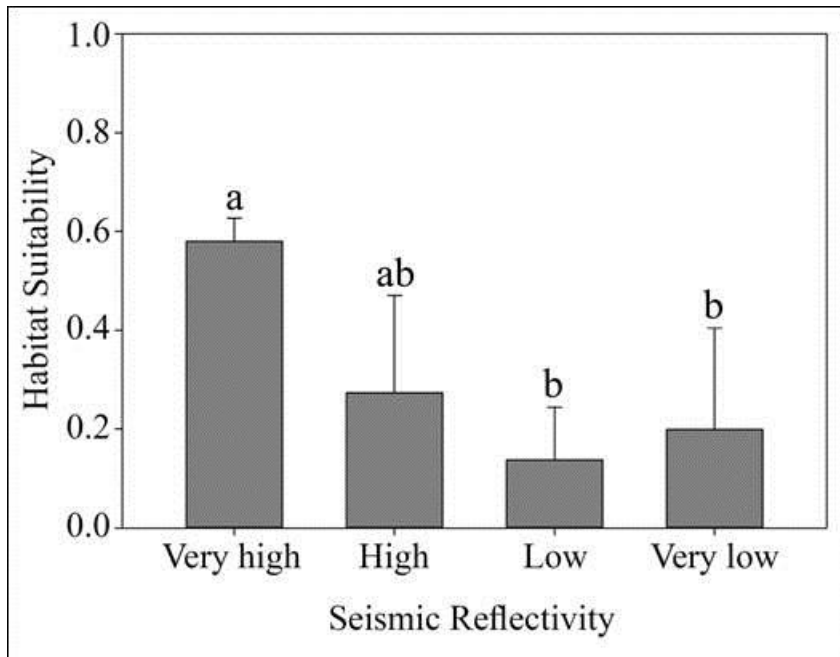
Figure 12-4. Response of the predicted habitat suitability for *L. pertusa* to changes in seismic reflectivity data, averaged across all sites. Higher reflectivity values indicate the presence of hard substrata. Locations with very high reflectivity values had significantly higher suitability indices than sites with low or very low reflectivity values (Kruskal- Wallis p<0.01, post-hoc Tukey p<0.05). Error bars indicate standard deviation.

An additional *L. pertusa* model was constructed at VK826 using only the occurrences obtained from *Sentry* transects as a general test of model accuracy. This test model had an AUC of 0.956 ± 0.012 and significantly outperformed a random model (exact binomial test, p<0.01; Table 12-1). The test model was significantly correlated with the original VK826 model (Pearson's correlation, r=0.91, p<0.01), and the models were not significantly different from each other under the identity test (I=0.95, p>0.05). The high degree of similarity between the original model and a test model built with more structured transect data verifies the accuracy of the original model and strongly suggests that the potentially deleterious effects of bias caused by user-directed ROV and HOV sampling were minimal or non-existent. When compared to the original VK826 habitat suitability map (Figure 12-5), the test model and original model appeared to predict similar locations to be the most suitable, but the test model tended to over-predict large areas as being highly suitable. In part, this may have resulted from the lower sample size (test n=454, original n=1242) and reduced spatial coverage of the transect sampling, or because dead colonies were included as occurrences in the analysis of transect photographs. Including dead colonies as occurrences may have caused unsuitable or barely suitable areas to be predicted as highly suitable. The presence of dead skeletal structures may indicate that the location was previously suitable due to unknown historical or stochastic factors, but recently became unsuitable. Alternatively, they may represent areas with relatively poor environmental conditions but high propagule pressure, a combination that might allow recruitment but inhibit the growth and long-term success of adults. Therefore, the re-analysis

of this dataset to remove dead colonies as occurrences may even further increase the similarity between the original model and the test model.
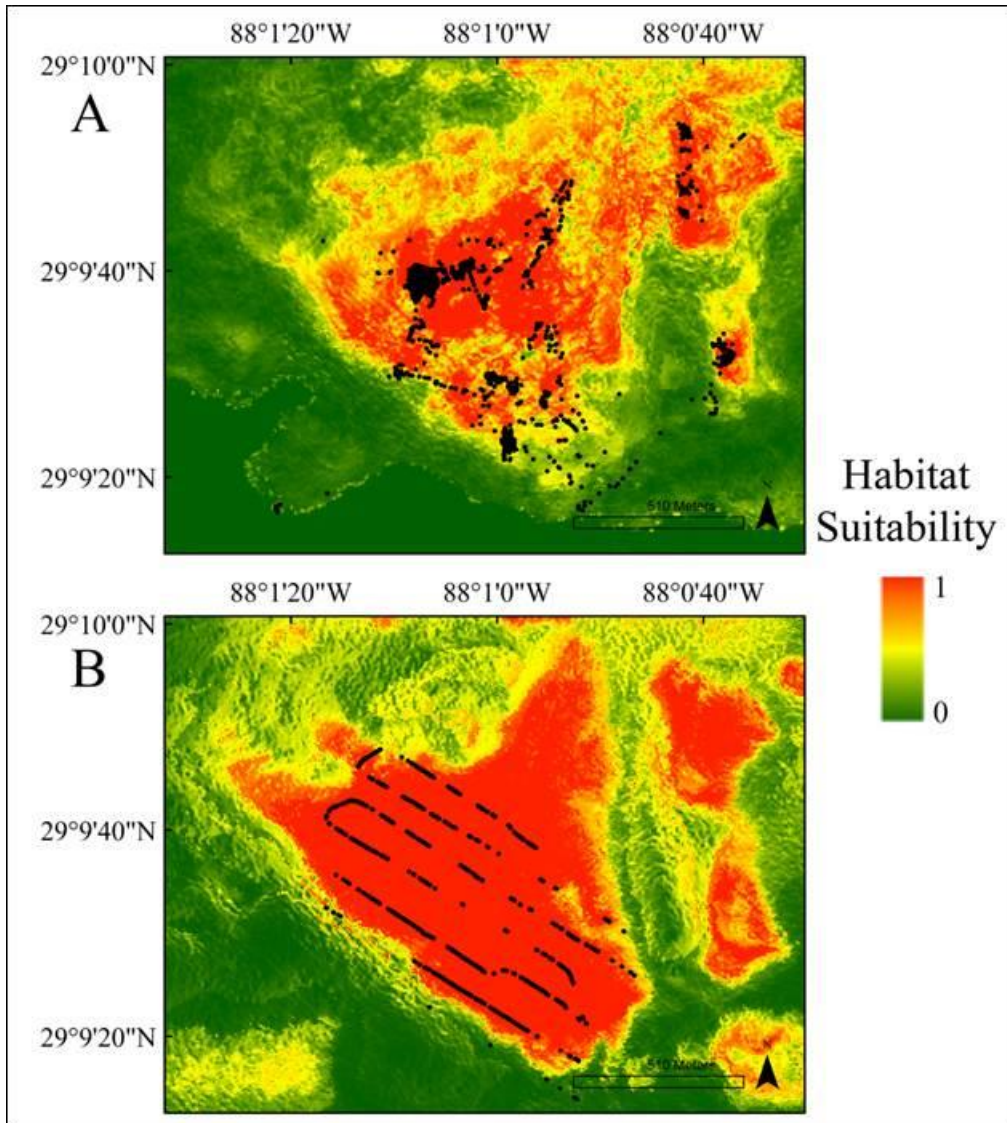


Figure 12-5. Enlarged view of habitat suitability maps for local scale *L. pertusa* models at VK826. A) Original VK826 model. B) Test model trained using only the transect occurrence data from *Sentry*. The two models were highly correlated (Pearson's correlation, r=0.91, p<0.01) and were not significantly different from each other under the identity test (I=0.95, p>0.05). Warmer colors indicate locations that are predicted to be more suitable. Black points indicate occurrences used to train the models.

Models were constructed for *Leiopathes glaberrima* at two sites: VK826 and VK906 (Figure 12-6). Both models performed well, with an average AUC of 0.958±0.011 at VK826 and 0.983±0.003 at VK862/906 (Table 12-2). At both sites, BPI calculated at a large scale (500 m) was the primary explanatory variable, contributing 50.4% of information at VK826 and 49.7% at VK862/906.

Response curves revealed that suitability indices were generally higher at BPI values greater than 20 (Figure 12-7). Interestingly, at VK826 suitability decreased when BPI was greater than 20, while at VK862/906, suitability did not peak until 60, the maximum BPI value found at the site. Depth was the secondary explanatory variable for both models, contributing 43.8% of information at VK826 and 43.9% at VK862/906. Suitability at VK826 was highest at depths between 450-475 m (Figure 12-8). At VK862/906, there was a peak in suitability at a depth of approximately 300 m corresponding with the top of the mound in VK862, and a second peak between 400-450 m corresponding with the Roberts' Reef cold-water coral mound in VK906 (Figure 12-8). Averaged across both sites, suitability was significantly higher when seismic reflectivity was very high (ANOVA, $p<0.01$, post-hoc Holm-Sidak $p<0.01$; Figure 12-9). The *L. glaberrima* model at each site was highly similar to its corresponding *L. pertusa* model, suggesting that the species occupy a similar niche at these sites; consistent with frequent observations of *L. glaberrima* growing on or immediately adjacent to *L. pertusa* structures, particularly around the periphery of Roberts' Reef. Niche breadth varied widely between the two sites, ranging from $39.12 \times 10^{-3}$ at VK862/906 to $112.52 \times 10^{-3}$ at VK826; mirroring the pattern observed for *L. pertusa* at these sites.
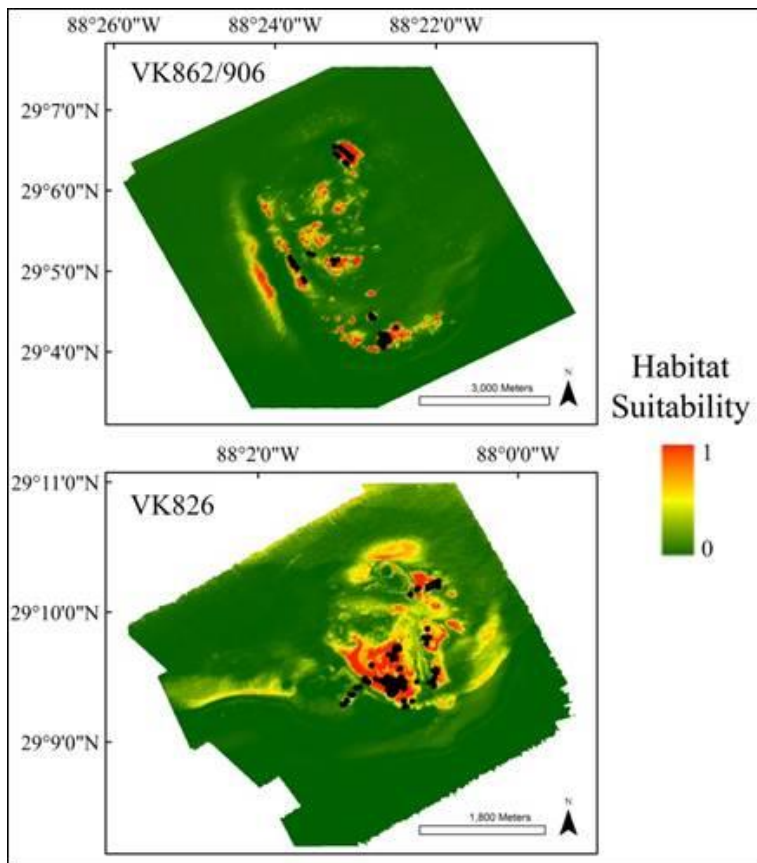


Figure 12-6.  Local scale habitat suitability models for *L. glaberrima*. Warmer colors indicate locations that are predicted to be more suitable. Black points indicate occurrences used to train and test the models. Note difference in scale.

536

Table 12-2.

Input data and model evaluation for *L. glaberrima* local scale models. The number of spatially explicit occurrences and the average AUC±s.d. are shown with significance marked (exact binomial test, ** p<0.001). The two primary explanatory variables for each model are listed along with the percentage of information contributed by each variable, as determined by jackknifing

| Site | No. of occurrences | Average AUC ± s.d. | Niche breadth (x $10^{-3}$) | Variable 1 | Variable 2 |
|---|---|---|---|---|---|
| VK826 | 386 | 0.958±0.011** | 112.52 | BPI-500 m (50.4%) | Depth (43.8%) |
| VK862/906 | 253 | 0.983±0.003** | 39.12 | BPI-500 m (49.7%) | Depth (43.9%) |
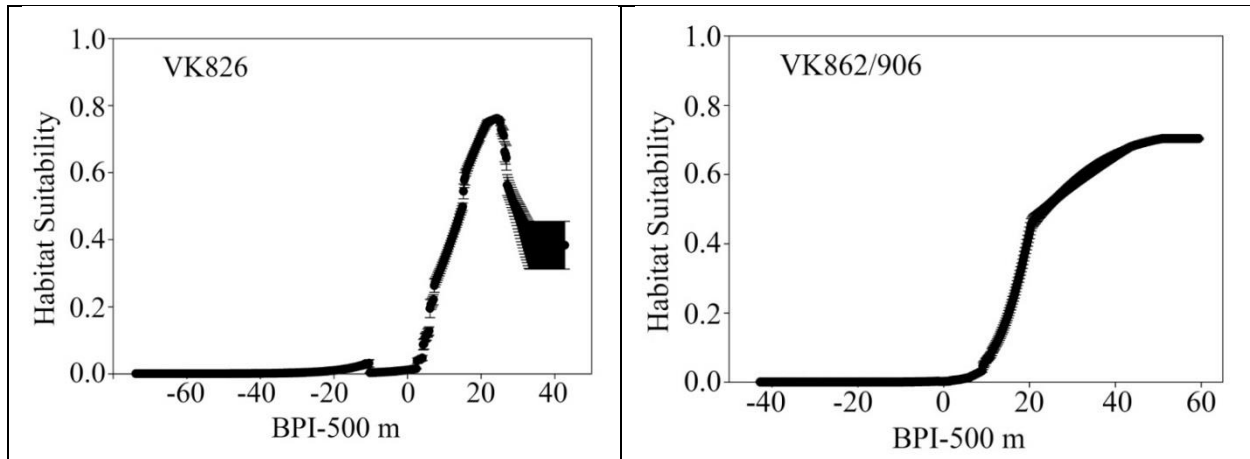


Figure 12-7. Response of the predicted habitat suitability for *L. glaberrima* to changes in bathymetric position index (BPI) calculated at the 500 m scale for local scale models. Error bars indicate standard deviation.

Figure 12-8. Response of the predicted habitat suitability for *L. glaberrima* to changes in depth (m) for local scale models. Error bars indicate standard deviation.
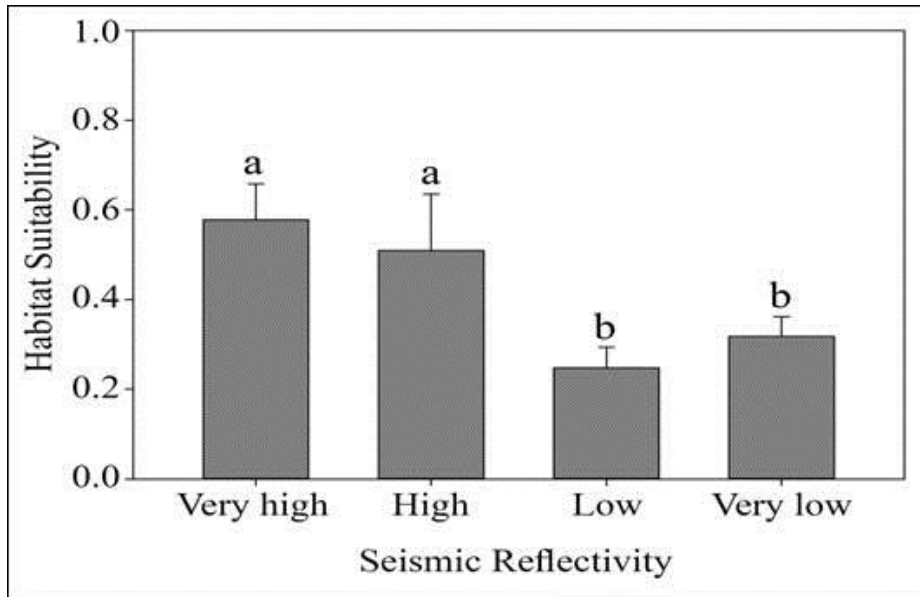


Figure 12-9. Response of the predicted habitat suitability for *L. glaberrima* to changes in seismic reflectivity data, averaged across VK862/906 and VK826. Error bars indicate standard deviation.

We constructed a single model for *C. gracilis* at GC140 (Figure 12-10), the only site in the GoM where it has been confirmed to be present. The model outperformed a random model (exact binomial test, 1-tailed p<0.01) and had an average test AUC of 0.931±0.018 (Table 12-3). Depth contributed the most information to the model (44.4%), followed by BPI-500 m (34.7%). Response curves revealed that the highest suitability indices were between depths of 250-300 m (Figure 12-11) and BPI-500 m values greater than 20 (Figure 12-12). *C. gracilis* had the largest niche breadth of any species with an inverse concentration of 207.55 (Table 12-3). Accordingly, a large portion of the shallow, southern portion of the site was predicted to be suitable, with peaks in suitability generally tracking with shallow ridges. Areas within the modeled optimum depth range (250-300 m) of *C. gracilis* were generally predicted to contain suitable habitat, reflecting its wide niche breadth and suggesting that depth is the primary factor structuring its distribution at this site. While it is possible that factors not included in model creation (eg. $\Omega_{calcite}$, water chemistry, currents, food supply) restrict its dispersal to, or recruitment and growth at other sites in the GoM, *C. gracilis'* wide niche breadth indicates that this species should occur more frequently at sites within its depth range. Therefore, while *C. gracilis* is currently only known to exist in the GoM at GC140, it seems likely that other shallow (<300 m) sites may contain undiscovered *C. gracilis* populations).

Table 12-3.

*Callogorgia spp.* Local-scale niche modeling results. The average test AUC of each model is listed along with model significance (exact binomial test, * p<0.05, ** p<0.01). The two primary explanatory variables for each model are listed along with the percentage of information contributed by each variable, as determined by jackknifing

| Species | Site | Bathymetry Resolution | No. of Occurrences | Mean AUC ± S.D. | Niche breadth (x 10⁻³) | Variable 1 | Variable 2 |
|---|---|---|---|---|---|---|---|
| *C. a. americana* | VK862/906 | 5 | 5 | 0.811 ± 0.246 | NA | NA | NA |
| *C. a. americana* | GB299 | 25 | 86 | 0.986 ± 0.006** | 45.64 | Depth (81.6%) | Rugosity (13.3%) |
| *C. gracilis* | GC140 | 5 | 152 | 0.931 ± 0.018** | 207.55 | Depth (44.4%) | BPI-500 m (34.7%) |
| *C. a. delta* | VK826 | 5 | 26 | 0.913 ± 0.148** | 145.85 | Depth (68.8%) | BPI-500 m (17.6%) |
| *C. a. delta* | GC234 | 8 | 15 | 0.966 ± 0.028* | 153.17 | Depth (42.6%) | Hard bottom (22.1%) |
| *C. a. delta* | GC246 | 8 | 8 | 0.949 ± 0.056 | NA | NA | NA |
| *C. a. delta* | MC751 | 5 | 83 | 0.985 ± 0.018** | 34.40 | Depth (41.4%) | Hard bottom (30.4%) |
| *C. a. delta* | MC885 | 8 | 40 | 0.979 ± 0.008** | 59.55 | Depth (44.9%) | BPI-500 m (33.5%) |
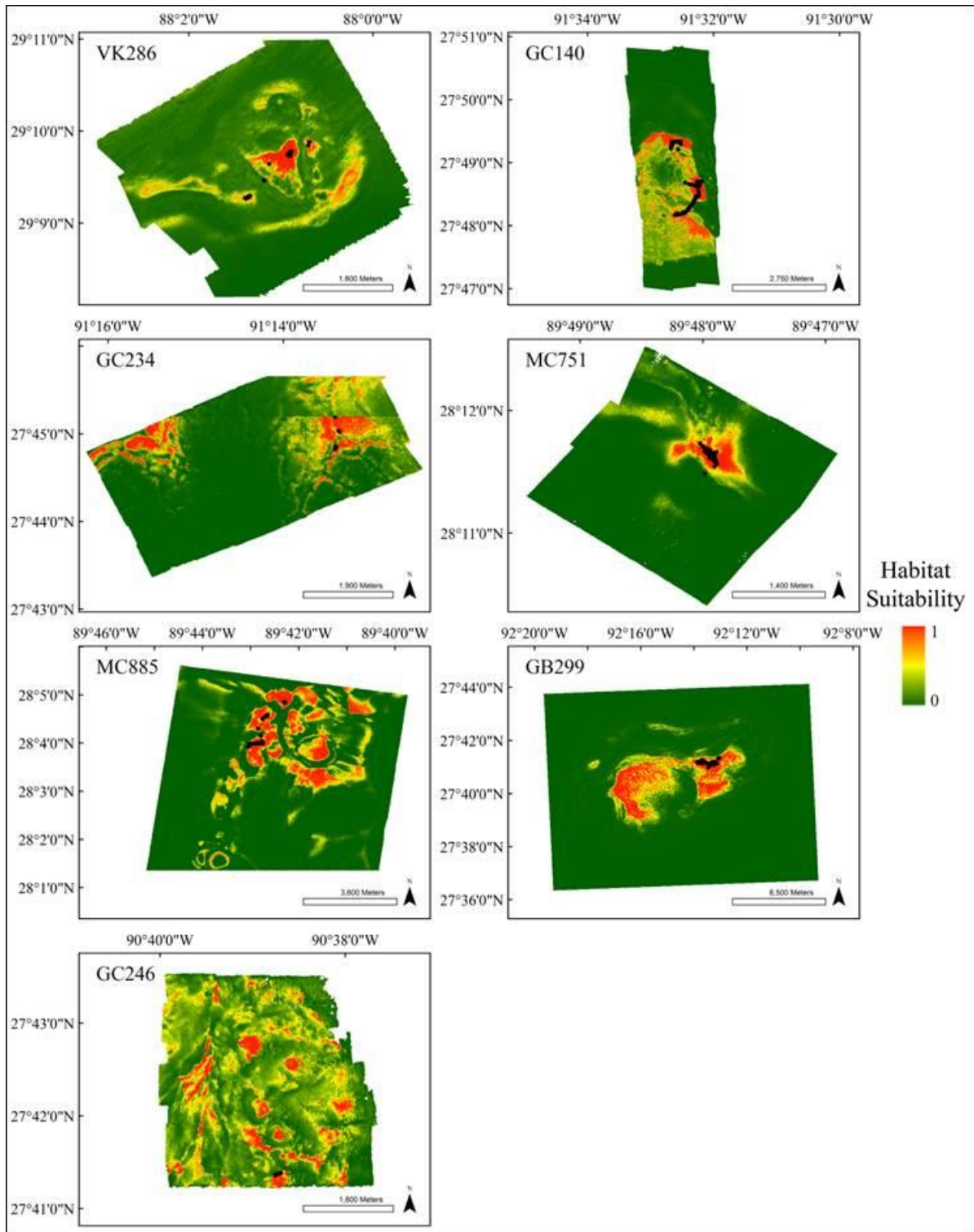
Figure 12-10. Local scale habitat suitability models for *Callogorgia spp.* Warmer colors indicate locations that are predicted to be more suitable. Black points indicate occurrences used to train and test the models. Note differences in scale. GC140 = *C. gracilis*, VK862/906, GB299 = *C. a. americana*, VK826, GC234, MC751, MC885, GC246 = *C. a. delta*.
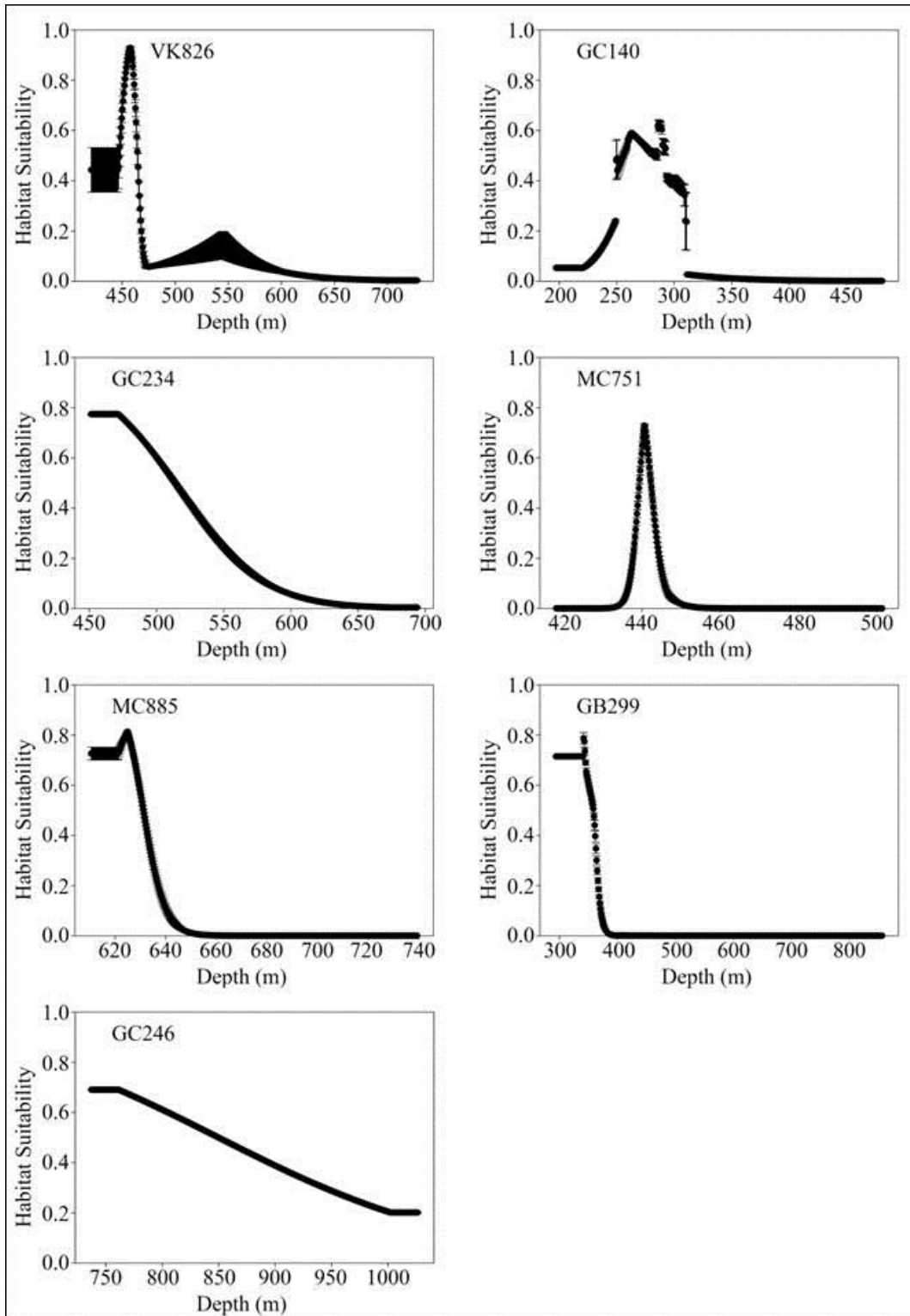
Figure 12-11. Response of the predicted habitat suitability for *Callogorgia spp.* to changes in depth (m) for local scale models. Error bars indicate standard deviation. GC140 = *C. gracilis*, VK862/906, GB299 = *C. a. americana,* VK826, GC234, MC751, MC885, GC246 = *C. a. delta*.

541
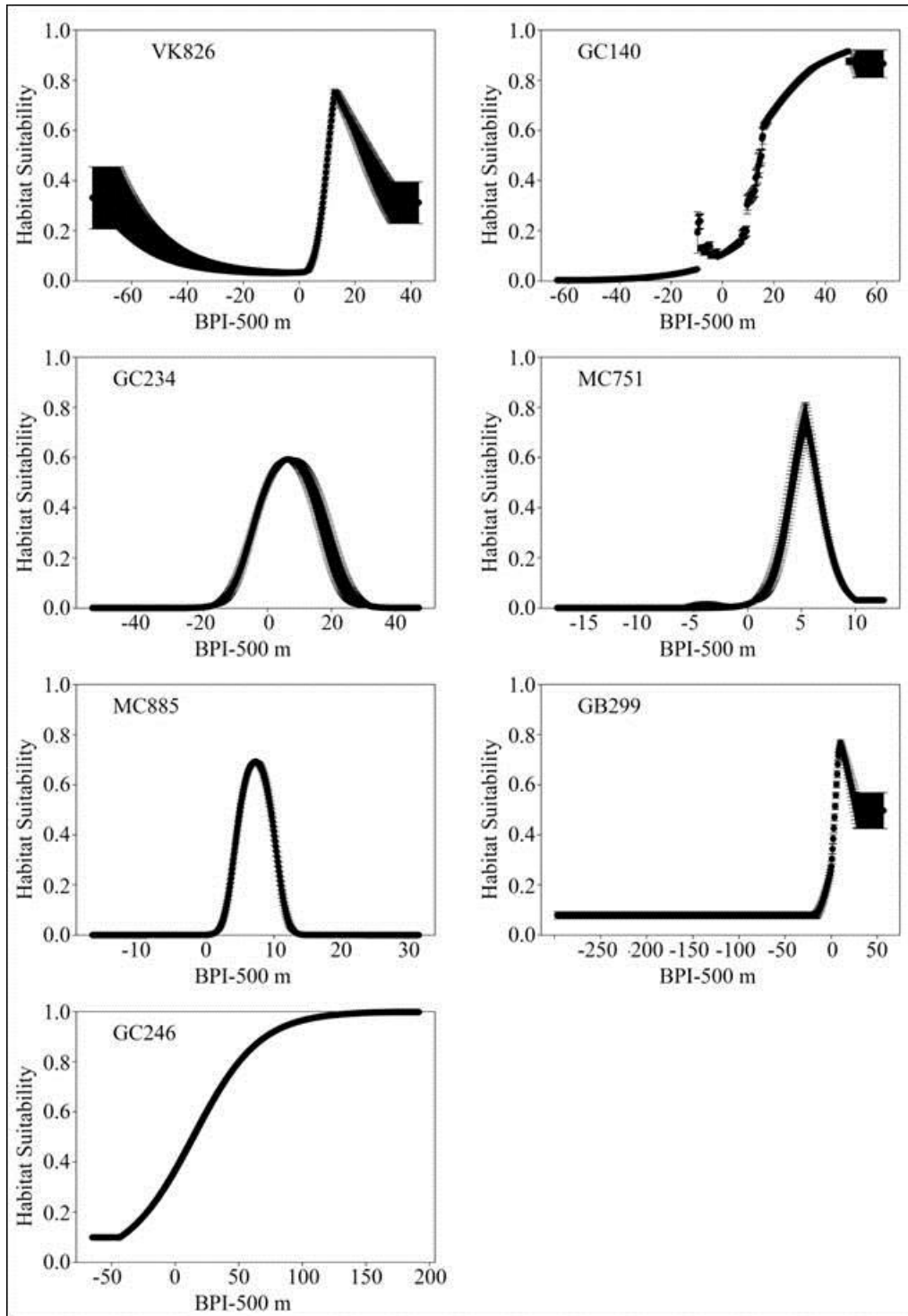
Figure 12-12.  Response of the predicted habitat suitability for *Callogorgia spp.* to
changes in BPI calculated at the 500 m scale for local scale models.
Error bars indicate standard deviation. GC140 = *C. gracilis*,
VK862/906, GB299 = *C. a. americana,* VK826, GC234, MC751,
MC885, GC246 = *C. a. delta.*

542

Models were constructed for *C. a. americana* at VK862/906 and GB299 (Figure 12-10). Only five spatially explicit colonies were observed at VK862/906, resulting in poor model performance (AUC of 0.811±0.246) that was not significantly better than a random model (exact binomial test, 1-tailed p>0.10; Table 12-3). Since the model was statistically no better than random, no additional statistical tests were conducted. The GB299 model was constructed using bathymetry from the National Oceanographic Data Center gridded at 25 $m^2$ because higher resolution bathymetry data were not available for this site. The model outperformed a random model (exact binomial test, 1-tailed p<0.01) and had a high AUC of 0.986±0.006. Depth contributed 81.6% of information to the model, with the highest suitability indices occurring below depths of 350 m (Figure 12-11). Rugosity contributed 13.3% of information to the model, with the suitability indices peaking at approximately 1.2. *C. a. americana* had an intermediate niche breadth of $45.64 \times 10^{-3}$ at GB299, likely reflecting its apparent restriction to sites deeper than 350 m. A comparison of model predictions to the bathymetry of GB299 suggests that *C. a. americana* is restricted to the slopes and summits of two large knolls in the center of the site, either reflecting a preference for large-scale elevated features, or simply a restriction to shallower depths. Within its suitable depth range, *C. americana* appeared to prefer more complex topographical features as evidenced by higher suitability indices at larger rugosity values. Therefore, other sites in the GoM within this depth range and containing complex topographical features may contain additional *C. a. americana* colonies.

Local-scale models were constructed for *C. a. delta* at VK826, GC234, GC246, MC751, and MC885. With the exception of GC246, all models outperformed a random model (exact binomial test, |p|<0.05) and exhibited high performance with AUC values ranging from 0.966±0.028 at GC234 to 0.985±0.018 at MC751 (Table 12-3). The GC246 model had a paucity of spatially unique occurrences (n=8) and performed relatively poorly with an AUC of 0.949±0.056. It was not significantly better than a random model (exact binomial test, p>0.05), therefore no additional statistics were calculated. Niche breadth varied greatly among sites, ranging from $34.40 \times 10^{-3}$ at MC751 to $153.17 \times 10^{-3}$ at GC234. Depth was the primary variable in all four significant models, contributing between 41.4% and 68.8% of information (Table 12-3). Response curves for all sites revealed that *C. a. delta* had the highest predicted suitability in a relatively broad depth range between approximately 440-625 m (Figure 12-11). At VK826 and MC885, BPI-500 m was the secondary variable, with contributions of 17.6% and 33.5% respectively. At all sites, suitability indices peaked between BPI-500 m values of 5-15, with decreasing suitability at maximal BPI values (Figure 12-12). At GC234 and MC751, hard bottom was the secondary explanatory variable, contributing 22.1% and 30.4% of information respectively. Across all sites, suitability indices were significantly higher at locations with very high seismic reflectivity values (ANOVA, p<0.01, post-hoc Holm-Sidak p<0.05: Figure 12-13) These results suggest that the presence of local topographic highs alone is not a good predictor of *C. a. delta* presence and abundance at all sites, and that depth and the availability of hard substrate are likely the determining factors that structure this species' distribution in the GoM.
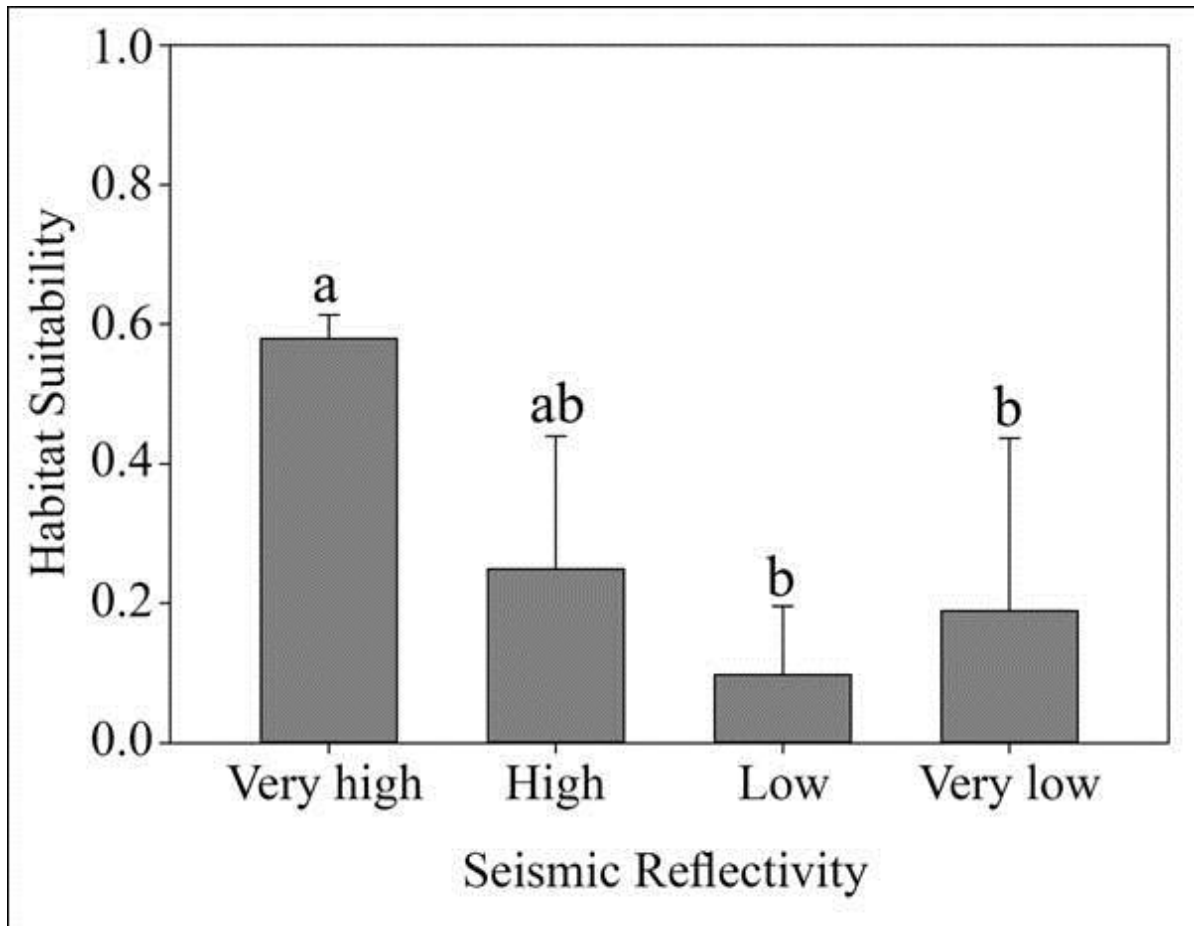
Figure 12-13. Response of the predicted habitat suitability for *C. a. delta* to changes in seismic reflectivity data, averaged across VK826, MC751, MC885, and GC234. Locations with very high reflectivity values had significantly higher suitability indices (ANOVA, p<0.01, post-hoc Holm-Sidak p<0.05) than sites with low and very low reflectivity values. Error bars indicate standard deviation.

## 12.3.2 *Callogorgia* spp. Mosaic Models

MAXENT models were also constructed for *C. a. americana*, *C. gracilis*, and *C. a. delta* from a mosaic of all sites where any *Callogorgia* species was found (GC140, GC234, GC246, MC751, MC885, VK826, VK862/906). GB299 was not included in mosaics because the available bathymetry was considerably courser than the additional variables included in the mosaic models (salinity, temperature, dissolved oxygen, and $\Omega_{calcite}$). The *C. a. americana* model had an average AUC of 0.781±0.266 s.d. and did not significantly outperform a random model (exact binomial test, 1-tailed, p=0.25; Table 12-4). The low performance of this model was likely because only five spatially explicit presence points were available for sites with high resolution bathymetry. No additional statistics were calculated for this model.

Table 12-4.

Model input and evaluation for *Callogorgia spp*. mosaic models. The average test AUC of each model is listed along with model significance (exact binomial test, * p<0.05, ** p<0.01). The two primary explanatory variables for each model are listed along with the percentage of information contributed by each variable, as determined by jackknifing

| Species | Sites | No. of Occurrences | Mean AUC ± s.d. | Variable 1 | Variable 2 |
|---|---|---|---|---|---|
| *C. gracilis* | GC140 | 152 | 0.977 ± 0.004[**] | Depth (70.6%) | Salinity (10.7%) |
| *C. a. americana* | VK864/906 | 5 | 0.781 ± 0.266 | NA | NA |
| *C. a. delta* | GC234,GC246, MC751, MC885 VK826 | 178 | 0.995 ± 0.002[**] | Seep (58.3%) | $\Omega_{calcite}$ |

The *C. gracilis* model significantly outperformed a random model (exact binomial test, 1-tailed, p<0.001) with an average AUC of 0.977±0.004 s.d. (Table 12-4). The variable that contributed the most information to the model was depth (percent contribution of 70.6%) followed by salinity (10.7%), and dissolved oxygen (9.3%). Salinity was highly correlated with depth (Pearson correlation r = -0.83, p<0.001) within the sampled area and provided minimal additional predictive power not already provided by depth as determined by a lack of reduction in AUC. Dissolved oxygen had a weaker correlation with depth (Pearson correlation, r = -0.30, p<0.001); however an additional model run without dissolved oxygen did not reduce the AUC, indicating that dissolved oxygen also provided minimal predictive power. Suitability indices were highest between depths of 220 and 300 m, with a maximum index value of 0.96 at a depth of 253 m (Figure 12-14). This species is known to have a shallower distribution, with an individual in the Smithsonian collection documented from 87 m depth in the GoM, and is found throughout the Caribbean (Cairns and Bayer 2002). Therefore, the records used for the modeling only cover a small portion of its realized niche, and the large niche breadth is an indication that it is likely to be relatively common in the shallower (80-200 m) waters of the GoM.
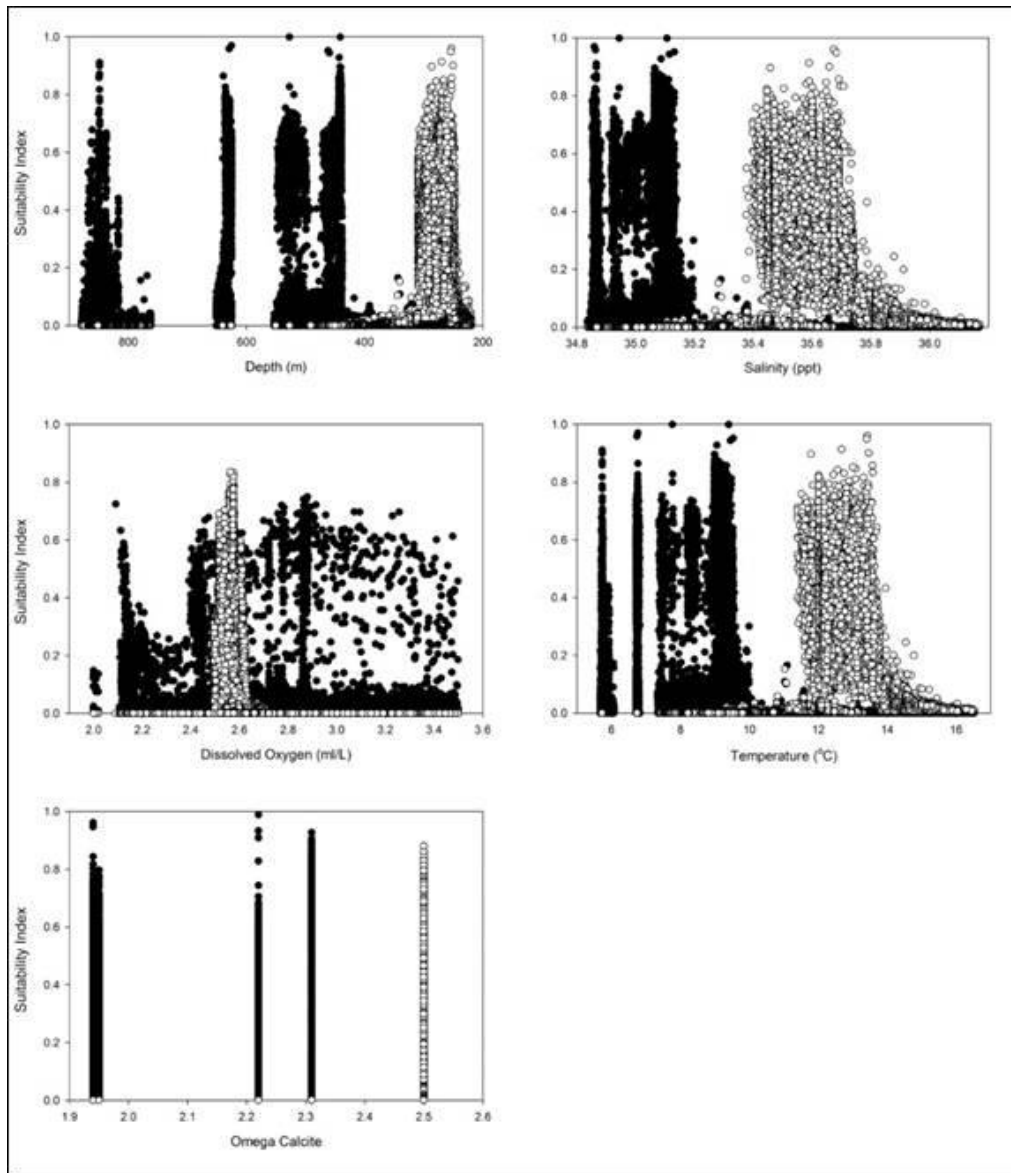
Figure 12-14.  Suitability indices of *Callogorgia spp.* relative to various
environmental parameters for mosaic models. Open circles = *C.
gracilis*, closed circles = *C. a. delta*.

The *C. a. delta* model was similarly robust, significantly outperforming a random model (exact
binomial test, 1-tailed, p<0.001) with an average AUC of 0.989±0.01 SD (Table 12-4). Jackknifing
revealed that seep activity (58.3%) contributed the most information to the model, followed by
calcite (19.8%), and salinity (9.4%). *C. a. delta* occurrences had significantly higher suitability
indices at localities with seep activity (average suitability index = 0.61) than at non-seep localities
(average suitability index = 0.37) (t-test, t=14.1, p<0.001). The highest suitability index (0.99)
corresponded with an $\Omega_{calcite}$ value of 2.2; however, high suitability indices (>0.9) occurred at all
$\Omega_{calcite}$ values encountered in the *C. a. delta* range (Figure 12-14).

546

Together, identity and background tests suggested that niche use differed significantly between *C. a. delta* and *C. gracilis* and was primarily driven by depth for *C. gracilis* and the presence of seeps for *C. a. delta*. The niche models of *C. gracilis* and *C. a. delta* had a very low degree of overlap (*I metric* = 0.014), and the identity test revealed that this overlap was significantly lower than the null distribution (p<0.01). Under the background test, the observed overlap between niche models (*I* metric) was significantly lower than the null distributions (p<0.01), rejecting the possibility that these species artificially show divergence due to differences in their access to environmental conditions. Therefore, these species appear to exhibit a high degree of niche divergence driven primarily by adaptation to a specific depth range, with *C. a. delta* occurring over a wider, deeper range than *C. gracilis*. While MAXENT has been shown to be robust with regard to correlated inputs (Phillips et al. 2006), correlated variables should be treated with caution when interpreting the percent contribution of variables to models. It is likely that one or more factors that covary with depth, including pressure, temperature, salinity, dissolved oxygen, pH, $\Omega_{calcite}$, resource availability, and distance from shore, are the causal factor of the observed divergence rather than depth itself.

Interestingly, the presence of seep activity significantly increased the suitability of *C. a. delta* habitat. There is also some indication that *C. a. delta* may gain nutritional input from seep activity (see Section 4.2.2 but also Becker et al. 2009). While the correlation with the areas of seep activity may primarily be due to the increased availability of substrate in the form of authigenic carboncarbonate, this species also appears to be more tolerant to seep conditions than its competitors, thereby giving it access to increased levels of local, deep-sea productivity.

Topography was surprisingly unimportant in the mosaic *Callogorgia spp.* models given that it is frequently stated that octocorals prefer local topographic highs (Bryan and Metaxas 2006; Tong et al. 2012). Colonies of *Callogorgia* were repeatedly observed in dense patches on fairly flat substrates, particularly at MC885 and GB299, indicating that relatively flat surfaces are also suitable habitat for some octocoral species. Our tactic of using a mosaic of sites across a large depth gradient may have dampened the role topography may play at smaller scales, but even in the local scale *Callogorgia spp.* models (Table 12-3), depth was the primary contributing variable at every site. BPI calculated at the 500 m scale did contribute between 17 and 34% of information at GC140, VK826, and MC885, however when these models were generated excluding BPI, there was no reduction in AUC. Therefore, while topographic variables were generally informative, they did not contain considerable predictive information not already provided by other variables, and likely did not strongly influence niche divergence among these species.

## 12.3.3 Large-Scale Models

A single model was constructed for each species at a coarser resolution (25 m$^2$) for an area of the northern GoM covering approximately 67,000 km$^2$ (Figure 12-15). Model performance was excellent, with AUC values ranging from 0.976 to 0.997 (Table 12-5). All models significantly outperformed a random model (exact binomial test, |p|<0.05; Table 12-5). *C. a. americana* was the most specialized species with a niche breadth of 5.74 x 10$^{-3}$, and *L. pertusa* occupied the broadest niche with a breadth of 43.58 x 10$^{-3}$. *L. glaberrima*, *C. a. delta*, and *C. gracilis* all had similar, intermediate niche breadths of 21.41 x 10$^{-3}$, 26.98 x 10$^{-3}$, and 21.41 x 10$^3$ respectively. In agreement with its wide niche breadth, *L. pertusa* was predicted to be the most prevalent species in the GoM, filling 76.3% of the largest range size (10,067 km$^2$). *C. gracilis* had the smallest

predicted range size (1,358 km$^2$) but filled 91.7% of its suitable habitat. For all species, there were relatively large regions that were predicted to be suitable but not known to be inhabited. It is possible that models simply overestimated the suitable habitat for each species. Niche models rely on the theory that a species' distribution is largely driven by the portions of its ecological niche that can be readily quantified. While there is ample evidence for this theory (see James et al. 1984; Schoener 1989), it is also clear that other factors, such as seawater chemistry, temperature, biotic interactions, disease, seasonal variability, or resource availability, may partially structure distributions but are intractable in modeling efforts (e.g., MacArthur 1972; Case and Taper 2000). It is plausible that unoccupied regions that were predicted to be suitable may in reality be unsuitable due to any number of ecological factors that could not be included during model creation. However many unfilled locations occurred in regions that have not been well surveyed, and it seems likely that extensive cold-water coral populations remain to be discovered in the GoM. Modeling efforts, while useful, should not replace extensive field explorations. Instead, models should support field operations by quantitatively assessing collected data and informing research efforts in unexplored regions; in turn, field studies should be used to ground truth, verify, and refine model predictions.
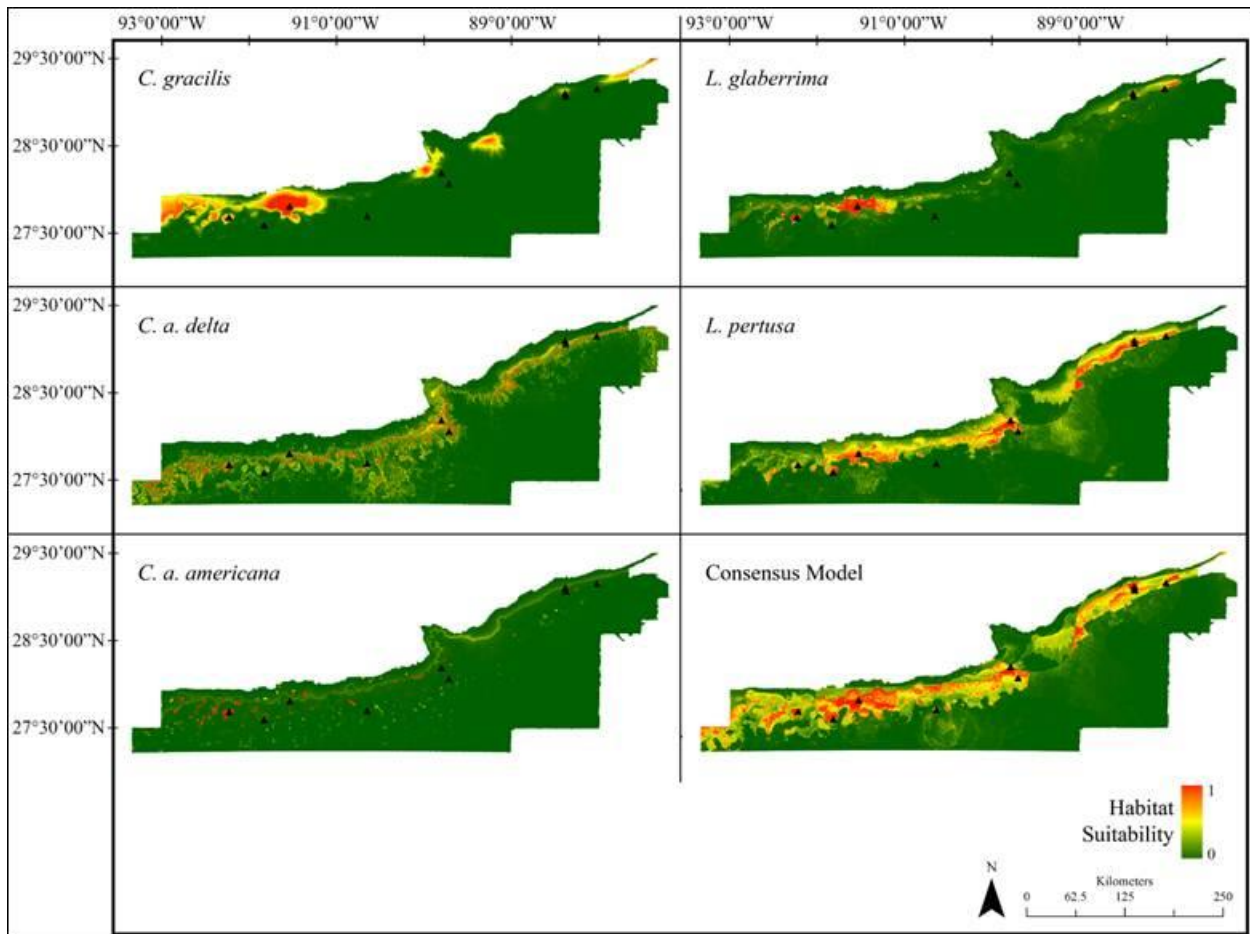


Figure 12-15.  Large scale habitat suitability model for cold-water corals in the northern GoM. Warmer colors indicate locations predicted to be more suitable. Black triangles indicate the most intensively surveyed sites (west to east: GB299, GC354, GC140, GC246, GC249, MC751, MC885, VK862, VK906, VK826).

548

When all large-scale models were considered in conjunction, AUC had a significant negative correlation with range size (Pearson correlation, r = -0.90, p=0.037), and a non-significant but negative correlation with niche breadth (Pearson correlation, r = -0.67, p=0.22). *L. pertusa* had the lowest AUC (0.976±0.004) despite having the greatest number of occurrence points, likely because it occupies the largest range (10,067 km$^2$) and has the widest niche breadth (43.58 x 10$^{-3}$). This was not surprising, since AUC is expected to be artificially inflated when species have small ranges and are more specialized (Guisan and Hofer 2003; Elith et al. 2006). Niche breadth was not well correlated with niche filling (Pearson's correlation, r = 0.10, p=0.87), but had a marginally significant positive correlation with range size (Pearson's correlation, r = 0.82, p=0.09). This relationship was expected as larger ranges generally encompass a wider range of environmental conditions (Nakazato et al. 2010). The small sample size (n=5) likely inhibited achieving significance for some niche metrics comparisons; the addition of more taxa may resolve these relationships.

Table 12-5.

Large scale modeling results and niche characteristics for each species. The average test AUC of each model is listed along with model significance (exact binomial test, ** p<0.01). The two primary explanatory variables for each model are listed along with the percentage of information contributed by each variable, as determined by jackknifing.

| Species | No. of Occurrences | Average AUC ± s.d. | Niche breadth (x 10$^{-3}$) | Niche filling (%) | Range size (km$^2$) | Variable 1 | Variable 2 |
|---|---|---|---|---|---|---|---|
| *L. pertusa* | 450 | 0.976±0.004** | 43.58 | 76.3% | 10,067 | Hard bottom (40%) | Depth (24%) |
| *L. glaberrima* | 242 | 0.985±0.009** | 21.41 | 72.3% | 6,644 | Hard bottom (65%) | Depth (21%) |
| *C. a. delta* | 111 | 0.993±0.004** | 26.98 | 35.3% | 7,054 | Depth (82%) | BPI-1000 m (8%) |
| *C. a. americana* | 88 | 0.996±0.001** | 5.74 | 44.4% | 2,683 | Hard bottom (71%) | Depth (21%) |
| *C. gracilis* | 76 | 0.997±0.001** | 21.41 | 91.7% | 1,358 | Depth (88%) | $\Omega_{arag}$ (8%) |

Depth was the primary or secondary variable in every large scale model, explaining between 21% and 88% of the distribution of each species (Table 12-5). The highest suitability indices for *L. pertusa* and *L. glaberrima* occurred between depths of 300-600 m, between 450-850 m for *C. a. delta*, between 350-400 m for *C. a. americana*, and between 200-400 m for *C. gracilis* (Figure 12-16). BPI calculated at the 1000 m scale contributed 8% of information to the *C. a. delta* model, but BPI calculated at any scale was generally uninformative in large scale models. Given its importance in *L. pertusa* and *L. glaberrima* local scale models, this may indicate that the effects of topography are predominantly localized and influence distributions on small spatial scales, as evidenced by the lack of importance of current flow and related variables in low resolution global modeling efforts (e.g., Tittensor et al. 2009). Depth was significantly but weakly correlated with BPI calculated at the 1000 m scale (Pearson's correlation, r = 0.05, p<0.05: Figure 12-16 Table 12-6), the 100 m scale (Pearson's correlation, r = 0.077, p<0.05), and the 25 m scale (Pearson's

correlation, r = -0.003, p<0.05), indicating that the importance of depth in models was likely attributable to other depth-related variables such as pressure, salinity, temperature, or $\Omega_{arag}$ rather than a factor related to the topography of the seafloor. The presence of hard substrata explained 40% of the distribution of *L. pertusa*, 65% of the distribution of *L. glaberrima*, and 71% of the distribution of *C. a. americana*. At all sites, the presence of hard substrata resulted in significantly higher suitability indices than locations with unknown or soft substrata (t-test, two-tailed |p|<0.05; Figure 12-17), again confirming that hard substrate is a necessary prerequisite for cold-water coral recruitment.
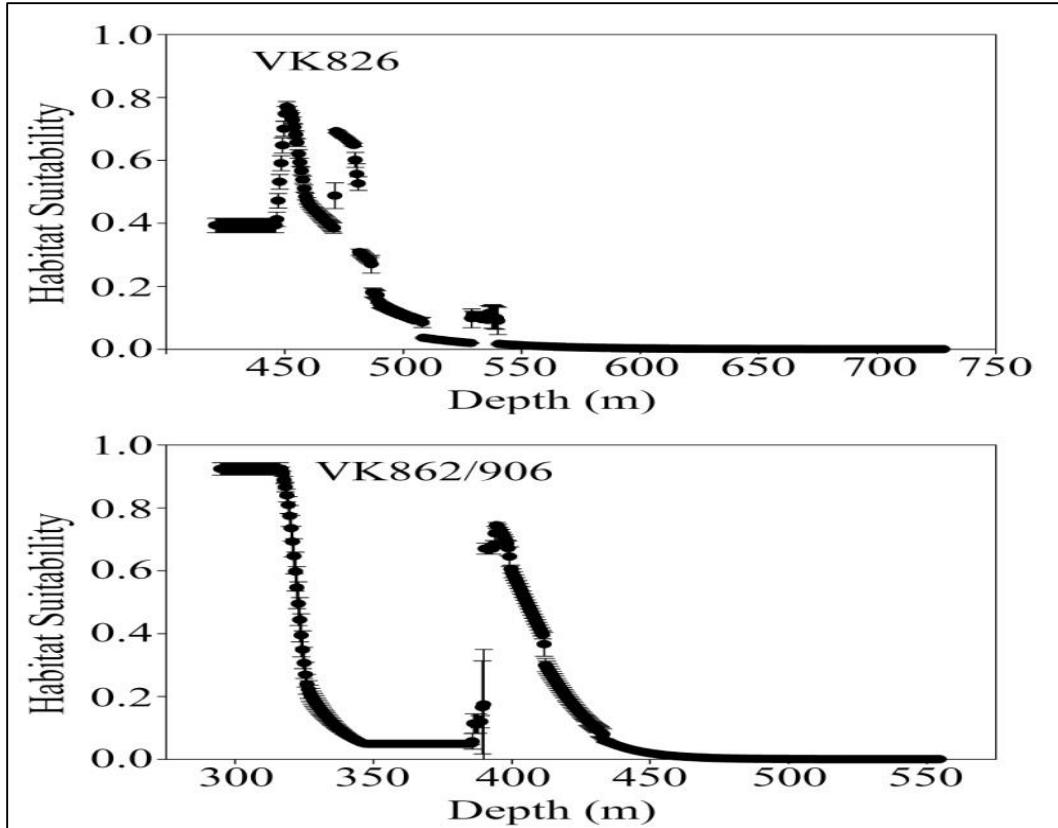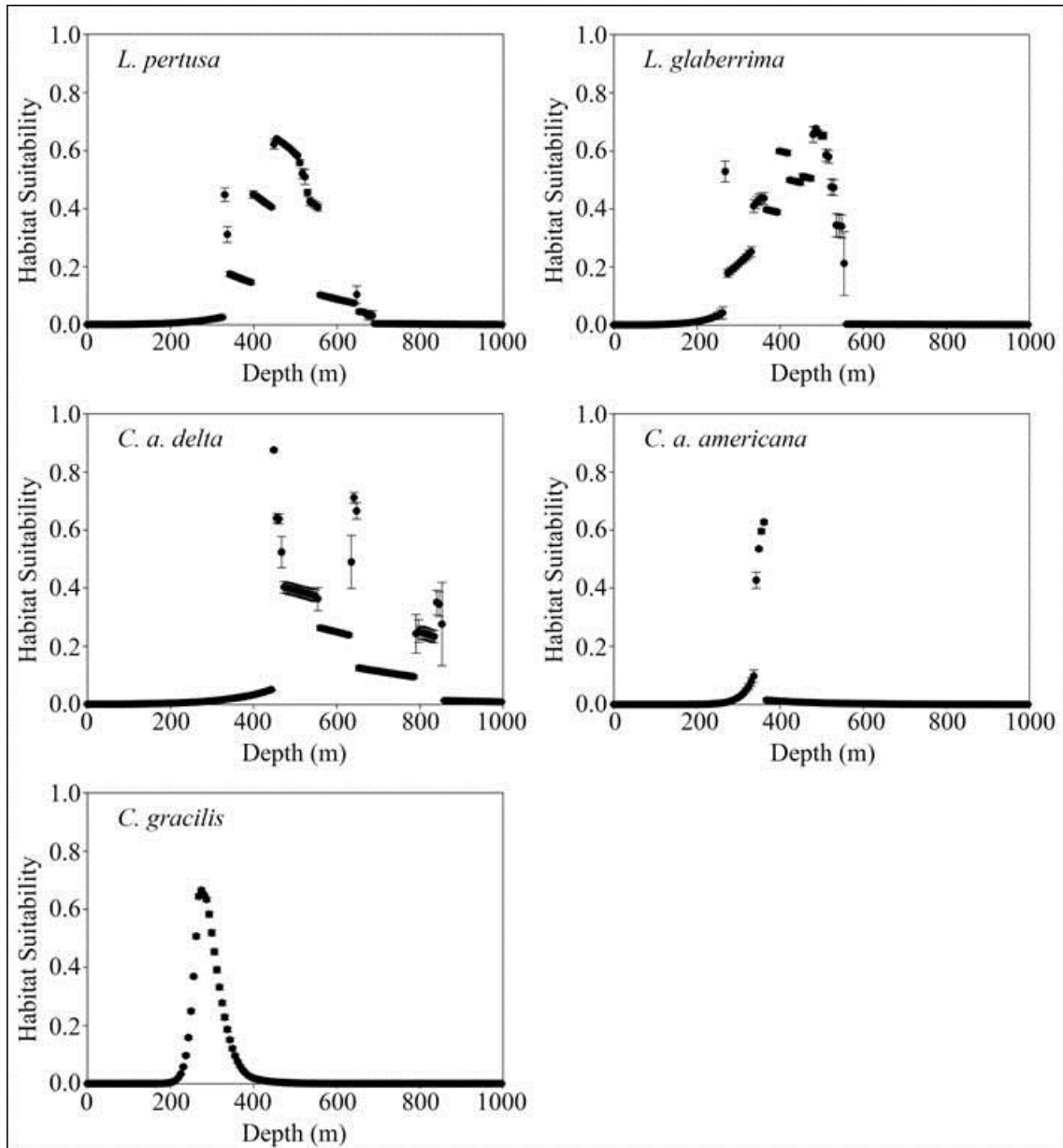


Figure 12-16.  Response of the predicted habitat suitability for cold-water coral species to changes in depth (m) for large scale models. Error bars indicate standard deviation. Only depths shallower than 1000 m are shown.

# Table 12-6.

Pearson's correlation values (r) among environmental variables used to train large scale models. Significant correlations (two-way p<0.05) are indicated with an asterisk. Significant correlations with an r>0.10 are highlighted in grey- N=673,646

| | BPI-1000 | Ω_arag | Chl *a* | Plan | Profile | Curvature | Depth | Eastness | NO₃⁻ | Northness | PO₄³⁻ | Rugosity | Seismic | Slope | BPI-25 | BPI-100 |
|---|---|---|---|---|---|---|---|---|---|---|---|---|---|---|---|---|
| BPI-1000 | | -0.003* | -0.009* | .204* | -0.207* | -.249* | .052* | .000 | -0.004* | .015* | -0.006* | .188* | -0.052* | -0.011* | 0.215* | 0.374* |
| Ω_arag | 0 | 1 | .426* | 0.002 | 0.001 | -.000 | 0.132* | .000 | .645* | .050* | .399* | 0.010* | 0.028* | 0.077* | 0.000 | -0.000 |
| Chl A | 0 | 0 | 1 | 0.000 | 0.001 | -.000 | .445* | .000 | .543* | .076* | .488* | .001 | 0.015* | 0.097* | -0.000 | -0.001 |
| Plan | 0 | 0 | 0 | 1 | 0.359* | .769* | -.004* | 0.000 | 0.002 | -0.006* | 0.001 | -.101* | -0.004* | 0.020* | 0.687* | 0.701* |
| Profile | 0 | 0 | 0 | 0 | 1 | 0.871* | 0.004* | -.000 | 0.001 | -.000 | 0.001 | -.078* | 0.000 | 0.004* | -0.744* | -0.739* |
| Curvature | 0 | 0 | 0 | 0 | 0 | 1 | -.004* | 0.000 | -0.000 | -0.003* | -.000 | 0.001 | 0.002* | 0.007* | 0.869* | 0.874* |
| Depth | 0 | 0 | 0 | 0 | 0 | 0 | 1 | .000 | 0.421* | -0.054* | -0.547* | .001 | 0.088* | -0.067* | 0.004* | 0.008* |
| Eastness | 0 | 0 | 0 | 0 | 0 | 0 | 0 | 1 | 0.000 | -0.001 | .001 | 0.000 | -0.000 | -0.001 | -0.000 | -0.000 |
| NO₃⁻ | 0 | 0 | 0 | 0 | 0 | 0 | 0 | 0 | 1 | 0.068* | .681* | 0.011* | 0.018* | 0.099* | -0.000 | -0.000 |
| Northness | 0 | 0 | 0 | 0 | 0 | 0 | 0 | 0 | 0 | 1 | .105* | 0.079* | 0.031* | 0.531* | -0.002 | 0.008* |
| PO₄³⁻ | 0 | 0 | 0 | 0 | 0 | 0 | 0 | 0 | 0 | 0 | 1 | 0.012* | -0.000 | 0.152* | 0.000 | -0.000 |
| Rugosity | 0 | 0 | 0 | 0 | 0 | 0 | 0 | 0 | 0 | 0 | 0 | 1 | 0.006* | 0.305* | 0.026* | 0.078* |
| Seismic | 0 | 0 | 0 | 0 | 0 | 0 | 0 | 0 | 0 | 0 | 0 | 0 | 1 | 0.048* | -0.002 | -0.005* |
| Slope | 0 | 0 | 0 | 0 | 0 | 0 | 0 | 0 | 0 | 0 | 0 | 0 | 0 | 1 | 0.005* | 0.020* |
| BPI-25 | 0 | 0 | 0 | 0 | 0 | 0 | 0 | 0 | 0 | 0 | 0 | 0 | 0 | 0 | 1 | 0.794* |
| BPI-100 | 0 | 0 | 0 | 0 | 0 | 0 | 0 | 0 | 0 | 0 | 0 | 0 | 0 | 0 | 0 | 1 |
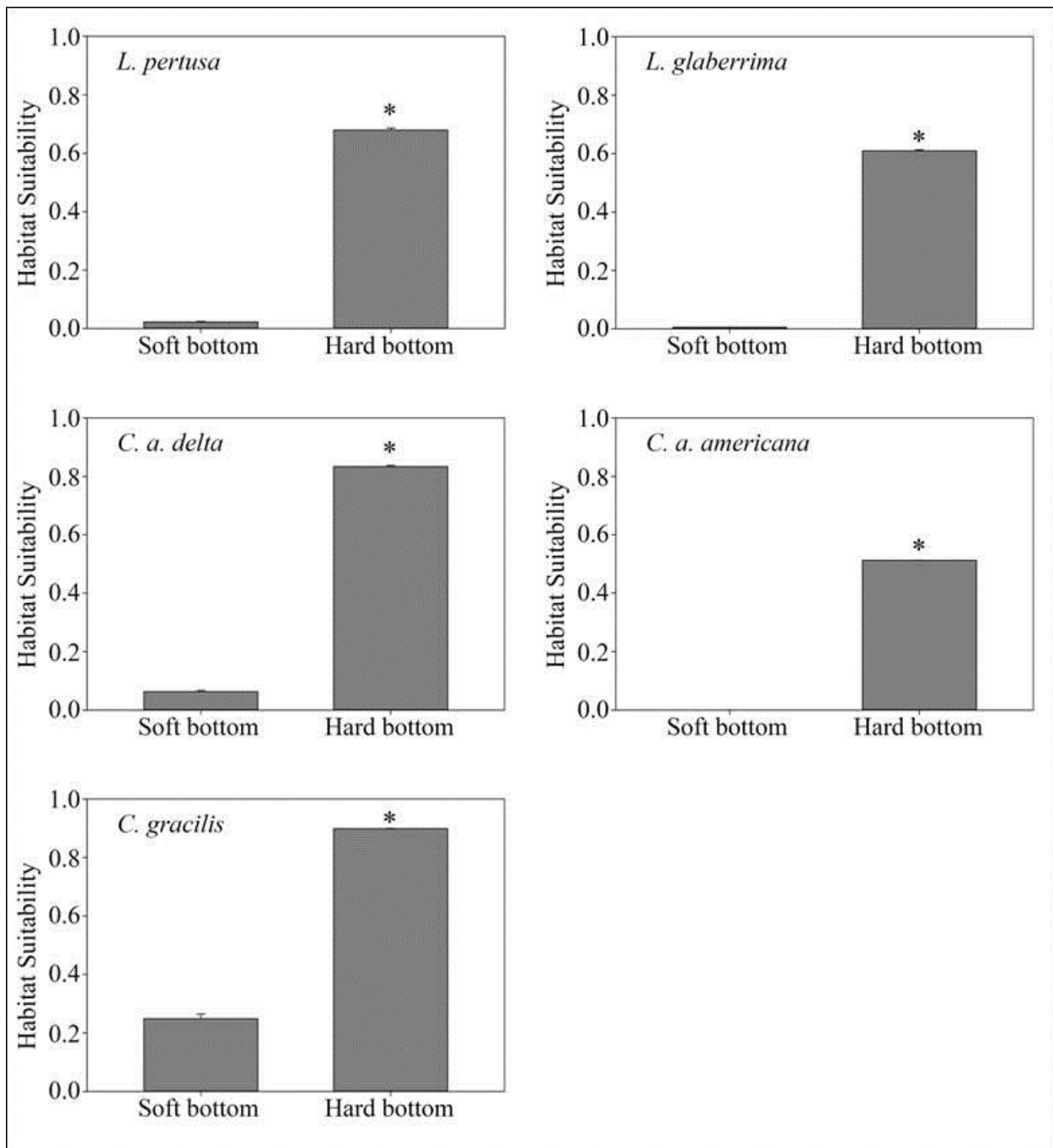
Figure 12-17. Response of the predicted habitat suitability for cold-water coral species to the presence or absence of hard bottom for large scale models. Error bars indicate standard deviation. Suitability was significantly higher at locations with hard bottoms at all sites (t-test, two-tailed |p|<0.05).

All species pairs were significantly more ecologically divergent than expected by chance (identity test, |p|<0.05; Table 12-7), however the degree of niche overlap ($I$ metric) varied considerably among species. *L. pertusa* and *L. glaberrima* occupied the most similar niches, with an $I$ metric value of 0.724, which suggests a high degree of niche overlap. The large degree of overlap supports the similarity of *L. glaberrima* and *L. pertusa* local scale models at VK862/906 and VK826, as

well as numerous field observations of *L. glaberrima* colonies growing on or near *L. pertusa* aggregations. In general, *Callogorgia spp.* had low overlaps with each other despite their greater relatedness. *C. a. delta* and *C. gracilis* were the most divergent species, with an overlap value of 0.162, supporting the high degree of divergence observed between their respective mosaic models. *C. gracilis* and *C. a. americana* had an overlap value of 0.291, and *C. a. delta* and *C. a. americana* had a slightly higher overlap value of 0.429. In conjunction with variable contributions and associated response curves, it appeared that this divergence was primarily driven by changes in depth, with *C. gracilis* occurring at the shallowest depths, *C. a. americana* at intermediate depths, and *C. a. delta* across the broadest depth range including deeper sites.

Table 12-7.

Niche overlap (I metric) between the large scale niche models of each species pair. Values closer to one indicate greater niche overlap and values closer to zero indicate greater divergence.

Asterisk indicates that species were more divergent than expected by chance under the identity test ($\alpha = 0.05$).

|  | *L. pertusa* | *L. glaberrima* | *C. a. delta* | *C. a. americana* | *C. gracilis* |
|---|---|---|---|---|---|
| *L. pertusa* | 1 |  |  |  |  |
| *L. glaberrima* | 0.724[*] | 1 |  |  |  |
| *C. a. delta* | 0.678[*] | 0.484[*] | 1 |  |  |
| *C. a. americana* | 0.471[*] | 0.658[*] | 0.429[*] | 1 |  |
| *C. gracilis* | 0.366[*] | 0.643[*] | 0.162[*] | 0.291[*] | 1 |

# 13 UNDERSTANDING DEEP CORAL DISTRIBUTION PATTERNS

The results of this study have significantly improved our understanding of deepwater coral ecosystems in the GoM and beyond. The first cold-water coral mound in the GoM was discovered, but in an area of low seismic reflectivity. The geology of this mound revealed that it has been developing intermittently for over 300,000 years (Section 9). The shallowest and deepest records for *Lophelia pertusa* in the GoM were located, but on artificial substrata (Section 8). The physiological limits of *L. pertusa* growth and survival with respect to oxygen, temperature and pH were determined in the laboratory (Section 7). Significant new archaeological sites were discovered, documented, and some were identified, including the *Gulfoil* wreck that supports one of the largest *L. pertusa* reefs in the Gulf (Section 10). The genetic patterns of deepwater coral relationships were revealed in the GoM for the first time (Sections 5.2 and 5.3). Several new species of corals and associates were identified and phylogenetic studies have increased our understanding of the taxonomy of all corals (Sections 5.1 and 5.2). The communities of animals living with the corals were described, and now include over 90 species living with *L. pertusa* alone (Section 4.1 – 4.4). The biogeographic and depth-driven patterns of occurrence of different corals and communities in the GoM are described (Section 4.2 to 4.4). The food webs of these communities were examined. We confirmed that most corals and associates are not obtaining any significant nutrition from seep-derived sources and therefore are not likely to be exposed to seep effluent (Section 6). In parallel but separate analyses we also found the first example of a coral species that appears to utilize seep production and found its distribution to be tied to seepage (Sections 5.1 and 6; Quattrini et al., 2013).

This study also contributed significantly to our understanding human impacts in the deep GoM. In addition to the laboratory studies constraining the sensitivity of *L. pertusa* to the effects of ocean acidification (Section 7) we provide the first data on the progress of ocean acidification in the deep GoM (Section 3.1). Although designed for long-term monitoring of natural change in deep water coral communities (Section 4.1 and 4.2) our monitoring stations proved quite valuable for analysis of the impact from the *Deepwater Horizon* oil spill to deep water coral communities (Section 4.5). Additionally, in response to the spill we explored for and discovered a coral community 7 miles from the Macondo well and documented serious impact from the blowout to the corals and ophiuroids at this site (White et al., 2012). Continued study of this site has provided the first data on the response of corals to impact from the spill and is providing data that allows us to constrain the ultimate outcome on the communities (Appendix C-4)

Building on these accomplishments, perhaps the greatest contribution of this study comes from the synthesis of these data. The primary objective of this project was to obtain a robust predictive capability for the occurrence of rich cnidarian (primarily scleractinian coral) hard-ground communities in the deep GoM. It is only through an examination of everything that we have learned that we can achieve this goal: from the site selection process, to the field observations, the gathering of oceanographic data, the genetic patterns in coral populations and the lab experiments, to the modeling of coral distribution patterns.

It is commonly held that deep-sea corals colonize hard substrata in areas of high local relief and high food availability. While these general statements have held true, they can be greatly refined by the knowledge gained in this study. The most important factor in determining the suitability of habitat for development of particular coral community types was depth, especially for *L. pertusa*.

In the modeling, depth is essentially a proxy for a variety of other factors that could be affecting the corals, including temperature, dissolved oxygen, pressure, and aragonite saturation state. In the laboratory experiments with *L. pertusa*, the corals ceased growth at an aragonite saturation state of 1.06, suffered complete mortality after being exposed to a temperature of 14°C, and complete mortality after prolonged exposure to dissolved oxygen concentrations of approximately 1.5 mL·L$^{-1}$. From our field measurements, *L. pertusa* often occupies habitats that are very near these critical thresholds (particularly at the western Green Canyon and Garden Banks sites for aragonite saturation state, VK862 for temperature, and the 500-600 m GC and GB sites for DO). These findings indicate that the available coral habitat may be severely reduced as anthropogenic impacts to these oceanographic variables intrude on the deeper waters of the Gulf.

The next factor was typically the presence of hard-grounds, as determined from the relative seismic reflectivity of the seafloor. This was a primary tool used in the site selection process, and was highly successful. Reflectivity was particularly significant for *Callogorgia americana americana*, likely due to its preference for authigenic carbonate substrate near seeps. However, there were a few notable exceptions to the link between seismic reflectivity and coral presence. The first is the Roberts' Reef cold-water coral mound in VK906. This mound and the other less well-developed mounds in the immediate vicinity were characterized by anomalously low seismic reflectivity. While the sub-bottom seismic profile revealed hard substrate at the base of the mounds, the thick accumulation of coral fragments that form the mounds acted to scatter the acoustic signal resulting in the low return. The other exception was exemplified at the GB201 site surveyed during the first cruise in 2008. This site looked promising from the seismic data, but the hard-grounds apparent in the seismic data were covered in a fairly thin layer of sediment. The multibeam bathymetry revealed numerous pockmarks around the site, suggesting recent and ongoing sediment expulsion. When interpreting the seismic data for indications of habitat suitable for corals, both of these features – pockmarks and low-reflectivity mounds – should be taken into consideration.

The next factor revealed by the modeling effort was local topography, represented by the bathymetric position index. This supports the notion that corals prefer locations that are elevated above their immediate surroundings. This factor was particularly significant for the black coral, *Leiopathes glaberrima*. Locally elevated patches of hard substrate will provide enhanced current flow, which will allow for sediment removal from the corals and resuspension of particulate matter that may contribute to the corals' diet. However, this factor was not significant at the larger scale considered in the models. This indicates that it operates at very localized spatial scales, and even a small elevation above the surrounding area may be sufficient to render a habitat patch suitable for coral growth.

The consistent finding that depth, seismic reflectivity, and local elevation were the most significant factors controlling coral distribution is quite useful to managers and deep-sea explorers alike. Potential coral sites may be predicted from the archive of 3D seismic data housed at BOEM along with high-resolution, multibeam bathymetry. At the largest scale, models suggest that areas of the northern Gulf in the western portion of the Green Canyon area appear to be the most suitable for coral growth (Fig. 12-15). Although many of the sites in this study were in that region, more emphasis has been placed on the seep communities there, and it remains ripe for exploration for additional coral habitats. Once certain areas are identified for exploration or management (i.e. lease blocks), smaller, well-defined targets where corals are likely to be present can be generated from the models and higher resolution AUV surveys for eventually ground-truthing by AUV or ROV visual surveys.

Scientific Services on a Global Basis
**TDI-Brooks International, Inc.**

14391 S. Dowling, College Station, TX 77845
Ph: (979) 693-3446    Fax: (979) 693-6389
www.tdi-bi.com

# Commercial Fisheries in the Gulf of Mexico and Potential Impacts to Deepwater Corals
## Report
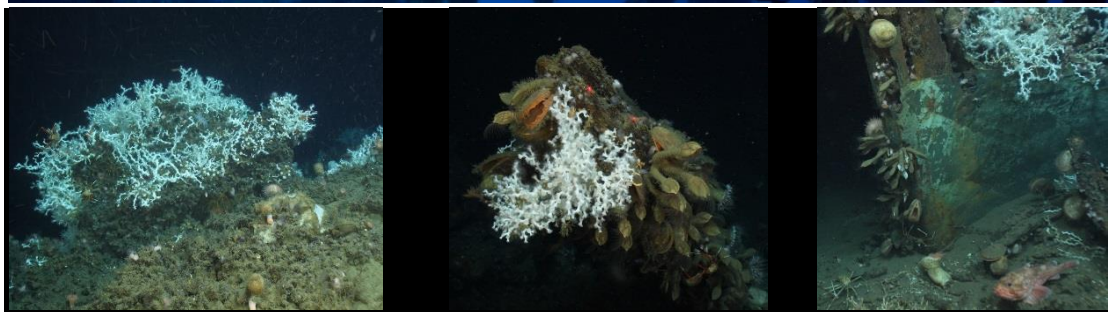


# January 2010

# Commercial Fisheries in the Gulf of Mexico and Potential Impacts to Deepwater Corals

BY

## TDI-BROOKS INTERNATIONAL, INC.

**PREPARED UNDER BOEM CONTRACT**

**M08PC20028**

*JANUARY 2010*

TDI-Brooks International Inc.
14391 South Dowling
College Station, TX  77845, USA.

## Acknowledgements

## 14.1 INTRODUCTION

### 14.1.1 Overview

This document represents an internal Report for contract number: **M08PC20038**, issued by the U.S.Department of the Interior, Minerals Management Service "**Deepwater Program: Exploration and Research of Northern Gulf of Mexico Deepwater Natural and Artificial Hard Bottom Habitats with Emphasis on Coral Communities: Reef, Rigs and Wrecks**". This report focuses on deepwater fishery practices in the Gulf of Mexico and potential for interactions with deepwater coral communities.

### 14.1.2 Overall Project Background

Over the last half century, offshore exploration for hydrocarbons in the northern Gulf of Mexico (GoM) has advanced from the bay and inner shelf to the continental slope-to-continental rise transition. Geophysical and geotechnical data collected in support of both exploration and production has been largely responsible for the foundation of our present understanding of slope geology. This database emphasizes the extremely complex geological framework of the northern Gulf's continental slope and the surprisingly important role that the expulsion of subsurface fluids and gases has on shaping surficial geology and biology of the modern seafloor. Regional topography of the slope consists of basins, knolls, ridges, and mounds derived from the dynamic adjustments of salt to the introduction of large volumes of sediment over long time scales. Superimposed on this underlying topography is a smaller class of mounds, flows, and hard grounds that are the products of the transport of fluidized sediment, mineral-rich formation fluids, and hydrocarbons to the present sediment-water interface. The geologic response to the expulsion process is related both to the products being transported and the rate at which they arrive at the seafloor. Mud volcanoes and mudflows are typical of rapid flux settings where fluidized sediment is involved. Slow flux settings are mineral-prone. Authigenic carbonate mounds, hard grounds, crusts, and nodules are common to settings where hydrocarbons are involved.

Recent manned submersible and ROV dives to the middle and lower continental slope confirm the existence of these hard substrates to the deepest parts of the slope. Direct observation and sampling of expulsion sites started in the mid-1980s on the upper slope. We now know from analysis of 3D-seismic data and submersible-ROV dives that numerous expulsion sites with hard substrates provide habitat for deep water corals over the full depth range of the slope.

In the context of this study, deep hardground communities of the Gulf of Mexico comprise all of the biological communities inhabiting natural or artificial hard substrates, excluding the chemosynthetic seep communities. These communities consist of foundation species, those species that form large complex habitats at these sites, and the associated fauna ranging in size from large mobile fishes to microscopic meiofauna. The most prominent foundation species in these communities are the deep-water ("cold-water") corals. The terms "deep-water corals" or "cold-water corals" include relatives of the tropical reef-forming scleractinian corals, but also refer to a variety of other cnidarian taxa including antipatharians (black corals), gorgonians (including bamboo corals), alcyonaceans (soft corals), and stylasterine hydrocorals. Other taxa, including

anemones and sponges are also significant contributors to the biogenic framework of these deep-water reef systems.

In the Gulf of Mexico, deep-water corals are commonly found on seep-related authigenic carbonates, but have also been observed on anthropogenic structures, ship wrecks and oil platforms in particular. The most common species of reef-forming deep-water coral in the Gulf of Mexico (GoM) is *Lophelia pertusa* (=*prolifera*). This species was first recovered in the late 1800s by the *U.S. Coast Survey Steamer Blake.*

Increasing industry activity in deepwater has resulted in the creation of numerous platforms in water depths exceeding 300 m. In areas where hard substrates are limiting, these platforms may significantly increase the potential range of corals and other hardground fauna. Growth of *Lophelia pertusa* has been noted on the Pompano platform in VK 989 (Schroeder et al. 2005). In addition, the Joliet platform in GC 184 near Bush Hill and the Neptune platform near the large *L. pertusa* site in VK 826 are very likely to host coral populations. This study will focus on the exploration and characterization of these communities and examination of their potential connection to other coral populations and surrounding deep-water communities.


## 14.1.3 Objectives of the Project

A primary goal of this study is to obtain a robust predictive capability for the occurrence of rich cnidarian (primarily scleractinian coral) hard ground communities in the deep Gulf of Mexico. To achieve this long-term goal, this study will accomplish three interrelated and interdependent objectives:

1) Discover and describe new locations at greater than 300m depth in the GoM with extensive coral community development, particularly including *Lophelia pertusa*.

2) Gain a more comprehensive understanding of the fundamental processes that control the occurrence and distribution of *Lophelia* and other extensive coral communities at depths greater than 300 m in the GoM through both laboratory experiments and field data collection.

3) Document and understand the relations between coral communities on artificial and natural substrates with respect to community composition and function, phylogeographic and population genetics, and growth rates of the key cnidarian foundation fauna.

4) As a supplement to the general program objectives listed above, this report will focus on the current status of deepwater fishing activities in the Gulf of Mexico to identify potential impacts of deepwater coral and other hard bottom communities.

## 14.2 DEEPWATER FISHERIES IN THE GULF OF MEXICO

### 14.2.1 Background

The Minerals Management Service (MMS) has requested a review of commercial fishery activities that have the potential for negative interaction with deepwater coral communities, with primary emphasis on *Lophelia* or *Madrepora* in depths below 200 m. Few reports have documented the frequency and location of deepwater fishing practices in the Gulf of Mexico (GOM), particularly for the deep reef fish assemblage (primarily groupers, tilefishes and snappers) or have reported these practices to be relatively rare when compared to pelagic longlining (CSA 2002).

The lack of a significant deepwater fishery in the GOM also makes this an ideal setting for the study of deepwater coral habitats in relatively pristine condition. In other regions of the world, the past and ongoing depletion of populations of deepwater fishes with long life spans such as rockfish (*Sebastes* spp.), orange roughy (*Hoplostethus atlanticus*), alfonsinos (*Beryx* spp.) and pelagic armourhead (*Pseudopentaceros wheeleri*) has resulted in significant damage to deepwater coral communities on Atlantic and Pacific seamounts and *Lophelia* reefs of the north Atlantic (Rogers 1999, Koslow *et al*. 2001, Hall-Spencer 2002, Fosså 2002). In the southeastern U.S., trawling operations for rock shrimp and brown shrimp resulted in severe damage to the *Oculina* banks on the Atlantic coast of Florida (Reed et al. 2007).

The deepest commercial trawl fisheries for bottom-dwelling fishes in the GOM remain on the continental shelf <200 m. However, the presence of potentially viable fishery species such as the red, white or longfin hake (*Urophycis spp.*), blackbelly rosefish (*Heliocolenus dactylopterus*) and numerous grenadiers (Macrouridae) in deeper waters suggests that there may be a limited fishery that has been largely undocumented, and that a larger commercial deepwater fishery in the GOM may yet develop (McEachran and Fechelm 1998). The golden crab (*Chaceon fenneri*) and deepsea red crab (*C. quinquedens*) support an active pot fishery in deepwater off the Atlantic coast of the U.S. with annual landings of several hundred thousand pounds (Steimle et al. 2001). Both species occur throughout the eastern and northern Gulf ( Lockhart et al. 1990, Waller et al 1995, Trigg et al. 1997). Limited golden crab fishing has historically occurred in the GOM; however crab fishing vessels have reportedly left the Gulf and the current potential of a focused fishery is marginal (NMFS 2004, S. Branstetter, *pers. comm.*). Therefore heavy deepwater crab pots do not currently appear to be a threat to deepwater corals, although future trapping efforts for both deepwater crabs and royal red shrimp could occur (GMFMC 2005a). Pelagic fishing practices such as longlining and midwater trawls can also impact deep sea corals due to entanglement with lost or abandoned fishing gear and accidental contact with the sea floor. Lost longlines have the potential to "ghost fish" for an extended period until the hooks are lost to corrosion. There is also a recent tendency of recreational or charter vessel fishers to "deep drop" on natural or artificial structures using 2-3 lb lead weights, but this effort appears to be relatively rare and typically occurs at the shallow limit of deepwater coral occurrence.

### 14.2.2 Deepwater Coral Ecosystems

Deepwater or deep sea coral ecosystems (DCES) in the southeastern U.S. and northern GOM often support populations of deepwater groupers (snowy grouper, yellowedge grouper, warsaw grouper), tilefish, wreckfish, barrelfish, and alfonsinos that could potentially be targeted by

longline or bandit reel fisheries (Reed et al. 2005, Reed et al. 2006, CSA 2007, Ross and Quattrini 2007, Sulak 2008, Goldman and Sedberry *in review*) (Figure 14-1).

Finely branched corals, including *Oculina* and *Lophelia*, are vulnerable to entanglement in bottom longlines and may be broken and crushed by heavy weights and anchors as fishing gear is dragged across the seafloor upon retrieval, leading to colony breakage or lost equipment (Barnette 2001). Repeated trawling activities using heavy tickler chains, lead lines, and weighted doors can crush living colonies, remove the epibenthos, and reduce topographic complexity (Barnette 2001, Reed et al. 2007, Wells et al. 2008) (Figures 14-2, 14-3). Barnette (2006) observed extensive areas of entangled, overgrown, or abandoned longline gears in the vicinity of colonies of *Oculina* in the NW GOM, the result of commercial grouper fishing activities. Numerous deepwater gears deployed for deepwater groupers, golden crab, or royal red shrimp in the GOM could cause extensive damage to deepwater coral communities (Perry et al. 1995, Barnette 2001, CSA 2002, SAFMC 2009).

Previous reviews of deepwater fishing practices in the northern GOM indicate that the primary deepwater commercial fishery is pelagic longlining for tuna, followed by bottom longlining for deepwater groupers, snappers, and tilefishes (CSA 2002). Commercial deepwater trapping for golden crab and bottom trawling for royal red shrimp, two activities most likely to impact benthic communities, historically have been at much lower levels than bottom longlining, and geographically concentrated in south Florida and Alabama/Mississippi, respectively (Lockhart et al. 1990, Jones et al. 1994, Perry et al. 1995, Harper et al. 2000, CSA 2002). Current analysis will focus on identifying geographic trends of deepwater fishing activities and/or changes in effort for bottom fisheries associated with known hard bottom marine communities, including *Lophelia* reefs.

### 14.2.3 Lophelia pertusa distribution

Schroeder et al. (2005) reviewed the distribution of *Lophelia pertusa* and *Madrepora oculata* to provide an assessment of the occurrence of these species in waters greater than 200 m in the GOM. *Lophelia* occurred at depths ranging from 343 to 878 m, with the majority of sites occurring between 450 and 650 m. *Madrepora* reef sites were reported from slightly deeper locations, up to 937 m, and in more southerly locations (including sites below 25° N). Currently known *Lophelia* locations occur north of 26° 30' N, and are primarily distributed in a small region on the west Florida slope, the Mississippi-Alabama slope, and the Texas-Louisiana slope. While *Lophelia pertusa* occurs to depths of over 800 m, the most well-developed and intensively studied reef sites occur at Viosca Knoll and Green Canyon Lease Blocks, at depths between 313 and 525 m (CSA 2007, Cordes et al. 2008, Sulak 2008). In addition to natural deepwater coral assemblages, numerous *Lophelia* colonies have been observed on the Pompano platform in VK 989 at depths ranging from 204 to 385 m (Schroeder et al. 2005, J. Reed *pers. comm.*, D. Weaver *pers. observ.*). To identify potential impacts of deepwater fishery gears on deep coral reef assemblages, including populations that colonize artificial structures (primarily production platforms and shipwrecks), we will focus on the review of existing fishery data occurring from 200 to 600 m.

### 14.2.4 Commercial Fishing Activities and Data Acquisition

The recent patterns in commercial deepwater fisheries (2000 to 2009) were reviewed to complement a previous assessment of bluewater/deepwater fisheries in the GOM (CSA 2002).

The deepwater fishing industry was described from data provided by the NOAA Fisheries (previously known as the National Marine Fisheries Service or NMFS) labs from the reef fish and shrimp logbooks, and landings data reported from seafood dealers of individual Gulf states. Datasets for the deepwater (200 to 600 m) fishing activities were extracted for comparison to the shallow water (< 200 m) for reef fishes (deepwater groupers, tilefish, barrelfish, golden crab) to identify the relative importance of the deepwater fishery. Mandatory reporting of Gulf reef fish and shrimp fishery information is collected by NOAA under the authority of the Magnuson Fishery Conservation and Management Act to effectively manage these fisheries. The reef fish logbook program has only recently included detailed information on depth of gear deployment, NMFS statistical grid, and specific location of gear sets. Data collected prior to 2005 often do not provide location or depth. The shrimp fishery was historically monitored through data collection by port agents who collected statistical information from vessel captains and port agents. The recent development of the electronic logbook system (ELB) has allowed more detailed records of shrimp trawling in the GOM, and has been installed on 450 of approximately 1,900 vessels operating in the GOM, including vessels fishing for royal red shrimp (J. Nance, *pers. comm.,* B. Gallaway *pers. comm.*).

The reef fish logbook database, maintained by the NOAA's Southeastern Science Center, Miami, only requires fisherman to report the numeric code of the NMFS statistical area, and not lat/long coordinates. Therefore data can only be assigned to statistical grids (individual grid cells cover one degree of longitude), but may be further limited to specific depth horizons of limited geographic area when depths are reported. Fishing effort and landings may be further extrapolated to occur in areas of natural hard bottom or artificial reef structures (deepwater platforms, shipwrecks), where many of the target species are known to associate. Statistical grid maps established by NMFS in the GOM are based on 21 individual cells established for the monitoring of the penaeid shrimp fishery, ranging from number 1 in the area of the Florida Keys/Dry Tortugas to 21 in Brownsville, TX (Figure 14-5). Grids no. 22 and 23 are located immediately south of the U.S./Mexico Border. The statistical grids continue from the Florida Keys northward along the east coast as four digit grid numbers, the first two digits designating latitude and the second two digits longitude (e.g. SAFMC grid 2481 is the equivalent of GOM grid no. 1 in the western Florida Keys). In the GOM, deepwater fishing activities occurring beyond the seaward boundary of the grid cell are included in the corresponding statistical area. Access to reef fish and shrimp logbook data are further limited when fewer than 3 vessels report landings per statistical grid, and the data are classified as confidential. Unfortunately, all three deepwater fisheries (bottom longlining for deepwater fishes, royal red shrimp trawling and deepwater crab traps) typically fall into this category, resulting in low spatial resolution of fishing activity or a complete lack of data.

## 14.2.5 Deepwater Fishery Species

Most fishes occurring in deepwater marine ecosystems are considered to be extremely vulnerable to overfishing based on life history traits and relatively low natural abundance. The American Fisheries Society (AFS) recognizes the increased vulnerability of many reef fishes, particularly those species dwelling in deepwater environments, due to their slow growth, long lifespan and late age of maturation (Coleman et al. 2000, Musick et al. 2000). Many deepwater groupers, wreckfish, and barrelfish enter the fishery at a relatively late age and can reach ages in excess of 60 years (Sedberry et al. 1993, 1999, Filer and Sedberry 2008, Shipp and Sedberry 2008). Deep-water marine fishes in general attain long lifespans (some up to 130 yrs), and an analysis of scorpaenid

fishes indicates increased longevity with greater depth of occurrence (Caillet et al. 2001). Reef-associated fishes in the GOM and S.E. Atlantic also appear to follow this pattern. Deep-dwelling species are also subject to severe barotrauma upon capture, resulting in 100% mortality of undersized fish or bycatch species. Many species of reef fish form localized spawning aggregations that result in an even greater risk of overfishing. In addition, groupers first mature as female and as larger adults and later switch to male, resulting in the potential skewing of sex ratios through fisheries that target large individuals (Coleman et al. 2000, Koenig et al. 2000).

By definition, the GMFMC recognizes five species in the deepwater grouper (DWG) complex, including yellowedge grouper, misty grouper, warsaw grouper, snowy grouper, and speckled hind (NOAA 2009). For regulatory purposes scamp (*Mycteroperca phenax*) and tilefishes are also included in this category. For the purposes of this review, we will focus on the DWG species that make up the majority of the catch for the GOM below 200 m, as well as large fishes commonly associated with *Lophelia* reefs that could sustain a multi-species fishery. The following brief species descriptions have been described from Heemstra and Randall (1993), McEachran and Fechhelm (1998, 2005), Musick et al. (2000), CSA (2002) and Fishbase (www.fishbase.org).

## Snowy Grouper: *Epinephelus niveatus*
### Geographic Distribution
The snowy grouper occurs along the outer continental shelf from North Carolina to southern Brazil in the western Atlantic, including the GOM, Bermuda, and Caribbean Sea.

### Habitat and Biology
Snowy grouper occur in depths of 30 to 525 m, over rocky habitats or artificial structures, and are often associated with *Lophelia* reefs and other deep coral ecosystems. This species reaches a maximum length of 120 cm, and a weight of 30 kg. Maximum estimated age is 27 years (Heemstra and Randall 1993).

### Fishery Importance
Snowy grouper are an important and abundant deep reef species in the GOM and western Atlantic, and are fished by commercial longlining and electric reels throughout the northern GOM. As with other deepwater groupers, this species is considered by the American Fisheries Society to be "at risk of extinction" due to its vulnerability to overfishing (Musick et al., 2000).

## Warsaw Grouper: *Epinephelus nigritus*
### Geographic Distribution
The warsaw grouper occurs along the outer continental shelf and upper continental slope from Massachusetts to Brazil in the western Atlantic, including the GOM.

### Habitat and Biology
Warsaw grouper occur in depths of 50 to 400 m, over natural rocky habitats or artificial structures (Olander 1991, 1999). This species is the largest deep-dwelling grouper in the western Atlantic, reaches a maximum length of 230 cm, and a weight of 200 kg. Maximum estimated age is 40 years.

**Fishery Importance**

The Warsaw grouper is incidental to fisheries targeting other deepwater species, as it typically occurs as solitary individuals or in small groups. As with other deepwater groupers, this species is considered by the American Fisheries Society to be "at risk of extinction" due to its vulnerability to overfishing (Musick et al., 2000).

**Yellowedge Grouper:** *Epinephelus flavolimbatus*
**Geographic Distribution**
The yellowedge grouper occurs along the outer continental shelf and upper continental slope from North Carolina to southern Brazil in the western Atlantic, including the GOM and Caribbean Sea.
**Habitat and Biology**
Yellowedge grouper occur in depths of 64 to 275 m, over rocky habitats or sand/clay bottoms. They are occasionally found in burrows or depressions in soft bottom sediments. This species reaches a maximum length of 110 cm, with males reaching larger sizes than females. Maximum estimated age is between 15 and 20 years (Bullock et al. 1996).

**Fishery Importance**
Yellowedge grouper are one of the most important and abundant deep reef species in the GOM and western Atlantic, and is fished by commercial longlining throughout the northern GOM. This species constitutes the majority of the deepwater grouper catch in the GOM. As with other deepwater groupers, this species is considered by the American Fisheries Society to be "at risk of extinction" due to its vulnerability to overfishing (Musick et al., 2000).

**Tilefish:** *Lopholatilus chamaeleonticeps*
**Geographic Distribution**
The tilefish occurs along the outer continental shelf and upper continental slope from the Scotian shelf, the entire eastern U.S. Coast, and the GOM to Campeche Bank.

**Habitat and Biology**
Tilefish occur in depths of 165 to 411 m in the GOM. They prefer soft bottom sediments where it constructs burrows. This species reaches a maximum length of 110 cm, and a weight of 18 kg (CSA 2002).

**Fishery Importance**
Tilefish are an important deepwater species in the GOM and Atlantic coast, and is fished by commercial longlining and electric reels throughout the northern GOM. This species is vulnerable to overfishing, but not officially listed. Tilefish are often caught as part of a mixed species assemblage that included yellowedge and other deepwater groupers. The commercial quota of tilefish is set at 440,000 lbs.

**Barrelfish:** *Hyperoglyphe perciformes*
**Geographic Distribution**
The barrelfish occurs off the Atlantic coast of North America from Nova Scotia to the Florida Keys, and the eastern GOM. This species also occurs in the eastern North Atlantic and western Mediterranean.

**Habitat and Biology**
Barrelfish occur at depths between 200 to 800 m, over natural hard bottom or artificial habitats. This species reaches a maximum length of 104 cm, a weight of 12 kg, and can live up to 85 years (Filer and Sedberry 2008). Barrelfish enter the fishery between 12-16 yrs of age.

**Fishery Importance**
Barrelfish are primarily caught as bycatch in the deepwater wreckfish fishery of the Charleston Bump and Blake Plateau off the coast of the southeast United States. There also appears to be a limited fishery for this species in the GOM, possibly as bycatch in the longline fishery for tilefish, yellowedge and snowy groupers (Cass-Calay and Bahnick 2002), or specifically targeted on a limited basis by recreational or small charter vessels, particularly around deepwater petroleum platforms (Olander 2001).

**Red Bream:** *Beryx decadactylus*
**Geographic Distribution**
The red bream occurs worldwide in tropical and temperate latitudes.

**Habitat and Biology**
Red bream occur at depths between 110 to 1000 m, usually between 200 and 400 m over natural hard bottom, sand or muddy bottoms. This species reaches a maximum length of 100 cm, and a weight of 10 kg.

**Fishery Importance**
The red bream is primarily caught as bycatch in the deepwater wreckfish fishery of the Charleston Bump off the coast of the southeast United States (Goldman and Sedberry *In Review*). This species has been observed during submersible surveys in associated with *Lophelia* coral mounds and other high profile hard bottom features (Reed et al. 2006, Ross and Quattrini 2007, D. Weaver *personal observation*). Red bream are also a small component of a deepwater fishery worldwide that focuses on populations of the splendid alfonsino, *B. splendens*, on deep slopes and seamounts.

**Splendid Alfonsino:** *Beryx splendens*
**Geographic Distribution**
The splendid alfonsino occurs worldwide in tropical and temperate latitudes.

**Habitat and Biology**
Splendid alfonsinos occur at depths between 25 to 1240 m, and are commonly fished over seamounts in the Pacific at depths between 500 and 900 m. This species reaches a maximum length of 60 cm, and a weight of 2.5 kg, and reach an age of at least 17 years.

**Fishery Importance**
The splendid alfonsino is caught as bycatch in the deepwater wreckfish fishery of the Charleston Bump off the coast of the southeast United States (Goldman and Sedberry *In Review*). There are directed deepwater longlining fisheries, trawl fisheries, and artisanal handline fisheries for this species throughout the world, particularly on seamounts and isolated islands bearing limited continental shelves (Vinnichenko 1997, Dürr and González 2002). This species does not appear to be abundant on *Lophelia* reefs in the GOM, but could be caught as bycatch for other deepwater species such as barrelfish.

<u>**Wreckfish:**</u> *Polyprion americanus*
**Geographic Distribution**
Wreckfish have an antitropical distribution and are found in temperate waters of the northern and southern hemisphere, from Newfoundland to the Florida Keys, Southern Brazil to Argentina, and Bermuda. Wreckfish also occur throughout deepwater of the eastern North Atlantic including the Azores, Madeira, and the Mediterranean and in the Pacific waters of South Africa, Australia and New Zealand (Sedberry et al. 1999, Vaughn et al. 2001, Shipp and Sedberry 2008). Wreckfish have only recently been reported from the GOM (Sulak et al. 2008, Shipp and Sedberry 2008).

**Habitat and Biology**
Adult wreckfish occur at depths between 42 to 1000 m, and are the primary species of the deepwater fishery at the Charleston Bump and Blake Plateau of the southeastern United States (Vaughn et al. 2001). This species reaches a maximum length of 146 cm, a weight of 47 kg, and reach an age of at least 31 years (Sedberry et al. 1999).

**Fishery Importance**
Wreckfish fisheries of the southeastern United States and Bermuda are one of the few fishes supporting a deepwater fishery at *Lophelia* depths, and illustrate the typical problems associated with managing a deepwater fishery. An extensive wreckfish fishery developed on the Blake Plateau in the mid 1980s using vertical lines on hydraulic reels (Sedberry et al. 1999). Wreckfish landings exceeded 4 million pounds annually before dramatically declining in the mid 1990's. The fishery has been successfully managed since 1990 under an Individual Transferable Quota (ITQ) system with an annual total quota set at 2 million pounds and a seasonal closure on the fishery during the January to April spawning period (Vaughn et al. 2001, Sedberry et al. 1999). The wreckfish fishery in Bermuda peaked at 5 metric tons (11,000 lbs) annually, and subsequently collapsed over a ten year period to a level that can no longer support a fishery (Sedberry et al. 1999). Although significant populations of wreckfish are currently unknown from the GOM, they are relatively abundant on the Pourtales Terrace in the Straits of Florida (Reed et al. 2006, Weaver *personal observation*). A single individual caught off of Alabama was a large, gravid female 119 cm in length, 31 kg in weight, and estimated to be 57 years old (Shipp and Sedberry 2008), indicating the possibility of a spawning population in the northern GOM. A review of yellowedge grouper handline trips in the GOM and associated fishes indicated 41 trips landing wreckfish out of a total of 118,000 logged trips (Cass-Calay and Bahnick 2002).

## Invertebrate Fishery Species
Deepwater invertebrate fishery species include royal red shrimp, golden crab, and red crab. The following brief species descriptions have been described from Bullis (1956), Anderson and Lindner (1971), Lockhart et al. (1990), Jones et al. (1994), Perry et al. (1995), Waller et al. (1995), CSA (2002), and Kilgour and Shirley (2008).

<u>**Royal red shrimp:**</u> *Pleoticus* (*Hymenopenaeus*) *robustus*
**Geographic Distribution**
Royal red shrimp occur from Massachusetts to Central America and northern South America, including the GOM.

**Habitat and Biology**

Royal red shrimp prefer sand, clay or mud bottoms in water depths ranging from 180 to 730 m, with highest densities in the GOM at depths ranging between 350 and 500 m. Unlike shallow-water penaeid shrimp, which complete their life cycle in a single year, royal red shrimp have a lifespan of several years (Jones et al. 1994).

**Fishery Importance**

Primary fishing grounds for royal red shrimp occur over sand, silt, and muds of the Mississippi Delta and calcareous muds of the Dry Tortugas (Anderson and Lidner 1971). This species requires specialized equipment for capture and storage, including storage in brine and quicker freezing, contributing to the relatively limited fishery. Fishing gear requires larger vessels than shallow water shrimp species, and trawling gear includes a configuration that may include one, two, or four nets towed simultaneously behind two benthic sleds (Figure 14-3). Megalops or pinspeckled shrimp (*Penaeopsis serrata*) have also been reported in landings of royal red shrimp (Jones et al. 1994). Ten other species of large deepwater shrimps are known to occur throughout the western Atlantic Ocean (Table 14-5), and could also contribute to regional fisheries.

**Golden Crab: *Chaceon fenneri***

**Geographic Distribution**

Golden crabs occur on the upper continental slope from New England to Brazil, including the GOM. The species is reported to be rare in the northern Gulf, where red crabs are the dominant large crab on slope habitats.

**Habitat and Biology**

Golden crabs prefer soft or hard bottom in water depths ranging from 200 to 800 m, with primary depths in the GOM ranging between 300 and 500 m. They have been reported to occur on natural hard bottom among sea fans and other sessile invertebrates.

**Fishery Importance**

Primary fishing grounds for golden crab occur along the east coast of the U.S. from North Carolina to the Florida Keys. Demand for golden crab is variable, as this species is mainly marketed as a substitute for snow crab. Gulf Coast fisheries were historically limited to the West Florida slope south of Tampa, FL, but currently appear to be nonexistent in the GOM. Commercial fishing for golden crab is currently unregulated, although they have been recognized as a potential fishery species and may be taken by trap only.

**Deepsea Red Crab: *Chaceon quinquedens***

Geographic Distribution

Deepsea red crabs occur on the upper continental slope from New England to Brazil, including the GOM. This species is the dominant large crab on slope habitats in the northern GOM (Waller et al. 1995, Kilgour and Shirley 2008).

**Habitat and Biology**

Deepsea red crabs prefer silty bottom habitats in water depths ranging from 300 to 2000 m, with primary depths in the GOM ranging between 670 and 1,000 m. Minimum depths are reported to be 860 m to the west of the Mississippi River delta and 677 m east of the river, deeper than most of the well-developed *Lophelia* sites in the northern GOM.

**Fishery Importance**

Primary fishing grounds for red crab occur along the East coast of the U.S. north of Cape Hatteras, N.C., in depths of 400 to 800 m. Red crab populations have been reported to reach densities capable of supporting a fishery in the northern GOM but this species is not currently exploited, and the increased depth of occurrence may make it economically unfeasible for a fishery to develop. As a result this fishery is unregulated.

## 14.2.6 Historical Development of the Deepwater Grouper and Tilefish Fishery

The fishery for shallow water snappers and groupers in the GOM has been well established since the 1870's, expanding shortly after the end of the Civil War (Jarvis 1935, Prytherch 1983). The availability of natural ice, delivered by schooners from Maine, for shipping food led the development of a commercial fishery in Pensacola, FL, (Prytherch 1983). Fish were initially held onboard in live wells and later packed in ice at sea. By the 1920s over 85 vessels were engaged in the reef fish fishery throughout the GOM to depths of 170 m, the harvest of red snapper and groupers reached almost 15 million pounds annually, and the fishery showed signs of overfishing (Jarvis 1935). Beginning in the 1930s, investigations by the U.S. Bureau of Fisheries focused on the development of alternative fishing methods at different depths across the continental shelf, including experimental longlines and fish traps, to improve the efficiency of the fishery. The results of longline experiments indicated that this was a promising and effective method for the landing of groupers. Research cruises conducting exploratory bottom longline fishing were conducted in the 1950's and 1960's, and resulted in high catch rates of tilefish, which were not commercially important species at that time (CSA, 2002).

Early use of handlines was replaced with by vertical lines passing through a rail-mounted davit with an attached motor, named a "One Arm Bandit" or "Bandit Rig" (Prytherch 1983, CSA 2002). Bandit rig fishing became common through the Gulf, and was supplemented with longlining on a commercial basis beginning in the late 1970's. Bottom longlining activity reached a peak in the early 90's, although most vessels were also equipped with bandit rigs (Prytherch 1983). The rapid development of bottom longline fishing in the Gulf caused concern over heavy impacts to the grouper and snapper fishery, coupled with the easy conversion of shrimp vessels to bottom longliners and rapid entry into the fishery in years where demand for shrimp was low (Prytherch 1983).

An analysis of reef fish longlining practices was later conducted by the NMFS in the 1960's on fishing vessels to depths of 340 m (Prytherch 1983) to investigate gears and effectiveness of harvest for different species, and provide information to the Gulf of Mexico Fishery Management Council for the development of the first Reef Fish Management Plan. The reef fish management plan has repeatedly been amended to prevent the overfishing of many species, including groupers and red snapper. The initial quota was set at 1.8 million pounds, and was twice reduced to the current quota of 1.02 million pounds.

## 14.2.7 Current status of the Deepwater Reef Fish Fishery

Large predatory reef fishes in the GOM, including groupers and snappers, are highly susceptible to overfishing, and populations have dramatically declined in both GOM and Atlantic shelf-edge reef sites (Coleman et al. 2000, Koenig et al., 2000, Reed et al. 2007). Fishing on hard bottom reef

ecosystems below approximately 50 m results in elevated mortality of juveniles and undersized adults due to barotrauma, further complicating management of the fishery. At greater depths, including *Lophelia* coral sites, reported populations of deepwater groupers and other fishery species (wreckfish, barrelfish, alfonsinos) are typically small (Reed et al. 2005, Sulak 2008), and would be vulnerable to depletion by very few fishing vessels. Submersible and remotely operated vehicle surveys also have documented lost longlines between 200 and 500 m, indicating fishing activity on *Lophelia* communities.

A preliminary analysis of *Lophelia* distribution and the NOAA reef fish logbook data indicates relatively low deepwater (200 to 600 m) fishing activity in the management grid areas with known *Lophelia* reefs, particularly those in the northern GOM (Figures 14-5 – 14-7). Deepwater reef fish effort appears to be concentrated along the west Florida shelf, in statistical grids 1-9. Recent (2007 to 2009) patterns indicated increased fishing activity in depths of less than 200 m in grids 10 and 11, the region of Viosca Knoll reef sites, but current efforts below 200 m appears to be relatively low or are confidential in nature (Figure 14-11). The current pattern of fishing effort appears to be concentrated in the region of the west Florida slope *Lophelia* sites and the Florida Keys (Figure 14-11).

Landings of deepwater groupers and tilefish appear to be relatively stable during the last 20 years (Figures 14-12 - 14-14). A gradual increase in number of reef fish trips that landed these species in the GOM was reported from 1990 to 2003 (Figure 14-12). The number of trips declined between 2004 and 2009, likely due to early closures in the fishery, rising fuel costs, and the implementation of Secretarial Amendment 1, which established a rebuilding plan and reduced commercial quotas for shallow and deepwater groupers (decreasing the deepwater grouper quota from 1.35 to 1.02 million lbs gutted weight). While the number of trips during this period was reduced, reported landings per trip increased slightly, for both total landings of reef fishes and deepwater species (Figure 14-12, 14-15), and in 2009 was the highest for the entire 1990-2009 period. State reported landings display a slightly different pattern, with peaks in deepwater grouper landings in 2000 and 2003, and relatively constant landings of ~ 1.2 million pounds in other years from 2001 to 2009.

Deepwater fisheries in the GOM are limited in both number of vessels engaged in the fishery and number of trips taken annually. Early closure of the 2009 deepwater grouper and tilefish fishery in the GOM and subsequent implementation of an Individual Fishery Quota (IFQ) system reflects ongoing difficulties with management of the resource and a need for more restrictive management actions to regulate the fishery (GMFMC 2008, NMFS 2009a, b, NOAA 2009). During the 2009 season, deepwater grouper fisheries were closed on June 27 and the tilefish fishery closed on May 15th due to the early harvest of the commercial quota. Reef fish trips for deepwater groupers, snappers, and tilefish are now of limited entry and managed through an IFQ system, established on August 31st, 2009 by the NOAA Fisheries Service. Individual IFQ allocations will eliminate the need for early closure of the fishery and improved records of fishing activity, and the 2010 commercial quota remained set at 1.02 million pounds. NOAA is currently considering, through Amendment 31 to the reef fish FMP, the reduction in number of commercial longline vessels in the eastern GOM through a longline endorsement, and also limiting the number of total hooks on vessels to 1,000 with a maximum of 750 rigged or fished at a time. The possible shift in effort to deepwater longlining could be hindered by the IFQ system.

## 14.2.8 History of the Deepwater Shrimp Fishery

The commercial shrimp industry began in the early 1800s along the southeastern U.S. Coast, using cast nets and seines, and shrimping began in Galveston in the 1830s. Sailboats were positioned in tidal inlets to harvest shrimp as they migrated out of estuaries into the GOM. Shrimp were salted and shipped in barrels to distant markets. In 1910, shrimp were shipped in ice or frozen and sent to cities as far as Chicago and New York. During World War 1, gasoline powered vessels and otter trawls were used and international markets developed with Japan, as well as domestic markets with other Gulf coast states. Shrimping activity further increased after World War II through the 1970s. In recent years high fuel costs and the import of farmed shrimp has led to fluctuations in the market, but the fishery remains one of the most valuable in the United States, in terms of economic value and weight (Table 14-6).

As with bottom longlining, deepwater exploratory trawling by the Bureau of Commercial Fisheries, Pascagoula lab identified exploitable populations of royal red shrimp in the 1950's in 300 to 800 m (Bullis 1956, CSA 2002). Commercial fishing for royal red shrimp began in 1960 (Figure 14-9), but landings have been very small compared to the shallow water penaeid shrimp fishery. Fewer than 25 vessels have fished for royal red shrimp in any given year, compared to an estimated 20,000 shrimp vessels operating in state or federal waters for brown, white and pink shrimp.   `

## 14.2.9 Current status of the Deepwater Invertebrate Fishery

The red and golden crab fishery is managed by fishery management plans in North and South Atlantic Coast regions, but management plans are lacking for the GOM (Kilgour and Shirley 2008, S. Branstetter *personal communication*). The initial development of a management plan to avoid potential conflicts with the royal red shrimp trawl fishery was discontinued when the value of the fishery was considered to be too low (GMFMC 1995, 2001, 2005). Despite suggestions of a viable fishery for red and golden crab in the literature, there appears to be no active vessels fishing for either species in the GOM. Only three reports of catch of golden crab were reported in the NMFS fishery logbook databases from 1990 to 2009, although there are reports of over 220,000 pounds per year harvested in the GOM Commercial fisheries (Table 14-6). These landing may occur as bycatch during the royal red shrimp fishery. Population densities of golden crab and deepsea red crab appear to be too low for an economically viable entry into the fishery (S. Branstetter, *personal communication*).

The royal red shrimp trawl fishery currently appears to be limited to three full time vessels in the GOM with up to sixteen vessels historically participating on a part-time basis in recent years (Jones et al. 1993, GMFMC 2001, GMFMC 2005, Stiles et al. 2007) (Table 14-1). Current trawling activity primarily occurs on the west Florida slope and the area surrounding the DeSoto Canyon, including the Viosca Knoll region (Stiles 2008, J. Nance, NOAA Fisheries, *personal communication*) (Figures 14-8, 14-10). Fishing historically has concentrated in NMFS Statistical Grid 2, 4 and 5 off the west coast of Florida, and grids 9-11 in the northeastern GOM. Recent fishing activity is concentrated in the Dry Tortugas and northern GOM around the Mississippi Delta and DeSoto Canyon, in both number of trips and landings (Figure 14-10). Trawling for royal red shrimp occurs in the depth range of known *Lophelia* communities, and could have considerable impacts on the region of the central west Florida slope and northern Gulf where

deep coral reefs occur. Unfortunately the exact locations of trawls in this fishery are classified as confidential, and a more detailed analysis of fishing effort will have to be made to identify potential interaction with deepwater coral sites.

The following data are based on 520 tows from 16 ELB trips where royal red shrimp were the primary catch: The total catches were 512,948 pounds of tails equivalent of royal red shrimp. Mean tow time: 6.71 hours, standard error of tow time: 0.089 hours (J. Cole, L.G.L. *pers. comm.*). Royal red shrimp boats are typically larger than shallow water vessels, in excess of 40 m in length, to accommodate extra cable for deep trawling. Fishermen typically deploy the quad net arrangement common in the shallow penaeid shrimp fisheries (B. Gallaway, LGL, *pers. comm.*).

Table 14-1.

Number of vessels and trips for royal shrimp in the Gulf of Mexico, 2004-2008, from the NMFS logbook system SEFSC.

| Year Unloaded | Vessels | Dedicated Vessels | Unique Triptickets | Unique Trips |
|---------------|---------|-------------------|--------------------|--------------|
| 2004 | 16 | 12 | 44 | 56 |
| 2005 | 11 | 4 | 27 | 31 |
| 2006 | 6 | 0 | 25 | 25 |
| 2007 | 8 | 0 | 30 | 30 |
| 2008 | 8 | 3 | 24 | 27 |

Impacts of fuel costs on the shallow water shrimp fleet and fluctuating imports of farmed shrimp could lead to increased levels of activity in the royal red shrimp fishery by dedicated vessels (GMFMC 2005). The GMFMC and NOAA Fisheries have also considered increasing the total allowable catch (TAC) above the current level of 392,000 lbs, an action that could stimulate conversion to the fishery. Historically the overall harvest has been relatively low, has declined in recent years and is at approximately 50% of the quota (Figure 14-4).

## 14.2.10    Oculina Banks Ecosystem Impacts

While current deepwater fisheries in the GOM appear to be conducted by a limited number of vessels in fairly restricted geographic areas, the potential impact of commercial longline and trawl fisheries to deep coral communities have been well documented in the *Oculina* ecosystems along the east coast of Florida (Koenig et al. 2000, Reed et al. 2007). Heavy commercial and recreational fishing pressure resulted in removal of large populations of adult groupers, and resulted in a drastic change in ecosystem structure of the resident fish communities. Commercial trawling for rock shrimp and brown shrimp in unprotected areas resulted in a nearly complete removal of living coral, with live coral remaining only in areas protected as a habitat area of particular concern (HAPC) established in 1984 (Reed et al. 2007, Stiles et al. 2007).

Because of the potential for future expansion of deepwater shrimp and crab fisheries, and possible targeting of high profile coral banks for deepwater fishes, the establishment of deepwater coral HAPCs for future protection of these areas is warranted. Currently regulated HAPC's in the GOM

are limited to the shelf edge reefs and banks of the northwestern Gulf and West Florida Shelf (GMFMC 2005), and reef fish Essential Fish Habitat (EFH) is only considered to depths of 200 m. The only exception is the Tortugas South Ecological Reserve of the Florida Keys National Marine Sanctuary, which extends from depths of 30 to 1000 m, and protects known spawning habitat for reef fishes on Riley's Hump coral reef ecosystem and a number of deepwater groupers (Weaver et al. 2006). An extensive hard bottom community occurs between depths of 80 and 145 m throughout the reserve, but no deepwater coral ecosystems are known to occur below 200 m. Although the EFH Amendment to the Reef Fish Management plan does not consider habitat below 200 m, many species listed in the amendment occur below these depths on deepwater coral ecosystems (Table 14-7).

### 14.2.11 Coral Habitat HAPCs in the South Atlantic

The South Atlantic Fishery Management Council has identified deep sea coral ecosystems (DSCE) off the east coast of the U.S. as Coral Habitat Areas of Particular Concern (CHAPCs), and recommended designation of four areas (Figure 14-16) to protect against destructive impacts of trawling for royal red shrimp and benthic finfish (SAFMC 2009). Approved by the SAFMC in September, 2009, the action is part of the Comprehensive Ecosystem-Based Amendment 1, is awaiting final approval by the Secretary of Commerce, and expected to be effective in early 2010. The council has justified this action to protect potential fisheries and the discovery of pharmaceutical compounds from the diverse deepwater reef fauna in depths of 400 to 700 m, while maintaining deepwater fisheries in the region. Council members worked closely with golden crab and royal red shrimp fisherman to insure both protection of deepwater coral areas and continuation of the deepwater fisheries by establishing both "Allowable Golden Crab Fishing Areas" and "Shrimp Fishery Access Areas" within two of the proposed HAPCs (SAFMC 2009).

Designation of CHAPC zones for known *Lophelia* sites in the GOM would provide the equivalent protection for these ecosystems, and the collaborative process followed by the SAFMC serves as a guideline for the GMFMC, MMS, and collaborating agencies.

### 14.3 SUMMARY

1. Deepwater fisheries in the GOM are limited with respect to number of vessels engaged in the fishery and number of trips taken annually. Regulatory closures also constrain the fishery. During the 2009 season, deepwater grouper fisheries were closed on June 27 and the tilefish fishery closed on May 15th due to the early harvest of the commercial quota. Reef fish trips for deepwater groupers, snappers, and tilefish are now of limited entry and managed through an Individual Fishing Quota (IFQ) system, established on August 31st, 2009 by the NOAA Fisheries Service. Individual IFQ allocations will eliminate the need for early closure of the fishery and improve regulation of the industry. An amendment under review to reduce shallow water bottom longlining activity in the eastern Gulf could cause vessels to shift to deeper waters, but an increase in the overall harvest of deepwater groupers and tilefish will be prevented by the IFQ system. It is possible that vessels could target barrelfish on *Lophelia* reefs, as landings are unregulated for this species, to increase the overall catch.

2. The spatial distribution of deepwater grouper and tilefish trips primarily occurs on the west Florida shelf, based on the non-confidential component of the reef fish log books. Confidential records include between 30 and 100 trips per year that occur between the Mississippi River Delta and Brownsville. Based on the percent of landings, most of these trips appear to target yellowedge grouper at depths less than 300 m (maximum reported depth for this species is 275 m), and to a lesser extent snowy and warsaw groupers. Few vessels appear to target deeper communities where *Lophelia* reefs occur, based on the low catch of barrelfish, which regularly occurs as bycatch in the deepwater grouper fishery. (Note: A breakdown of reef fish trips and landings by 100 m depth horizons will be provided by J. Bennett, NOAA Fisheries, for inclusion in a future draft).

3. Royal red shrimp fisheries have historically been conducted by 3 to 12 full time vessels in the GOM per year, and primarily in the areas of the Dry Tortugas and east of the Mississippi Delta. Electronic logbook records for 2008 indicate trawling activity in the vicinity of known *Lophelia* reefs, most likely by a single vessel. Recent trends in the fishery show a decline in fishing effort and harvest, but the fishery for this species has been highly variable over the last 50 years. NOAA Fisheries has considered raising the quota to accommodate expansion of the fishery under favorable market conditions, and low demand for or restrictions on shallow penaeid shrimp species could shift efforts to deeper waters. Because of the restricted depth range of royal red trawling between ~350 and 500 m, this activity could have significant effects on known *Lophelia* communities.

4. The focused golden and deepsea red crab fishery currently appears to be extremely limited or nonexistent, other than as possible bycatch in the royal red shrimp fishery. NOAA Fisheries has limited gear to traps for deepwater geryonid crabs, but the fishery is otherwise unregulated. Although golden crab populations appear to be south of the main area of known *Lophelia* beds, and red crabs in deeper slope waters of the northern Gulf, exploratory trap fishing for these species could significantly damage deepwater corals.

5. The South Atlantic Fishery Management Council has identified deep sea coral ecosystems (DSCE) of the east coast of the U.S. as Habitat Areas of Particular Concern (HAPCs), and recommended designation of four areas to protect against potentially destructive impacts of trawling for royal red shrimp and benthic finfish. The council has justified this action to protect potential fisheries and the discovery of pharmaceutical compounds from the diverse deepwater reef fauna. Designation of DSCE areas for the GOM therefore has precedent as a management option for protection of *Lophelia pertusa* and other deepwater coral ecosystems.

## 14.4 REFERENCES:

Anderson, W. W. and M. J. Lindner. 1971. Contributions to the biology of the royal red shrimp, *Hymenopenaeus robustus* Smith. Fishery Bulletin 69(2):313-336.

Auster, P. A, J. Moore, K. B. Heinonen, and L. Watling. 2005. A habitat classification scheme for seamount landscapes: assessing the functional role of deep-water corals as fish habitat. Pp. 761-769 in Friewald, A., and Roberts, J.M. (eds.), Cold-water Corals and Ecosystems. Springer-Verlag, Berlin Heidelberg.

Balmford, A., P. Gravestock, N. Hockley, C. J. McClean, and C. M. Roberts. 2004. The worldwide costs of marine protected areas. PNAS 2004:1-4.

Barnette, M. C. 2001. A review of the fishing gear utilized within the Southeast Region and their potential impacts on essential fish habitat. NOAA Tech. Memo. NMFSSEFSC- 449. 62 pp.

Barnette, M. C. 2006. [Observations of the Deep-Water Coral *Oculina varicosa* in the Gulf of Mexico](). NOAA Technical Memorandum NMFS-SEFSC-535. 12 pp.

Bohnsack, J. A. 2003. Shifting baselines, marine reserves, and Leopold's biotic ethic. Gulf and Caribbean Research 14(2):1-7.

Brooke, S. D., M. W. Holmes, and C. M. Young. 2009. Sediment tolerance of two different morphotypes of the deep-sea coral *Lophelia pertusa* from the Gulf of Mexico. Mar. Ecol. Prog. Ser. 390:137-144.

Bullis, H. R., Jr. 1956. Preliminary results of deep-water exploration for shrimp in the Gulf of Mexico by the M/V OREGON (1950-1956). Comm. Fish. Rev.18(12):1-12.

Bullock, L. H. and G. B. Smith. 1991. Seabasses (Pisces: Serranidae). Memoirs of the *Hourglass* Cruises. Florida Marine Research Institute Dept. Nat. Res., St. Petersburg, FL, Vol. 8, 243 pp.

Bullock, L. H., M. F. Godcharles, and R. E. Crabtree. 1996. Reproduction of yellowedge grouper, *Epinephelus flavolimbatus*, from the Gulf of Mexico. Bull. Mar. Sci. 59(1):216-244.

Caillet, G. M., A. H. Andrews, E. J. Burton, D. L. Watters, D. E. Kline, and L. A. Ferry-Graham. 2001. Age determination and validation studies of marine fishes: do deep-dwellers live longer? Exp. Ger. 36(2001): 739-764.

Cass-Calay, S. L. and M. Bahnick. 2002. Status of the yellowedge grouper fishery in the Gulf of Mexico. Southeastern Fisheries Division Contribution No. SFD-02/03-172

Chittenden, M. E., and J. D. McEachran. 1976. Composition, ecology, and dynamics of demersal fish communities on the northwestern Gulf of Mexico continental shelf, with a similar

synopsis for the entire Gulf.  Texas A&M University Sea Grant College TAMU-SG-76-208.

Coleman, F. C., C. C. Koenig, G. R. Huntsman, J. A. Musick, A. M. Eklund, J. C. McGovern, R. W. Chapman, G. R. Sedberry, and C. B. Grimes.  2000.  Long-lived Reef Fishes: the Grouper-Snapper Complex.  Am. Fisheries Soc. 25(3):14-20.

Continental Shelf Associates, Inc.  2002.  Deepwater Program: Bluewater Fishing and Deepwater OCS Activity, Interactions between the Fishing and Petroleum Industries in Deepwaters of the Gulf of Mexico.  A Final Report for the U.S. Department of the Interior, Minerals Management Service, Gulf of Mexico OCS Region, Metairie, LA.  OCS Study MMS-2002-78.

Continental Shelf Associates International, Inc.  2007.  Characterization of northern Gulf of Mexico deepwater hardbottom communities with emphasis on *Lophelia* coral.  U.S. Department of the Interior, Minerals Management Service, Gulf of Mexico OCS Region, Metairie, LA.  OCS Study MMS-2007-44.

Cordes E. E., D. C. Berquist, C. R.  Fisher.  2009.  Macro-ecology of Gulf of Mexico cold seeps.  Annu Rev Mar Sci 1:143-168.

Cordes, E. E., M. P. McGinley. E. L. Podowski, E. L. Becker, S. Lessard-Pilon, S. T. Viada, and C. R. Fisher.  2008.  Coral communities of the deep Gulf of Mexico.  Deep-Sea Res. I 55(2008): 777-787.

Costello, M. J., M. McCrea, A. Friewald, T. Lundalv, L. Jonsson, B. J. Bett, T. C. E. van Weering, H. de Haas, J. M. Roberts, and D. Allen.  2005.  Role of cold-water *Lophelia pertusa* coral reefs as fish habitat in the NE Atlantic.  Pages 771-805 in Friewald, A. and Roberts, J. M. (eds) Cold-water corals and Ecosystems.  Springer-Verlag, Berlin Heidelberg.

Dürr and González.  2002.  Feeding habits of *Beryx splendens* and *Beryx decadactlyus* (Berycidae) off the Canary Islands.  Fisheries Research (2002): 363-374.

Erdman, R. B. and N. J. Blake.  The Golden Crab (*Chaceon fenneri*) fishery of southeast Florida.

Filer, K. R. and G. R. Sedberry.  2008.  Age, growth, and reproduction of the barrelfish *Hyperoglyphe perciformis* (Mitchill) in the western North Atlantic.  J. Fish Biol. 72:861-882.

Fosså, J. H., P. B. Mortenson, and D. M. Furevik.  2002.  The deep-water coral *Lophelia pertusa* in Norwegian waters: distribution and fishery impacts.  Hydrobiol. 471: 1-12.

Gallaway, B. J., J. G. Cole, R. X. Nguyen.  2009.  Gulf of Mexico ELB Tows.  L.G.L. Ecological Research Associates, Inc.(Paper Map)

Gallaway, B. J., L. R. Martin, R. L. Howard, G. S. Boland, and G. D. Dennis. 1981. Effects on artificial reefs and demersal fish and macrocrustacean communities. In: Environmental effects of offshore oil production, B. S. Middleitch, ed. pp. 237- 299.

Gass S. E., M. Roberts (2006) The occurrence of the cold-water coral *Lophelia pertusa* (Scleractinia) on oil and gas platforms in the North Sea: Colony growth, recruitment and environmental controls on distribution. Mar Pollut. Bull. 52:549-559.

Gauvin, J. R., J. M. Ward and E. E. Burgess. 1994. Description and evaluation of the wreckfish (*Polyprion americanus*) fishery under individual transferable quotas. Mar. Res. Economics 9(2):99-118.

Genin, A. 2004. Bio-physical coupling in the formation of zooplankton and fish aggregations over abrupt topographies. J. of Mar. Syst. 50(2004): 3-20.

Gilmore, R. G. and R. S. Jones. 1992. Color variation and associated behavior in the epinepheline groupers, Mycteroperca microlepis (Goode and Bean) and M. phenax Jordan and Swain. Bull. Mar. Sci. 51(1):83-103.

Glover, A. G. and C. R. Smith. 2003. The deep-sea floor ecosystem: current status and prospects of anthropogenic change by the year 2025. Environmental Conservation 30(3):219-241.

GMFMC. 1995. Amendment 8 to the Fishery Management Plan for the Shrimp Fishery of the Gulf of Mexico, United States Waters. Gulf of Mexico Fishery Management Council, 5401 West Kennedy Boulevard, Tampa, Florida 33609. 25 pp.

GMFMC. 2001. Amendment Number 11 to the Fishery Management Plan for the Shrimp Fishery of the Gulf of Mexico, United States Waters. Gulf of Mexico Fishery Management Council, 3018 U.S. Highway 301 North, Suite 1000, Tampa, Florida 33619. 42 pp.

GMFMC. 2005a. Final Amendment Number 13 to the Fishery Management Plan for the Shrimp Fishery of the Gulf of Mexico, United States Waters. Gulf of Mexico Fishery Management Council, 2203 North Lois Avenue, Suite 1100, Tampa, Florida 33607. 273 pp.

GMFMC. 2005b. Generic Amendment Number 3 for Addressing Essential Fish Habitat Requirements, Habitat Areas of Particular Concern, and Adverse Effects of Fishing in the following Fishery Management Plans in the Gulf of Mexico: Shrimp Fishery of the Gulf of Mexico, Red Drum Fishery of the Gulf of Mexico, Reef Fish Fishery of the Gulf of Mexico, Coastal Migratory Pelagic Resources (Mackerels) in the Gulf of Mexico and South Atlantic, Stone Crab Fishery of the Gulf of Mexico, Spiny Lobster in the Gulf of Mexico and South Atlantic, Coral and Coral Reefs of the Gulf of Mexico. Gulf of Mexico Fishery Management Council, 3018 U.S. Highway 301 North, Suite 1000, Tampa, Florida 33619. 104 pp.

GMFMC. 2008. Amendment 29 to the Fishery Management Plan for the Reef Fish Management Plan, Effort Management in the Commercial Grouper and Tilefish Fisheries, United States

Waters. Gulf of Mexico Fishery Management Council, 2203 North Lois Avenue, Suite 1100, Tampa, Florida 33607. 300 pp.

Hall-Spencer, J., V. Allain, and J. H. Fosså. 2002. Trawling damage to northeast Atlantic ancient coral reefs. Proc. R. Soc. Lond. B 269: 507-511.

Harper, D. E., P. B. Eyo and G. P. Scott. 2000. Updated golden crab fishery trends and production model analysis based on trip report logbook and trip interview data collection programs. Contribution Number PRD-99/00-12. NMFS Southeastern Fisheries Science Center. Miami, Florida.

Heemstra, P. C. and J. E. Randall. 1993. Groupers of the World (Family Serranidae, Subfamily Epinephelinae). An annotated and illustrated catalogue of the grouper, rockcod, hind, coral grouper and lyretail grouper species known to date. FAO Fisheries Synopsis No. 125, Vol. 16. Food and Agriculture Organization of the United Nations, Rome. 382 pp.

Husebo, A., L. Nottestad, J. H. Fossa, D. M. Furevik and S. B. Jorgensen. 2002. Distribution and abundance of fish in deep-sea coral habitats. Hydrobiol. 471: 91-99.

Jarvis, N. D. 1935. Fishery for red snappers and groupers in the Gulf of Mexico. U.S. Department of Commerce, Bureau of Fisheries Investigational Report No. 26(1):1-29.

Jones, A. C., J. M. Nance, and W. O. Antozzi, Jr. 1994. A review of the royal red shrimp resource and fishery in the Gulf of Mexico. A report to the Gulf of Mexico Fishery Management Council. 31 pp.

Kilgour, M. J. and T. C. Shirley. 2008. Disribution of red deepsea crab (*Chaceon quinquedens*) by size and sex in the Gulf of Mexico. Fishery Bull. 106: 317-320.

Koenig, C. C., F. C. Coleman, C. B. Grimes, G. R. Fitzhugh, K. M. Scanlon, C. T. Gledhill, and M. W. Grace. 2000. Protection of fish spawning habitat for the conservation of warm-temperate reef-fish fisheries of shelf-edge reefs of Florida. Bull. Mar. Sci. 66(3):593-616.

Koslow, J. A., K. Gowlett-Holmes, J. K. Lowry, G. C. B. Poore, and A. Williams. 2001. Seamount benthic macrofauna off southern Tasmania: community structure and impacts of trawling. Marine Ecology Progress Series 213: 111-125.

LGL Ecological Research Associates, Inc. 2009. Gulf of Mexico Cooling Water Intake Structure: Source Water Biological Baseline Characterization Study. Prepared for the Offshore Operators Committee, Environmental Sciences Subcommittee. 142 pp.

Lockhart, F. D., W. J. Lindberg, N. J. Blake, R. B. Erdman, H. M. Perry, and R. S. Waller. 1990. Distributional differences and population similarities for two deep-sea crabs (Family Geryonidae) in the northeastern Gulf of Mexico. Canadian Journal of Fisheries and Aquatic Sciences 47: 2112-2122.

Matlock, G. C., W. R. Nelson, R. S. Jones, A. W. Green, T. J. Cody, E. Gutherz and J. Doerzbacher. 1990. Comparison for two techniques for estimating tilefish, yellowedge grouper, and other deepwater fish populations. Fishery Bulletin 89:91-99.

McEachran, J. D. and J. D. Fechelm. 1998. Fishes of the Gulf of Mexico: Vol. 1: Myxiniformes to Gasterosteiformes. 997 pp.

McEachran, J. D. and J. D. Fechelm. 2005. Fishes of the Gulf of Mexico: Scorpaeniformes to Tetraodontiformes. 997 pp.

Messing, C. G., J. K. Reed, S. D. Brooke, and S. W. Ross. 2008. Deepwater Coral Reefs of the United States. Pages 767 - 791 in B. M. Riegl and R. E. Dodge (eds.), Coral Reefs of the USA. Springer Science.

Moore, D. R. and H. R. Bullis, Jr. 1960. A deep-water coral reef in the Gulf of Mexico. Bull. Mar. Sci. 10(1):125-128.

Morato, T., R. Watson, T. J. Pitcher and D. Pauley. 2006. Fishing down the deep. Fish and Fisheries 7:24-34.

Musick, J. A., M. M. Harbin, S. A. Berkely, G. H. Burgess, A. M. Eklund, L. Findley, R. G. Gilmore, J. T. Golden, D. S. Ha, G. R. Huntsman, J. C. McGovern, S. J. Parker, S. G. Poss, E. Sala, T. W. Schmidt, G. R. Sedberry, H. Weeks, and S. G. Wright. 2000. Marine, estuarine, and diadromous stocks at risk of extinction in North America (exclusive of Pacific salmonids). Fisheries 25(11):6-30.

Myers, R. A. and B. Worm. 2003. Rapid worldwide depletion of predatory fish communities. Nature 423:280-283.

Nance, J. M. 2007. Review of the Status and Health of the Shrimp Stocks for 2007. NMFS.

Nelson, W. R. and J. S. Carpenter. 1968. Bottom longline explorations in the Gulf of Mexico. Comm. Fish. Rev. 30(10):57-62

Newton, C. R., H. T. Mullins, A. F. Gadulski, A. C. Hine, and G. R. Dix. 1987. Coral mounds on the West Florida Slope: Unanswered questions regarding the development of deepwater banks. Palaios 1987(2):359-367.

NMFS. Royal Red Shrimp Life History. http://www.nmfs.noaa.gov/habitat/habitatprotection/profile/gulfofmexico/royal_red_shrimphome.htm

NMFS. 2004. SAFE report for the Golden Crab fishery of the South Atlantic region - 2004. National Marine Fisheries Service, Southeastern Regional Office, 9721 Executive Center Drive North, St. Petersburg, FL 33702. 14 pp.

NMFS 2008. Fisheries Statistics. http://www.st.nmfs.gov/st1/

NMFS. 2009a.  Clarification of Selected Reef Fish Regulations in the Gulf of Mexico for 2010.  Southeastern Fishery Bulletin, 16 December 2009.

NMFS. 2009b.  Deepwater Grouper Commercial Fishery Closed to Vessels Fishing in the Gulf of Mexico Federal Waters.  Southeastern Fishery Bulletin, 17 June 2009.

NOAA.  2001.  Fisheries of the Caribbean, Gulf of Mexico, and South Atlantic; Golden Crab Fishery of the Southern Atlantic States; Amendment 3.  Federal Register 66(228): 59221

NOAA.  2009.  Fisheries of the Caribbean, Gulf of Mexico, and South Atlantic; Reef Fish Fishery of the Gulf of Mexico.  Federal Register 74(167): 44732-44750.

Olander, D.  2001.  Down the tubes: deep-dropping Gulf oil rigs.  Sport Fishing 16(6):48-55.

Olander, D.  2009.  Deep-dropping in the Gulf.  Sport Fishing.  31 August 2009.

Perry, H., R. Waller, C. Trigg, J. McBee, R. Erdman, and N. Blake.  1995.  A note on bycatch associated with deepwater trapping of *Chaceon* in the northcentral Gulf of Mexico.  Gulf Research Reports 9(2):139-142.

Powell, S. M., R. L. Haedrich, and J. D. McEachran.  2003.  The Deep-sea Demersel Fish Fauna of the Northern Gulf of Mexico.  J. North. Atl. Fish. Sci., Vol. 31:19-33

Prytherch, H. F.  1983.  A Descriptive Survey of the Bottom Longline Fishery in the Gulf of Mexico.  NOAA Technical Memorandum NMFS-SEFC-122

Reed, J. K.  2002.  Comparison of deep-water coral reefs and lithoherms off southeastern USA.  Hydrobiol. 471:57-69.

Reed, J. K.  2006.  Habitat and fauna of deep-water coral reefs off the southeastern USA.  A Report to the South Atlantic Fishery Management Council Addendum to the 2004 Report.  2005-2006 Update- East Florida Reefs.  8 pp.

Reed, J. K., C. C. Koenig, and A. N. Shepard.  2007. Impacts of bottom trawling on a deep-water *Oculina* coral ecosystem off Florida. Bulletin of Marine Science 81(3): 481-496.

Reed, J. K., D. C. Weaver, and S. A. Pomponi.  2006.  Habitat and fauna of deep-water *Lophelia pertusa* coral reefs off the southeastern U.S.: Blake Plateau, Straights of Florida, and Gulf of Mexico.  Bulletin of Marine Science 78(2): 343-375.

Reed, J. K., S. A. Pomponi, D. C. Weaver, C. K. Paull, and A. E. Wright.  2005.  Deep-water sinkholes and bioherms of South Florida and the Pourtales Terrace- Habitat and Fauna.  Bulletin of Marine Science 77(2):267-296.

Roberts, C. M.  2002.  Deep impact: the rising toll of fishing in the deep sea.  Tr. Ecol. Evol. 17(5): 242-245.

Roberts, J. M., A. J. Wheeler, and A. Friewald. 2006. Reefs of the Deep: the Biology and Geology of Cold-Water Coral Ecosystems. Science 312:543-547.

Rogers, A. D. 1999. The biology of *Lophelia pertusa* (Linnaeus 1758) and other deep-water reef-forming corals and impacts from human activities. International Revue of Hydrobiology (84)4:315-406.

Ross, S. W. and A. M. Quattrini. 2007. The fish fauna associated with deep coral banks off the southeastern United States. Deep-Sea Research I 54: 975-1007.

Russell, G. M., E. J. Gutherz, and C. A. Barans. 1988. Evaluation of demersal longline gear off South Carolina and Puerto Rico with Emphasis on Deep-water Reef Fish Stocks. Marine Fisheries Review 50(1):26-31.

SAFMC. 2009. Council Approves Measure to Protect Largest Deepwater Coral Reef in the South Atlantic. South Atlantic Fishery Management Council News Release. September 24, 2009. http://www.safmc.net.

Schroeder, W. W., S. D. Brooke, J. B. Olson, B. Phaneuf, J. J. MacDonough III, and P. Etnoyer. 2005. Occurrence of deep-water *Lophelia pertusa* and *Madrepora oculata* in the Gulf of Mexico. Pp. 297-307 in Friewald, A., and Roberts, J.M. (eds.), Cold-water Corals and Ecosystems. Springer-Verlag, Berlin Heidelberg.

Sedberry, G. R., C. A. P. Andrade, J. L. Carlin, R. W. Chapman, B. E. Luckhurst, C. S. Manooch, III, G. Menzes, B. Thomsen, and G. F. Ulrich. 1999. Wreckfish *Polyprion americanus* in the North Atlantic: fisheries, biology, and management of a widely distributed and long-lived fish. Am. Fish. Soc. Symp. 23:27-50.

Sedberry, G. R., G. F. Ulrich and A. J. Applegate. 1993. Development and status of the fishery for wreckfish (*Polyprion americanus*) in the southeastern United States. Proc. Gulf and Caribb. Fish. Inst. 58:118-129.

Shipp, R. L. and G. Sedberry. 2008. First capture of a wreckfish, *Polyprion americanus*, from the Gulf of Mexico. Gulf of Mexico Science 2008(2):133-135.

Smith-Vaniz, W. F., B. B. Collette, and B. E. Luckhurst. 1999. Fishes of Bermuda. Amer. Soc. Ichthy. Herpet. Spec. Publ. 20. 183 pp.

Steimle, F. W., C. A. Zetlin and S. Chang (2001) Red deepsea crab, *Chaceon* (*Geryon*) *quinquedens*, life history and habitat characteristics. January 2001, 36, U.S. Dept. Commerce, NOAA, NOAA Technical Memorandum NMFS-NE-163.

Stiles, M. L., E. Harrould-Kolieb, P. Faure, H. Ylitalo-Ward, M. F. Hirschfield. 2007. Deep sea trawl fisheries of the southeast US and Gulf of Mexico: Rock shrimp, royal red shrimp, calico scallops. Oceana. Washington D.C.

Sulak, K. J. 2008. Characterization of Northern Gulf of Mexico Deepwater Hardbottom Communities with Emphasis on *Lophelia* Coral- *Lophelia* Reef Megafaunal Community Structure, Biotopes, Genetics, Microbial Ecology, and Geology. USGS Open-File Report 2008-1148. OCS Study MMS 2008-015.

Thresher, R. E. and P. L. Colin. 1986. Trophic structure, diversity, and abundance of fishes of the deep reef (30-300 m) at Enewetak, Marshall Islands. Bull. Mar. Sci. 38253-272.

Trigg, C., H. Perry, and W. Brehm. 1997. Size and weight relationships for the Golden crab, *Chaceon fenneri*, and the red crab, *Chaceon quinquedens*, from the eastern Gulf of Mexico. Gulf Res. Rep. 9(4): 339-343.

Vaughn, D. S., C. S. Manooch III, and J. C. Potts. 2001. Assesment of the wreckfish fishery on the Blake Plateau. Am. Fish. Soc. Symp. 25:105-120.

Vecchione, M. 1987. Commercial Fishing for Gulf Butterfish, *Peprilus burti*, in the Gulf of Mexico. Mar. Fish. Rev. 49(4):14-22.

Vinnichenko V. I. 1997. Vertical diurnal migrations of the Slender Alfonsino *Beryx splendens* (Berycidae) at the underwater rises of the open North Atlantic. J. Ichthyol. 37(4):490-496

Waller, R., H. Perry, C. Trigg, J. McBee, R. Erdman, and N. Blake. 1995. Estimates of harvest potential and distribution of the deep sea red crab, *Chaceon quinquedens*, from the northcentral Gulf of Mexico. Gulf Res. Rep. 9(2): 75-84.

Weaver, D. C. and G. R. Sedberry. 2001. Trophic subsidies at the Charleston Bump: Food web structure of reef fishes on the continental slope of the southeastern United States. *In* Islands in the Steam: oceanography and fisheries of the Charleston Bump (G. R. Sedberry, ed.). Pp. 137-152. American Fisheries Society Symposium 25, Bethesda, MD.

Weaver, D. C., D. F. Naar, and B. T. Donaue. 2006. Deepwater reef fishes and multibeam bathymetry of the Tortugas South Ecological Reserve, Florida Keys National Marine Sanctuary, Florida. NMFS Professional Paper 5:48-68.

Weaver, D. C., E. L. Hickerson, and G. P. Schmahl. 2006. Deep reef fish surveys by submersible on Alderdice, McGrail, and Sonnier Banks in the northwestern Gulf of Mexico. NMFS Professional Paper 5:69-87.

Wells, R. J. D., J. H. Cowan Jr., and W. F. Patterson III. 2008. Habitat use and the effect of shrimp trawling on fish and invertebrate communities over the northern Gulf of Mexico continental shelf. ICES Journal of Marine Science 65:1610-1619.

White, M., C. Mohn, H. de Stigter, G. Mottram. 2005. Cold-water coral development as a function of hydrodynamics and surface productivity around the submarine banks of Rockall Trough, NE Atlantic. Pages 503-514 in Friewald, A. and Roberts, J. M. (eds) Cold-water corals and Ecosystems. Springer-Verlag, Berlin Heidelberg.

Yoerger, D. R., J. Kinsey, J. Stanway, R. Catanach, A. Duester, and A. Billings.  2009.  *Lophelia* II-2 Sentry Dive Summaries.  Woods Hole Oceanographic Institute, Woods Hole, MA.  38 pp.

Bottom Long Line

Seafloor
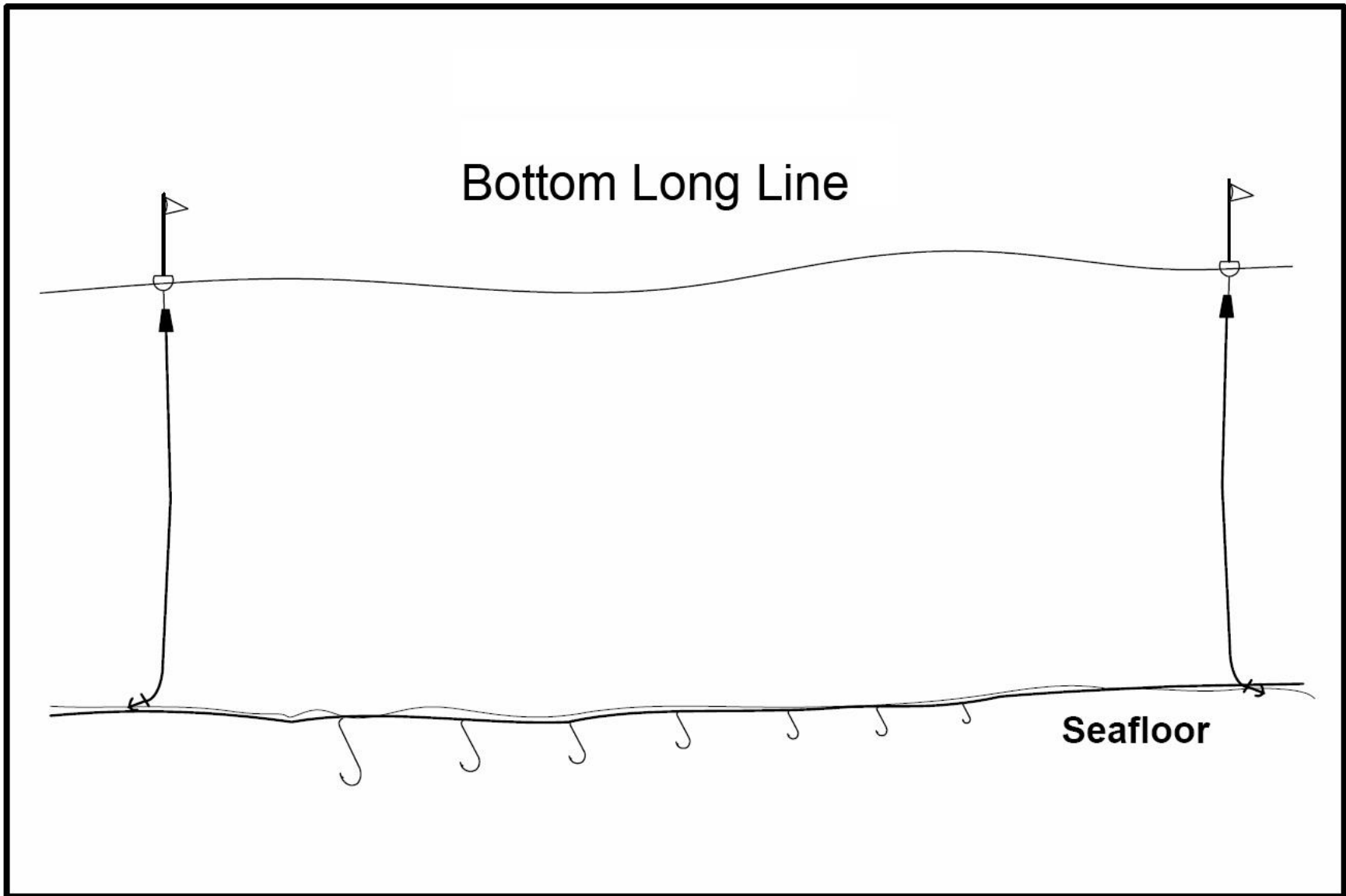
Figure 14-1.  A typical bottom longline used for reef fish in the Gulf of Mexico (from CSA 2002).

# OTTER TRAWL COMPONENTS
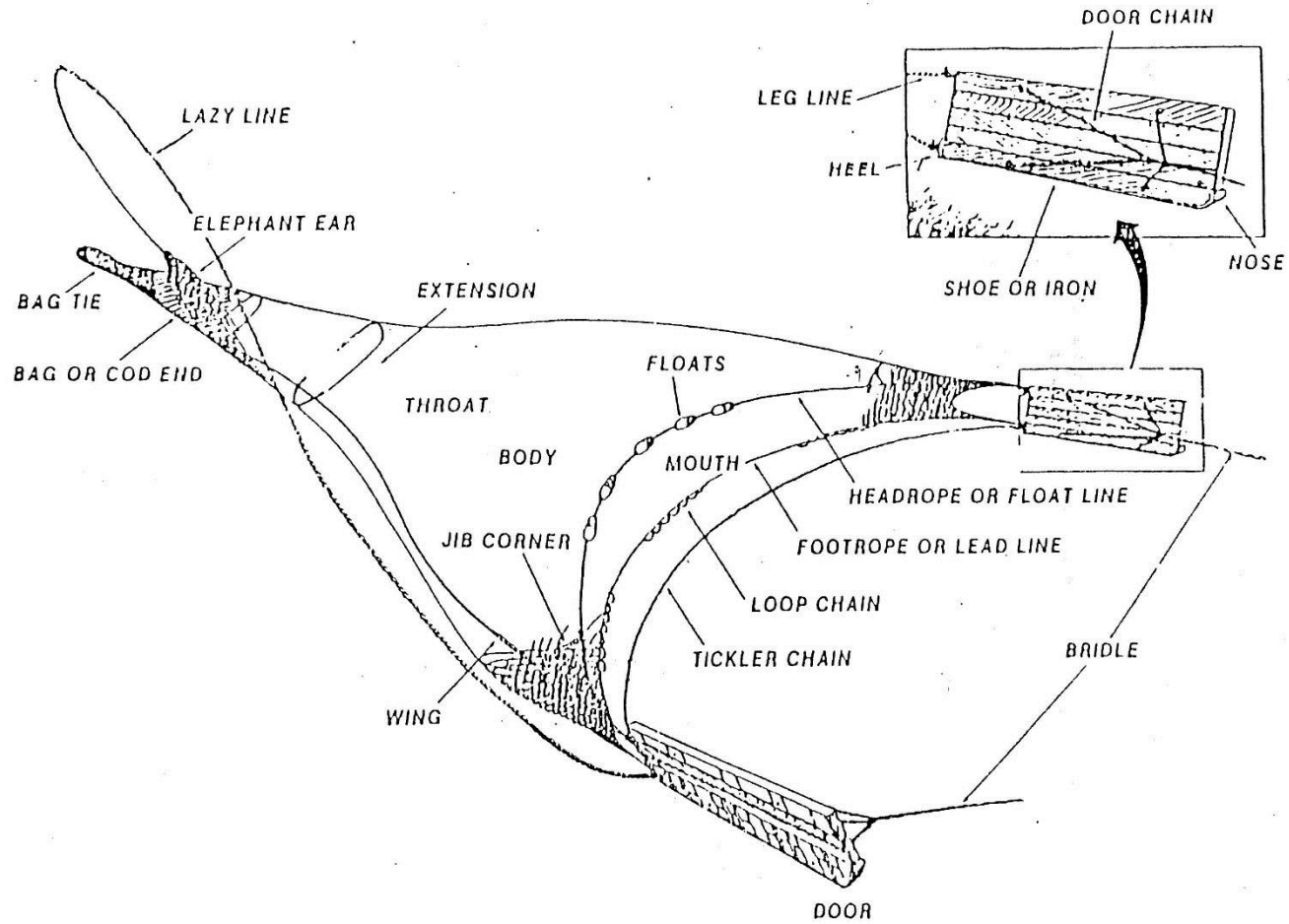


Figure 14-2. Configuration of a standard shrimp trawl used for shallow water penaeid shrimp in the Gulf of Mexico. Image courtesy NOAA Fisheries.
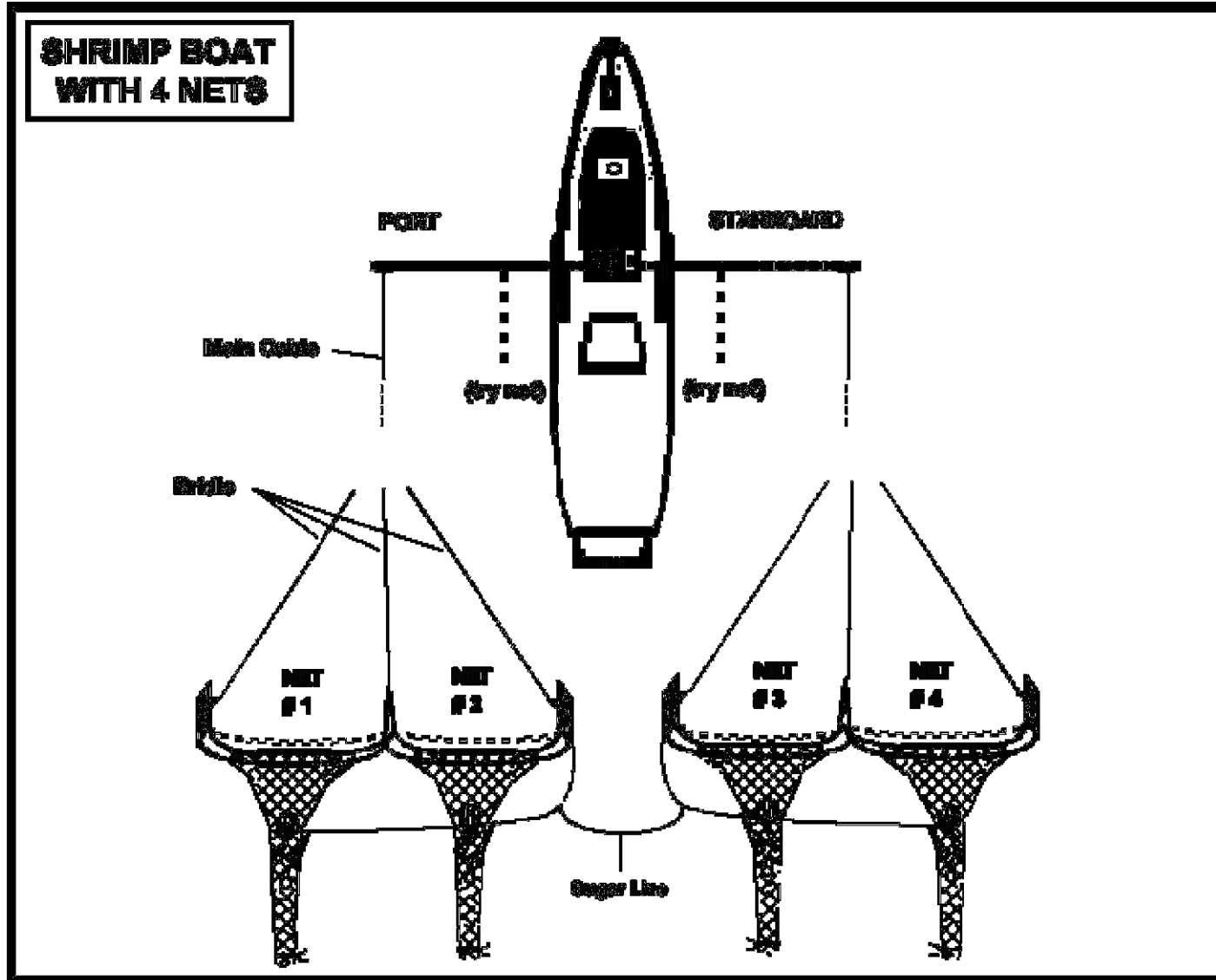
Figure 14-3. . Diagram of shrimp trawl configuration typically used for shallow water penaeid shrimp in the Gulf of Mexico. This arrangement is also used in deepwater trawling for royal red shrimp. Image courtesy NOAA Fisheries.
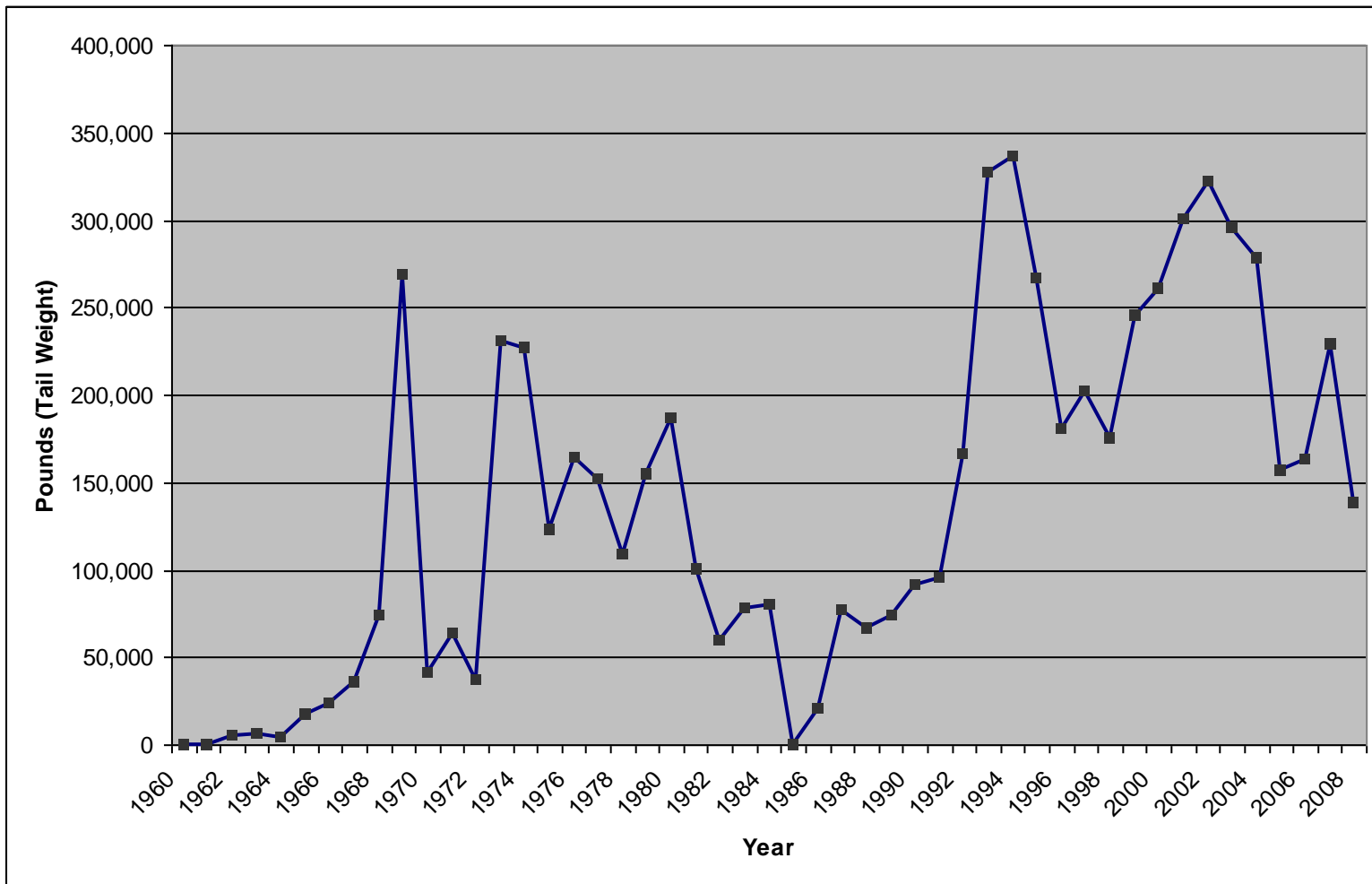
Figure 14-4.  Historical landings for royal red shrimp in the Gulf of Mexico.
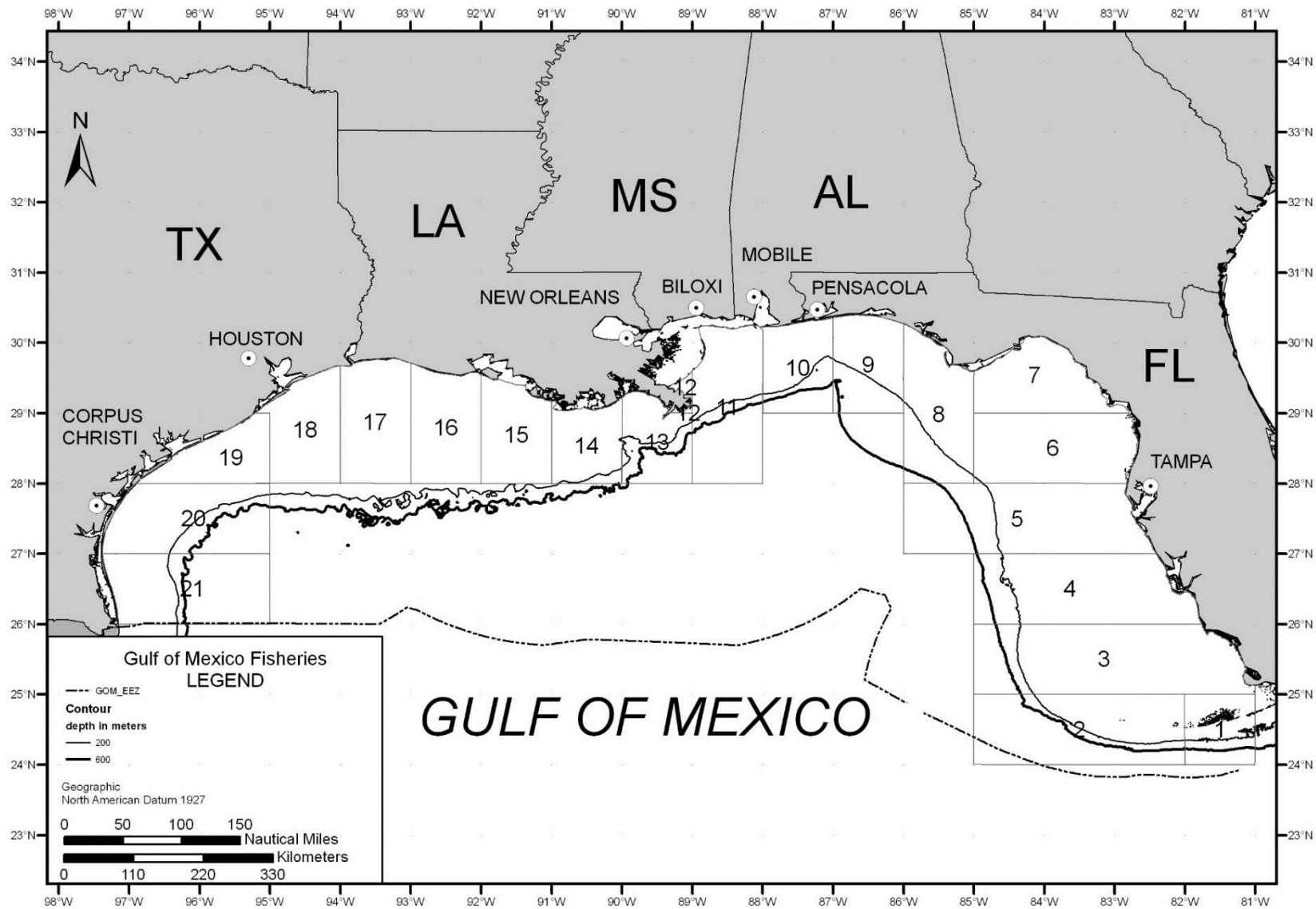
Figure 14-5. NMFS statistical areas for the Gulf of Mexico, grids 1 to 21.
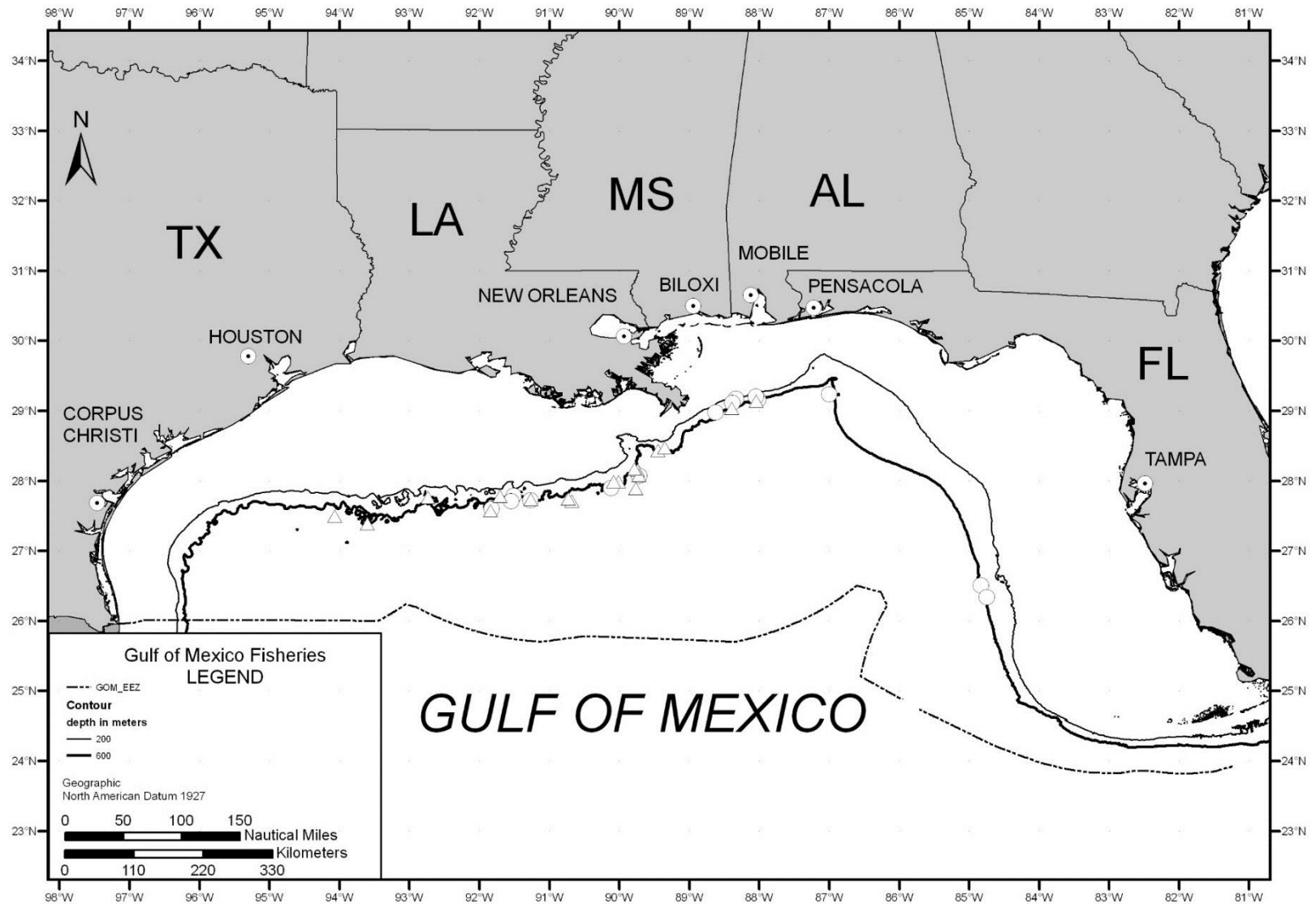
Figure 14-6. Known *Lophelia pertusa* sites in the Gulf of Mexico, with 200 and 600 m contours. Open circles represent sites discussed in Shroeder et al. 2005. Open triangles are sites visited during Lophelia II cruises
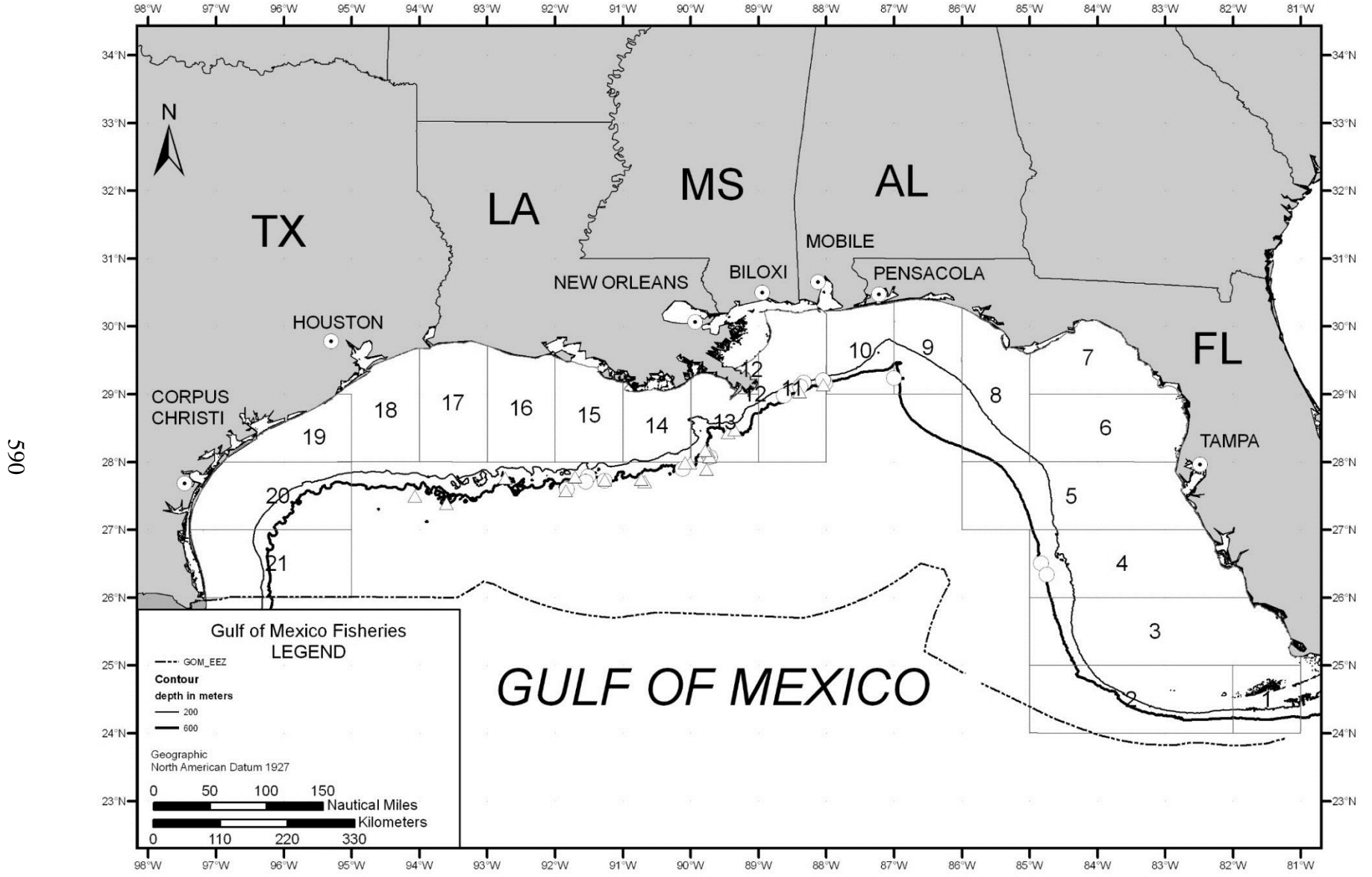
Figure 14-7. Known Lophelia pertusa sites in the Gulf of Mexico with NMFS grid overlay.
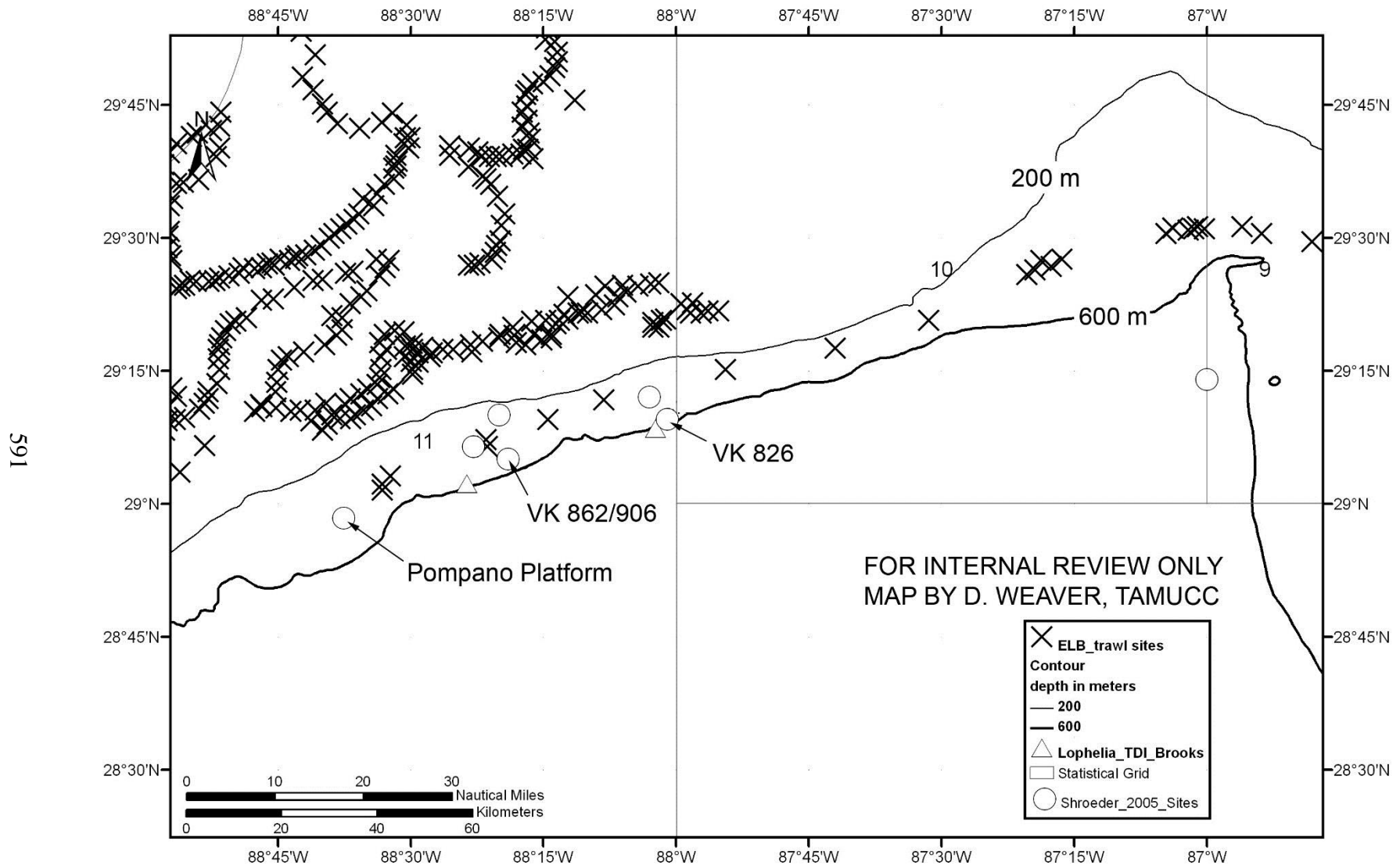
Figure 14-8. Electronic Logbook (ELB) records of shrimp trawl locations for the Gulf of Mexico made in 2008. The deep locations suggests trawling for royal red shrimp in the vicinity of known Lophelia coral sites. Data from Gallaway et al. 2009.

591
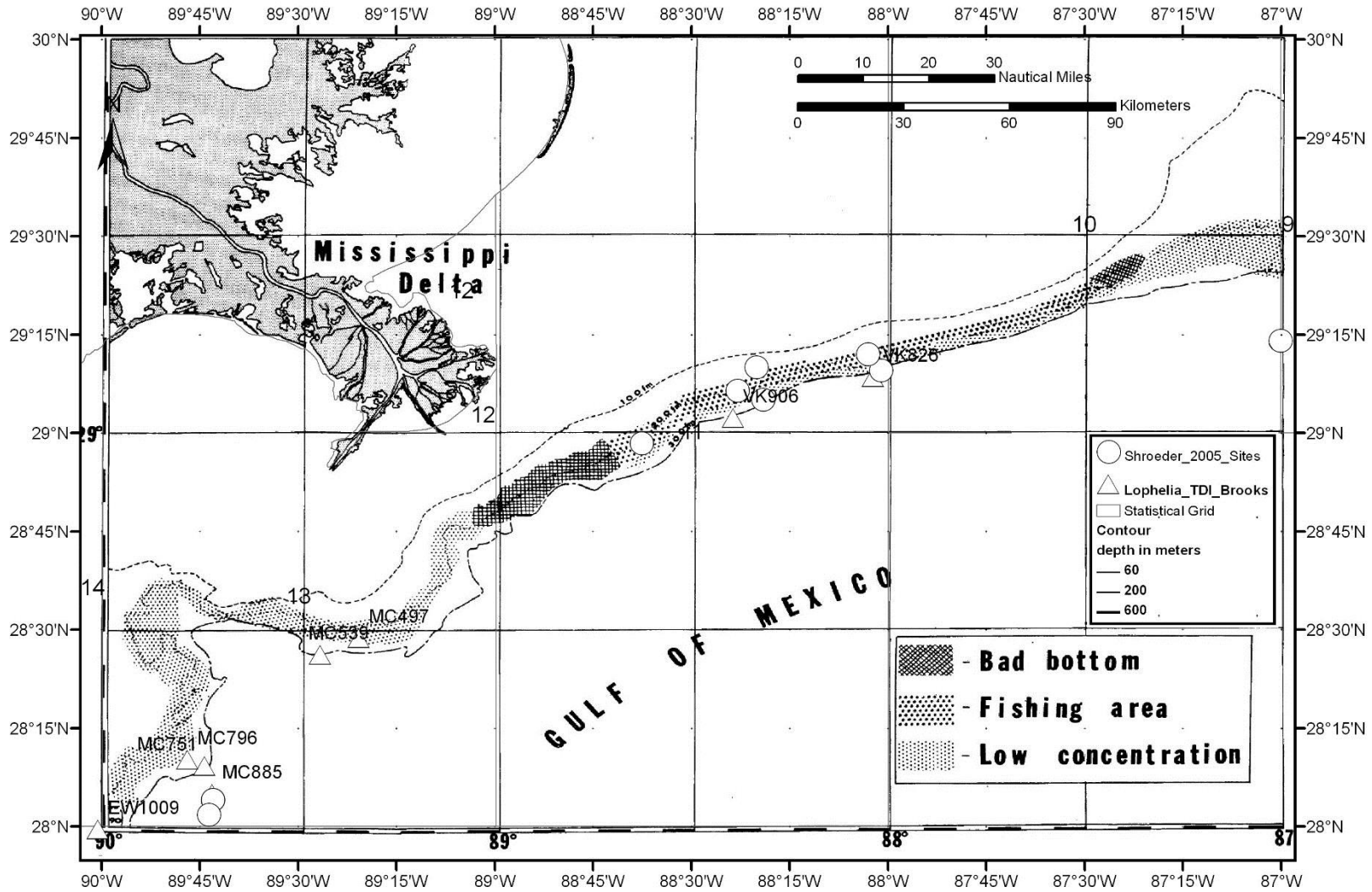
Figure 14-9. Royal red shrimp trawling grounds in the vicinity of known Lophelia coral sites. From Bullis 1956.

**Royal Red Shrimp Landings from 2000 -2008 by NMFS Statistical Grid**



**Royal Red Trips from 200 - 2008 by NMFS Statistical Grid**
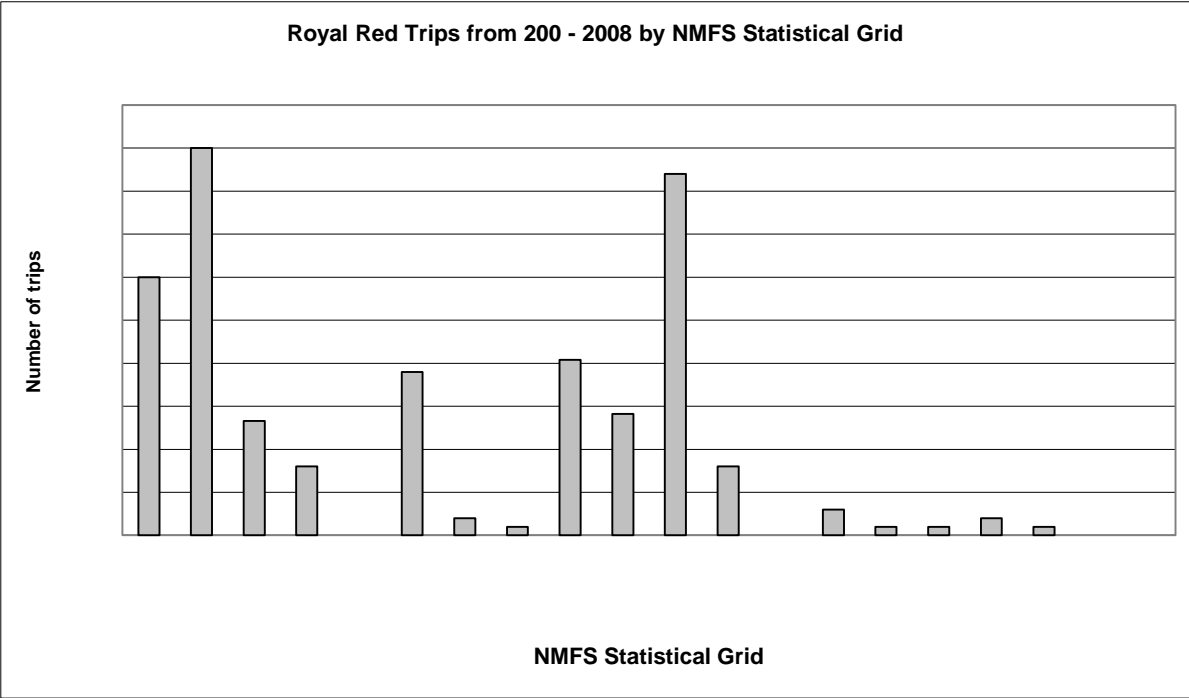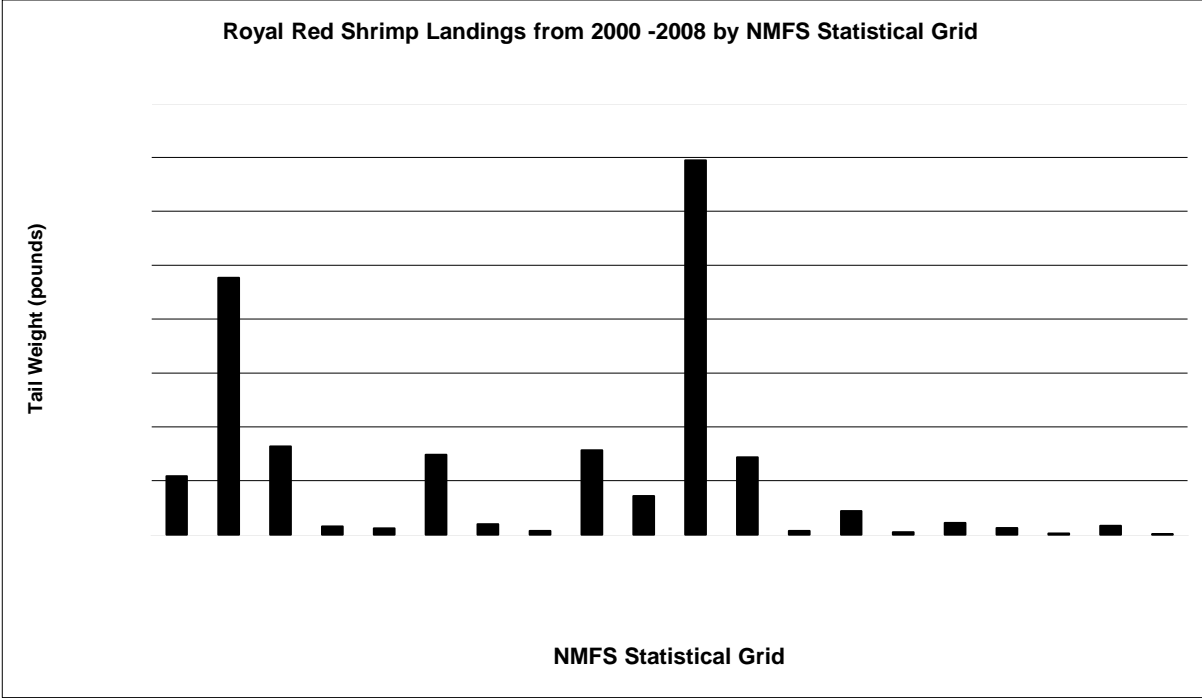
Figure 14-10. Summary of landings and trips for royal red shrimp, 2000-2008, by NMFS Statistical Grid. Data provided by J. Nance, NOAA Fisheries Galveston Lab. Highest activity occurs in the Dry Tortugas (1) and Mississippi Delta/DeSoto Canyon (10) regions.
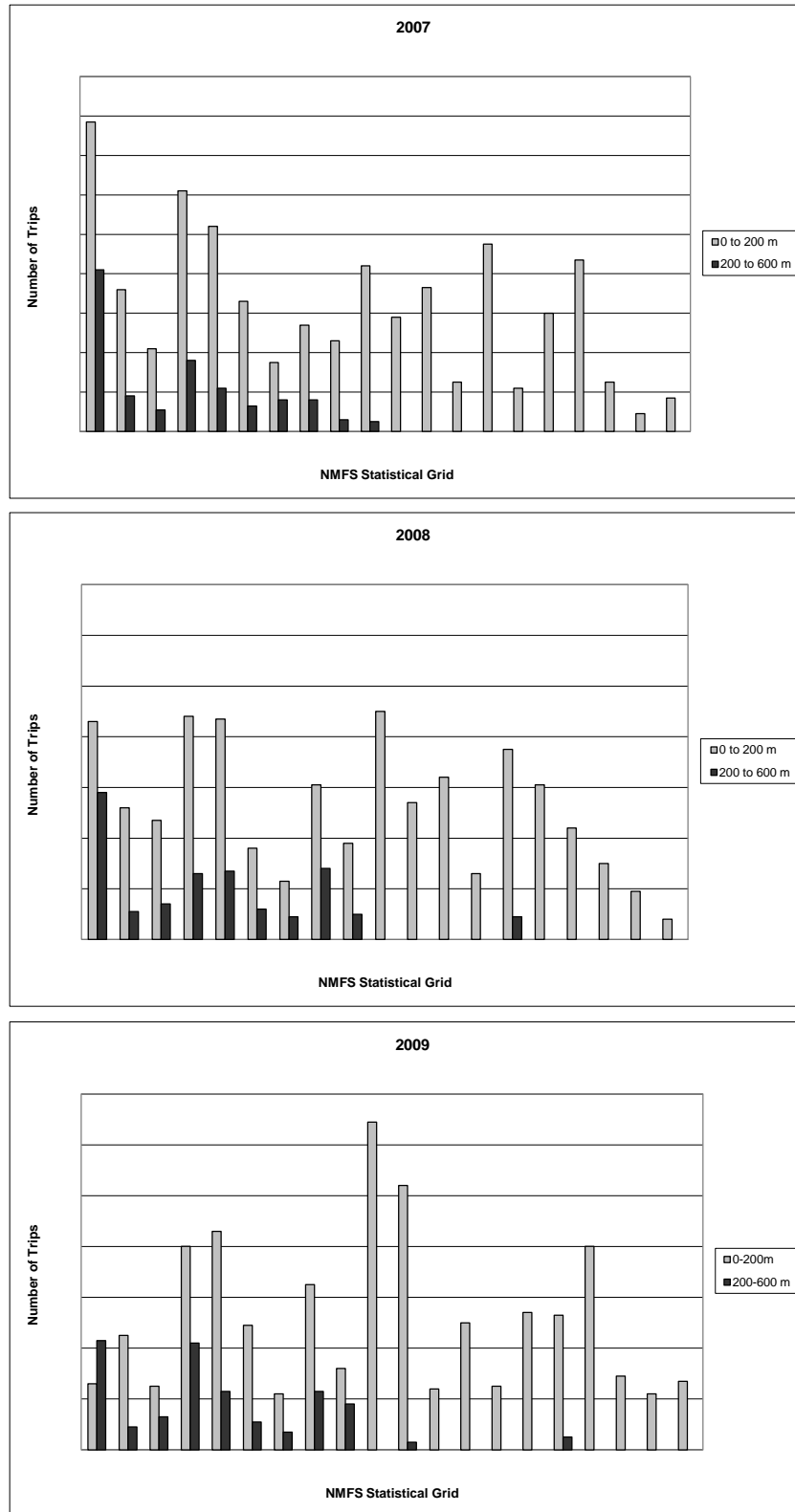
Figure 14-11. Summary of trips targeting deepwater reef fishes, per NMFS statistical grid 2007-2009, from the non-confidential portion of the reef fish logbooks.

**Reef Fish Trips in GOM from Logbook Database**



**Landings per trip**
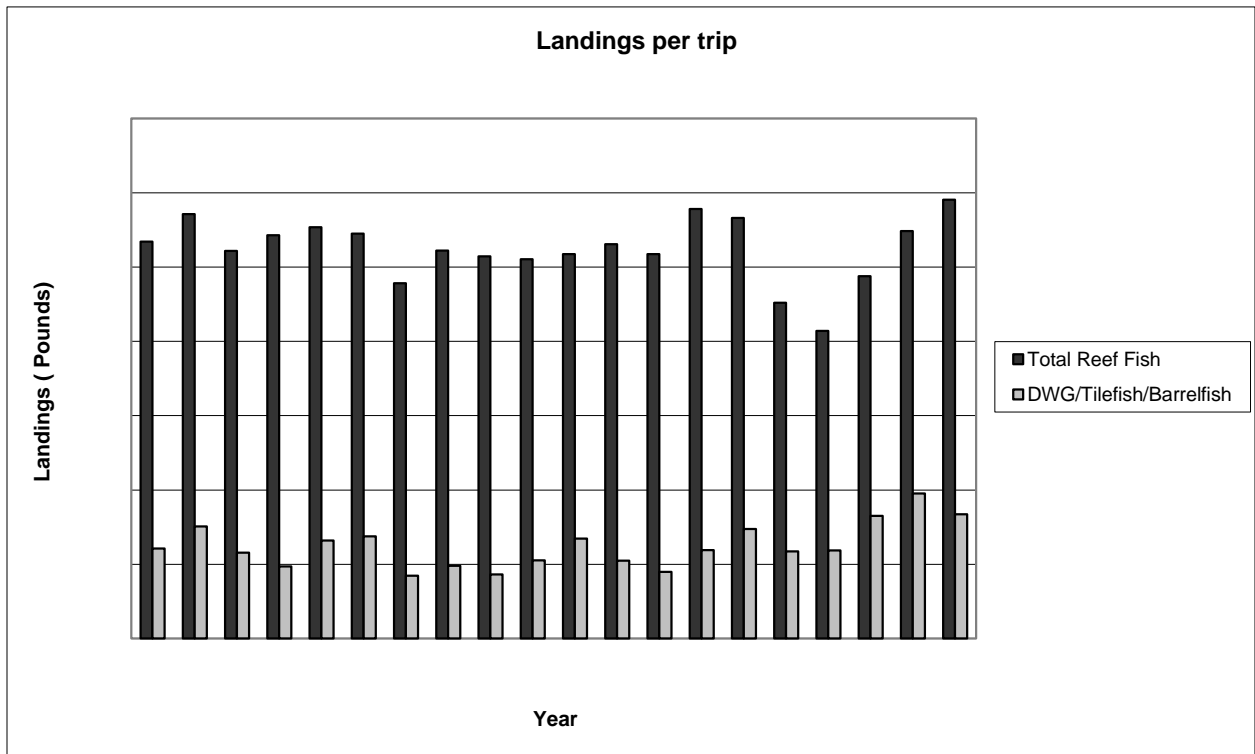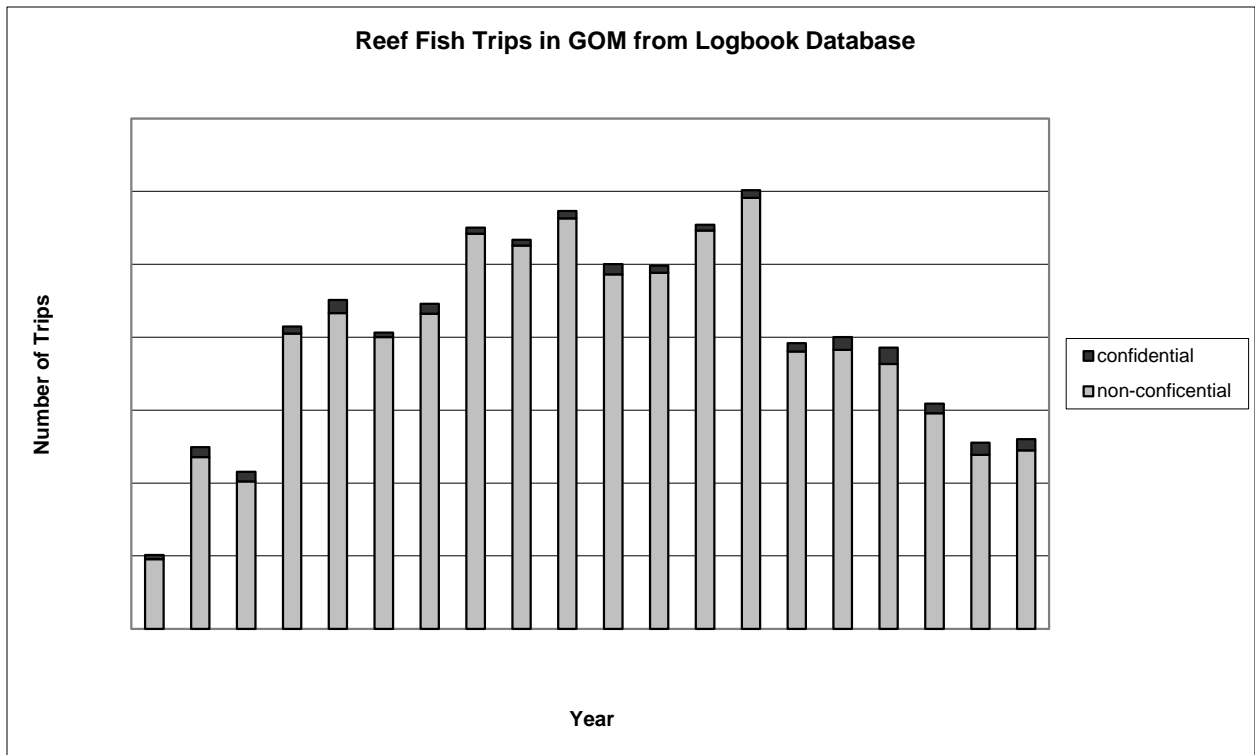


Figure 14-12. Summary of trips targeting deepwater reef fishes from the reef fish log book (top), and catch in pounds per trip, 1990-2009 summed across the Gulf of Mexico.

595

Table 14-2.

Effort in miles of line and number of hooks from reef fish longline records showing depth information and landing selected species of deepwater grouper and tilefish.  Data are from the NMFS logbook system, SEFSC.

| YEAR | Depth (m) | Max (mi) | Min (mi) | Avg (mi) | Mode (mi) | Max no. hooks | Min no. hooks | Ave no. hooks | Mode hooks | No. records |
|------|-----------|----------|----------|----------|-----------|---------------|---------------|---------------|------------|-------------|
| 2004 | 0-200m    | 7        | 2        | 4.81     | 2         | 1000          | 200           | 687.5         | 1000       | 8           |
| 2005 | 0-200m    | 26       | 1        | 6.32     | 4         | 2500          | 100           | 1018.7        | 1000       | 308         |
| 2006 | 0-200m    | 20       | 1        | 6.23     | 5         | 2500          | 100           | 1151.8        | 1500       | 456         |
| 2007 | 0-200m    | 24       | 1        | 6.09     | 5         | 3000          | 50            | 1177.29       | 1000       | 329         |
| 2008 | 0-200m    | 15       | 1        | 6.1      | 5         | 3000          | 5             | 977.13        | 500        | 379         |
| 2009 | 0-200m    | 17       | 1        | 5.26     | 6         | 3000          | 60            | 911.73        | 1000       | 356         |
| 2005 | 201-600m  | 18       | 1.5      | 6.17     | 5         | 3500          | 300           | 1075          | 500        | 60          |
| 2006 | 201-600m  | 16       | 1        | 6.99     | 5         | 2200          | 12            | 1132.99       | 1500       | 91          |
| 2007 | 201-600m  | 16       | 1        | 6.9      | 5         | 2500          | 50            | 1197.63       | 1200       | 158         |
| 2008 | 201-600m  | 14       | 1        | 6.98     | 10        | 3000          | 16            | 1224.1        | 1000       | 149         |
| 2009 | 201-600m  | 15       | 2.5      | 6.99     | 5         | 3000          | 200           | 1185.78       | 1000       | 147         |
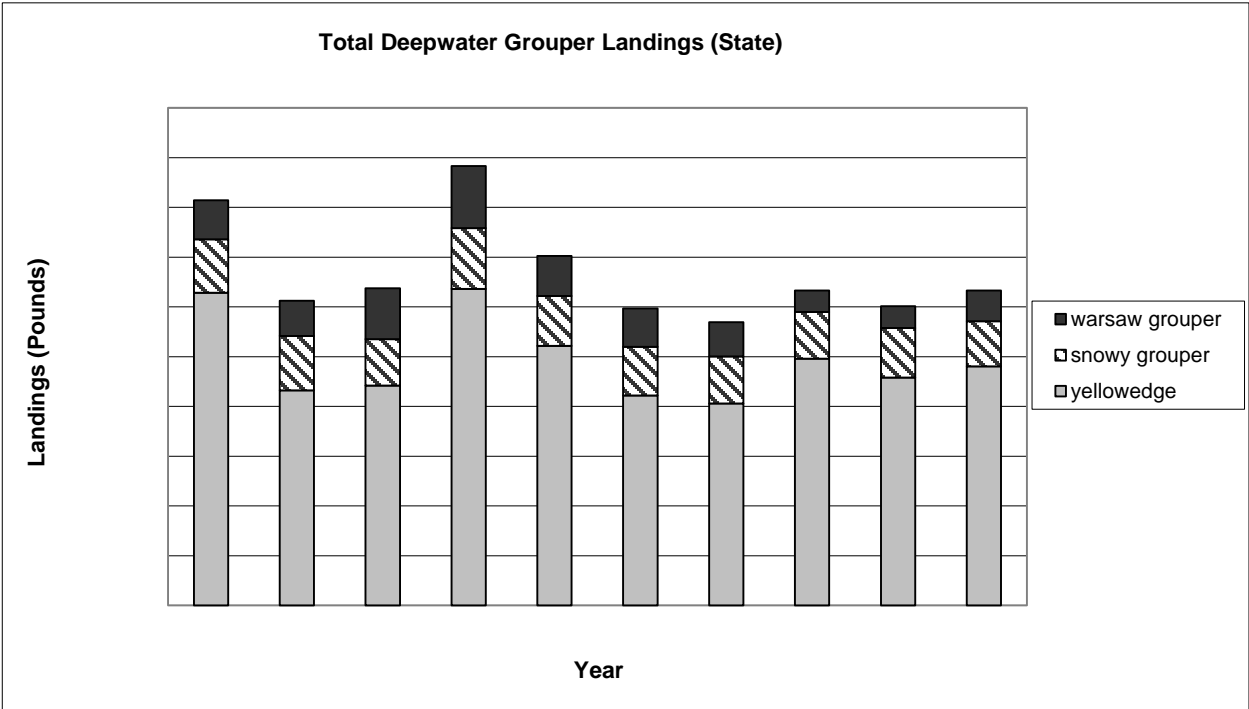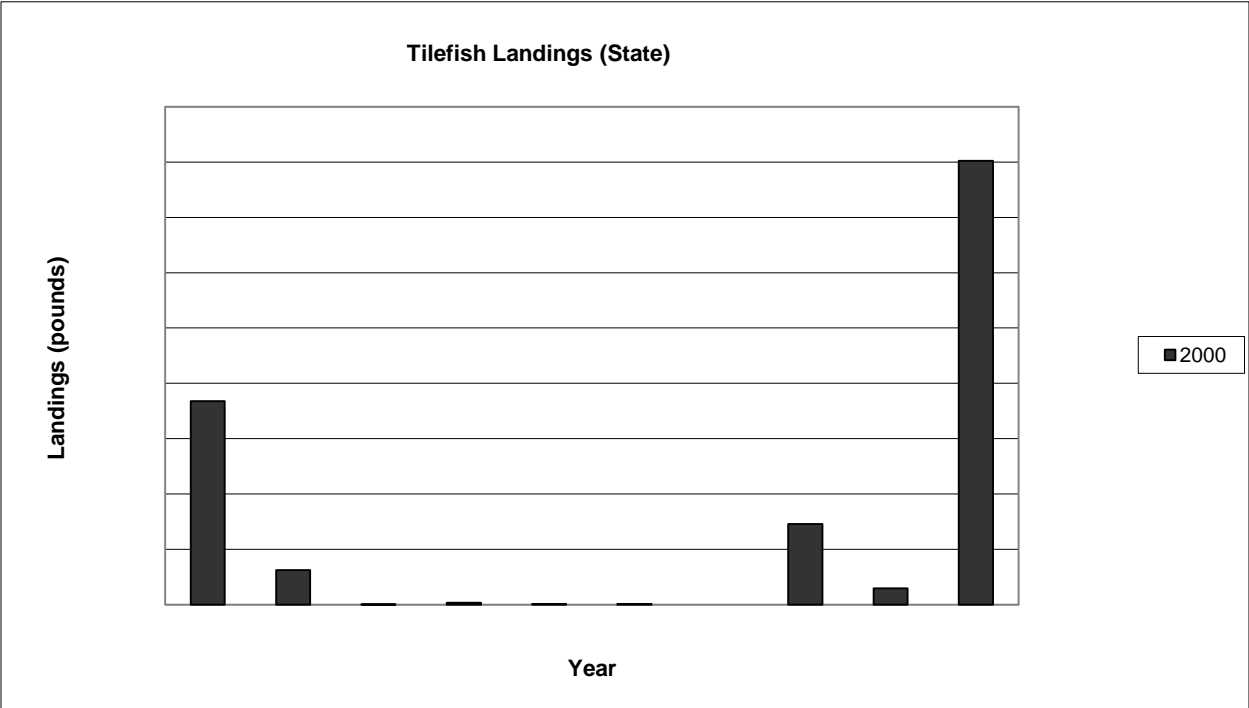
Figure 14-13. Landings in pounds for deepwater groupers (top) and tilefish (bottom), total catch from 2000 through 2009, based on reported state landings summed across the Gulf of Mexico.

597
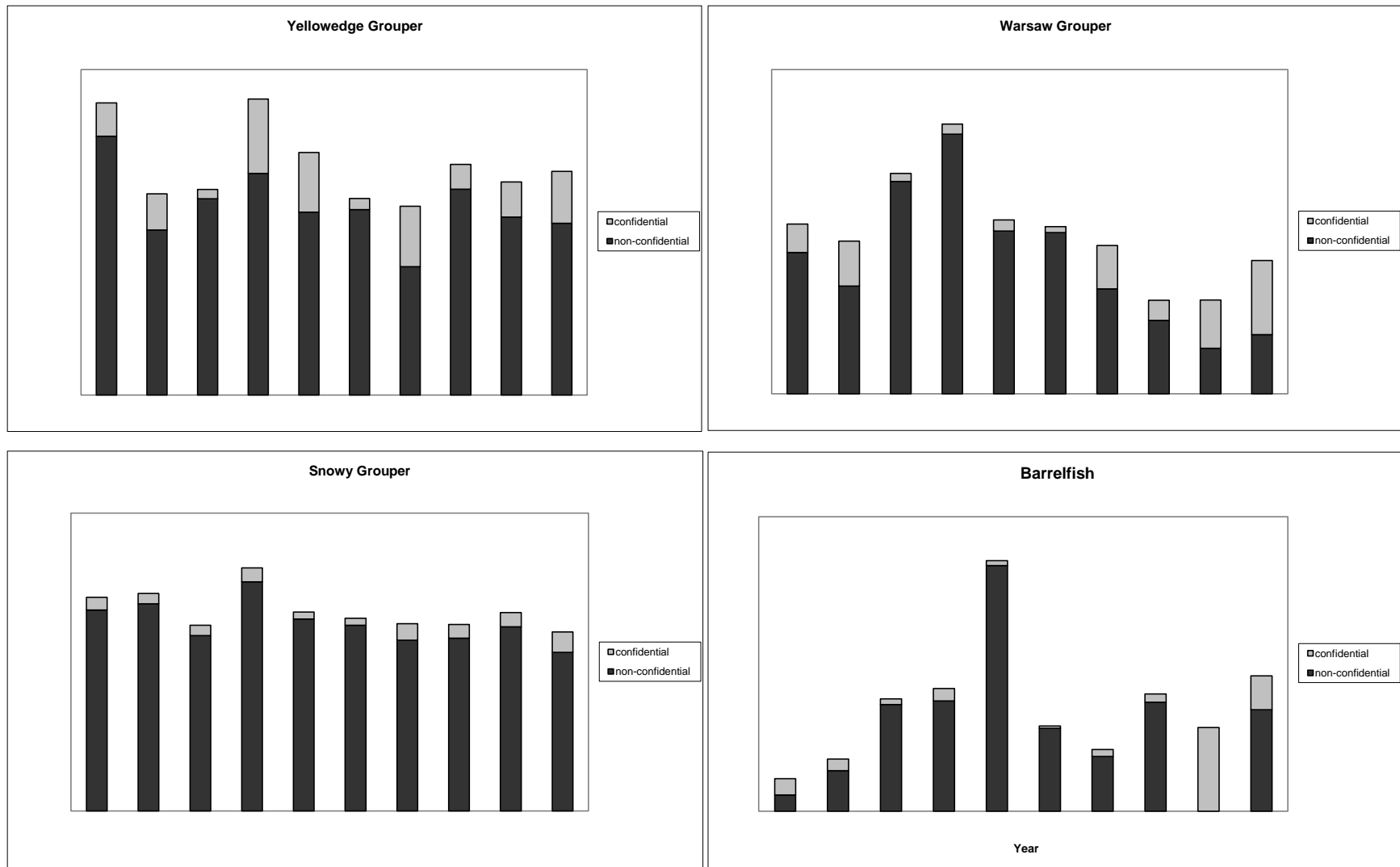
Figure 14-14.  Landings in pounds for select deepwater species, total catch from 2000 through 2009, based on reported state landings summed across the Gulf of Mexico.
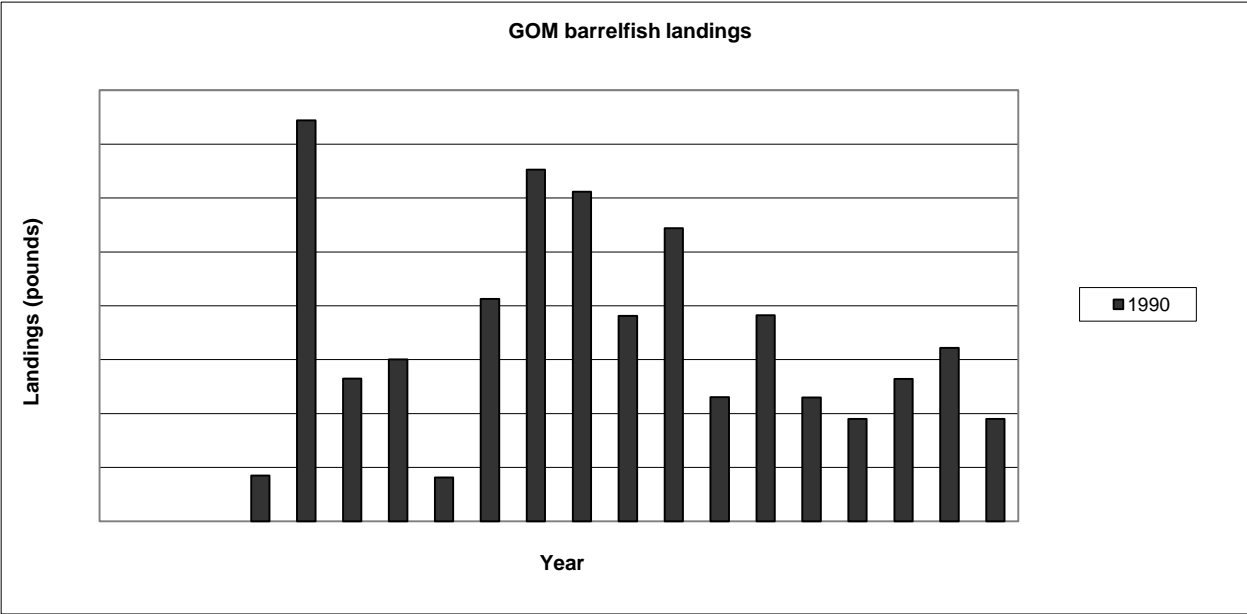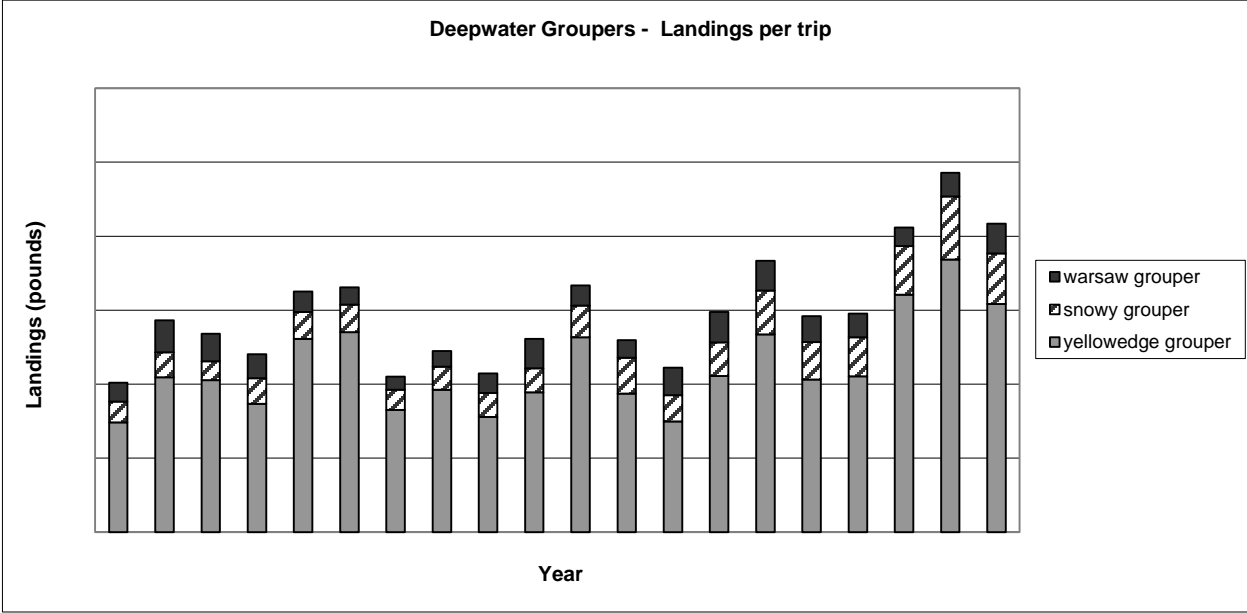
Figure 14-15. Summary of deepwater grouper landings in pounds per trip, (top), and total barrelfish landings (bottom) summed across the Gulf of Mexico for years 1990-2009.
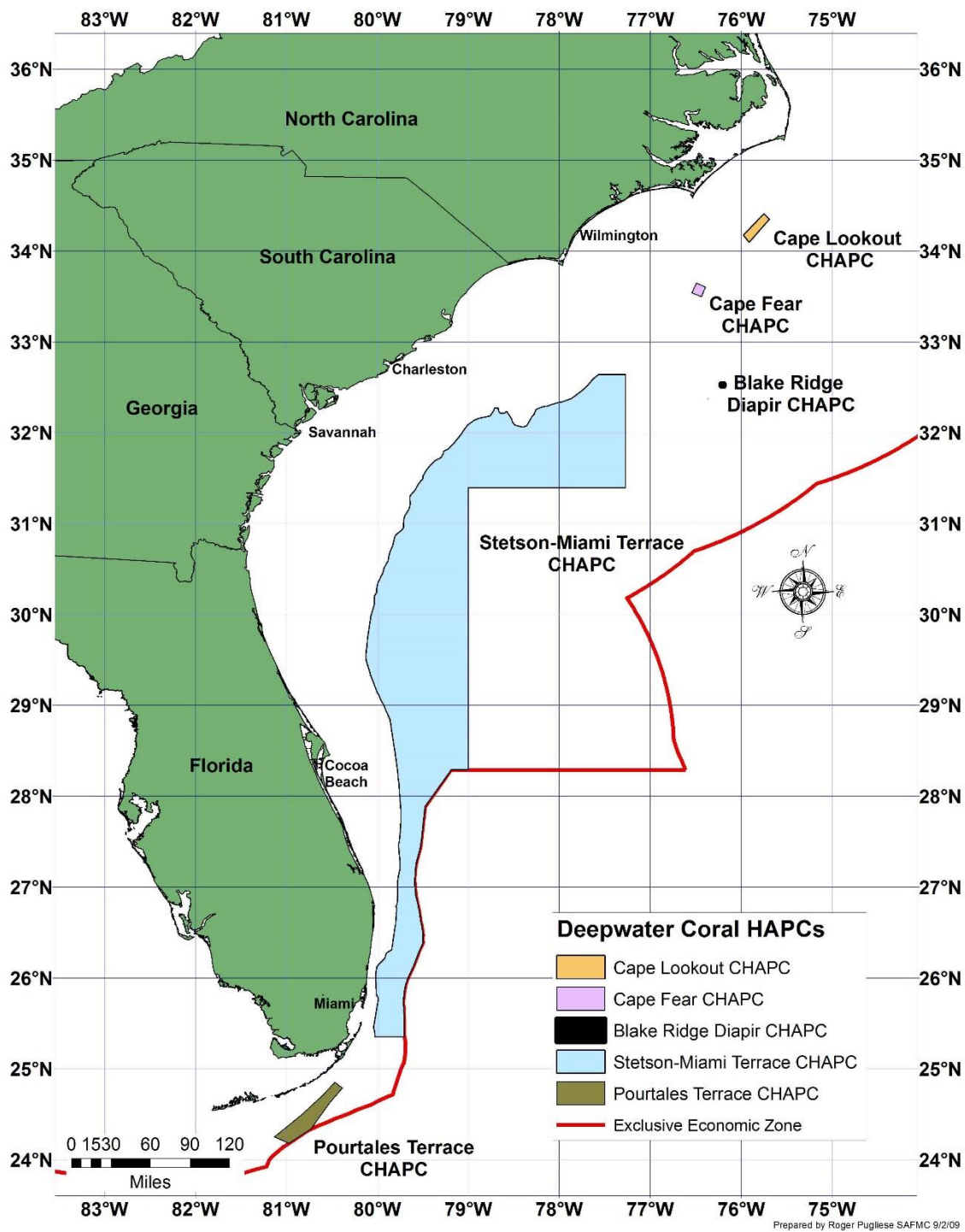
Figure 14-16. Habitat Areas of Particular Concern (HAPCs) designated in the Comprehensive Ecosystem-Based Amendment 1, by the South Atlantic Fisheries Management Council in September 2009, pending final approval by the Secretary of Commerce. From SAFMC 2009.

Table 14-3.

Lophelia sites known from the Gulf of Mexico.  Sites no. 1 to 24 taken from Schroeder et al. 2005.  Sites 25 to 42 visited during Lophelia II project cruises.

| Site | Species | Area | Lat | Long | Depth_m | Source |
|---|---|---|---|---|---|---|
| 1 | *Lophelia pertusa* | W. Florida Slope | 26.500000 | -84.833333 | 640 | (Cairns, 2000) |
| 1 | *Madrepora oculata* | W. Florida Slope | 26.500000 | -84.833333 | 640 | (Cairns, 2000) |
| 2 | *Lophelia pertusa* | DeSoto Canyon | 29.233333 | -87.000000 | 878 | (Cairns, 1979) |
| 3 | *Lophelia pertusa* | Mississippi  Canyon | 29.158333 | -88.016667 | 430-520 | (Schroeder,2002) |
| 4 | *Lophelia pertusa* | Mississippi  Canyon | 29.200000 | -88.050000 | 457-549 | (Cairns, 1979) |
| 5 | *Lophelia pertusa*** | Mississippi  Canyon | 29.083333 | -88.316667 | 421-512 | (Moore and Bullis, 1960) |
| 6 | *Lophelia pertusa* | Mississippi  Canyon | 29.166667 | -88.333333 | 519 | (Cairns, 2000) |
| 7 | *Lophelia pertusa* | Mississippi  Canyon | 29.106667 | -88.381667 | 343 | NOAA RON BROWN |
| 8 | *Lophelia pertusa* | Mississippi  Canyon | 28.066667 | -89.716667 | 616-630 | NOAA RON BROWN |
| 8 | *Madrepora oculata* | Mississippi  Canyon | 28.066667 | -89.716667 | 616-630 | NOAA RON BROWN |
| 9 | *Madrepora oculata* | Mississippi  Canyon | 28.028333 | -89.726667 | 650 | JSL3340 |
| 10 | *Lophelia pertusa* | Mississippi  Canyon | 27.893333 | -90.118333 | 635 | Boland 1986 |
| 11 | *Madrepora oculata* | Green Canyon | 27.733333 | -91.045000 | 720 | JSL4398 |
| 12 | *Lophelia pertusa* | Green Canyon | 27.716667 | -91.266667 | N/A | (Cairns, 2000) |
| 13 | *Lophelia pertusa* | Green Canyon | 27.781667 | -91.506667 | 540-570 | (MacDonald et al, 1989) |
| 14 | *Lophelia pertusa* | Green Canyon | 27.705000 | -91.548333 | 543-783 | (Viada and Cairns, 1987) |
| 15 | *Madrepora oculata* | Green Canyon | 27.783333 | -91.550000 | 300 | JSL2064 |
| 16 | *Madrepora oculata* | Green Canyon | 27.783333 | -91.550000 | 524-539 | JSL 4577 |
| 16 | *Lophelia pertusa* | Green Canyon | 27.596667 | -91.826667 | 524-539 | NOAA RON BROWN |
| 17 | *Madrepora oculata* | Garden Banks | 27.533333 | -93.033333 | 732-823 | (Cairns, 1979) |
| 18 | *Madrepora oculata* | Tuxpan | 23.916667 | -97.000000 | 937 | (Cairns, 1979) |
| 19 | *Madrepora oculata* | Tuxpan | 23.500000 | -97.183333 | 732 | NMNH Database |
| 20 | *Madrepora oculata* | Yucatan | 24.366667 | -87.783333 | 549 | NMNH Database |
| 21 | *Madrepora oculata* | Yucatan | 23.300000 | -86.550000 | 914 | (Cairns, 1979) |
| 22 | *Madrepora oculata* | Yucatan | 23.183333 | -86.466667 | 914 | (Cairns, 1979) |
| 23 | *Lophelia pertusa* | W. Florida Slope | 26.333525 | -84.750075 | 428-466 | HBOI-Reed |
| 24 | *Lophelia pertusa* | B.P. Pompano | 28.973033 | -88.625983 | 204-292 | HBOI-Reed |
| 25 | *Lophelia pertusa* | VK826 | 29.142 | -88.037833 | 610 | Lophelia II_Cruise 2 |
| 26 | *Lophelia pertusa* | GC140 | 27.786 | -91.703333 | 330 | Lophelia II_Cruise 2 |
| 27 | *Lophelia pertusa* | GB201 | 27.761167 | -92.729833 | na | Lophelia II_Cruise 2 |
| 28 | *Lophelia pertusa* | EB478 | 27.3895 | -93.600167 | 627 | Lophelia II_Cruise 2 |
| 29 | *Lophelia pertusa* | GB535 | 27.498167 | -94.065667 | nr | Lophelia II_Cruise 2 |
| 30 | *Lophelia pertusa* | GC234 | 27.7355 | -91.263833 | 555 | Lophelia II_Cruise 2 |
| 31 | *Lophelia pertusa* | GC246 | 27.711333 | -90.676 | 755 | Lophelia II_Cruise 2 |
| 32 | *Lophelia pertusa* | GC535 | 27.578333 | -91.8355 | nr | Lophelia II_Cruise 2 |
| 33 | *Lophelia pertusa* | MC751 | 28.154 | -89.738 | nr | Lophelia II_Cruise 2 |
| 34 | *Lophelia pertusa* | AT47 | 27.893333 | -89.762333 | nr | Lophelia II_Cruise 2 |
| 35 | *Lophelia pertusa* | MC885 | 28.0825 | -89.7185 | nr | Lophelia II_Cruise 2 |
| 36 | *Lophelia pertusa* | VK906 | 29.037833 | -88.393333 | 500 | Lophelia II_Cruise 2 |
| 37 | *Lophelia pertusa* | EW1009 | 27.991667 | -90.00929 |  | Lophelia II_Cruise 2 |
| 38 | *Lophelia pertusa* | MC539 | 28.436667 | -89.443333 |  | Lophelia II_Cruise 2 |
| 39 | *Lophelia pertusa* | EW1008 | 27.991667 | -90.081667 |  | EW Shipwreck |
| 40 | *Lophelia pertusa* | GC245 | 27.743333 | -90.725 |  | Green Lantern Shipwreck |
| 41 | *Lophelia pertusa* | MC497 | 28.478333 | -89.345 |  | Gulfpenn Shipwreck |
| 42 | *Lophelia pertusa* | MC796 | 28.17 | -89.781667 |  | Gulfoil Shipwreck |

Table 14-4.

Fishes with potential commercial value associated with deep hard bottom or coral communities below 200 m.

| Family | Name | Common Name | Depth Reported (m) | Source |
|---|---|---|---|---|
| Carcharhinidae | | | | |
| | *Carcharhinus falciformis* | silky shark | 335-522 | Reed et al. 2006 |
| | *Carcharhinus signatus* | night shark | | Cass-Calay and Bahnick 2002 |
| | *Carcharhinus obscurus* | dusky shark | | Cass-Calay and Bahnick 2002 |
| Lamnidae | | | | |
| | *Isurus paucus* | longfin mako | | Cass-Calay and Bahnick 2002 |
| Alopiidae | | | | |
| | *Alopias superciliosus* | bigeye thresher | 0 - 500 m | Weaver, *pers. obs.* |
| Squalidae | | | | |
| | *Squalus cubensis* | Cuban dogfish | 267-525 | Reed et al. 2006, Matlock et al. 1990 |
| Triakidae | | | | |
| | *Mustelus sp.* | dogfish | | Reed et al. 2006 |
| Congridae | | | | |
| | *Conger oceanicus* | conger eel | | Reed et al. 2006 |
| Macrouridae | | | | |
| | *Nezumia sp.* | grenadiers | 322-752 | Reed et al. 2006 |
| Moridae | | | | |
| | *Laemonema barbatulum* | shortbeard codling | 521 | Reed et al. 2006 |
| | *Laemonema melanurum* | codling | 186-770 | Reed et al. 2006 |
| Phycidae | | | | |
| | *Phycis spp.* | hakes | 557-767 | Reed et al. 2006 |
| | *Urophycis floridana* | southern hake | 267-311 | Reed et al. 2006, Matlock et al. 1990 |
| | *Urophycis cirrata* | gulf hake | 267-311 | Matlock et al. 1990 |
| | *Urophycis chuss* | red hake | | Matlock et al. 1990 |
| Polymixidae | | | | |
| | *Polymixia lowei* | beardfish | 267-414 | Reed et al. 2006, Matlock et al. 1990 |
| Berycidae | | | | |
| | *Beryx decadactylus* | red bream | 287-671 | Reed et al. 2006 |
| Trachichthyidae | | | | |
| | *Gephyroberyx darwinii* | big roughy | 392-518 | Reed et al. 2006 |
| Centrolophidae | | | | |
| | *Hyperoglyphe perciformis* | barrelfish | 267-311 | Reed et al. 2006, Matlock et al. 1990 |
| Serranidae | | | | |
| | *Antias nicholsi* | yellowfin bass | 179-283 | Reed et al. 2006 |
| | *Epinephelus flavolimbatus* | yellowedge grouper | 267-311 | Matlock et al. 1990 |
| | *Epinephelus niveatus* | snowy grouper | 70-308 | Reed et al. 2006 |
| | *Epinephelus mysticinus* | misty grouper | | Cass-Calay and Bahnick 2002 |
| | *Hemanthias leptus* | longfin bass | 267-311 | Matlock et al. 1990 |
| Polyprionidae | | | | |
| | *Polyprion americanus* | wreckfish | 283-693 | Reed et al. 2006 |

Table 14-4    Continued.

| Family | Name | Common Name | Depth Reported (m) | Source |
|---|---|---|---|---|
| Lujanidae | | | | |
| | *Etelis oculatus* | queen snapper | | Cass-Calay and Bahnick 2002 |
| | *Lutjanus buccanella* | blackfin snapper | | Cass-Calay and Bahnick 2002 |
| | *Lutjanus vivanus* | silk snapper | | Cass-Calay and Bahnick 2002 |
| Lophiidae | | | | |
| | *Lophiodes reticulatus* | reticulate goosefish | 267-311 | Matlock et al. 1990 |
| Malacanthidae | | | | |
| | *Caulolatilus microps* | blueline tilefish | | Reed et al. 2006 |
| Scorpaenidae | | | | |
| | *Helicolenus dactylopterus* | blackbelly rosefish | 179-754 | Reed et al. 2006 |
| | *Pontinus longispinus* | longspine scorpionfish | 267-311 | Matlock et al. 1990 |
| Xiphiidae | | | | |
| | *Xiphias gladius* | swordfish | | Reed et al. 2006 |

Table 14-5.

Deepwater shrimps of the western Atlantic Ocean associated soft bottom communities below 200 m.  From Jones et al. 1994, originally described in Cervignon et al. 1993).

| Family | Name | Maximum Inches | size cm | Distribution | Habitat | Depth/Temperature Range |
|--------|------|---------|---------|--------------|---------|-------------------------|
| Solenoceridae | | | | | | |
| | Royal Red Shrimp *Pleoticus (Hymenopenaeus) robustus* (Smith, 1885) | 8.9 | 22.5 | Massachusetts to northern South America including Gulf of Mexico and coasts of central America. | Sand, clay, mud and muddy clay bottoms | 70-915 m (250-475 m) 9 -12° C |
| | Salmon shrimp *Mesopenaeus tropicalis* (Bouvier, 1905) | 4.3 | 11 | North Carolina to Brazil including Florida, Gulf of Mexico and Caribbean Sea | n/a | 30-915 m (>200 m) |
| Penaeidae | | | | | | |
| | Rose shrimp *Parapenaeus politus* Smith, 1881 | 4.9 | 12.5 | Massachusetts to Venezuela | Mud and sandy mud bottoms | 3-752 m (65-275 m) |
| | Megalops or pinkspeckled shrimp *Penaeopsis serrata* Bate, 1881 | 5.9 | 15 | Massachusetts to Brazil including the Bahamas, Gulf of Mexico, and Caribbean Sea | Sandy and Muddy bottoms | 120-750 m |
| Pandalidae | | | | | | |
| | Armed nylon shrimp *Heterocarpus ensifer* A. Milne Edwards, 1881 | 4.9 | 12.4 | North Carolina to Guianas including the Caribbean Sea | Muddy bottoms | 40-880 m |
| | Lesser striped shrimp *Plesionika acanthonotus* (S. I. Smith, 1882) | 3.3 | 8.4 | South Carolina to Brazil | Muddy bottoms | 190-1350 m |
| | Striped soldier shrimp *Plesionika edwardsii* (Brandt, 1851) | 6.5 | 16.6 | North Carolina to Surinam including the Gulf of Mexico & Antilles | Muddy bottoms | 50-690 m |
| | Striped gladiator shrimp *Plesionika ensis* (A. Milne Edwards, 1881) | 4.7 | 12 | Florida, Western Gulf of Mexico, Antilles, Guianas, & Brazil | Muddy bottoms | 100-1250 m |
| | Longtail shrimp *Plesionika longicauda* (Rathbun, 1901) | >3.1 | >8 | Gulf of Mexico to northern South America | Soft bottoms | 55-410 m |

Table 14-5. Continued

| Family | Name | Maximum | size | Distribution | Habitat | Depth/Temperature Range |
|---|---|---|---|---|---|---|
| | | Inches | cm | | | |
| Aristeidae | | | | | | |
| | Giant red shrimp | 8.9 | 22.5 | Massachusetts to northern South | Muddy bottoms | 170-1350 m |
| | *Aristaeomorpha foliacea* | | | America including the Gulf of Mexico | | |
| | (Risso, 1827) | | | & Caribbean Sea | | |
| | Purplehead gamba prawn | 7.6 | 19.3 | North Carolina to Surinam including | Soft bottoms | 200-820 m |
| | *Aristeus antillensis* | | | the Gulf of Mexico & Caribbean Sea | | |
| | (Milne Edwards and Bouvier, 1909) | | | | | |
| | Scarlet shrimp | 13.1 | 33.4 | Newfoundland to northern South | Muddy bottoms | 270-1850 m |
| | *Plesiopenaeus edwardsianus* | | | America including the Gulf of Mexico | | (400-900 m) |
| | (Johnson, 1868) | | | & Caribbean Sea | | |

Table 14-6.
Fish and invertebrate taxa taken commercially in the northern GOM (U.S. waters) in decreasing order of commercial dollar value. Deepwater Species designated in bold. All values are annual averages for the period 2000-2007. Source: Fisheries Statistics Division ST1 (FSD) of the NMFS (NMFS 2008). From LGL 2009.

| Common Name | Scientific Name | Pounds | Dollar Value (US) | Percent Dollar Value (US) |
|---|---|---|---|---|
| Shrimp, Brown | *Farfantepenaeus aztecus* | 127,426,610 | 203,525,795 | 28.4 |
| Shrimp, White | *Litopenaeus setiferus* | 101,305,075 | 177,981,856 | 24.8 |
| Oyster, Eastern | *Crassostrea virginica* | 23,681,186 | 58,168,167 | 8.1 |
| Menhaden, Gulf | *Brevoortia patronus* | 1,081,127,556 | 54,144,592 | 7.6 |
| Crab, Blue | *Callinectes sapidus* | 61,128,125 | 43,619,711 | 6.1 |
| Shrimp, Pink | *Farfantepenaeus duorarum* | 13,237,192 | 27,809,743 | 3.9 |
| Crab, Florida Stone Claws | *Menippe mercenaria* | 5,800,380 | 24,171,885 | 3.4 |
| Lobster, Caribbean Spiny | *Panulirus argus* | 3,932,025 | 20,156,482 | 2.8 |
| Grouper, Red | *Epinephelus morio* | 6,300,903 | 12,944,474 | 1.8 |
| Snapper, Red | *Lutjanus campechanus* | 4,394,552 | 10,945,823 | 1.5 |
| Tuna, Yellowfin | *Thunnus albacares* | 3,349,396 | 10,491,828 | 1.5 |
| Shrimp, Dendrobranchiata | Shrimp Suborder | 2,762,392 | 8,407,760 | 1.2 |
| Mullet, Striped (Liza) | *Mugil cephalus* | 12,401,802 | 8,358,186 | 1.2 |
| Gag | *Mycteroperca microlepis* | 2,510,539 | 6,441,548 | 0.9 |
| Snapper, Vermilion | *Rhomboplites aurorubens* | 1,957,037 | 3,902,361 | 0.5 |
| Drum, Black | *Pogonias cromis* | 5,095,562 | 3,575,429 | 0.5 |
| Snapper, Yellowtail | *Ocyurus chrysurus* | 1,258,740 | 2,717,862 | 0.4 |
| **Grouper, Yellowedge** | ***Epinephelus flavolimbatus*** | **1,017,550** | **2,658,727** | **0.4** |
| Shrimp, Rock | *Sicyonia brevirostris* | 1,681,983 | 2,249,763 | 0.3 |
| Sharks | | 874,311 | 2,019,884 | 0.3 |
| Shrimp, Seabob | *Xiphopenaeus kroyeri* | 4,653,430 | 1,970,282 | 0.3 |
| Swordfish | *Xiphias gladius* | 814,694 | 1,822,322 | 0.3 |
| Catfish, Blue | *Ictalurus furcatus* | 3,433,441 | 1,614,270 | 0.2 |
| Mackerel, King and Cero | *Scomberomorus cavalla/regalis* | 1,317,458 | 1,466,095 | 0.2 |
| Mackerel, King | *Scomberomorus cavalla* | 985,712 | 1,211,584 | 0.2 |
| Amberjack, Greater | *Seriola dumerili* | 1,087,468 | 1,056,163 | 0.1 |
| Grouper, Black | *Mycteroperca bonaci* | 417,192 | 1,054,001 | 0.1 |
| **Shrimp, Royal Red** | ***Pleoticus robustus*** | **470,095** | **1,048,030** | **0.1** |
| Pompano, Florida | *Trachinotus carolinus* | 308,544 | 995,822 | 0.1 |
| Ladyfish | *Elops saurus* | 1,437,907 | 862,799 | 0.1 |
| Scamp | *Mycteroperca phenax* | 325,697 | 846,620 | 0.1 |
| Flatfish | Pleuronectiformes | 407,373 | 797,752 | 0.1 |
| Finfishes, Unc General | | 2,098,136 | 794,144 | 0.1 |
| Mackerel, Spanish | *Scomberomorus maculatus* | 1,335,034 | 731,828 | 0.1 |
| **Tilefish** | **Malacanthidae** | **439,419** | **682,412** | **0.1** |
| Sheepshead | *Archosargus probatocephalus* | 2,037,239 | 671,438 | 0.1 |
| Catfish, Channel | *Ictalurus punctatus* | 1,315,173 | 662,955 | 0.1 |
| Buffalofishes | *Ictiobus spp.* | 3,370,904 | 581,891 | 0.1 |
| Shrimp, Marine, Other | | 214,729 | 581,576 | 0.1 |
| Snapper, Gray | *Lutjanus griseus* | 312,223 | 578,521 | 0.1 |
| Finfishes, Unc Bait/Animal Food | | 1,700,423 | 570,156 | 0.1 |
| **Grouper, Snowy** | ***Epinephelus niveatus*** | **243,299** | **547,017** | **0.1** |
| Ballyhoo | *Hemiramphus brasiliensis* | 657,657 | 504,102 | 0.1 |
| Scads | Carangidae | 721,776 | 484,118 | 0.1 |
| Dolphinfish | *Coryphaena hippurus* | 349,132 | 455,029 | 0.1 |
| Croaker, Atlantic | *Micropogonias undulatus* | 86,695 | 451,349 | 0.1 |
| Snapper, Mutton | *Lutjanus analis* | 215,000 | 403,587 | 0.1 |
| Sardine Spanish | *Sardinella aurita* | 1,589,857 | 378,855 | 0.1 |
| Butterfish, Gulf | *Peprilus burti* | 802,857 | 361,029 | 0.1 |
| Tuna, Bluefin | *Thunnus thynnus* | 76,600 | 345,746 | 0.0 |
| Shrimp, Atlantic & Gulf, Roughneck | *Trachypenaeus similis* | 568,143 | 331,652 | 0.0 |
| **Grouper, Warsaw** | ***Epinephelus nigritus*** | **164,097** | **316,489** | **0.0** |
| Shark, Blacktip | *Carcharhinus limbatus* | 1,201,625 | 313,022 | 0.0 |
| Grunts | Haemulidae | 435,912 | 309,195 | 0.0 |
| Herring, Atlantic Thread | *Opisthonema oglinum* | 1,950,158 | 277,850 | 0.0 |
| **Crab, Deepsea Golden** | ***Chaceon fenneri*** | **233,354** | **258,468** | **0.0** |
| Shad, Gizzard | *Dorosoma cepedianum* | 1,149,656 | 252,390 | 0.0 |
| Cobia | *Rachycentron canadum* | 115,774 | 241,807 | 0.0 |

Table 14-6.  Continued

| Common Name | Scientific Name | Pounds | DollarValue (US) | Percent Dollar Value (US) |
|---|---|---|---|---|
| Mullets | *Mugil* spp. | 300,736 | 235,563 | 0.0 |
| Shark, Sandbar | *Carcharhinus plumbeus* | 822,699 | 235,166 | 0.0 |
| Jack, Crevalle | *Caranx hippos* | 387,572 | 233,819 | 0.0 |
| Scups or Porgies | Sparidae | 243,998 | 231,214 | 0.0 |
| Pinfish | *Lagodon rhomboides* | 44,340 | 215,985 | 0.0 |
| Finfishes, Unc For Food | | 674,433 | 197,774 | 0.0 |
| Mojarras | Gerreidae | 249,333 | 187,975 | 0.0 |
| **Snapper, Silk** | ***Lutjanus vivanus*** | **80,838** | **177,109** | **0.0** |
| **Hind, Speckled** | ***Epinephelus drummondhayi*** | **79,726** | **165,502** | **0.0** |
| Seatrout, Spotted | *Cynoscion nebulosus* | 82,966 | 160,853 | 0.0 |
| Wahoo | *Acanthocybium solandri* | 135,889 | 158,912 | 0.0 |
| Herrings | Clupeidae | 1,007,150 | 156,300 | 0.0 |
| Tuna, Little Tunny | *Euthynnus alletteratus* | 392,580 | 144,981 | 0.0 |
| Tuna, Bigeye | *Thunnus obesus* | 38,511 | 132,672 | 0.0 |
| Leatherjackets | Carnagidae | 103,665 | 127,437 | 0.0 |
| Catfish, Flathead | *Pylodictis olivaris* | 255,478 | 121,971 | 0.0 |
| Mackerel, Chub | *Scomber colias* | 204,110 | 121,699 | 0.0 |
| Runner, Blue | *Caranx crysos* | 253,723 | 120,967 | 0.0 |
| Bowfin | *Amia calva* | 137,670 | 113,640 | 0.0 |
| Bonito, Atlantic | *Sarda sarda* | 80,325 | 112,630 | 0.0 |
| Tilefish, Blueline   (DW) | *Caulolatilus microps* | 122,561 | 109,760 | 0.0 |
| Sea Bass, Black | *Centropristis striata* | 161,843 | 109,325 | 0.0 |
| Porgy, Red | *Pagrus pagrus* | 96,938 | 103,239 | 0.0 |
| Flounder, Southern | *Paralichthys lethostigma* | 83,869 | 99,322 | 0.0 |
| Snapper, Lane | *Lutjanus synagris* | 52,884 | 90,369 | 0.0 |
| **Escolar** | ***Lepidocybium flavobrunneum*** | **121,980** | **87,031** | **0.0** |
| Groupers | Serranidae | 38,315 | 84,480 | 0.0 |
| Mullet, white | *Mugil curema* | 149,670 | 83,001 | 0.0 |
| Drum, Freshwater | *Apoldinotus grunniens* | 541,676 | 82,136 | 0.0 |
| Pigfish | *Orthopristis chrysoptera* | 28,247 | 80,737 | 0.0 |
| Hogfish | *Lachnolaimus maximus* | 36,141 | 79,411 | 0.0 |
| Amberjack, Lesser | *Seriola fasciata* | 66,655 | 73,224 | 0.0 |
| King Whiting | *Menticirrhus americanus* | 126,338 | 73,057 | 0.0 |
| Triggerfish, Gray | *Balistes capriscus* | 68,194 | 70,827 | 0.0 |
| Seatrout, Sand | *Cynoscion arenarius* | 105,370 | 67,330 | 0.0 |
| Shark, Atlantic Sharpnose | *Rhizoprionodon terraenovae* | 140,138 | 55,309 | 0.0 |
| **Tilefish, Goldface** | ***Caulolatilus chrysops*** | **36,846** | **52,706** | **0.0** |
| Jack, Almaco | *Seriola rivoliana* | 52,718 | 48,527 | 0.0 |
| Lobster, Slipper | *Scyllarides squammosus* | 10,512 | 46,370 | 0.0 |
| **Snapper, Queen** | ***Etelis oculatus*** | **19,694** | **41,868** | **0.0** |
| Shark, Finetooth | *Carcharhinus isodon* | 77,303 | 41,690 | 0.0 |
| Scad, Bigeye | *Selar crumenophthalmus* | 247,372 | 40,873 | 0.0 |
| Bluefish | *Pomatomus saltatrix* | 126,246 | 39,503 | 0.0 |
| Oilfish | *Ruvettus pretiosus* | 44,373 | 36,005 | 0.0 |
| Jacks | Carangidae | 59,810 | 34,820 | 0.0 |
| Drum, Red | *Sciaenops ocellatus* | 24,317 | 34,414 | 0.0 |
| Cutlassfish, Atlantic | *Trichiurus lepturus* | 35,776 | 33,237 | 0.0 |
| Suckers | Catostomidae | 81,078 | 31,501 | 0.0 |
| Jack, Bar | *Caranx ruber* | 38,080 | 31,259 | 0.0 |
| **Barrelfish** | ***Hyperoglyphe perciformis*** | **14,912** | **29,069** | **0.0** |
| Snapper, Black | *Apsilus dentatus* | 14,888 | 25,052 | 0.0 |
| Permit | *Trachinotus falcatus* | 17,361 | 24,949 | 0.0 |
| Snappers | Lutjanidae | 13,304 | 24,053 | 0.0 |
| Anchovies | Engraulidae | 106,489 | 23,212 | 0.0 |
| Shark, Great Hammerhead | *Sphyrna mokarran* | 89,196 | 21,795 | 0.0 |
| Wenchman | *Pristipomoides aquilonaris* | 16,674 | 21,318 | 0.0 |
| Tuna, Blackfin | *Thunnus atlanticus* | 31,901 | 21,077 | 0.0 |
| Shark, Shortfin Mako | *Isurus oxyrinchus* | 23,747 | 20,444 | 0.0 |
| Shark, Bull | *Carcharhinus leucas* | 70,871 | 19,604 | 0.0 |
| Brotula, Bearded | *Brotula barbata* | 16,608 | 18,401 | 0.0 |
| Spadefish, Atlantic | *Chaetodipterus faber* | 36,118 | 15,995 | 0.0 |
| **Black Driftfish** | ***Hyperoglyphe bythites*** | **11,137** | **15,591** | **0.0** |
| Margate | *Haemulon album* | 22,334 | 13,481 | 0.0 |

Table 14-6. Continued

| Common Name | Scientific Name | Pounds | Dollar Value (US) | Percent Dollar Value (US) |
|---|---|---|---|---|
| **Grouper, Yellowfin** | *Mycteroperca venenosa* | **5,948** | **13,415** | **0.0** |
| Scorpionfishes | *Scorpaeniformes* | 11,904 | 13,033 | 0.0 |
| Porgy, Knobbed | *Calamus nodosus* | 19,803 | 13,020 | 0.0 |
| Spot | *Leiostomus xanthurus* | 32,853 | 12,550 | 0.0 |
| Shark, Lemon | *Negaprion brevirostris* | 44,990 | 12,211 | 0.0 |
| Tilefishes  (DW) | Malacanthidae | 26,584 | 12,128 | 0.0 |
| Rudderfish, Banded | *Seriola zonata* | 12,880 | 11,028 | 0.0 |
| Snapper, Blackfin  (DW) | *Lutjanus buccanella* | 4,987 | 10,551 | 0.0 |
| Shark, Spinner | *Carcharhinus brevipinna* | 30,884 | 10,359 | 0.0 |
| Tuna, Albacore | *Thunnus alalunga* | 15,321 | 10,022 | 0.0 |
| Mackerel, (Scomber) | Scombridae | 15,479 | 9,363 | 0.0 |
| Barracudas | *Sphyraena* spp. | 14,835 | 9,324 | 0.0 |
| Hind, Red | *Epinephelus guttatus* | 5,447 | 9,202 | 0.0 |
| Amberjack | *Seriola* spp. | 8,738 | 7,778 | 0.0 |
| Shark, Blacknose | *Carcharhinus acronotus* | 21,928 | 7,656 | 0.0 |
| **Grouper, Marbled** | ***Dermatolepis inermis*** | **3,009** | **5,953** | **0.0** |
| **Grouper, Misty** | ***Epinephelus mystacinus*** | **2,557** | **5,557** | **0.0** |
| **Hake, Atlantic, Red/White** | ***Urophycis chuss/tenuis*** | **5,178** | **5,313** | **0.0** |
| Tunas | Scombridae | 2,298 | 5,212 | 0.0 |
| Porgy, Whitebone | *Calamus leucosteus* | 4,815 | 4,953 | 0.0 |
| Flyingfishes | Exocoetidae | 33,991 | 4,829 | 0.0 |
| Porgy, Jolthead | *Calamus bajonado* | 5,251 | 4,340 | 0.0 |
| Tripletail, Atlantic | *Lobotes surinamensis* | 3,755 | 3,448 | 0.0 |
| Sea Catfishes | Ariidae | 12,567 | 3,411 | 0.0 |
| Puffers | Tetradontidae | 4,997 | 3,394 | 0.0 |
| Rays | *Rajiformes/Myliobatiformes* | 19,400 | 3,383 | 0.0 |
| Shark, Longfin Mako | *Isurus paucus* | 4,037 | 3,083 | 0.0 |
| Drums | Sciaenidae | 4,864 | 2,267 | 0.0 |
| Snapper, Dog | *Lutjanus jocu* | 1,699 | 1,889 | 0.0 |
| Rosefish, Blackbelly   (DW) | *Helicolenus dactylopterus* | 1,590 | 1,789 | 0.0 |
| Scorpionfish, Spotted | *Scorpaena plumieri* | 1,208 | 1,780 | 0.0 |
| Snapper, Cubera | *Lutjanus cyanopterus* | 1,476 | 1,603 | 0.0 |
| Creolefish, Atlantic | *Paranthias furcifer* | 2,193 | 1,546 | 0.0 |
| Ray, Stingrays | *Rajiformes/Myliobatiformes* | 4,953 | 1,360 | 0.0 |
| Shark, Silky | *Carcharhinus falciformis* | 4,152 | 1,357 | 0.0 |
| Parrotfishes | Scaridae | 1,207 | 1,192 | 0.0 |
| Shark, Tiger | *Galeocerdo cuvier* | 3,708 | 1,157 | 0.0 |
| Bigeye | *Priacanthus arenatus* | 1,964 | 1,149 | 0.0 |
| Sand Perch | *Diplectrum formosum* | 612 | 1,141 | 0.0 |
| Grouper, Yellowmouth | *Mycteroperca interstitialis* | 489 | 1,061 | 0.0 |
| Pompano, African | *Alectis ciliaris* | 795 | 971 | 0.0 |
| Scorpionfish, Spinycheek | *Neomerinthe hemingwayi* | 838 | 898 | 0.0 |
| **Eel, Conger** | **Congridae** | **1,004** | **876** | **0.0** |
| Hind, Rock | *Epinephelus adscensionis* | 425 | 791 | 0.0 |
| Snapper, Caribbean Red | *Lutjanus purpureus* | 816 | 749 | 0.0 |
| **Bass, Longtail          (** | ***Hemanthias leptus*** | **680** | **667** | **0.0** |
| Triggerfish, Queen | *Balistes vetula* | 582 | 599 | 0.0 |
| Tuna, Skipjack | *Katsuwonus pelamis* | 572 | 469 | 0.0 |
| Lookdown | *Selene vomer* | 680 | 467 | 0.0 |
| Opah | *Lampris guttatus* | 346 | 445 | 0.0 |
| Squirrelfishes | Holocentridae | 607 | 357 | 0.0 |
| Runner, Rainbow | *Elagatis bipinnulata* | 560 | 315 | 0.0 |
| Eels, Snake | Ophichthidae | 231 | 312 | 0.0 |
| Sea Chubs | Kyphosidae | 538 | 283 | 0.0 |
| Tilefish, Sand | *Malacanthus plumieri* | 166 | 244 | 0.0 |
| Shark, Thresher | *Alopias vulpinus* | 531 | 214 | 0.0 |
| Jack, Horse-eye | *Caranx latus* | 248 | 172 | 0.0 |
| Graysby | *Cephalopholis cruentata* | 64 | 117 | 0.0 |
| Snapper, Schoolmaster | *Lutjanus apodus* | 82 | 111 | 0.0 |
| Shark, Bonnethead | *Sphyrna tiburo* | 338 | 96 | 0.0 |
| Pomfrets | Bramidae | 82 | 78 | 0.0 |
| Jack, Black | *Caranx lugubris* | 139 | 76 | 0.0 |

Table 14-7.

Species listed in the Essential Fish Habitat Amendment to Gulf of Mexico Fishery Management Plans.  Deepwater species in bold. Source: GMFMC (2005b).  Used with permission from LGL 2009.

| FMP | Common name | Scientific Name |
|---|---|---|
| **Red Drum (1)** | Drum, Red | *Sciaenops ocellatus* |
| **Reef Fish (43)** | **Balistidae - Triggerfishes (1)** | |
| | Triggerfish, Gray | Balistes capriscus |
| | **Carangidae - Jacks (4)** | |
| | Amberjack, Greater | *Seriola dumerili* |
| | Amberjack, Lesser | *Seriola fasciata* |
| | Jack, Almaco | *Seriola rivoliana* |
| | Rudderfish, Banded | *Seriola zonata* |
| | **Labridae - Wrasses (1)** | |
| | Hogfish | Lachnolaimus maximus |
| | **Lutjanidae - Snappers (14)** | |
| | **Snapper, Queen** | ***Etelis oculatus*** |
| | Snapper, Mutton | *Lutjanus analis* |
| | Snapper, Schoolmaster | *Lutjanus apodus* |
| | **Snapper, Blackfin** | ***Lutjanus buccanella*** |
| | Snapper, Red | *Lutjanus campechanus* |
| | Snapper, Cubera | *Lutjanus cyanopterus* |
| | Snapper, Gray | *Lutjanus griseus* |
| | Snapper, Dog | *Lutjanus jocu* |
| | Snapper, Mahogany | *Lutjanus purpureus* |
| | Snapper, Lane | *Lutjanus synagris* |
| | **Snapper, Silk** | ***Lutjanus vivanus*** |
| | Snapper, Yellowtail | *Ocyurus chrysurus* |
| | **Wenchman** | ***Pristipomoides aquilonaris*** |
| | Snapper, Vermilion | *Rhomboplites aurorubens* |
| | **Malacanthidae - Tilefishes (5)** | |
| | **Tilefish, Goldface** | ***Caulolatilus chrysops*** |
| | **Tilefish, Blackline** | ***Caulolatilus cyanops*** |
| | **Tilefish, Anchor** | ***Caulolatilus intermedius*** |
| | **Tilefish, Blueline** | ***Caulolatilus microps*** |
| | **Tilefish, Golden** | ***Lopholatilus chamaeleonticeps*** |
| | **Serrinidae - Groupers (18)** | |
| | Sand Perch, Dwarf | *Diplectrum bivittatum* |
| | Sand Perch | *Diplectrum formosum* |
| | Hind, Rock | *Epinephelus adscensionis* |
| | **Hind, Speckled** | ***Epinephelus drummondhayi*** |
| | **Grouper, Yellowedge** | ***Epinephelus flavolimbatus*** |
| | Hind, Red | *Epinephelus guttatus* |
| | Grouper, Goliath | *Epinephelus itajara* |
| | Grouper, Red | *Epinephelus morio* |
| | **Grouper, Misty** | ***Epinephelus mystacinus*** |

Table 14-7. Continued.

| FMP | Common name | Scientific Name |
|---|---|---|
| | **Grouper, Warsaw** | ***Epinephelus nigritus*** |
| | **Grouper, Snowy** | ***Epinephelus niveatus*** |
| | Grouper, Nassau | *Epinephelus striatus* |
| | Grouper, Marbled | *Dermatolepis inermis* |
| | Grouper, Black | *Mycteroperca bonaci* |
| | Grouper, Yellowmouth | *Mycteroperca interstitialis* |
| | Gag | *Mycteroperca microlepis* |
| | Scamp | *Mycteroperca phenax* |
| | Grouper, Yellowfin | *Mycteroperca venenosa* |
| **Coastal Migratory Pelagic (3)** | Mackerel, King | *Scomberomorus cavalla* |
| | Mackerel, Spanish | *Scomberomorus maculatus* |
| | Cobia | *Rachycentron canadum* |
| **Shrimp (4)** | Shrimp, Brown | *Farfantepenaeus aztecus* |
| | Shrimp, White | *Farfantepenaeus setiferus* |
| | Shrimp, Pink | *Farfantepenaeus duorarum* |
| | **Shrimp, Royal Red** | ***Pleoticus robustus*** |
| **Stone Crab (2)** | Crab, Florida Stone Claws | *Menippe mercenaria* |
| | Crab, Florida Stone Claws (Ceder Key N) | *Menippe adina* |
| **Spiny Lobster (2)** | Lobster, Caribbean Spiny | *Panulirus argus* |
| | Lobster, Slipper | *Sycllarides squammosus* |

# 15 REFERENCES

Álvarez, I. and J.F. Wendel. 2003. Ribosomal ITS sequences and plant phylogenetic inference. Molecular Phylogenetics and Evolution 293:417-434.

Andersson, A.J., F.T. Mackenzie, and J.-P. Gattuso,. 2011. Effects of ocean acidification on benthic processes, organisms, and ecosystems. In: Gattuso, J.P., and L. Hansson, eds. Ocean Acidification. New York: Oxford University Press. Pp. 122-153.

Barnett, T., D. Pierce, K. AchutaRao, P. Gleckler, B.D. Santer, J. Gregory and W.M. Washington. 2005. Penetration of human-induced warming into the world's oceans. Science 309:284-287.

Barrow, H.S., and A. Kelson. 1993. Problem-based learning in secondary education and the Problem-based Learning Institute Monograph. Springfield: Southern Illinois University School of Medicine.

Bayer, F. 1956. Octocorallia. Treatise on invertebrate paleontology. 166-231.

Baums, I.B., C.B. Paris, and L.M. Cherubin. 2006. A bio-oceanographic filter to larval dispersal in a reef-building coral. Limnology and Oceanography 515:1969-1981.

Baums, I. B., C.R. Hughes, and M.H. Hellberg. 2005. Mendelian microsatellite loci for the Caribbean coral Acropora palmata. Mar. Ecol. Prog. Ser. 288:115-127.

Becker, E.L., E. E. Cordes, S.A. Macko, and C. R. Fisher. 2009. Importance of seep primary production to *Lophelia pertusa* and associated fauna in the Gulf of Mexico. Deep-Sea Research Part I: Oceanographic Research Papers 56:786-800.

Bell, N., and J. Smith. 1999. Coral growing on North Sea oil rigs. Nature. 402: 601.

Benson, G. 1999. Tandem repeat finder: a program to analyze DNA sequences. Nucleic Acid Research 272:573-580.

Blair, C. 2000. Hitler's U-boat War: The Hunters, 1939-1942. New York: Modern Library.

Bloomster, E. 1940. Sailing and Small Craft Down the Ages. Annapolis, MD: Naval Institute Press.

Bodsworth, C. 1998. Sir Henry Bessemer: Father of the steel industry. London: IOM Communications.

Boulay, J.N., J. Cortés, M. Hellberg, and I.B. Baums. 2014. Unrecognized coral species diversity masks differences in functional ecology. Proc Roy Acad Sci Series B. 281:20131580.

Bouma, A.H., J.M. Coleman, and DPSP Leg 96 Shipboard Scientists. 1985. Mississippi Fan: Leg 96 program and principal results, Chapter 36. In: Bouma, A.H., W.R. Normark, and N.E. Barnes, eds. Submarine Fans and Related Turbidite Sequences. New York: Springer-Verlag.

Bradshaw, J. 2002. Louisiana Purchase: A pictorial retrospective celebrating Louisiana. Vancouver: Pediment Publishing.

Brawley S.H., and W.H. Adey. 1982. Coralliophila abbreviate: A significant coralliovore. Bull Mar Sci 32:595-599.

Breitburg, D.L., T. Loher, C.A. Pacey, and A. Gerstein. 1997. Varying effects of low dissolved oxygen on trophic interactions in an estuarine food web. Ecol. Monogr. 67:489-507.

Broecker, W. 1991. The great ocean conveyor. Oceanography 4:79-89.

Brooke, S. and W.W. Schroeder. 2007. State of deep coral Ecosystems in the Gulf of Mexico Region: Texas to the Florida Straits. In: Lumsden, S.E., T.F. Hourigan, A.W. Bruckner, G. Dorr, eds. The State of Deep Coral Ecosystems of the United States. Silver Spring, MD. NOAA Tech. Memo. CRCP-3. Pp. 271–306.

Brooke, S., S.W. Ross, J.M. Bane, H.E. Seim, and C.M. Young. 2013. Temperature tolerance of the deep-sea coral *Lophelia pertusa* from the southeastern United States. Deep-Sea Res. II 92:240-248

Brooke, S.D. and C.M. Young. 2009. In situ measurement of survival and growth of *Lophelia pertusa* in the northern Gulf of Mexico. Mar. Ecol. Prog. Ser. 397:153-161.

Brooke, S.D., Holmes, M.W., and Young, C.M. 2009. Sediment tolerance of two different morphotypes of the deep-sea coral *Lophelia pertusa* from the Gulf of Mexico. Mar. Ecol. Prog. Ser. 390:137-144.

Browning, R.M., Jr. 1996. U.S. merchant vessel war casualties of World War II. Annapolis, MD: Naval Institute Press.

Brugler, M.R. and S.C. France. 2007. The complete mitochondrial genome of the black coral Chrysopathes formosa Cnidaria:Anthozoa:Antipatharia supports classification of antipatharians within the subclass Hexacorallia. Molecular phylogenetics and evolution 42:776-788.

Bryan T.L. and A. Metaxas. 2007. Predicting suitable habitat for deep-water gorgonian corals on the Atlantic and Pacific Continental Margins of North America. MEPS 330:113-126.

Bryan, T.L. and A. Metaxas. 2006. Distribution of deep-water corals along the North American continental margins: relationships with environmental factors. Deep-Sea Res. I 53:1865-1879.

Buhl-Moretensen, L., A. Vanreusel, A. Gooday, L.A. Levin, I. Priede, P. Buhl-Mortensen, H. Gheerardyn, N. King, and M. Raes. 2010. Biological structures as a source of habitat heterogenety and biodviersity on the deep deep ocean margins. Mar. Ecol. 31:21-50.

Buhl-Mortensen, L. and P.B. Mortensen. 2004a. Crustaceans associated with the deep-water gorgonian corals Paragorgia arborea (L., 1758) and Primnoa resedaeformis (Gunn., 1763). Journal of Natural History 38:1233-1247.

Buhl-Mortensen, L. and P.B. Mortensen. 2005. Distribution and diversity of species associated with deep-sea gorgonian corals off Atlantic Canada. In: Freiwald, A. and J. M. Roberts, eds. Cold-water Corals and Ecosystems. Springer-Verlag. Pp. 849-879

Buhl-Mortensen, L. A. Vanreusel, A.J. Gooday, L.A. Levin, I.G. Priede, P. Buhl-Mortensen, H. Gheerardyn, N.J. King and M. Raes. 2010. Biological structures as a source of habitat heterogeneity and biodiversity on the deep ocean margins. Mar. Ecol. 31:21-50.

Burch, H.A. 1942a. Summary of Statements by Survivors of the SS Gulf Penn, U.S. Tanker. Navy department, Office of the Chief of Naval Operations. May 22.

Busch, R. and H.J. Röll. 1999. German U-boat commanders of World War II: A biographical dictionary. Annapolis, MD: Naval Institute Press.

Cairns, S. 1979. The deep-water Scleractinia of the Caribbean Sea and adjacent waters. Stud Fauna Curaqao 57(180): 341 pp.

Cairns, S. 2001 Deep-water corals: an overview with special reference to diversity and distribution of deep-water scleractinian corals. Bulletin of Marine Science, 81: 311-322.

Cairns, S.D. and D.M. Opresko. 1993. New records of deep-water cnidaria Scleractinia and Antipatharia from the Gulf of Mexico. Northeast Gulf Science 13:1-11.

Camilli, R., C.M. Reddy, D.R. Yoerger, B.A.S. Van Mooy, M.V. Jakuba, J.C. Kinsey, and C.P. McIntyre, S. P. Sylva, and J. V. Maloney. 2012 Tracking hydrocarbon plume transport and 380 biodegradation at *Deepwater Horizon*. Science 330:201-204.

Carney, S.L., M.I. Formica, H. Divatia, K. Nelson, C.R. Fisher, and S.W. Schaeffer. 2006. Population structure of the mussel Bathymodiolus childressi from Gulf of Mexico hydrocarbon seeps. Deep-Sea Research Part I 536:1061-1072.

Cartes, J.E. and F. Sarda. 1993. Zonation of deep-sea decapod fauna in the Catalan Sea Western Mediterranean. Mar. Ecol. Prog. Ser. 94:27-34.

Case, T.J. and M. Taper. 2000. Interspecific competition, environmental gradients, gene flow, and the coevolution of species' borders. Am. Nat. 155:583–605.

Chapelle, H.I. 1973. The American fishing schooners, 1825-1935. New York: W.W. Norton & Company

Chapman, F.H. af. 2006.  Architecturanavalismercatoria:  The classic of eighteenth-century naval architecture.  Originally published by Holmiae, Stockholm in 1768. Dover ed.  Mineola, NY: Dover Publications.

Charlton, M.J. 2003. Interview by M. K. Morgan at Mr. Charlton's home, Monroe, Louisiana, January 31, 2003 Church, R. A., D. J. Warren, A. W. Hill, and J. S. Smith.  2002.  In: The Discovery of *U-166*: Rewriting History with New Technology.  Offshore Technology Conference. May 2003.

Cho, W. 2008. Faunal biogeography, community structure, and genetic connectivity of North Atlantic Seamounts. PhD thesis, Massachusetts Institute of Technology/Woods Hole Oceanographic Institution Joint Program.

Church, R.A., D.J. Warren, A.W. Hill, J.S. Smith. 2002. The Discovery of U-166: Rewriting History with New Technology. Offshore Technology Conference, 6-9 May, Houston, Texas, OTC-14136-MS.

Church, R.A. and D.J. Warren. 2008. Viosca Knoll Wreck: Discovery and investigation of an early 19th century sailing ship in 2000 feet of water.  U.S. Dept. of the Interior, Minerals Management Service, Gulf of Mexico OCS Region, New Orleans, LA. OCS Study MMS 2008-018.

Church, R.A., D.J. Warren, J.B. Weirich, and D.A. Ball. 2004. Return to the *U-166*: Working Together to Meet the Challenge of Deepwater Archaeology. Proceedings of the Underwater Intervention Conference. February.

Church, R., D. Warren, R. Cullimore, L. Johnston, W. Schroeder, W. Patterson, T. Shirley, M. Kilgour, N. Morris, and J. Moore. 2007. Archaeological and biological analysis of World War II shipwrecks in the Gulf of Mexico: Artificial reef effect in deep water. U.S. Dept. of the Interior, Minerals Management Service, Gulf of Mexico OCS Region, New Orleans, LA.  OCS Study MMS 2007-015.

Church, R.A. 2003. Archaeological assessment for a proposed 6-inch gas and 6-inch oil pipeline routes from Block 962 to Block 786, Viosca Knoll Area.  Prepared by C & C Technologies, Inc. for Geoscience Earth & Marine Services, Inc. on behalf of Mariner Energy.  Report submitted to the U.S. Dept. of the Interior, Minerals Management Service, Gulf of Mexico OCS Region, New Orleans, LA.

Church, R.A., D.J. Warren, and J.B. Irion.2009.Analysis of deepwater shipwrecks in the Gulf of Mexico: Artificial reef effect of six World War II shipwrecks. Oceanography 22(2):50-63.

Clark, A.H. 1910. The clipper ship era: An epitome of famous American and British clipper ships, their owners, builders, commanders, and crews 1843-1869. New York, NY: G.P. Putnam's Sons.

Clark, J.A. and M. Odintz, 2012. Gulf Oil Corporation. Texas State Historical Association. Internet website: http://www.tshaonline.org. January 20, 2012.

Clarke, K.R., and R.M. Warwick. 2001. Change in marine communities: An approach to statistical analysis and interpretation, 2nd ed. PRIMER-E.

Clarke, K. R., and R. N. Gorley. 2001. "PRIMER v6 PRIMER-E Ltd." *Plymouth, UK.*.

Clarke, K.R., and R.N. Gorley. 2006. PRIMER v6: User manual/tutorial. PRIMER-E.

Commissioner of Navigation. 1897. Report of the Commissioner of Navigation to the Secretary of the Treasury. Washington, D.C.: Government Printing Office.

Cordes, E.E., M.P. McGinley, E.L. Podowski, E.L. Becker, S. Lessard-Pilon, S.T. Viada, and C.R. Fisher. 2008. Coral communities of the deep Gulf of Mexico. Deep Sea Res. Part I. Oceanogr. Res. Pap. 55(6): 777-787.

Davies, A.J. and J.M. Guinotte. 2011. Global habitat suitability for framework-forming cold-water corals. Plos One 64:e18483. doi:10.1371/journal.pone.0018483

Davies, A.J., G.C.A. Duineveld, M.S.S. Lavaleye, M.J.N. Bergman, H. van Haren, and J.M. Roberts. 2009. Downwelling and deep-water bottom currents as food supply mechanisms to the cold-water coral *Lophelia pertusa* Scleractinia at the Mingulay Reef complex. Limnol. Oceanogr. 54:620-629.

Davies, A.J., G. Duineveld, G., T. van Weering, F. Mienis, A.M. Quattrini, H.E. Seim, J.M. Bane, and S.W. Ross. 2010. Short-term environmental variability in cold-water coral habitat at Viosca Knoll, Gulf of Mexico. Deep-Sea Res. Pt. I 57:199-212.

Davies, A.J., M. Wisshak, J.C. Orr, and J.M. Roberts. 2008. Predicting suitable habitat for the cold-water coral *Lophelia pertusa* Scleractinia. Deep-Sea Res. I 558:1048-1062.

Davies, P.S. 1989. Short-term growth measurements of corals using an accurate buoyant weighing technique. Mar. Biol. 101:389-395.

Delbeek, J.C. and J. Sprung. 2005. The reef aquarium volume three: science, art, and technology. Miami Gardens, FL: Two Little Fishies, Inc.

Desmond, C. 1998. Wooden ship-building. Reprint. Originally published: New York: Rudder Publishing Company, 1919

Deuser, W.G. 1986. Seasonal and interannual variations in deep-water particle fluxes in the Sargasso Sea and their relation to surface hydrography. Deep-Sea Res. I 332:225-246.

Dickson, A.G. 2010. The carbon dioxide system in seawater: equilibrium chemistry and measurements. In: Riebesell, U., V.J. Fabry, L. Hansson, and J.-P. Gattuso, eds. Guide to Best Practices for Ocean Acidification Research and Data Reporting. Luxembourg: Publications Office of the European Union. Pp. 17-40.

Dickson, A.G., C.L. Sabine, and J.R. Christian, eds. 2007. Guide to best practices for ocean CO2 measurements. PICES Special Publication 3. 191 pp.

Dickson, A.G. and F.J. Millero. 1987. A comparison of the equilibrium constants for the dissociation of carbonic acid in seawater media. Deep Sea Research Part A. Oceanographic Research Papers: 34(10):1733–1743.

Dixon, B.T. and P. Weimer. 1998. Sequence stratigraphy and depositional history of the Eastern Misssissippi Fan Pleistocene, Northeastern Deep Gulf of Mexico. AAPG Bulletin 82(6):1207-1232.

Dodds, L.A., J.M. Roberts, A.C. Taylor, and F. Marubini. Metabolic tolerance of the cold-water coral *Lophelia pertusa* Scleractinia to temperature and dissolved oxygen change. J. Exp. Mar. Biol. Ecol. 349:205–214.

Dolan, M.F.J., A.J. Grehan, J.C. Guinan, and C. Brown. 2008. Modelling the local distribution of cold-water corals in relation to bathymetric variables: adding spatial context to deep-sea video data. Deep-Sea Research I 5511:1564-1579.

Doney, S.C., V.J. Fabry, R.A. Feely, and J.A. Kleypas. 2009. Ocean acidification: the other CO2 problem. Annu. Rev. Mar. Sci. 1:169-192.

Doughty, C. L., A.M. Quattrini, and E.E. Cordes. In press. Insights into the population dynamics of the deep-sea coral genus *Paramuricea* in the Gulf of Mexico. Deep Sea Research I.

Drummond, A.J., B. Ashton, S. Buxton, M. Cheung, A. Cooper, J. Heled, M. Kearse, R. Moir, S. Stones-Havas, S. Sturrock, T. Thierer, and A. Wilson et al. 2010. Geneious v5.1.

Dudley, W.S. 1992. The Naval War of 1812: A documentary history. Vol. II. Washington, D.C.: Naval Historical Center, Dept. of Navy.

Duffy, J. 1971. The history of Asiatic Cholera in the United States. Bulletin of the New York Academy of Medicine 47(10):1152-1167.

Duineveld, G.C.A., R.M. Jeffreys, M.S.S. Lavaleye, A.J. Davies, M.J.N. Bergman, T. Watmough, and R. Witbarrd. 2012. Spatial and tidal variation in food supply to shallow cold-water coral reefs of the Mugulay Reef complex Outer Hebries, Scotland. Mar. Ecol. Prog. Ser. 444:97-115.

Duncan, P.M. 1877. On the rapidity of growth and variability of some *Madrepora*ria on an Atlantic Cable, with remarks upon the rate of accumulation of foraminiferal deposits. Proceedings of the Royal Society of London 26: 179-184, 133-137.

Earl, D.A. and B.M. von Holdt. 2012. Structure harvester: a website and program for visualizing structure output and implementing the Evanno method. Conservation Genetics Resources 42:359-361.

Edmunds, P. 2012. Effects of pCO2 on the growth, respiration, and photophysiology of massive Porites spp. in Moorea, French Polynesia. Mar. Biol. 159:2149-2160.

Elith, J., C.H. Graham, R.P. Anderson, M. Dudik, S. Ferrier, A. Guisan, R.J. Hijmans, F. Huettmann, J.R. Leathwick, A. Lehmann, J. Li, L.G. Lohmann, B.A. Loiselle, G. Manion, C. Moritz, M. Nakamura, Y. Nakazawa, J.M.M. Overton, A.T. Peterson, S.J. Phillips, K. Richardson, R. Scachetti-Pereira, R.E. Schapire, J. Soberon, S. Williams, M.S. Wisz, and N.E. Zimmermann. 2006. Novel methods improve prediction of species' distributions from occurrence data. Ecography 292:129-151.

Elkins, P., R. Vanner, J.Firebrace. 2006. Decommissioning of offshore oil and gas facilities: A comparative assessment of different scenarios. Journal of Environmental Management: 79(4) 420–438.

Eller, E.M., W.J. Morgan, and R.M. Basoco. 1965. The Battle of New Orleans: Sea power and the Battle of New Orleans. The Battle of New Orleans, 150th Anniversary Committee of Louisiana, New Orleans, LA.

Emson, R. and J. Woodley. 1987. Submersible and laboratory observations on Asteroschema tenue, a long-armed euryaline brittle star epizoic on gorgonians. Mar Biol 96:31-45.

Fielding, A.H. and J.F. Bell. 1997. A review of methods for the assessment of prediction errors in conservation presence/absence models. Environmental Conservation 241:38-49.

Fine, M. and D. Tchernov. 2007. Scleractinian coral species survive and recover from decalcification. Science 315:1811.

Fleming, M.D. and R.M. Hoffer. 1979. Machine processing of landsat MSS data and DMA topographic data for forest over type mapping. LARS Technical Report 062879. Laboratory for Applications of Remote Sensing, Purdue University, West Lafayette, Indiana.

Flodin, John. 1919. "Annalysis of Isherwood System," Transactions of the Society of Naval Architects and Marine Engineers proceedings of the Twenty-Seventh General Meeting Nov. 13 and 14, 1919. Principal office of the Society. New York, NY. Pp. 95-85.

Form, A.U. and U. Riebesell. 2012. Acclimation to ocean acidification during long-term $CO_2$ exposure in the cold-water coral *Lophelia pertusa*. Global Change Biol. 18:843-853.

Forsman, Z.H., C.L. Hunter, G.E. Fox, and G.M. Wellingon. 2006. Is the ITS region the solution to the "species problem" in corals? Intragenomic variation and alignment permutation in Porites, Siderastrea and outgroup taxa. Proceedings of the 10th international coral reef symposium.

Frazier, D.E. 1967. Recent deltaic deposits of the Mississippi River. Gulf Coast Association of Geological Societies Transactions. Vol. XVII.

Frederiksen, R., A. Jensen, and H. Westerberg. 1992. The distribution of the scleractinian coral *Lophelia pertusa* around the Faroe Islands and the relation to internal tidal mixing. Sarsia 77:157-171.

Freiwald, A. 2002. Reef-forming cold-water corals. In: Wefer G.,D. Billett, D. Hebbeln, B.B.. Jorgensen, M. Schluter, and T. van Weering, eds. Ocean Margin Systems. Berlin: Springer. Pp. 365-385.

Freiwald, A., R. Henrich. and J. Patzold. 1997. Anatomy of a deep-water coral reef mound from Stjernsund, west Finnmark, northern Norway. Special Publication-SEPM 56:141-162.

Freiwald, A., J.B. Wilson, and R. Henrich. 1999. Grounding Pleistocene icebergs shape recent deep-water coral reefs. Sedimentary Geology 125:1-8.

Fuel Oil. 1914. Vessel Shipments from U.S. Gulf Ports. Fuel Oil Journal 5(1-12). Houston, TX.

Fuel Oil. 1915. Vessel Shipments from U.S. Gulf Ports. Fuel Oil Journal 6(1-12). Houston, TX.

Fuel Oil. 1916. Vessel Shipments from U.S. Gulf Ports. Fuel Oil Journal 7(1-12). Houston, TX.

Fujita, T. and S. Ohta. 1988. Photographic observations of the live style of a deep-sea ophiuroid Asteronyx loveni Echinodermata. Deep-Sea Research 35:2029-2043.

Gage, J.D. and P.A. Tyler. 1991. Deep-sea biology: a natural history of organisms at the deep-sea floor. Cambridge, New York: Cambridge University Press. Pp. 1-504.

Gage, J.D. 2004. Diversity in deep-sea benthic macrofauna: the importance of local ecology, the larger scale, history and the Antarctic. Deep-Sea Research II 51:1689-1708.

Garrard, S.L., R.C. Hunter, A.Y. Frommel, A.C. Lane, J.C. Phillips, R. Cooper, R. Dineshram, U. Cardini, S.J. McCoy, M. Arnberg, B.G. Rodrigues Alves, S. Annane, M.R. de Orte, A. Kumar, G.V. Aguirre-Martetínez, R.H. Maneja, M.D. Basallote, F. Ape, A. Torstensson, and M.M. Bjoerk. 2012. Biological impacts of ocean acidification: a postgraduate perspective on research priorities. Mar. Biol. DOI 10.1007/s00227-012-2033-3

Gass, S.E. and J.M. Roberts. 2006. The occurrence of the cold-water coral *Lophelia pertusa* Scleractinia on oil and gas platforms in the North Sea: colony growth, recruitment and environmental controls on distribution. Mar. Pollut. Bull. 52(5):549-59.

Gaston, K.J. 2003. The structure and dynamics of geographic ranges. Oxford: Oxford University Press.

Gattuso, J.-P., K. Gao, K. Lee, B. Rost, and K.G. Schulz. 2010. Approaches and tools to manipulate the carbonate chemistry. In: Riebesell, U., V.J. Fabry, L. Hansson, and J.-P, Gattuso, eds. Guide to Best Practices for Ocean Acidification Research and Data Reporting. Publications Office of the European Union: Luxembourg, Pp. 41-52.

Gearing, J.N., P.J. Gearing, D.T. Rudnick, A.G. Requejo, and M.J. Hutchins. 1984. Isotopic variability of organic carbon in a phytoplankton-based, temperate estuary. Geochimica et Cosmochimica Acta 48:1089-1098.

Geist, D.R., C.S. Abernethy, K.D. Hand, V.I. Cullinan, J.A. Chandler, and P.A. Groves. 2006. Survival, development, and growth of fall Chinook salmon embryos, alevins, and fry exposed to variable thermal and dissolved oxygen regimes. T. Am. Fish Soc. 135:1462-1477.

Genin, A., P.K. Dayton, P.F. Lonsdale, and F.N. Spiess. 1986. Corals on seamount peaks provide evidence of current acceleration over deep-sea topography. Nature 322:59-61.

Gjerde, K.M. 2006. Ecosystems and biodiversity report in deep waters and high seas. UNEP Regional Seas Reports and Studies No. 178. UNEP/ICUN, Gland, Switzerland.

Groner, J. 1922. Isherwood System Upheld in U. S. Court. American Shipping. Shipping Publishing Company, Inc., New York, NY. 24:6:18-23.

Guinan, J., C. Brown, M.F.J. Dolan, A.J. Grehan. 2009. Ecological niche modelling of the distribution of cold-water coral habitat using underwater remote sensing data. Ecological Informatics 42:83-92.

Guinotte, J.M., J. Orr, S. Cairns. 2006. Will human-induced changes in seawater chemistry alter the distribution of deep-sea scleractinian corals? Front. Ecol. Environ. 4:141-146.

Guisan, A. and U. Hofer. 2003. Predicting reptile distributions at the mesoscale: relation to climate and topography. J. Biogeorgr. 30:1233-1243.

Gulf Oil International. 2011. A Brief History of Gulf Oil. Internet website: http://www.gulfoilltd.com/about_gulf/history_of_gulf_oil/index.html. December 14.

Gulfpenn. 1921. Application of owner or master for official number. Department of Commerce, Bureau of Navigation. National Archives and Records Administration, Washington, DC. April 25.

Gulfpenn. 1942. Consolidated certificate of enrollment and license. The United States of America Treasury Department of Customs. National Archives and Records Administration, Washington, DC. March 11.

Haedrich, R.L., G.T. Rowe, and P.T. Polloni. 1980. The megabenthic fauna in the deep sea south of New England, USA. Mar. Biol. 57:165-179.

Hamilton, P. 1990. Deep currents in the Gulf of Mexico. Journal of Physical Oceanography 20:1087-1104.

Hamilton, P.T., J. Berger, J. H. Churchill, R. R. Leben, T. N. Lee, J. Singer, W. Sturges, E. Waddell. 2000. Desoto Canyon Eddy Intrusion Study; Final Report, Volume II: Technical Report, OCS Study MMS 2000-080, U. S. Dept. of the Interior, Minerals Management Service, Gulf of Mexico OCS Region, New Orleans, LA.

Hellberg, M. 2006. No variation and low synonymous substitution rates in coral mtDNA despite high nuclear variation. BMC Evolutionary Biology 61:24.

Hellberg, M.E. 2006. No variation and low synonymous substitution rates in coral mtDNA despite high nuclear variation. BMC Evolutionary Biology 624:1471-2148.

Helmuth, B., B.R. Broitman, C.A. Blanchette, S. Gilman, P. Halpin, C.D.G. Harley, M.J. O'Donnell, G.E. Hofmann, B. Menge, and D. Strickland. 2006. Mosaic patterns of thermal stress in the rocky intertidal zone: Implications for climate change. Ecol. Monogr. 76:461–479.

Henderson, E.D. 1942. Summary of statements by survivors of the SS Robert E. Lee, U.S. Cargo-Passenger Vessel. Navy department, Office of the Chief of Naval Operations. August 13.

Henry, L. and J Roberts. 2007. Biodiversity and ecological composition of macrobenthos on cold-water coral mounds and adjacent off-mound habitat in the bathyal Porcupine Seabight, NE Atlantic. Deep Sea Research Part I: Oceanographic Research Papers, 54 (4):654–672.

Hocking, C. 1969: Dictionary of disasters at sea during the age of steam, including sailing ships and ships of war lost in action, 1824-1962. Lloyd's Register of Shipping.

Henkel, S.K., H. Kawai, and G.E. Hofmann. 2009. Interspecific and interhabitat variation in hsp70 gene expression in native and invasive kelp populations. Mar. Ecol. Prog. Ser. 386:1-13.

Hirzel, A.H., J. Hausser, D. Chessel, and N. Perrin. 2002. Ecological-niche factor analysis: how to compute habitat-suitability maps without absence data? Ecology 837:2027-2036.

Hoff, G.R. and B. Stevens. 2005. Faunal Assemblage Structure on the Patton Seamount Gulf of Alaska, USA. Alaska Fishery Research Bulletin 11: 27-36.

Hofmann, G. and Todgham, A. 2010. Living in the now: Physiological mechanisms to tolerate a rapidly changing environment. Annu. Rev. Physiol. 72:127-145.

Hofmann, G.E., J.P Barry, P.J. Edmunds, R.D. Gates, D.A. Hutchins, T. Klinger, and M.A. Sewell. 2010. The effect of ocean acidification on calcifying organisms in marine ecosystems: An organism-to-ecosystem perspective. Annu. Rev. Ecol. Evol. Syst. 41:127-147.

Holcomb, M., A. Cohen, R.I. Gabitov, J.L. Hutter. 2009. Compositional and morphological features of aragonite precipitated experimentally from seawater and biogenically by corals. Geochim. Cosmochim. Ac. 73:4166-4179.

Horn, B.K.P. 1981. Hill shading and the reflectance map. Proceedings of the IEEE 691:14-47.

Hovland, M. and M. Risk. 2003. Do Norwegian deep-water coral reefs rely on seeping fluids? Marine Geology 198:83-96.

Howell, K.L., D.S.M. Billett, and P.A. Tyler. 2002. Depth-related distribution and abundance of seastars Echinodermata: Asteroidea in the Porcupine Seabight and Porcupine Abyssal Plain, NE Atlantic. Deep-Sea Research I 49:1901-1920.

Howell, K.L., R. Holt, I.P. Endrino, and H. Stewart. 2011. When the species is also a habitat: comparing the predictively modelled distributions of *Lophelia pertusa* and the reef habitat it forms. Biological Conservation 14411:2656-2665.

Hughes, T.P., A.H. Baird, D.R. Bellwood, M. Card, S. R. Connolly, C. Folke, R. Grosberg, O. Hoegh-Guldberg, J. B. C. Jackson, J. Kleypas, J.M. Lough, P. Marshall, M. Nyström, S.R. Palumbi, J.M. Padolfi, B. Rosen, and J. Roughgarden. 2003. Climate change, human impacts, and the resilience of coral reefs. Science 301:929-933.

Hughes, V. 2004. Edgar Anguish McKinnon: The Hughes family History. Internet Website: http://worldconnect.genealogy.rootsweb.com. May 14.

International Marine Engineering. 1912. New tank steamer for the Gulf Refining Company. International Marine Engineering March 1912. New York, NY: Aldrich Publishing Company. Pp. 109-112.

James, F.C., R.F. Johnston, N.O. Wamer, G.J. Niemi, and W.J. Boecklen. 1984. The Grinnellian niche of the Wood Thrush. Am. Nat. 124:17-30.

Jaubert, J. 1989. An integrated nitrifying-denitrifying biological system capable of purifying seawater in a closed circuit system. In Deuxieme International d'Aquariologie 1988 Monaco. Bulletin de l'Institut Oceanographique, Monaco, 5:195-204.

Jenness, J.S. 2004. Calculating landscape surface area from digital elevation models. Wildlife Society Bulletin 323:829-839.

Jenness, J.S. 2013. DEM Surface Tools for ArcGIS. Jenness Enterprises. Available at: http://www.jennessent.com/

Jensen, A. and R. Frederiksen. 1992. The fauna associated with the bank-forming deep-water coral *Lophelia pertusa* Scleractinaria on the Faroe Shelf. Sarsia 77(1):53-69.

Jones, K.H. 1998. A comparison of algorithms used to compute hill slope as a property of the DEM. Computers & Geosciences 244:315-323.

Jones, T.N. 2004. The Mica shipwreck deepwater nautical archaeology in the Gulf of Mexico. College Station, TX: Texas A&M University.

Kavanagh, D., J. Curdy, and A. McCarron. 2001. Sun Shipbuilding history log from 1916 thru 1919 and Sun Shipbuilding& Dry Dock Company hull data. http://www.sunshiporg.homestead.com/files/hullmas.pdf. Internet website: http://www.sunshiporg.homestead.com/files/1916_1919.htm. October 22.

Keeling, R., A. Körtzinger, and N. Gruber. 2010. Ocean deoxygenation in a warming world. Annu. Rev. Mar. Sci. 2:199-229.

Knowlton, N. 1993. Sibling species in the sea. Annual Review of Ecology and Systematics. 24:189-216.

Kohavi, R. 1995. A study of cross-validation and bootstrap for accuracy estimation and model selection. Appears in: The International Joint Conference on Artificial Intelligence IJCAI.

Koslow, J., K. Gowlett-Holmes, J. K. Lowry, T. O'Hara, G. C. B. Poore and A. Williams. 2001. Seamount benthic macrofauna off southern Tasmania: community structure and impacts of trawling. Mar Ecol, 213: 111–125.

Kube-McDowell, Michael. 2009. A Place Called Yorkship, Internet website: http://yorkship.us. Deccember 12, 2011.

Landry, L. 1994. Archaeological Assessment for the Nakika Pipeline Project. Prepared by John E. Chance and Associates for Shell International Exploration and Production, Inc. December.

Langer, G., G. Nehrke, I. Probert, J.Ly, and P. Ziveri. 2009. Strain-specific responses of Emiliania huxleyi to changing seawater carbonate chemistry. Biogeosciences 6:2637-2646.

Lavery, B. 2000. The arming and fitting of english ships of war, 1600-1815. Annapolis, MD: Naval Institute Press.

Lessard-Pilon, S.A., E.L. Podowski, E. E. Cordes, C.R. Fischer. 2010. Megafauna community composition associated with *Lophelia pertusa* colonies in the Gulf of Mexico. Deep Sea Res. Part II: Top. Stud. Oceanogr. 57:21-23, 1882-1890.

Leverette, T.L. and A. Metaxas. 2005. Predicting habitat for two species of deep-water coral on the Canadian Atlantic continental shelf and slope. In: Freiwald A. and J.M. Roberts, eds. Cold-water Corals and Ecosystems. Springer-Verlag Berlin Heidelberg. Pp. 467-479.

Levins, R. 1968. Evolution in changing environments: some theoretical explorations. Princeton, NJ: Princeton University Press.

Levitus, S., J. Antonov, and T. Boyer. 2005. Warming of the world ocean, 1955-2003. Geophys. Res. Lett. 32:L02604.

Levitus, S., J.I. Antonov, T.P. Boyer, and C. Stephens. 2000. Warming of the world ocean. Science 287:2225-2229.

Liu, C.R., P.M. Berry, T.P. Dawson, and R.G. Pearson. 2005. Selecting thresholds of occurrence in the prediction of species distributions. Ecography 28:385-393.

Lunblad, E.R., D.J. Wright, J. Miller, E.M. Larkin, R. Rinehart, D.F. Naar, B.T. Donahue, S.M. Anderson, and T. Battista. 2006. A benthic terrain classification scheme for American Samoa. Marine Geodesy 292:89-111.

Lunden, J.J., S.E. Georgian, and E.E. Cordes. 2013. Aragonite saturation states at cold-water coral reefs structured by *Lophelia pertusa* in the northern Gulf of Mexico. Limnol. Oceanogr. 58:354-362.

MacArthur, R.H. 1972. Geographical Ecology. New York: Harper & Row. 269 pp.

Maier, C., J. Hegeman, M.G. Weinbauer, et al. 2009. Calcification of the cold-water coral *Lophelia pertusa* under ambient and reduced pH. Biogeosciences 6:1671-1680.

Maier, C., P. Watremez, M. Taviani, M.G. Weinbauer, and J.-P. Gattuso. 2012. Calcification rates and the effect of ocean acidification on Mediterranean cold-water corals. Proc. R. Soc. B. 279:1716-1723.

Maier, C., F. Bils, M.G. Weinbauer, P. Watremez, M.A. Peck, and J.-P Gattuso. 2013a. Respiration of Mediterranean cold-water corals is not affected by ocean acidification as projected for the end of the century. Biogeosciences Discussions 10:7617-7640.

Maier, C., A. Schubert, M.M. Berzunza Sànchez, M.G. Weinbauer, P. Watremez, and J.-P. Gattuso. 2013b. End of the century pCO2 levels do not impact calcification in Mediterranean cold-water corals. PLoS ONE 8: e62655.

Masson, D.G., B.J. Bett, D.S.M. Billett, C.L. Jacobs, A.J. Wheeler, and R.B. Wynn. 2003. The origin of deep-water, coral-topped mounds in the northern Rockall Trough, Northeast Atlantic. Marine Geology 194:159-180.

McCarthy, M. 2005. Ship's fastenings: from sewn boat to steamship. College Station: Texas A&M University Press.

McCulloch, M., J. Trotter, P. Montagna, J. Falter, R. Dunbar, A. Freiwald, G. Försterra, M. López Correa, C. Maier, A. Rüggeberg, and M. Taviani. 2012. Resilience of cold-water scleractinian corals to ocean acidification: Boron isotopic systematics of pH and saturation state up-regulation. Geochim. Cosmochim. Ac. 87:21-34.

McFadden, C.S., SC France and JA Sánchez. 2006. A molecular phylogenetic analysis of the Octocorallia (Cnidaria: Anthozoa) based on mitochondrial protein-coding sequences. Molecular Phylogenetics and Evolution 41(3)513–527.

McMullin, E.R., K. Nelson, C.R. Fisher, and S.W. Schaeffer. 2010. Population structure of two deep sea tubeworms, Lamellibrachia luymesi and Seepiophila jonesi, from the hydrocarbon seeps of the Gulf of Mexico. Deep Sea Research Part I: Oceanographic Research Papers 5711:1499-1509.

Metaxas, A. and J. Davis. 2005. Megafauna associated with assemblages of deep-water gorgonian corals in Northeast Channel, off Nova Scotia, Canada. J. Mar. Biol. Assoc. UK 85: 1381-1390.

Messing, C., A. Conrad Neumann, and Judith C. Lang. 1990. Biozonation of deep-water lithoherms and associated hardgrounds in the northeastern Straits of Florida. Palaios :: 15-33.

Mienis, F., G.C.A. Duineveld, A.J. Davies, et al. 2012. The influence of near-bed hydrodynamic conditions on cold-water corals in the Viosca Knoll area, Gulf of Mexico. Deep-Sea Res. Pt. I 60:32-45.

Mikkelsen, N., H. Erlenkeuser, J. Killingley, and W. Berger. 1982. Norwegian corals: radiocarbon and stable isotopes in *Lophelia pertusa*. Boreas 11(2):163.

Miller, D. 2000. U-Boats: History, development and equipment, 1914-1945. London: Conway Maritime Press.

Miller, K.J. 1997. Genetic structure of black coral populations in New Zealand's fiords. Mar. Ecol. Prog. Ser. 161:123-132.

Miller, K.J. 1998. Short-distance dispersal of black coral larvae: inference from spatial analysis of colony genotypes. Mar. Ecol. Prog. Ser. 163: 225-233.

Minagawa, M. and E. Wada. 1984. Stepwise enrichment of 15N along food chains: Further evidence for the relation between d15N and animal age. Geochimica et Cosmochimica Acta 48:1135-1140.

Millero, F., J., K. Lee, M. Roche. 1998. Distribution of alkalinity in the surface waters of the major oceans. Marine Chemistry60 (1–2) 111–130.

Morgan, M. and C.J. Christ. 2003. Demise of *U-166*. World War II Magazine. July.

Morrison, C.L., S.W. Ross, M.S. Nizinski, S. Brooke, J. Järnegren, R.G. Waller, R.L. Johnson, and T.L. King. 2011. Genetic discontinuity among regional populations of *Lophelia pertusa* in the North Atlantic Ocean. Conservation Genetics 12:713-729.

Mortensen, P.B. and L. Buhl-Mortensen. 2004. Distribution of deep-water gorgonian corals in relation to benthic habitat features in the Northeast Channel Atlantic Canada. Mar. Biol. 144:223-1238.

Mortensen, P.B. 2001. Aquarium observations on the deep-water coral *Lophelia pertusa* (L., 1758) (Scleractinia) and selected associated invertebrates. Ophelia 54:83-104.

Mortensen, P., M. Hovland, T. Brattegard, and R. Farestveit. 1995. Deep water bioherms of the scleractinian coral *Lophelia pertusa* L. at 64° N on the Norwegian shelf: Structure and associated megafauna. Sarsia 80(2):145-158.

Mortensen, P., H. Rapp, 1998. Oxygen and carbon isotope ratios related to growth line patterns in skeletons of *Lophelia pertusa* (L) (Anthozoa, Scleractinia): Implications for determination of linear extension rate. Sarsia 83:433-446.

Mortensen, P.B., M.T. Hovland, J.F. Fosså, and D.M. Furevik. 2001. Distribution, abundance, and size of *Lophelia pertusa* coral reefs in mid-Norway in relation to seabed characteristics. J. Mar. Biol. Assoc. U.K. 81:581-597.

Mucci, A. 1983. The solubility of calcite and aragonite in seawater at various salinities, temperatures, and one atmosphere total pressure. Am. J. Sci. 283:780-799.

Mueller, C., T. Lundälv, J. Middelburg, and D. van Oevelen. 2013. The symbiosis between *Lophelia pertusa* and Eunice norvegica stimulates coral calcification and worm assimilation. PLoS ONE 8:e58660.

Mullineaux, L.S. and E.D. Garland. 1993. Larval recruitment in response to manipulated field flows. Mar. Biol. 116:667-683.

Nakajima, Y., A. Nishikawa, et al. 2012. The population genetic approach delineates the species boundary of reproductively isolated corymbose acroporid corals. Molecular phylogenetics and evolution 632:527-531.

Nakazato, T., D.L. Warren, and L.C. Moyle. 2010. Ecological and geographic modes of species divergence in wild tomatoes. American Journal of Botany 97:680-693.

Naumann, M.S., C. Orejas, C. Wild, and C. Ferrier-Pagès. 2011. First evidence for zooplankton feeding sustaining key physiological processes in a scleractinian cold-water coral. J. Exp. Biol. 214:3570-3576.

Neigel, J.E. 2009. Population Genetics and Biogeography of the Gulf of Mexico. In: Darryl, D.K.C. and L. Felder, eds. Gulf of Mexico origin, waters, and biota. Texas A&M University Press. Pp. 1353-1369.

Nemzer, B.V. and A.G. Dickson. 2005. The stability and reproducibility of Tris buffers in synthetic seawater. Mar. Chem. 96:237-242.

Neulinger, S., J. Järnegren, M. Ludvigsen, K. Lochte, W.-C. Dullo. 2008. Phenotype-specific bacterial communities in the cold-water coral *Lophelia pertusa* Scleractinia and their implications for the coral's nutrition, health, and distribution. Applied and Environmental Microbiology 74(23):7272–7285.

Neumann, A., J. W. Kofoed, and G. H. Keller. 1977. Lithoherms in the Straits of Florida. Geology, January, 1977, v. 5: 4-10

Newton, C., H. T. Mullins, A. F. Gardulski, A. C. Hine, and G. R. Dix. 1987. Coral mounds on the west Florida slope: unanswered questions regarding the development of deep-water banks." Palaios : 359-367.

New York Shipbuilding. 1911. "*Gulfoil*," Contract No. 125 Specifications for the Construction of a Single Screw Oil Steamer. Camden, NJ.

New York Shipbuilding. 1949. 50 Years. New York Shipbuilding Corporation. Camden, New Jersey.

Oil Trade,1918. Vessel Shipments of Oil from the U.S. Gulf Coast.Oil Trade Journal 9;1-12. Houston, TX.

Oil Trade,1920. Movements of the Mexican Oil Fleet. Oil Trade Journal 11;1-12. Houston, TX.

Olariaga, A., A. Gori, C. Orejas, and J.-M. Gili. 2009. Development of an autonomous aquarium system for maintaining deep corals. Oceanography 22:44-45.

Opresko, D.M. 2009. Antipatharia Cnidaria of the Gulf of Mexico. Corpus Christi, TX: Texas A&M University Press.

Orejas, C., C. Ferrier- Pagès, S. Reynaud, G. Tsounis, D. Allemand, and J. Maria. 2011. Experimental comparison of skeletal growth rates in the cold-water coral *Madrepora* oculata Linnaeus, 1758 and three tropical scleractinian corals. J. of Experimental Mar. Biol. and Ecol. 405(1-2):1-5.

Orejas, C., C. Ferrier-Pages, S. Reynaud, A. Gori, E. Beraud, G. Tsounis, D. Allemand, and J.-M. Gili. 2011b . Long-term growth rates of four Mediterranean cold-water coral species maintained in aquaria. Mar. Ecol. Prog. Ser. 429:57-65.

Orejas, C., A. Gori, and J.-M. Gili. 2007. Growth rates of live *Lophelia pertusa* and *Madrepora* oculata from the Mediterranean Sea maintained in aquaria. Coral Reefs 27(2):255.

Orth, R.J., T.J.B. Carruthers, W.C. Dennison, C. M. Duarte, J.W. Fourqurean, K.L. Heck Jr., A. R. Hughes, G.A. Kendrick, W.J. Kenworthy, S. Olyaarnik, F.T. Short, M. Waycott, and S.L. Williams. 2006. A global crisis for seagrass ecosystems. BioScience 56:987-996.

Palumbi, S.R. 2003. Population genetics, demographic connectivity, and the design of marine reserves. Ecological Applications 131:S146-S158.

Pane, E.F. and J.P. Barry. 2007. Inefficient acid-base regulation in the deep-sea decapod crab Chionoecetes tanneri during short-term hypercapnia. Mar. Ecol. Prog. Ser. 334:1-9.

Parker, L.M., P.M. Ross, W.A. O'Connor, L.Borysko, D.A. Raftos, and H.-O. Pörtner. 2012. Adult exposure influences offspring responses to ocean acidification in oysters. Global Change Biol. 18:82-92.

Paull, C.K., A.C. Neumann, B.A. am Ende, W. Ussler, and N.M. Rodriguez. 2000. Lithoherms on the Florida-Hatterasslope. Mar. Geol. 166:83-101.

Peakall, R.O.D. and P.E. Smouse. 2006. Genalex 6: genetic analysis in Excel. Population genetic software for teaching and research. Molecular Ecology Notes 6(1):288-295.

Pearce, J. and S. Ferrier. 2000. An evaluation of alternative algorithms for fitting species distribution models using logistic regression. Ecological Modelling 128:127-147.

Pearson, C.E., G.J. Castille, D.Davis, T.E. Redard, A.R. Saltus. 1989. A history of Waterborne Commerce and Transportation with in the U.S. Army Corps of Engineers New Orleans District and an inventory of known underwater cultural resources. New Orleans District, U.S. Army Corps of Engineers. New Orleans, Louisiana.

Peterson, C.H., M C Kennicutt II, R H Green, P Montagna, D E Harper, Jr., E N Powell, P F Roscigno. 1996. Ecological consequences of environmental perturbations associated with offshore hydrocarbon production: a perspective on long-term exposures in the Gulf of Mexico. Canadian Journal of Fisheries and Aquatic Sciences, 53(11): 2637-2654.

Phillips, S.J. and M. Dudik. 2008. Modeling of species distributions with Maxent: new extensions and a comprehensive evaluation. Ecography 312:161-175.

Phillips, S.J., R.P. Anderson, and R.E. Schapire. 2006. Maximum entropy modeling of species geographic distributions. Ecological Modelling 190:231-259.

Piepenburg, D. and B. Müller. 2004. Distribution of epibenthic communities on the Great Meteor seamount North-East Atlantic mirrors pelagic processes. Arch. Fish. Mar. Res. 51:55-70.

Pierrat, B., T. Saucède, R. Laffont, C. De Ridder, A. Festeau, and B. David. 2012. Large-scale distribution analysis of Antarctic echinoids using ecological niche modelling. MEPS 163:215-230.

Pierrot, D., E. Lewis, and D.W.R. Wallace. 2006. MS Excel Program Developed for CO2 System Calculations ORNL/CDIAC-105, Carbon Dioxide Inf. Anal. Cent., Oak Ridge Natl. Lab., U.S. Dept. of Energy, Oak Ridge, Tenn.

Pinzón, J.H., E. Sampayo, E. Cox, L.J. Chauka, C.A. Chen, C.R. Voolstra, and T.C. LaJeunesse. 2013. Blind to morphology: genetics identifies several widespread ecologically common species and few endemics among Indo-Pacific cauliflower corals Pocillopora, Scleractinia. Journal of Biogeography.

Pistevos, J.C.A., P. Calosi, S. Widdicombe, and J.D.D. Bishop. 2011. Will variation among genetic individuals influence species responses to global climate change? Oikos 120:675-689.

Pritchard, J. K., M. Stephens, and P. Donnelly. 2000. Inference of population structure using multilocus genotype data. Genetics 155(2):945-959.

Prouty, N., E. Roark, N. Buster, and S. Ross. 2011. Growth rate and age distribution of deep-sea black corals in the Gulf of Mexico. Mar. Ecol. Prog. Ser. 423:101-115.

Purser, A., A.I. Larsson, and D. van Oevelen. 2010. The influence of flow velocity and food concentration on *Lophelia pertusa* Scleractinia zooplankton capture rates. J. of Experimental Mar. Biol. and Ecol. 395:55-62.

Quattrini A., S.E. Georgian, L. Byrnes, A. Stevens, R. Falco, and E.E. Cordes. In press. Niche divergence by deep-sea octocorals in the genus Callogorgia across the continental slope of the Gulf of Mexico. Molecular Ecology.

Quattrini, A.M., S.E. Georgian, L. Byrnes, A. Stevens, R. Falco, and E.E. Cordes. 2013. Niche divergence by deep-sea octocorals in the genus Callogorgia across the continental slope of the Gulf of Mexico. Molecular Ecology.

Raven, J., K. Caldeira, H. Elderfield, O. Hoegh-Guldberg, P. Liss, U. Riebesell, J. Shepherd, C. Turley, A. Watson. 2005. Ocean acidification due to increasing atmospheric carbon dioxide. The Royal Society policy document 12/05. Cardiff, UK: The Clyvedon Press Ltd.

Recknagel, F. 2001. Applications of machine learning to ecological modelling. Ecological Modelling 146:303-310.

Rex, M.A. 1981. Community structure in the deep-sea benthos. Annual Review of Ecology and Systematics 12:331-353.

Ridgway, T. 2002. Testing the applicability of molecular genetic markers to population analyses of scleractinian corals. Symbiosis 333:243-262.

Roark, E.B., T.P. Guilderson, R.B. Dunbar, S.J. Fallon, and D.A. Mucciarone. 2009. Extreme longevity in proteinaceous deep-sea corals. PNAS. 106(13):5204-5208.

Roberts, H.H., C. V. Phipps and L. Effendi. 1987. *Halimeda* bioherms of the eastern Java Sea, Indonesia. Geology 15 (4)371-374.

Roberts, H. H., R. Fillon, B. Kohl, J. Robalin and J. Sydow. 2004. Depositional architecture of the Lagniappe Delta: sediment characteristics, timing of depositional events, and temporal relationship with adjacent shelf-edge deltas. SEPM (Society for Sedimentary Geology), Special Pub. 79: 143–188

Roberts, J.M. 2002. The occurrence of the coral *Lophelia* pertusea and other conspicuous epifauna around an oil platform in the North Sea. The International J. of Society of Underwater 25(2):83-92.

Roberts, J.M. 2005. Reef-aggregating behavior by symbiotic eunicid polychaetes from cold-water corals: Do worms assemble reefs? J. Mar. Biol. Ass. U.K. 85:813-819.

Roberts, J.M., D. Long, J.B. Wilson, P.B. Mortensen, and J.D. Gage. 2003. The cold-water coral *Lophelia pertusa* (Scleractinia) and enigmatic seabed mounds along the north-east Atlantic margin: are they related? Mar. Pollution Bull. 46(1):7-20.

Roberts, J.M., A.J. Wheeler, and A. Freiwald. 2006. Reefs of the deep: The biology and geology of cold-water coral ecosystems. Science 312:543-547.

Roberts, H., R. Carney, M.Kupchik, C. Fisher, K. Nelson, E.Becker, L. Goehring, S. Lessard-Pilon, G.Telesnicki, B.Bernard, J.Brooks, M. Bright, E. Cordes, ; S. Hourdez, J.Hunt Jr., W.Shedd, .G. Boland, ; S. Joye, V. Samarkin, M. Bernier, and M. Bowles, I. MacDonald, H. Niemann, C. Petersen, C. Morrison, J. Potter. 2007. Alvin Explores the Deep Northern Gulf of Mexico Slope. EOS 88:341–348.

Roberts, J.M., A.J. Wheeler, A. Freiwald, and S.D. Cairns. 2009. Cold-water corals: the biology and geology of deep-sea coral habitats. Cambridge, NY: Cambridge University Press.

Rödder D. and J.O. Engler. 2011. Quantitative metrics of overlaps in Grinnellian niches: advances and possible drawbacks. Global Ecology and Biogeography 20:915-927.

Rodolfo-Metalpa, R., F. Houlbreque, E. Tambutte, F. Boisson, C. Baggini, F.P. Patti, R. Jeffree, M. Fine, A. Foggo, J.-P., Gattuso, and J.M. Hall-Spencer. 2011. Coral and mollusc resistance to ocean acidification adversely affected by warming. Nat. Clim. Change 1:308-312.

Rogers, A.D. 1994. The biology of seamounts. Advances in Marine Biology 30:305-350.

Rogers, A.D. 1999. The biology of *Lophelia pertusa* (Linnaeus, 1758) and other deep-water reef-forming corals and impacts from human activities. Int. Rev. Hydrobiol. 844:315–406.

Ronquist, F. and J.P. Huelsenbeck. 2003. Mr.Bayes 3: Bayesian phylogenetic inference under mixed models. Bioinformatics 19:1572-1574.

Ross, S.W. and A.M. Quattrini. 2007. The fish fauna associated with deep coral banks off the southeastern Unites States. Deep Sea Res. Part I. Oceanogr. Res. Pap. 54(6): 975-1007.

Rössler, E. 2001. The U-boat: The evolution and technical history of German submarines. London: Arms and Armour Press, reprint.

Rozen, S. and H. Skaletsky. 2000. Primer3 on the WWW for general users and for biologist programmers. Totowa, NJ: Humana Press.

Rybka, W. and D. Moreland. 1994. U.S. Brig Niagara: Crew handbook. Third edition. A. McMamy, ed. Pennsylvania Museum and Historical Commission. Flagship Niagara League, Inc., Erie, PA.

Sabater, M.G. and H.T. Yap. 2002. Growth and survival of coral transplants with and without electrochemical deposition of CaCO3. J. Exp. Mar. Biol. Ecol. 272:131-146.

Sabatier, P., J. Reyss, J. Hall-Spencer, C. Colin, N. Frank, N. Tisnérat-Laborde, L. Bordier, and E. Douville. 2012. 210Pb-226Ra chronology reveals rapid growth rate of *Madrepora* oculata and *Lophelia pertusa* on world's largest cold-water coral reef. Biogeosciences 9:1253-1265.

Samadi, S., T. Schlacher, and B.R. De Forges. 2007. Seamount benthos. In: Pitcher, T.J., T. Morato, P.J.B. Hart, M.R. Clark, N. Haggan, and R.S. Santos, eds. Seamounts: Ecology, Fisheries, & Conservation. Fish and Aquatic Resources Series. Blackwell Publishing. Pp. 119-140.

Sammarco, P.W. 1982. Polyp bail-out: an escape response to environmental stress and a new means of reproduction in corals. Mar. Ecol. Prog. Ser. 10(1): 57-65.

Sayenga, D. Modern history of wire rope. Internet website: http://atlantic-cable.com/Article/WireRope/Sayenga/wirerope4.htm. July 2, 1998.

Schacht, H. 1942. War-Diary. Oberkommando Kriegsmarine Kriegstagebuch, Akten betreffend U-506, from March 26, 1942 through June 4, 1942. National Archives and Records Administration, Washington DC.

Schaum, E., B. Rost, A. Millar, and S. Collins. 2013. Variation in plastic responses of a globally distributed picoplankton species to ocean acidification. Nature Clim. Change 3:298-302.

Schoener, A. 1989. The ecological niche. In: Cherret, J.M., ed. Ecological Concepts. Oxford, UK: Blackwell Science. Pp. 79-114.

Schroeder, W.W. 2002. Observations of *Lophelia pertusa* and the surficial geology at a deep-water site in the northeastern Gulf of Mexico. Hydrobiologia 471:29-33.

Schroeder, W.W., S. Brooke, J. Olson, et al. 2005a. Occurrence of deep-water *Lophelia pertusa* and *Madrepora* oculata in the Gulf of Mexico. In: Freiwald, A. and J.M. Roberts, eds. Berlin Heidelberg cold-water corals and ecosystems. Springer. Pp. 297-307.

Schroeder, W.W., S.D. Brooke, J.B. Olson, B. Phaneuf, J.J. McDonough III, and P. Etnoyer. 2005b. Occurrence of deep-water *Lophelia pertusa* and *Madrepora oculata* in the Gulf of Mexico. In: Freiwald, A. and J.M. Roberts, eds. Cold-water corals and ecosystems. Springer-Verlag Berlin Heidelberg, Pp. 297-307.

SeaWaves. 2005. Gulfpenn 1942. SeaWaves Today in History. Internet website http://www.seawaves.com/newsletters/. May 13.

Shank, T.M. 2010. Seamounts: deep-ocean laboratories of faunal connectivity, evolution, and endemism. Oceanography 23:108–122.

Shearer, T.L., M.J.H. van Oppen, S.L. Romano, and G. Worheide. 2002. Slow mitochondrial DNA sequence evolution in the Anthozoa Cnidaria. Molecular Ecology 11(12):2475-2487.

Shepard, A.N., R.B. Theroux, R.A. Cooper, and J.R. Uzmann. 1986. Ecology of Ceriantharia Coelenterata, Anthozoa of the northwestern Atlantic from Cape Hatteras to Nova Scotia. Fish. Bull. 84:625–646.

Sinniger, F. and J. Pawlowski. 2009. The partial mitochondrial genome of *Leiopathes glaberrima* Hexacorallia: Antipatharia and the first report of the presence of an intron in COI in black corals. Galaxea, Journal of Coral Reef Studies 11:21-26.

Smith, S.O. 2007. Personal correspondence with authors January to July 2007.

Smith, S.O. 2005. The Frolic Archaeological Survey. Submitted to the California Department of Parks and recreation, Cultural Heritage Division. PAST Foundation, Columbus.

Souter, P. 2010. Hidden genetic diversity in a key model species of coral. Mar. Biol. 1574:875-885.

Staton, J.L., and D.L. Felder. 1995. Genetic variation in populations of the ghost shrimp genus Callichirus Crustacea, Decepoda, Thalassinoidea in the western Atlantic and Gulf of Mexico. Bull. Mar. Sci. 56:523-536.

Steffy, J.R. 1994. Wooden ship building and the interpretation of shipwrecks. College Station: Texas A&M University Press.

Sternhell, C.M. and A.M. Thorndike. 1946. Antisubmarine Warfare in World War II. Operations Evaluation Group report number 51. Office of the Chief of naval Operations Navy Department. Washington, DC.

Stocks, K.I. 2004. Seamount invertebrates: composition and vulnerability to fishing. In: Morato, T. and D. Pauly, eds. Seamounts: Biodiversity and fisheries. Fisheries Centre, University of British Columbia. Pp. 17-24

Stockwell, D.R.B. and I.R. Noble. 1991. Induction of sets of rules from animal distribution data: a robust and informative method of data analysis. Math. Comp. Simul. 32:249-254.

Strömberg, S.M., T. Lundälv, T. J. Goreau. 2010. Suitability of mineral accretion as a rehabilitation method for cold-water coral reefs. J. Mar. Biol. Ecol. 395:153-161.

Sulak, K. J., Brooks, R. A., Luke, K. E., Norem, A. D., Randall, M., A. J. Quaid, G.E. Yeargin,.; J.M. Miller, ; W.M. Harden, J.H. Caruso; S.W. Ross. 2007. Demersal fishes associated with Lophelia pertusa coral and hard-substrate biotopes on the continental slope, northern Gulf of Mexico. Bulletin of Marine Science, 81(Supplement 1), 65-92.

Sulak, K.J. 2008. Origins, composition, age, and structural diversification of Viosca Knoll *Lophelia* coral reefs and substrates – a synopsis of preliminary results. In: Sulak, K.J., M.T. Randall, K.E. Luke, A.D. Norem, and J.M. Miller, eds. Characterization of Northern Gulf of Mexico deepwater hard bottom communities with emphasis on *Lophelia* coral - *Lophelia* reef megafaunal community structure, biotopes, genetics, microbial ecology, and geology. USGS Open-File Report Pp.1-53.

Swanson, C.E. 1991. Predators and prizes: American privateering and imperial warfare 1739-1748. Columbia: South Carolina University Press.

Tent, J.F. 2003.Translation of war diary for German submarine "U-506" patrol duration: 26 March to 15 June 1942. Birmingham, AL.

Thiem, Ø., E. Ravagnan, J.H. Fossà, and J. Berntsen.2006. Food supply mechanisms for cold-water corals along a continental shelf edge. Journal of Marine Systems 60:207-219.

Thresher, R.E., B. Tilbrook, S. Fallon, N.C. Wilson, and J. Adkins. 2011. Effects of chronic low carbonate saturation levels on the distribution, growth and skeletal chemistry of deep-sea corals and other seamount megabenthos. MEPS 442:87-99.

Tindall, G.B. 1988. America, a narrative history. Vol. I. New York: W. W. Norton and Company.

Tittensor, D.P., A.R. Baco, P.E. Brewin, M.R. Clark, M. Consalvey, J. Hall-Spencer, A.A. Rowden, T. Schlacher, K.I. Stocks, and A.D. Rogers. 2009. Predicting global habitat suitability for stony corals on seamounts. Journal of Biogeography 366:1111-1128.

Todd, P.A. 2008. Morphological plasticity in scleractinian corals. Biological Reviews 83:315 - 337.

Tong, R., A. Purser, V. Unnithan, and J. Guinan. 2012. Multivariate statistical analysis of distribution of deep-water gorgonian corals in relation to seabed topography on the Norwegian margin. PLoS ONE, 78:e43534. doi:10.1371/journal.pone.0043534

Turley, C.M., J.M. Roberts, and J.M. Guinotte. 2007. Corals in deep-water: will the unseen hand of ocean acidification destroy cold-water ecosystems? Coral Reefs 26:445-448.

Turner, R.D. 1966. A survey and illustrated catalogue of the Teredinidae Mollusca: Bivalvia. Cambridge: Museum of Comparative Zoology, Harvard University.

U.S. Dept. of the Treasury, Bureau of Statistics.1886. Annual list of merchant vessels of the United States. Washington, D.C.: Government Printing Office.

USS PC-566. 1942. Report of Action with Enemy Submarine Which Torpedoed SS Robert E. Lee, Rescue of Survivors. Statements by H. C. Claudius and K. Howard.National Archives and Records Administration, Washington DC.

van der Vaart, A.W. 1998. Asymptotic statistics. Cambridge, UK: Cambridge University Press.

Wagner, D., R.G. Waller, R. J. Toonen. 2011. Sexual reproduction of Hawaiian black corals, with a review of the reproduction of antipatharians Cnidaria: Anthozoa: Hexacorallia. Invertebrate Biology 1303: 211-225.

Waller, R. and P. Tyler. 2005. The reproductive biology of two deep-water, reef-building scleractinians from the NE Atlantic Ocean. Coral Reefs 24:514-522.

Wang, Z.A., R. Wanninkhof, W. Cai, R.H. Byrne, X. Hu, T. Peng, and W. Huang. 2013. The marine inorganic carbon system along the Gulf of Mexico and Atlantic coasts of the United States: insights from a transregional coastal carbon study. Limnol. Oceanogr.  581:325-342.

Warren, D.J., R.A Church, R. Cullimore, and L. Johnston. 2004. ROV Investigations of The DKM *U-166* Shipwreck Site to Document the Archaeological and Biological Aspects of the Wreck Site: Final Performance Report.  U.S. Department of Commerce, National Oceanic and Atmospheric Administration, Office of Ocean Exploration.  Silver Spring, Maryland.

Warren, D.L., R.E. Glor, and M. Turelli. 2008. Environmental niche equivalency versus conservatism: quantitative approaches to niche evolution. Evolution 62:2868-2883.

Warren, D.L., R.E. Glor, and M. Turelli. 2010. ENMTools: a toolbox for comparative studies of environmental niche models. Ecography 33:607-611.

Watling, L. 2012. Biology of Deep-Water Octocorals. In: Michael Lesser, ed. Advances in marine biology. Academic Press. Pp. 41-122.

Watts, G.P., Jr. 1988. The Civil War at sea: Dawn of an age of iron and engineering. In: Bass. G.F., ed. Ships and Shipwrecks of the Americas: A History Based on Underwater Archaeology.  Thames and Hudson Ltd., London.

Wei, C.L., G.T. Rowe, G.F Hubbard, A.H. Scheltema and others (2010) Bathymetric zonation of deep-sea macrofauna in relation to export of surface phytoplankton production. Mar Ecol Prog Ser 399:1-14.

White, H.K., P.-Y. Hsing, W. Cho, T.M. Shank, E.E. Cordes, A.M. Quattrini, R.K. Nelson, R.Camilli, A.W.J. Demopoulos, C.R. German, J.M. Brooks, H.H. Roberts, W. Shedd, C.M. Reddy, and C.R. Fisher. 2012. Impact of the *Deepwater Horizon* oil spill on a deep-water coral community in the Gulf of Mexico. Proceedings of the National Academy of Sciences 109: E2648.

White, M., C. Mohn, H. de Stigter, and G. Mottram. 2005. Deep-water coral development as a function of hydrodynamics and surface productivity around the submarine banks of the

Rockall Trough, NE Atlantic. In: A. Freiwald and J.M. Roberts, eds. Cold-water Corals and Ecosystems. Springer-Verlag Berlin Heidelberg. Pp. 503-514.

Wiggins, M. 1995. Torpedoes in the Gulf Galveston and the U-Boats 1942-1943. College Station, TX: Texas A&M University Press.

Wilson, J.B. 1979. Patch Development of the deep-water coral *Lophelia pertusa* (L.) on Rockall Bank. J. Mar. Biol. Assoc. UK 591:165-172.

Wilson, M.F.J., B. O'Connell, C. Brown, J.C. Guinan, and A.J. Grehan. 2007. Multiscale terrain analysis of multibeam bathymetry data for habitat mapping on the continental slope. Marine Geodesy 30:3-35.

Winnier, J. 2003. Interview by F. Beierl and O. Halmburger at the National D-Day Museum, New Orleans, Louisiana, September 2003. In: History Uncovered Legend of *U-166*. History Channel. December 19, 2004.

Würdemann, E.K. Lt. 1942. Kriegstagebuch KTB or War Diary for German Submarine "U-506" Patrol Duration: 26 March to 15 June 1942. Translated by James F. Trent. Birmingham, AL.

Yesson C., M.L. Taylor, D.P. Tittensor, A.J. Davies, J. Guinotte, A. Baco, J. Black, J.M. Hall-Spencer, and A.D. Rogers. 2012. Global habitat suitability of cold-water octocorals. Journal of Biogeography 39:1278-1292.

zu Mondfeld, W. 2005. Historic ship models. New York: Sterling.

## The Department of the Interior Mission

As the Nation's principal conservation agency, the Department of the Interior has responsibility for most of our nationally owned public lands and natural resources. This includes fostering the sound use of our land and water resources, protecting our fish, wildlife and biological diversity; preserving the environmental and cultural values of our national parks and historical places; and providing for the enjoyment of life through outdoor recreation. The Department assesses our energy and mineral resources and works to ensure that their development is in the best interests of all our people by encouraging stewardship and citizen participation in their care. The Department also has a major responsibility for American Indian reservation communities and for people who live in island communities.

## The Bureau of Ocean Energy Management

The Bureau of Ocean Energy Management (BOEM) works to manage the exploration and development of the nation's offshore resources in a way that appropriately balances economic development, energy independence, and environmental protection through oil and gas leases, renewable energy development and environmental reviews and studies